DOCUMENT RELEASE

FOR RELEASE OF NEW OR REVISED DOCUMENTS & TEST REPORTS

THE BOEING COMPANY - VERTOL DIVISION

SHEET 1 OF 1 | RELEASE NO.

CLASSIFIED TITLE: WIND TUNNEL TESTS OF A FULL SCALE HINGELESS PROP/ROTOR DESIGNED FOR THE BOEING MODEL 222 TILT ROTOR AIRCRAFT

REL. DATE

EO NO.

DOCUMENT OR REPORT NO.: D222-10059-1

SECURITY CLASS: [ ] LIMITED [ ] DEFENSE LIMITED [ ] CONFIDENTIAL [X] UNCLASSIFIED

MODEL (IF APPLICABLE): MODEL 222

CONTRACT REQUIREMENT: [X] YES [ ] NO

CONTRACT NO.: NAS2-6505

DISTRIBUTION CATEGORY: [ ] A [ ] B [ ] C

REV. [ ] NEW [X]

DISTRIBUTION INFORMATION

ISSUED TO — GIVE NAME, ORGANIZATION AND ORGANIZATION NUMBER	MAIL STOP	QTY.	ISSUE NO.	KEEP UP TO DATE
ENGINEERING LIBRARY, 7214	P32-01	2		
RECORDS MANAGEMENT, 1543	P30-70	1		-
ENGINEERING RELEASE, 7213	P15-19	1 + 1 Vellum		
H. Klein	P32-23	1		
K. Grina	P32-04	1		
W. Peck	P30-12	1		
J. Magee	P32-23	5		
H. Alexander	P32-23	1		
J. Hooper	P32-75	1		
R. Gabel	P32-40	1		
J. Liiva	P31-75	1		
D. Richardson	P30-26	1		
K. Gillmore	P30-03	1		
R. Taylor	P32-48	1		
G. Walsh	P32-71	1		
J. Duvivier	P31-38	1		
C. Ellis	P30-18	1		
H. Bishop	P32-48	1		
B. Blake	P30-31	1		
J. Morris	P30-31	1		
J. O'Leary	P32-71	1		
L. Hengen	P32-71	1		
F. Leone	P32-48	1		
E. Tarzanin	P32-48	1		
W. Eason	P30-31	1		
F. Harris	P38-07	1		
D. Ekquist	P38-07	1		
NASA - CALIFORNIA		20 + 1 Vellum		

SHEETS ADDED

SHEETS REVISED

ORIGINATOR & DATE

CONTROLLING ORG.: Preliminary Design - 7040

MAIL STOP: P32-23 | PHONE: 2238

AUTHORIZATION SIGNATURE: J. P. Magee

CONTROL POINT SIGNATURE

CUSTOMER SIGNATURE

REMARKS

54 TOTAL DOCUMENTS/EO'S

54 TOTAL RELEASE FORMS

REV LTR

A B

THE BOEING COMPANY

VERTOL DIVISION · PHILADELPHIA, PENNSYLVANIA

CODE IDENT. NO. 77272

NUMBER D222-10059-1

TITLE Wind Tunnel Tests of a Full Scale Hingeless Prop/Rotor Designed for the Boeing Model 222 Tilt Rotor Aircraft

ORIGINAL RELEASE DATE _____. FOR THE RELEASE DATE OF SUBSEQUENT REVISIONS, SEE THE REVISION SHEET. FOR LIMITATIONS IMPOSED ON THE DISTRIBUTION AND USE OF INFORMATION CONTAINED IN THIS DOCUMENT, SEE THE LIMITATIONS SHEET.

MODEL 222 CONTRACT NAS2-6505

ISSUE NO. _____ ISSUED TO: _____

PREPARED BY	J. P. Magee	DATE	4/12/73
PREPARED BY	H. R. Alexander	DATE	4/12/73
APPROVED BY	K. B. Gilmore	DATE	
APPROVED BY	D. A. Richardson	DATE	4/13/73
APPROVED BY	W. B. Peck	DATE	4-16-73

LIMITATIONS

This document is controlled by Organization 7810

All revisions to this document shall be approved by the above noted organization prior to release.

ACTIVE SHEET RECORD

SHEET NUMBER	REV LTR	ADDED SHEETS				SHEET NUMBER	REV LTR	ADDED SHEETS			
		SHEET NUMBER	REV LTR	SHEET NUMBER	REV LTR			SHEET NUMBER	REV LTR	SHEET NUMBER	REV LTR
i	A			—		XLV	A				
ii	A	iia	A	—		XLVI	A				
iii	A					XLVII	A				
iv	A					XLVIII	A				
v	A					XLIX	A				
vi	A					L	A				
vii	A					LI	A				
viii	A					LII	A				
ix	A					LIII	A				
x	A					LIV	A	LIVa	A		
xi	A	xia	A					LIVb	A		
xii	A							LIVc	A		
xiii	A					LV	A				
xiv	A					LVI	A				
xv	A					LVII	A				
xvi	A					LVIII	A				
xvii	A										
xviii	A										
xix	A										
xx	A										
xxi	A										
xxii	A										
xxiii	A										
xxiv	A										
xxv	A										
xxvi	A										
xxvii	A										
xxviii	A										
xxix	A										
xxx	A										
xxxi	A										
xxxii	A										
xxxiii	A										
xxxiv	A										
xxxv	A										
xxxvi	A										
xxxvii	A										
xxxviii	A										
xxxix	A										
XL	A										
XLI	A										
XLII	A										
XLIII	A										
XLIV	A										

ACTIVE SHEET RECORD

SHEET NUMBER	REV LTR	ADDED SHEETS				SHEET NUMBER	REV LTR	ADDED SHEETS			
		SHEET NUMBER	REV LTR	SHEET NUMBER	REV LTR			SHEET NUMBER	REV LTR	SHEET NUMBER	REV LTR
1						41					
2	A					42	A				
3	A					43					
4	A					44	A				
5						45	A				
6						46					
7						47					
8	A,B					48					
9						49					
10						50					
11						51					
12						52					
13	A					53					
14	A					54	A				
15	A					55	A				
16						56					
17						57					
18						58					
19	B					59					
20	A.					60					
21						61					
22						62					
23						63					
24						64					
25	A					65					
26						66					
27						67					
28						68	A				
29						69	A				
30						70					
31						71					
32						72					
33						73					
34	A,B					74					
35	B					75					
36						76					
37						77					
38						78					
39						79					
40						80					

FORM 48283 (12/65)

ACTIVE SHEET RECORD

SHEET NUMBER	REV LTR	ADDED SHEETS				SHEET NUMBER	REV LTR	ADDED SHEETS			
		SHEET NUMBER	REV LTR	SHEET NUMBER	REV LTR			SHEET NUMBER	REV LTR	SHEET NUMBER	REV LTR
81						121					
82						122					
83	A					123					
84						124	A				
85	A					125					
86	A					126					
87						127					
88						128					
89						129					
90						130					
91						131					
92						132					
93						133					
94						134					
95	A					135					
96						136					
97						137					
98						138					
99						139					
100						140					
101						141					
102						142					
103						143					
104						144					
105		—				145					
106	A					146					
107						147					
108						148					
109				—	—	149					
110						150	A				
111						151	A				
112						152				—	—
113						153	A				
114						154					
115						155					
116		—	—	—	—	156	—	—	—	—	—
117	A					157					
118						158					
119	A					159					
120						160	A				

FORM 46283 (12-65)

ACTIVE SHEET RECORD

SHEET NUMBER	REV LTR	ADDED SHEETS				SHEET NUMBER	REV LTR	ADDED SHEETS			
		SHEET NUMBER	REV LTR	SHEET NUMBER	REV LTR			SHEET NUMBER	REV LTR	SHEET NUMBER	REV LTR
161	A					201					
162	A					202					
163						203					
164	A					204					
165	A					205					
166	A					206					
167	A					207					
168						208					
169						209					
170	A					210					
171						211					
172						212					
173						213					
174						214					
175						215					
176						216					
177						217					
178						218					
179						219					
180						220					
181						221	A				
182						222					
183						223					
184						224					
185						225					
186						226					
187						227					
188						228					
189						229					
190						230					
191						231					
192						232					
193						233					
194						234					
195						235					
196						236					
197						237					
198						238					
199						239					
200						240					

FORM 46268 (7/67)

ACTIVE SHEET RECORD

SHEET NUMBER	REV LTR	ADDED SHEETS				SHEET NUMBER	REV LTR	ADDED SHEETS			
		SHEET NUMBER	REV LTR	SHEET NUMBER	REV LTR			SHEET NUMBER	REV LTR	SHEET NUMBER	REV LTR
241						281					
242						282					
243						283					
244						284					
245						285					
246						286					
247						287					
248						288					
249	A					289					
250						290					
251	A					291					
252						292					
253	A					293					
254						294					
255						295					
256						296					
257						297					
258						298					
259						299					
260						300	A				
261						301					
262						302					
263						303					
264						304					
265						305					
266						306	A				
267						307	A				
268						308					
269						309					
270						310					
271						311	A				
272						312					
273						313					
274						314	A, B				
275						315					
276						316					
277						317					
278						318					
279						319					
280						320					

FORM 46282 (7/67)

ACTIVE SHEET RECORD

SHEET NUMBER	REV LTR	ADDED SHEETS				SHEET NUMBER	REV LTR	ADDED SHEETS			
		SHEET NUMBER	REV LTR	SHEET NUMBER	REV LTR			SHEET NUMBER	REV LTR	SHEET NUMBER	REV LTR
321	B					361					
322						362					
323	B					363	B				
324	B					364	B				
325	B					365	B				
326	B					366					
327						367					
328						368	B				
329						369					
330						370	B				
331	B					371	B				
332						372	B				
333						373	B				
334						374					
335						375					
336						376					
337						377					
338						378	B				
339						379	B				
340						380	B				
341						381	B				
342						382					
343						383	B				
344						384					
345						385					
346						386					
347						387					
348						388					
349						389					
350						390					
351						391					
352						392					
353						393					
354						394					
355						395					
356	B					396					
357	B					397					
358						398					
359	B					399					
360						400					

FORM 46283 (7/67)

ACTIVE SHEET RECORD

SHEET NUMBER	REV LTR	ADDED SHEETS				SHEET NUMBER	REV LTR	ADDED SHEETS			
		SHEET NUMBER	REV LTR	SHEET NUMBER	REV LTR			SHEET NUMBER	REV LTR	SHEET NUMBER	REV LTR
401						441					
402						442					
403						443					
404						444					
405						445					
406						446					
407						447					
408						448					
409						449					
410						450					
411						451					
412						452					
413						453					
414						454					
415						455					
416						456					
417						457					
418						458					
419						459					
420						460					
421						461					
422						462					
423						463					
424						464	A				
425						465					
426						466	A				
427						467					
428						468					
429						469					
430						470					
431						471					
432						472					
433						473					
434						474					
435						475					
436						476					
437						477					
438						478					
439						479					
440						480					

FORM 46283 (7/67)

ACTIVE SHEET RECORD

SHEET NUMBER	REV LTR	ADDED SHEETS				SHEET NUMBER	REV LTR	ADDED SHEETS			
		SHEET NUMBER	REV LTR	SHEET NUMBER	REV LTR			SHEET NUMBER	REV LTR	SHEET NUMBER	REV LTR
481						521					
482						522	A				
483						523	A				
484						524	A ,B				
485						525	A ,B				
486						526	A				
487						527	A				
488						528	A				
489						529	A				
490						530	A	530a,b			
491						531					
492						532					
493						533					
494						534					
495						535					
496						536					
497	A					537	A				
498						538					
499						539					
500						540					
501						541					
502	A					542					
503						543					
504						544					
505						545					
506	A					546					
507	A					547					
508	A ,B					548	A	548a			
509	A ,B					549	A				
510	A					550	A				
511	A	511a,b				551					
512						552	A				
513						553					
514	A					554					
515	A					555					
516						556					
517						557					
518						558					
519						559					
520						560					

FORM 46263 (12/65)

ACTIVE SHEET RECORD

SHEET NUMBER	REV LTR	ADDED SHEETS				SHEET NUMBER	REV LTR	ADDED SHEETS			
		SHEET NUMBER	REV LTR	SHEET NUMBER	REV LTR			SHEET NUMBER	REV LTR	SHEET NUMBER	REV LTR
561						601					
562	A					602					
563	A					603	A				
564						604	A				
565						605	A				
566	A					606	A				
567	A					607	A				
568						608	A				
569						609	A				
570	A					610					
571	A					611					
572						612	A				
573						613	A				
574	A					614					
575	A					615					
576	A					616					
577	A					617					
578	A					618					
579	A					619					
580						620					
581	A					621					
582	A					622					
583						623					
584						624					
585						625					
586						626					
587						627					
588						628					
589						629					
590						630					
591						631					
592						632					
593						633					
594						634					
595						635					
596						636					
597						637					
598						638					
599						639					
600						640					

ACTIVE SHEET RECORD

SHEET NUMBER	REV LTR	ADDED SHEETS				SHEET NUMBER	REV LTR	ADDED SHEETS			
		SHEET NUMBER	REV LTR	SHEET NUMBER	REV LTR			SHEET NUMBER	REV LTR	SHEET NUMBER	REV LTR
641						681	A				
642						682	A				
643						683	A				
644						684	A				
645						685	A				
646						686	A				
647						687	A				
648						688	A				
649						689	A				
650						690	A				
651						691	A				
652						692	A				
653						693	A				
654						694	A				
655						695	A				
656						696	A				
657						697	A				
658						698	A				
659						699	A				
660						700	A				
661						701	A				
662						702	A				
663						703	A				
664						704	A				
665						705	A				
666						706	A				
667						707	A				
668						708	A				
669						709	A				
670						710	A				
671						711	A				
672						712	A				
673						713	A				
674	A					714	A				
675	A					715	A				
676	A					716	A				
677	A					717	A				
678	A					718	A				
679	A					719	A				
680	A					720	A				
						721	A				
						722	A				
						723	A				
						724	A				
						725	A				

FORM 46283 (12/65)

ACTIVE SHEET RECORD

SHEET NUMBER	REV LTR	ADDED SHEETS				SHEET NUMBER	REV LTR	ADDED SHEETS			
		SHEET NUMBER	REV LTR	SHEET NUMBER	REV LTR			SHEET NUMBER	REV LTR	SHEET NUMBER	REV LTR
726	A					771	A				
727	A					772	A				
728	A					773	A				
729	A					774	A				
730	A					775	A				
731	A					776	A				
732	A					777	A				
733	A					778	A				
734	A					779	A				
735	A					780	A				
736	A					781	A				
737	A					782	A				
738	A					783	A				
739	A					784	A				
740	A					785	A				
741	A					786	A				
742	A					787	A				
743	A					788	A				
744	A					789	A				
745	A					790	A				
746	A					791	A				
747	A										
748	A										
749	A										
750	A										
751	A										
752	A										
753	A										
754	A										
755	A										
756	A										
757	A										
758	A										
759	A										
760	A										
761	A										
762	A										
763	A										
764	A										
765	A										
766	A										
767	A										
768	A										
769	A										
770	A										

FORM 46283 (7/67)

REVISIONS Rev. B

LTR	DESCRIPTION	DATE	APPROVAL
A	Revision A is issued to incorporate comments received from NASA. Revision A is also issued to make changes in the Appendices as follows: Appendix 1 - no changes Appendix 2 - no changes Appendix 3 - revised Appendix 3 and added Appendix A3b and and Appendix A3c Appendix 4 - revised page numbers Appendix 5 - this is a new Appendix in its entirety Active Sheet Record Page ii(a) has been added to list the Roman Numeral sheets which were omitted from previous submittal		
B	Revision B is issued to incorporate comments received from NASA, and also add some additional comments of Boeing-Vertol.		

FOREWORD

This document was prepared by The Boeing Vertol Company of Philadelphia, Pa., for the National Aeronautics and Space Administration, Ames Research Center, under NASA Contract NAS2-6505 and was jointly funded by NASA and U. S. Army Air Mobility Research and Development Laboratory, Ames Directorate. The report presents the results of two wind tunnel tests of the Boeing Model 222 rotor in the NASA Ames 40' x 80' wind tunnel. Mr. D. Giulianetti of Ames Research Center was the technical monitor. Control feedback testing was also performed. Mr. G. Churchill was the technical monitor for this work.

Mr. J. P. Magee was the Boeing Vertol project engineer.

ABSTRACT

The rotor system designed for the Boeing Model 222 tilt rotor aircraft is a soft-in-plane hingeless rotor design, 26 feet in diameter. This rotor has completed two test programs in the NASA Ames 40' X 80' Wind Tunnel under NASA Contract NAS2-6505. The first test was a windmilling rotor test on two dynamic wing test stands. The rotor was tested up to an advance ratio equivalence of 400 knots. The second test used the NASA powered propeller test rig and data was obtained in hover, transition and low speed cruise flight.

Test data was obtained in the areas of wing-rotor dynamics, rotor loads, stability and control, feedback controls, and performance to meet the test objectives and are presented herein.

KEY WORDS

Model 222
Hingeless Rotor
Wind Tunnel Test
Wing-Rotor Dynamics
Rotor Loads
Rotor Stability Derivatives
Rotor Performance
Feedback Control
Frequency Response

TABLE OF CONTENTS

TABLE OF CONTENTS (CONT'D)

LIST OF FIGURES

LIST OF FIGURES (CONT'D)

LIST OF FIGURES

LIST OF FIGURES (CONT'D)

LIST OF FIGURES (CONT'D)

LIST OF FIGURES

LIST OF FIGURES (CONT'D)

LIST OF FIGURES (CONT'D)

LIST OF FIGURES (CON'T'D)

LIST OF FIGURES (CONT'D)

LIST OF FIGURES (CONT'D)

LIST OF FIGURES (CONT'D)

LIST OF FIGURES (CONT'D)

LIST OF FIGURES

LIST OF FIGURES (CONT'D)

LIST OF FIGURES (CONT'D)

LIST OF FIGURES (CONT'D)

LIST OF FIGURES (CONT'D)

LIST OF FIGURES

LIST OF FIGURES (CONT'D)

LIST OF FIGURES (CONT'D)

LIST OF FIGURES (CONT'D)

LIST OF FIGURES (CONT'D)

LIST OF FIGURES (CONT'D)

LIST OF FIGURES (CONT'D)

LIST OF FIGURES (CONT'D)

LIST OF FIGURES (CONT'D)

LIST OF FIGURES (CONT'D)

LIST OF FIGURES (CONT'D)

LIST OF FIGURES (CONT'D)

LIST OF FIGURES

LIST OF FIGURES (CONT'D)

LIST OF FIGURES (CONT'D)

LIST OF FIGURES

LIST OF FIGURES (CONT'D)

LIST OF FIGURES (CONT'D)

LIST OF FIGURES (CONT'D)

LIST OF FIGURES (CONT'D)

LIST OF FIGURES (CONT'D)

LIST OF FIGURES

LIST OF FIGURES (CONT'D)

LIST OF FIGURES (CONT'D)

LIST OF FIGURES (CONT'D)

LIST OF TABLES

NOMENCLATURE

A_1 - Lateral Cyclic Blade Angle ($\Delta\Theta = -A_{1}\cos(\psi + 20) - B_{1}\sin(\psi + 20)$

Aq - Product of Incidence Angle and Dynamic Pressure

B_1 - Longitudinal Cyclic Blade Angle ($\Delta\Theta = -A_{1}\cos(\psi + 20) - B_{1}\sin(\psi + 20)$

Bq - Product of Sideslip Angle and Dynamic Pressure

C_{T_P} - Propeller Thrust Coefficient $T/\rho n^2 D^4$

C_{T_R} - Rotor Thrust Coefficient $T/\rho \pi R^2 (\Omega R)^2$

C_M - Propeller Pitch Moment Coefficient $PM/\rho n^2 D^5$

C_{YAW} - Propeller Yaw Moment Coefficient $YM/\rho n^2 D^5$

C_N - Propeller Normal Force Coefficient $NF/\rho n^2 D^4$

C_{SF} - Propeller Side Force Coerficient $SF/\rho n^2 D^4$

C_{P_P} - Propeller Power Coefficient $HP/\rho n^3 D^5$

C_{P_R} - Rotor Power Coefficient $HP/\rho \pi R^2 (\Omega R)^3$

D - Diameter

EI_{FLAP} - Flapwise Bending Stiffness

EI_{CHORD} - Chordwise Bending Stiffness

FM - Figure of Merit

GJ - Torsional Stiffness

G_P - Pitch Gain Potentiometer Setting

G_Y - Yaw Gain Potentiometer Setting

HP - Horse Power

HZ - Hertz

i_N - Powered Test Thrust Line Incidence

$I_{cg_{pitch}}$ - Nacelle Pitch Inertia, Test 410

NOMENCLATURE (CONT'D)

$I_{cg_{yaw}}$	- Nacelle Yaw Inertia, Test 410
$I_{cg_{roll}}$	- Nacelle Roll Inertia, Test 410
I_{xx}	- Nacelle Roll Inertia, Test 416
I_{yy}	- Nacelle Pitch Inertia, Test 416
I_{zz}	- Nacelle Yaw Inertia, Test 416
I_p	- Acceleration Pitch Inertia
I^*_p	- Centrifugal Pitch Inertia
J	- Propeller Advance Ratio $V/n D$
n	- Revs/Sec
NF	- Normal Force
NA	- Neutral Axis
PM	- Pitching Moment
q	- Dynamic Pressure
R	- Radius
SF	- Side Force
SAS	- Electrohydraulic Servo Actuator
T	- Thrust
t/c	- Thickness/Chord Ratio
$V_{or}\ V_T$	- Tunnel Speed
V_1	- Command Voltage Pitch Loop (Figure 8.1)
V_2	- Command Voltage Yaw Loop (Figure 8.1)
V_1^1	- B_1 Actuator Voltage
V_2^1	- A_1 Actuator Voltage
W	- Running Weight

NOMENCLATURE (CONT'D)

WTP	- Wing Tip Pitch Moment
WTY	- Wing Tip Yaw Moment
WTL	- Wing Tip Lift
WRP	- Wing Root Pitch Moment
X/R or r/R	- Non-Dimensional Radius
YAW or YM	- Yaw Moment
α	- Angle of Attack
α_w	- Wing Angle of Attack
∂	- Partial Derivative Operator
ζ_V	- Wing Vertical Bending Damping % Critical
ζ_C	- Wing Chord Bending Damping % Critical
ζ_α	- Wing Torsion Damping % Critical
θ_{75}	- Blade Collective Pitch Angle
$\Delta\theta$	- Incremental Blade Pitch
ρ	- Density
ψ	- Azimuthal Angle, Figure 4.24
ψ_{rot}	- Incremental Azimuth Angle Defined in Figure 8.7
ω_{β}	- 2nd Mode Bending Blade Frequency
ω_L	- 1st Mode Bending Blade Frequency
ω_V	- Wing Vertical Bending Frequency
ω_C	- Wing Chord Bending Frequency
ω_α	- Wing Torsion Frequency
Ω	- Rotational Frequency

SUMMARY

The rotor system designed for the Boeing Model 222 tilt rotor research aircraft has been tested on two programs in the NASA Ames 40' X 80' wind tunnel under NASA contract NAS2-6505. This rotor is a soft in-plane hingeless composite (fiberglass boron) design. The first test program was a windmilling configuration mounted on two dynamic wing test stands. The aeroelastic data obtained on this program correlated well with predicted behavior and demonstrated the Boeing dynamics technology used in the Model 222 design. Testing was performed up to an advance ratio equivalence of 400 knots.

The second test program was a powered test program and covered hover, transition and cruise flight. A summary of the range of test conditions achieved is shown in Figure 1.

The rotor loads obtained on both programs in conjunction with structural test data indicate an adequate blade fatigue life with no load alleviation systems operating.

Performance data met or exceeded anticipated performance and stability and control data were obtained sufficient to provide design verification and correlation.

Two feedback control systems were tested: a load alleviation system and a damping augmentation system. The Boeing Model 222 does not require either of these systems. The load alleviation system attenuated the blade loads due to angle of attack by more than a factor of two, and the damping augmentation system increased the wing vertical bending modal damping as much as 500%.

The results of these tests provide confidence in the technology upon which the Boeing Model 222 tilt rotor aircraft design is based.

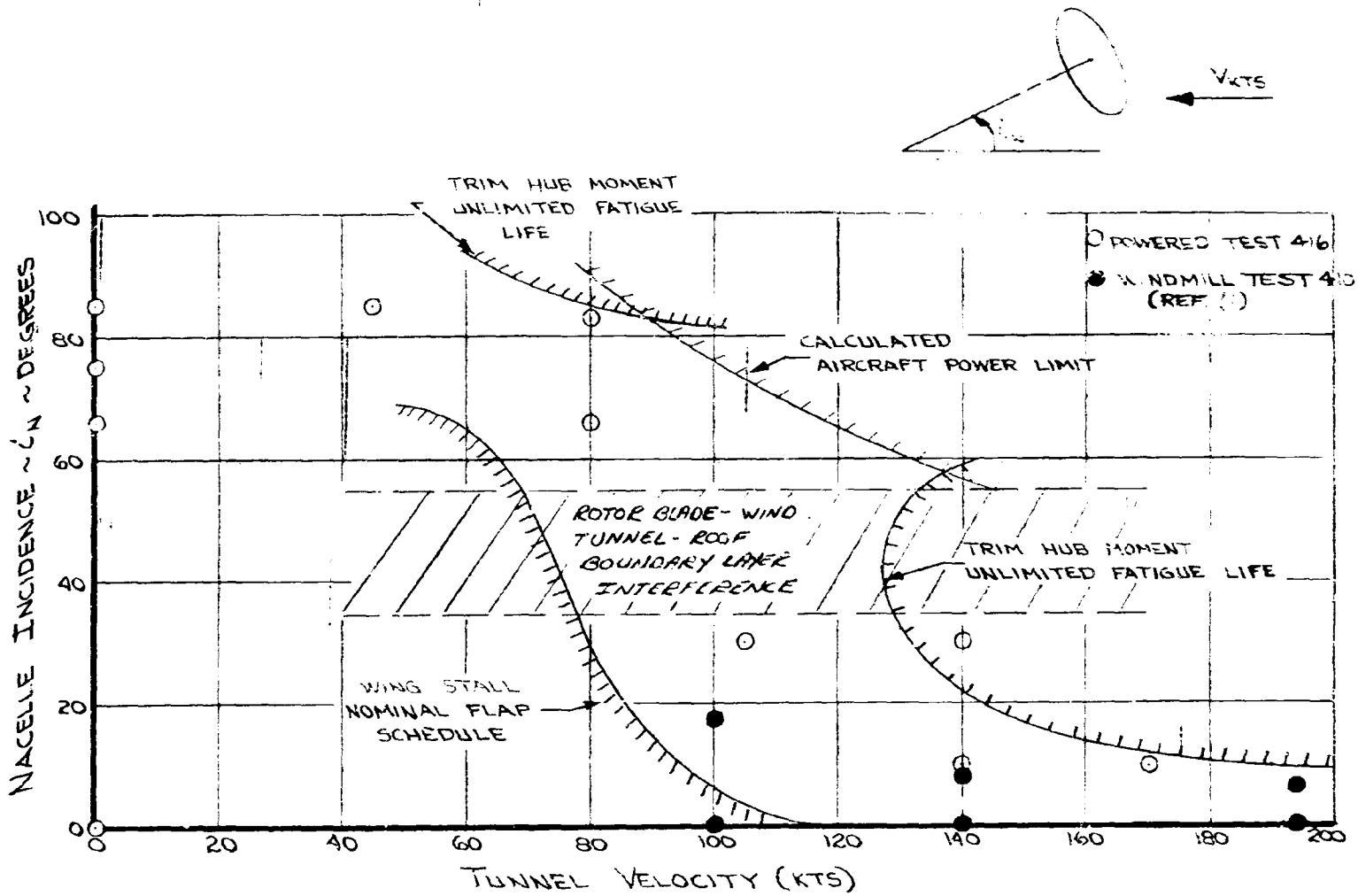

FIGURE 1. MODEL 222 WIND TUNNEL TEST CONDITIONS

1. INTRODUCTION

1.0 INTRODUCTION

The tilt rotor concept is the most promising candidate for a variety of future V/STOL aircraft applications. Many vehicle trend, comparison and preliminary design studies support this view, for example, References 1 to 6. The aircraft combines the hover and low speed advantages of the helicopter with the cruise capability of a propeller driven conventional aircraft. This airplane concept has been researched by Boeing and other companies for several years in addition to research initiated by NASA (Ames Research Center, Advanced Aircraft Programs Office), the U. S. Army Aeronautical Research Laboratory and the U. S. Air Force (AFRDL), References 7 to 12. This effort culminated in the NASA/Army proof of concept research aircraft program.

The Model 222 Tilt Rotor Research Aircraft was designed and proposed by the Boeing Company for this program. The rotor is a 26 ft. diameter soft in-plane hingeless composite (fiberglass/boron) design.

The rotor system to be used on this aircraft has been demonstrated and tested in the NASA 40' X 80' wind tunnel on two test programs. A dynamic test program (NASA 40'

by 80' wind tunnel test 410) where the rotor system was mounted on two dynamic wing test stands was performed in August-September 1972. For this test the rotor was unpowered and the objectives were to investigate the wing-rotor aeroelastic behavior. This test also incorporated additional research objectives concerning feedback to the rotor controls for load alleviation and aeroelastic damping augmentation.

The second test program (NASA 40' by 80' wind tunnel test 416) was performed in November-December 1972. For this test the rotor was mounted on the NASA powered propeller test rig and tested over a wide range of static, transition and low speed cruise conditions. The objectives of this program were to measure rotor loads, stability derivatives, control loads and performance.

The test data obtained on these two test programs is given in succeeding sections of this volume and provides experimental verification of the technology base on which the Boeing Model 222 Tilt Rotor Research Aircraft rests.

2.0 TEST INSTALLATIONS AND MODELS

2.0 TEST INSTALLATIONS AND MODEL DESCRIPTION

2.1 General

The model consists of a test stand and a flightworthy 26 foot diameter hingeless soft-in-plane rotor. The test stand (in the form of a nacelle) includes the necessary components for testing the rotor under varying conditions of collective and cyclic blade angles. The test stand and rotor was mounted on the NASA dynamic wing test stands (Figure 2.1) and the NASA propeller test rig for powered testing (Figure 2.2).

2.2 Dynamic Test Installation

During dynamic tests (NASA 40' x 80' test number 410) the Model 222 prop/rotor with its test stand nacelle and controls was mounted on two NASA furnished wing stands representing a prop/rotor aircraft semi-span wing. The aeroelastic properties of the two wings are given in Table 2.1. The full stiffness wing has stiffnesses designed to be optimum for a teetering rotor and as such is not optimal for the M-222 soft in-plane hingeless design, but is adequate to provide validation of analyses and to explore the rotor characteristics. The wing torsion frequency is higher than required and the wing vertical bending frequency is lower than the Model 222 design. The one quarter stiffness wing has natural frequencies of one half of the full stiffness wing.

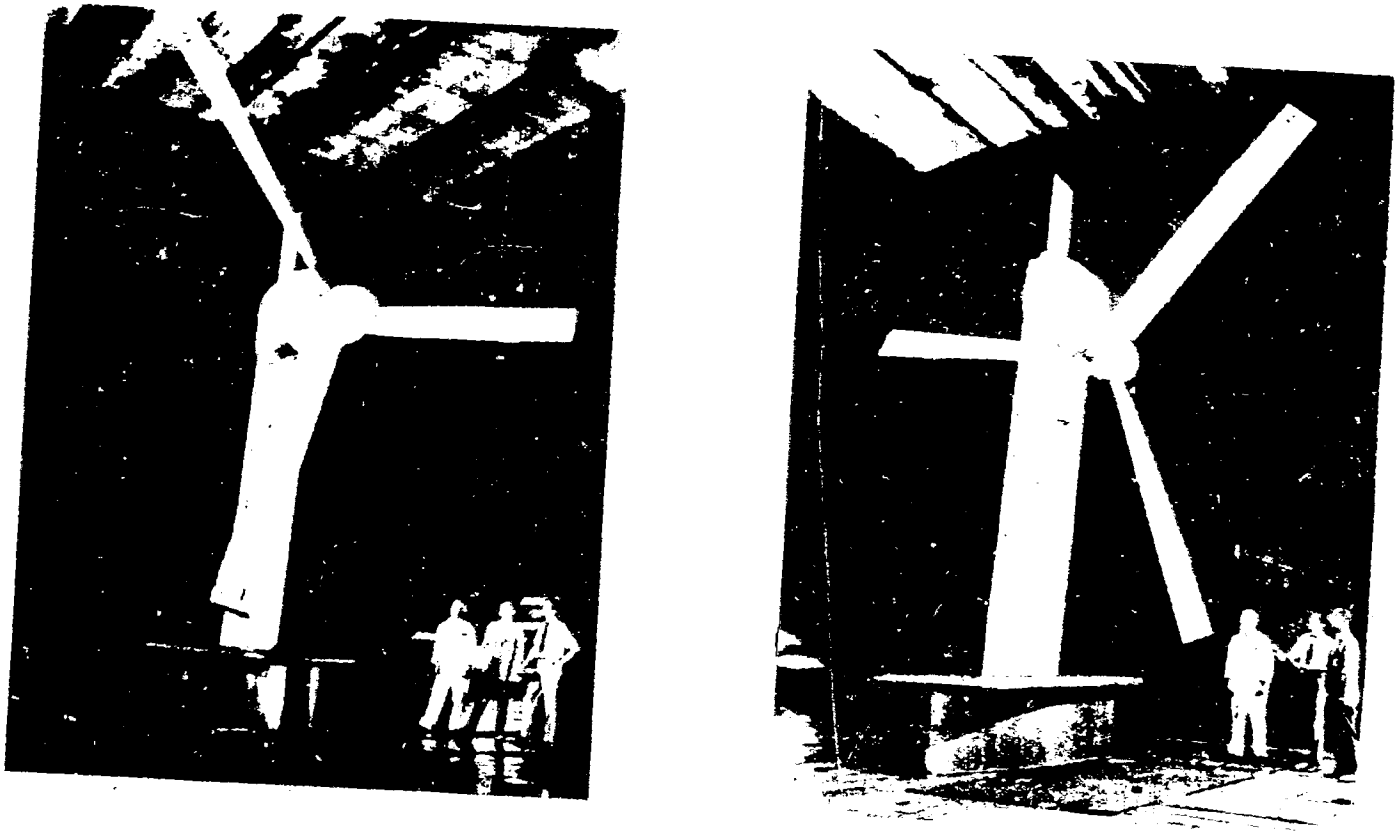

FIGURE NO. V-1
M222 26 Ft. Diameter Rotor System
Mounted on the NASA Dynamic Wing Test Stand
40' x 80' Tunnel
Test 410

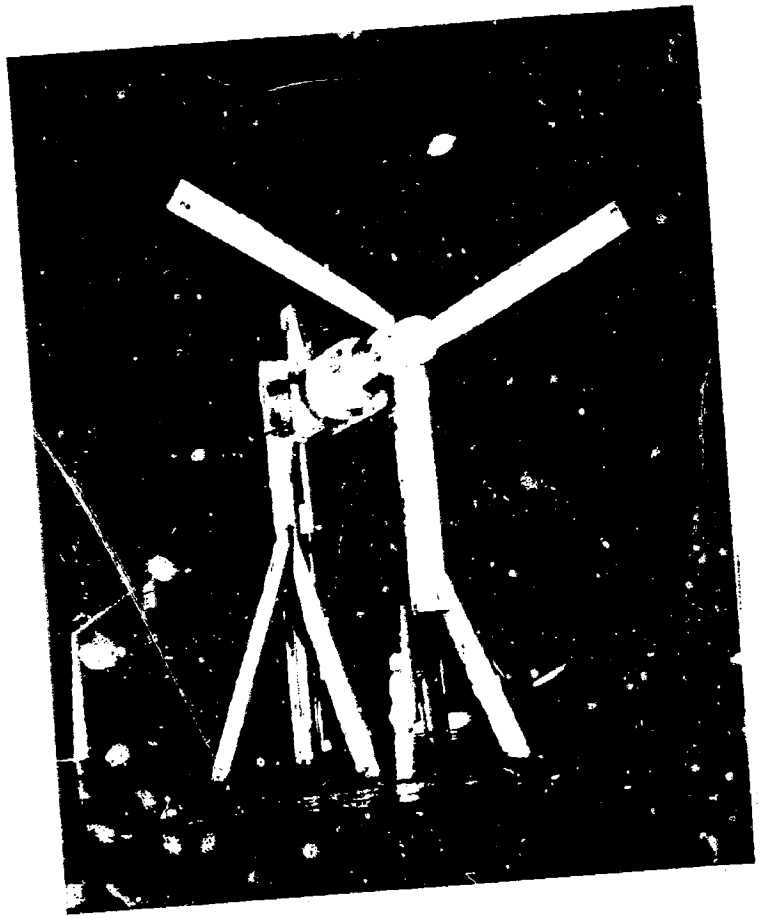

$I_N = 0°$

$i_N = 85°$

FIGURE NO. 2-2
M222 26 Ft. Diameter Rotor System
Mounted on the NASA Ames 40' x 80' Wind Tunnel
Powered Test Rig
Test 416

The construction of the full stiffness wing is a torque box with light non-structural nose and tail fairings resulting in a 13.5% thickness/chord ratio section. The installation is shown schematically including major dimensions in Figure 2.3. The nacelle mass and balance data in the dynamic test configuration with and without blades is given in Table 2.1.

Wing instrumentation consisted of two sets of strain gages. The wing "root" gages were located 150.62" inboard of the rotor shaft and a little aft of the ¼ chord (62.55" aft of rotor plane). These gages were arranged to measure wing flap bending, wing chord bending and wing torsion.

The wing "tip" gages were located 54.62" inboard of the rotor shaft and 51.67" aft of the rotor plane. These gages recorded wing tip chord bending (yaw), wing tip torsion (pitch), wing tip lift (normal force) and wing tip drag.

To provide excitation during rotating testing a shaker vane was mounted outboard of the nacelle which could be made to oscillate through various amplitudes at frequencies ranging from 2.0 Hz to 20 Hz. The vane was driven by a hydraulic motor.

TABLE 2.1
NASA AMES TEST-FULL AND
1/4 STIFFNESS WINGS-PROPERTIES

	Full Stiffness	1/4 Stiffness
Weight (LB) —	515.	1026.
Torsional Inertia (SLUG-FT^2)	6.47	4.20
Semichord (FT)	2.583	2.583
*Frequencies (coupled blades off)		
ω_v - vertical bending (cps)	2.5	1.2
ω_c - chordwise bending (cps)	4.5	2.2
ω_α - torsion (cps)	11.3	4.5

*Note: Frequencies checked out against test data

Nacelle Weight Data

Note: Data is without blades

Weight = 2000 LB.

$I_{cgpitch}$ = 250 SLUG-FT^2

I_{cgyaw} = 250 SLUG-FT^2

I_{cgroll} = 30 SLUG-FT^2

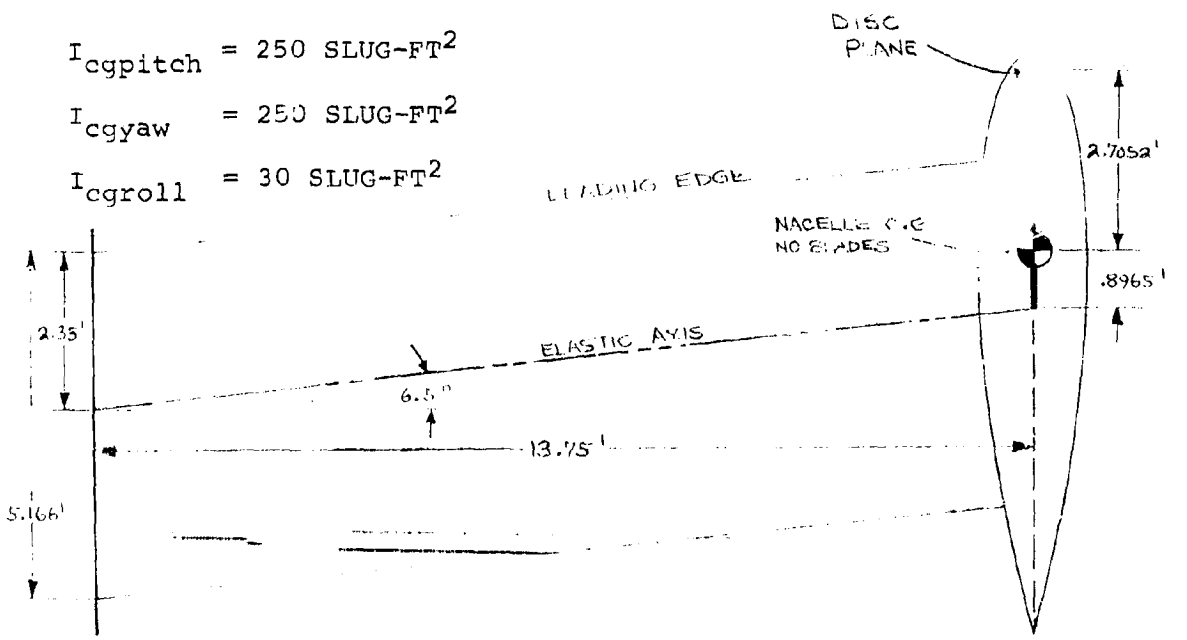

TABLE 2.1 (CONT'D)
1/4 AND FULL STIFFNESS WINGS
NASA TEST STAND MODE SHAPES

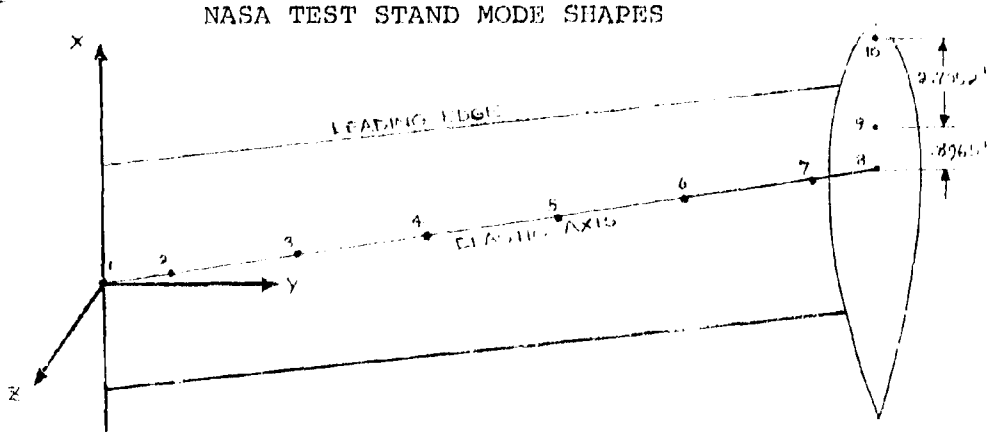

1. Wing Vertical Bending
   Full Stiff = 2.5 cps
   1/4 Stiff = 1.2 cps

MASS PT.	Y DISTANCE(IN.)	X(IN)	Y(IN)	Z(IN)	θX(RAD)	θY(RAD)	θZ(RAD)
1	0	0	0	0	0	0	Small
2	13.75	Small	Small	.005	.001	Small	Small
3	41.25	-.001	Small	.040	.002	Small	Small
4	68.75	-.002	Small	.104	.003	-.001	Small
5	96.25	-.004	Small	.191	.003	-.001	Small
6	123.75	-.006	.001	.293	.004	-.001	Small
7	151.25	-.008	.001	.405	.004	-.001	Small
8	165.0	-.009	.001	.463	.004	-.001	Small
9	165.0	-.009	.002	.475	.004	-.001	Small
10	165.0	-.009	.005	.511	.004	-.001	Small

2. Wing Chordwise Bending
   Full Stiff = 4.5 cps
   1/4 Stiff = 2.2 cps

MASS PT.	Y DISTANCE(IN.)	X(IN)	Y(IN)	Z(IN)	θX(RAD)	θY(RAD)	θZ(RAD)
1	0	0	0	0	0	0	0
2	13.75	-.005	.001	Small	Small	Small	.001
3	41.25	-.039	.005	-.001	Small	Small	.002
4	68.75	-.103	.012	-.002	Small	Small	.003
5	96.25	-.188	.022	-.004	Small	Small	.003
6	123.75	-.290	.033	-.006	Small	Small	.004
7	151.25	-.402	.046	-.008	Small	Small	.004
8	165.0	-.460	.053	-.009	Small	Small	.004
9	165.0	-.460	.099	-.009	0	Small	.004
10	165.0	-.460	.236	-.011	0	Small	.004

TABLE 2.1 (CONT'D)

3. Wing Torsion

Full Stiff = 11.3 cps
1/4 Stiff = 4.5 cps

MASS PT.	Y DISTANCE(IN.)	X(IN)	Y(IN)	Z(IN)	$\Theta_{X(RAD)}$	$\Theta_{Y(RAD)}$	$\Theta_{Z(RAD)}$
1	0	0	0	0	0	0	0
2	13.75	Small	Small	-.005	-.001	-.002	Small
3	41.25	Small	Small	-.036	-.002	-.007	Small
4	68.75	Small	Small	-.089	-.003	-.011	Small
5	96.25	Small	Small	-.153	-.004	-.016	Small
6	123.75	Small	Small	-.217	-.005	-.020	Small
7	151.25	-.001	Small	-.276	-.005	-.025	Small
8	165.0	-.001	Small	-.301	-.005	-.027	Small
9	165.0	-.001	Small	-.012	0	-.027	Small
10	165.0	-.001	.001	-.866	0	-.027	Small

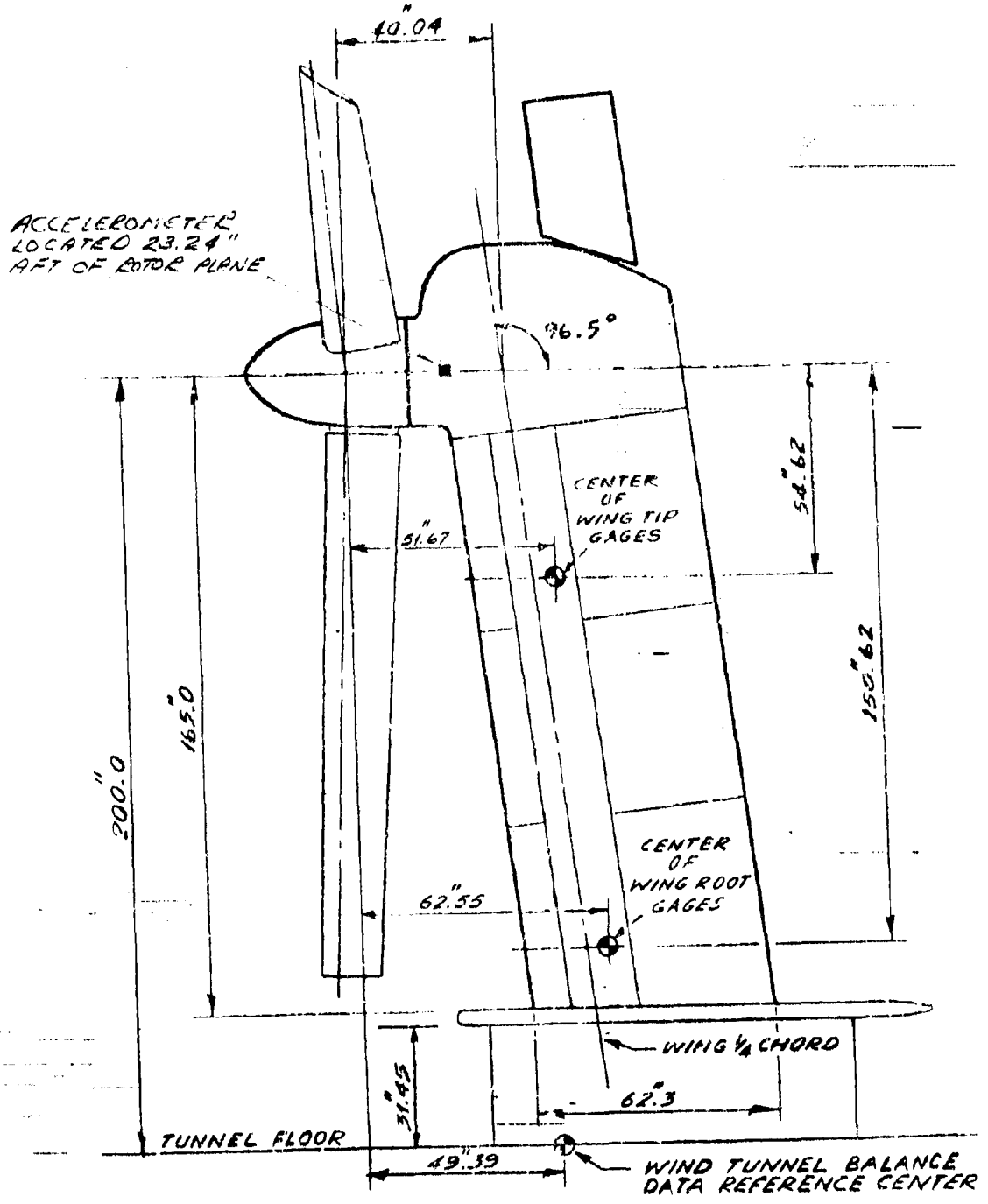

FIGURE 2.3. WINDMILLING TEST RIG GENERAL ARRANGEMENT AND CALIBRATION POINTS

The sign conventions used during test 410 for positive wing forces and moments are shown in Figure 2.4.

2.3 Powered Test Installation

The Model 222 rotor and nacelle used during dynamic tests were mounted on the NASA 40' X 80' wind tunnel propeller test rig for powered testing (NASA 40' X 80' wind tunnel test number 416). This installation is shown in Figures 2.2 and 2.5. The centerline of the rotor was mounted close to the tunnel centerline at zero incidence. Incidence could be changed by a remotely actuated tail strut. The angle range available was from 0 to 35° and 55° to 85°, the increment from 35° to 55° was not tested because in this range the blade tip would come within 2 feet of the tunnel roof.

The mass and cg data for the rotor and nacelle is given in Table 2.2. The sign convention for positive forces and moments on test 416 is shown in Figure 2.6.

The rotor was powered by two electric motors through a 0.45 to 1 ratio gear box. The motors generated a nominal 3000 HP at 3000 RPM and the maximum power available is a function of RPM. At normal operating RPM in hover (551) 1200 HP was available to drive the rotor.

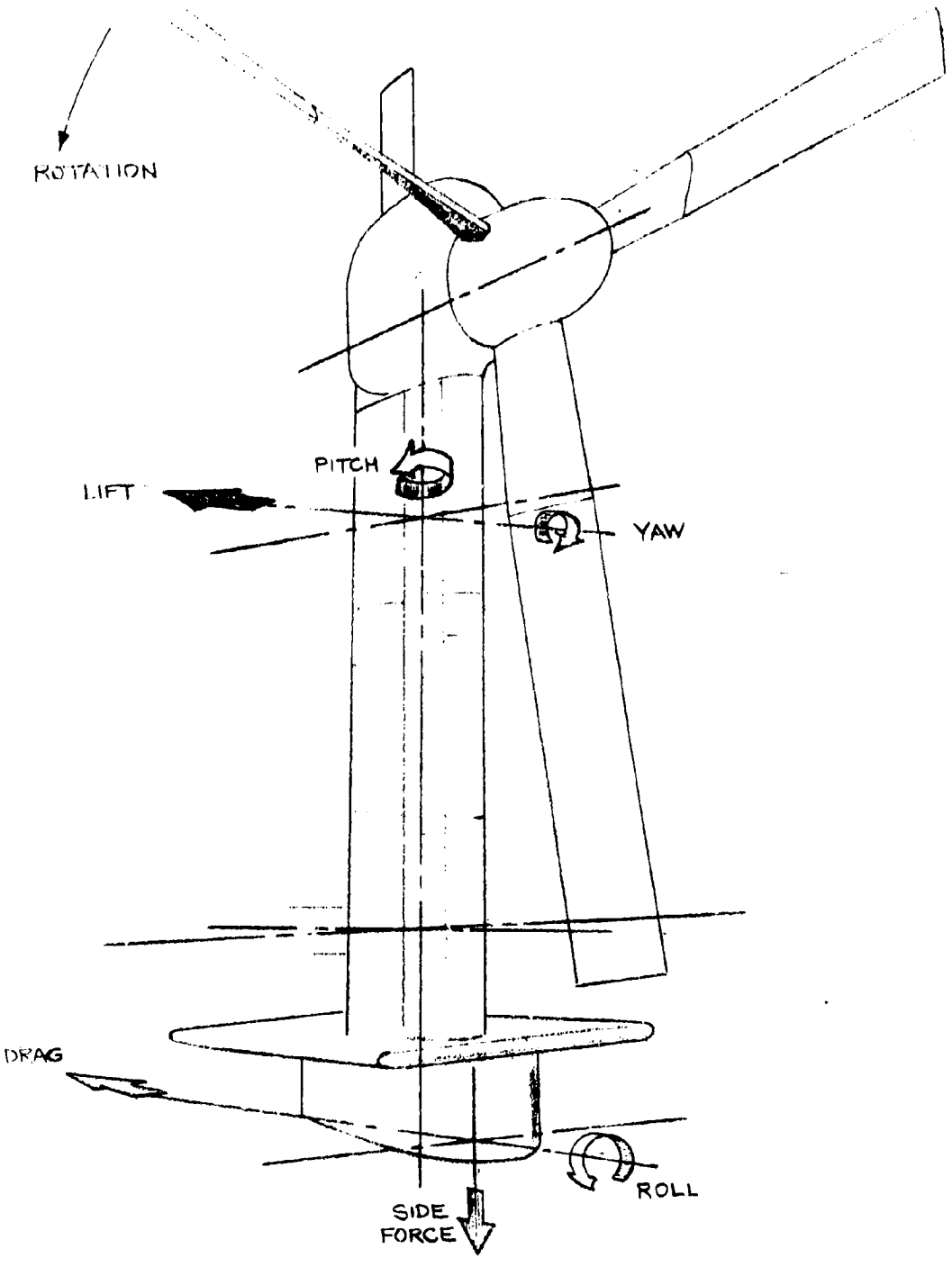

FIGURE 2.4 DYNAMIC TEST 410 POSITIVE WING LOAD SIGN CONVENTION. (PORT WING SYMMETRICAL)

TABLE 2.2
NACELLE MASS AND BALANCE DATA
POWERED TEST 416 (1)

Items	Wt. (Lbs)	A (2) (In.)	Moments of Inertia (Slug Ft^2) (3)		
			I_{XX}	I_{YY}	I_{ZZ}
Nacelle and Contents (With Blades)	1702	25.5	30	207	207
Nacelle and Contents (Without Blades)	1330	19.5	28	158	158

Notes:

1. Mass and balance data are for Boeing nacelle and blades only (shaded portion of Figure 2-5).

2. For C.G. location, dimension "A", see Figure 2-5.

3. Axes for moments of inertia given in Figure 2-5.

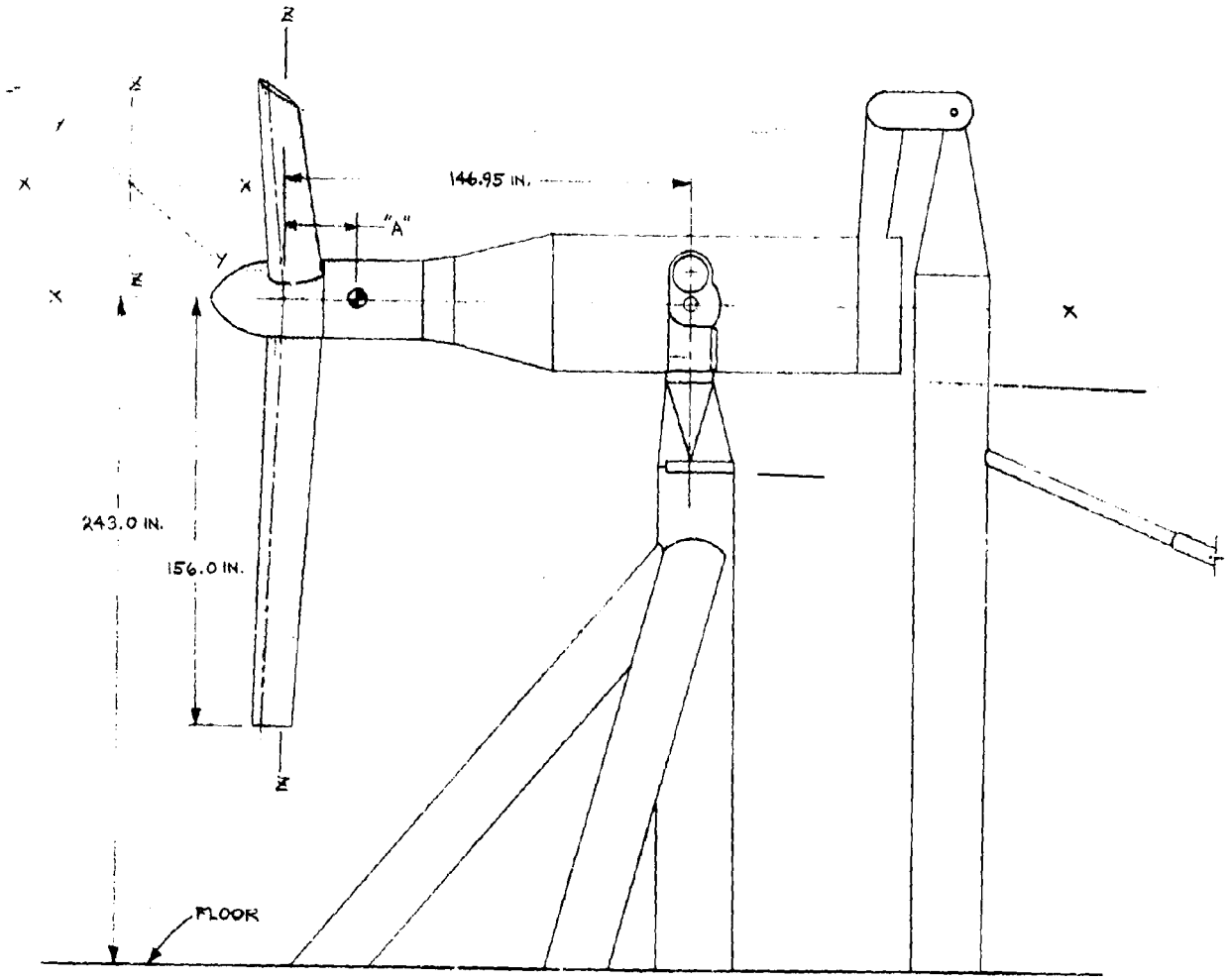

FIGURE 2.5 MODEL 222 26 FT. ROTOR MOUNTED ON NASA AMES POWERED TEST RIG.

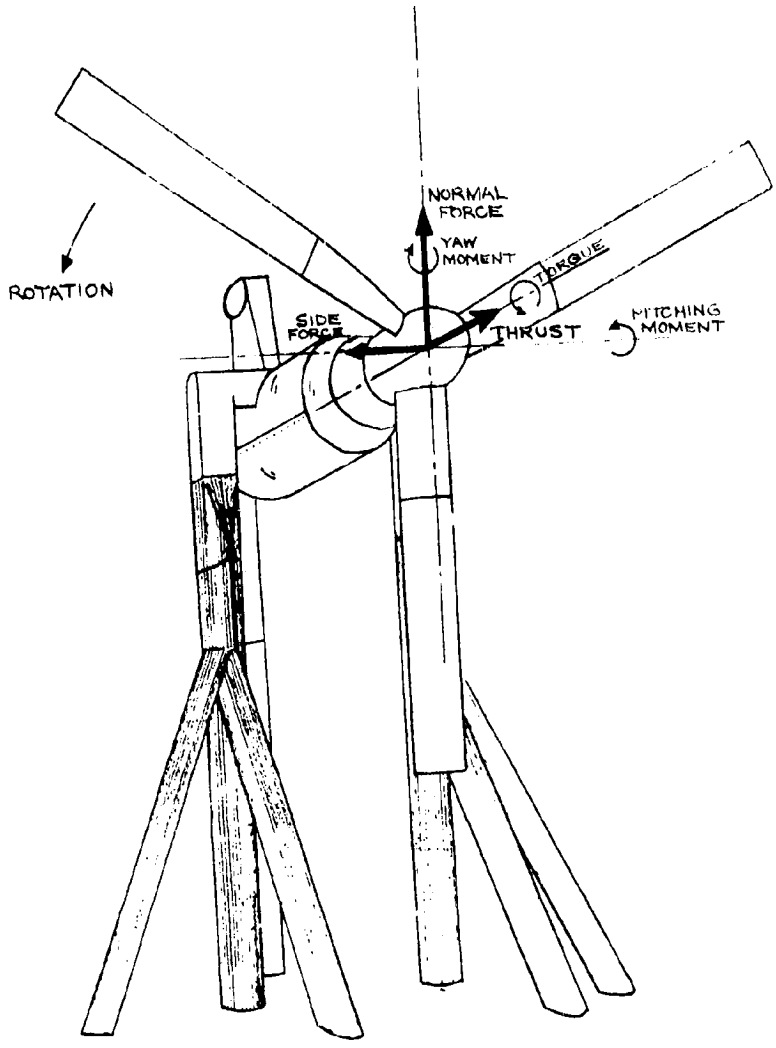

FIGURE 2-6 POWERED TEST 416 POSITIVE ROTOR HUB LOAD SIGN CONVENTION.

The rotor, nacelle and motors were carried on the tunnel balance although the fairings surrounding the model supports and the motor case were not. This was to reduce the magnitude of blade off tares.

2.4 Rotor System Data

The Model 222 prop/rotor blade design is a soft in-plane non-articulated rotor blade with pitch bearings to provide cyclic and collective control. The first in-plane bending frequency is placed less than 1/rev. A summary of the rotor system description is shown in Table 2.3.

The Model 222 prop/rotor blade is a composite structure consisting of a built up unidirectional fiberglass epoxy and crossply boron epoxy spar and skins, aluminum honeycomb fairing core and a titanium leading edge erosion strip. Fiberglass was selected for the spar material to obtain high torsional stiffness consistent with low bending stiffness. Torsional stiffness is required to maintain low blade twisting under operating conditions and to achieve a satisfactory torsional frequency for stall flutter considerations. The blade length from the centerline of rotation is 156 inches. The blade chord is a constant 18.85 inches from the tip to station .072R The airfoil shape is the

TABLE 2.3

ROTOR SYSTEM DESCRIPTION

Number of Rotors/Aircraft	2
Number of Blades/Rotor	3
Rotor Diameter	26 Ft.
Blade Chord	18.85 In.
Blade Airfoil	See Figure 2.8
Blade Twist	See Figure 2.8
Helicopter Flight Normal Design Rotor Speed	551 RPM
Airplane Flight Normal Design Rotor Speed	386 RPM
Hub Configuration	Hingeless
Torque Offset (Lead)	.65 In.
Precone Angle	2.5 Deg.
Hover Download Factor	1.05
Disc Loading at Design Gross Weight	12 Lb/Ft^2
Rotor Solidity	.115

Boeing-Vertol 23010-1.58 section. An aerodynamic fairing (cuff) is attached over the inboard section of the blade starting at station 15.6 and ending at station 54.6. The blade is twisted 41.08° between the tip and station 15.6.

The tubular spar section is circular at .072R rapidly becoming elliptical up to .30R. The section consists of a unifiberglass core sandwiched by boron crossply inner and outer torsion wraps. The spar is constructed in two precured halves spliced together by fiberglass crossply inner and outer bonded plates. The cross section is tailored so that the desired blade bending frequencies in both hover and airplane flight modes are achieved. The section taper from .10R to .30R is designed to minimize spar stresses due to spar bending moments.

The root end retention assembly consists of five basic components. These are namely a steel socket (SK222-10015), a glass composite spar (SK222-10007 and 10009), a conically shaped steel fitting (SK222-10008), an elastomeric bearing (SK222-10024) and a tension pin (SK222-10021), Figure 2.7. The spar assembly is a composite of 1002S unidirectional glass fibers, 1002S crossplied (45°) splices and boron crossplied (45°) torsion wraps. The spar is fabricated into

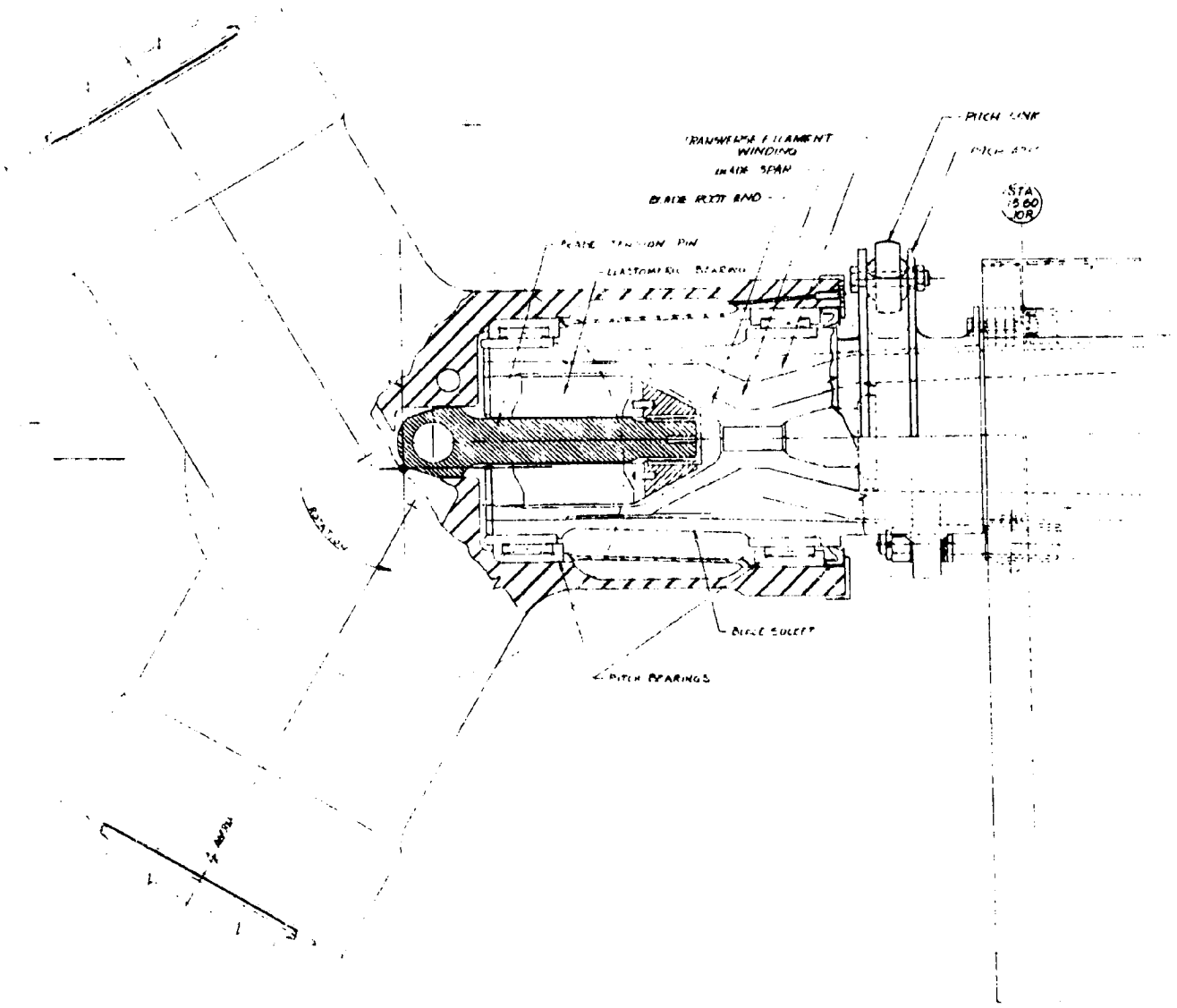

Figure 2.7. Blade Root and Hub Assembly

two half sections of the unifibers (.3255t) which are sandwiched between and bonded to the steel fitting. The two half sections and the outer splice are layed up next and cured to complete the fabrication process. Pre-loaded 1014S glass rovings are wound around the fitting and spar to give hoop restraints to the spar under the action of centrifugal force. Centrifugal forces are transmitted to the hub through the elastomeric bearing and tension pin. The elastomeric bearing is threaded on to the fitting and is supported by the tension pin.

The blade spar structure from 10 to 45% blade radius does not include the complete airfoil section. The spar was designed in this manner in order to achieve the required blade lag bending frequencies. The blade airfoil section is maintained by a cuff which fits over the spar root area. The cuff (Drawing SK222-10016) consists of two parts, one from station 14.60 to 54.6 which is free to flap and lag with the blade and the other from station 55 to 70 which is fixed to the blade structure. The inboard end of the free cuff is hinged to the blade socket at station 15.2 by an eye bolt assembly, SK222-10016-7. The outboard end is supported by the spar through the flexible rubber seal

and assembly, SK222-10016-16. The cuff is basically a shell constructed of BP907-143/1305 prepregrated glass woven cloth. The trailing box aft of 50 percent chord also includes a urethane core (NOPCO foam C500 series 4.5 PCF density). The shell is built in two halves which are fitted over the spar and bonded together at the final blade assembly (Drawing SK222-10001). Torsional loads on the cuff are reacted at the inboard end by a self aligning link, SK222-10016-21, so that the cuff is free to move with the blade flap and lag motion, without contributing appreciably to the blade stiffness.

The blade twist distribution and thickness chord ratio distribution is given in Figure 2.8. The design stiffness and mass properties for the blade are shown plotted in Figures 2.9 to 2.15. The cuff stiffness and mass properties are given in Table 2.4. Figures 2.16 and 2.17 show comparisons of bending stiffnesses and torsional deflections measured prior to the wind tunnel tests with design data. The blade design is discussed more fully in Reference 13.

2.5 Nacelle and Controls

The test stand (in the form of a nacelle) provides the necessary inputs for testing the rotor under varying

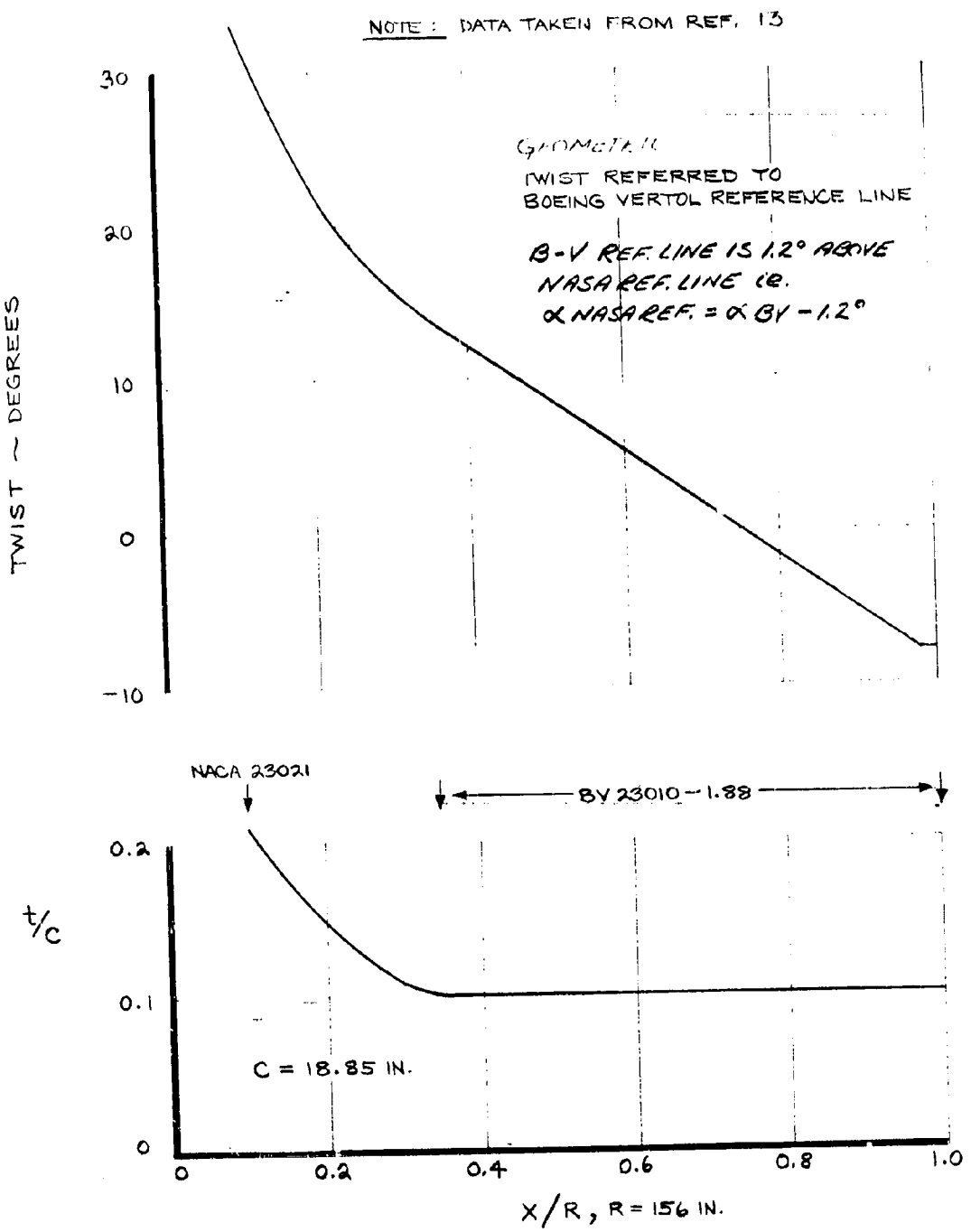

FIGURE 2.8 MODEL 222 TILT ROTOR BLADE DESIGN 3F-6, BLADE TWIST AND THICKNESS CHARACTERISTICS

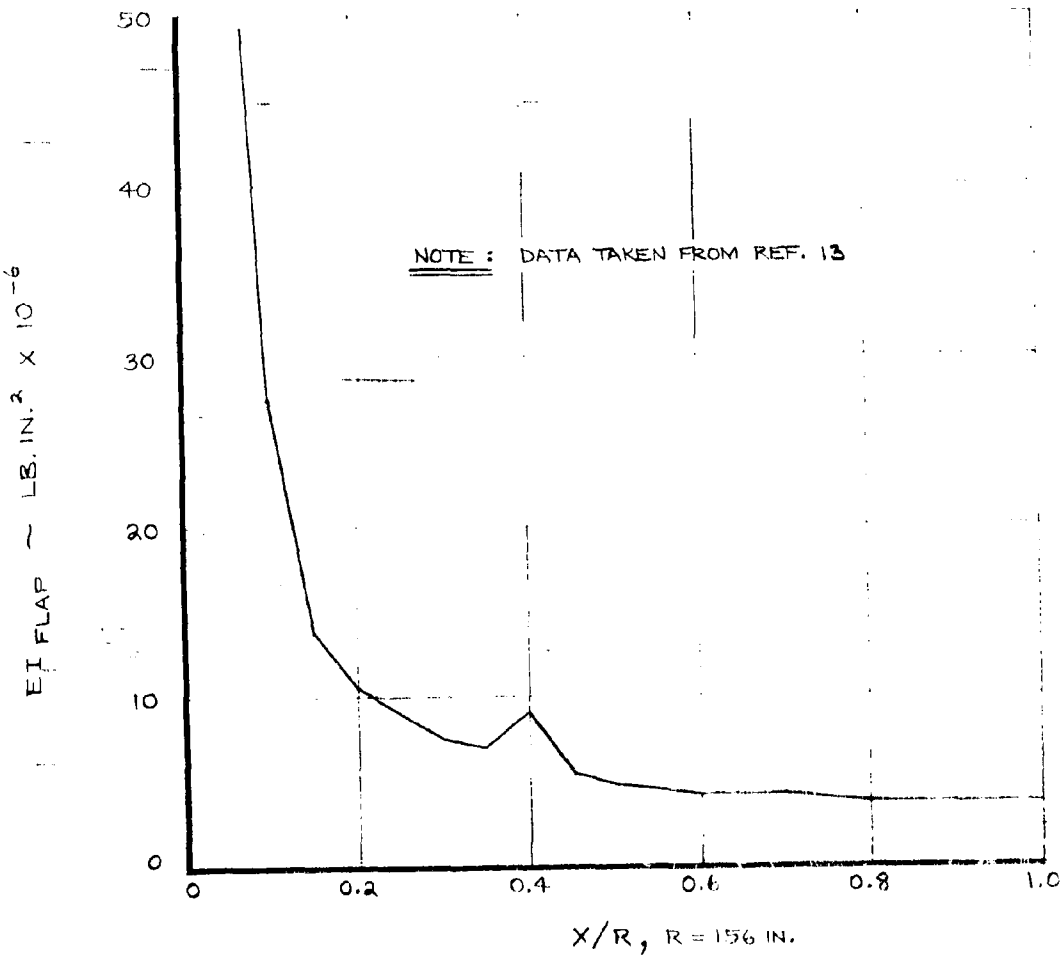

FIGURE 2.9 MODEL 222 TILT ROTOR BLADE DESIGN 3F-6, SPANWISE DISTRIBUTION OF FLAPWISE STIFFNESS

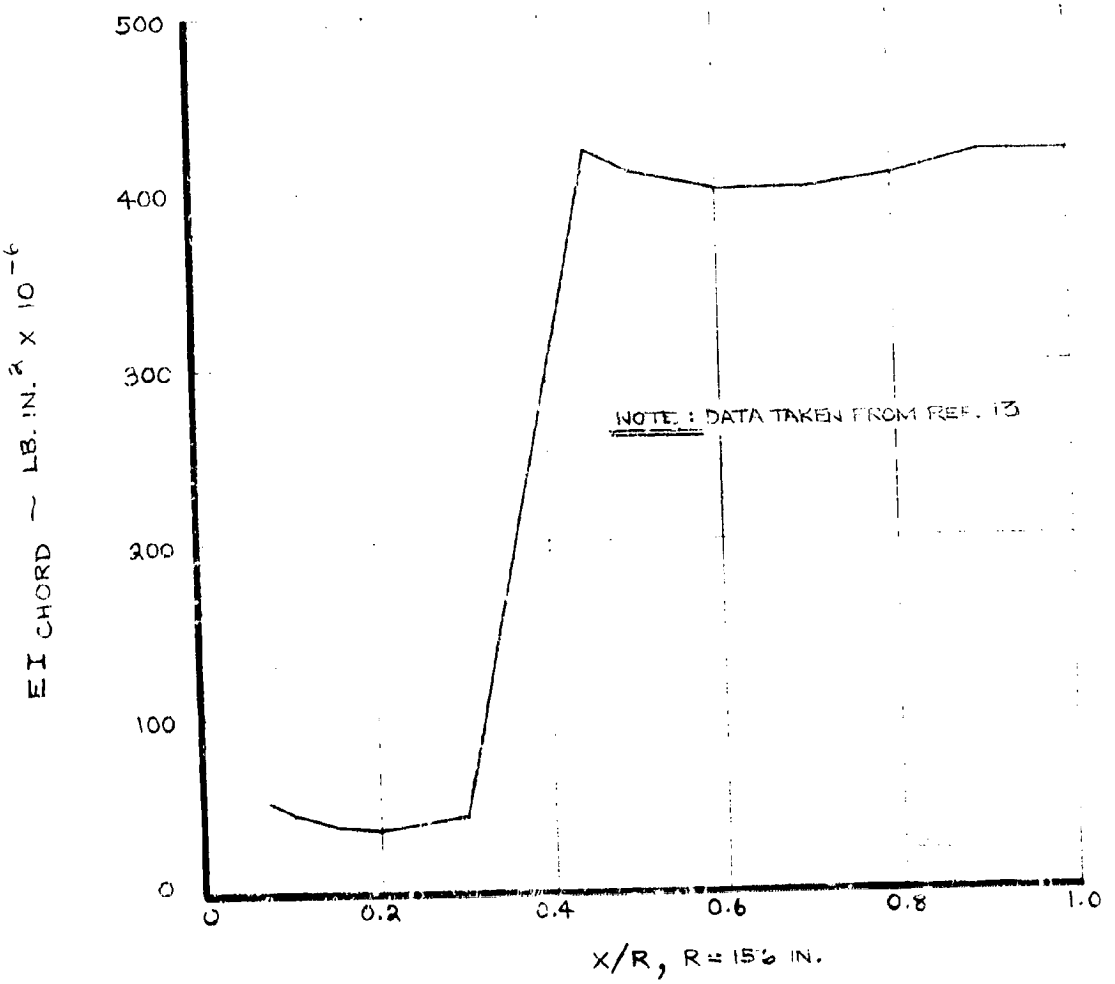

FIGURE 2.10 MODEL 222 TILT ROTOR BLADE DESIGN 3F-6, SPANWISE DISTRIBUTION OF CHORDWISE STIFFNESS

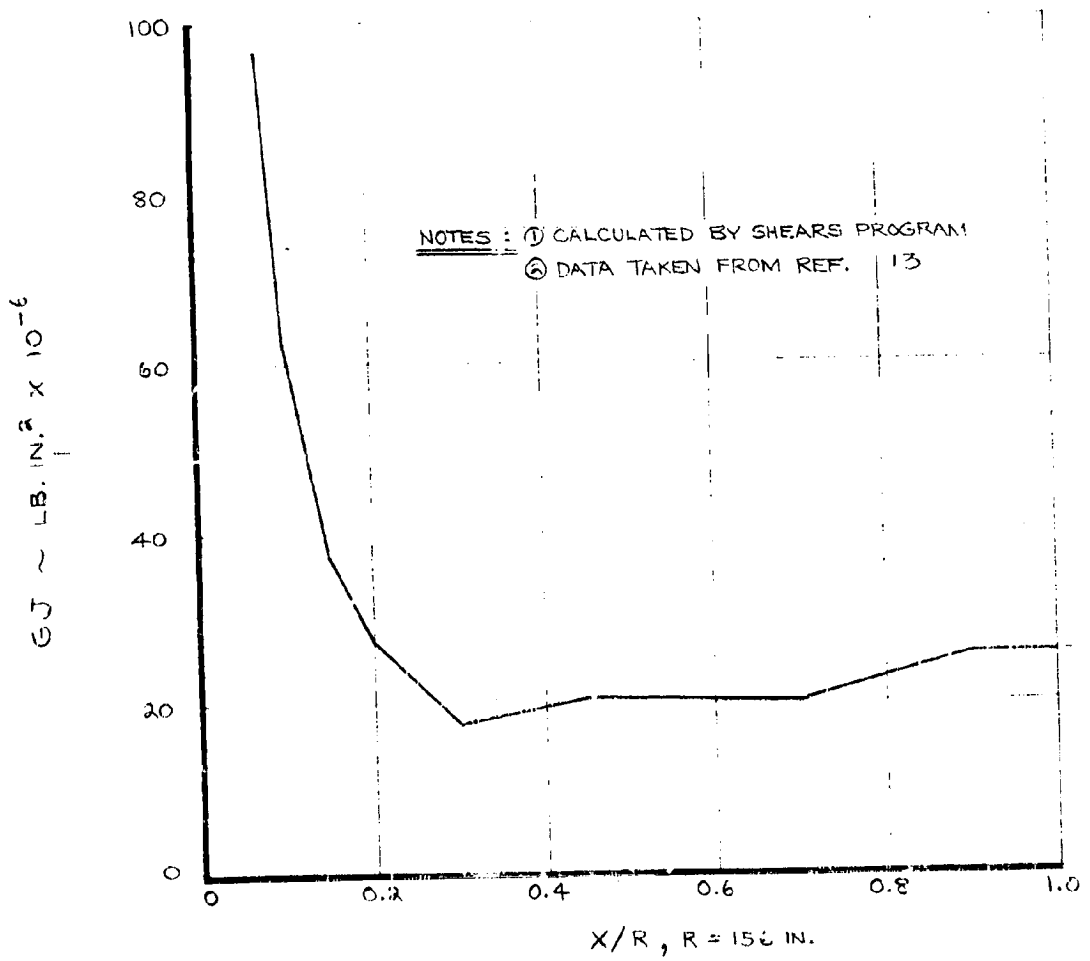

FIGURE 2.11 MODEL 222 TILT ROTOR BLADE DESIGN 3F-6, SPANWISE DISTRIBUTION OF TORSIONAL STIFFNESS

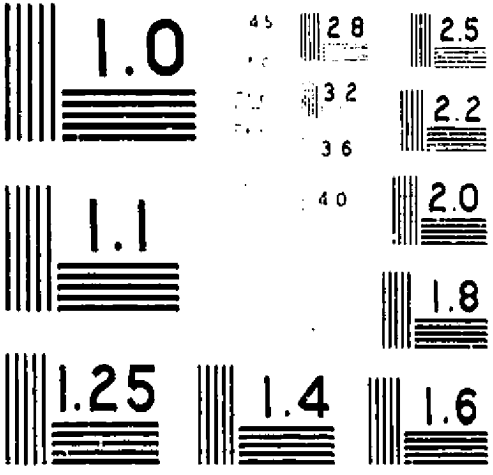

MICROCOPY RESOLUTION TEST CHART

NATIONAL BUREAU OF STANDARDS - 1963

NOTES : ① CALCULATED BY SHEARS PROGRAM
② DATA TAKEN FROM REF. 13

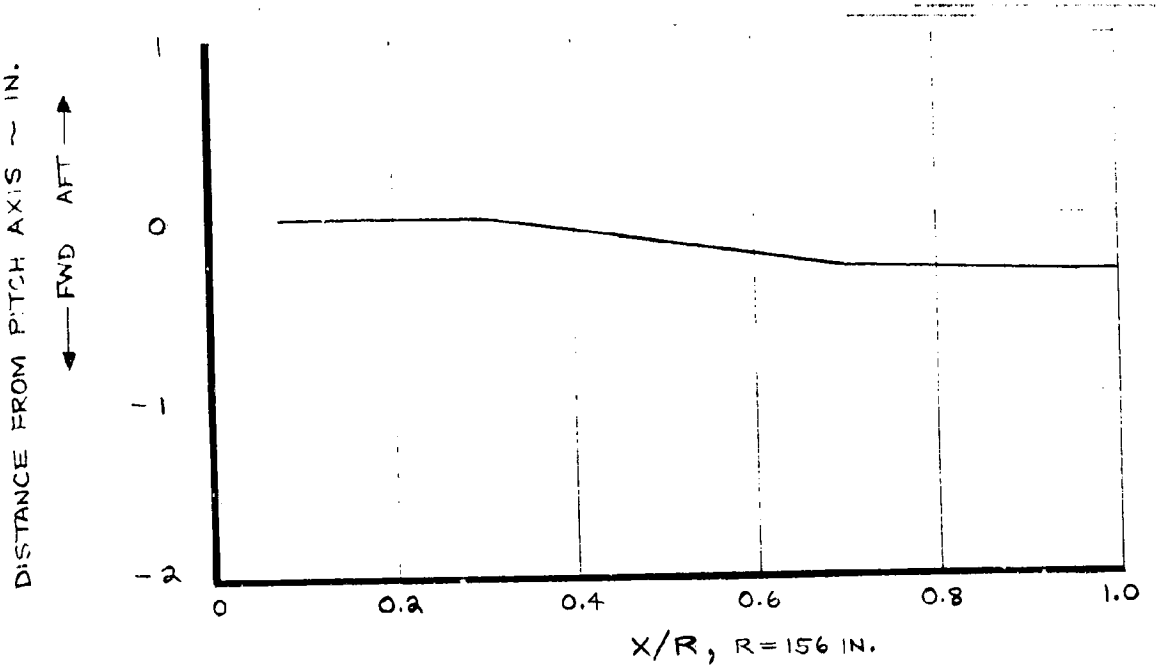

FIGURE 2.12 MODEL 222 TILT ROTOR BLADE DESIGN 3F-6, SPANWISE DISTRIBUTION OF SHEAR CENTER

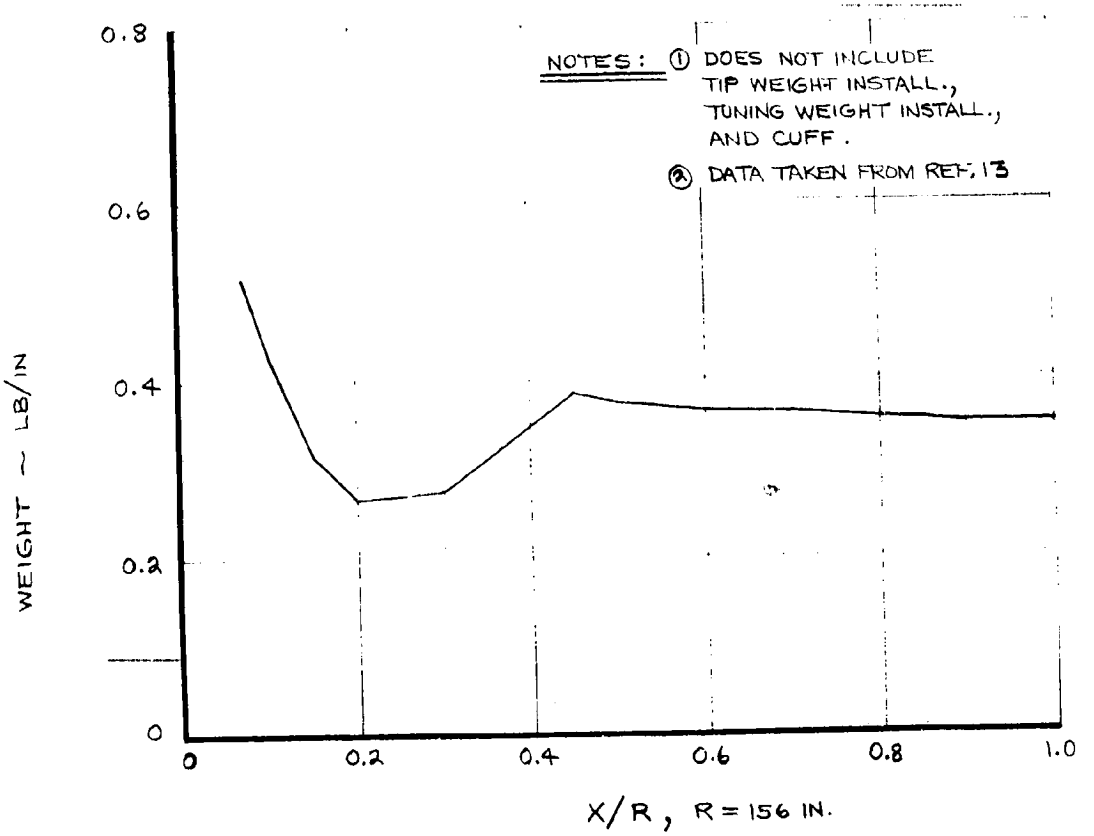

FIGURE 2-13 MODEL 222 TILT ROTOR BLADE DESIGN 3F-6, SPANWISE DISTRIBUTION OF BLADE WEIGHT

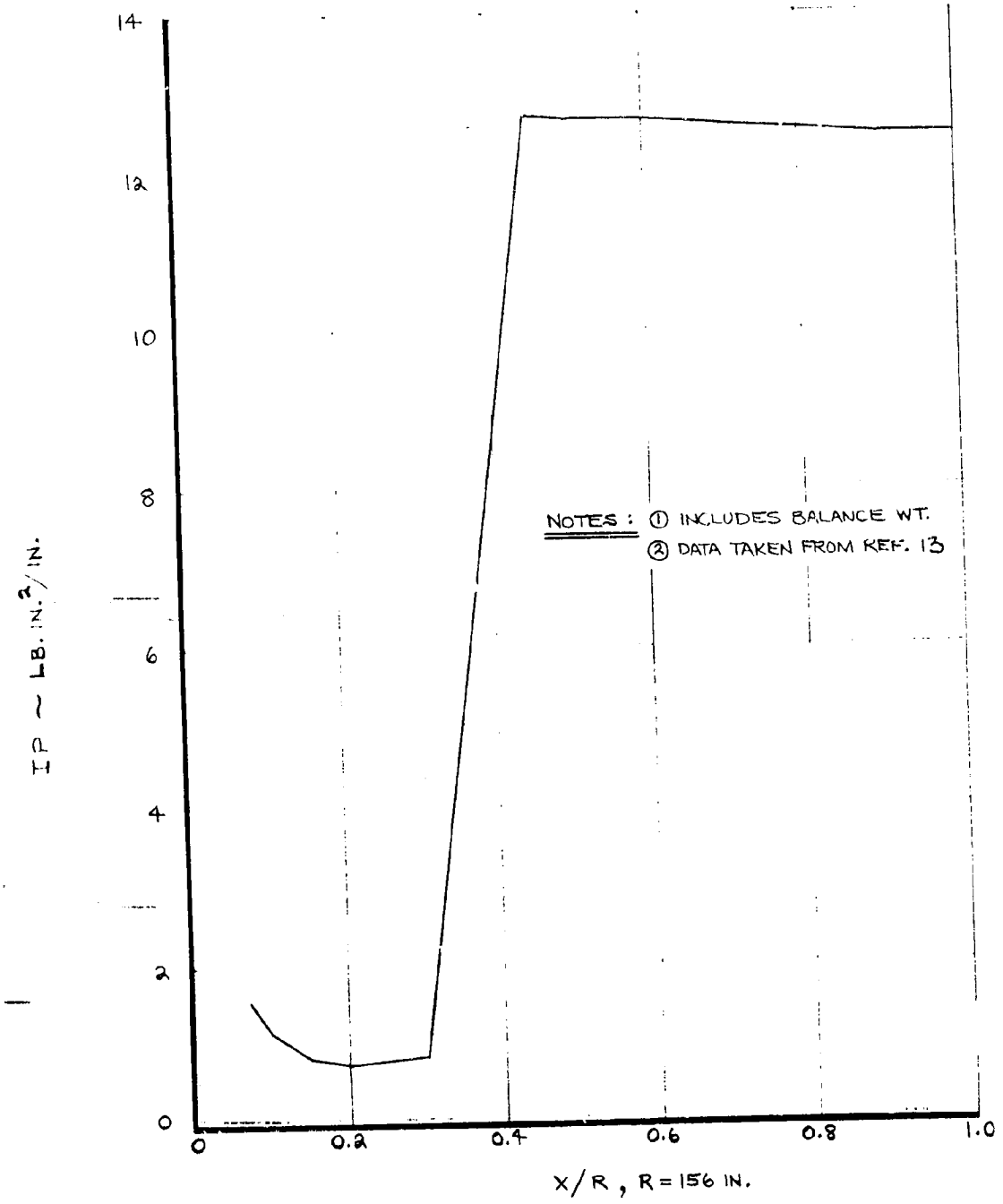

FIGURE 2.14 MODEL 222 TILT ROTOR BLADE DESIGN 3F-6, SPANWISE DISTRIBUTION OF ACCELERATION PITCH INERTIA

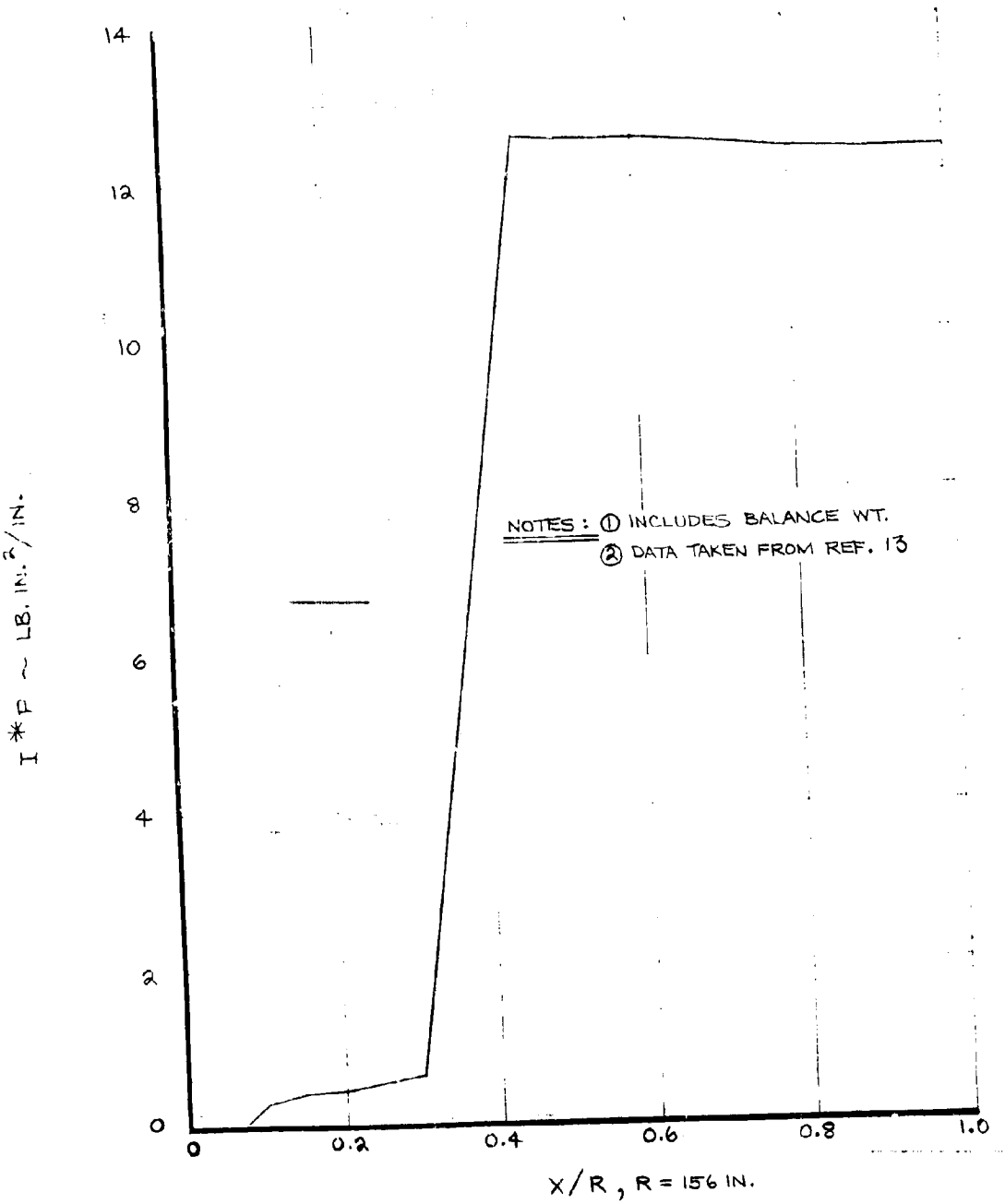

FIGURE 2-15 MODEL 222 TILT ROTOR BLADE DESIGN 3F-6, SPANWISE DISTRIBUTION OF CENTRIFUGAL PITCH INERTIA

TABLE 2.4

M222 BLADE CUFF PROPERTIES

Blade Station	w Lb/In	EA $Lbx10^{-6}$	EI Flap Lb. $In^2 x10^{-6}$	EI Chord Lb. $In^2 x10^{-6}$	I_p Lb Sec^2 In/In	GJ $Lb/In^2 x10^{-6}$
15.2	.302	5.1	14.8	102	.0149	7.22
54.6	.117	4.07	4.23	95	.0136	2.25

Chordwise N.A. 1.9 In. Aft of Pitch Axis
I_p = .556 Lb. Sec^2 In.
Weight = 8.3 Lb. (Inboard Cuff)
Weight = .9 Lb. (Fixed Cuff)
C.G. = Sta. 32
Chordwise CG = 7.57 In. Aft of Leading Edge

NOTES: (1) GRAPH TAKEN FROM REF.
(2) MEASURED DATA
⊙ — FLAP - #2 BLADE
⊡ — CHORD - "
⊙ — FLAP - #3 BLADE - "
⊡ — CHORD - "

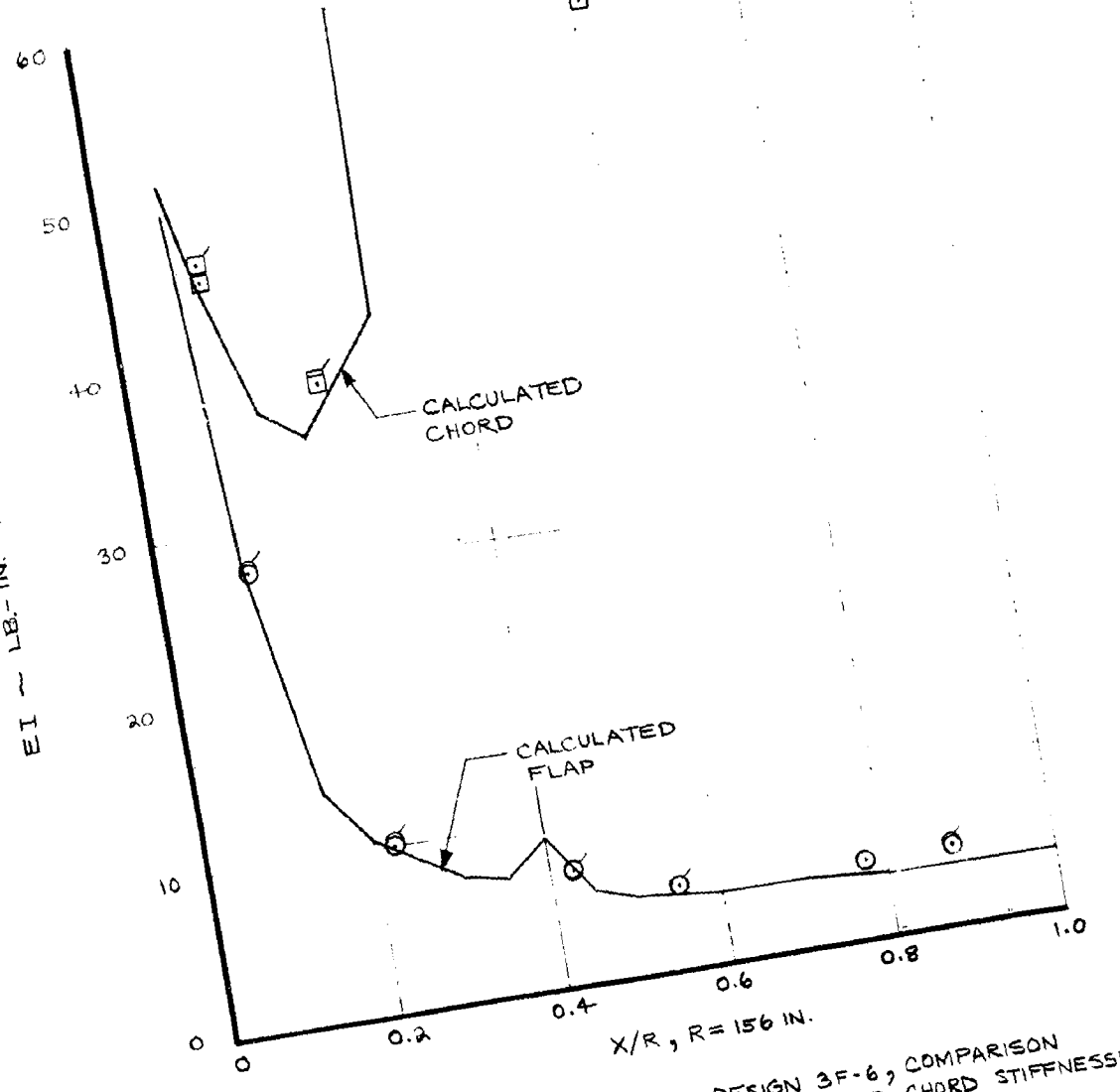

FIGURE 2-16 MODEL 222 TILT ROTOR BLADE DESIGN 3F-6, COMPARISON OF MEASURED AND CALCULATED BLADE FLAP AND CHORD STIFFNESSES

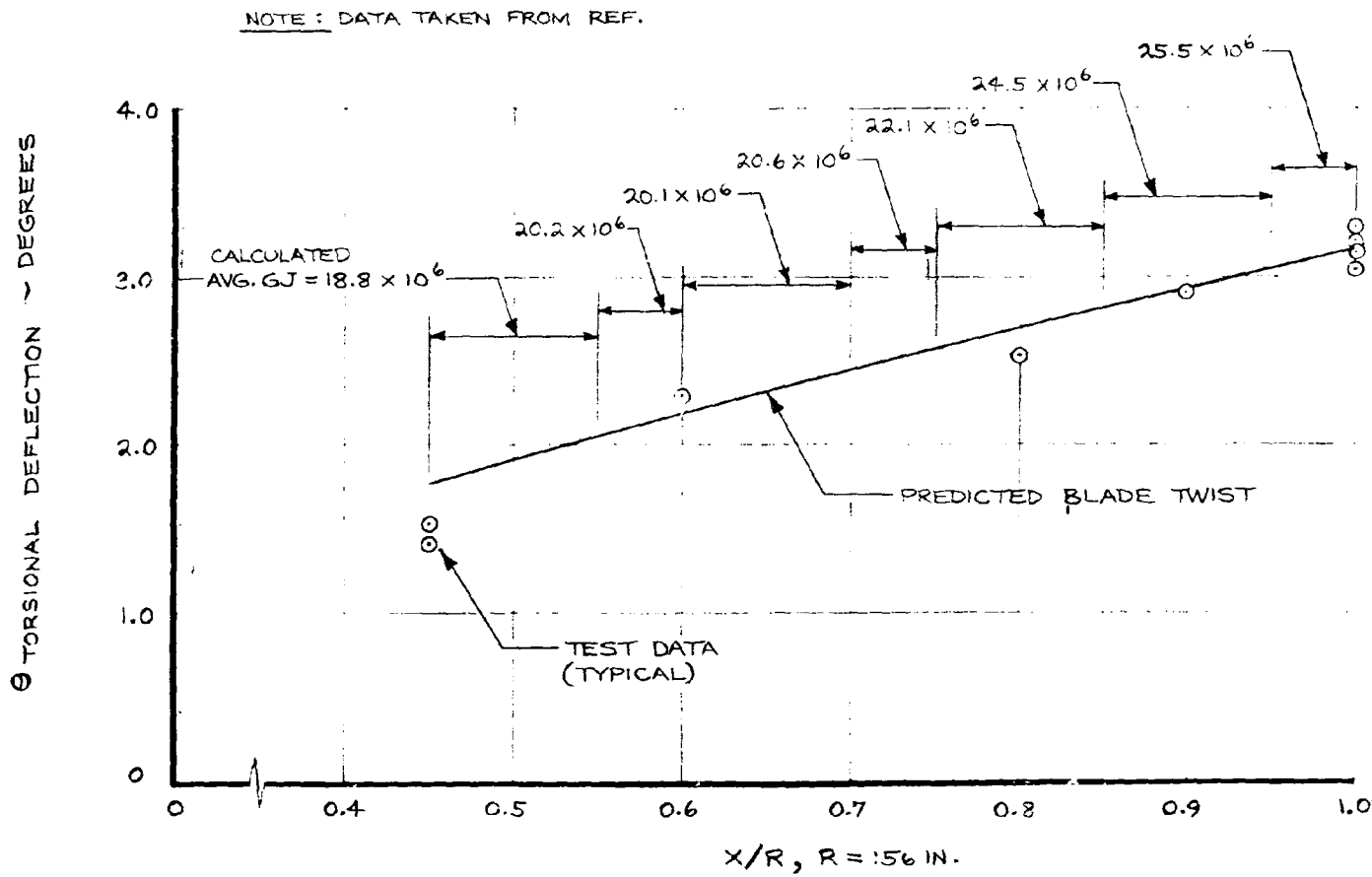

FIGURE 2-17 MODEL 222 TILT ROTOR BLADE DESIGN 3F-6, COMPARISON OF MEASURED AND CALCULATED TORSIONAL DEFLECTIONS.

conditions of collective and cyclic blade angles. The test stand and rotor can be mounted on a wing for windmilling tests or on the NASA Ames propeller test rig for powered testing. Rotor rotation is provided by a two bearing shaft which also carries a slip ring stack necessary to provide electrical continuity between stationary and rotating components. One end of the shaft has a splined bore to provide drive to the rotor during the power test only. The other end has a detachable flange that mounts the rotor hub. Support for the rotor shaft bearings is provided by a support casing that also provides the necessary features for mounting the test stand to the wind tunnel fixtures. Actuator and mechanism ground points for the upper and lower controls are also provided for on the support casing. Collective and cyclic blade angle motions are obtained through a lower control mixing system which provides the necessary inputs to upper boost actuator servovalves. Input to the mixing system is by an electric control actuator, with one actuator for each control mode (collective, A_1 and B_1 cyclic), three actuators in all. SAS units are "piggybacked" on the electric actuators to provide a feedback capability, Figure 2.17. The electrical control inputs to the actuators were made using a control

panel which had in addition to the primary controls the equipment (filters, sign reversals and resolvers) to provide electrical feedback from any of the fixed system sensors (accelerometers or strain gages) to the rotor controls.

The upper controls (which are powered by the upper boost actuator) consist of a gimbal mounted swashplate incorporating a large diameter double row ball bearing (CH-47 swashplate bearing). This provides rotational freedom between the non-rotating lower ring and the rotating upper ring. The gimbal ring mounting which supports the lower ring of the swashplate provides a universal action which permits tilting of the swashplate about mutually perpendicular axes for cyclic pitch control. The gimbal ring mount is completed by its attachment to the slider assembly. Dry bearings in each end of the slider assembly permits the assembly to traverse the slider guide. This motion provides the collective pitch control. The slider assembly is restrained from rotating by the slide scissors linkage which is grounded out on the slider guide - this in turn being attached to the support casing. The rotating upper ring of the swashplate is driven by the drive scissors linkage which is attached to the rotor shaft hub flange.

The swashplate motions are transmitted to the rotor blades by the pitch links which connect the rotor blade integral pitch arms to the upper swashplate ring.

The engineering drawings of the total assembly and compound parts can be found in Reference 14.

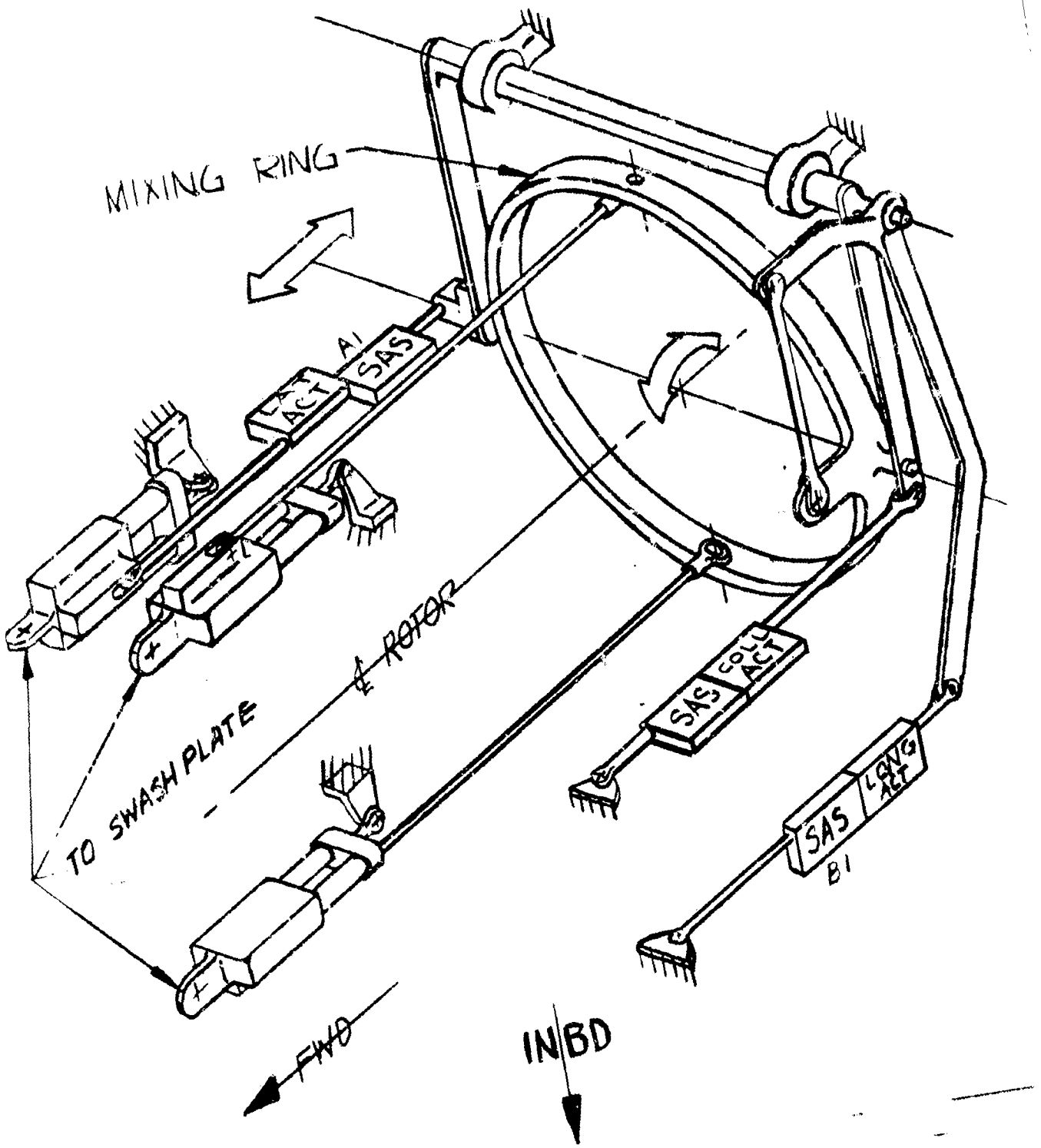

FIGURE 2-18 LOWER CONTROLS (SCHEMATIC)

3.0 DYNAMICS

3.0 DYNAMICS

The primary objective of the dynamic test (NASA Ames 40' X 80' Wind Tunnel Test 410) was to investigate the aeroelastic characteristics of a hingeless rotor and wing and to compare this experimental data with pretest analytical predictions.

The soft in-plane rotor was tested on two NASA furnished wing test stands of different stiffnesses in order to meet this objective. The stiff wing was designated "full stiffness" and the less stiff wing "¼ stiffness" since its first mode bending and torsion frequencies were one half of the former. These wing test stands were specifically designed for a teetering rotor test and resulted in non-optimum rotor-wing aeroelastic characteristics when used with a soft in-plane hingeless rotor. A comparison of test full stiff wing frequencies and M-222 airplane design wing frequencies is shown in Table 3.1. The airplane wing has higher wing vertical bending and wing chord bending frequencies than the test "full stiff" model and a lower torsional frequency.

Two types of instability are possible on this type of rotor-wing configuration. One of these is "whirl flutter" which involves pitching and/or yawing of the nacelle and blade flapping out of plane of the rotor. This is generally a high

TABLE 3.1

WING FREQUENCY COMPARISON (Hz)

Mode	Full Stiff	½ Stiff	M-222
Wing Vertical Bending	2.5	1.2	3.6
Wing Chord Bending	4.6	2.2	5.4
Wing Torsion	11.4	4.5	6.1

speed condition to which the soft in-plane rotor has a low susceptibility (i.e. less wing torsional stiffness per slug ft^2 of inertia). The other instability is "air resonance" which involves hub motion in the plane of the rotor and the lead-lag motion of the blades. The low wing vertical bending frequency of the full stiff wing model offered a unique opportunity to study this mode.

3.1 Full Stiffness Wing Test Stand

The predicted air resonance instability boundary and contours of constant modal damping for the full stiffness wing are shown in Figure 3.1 and superimposed on Figure 3.1 are the test conditions at which damping measurements were taken. The open symbols represent stable conditions and the solid symbols represent conditions of neutral stability (i.e. zero damping). The figure shows the instability boundary to be accurately predicted.

The test procedure used to establish this data was to increase RPM at constant airspeeds using the nacelle shaker vane to excite the wing vertical bending mode. The modal damping was determined from the oscillatory decay of the signal from the wing vertical bending bridges. In this instance the air resonance instability arises from the coalescence of the lower blade lag mode and wing vertical

bending mode. The lower blade lag frequency ($\Omega - \omega_L$) increases as RPM increases and approaches the wing vertical bending modal frequency which is unaffected by RPM. At these conditions "air resonance" is possible though other physical parameters (e.g., nacelle mass, wing structural damping, etc.) play a large part in defining the level of modal damping.

Figures 3-2 to 3-5 show the predicted modal damping as a function of RPM at four airspeeds. The damping of the wing vertical bending mode decreases as RPM increases until the stability boundary is reached. Data obtained from damping measurements is superimposed on the predictions and shows close agreement. The data scatter obtained decreases as the mode becomes more lightly damped. At 60 kts and 100 kts it was possible to achieve neutral stability and define precisely the experimental stability boundary. At higher speeds 140 kts and 192 kts the mode is stable.

The predicted modal frequencies for 100 kts, 150 kts and 200 kts are shown in Figures 3-6 to 3-8. The experimental wing vertical bending frequency data is superimposed and confirms the modal frequency. For Figure 3-6 two experimental

points for the lower blade lag frequency are available (see Section 4.1). These data points show the first mode bending frequency of the blade to be low resulting in a higher lower blade lag frequency. The effect of this small discrepancy is to reduce the RPM at which zero damping will occur and is thought to be the reason for the 2% discrepancy between predicted and measured boundaries. Figure 3-9 is a calculated frequency plot showing all of the modes at 200 knots.

It is noted that the modal frequencies shown in all figures are fully coupled. The blade lead-lag mode which is generally defined in terms of a cantilevered root end condition gives rise to two distinct types of rotor mode. In one the blades vibrate in phase and apply a summed torque to the hub. Since the hub inertia is small and there is no drive system constraint, a high frequency collective bending mode results in which the blades behave as if pinned at the hub center. There is no simple relationship between the frequency of this mode and the calculated frequency of the cantilevered mode. In the other type of mode the blades vibrate out of phase so that the root bending moments are reacted in the hub structure. Thus, the frequencies of these modes are approximately related to the cantilevered mode frequencies by the formula $(\Omega \pm \omega_L)$ where ω_L is the cantilevered lag frequency.

The static wing frequencies measured on test are shown in Table 3-2. These data were taken by manually exciting the wing mode (bang tests). The data agree closely with the values used in

the calculations shown on Figure 3-1.

The rotor off wing frequencies and damping are plotted as a function of airspeed in Figures 3-10 to 3-12. Alternating wing loads measured on RPM sweeps are given in Figures 3-13 to 3-15. These data indicate that the wing vertical bending frequency and the wing chordwise bending frequency become coincident with one per rev at 140 cpm and 235 cpm respectively. These points are included on Figure 3-6.

The full stiffness wing-rotor configuration was predicted to be stable to speeds in excess of 400 knots at design cruise RPM. Tests were performed up to the maximum tunnel speed and over a wide range of RPM as shown in Figure 3-1 and confirmed system stability. The wing chord bending and wing torsion modes, predicted to be highly damped, could not be excited to a large enough amplitude to permit data analysis. Further investigations using spectral analysis technique may yield further information. The difficulty experienced in exciting these modes is an indication of high modal damping.

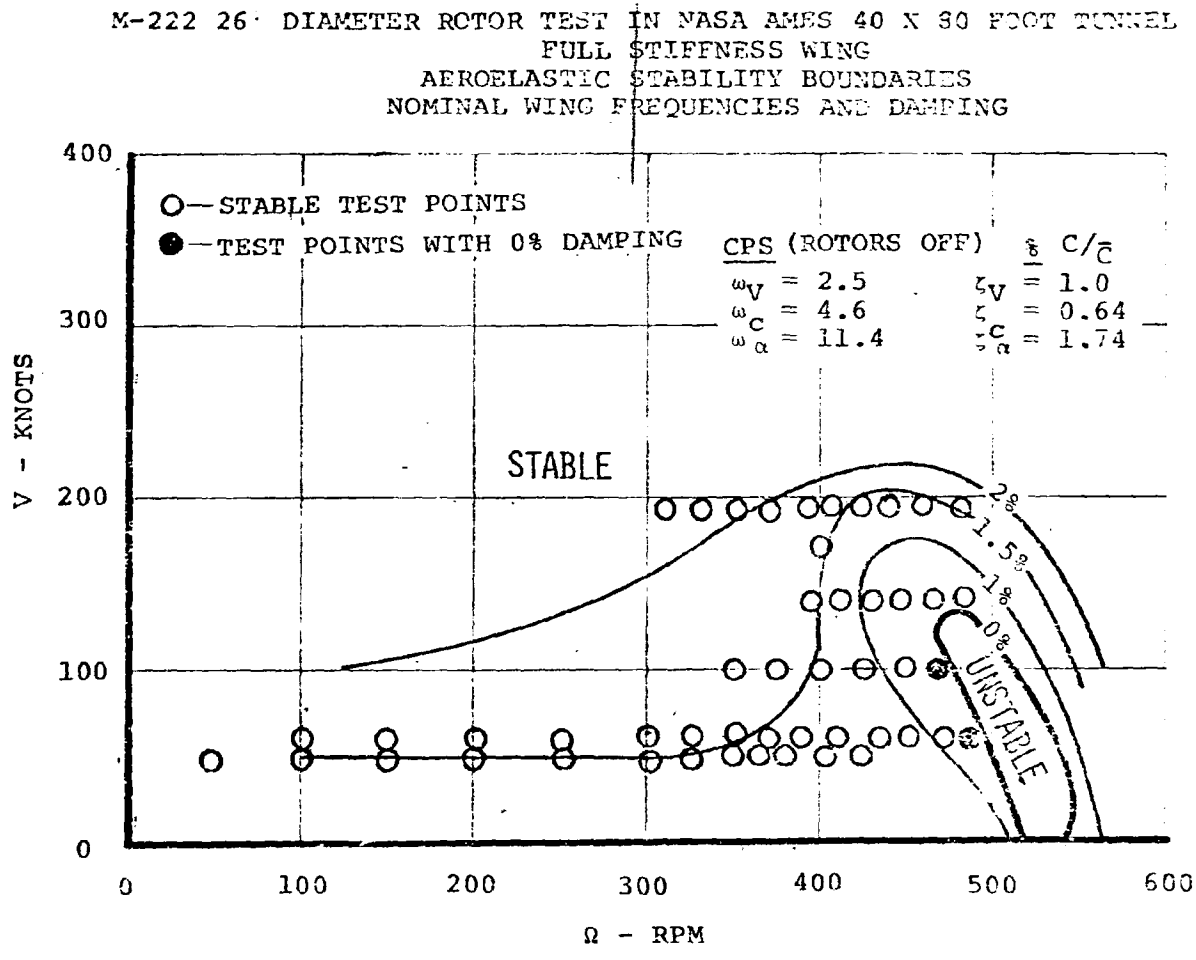

FIGURE 3-1. COMPARISON OF PREDICTED AIR RESONANCE BOUNDARY AND TEST DATA

MODEL-222 FULL SCALE ROTOR TEST IN NASA AMES 40 X 80 FOOT TUNNEL: FULL STIFF WING

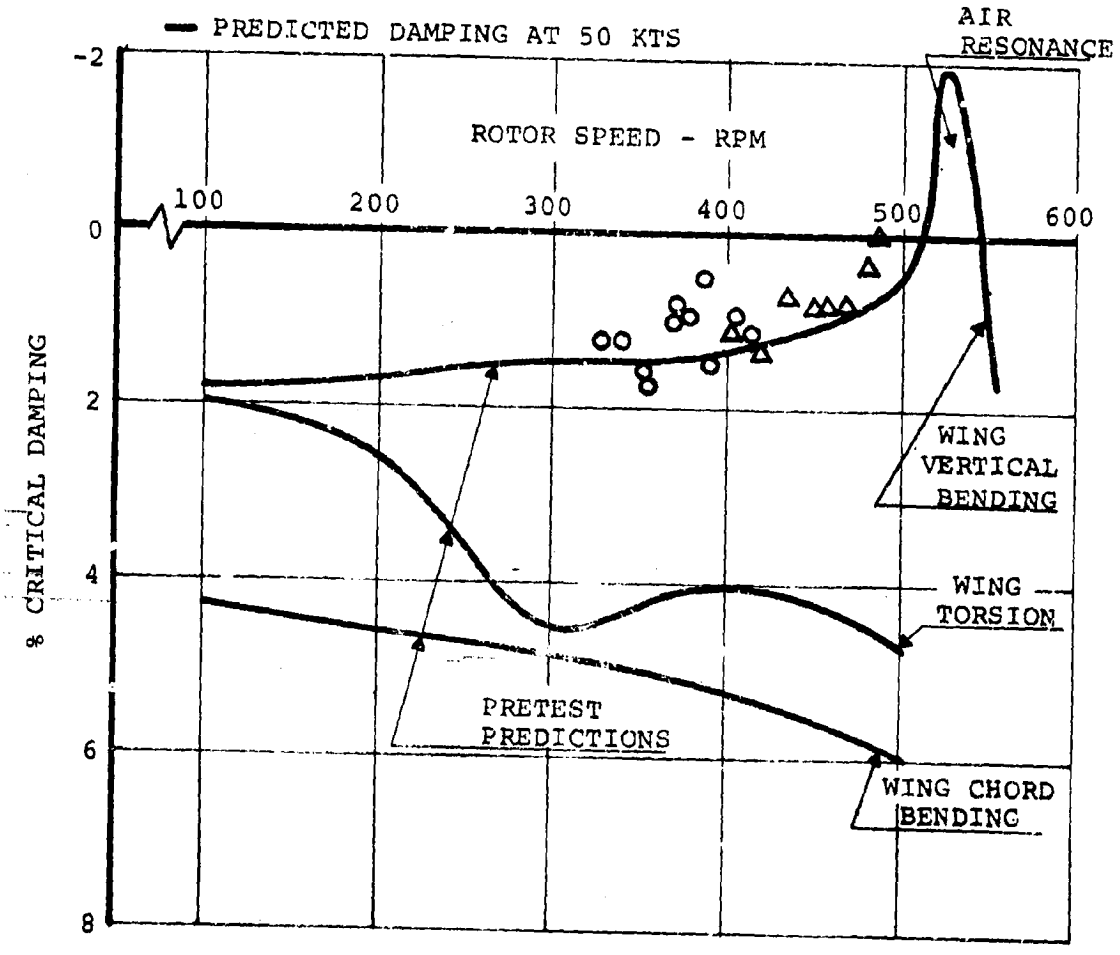

FIGURE 3-2. CORRELATION OF PREDICTED AIR RESONANCE MODE DAMPING AND MEASURED DAMPING OF THIS MODE DURING TEST. V = 50 KNOTS AND 60 KNOTS.

MODEL-222 FULL SCALE ROTOR TEST IN NASA
AMES 40 X 80 FOOT TUNNEL: FULL STIFF WING

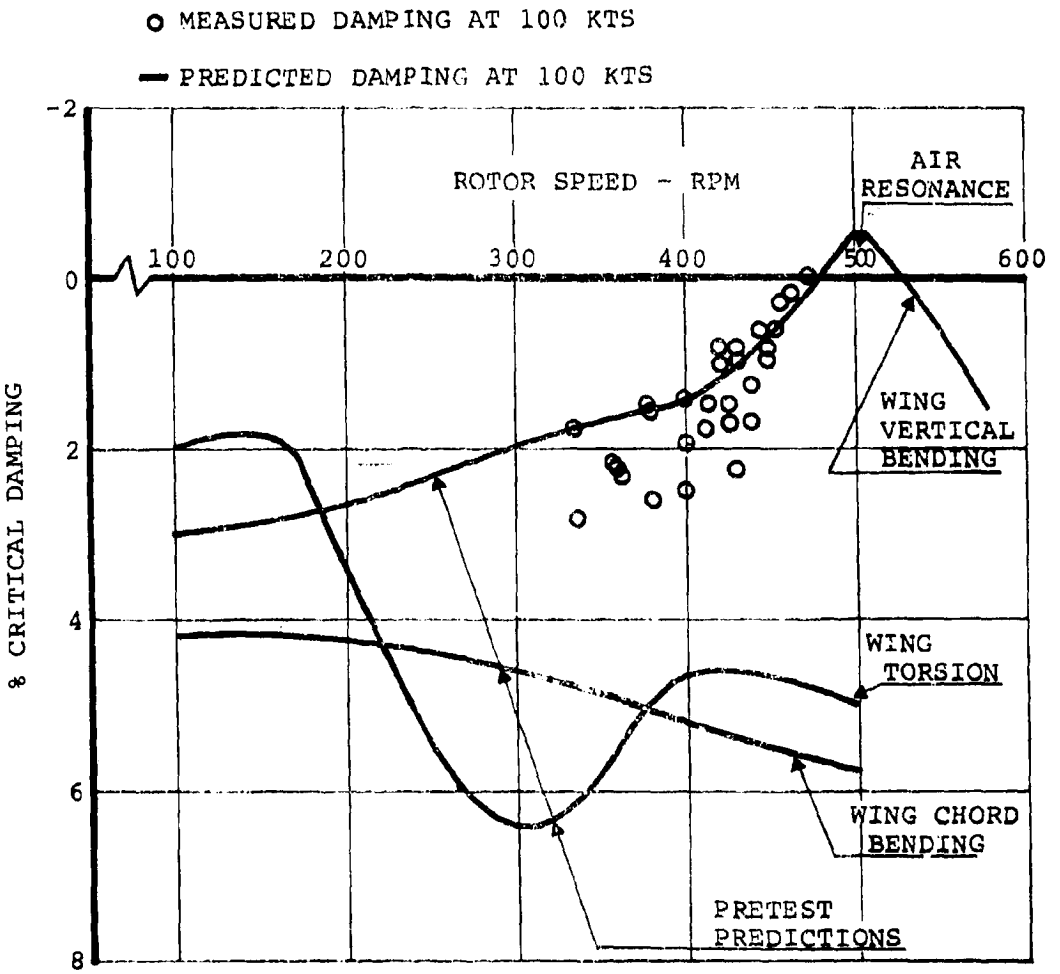

FIGURE 3-3. CORRELATION OF PREDICTED AIR RESONANCE MODE DAMPING AND MEASURED DAMPING OF THIS MODE DURING TEST. V = 100 KNOTS.

MODEL-222 FULL SCALE ROTOR TEST IN NASA AMES 40x80 FOOT TUNNEL: FULL STIFF WING

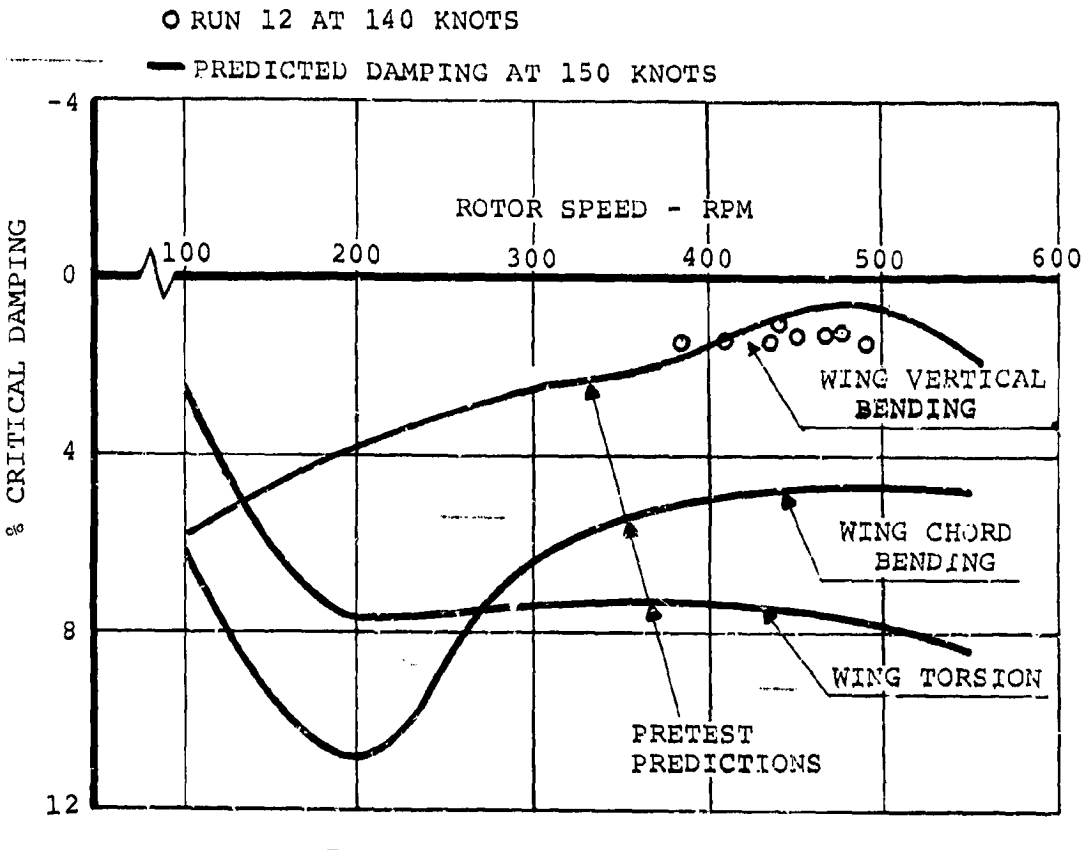

FIGURE 3-4. CORRELATION OF PREDICTED AIR RESONANCE MODE DAMPING AND MEASURED DAMPING OF THIS MODE DURING TEST. V = 140 KNOTS AND 150 KNOTS.

MODEL-222 FULL SCALE ROTOR TEST IN NASA AMES 40x80 FOOT TUNNEL: FULL STIFF WING

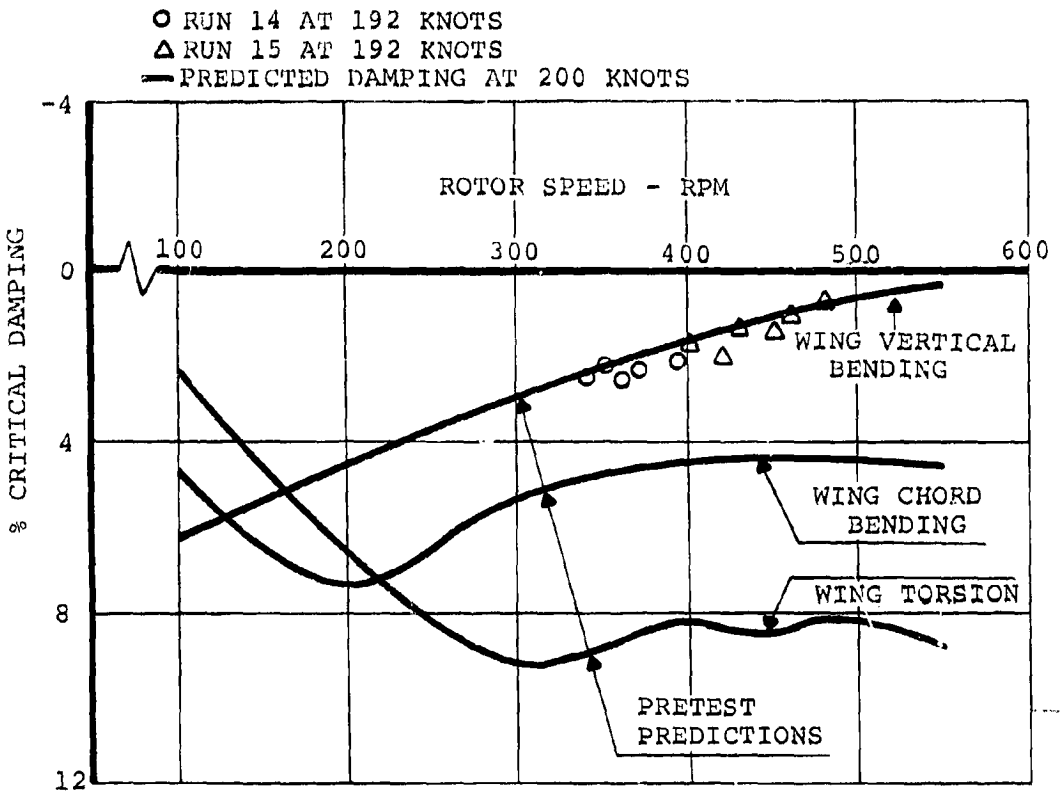

FIGURE 3-5. CORRELATION OF PREDICTED AIR RESONANCE MODE DAMPING AND MEASURED DAMPING OF THIS MODE DURING TEST. V = 192 KNOTS AND 200 KNOTS.

NASA AMES 40 X 80 WIND TUNNEL
TEST 410

100 KNOTS

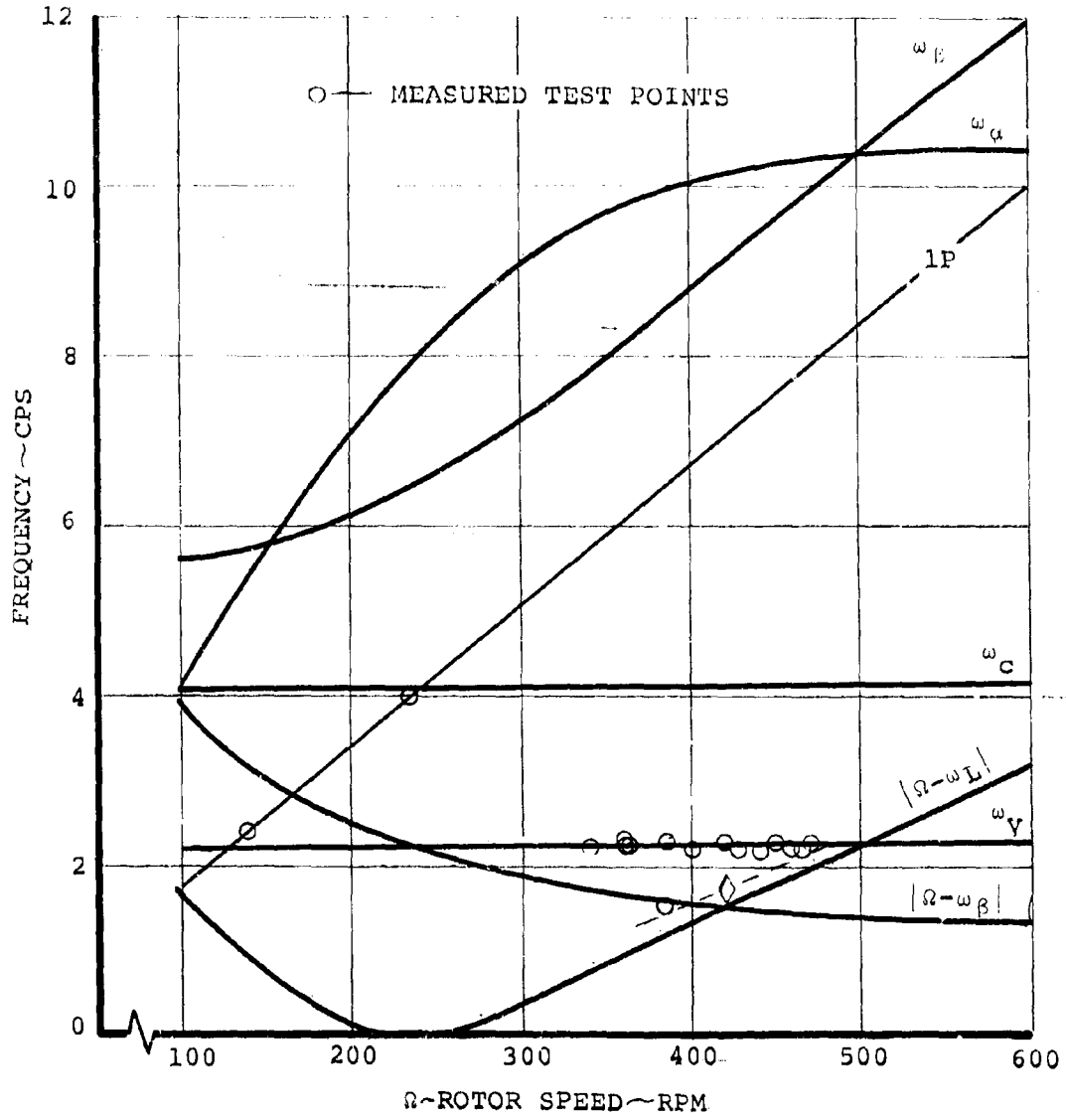

FIGURE 3-6. 26 FT. ROTOR - FULL STIFFNESS WING - MODAL FREQUENCIES AT V = 100 KNOTS.

NASA AMES 40 X 80 WIND TUNNEL
TEST 410

150 KNOTS

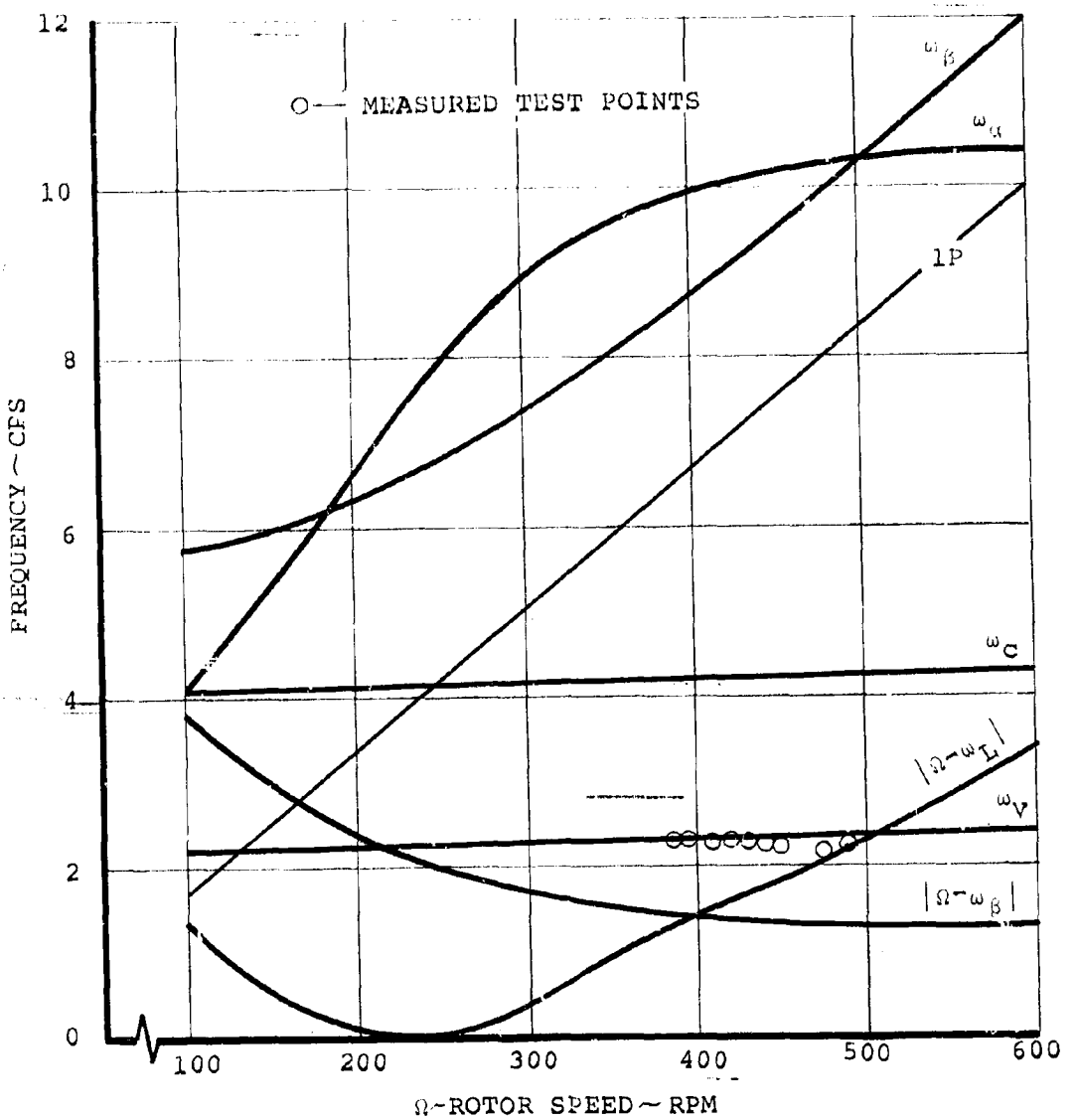

FIGURE 3-7. 26 FT. ROTOR - FULL STIFFNESS WING - MODAL FREQUENCIES AT V = 150 KNOTS.

NASA AMES 40 X 80 WIND TUNNEL
TEST 410

200 KNOTS

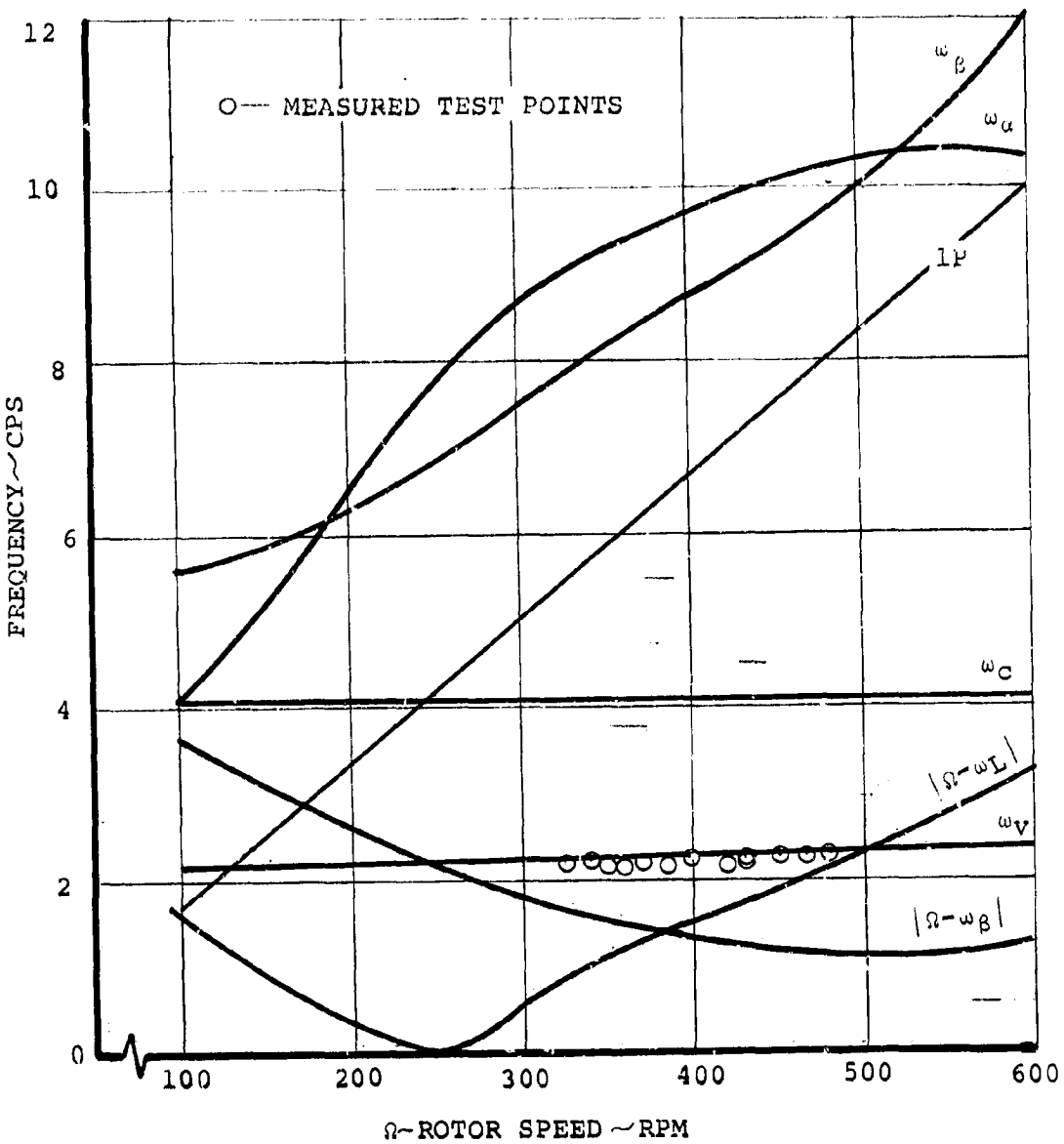

FIGURE 3-8. 26 FT. ROTOR - FULL STIFFNESS WING - MODAL FREQUENCIES AT V = 200 KNOTS.

NASA AMES 40 X 80 WIND TUNNEL
TEST 410

200 KNOTS

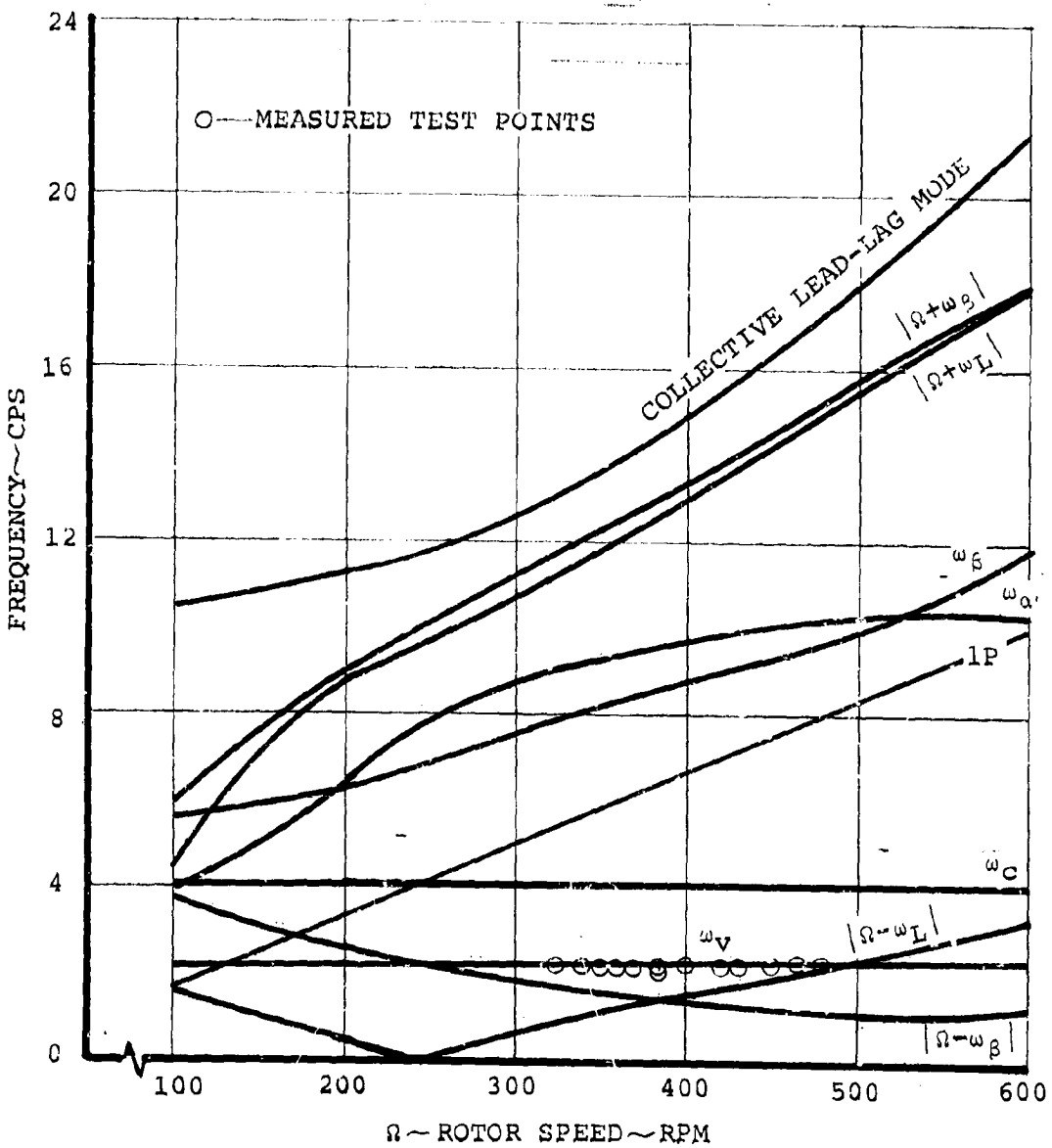

FIGURE 3-9. 26 FT. ROTOR - FULL STIFFNESS WING - MODAL FREQUENCIES AT V = 200 KNOTS.

TABLE 3.2

FULL STIFFNESS WING STATIC FREQUENCIES

(SUMMARY OF 3 MEASUREMENTS FOR EACH MODE)

Mode	ω - Hz	Structural Damping - %
Wing Vertical Bending	2.50	1.02
	2.49	1.16
	2.50	0.986
Wing Chord Bending	4.54	0.79
	4.49	0.80
	4.50	0.80
Wing Torsion	11.3	1.99
	11.42	2.18
	11.3	1.86

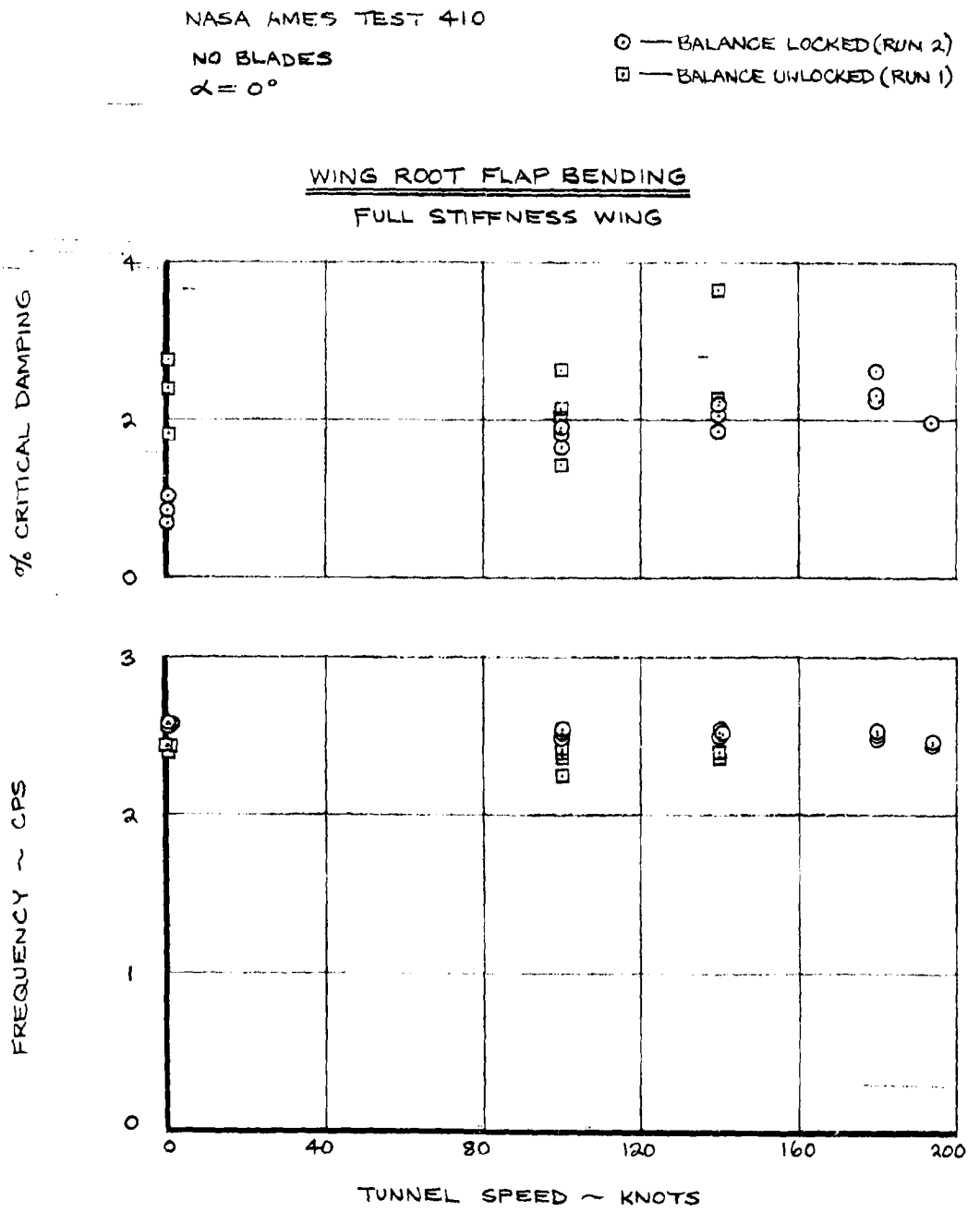

FIGURE 3-10 EFFECT OF TUNNEL SPEED ON WING ROOT FLAP BENDING FREQUENCY AND DAMPING DURING SHAKE TESTS - NO BLADES

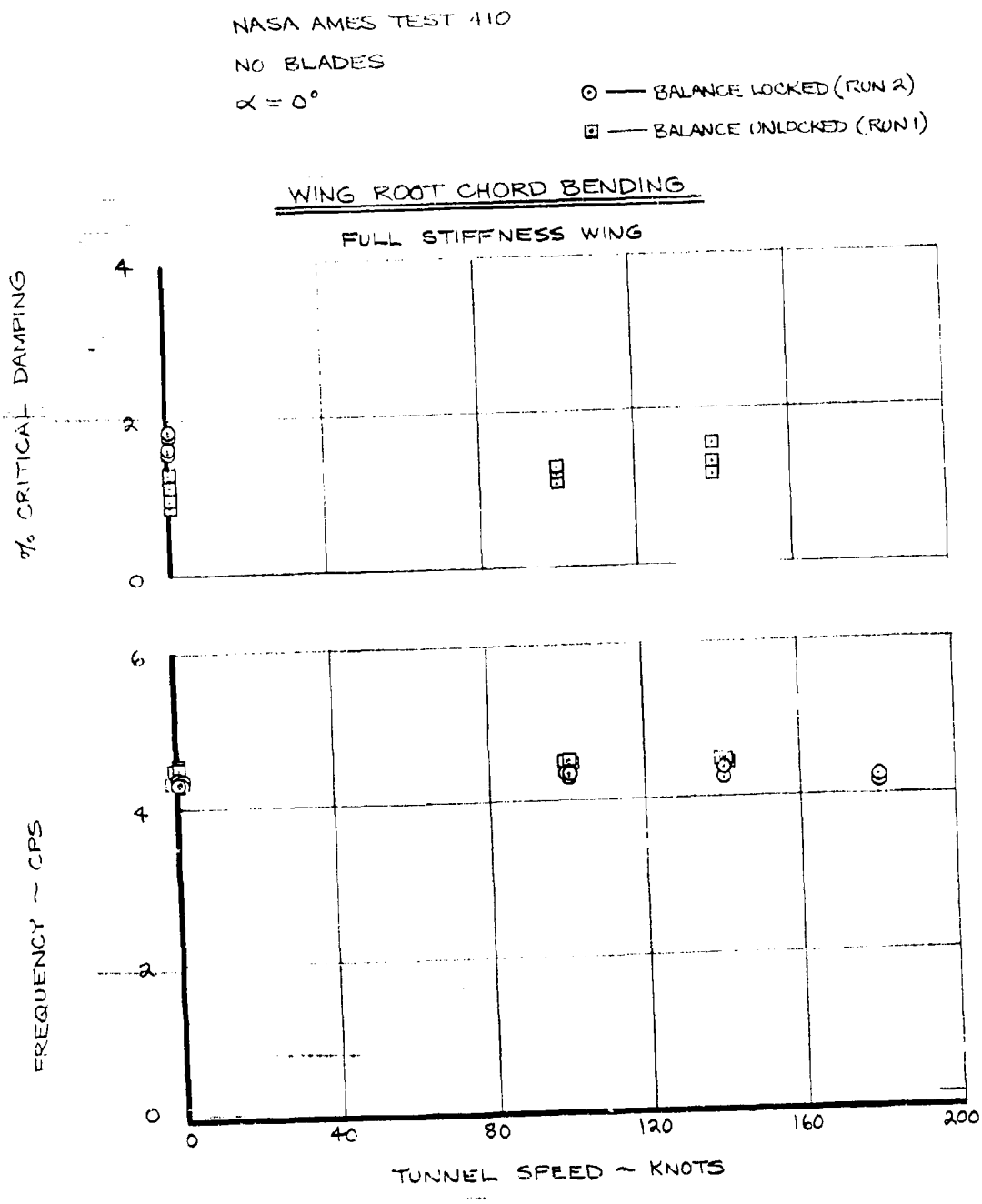

FIGURE 3-11 EFFECT OF TUNNEL SPEED ON WING ROOT CHORD BENDING FREQUENCY AND DAMPING DURING SHAKE TESTS - NO BLADES

NASA AMES TEST 410
NO BLADES
$\alpha = 0°$

⊙ —— BALANCE LOCKED (RUN 2)
⊡ —— BALANCE UNLOCKED (RUN 1)

WING ROOT TORSION

FULL STIFFNESS WING

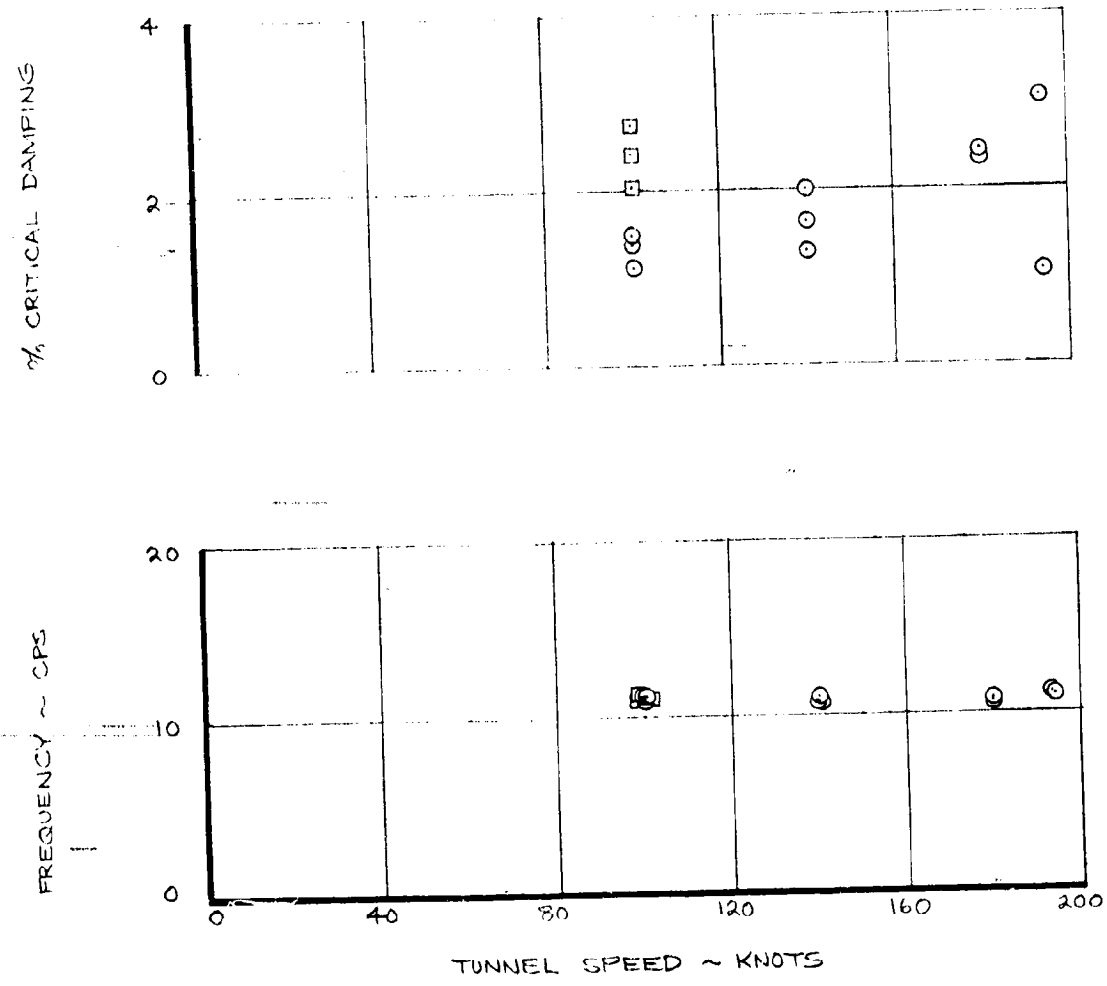

FIGURE 3-12 EFFECT OF TUNNEL SPEED ON WING ROOT TORSION FREQUENCY AND DAMPING DURING SHAKE TESTS - NO BLADES

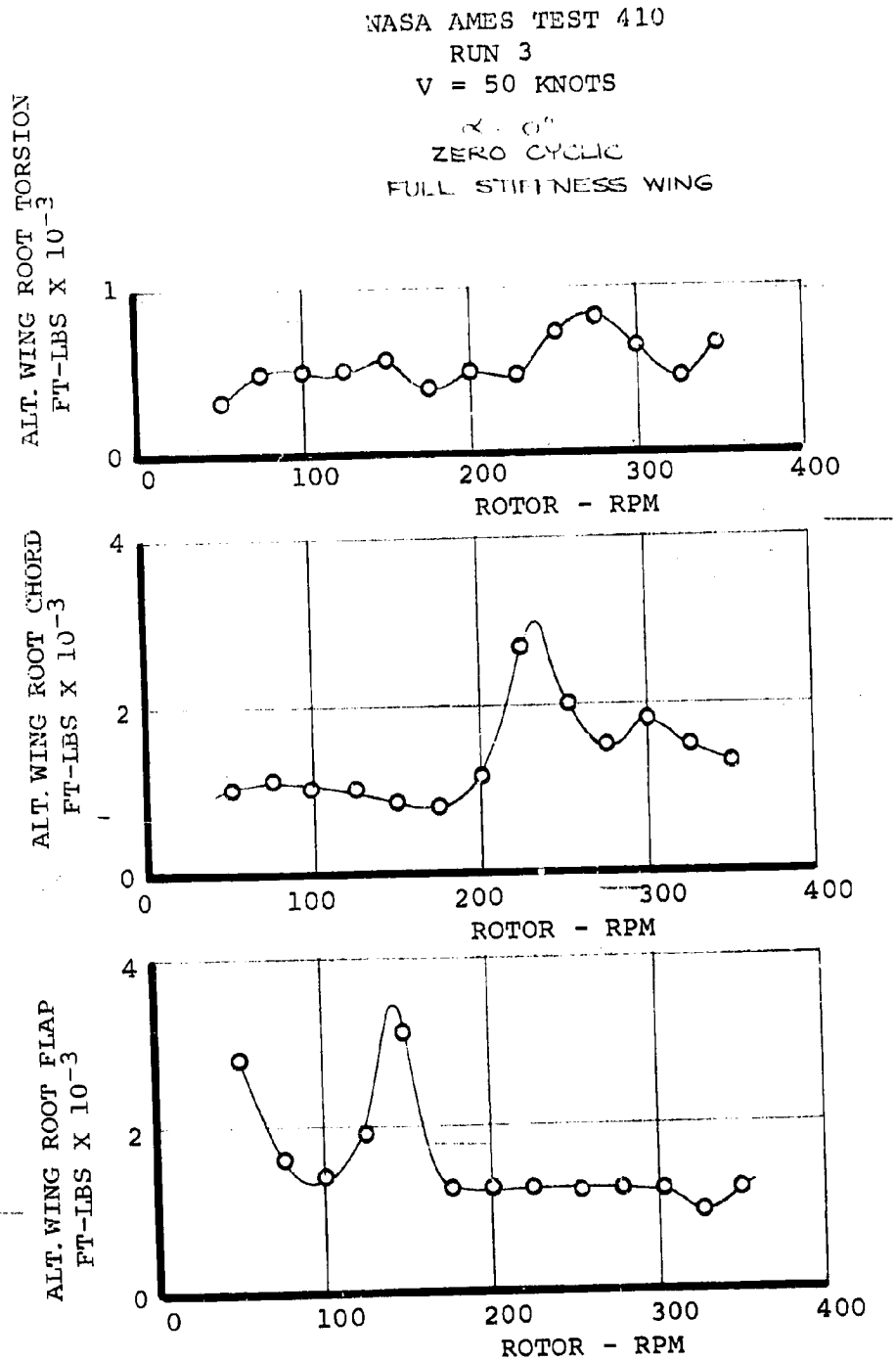

FIGURE 3-13 ALTERNATING WING LOADS DUE TO ROTOR RPM - V = 50 KNOTS

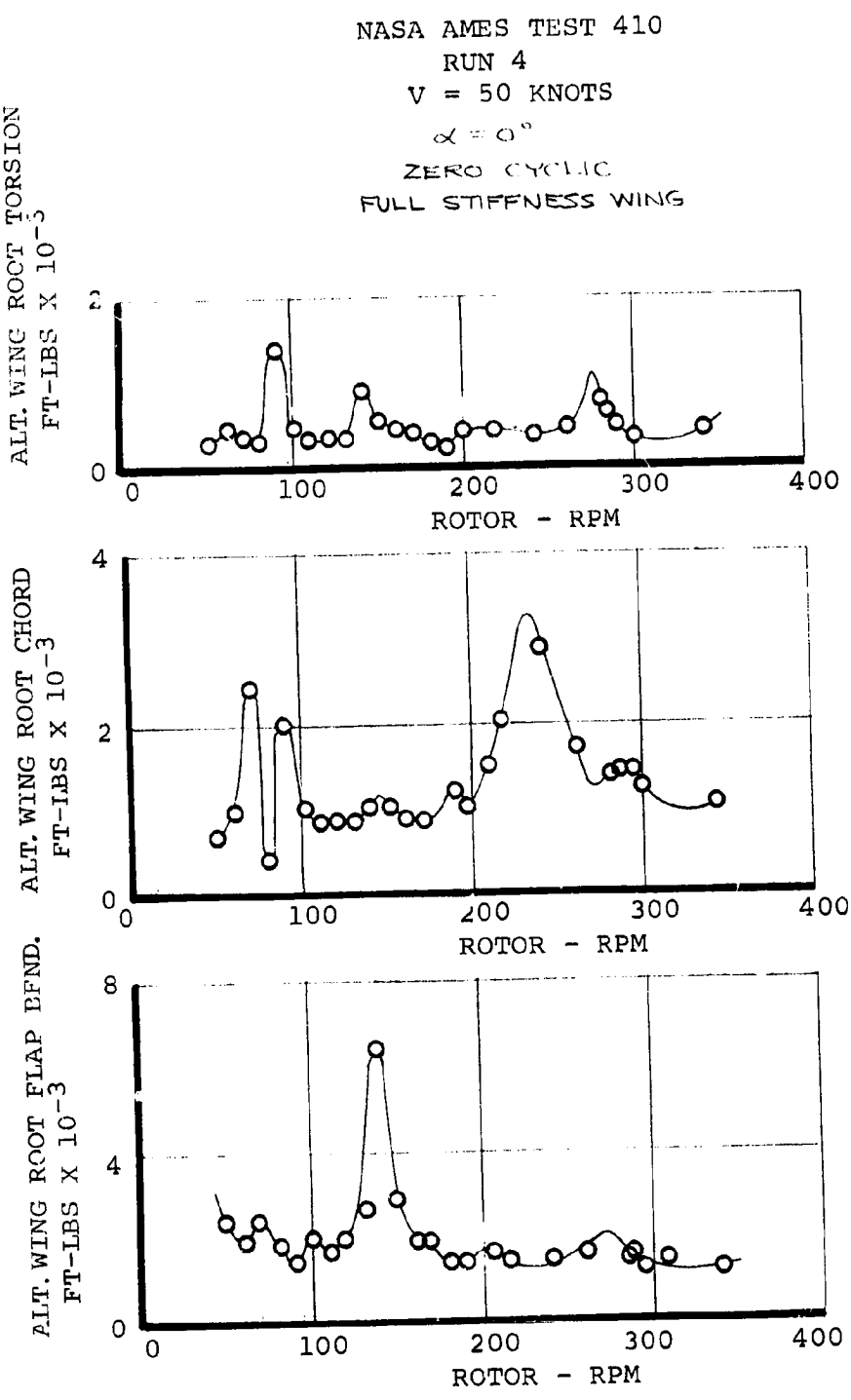

FIGURE 3-14 ALTERNATING WING LOADS DUE TO ROTOR RPM – V = 50 KNOTS

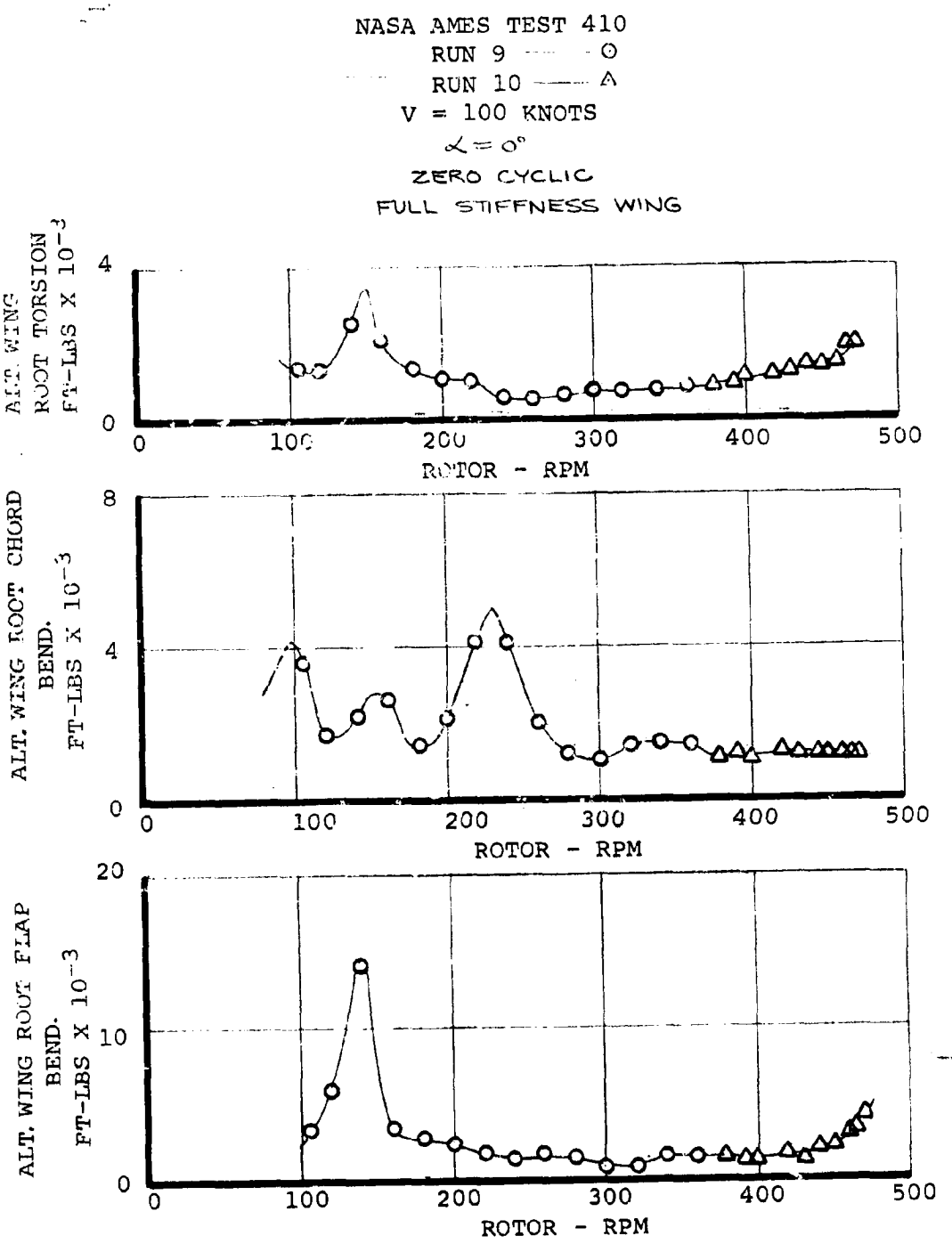

FIGURE 3-15 ALTERNATING WING LOADS DUE TO ROTOR RPM – V = 100 KNOTS

3.2 ¼ Stiffness Wing Test Stand

The objective in testing the Model 222 rotor on the ¼ stiffness wing was to simulate conditions at high forward speed. The 40' X 80' tunnel has a maximum speed of about 200 knots. The advance ratio equivalence of 400 knots was simulated by operating the rotor at one half design RPM. This provides correct simulation of the rotor aerodynamics with the exception of Mach No. The Mach No. effect is small up to the simulated speed and its effect on the aeroelastic behavior of the model is insignificant. The wing frequencies were one half the "full stiffness wing" resulting in correct simulation of wing characteristics. The simulation of the blade frequencies is less satisfactory since at one half design RPM the rotor operates close to the one per rev - first mode bending frequency crossing. This mismatch of blade frequencies produces aeroelastic characteristics not normally found at 400 knots and design RPM.

The predicted stability boundaries for this configuration are shown in Figure 3.16. The analysis predicts instabilities of two modes at a little over two hundred knots. One is a "whirl flutter" mode and the other an air resonance mode.

Two test investigations were performed. An RPM sweep was made at 80 knots to show that the air resonance instability previously experienced on the full stiffness wing was now stabilized. At 192 RPM an airspeed sweep was made to track the damping of the "whirl flutter" mode up to maximum tunnel speed. Unlike the air resonance mode previously investigated the whirl flutter mode has a "hard" flutter boundary in the sense that the modal damping changes rapidly with speed as shown in Figure 3.17. Testing under such conditions involves some element of risk. If the prediction had been unconservative flutter would have occurred below 200 knots and within the test speed range. Careful excitation of the critical modes and on line tracking of the modal damping was necessary to ensure that the finite speed increments associated with large scale tunnel operation did not bring about inadvertent deep penetration of an unstable region.

The modal damping data measured for both the whirl flutter mode and the air resonance mode are shown superimposed on Figure 3.17. Damping of the whirl flutter mode ($\Omega - \omega_\beta$) follows the predicted sharply reducing trend. Extrapolation of the test data to zero damping indicates a stability boundary at 215 knots and is shown for comparison on Figure 3.16.

For this airspeed sweep the air resonance mode is more highly damped; however, the data show good agreement with the predicted line.

The wing vertical bending modal damping is plotted against RPM at 80 knots, Figure 3.18. The predicted damping shows a tendency to reduce at about 370 RPM (i.e., just before the intersection of the $(\Omega - \omega_L)$ frequency and wing vertical bending frequency (ω_V). The mode is not predicted to go unstable. The experimental damping data closely follow the predicted trend and exhibit the same reduction in damping at 370 RPM.

The ¼ stiffness wing frequency spectrum is shown in Figure 3.19 and the measured modal frequencies are superimposed.

The degree of correlation obtained in both damping and frequency measurements clearly demonstrate the capability of the Boeing methodology.

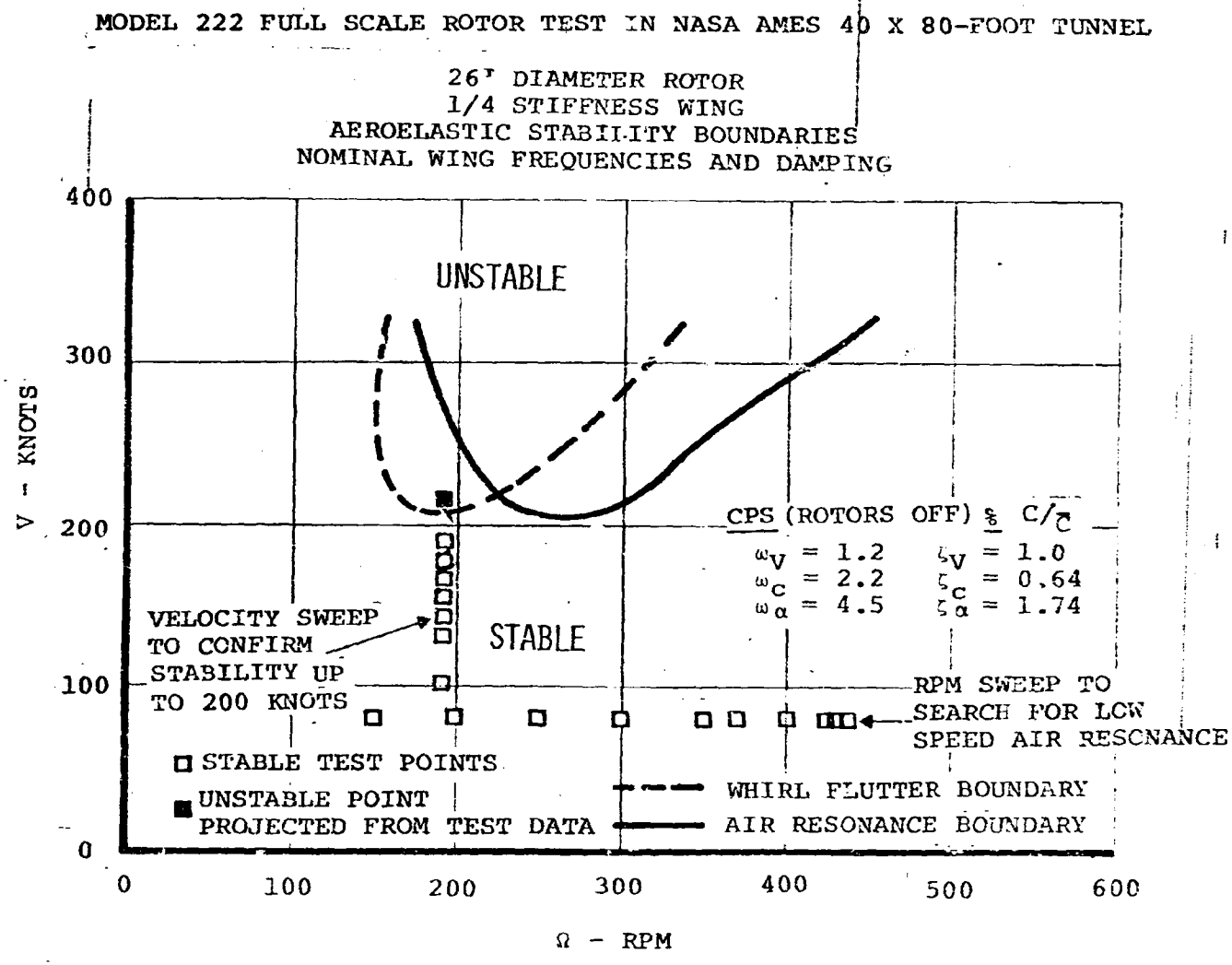

FIGURE 3-16 TEST POINTS RELATIVE TO PREDICTED BOUNDARIES FOR 1/4 STIFF WING TEST.

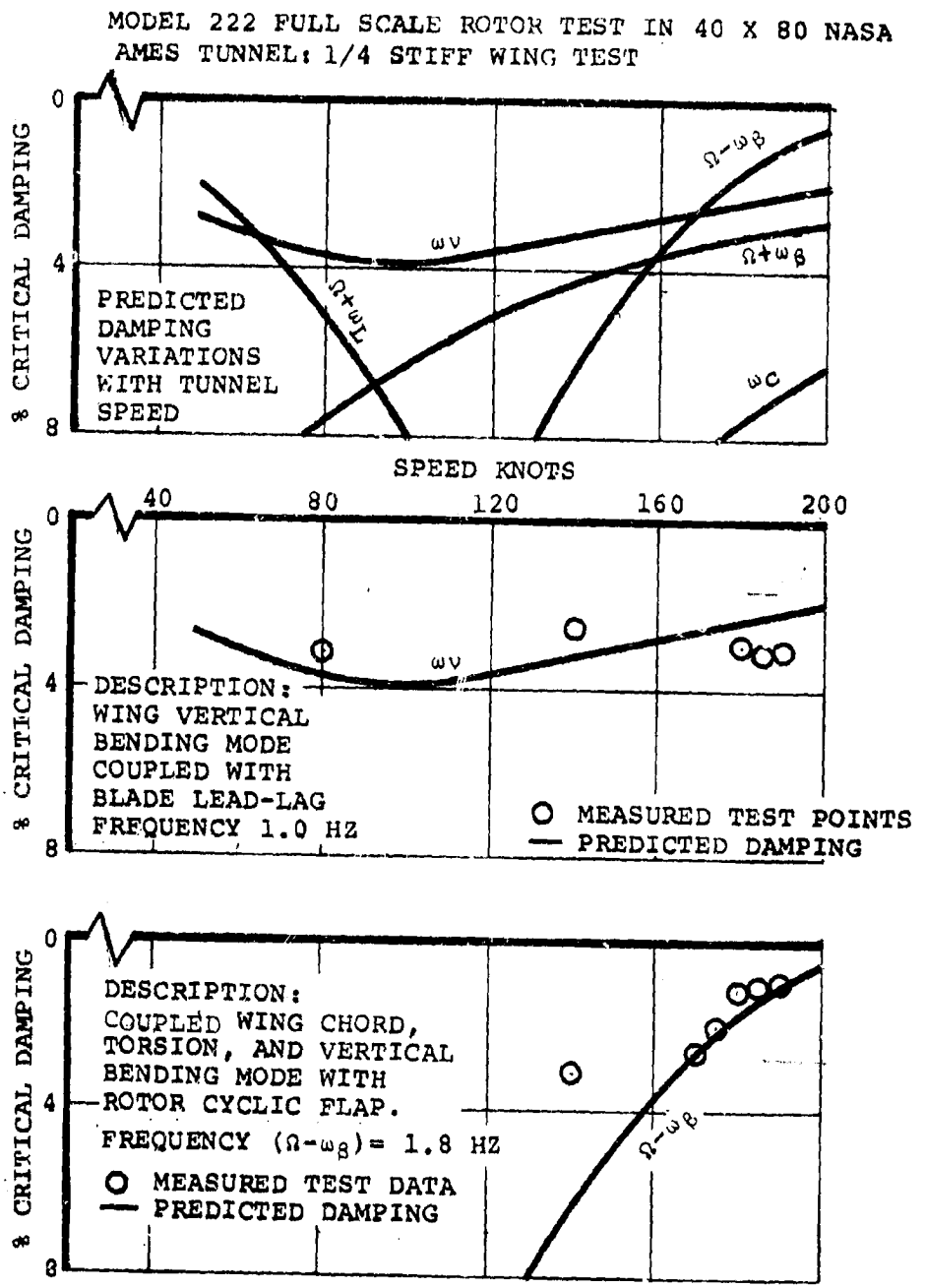

FIGURE 3-17 COMPARISON OF STABILITY PREDICTIONS AND TEST DATA FOR BOEING-VERTOL M222 26-FOOT ROTOR MOUNTED ON NASA-AMES 1/4 STIFF WING.

MODEL 222 FULL SCALE ROTOR TEST IN NASA AMES
40 X 80-FOOT TUNNEL

26-FOOT DIAMETER ROTOR: 1/4 STIFF WING

V = 80 KNOTS

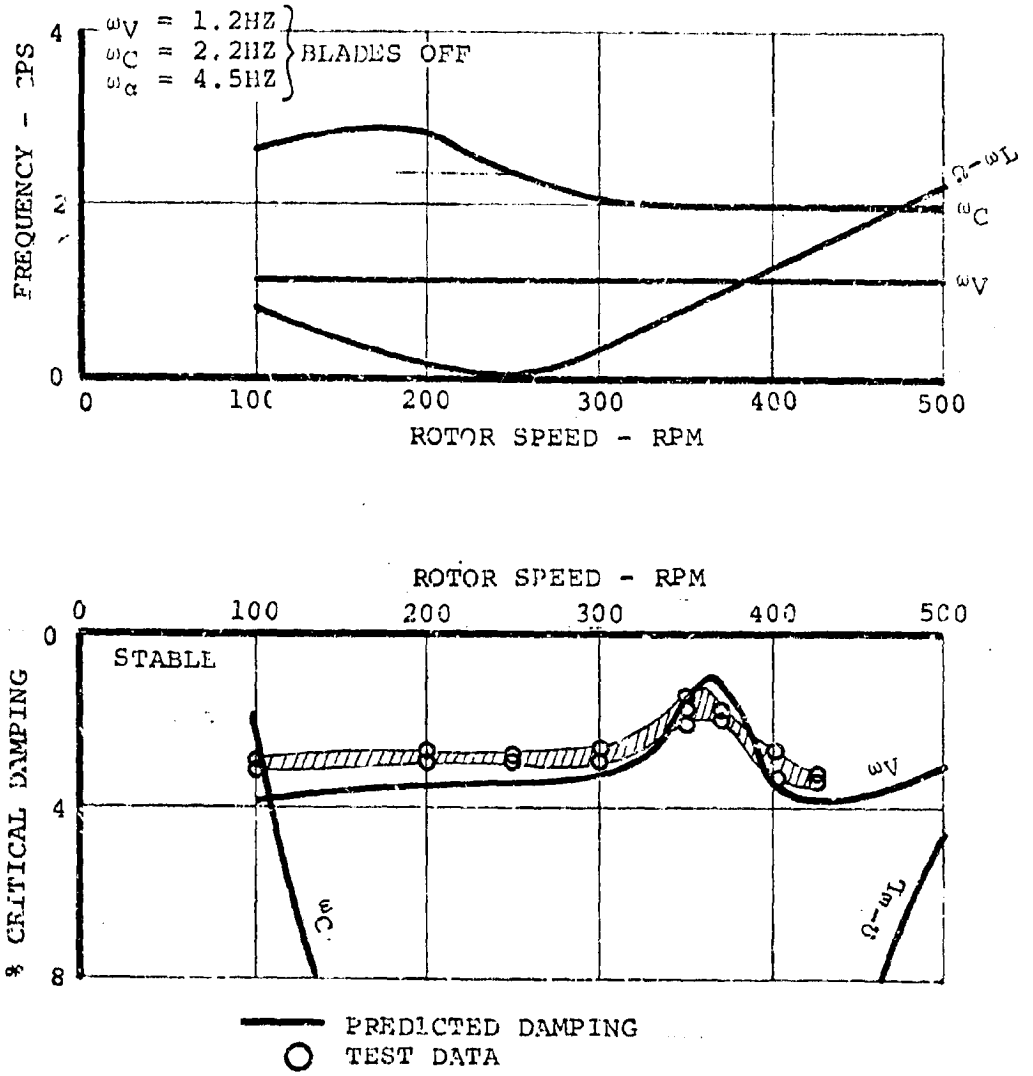

FIGURE 3-18 COMPARISON OF PREDICTED AND MEASURED DAMPING IN STABLE AIR RESONANCE MODE AT 80 KNOTS

MODEL 222 FULL SCALE ROTOR TEST IN
NASA/AMES 40x80 TUNNEL: 1/4 STIFF WING TEST

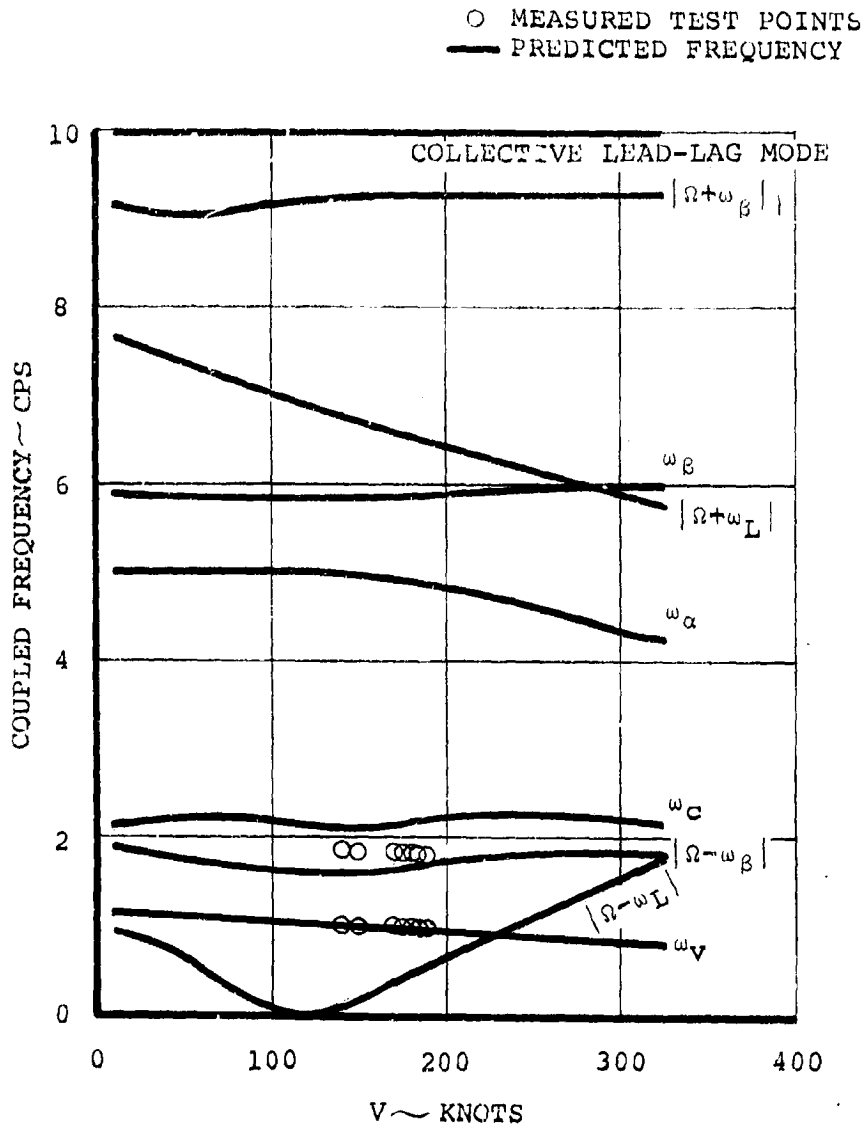

FIGURE 3-19 1/4 STIFFNESS WING FREQUENCY SPECTRUM

3.3 Powered Test Stand Stability

Background

The power test stand had been analyzed using a combination of empirical and analytical data and found to be stable. In the cruise and low tilt angle tests this was confirmed. However, at 83-degrees tilt it was found that a 0.33 per rev beat was present in the nacelle vertical accelerometer at 534 rpm and that the blade loads also showed signs of frequencies which were not integer multiples of rpm, see Figure 3.20. This was identified as a resonance condition and indicated that some essential degree of freedom had been omitted from the prediction analysis. Re-examination of the layout drawings indicated that the nacelle pitching constraint would become progressively less stiff as the nacelle tilted, since the goose neck eventually becomes horizontal and provides substantially less stiffness than in the untilted configuration. This offered an explanation of the source of an additional degree of freedom which was not identified by the structural analysis and shake testing conducted in 1969, which had both been restricted to the untilted case. The changes in the geometry of the pitch restraint mechanism are shown in Figures 3.21 and 3.22. A rudimentary shake test using hub out-of-balance conducted

at the conclusion of the subject test confirmed that such a mode existed and that its frequency was such as to explain the resonance condition encountered at 535 rpm.

Test Data

The data from the nacelle accelerometers and gages are shown in Figure 3.20. The gage on the rotor hub measuring in-plane bending moment was filtered to attenuate 1 per rev components and to eliminate higher frequencies. The same process was applied to the nacelle accelerometer mounted near the rotor hub and the nacelle moment. The results of this process are shown in Figure 3.23. The following conclusions may be drawn:

1. There is a significant 0.33 per rev vertical motion (in rotor axes) at the rotor hub, but no such indication at the nacelle pitch axis. Thus the oscillation is a pitching motion about the tilt axis.
2. There is no significant amount of lateral 0.33 per rev motion at the rotor or the pivot axis, confirming that the nacelle motion is almost pure pitch.
3. The hub gage trace shows a 0.66 per rev oscillation with a 1 per rev component added. This waveform was synthesized exactly by combining a 1 per rev trace with a 0.66 per rev trace.

As a result of these studies of the test data it was concluded that the oscillation was nothing more serious than a mechanical resonance condition and the test proceeded avoiding this region.

Analytical Studies

Concurrently with the study of the test data an analysis was made incorporating a pitch degree of freedom. This was done for two reasons:

1. To demonstrate analytically that the oscillation was a mechanical resonance with predictable behavior and which therefore presented no substantial risk in further testing.
2. To demonstrate that the incident would have been anticipated and preventive steps taken if information on the stand frequencies at high tilt angles had been available prior to the test.

Since at this point the nacelle pitch frequency was indicated only by the oscillation frequency and its damping unknown, a range of pitch frequencies and dampings were investigated. Frequencies of 2.4, 2.9 and 3.6 were investigated with the results shown in Table 3.3.

These results indicate that the onset of the instability is relatively insensitive to damping and that the frequency of

Table 3.3. RPM and Oscillation Frequency at Onset of Instability

Pitch Frequency	0% Damping RPM/Hz	1% Damping RPM/Hz	2% Damping RPM/Hz
2.4 Hz	517/2.3	517/2.3	520/2.4
2.9 Hz	560/2.85	565/2.9	565/2.95
3.6 Hz	595/3.25	600/3.25	--

the instability is approximately the same as the pitch mode frequency. However, the observed frequency of 2.95 Hz for the instability implies a pitch frequency of around 2.9 Hz; this in turn implies a stability boundary at 565 RPM and not the observed stability boundary of 535 RPM. Thus there is a 6% discrepancy in the correlation. An error in the predicted rpm of this magnitude could be accounted for by differences between the actual and assumed blade frequencies. Differences between predicted and actual blade frequency of the required order of magnitude are shown in Figure 4.11 in Section 4.1. The effect of this reduction in blade frequency is shown in Figure 3.24.

Post Test Shake

The above conclusions were reached with only deductive knowledge of the pitch mode. At the end of the test the blades were removed and an out of balance mass added to the hub. The system was then run up at two tilt angles and the vibration levels were noted as shown in Figures 3.25, 3.26 and 3.27. These responses in the nacelle vertical accelerometer, the trunnion and the goose neck accelerometer clearly indicate the existence of a pitch resonance of approximately 2.9 Hz.

Conclusions

The analytical studies and test data analysis and post test

resonance investigation all confirm the original conclusion that the oscillation observed at 85-degrees was an incipient mechanical instability, the mechanism of which is well understood.

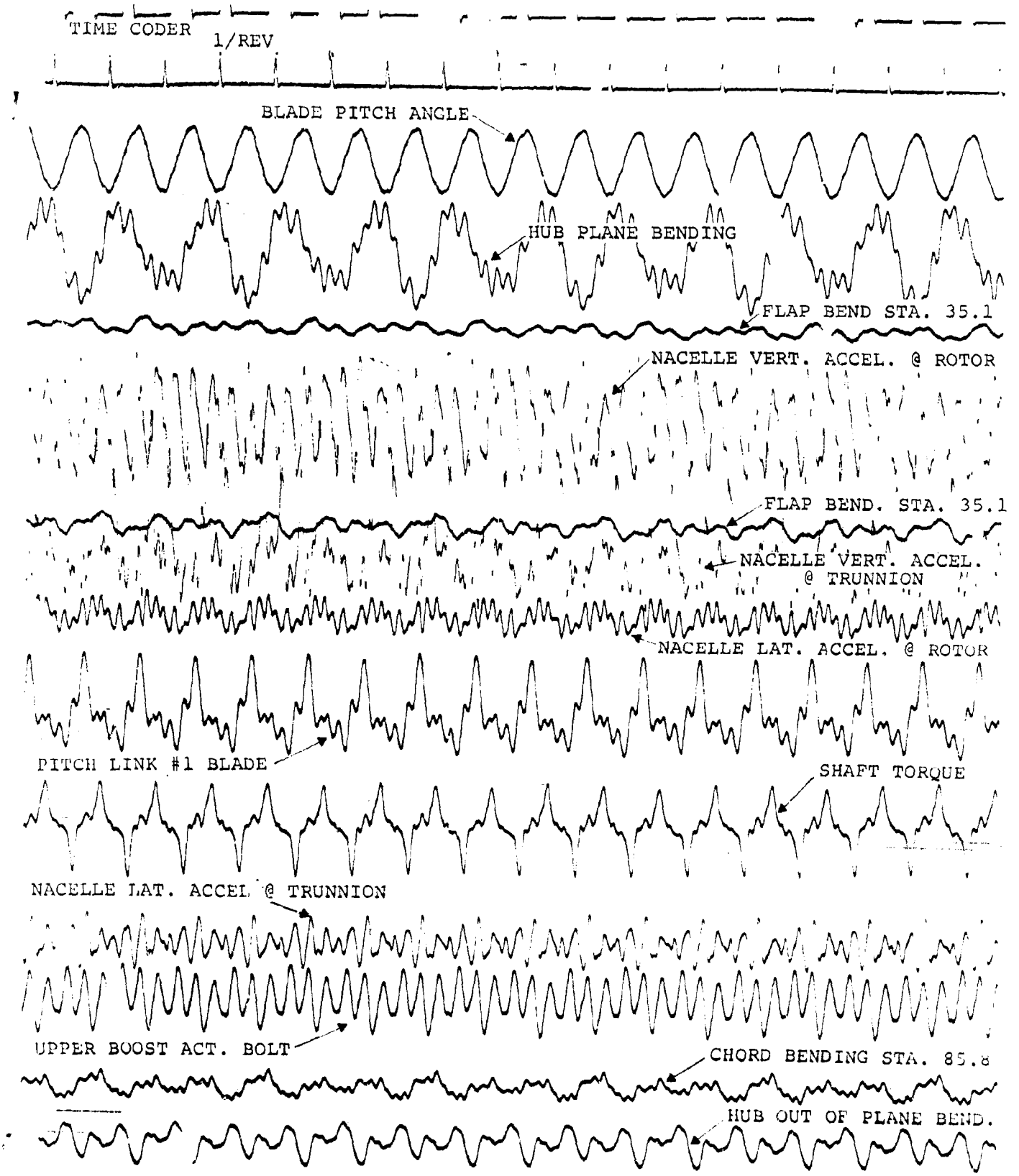

FIGURE 3.20 NACELLE ACCELEROMETER TRACES AT 83° TILT ANGLE AND 534 RPM

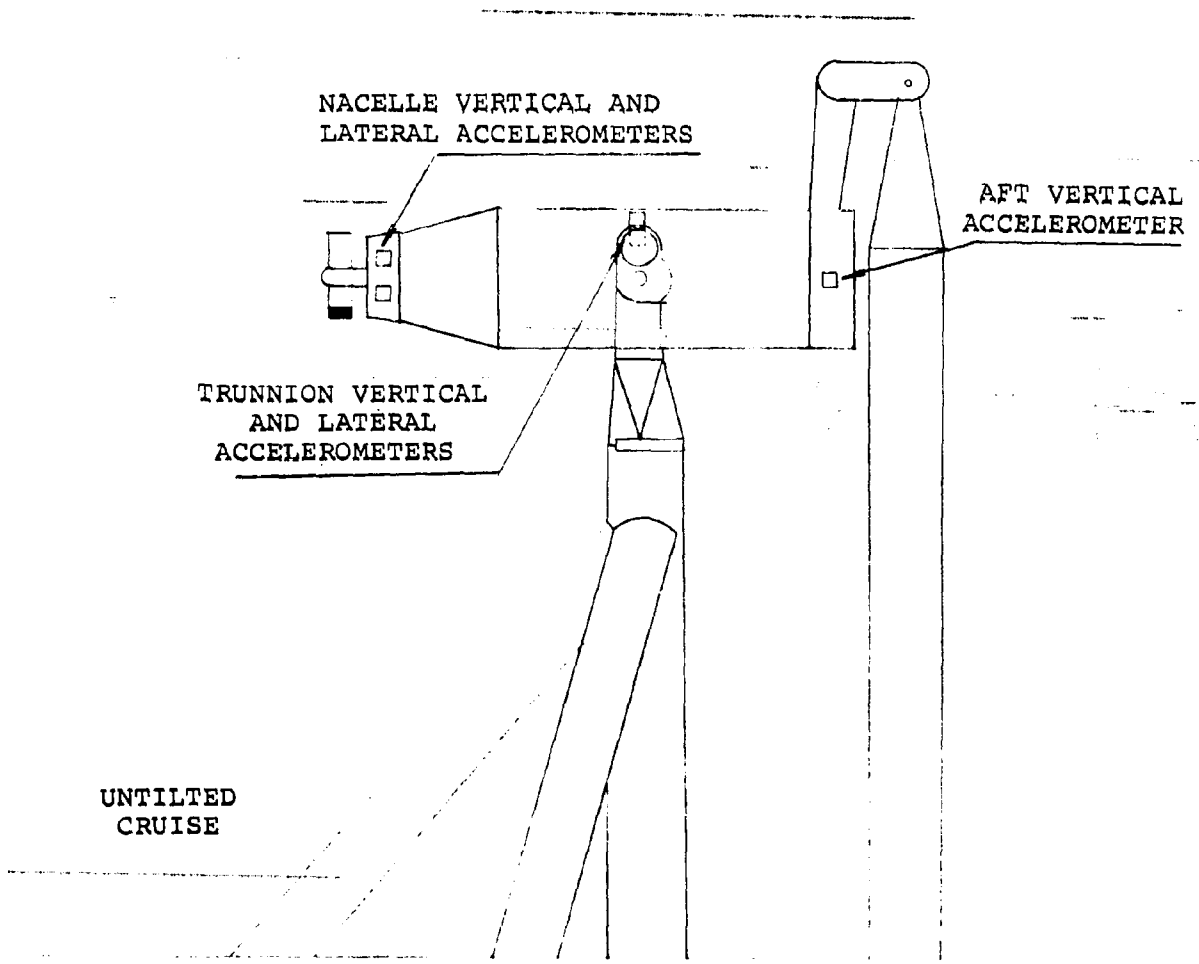

FIGURE 3.21 SCHEMATIC OF POWER TEST STAND
SHOWING PITCH RESTRAINT GEOMETRY

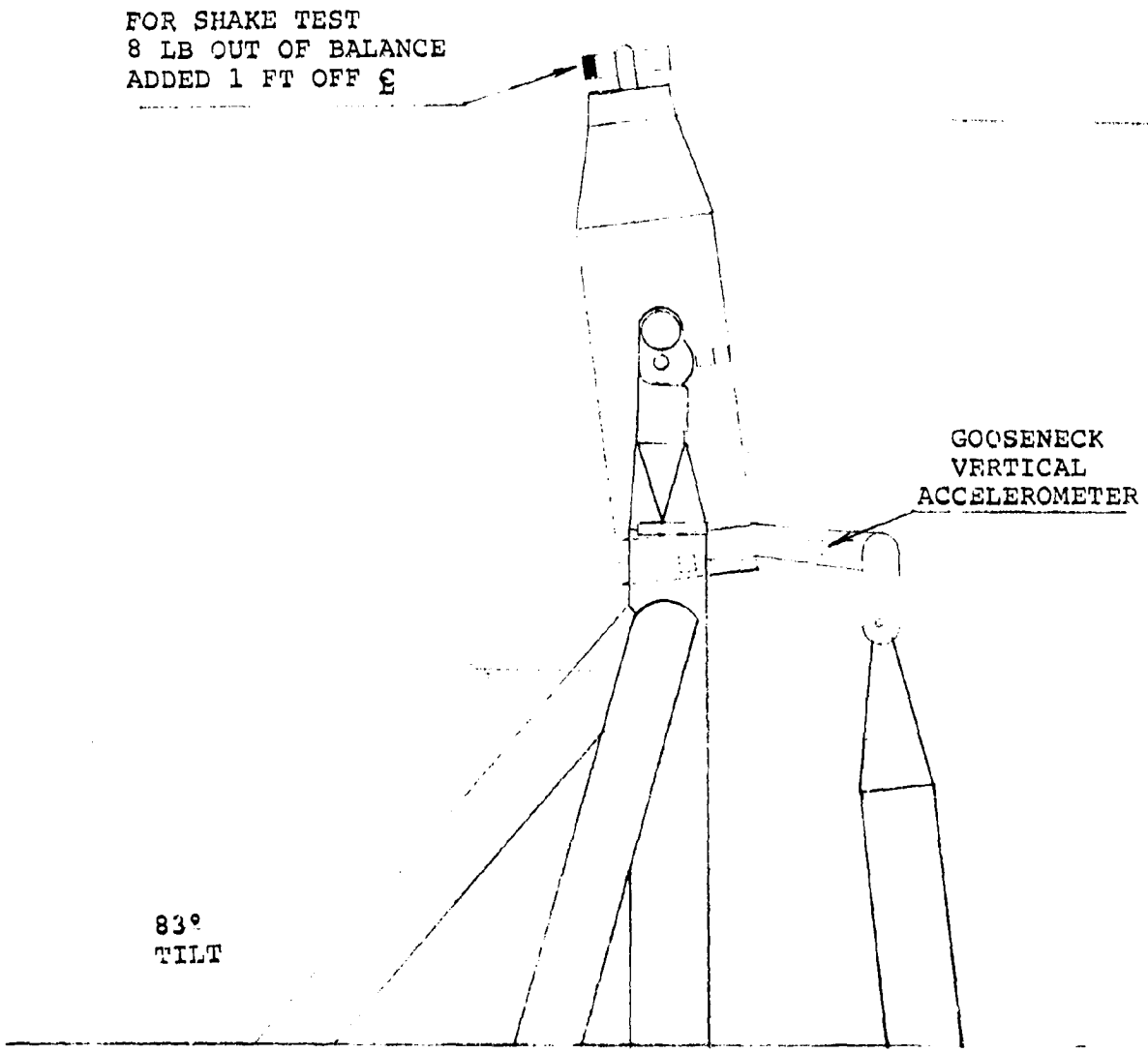

FIGURE 3.22 SCHEMATIC OF POWER TEST STAND SHOWING CHANGE IN PITCH RESTRAINT GEOMETRY WITH TILT ANGLE

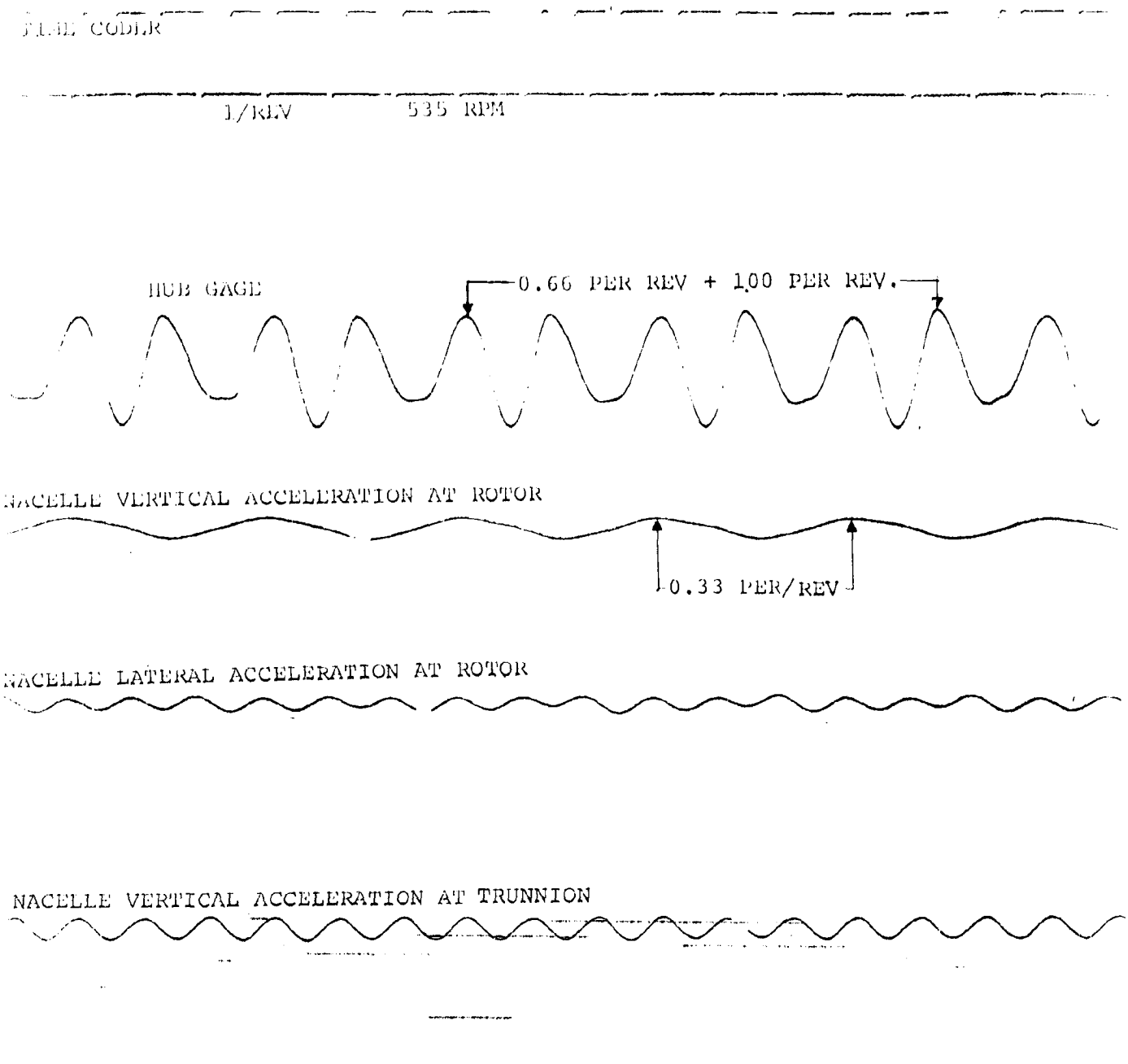

FIGURE 3.23 FILTERED TRACES OF HUB IN PLANE BENDING MOMENT AND NACELLE ACCELEROMETERS

M222 26FT DIAMETER ROTOR ON NASA-AMES POWERED TEST STAND

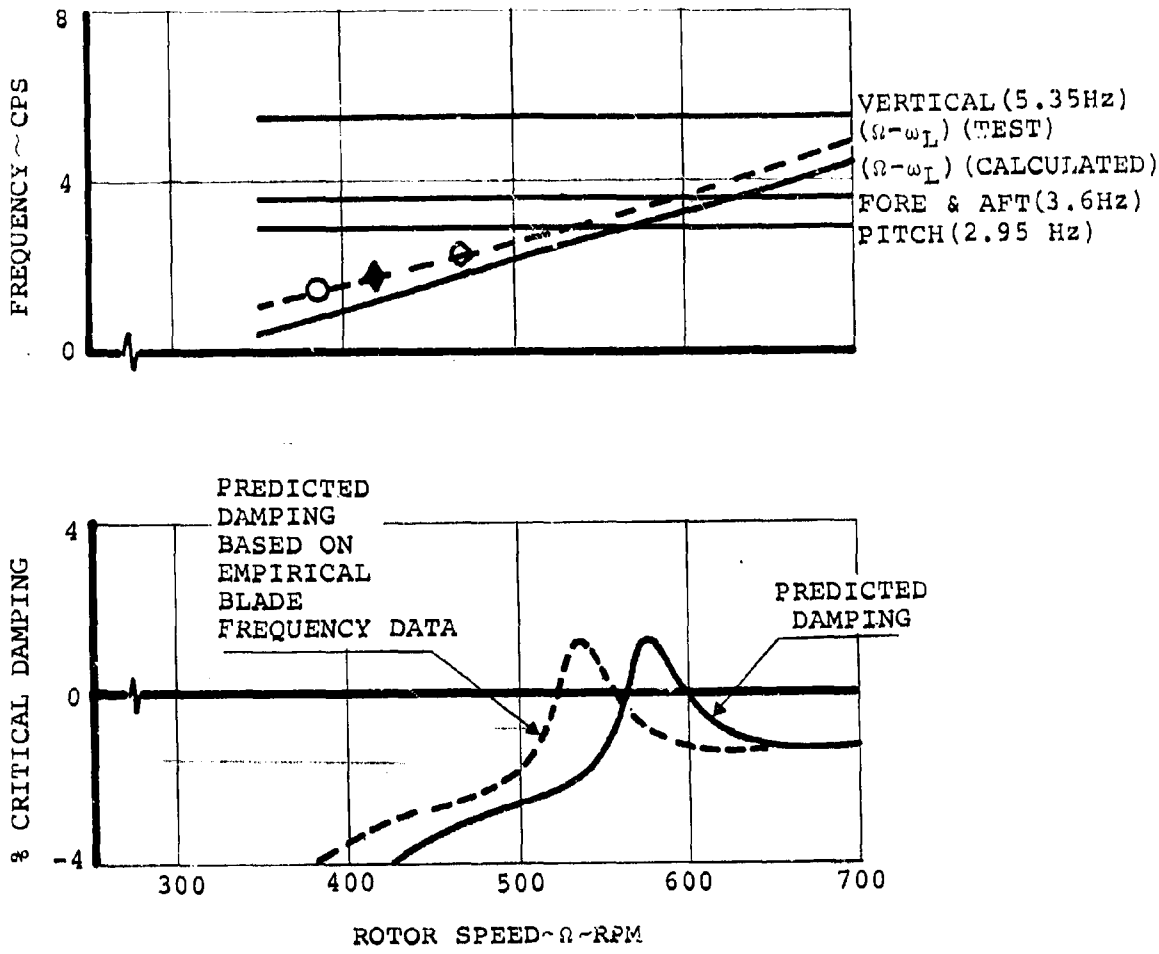

FIGURE 3.24 POWER TEST STAND 83° TILT COMPARISON OF DAMPING PREDICTIONS USING BLADE EXPERIMENTAL AND BLADE CALCULATED DATA

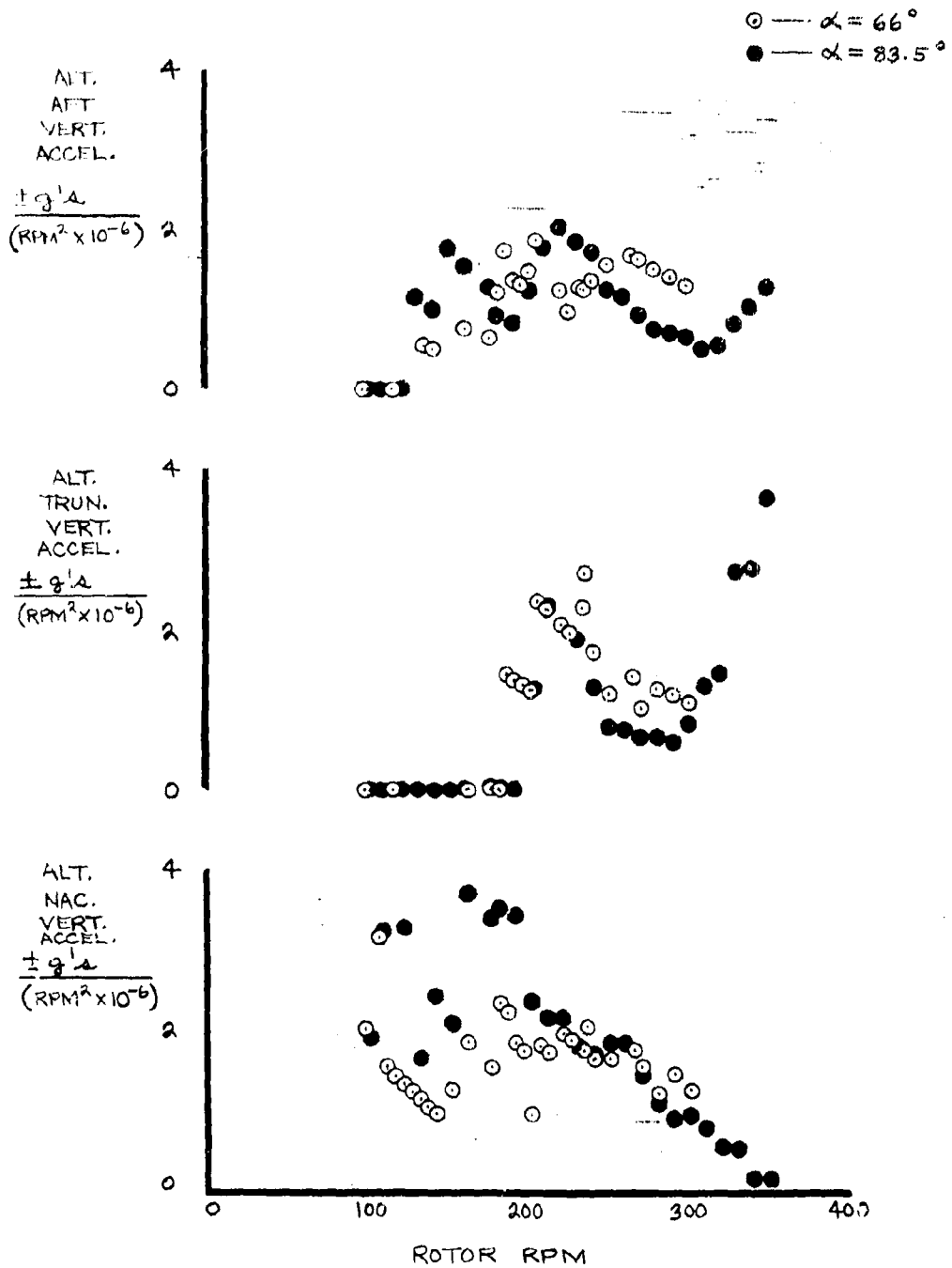

FIGURE 3.25 NASA-AMES POWERED TEST STAND RESULTS OF POST TEST ROTATING MASS SHAKE TEST. NACELLE VERTICAL ACCELEROMETERS AT ROTOR, TRUNNION AND REAR.

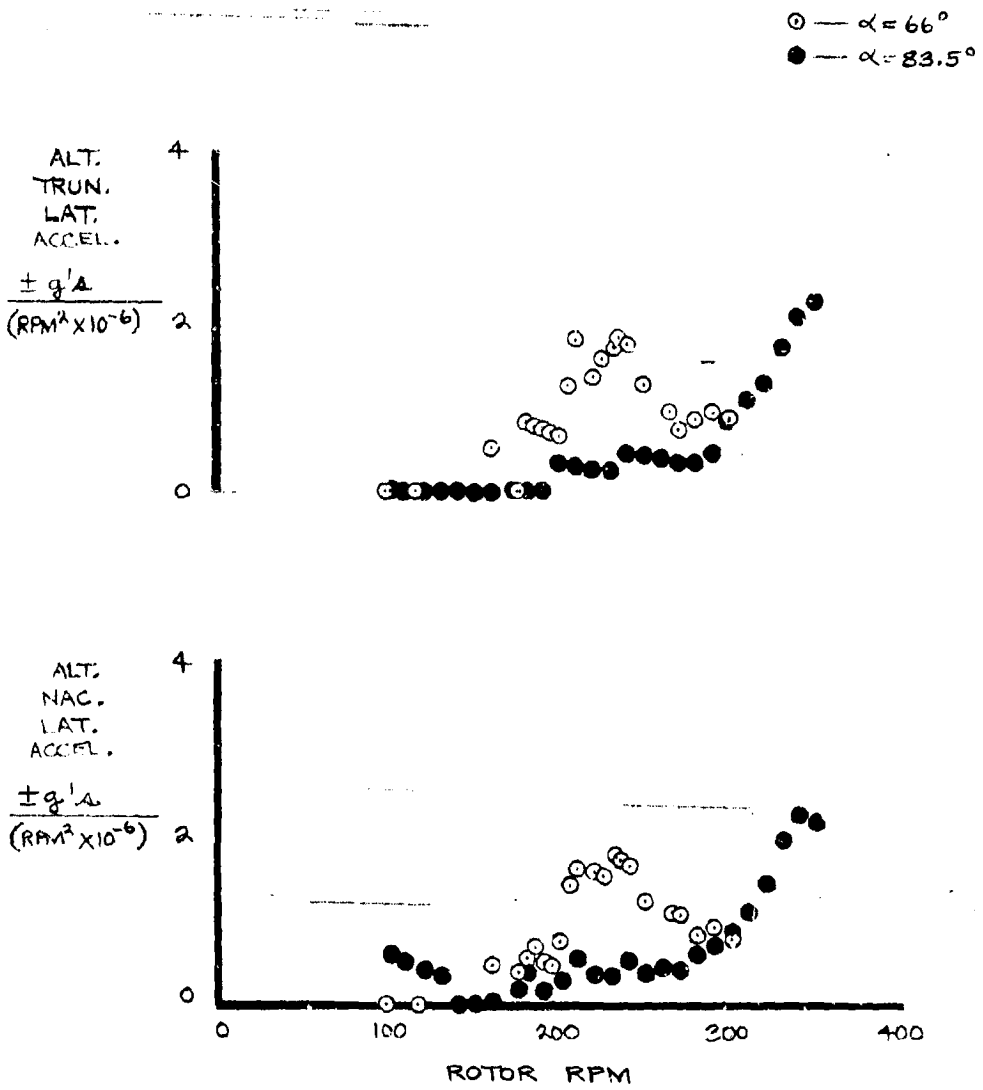

FIGURE 3.26 NASA-AMES POWERED TEST STAND RESULTS OF POST TEST ROTATING MASS SHAKE TEST. NACELLE LATERAL ACCELEROMETERS AT ROTOR AND TRUNNION.

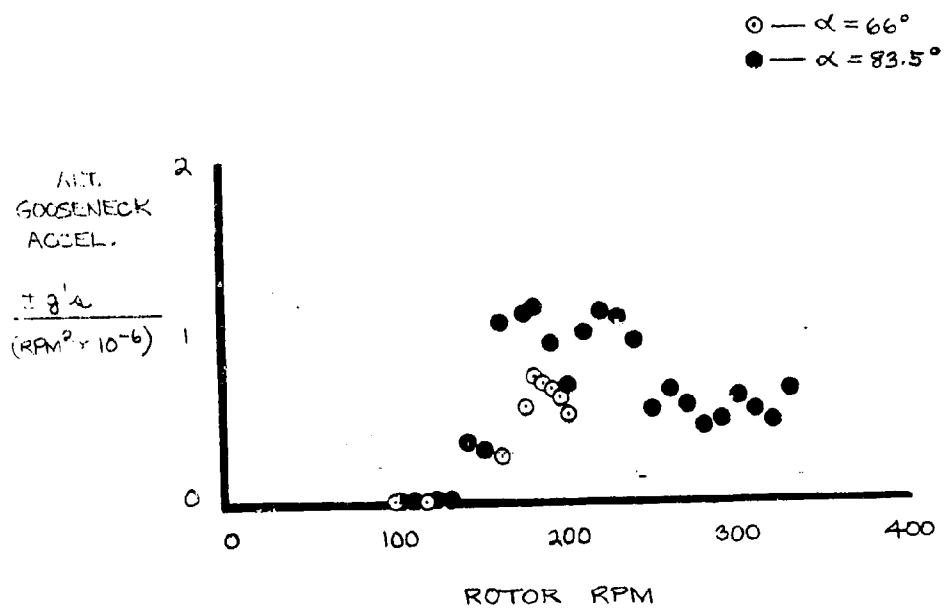

FIGURE 3.27 NASA-AMES POWERED TEST STAND RESULTS OF POST TEST ROTATING MASS SHAKE TEST. GOOSENECK VERTICAL ACCELEROMETERS.

4.0 ROTOR LOADS

4.0 ROTOR LOADS

The Model 222 rotor is a hingeless, soft-in-plane design. The name soft-in-plane implies that the first bending modal frequency is less than one per revolution. The second bending frequency is greater than one per revolution. This type of rotor was selected for several reasons. For example, the hingeless blade design provides a simple hub design with fewer moving parts than its hinged or teetering counterpart, providing improved reliability and maintenance. Hub drag is reduced and also the reduced blade flapping excursions of the hingeless rotor enable the rotor-pivot dimension to be held to a minimum.

Analysis and tests indicate that the aeroelastic behavior of the individual hingeless rotor blade including stall flutter characteristics are acceptable. Rotor-wing dynamics provide low susceptibility to whirl flutter instabilities and although the lower blade lag mode can drive air/ground resonance, the damping of these modes can be predicted accurately by Boeing's analytical dynamics methodology as shown in Section 3.

The flight envelope of the aircraft is limited by power and alternating blade loads.

The first harmonic of the alternating blade loads, due to angle of attack and advance ratio, can be counteracted by the application of cyclic pitch control and the limits of the rotor are reached when either the alternating blade loads

at frequencies other than one per revolution reach the blade allowable loads or when the cyclic pitch control input to negate the bending loads causes pitch link loads to reach their fatigue allowables.

The tests ran on this rotor were aimed at providing experimental verification of the rotor limits and the sensitivities of blade loads to attitude and cyclic pitch throughout the flight envelope.

4.1 BLADE FREQUENCIES

The first mode bending frequency of the soft-in-plane rotor is designed to be in the region of 0.7 to 0.8 per revolution throughout its operating envelope. This design requirement is a compromise between decreased loads obtained by lowering the blade frequency and increased air resonance modal damping obtained by increased blade frequency.

Testing was performed on both windmilling and powered tests to verify the design blade frequencies and these data are given in Figures 4.1 to 4.11.

Static Frequencies

The blades were mounted in a dummy hub barrel fixture and cantilevered from a "strongback". Two types of static frequency tests were run prior to the windmilling tests: shake tests and bang tests. For the shake tests a ±5 lb. shaker was used, the armature of which weighed 1.7 lbs. An accelerometer (located at the blade tip) was used to measure the blade frequency for initial tests. The location of the accelerometer was varied in later tests to define the mode shapes. Since the first mode bending frequency of the blade was below the recommended shaker operating range, "bang" tests were also performed. The accelerometer signal was recorded on oscillograph and the blade given a sharp rap at the tip. The resulting oscillatory signal was compared with a 60 Hz trace to determine frequency. These tests were performed prior to balancing the rotor and were performed with both no balance weights and with 5 lbs. of tip balance weights installed.

Blade static frequency data obtained on these tests and subsequent blade bang tests are presented in Table 4.1. The data marked "interpolated" are deduced from the zero and 5 lb. tip weight data after the rotor balance had been performed and are the operating condition blade static frequencies. The design blade static and rotating frequencies are given in Table 4.2.

TABLE 4-1

MODEL 222 BLADE STATIC FREQUENCIES

FROM SHAKE AND BANG TESTS

TEST METHOD	BLADE NO.	TIP WT CONFIG (LBS)	BENDING MODES			Torsion	REFERENCE
			1 Hz	2 Hz	3 Hz	Hz	
Bang	1	5	2.34	4.66			TMR 1353
Shake	1	5	2.34	4.80	12.5	42.5	" "
Bang	1	0	2.43	5.09			" "
Bang	2	5	2.32	4.76			" "
Shake	2	5	2.32	5.4	13.4	40.3	" "
Bang	2	0	2.43	5.06			" "
Bang	3	5	2.28	4.65			" "
Shake	3	5	2.28	5.20	11.65/ 14.35	41.6	" "
Bang	3	0	2.43	4.88			" "
Bang	2	0.0354	2.35	4.74			IOM 8-7310-5-12
Bang	2	0.0354	2.36	4.73			
Bang	2	0.0354	2.358	4.74			
Bang	3	0.0	2.33	4.70			
Bang	3	0.0	2.34	4.70			
Interpolated	1	0.533	2.41	5.081			
"	2	0.0354	2.428	5.056			
"	3	0.0	2.43	4.88			

TABLE 4-2

MODEL 222 ROTOR DESIGN FREQUENCIES

$\Theta_{.75}$	RPM	1	2	3	4
0	0	2.323	5.25	13.782	
16°	551	6.625	11.23	30.34	52.18
21°	551	6.509	11.230	30.25	52.14
31°	551	6.284	11.424	30.03	52.06
36°	386	5.104	8.768	23.25	44.026
54°	386	4.743	8.968	22.96	43.92

Data Taken from Reference 13 (D222-10009-1).

Rotating Frequencies

The natural frequencies of a soft-in-plane hingeless rotor are a function of RPM since there is a significant portion of the blade stiffness derived from centrifugal stiffening. The rotating natural frequencies of the lower bending modes have been determined in two ways. First, RPM sweeps with small amounts of one/rev excitation (cyclic or angle of attack) were performed. As the blade first mode bending frequency coincides with the rotational frequency a load amplification is observed which is particularly noticeable at low collective and airspeed (low lag mode damping) and is more difficult to determine as airspeed and collective increase (high lag mode damping). The one/rev frequency decreases as collective increases. Data obtained in near hover conditions on the powered test are given in Figures 4-1 and 4-2 for a constant collective (θ_{75} = 8.8°) and also for windmilling conditions at 50 knots and 100 knots tunnel velocity in Figures 4-3 to 4-5. For these latter plots the blade collective is a function of RPM and tunnel speed and is defined in Section 7 of this report.

The first mode bending, one per revolution frequency crossing, is shown to be at 285 RPM for a collective of 8.8° in Figures 4-1 and 4-2, data obtained in near hover powered runs.

Figures 4.3, 4.4 and 4.5 show similar RPM sweeps for the windmilling case. For the 50 knot condition, Figures 4.3 and 4.4, the first mode, one per revolution frequency crossing, is seen to be at about 286 RPM. The small increase in collective and 50 knots of airspeed have increased the damping of this mode as can be seen by comparing the load magnification curves. The modal damping indicated by Figures 4.1 and 4.2 is 5.6% and this is increased to 9.3% for Figures 4.3 and 4.4. At 100 knots the one per revolution crossing had decreased to about 215 RPM as shown in Figure 4.5.

The one per revolution, first mode bending frequency coincidence, has been plotted as a function of collective in Figures 4.6 and compared with the pretest prediction of Reference 13. The correlation indicates correct theoretical analysis.

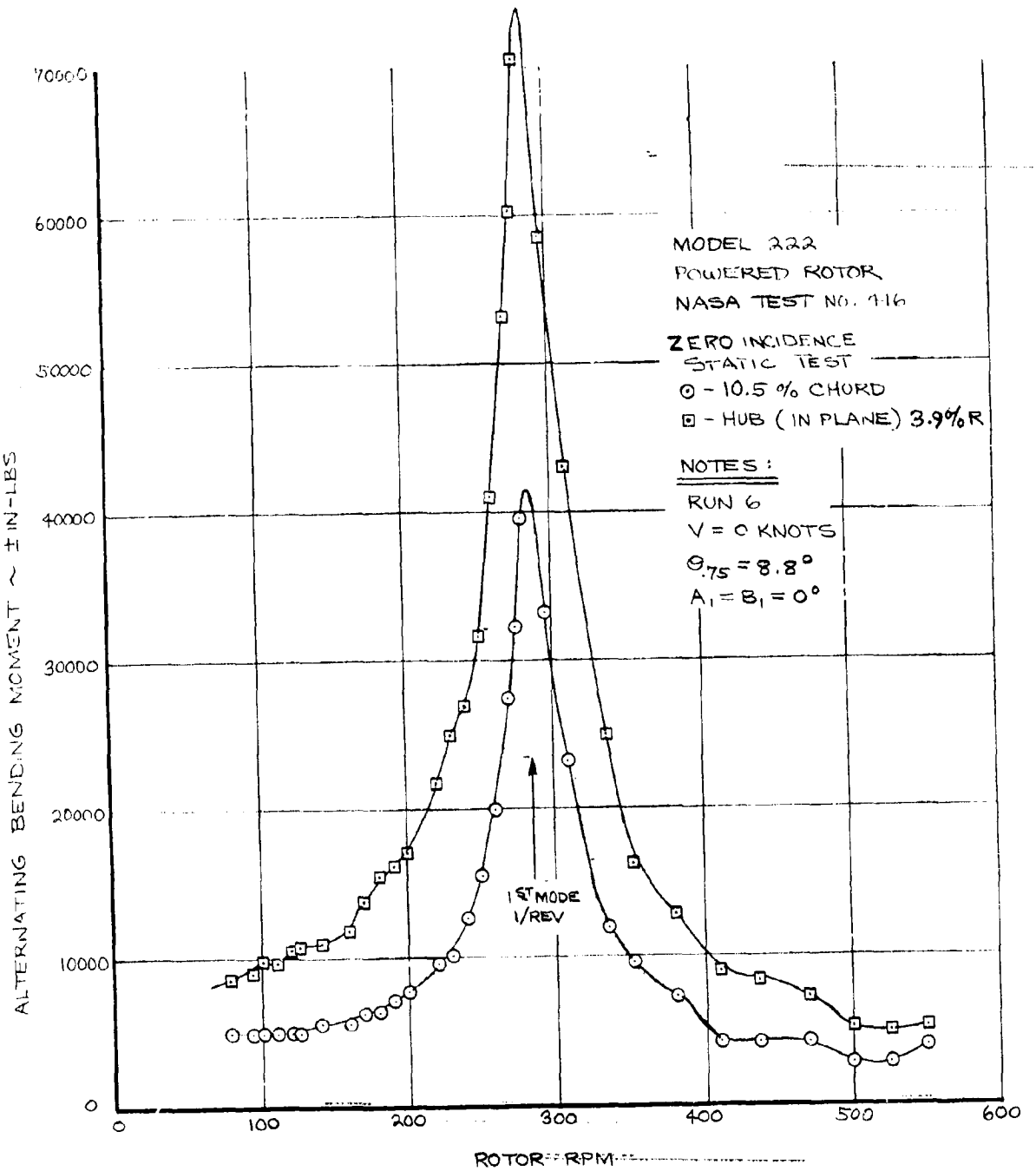

FIGURE 4.1 EFFECT OF ROTOR RPM ON ALTERNATING CHORD BENDING MOMENTS

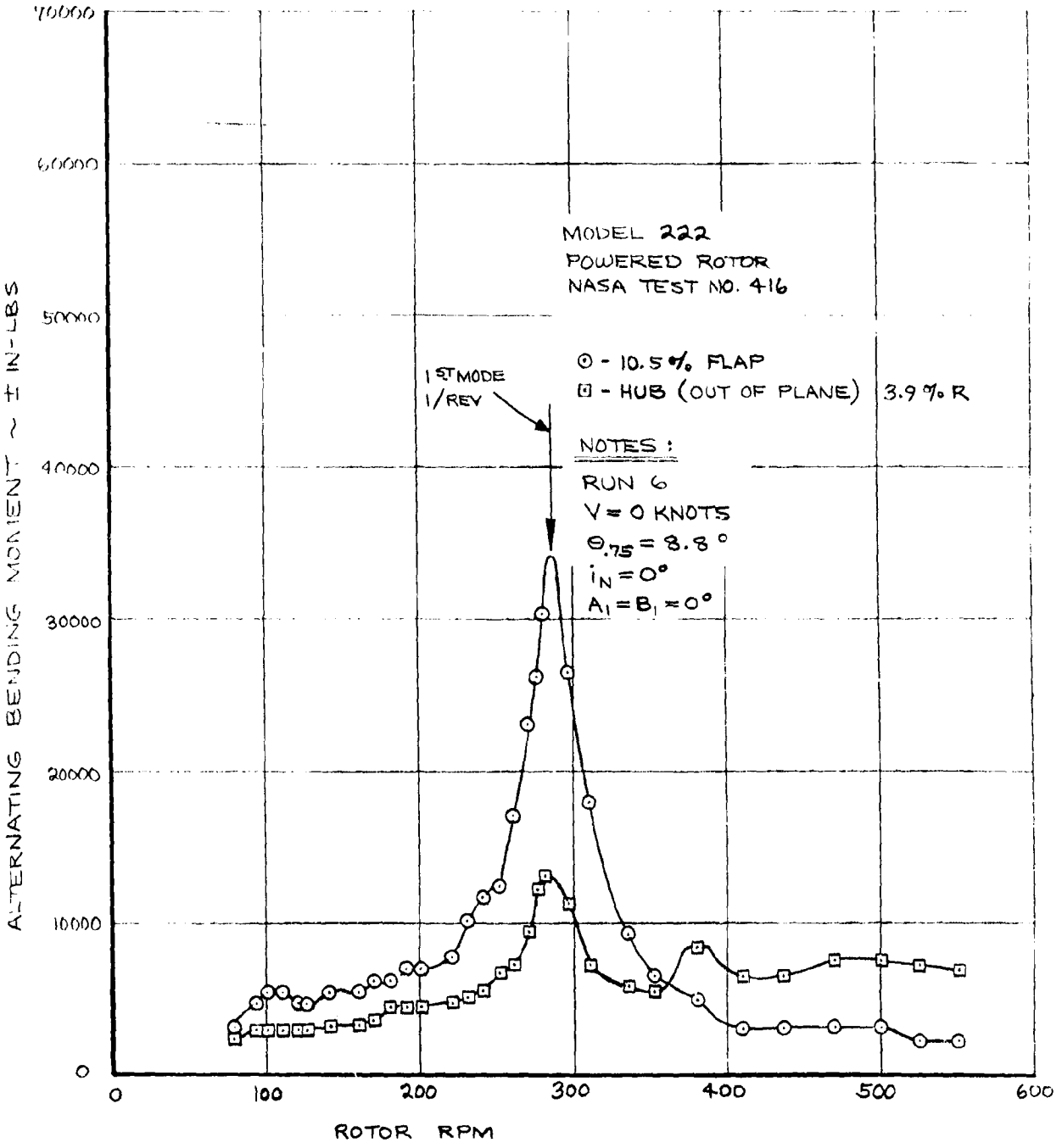

FIGURE 4.2 EFFECT OF ROTOR RPM ON ALTERNATING FLAP BENDING MOMENTS

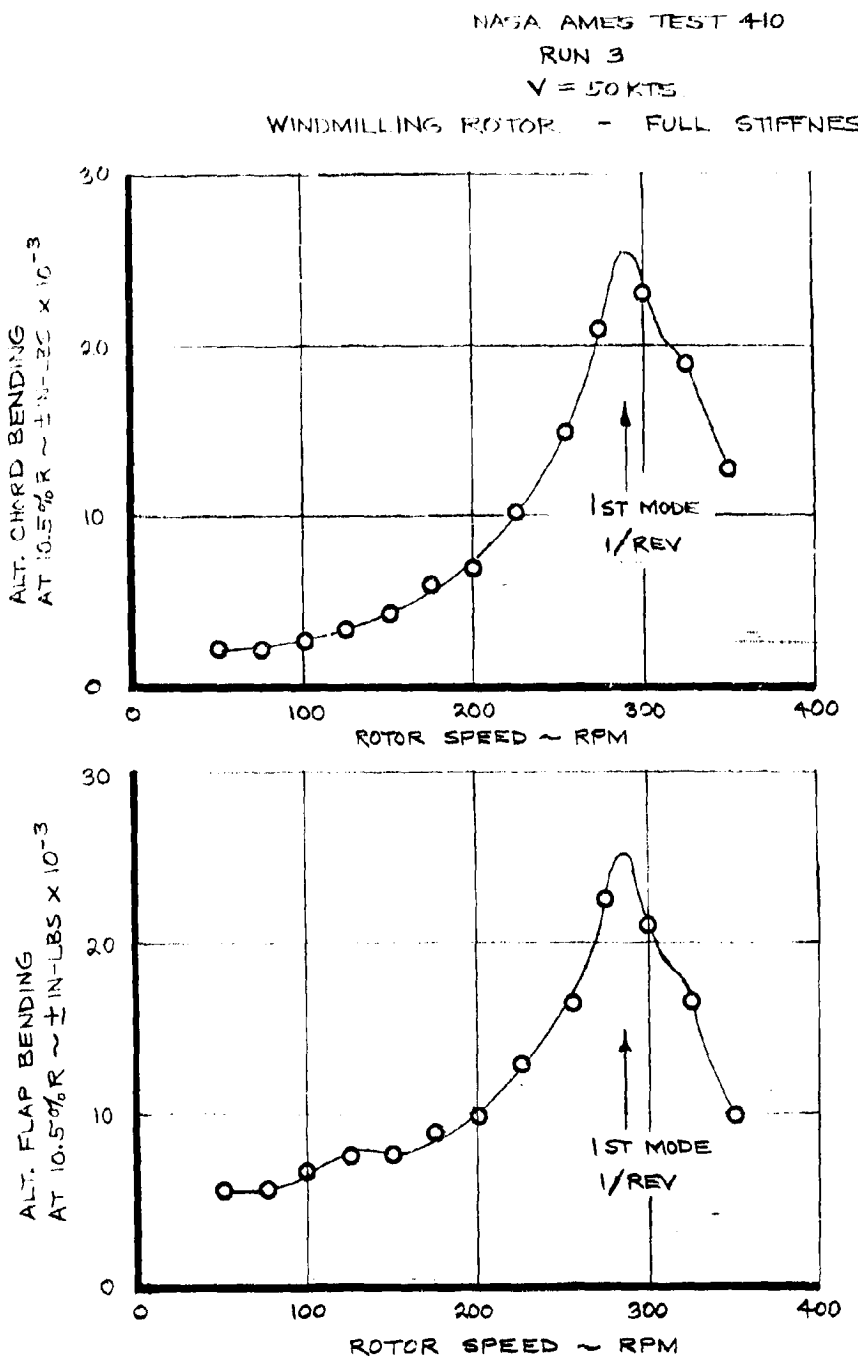

FIGURE 4.3 EFFECT OF ROTOR RPM ON ALTERNATING BLADE LOADS - WINDMILLING, V = 50 KTS.

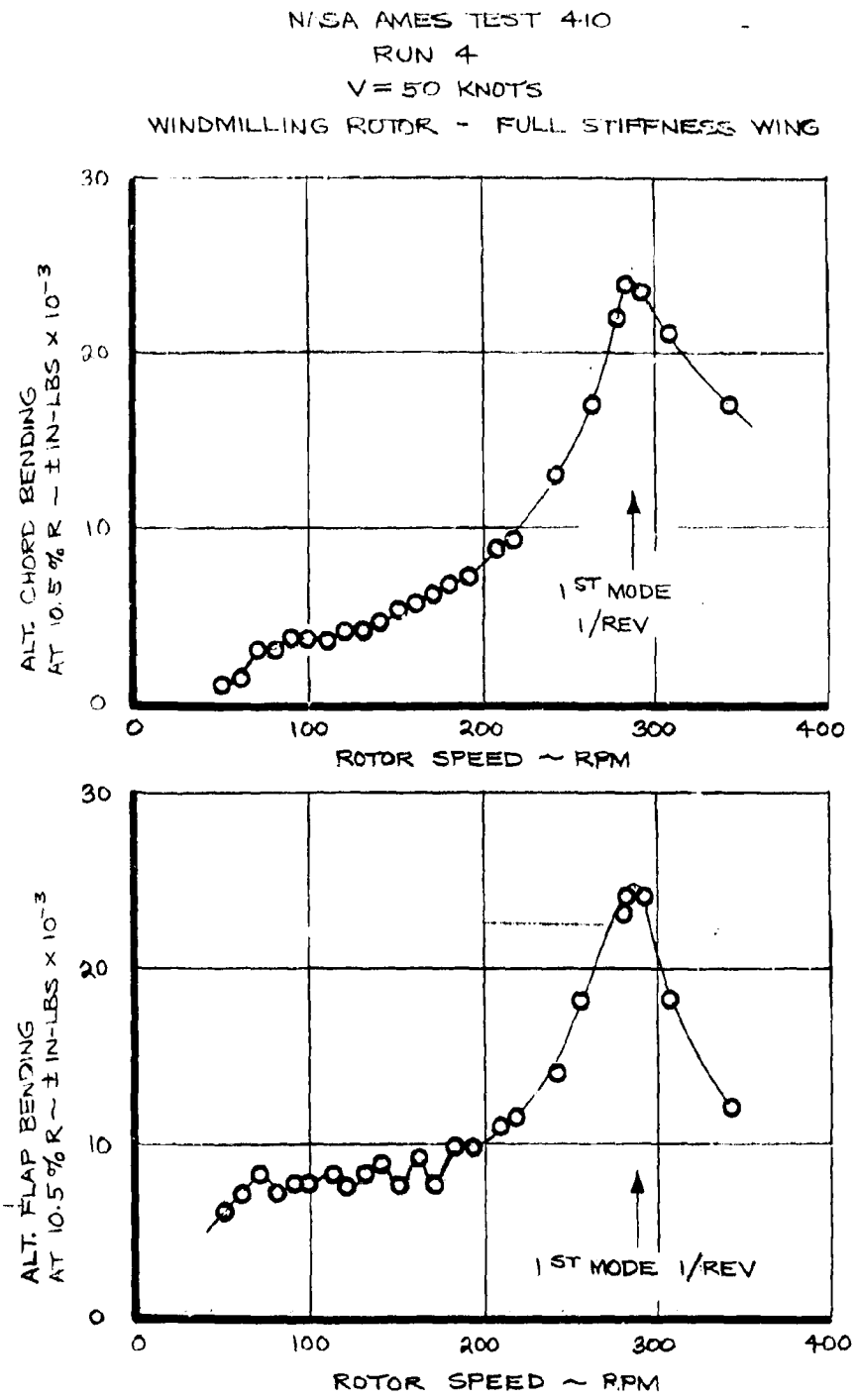

FIGURE 4.4 EFFECT OF ROTOR RPM ON ALTERNATING BLADE LOADS - WINDMILLING, V = 50 KTS.

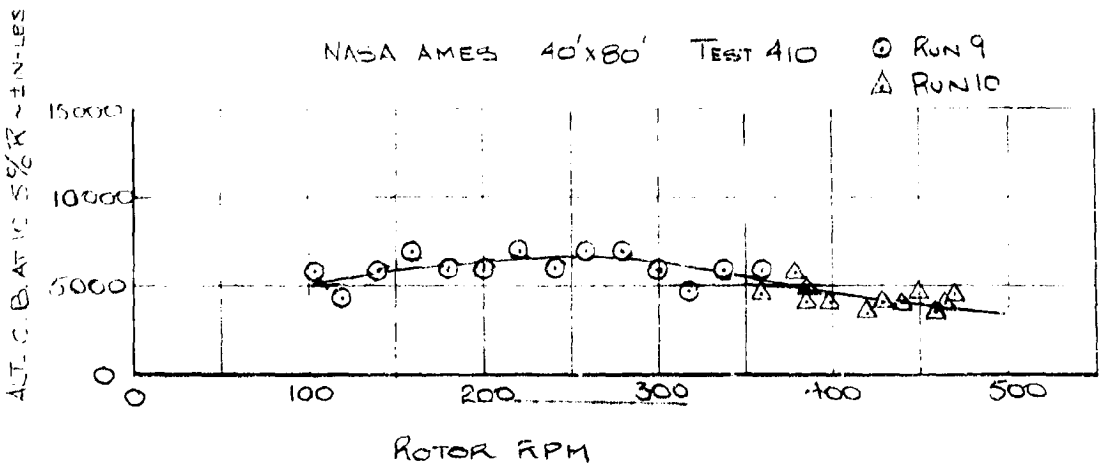

TUNNEL SPEED = 100KTS.
WINDMILLING ROTOR. - FULL STIFFNESS WING

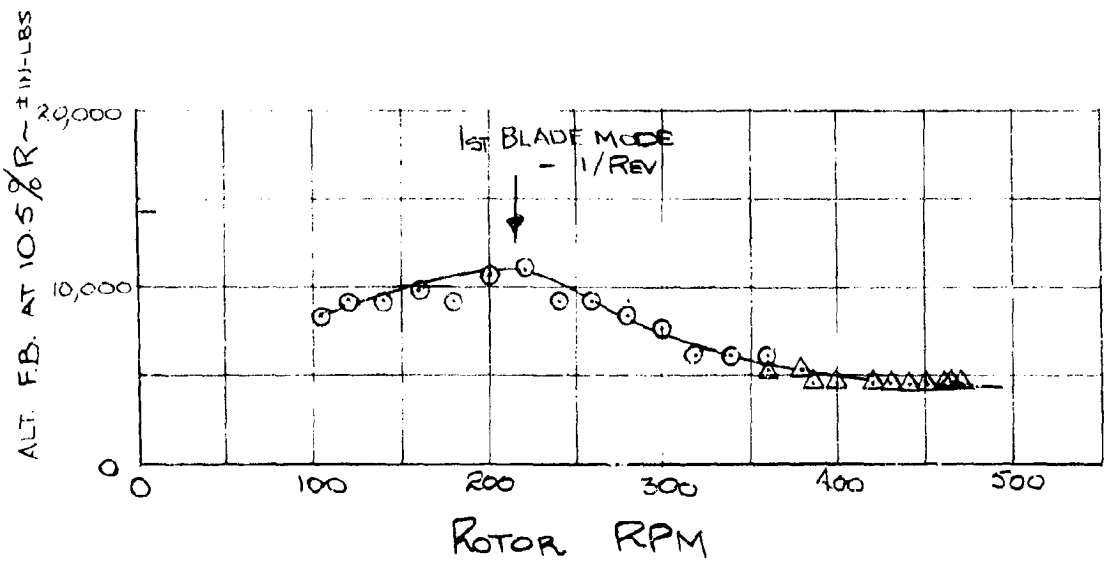

FIGURE 4.5 EFFECT OF ROTOR RPM ON ALTERNATING BLADE LOADS - WINDMILLING, 100 KTS.

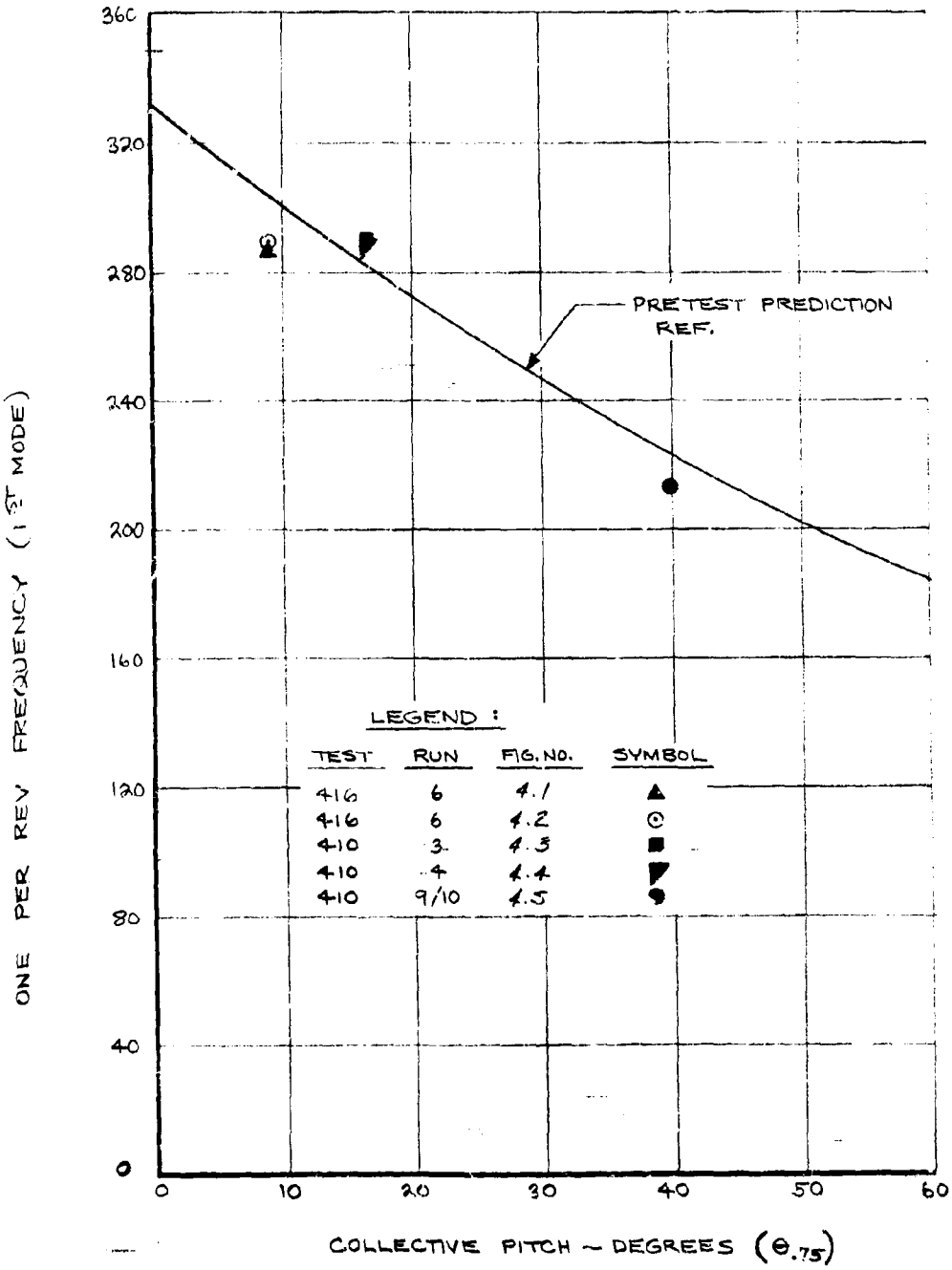

FIGURE 4.6 VARIATION OF FIRST BENDING MODE ONE PER REV FREQUENCY WITH COLLECTIVE PITCH

Cyclic Shake Tests

Oscillatory cyclic shaking was tried as a means of exciting the first two blade modes. The transformation of the fixed to the rotating system demodulates the command frequency by the rotational frequency such that a cyclic command of $(\Omega - \omega_L)$ frequency excites the blade at $(\Omega - (\Omega - \omega_L))$ or ω_L. A similar logic applies to the second mode where the command frequency was aimed at $(\Omega - \omega_B)$. These experiments were conducted at 100 knots, 386 and 420 RPM and also 190 knots, 386 RPM. The alternating blade loads due to oscillatory cyclic excitation are given in Figures 4-7 to 4-10. These tests were performed on the windmill test using the full stiffness wing.

The alternating flap bending data of Figure 4-7 shows two small amplifications at excitation frequencies of 1.55 Hz and 1.8 Hz and a further more pronounced "hump" at 2.2 Hz. This latter case is undoubtedly the wing vertical bending natural frequency and this data agrees with that given in Section 3. The $(\Omega - \omega_L)$ and $(\Omega - \omega_B)$ frequencies are well damped and not easily excited.

Similar data was taken at 420 RPM on Run 28. The objective of this run was to establish the wing vertical mode. As a result, no data points were taken in the frequency range 1.3 to 2 Hz. The data points do, however, indicate a load amplification peak

between 1.5 Hz and 1.75 Hz. These experiments were repeated at both 386 RPM and 420 RPM at 100 knots airspeed on Run 71 of test 410 and the data obtained is presented in Figure 4.9. On Run 71 the inboard blade gages were inoperative such that the gages available lack the sensitivity of those previously used at 10.5%R. At 386 RPM there is a significant load amplification at 1.5 Hz. At 420 RPM there is little or no evidence of frequency crossings. A small load amplification occurs in the flap bending; however, repeat points do not show this effect.

Cyclic shake data at 190 knots, 386 RPM, was obtained on Run 33 of the windmill test and is given in Figure 4.10.

The objective of the RPM sweeps and cyclic shake tests was to generate data points for correlation with the predicted blade frequencies. Figure 4.11 shows the predictions of the first two bending modes as a function of RPM. The solid lines correspond to a 100 knot windmilling cruise flight condition and the broken lines are the hover flight condition. Superimposed are lines of constant per revolution frequency (.75, 1, 2, 3) and also for the cruise predictions the demodulated fixed system frequencies ($\Omega - \omega_{\zeta_L}$) and ($\Omega - \omega_{\beta}$) are shown.

The solid triangle symbols are taken from the static frequency data of Table 4-1 and show that the first bending mode static frequency is on its design value. The second bending mode is about 9% lower than calculated. The solid square symbol is the 1/rev crossing of Figure 4-5 (100 knots windmilling) and the open ellipse symbol is the 1/rev crossing of Figures 4-1 and 4-2. These 1/rev data correlate closely with the predicted one per revolution frequencies. The frequencies implied by the cyclic shake data of Figure 4-7 are shown as open circle symbols. These data indicate that at 386 RPM the $(\Omega - \omega_\zeta)$ frequency is a little higher than predicted and the $(\Omega - \omega_\beta)$ is lower than predicted. The first and second mode bending frequencies deduced from the lower blade lag and flap frequencies show that the predicted values are a little higher than the experimental data. The peak drawn in Figure 4-8 (solid diamond symbol) would give an $(\Omega - \omega_\zeta)$ frequency of 107 cpm and correlates with the 386 RPM data and also with the data deduced from the onset of air resonance discussed in Section 3. At 100 knots the air resonance root for the full stiffness wing reached zero damping at approximately 475 RPM. This condition requires that the lower blade lag mode frequency be almost coincident with the wing vertical bending frequency and allows a further blade first mode frequency

point to be deduced. These data taken from several different test runs seem to agree and indicate that the rotating blade first mode bending frequency is about 5% lower than predicted in the cruise mode at 386 RPM. The second mode bending rotating frequency is also about 5% low. The one per revolution frequency data indicate that the trend of frequency with collective predicted is correct.

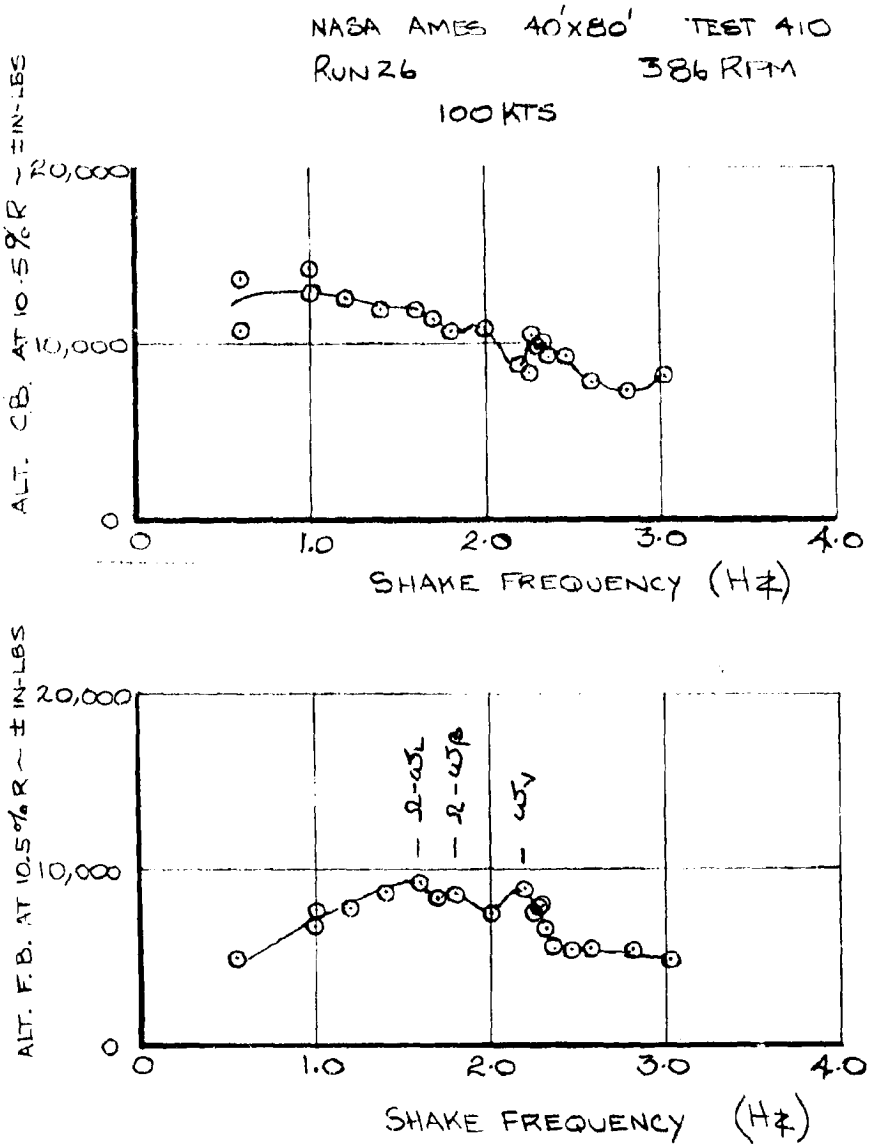

WINDMILLING ROTOR - FULL STIFFNESS WING
OSCILLATORY CYCLIC EXCITATION

FIGURE 4.7 ALTERNATING BLADE LOADS DUE TO CYCLIC SHAKING - 386 RPM, 100 KTS.

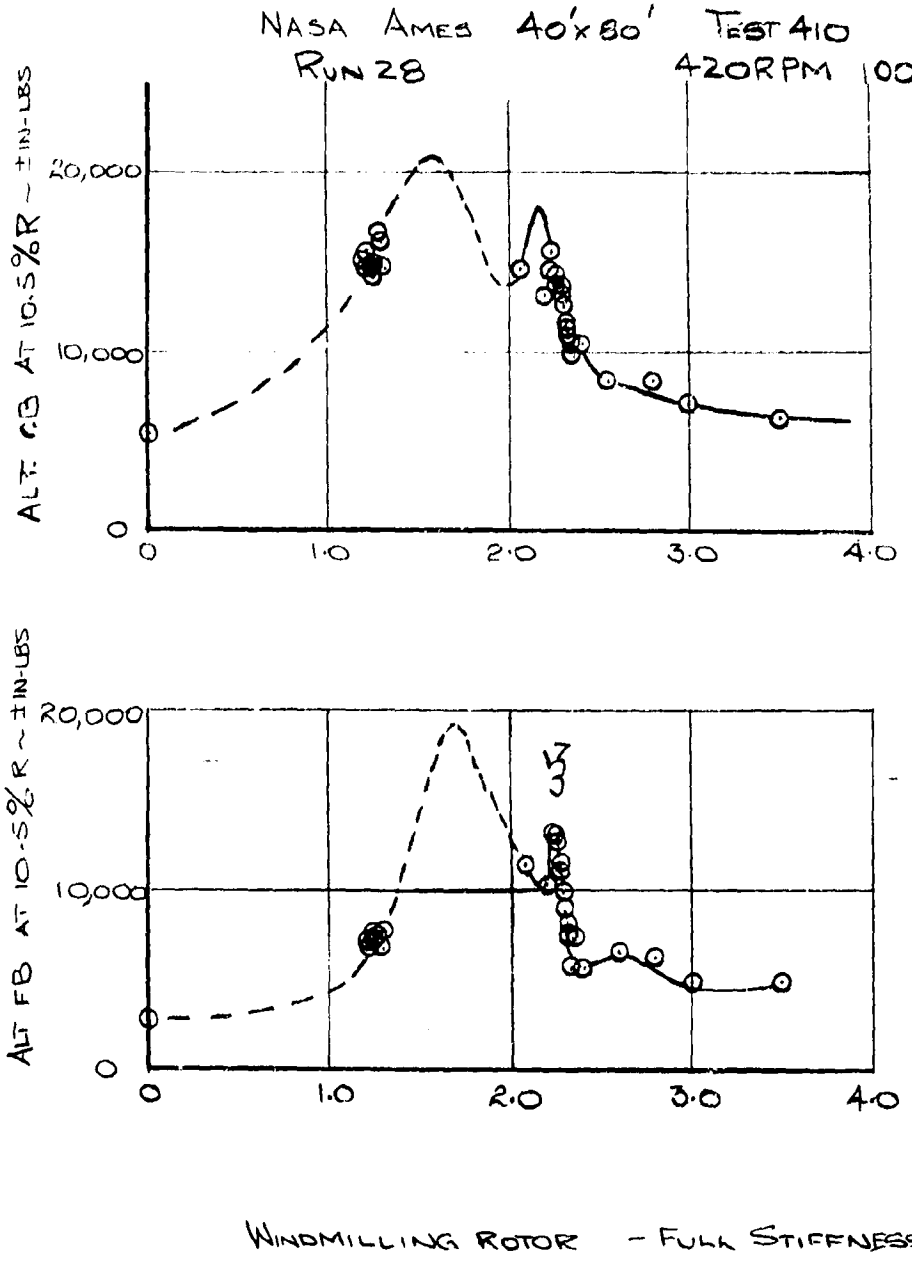

WINDMILLING ROTOR - FULL STIFFNESS WING

FIGURE 4.8 ALTERNATING BLADE LOADS DUE TO CYCLIC SHAKING - 420 RPM, 100 KTS.

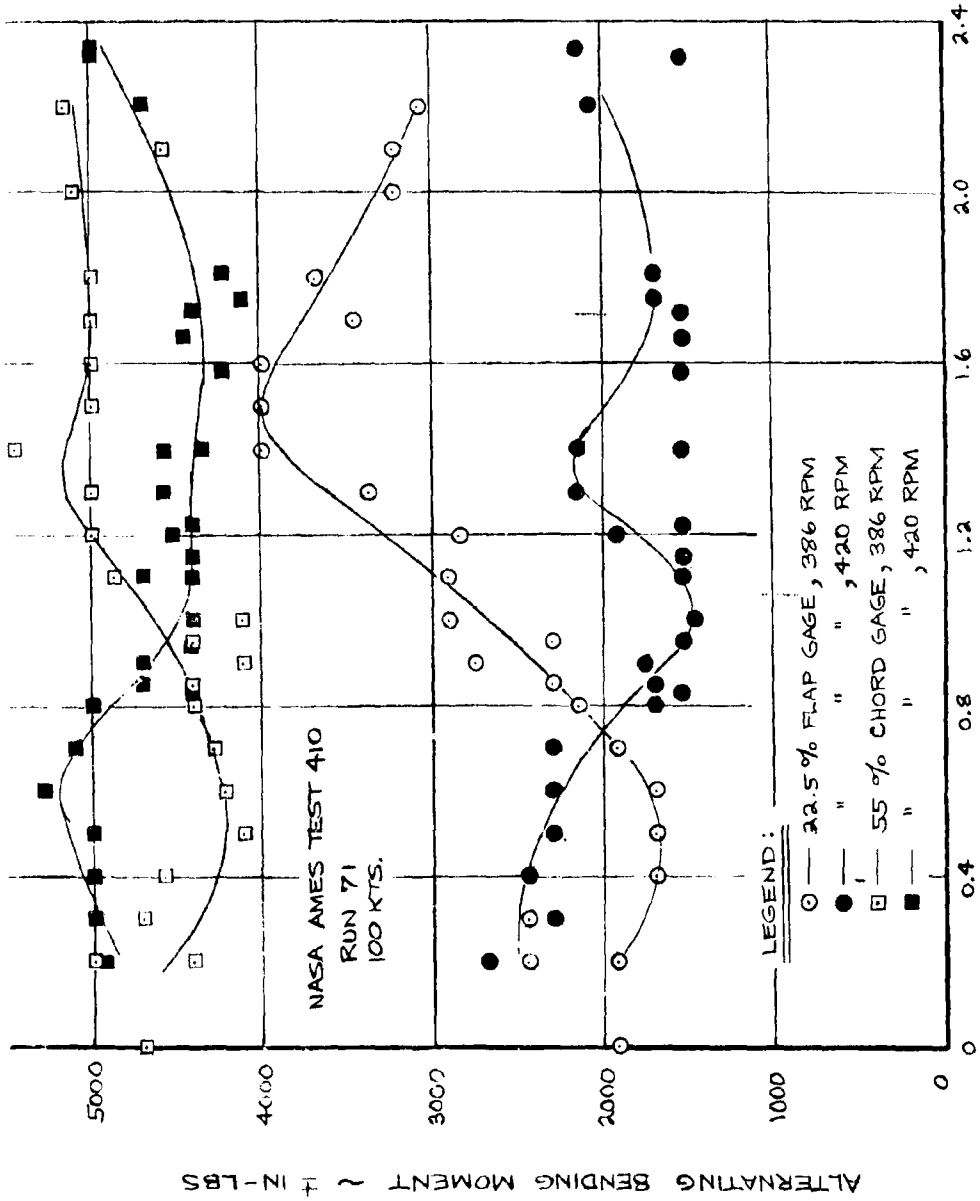

FIGURE 4.9 ALTERNATING BLADE LOADS DUE TO CYCLIC SHAKING - 100 KTS.

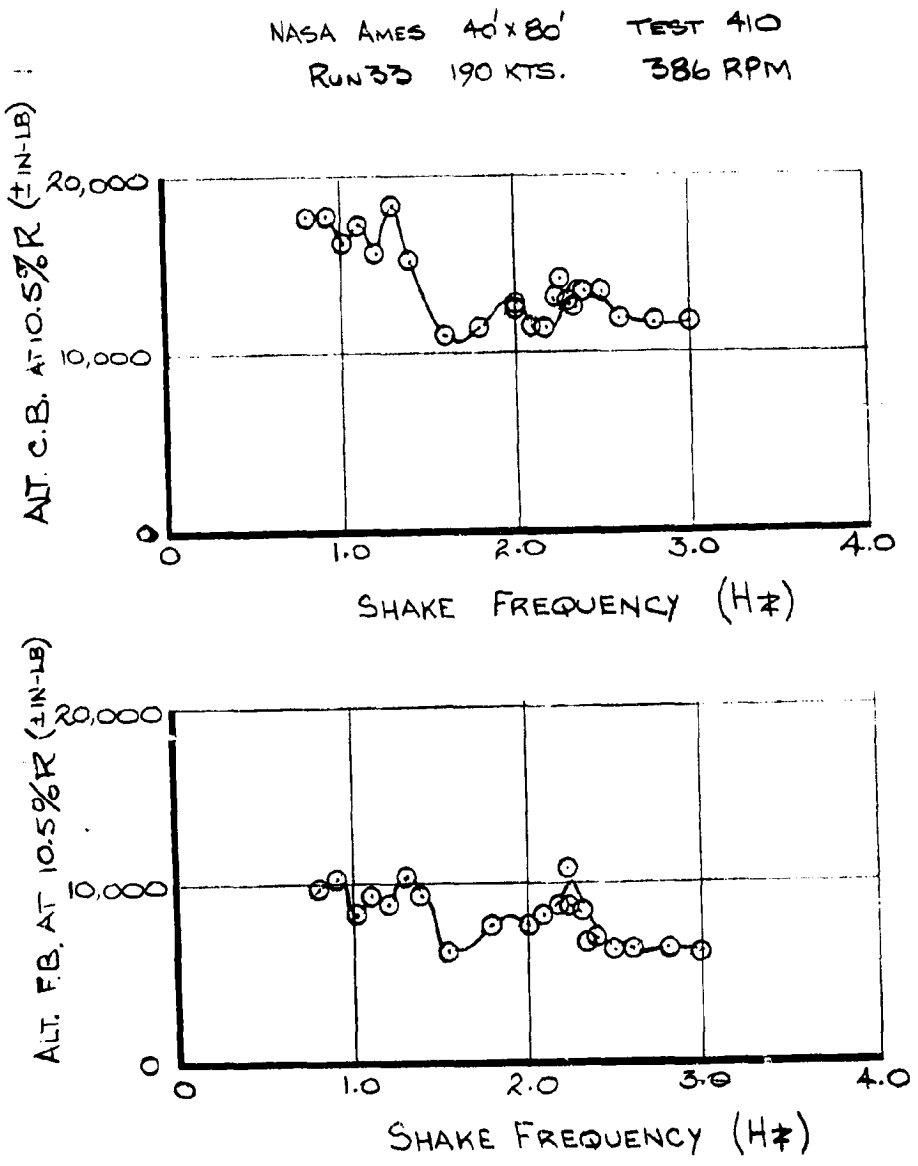

FIGURE 4.1b ALTERNATING BLADE LOADS DUE TO CYCLIC SHAKING - 386 RPM, 190 KNOTS

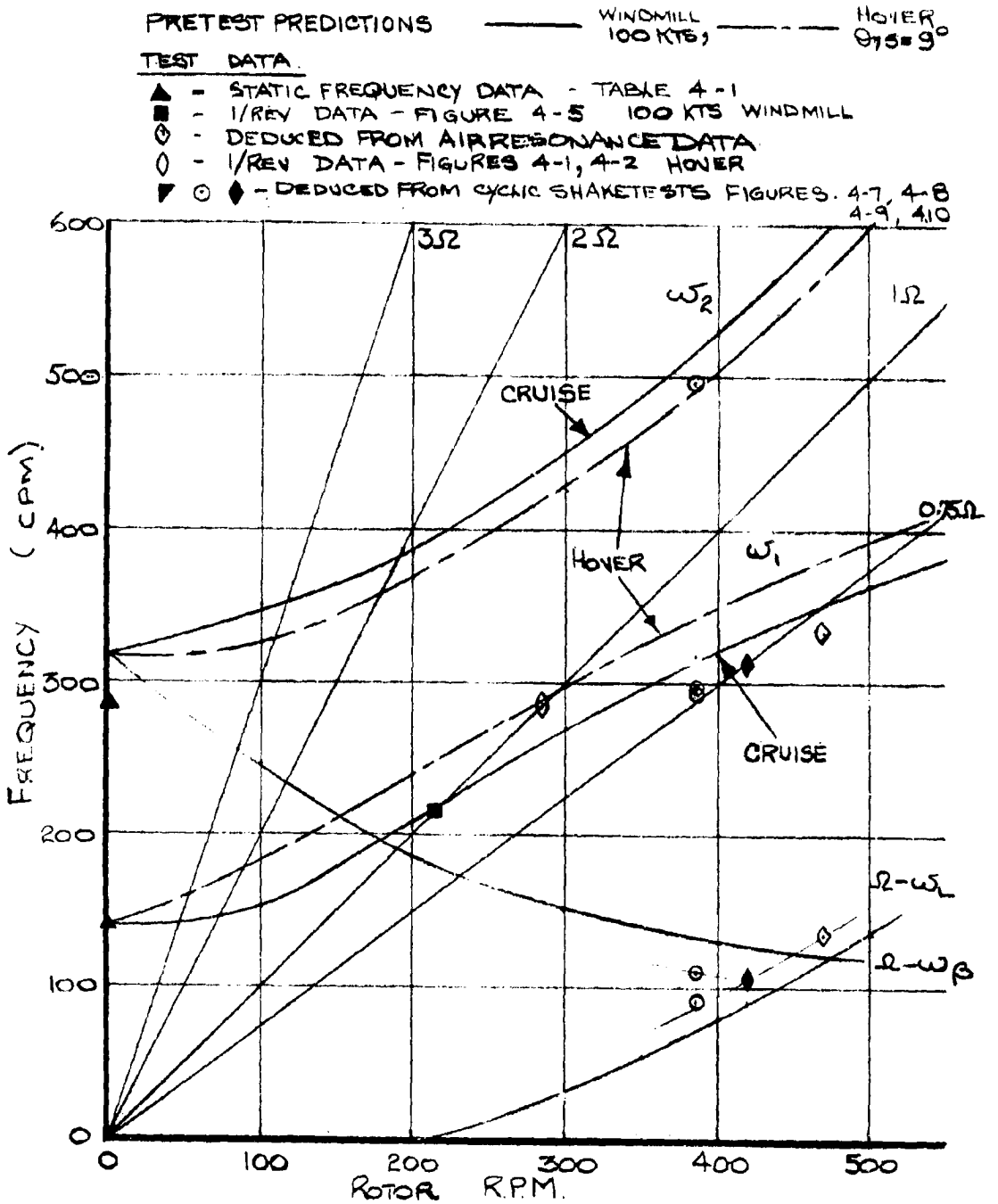

FIGURE 4.11 BLADE FREQUENCY CORRELATION SUMMARY. - M222 26 FT. DIA.

4.2 HOVER ROTOR BLADE LOADS

In hover alternating blade loads are caused by cyclic pitch used for trim or control and also by sidewinds. The rotor design incorporates a precone of 2½° and also a torque offset (lead) of 0.65". These features are included to reduce the steady bending loads at the blade root by balancing the centrifugal force, thrust and airloads at a nominal condition. The most difficult axis of control to achieve good handling qualities in hover is aircraft yaw which is in part achieved by the application of cyclic pitch to generate inplane forces fore and aft. This cyclic pitch is limited by the alternating loads produced.

Effect of Cyclic Pitch

The alternating blade bending loads due to cyclic pitch in near hover conditions (vertical climb, Run 7, Test 416) are given in Figures 4.12 to 4.15. Data are given for various radial positions on the blade and the predicted loads at 10.5%R are superimposed for correlation. The alternating chord bending loads due to cyclic, Figures 4.12 and 4.13, are less than predicted at 10.5% radius. A residual load of ±4500 in.-lbs. exists at zero cyclic and the growth of alternating chord bending with cyclic pitch is lower than the theoretical slope.

The correlation of alternating flap bending at 10.5% radius given in Figures 4.14 and 4.15 shows theory and test results to be in close agreement.

The alternating flap bending and alternating chord bending loads have been expressed in terms of resultant alternating strain at 10.5% radius and these data are shown in Figure 4.16. The alternating loads due to longitudinal cyclic agree very closely with prediction. The growth of alternating strain with lateral cyclic is also in good agreement with the theoretical data; however, there appears to be a lateral cyclic offset of the order of four tenths of a degree. The cycles to failure from the (mean -3σ) line are given for various load levels in Figure 4.16.

The data shown in Figures 4.12 to 4.15 have been plotted against radial distance in Figure 4.17 for 3.0° cyclic and compared with predicted load distributions.

The data shown at 3.9%R is deduced from the hub barrel gages. The data taken from the blade gages is referred to the blade axis system (i.e., normal and parallel to the blade chord). The hub gages record in and out of plane bending and require resolution to compare with other blade data. This explains why the hub (in plane) data of Figures 4.12 and 4.13 is lower than the 10.5% data.

The alternating blade loads obtained during collective sweeps are given in Figures 4.18, 4.19 and show low load levels unaffected by collective pitch. Figure 4.20 shows a time history of RPM and blade loads during a shut down. The power was chopped at 551 RPM and the recorders left running. The polar inertia of the motors and drive system is estimated at 100 slug ft^2, with a gearing ratio of 0.45:1.

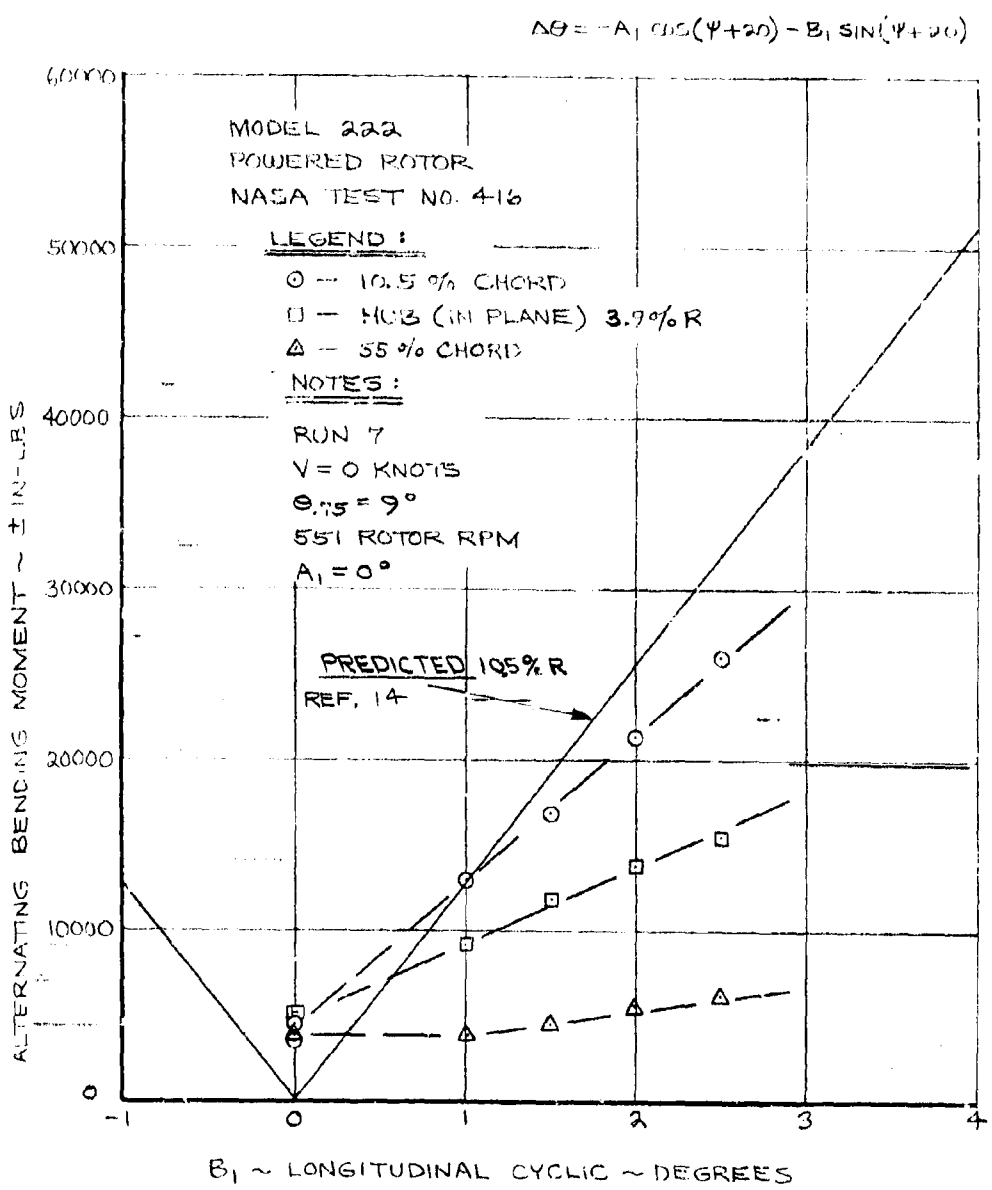

FIGURE 4.12. EFFECT OF B_1 CYCLIC ON CHORD BENDING MOMENTS

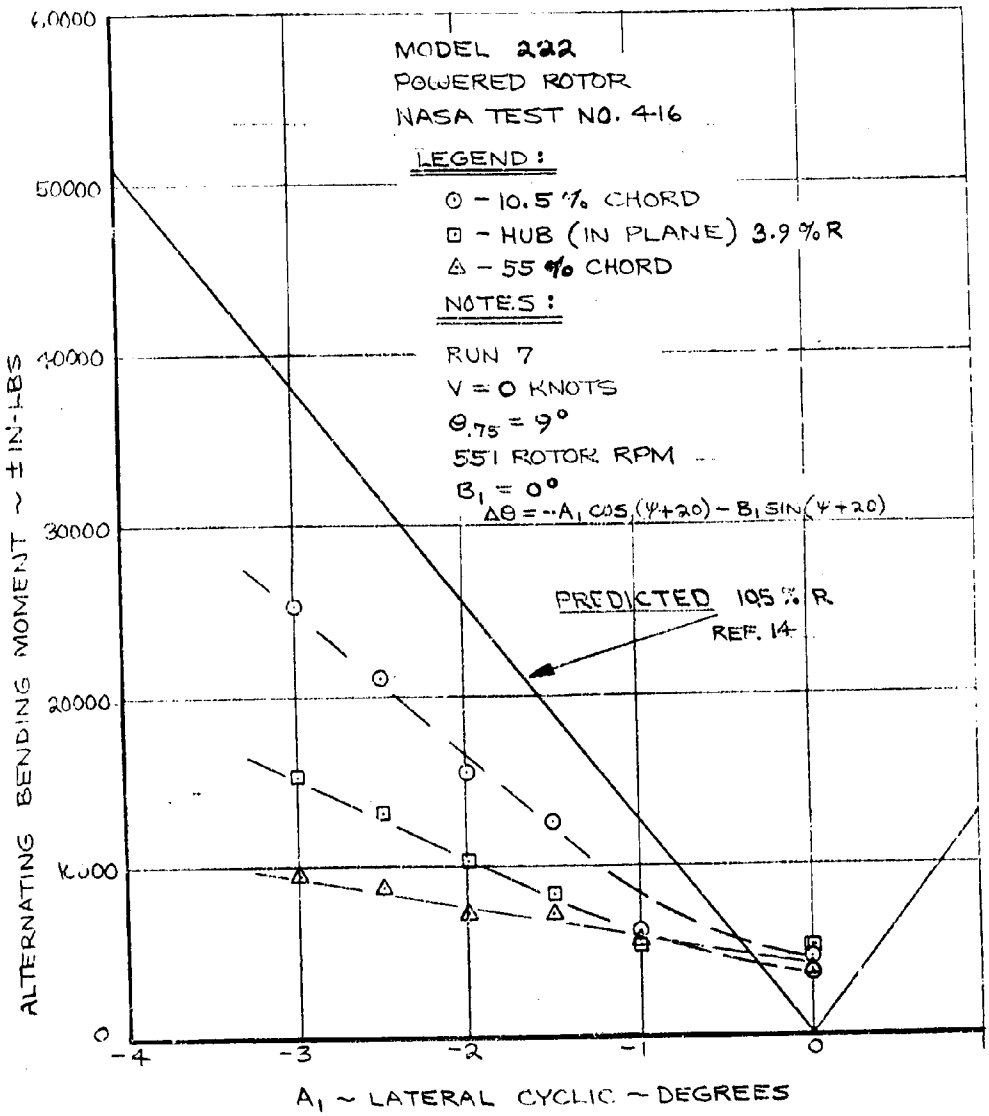

FIGURE 4.13. EFFECT OF A_1 CYCLIC ON CHORD BENDING MOMENTS

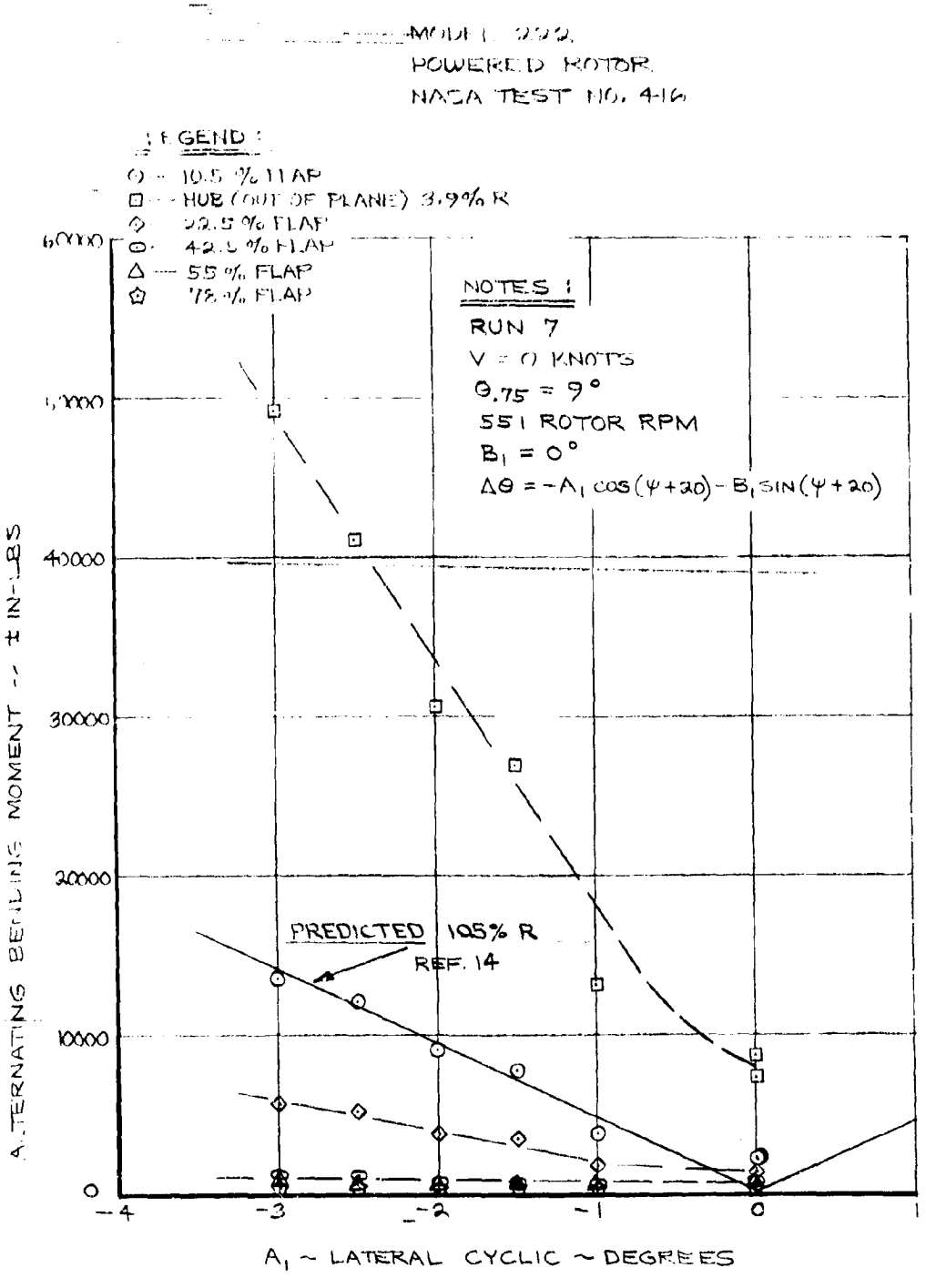

FIGURE 4.14. EFFECT OF A_1 CYCLIC ON FLAP BENDING MOMENTS

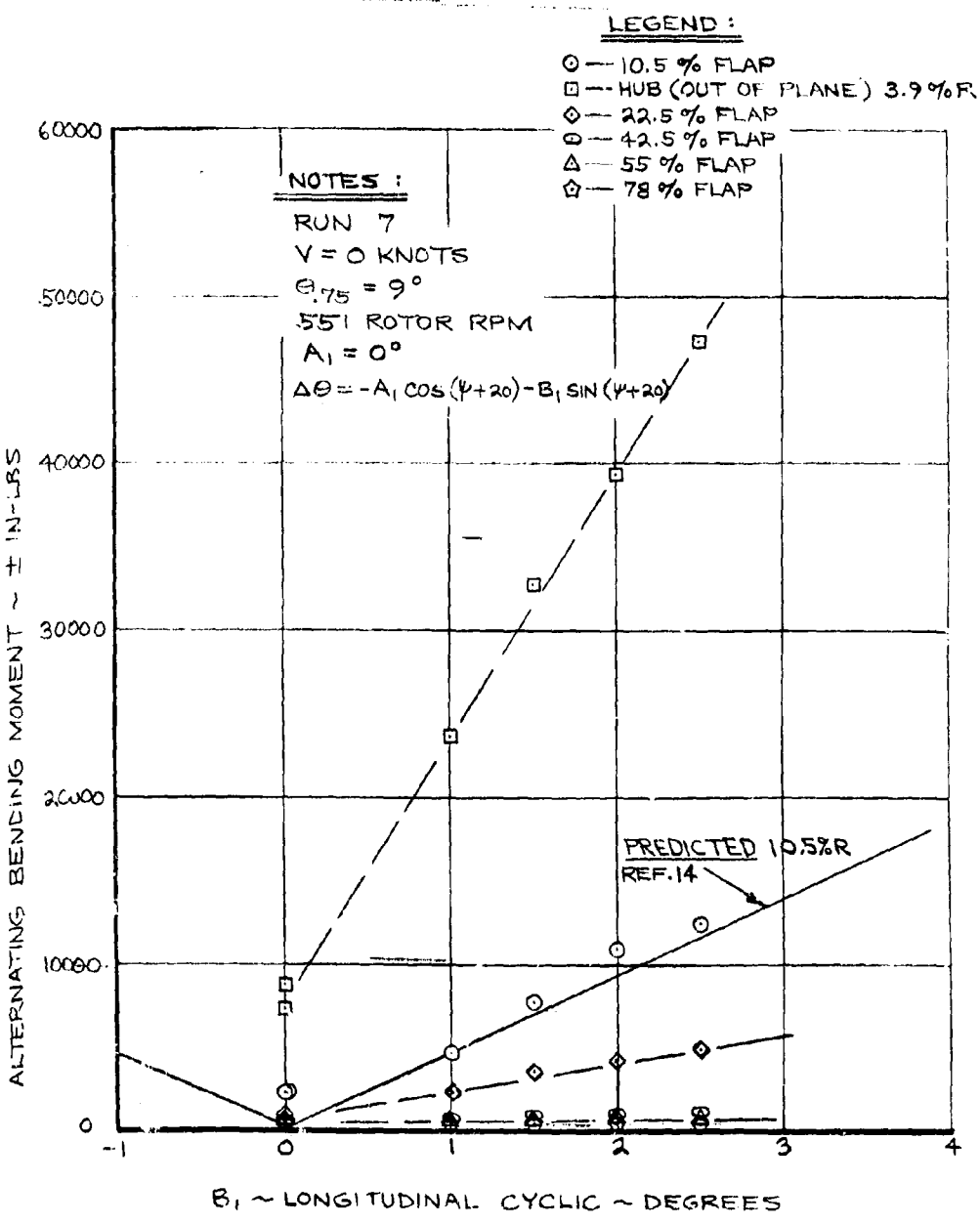

FIGURE 4.15. EFFECT OF B_1 CYCLIC ON FLAP BENDING MOMENTS

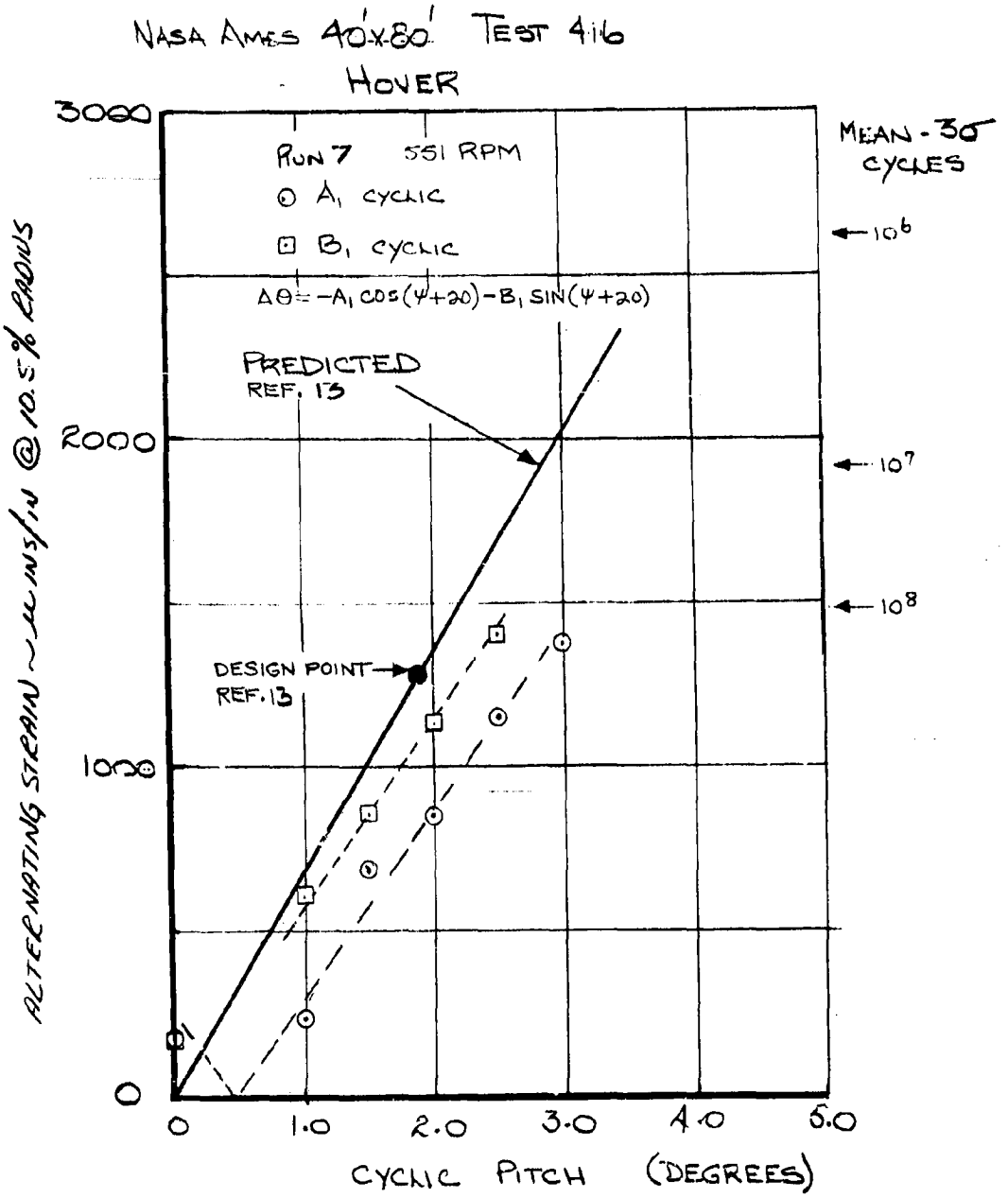

FIGURE 4.16 ALTERNATING BLADE ROOT STRAIN DUE TO CYCLIC — HOVER 551 RPM

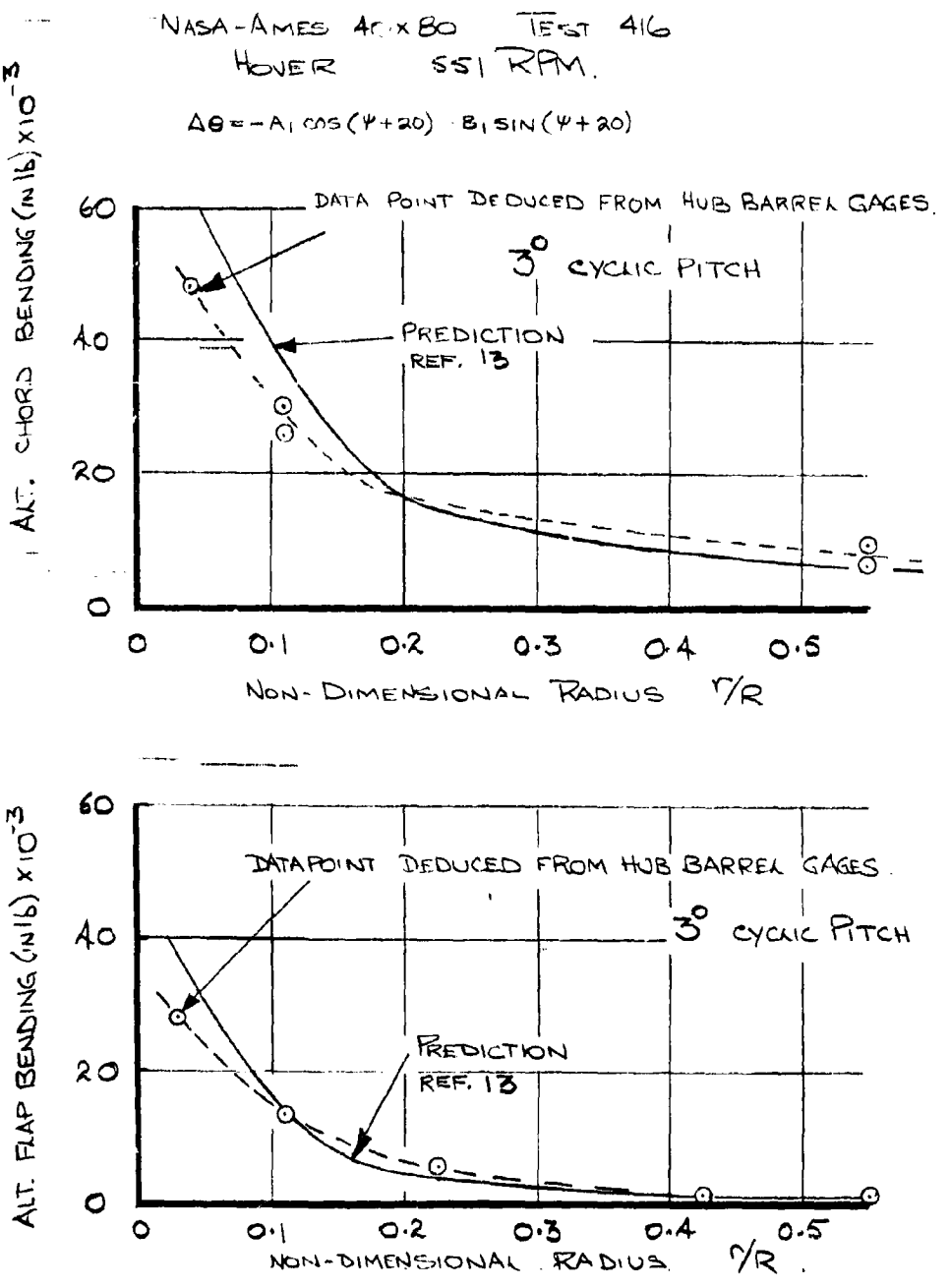

FIGURE 4.17 RADIAL DISTRIBUTION OF ALTERNATING BENDING MOMENTS DUE TO HOVER CYCLIC

NASA AMES TEST 416
RUN 7
551 RPM
$i_N = 0°$
V = 0 KNOTS
$A_1 = 0°$
$B_1 = 0°$

⊙ — 10.5% CHORD
⊡ — HUB (IN PLANE) 3.9%R
△ — 55% CHORD

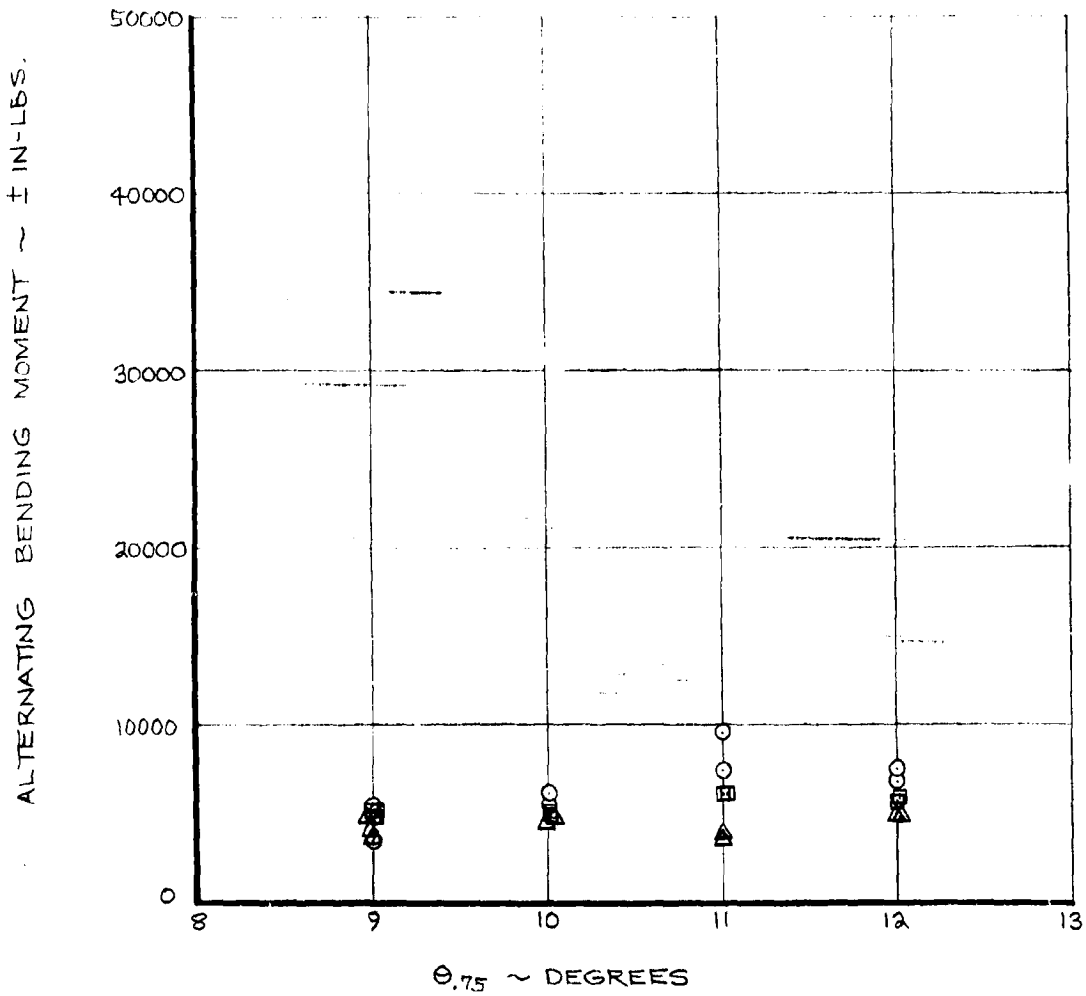

FIGURE 4.18 EFFECT OF COLLECTIVE PITCH ON ALTERNATING CHORD BENDING MOMENT

NASA AMES TEST 416
RUN 7
551 RPM
$i_N = 0°$
V = 0 KNOTS
$A_1 = 0°$
$B_1 = 0°$

⊙ — 10.5 % FLAP
⊡ — HUB (OUT OF PLANE) 3.9%R
◈ — 22.5 % FLAP
⊕ — 42.5 % FLAP
△ — 55 % FLAP

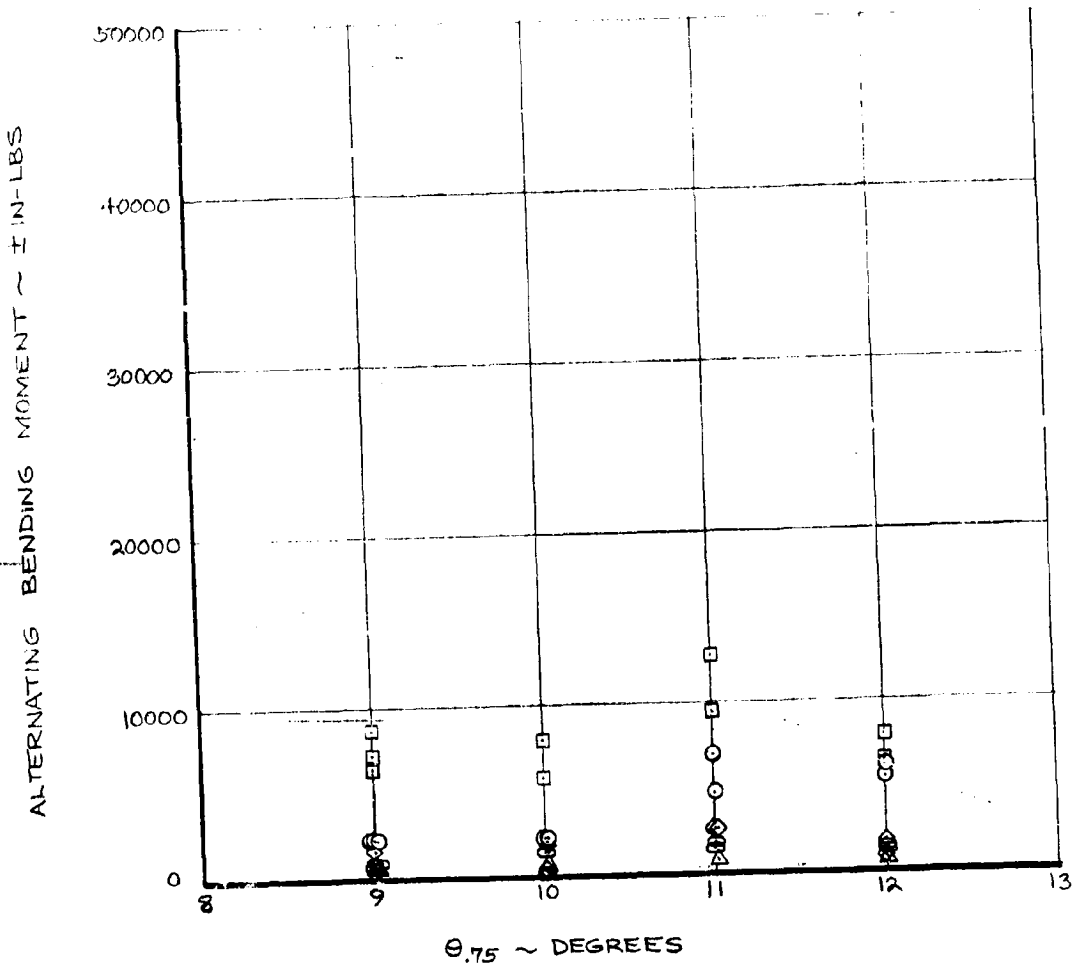

FIGURE 4.19 EFFECT OF COLLECTIVE PITCH ON ALTERNATING FLAP BENDING MOMENT

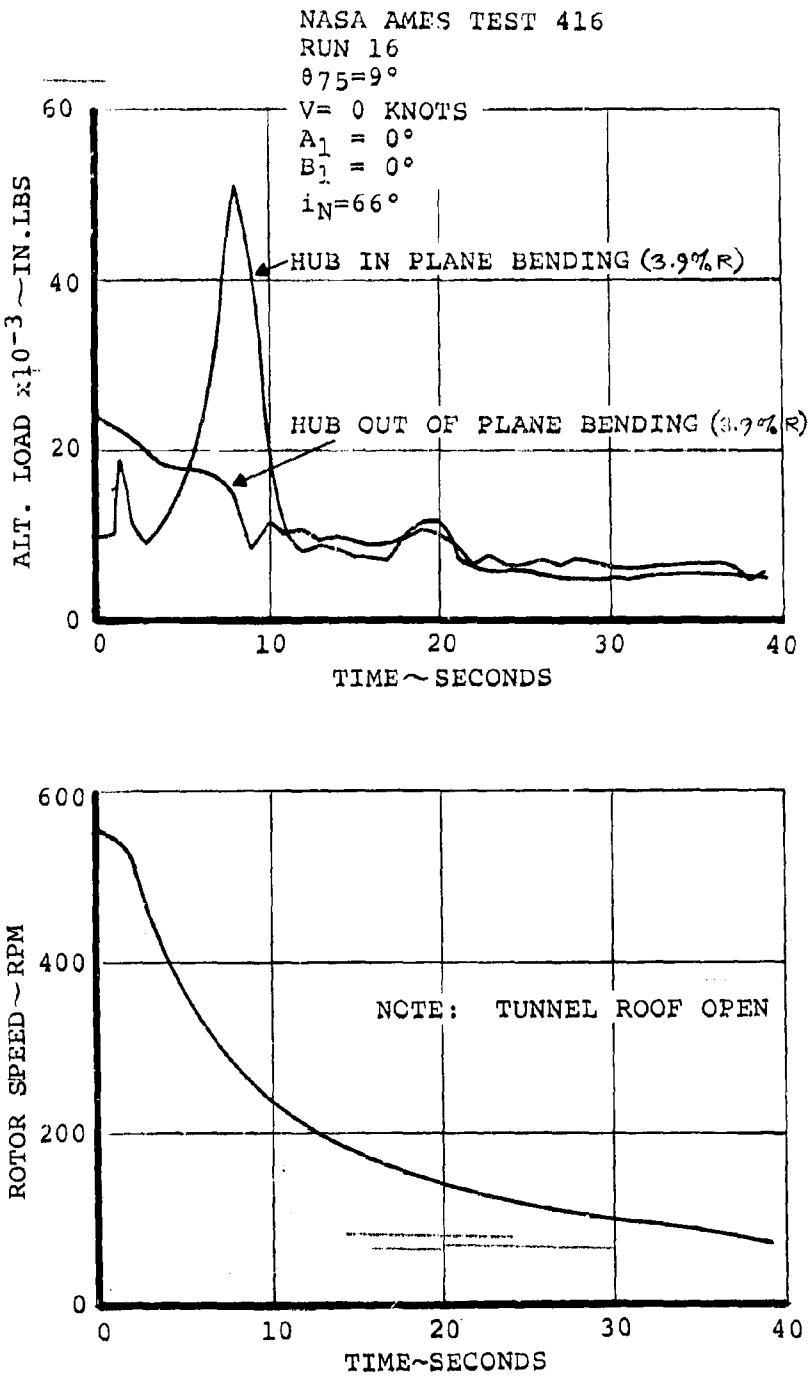

FIGURE 4.20 TIME HISTORY OF SHUTDOWN IN HOVER.

4 3 Transition Rotor Loads

The blade bending loads in transition are made up of components at various frequencies, each frequency in general being an integer times RPM. The largest component is due to the one per rev terms. These terms result from the one per rev excitation provided primarily by shaft angle and airspeed and by blade coning and airspeed. Higher harmonic terms result from the reverse flow region on the retreating side of the disc, the effects of blade motion due to first harmonic forcing and hub motions.

On the test rig the first harmonic of the rotor loads can be trimmed out with cyclic pitch.

For the Model 222 design the alternating blade loads are a function of the cyclic required to trim the aircraft. In the early part of transition the rotors provide the primary control since the aircraft control surfaces are ineffective at low speed and the required cyclic differs from that required for minimum loads giving an increment in one per rev loads. As airspeed increases it is possible to use cyclics closer to minimum loads cyclic by providing trim moments from the airplane control surfaces. The aircraft transition loads are thus a function of the control configuration and would be lower with the load alleviation system on than with the system inoperative for the M-222 control configuration. All of the data in this section is taken

from NASA 40' x 80' wind tunnel test 416. The data shown in Figures 4-21 to 4-23 were taken on Run 19 at a shaft incidence of 85° and a flight speed of 45 kts. These data were run at an RPM of 500 to avoid a ground resonance (rotor-test stand) observed at high incidence. The subject is discussed in Section 3.

The flap and chord bending loads at 55% radius are low, Figure 4-21, and relatively insensitive to collective pitch. The alternating loads measured on the hub barrel at 3.9% radius show low in-plane loads at all collectives. The out-of-plane bending loads increase as collective is either increased or decreased about the minimum load point set up. (As the blade increases collective, coning is increased providing additional one per rev loads and as thrust is decreased the cyclic pitch previously required is excessive and results in an increase in load due to cyclic pitch.) At a collective of 8.9° the cyclics required to minimize the blade root alternating loads were -5.03° A_1 and 1.41° B_1. The cyclics quoted are in the test axes such that the first harmonic increment of blade angle is given by:

$$\Delta\Theta = -A_{1}\cos(\psi + 20) - B_{1}\sin(\psi + 20)$$

where azimuth and direction of rotation are defined in Figure 4-24 and $\Delta\Theta$ is positive nose up.

A summary of all minimum loads cyclics required in transition is given in Table 4.3.

Figures 4-22 and 4-23 show the alternating blade loads due to cyclic excursions about the minimum load point. As A_1 is reduced from -5° to -3.4° the alternating blade root out-of-plane loads increase at about 13,000 in-lbs/° at r/R = 3.9%. The in-plane loads remain low but exhibit a minimum at -4.4° A_1 or 0.6° less than minimum out-of-plane loads.

As longitudinal cyclic B_1 is increased from the minimum loads value of 1.41° both out-of-plane and in-plane loads increase though the out-of-plane loads show the more pronounced rate of increase (11,500 in-lbs/°). The bending loads at 55% radius are insensitive to either axes of cyclic.

Figures 4-25 through 4-27 show similar data taken from Run 22 at 83° incidence, 76 kts and 500 RPM.

The alternating bending load out-of-plane at 3.9%R increased to 30,000 in-lbs compared with 17,000 in-lbs at 45 kts. A large proportion of this increased load appears to be 2/rev and 3/rev. The load level observed on test was not limiting from a fatigue stand point and testing was limited by alternating pitch link loads for the pitch links as shown

in Section 5. The in-plane bending loads increased to 15,000 in-lbs compared with 11,000 in-lbs at 45 kts. The blade root loads again increase as collective is increased or decreased away from the trimmed case due to changes in blade coning. The effects of A_1 and B_1 cyclic pitch are shown in Figures 4-26 and 4-27. The minimum loads cyclic settings at this condition were -4.8° A_1 and 2.79° B_1.

As A_1 was reduced to -4.1° the alternating out-of-plane loads increase at a rate of 10,000 in-lbs/°. The in-plane loads which are low at 14,500 in-lbs reduce to 11,000 in-lbs at -4.1° A_1. The blade root bending loads increase as B_1 is increased or decreased away from the trim point. The in-plane loads have a minimum at about 0.4° cyclic higher than the minimum out-of-plane loads. Out-of-plane bending loads at 3.9%R increase at 9000 in-lbs/° B_1 and in-plane loads (3.9%R) at 4800 in-lbs/° B_1. The blade loads at 55%R are insensitive to cyclic pitch changes.

Run 21 was at 66° incidence and 80 kts and 550 RPM. It was possible at this angle to operate at full RPM. The alternating blade loads obtained at this condition are shown in Figures 4-28 to 4-30.

The out-of-plane bending loads increase as collective increases or decreases away from the minimum loads condition as previously

observed at 83° incidence. The increase in alternating load per degree of collective is increased to 8500 in-lbs/° θ_{75} at 3.9%R. This effect results from increased velocity ratio and the increase in thrust per degree of collective (and hence coning angle). The in-plane root (3.9%R) bending moments and the blade flap and chord bending at 55%R are low and insensitive to collective pitch.

The cyclic pitch settings to obtain minimum loads at this condition were -2.78° A_1 and 2.16° B_1. The alternating blade root loads due to excursions in cyclic away from these values are seen to increase in Figures 4-29 and 4-30. At 3.9%R the out-of-plane load increases at 17,600 in-lbs/° A_1 and in-plane load at 4500 in-lbs/° A_1. The corresponding rates with B_1 are 19,500 and 4000 in-lbs/° B_1 respectively. The blade loads at 55% again show little dependence on cyclic pitch.

The data presented in Figures 4-31 to 4-33 are at the same conditions as Figures 4-28 to 4-30 but at 500 RPM. The effect of reducing RPM reduced the rate of growth of the blade root out-of-plane load and made little difference to the in-plane loads.

Run 9 was performed at 105 kts 27° i_N and 550 RPM. The alternating blade loads measured at this condition due to collective and cyclic pitch are given in Figures 4-34 to 4-39. Figures 4-40 and 4-41 show loads due to an incidence excursion away from the minimum load point. At higher incidences this was not performed since in changing incidence the test rig inertia was increased by the fairing inertia (jacks pick up the fairing while changing i_N). This inertia change was considered to be enough to aggravate the ground resonance instability and was hence avoided at high incidence.

Figures 4-34 and 4-35 show the alternating blade loads due to collective pitch. The loads are lower at this condition than previously observed. As zero incidence is approached the effect of coning on alternating blade loads tends to zero. The effects of cyclic pitch are shown in Figures 4-36 to 4-39. At this flight condition the minimum load cyclic settings were -2.12° A_1 and 2.56° B_1. The alternating in-plane loads reach a minimum at 0.35° less A_1 (i.e., -1.77). The out-of-plane bending increases at 19,000 in-lbs/° A_1 cyclic away from the minimum loads whereas in-plane bending is lower at 7500 in-lbs/° A_1. The corresponding rates for B_1 are 17,500 in-lbs/° B_1 and 9000 in-lbs/° B_1 respectively.

Figures 4-40 and 4-41 show increasing alternating bending loads as incidence decreases from 27° to 15°. This is because the minimum load cyclic settings for 27° were used and as the one per rev excitation from incidence is reduced the cyclic required to produce minimum loads is reduced resulting in an excess of cyclic. This excess cyclic causes the loads to increase. The blade root (3.9%R) out-of-plane loads increase at 1750 in-lbs/° and appear to be slightly nonlinear (Figure 4-40). Out-of-plane loads increase at 500 in-lbs/°. The blade flap bending loads show low loads (< 5000 in-lbs). Chord bending at 55%R is low and about 5000 in-lbs.

The last transition point was at 27° i_N and 140 kts, 550 RPM. The loads measured on Run 13 are shown in Figures 4-42 to 4-44. The minimum loads cyclic at this flight condition were -3.23° A_1 and 4.31° B_1. Figure 4-42 shows both flap and chord loads due to A_1 cyclic. Out-of-plane bending at the hub 3.9%R increases at 16,000 in-lbs/° A_1 and the other loads are insensitive to A_1 cyclic. The in-plane loads show a slight variation indicating a minimum in-plane bending load at about 0.5° less A_1 than for minimum out-of-plane loads. The sensitivity of out-of-plane bending to B_1 (Figure 4-43) is high (24,300 in-lbs/°). The

in-plane loads show a minimum at 0.75° less B_1 than out-of-plane bending. The outboard gages indicate low bending moments.

The loads due to incidence are given in Figure 4.44 and show increased loads as incidence is reduced as observed previously at 105 knots. The loads grow more rapidly than the 105 knot case. Out-of-plane bending increases at 4500 in-lbs/° (1750 in-lbs/° at 105 knots) and in-plane at 2100 in-lbs/° (500 in-lbs/° at 105 knots.

For the transition conditions tested values of longitudinal and lateral cyclic were found (using blade load monitoring) which kept the alternating blade loads below 50% of the endurance limit except one condition at 76 knots and 8° incidence (high thrust and hence high g's) where the loads were about equal to the endurance limit. Figure 1 shows a test point past the boundary at 27° incidence. This boundary is only a function of the control configuration and can be moved out by increasing cyclic authority. This test point demonstrates this fact.

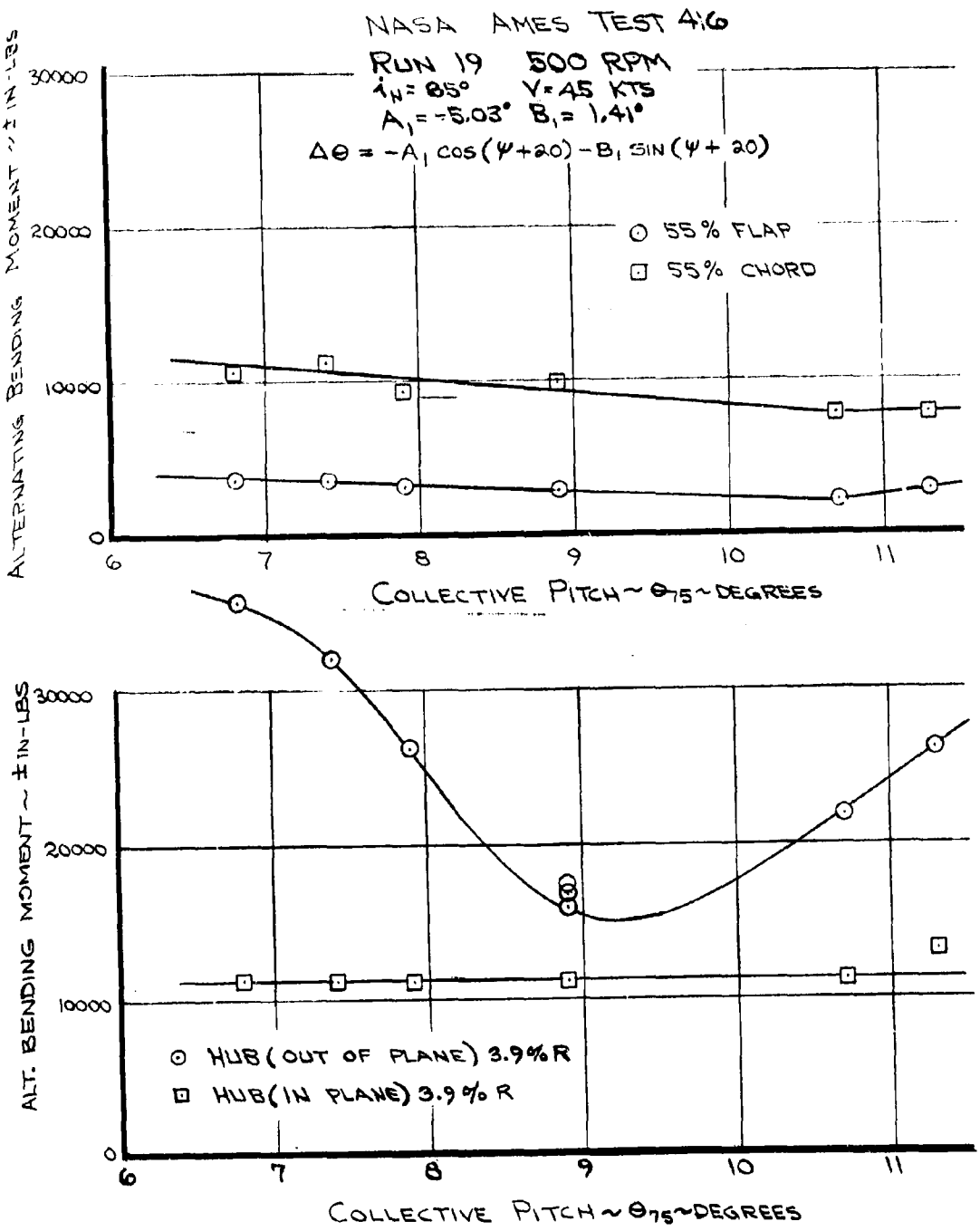

FIGURE 4.21. ALTERNATING BLADE LOADS DUE TO COLLECTIVE PITCH - V = 45 KNOTS, i_N = 85°

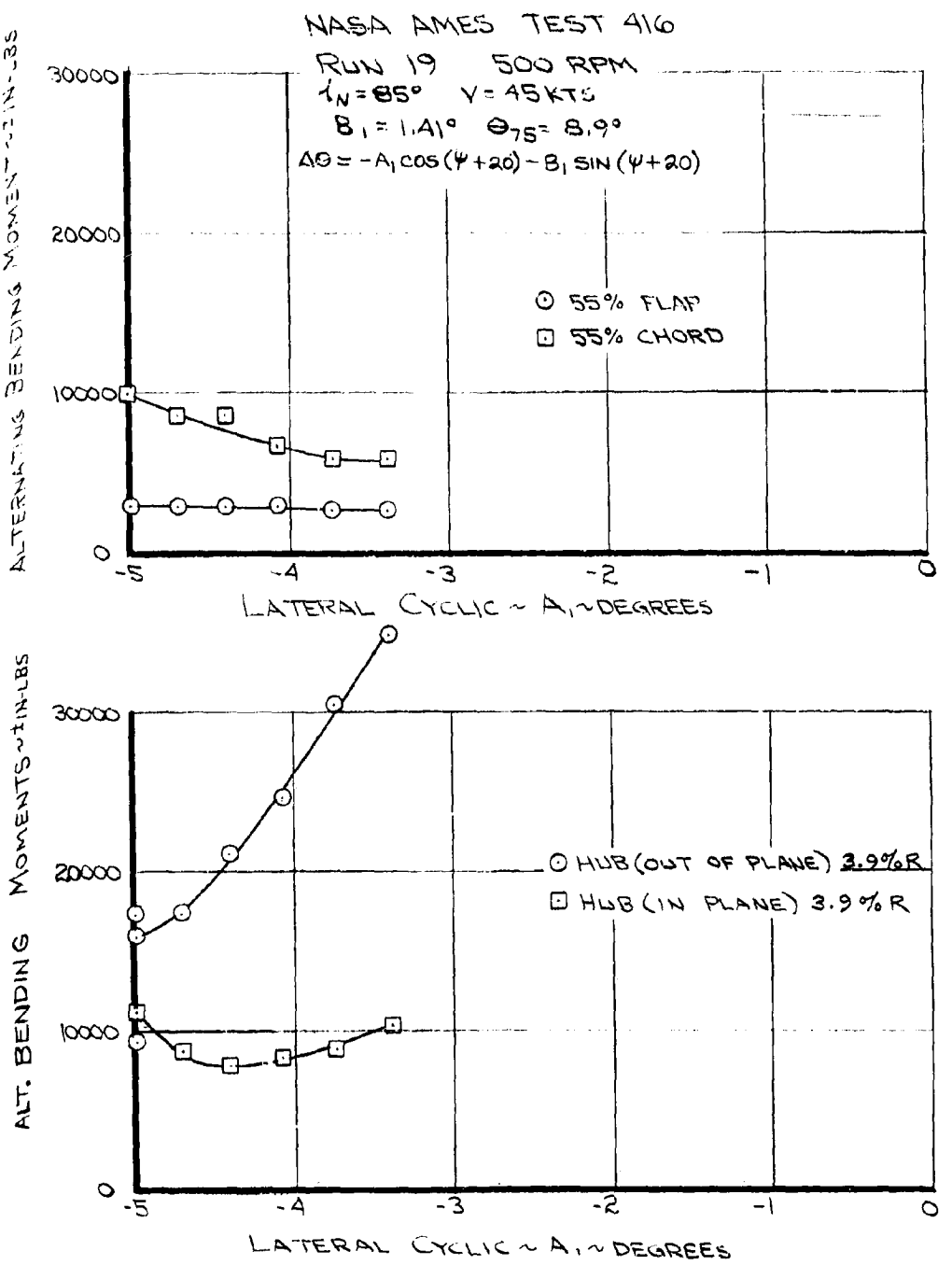

FIGURE 4.22. ALTERNATING BLADE LOADS DUE TO A_1 CYCLIC - V = 45 KNOTS, i_N = 85°

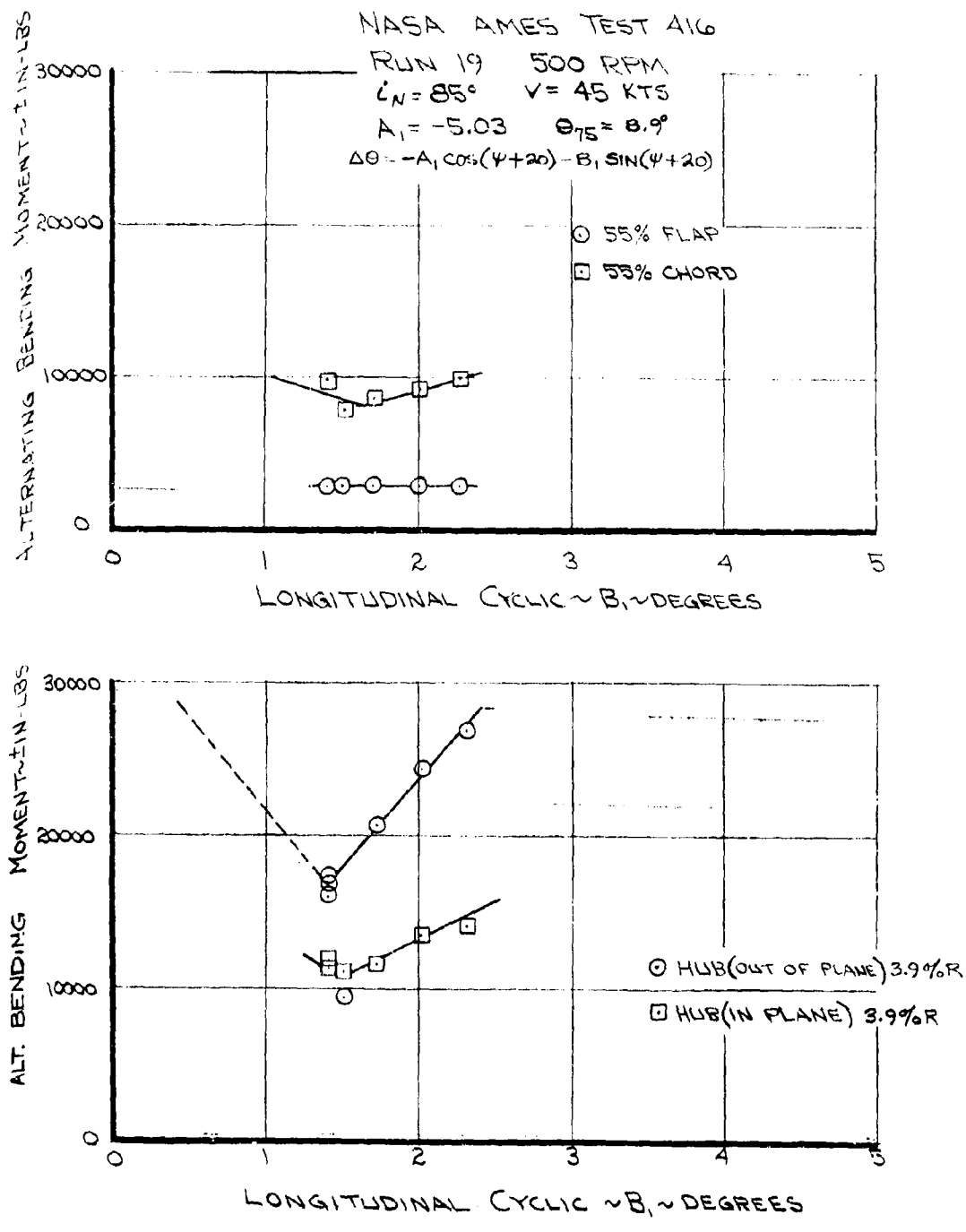

FIGURE 4.23. ALTERNATING BLADE LOADS DUE TO B_1 CYCLIC - V = 45 KNOTS, i_N = 85°

$$\Delta\theta = -A_1 \cos(\psi + \phi) - B_1 \cos(\psi + 2\phi)$$

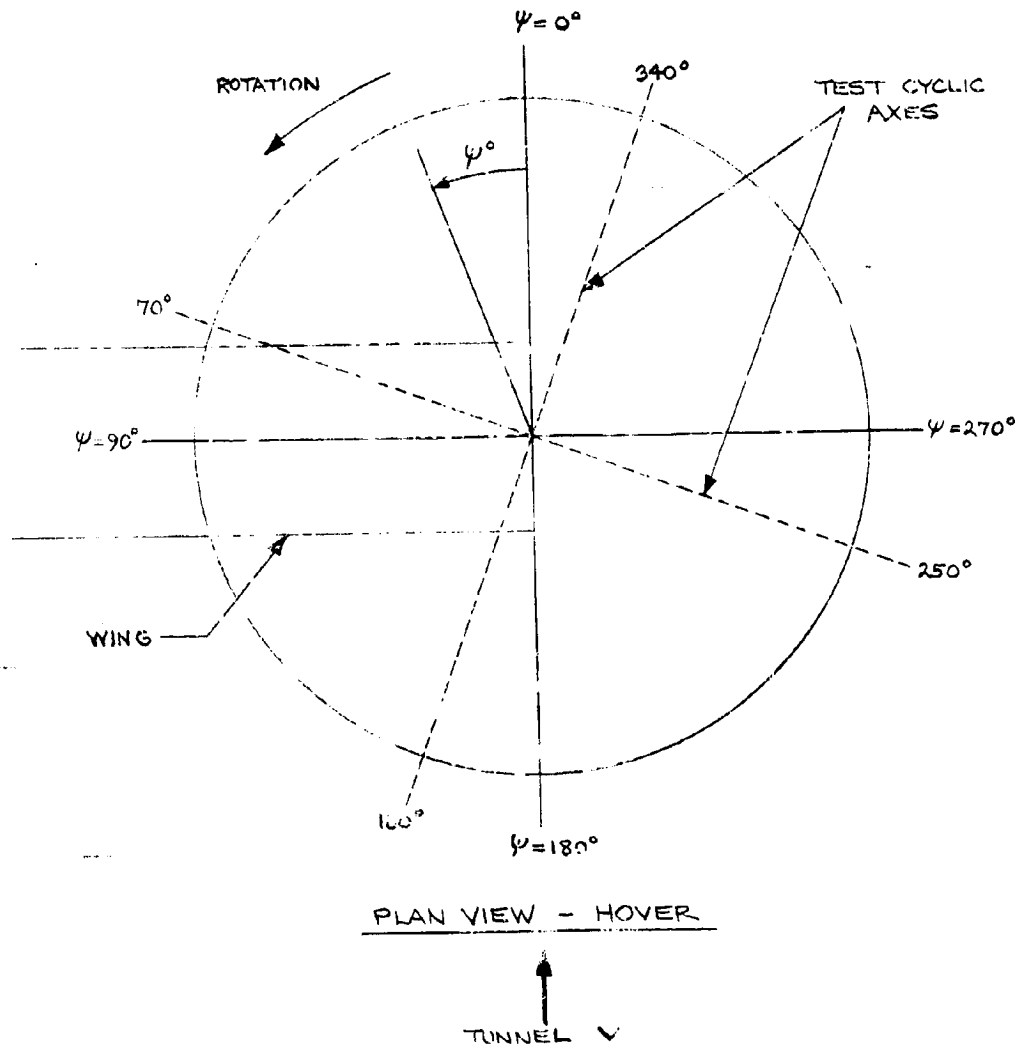

FIGURE 4.24 CYCLIC AXES DEFINITION

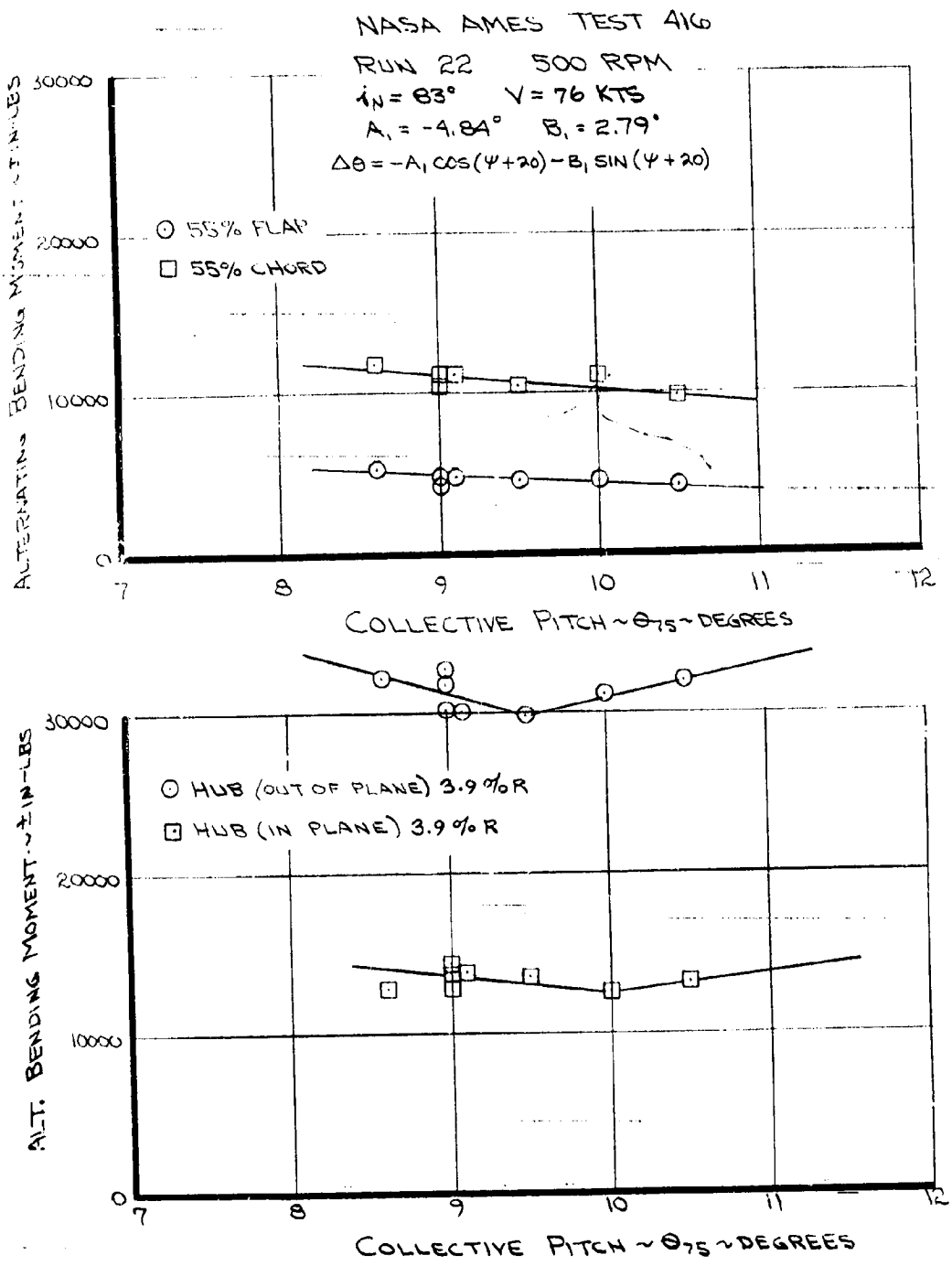

FIGURE 4.25. ALTERNATING BLADE LOADS DUE TO COLLECTIVE PITCH - V = 76 KNOTS, $i_N = 83°$

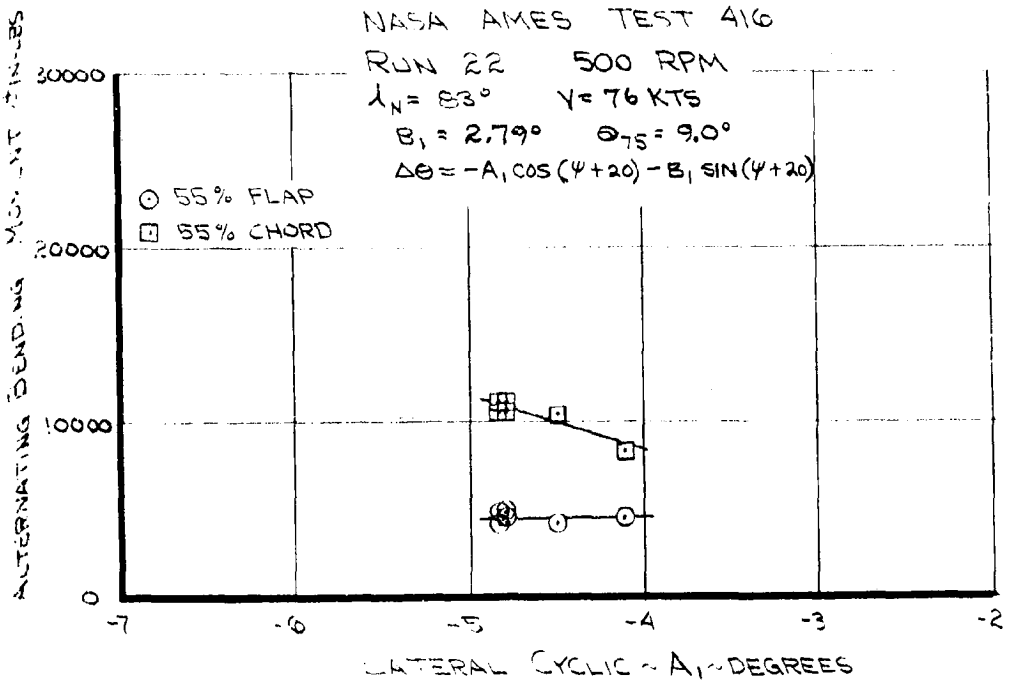

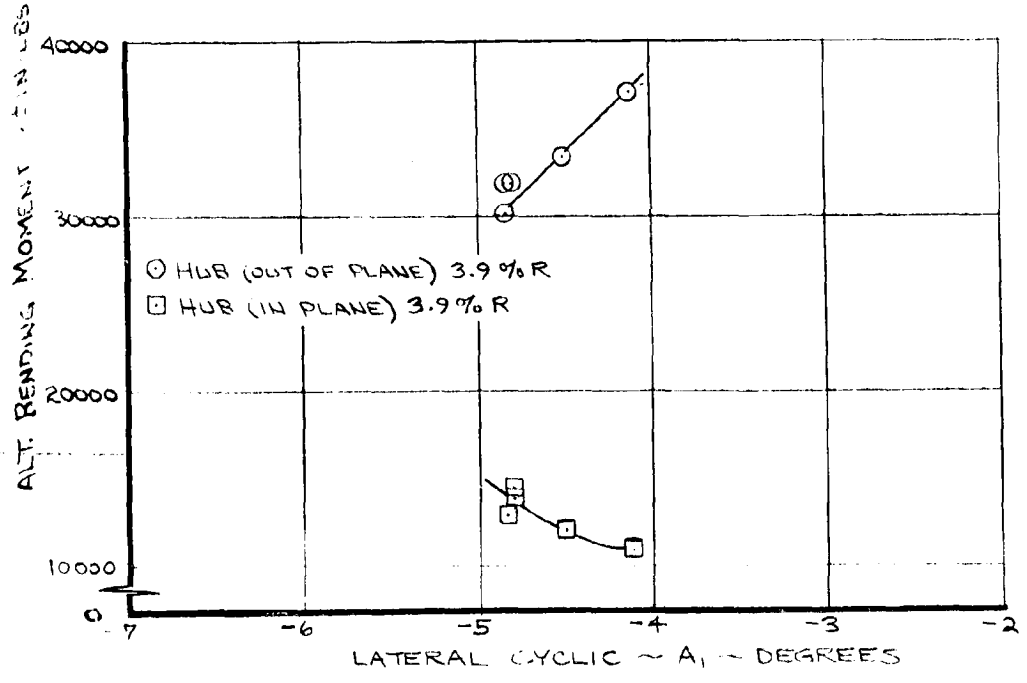

FIGURE 4.26. ALTERNATING BLADE LOADS DUE TO LATERAL CYCLIC - V = 76 KNOTS, $i_N = 83^\circ$

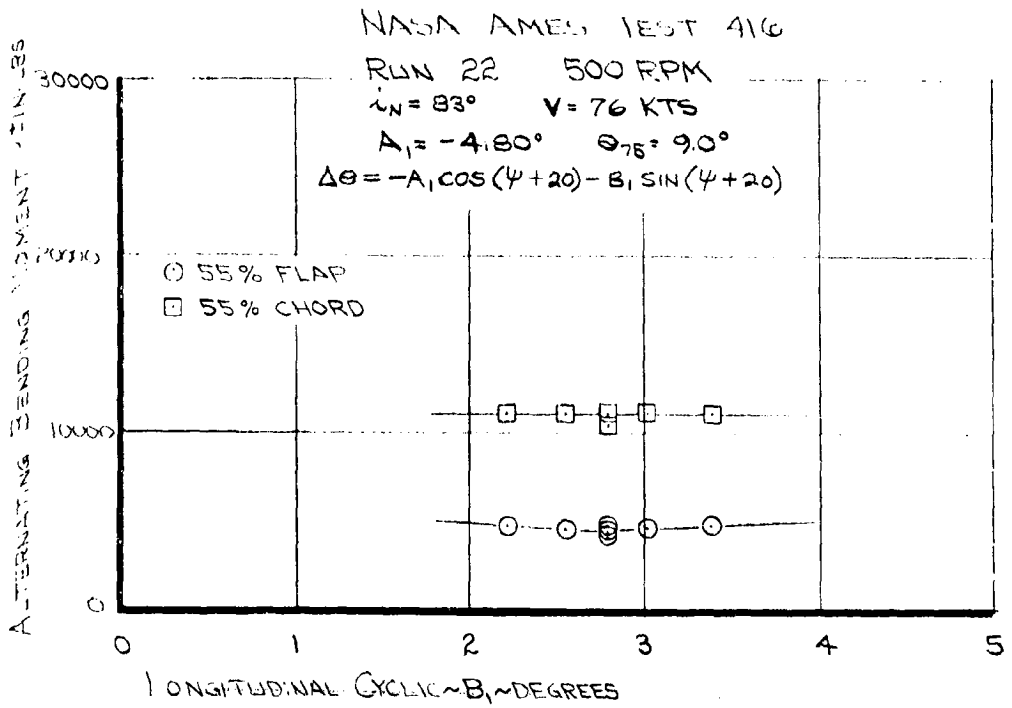

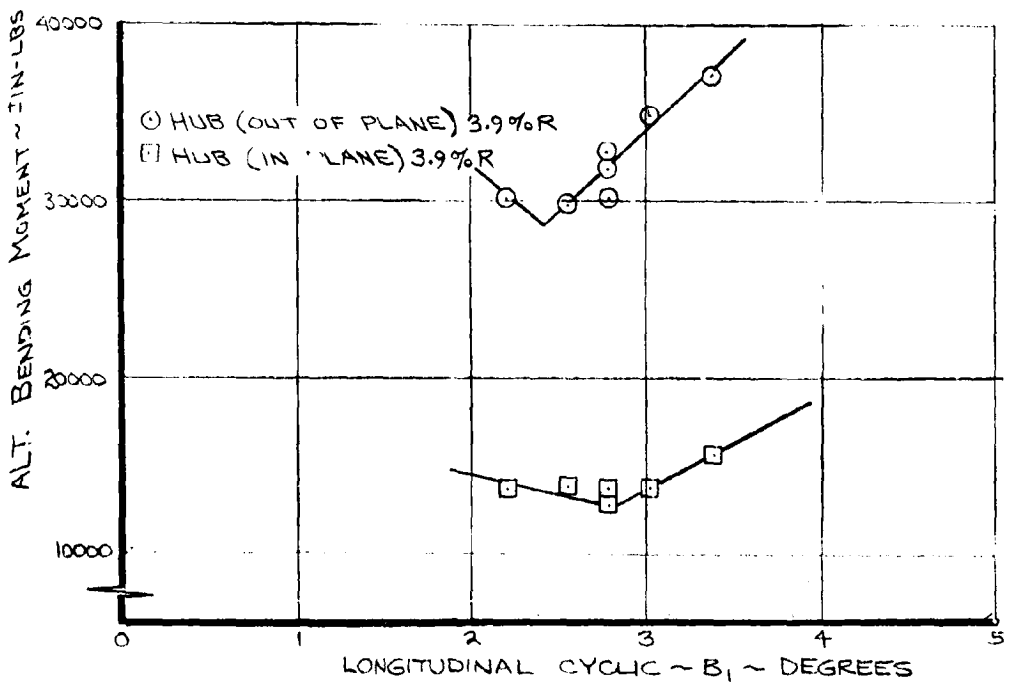

FIGURE 4.27. ALTERNATING BLADE LOADS DUE TO LONGITUDINAL CYCLIC - V = 76 KNOTS, $i_N = 83°$

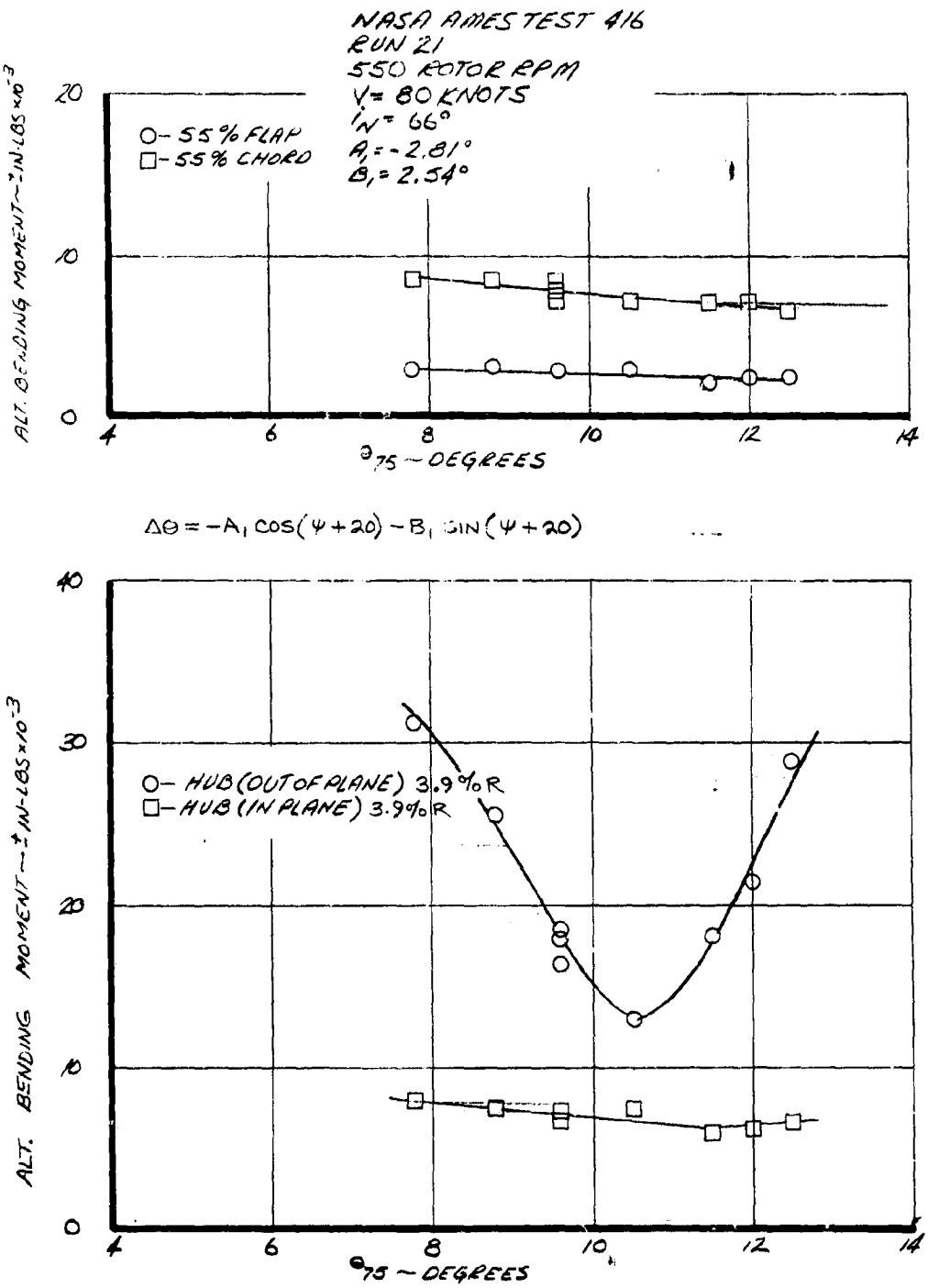

FIGURE 4.28. ALTERNATING BLADE LOADS DUE TO COLLECTIVE PITCH V = 80 KNOTS, i_N = 66°

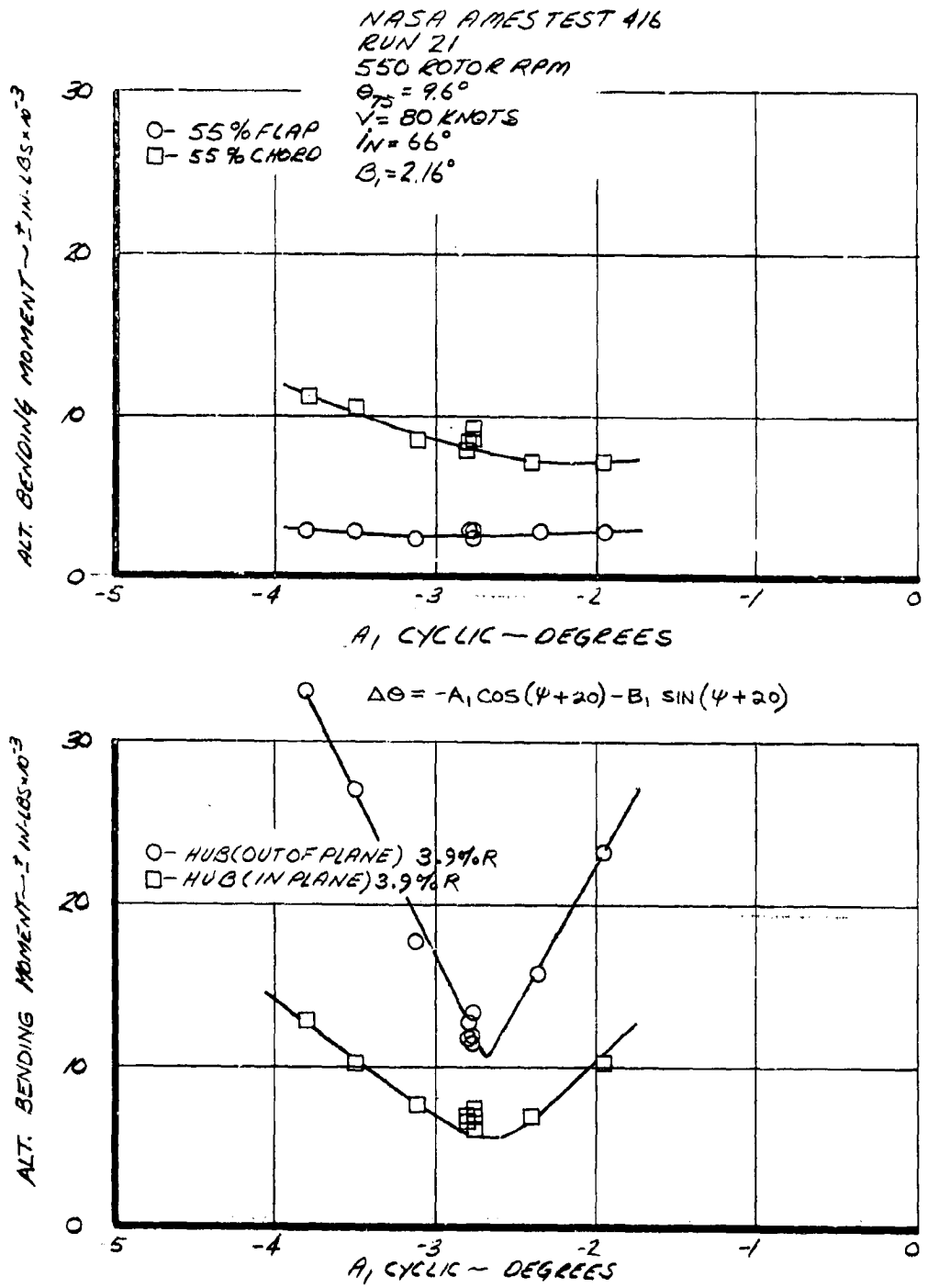

FIGURE 4.29. ALTERNATING BLADE LOADS DUE TO A_1 CYCLIC - V = 180 KNOTS, i_N = 66°

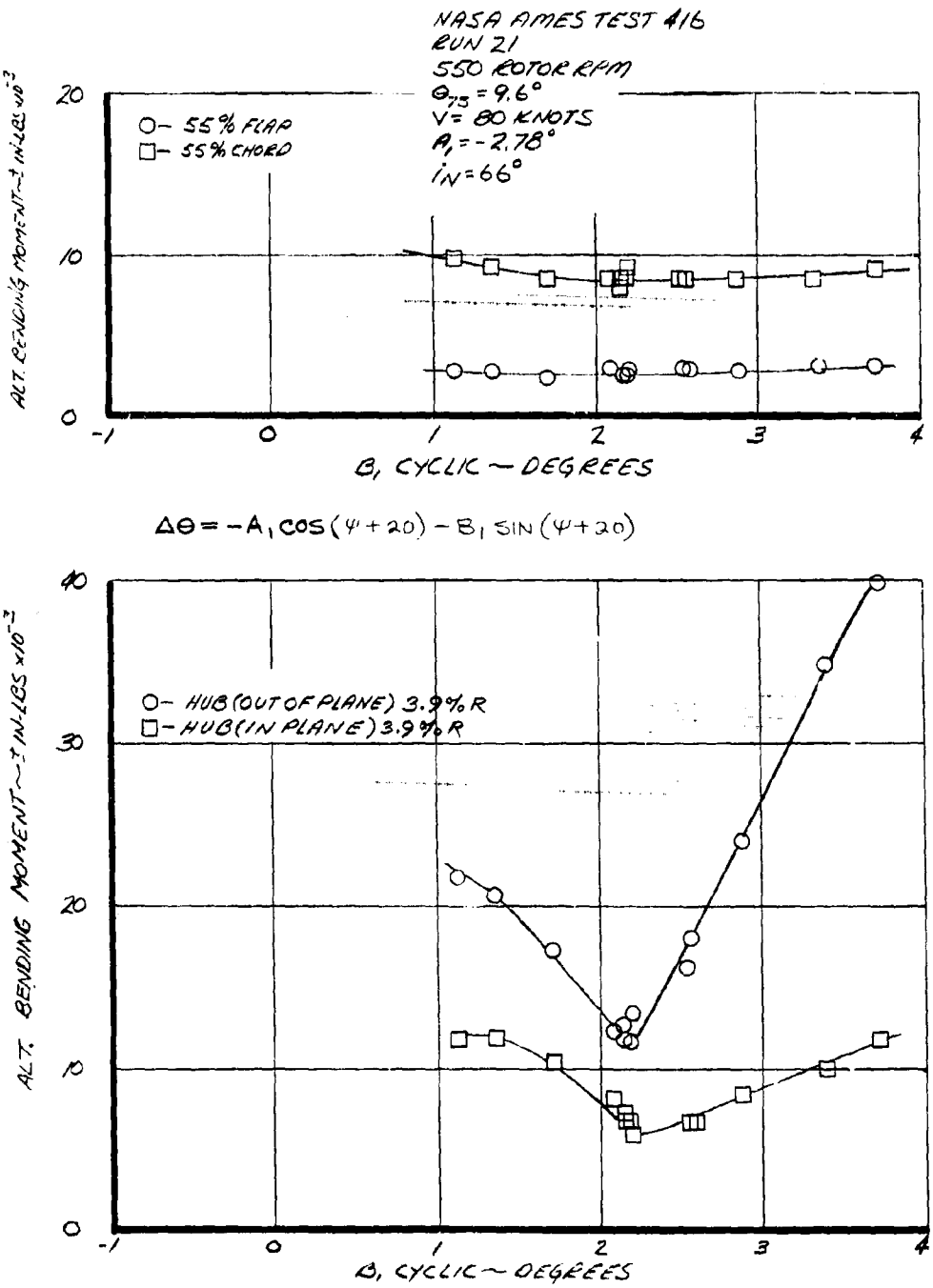

FIGURE 4.30. ALTERNATING BLADE LOADS DUE TO B_1 CYCLIC - V = 180 KNOTS, i_N = 66°

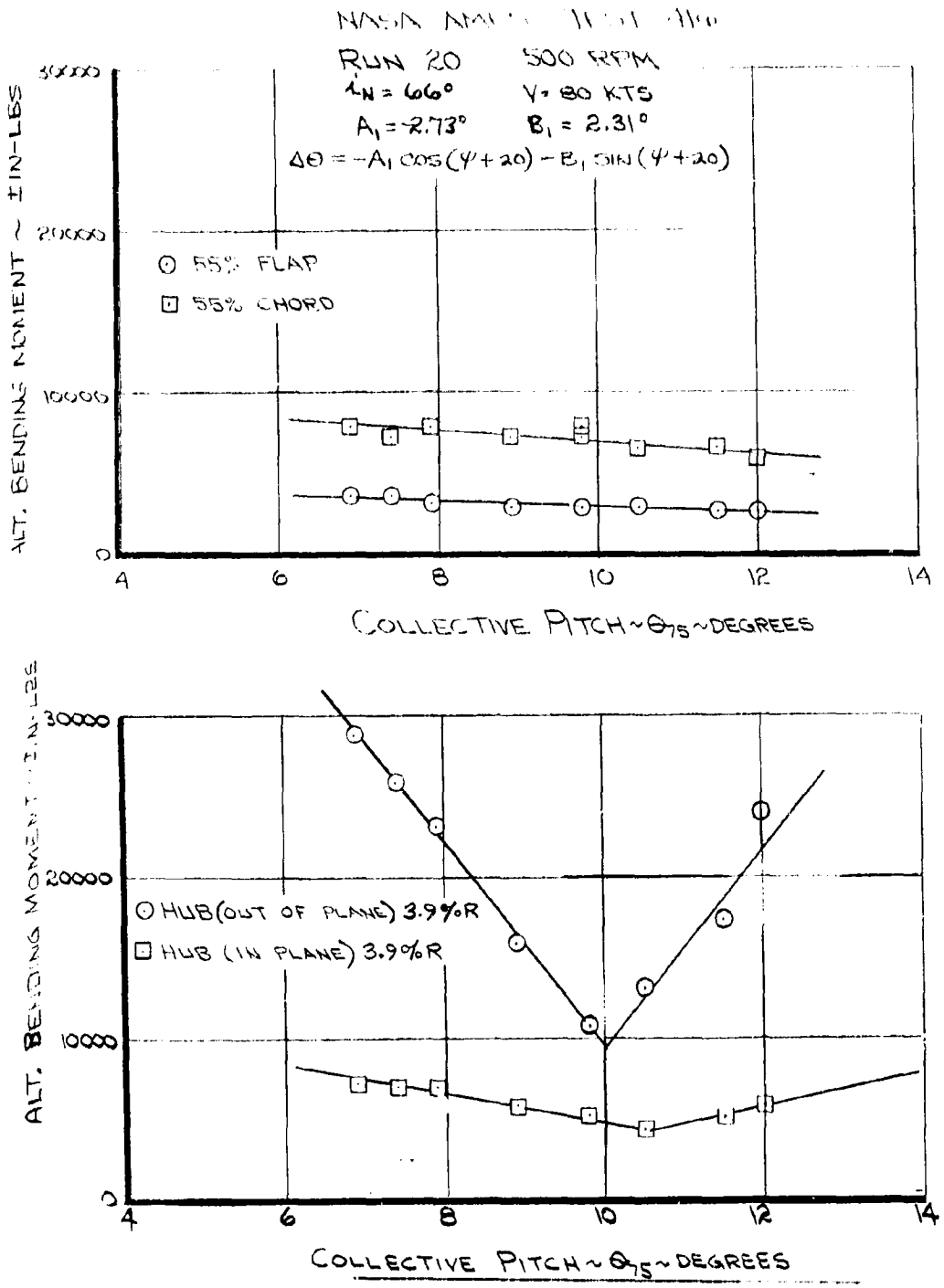

FIGURE 4.31. ALTERNATING BLADE LOADS DUE TO COLLECTIVE PITCH - V = 80 KNOTS, $i_N = 66°$

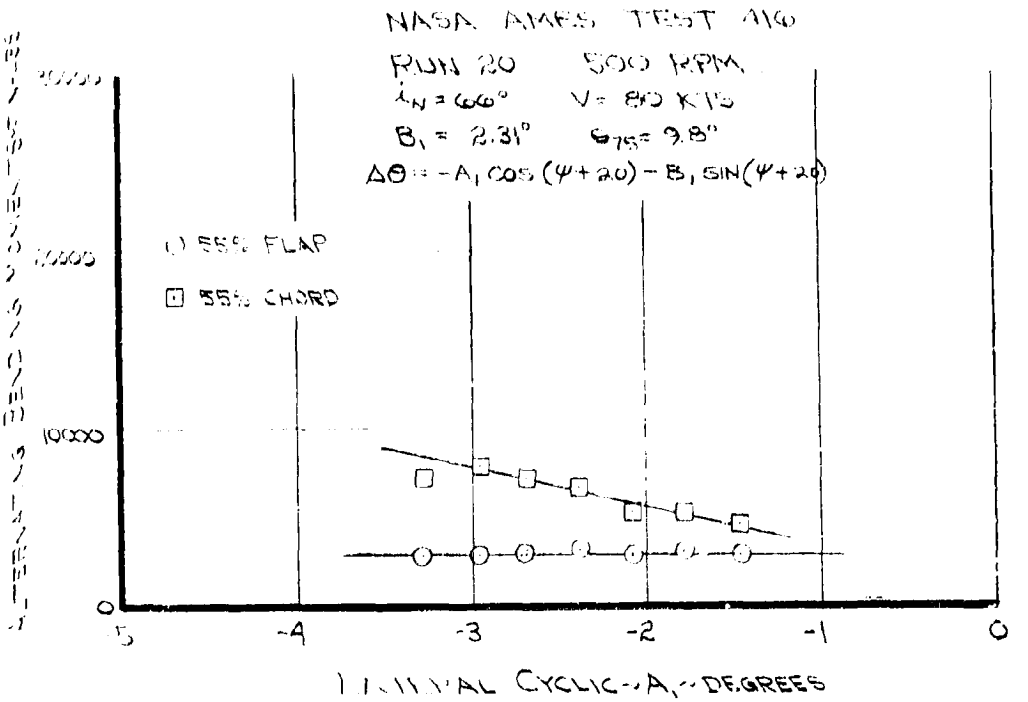

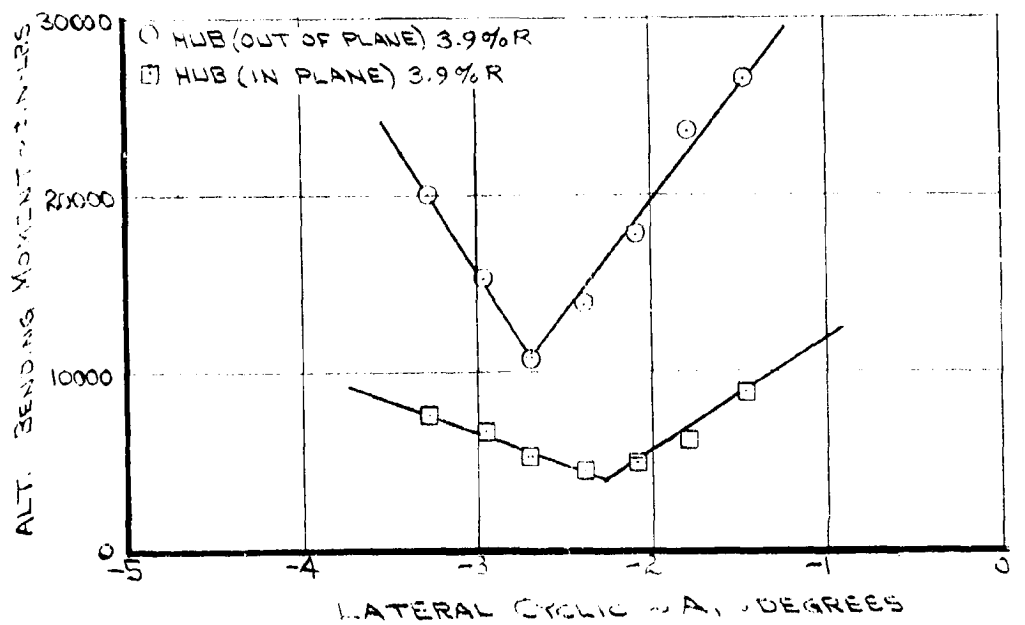

FIGURE 4.32. ALTERNATING BLADE LOADS DUE TO LATERAL CYCLIC - V = 180 KNOTS, i_N = 66°

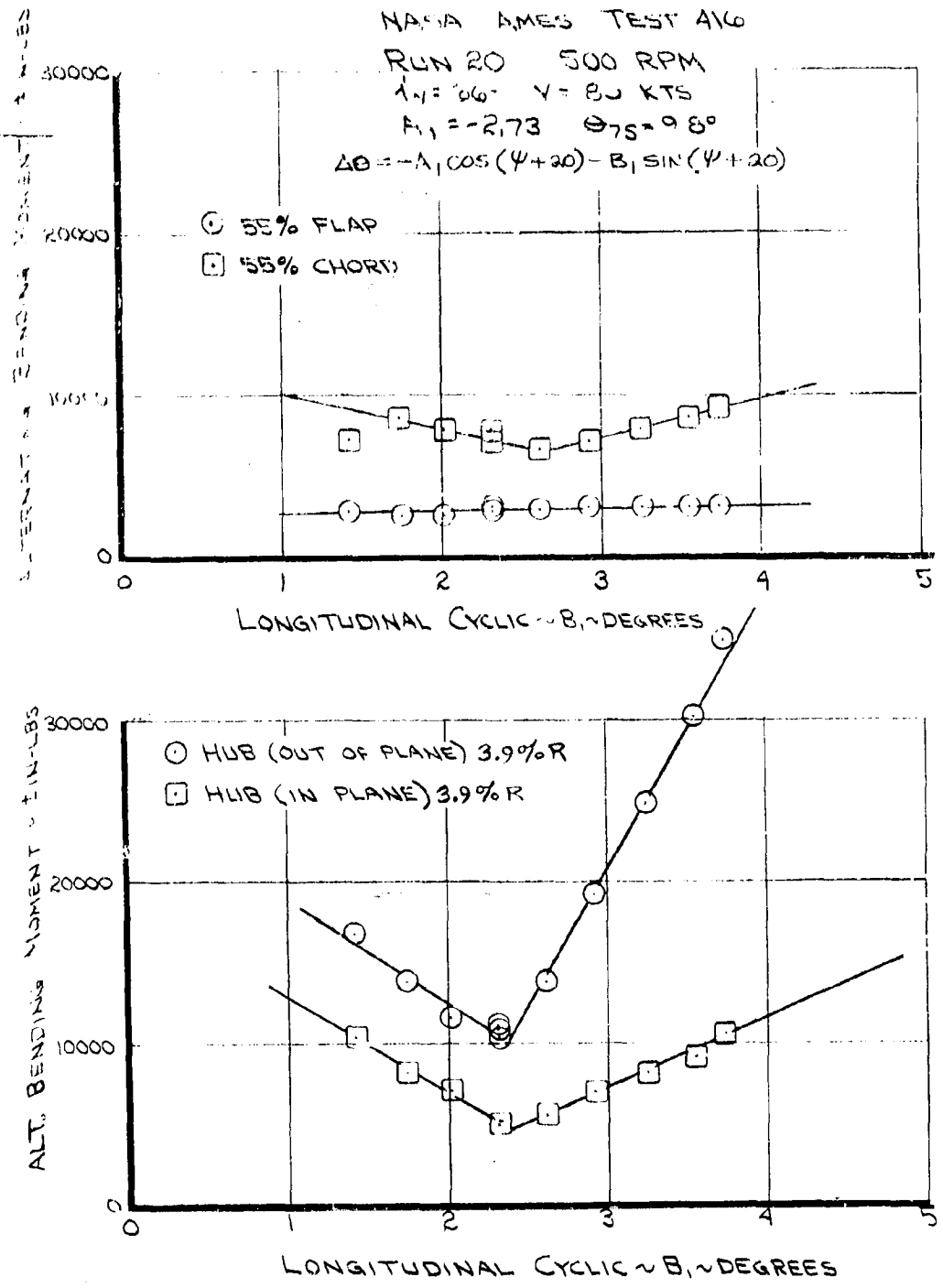

FIGURE 4.33. ALTERNATING BLADE LOADS DUE TO LONGITUDINAL CYCLIC - V = 80 KNOTS, $i_N = 66^\circ$

NASA AMES TEST #16
RUN 9
551 ROTOR RPM
$i_N = 27°$
V = 105 KNOTS
$A_1 = -2.16°$
$B_1 = 2.56°$

⊙ — 10.5 % FLAP
⊡ — HUB (OUT OF PLANE) 3.9%R
◈ — 22.5 % FLAP
△ — 55 % FLAP

$\Delta Q = -A_1 \cos(\psi + 20) - B_1 \sin(\psi + 20)$

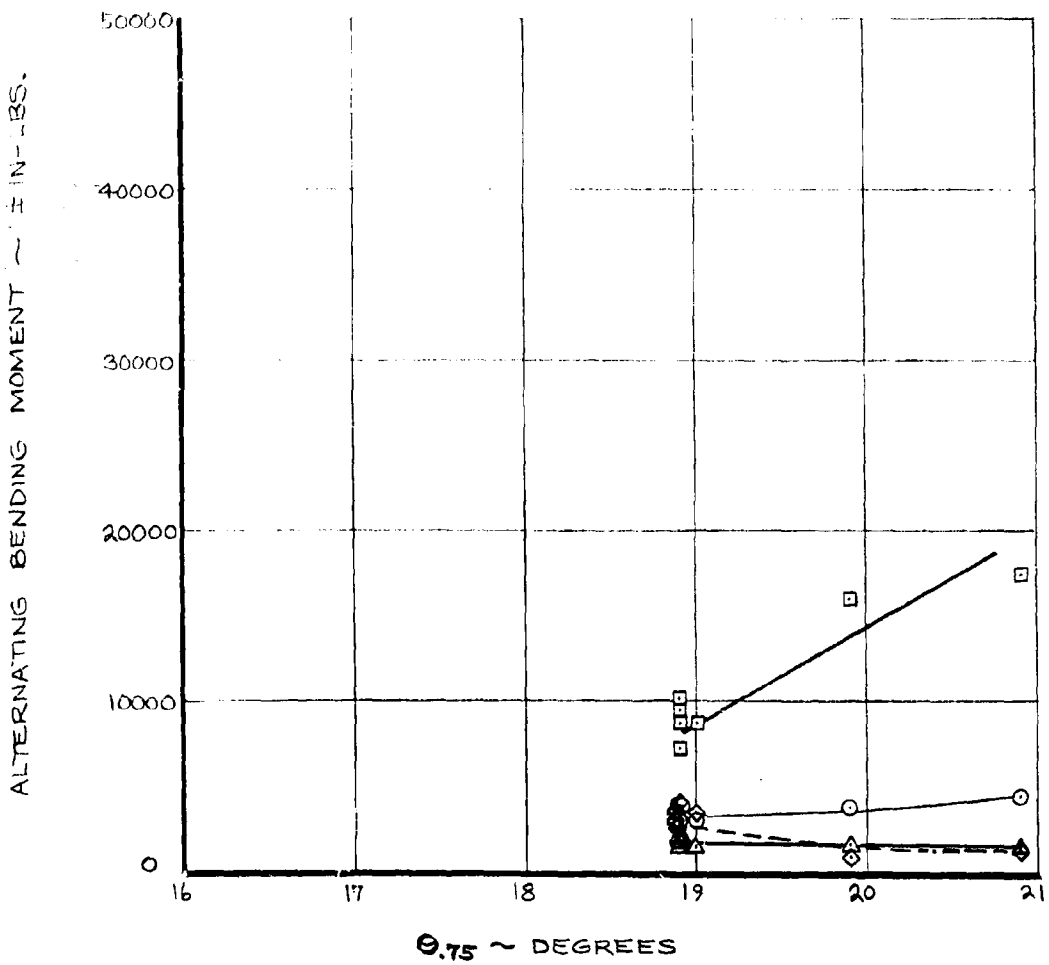

FIGURE 4.34 ALTERNATING BLADE FLAP LOADS DUE TO COLLECTIVE PITCH - V = 105 KNOTS, $i_N = 27°$

NASA AMES TEST 416
RUN 9
551 ROTOR RPM
$i_N = 27°$
$V = 105$ KNOTS
$A_1 = -2.16°$
$B_1 = 2.56°$

$\Delta\theta = -A_1 \cos(\psi + 20) - B_1 \sin(\psi + 20)$

⊙ —— HUB (IN PLANE) 3.9%R
△ —— 55% CHORD

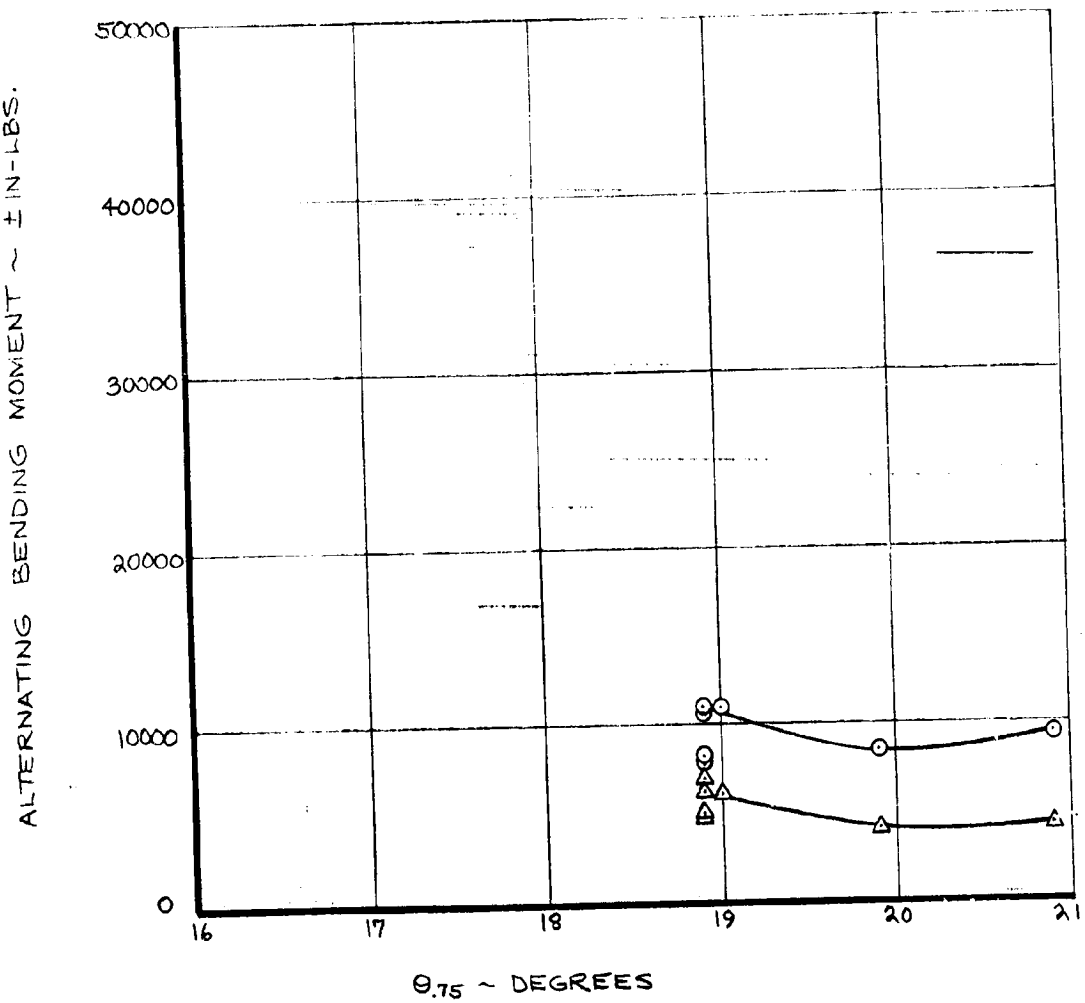

FIGURE 4.35 ALTERNATING BLADE CHORD LOADS DUE TO COLLECTIVE PITCH - $V = 105$ KNOTS, $i_N = 27°$

NASA AMES TEST 4-16

RUN 9
551 ROTOR RPM
$\theta_{.75} = 18.9°$
105 KNOTS
$i_{TT} = 27°$
$B_1 = 2.56°$

⊙ — 10.5 % FLAP
⊡ — HUB (OUT OF PLANE) 3.9%R
◇ — 22.5 % FLAP
△ — 55 % FLAP

$\Delta\theta = -A_1 \cos(\psi + 20) - B_1 \sin(\psi + 20)$

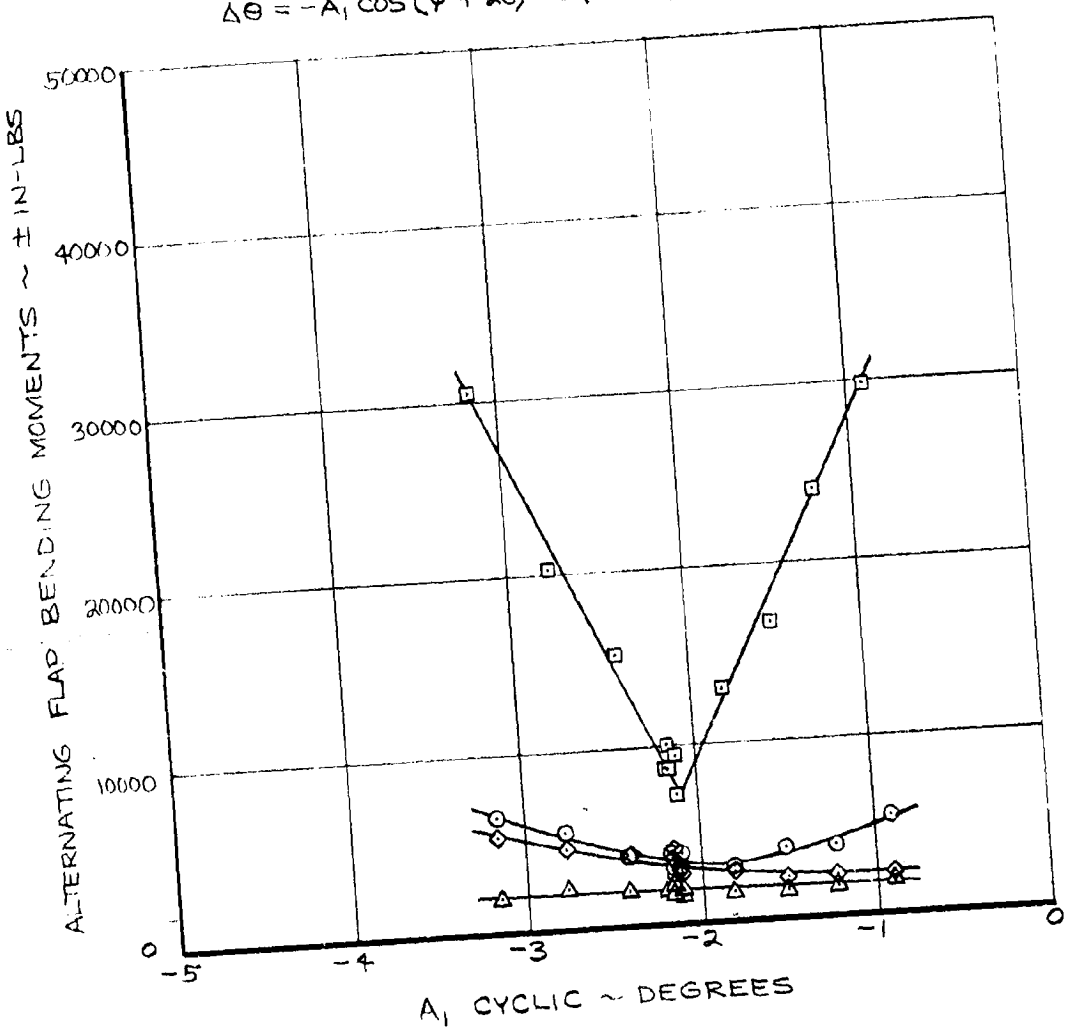

FIGURE 4.36 ALTERNATING FLAP BENDING LOADS DUE TO A_1 CYCLIC. V = 105 KNOTS, $i_N = 27°$

NASA AMES TEST 416
RUN 9
551 ROTOR RPM
$\theta_{.75} = 18.9°$
105 KNOTS
$i_N = 27°$
$B_1 = 2.56°$

⊙ — 55% CHORD
⊡ — HUB (IN PLANE) 3.9%R

$\Delta\theta = -A_1 \cos(\psi + 20) - B_1 \sin(\psi + 20)$

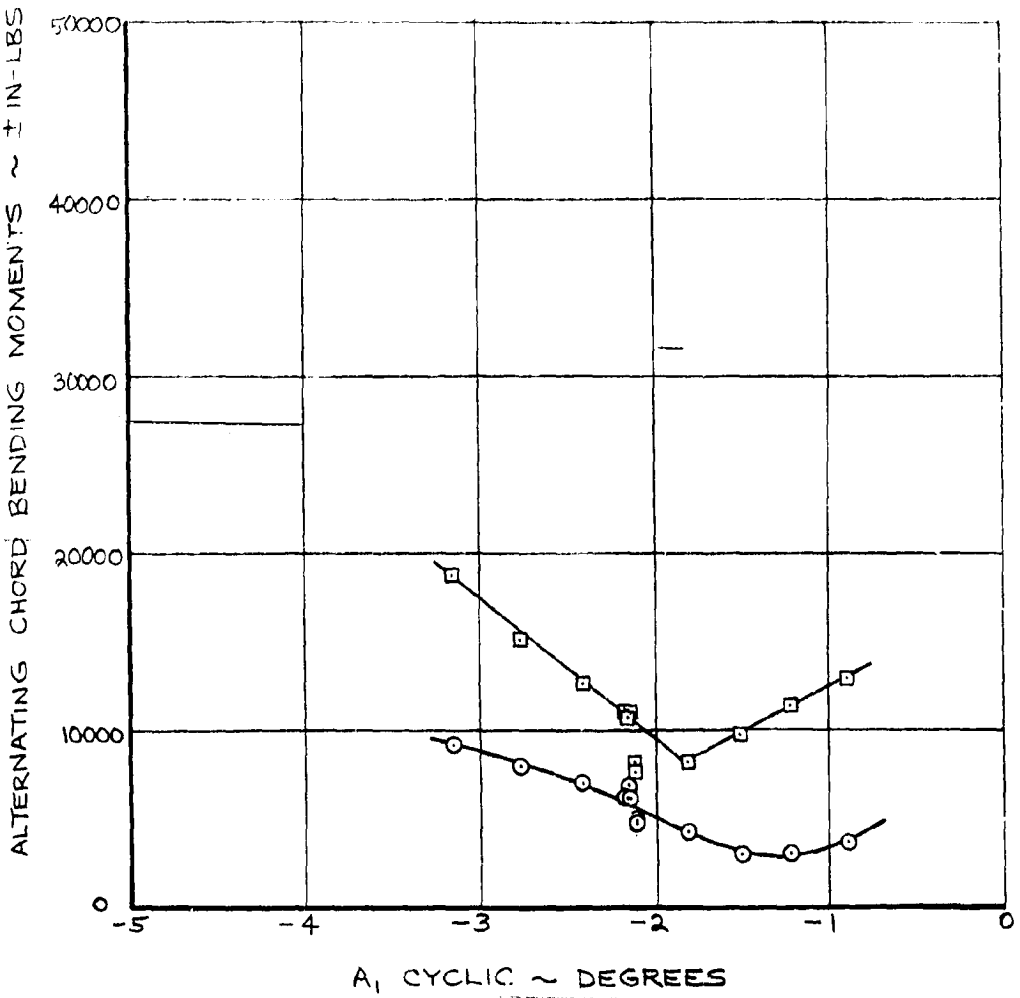

FIGURE 4.37 ALTERNATING CHORD BENDING LOADS DUE TO A_1 CYCLIC . V = 105 KNOTS, $i_N = 27°$

NASA AMES TEST 416
RUN 9
551 ROTOR RPM
$\theta_{.75} = 18.9°$
105 KNOTS
$i_N = 27°$
$A_1 = -2.12°$

⊙ — 10.5 % FLAP
⊡ — HUB (OUT OF PLANE) 3.9%R
◈ — 22.5 % FLAP
△ — 55 % FLAP

$\Delta\theta = -A \cos(\psi + 20) - B_1 \sin(\psi + 20)$

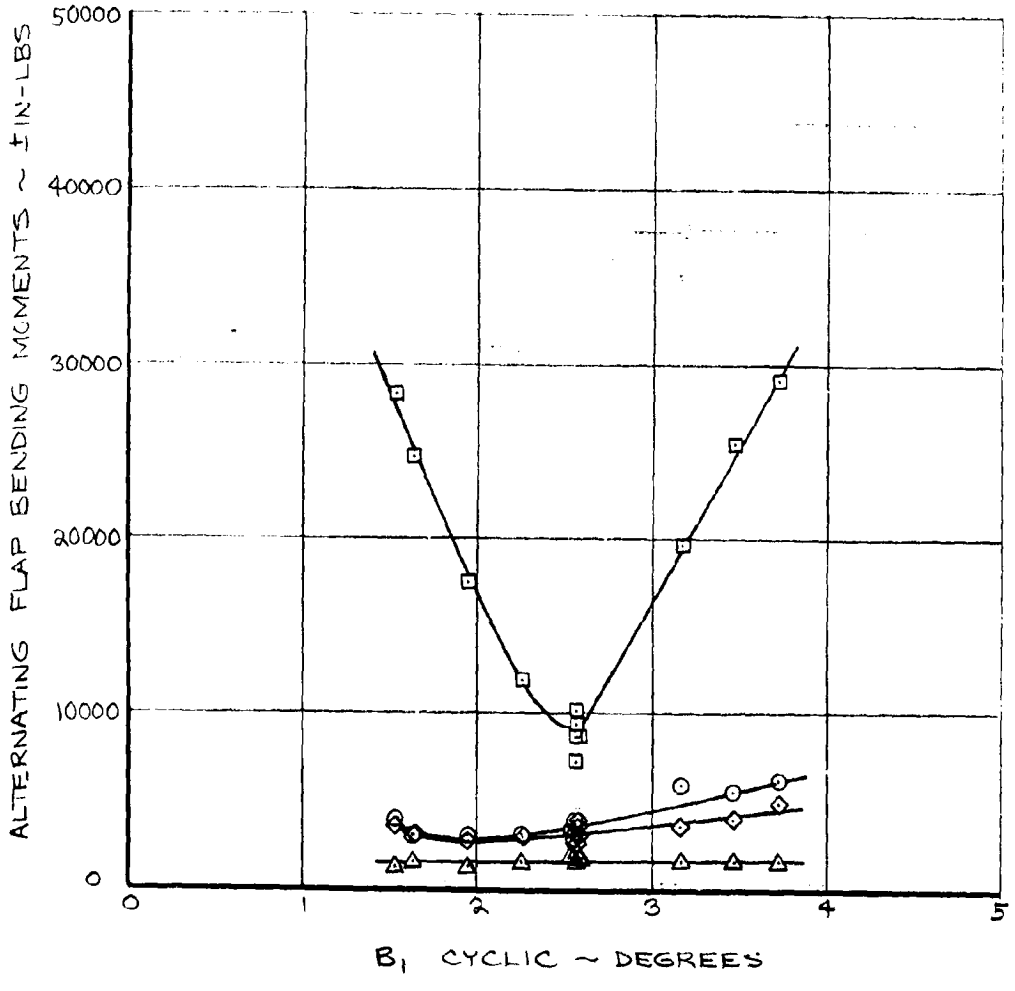

FIGURE 4.38 ALTERNATING FLAP BENDING LOADS DUE TO B_1 CYCLIC, V = 105 KNOTS, $i_N = 27°$

NASA AMES TEST 416
RUN 9
551 ROTOR RPM
$\theta_{.75} = 18.9°$
105 KNOTS
$i_N = 27°$
$A_1 = -2.12°$

⊙ — 55 % CHORD
⊡ — HUB (IN PLANE) 3.9 %R

$\Delta\theta = -A_1 \cos(\psi + 20) - B_1 \sin(\psi + 20)$

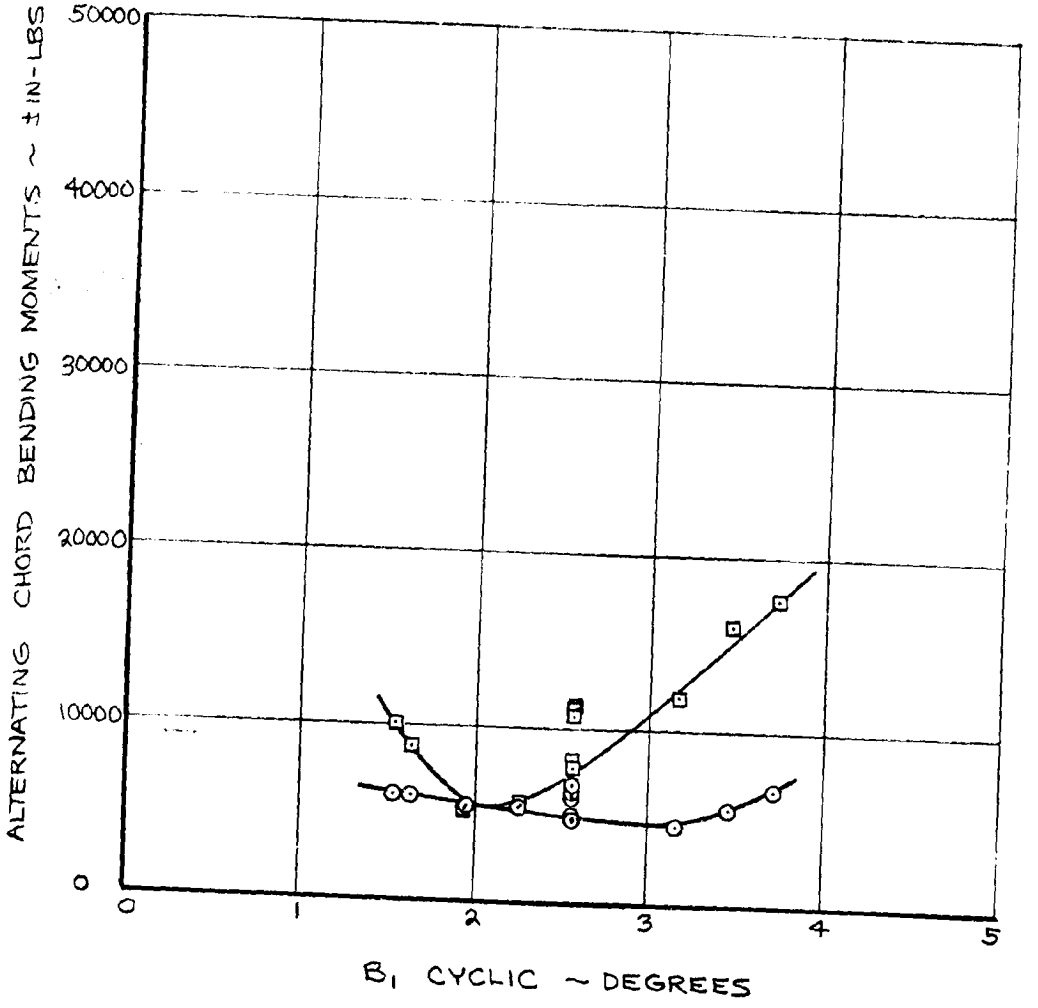

FIGURE 4.39 ALTERNATING CHORD BENDING LOADS DUE TO B_1 CYCLIC . V = 105 KNOTS, $i_N = 27°$

NASA AMES TEST 416

RUN 9

551 ROTOR RPM

$\theta_{.75} = 18.9°$

105 KNOTS

$A_1 = -2.12°$

$B_1 = 2.56°$

⊙ — 10.5 % FLAP

⊡ — HUB (OUT OF PLANE) 3.9 %R

◇ — 22.5 % FLAP

△ — 55 % FLAP

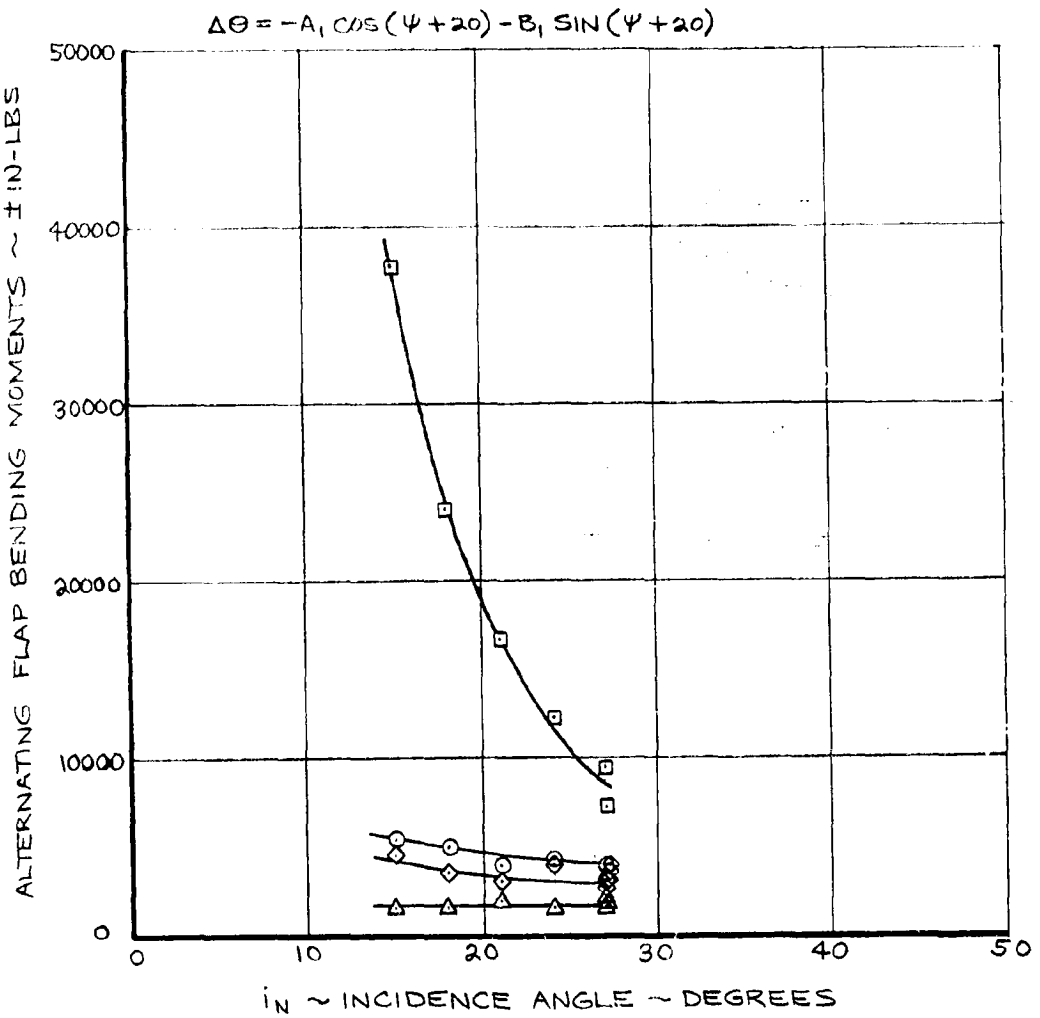

FIGURE 4.40 ALTERNATING FLAP BENDING LOADS DUE TO INCIDENCE ANGLE. V = 105 KNOTS

NASA AMES TEST 416

RUN 9

551 ROTOR RPM

$\theta_{.75} = 18.9°$

105 KNOTS

$A_1 = -2.12°$

$B_1 = 2.56°$

⊙ — 55 % CHORD

⊡ — HUB (IN PLANE) 3.9% R

$\Delta\theta = -A_1 \cos(\psi + 20) - B_1 \sin(\psi + 20)$

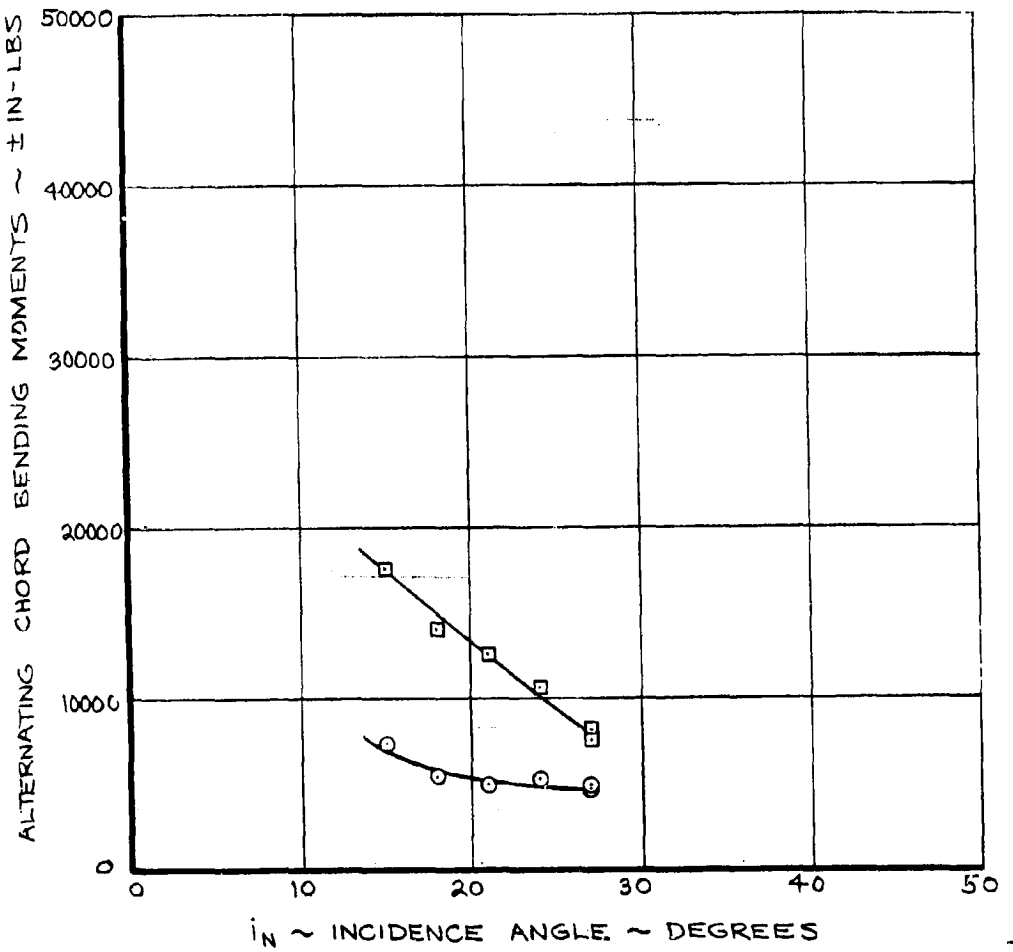

FIGURE 4.41 ALTERNATING CHORD BENDING LOADS DUE TO INCIDENCE ANGLE. V = 105 KNOTS

NASA AMES TEST 416

RUN 13

551 ROTOR RPM

$\theta_{.75} = 25.1°$

140 KNOTS

$i_N = 27°$

$B_1 = 4.31°$

⊙ — HUB (OUT OF PLANE) 3.9%R

⊡ — HUB (IN PLANE) 3.9%R

● — 55% FLAP

■ — 55% CHORD

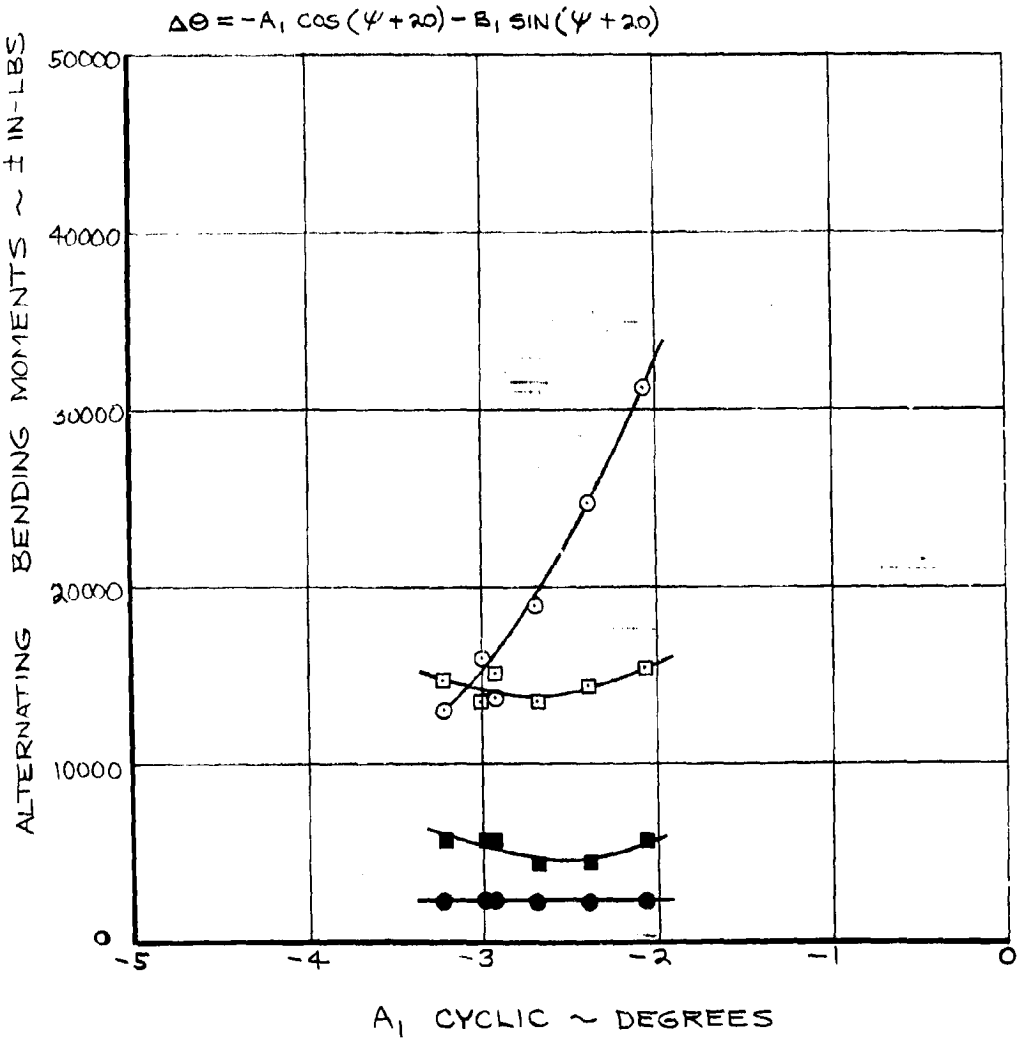

FIGURE 4.42 ALTERNATING BLADE LOADS DUE TO A_1 CYCLIC
$V = 140$ KNOTS, $i_N = 27°$

NASA AMES TEST 416
RUN 13
551 ROTOR RPM
$\theta_{.75} = 25.1°$
140 KNOTS
$i_N = 27°$
$A_1 = -3.23°$

⊙ — HUB (OUT OF PLANE) 3.9%R
⊡ — HUB (IN PLANE) 3.9%R
● — 55% FLAP
■ — 55% CHORD

$\Delta\theta = -A_1 \cos(\psi+20) - B_1 \sin(\psi+20)$

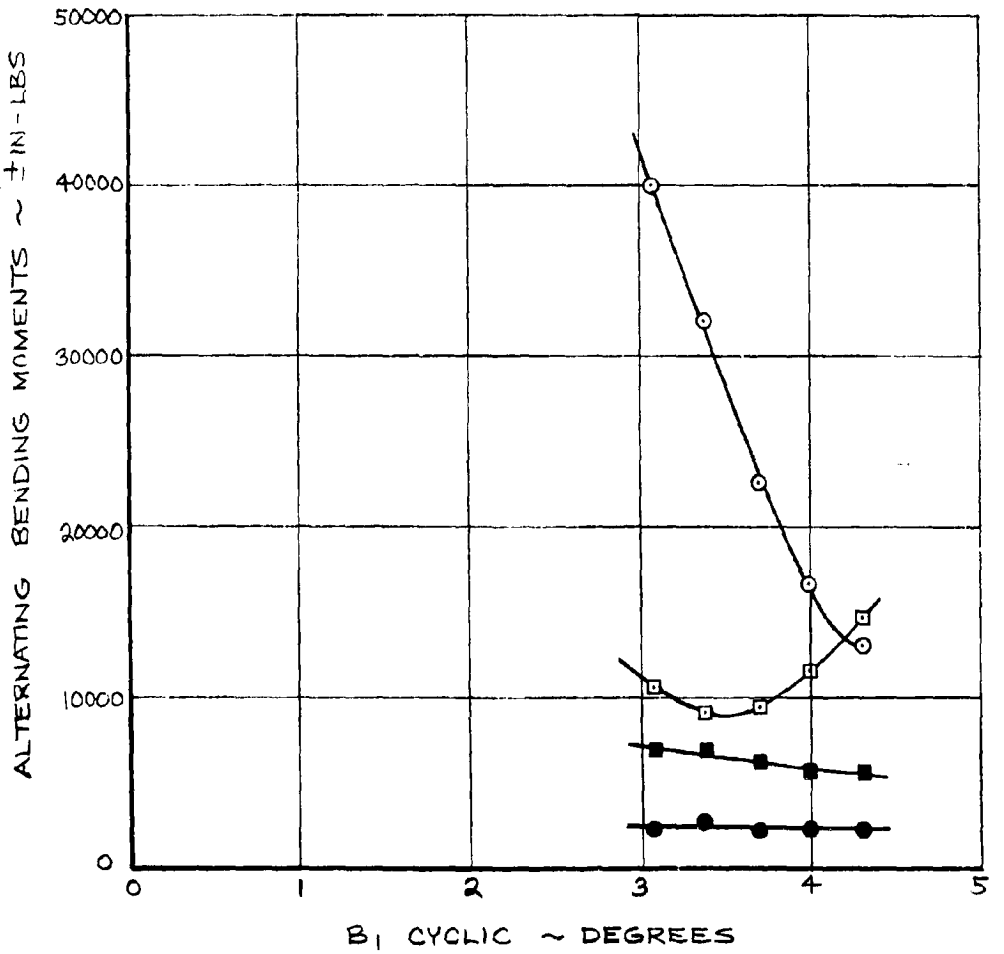

FIGURE 4.43 ALTERNATING BLADE LOADS DUE TO B_1 CYCLIC
$V = 140$ KNOTS, $i_N = 27°$

NASA AMES TEST 416
RUN 13
551 ROTOR RPM
$\theta_{.75} = 25.1°$
140 KNOTS
$A_1 = -3.23°$
$B_1 = 4.31°$

⊙ — HUB (OUT OF PLANE) 3.9%R
⊡ — HUB (IN PLANE) 3.9%R
● — 55% FLAP
■ — 55% CHORD

$\Delta\theta = -A_1 \cos(\psi + 20) - B_1 \sin(\psi + 20)$

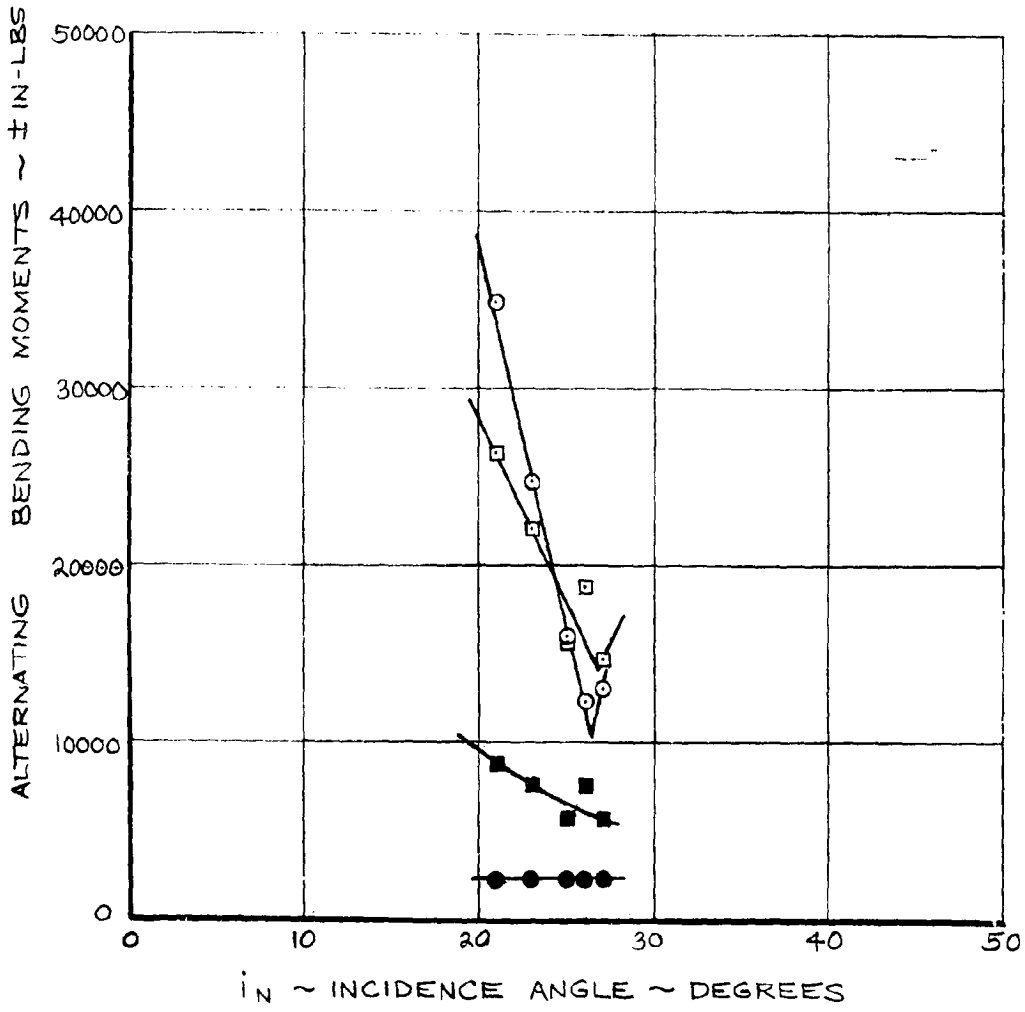

FIGURE 4.44 ALTERNATING BLADE LOADS DUE TO INCIDENCE ANGLE - V = 140 KNOTS

TABLE 4.3

CYCLIC PITCH SETTINGS FOR MINIMUM LOADS

RUN NO.	V TUNNEL SPEED (KNOTS)	ROTOR RPM	i_N INCIDENCE ANGLE (DEGREES)	TEST AXIS SYSTEM		CLASSICAL AXIS SYSTEM	
				$A_1°$	$B_1°$	A_1	B_1
				(DEGREES)		(DEGREES)	
7	0	551	0	0	0	0	0
19	45	500	85	-5.03	1.41	-4.24	3.05
22	76	500	83	-4.84	2.79	-3.59	4.28
21	80	550	66	-2.81	2.54	-1.77	3.35
20	80	500	66	-2.73	2.31	-1.78	3.10
9	105	551	27	-2.16	2.56	-1.15	3.14
13	140	551	27	-3.23	4.31	-1.56	5.15
11	140	386	10	-2.66	2.31	-1.71	3.08
14	170	386	10	-2.97	3.38	-1.63	4.19

4.4 Rotor Loads in Cruise

Alternating blade loads in cruise flight arise because of aircraft attitude (incidence or yaw), aircraft motions normal to body waterline axis or extraneous disturbances, e.g., gusts or turbulence. With the exception of high frequency gusts or turbulence all of these effects induce one per rev blade excitation primarily. These blade loads can constitute a limit to the flight envelope. On the Model 222 aircraft cyclic pitch (by means of the load alleviation system) is used to effectively neutralize the one per rev loads. In this section of the report cruise condition blade loads obtained from both tests 410 and 416 are presented to show the effects of angle of attack, cyclic, RPM and the application of power.

Effect of Angle of Attack

The alternating blade loads obtained at cruise design RPM from the windmilling test (test no. 410) are summarized in Figures 4-45 to 4-48. These data are measured in the blade reference axes, normal to and parallel with the local blade chord.

Alternating blade flap and chord data at radial locations 10.5%R, 22.5%R and 55%R are shown in Figures 4-45, 4-46 and 4-47 respectively. Flap bending data for stations 42.5%R,

78%R and 55%R are given in Figure 4-48. The effect of increasing angle of attack is to increase the alternating flap and chord bending particularly at the blade root. The extreme outboard gages show alternating flap bending to be insensitive to angle of attack.

At the 10.5% radial station the alternating chord bending increases at 3750 in-lbs/° at 100 kts and flap bending at 1375 in-lbs/°. These load sensitivities increase to 5500 in-lbs/° and 2625 in-lbs/° respectively at 140 kts. At 192 kts the bending moments increase at 10,000 in-lbs/° alternating chord bending and 5750 in-lbs/° alternating flap bending. At four degrees incidence at 192 kts the test alternating allowable strain of 2000μ i/in was reached. This strain level corresponds to a fatigue life of 2.0 x 10^7 cycles from the mean -3σ curve of Reference 13.

At this flight condition (i.e., S.L.S. nacelle incidence zero, no flap and no load alleviation) four degrees of airplane angle of attack would produce a normal load factor of 1.58 g's. At constant angle of attack the normal load factor increases with airspeed squared. The alternating load sensitivities to angle of attack increase at less than the square of velocity indicating that higher load

factors can be attained as airspeed increases. Figure 4-49 shows calculated normal load factor as a function of airspeed for two flap settings assuming zero nacelle incidence relative to the wing and no load alleviation. The aircraft attitude has been limited to the angle producing blade loads equivalent to 2000 μ i/in blade root strain. The data indicate that the airplane can be adequately flown with no load alleviation without using significant amounts of blade life. These load factors should not be construed as the maximum attainable on the aircraft since much higher values can be attained at higher nacelle incidence where cyclic pitch maintains acceptable blade loads.

Figures 4-50 and 4-51 show cruise alternating blade loads obtained on Run 11 of test 416 (powered) at 140 kts. The chord bending and hub barrel in-plane bending data are given in Figure 4-50 and predicted in-plane loads using the Boeing computer program C-70, generated under Air Force contract, Reference 16.

This program was used to generate transition and low speed cruise loads prior to the powered test. At 3.9%R the in-plane loads are predicted to increase at a higher rate than measured (7000 in-lbs/° C-70 4500 in-lbs/° measured).

Blade flap bending and hub barrel out-of-plane data are presented in Figure 4-51. The C-70 prediction shows a lower growth rate of blade root out-of-plane bending (5500 in-lbs/° C-70 compared with 6500 in-lbs/° measured). The flap bending data at 10.5%R are shown to be over predicted.

At these conditions (140 kts, 10° i_N, 386 RPM) -2.66° A_1 and 2.31° B_1 were used to minimize alternating blade loads. With these cyclic settings the alternating blade root in-plane bending data, Figure 4-50, reached a minimum at about 11° incidence whereas the out-of-plane data minimized at about 9° incidence.

The minimum load levels observed are made up of the one per rev weight moment of the blade and air loads caused by hub motion or tunnel turbulence. In general these are low. The loads caused by angle of attack can be expressed as bending moment sensitivities, i.e., in-lbs/°. Figure 4-52 shows a summary of 140 kt blade load data from both tests with predictions as a function of blade radial station. The data shown at r/R = 0.039 are resolved into the blade system using hub barrel gage data. The C-70 predictions were done after the windmill test (410) and prior to the powered test (416). This method was not used for the

predictions of Reference 17 since the computer program was not operationally available at that time. At r/R = 10.5 the windmill test data indicate an increase in blade strain of 280 μi/in. per degree of angle of attack. C-70 overpredicts the strain increase at 325 μi/in. per degree of angle of attack (14% high). The predictions of Reference 17 predict a strain increase of 260 μi/in. per degree (8.9% low).

Blade load data measured at 170 knots on Run 14 of test 416 are shown in Figure 4.53. The cyclic settings used to minimize loads at 10° incidence were -2.97° A_1 and 3.38° B_1. The out-of-plane and in-plane bending loads again show minimum loads at different angles of attack 10° and 12° respectively.

Further blade load correlation at 140 knots and 192 knots is shown in Figures 4.54 to 4.57. The predicted data is taken from Reference 17. These predictions make no allowance for weight moment loads or hub motions, etc., and result in a theoretical zero load at zero incidence. The measured loads do not go to zero but a small finite value. If an allowance is made for non-zero minimum loads, i.e., the predicted line increased by the measured minimum loads, the maximum loads in the useful angle of attack range are adequately predicted to establish blade load limitations.

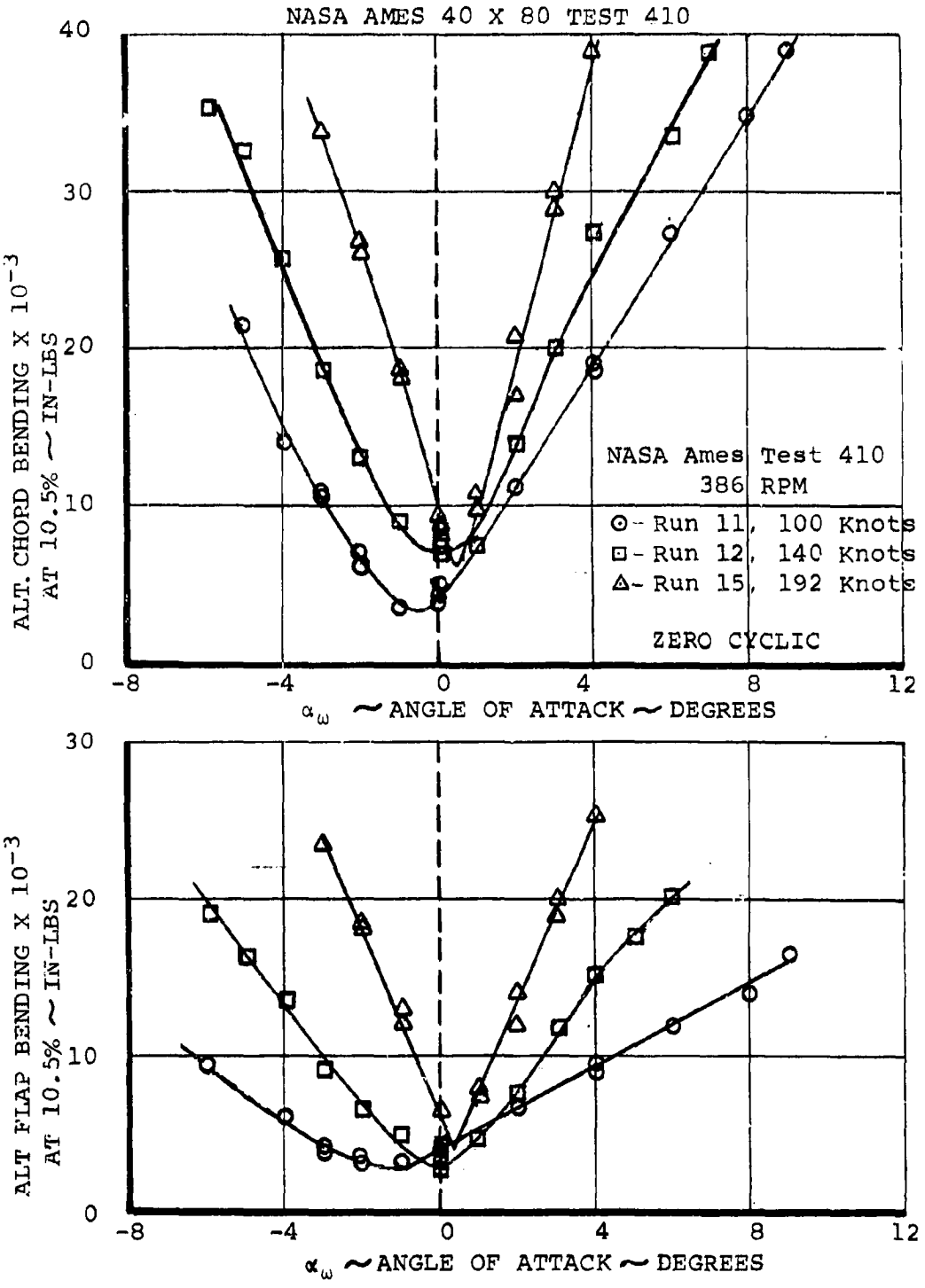

Figure 4.45 . Effect of Airspeed and Attack Angle on Alternating Blade Loads, r/R = 10.5%, 386 RPM

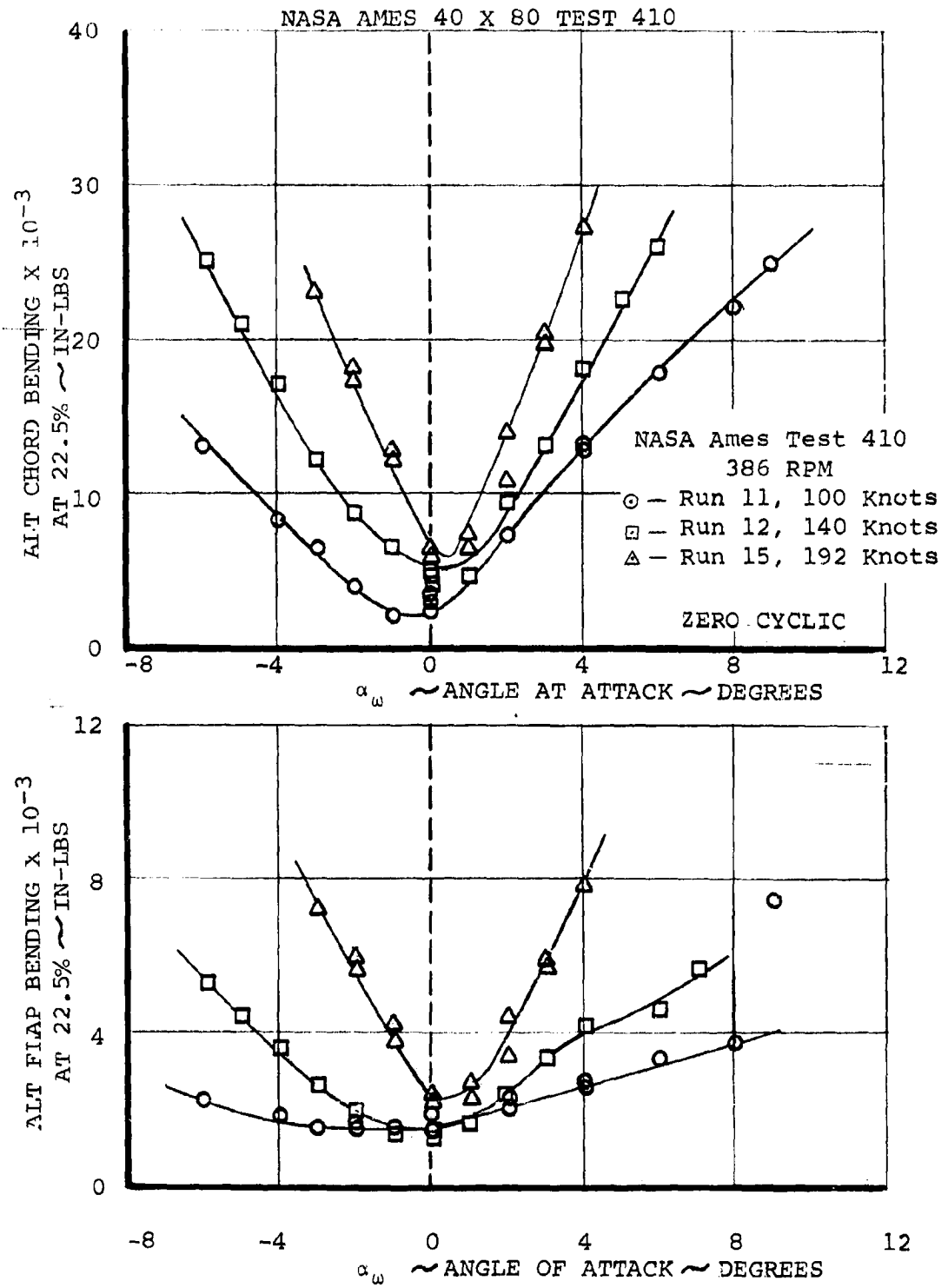

Figure 4.46. Effect of Airspeed and Attack Angle on Alternating Blade Loads, r/R = 22.5%, 386 RPM

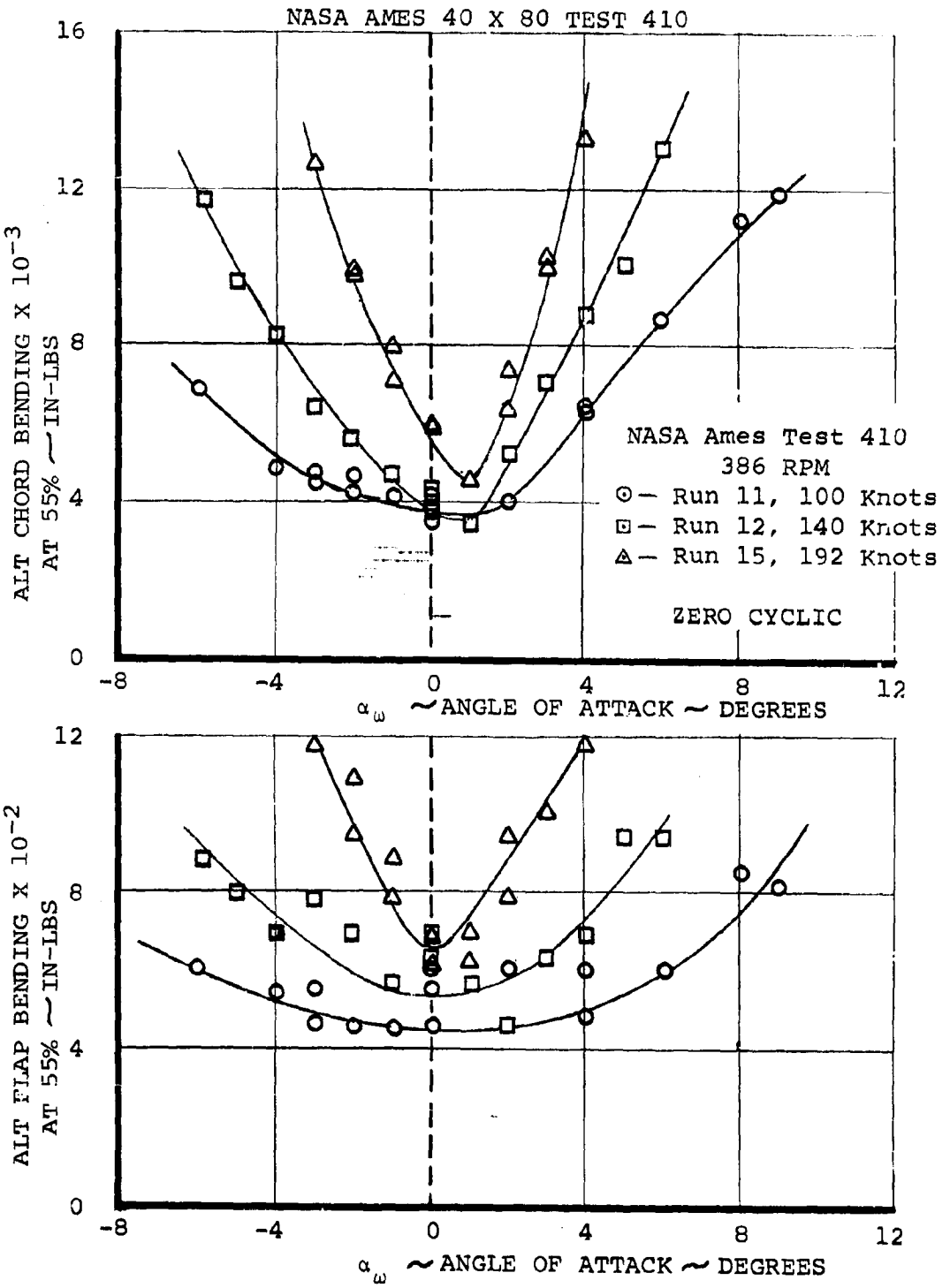

Figure 4.4.7. Effect of Airspeed and Attack Angle on Alternating Blade Loads, r/R = 55%, 386 RPM

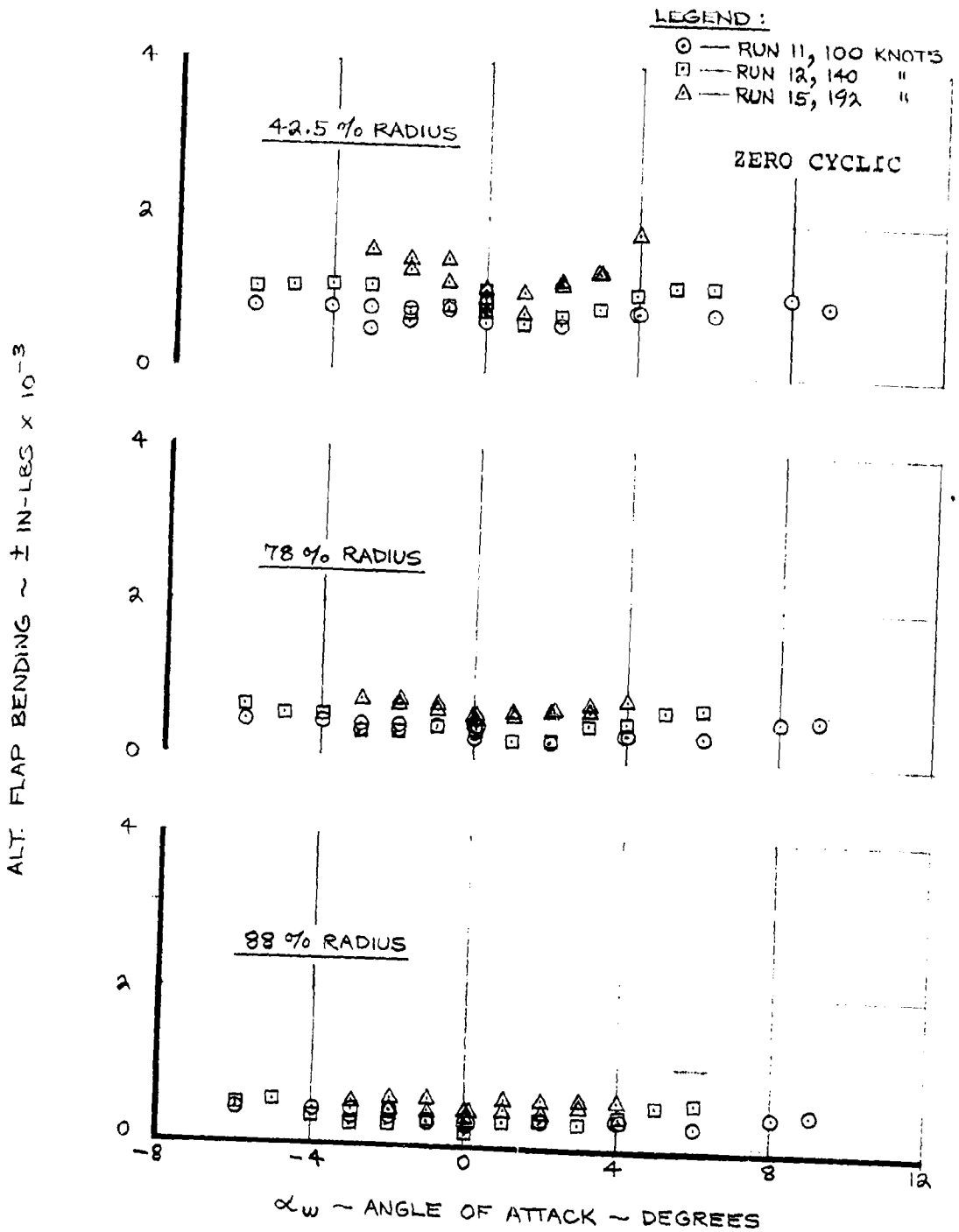

FIGURE 4.48 ALTERNATING BLADE FLAP BENDING DUE TO ANGLE OF ATTACK, 386 RPM

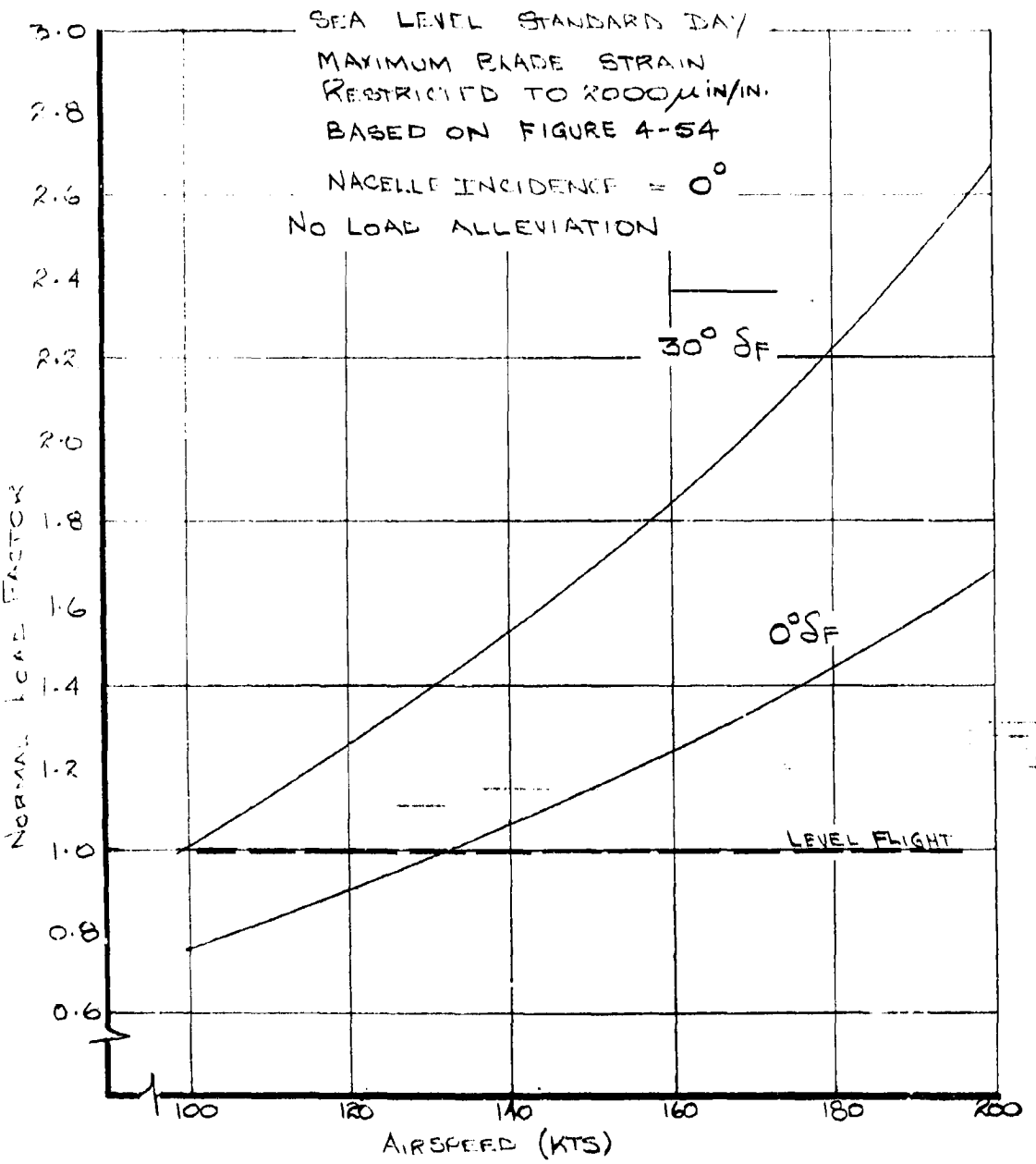

FIGURE 4.49. EFFECT OF MEASURED BLADE LOAD LIMITS ON AIRPLANE LOAD FACTOR-NACELLE INCIDENCE ZERO

NASA AMES TEST 4-16
RUN 11
386 ROTOR RPM
$\theta_{.75} = 35.1°$
140 KNOTS
$A_1 = -2.66°$
$B_1 = 2.31°$
$\Delta\theta = -A_1 \cos(\psi + 20) - B_1 \sin(\psi + 20)$

⊙ — 55 % CHORD
⊡ — HUB (IN PLANE) 3.9%R

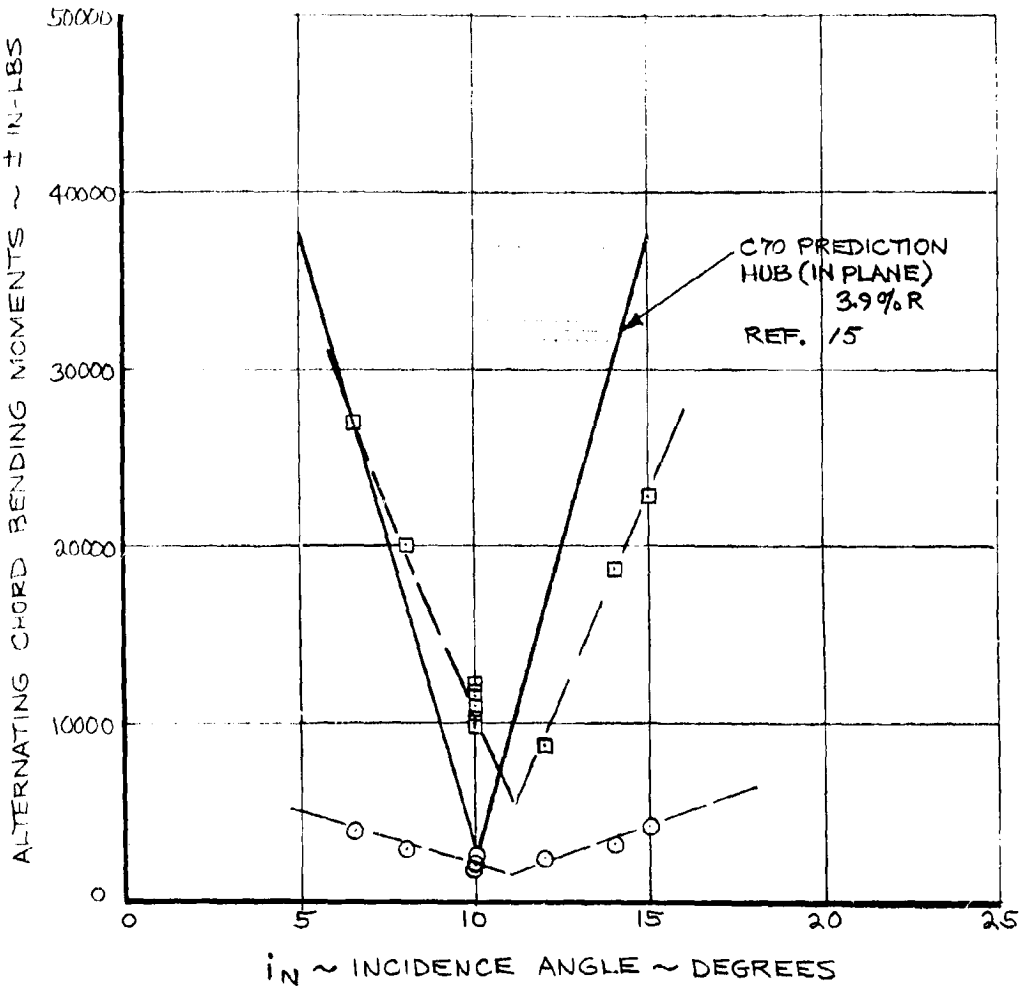

Figure 4.4.6. Alternating Blade Chord Bending Due to Incidence Angle 140 Knots, 386 RPM

NASA AMES TEST 416

RUN 11

386 ROTOR RPM

$\theta_{.75} = 35.1°$

140 KNOTS

$A_1 = -2.66°$

$B_1 = 2.31°$

⊙ —— 10.5 % FLAP

⊡ —— HUB (OUT OF PLANE) 3.9 %R

△ —— 55 % FLAP

$$\Delta\theta = -A_1 \cos(\psi + 20) - B_1 \sin(\psi + 20)$$

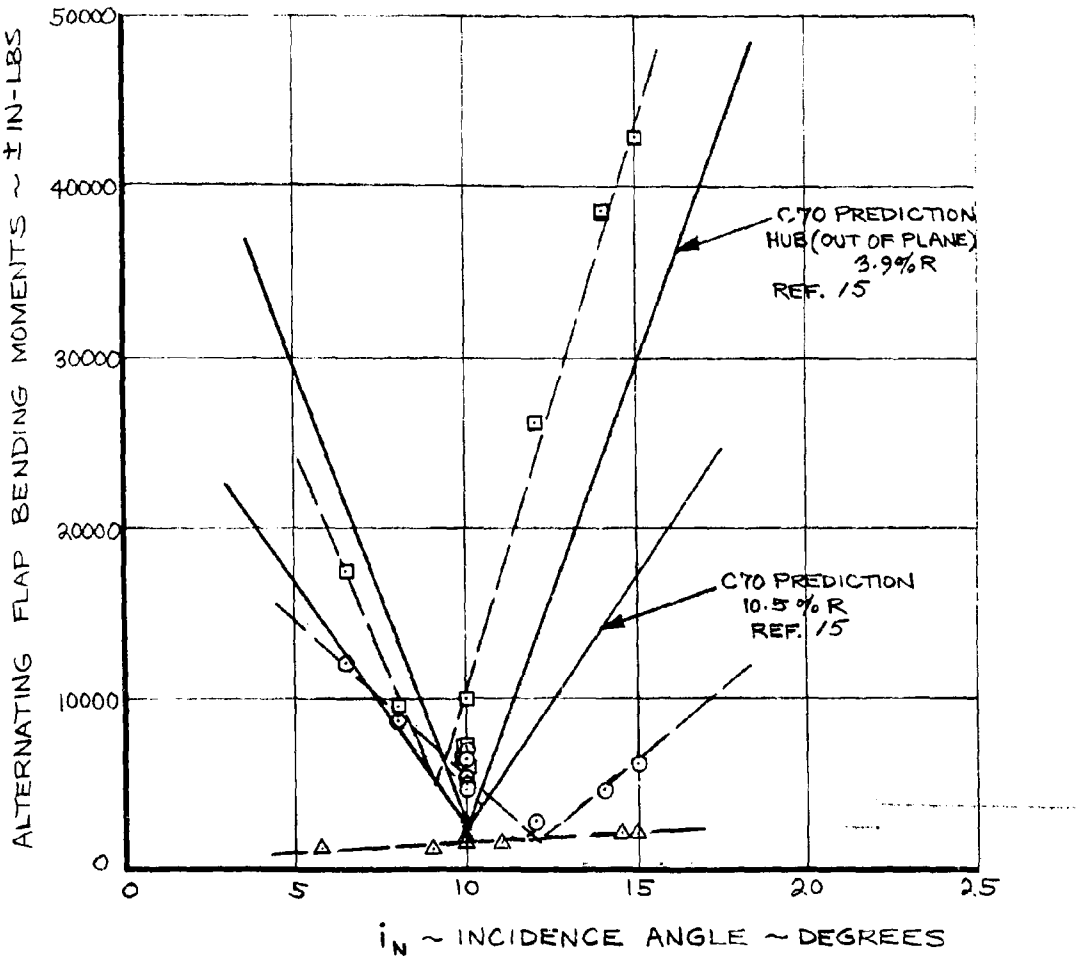

Figure 4.51 . Alternating Blade Flap Bending Due to Incidence Angle 140 Knots, 386 RPM

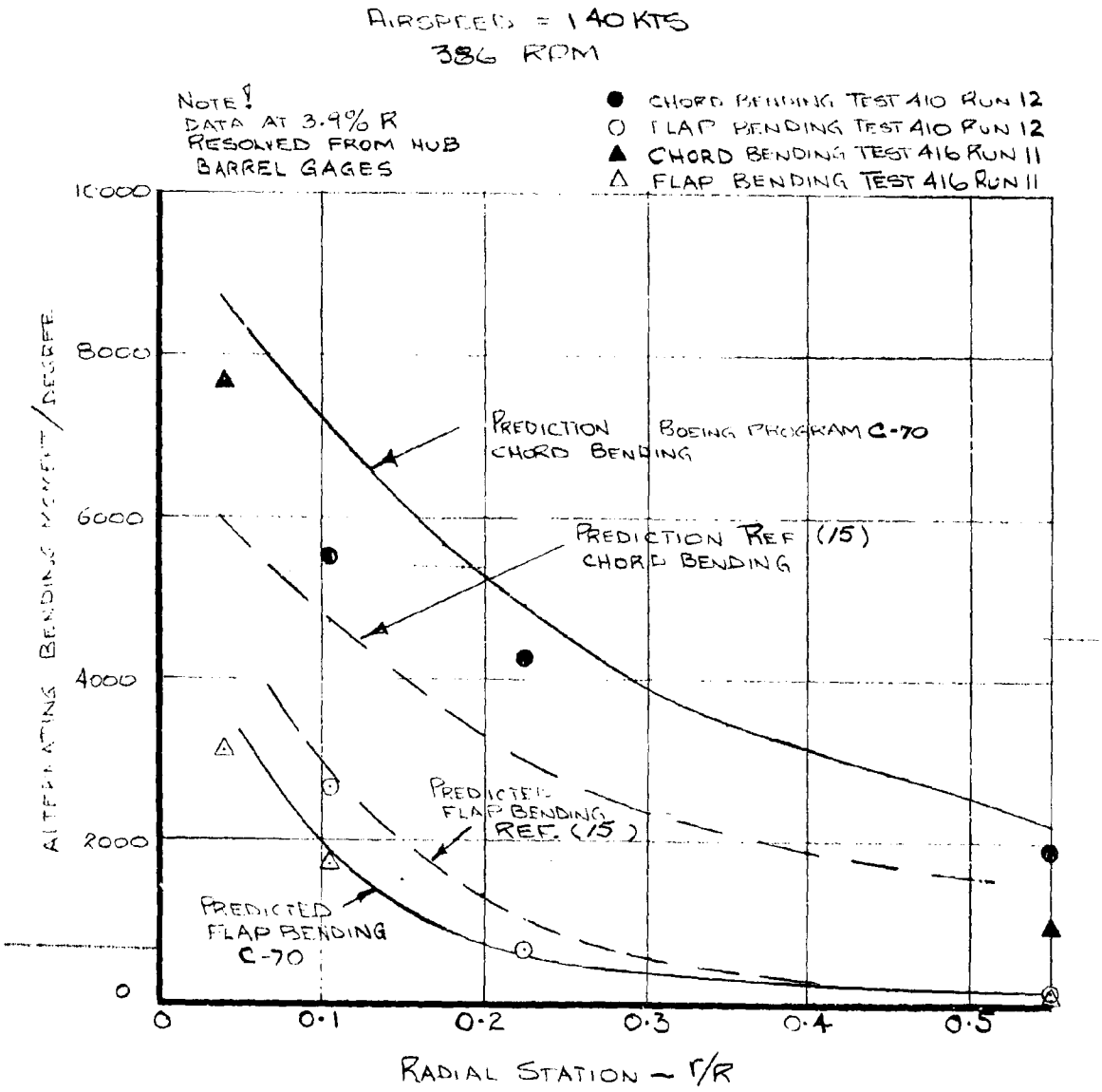

FIGURE 4.52 CORRELATION OF RADIAL DISTRIBUTION OF BLADE LOADS DUE TO ANGLE OF ATTACK, IN CRUISE

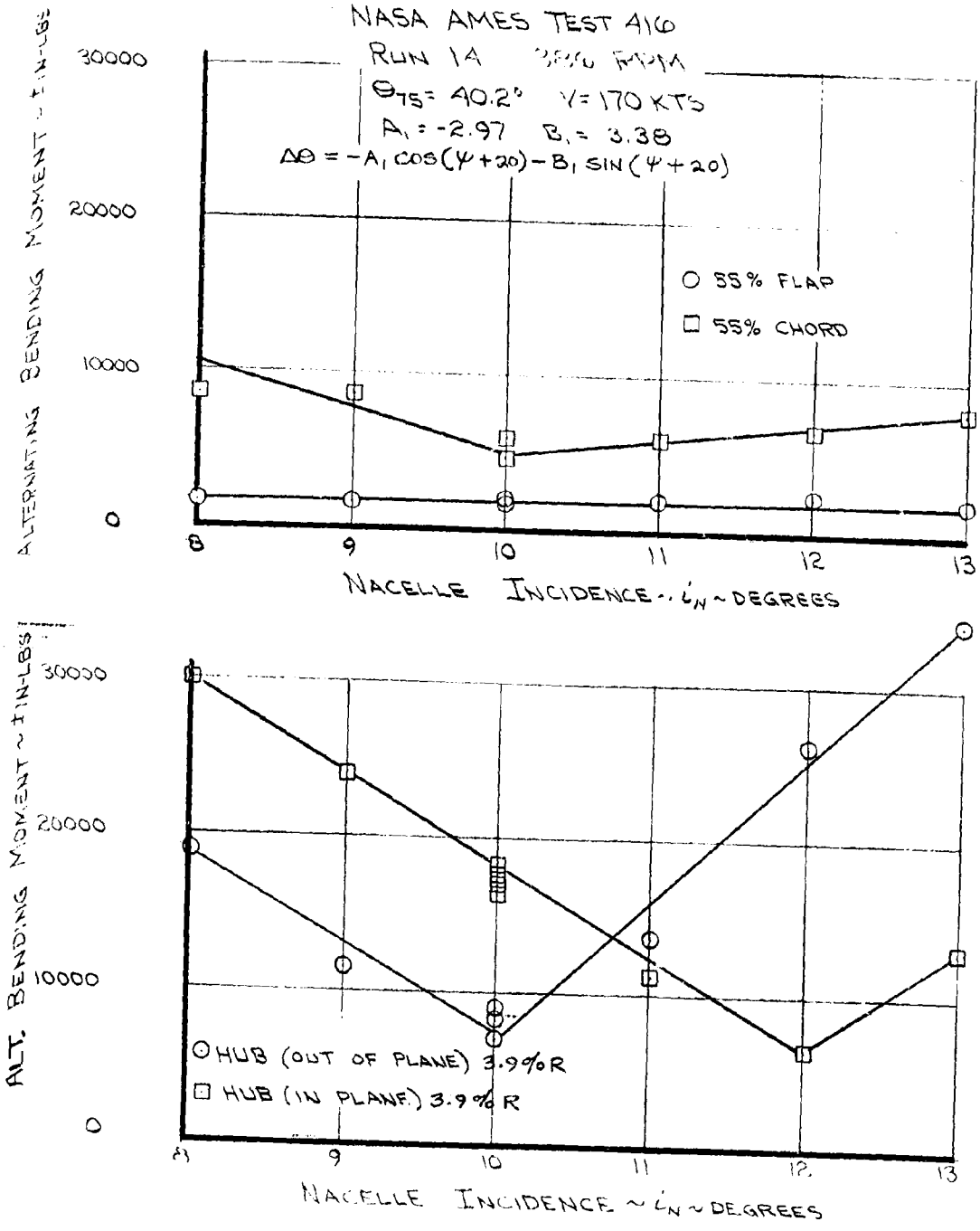

FIGURE 4.53 ALTERNATING BLADE LOADS DUE TO INCIDENCE ANGLE - V = 170 KNOTS

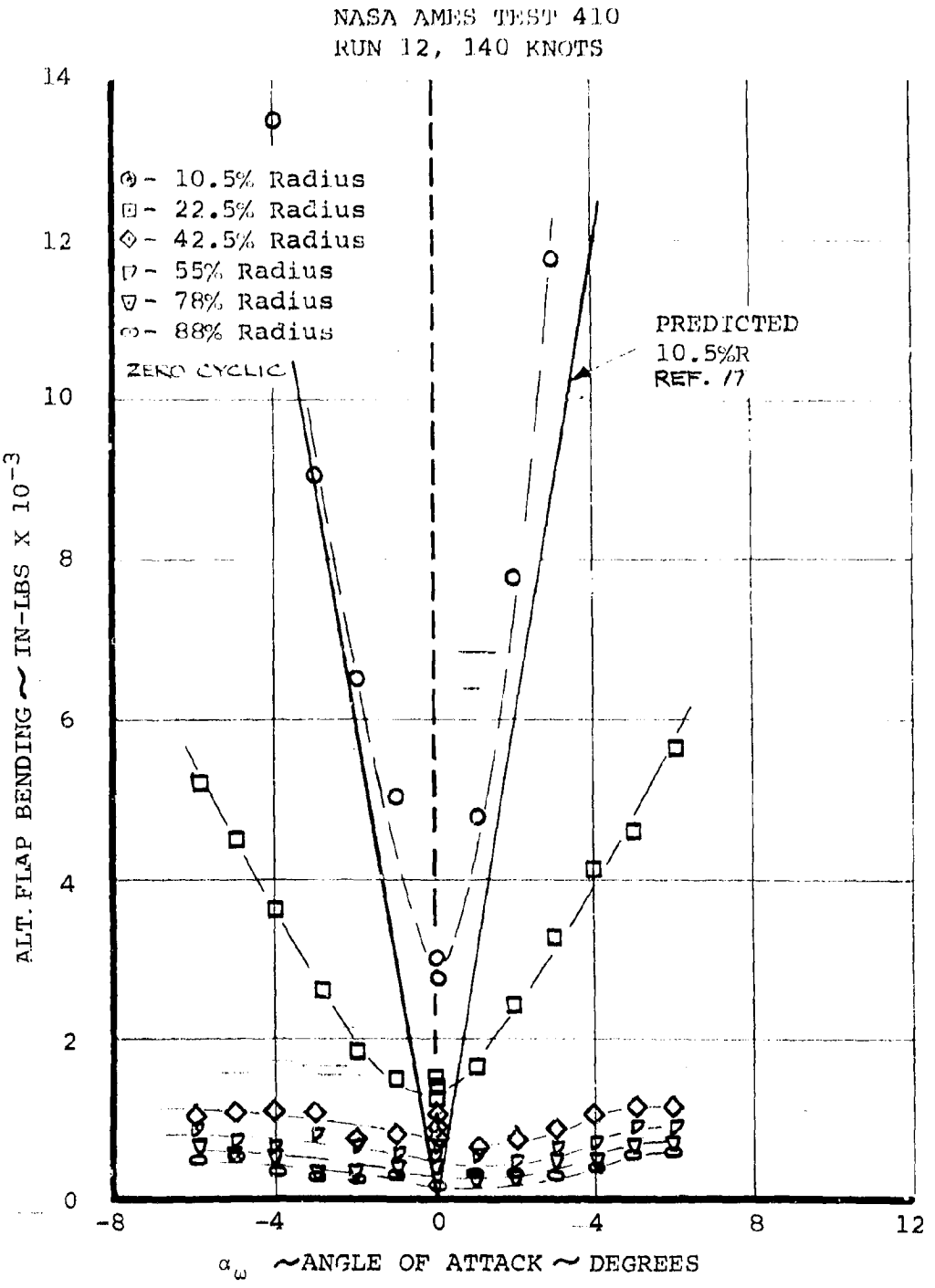

Figure 4.54. Alternating Blade Flap Bending Due to Angle of Attack, 140 Knots, 386 RPM

NASA AMES TEST 410
RUN 12, 140 KNOTS, 386 RPM

⊙- 10.5% Radius
□- 22.5% Radius
◇- 55% Radius

ZERO CYCLIC

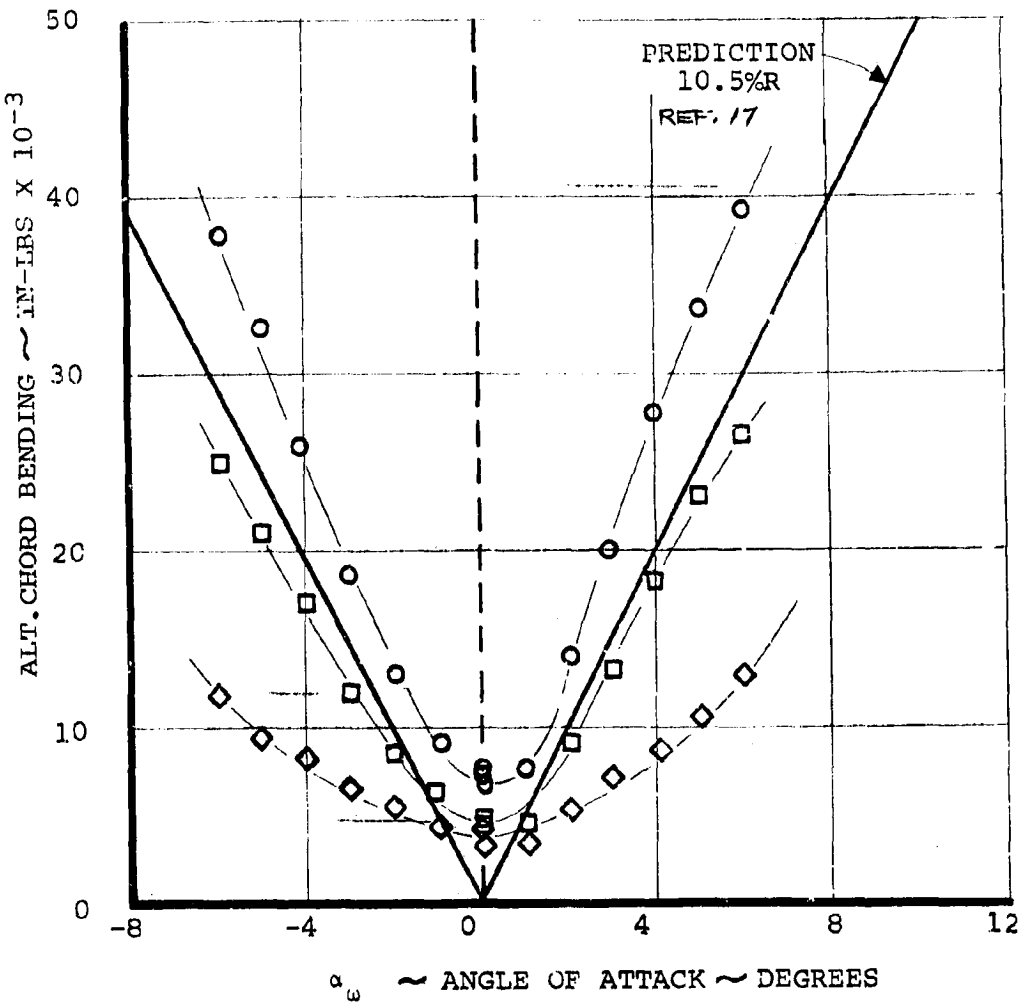

Figure 4.55. Alternating Blade Chord Bending Due to Angle of Attack, 140 Knots, 386 RPM

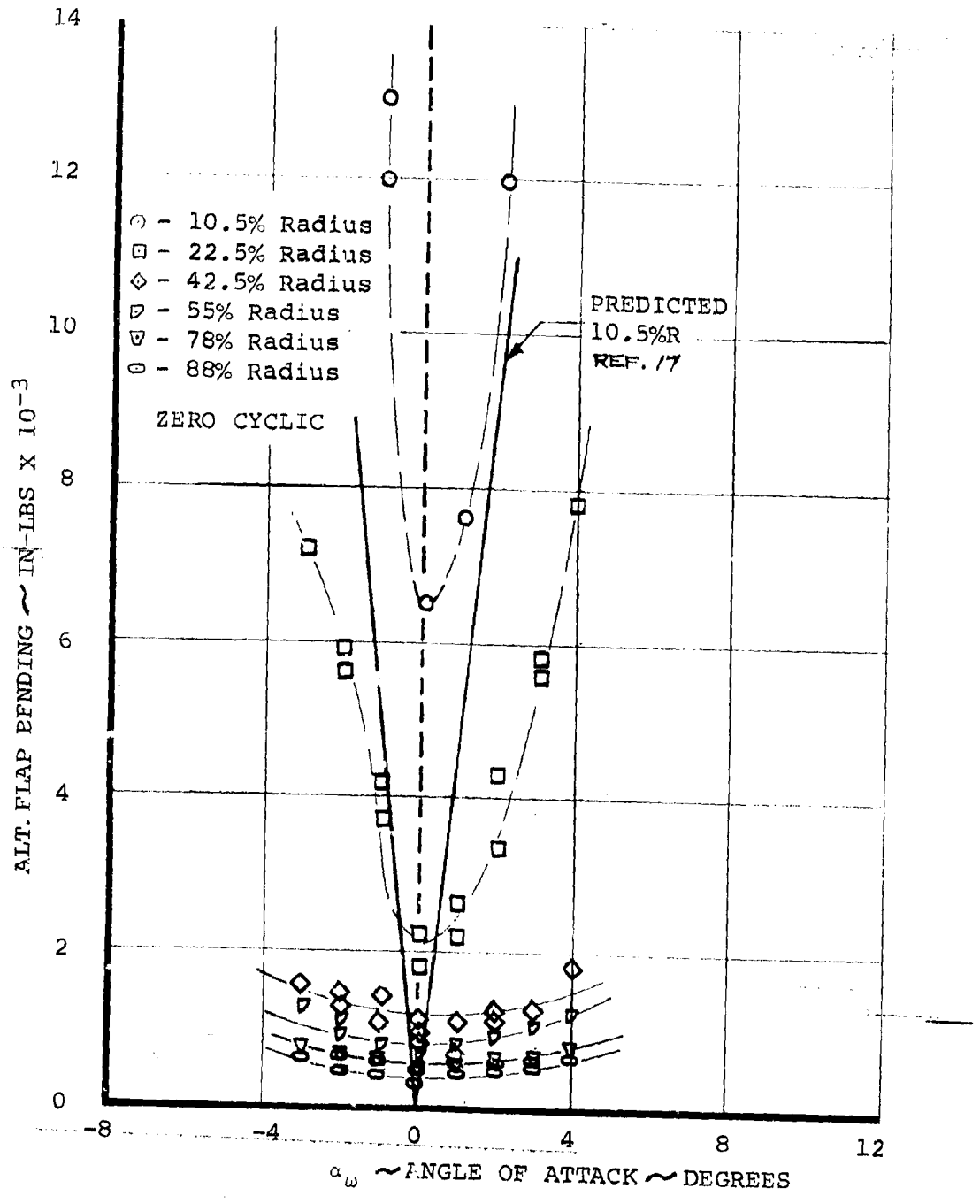

Figure 4.56. Alternating Blade Flap Bending Due to Angle of Attack, 192 Knots, 386 RPM

NASA AMES TEST 410
RUN 15, 192 KNOTS, 386 RPM

○- 10.5% Radius
⊡- 22.5% Radius
◇- 55% Radius

ZERO CYCLIC

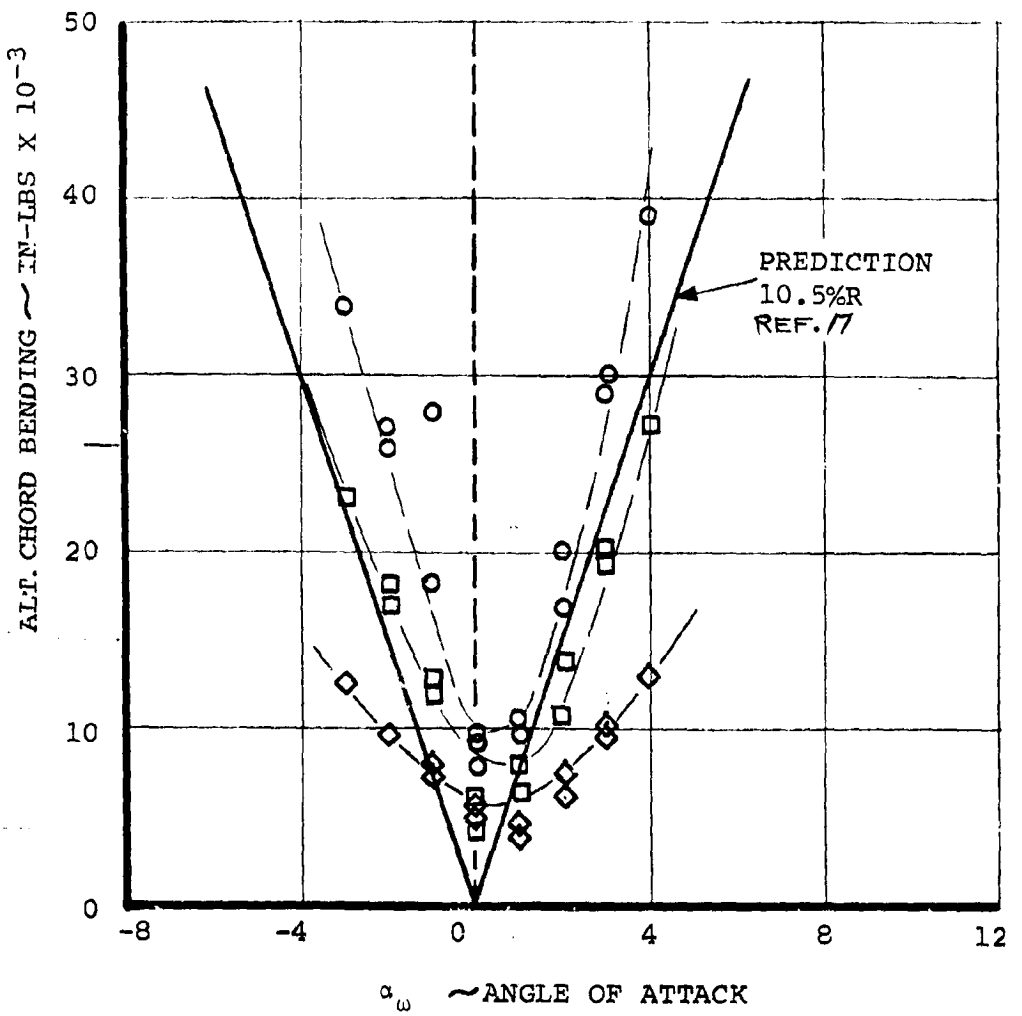

Figure 4.57. Alternating Blade Chord Bending Due to Angle of Attack, 192 Knots, 386 RPM

Effect of Cyclic Pitch

In the cruise flight mode cyclic pitch can be used to alleviate the blade loads caused by shaft incidence, maneuver load, factor and gusts. The sensitivities of alternating blade loads to cyclic pitch are summarized in Figures 4-58 to 4-63 for blade radial stations 10.5%R, 22.5%R and 55%R. The cyclic pitch inputs made during these tests were such that the first harmonic of blade angle is defined by

$$\Delta\theta = -A_{1\cos}(\psi + 20) - B_{1\sin}(\psi + 20)$$

(see Figure 4-24).

The effect of A_1 and B_1 at 10.5%R is shown in Figures 4-58 and 4-59. For A_1 inputs, Figure 4-58, the alternating chord bending increases with cyclic at a rate which appears to be independent of airspeed (18,000 in-lbs/deg). For B_1 inputs the 140 and 192 knot data show similar behavior (17,500 in-lbs/deg). The 100 kt data for B_1 inputs shows much lower loads. The alternating flap bending shows a rise in sensitivity to cyclic pitch as airspeed increases for both A_1 and B_1 applications. The alternating flap bending loads are generally about half of the alternating chord bending magnitudes resulting in a lesser effect on the blade root alternating strain.

At 22.5%R (Figures 4-60 and 4-61) the alternating blade loads are lower than at 10.5%R but exhibit similar variations. In Figure 4-61 the alternating chord bending shows a tendency to increase with airspeed not previously observed at 10.5%R.

At 55%R (Figures 4-62 and 4-63) the blade loads are lower still. The alternating chord bending is insensitive to airspeed for A_1 control inputs. B_1 control inputs show a slight increase in load sensitivity as airspeed increases. At 55%R the alternating flap bending loads are an order of magnitude less than alternating chord bending.

The outboard flap bending gages at 42.5, 78 and 88%R show low loads which are unaffected by cyclic pitch, Figures 4-64 to 4-66.

Figures 4-67 to 4-72 show correlation of alternating blade loads at 10.5% radius with A_1 and B_1 cyclic inputs. The predictions are taken from Reference 17.

The rate at which alternating chord bending loads increase with cyclic pitch is quite well predicted and if allowance were made for the minimum blade load levels the absolute loads would be overpredicted in the useful cyclic operating

range. The flap bending data show higher sensitivities to cyclic than do the predictions at higher speeds and the minimum load level of typically 3000 in-lbs does not help the correlation. The alternating flap bending loads are low compared with chord bending and have much less effect on absolute blade strain levels.

The radial distribution of measured blade loads due to cyclic pitch at 140 kts are shown in Figure 4-73. These measured distributions have been used to extrapolate the predicted data given at 10.5% radius in Reference 17 in order to provide a comparison with hub gage data obtained during test 416.

The alternating loads measured on Run 11 of test 416 at 10° incidence and 140 kts are shown in Figures 4-74 to 4-77.

For the purpose of comparison of cyclic effects the minimum predicted load is assumed to be at the minimum load cyclic value defined on test. The growth of alternating blade root loads as cyclic pitch is either increased or decreased about the minimum load cyclic settings are shown to correlate. At this flight condition -2.66° A_1 and 2.31° B_1 were required to keep the alternating blade loads at a minimum.

Experimental data at 170 kts and 10° incidence are shown in Figures 4-78 and 4-79. At this condition -2.97° A_1 and 3.38° B_1 were used to minimize blade loads.

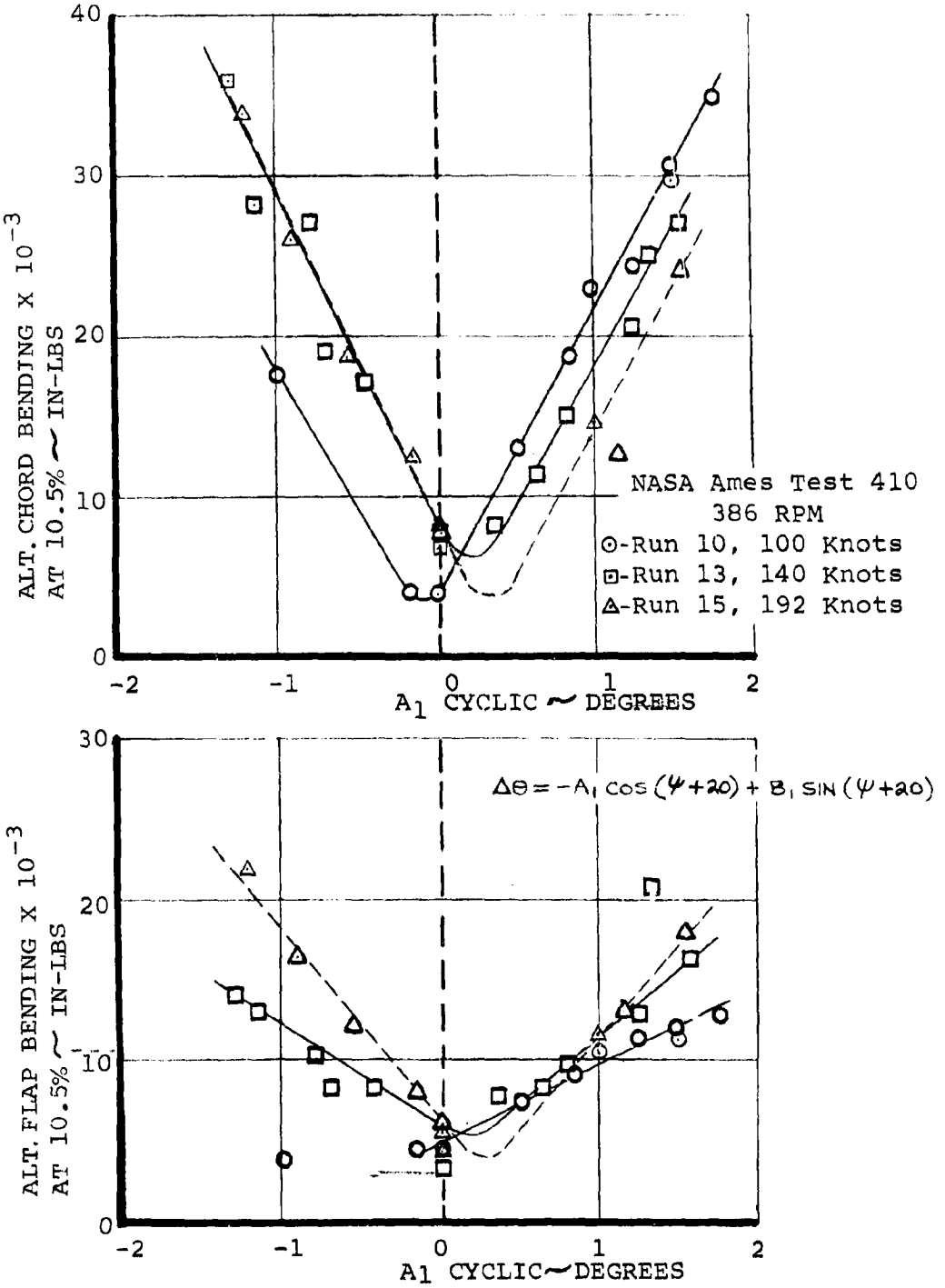

Figure 4.58. Effect of Lateral Cyclic and Airspeed on Alternating Blade Loads, 10.5%R, 386 RPM

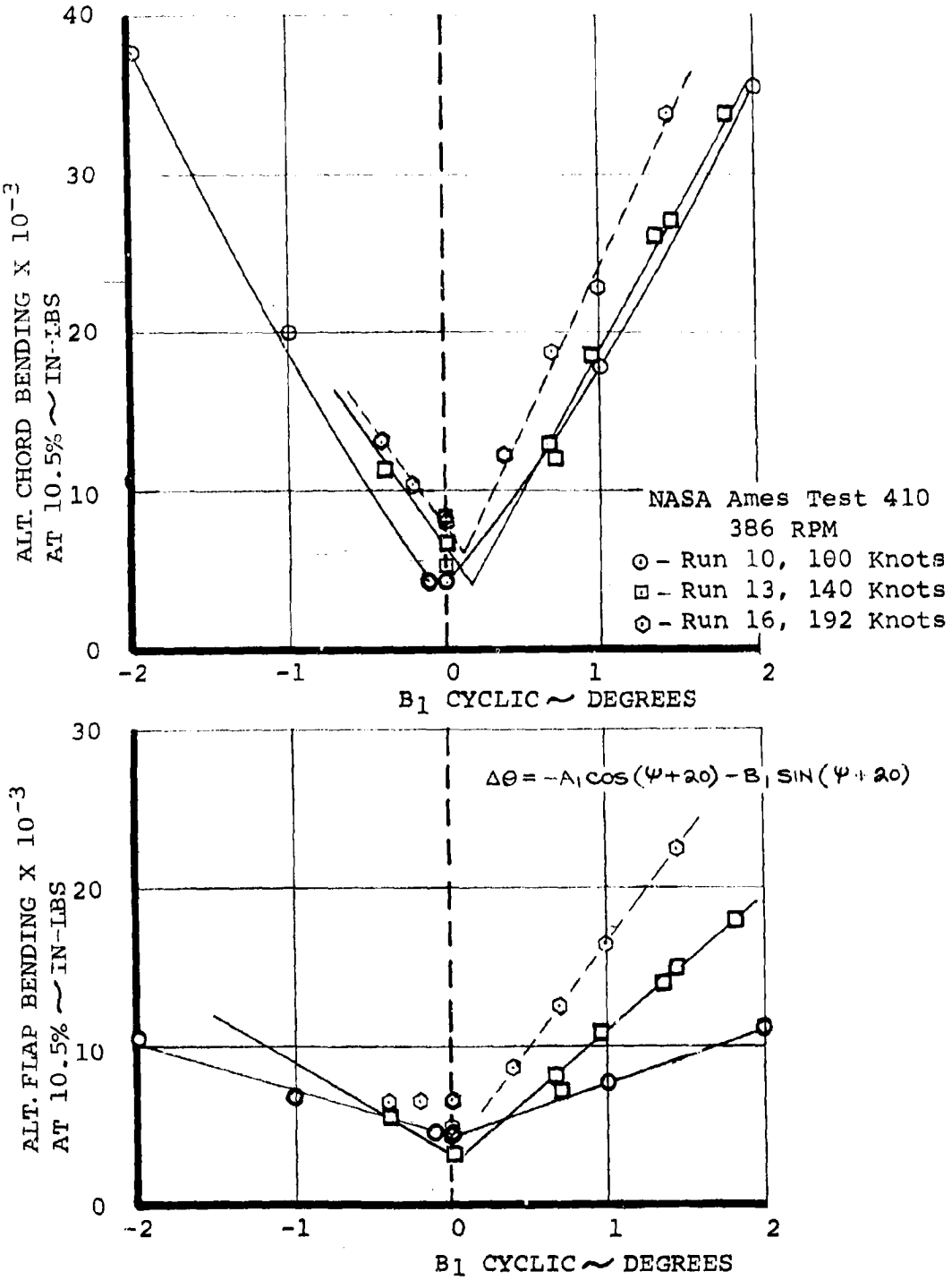

Figure 4.59 . Effect of Longitudinal Cyclic and Airspeed on Alternating Blade Loads, 10.5%R, 386 RPM

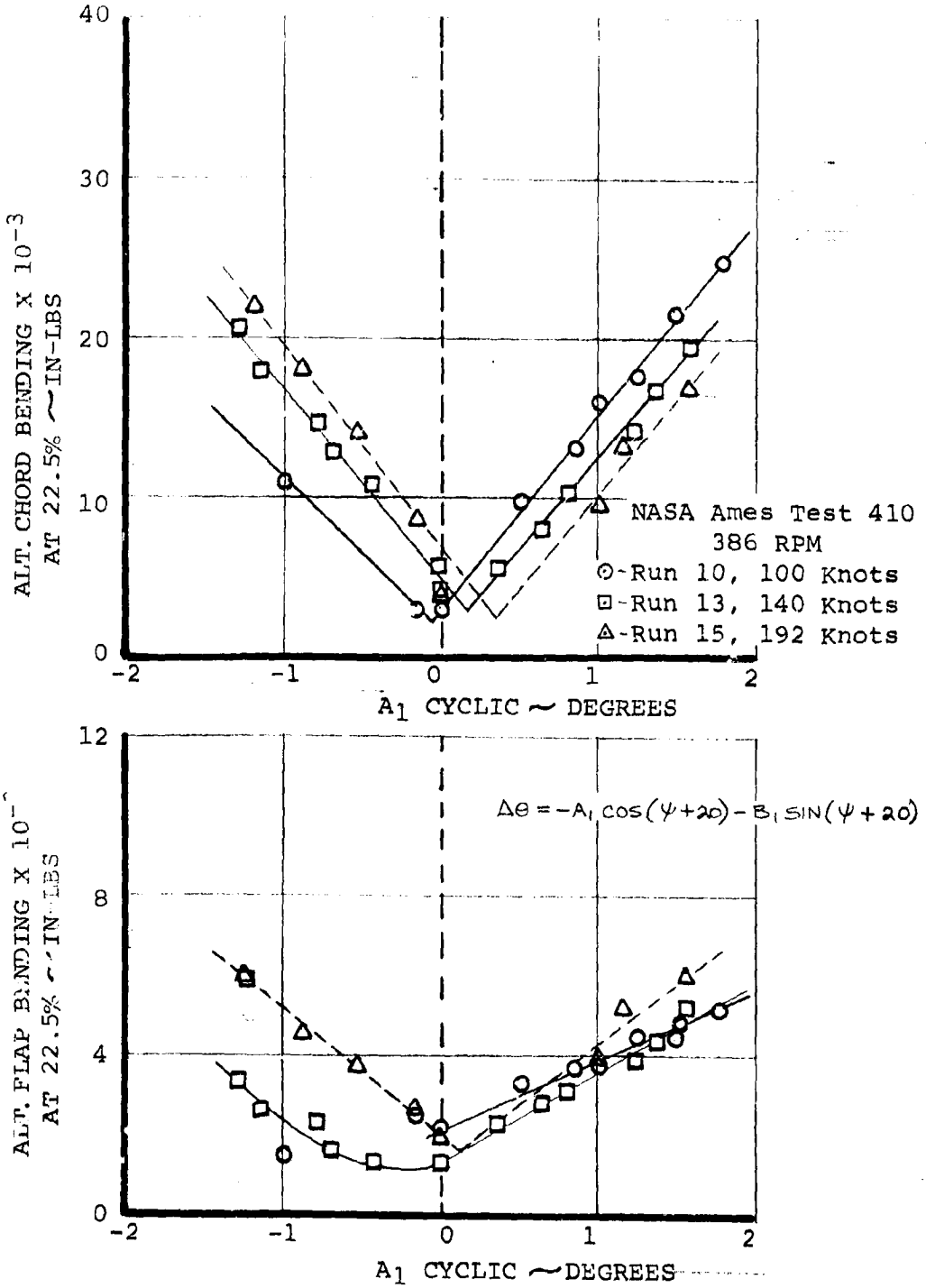

Figure 4.60. Effect of Lateral Cyclic and Airspeed on Alternating Blade Loads, 22.5%R, 386 RPM

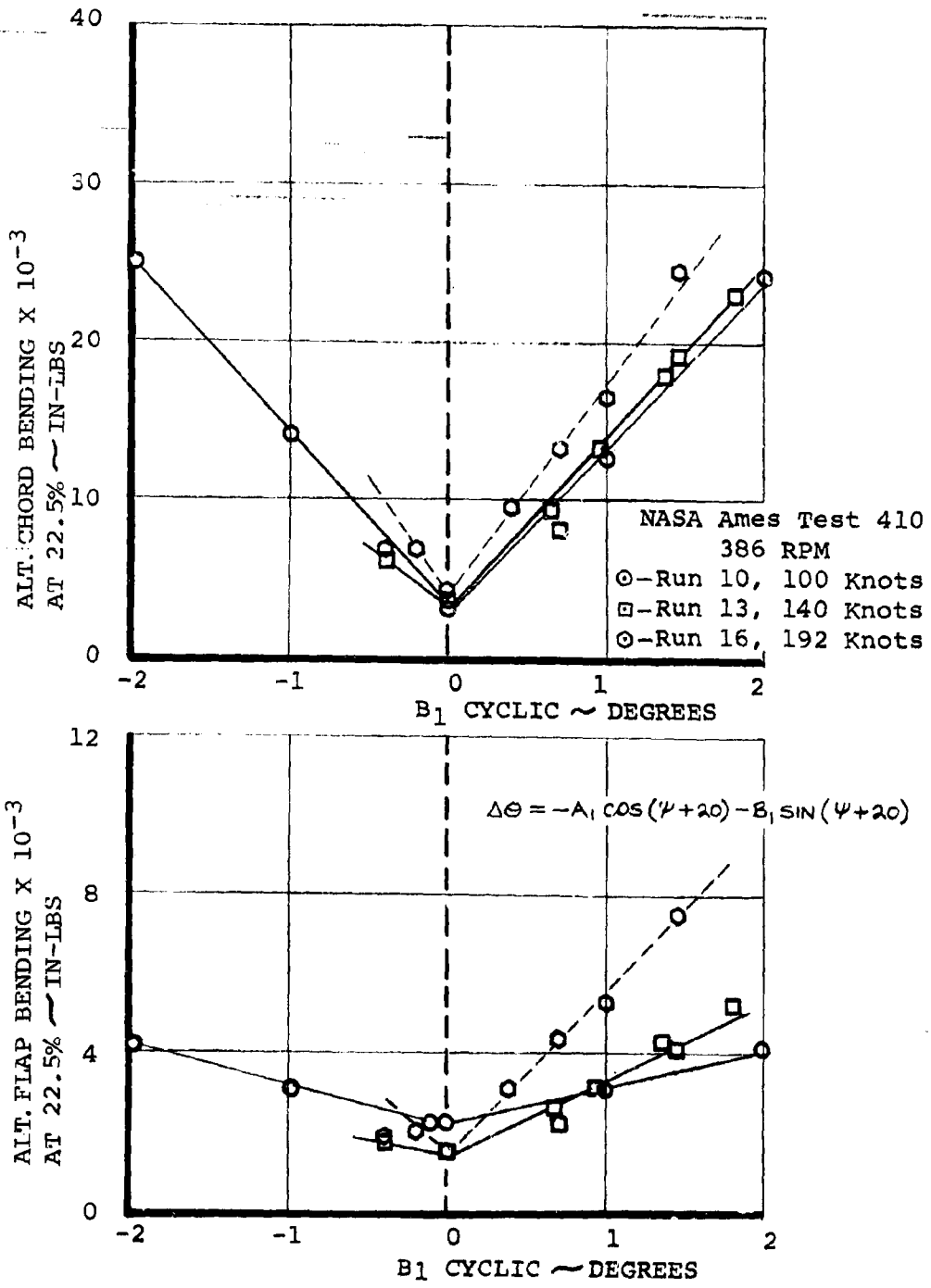

Figure 4.61 . Effect of Longitudinal Cyclic and Airspeed on Alternating Blade Loads, 22.5%R, 386 RPM

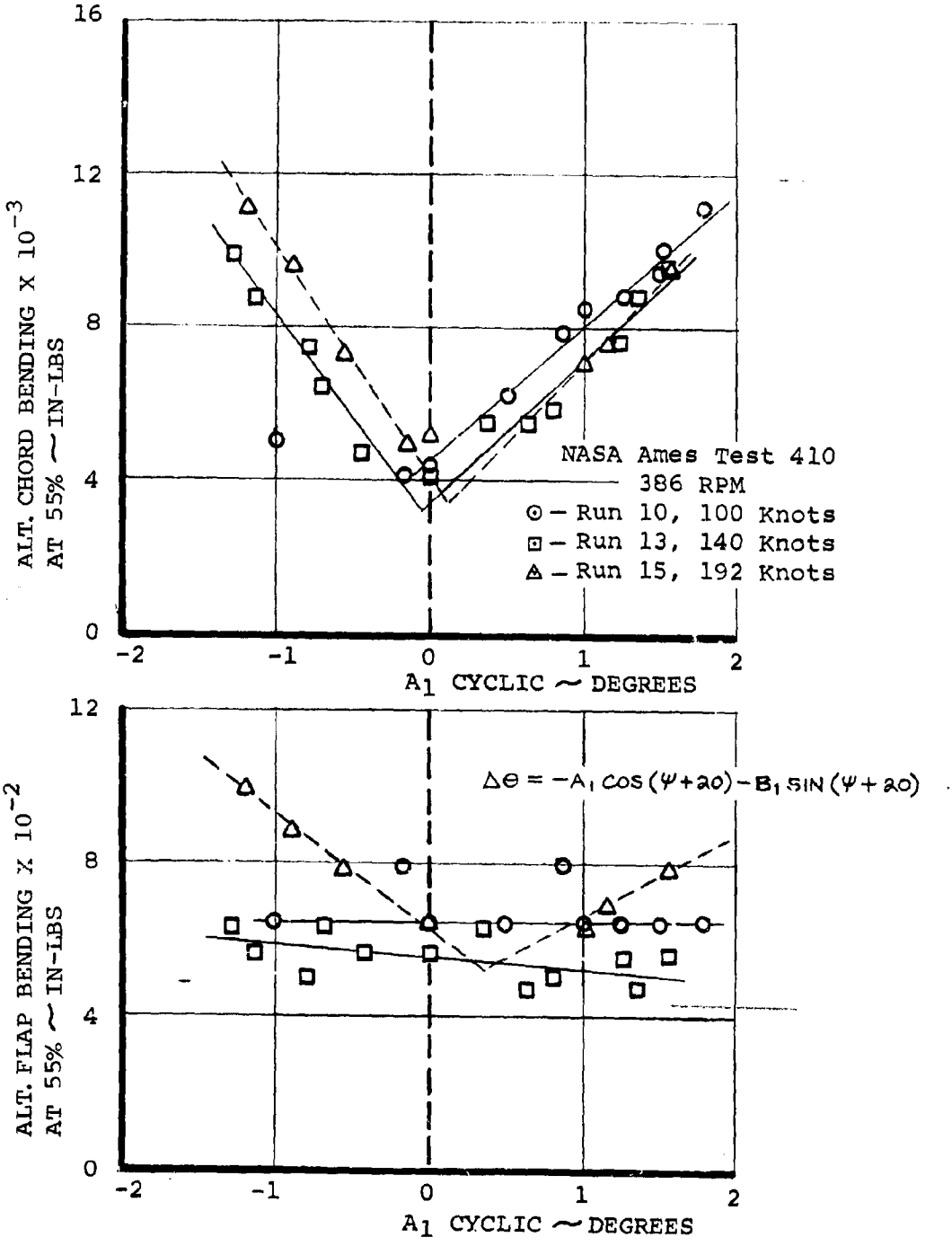

Figure 4.62 . Effect of Lateral Cyclic and Airspeed on Alternating Blade Loads, 55%R, 386 RPM

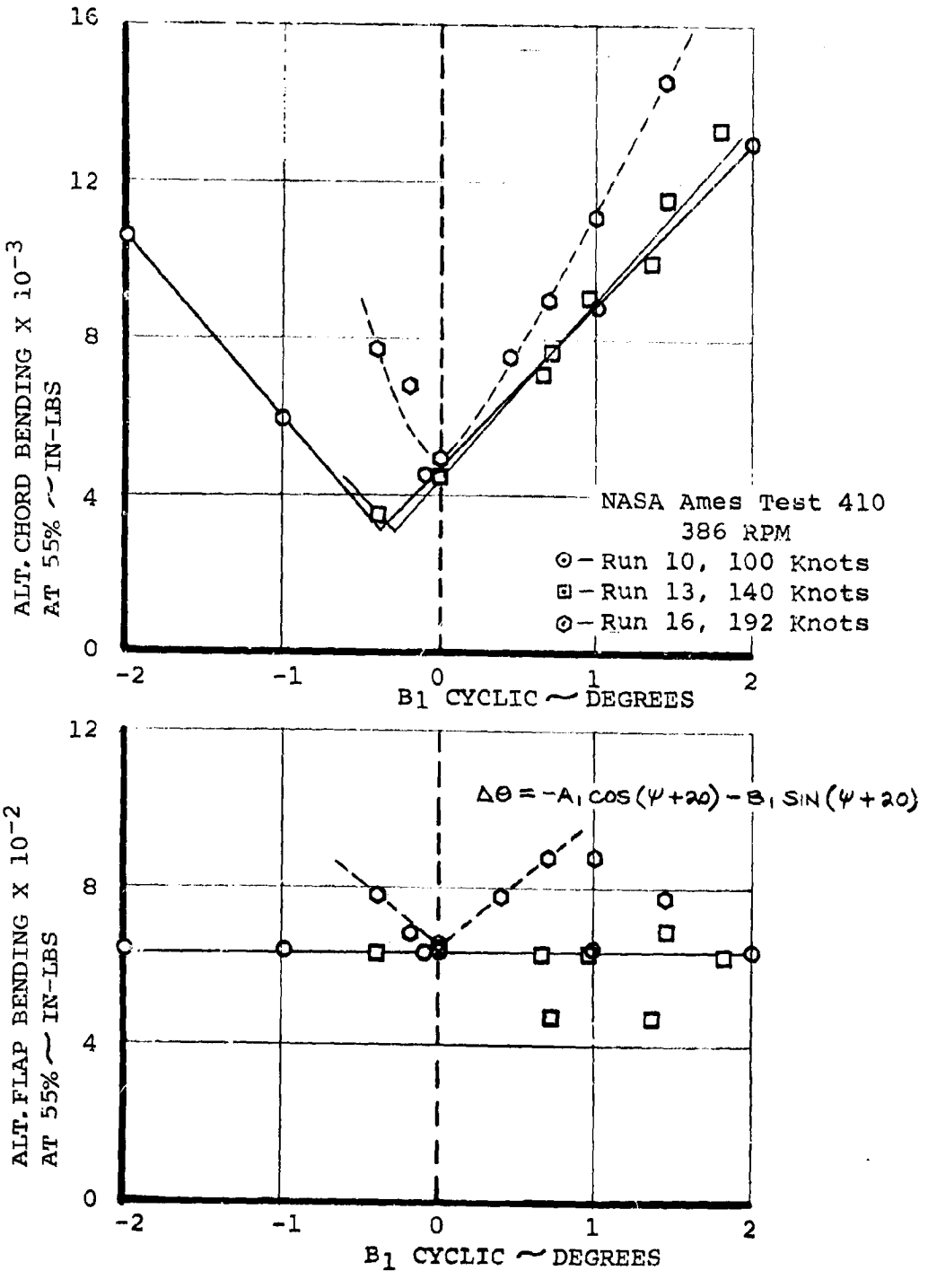

Figure 4.63. Effect of Longitudinal Cyclic and Airspeed on Alternating Blade Loads, 55%R, 386 RPM

NASA AMES TEST 410
RUN-10
100 KNOTS
386 RPM

$\Delta\theta = -A_1 \cos(\psi+20) - B_1 \sin(\psi+20)$

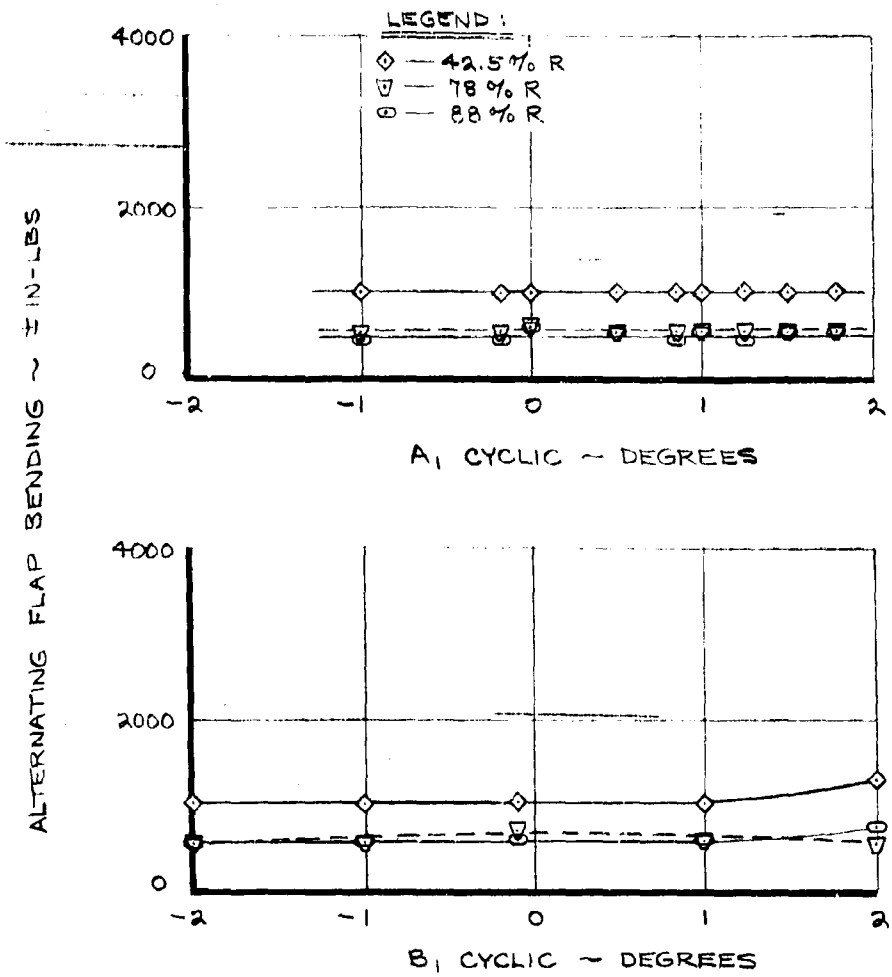

FIGURE 4.64 EFFECT OF A_1 AND B_1 CYCLIC ON ALTERNATING BLADE FLAP BENDING LOADS, 42.5% R, 78% R, 88% R - 100 KNOTS, 386 RPM

NASA AMES TEST 410

RUN 13

140 KNOTS

386 RPM

$\Delta\theta = -A_1 \cos(\psi + 20) - B_1 \sin(\psi + 20)$

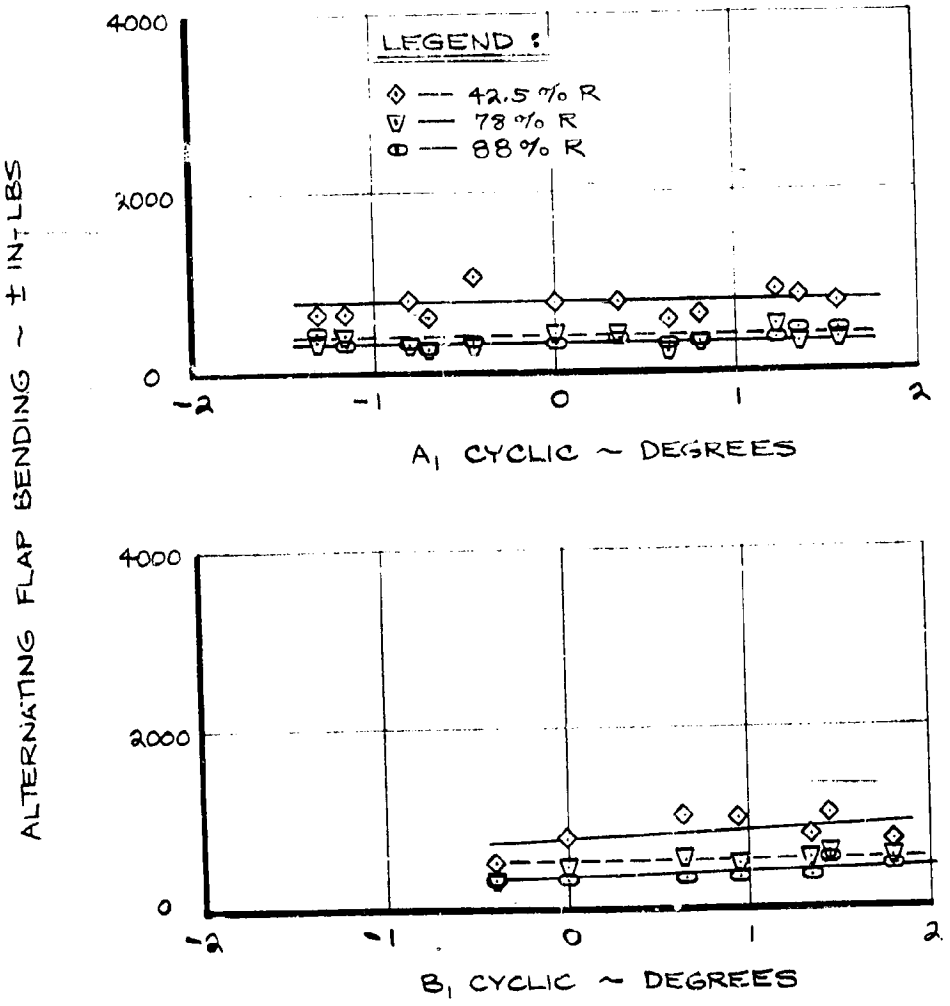

FIGURE 4.65 EFFECT OF A_1 AND B_1 CYCLIC ON ALTERNATING BLADE FLAP BENDING LOADS, 42.5 %R, 78 %R, 88 %R - 140 KNOTS, 386 RPM

NASA AMES TEST 410
192 KNOTS
386 RPM

$$\Delta\theta = -A_1 \cos(\psi + 20) - B_1 \sin(\psi + 20)$$

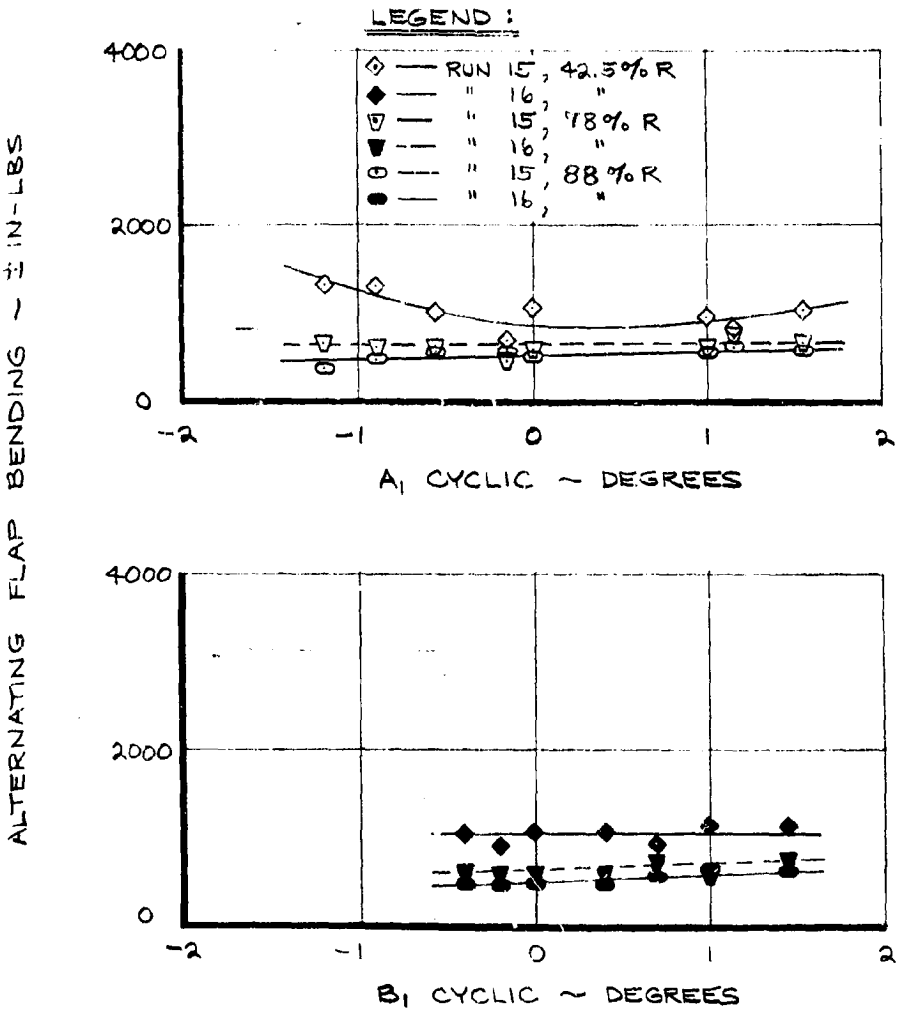

FIGURE 4.66 EFFECT OF A_1 AND B_1 CYCLIC ON ALTERNATING BLADE FLAP BENDING LOADS, 42.5%R, 78%R, 88%R - 192 KNOTS 386 RPM

NASA AMES TEST 410
RUN 10, 100 KNOTS, 386 RPM

$$\Delta\theta = -A_1 \cos(\psi + 20) - B_1 \sin(\psi + 20)$$

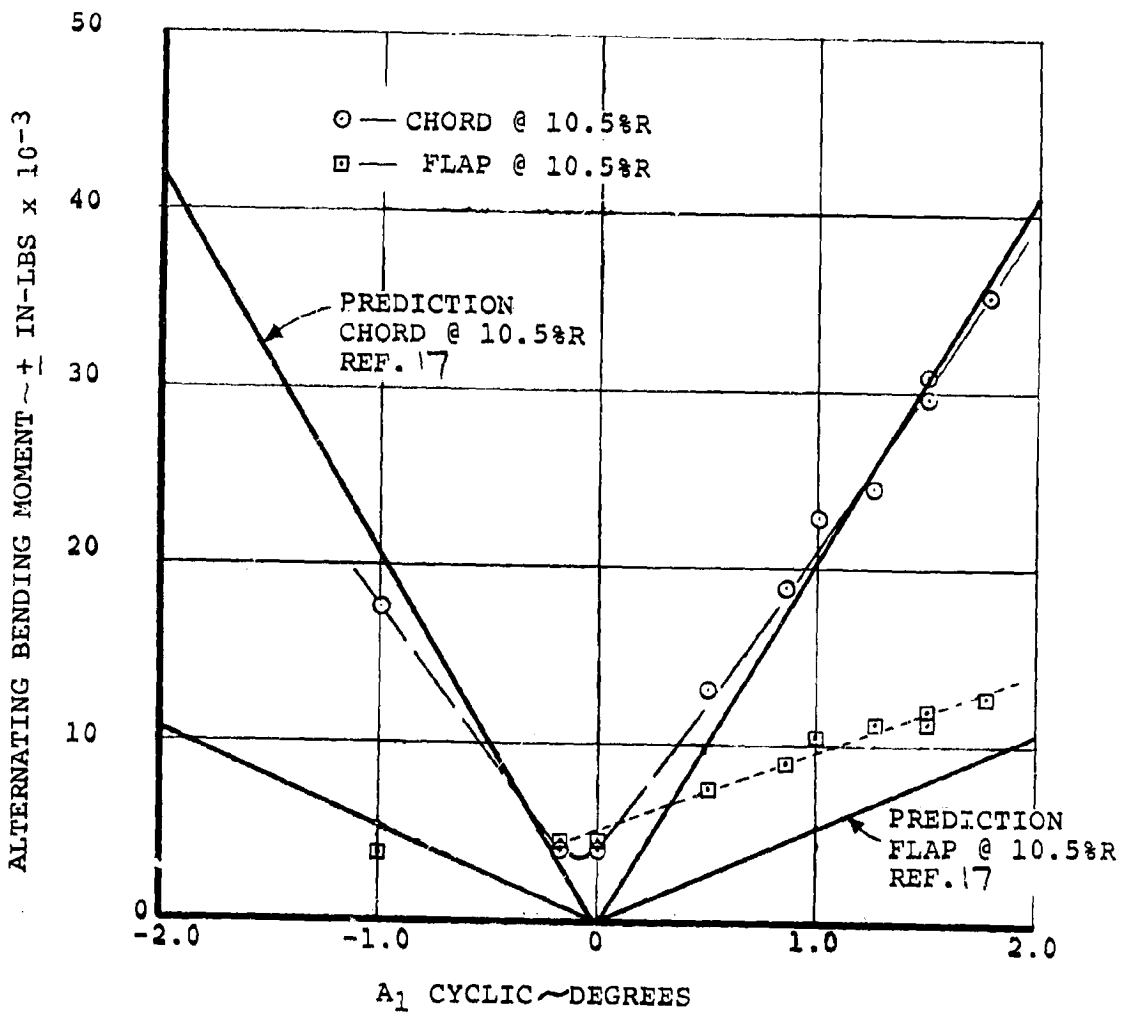

Figure 4.67. Effect of Lateral Cyclic on Alternating Flap and Chord Bending @ 10.5% R, 100 Knots, 386 RPM

NASA AMES TEST 410
RUN 10, 100 KNOTS, 386 RPM

$$\Delta\theta = -A_1 \cos(\psi + 20) - B_1 \sin(\psi + 20)$$

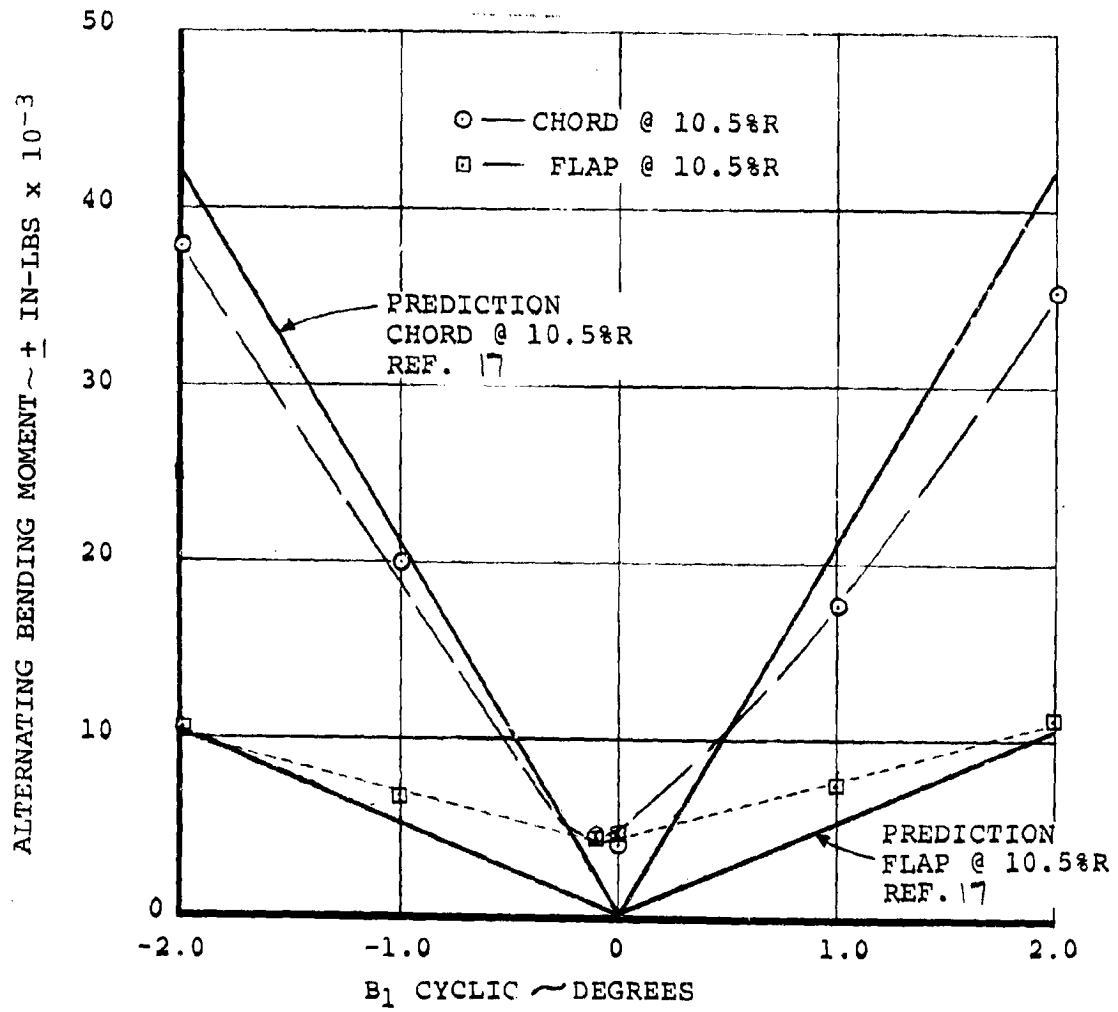

Figure 4.68 .Effect of Longitudinal Cyclic on Alternating Flap and Chord Bending @ 10.5% R, 100 Knots, 386 RPM

NASA AMES TEST 410
RUN 13, 140 KNOTS, 386 RPM

$$\Delta\Theta = -A_1 \cos(\Psi + 20) - B_1 \sin(\Psi + 20)$$

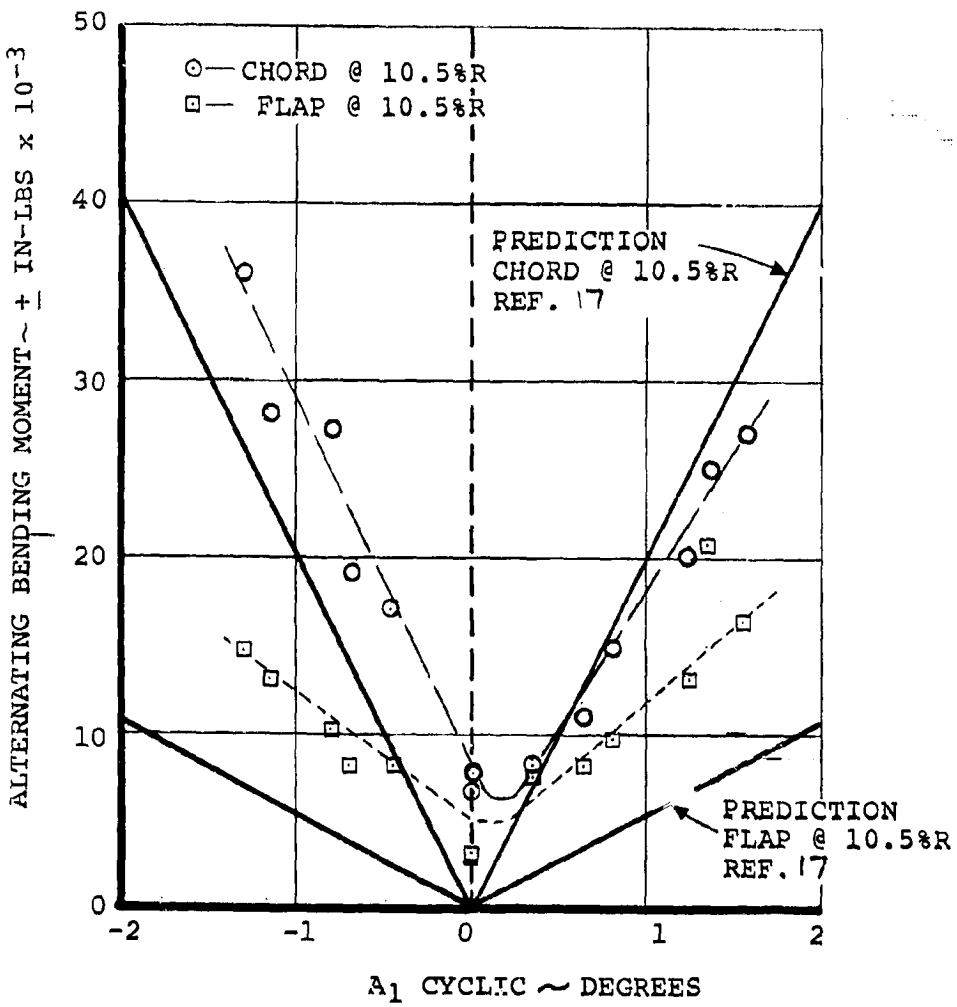

Figure 4.69 .Effect of Lateral Cyclic on Alternating Flap and Chord Bending @ 10.5% R, 140 Knots, 386 RPM

NASA AMES TEST 410
RUN 13, 140 KNOTS, 386 RPM

$$\Delta\Theta = -A_1 \cos(\Psi + 20) - B_1 \sin(\Psi + 20)$$

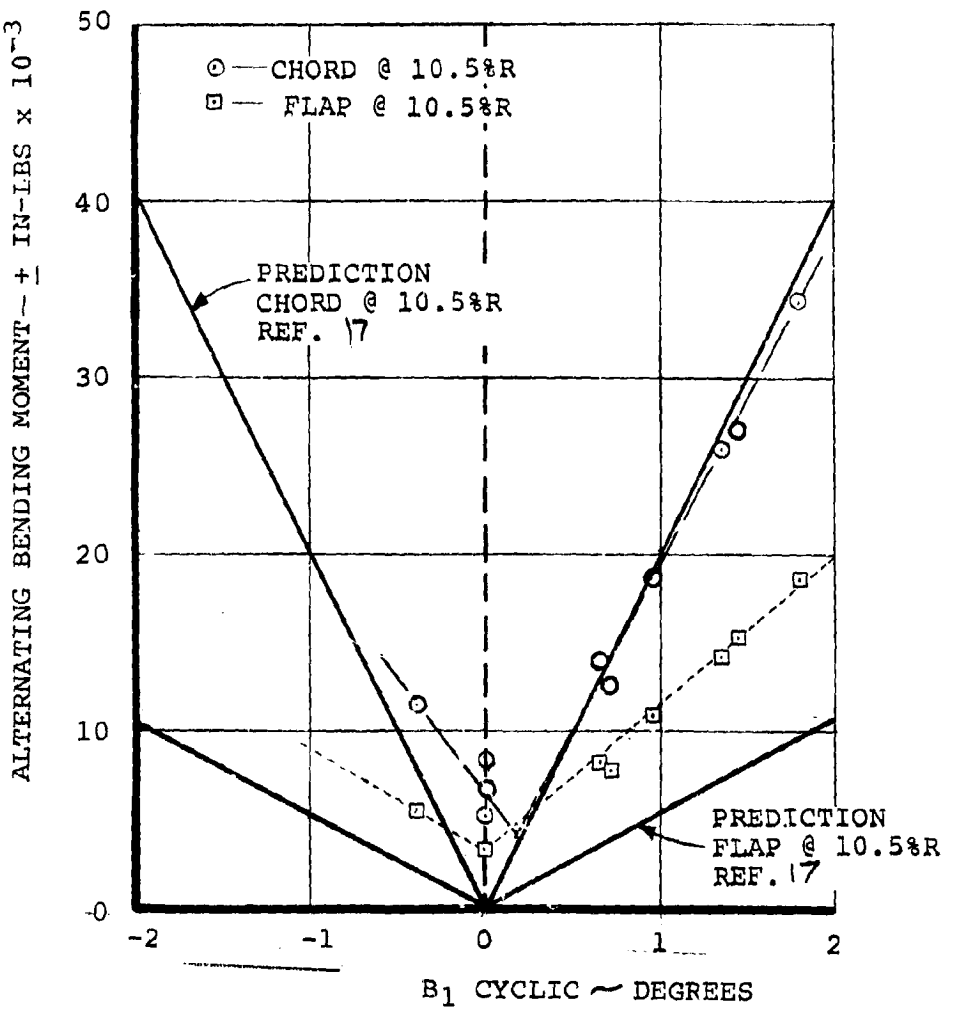

Figure 170 . Effect of Longitudinal Cyclic on Alternating Flap and Chord Bending @ 10.5%R, 140 Knots, 386 RPM

NASA AMES TEST 410
RUN 15, 192 KNOTS, 386 RPM

$$\Delta\theta = -A_1 \cos(\psi + 20) - B_1 \sin(\psi + 20)$$

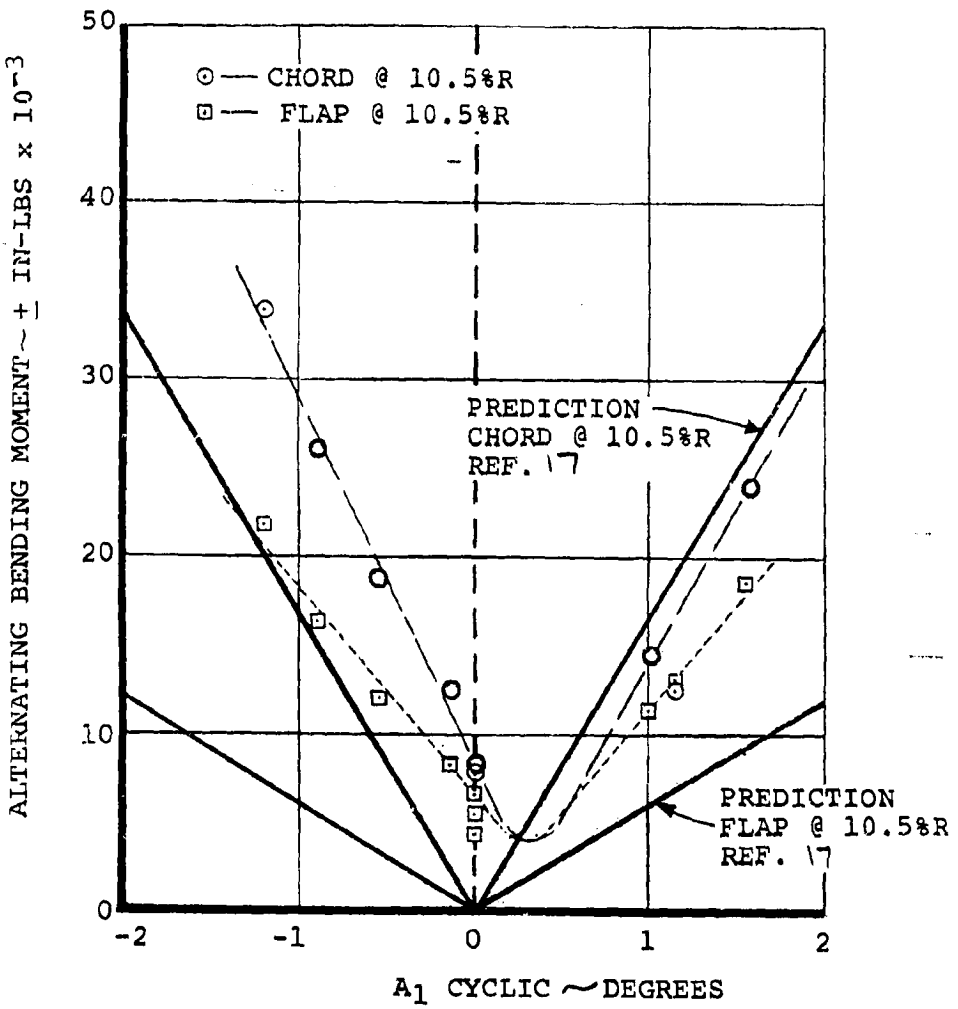

Figure 4.71 .Effect of Lateral Cyclic on Alternating Flap and Chord Bending @ 10.5%R, 192 Knots, 386 RPM

NASA AMES TEST 410
RUN 16, 192 KNOTS, 386 RPM

$$\Delta\Theta = -A_1 \cos(\Psi + 20) - B_1 \sin(\Psi + 20)$$

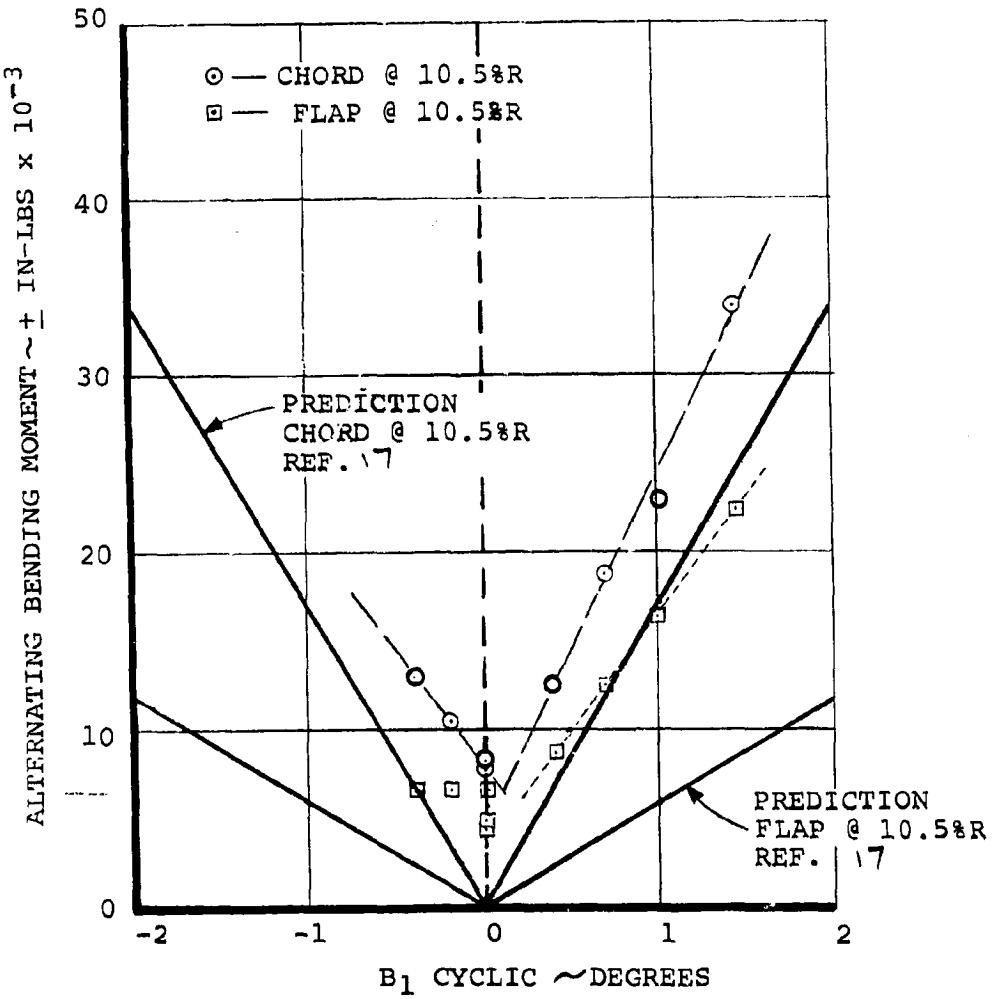

Figure 4.72 .Effect of Longitudinal Cyclic on Alternating Flap and Chord Bending @ 10.5%R, 192 Knots, 386 RPM

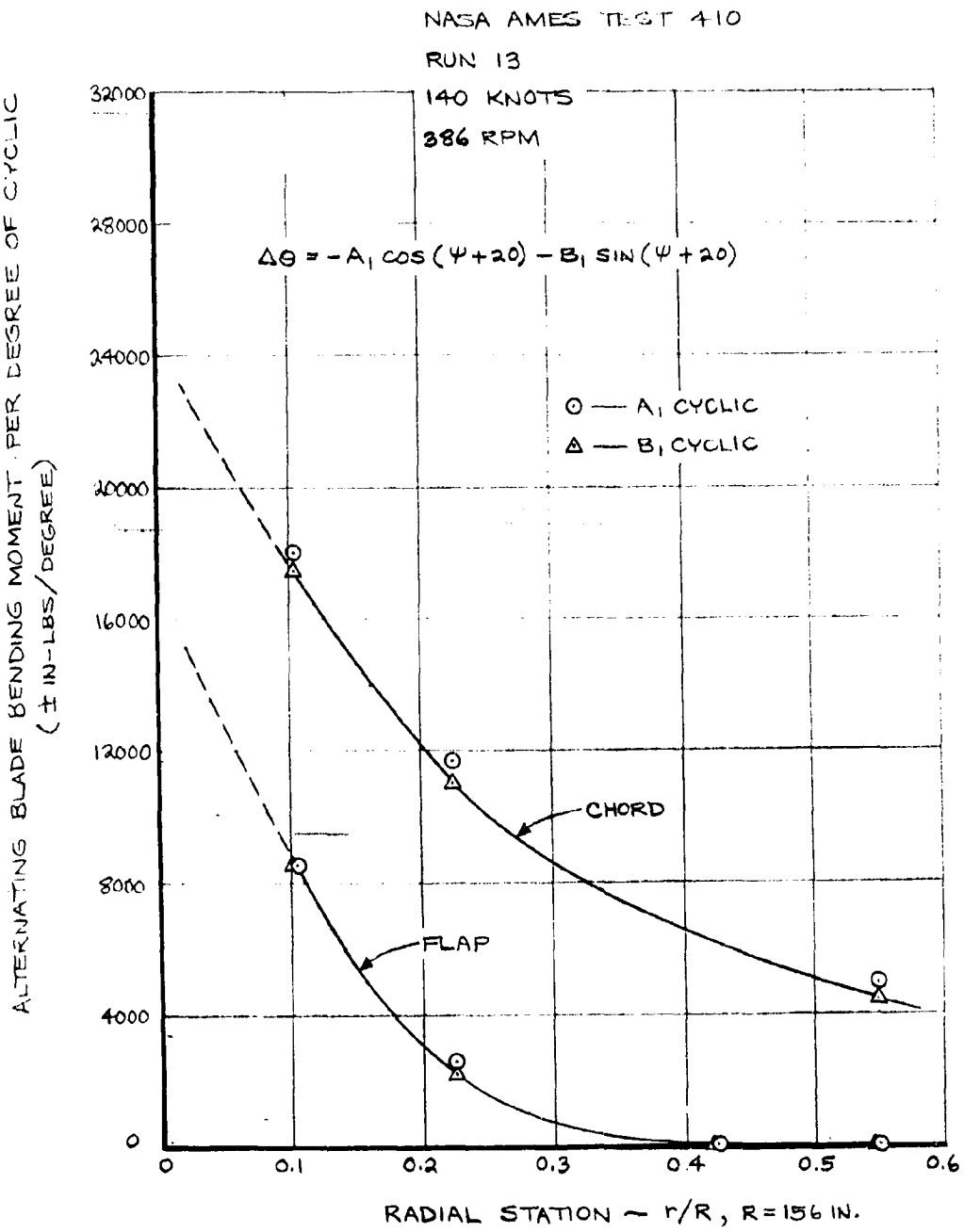

FIGURE 4.73 RADIAL DISTRIBUTION OF FLAP AND CHORD BLADE LOADS DUE TO CYCLIC - 140 KNOTS, 386 RPM

NASA AMES TEST 4.16
RUN 11
386 ROTOR RPM
$\theta_{.75} = 35.1°$
140 KNOTS
$i_N = 10°$
$B_1 = 2.31°$

⊙ —— 10.5% FLAP
⊡ —— HUB (OUT OF PLANE) 3.9%R
△ —— 55% FLAP

$\Delta\theta = -A_1 \cos(\psi + 20) - B_1 \sin(\psi + 20)$

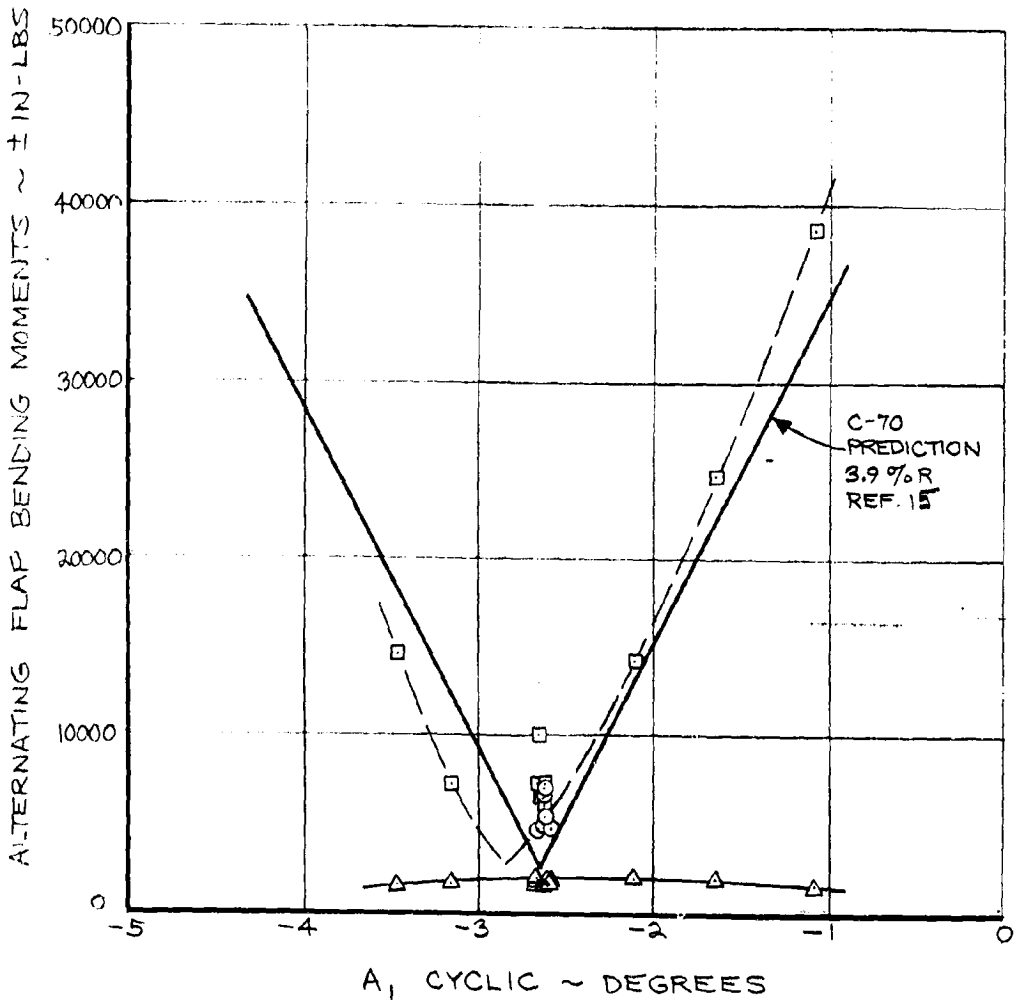

FIGURE 4.74 ALTERNATING BLADE FLAP LOADS DUE TO A_1 CYCLIC - V = 140 KNOTS, $i_N = 10°$.

NASA AMES TEST 416
RUN 11
386 ROTOR RPM
$\theta_{.75} = 35.1°$
140 KNOTS
$i_N = 10°$
$B_1 = 2.31°$

⊙ — 55% CHORD
⊡ — HUB (IN PLANE) 3.9%R

$\Delta\theta = -A_1 \cos(\psi + 20) - B_1 \sin(\psi + 20)$

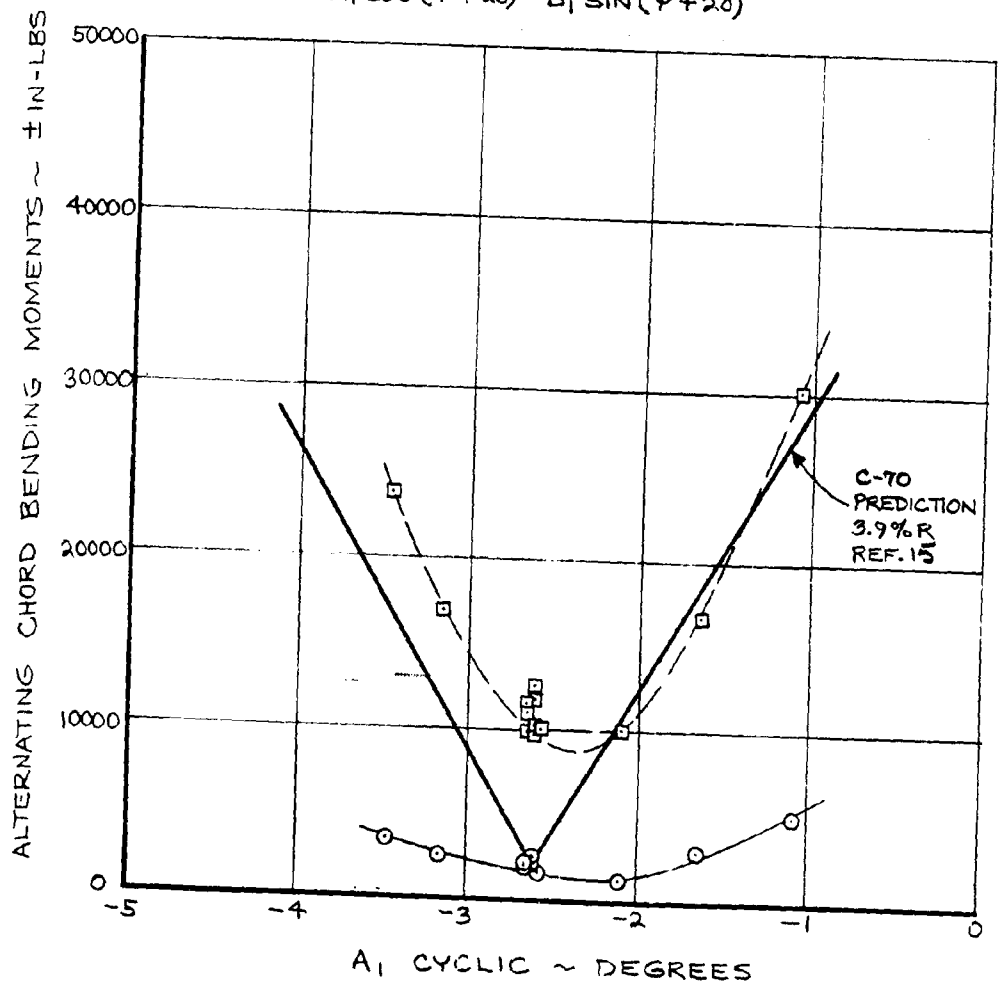

FIGURE 4.75 ALTERNATING BLADE CHORD LOADS DUE TO A_1 CYCLIC- V = 140 KNOTS, $i_N = 10°$

NASA AMES TEST 4-16
RUN 11
386 ROTOR RPM
$\theta_{.75} = 35.1°$
140 KNOTS
$i_N = 10°$
$A_1 = -2.66°$

⊙ —— 10.5 % FLAP
⊡ —— H. 3 (OUT OF PLANE) 3.9%R
△ —— 55 % FLAP

$\Delta\theta = -A_1 \cos(\psi + 20) - B_1 \sin(\psi + 20)$

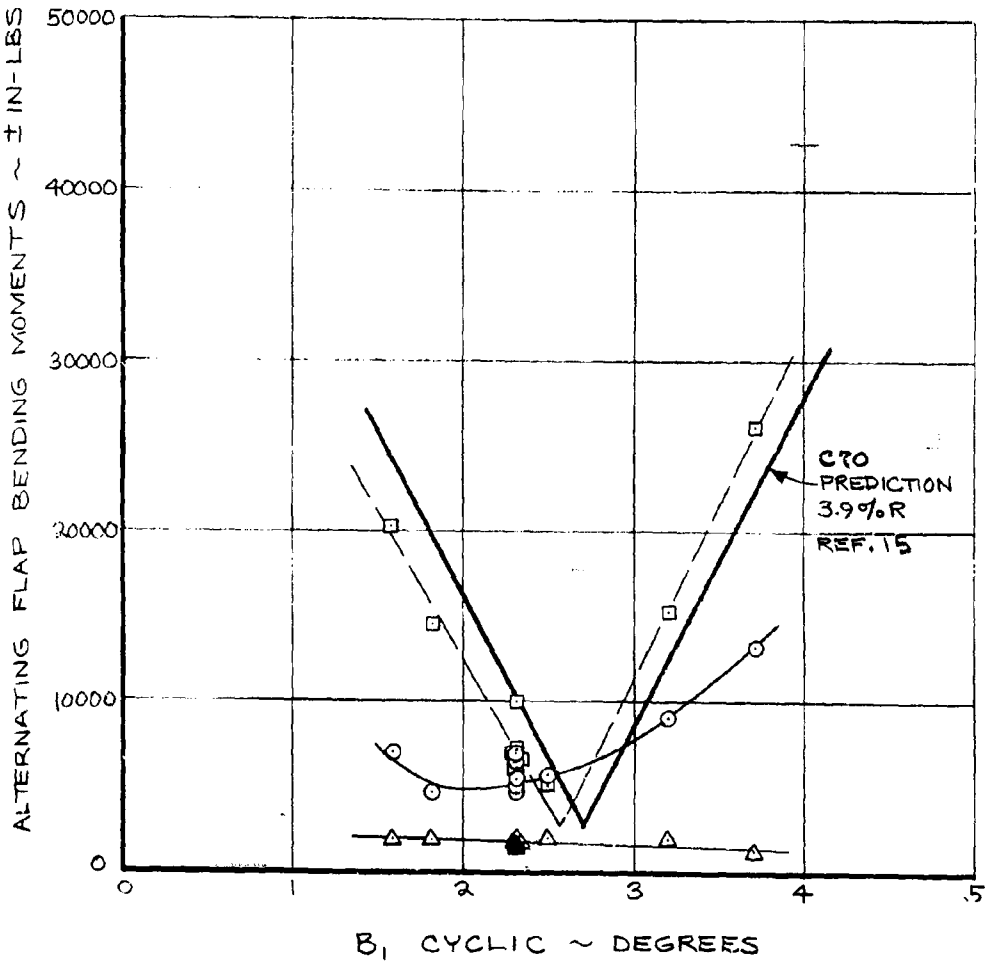

FIGURE 4.76 ALTERNATING BLADE FLAP LOADS DUE TO B_1 CYCLIC - $V = 140$ KNOTS, $i_N = 10°$

NASA AMES TEST 416
RUN 11
386 ROTOR RPM
$\theta_{.75} = 35.1°$
140 KNOTS
$i_N = 10°$
$A_1 = -2.66'$

⊙ — 55% CHORD
⊡ — HUB (IN PLANE) 3.9%R

$\Delta\theta = -A_1 \cos(\psi+20) - B_1 \sin(\psi+20)$

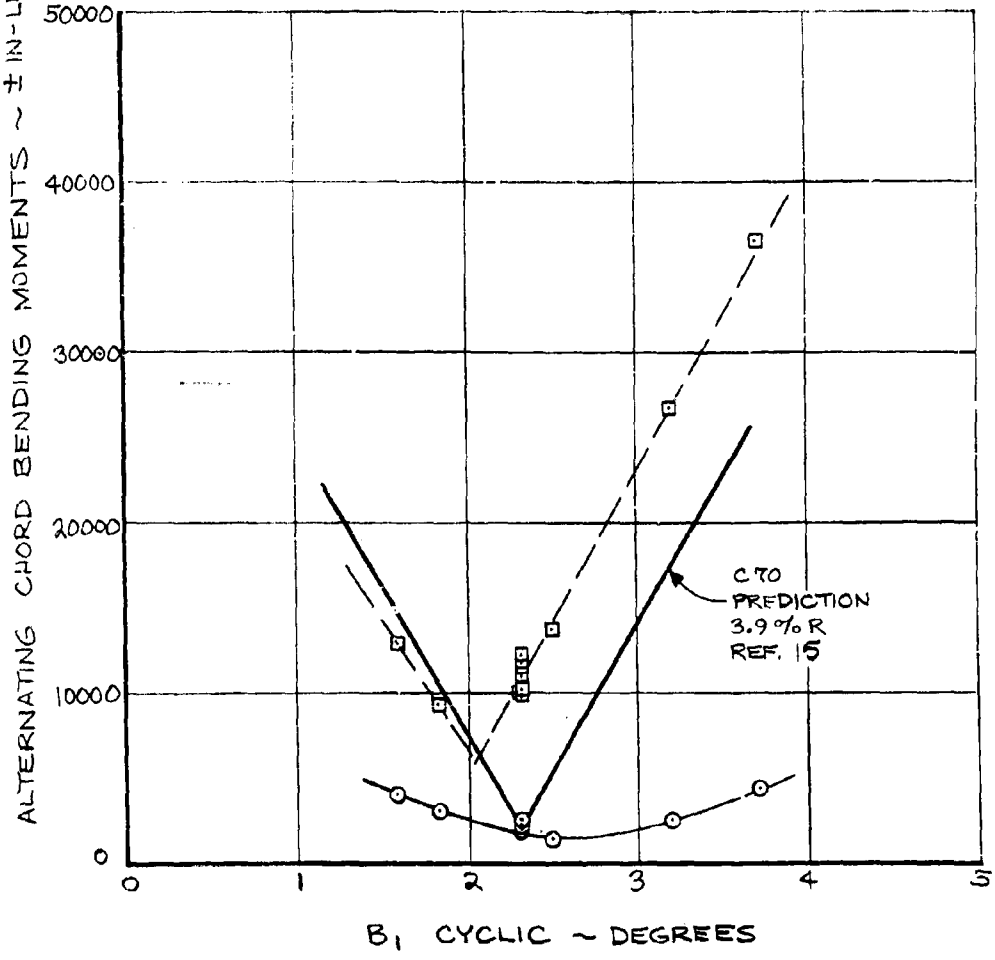

FIGURE 4.77 ALTERNATING BLADE CHORD LOADS DUE TO B_1 CYCLIC - V = 140 KNOTS, $i_N = 10°$

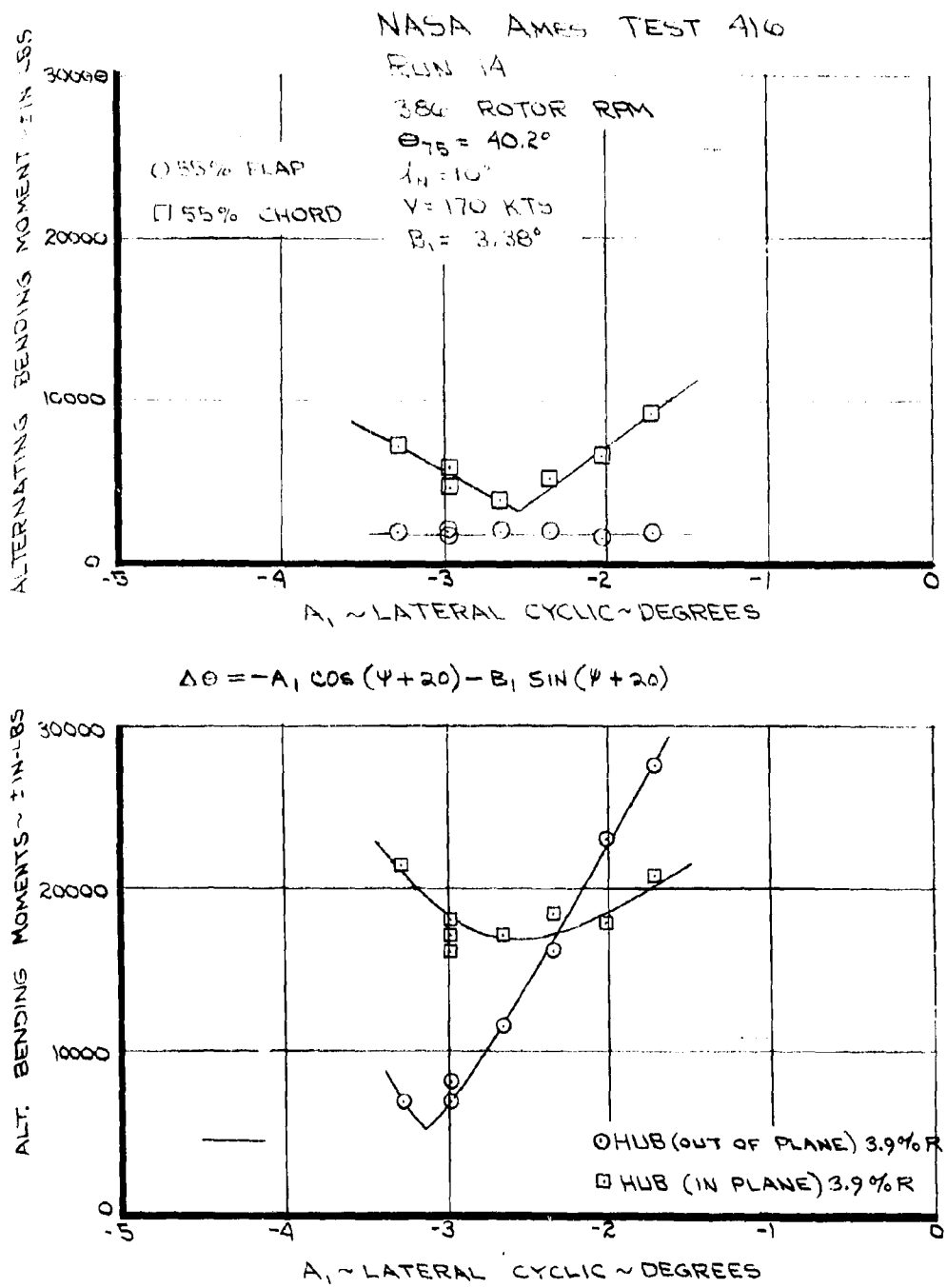

FIGURE 4.78 ALTERNATING BLADE LOADS DUE TO A_1 CYCLIC
V = 170 KNOTS, i_N = 10°

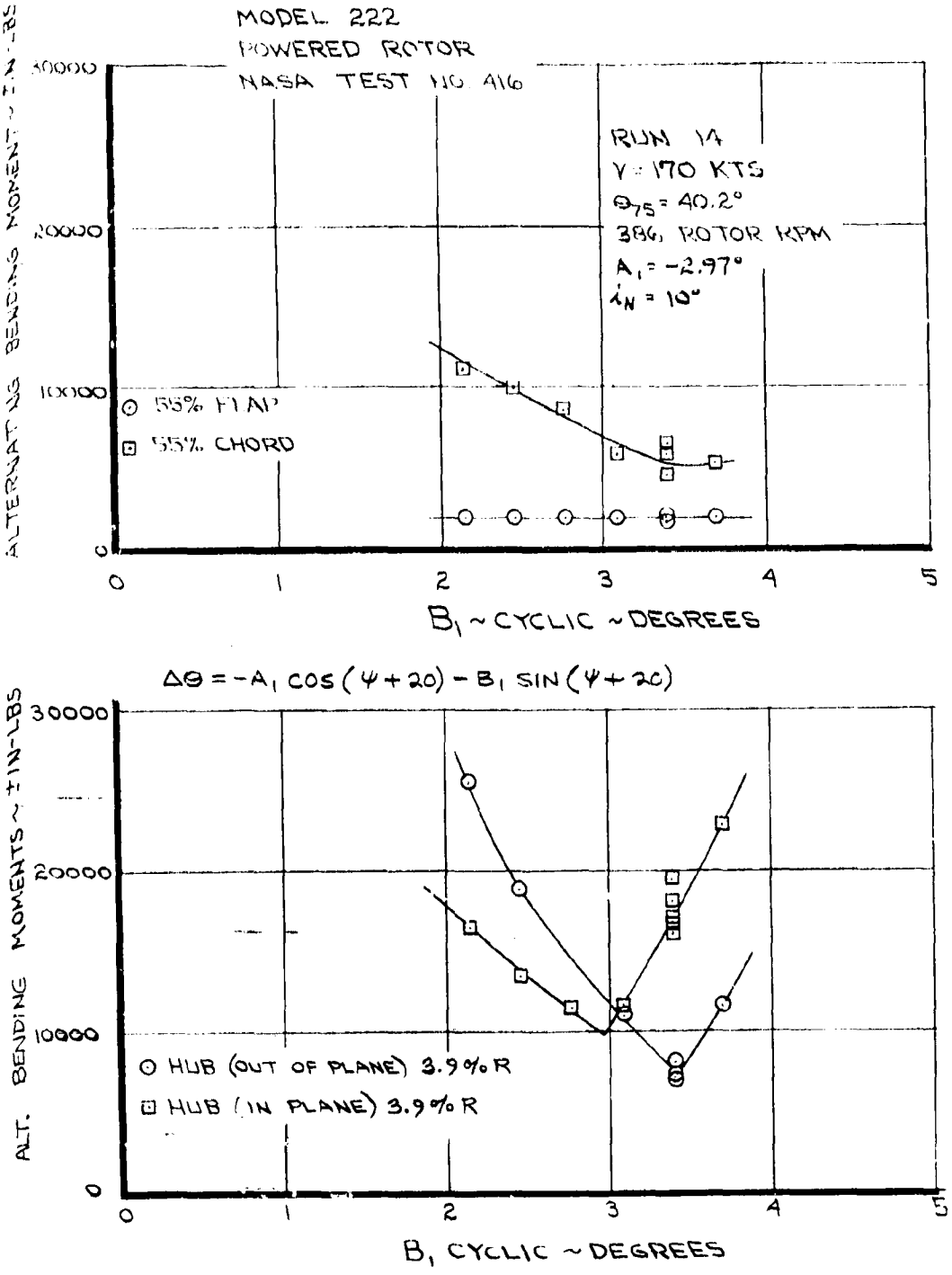

FIGURE 4.79 ALTERNATING BLADE LOADS DUE TO B_1 CYCLIC
V = 170 KNOTS, i_N = 10°

Effect of Collective Pitch

The alternating blade loads measured at 140 kts and 170 kts at 10° incidence in cruise are shown as a function of collective in Figures 4-80 to 4-82. These tests were performed at the minimum load cyclic conditions and represent a range of collective from zero thrust to maximum power (see Section 7). The alternating loads remain low and in general decrease as thrust is increased.

NASA AMES TEST 4-16
RUN 11
386 ROTOR RPM
$i_N = 10°$
V = 140 KNOTS
$A_1 = -2.62°$
$B_1 = 2.31°$

⊙ — 10.5% FLAP
⊡ — HUB (OUT OF PLANE) 3.9%R
△ — 55% FLAP

$\Delta\theta = -A_1 \cos(\psi+20) - B_1 \sin(\psi+20)$

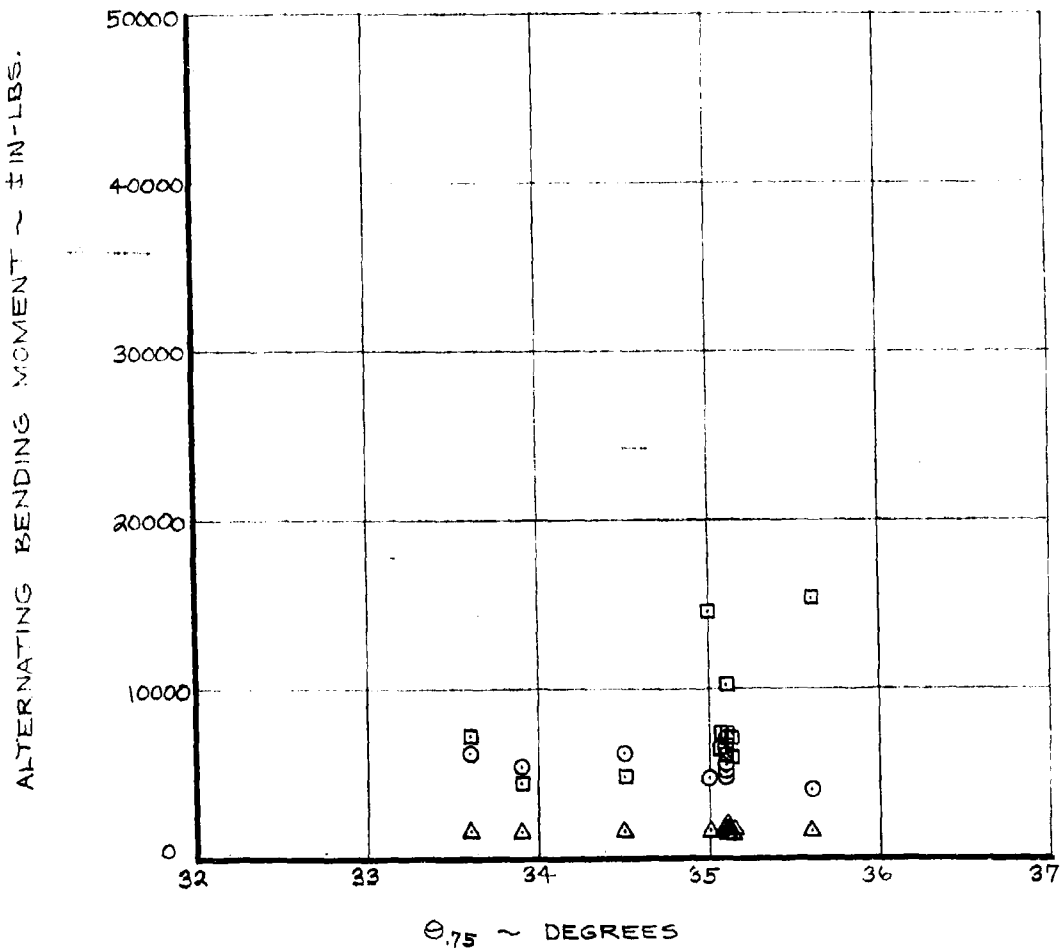

FIGURE 4.80 ALTERNATING BLADE FLAP LOADS DUE TO COLLECTIVE PITCH – V = 140 KNOTS, $i_N = 10°$

NASA AMES TEST 416
RUN 11
386 ROTOR RPM
$i_N = 10°$
V = 140 KNOTS
$A_1 = -2.62°$
$B_1 = 2.31°$

⊡ — HUB (IN PLANE) 3.9%R
△ — 55 % CHORD

$\Delta\theta = -A_1 \cos(\psi+20) - B_1 \sin(\psi+20)$

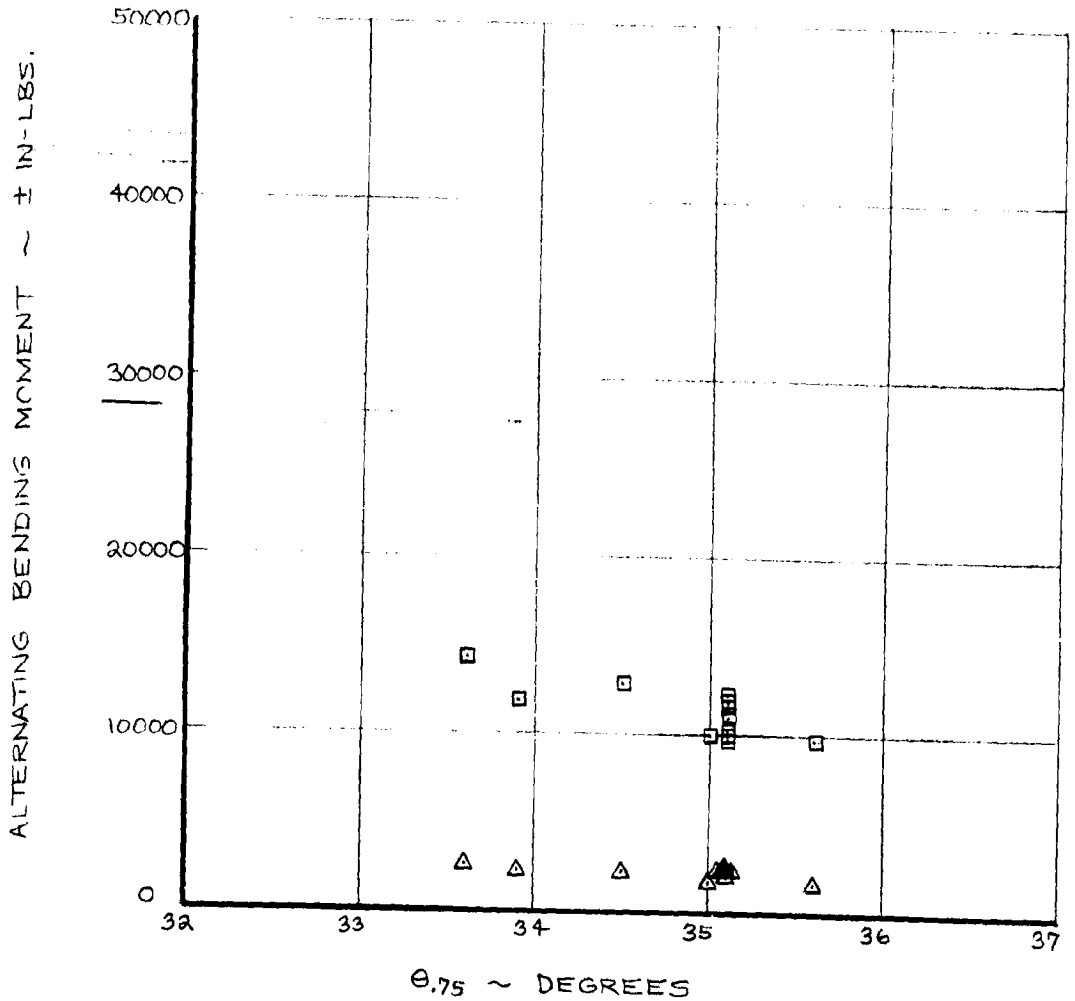

FIGURE 4.81 ALTERNATING BLADE CHORD LOADS DUE TO COLLECTIVE PITCH – V = 140 KNOTS, $i_N = 10°$

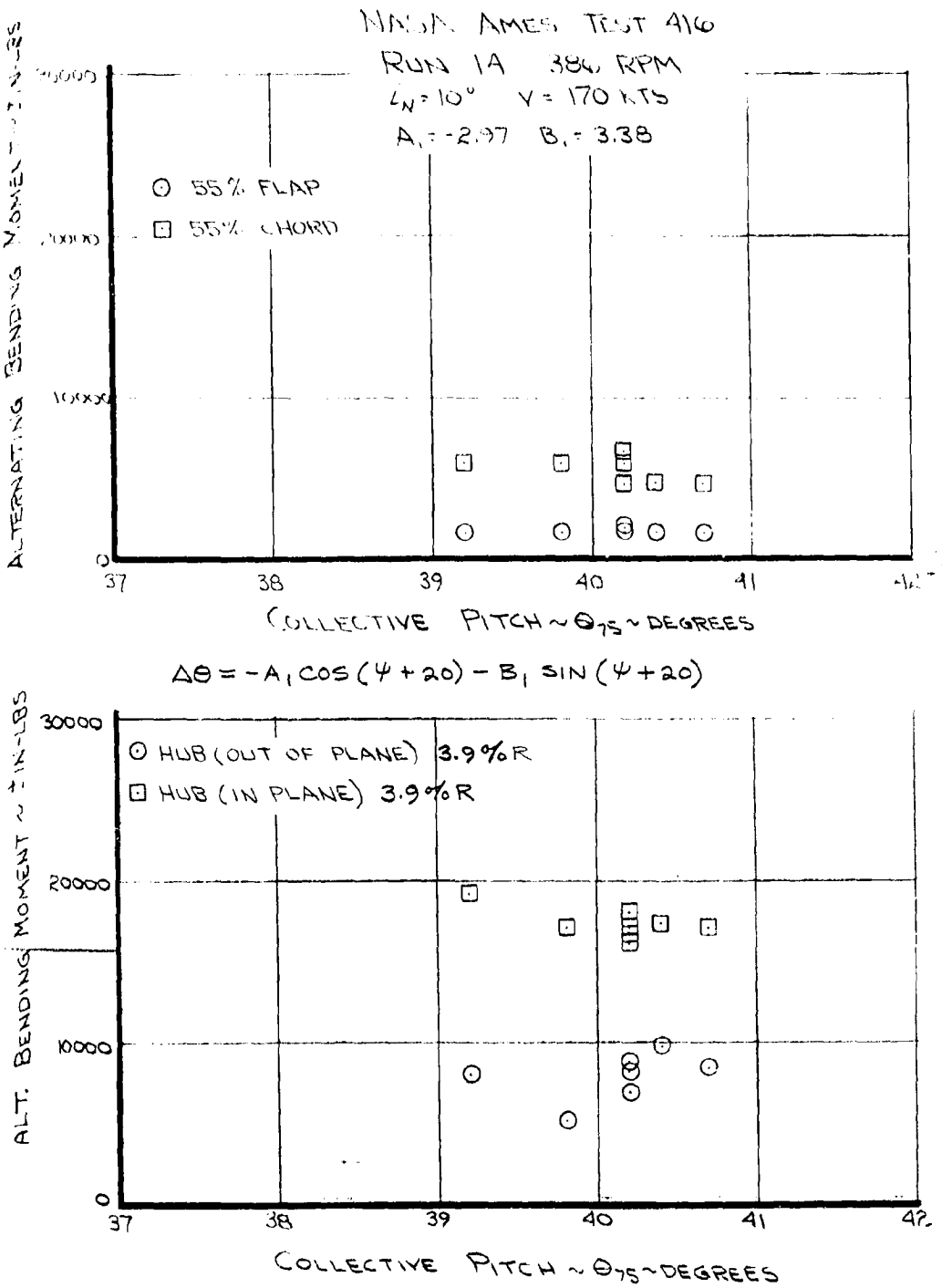

FIGURE 4.82. ALTERNATING BLADE LOADS DUE TO COLLECTIVE PITCH - V = 170 KNOTS, i_N = 10°

Effect of Off Design RPM

In addition to the data taken at design cruise RPM a number of cases were tested at higher and lower RPM conditions in order to establish an alternating blade loads sensitivity. As RPM increases the first bending mode decreases on a per rev basis (see Section 4.1) and as RPM decreases the one per rev frequency coincidence is approached. Also at low airspeed increasing RPM reduces the damping in the air resonance mode because of the frequency coalescence between the rotor $(\Omega-\omega_L)$ lower blade lag mode and wing vertical bending. This phenomena is discussed in Section 3.0.

Alternating blade load data obtained on test 410 due to angle of attack at off design RPM are shown in Figures 4-83 to 4-92. In some cases data points are not plotted. This is due to bad "spiking" on some instrumentation traces making the data untrustworthy.

At 100 kts and 445 RPM, Figures 4-83 and 4-84, the alternating blade loads at 10.5%R increase at about 2850 in-lbs chord bending/degree and 500 in-lbs flap bending/degree compared with 3750 in-lbs/degree and 1375 in-lbs/degree respectively at 386 RPM.

At 140 kts angle of attack data was obtained at two off design RPM's 330 and 420. The sensitivities of alternating chord and flap bending are increased at the lower RPM to 6500 in-lbs/° and 3300 in-lbs/° respectively at 10.5%R. The corresponding data at 386 RPM indicates 5500 in-lbs/° (chord) and 2625 in-lbs/° (flap). At 420 RPM Figures 4-87 and 4-88 show reduced loads at 4500 in-lbs/° chord bending and 2050 in-lbs/° flap bending. From these data it appears that the alternating loads reduce as the blade per rev frequency reduces and the decrease in air resonance modal damping does not reverse this trend.

Figures 4-89 and 4-90 contain data measured at 170 kts 400 RPM and data at 192 kts and 450 RPM are also included in Figures 4-91 and 4-92. These curves show similar behavior.

Figures 4-93 to 4-102 show the effects of cyclic pitch on alternating blade loads at off design cruise RPM. At 100 kts 445 RPM the alternating flap bending increases at about 4000 in-lbs/° of cyclic compared with 4970 in-lbs/° at 386 RPM. The chord bending is also reduced at 445 RPM, 14000 in-lbs/° compared with 18,000 in-lbs/° at 386 RPM.

At 420 RPM and 140 kts (Figures 4-97 and 4-98) A_1 cyclic inputs give 6800 in-lbs/° of alternating flap bending and 17,800 in-lbs/° alternating chord bending (8200 in-lbs/° and 18,000 in-lbs/° respectively at 386 RPM). This set of data does not show the marked reduction in alternating chord bending previously observed.

Figures 4-99 to 4-102 show cyclic data at 192 kts and 300 RPM. Unfortunately the most inboard gage stations were inoperative at this stage in the test. The 22.5% flap bending gages indicated 6800 in-lbs/° cyclic and the 55% chord bending gages about 4,000 in-lbs/°. These values compare with 4800 in-lbs/° 22.5% flap bending and 3100 in-lbs/° 55% chord bending at 386 RPM, again confirming the general trend of reduced alternating blade loads as RPM is increased in cruise.

NASA AMES TEST 410
RUN 53, 100 KNOTS, 445 RPM
ZERO CYCLIC

○ - 10.5% Radius
□ - 55% Radius

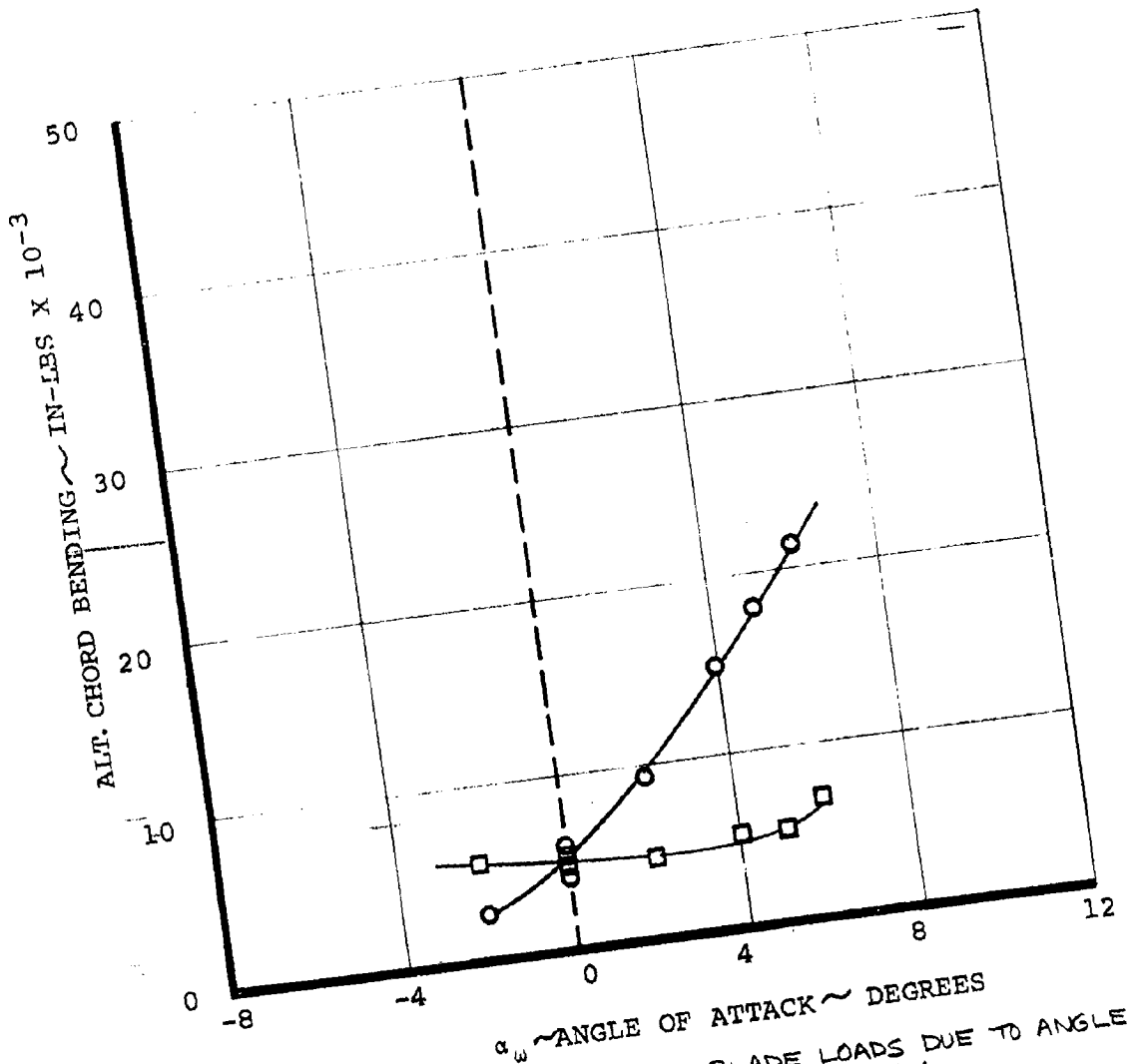

FIGURE 4.83 ALTERNATING CHORD BLADE LOADS DUE TO ANGLE OF ATTACK - V=100 KNOTS, 445 RPM

NASA AMES TEST 410
RUN 53, 100 KNOTS, 445 RPM
ZERO CYCLIC

○ - 10.5% Radius
□ - 22.5% Radius
◇ - 42.5% Radius
▽ - 55% Radius

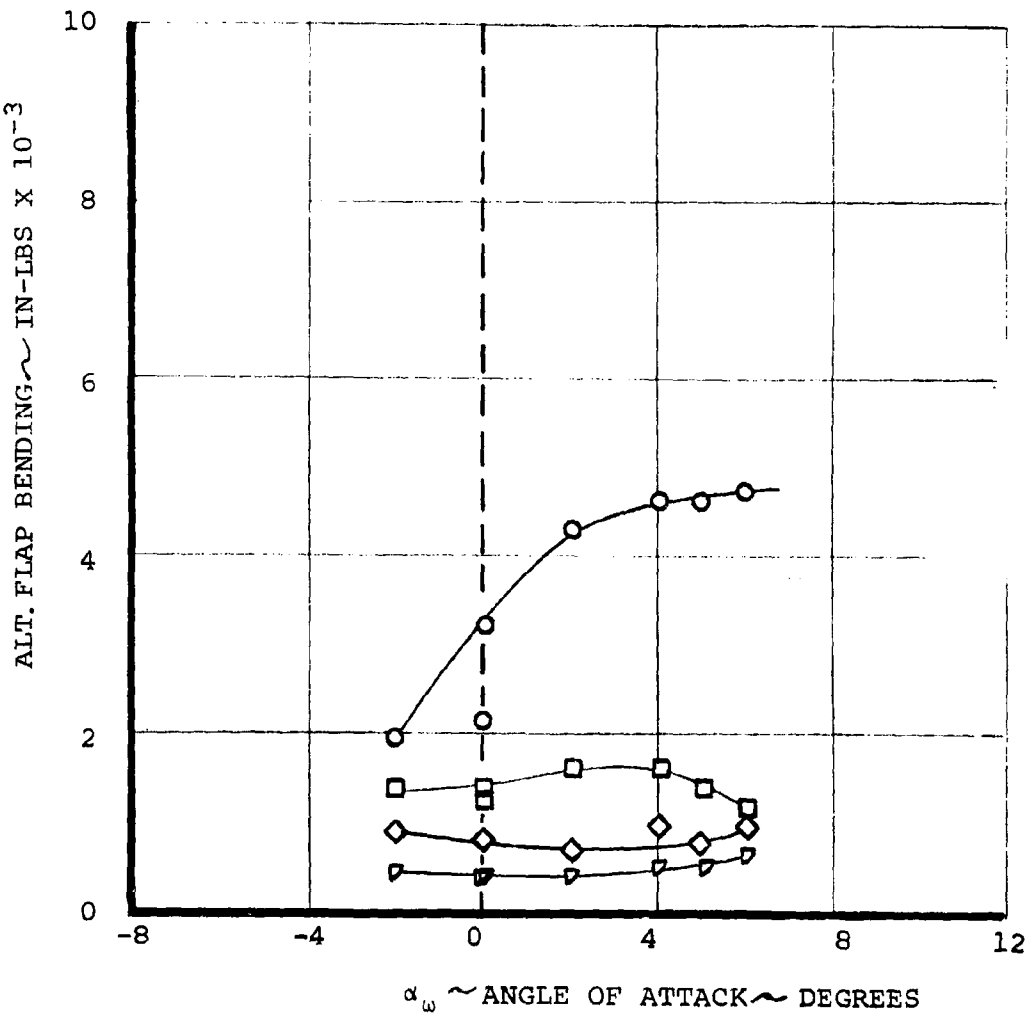

FIGURE 4.84 ALTERNATING FLAP BLADE LOADS DUE TO ANGLE OF ATTACK - V = 100 KNOTS, 445 RPM

NASA AMES TEST 410
RUN 52, 140 KNOTS, 330 RPM

ZERO CYCLIC

○ - 10.5% Radius
□ - 55% Radius

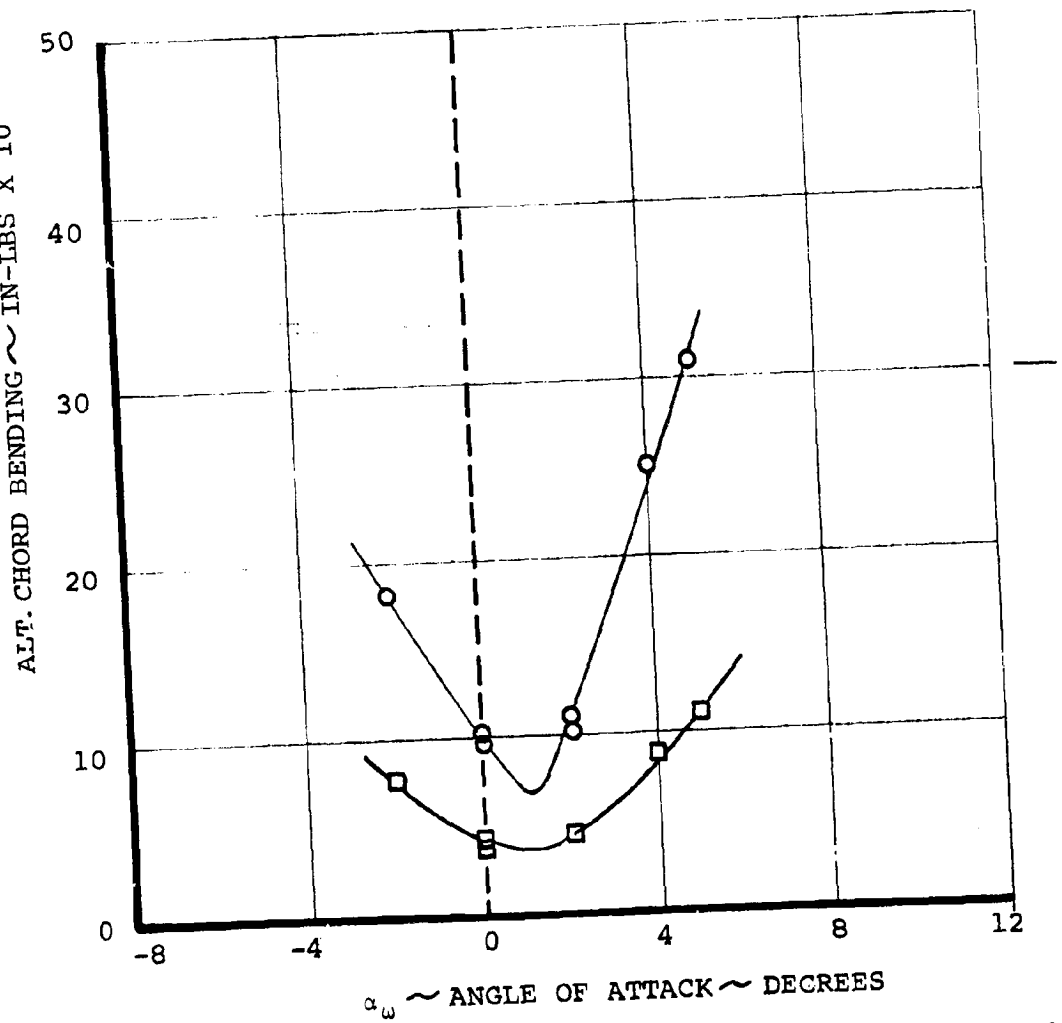

FIGURE 4.85 ALTERNATING CHORD BLADE LOADS DUE TO ANGLE OF ATTACK - V = 140 KNOTS, 330 RPM

NASA AMES TEST 410
RUN 52, 140 KNOTS, 330 RPM

ZERO CYCLIC

○- 10.5% Radius
□- 22.5% Radius
◇- 42.5% Radius
▽- 55% Radius

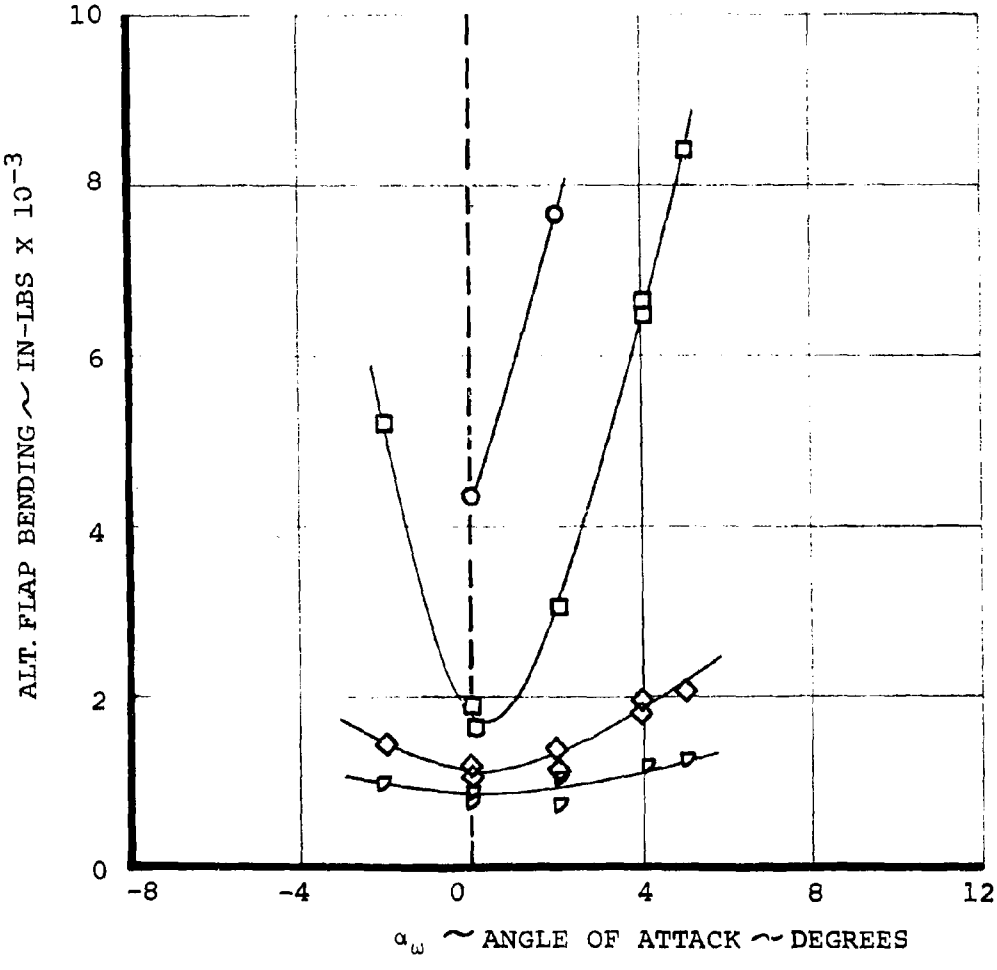

FIGURE 4.86 ALTERNATING FLAP BLADE LOADS DUE TO ANGLE OF ATTACK - V = 140 KNOTS, 330 RPM

NASA AMES TEST 410
RUN 52, 140 KNOTS, 420 RPM

ZERO CYCLIC

○ - 10.5% Radius
□ - 55% Radius

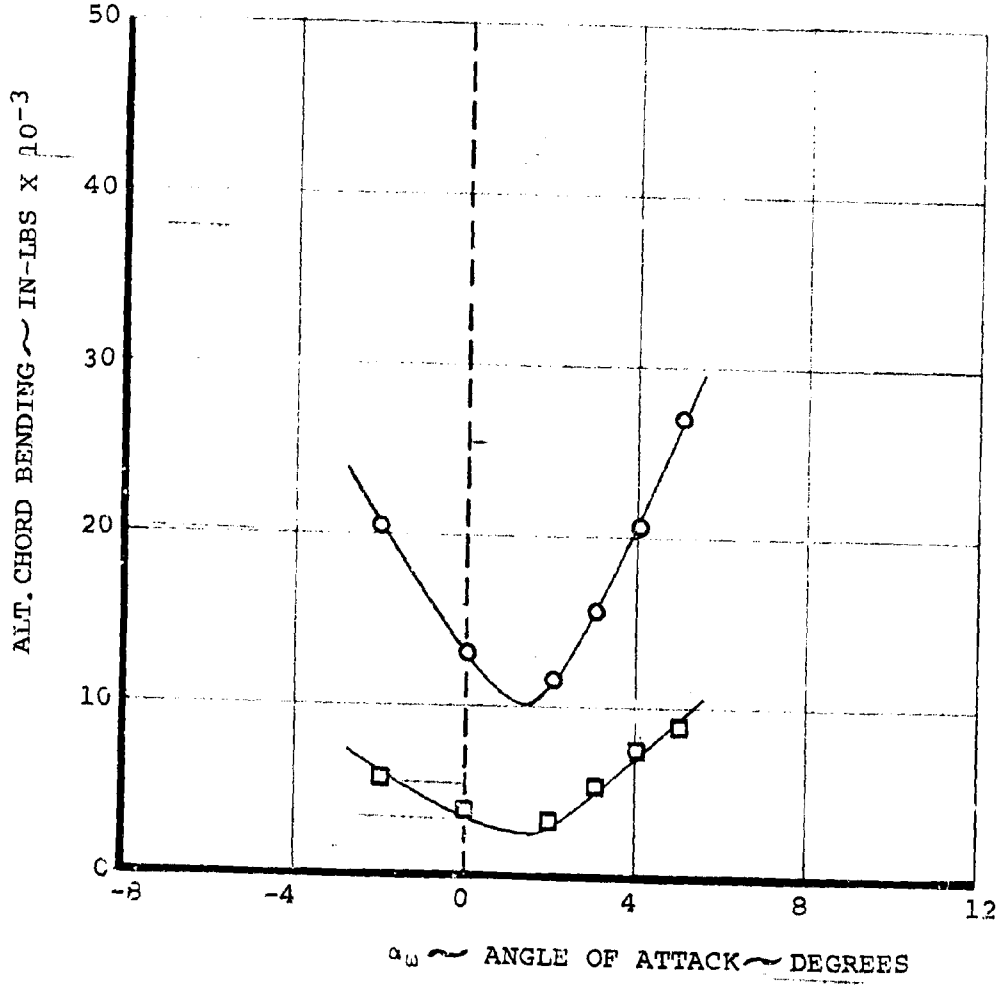

FIGURE 4.87 ALTERNATING CHORD BLADE LOADS DUE TO ANGLE OF ATTACK - V = 140 KNOTS, 420 RPM

NASA AMES TEST 410
RUN 52, 140 KNOTS, 420 RPM

ZERO CYCLIC

○ - 10.5% Radius
□ - 22.5% Radius
◇ - 42.5% Radius
▽ - 55% Radius

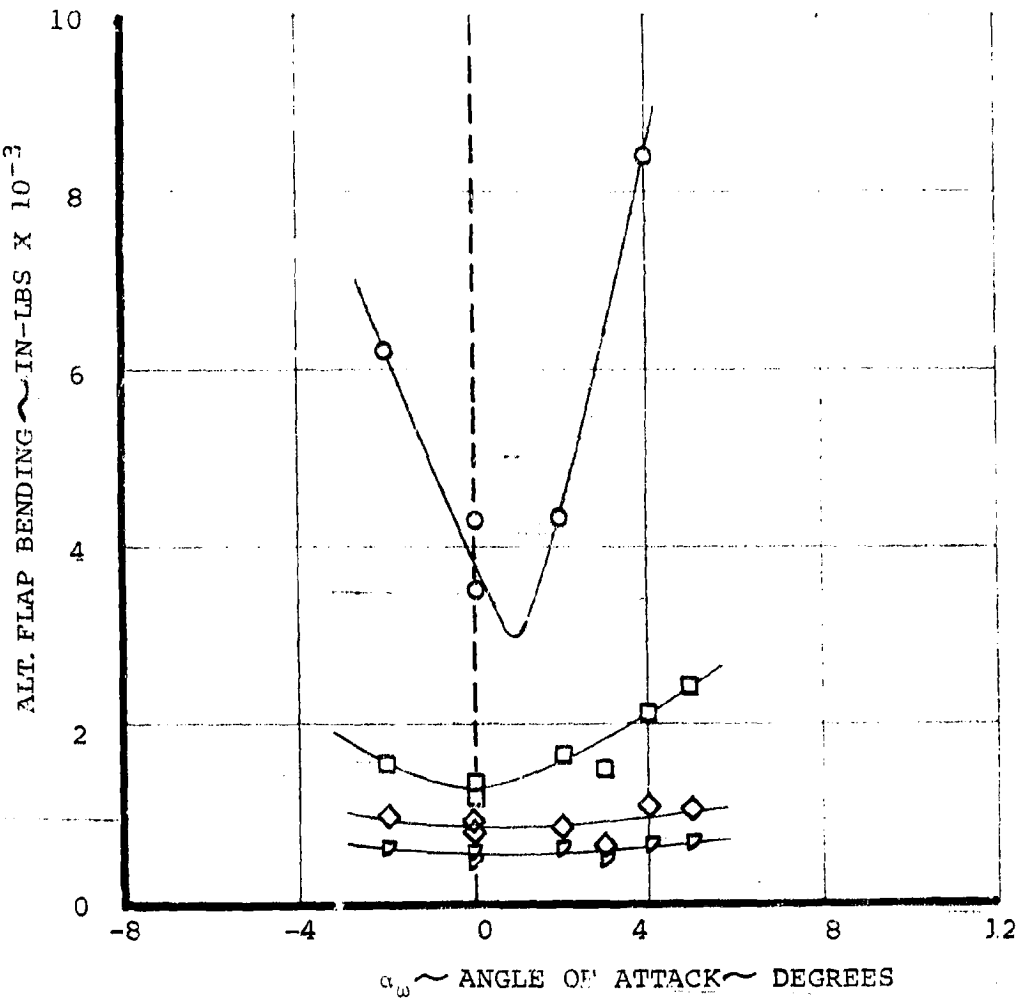

FIGURE 4.88 ALTERNATING FLAP BLADE LOADS DUE TO ANGLE OF ATTACK - V = 140 KNOTS, 420 RPM

NASA AMES TEST 410
RUN 58, 170 KNOTS, 400 RPM
ZERO CYCLIC

□ - 22.5% Radius
◇ - 42.5% Radius
▽ - 55% Radius

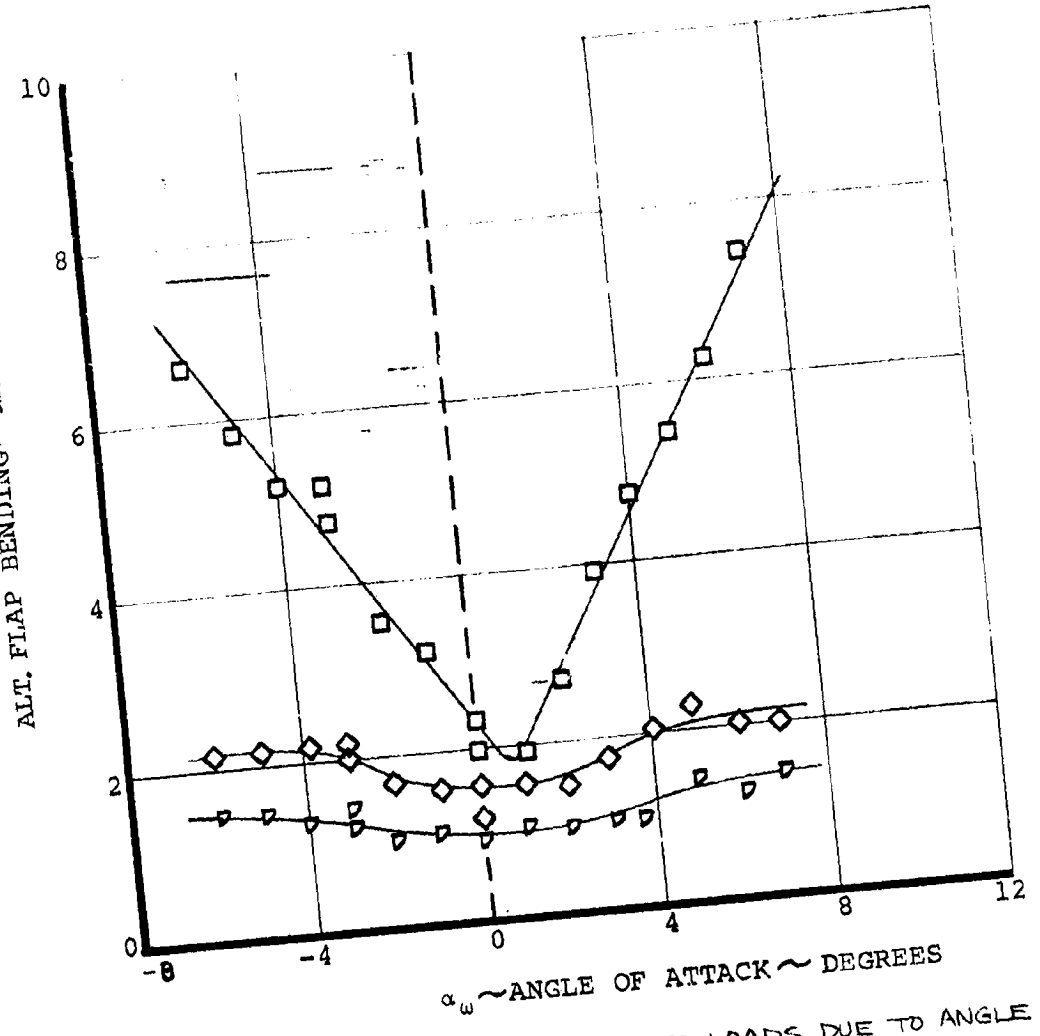

FIGURE 4.89 ALTERNATING FLAP BLADE LOADS DUE TO ANGLE OF ATTACK - V = 170 KNOTS, 400 RPM

NASA AMES TEST 410
RUN 58, V = 170 KNOTS, 400 RPM
ZERO CYCLIC

○ - 10.5% Radius
□ - 55% Radius

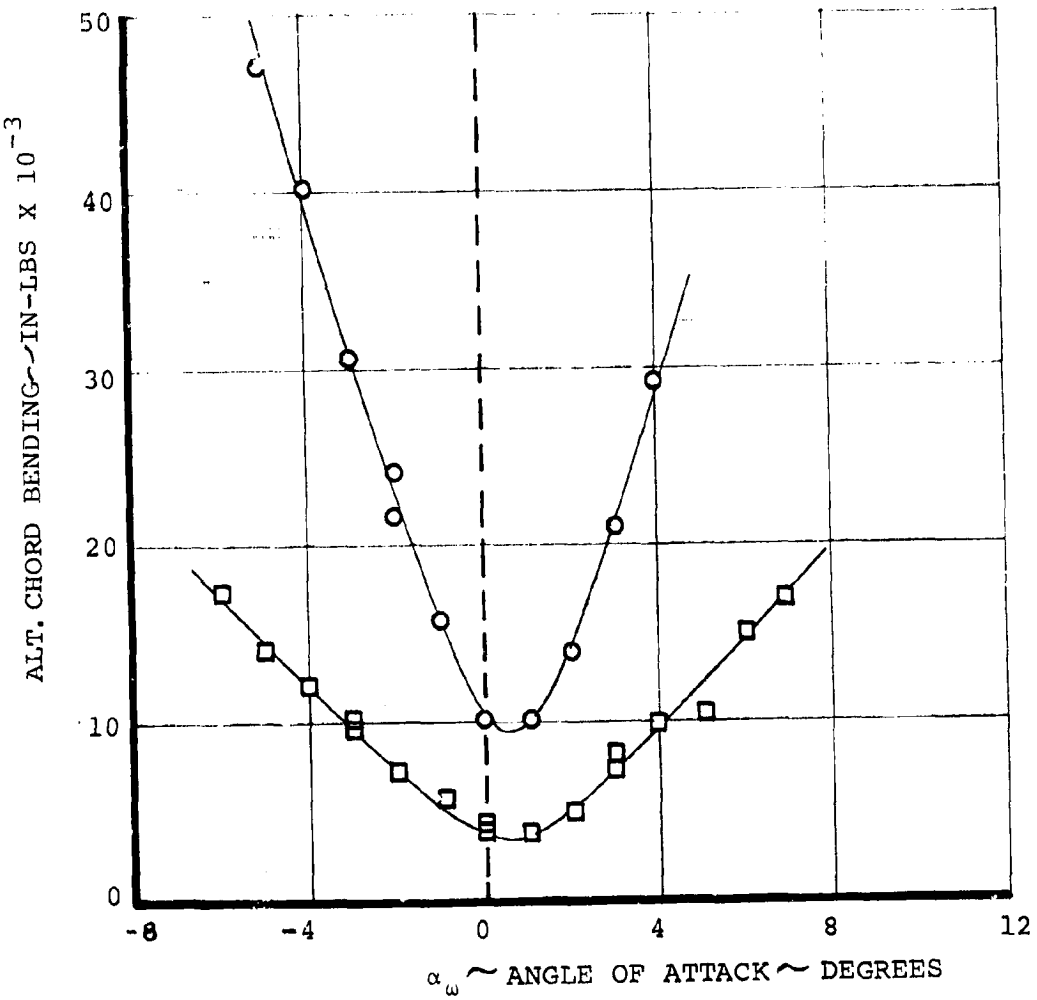

FIGURE 4.90 ALTERNATING CHORD BLADE LOADS DUE TO ANGLE OF ATTACK - V = 170 KNOTS, 400 RPM

NASA AMES TEST 410
RUN 58, V = 192 KNOTS, 450 RPM
ZERO CYCLIC

□ - 55% Radius

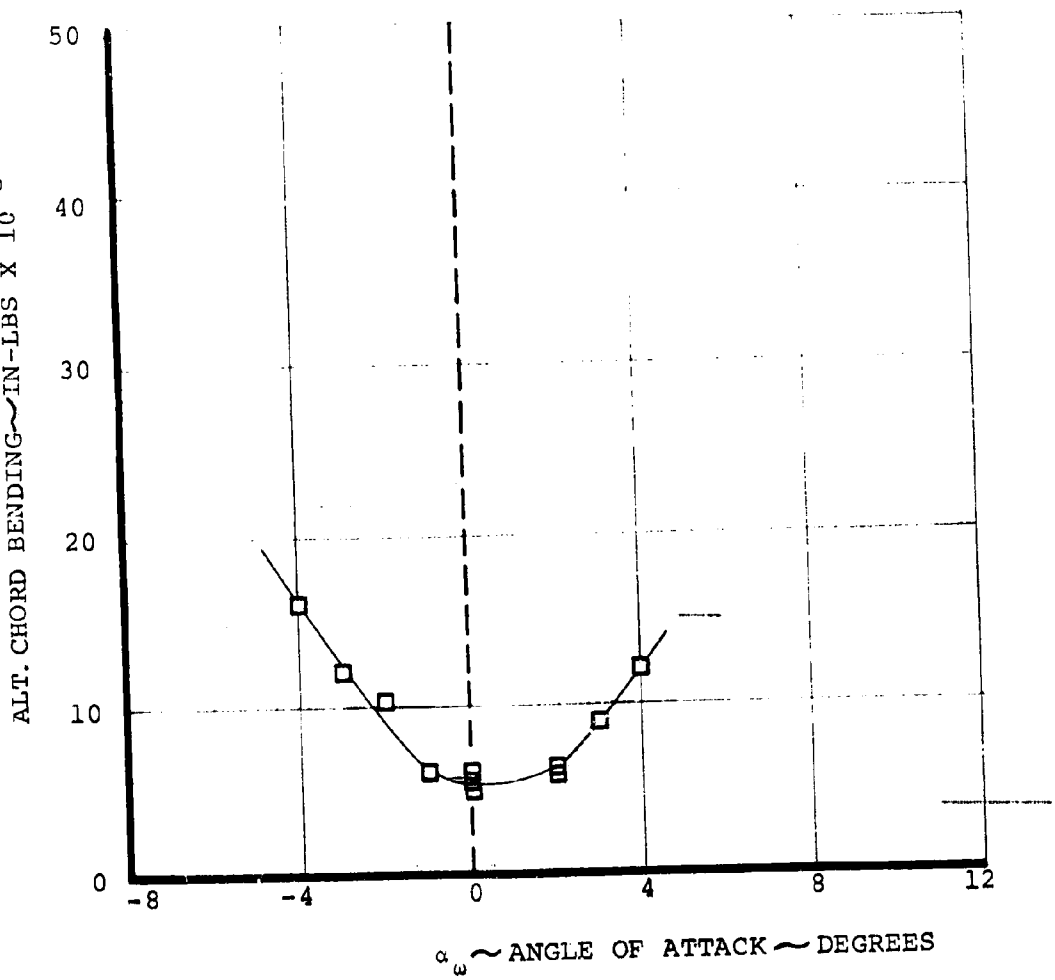

FIGURE 4.91 ALTERNATING CHORD BLADE LOADS DUE TO ANGLE OF ATTACK - V = 192 KNOTS, 450 RPM

NASA AMES TEST 410
RUN 58, V = 192 KNOTS, 450 RPM
ZERO CYCLIC

□ - 22.5% Radius
◇ - 42.5% Radius
▽ - 55% Radius

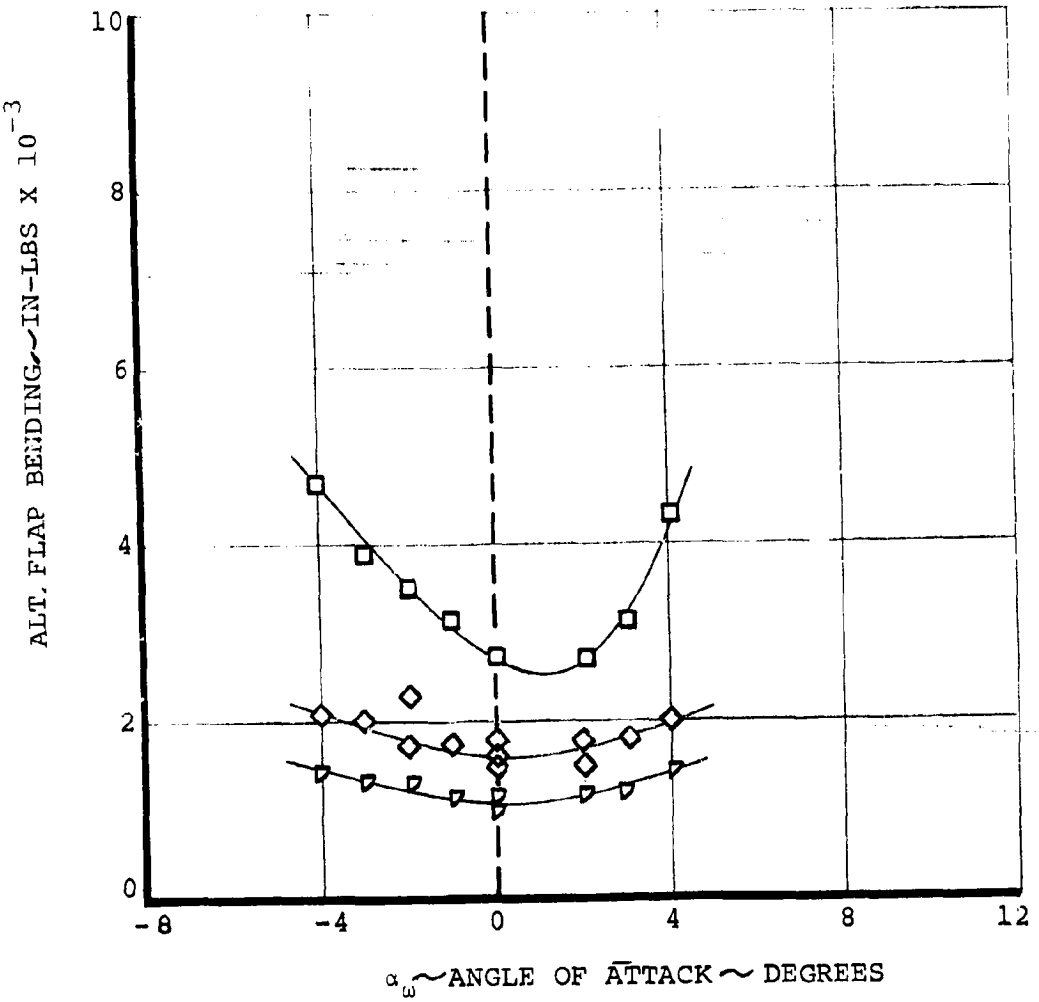

FIGURE 4.92 ALTERNATING FLAP BLADE LOADS DUE TO ANGLE OF ATTACK - V = 192 KNOTS, 450 RPM

NASA AMES TEST 410
RUN 53, 100 KNOTS, 445 RPM
$B_1 = 0°$

○ - 10.5% Radius
□ - 22.5% Radius
◇ - 42.5% Radius
▽ - 55% Radius

$$\Delta\theta = -A_1 \cos(\psi + 20) - B_1 \sin(\psi + 20)$$

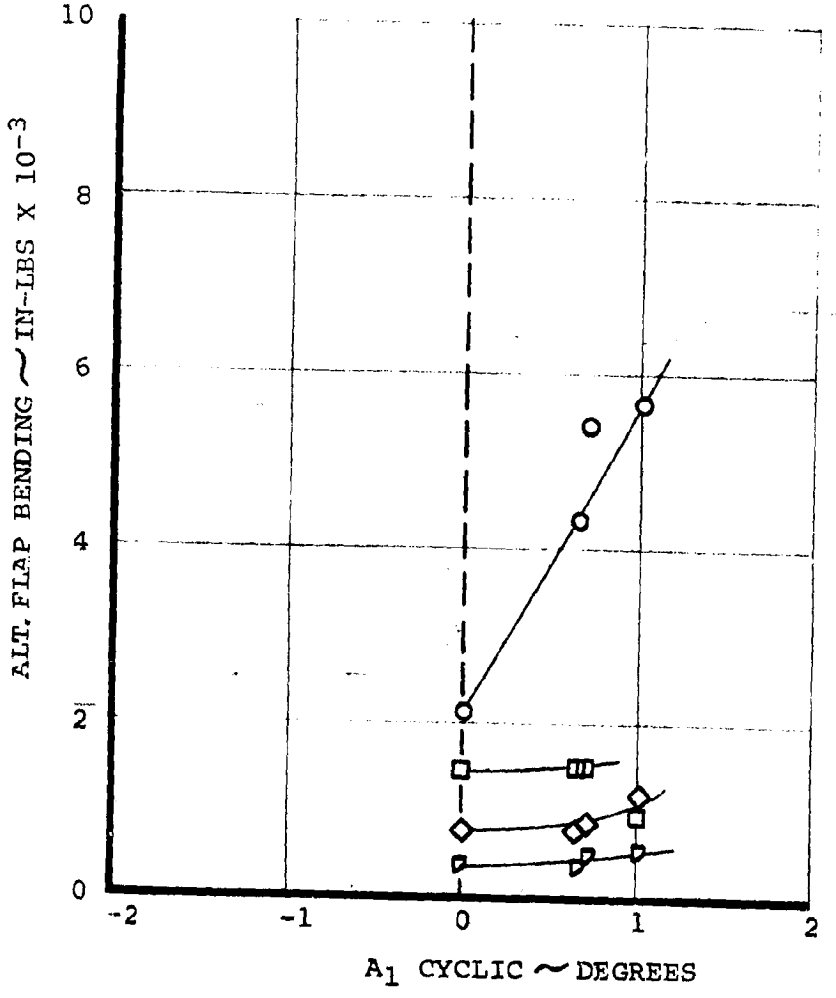

FIGURE 4.93 ALTERNATING FLAP BLADE LOADS DUE TO A_1 CYCLIC - V = 100 KNOTS, 445 RPM

NASA AMES TEST 410
RUN 53, 100 KNOTS, 445 RPM

$B_1 = 0°$

○ - 10.5% Radius
□ - 55% Radius

$$\Delta\Theta = -A_1 \cos(\psi + 20) - B_1 \sin(\psi + 20)$$

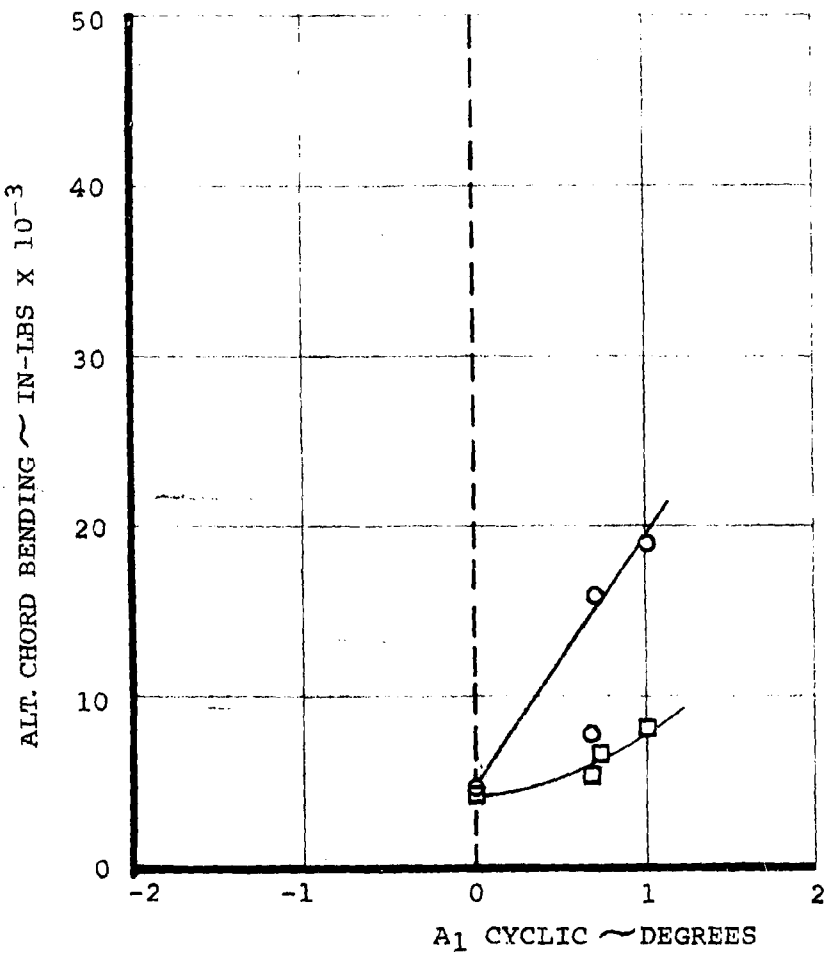

FIGURE 4.94 ALTERNATING CHORD BLADE LOADS DUE TO A_1 CYCLIC - V = 100 KNOTS, 445 RPM

NASA AMES TEST 410
RUN 53, 100 KNOTS, 445 RPM

$A_1 = 0°$

○ - 10.5% Radius
□ - 22.5% Radius
◇ - 42.5% Radius
▽ - 55% Radius

$$\Delta\theta = -A_1 \cos(\psi + 20) - B_1 \sin(\psi + 20)$$

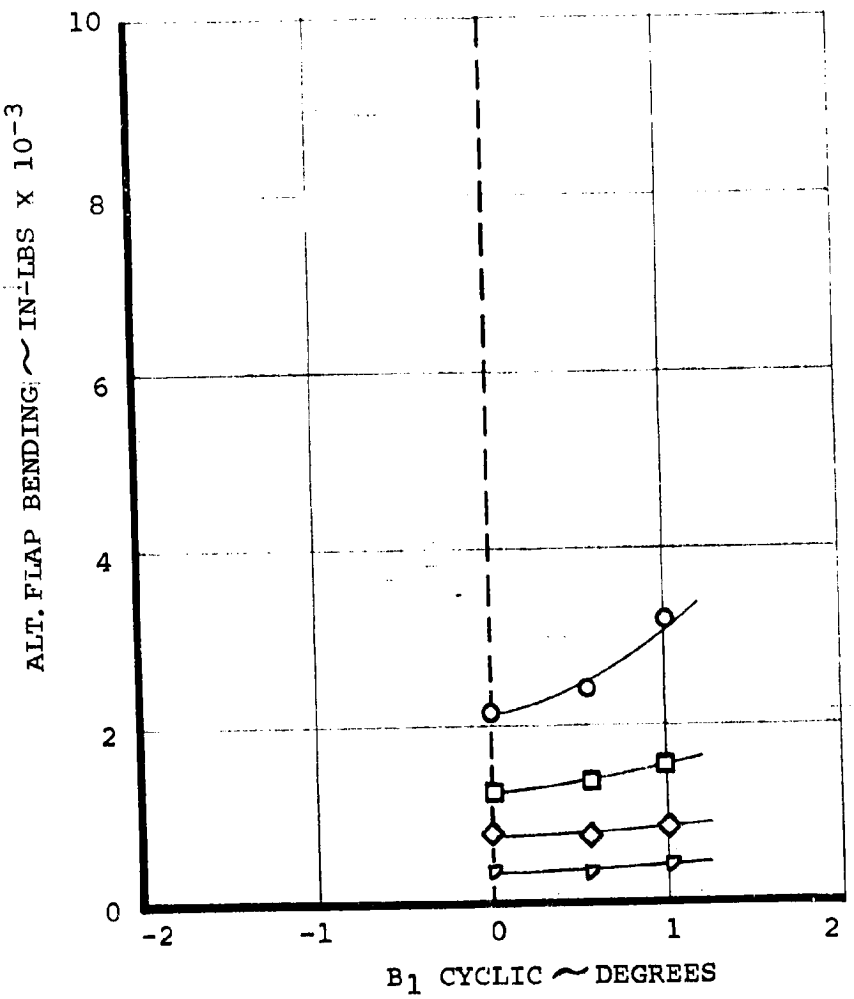

FIGURE 4.95 ALTERNATING FLAP BLADE LOADS DUE TO B_1 CYCLIC — V = 100 KNOTS, 445 RPM

NASA AMES TEST 410
RUN 53, 100 KNOTS, 445 RPM

$A_1 = 0°$

○ - 10.5% Radius
□ - 55% Radius

$$\Delta\theta = -A_1 \cos(\psi + 20) - B_1 \sin(\psi + 20)$$

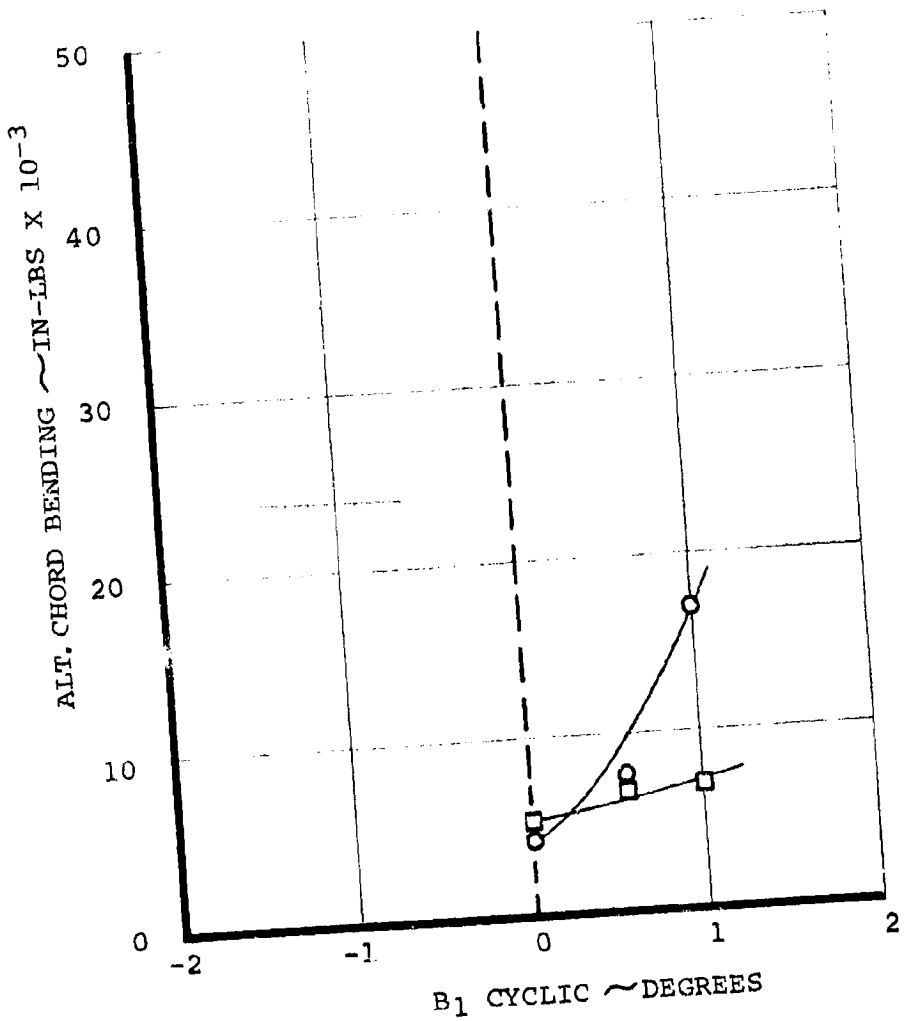

FIGURE 4.96 ALTERNATING CHORD BLADE LOADS DUE TO B_1 CYCLIC - V = 100 KNOTS, 445 RPM

NASA AMES TEST 410
RUN 52, 140 KNOTS, 420 RPM

$B_1 = 0°$

○ - 10.5% Radius
□ - 22.5% Radius
◇ - 42.5% Radius
▽ - 55% Radius

$$\Delta\theta = -A_1 \cos(\psi + 20) - B_1 \sin(\psi + 20)$$

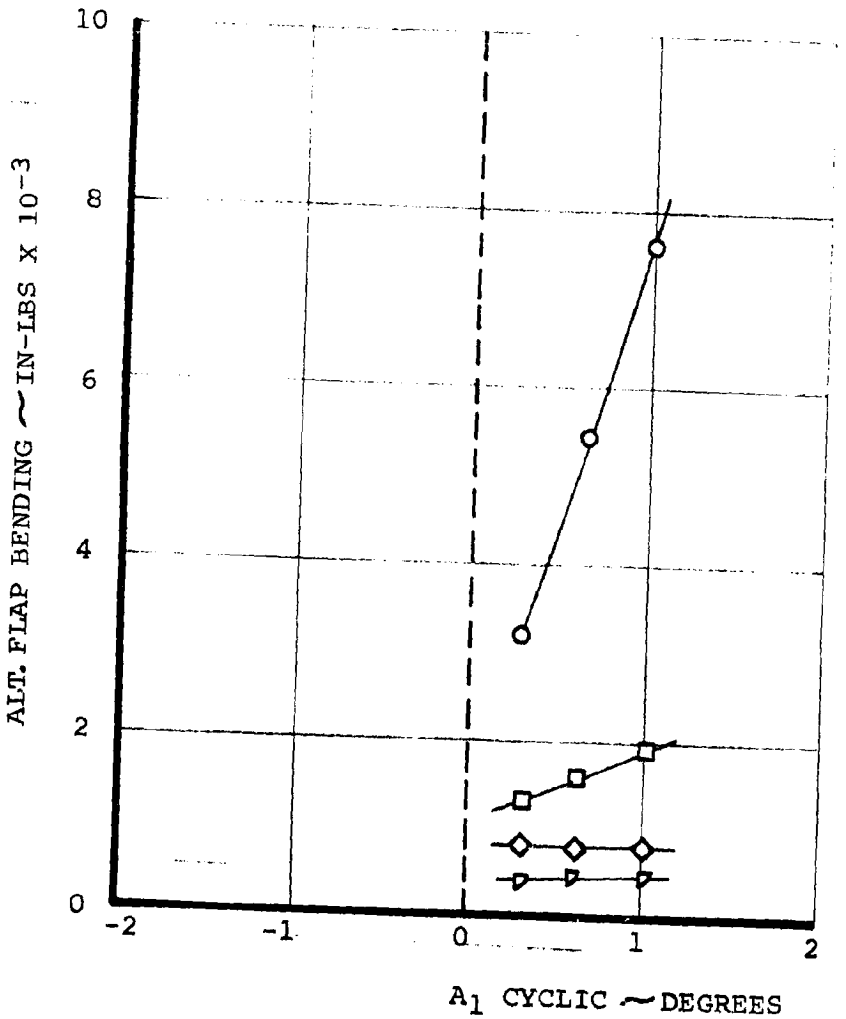

FIGURE 4.97 ALTERNATING FLAP BLADE LOADS DUE TO A_1 CYCLIC - V = 140 KNOTS, 420 RPM

NASA AMES TEST 410
RUN 52, 140 KNOTS, 420 RPM

$B_1 = 0°$

○ - 10.5% Radius
□ - 55% Radius

$$\Delta\theta = -A_1 \cos(\psi + 20) - B_1 \sin(\psi + 20)$$

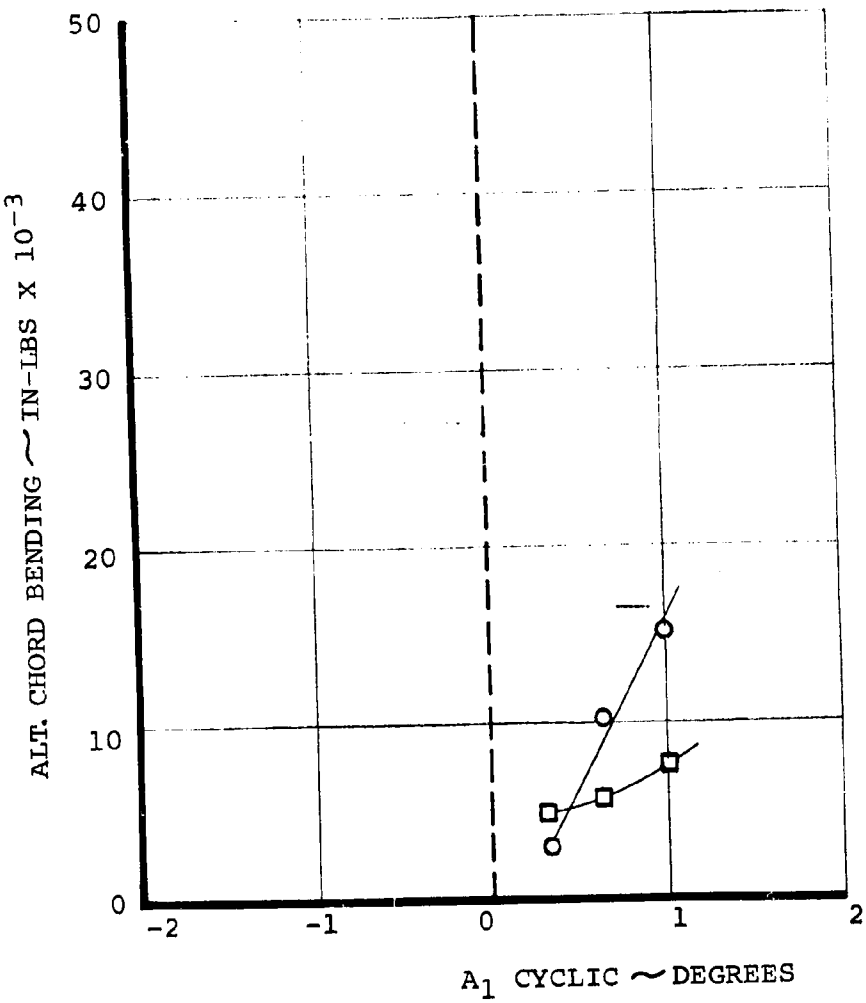

FIGURE 4.98 ALTERNATING CHORD BLADE LOADS DUE TO A_1 CYCLIC — V = 140 KNOTS, 420 RPM

NASA AMES TEST 410
RUN 59, 192 KNOTS, 300 RPM

$B_1 = 0°$

□ - 22.5% Radius
◇ - 42.5% Radius
▽ - 55% Radius

$$\Delta\theta = -A_1 \cos(\psi + 20) - B_1 \sin(\psi + 20)$$

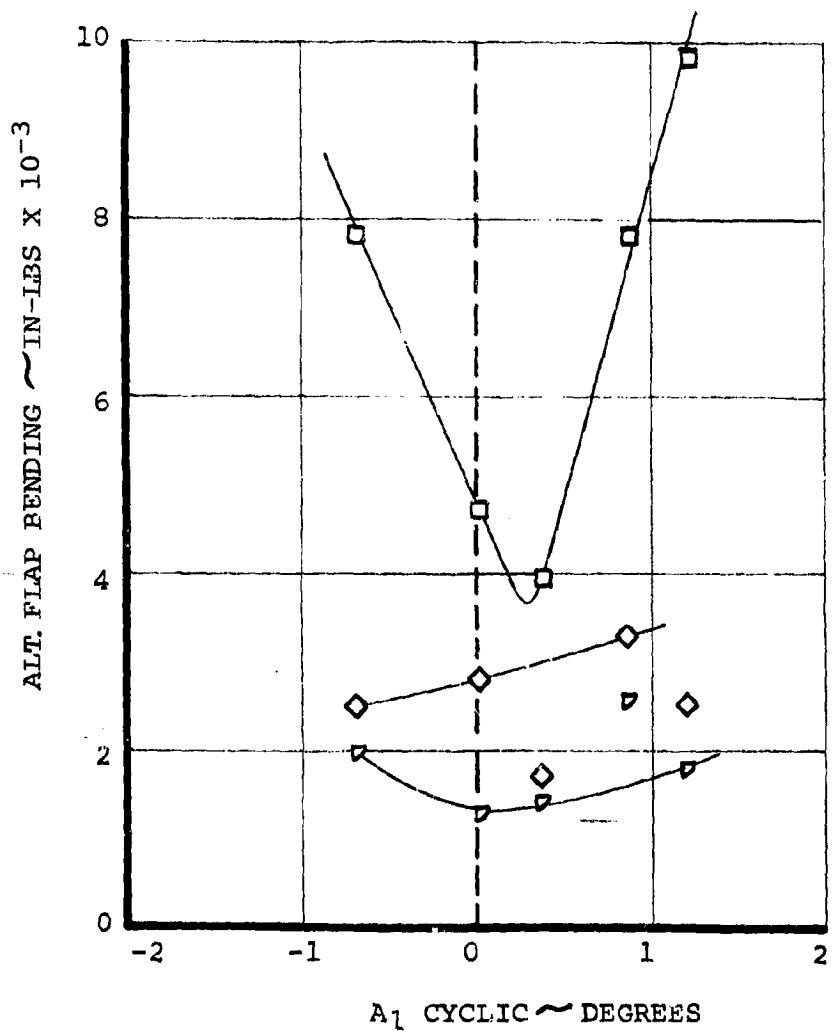

FIGURE 4.99 ALTERNATING FLAP BLADE LOADS DUE TO A_1 CYCLIC - $V = 192$ KNOTS, 300 RPM

NASA AMES TEST 410
RUN 59, 192 KNOTS, 300 RPM

$A_1 = 0°$

□ - 22.5% Radius
◇ - 42.5% Radius
▽ - 55% Radius

$$\Delta\theta = -A_1 \cos(\psi + 20) - B_1 \sin(\psi + 20)$$

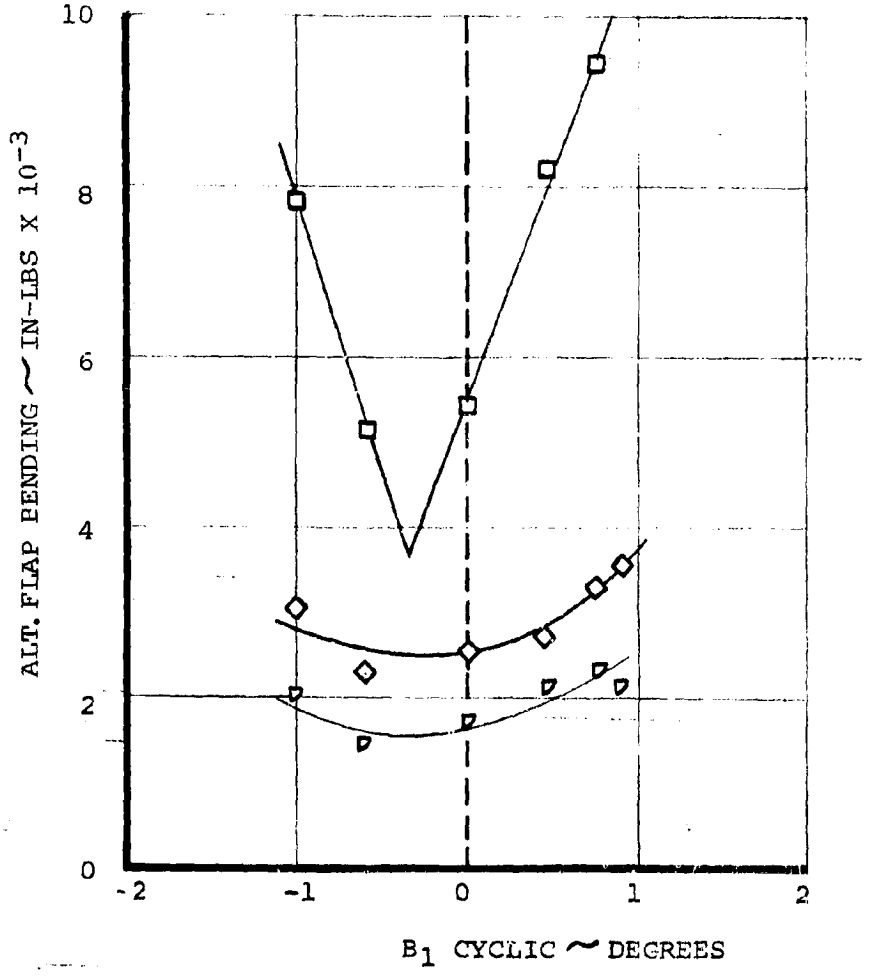

FIGURE 4.100 ALTERNATING FLAP BLADE LOADS DUE TO B_1 CYCLIC - V=192 KNOTS, 300 RPM

NASA AMES TEST 410
RUN 59, 192 KNOTS, 300 RPM

$B_1 = 0°$

□ - 55% Radius

$\Delta\theta = -A_1 \cos(\psi + 20) - B_1 \sin(\psi + 20)$

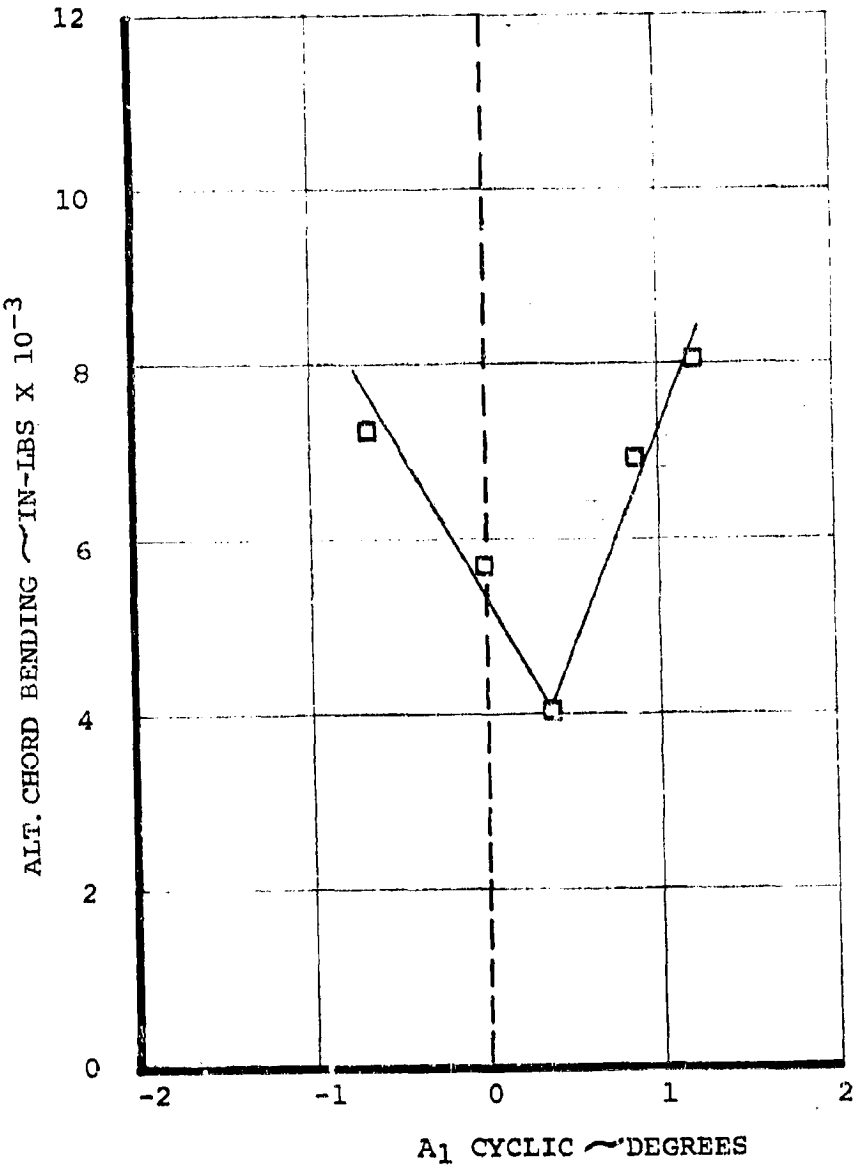

FIGURE 4.101 ALTERNATING CHORD BLADE LOAD @ 55% R DUE TO A_1 CYCLIC - V = 192 KNOTS, 300 RPM

NASA AMES TEST 410
RUN 59, 192 KNOTS, 300 RPM

$A_1 = 0°$

□ - 55% Radius

$\Delta\Theta = -A_1 \cos(\psi + 30) - B_1 \sin(\psi + 30)$

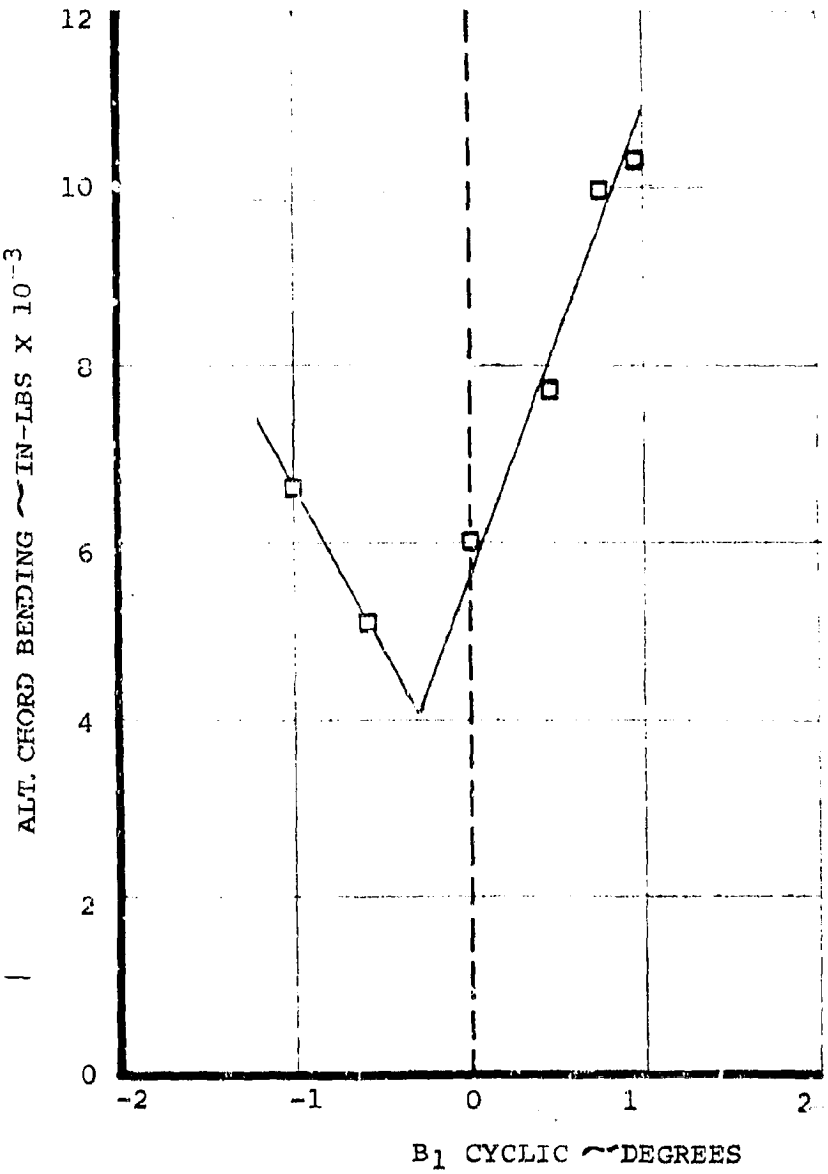

FIGURE 4.102 ALTERNATING CHORD BLADE LOAD @ 55%R DUE TO B_1 CYCLIC - V = 192 KNOTS, 300 RPM

Steady Loads in Windmilling Flight

Figures 4.103 and 4.104 show the steady blade root bending loads in windmilling flight. These loads are due to the precone (2½°) and torque offset (0.65" lead) built into the rotor.

NASA AMES TEST 410

$\alpha = 0°$

ZERO CYCLIC

O — RUN 4, BLADE 2, 50 KTS.

■ — RUN 9, BLADE 3, 100 KTS.

Δ — RUN 10, BLADE 3, 100 KTS.

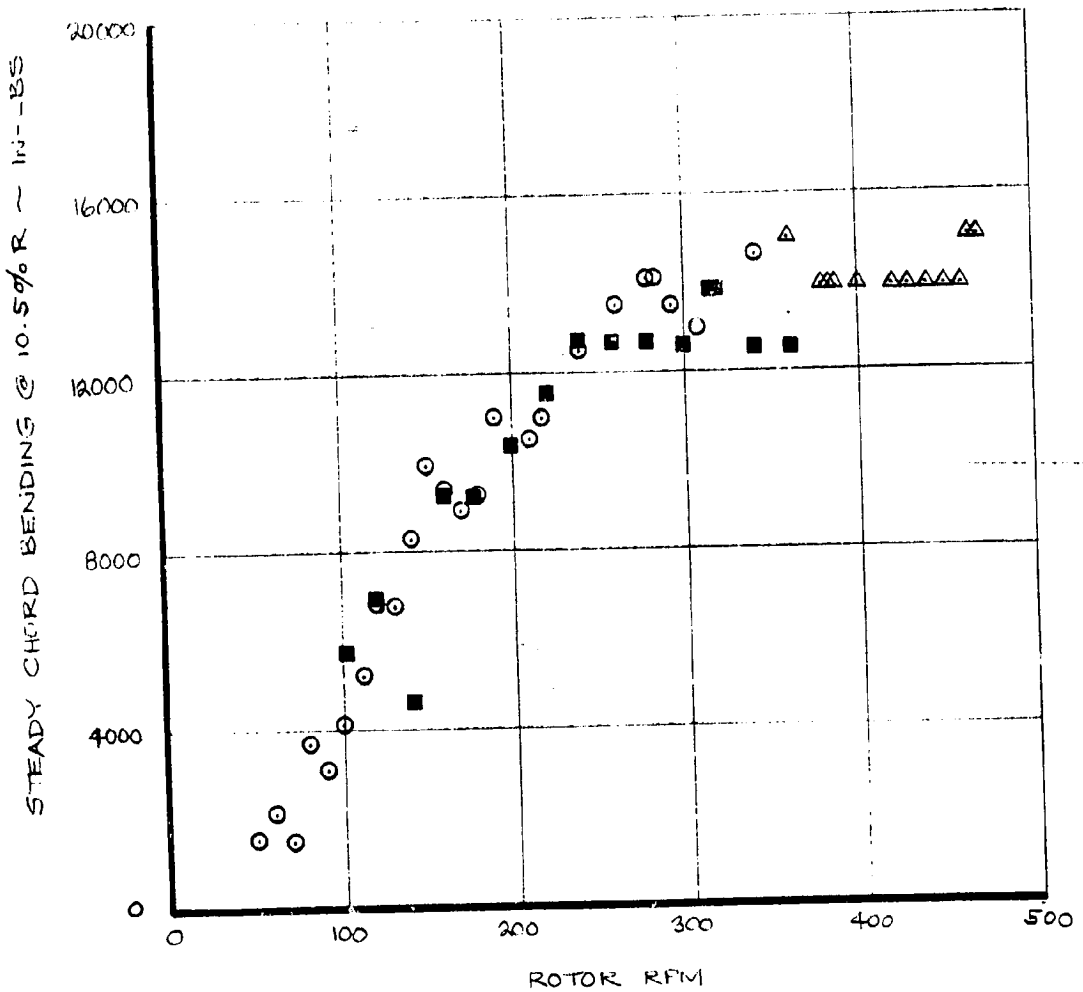

FIGURE 4.103 EFFECT OF ROTOR RPM AND AIRSPEED ON STEADY CHORD BENDING @ 10.5% R – $\alpha = 0°$

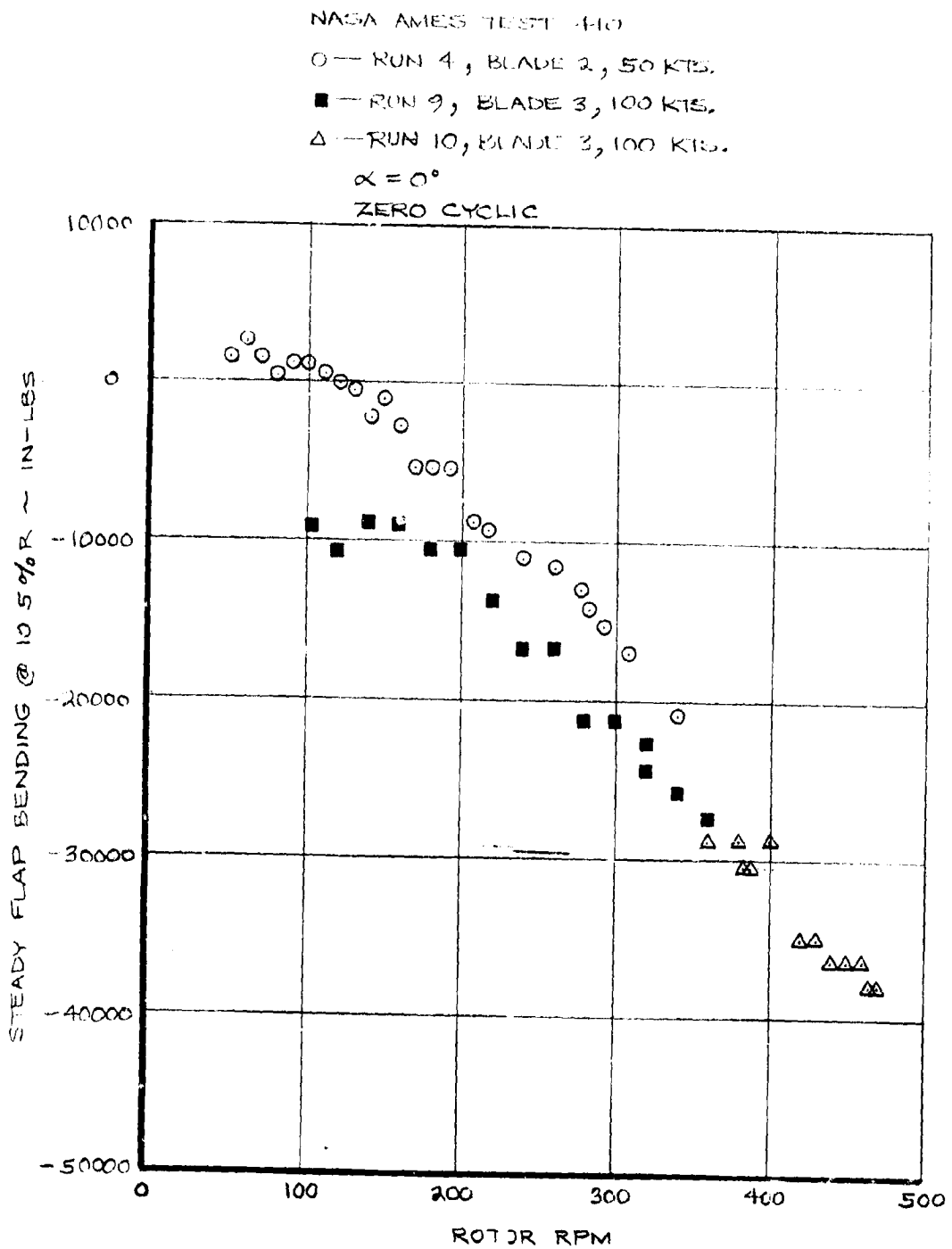

FIGURE 4.104 EFFECT OF ROTOR RPM AND AIRSPEED ON STEADY FLAP BENDING @ 10.5% R - α = 0°

5.0 CONTROL LOADS

5.0 CONTROL LOADS

The control loads data presented in this section are taken entirely from test 416 (powered). Two types of measurement were taken. The pitch links were strain gaged and the output of one of them taken through a slip ring to the signal conditioning equipment. The second measurement was the loads experienced on the longitudinal actuator ground point bolt. The bolt was a special STRAINCERT bolt which was bored out and contained a strain gage bridge. The actuator for which this bolt was used was located at an azimuthal location of $\psi = 90°$. Azimuthal axes definition is given in Figure 4.24.

The pitch link load data were recorded on oscillograph and the wave forms obtained contained a one per rev spike. This spike has been faired out of the alternating pitch link load data. Examples of the wave form and the rationale for disregarding the "spike" are given at the end of this section of the report.

5.1 Hover Control Loads

Pitch link steady loads result primarily from planipetal torsion which is a function of collective pitch and centrifugal force, i.e., (RPM^2). Figure 5.1 shows the steady pitch link load data obtained from Run 6. The steady loads increase as RPM squared and compare well with the predicted steady loads. At 285 RPM

the data show a reduction in pitch link load corresponding to the 1st blade mode bending one per rev frequency crossing. The steady loads measured on the longitudinal upper boost actuator ground point bolt are shown in the same figure. The relationship given in Reference 18 between the actuator ground point steady load and the pitch link load is

$$\text{ACT. STEADY LOAD} = 1.5\ (\text{P.L. STEADY}) + \frac{11.6}{18.56}\ (1.801)\ (\text{PL ALT.})$$

The alternating pitch link load in the above equation is the one per rev component which becomes a steady load in the fixed system. The alternating loads from Run 6 are given in Figure 5.2 and are low although a load amplification is again observed at an RPM corresponding to the blade 1st mode bending one per rev frequency crossing. Applying the above expression to the pitch link load data the actuator steady load would calculate to -1527 lbs. which compares well with the 1550 lbs. measured at 550 RPM.

Figures 5.3 and 5.4 show the effect of collective pitch on the steady and alternating control loads in hover at 551 RPM. The steady pitch link loads are 8% lower than predicted and increase as collective pitch increases at the same rate as the predicted line (Figure 5.3).

The steady actuator bolt data shown in Figure 5.3 is consistent with the pitch link load data. At $\theta_{.75} = 9.0°$ the actuator bolt

load calculated from the pitch link data is 1476 lbs. compared with 1450 lbs. measured and at $\theta_{75} = 12°$ the pitch link data indicate an actuator bolt load of 1775 lbs. compared with 1740 lbs. measured.

Cyclic pitch introduces a one per rev blade pitch inertial load to the pitch link. The alternating control loads due to cyclic pitch in hover are given in Figures 5.5 and 5.6. The alternating pitch link load data increase at slightly less than the predicted rate and are a little higher than predicted due to the residual alternating load at zero cyclic. These alternating loads are low. The endurance limit load for the socket pitch link bracket was $\pm$910 lbs. The alternating actuator bolt loads are approximately the same magnitude as the alternating pitch link loads. The endurance limit load for the STRAINCERT bolt was $\pm$810 lbs. and for the normal actuator ground point bolt $\pm$1440 lbs.

The steady control loads measured during the cyclic sweeps, Figures 5.7 and 5.8, give a steady pitch link load of 900 lbs. compression. The actuator bolt loads increase with A_1 cyclic pitch due to the increase in one per rev alternating cyclic pitch observed in Figure 5.5. The alternating pitch link load due to A_1 increases by 210 lbs. due to 3° cyclic and should

result in a 237 lb. increase in actuator bolt steady load. The measured bolt loads of Figure 5.7 confirm this.

The B_1 cyclic data, Figure 5.6, show the steady actuator bolt loads reducing with increased cyclic pitch. The one per rev alternating pitch link loads (Figure 5.6) increase in a similar manner to the A_1 data (Figure 5.5) and would be expected to result in an increase in steady actuator ground point bolt load.

The steady pitch link loads show a reduction in steady load at the higher B_1 inputs which could account for the drop in actuator load. The other possible explanation is swashplate or actuator fouling. The rotor loads (Section 4.2) and force and moment data (Section 6.1) as well as the alternating pitch link load data indicate that the cyclic pitch was in fact input to the swashplate and the rotor. The output of the blade angle potentiometer mounted on the root of blade no. 1 also indicate that the cyclic pitch was felt by the blades.

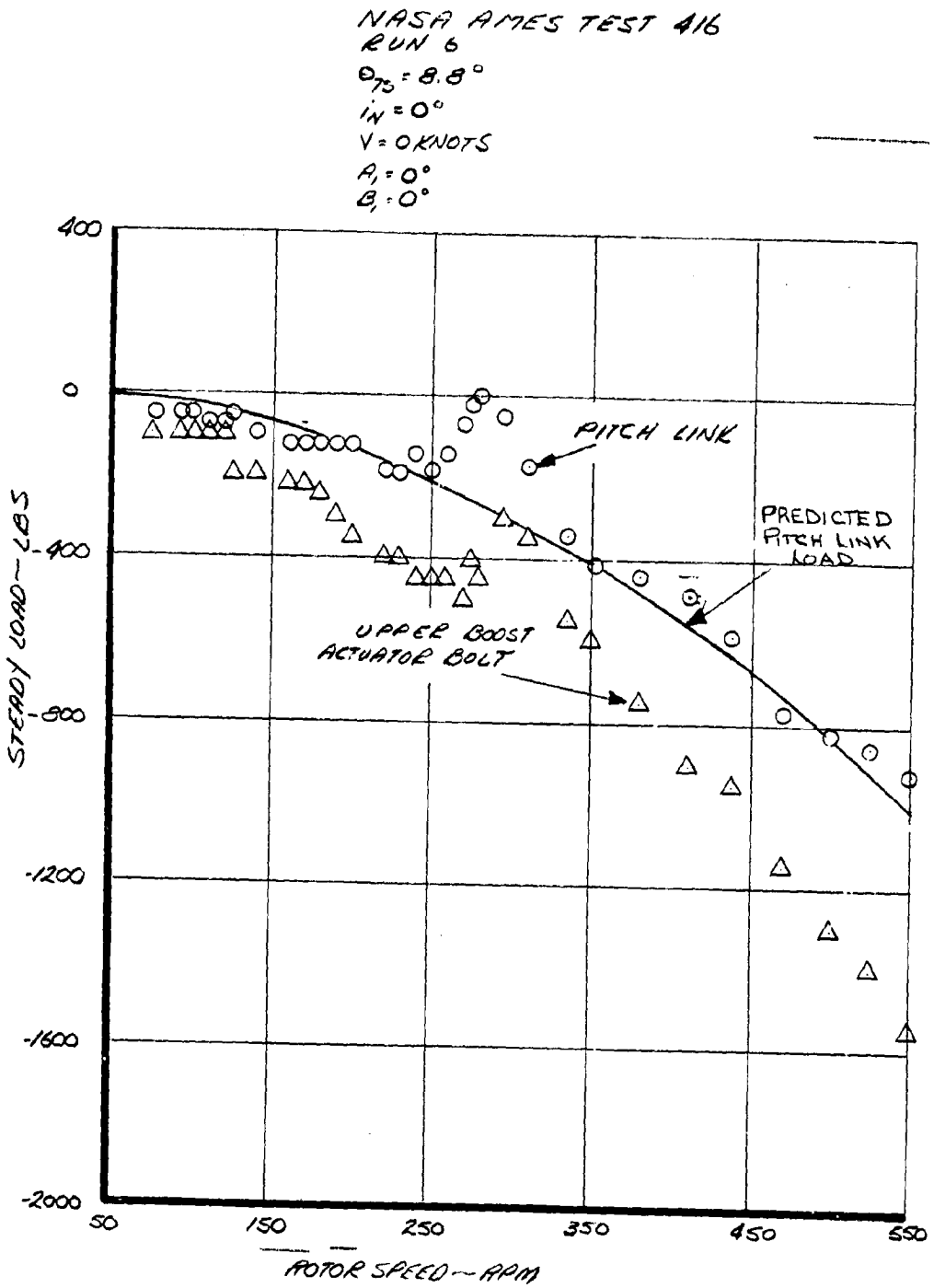

FIGURE 5-1 EFFECT OF RPM ON STEADY CONTROL LOADS IN HOVER. $\theta_{.75} = 8.8°$ ZERO CYCLIC

NASA AMES TEST 416
RUN 6
$\theta_{.75} = 8.8°$
$i_N = 0°$
V = 0 KNOTS
$A_1 = 0°$
$B_1 = 0°$

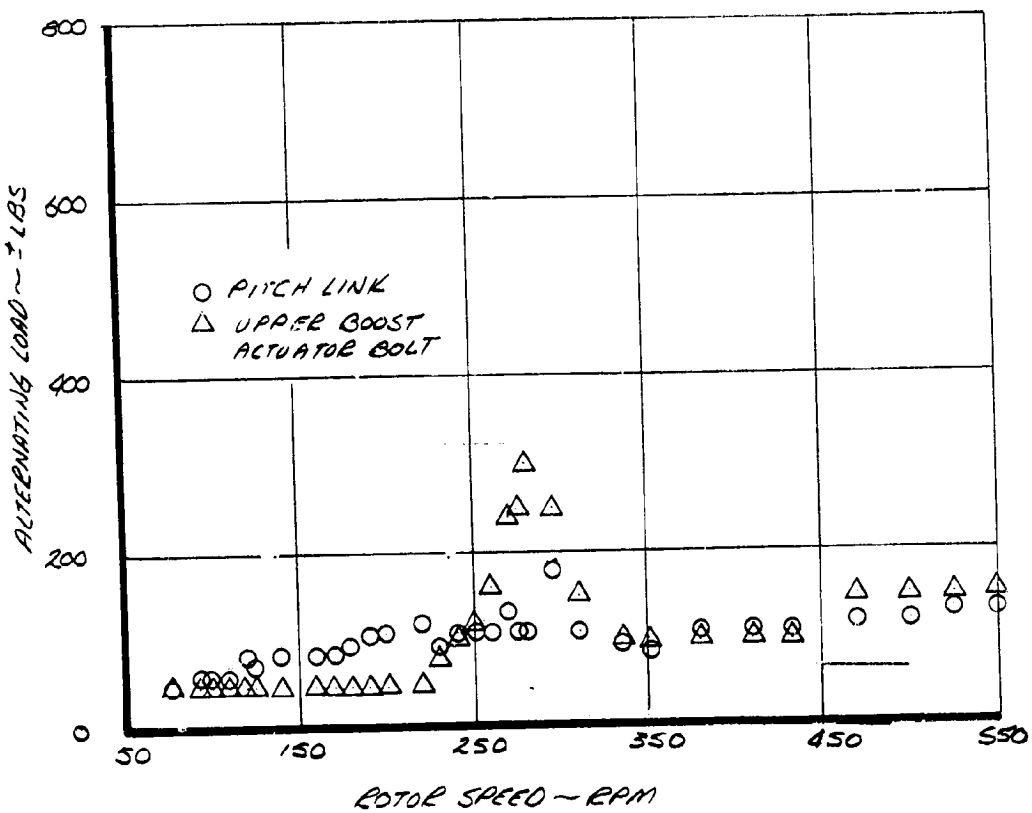

FIGURE 5-2 EFFECT OF RPM ON ALTERNATING CONTROL LOADS IN HOVER, $\theta_{.75} = 8.8°$ ZERO CYCLIC

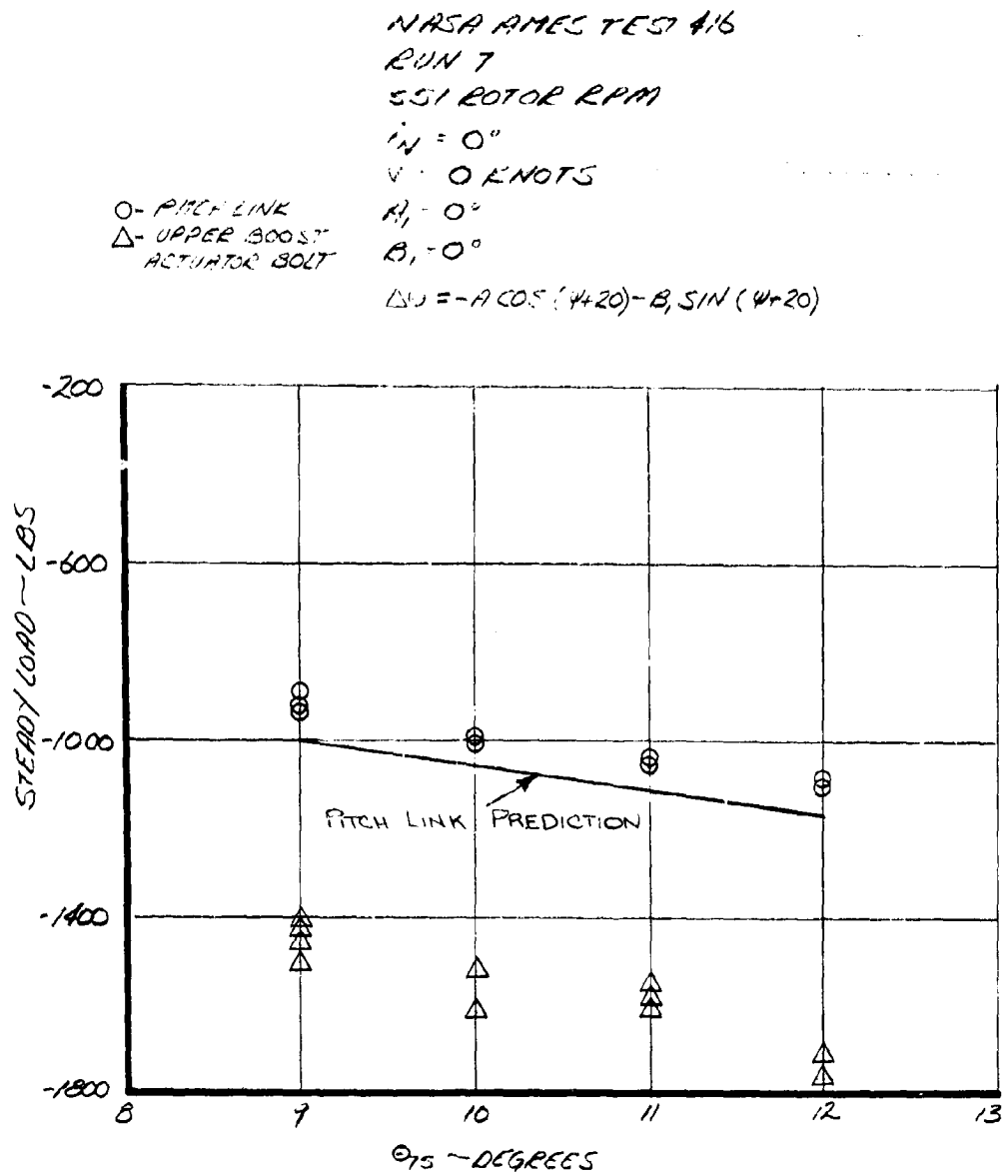

FIGURE 5-3 EFFECT OF COLLECTIVE PITCH ON STEADY CONTROL LOADS IN HOVER, 551 RPM ZERO CYCLIC

NASA AMES TEST 416
RUN 7
551 ROTOR RPM
$\psi_N = 0°$
V = 0 KNOTS
$A_1 = 0°$
$B_1 = 0°$
$\Delta\theta = -A_1 \cos(\psi+20) - B_1 \sin(\psi+20)$

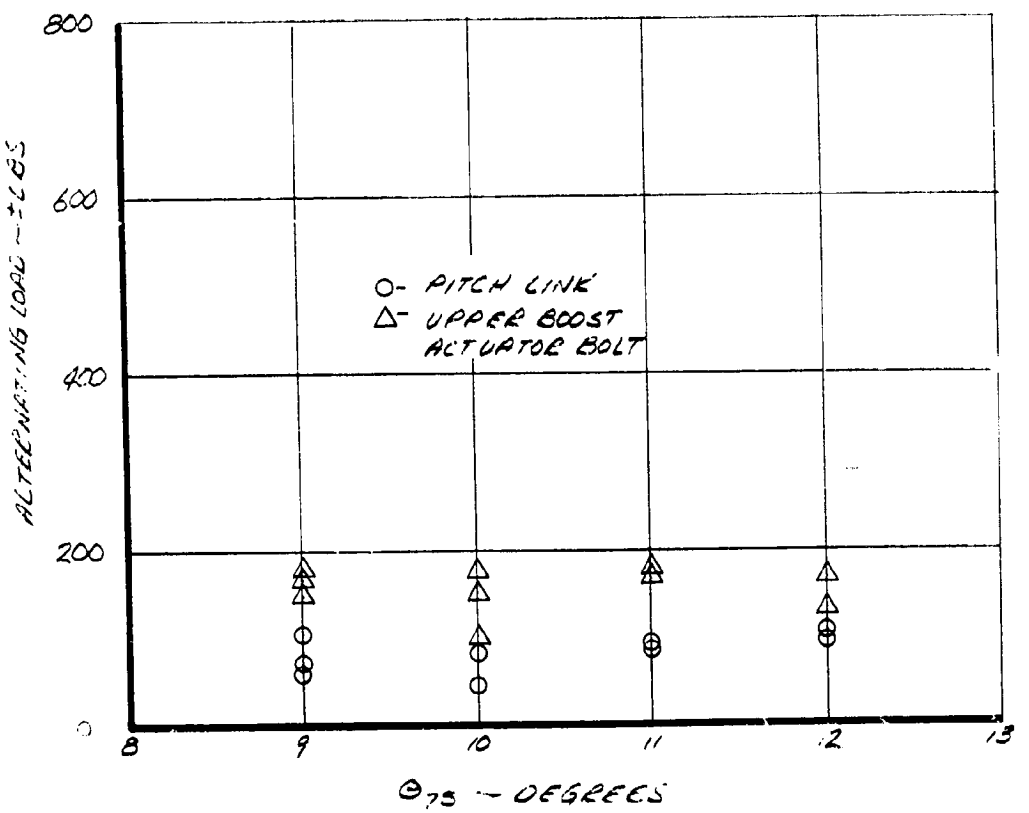

FIGURE 5-4 EFFECT OF COLLECTIVE PITCH ON ALTERNATING CONTROL LOADS IN HOVER, 551 RPM ZERO CYCLIC

NASA AMES TEST A/C
RUN 7
551 ROTOR RPM
$\theta_{.75} = 9°$
$i_N = 0°$
V = 0 KNOTS
$\theta_1 = 0°$
$\Delta\theta = -A_1 \cos(\psi+20) - B_1 \sin(\psi+20)$

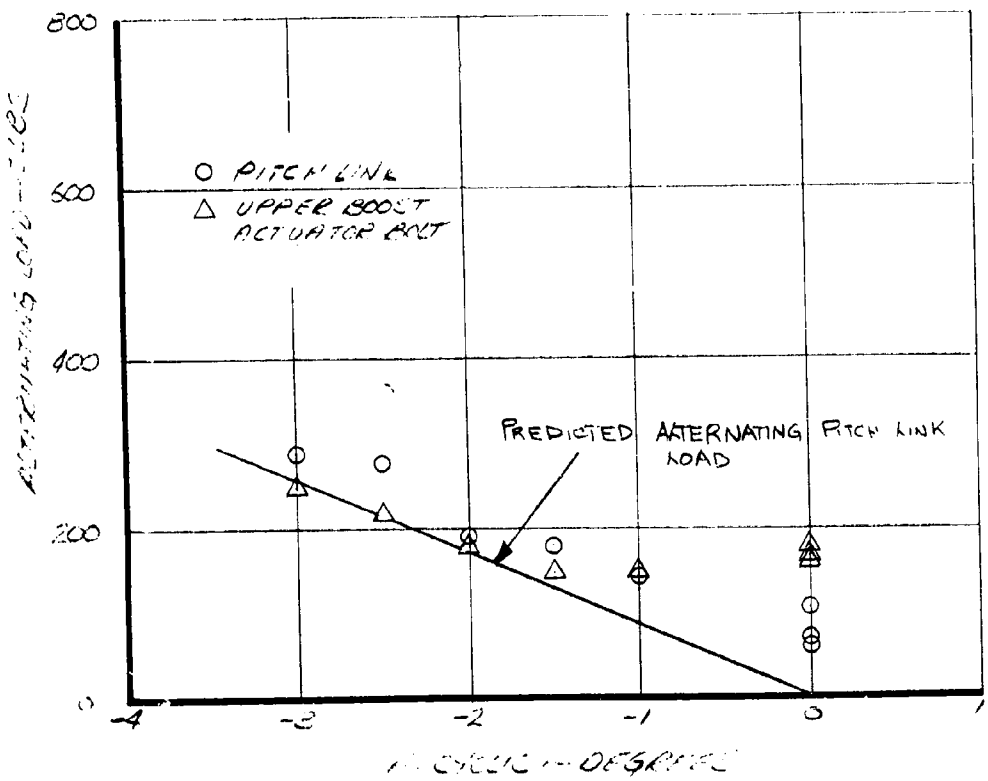

FIGURE 5-5 EFFECT OF LATERAL CYCLIC ON ALTERNATING CONTROL LOADS IN HOVER. 551 RPM $\theta_{.75} = 9°$

NASA AMES TEST 416
RUN 7
551 ROTOR RPM
$\Theta_{.75} = 9°$
$i_N = 0°$
V = 0 KNOTS
$A_1 = 0°$
$\Delta\Theta = -A_1 \cos(\psi - 20) - B_1 \sin(\psi + 20)$

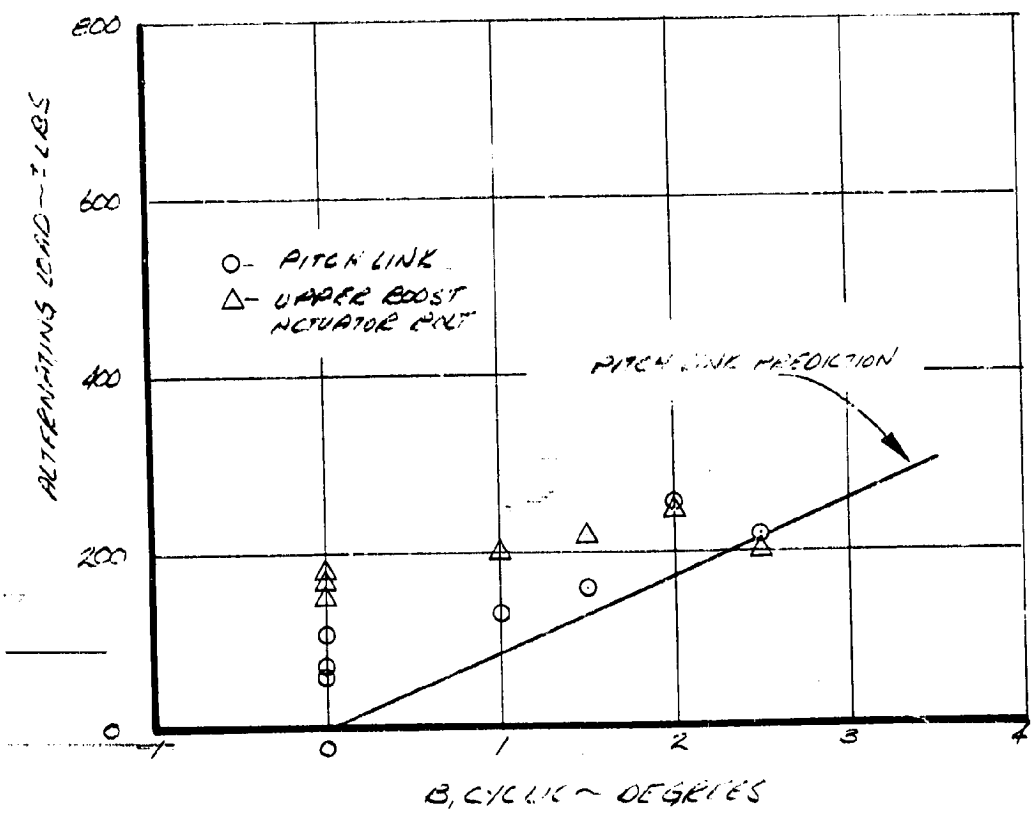

FIGURE F-6 EFFECT OF LONGITUDINAL CYCLIC ON ALTERNATING CONTROL LOADS IN HOVER. 551 RPM $\Theta_{.75} = 9°$

NASA AMES TEST 416
RUN 3
551 ROTOR RPM
$\theta_{.75} = 9°$
$i_N = 0°$
V = 0 KNOTS
$B_1 = 0°$
$\therefore \theta = -A_1 \cos(\psi+20) - B_1 \sin(\psi+20)$

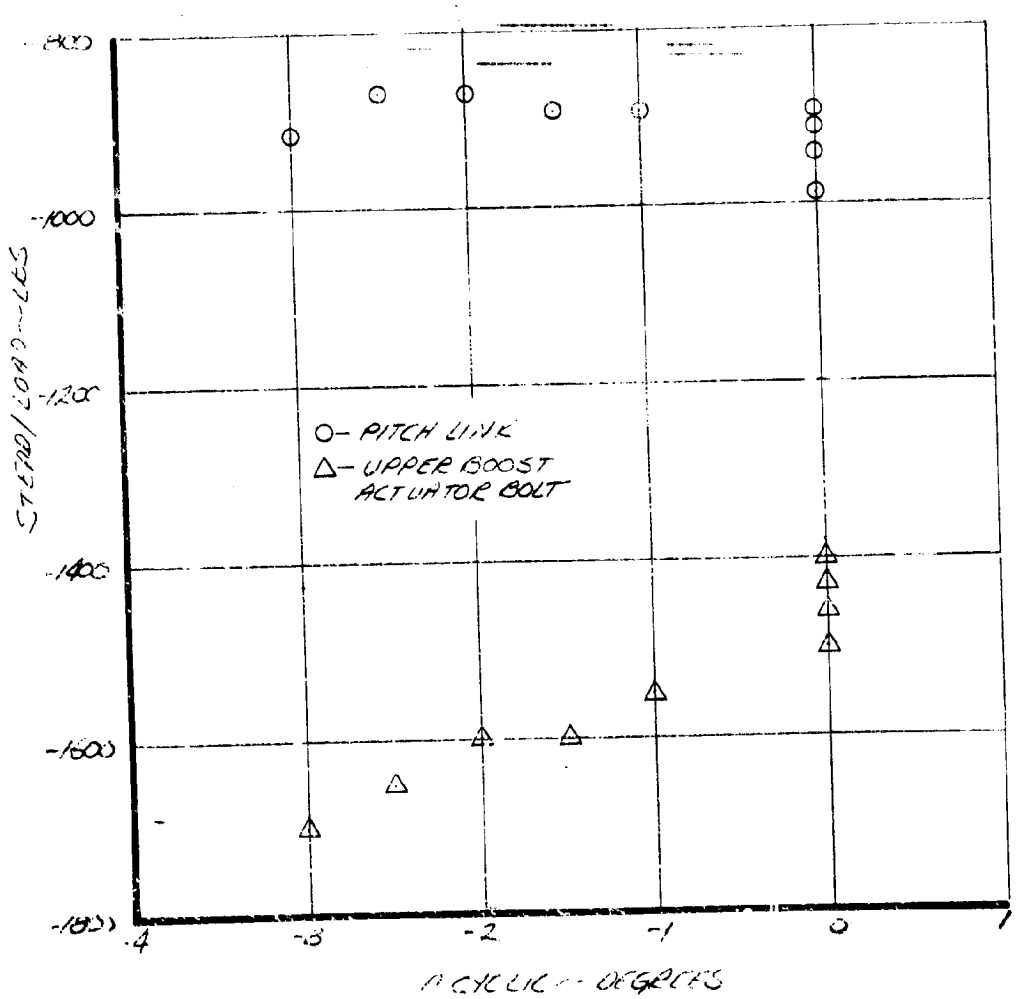

FIGURE 5-7 EFFECT OF LATERAL CYCLIC ON STEADY CONTROL LOADS IN HOVER. 551 RPM $\theta_{.75} = 9°$

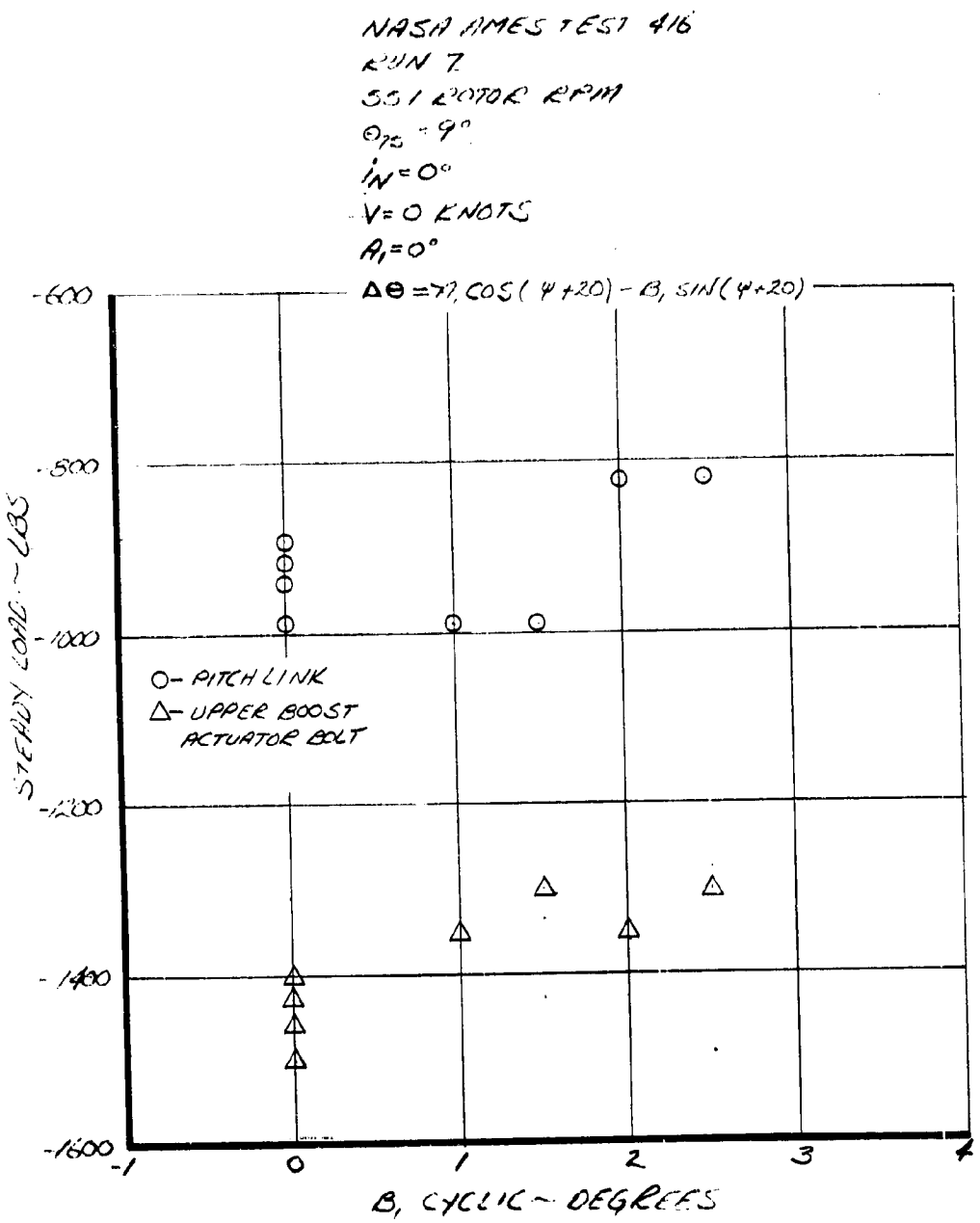

FIGURE 5-8 EFFECT OF LONGITUDINAL CYCLIC ON STEADY CONTROL LOADS IN HOVER. 551 RPM $\theta_{.75} = 9°$

5.2 Transition Control Loads

The test runs performed in transition consisted of control parameter variations about discrete test conditions at which the blade loads were minimized by the application of cyclic pitch.

The lowest velocity transition data was obtained at $i_N = 85°$ and 45 knots on Run 19. This run was done at 500 RPM to avoid a ground resonance which is discussed in Section 3.3. The steady and alternating control loads due to collective and cyclic control inputs are plotted in Figures 5.9 to 5.14. The steady pitch link loads increase with collective and are lower than predicted. The prediction is the 551 RPM case reduced by RPM squared. The alternating pitch link loads reduce as collective is increased. The alternating pitch link load at the nominal collective setting for this condition, $\theta_{75} = 8.9°$, is 310 lbs. Extrapolating the hover data to the cyclic values used on this run the alternating load would be expected to be higher. The difference is due to the reduced RPM. The variations of cyclic pitch given in Figures 5.11 to 5.14 show the steady and alternating control loads to be insensitive to cyclic over the range achieved.

Run 22 was performed at $i_N = 83°$ and 76 knots, again at 500 RPM. Control load data for collective and cyclic pitch sweeps about

the minimum blade load condition are plotted in Figures 5.15 to 5.20.

The steady control loads, Figure 5.15, increase slightly with collective and the upper boost actuator bolt loads are a little more than 50% greater than the pitch link steady loads despite the alternating pitch link loads shown in Figure 5.16. At this condition a high percentage of the pitch link alternating loads are three per rev, which would not affect the actuator steady loads. The alternating pitch link loads are about $\pm$1000 lbs. and are slightly higher than the endurance limit load for the test pitch link ($\pm$910 lbs.) but less than the maximum established for testing purposes (Ref. 19, $\pm$1100 lbs. maximum allowable).

The effects of cyclic pitch control on the steady and alternating control loads at this condition are given in Figures 5.17 to 5.20.

The A_1 cyclic data show a small increase in steady pitch link load as A_1 is reduced. The actuator bolt loads do not reflect the increase. The alternating loads are the same magnitude as for the collective sweep and are insensitive to the small A_1 variation obtained.

The steady pitch link loads increase as B_1 cyclic is input whereas the actuator load decreases. For this to occur an alternate load path must exist for the actuator load.

The blade angle potentiometer on No. 1 blade root indicates a resultant cyclic magnitudes and azimuths consistent with the cyclic values set using the actuator feedback potentiometer voltage. This in addition to the loads, stability and performance data of Sections 4, 6 and 7 provide confidence that the cyclic was applied to the rotor. The reason for making this point clear is that it is possible to read a change in feedback potentiometer voltage if the upper boost actuator had not moved since the upper boost actuator spool valve travel is 0.06" (equivalent to 1.02° B_1). This kind of problem highlights the importance of measuring control inputs as close to the blade as possible and makes the use of a blade angle potentiometer in conjunction with a resolver (such as was used for hub moment data, Section 6) attractive in future testing.

Frequent visual inspections of the swashplate and controls were made throughout the test because of difficulties in moving both the collective and B_1 cyclic with SAS off. No swashplate fouling was apparent. The other possible load path is the control input rod itself. This would require a damaged upper boost actuator and/or spool valve to allow the loads to be transferred to the lower controls and might possibly explain some of the difficulties experienced.

A further indicator of trouble is the alternating actuator bolt loads throughout this run. The alternating pitch link loads are high and contain a large percentage of three per rev loads. These loads would be expected to reach the actuator as alternating loads. Understanding the transfer of alternating loads from the rotating to non-rotating system in practice has always been difficult. In view of the steady measured loads it is reasonable to assume that the actuator alternating loads are artificially low in this case.

Two test runs were made at i_N = 66° and 80 knots, Run 20 at 500 RPM and Run 21 at 550 RPM. The control loads measured on Run 20 are given in Figures 5.21 to 5.26. Both the pitch link and actuator bolt steady loads increase with collective pitch (Figure 5.21) and the alternating loads show a tendency to increase a little as collective is increased or decreased away from the nominal value (9.8°) at which the cyclics reduced blade bending loads to a minimum. The A_1 cyclic sweep data, Figures 5.23 and 5.24, show steady and alternating loads to be relatively insensitive to cyclic control. The steady pitch link loads due to B_1 cyclic, Figure 5.25, increase slowly. The actuator bolt steady loads again reduce as B_1 is increased in spite of the increase in steady and alternating pitch link loads shown in Figures 5.25 and 5.26.

The cyclic pitch values are again confirmed by the blade angle pot trace and give us cause to doubt the loads, stability or performance data. The actuator bolt loads should be treated with caution.

For the 550 RPM i_N = 66° and 80 knots condition the control loads are shown in Figures 5.27 through 5.32. The steady pitch link loads increase with collective pitch as predicted and the alternating pitch link loads also show an increase (Figure 5.28). The steady actuator bolt loads are less than would be expected from the pitch link loads and probably contain fouling problems as previously discussed. The pitch link steady loads are insensitive to cyclic pitch, Figures 5.29 and 5.31. The alternating pitch link loads show a small decrease as A_1 cyclic increases. The B_1 alternating pitch link loads (Figure 5.32) increase with cyclic as expected.

Run 9 was performed at i_N = 27° 105 knots and 551 RPM. For this run and others at low incidence and high tunnel speed a low collective stop was installed to protect against the danger of a runaway actuator to low collective (and hence high RPM due to windmilling torque). The sensitivity of RPM to collective in this flight mode is high and shown from the windmill test in Figure 7.37. For this run the swashplate was fouling on the

collective stops at 18.9° and below. This coupled with apparent fouling associated with the B_1 actuator make the actuator bolt loads unintelligible and these data have been discarded. The steady pitch link loads due to collective agree with the prediction and the alternating loads are insensitive to the small collective range actually achieved. The steady pitch link loads are insensitive to cyclic pitch and the alternating loads increase with cyclic, Figures 5.35 to 5.38. Figures 5.39 and 5.40 are the pitch link loads for an incidence sweep from 15° to 27°.

Run 13 was also performed at i_N = 27° 551 RPM but at 140 knots. During this run the collective was fouled on the low collective stop and the actuator bolt data are invalid. The cyclic inputs are verified by the blade angle pot. The pitch link load data for cyclic and incidence sweeps are given in Figures 5.41 through 5.43 and give similar results as Run 9.

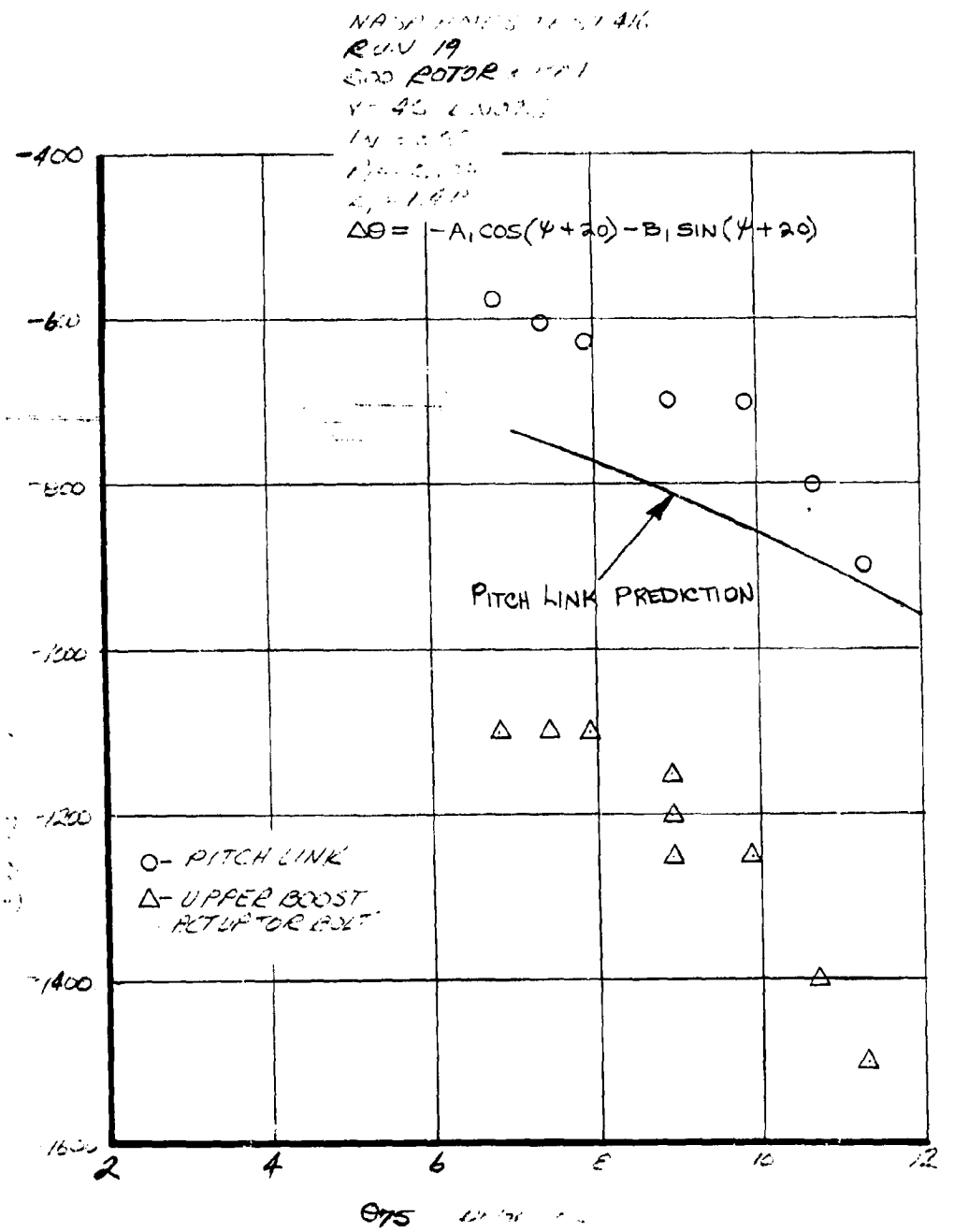

FIGURE 5-9 EFFECT OF COLLECTIVE PITCH ON STEADY CONTROL LOADS. 45 KNOTS, $i_N = 85°$, 500 RPM

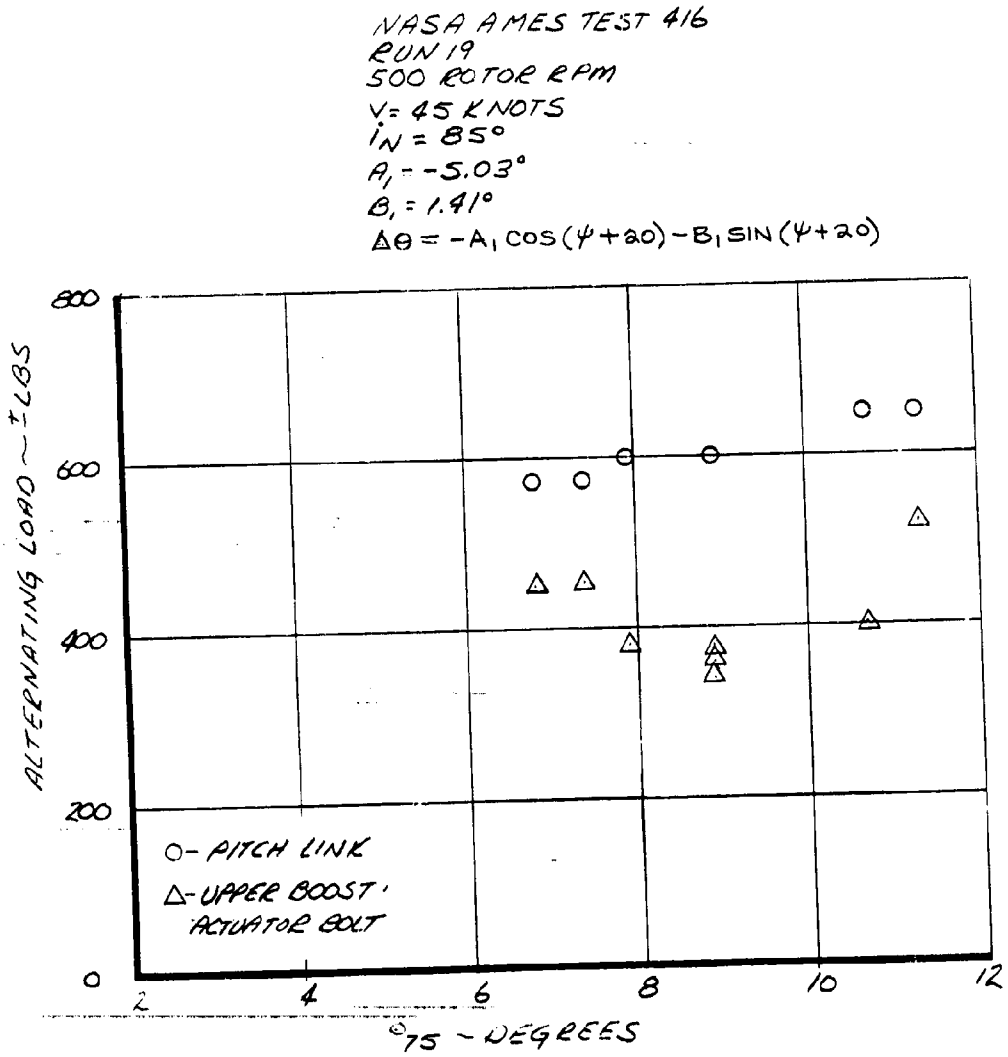

FIGURE 5-10 EFFECT OF COLLECTIVE PITCH ON ALTERNATING CONTROL LOADS. 45 KNOTS, i_N = 85°, 500 RPM

$$\Delta\theta = -A_1 \cos(\psi + 20) - B_1 \sin(\psi + 20)$$

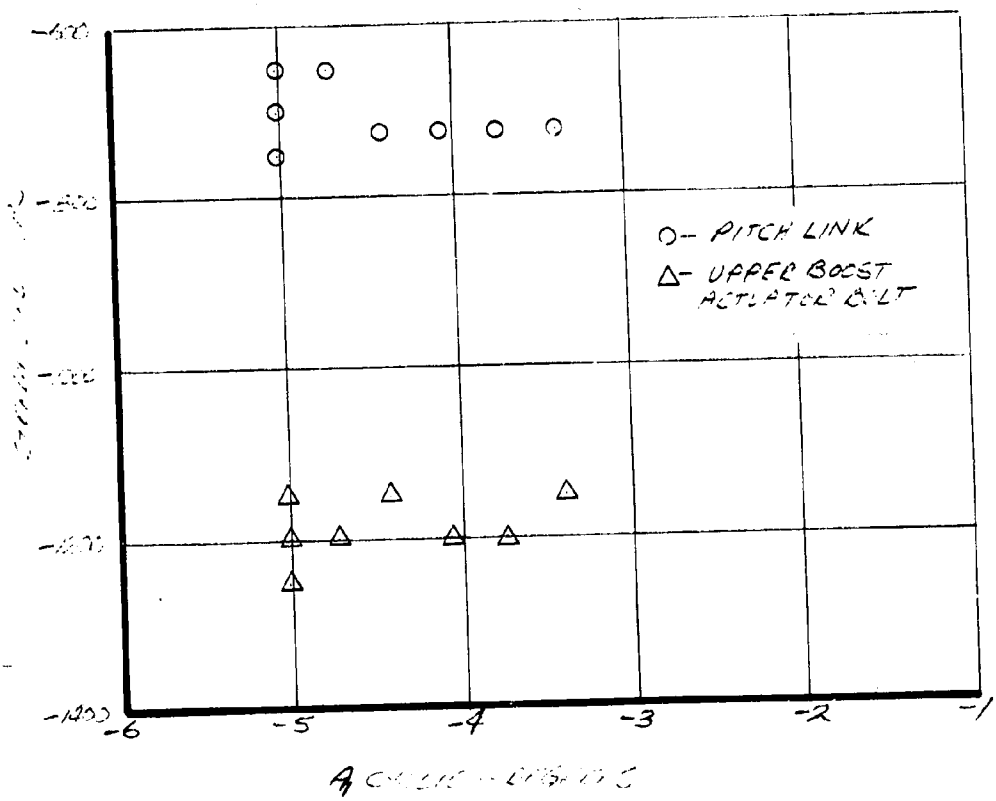

FIGURE 5-11 EFFECT OF LATERAL CYCLIC ON STEADY CONTROL LOADS. 45 KNOTS, $i_N = 85°$, 500 RPM, $\theta_{.75} = 8.9°$

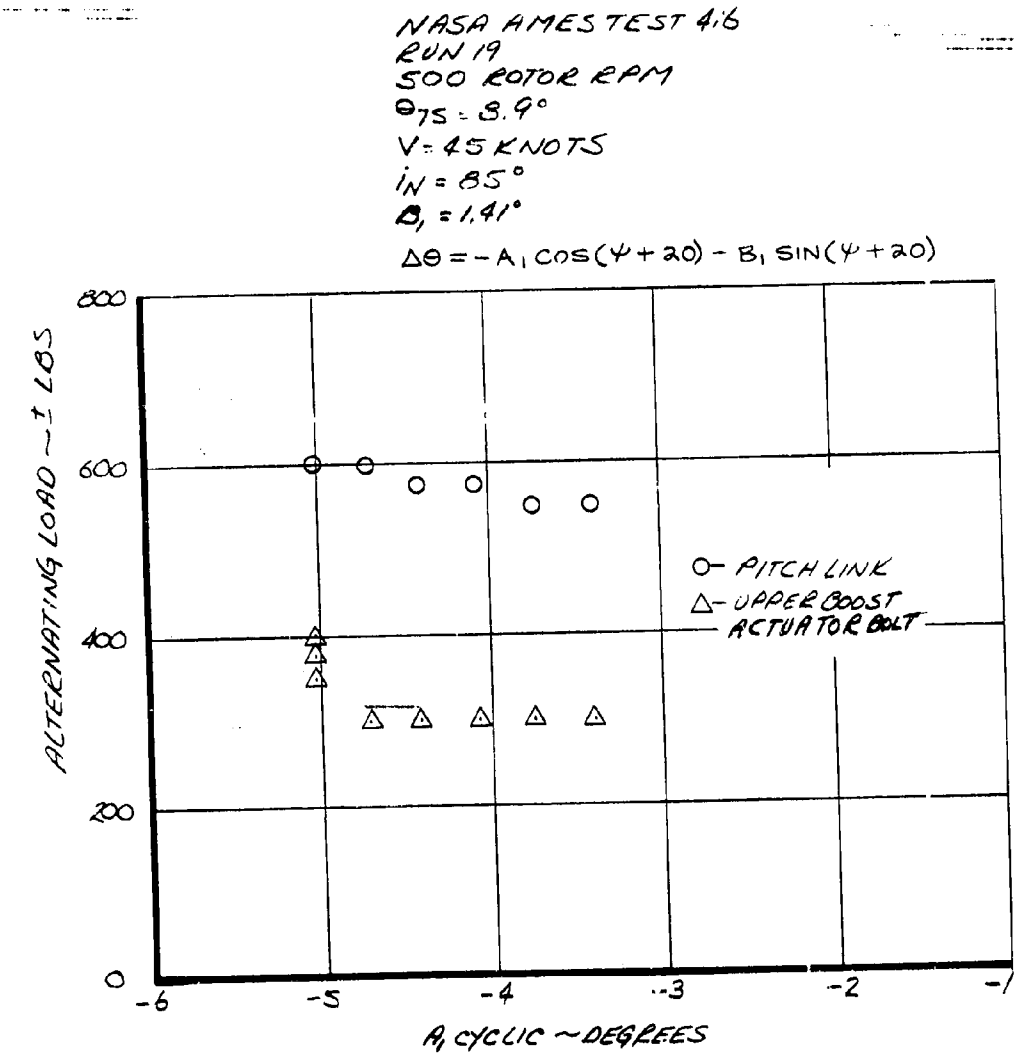

FIGURE 5-12 EFFECT OF LATERAL CYCLIC ON ALTERNATING CONTROL LOADS. 45 KNOTS, $i_N = 85°$, 500 RPM, $\theta_{.75} = 8.9°$

$\theta_{.75} = 8.9°$

$\Delta\theta = -A_1 \cos(\psi + 20) - B_1 \sin(\psi + 20)$

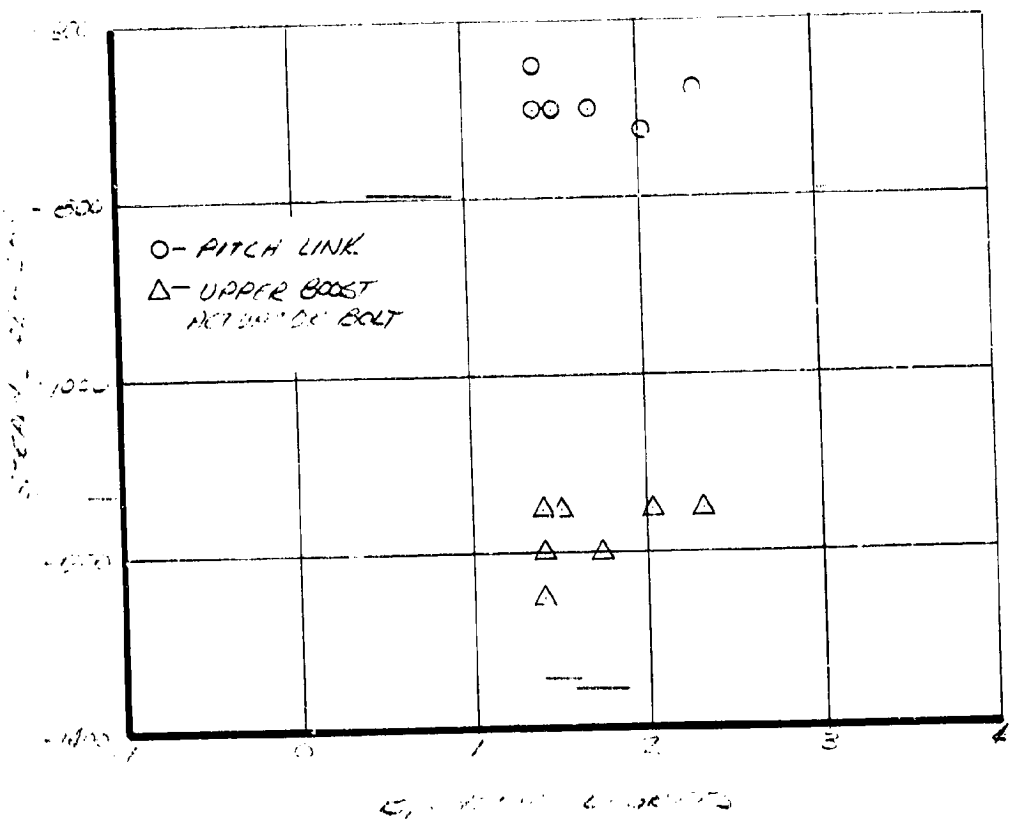

FIGURE 5-13 EFFECT OF LONGITUDINAL CYCLIC ON STEADY CONTROL LOADS. 45 KNOTS, $i_N = 85°$, 500 RPM, $\theta_{.75} = 8.9°$

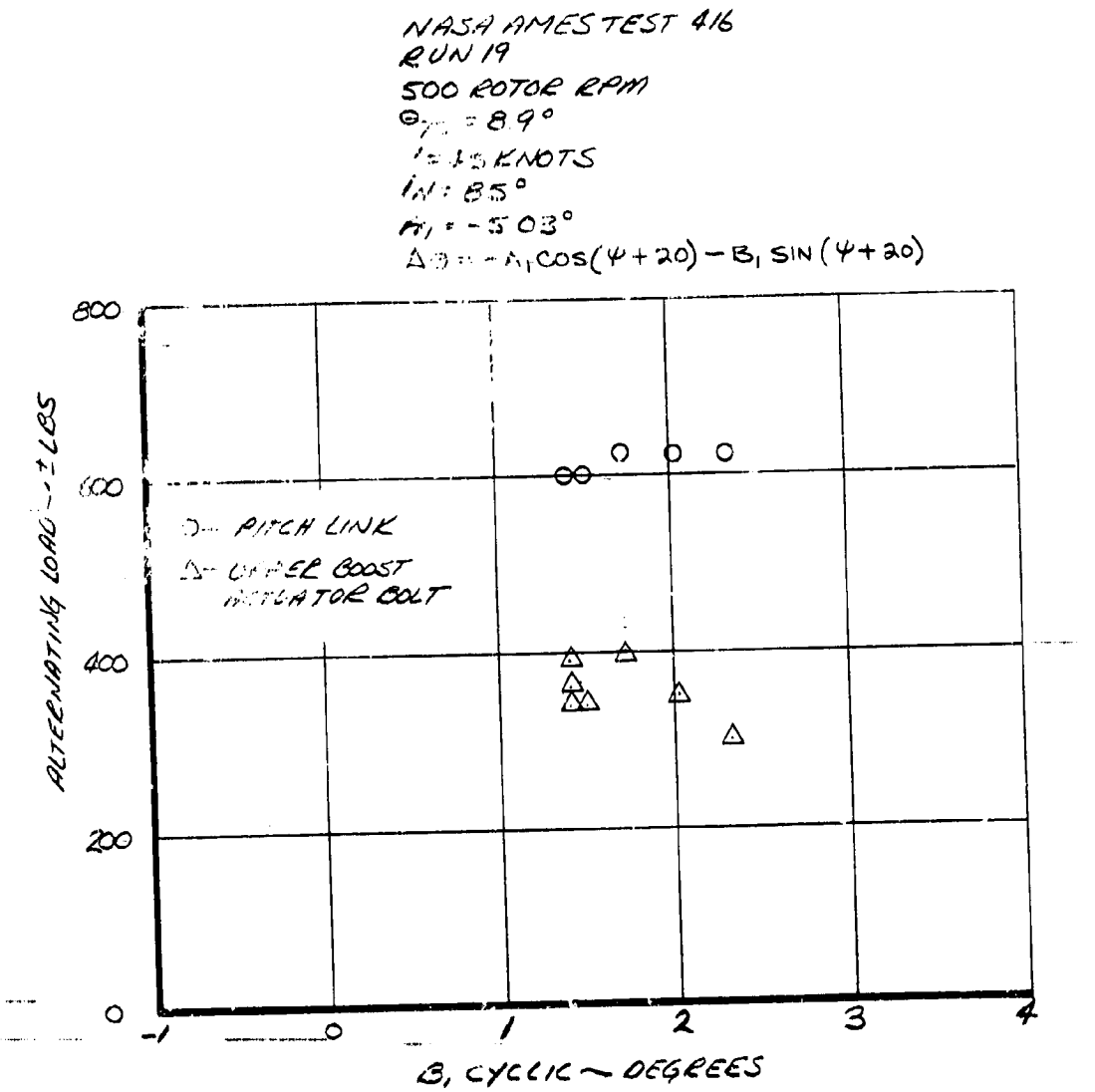

FIGURE 5-14 EFFECT OF LONGITUDINAL CYCLIC ON ALTERNATING CONTROL LOADS. 45 KNOTS, $i_N = 85°$, 500 RPM, $\theta_{.75} = 8.9°$

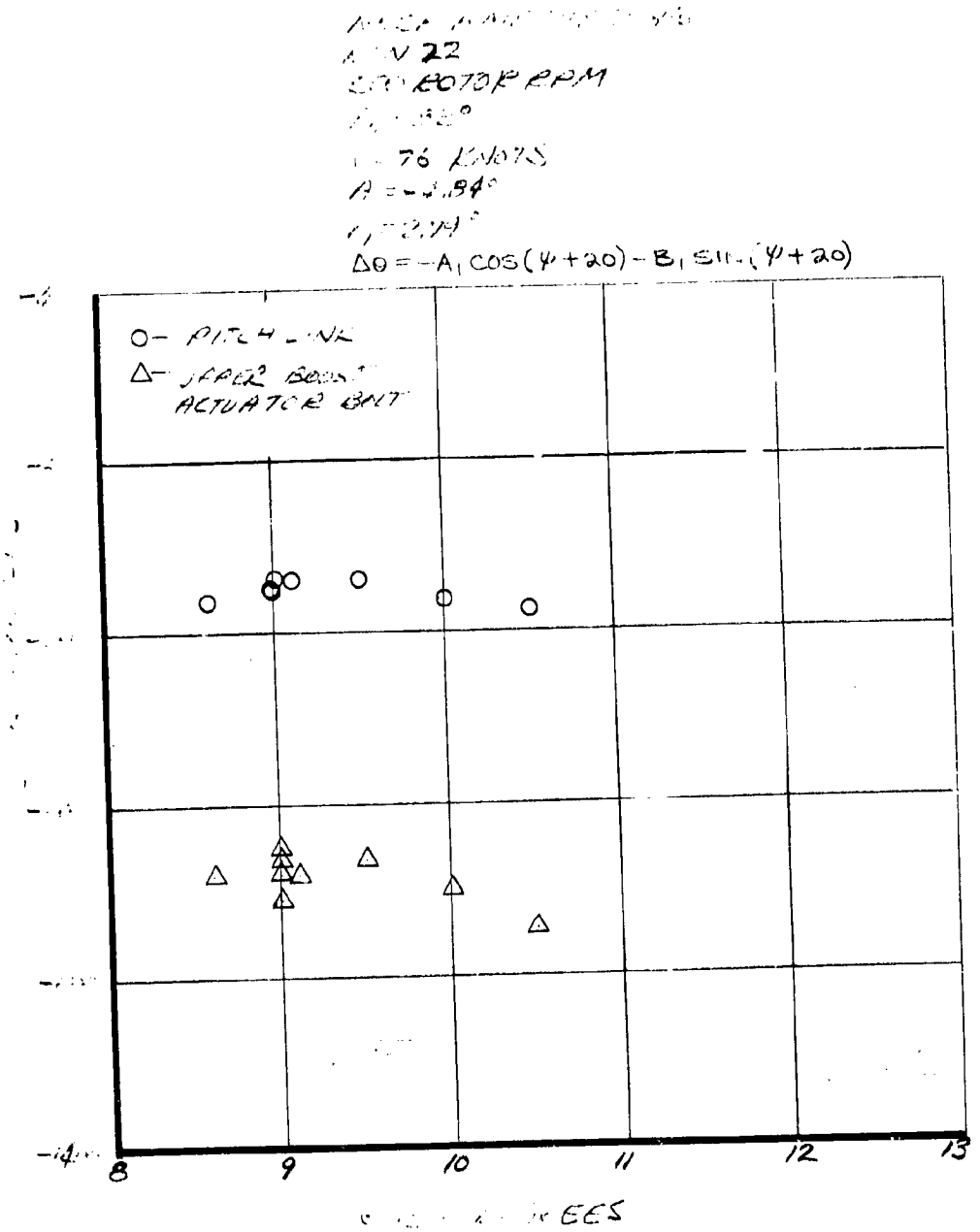

FIGURE 5-15 EFFECT OF COLLECTIVE PITCH ON STEADY CONTROL LOADS. 76 KNOTS, $i_N = 83°$, 500 RPM

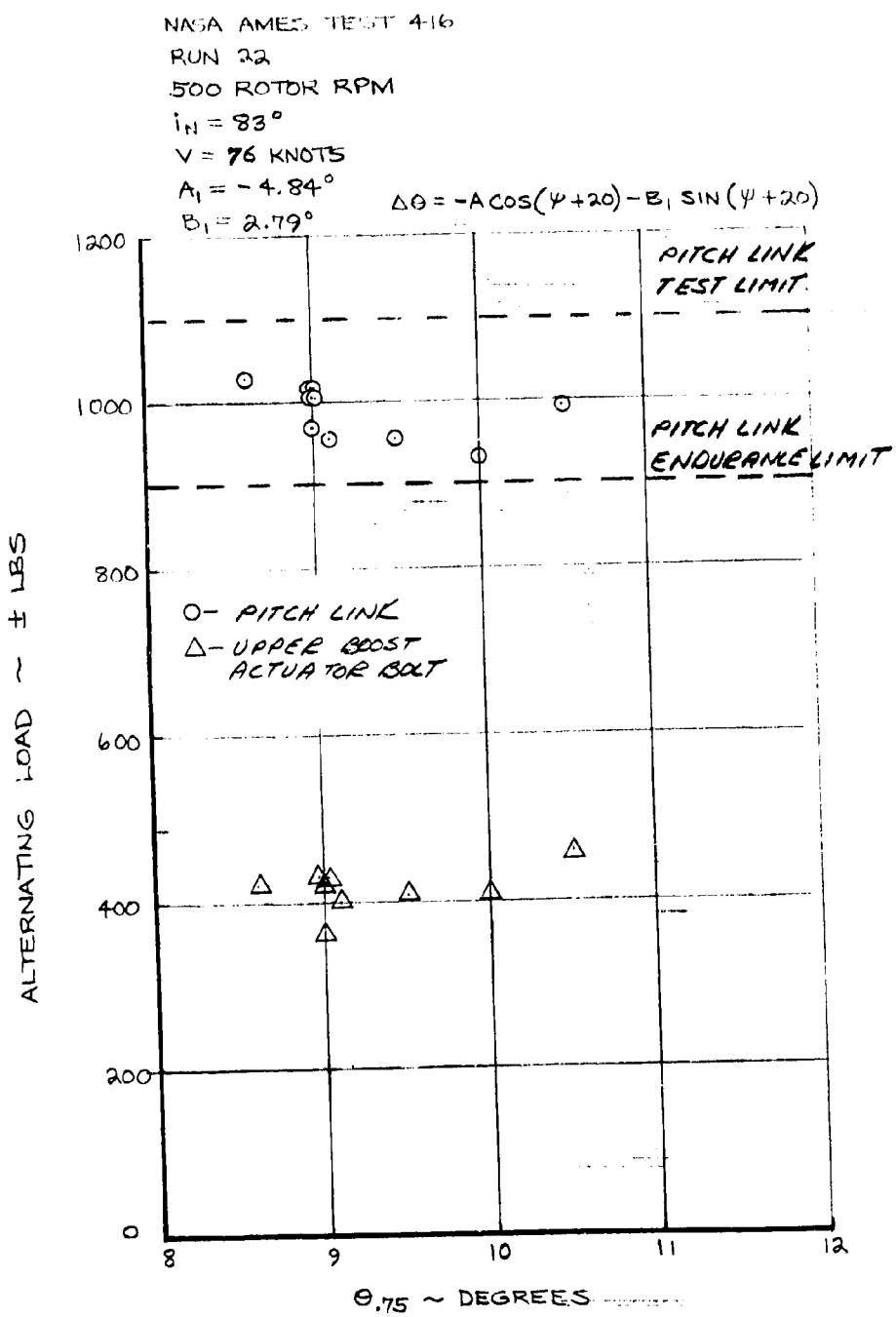

FIGURE 5-16 EFFECT OF COLLECTIVE PITCH ON ALTERNATING CONTROL LOADS. V = 76 KNOTS, 500 RPM, $i_N = 83°$

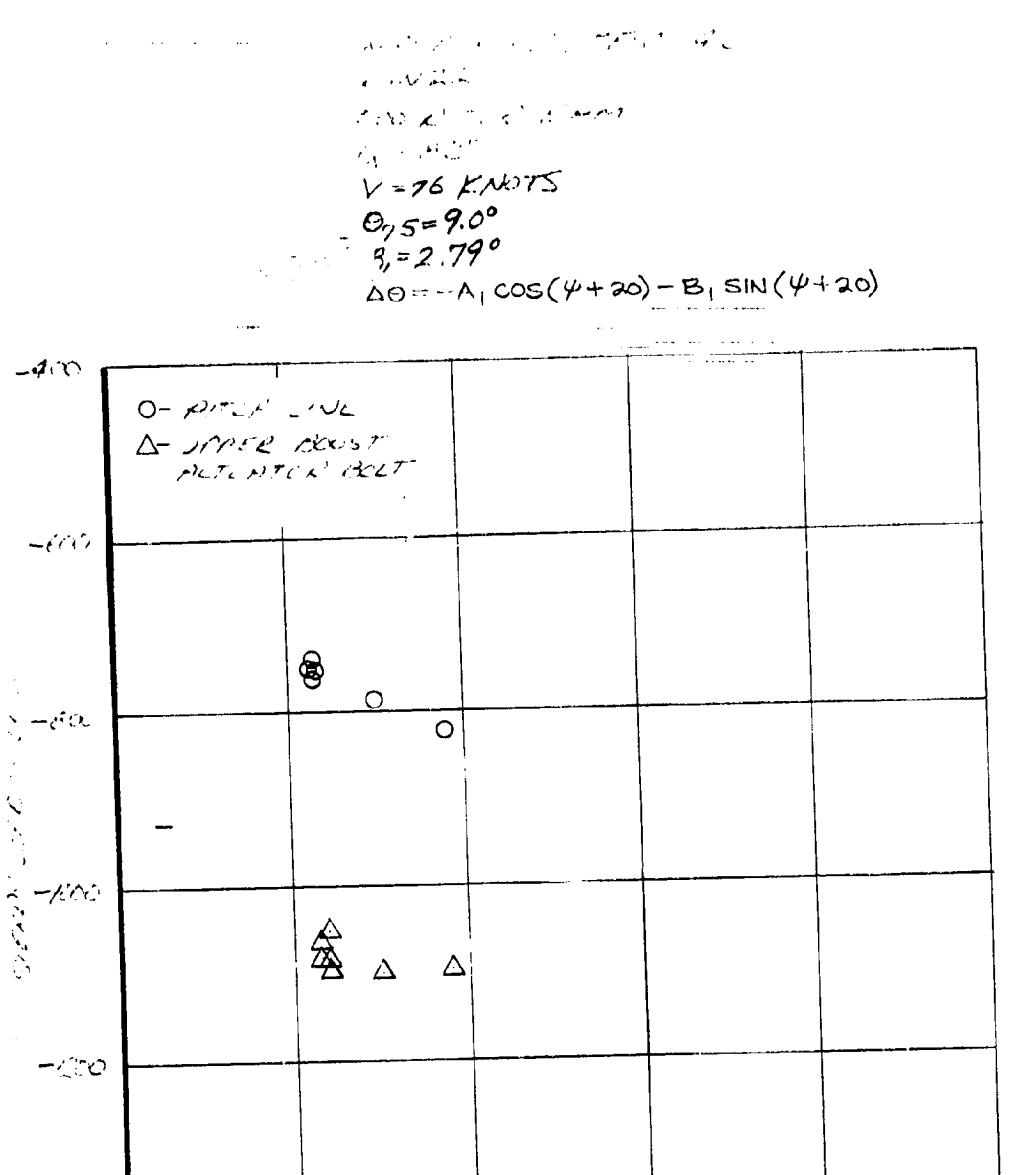

FIGURE 5-17 EFFECT OF LATERAL CYCLIC ON STEADY CONTROL LOADS. 76 KNOTS, $i_N = 83°$, 500 RPM, $\theta_{.75} = 9.0°$

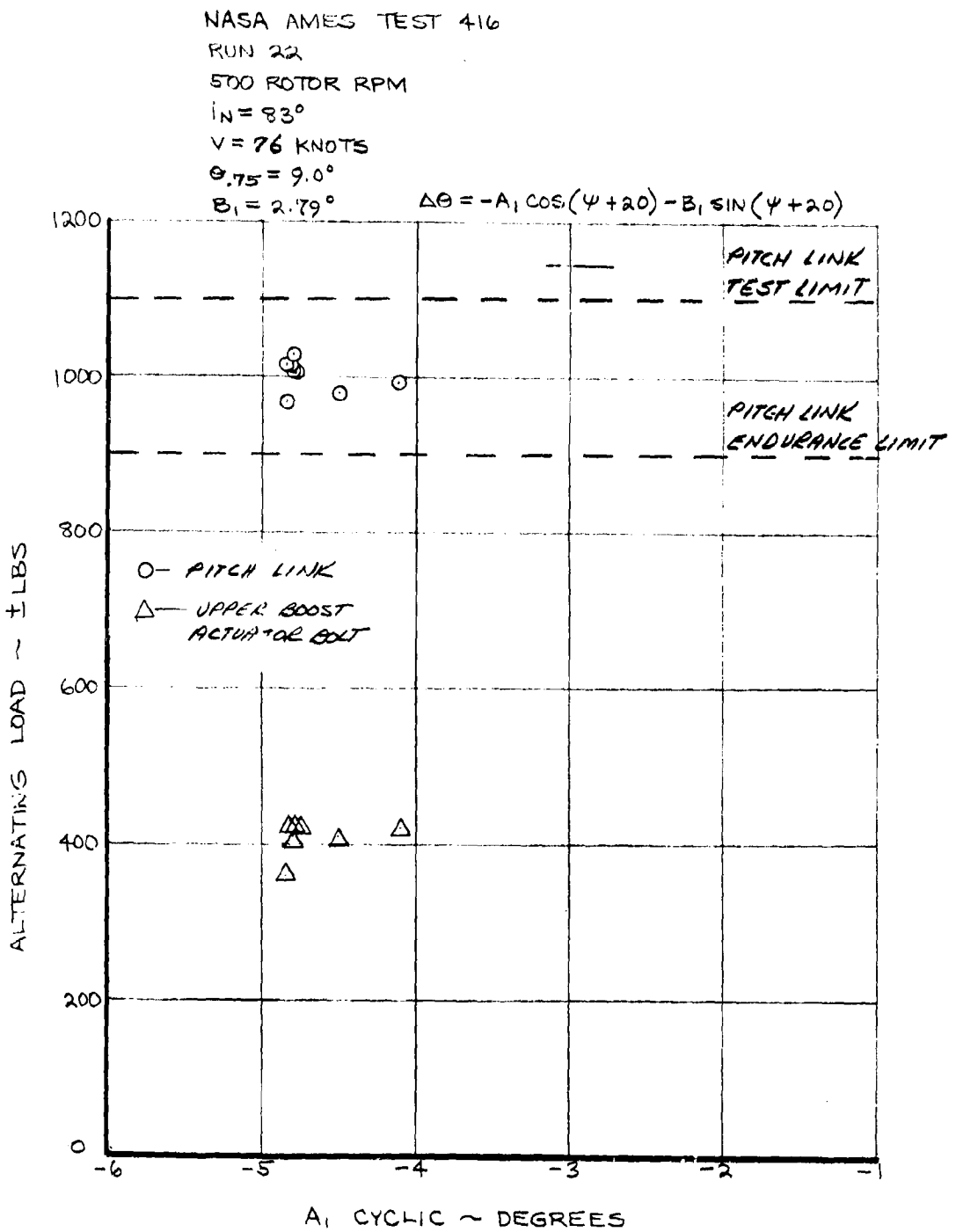

FIGURE 5-18 EFFECT OF LATERAL CYCLIC ON ALTERNATING STEADY CONTROL LOADS. V = 76 KNOTS, 500 RPM, $i_N = 83°$, $\theta_{.75} = 9.0°$

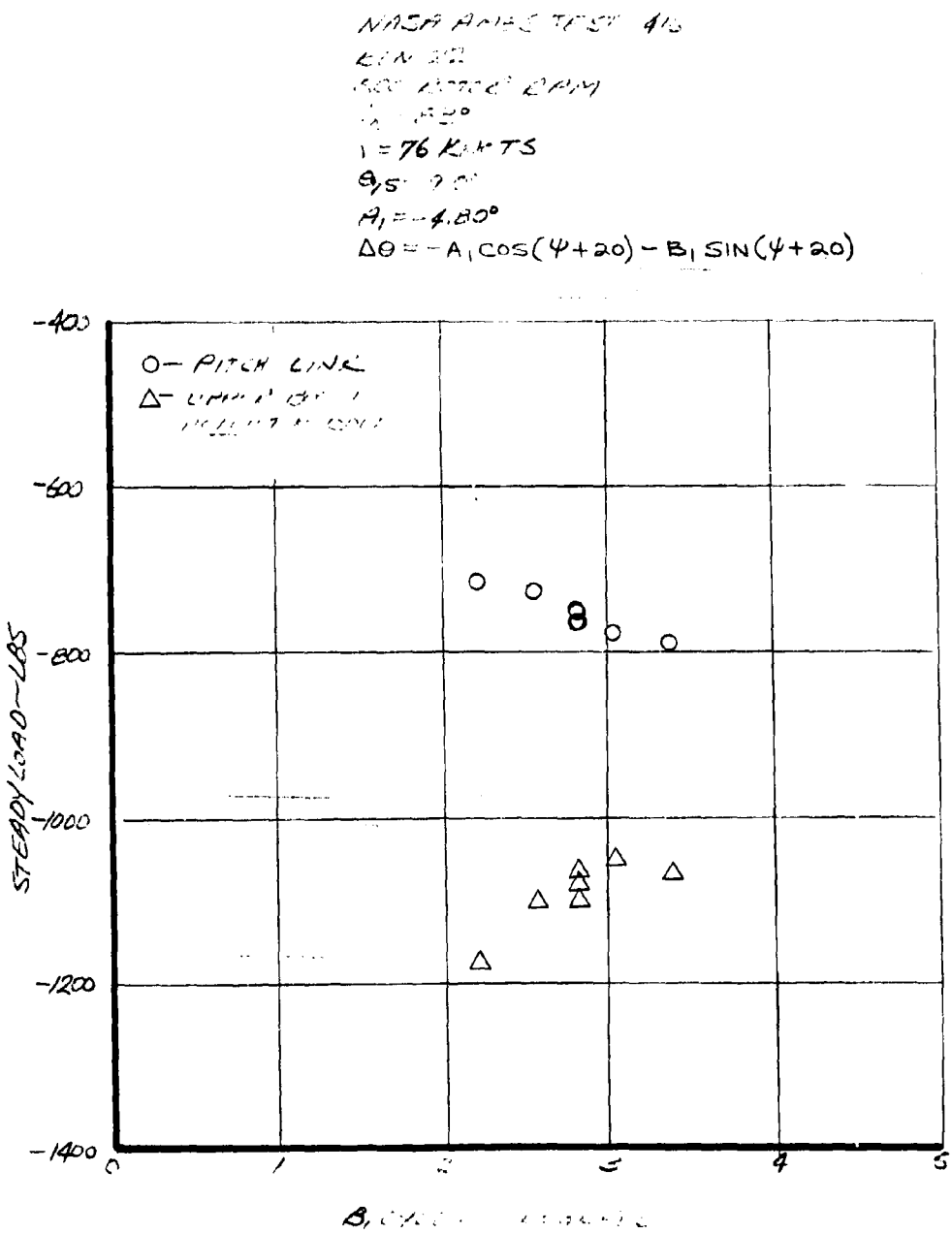

FIGURE 5-19 EFFECT OF LONGITUDINAL CYCLIC ON STEADY CONTROL LOADS. 76 KNOTS, $i_N = 83°$, 500 RPM, $\theta_{.75} = 9.0°$

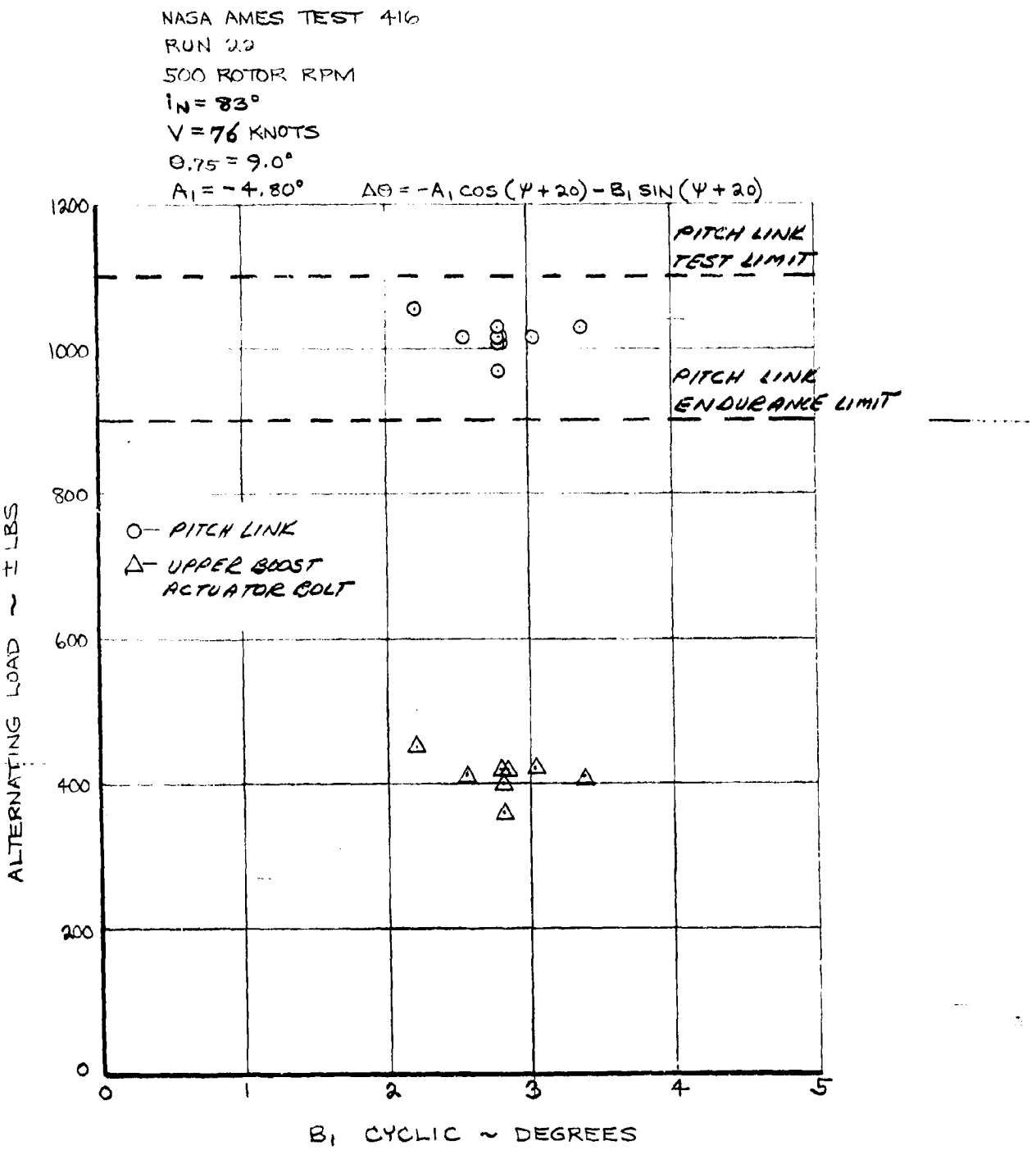

FIGURE 5.20 EFFECT OF B_1 CYCLIC ON ALTERNATING CONTROL LOADS. V= 76 KNOTS, 500 RPM, $i_N = 83°$, $\theta_{.75} = 9.0°$

$A_1 = -$

$B_1 =$

$\Delta\theta = -A_1 \cos(\psi+20) - B_1 \sin(\psi+20)$

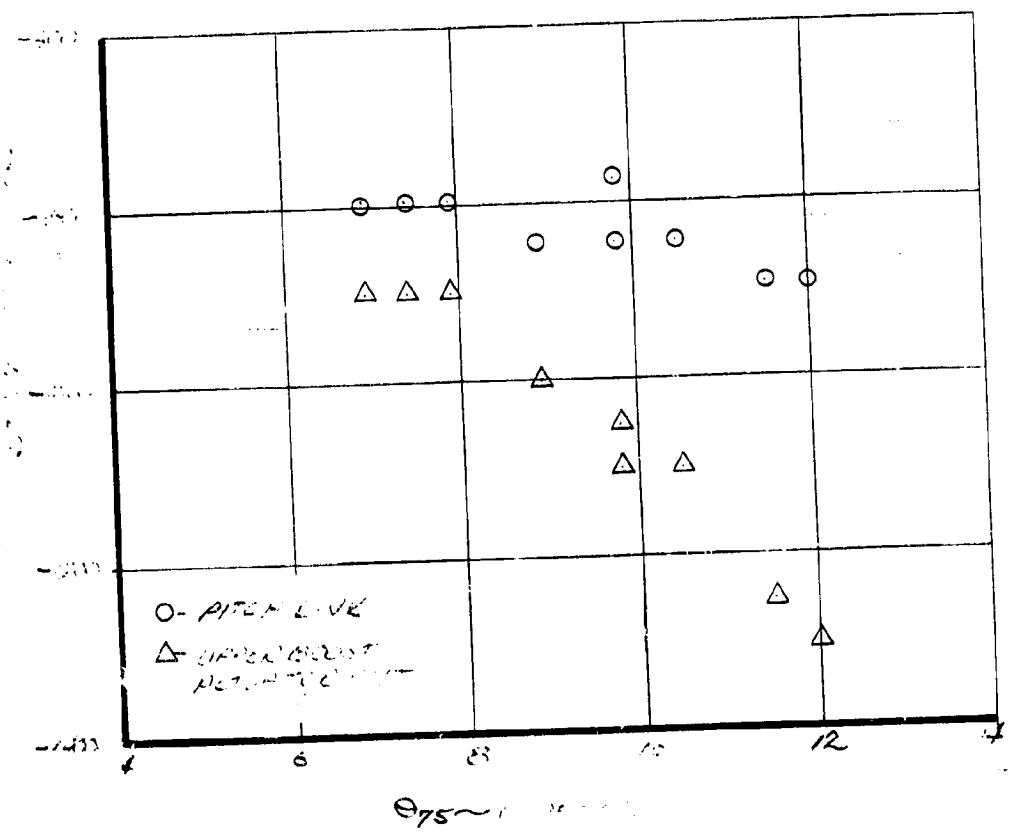

FIGURE 5-21 EFFECT OF COLLECTIVE PITCH ON STEADY CONTROL LOADS. 80 KNOTS, 500 RPM, $i_N = 66°$

$$\Delta\theta = -A_1 \cos(\psi+20) - B_1 \sin(\psi+20)$$

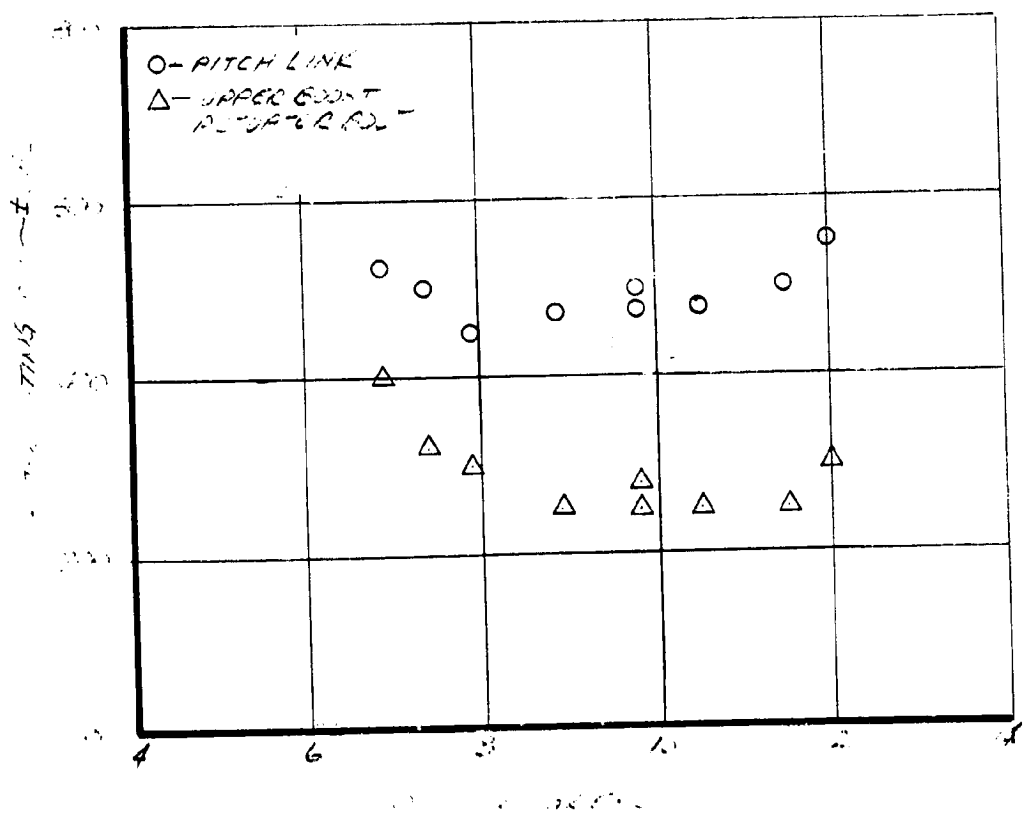

FIGURE 5-22 EFFECT OF COLLECTIVE PITCH ON ALTERNATING CONTROL LOADS. 80 KNOTS, 500 RPM, $i_N = 66°$

NASA AMES TEST 9/6
80 KNOTS
500 ROTOR RPM
$\theta_{.75}$ = 9.5°
V-22 GEOMETRY
i_N = 66°
θ_1 = 2.5°
$\Delta\theta = -A_1 \cos(\psi+20) - B_1 \sin(\psi+20)$

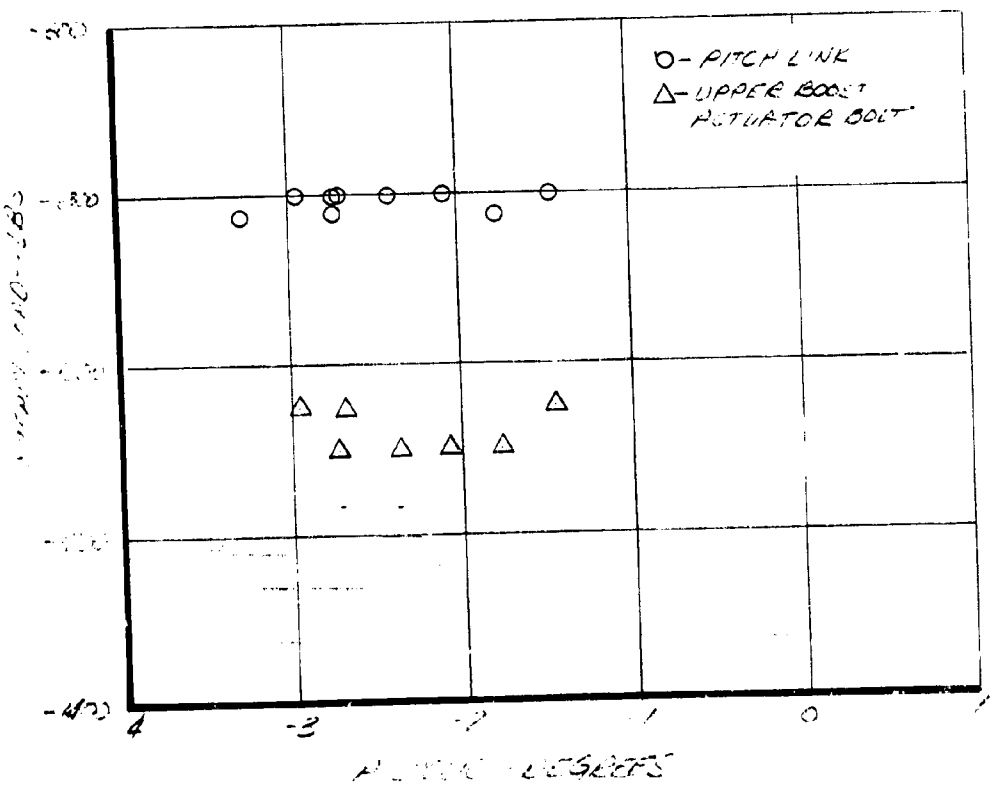

FIGURE 5-23 EFFECT OF LATERAL CYCLIC ON STEADY CONTROL LOADS. 80 KNOTS, 500 RPM, $i_N = 66°$, $\theta_{.75} = 9.8°$

NASA AMES TEST 416
RUN 20
500 ROTOR RPM
$\theta_{.75} = 9.8°$
V = 80 KNOTS
$i_N = 66°$
$B_1 = 2.31°$
$\Delta\theta = -A_1 \cos(\psi+20) - B_1 \sin(\psi+20)$

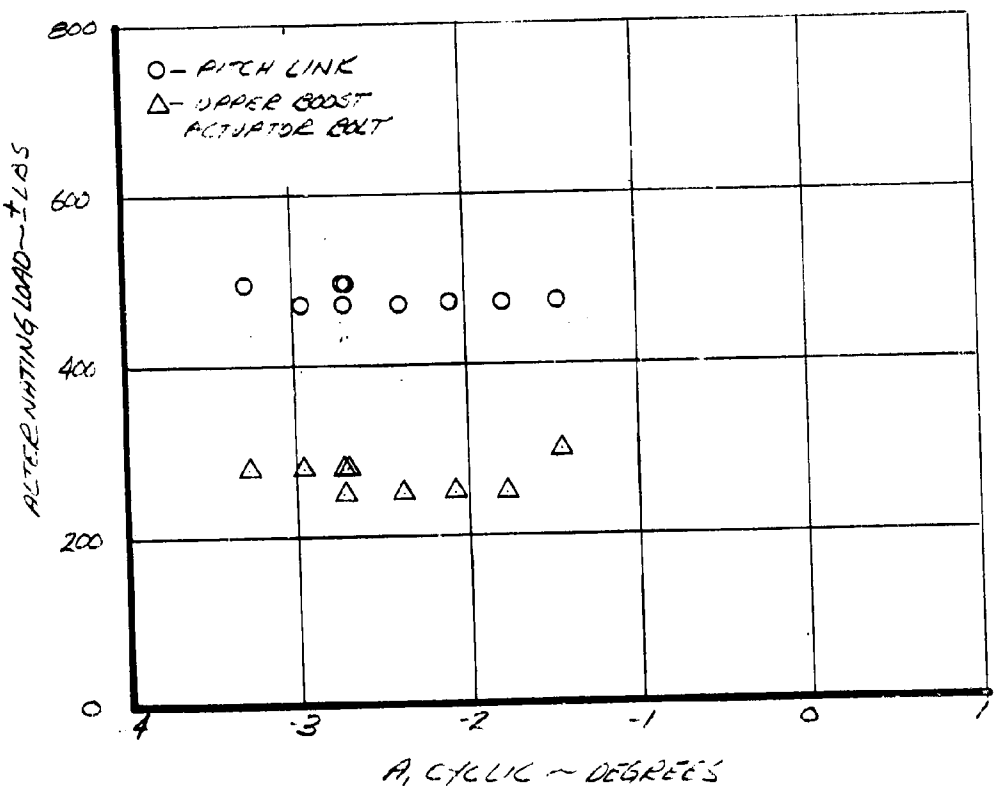

FIGURE 5-24 EFFECT OF LATERAL CYCLIC ON ALTERNATING CONTROL LOADS. 80 KNOTS, 500 RPM, $i_N = 66°$, $\theta_{.75} = 9.8°$

NASA AMES TEST #16
80 KNOTS
500 ROTOR RPM
$\theta_{.75} = 9.8°$
$V = 80$ KNOTS
$i_N = 66°$
$A_1 = -2.7°$
$\Delta\theta = -A_1 \cos(\psi+20) - B_1 \sin(\psi+20)$

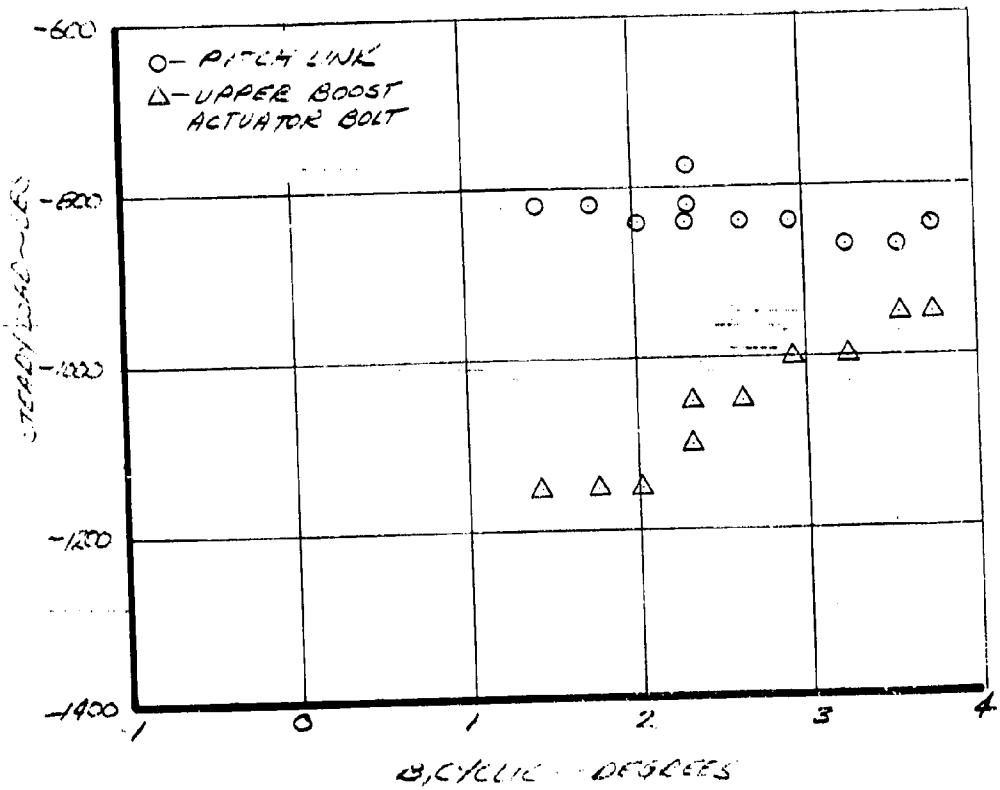

FIGURE 5-25 EFFECT OF LONGITUDINAL CYCLIC ON STEADY CONTROL LOADS. 80 KNOTS, 500 RPM, $i_N = 66°$, $\theta_{.75} = 9.8°$

NASA AMES TEST #16
[illegible]
500 [illegible] RPM
[illegible]
[illegible]
i_N [illegible]
[illegible]
$\Delta\theta = -A_1 \cos(\psi+20) - B_1 \sin(\psi+20)$

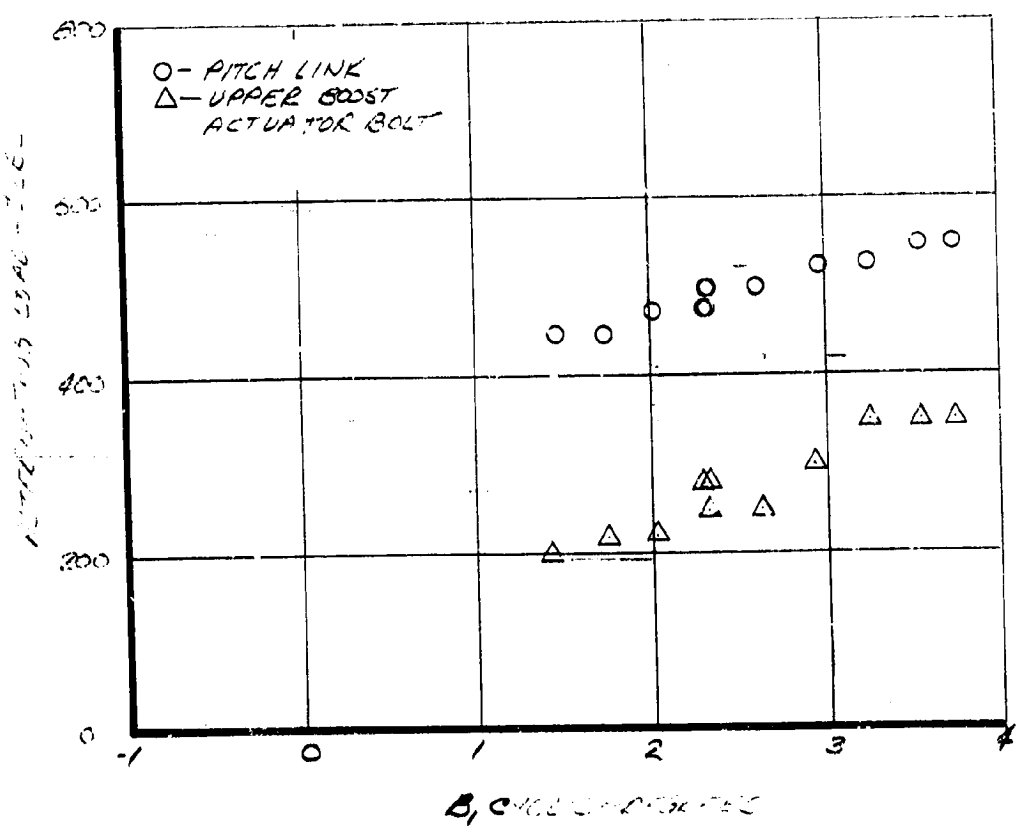

FIGURE 5-26 EFFECT OF LONGITUDINAL CYCLIC ON ALTERNATING CONTROL LOADS. 80 KNOTS, 500 RPM, $i_N = 6\frac{1}{2}°$, $\theta_{.75} = 9.8°$

$\Delta\theta = -A_1 \cos(\psi+20) - B_1 \sin(\psi+20)$

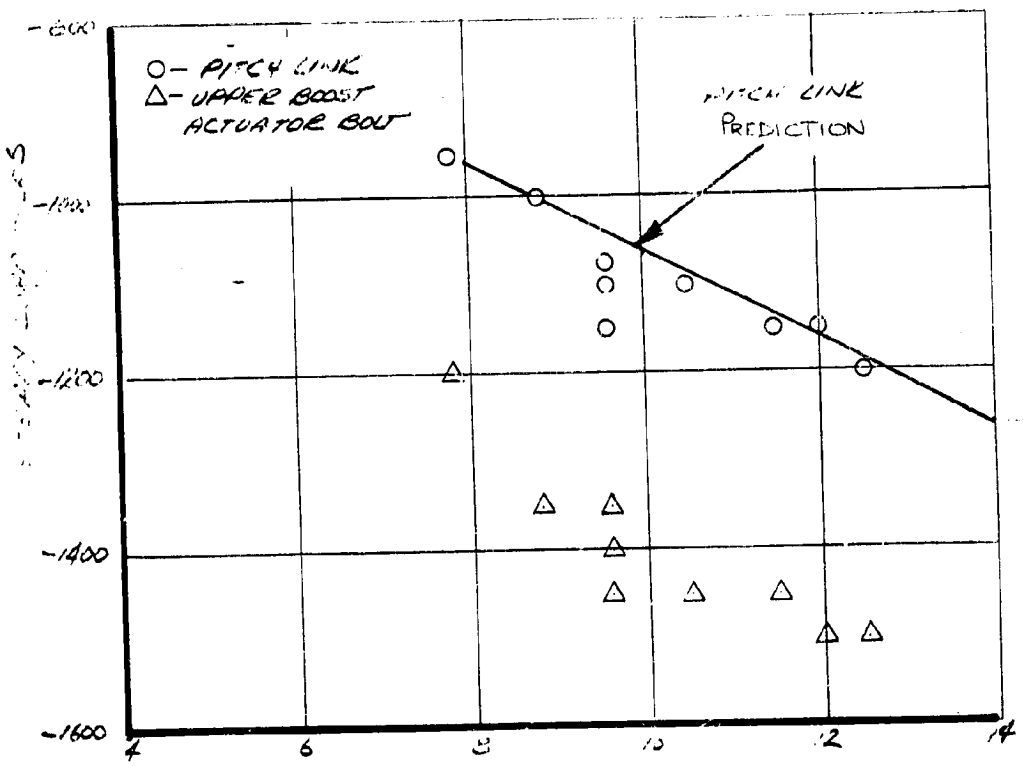

θ_{75} –

FIGURE 5-27 EFFECT OF COLLECTIVE PITCH ON STEADY CONTROL LOADS. 80 KNOTS, 550 RPM, $i_N = 66°$

NASA AMES TEST 416
RUN 21
550 ROTOR RPM
V = 80 KNOTS
i_N = 66°
A_1 = -2.81°
B_1 = 1.24°
$\Delta\theta = -A_1 \cos(\psi+20) - B_1 \sin(\psi+20)$

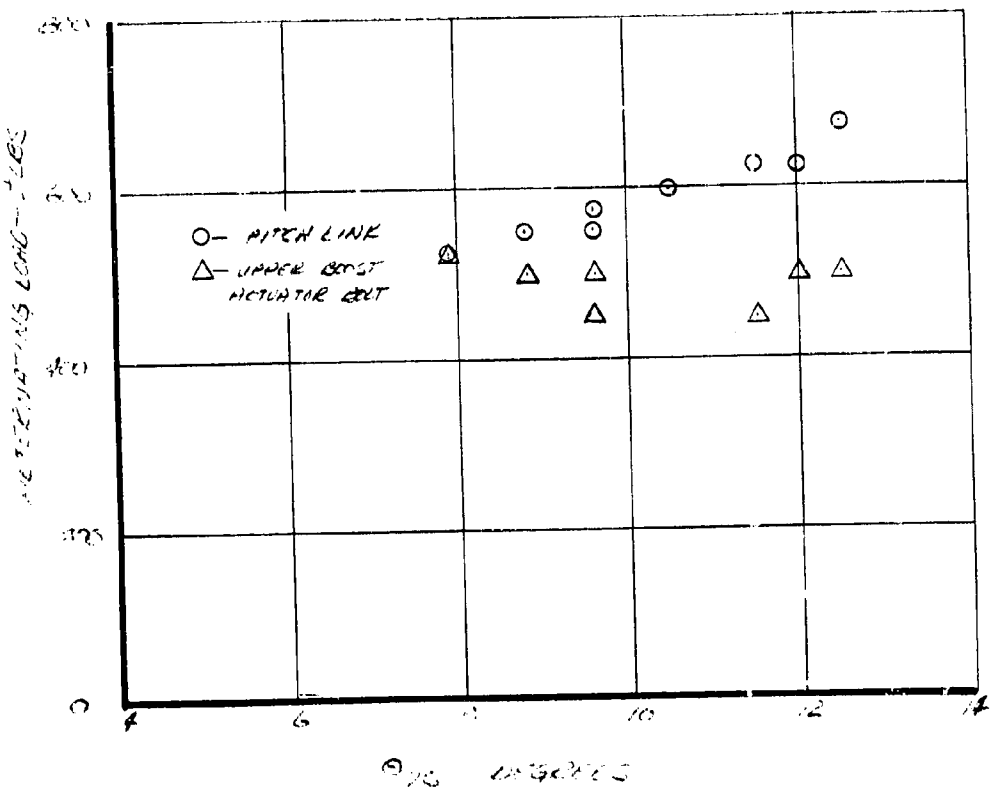

FIGURE 5-28 EFFECT OF COLLECTIVE PITCH ON ALTERNATING CONTROL LOADS. 80 KNOTS, 550 RPM, $i_N = 66°$.

$\Delta\theta = -A_1 \cos(\psi+20) - B_1 \sin(\psi+20)$

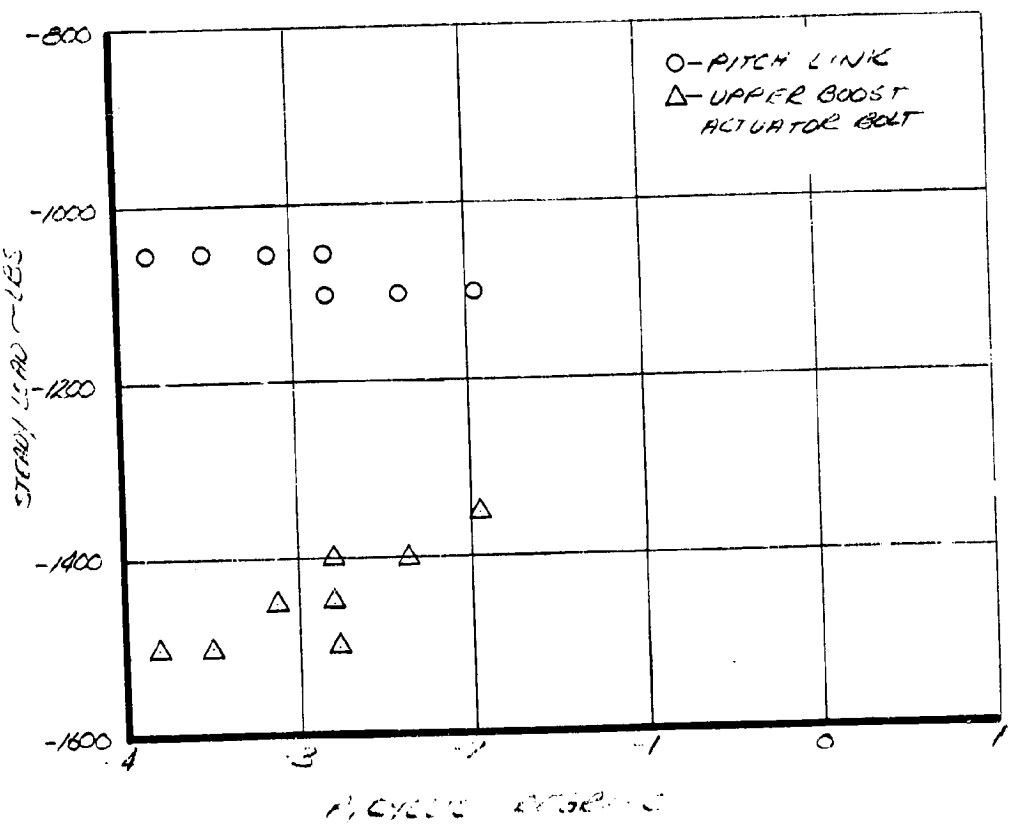

FIGURE 5-29 EFFECT OF LATERAL CYCLIC ON STEADY CONTROL LOADS. 80 KNOTS, 550 RPM, $i_N = 66°$, $\theta_{.75} = 9.6°$

NIKEN MAIFS TEST 416
RUN 21
550 RPM
$\theta_{.75}$ 9.6°
V: 80 KNOTS
i_N : 66°
θ_1 : 2.16°
$\Delta\theta = -A_1 \cos(\psi+20) - B_1 \sin(\psi+20)$

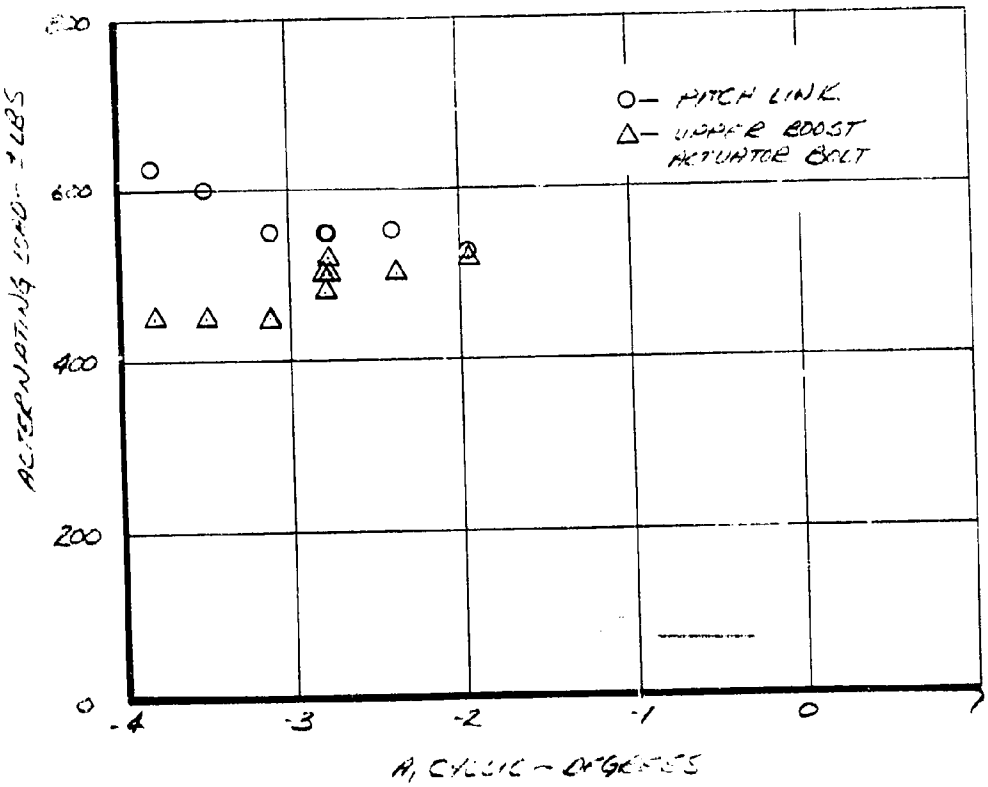

FIGURE 5-30 EFFECT OF LATERAL CYCLIC ON ALTERNATING CONTROL LOADS, 80 KNOTS, 550 RPM, $i_N = 66°$, $\theta_{.75} = 9.6°$

$\Delta\theta = -A_1 \cos(\psi+20) - B_1 \sin(\psi+20)$
$V = 80$ KNOTS

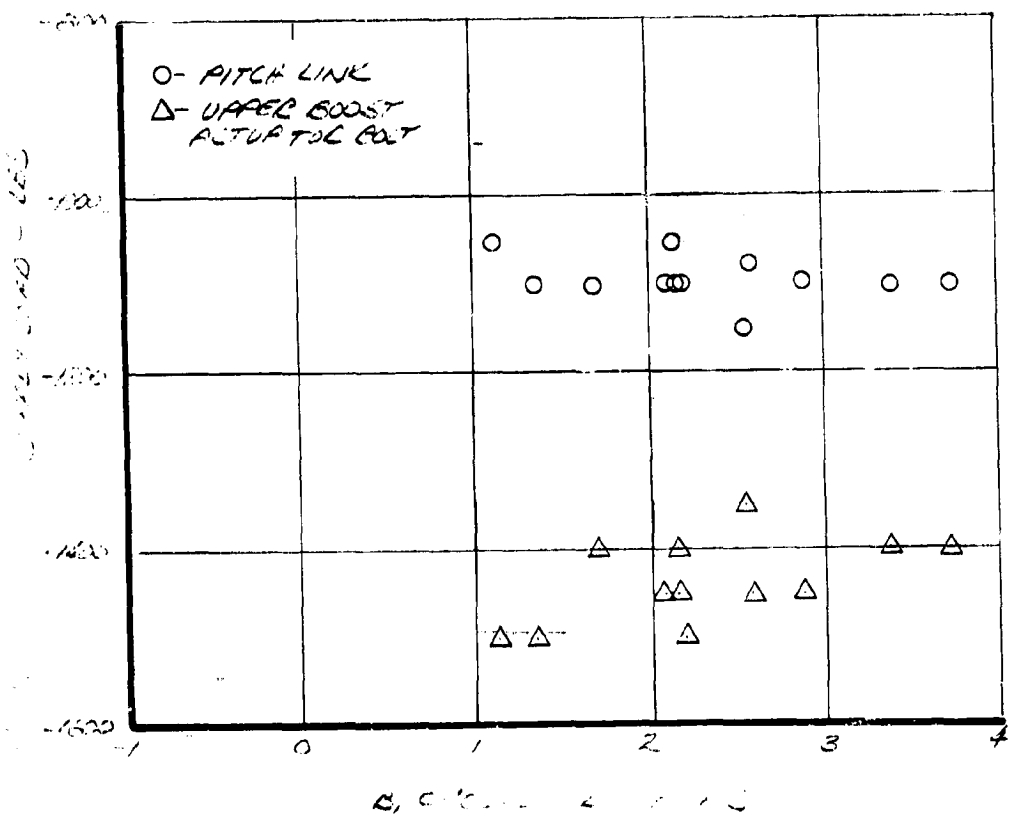

FIGURE 5-31 EFFECT OF LONGITUDINAL CYCLIC ON STEADY CONTROL LOADS. 80 KNOTS, 550 RPM, $i_N = 66°$, $\theta_{.75} = 9.6°$

$$\Delta\theta = -A_1 \cos(\psi + 20) - B_1 \sin(\psi + 20)$$

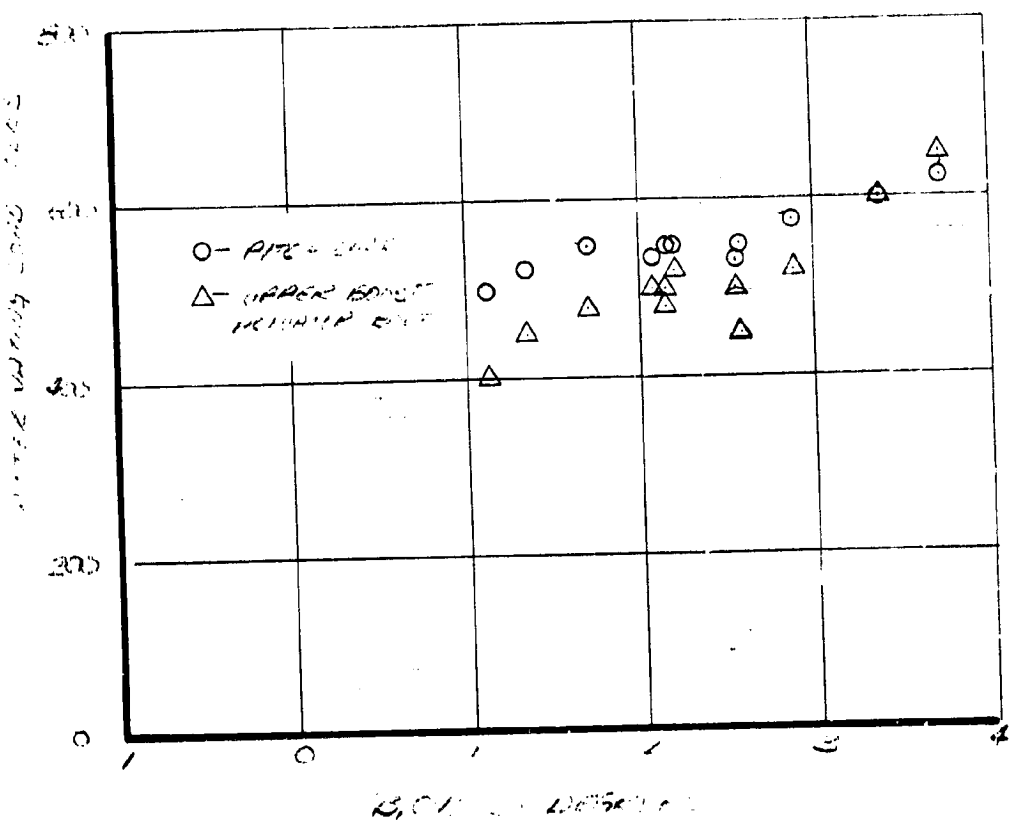

FIGURE 5-32 EFFECT OF LONGITUDINAL CYCLIC ON ALTERNATING CONTROL LOADS. 80 KNOTS, 550 RPM, $i_N = 66°$, $\theta_{.75} = 9.6°$

NASA AMES TEST 416
RUN 9
551 ROTOR RPM
$i_N = 2.7°$
V = 105 KNOTS
$A_1 = -2.16°$
$B_1 = 2.56°$
$\Delta\theta = -A_1 \cos(\psi+20) - B_1 \sin(\psi+20)$

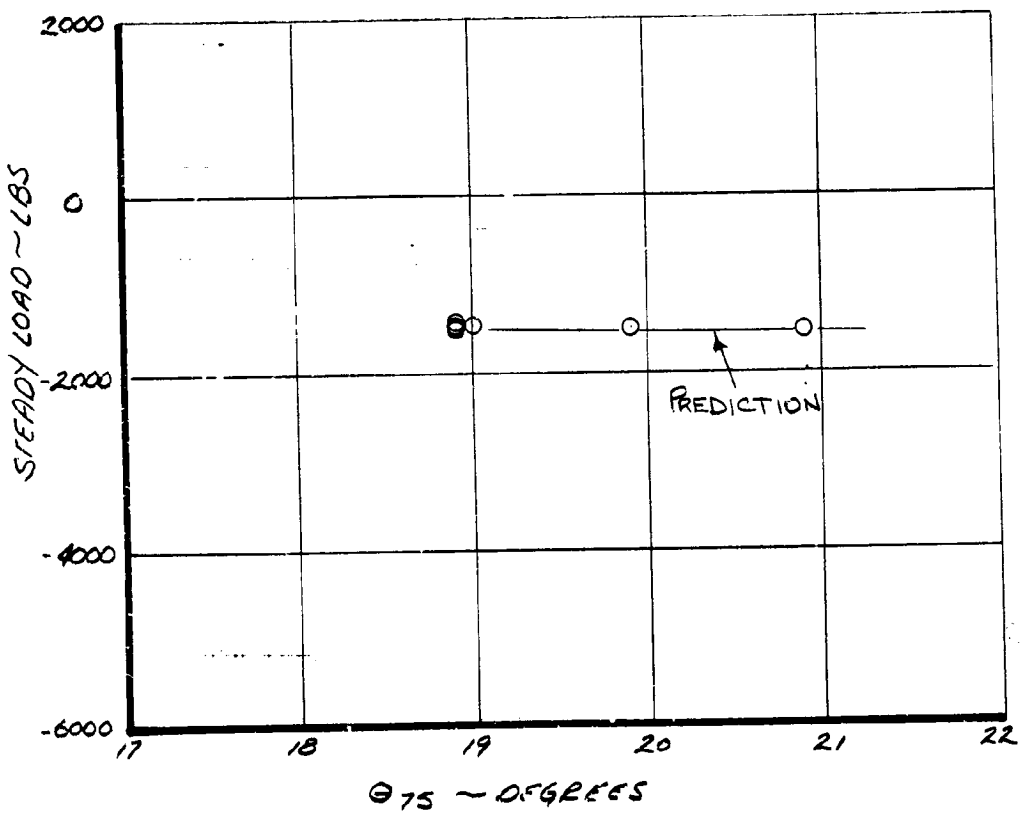

FIGURE 5-33 EFFECT OF COLLECTIVE PITCH ON STEADY PITCH LINK LOADS. $i_N = 2.7°$ V=105 KNOTS RPM=551

NASA AMES TEST 416
RUN 9
551 ROTOR RPM
V=105 KNOTS
$A_1 = -2.16°$
$B_1 = 2.56°$
$i_N = 27°$

$\Delta\theta = -A_1 \cos(\psi+20) - B_1 \sin(\psi+20)$

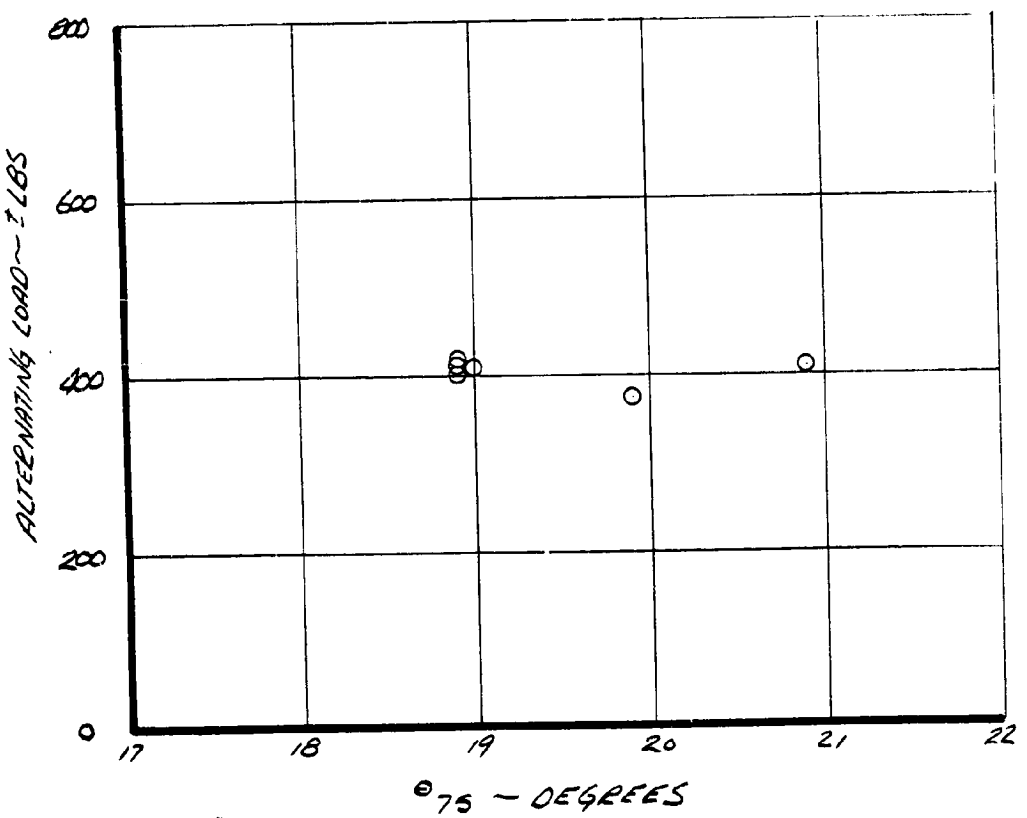

FIGURE 5-34 EFFECT OF COLLECTIVE PITCH ON ALTERNATING PITCH LINK LOADS. $i_N = 27°$ V=105 KNOTS RPM=551

NASA AMES TEST 416
RUN 9
551 ROTOR RPM
$\theta_{.75} = 18.9°$
$i_N = 2.7°$
V = 105 KNOTS
$A_1 = -2.16°$
$\Delta\theta = -A_1 \cos(\psi+20) - B_1 \sin(\psi+20)$

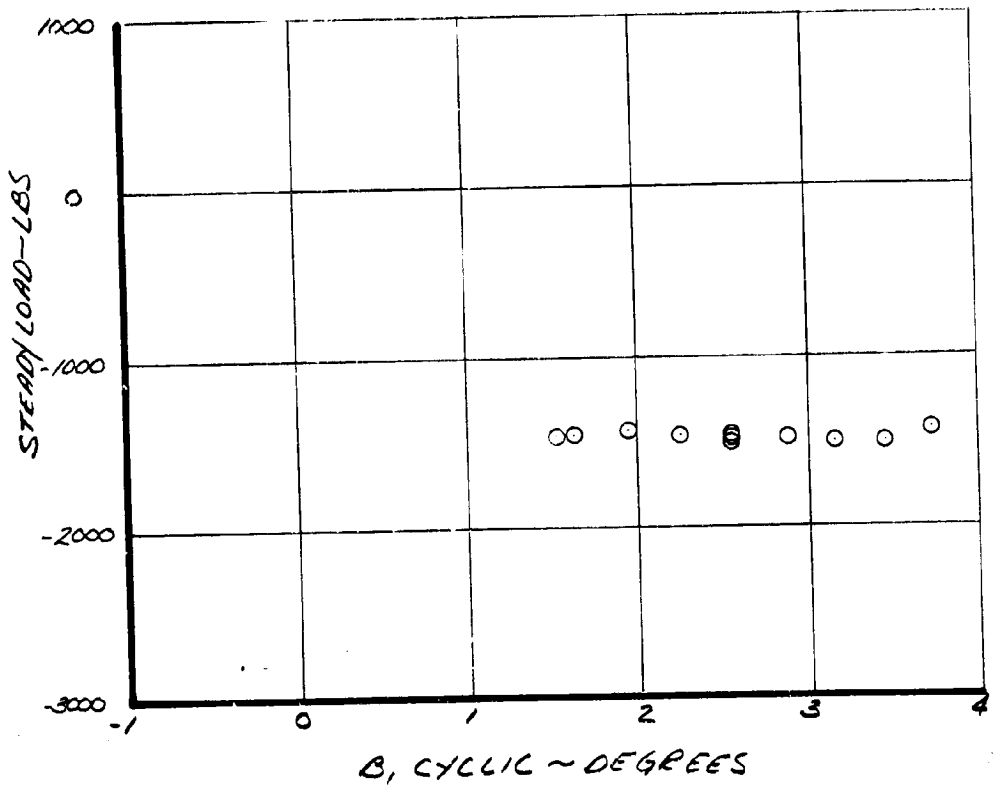

FIGURE 5-35 EFFECT OF B_1 CYCLIC ON STEADY PITCH LINK LOADS. $i_N = 2.7°$ V = 105 KNOTS RPM = 551

NASA AMES TEST 416
RUN 9
551 ROTOR RPM
$\Theta_{.75} = 18.9°$
$i_N = 2.7°$
$V = 105$ KNOTS
$A_1 = -2.16°$

$\Delta\Theta = -A_1 \cos(\psi+20) - B_1 \sin(\psi+20)$

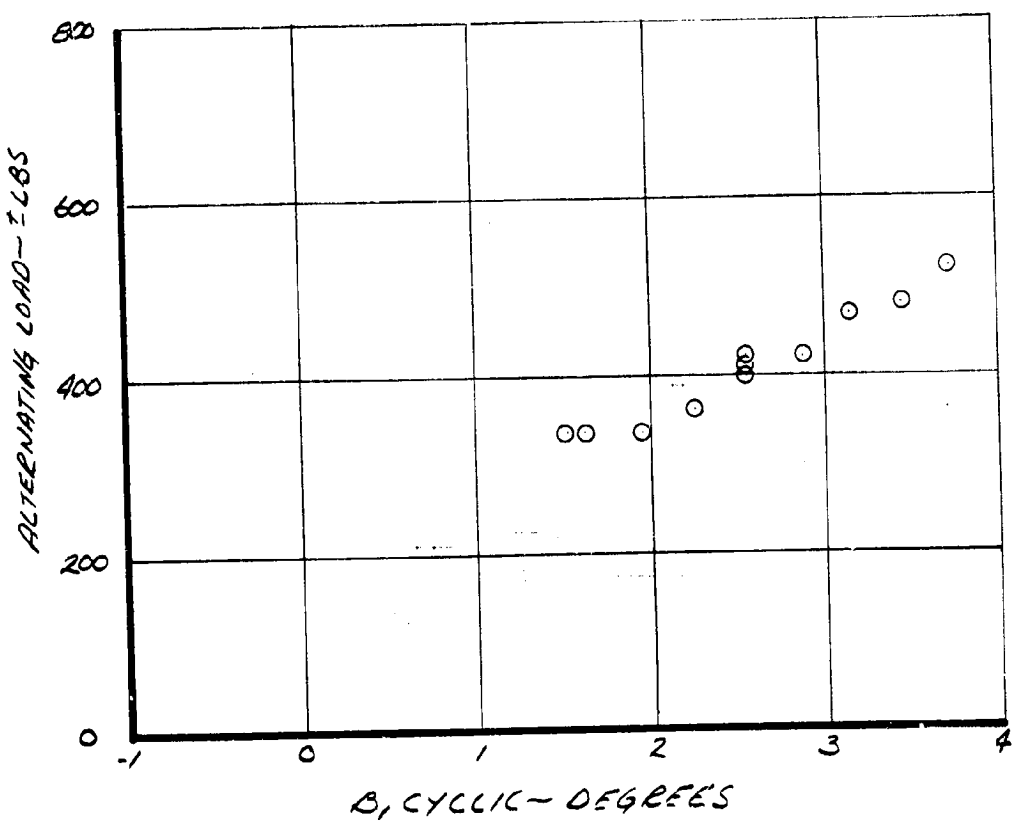

FIGURE 5-36 EFFECT OF B_1 CYCLIC ON ALTERNATING PITCH LINK LOADS $i_N = 2.7°$ V = 105 KNOTS RPM = 551

NASA AMES TEST 416
RUN 9
551 ROTOR RPM
$\theta_{.75} = 10.9°$
$i_N = 2.7°$
V = 105 KNOTS
$B_1 = 2.56°$

$\Delta\theta = -A_1 \cos(\psi+20) - B_1 \sin(\psi+20)$

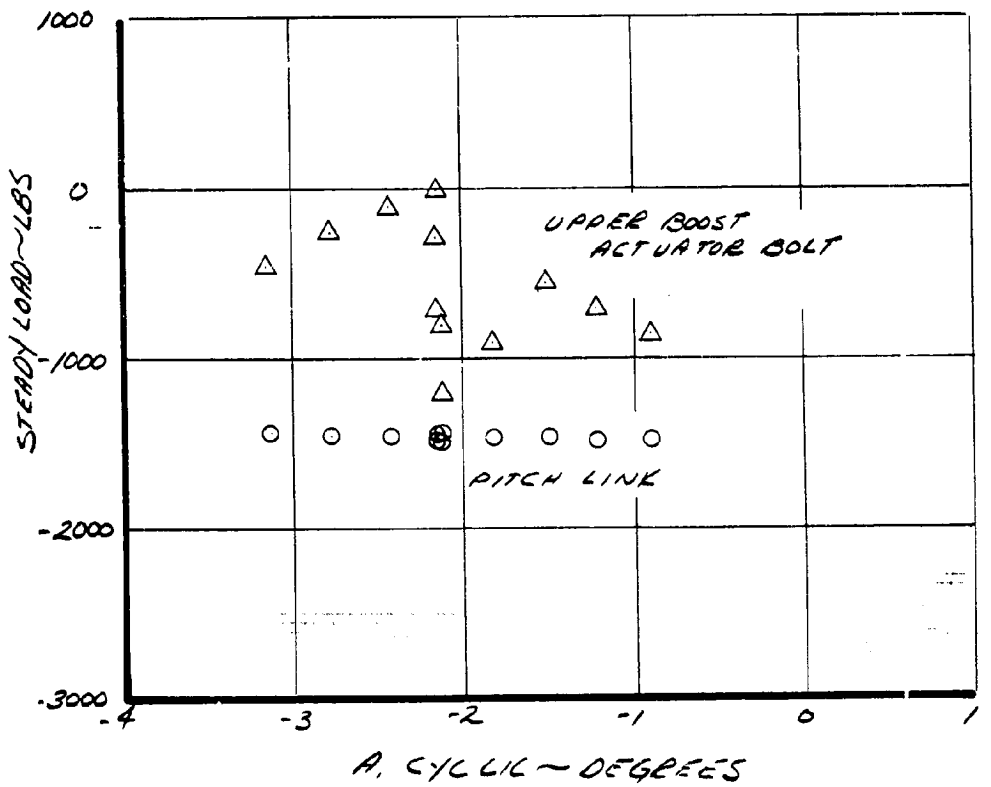

FIGURE 5-37 EFFECT OF A_1 CYCLIC ON STEADY PITCH LINK LOADS. $i_N = 2.7°$ V = 106 KNOTS RPM = 551

MAIN ROTOR LOADS
FLT 7
CS-1 ROTOR LOADS
$\Theta_{.75} = 18.9°$
$i_N = 2.7°$
$V = 105$ KNOTS
$\Theta_1 = 2.56°$
$\Delta\Theta = -A_1 \cos(\psi+20) - B_1 \sin(\psi+20)$

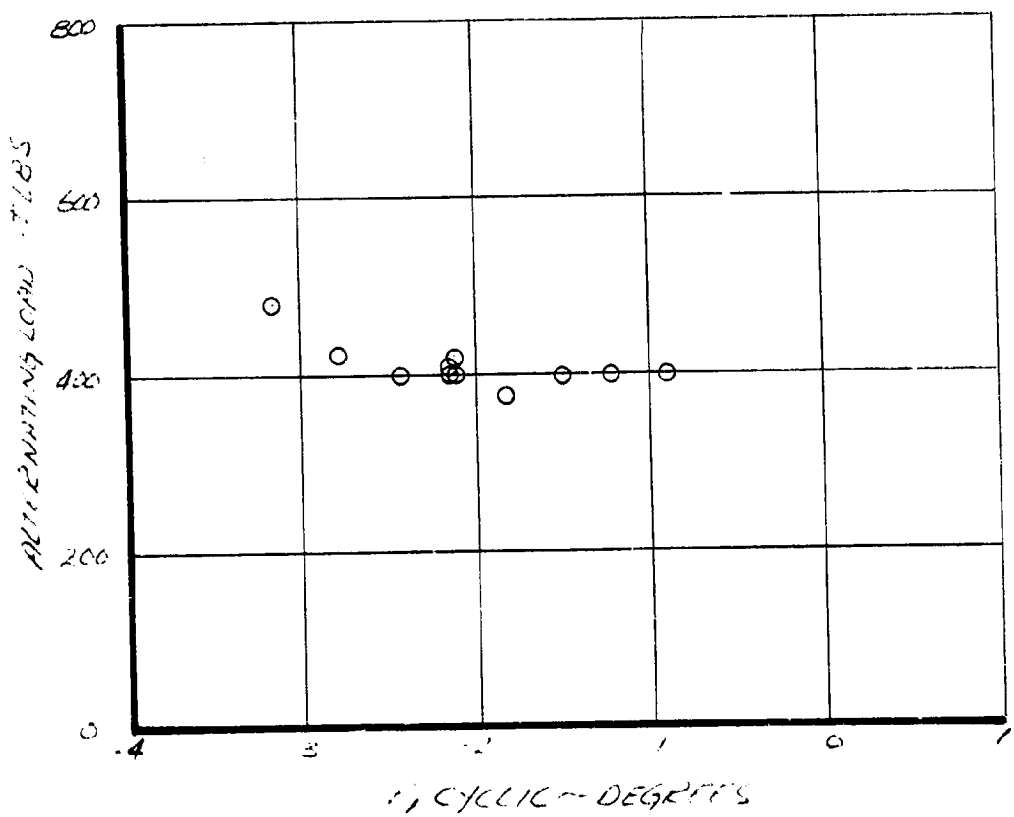

FIGURE 5-38 EFFECT OF A_1 CYCLIC ON FLAPWISE BENDING PITCH LINK LOADS. $i_N = 2.7°$, V KNOTS, FLT 7, CS-1

NASA AMES TEST 416
RUN 9
551 ROTOR RPM
$\theta_{.75} = 18.9°$
V = 105 KNOTS
$A_1 = -2.12°$
$B_1 = 2.56°$
$\Delta\theta = -A_1 \cos(\psi+20) - B_1 \sin(\psi+20)$

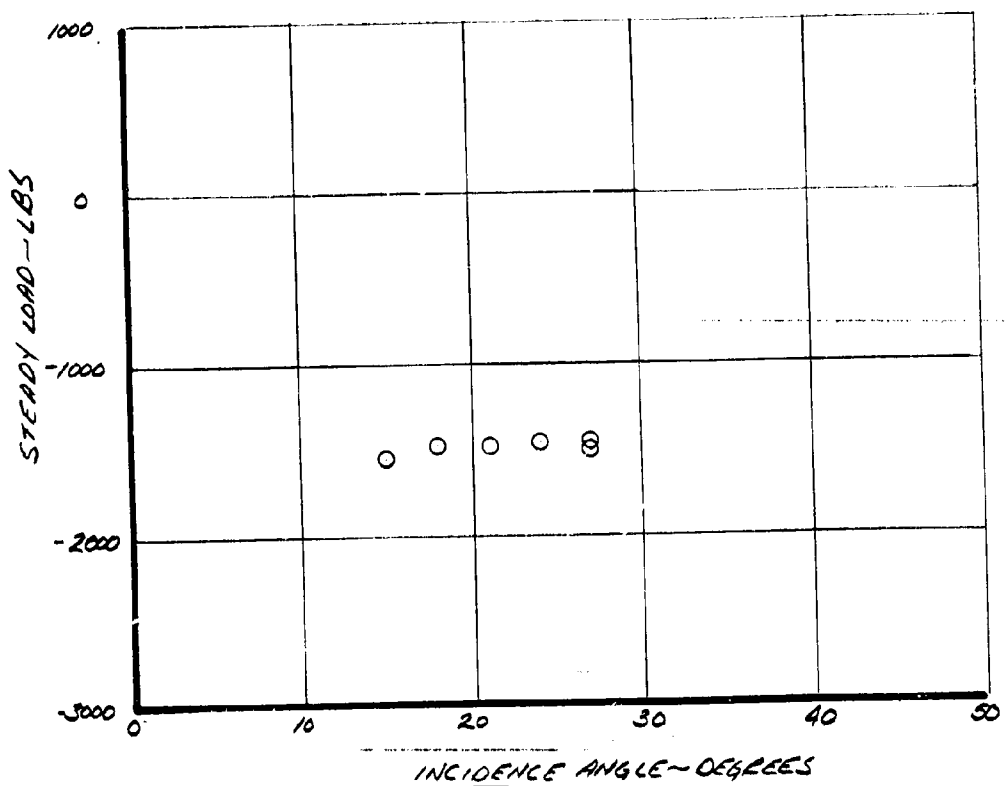

FIGURE 5-39 EFFECT OF INCIDENCE ANGLE ON STEADY PITCH LINK LOADS. $i_N = 27°$ V = 105 KNOTS RPM = 551

NASA AMES TEST 416
RUN 9
551 ROTOR RPM
$\Theta_{.75}$ 18.9°
V = 105 KNOTS
A_1 = -2.12°
B_1 = 2.56°
$\Delta\Theta = -A_1 \cos(\psi+20) - B_1 \sin(\psi+120)$

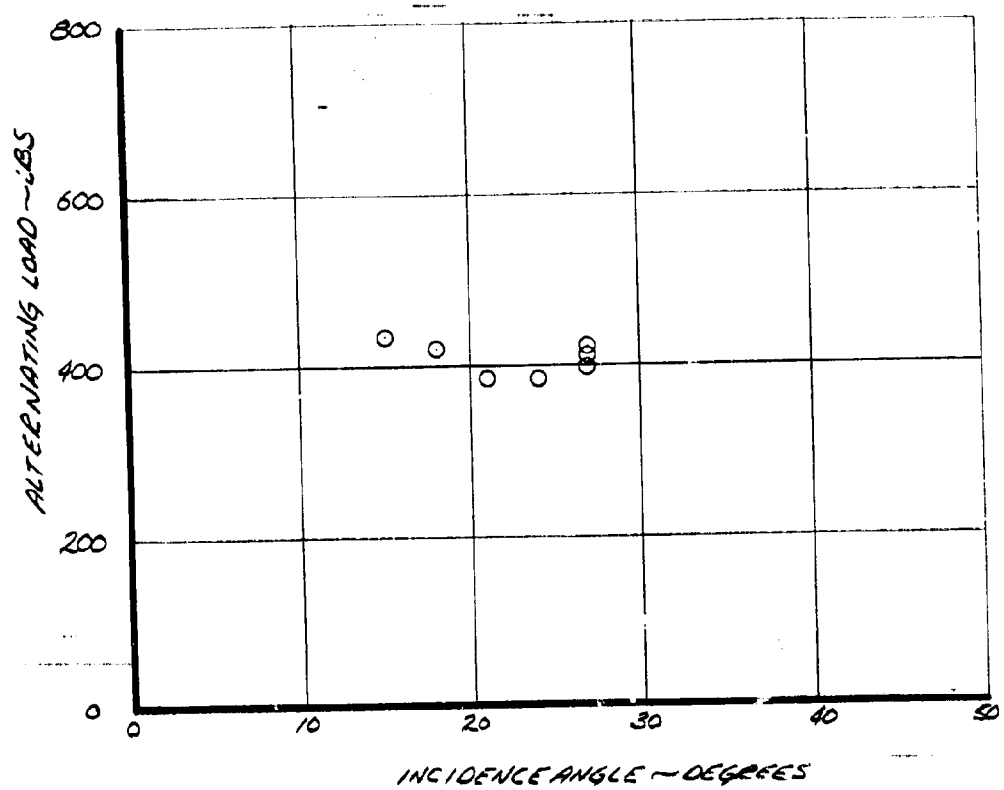

FIGURE 5-40 EFFECT OF INCIDENCE ANGLE ON ALTERNATING PITCH LINK LOADS. i_N = 2.7° V = 105 KNOTS RPM = 551

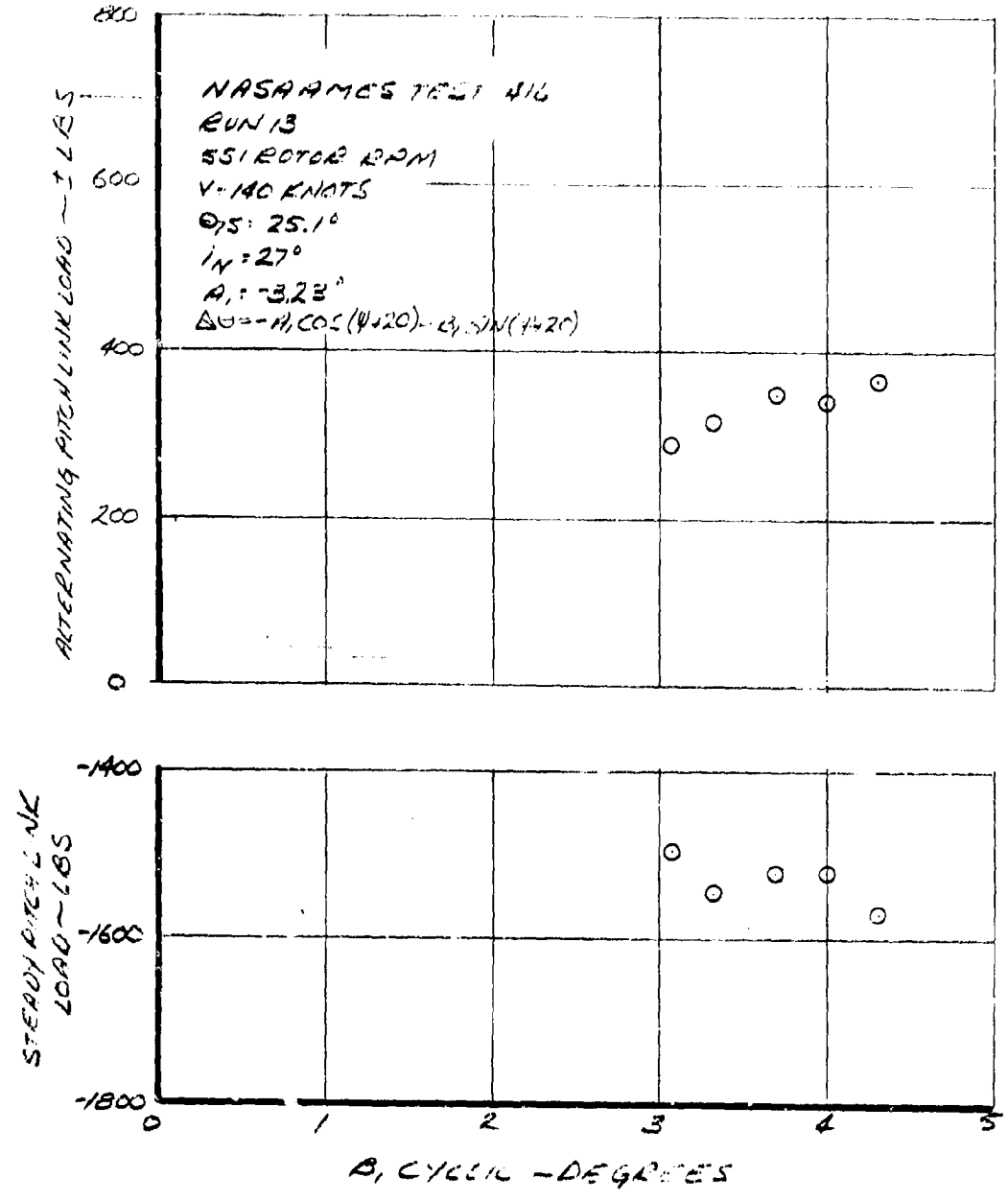

FIGURE 5-41 EFFECT OF B1 CYCLIC ON STEADY AND ALTERNATING PITCH LINK LOADS. i_N = 27° V = 140 KNOTS RPM = 551

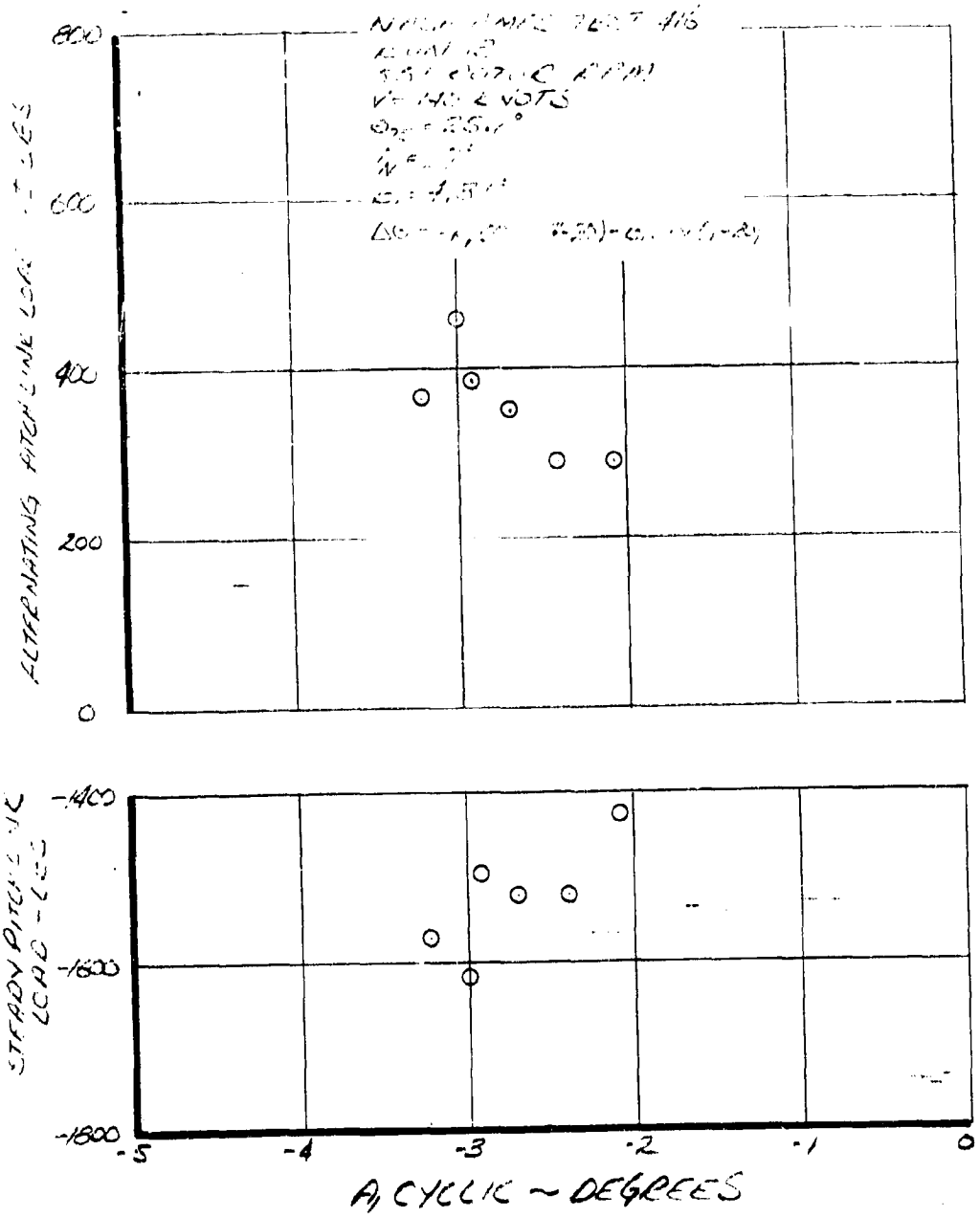
800
600
400
200
0
-1400
-1600
-1800
-5
-4
-3
-2
-1
0
A, CYCLIC ~ DEGREES

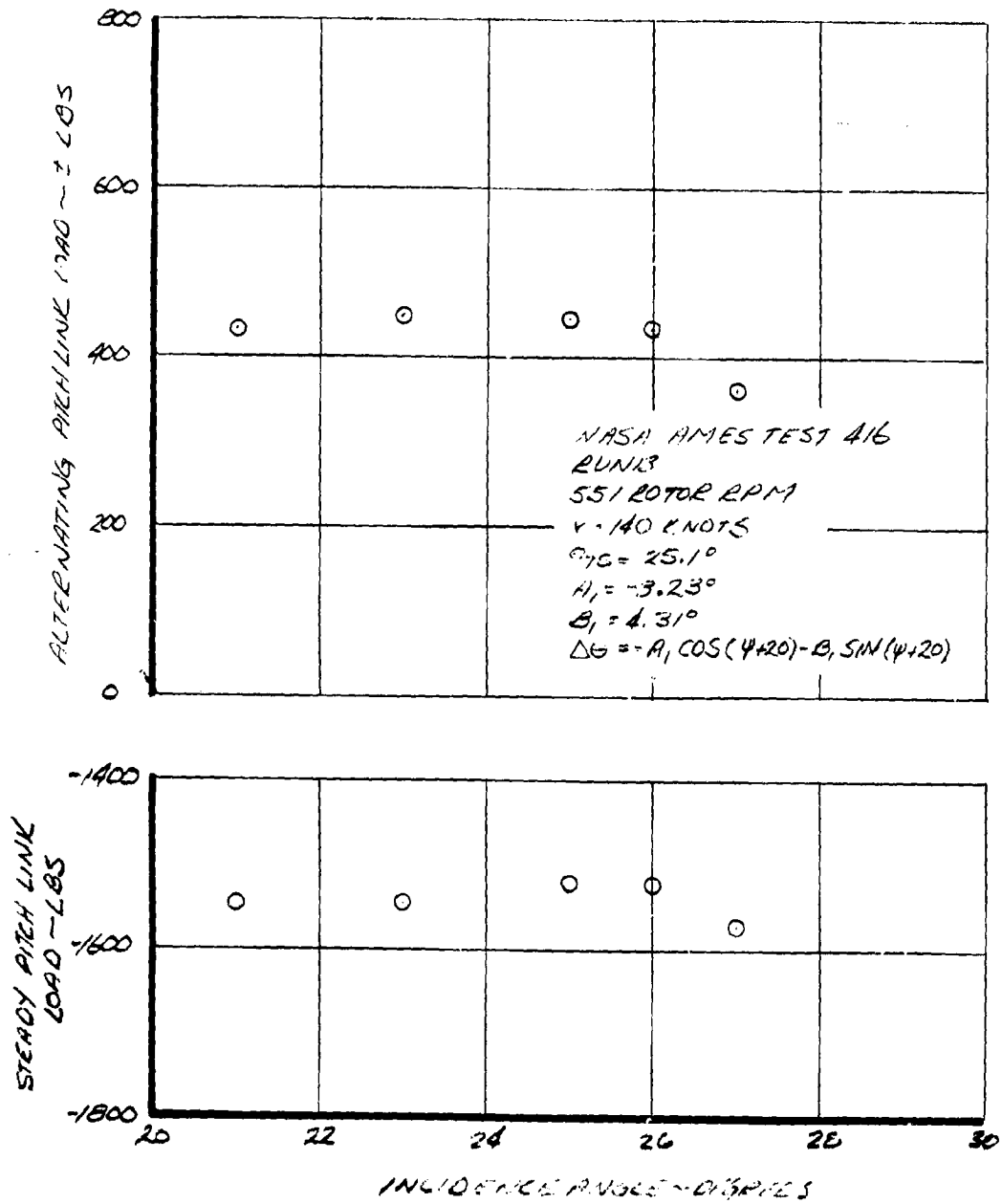

FIGURE 5-43 EFFECT OF INCIDENCE ANGLE ON STEADY AND ALTERNATING PITCHLINK LOADS. i_N = 1°
V = 140 KNOTS, RUN = 551

5.3 Cruise Control Loads

The data in this section were taken from test 416 and are designated cruise control loads since they were obtained at cruise design RPM. The primary impact of the reduction of RPM on control loads is to reduce the blade planipetal torsion load and hence the pitch link steady load by the RPM ratio squared.

The control load data at 140 knots 10° i_N and 386 RPM are given in Figures 5.44 to 5.51. The steady pitch link loads are a little higher than predicted (about 7%). The alternating pitch link loads increase with cyclic pitch. The actuator bolt loads are lower than the pitch link data would indicate and are not considered reliable in view of possible alternate load paths as discussed in Section 5.2.

Run 14 was done at 170 knots i_N = 10° and 386 RPM. The steady pitch link data are again higher than predicted (Figure 5.52) during the collective sweep. The alternating pitch link loads are insensitive to collective pitch (Figure 5.53). The effect of cyclic pitch is shown in Figures 5.54 to 5.57. The steady pitch link loads are unaffected and the alternating pitch link loads increase. The upper boost actuator loads do not agree with the pitch link load data and are considered unreliable. Resolution of this problem would require stripping down the

actuators and control system to determine the cause. This must be done if any further testing is to be performed using the test nacelle.

The steady pitch link loads at this condition (170 knots) are unaffected by incidence; however, the alternating loads increase as incidence increases, Figures 5.58 and 5.59.

The steady pitch link loads are summarized in Figure 5.60 and compared with prediction. The agreement is good over the range tested.

NASA AMES TEST 416
RUN 11
386 ROTOR RPM
i_N = 10°
V = 140 KNOTS
A_1 = -2.62°
B_1 = 2.31°
$\Delta\theta = -A_1 \cos(\psi+20) - B_1 \sin(\psi+20)$

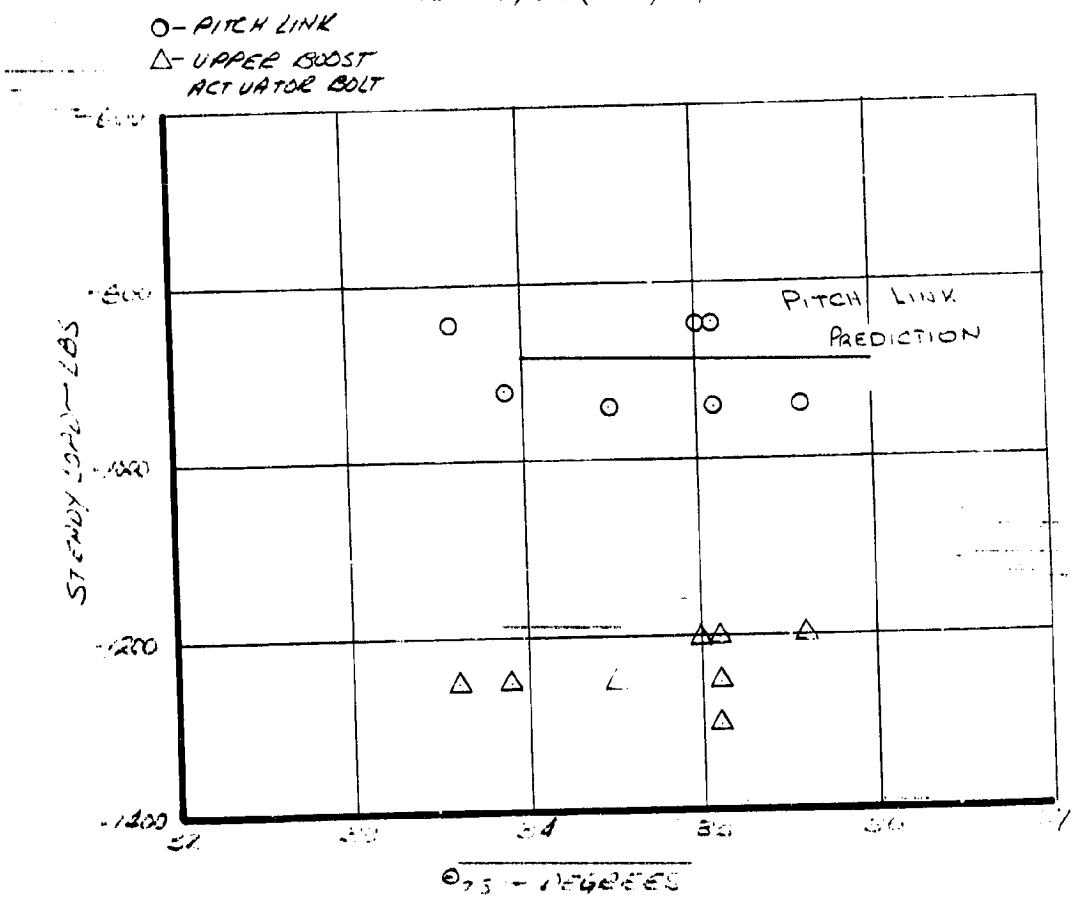

FIGURE 5-14 EFFECT OF COLLECTIVE PITCH ON STEADY CONTROL LOADS. i_N = 10° V = 140 KNOTS RPM = 386

NASA AMES TEST 416
RUN 11
356 ROTOR RPM
$i_N = 10°$
$V = 140$ KNOTS
$A_1 = -2.62°$
$B_1 = 2.31°$

O– PITCH LINK
Δ– UPPER BOOST ACTUATOR PIST

$\Delta\theta = -A_1 \cos(\psi+20) - B_1 \sin(\psi+20)$

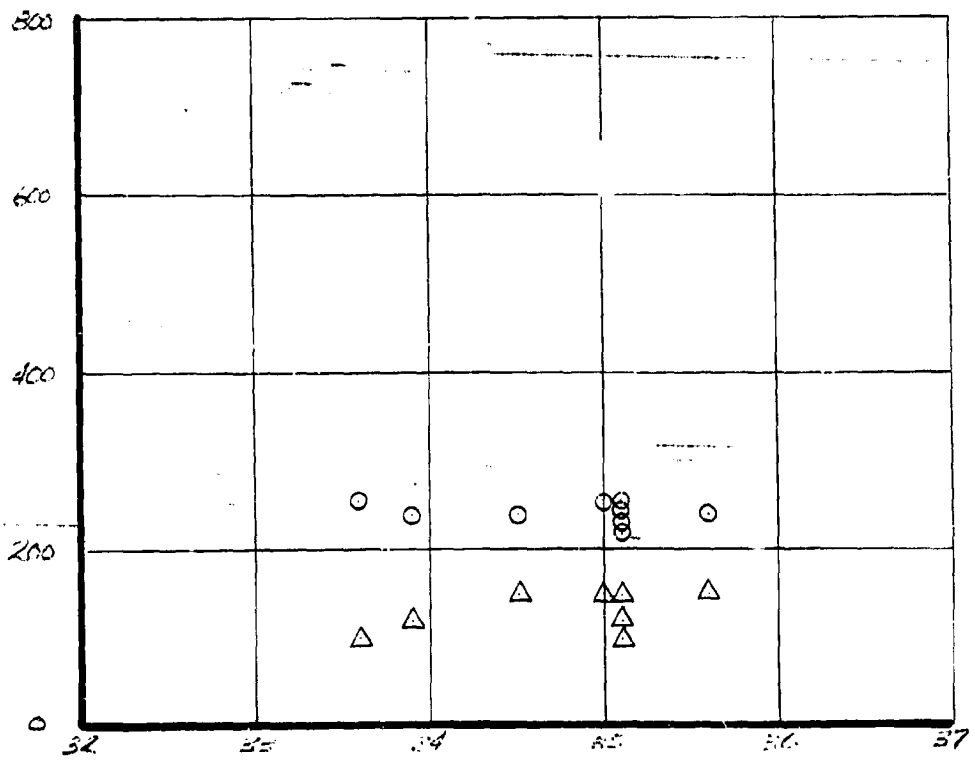

NASA AMES TEST 4/6
[illegible]
386 ROTOR RPM
Θ_{75} = 35.1°
i_N = 10°
V = 140 KNOTS
B_1 = 2.31°
$\Delta\theta = -A_1 \cos(\psi - 20) - B_1 \sin(\psi + 2)$

○ - [illegible]
△ - UPPER BOOST ACTUATOR BOLT

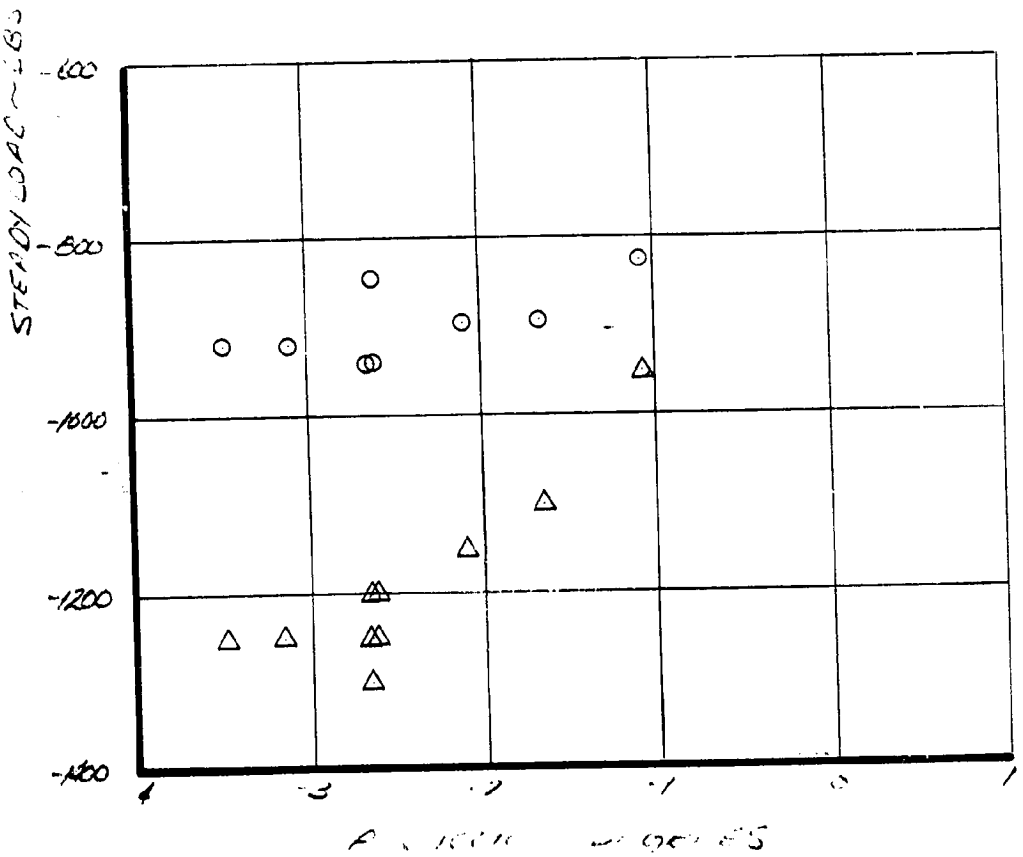

FIGURE 5-45 EFFECT OF [illegible] CONTROL LOADS. i_N = 10° V = 140 KNOTS RPM = 386

NASA AMES TEST 416
RUN 11
356 ROTOR RPM
θ_{75} = 35.1°
i_N = 10°
V = 180 KNOTS
θ_1 = 3.51°
$\Delta\theta = -A_1 \cos(\psi+20) - B_1 \sin(\psi+20)$

○ — PITCH CASE
△ — UPPER BOOST ACTUATOR CASE

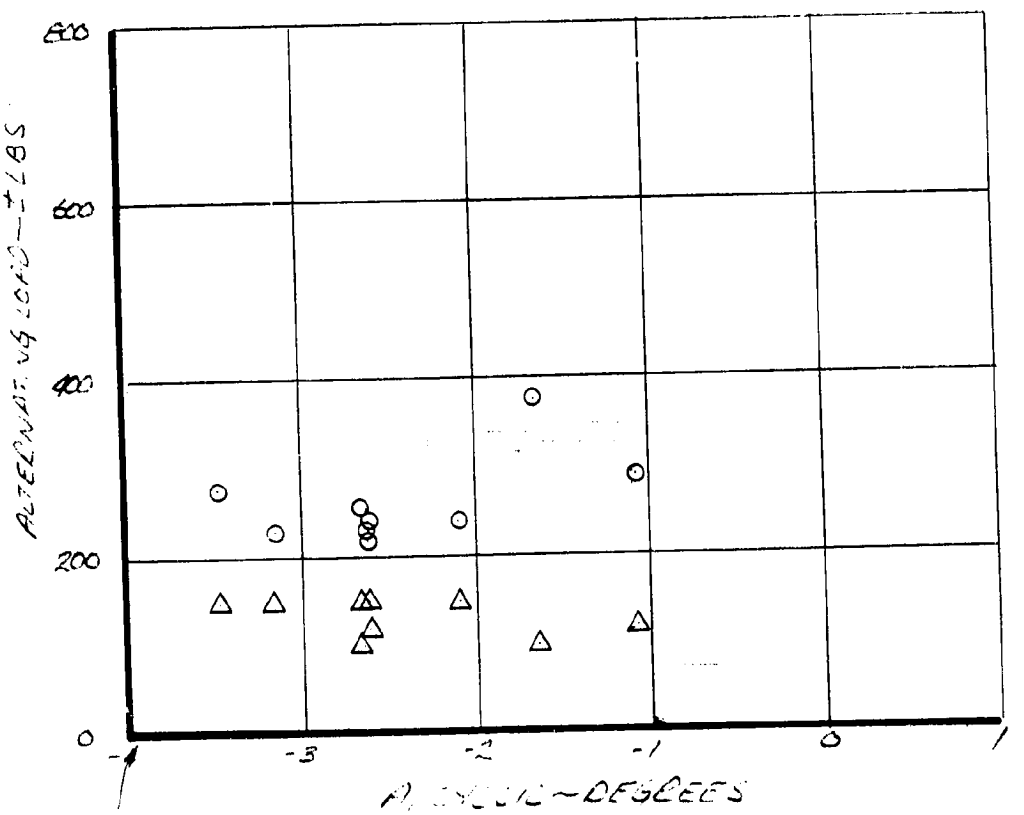

FIG. [illegible] PITCH CASE AND UPPER BOOST ACTUATOR CASE ALTERNATING LOADS VS CYCLIC PITCH

O- PITCH LINK

Δ- UPPER BOOST ACTUATOR ROD END

$\Delta U = A_1 \cos(\psi + 20) - B_1 \sin(\psi + 20)$

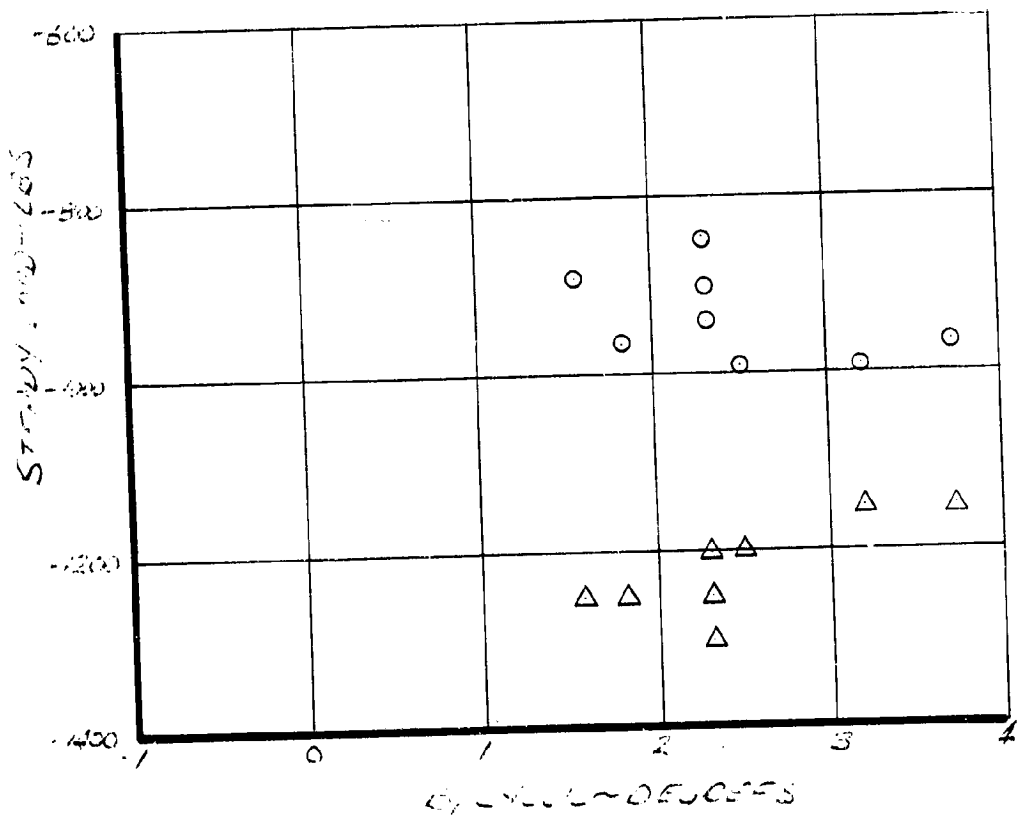

NASA AMES TEST 416

O– PITCH LINK
Δ– UPPER BOOST ACTUATOR BOLT

$\Delta\theta = -A_1 \cos(\psi+20) - B_1 \sin(\psi+20)$

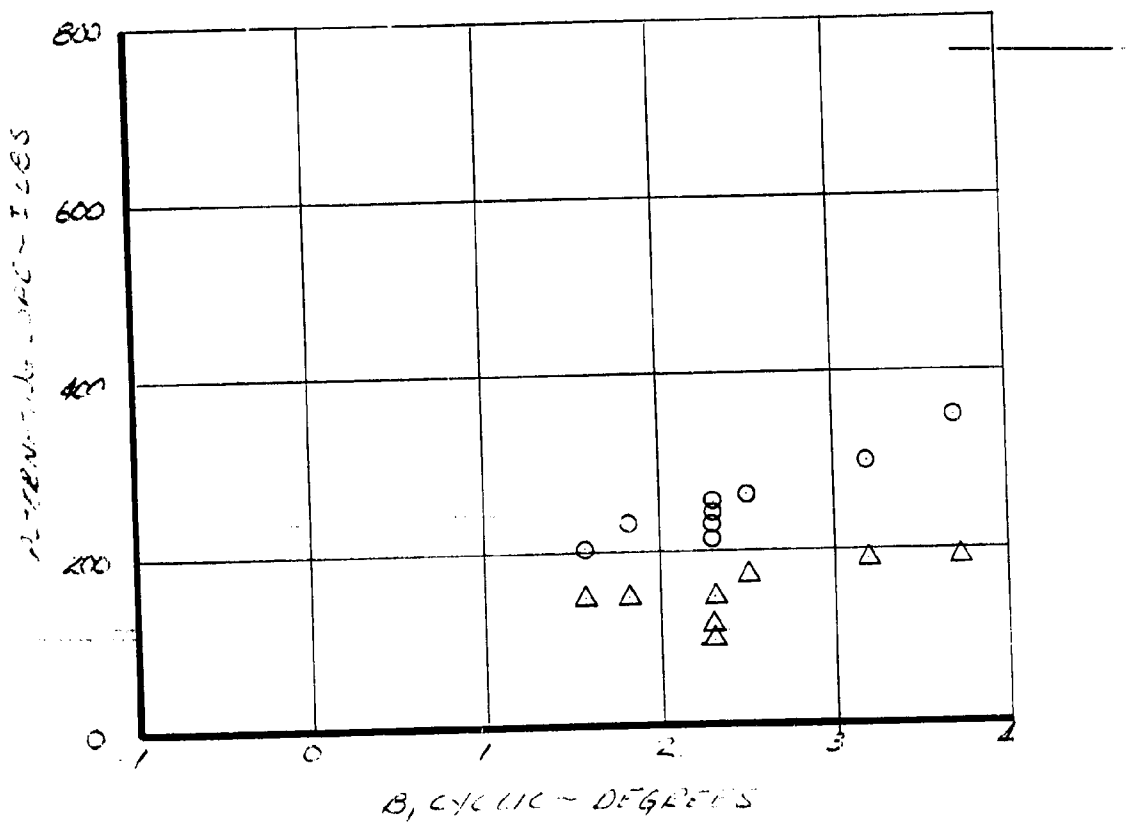

NASA AMES TEST 416
RUN 11
386 ROTOR RPM
Θ_{75} - 25.1°
V - 140 KNOTS
A_1 = 2.62°
B_1 = 2.31°
$\Delta L = -A_1 \cos(\psi+20) - B_1 \sin(\psi-20)$

○ - PITCH LINK
△ - (PROPELLER INPUT ROTATING SYSTEM)

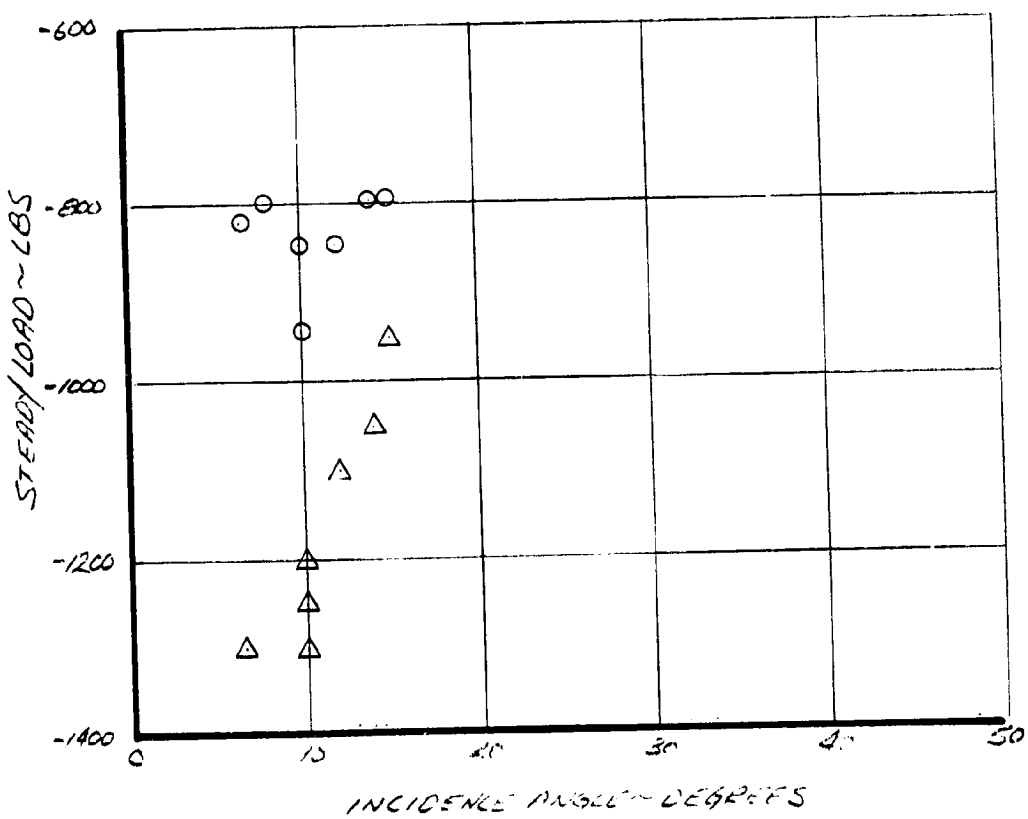

FIGURE 5.20 EFFECT OF INCIDENCE ON [illegible]

NASA AMES TEST 416
RUN 11
386 ROTOR RPM
Θ_{75} = 35.1°
V = 140 KNOTS
A_1 = -2.62°
B_1 = 2.31°

O - PITCH LINK
Δ - [illegible]

$\Delta\Theta = -A_1 \cos(\psi+20) - B_1 \sin(\psi+20)$

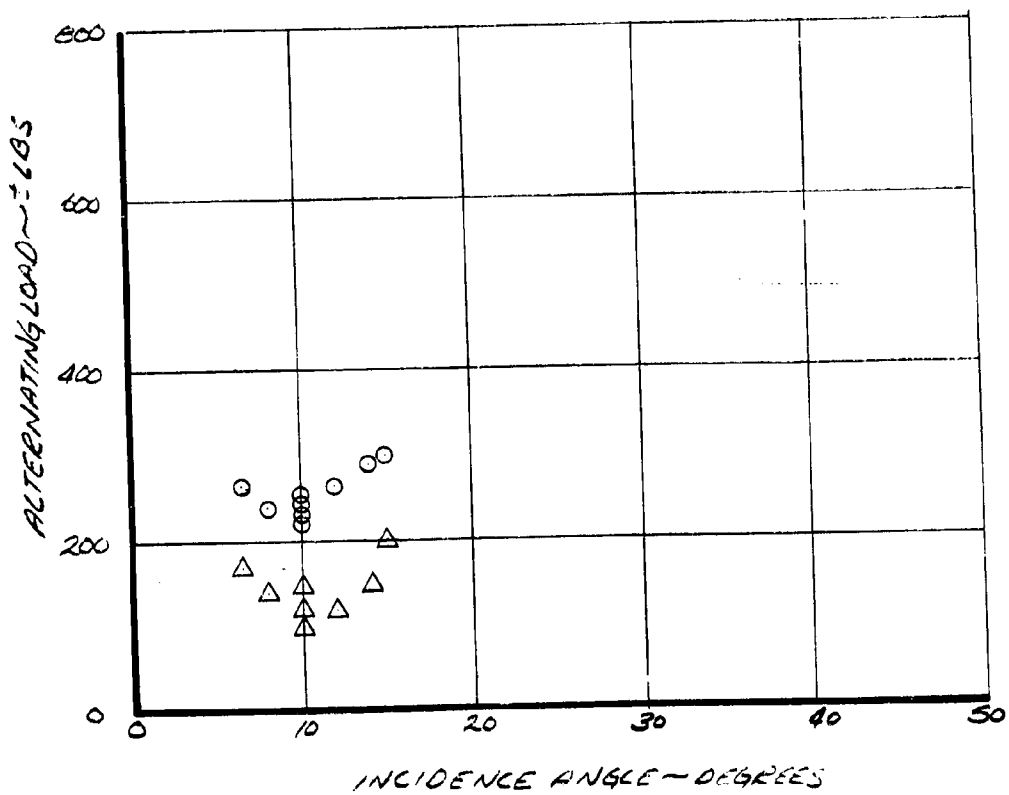

FIGURE 3-31 [illegible]

NASA AMES TEST RIG
ROTOR
3600 RPM TIP SPEED
IN = 10°
V = 170 KNOTS
$A_1 = -2.97°$
$B_1 = 3.84°$
$\Delta\theta = -A_1 \cos(\psi+20) - B_1 \sin(\psi+20)$

○— PITCH LINK
△— SWASH PLATE ACTUATOR ROD

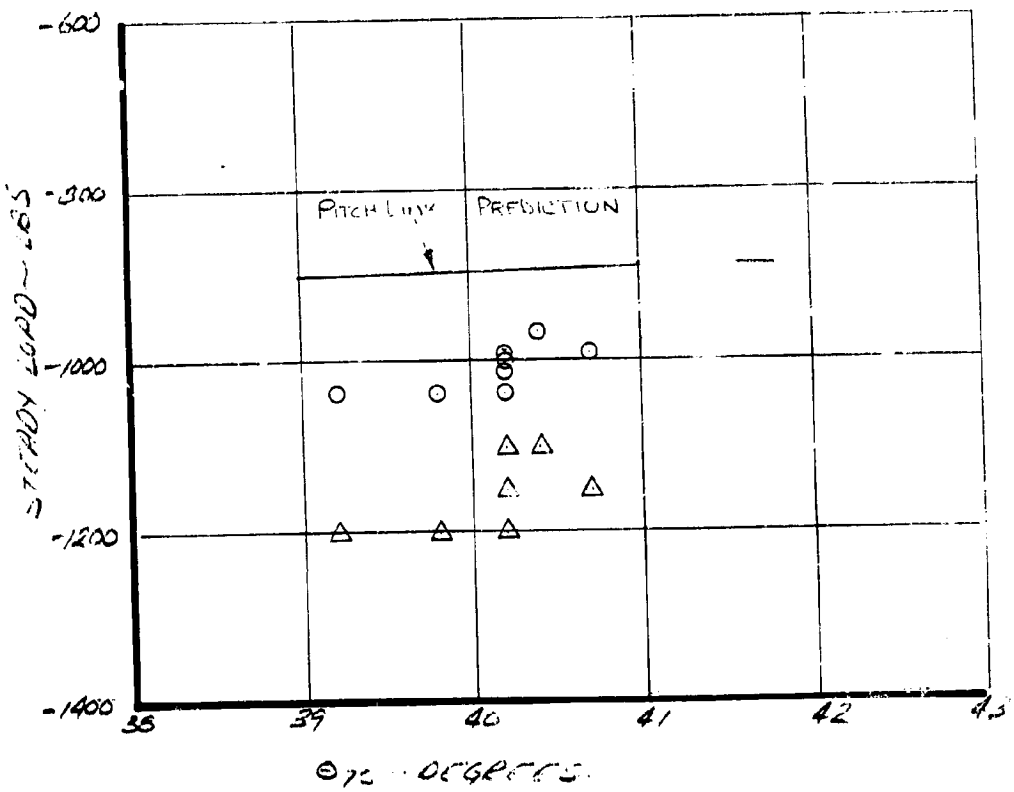

F 3 CC 3 CA ... IN = 10° V = 170 KNOTS RPM = 3600

NASA AMES TEST 416
RUN 14
ROTOR RPM
i_N = 1°
V = 100 KNOTS
○ – PITCH LINK R_1 = 2.97
△ – UPPER BOOST ACTUATOR BOLT R_2 = 3.20"
$\Delta\theta = -A_1 \cos(\psi - 20) - B_1 \sin(\psi - 20)$

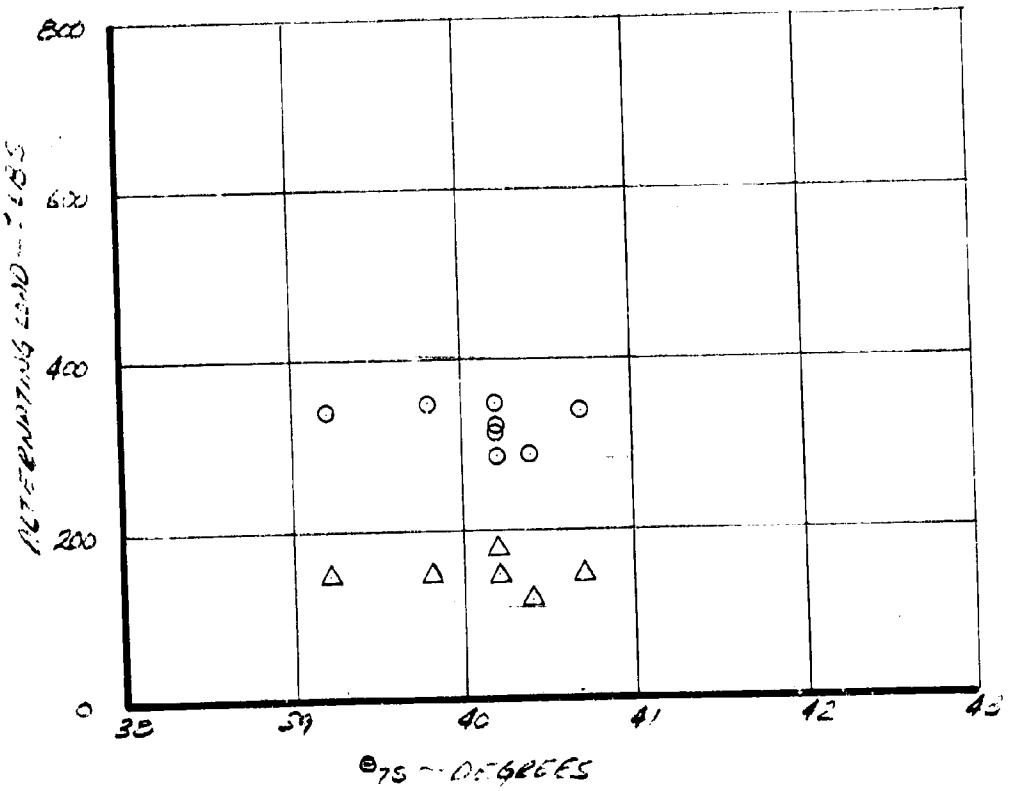

FIG. K-14 [illegible] VS. θ_{75} 100 KNOTS RPM 356

NASA AMES TEST 416
RUN 14
350 ROTOR RPM
$\theta_{.75} = 10.2°$
$i_N = 10°$
V = 170 KNOTS
$A_1 = -2.97°$
$B_1 = -1.20 - 2.5\sin(\psi + 20) - 2.5\sin(2\psi + 20)$

○ – PITCH LINK
△ – [illegible]

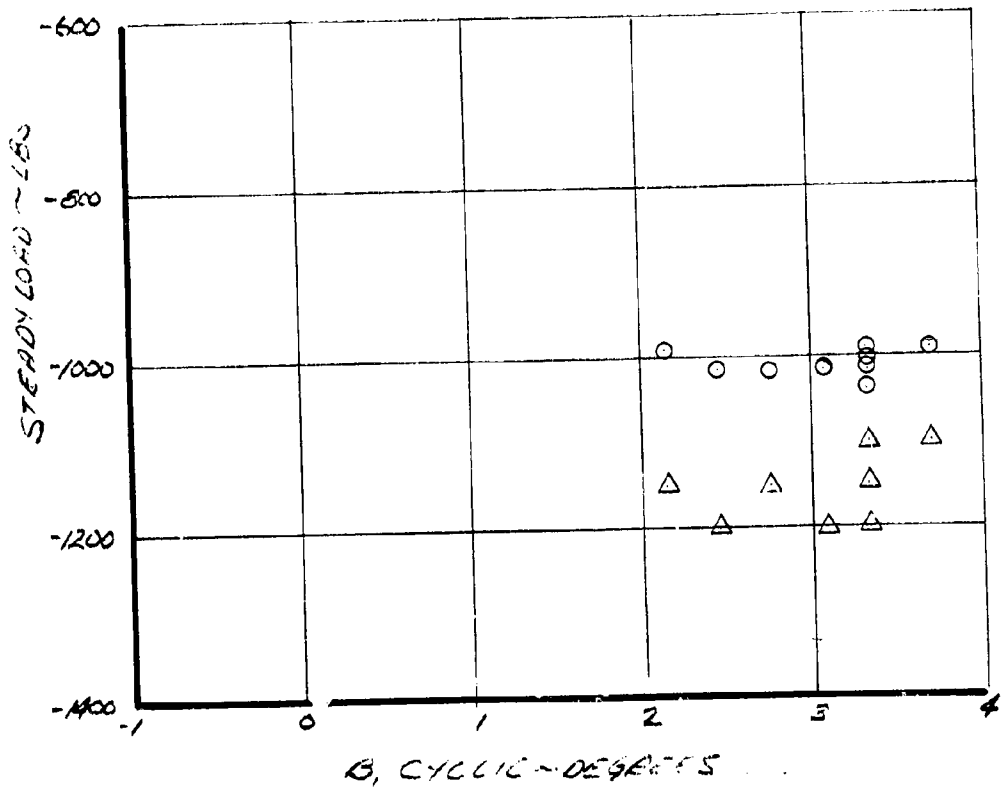

[illegible]

NASA AMES TEST 416
RUN 12
386 ROTOR RPM
$\theta_{75} = 40.2°$
V = 170 KNOTS
$i_N = .10°$
$A_1 = -2.97°$
$\Delta\theta = -A_1 \cos(\psi+20) - B_1 \sin(\psi+20)$

○ – PITCH LINK
△ – UPPER AXIS ROTATING ROTOR COUT

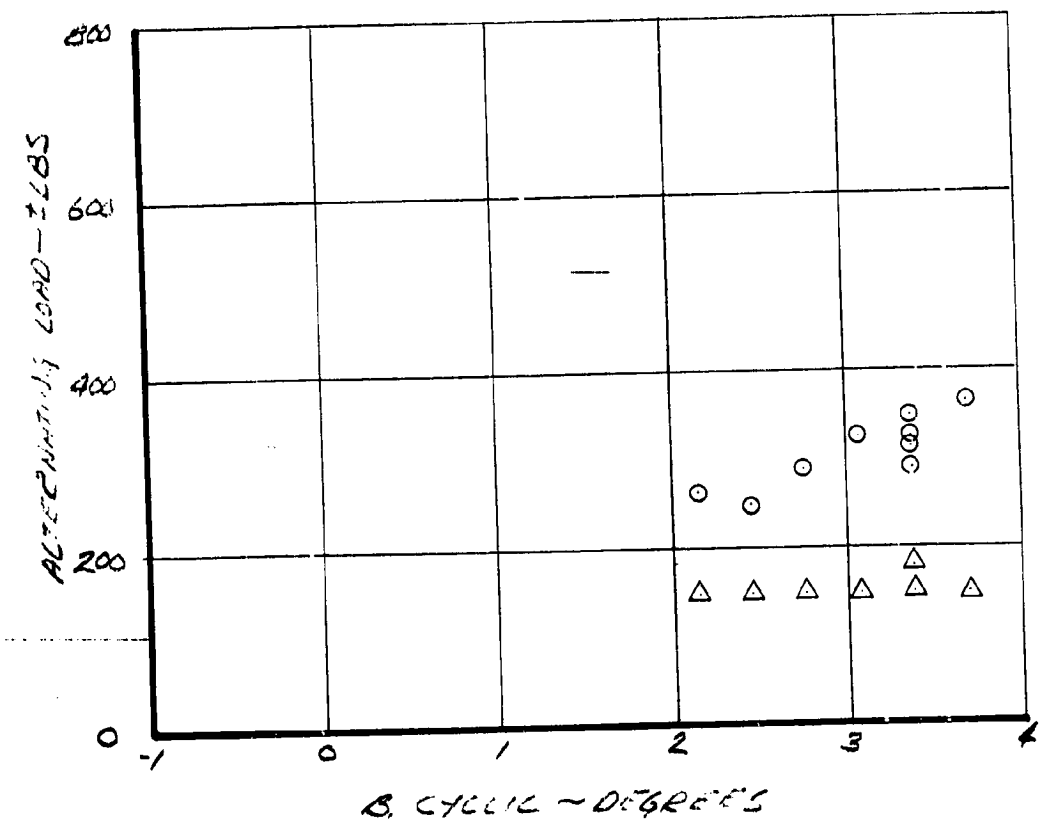

FIGURE C-6 [illegible]

NASA AMES TEST 416
RUN 14
360 ROTOR RPM
$\Theta_{.75}$ 40.2°
V - 170 KNOTS
i_N = 10°
B_1 = 3.30°

O - PITCH LINK
Δ - UPPER BOOST ACTUATOR ROD

$\Delta\theta = -A_1 \cos(\psi + 20) - B_1 \sin(\psi + 20)$

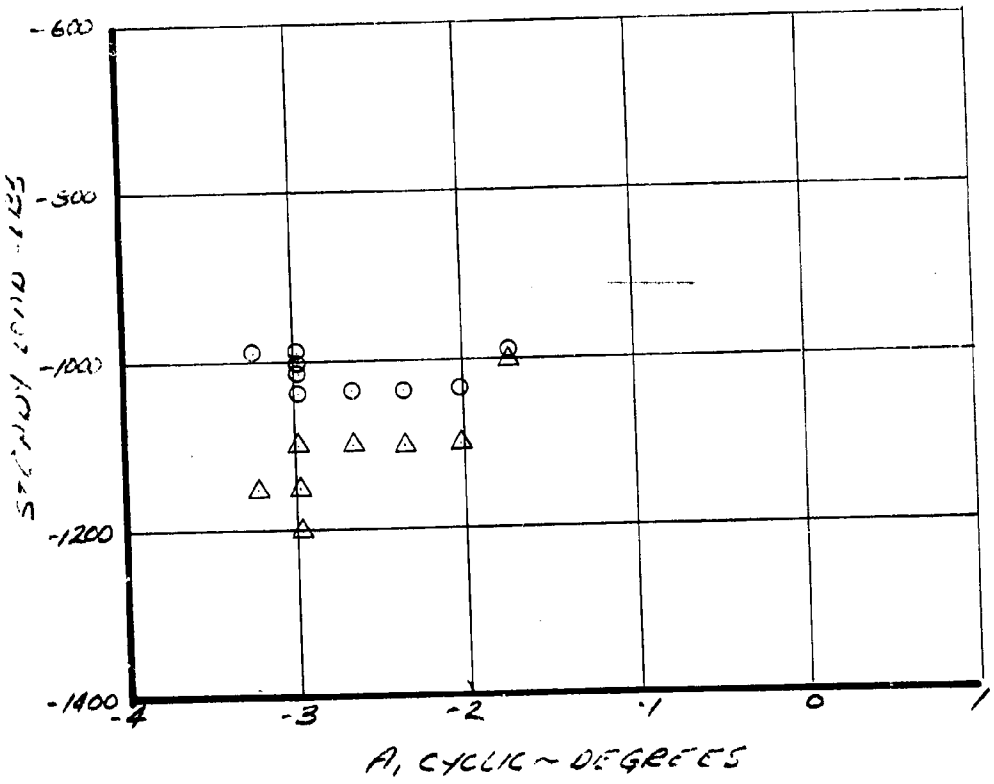

FIG 30 - C.G. EXCITATION AND [illegible] VS LONG. CYC. PITCH - V = 170 KNOTS, RPM = 360

NIKA AMES TEST 416
RUN 14
386 ROTOR RPM
$\theta_{.75} = 40.2°$
V = 170 KNOTS
$i_N = 10°$
$A_1 = 3.39°$
$\theta = -A_1 \cos(\psi+20) - B_1 \sin(\psi+20)$

○ – PITCH LINK
△ – UPPER BOOST ACTUATOR BOLT

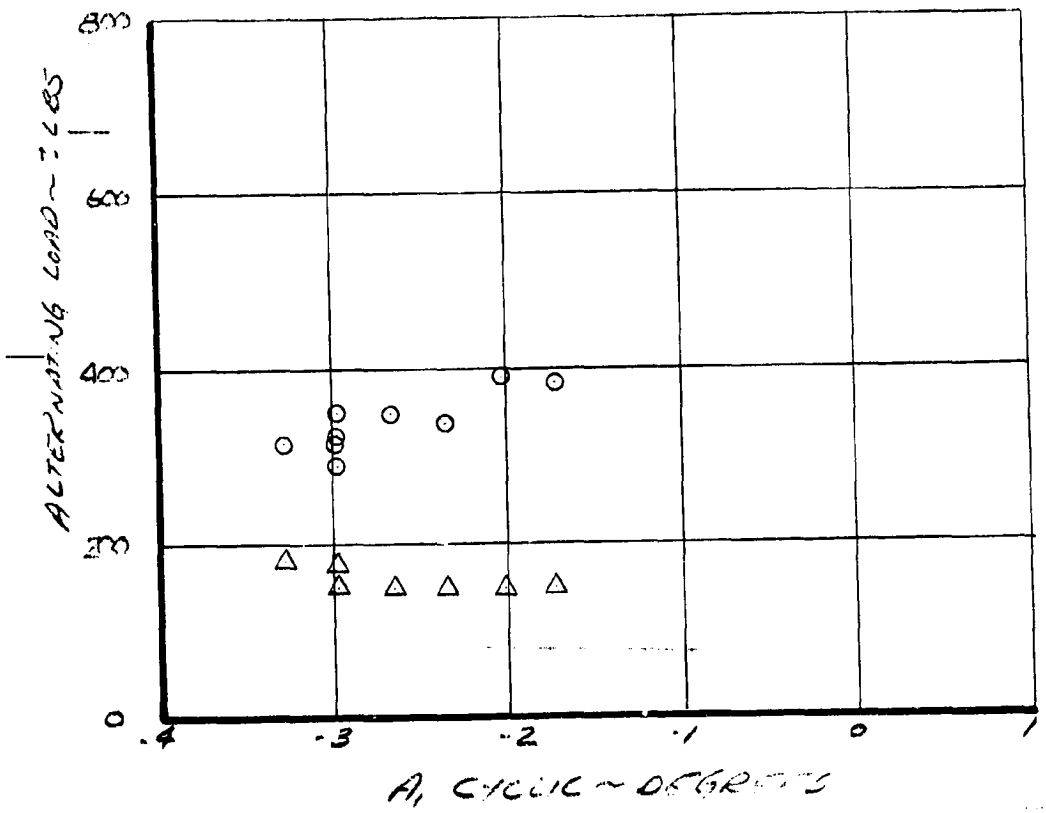

FIGURE 5.2.1 [illegible]

NASA AMES TEST 416
RUN 12
356 ROTOR RPM
θ_{TS} = 40.2°
V = 170 KNOTS
A_1 = 2.97°
B_1 = 3.38°
$\Delta\theta = -A_1 \cos(\psi + 20) - B_1 \sin(\psi + 20)$

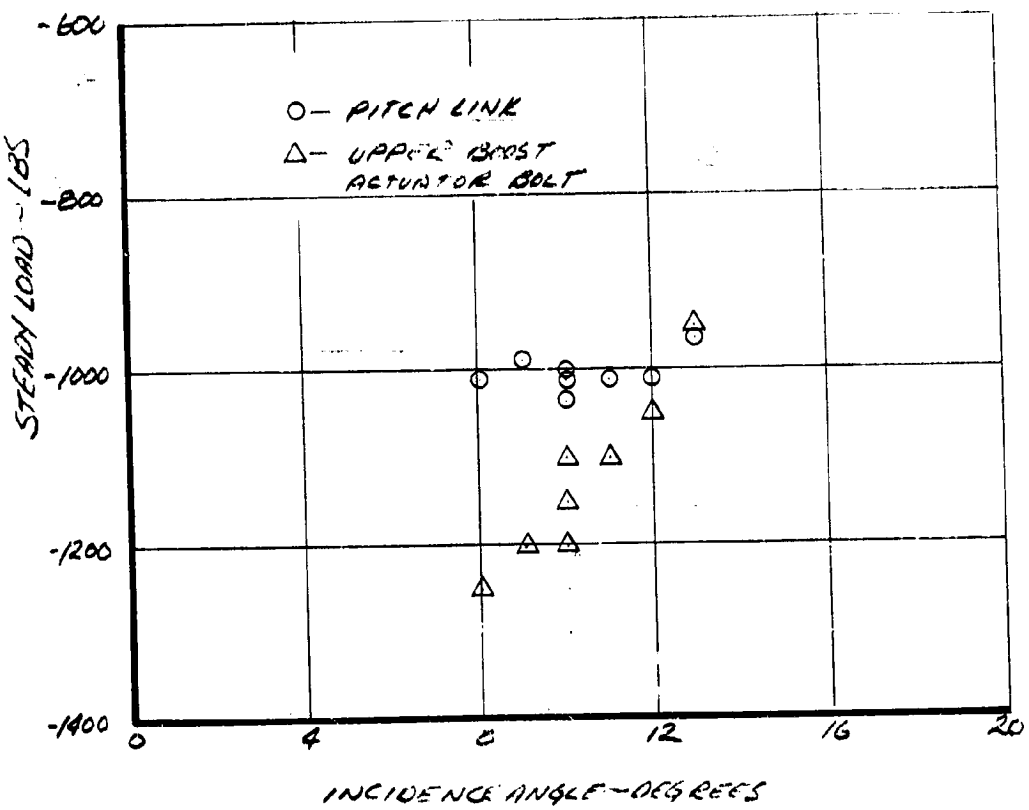

FIGURE 5-65 COLLECTIVE INCIDENCE ANGLE VS STEADY [illegible] AMES RPM-356

NASA AMES TEST 416
RUN 12
386 ROTOR RPM
i_N = 10°
V = 170 KNOTS
A_1 = -2.97°
B_1 = 3.38°
$\Delta\theta = -A_1 \cos(\psi+20) - B_1 \sin(\psi+20)$

O - PITCH LINK
Δ - UPPER BOOST ACTUATOR BOLT

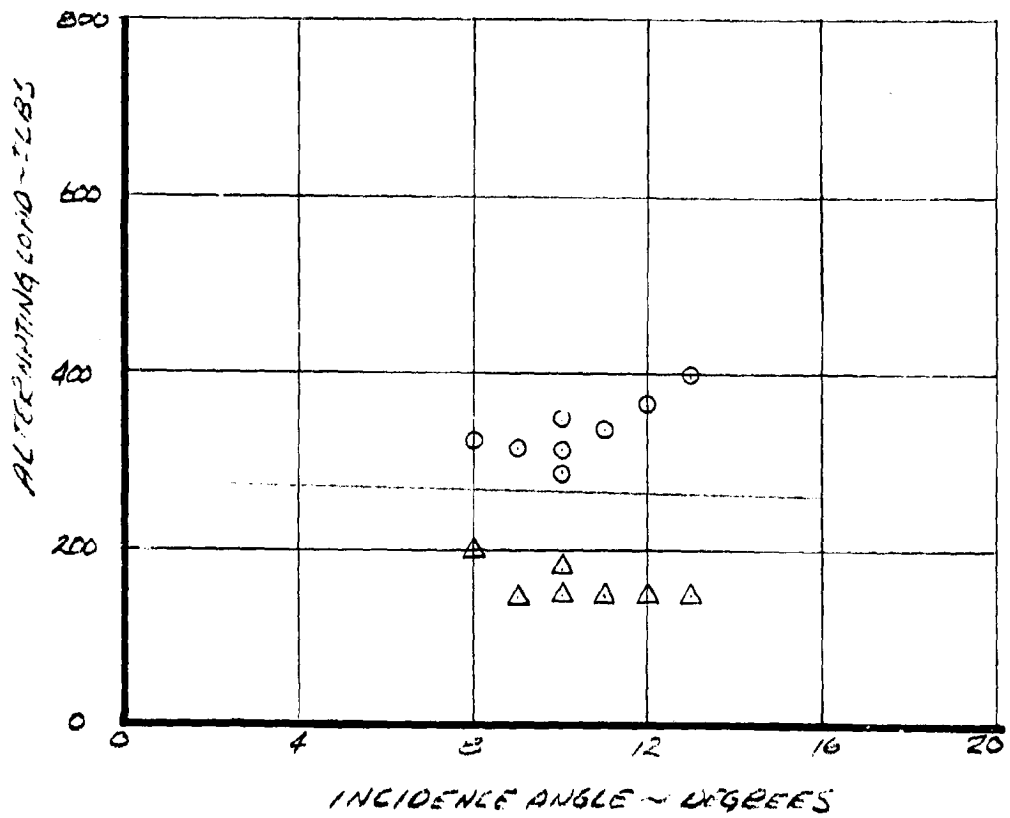

FIGURE 5-59 EFFECT OF INCIDENCE ANGLE ON ALTERNATING CONTROL LOADS. μ = .[illegible] V = 170 KNOTS RPM = 386

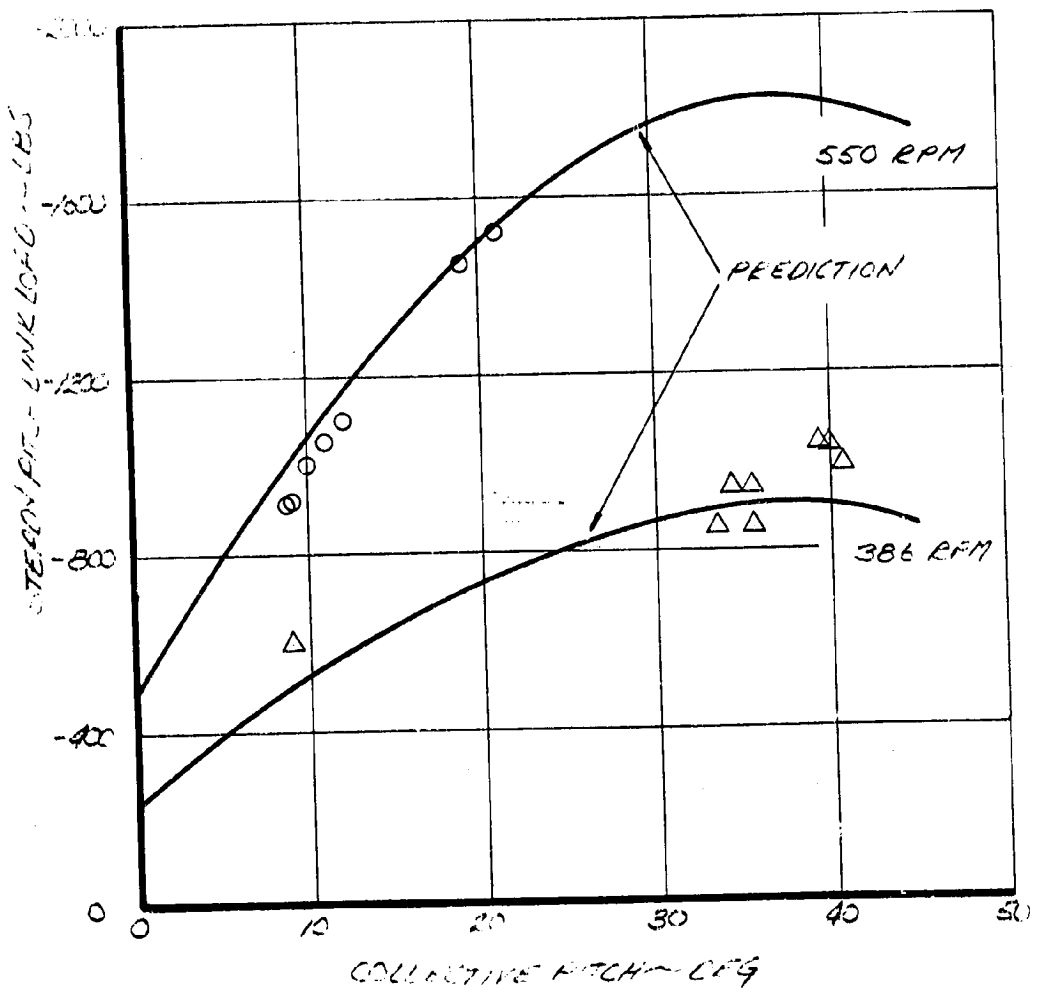

FIGURE 5.4 COMPARISON OF STEADY PITCH-LINK LOADS.

5.4 WAVEFORMS AND DATA REDUCTION

The pitch link wave forms obtained from CEC recordings contain a spike up and down once per revolution. This effect is most evident in the hover runs and an example of the waveform is given in Figure 5.61. A smaller spike on the trace is also evident and coincident with the one per rev marker. This smaller spike is attributed to electrical interference from this source. The larger pair of spikes are more difficult to identify. They always occur at the same azimuth position and appear to be independent of cyclic input, Figure 6.62. This would tend to rule out pitch link "slop" and inertial effects due to cyclic. This is also clear from the fact that the spike exists when no cyclic is input in axial flow (hence no pitch acceleration).

The blade angle trace shown in Figure 6.62 is taken from a rotary pot mounted right at the blade root. This traces shows no discontinuities or spikes and is indicative of smooth blade pitch motion. The spike was not coming from the blade.

This spike was in evidence but to a smaller extent on Test 410. On this test two pitch link gages were recorded and these data indicate a similar spike occurring at the same instant in time (not azimuth). This again rules out cyclic motion.

The shaft torque trace also contains a similar spike at the same time as the pitch link.

In reducing the alternating pitch link load data the spike was faired out for the following reasons:

1. The spike load is inexplicable in hover with no cyclic.
2. The blade angle contains no discontinuities.
3. The loads including the spike are less than the endurance limit except for Run 22.
4. On Run 22 the spike does not affect the alternating load read since it is 90-degrees out of phase with the peak load.

NASA AMES TEST 416
RUN 7
551 ROTOR RPM
$i_N = 0°$
V = 0 KNOTS
$\theta_{.75} = 9°$

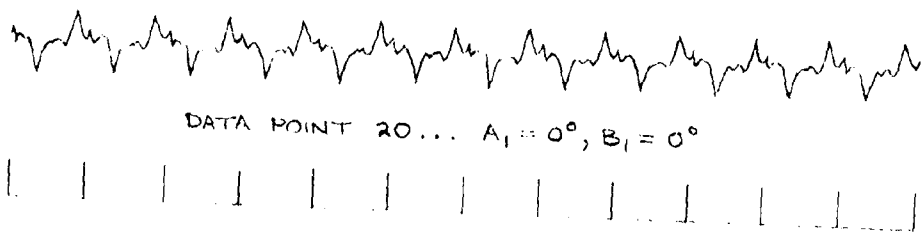

DATA POINT 20... $A_1 = 0°$, $B_1 = 0°$

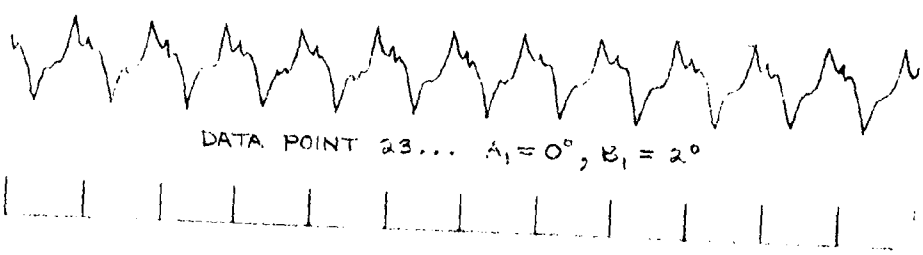

DATA POINT 23... $A_1 = 0°$, $B_1 = 2°$

FIGURE 5.61 SAMPLE PITCH LINK LOAD WAVEFORMS AT STATIC THRUST. $B_1 = 0°$ AND $B_1 = 2°$, 551 ROTOR RPM.

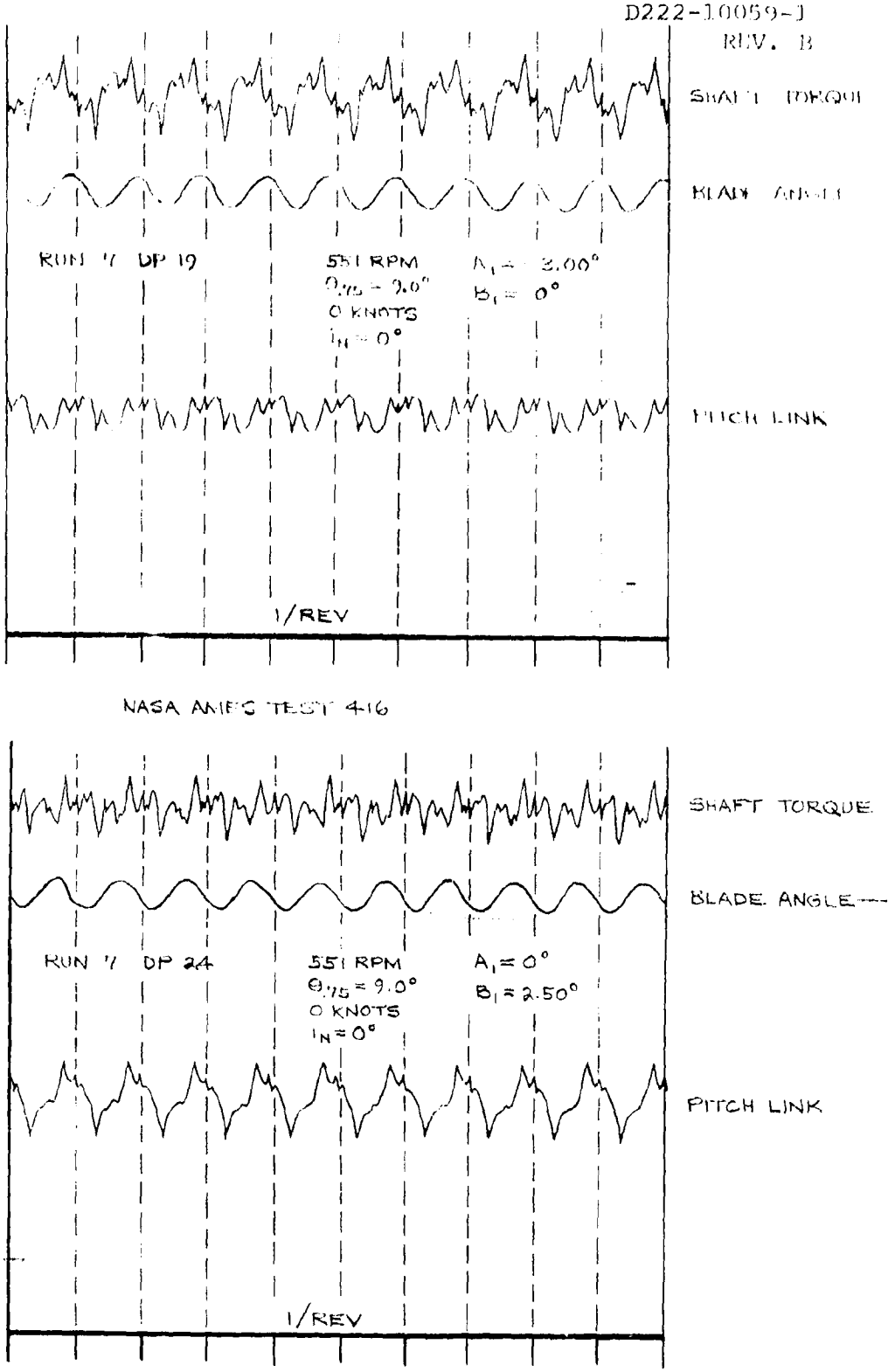

FIGURE 5.62 PITCH LINK, BLADE ANGLE AND SHAFT TORQUE WAVE FORMS

4.0 STABILITY AND CONTROL

6.0 STABILITY AND CONTROL

The Model 222 aircraft uses its rotors for control in hover and conventional airplane surfaces in cruise flight. In transition, control is maintained by a mixture of rotor and airframe controls. Though not used as a primary control in cruise the rotor significantly influences the flying qualities and static stability of the aircraft.

Measurements were taken on both windmilling and powered tests to provide an experimental data base for correlation and design verification.

In hover and transition the data are taken from test 416 (powered) and obtained from tunnel balance measurements. The hub moments were also derived and measured from the hub barrel "blade load" out of plane bending gage by electronic demodulation and resolution. (See Appendix 4).

Most of the data in the cruise mode is taken from test 410 (windmilling) and was obtained from wing strain gage readings.

6.1 Hover Control

The data presented in this section were obtained with the rotor shaft aligned with the tunnel axis and the tunnel fans stopped. This is not a pure static thrust condition but a vertical rate of climb as shown in Section 7.1 The sign convention used for positive forces and moments is as shown in Figure 2.6, and the

cyclic pitch axes are as described in Figure 4.24 such that

$$-/\cdot = -A_{1}\cos(\psi + 20) - B_{1}\sin(\psi + 20).$$

In hover the most difficult axis about which to achieve good handling qualities is yaw. This is obtained in part by generating rotor in plane forces fore and aft differentially. Figure 6-1 shows the effect of longitudinal cyclic on hub in plane forces. Figure 6-2 is similar data for lateral cyclic pitch. The B_1 cyclic data indicate a maximum in plane force of 1.7% of thrust per degree of cyclic pitch. This maximum force vector lies 241° of azimuth after the maximum blade angle input. For A_1 cyclic Figure 6.2 the maximum blade angle input is at 160° azimuth and gives a maximum in plane force vector of 1.96% thrust. This force vector lies 243.4° after the maximum blade angle input. Averaging these data gives a maximum force vector of 1.83% thrust at 242.2° after the maximum blade angle input. At the thrust level at which these data were taken (C_{T_P} = 0.0014) the predicted value is 1.86% thrust.

With no cyclic input the in plane forces are small and independent of collective and RPM, Figures 6.3 and 6.4.

The hub moments due to cyclic pitch are shown in Figures 6.5 and 6.6. Hub moments were measured two ways, the tunnel balance and by a resolved demodulated blade load strain gage signal. Both sets of measurements are shown and result in the derivatives:

$\partial C_M/\partial B_1 = -.000207/°$ (Tunnel Balance)

$\partial C_M/\partial B_1 = -.000182/°$ (Resolver)

$\partial C_{YAW}/\partial B_1 = +0.00109/°$ (Tunnel Balance)

$\partial C_{YAW}/\partial B_1 = 0.00097/°$ (Resolver)

$\partial C_M/\partial A_1 = 0.000915/°$ (Tunnel Balance)

$\partial C_M/\partial A_1 = 0.000885/°$ (Resolver)

$\partial C_{YAW}/\partial A_1 = 0.000135/°$ (Tunnel Balance)

$\partial C_{YAW}/\partial A_1 = 0.000140/°$ (Resolver)

The A_1 cyclic derivatives indicate a maximum hub moment coefficient of 0.000925/° whose vector lies 298.4° after the cyclic input. The hub moment resolver gives 0.000892/° and oriented 299° after the cyclic input.

The B_1 cyclic derivatives show a maximum moment of 0.00111/° at 300.75° after maximum input, based on balance data. The resolver data give a maximum moment coefficient of 0.000985/° occurring at 300.3° after the maximum blade angle.

Summarizing this data cyclic pitch produces a hub moment coefficient of 0.000978/° cyclic which is oriented such that the moment vector lies 299.61° after the azimuth for maximum blade angle. The predicted maximum hub moment derivative is 0.00136/°.

This discrepancy in hub moment is partially explained by the radial distribution of blade loads, Section 4.1. The alternating

out of plane loads are less at 3.9%R (55,000 in-lbs/3 degrees cyclic) than predicted (68,500 in-lbs per 3 degrees cyclic) though at 10.5% the correlation is better. The experimental loads increase more slowly than predicted as r/R tends to zero, producing lower hub moment than predicted.

Figure 6.7 shows that collective pitch has no effect on hub moment with zero cyclic input.

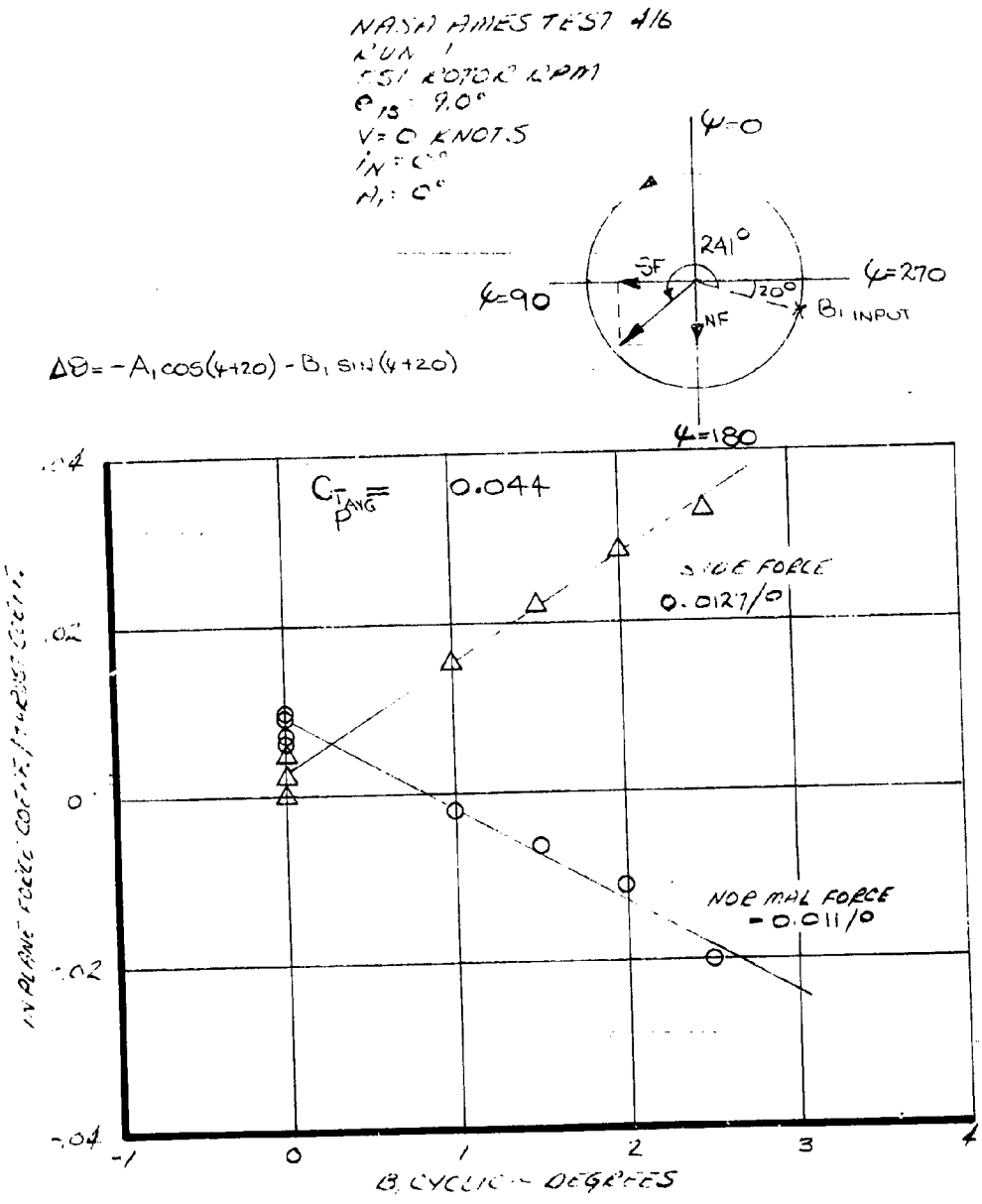

FIGURE 6.1 EFFECT OF LONGITUDINAL CYCLIC ON ROTOR HUB IN-PLANE FORCES 551 RPM TUNNEL FAN RPM = 0.

NASA AMES TEST 416
RUN 7
551 ROTOR RPM
$\Theta_{.75} = 9.0°$
V = 0 KNOTS
$i_N = 0°$
$\zeta_1 = 0°$

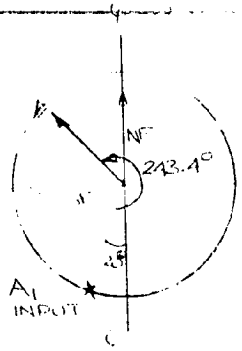

$$\Delta\Theta = -A_1\cos(\psi+270) - B_1\sin(\psi+270)$$

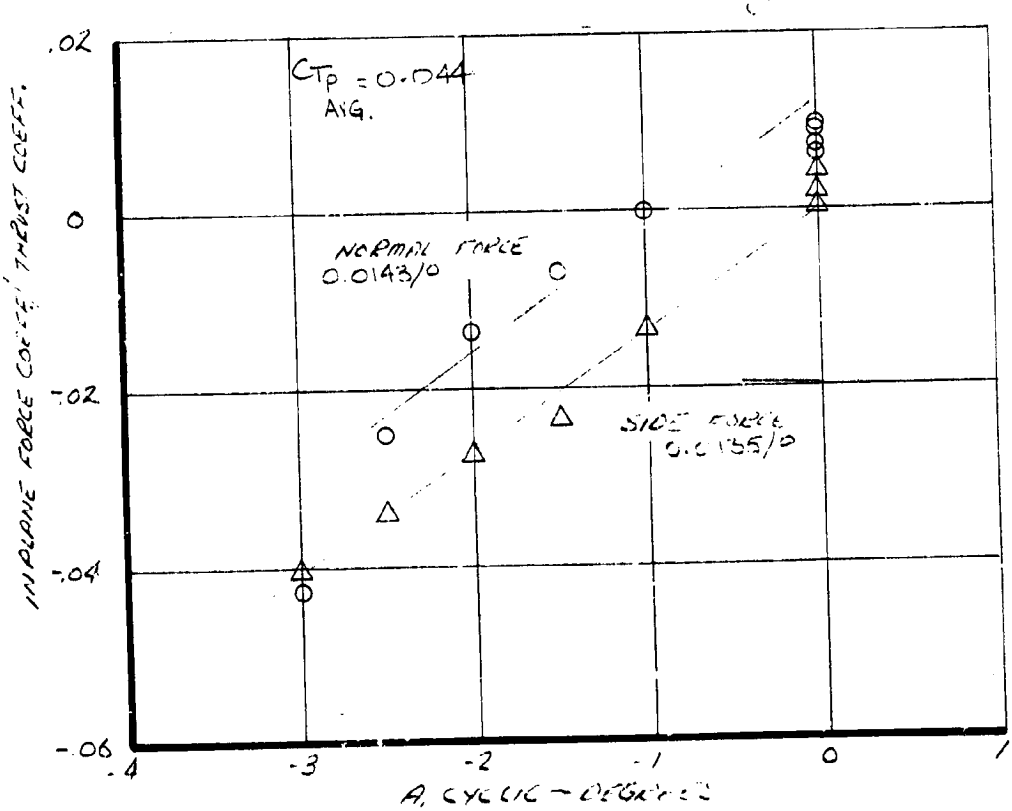

FIGURE 6-X EFFECT OF LATERAL [illegible] ON IN-PLANE FORCES [illegible] FAN RPM = 0

NASA AMES TEST 416
RUN 7
551 ROTOR RPM
V = 0 KNOTS
$i_N = 0°$
$A_1 = 0°$
$B_1 = 0°$

○ = NORMAL FORCE
△ = SIDE FORCE

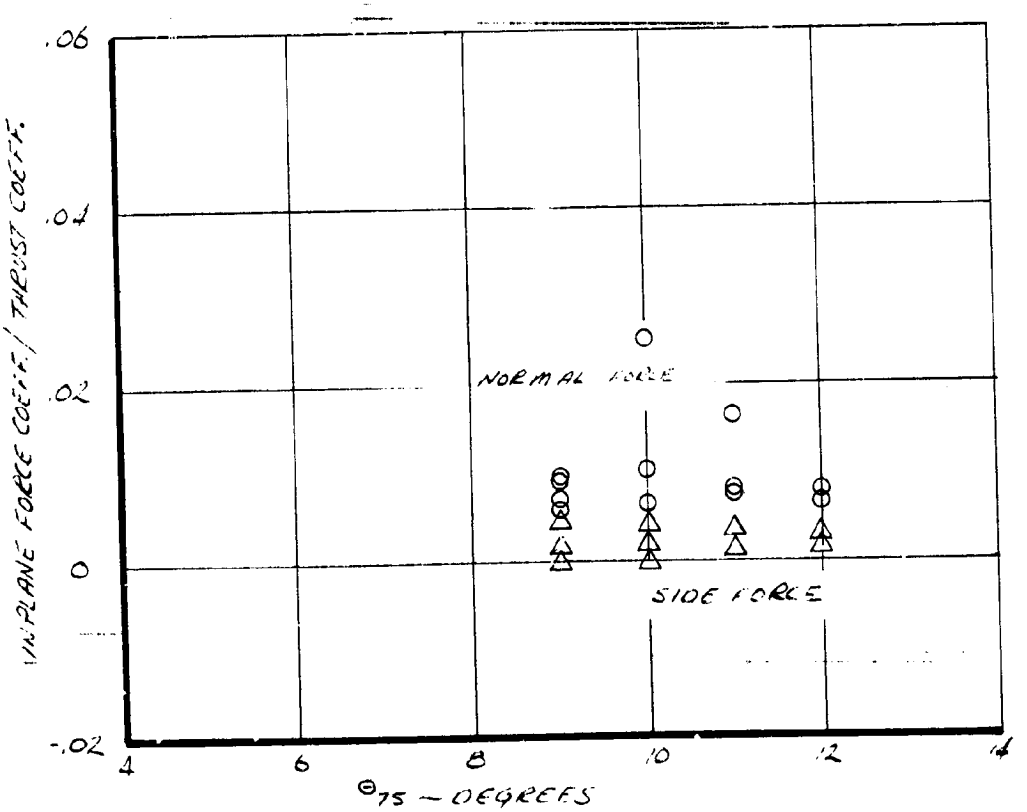

FIGURE 6.3 EFFECT OF COMPOUNDING ON IN-PLANE FORCES — SOLIDITY
ZERO CYCLIC — TUNNEL FAN RPM = 1750

NASA AMES TEST 4/6
RUN 6
$\Theta_{75} = 8.6°$
V = 0 KNOTS
$i_N = 0°$
$A_1 = 0°$
$B_1 = 0°$

C = NORMAL FORCE
C = SIDE FORCE

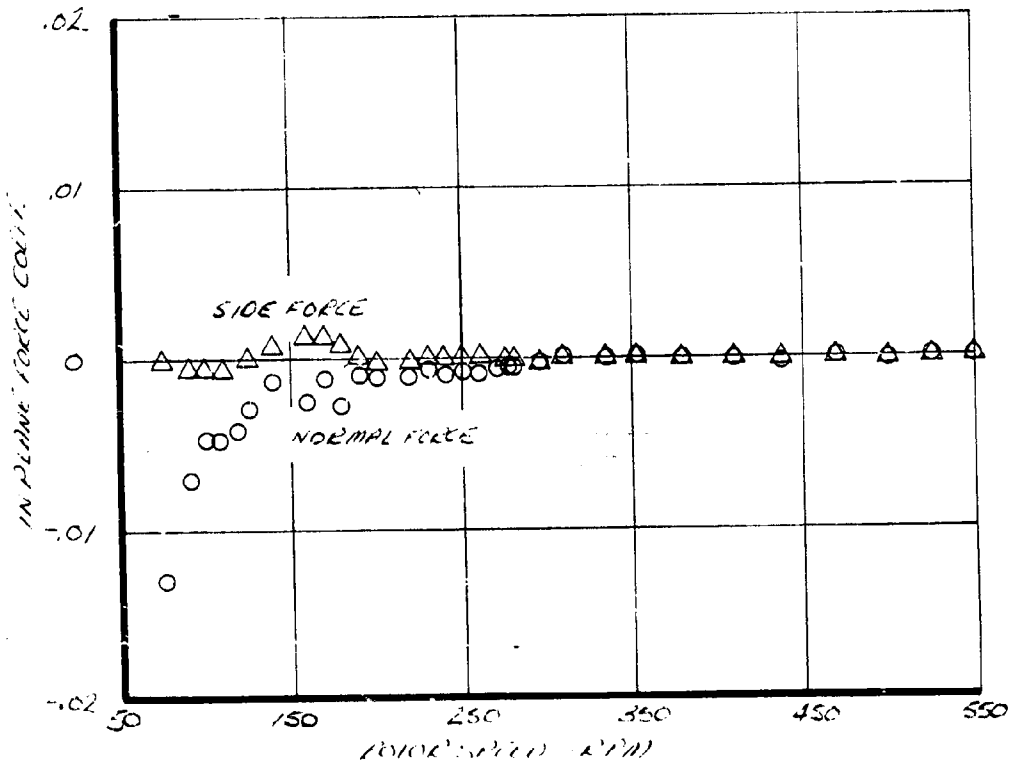

FIGURE 6.4 EFFECT OF ROTOR RPM ON IN PLANE FORCES 551 RPM
ZERO PITCH TUNNEL FAN RPM = 0.0

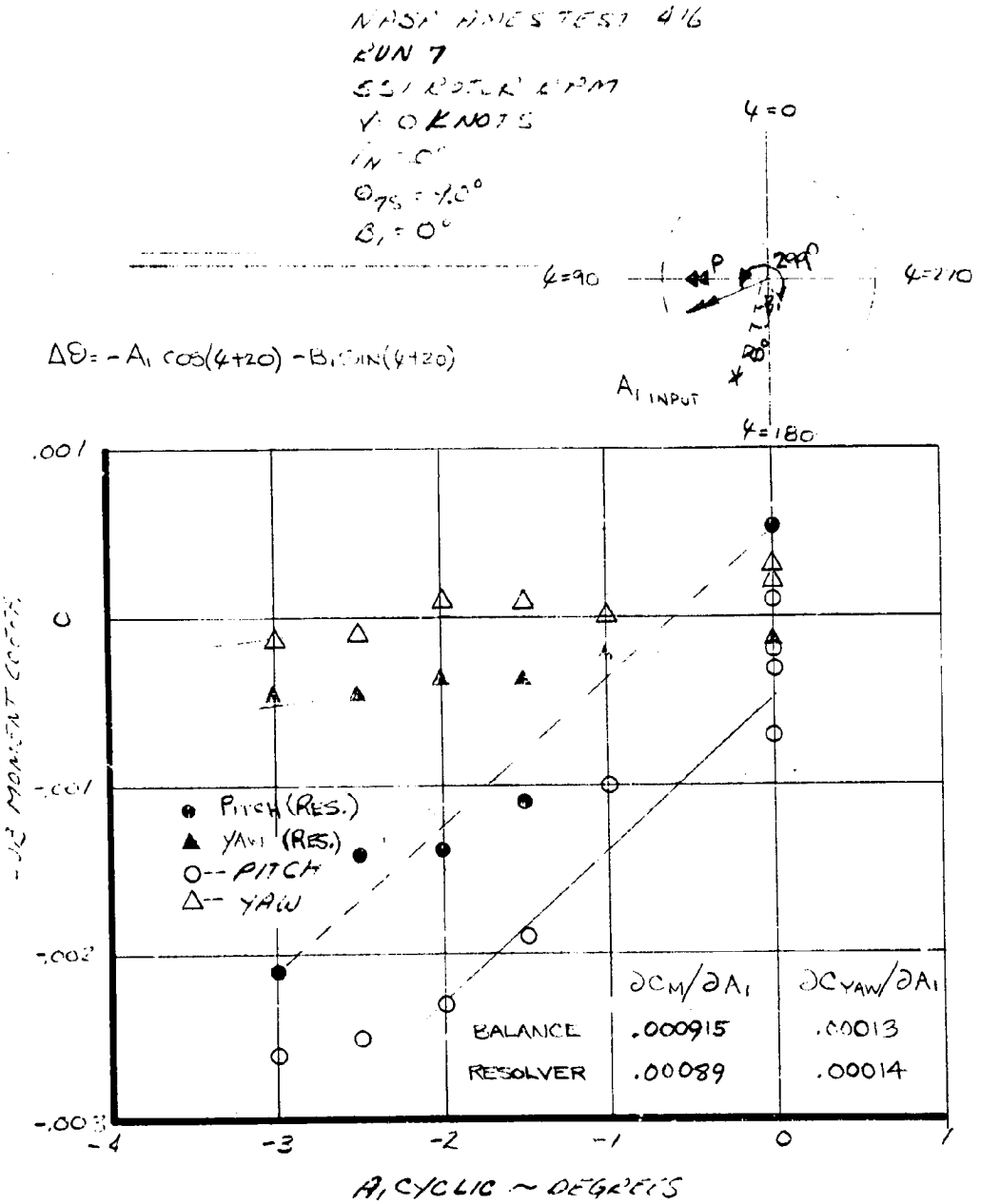

FIGURE 6-5 EFFECT OF LATERAL CYCLIC ON HUB MOMENTS. 551 RPM TUNNEL FAN PITCH = 0.

NASA AMES TEST #16
RUN 7
55' ROTOR RIG
V = 0 KNOTS
α_{TPP} 9.0°
i_N = 0°
η_1 = 0°

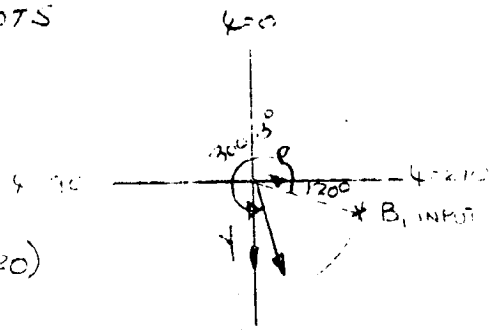

$$\Delta\Theta = -A_1 \cos(\psi + 2c) - B_1 \sin(\psi + 2c)$$

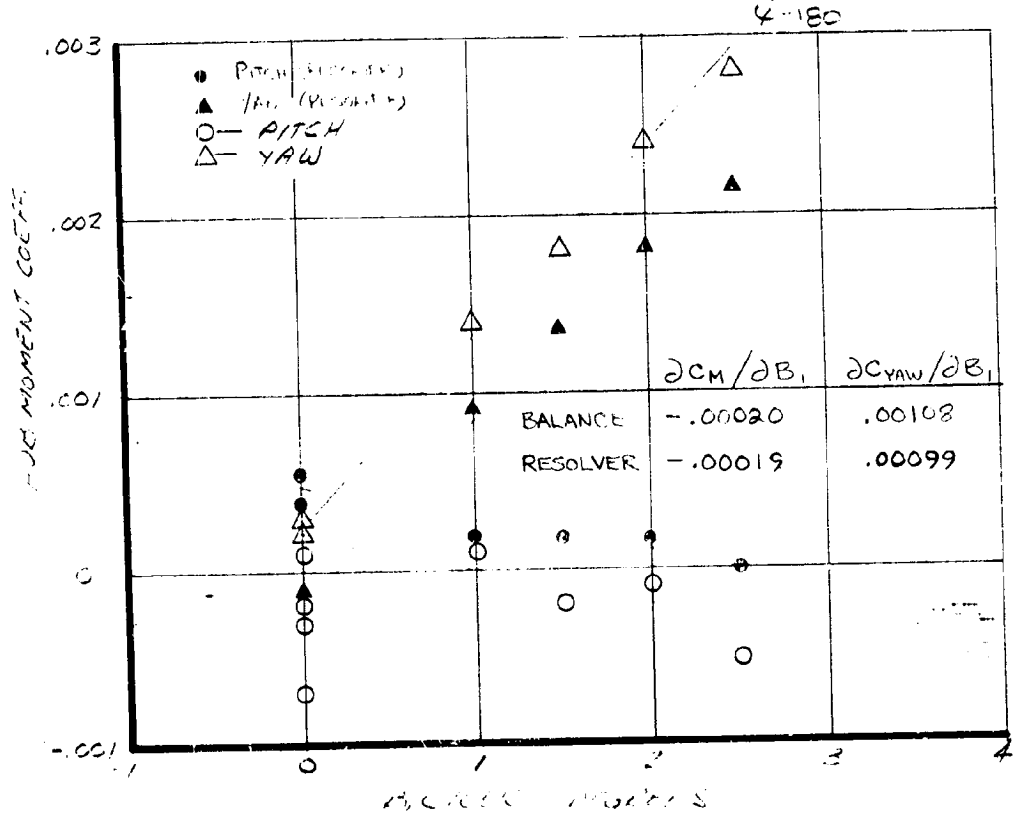

NASA AMES TEST 416
RUN 1
551 ROTOR RPM
V = 0 KNOTS
$i_N = 0°$
$\beta_1 = 0°$
$\beta_3 = 0°$

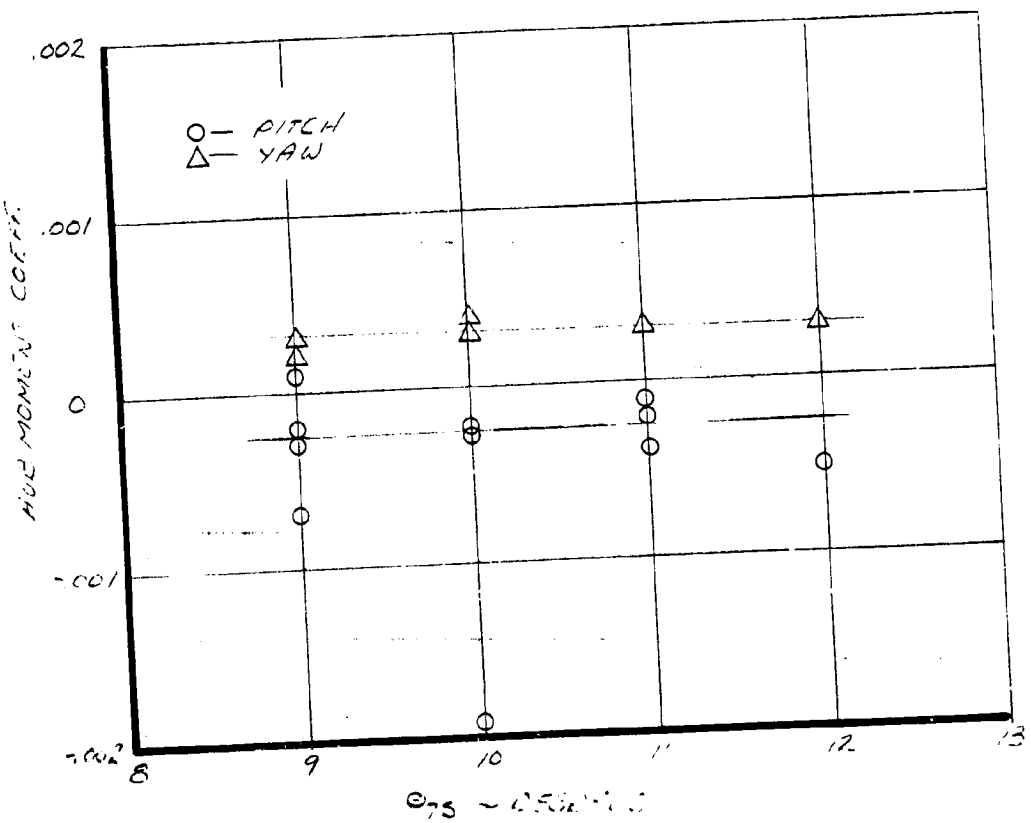

Figure 6.1 [illegible] PITCH AND ROTOR HUB MOMENT [illegible]

6.2 TRANSITION STABILITY AND CONTROL

The test data presented in this section was taken from the powered test 416 and consists of excursions of the control parameters about several test conditions. At each test condition the cyclic pitch values were adjusted to provide low alternating blade stresses. The two cyclic pitch controls and collective were then exercised to establish the hub force and moment derivatives.

At high shaft incidence i_N a rotor-test stand ground resonance instability was encountered which limited testing to 500 RPM at 85° incidence. This phenomena is discussed in Section 3.3 of this report. Figures 6.8 to 6.13 show the in plane forces and hub moments at 45 knots i_N = 85° and 500 RPM.

The minimum blade loads were obtained with cyclic values of A_1 = -5.03°, B_1 = 1.41° and at these cyclics the trim in plane forces were:

$$C_N = +.0023 \qquad C_{SF} = -0.002$$

These values are consistent for each of the repeat values taken. The trim yaw moment is slightly different for various repeat points and lies in the range $-.00027 \leq C_{YAW} \leq .0004$.

The resolver and the tunnel balance data show consistently different trim moments ($C_{M_{TRIM}} = -0.0003$, from balance; $C_{M_{TRIM}} = +0.0005$, from resolver).

The force and moment derivatives have been computed from the test data and are given next to the appropriate graph:

$\partial C_N/\partial B_1 = -0.00054/°$ $\quad -\partial C_N/\partial A_1 = +0.00087/°$

$\partial C_{SF}/\partial B_1 = 0.00066/°$ $\quad \partial C_{SF}/\partial A_1 = +0.0004/°$

(Figures 6.9 and 6.10)

The effect of B_1 on normal force has increased compared with hover ($\partial C_N/\partial B_{1_{HOVER}} = -.000485$) by 11.1%. The normal force due to A_1 cyclic increased more rapidly ($\partial C_N/\partial A_{1_{HOVER}} = +.00063$) by 13.8%. The side force due to B_1 also increased from 0.00054 in hover to 0.00066 at 45 knots 85°. Side force due to A_1 decreased from 0.000592/° in hover to 0.0004/°. The difference in RPM and thrust is partly responsible for these differences. The values of in plane force derivatives due to A_1 cyclic were obtained ignoring the slashed symbol data points which indicate a tunnel balance foul warning. The foul warning system is an electrical system and in some instances gives a foul warning due to an electrical problem. For this reason all the data are shown but points are identified where potential fouls exist. In this case the foul was probably real; see normal force data, Figure 6.10.

The in plane forces result mostly from thrust vector tilt in the early part of transition. The effect of collective pitch variation on the in plane forces is shown in Figure 6.11. The cyclic pitch settings are those for minimum blade loads at

8.9° θ_{75}. At 10.7° and 11.3° θ_{75} the foul warning was on and the normal force data again indicate a foul. These points were not used in establishing the sensitivities of in plane force to collective pitch:

$$\partial C_N/\partial \theta_{75} = 0.00035/°$$

$$\partial C_{SF}/\partial \theta_{75} = -0.000387/°$$

The hub moments due to cyclic are given in Figures 6.11 and 6.12. The yaw moment data due to B_1 cyclic from both tunnel balance and the blade load gauge resolver are identical and give a yaw derivative $\partial C_{YAW}/\partial B_1 = 0.00105/°$. The balance data for pitching moment due to B_1 give a derivative of zero $\partial C_M/\partial B_1 = 0$ whereas the resolver shows $\partial C_M/\partial B_1 = -0.00047/°$. The pitch derivative with B_1 in hover was -0.0002/° and at 76 knots 83° Figure 6.17 is -0.00043/° resolver or -0.00025/° balance which indicates the resolver value of pitch derivative from Figure 6.11 is closer to the truth.

The A_1 cyclic data of Figure 6.12 show derivatives of

$\partial C_M/\partial A_1 = 0.0012/°$ (Balance) $\quad \partial C_M/\partial A_1 = 0.00115/°$ (Resolver)

$\partial C_{YAW}/\partial A_1 = 0.00042/°$ (Balance) $\quad \partial C_{YAW}/\partial A_1 = 0.00055/°$ (Resolver)

which are reasonably consistent. These data indicate a maximum moment vector 313° after the maximum blade angle input and compares with 314° based on the B_1 data (assuming the resolver pitch derivative is correct in Figure 6.11).

The balance pitching moment is extremely sensitive to small errors in lift force on the fore and aft scales because of two effects. The distances over which the moments are transferred are large and also the lift forces measured are a small portion of the tunnel balance capability.

The effect of collective is shown in Figure 6.13 and gives derivatives

$\partial C_M / \partial \theta_{75}$ = 0.0005/° (Balance) 0.00041/° (Resolver)

$\partial C_{YAW} / \partial \theta_{75}$ = -0.000047/° (Balance) 0.000085/° (Resolver)

The effect on yaw is small but pitching moment is affected for the same reason that the blade loads of Figure 4.21 increase on either side of θ_{75} = 8.9°. The coning changes with thrust provide a longitudinal blade one per rev disturbance and gives an incremental pitching moment.

Run 22 of test 416 produced derivative data at 76 knots and a shaft incidence of 83° at 500 RPM. This condition is close to the airplane transition corridor boundary and represents vertical load factors up to about 1.8 g (see Section 7).

The normal force derivative with B_1 cyclic increased as airspeed increased from hover to 45 knots as previously shown. At 76 knots 83° the derivative is reduced to about its value in hover $\partial C_N / \partial B_1$ = -.000475/° (-0.000485 Hover). The side force derivative

increased further to $\partial C_{SF}/\partial B_1 = 0.00075/°$. Data taken from Figure 6.14.

Figure 6.15 shows the in plane forces due to A_1 cyclic at 500 RPM 83° incidence and 80 knots and give $\partial C_N/\partial A_1 = 0.00095/°$ and $\partial C_{SF}/\partial A_1 = 0.00058/°$. These data indicate an angle of 232° between the azimuth for maximum blade angle and the maximum force vector.

The values of cyclic used at this condition to minimize blade loads were $A_1 = -4.8$ and $B_1 = 2.79$. At these conditions the trim in plane forces were $C_N = 0.0035$, $C_{SF} = -0.0015$.

The collective pitch variation is given in Figure 6.16 and shows normal force and side force increasing as thrust or collective increases. $\partial C_N/\partial \theta_{75} = 0.00078/°$ and $\partial C_{SF}/\partial \theta_{75} = -0.0004/°$.

The hub moments due to B_1 cyclic at 76 knots 83° are shown in Figure 6.17. The pitch derivatives are small and negative: $\partial C_M/\partial B_1 = -0.00025/°$ (balance) and $\partial C_M/\partial B_1 = -0.00043/°$ (resolver) and are of similar magnitude to the resolver derivative at 45 knots, Figure 6.11. The yaw derivatives are not much different at 76 knots than 45 knots. At 76 knots $\partial C_{YAW}/\partial B_1 = 0.0012/°$ (balance) $0.00105/°$ (resolver).

The A_1 cyclic data are given in Figure 6.18 and indicate $\partial C_M/\partial A_1 = 0.00105/°$ (balance) and $\partial C_M/\partial A_1 = 0.00102/°$ (resolver),

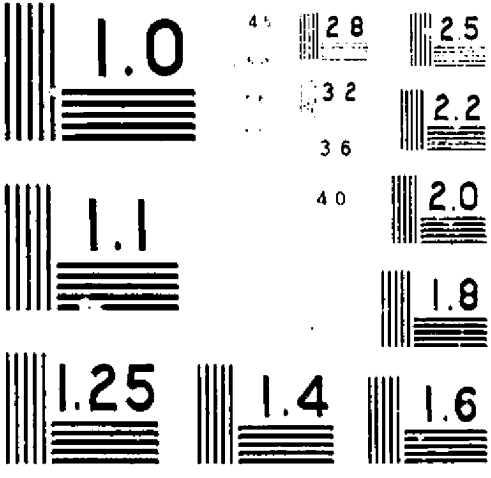

a little lower than was the case at 45 knots. The yaw derivatives with A_1 are given at $\partial C_{YAW}/\partial A_1 = 0.0004/°$ (balance) $0.0003/°$ (resolver).

The cyclic values for minimum blade loads at this flight condition were $A_1 = -4.84°$ $B_1 = 2.79°$ for a collective pitch of 9.0°. At these settings the trim yaw moment is between 0.0 and 0.0004 and pitch is estimated at 0.0003.

The resolver data from Figure 6.19 shows that collective has no effect on hub yaw at this condition. The balance data gives a negative derivative $\partial C_{YAW}/\partial \theta_{75} = -0.00095/°$. The pitch data from the balance and resolver agree and give derivatives:

$\partial C_M/\partial \theta_{75} = 0.00026/°$ (balance)

$\partial C_M/\partial \theta_{75} = 0.000285/°$ (resolver)

Run 21 was centered around a 66° incidence 80 knot test point and it was possible to operate at 550 RPM at this condition. Data was also taken at 500 RPM to provide some measure of RPM effect on the higher incidence data.

Figures 6.20 and 6.21 show the effect of cyclic pitch on in plane forces at 66°, 80 knots, 550 RPM and give the derivatives:

$\partial C_N/\partial B_1 = -0.00046/°$

$\partial C_{SF}/\partial B_1 = 0.00025/°$

$\partial C_N/\partial A_1 = 0.00013/°$

$\partial C_{SF}/\partial A_1 = 0.0004/°$

The B_1 derivatives give an angle of 261.5° between the maximum blade angle input and the maximum force vector. The A_1 data indicates 272°.

The angle between maximum cyclic blade angle input and the force vector has increased from the hover value of 242°.

The trim forces at cyclic pitch for minimum blade loads are $C_N = 0.0045$, $C_{SF} = 0$ ($A_1 = -2.84$, $B_1 = 2.16$).

The effect of collective pitch on in plane forces at this flight condition is shown in Figure 6.22. The side force gives -0.000165/° $\partial C_{SF}/\partial \vartheta_{75}$. The normal force, previously linear with ϑ_{75}, displays non-linearity. At the trim collective pitch of 9.55° and lower the derivative $\partial C_N/\partial \vartheta_{75} = 0$. As collective increases, the normal force increases until at $\vartheta_{75} = 12.5°$ the slope is $\partial C_N/\partial \vartheta_{75} = 0.0016/°$.

The balance data and the resolver moments show consistent moment derivatives with cyclic pitch in Figures 6.23 and 6.24 (80 knots, 66°, 550 RPM):

$\partial C_M/\partial B_1$ = -0.00038/° (Balance)	-0.0004/° (Resolver)
$\partial C_{YAW}/\partial B_1$ = 0.00123/° (Balance)	0.00104/° (Resolver)
$\partial C_M/\partial A_1$ = 0.00115/° (Balance	0.001/° (Resolver)
$\partial C_{YAW}/\partial A_1$ = 0.00031/° (Balance)	0.0004/° (Resolver)

These derivatives give a maximum moment vector 307.2° after the maximum blade angle input based on the B_1 balance data. The corresponding angles for the other derivative pairs are:

305.1° A_1 balance data

311° B_1 resolver data

312° A_1 resolver data

This orientation of the moment vector has increased slightly from 300.3° in hover.

The resolver data indicate trim hub moments close to zero.

The hub moment data with collective pitch, Figure 6.25, does not show the non-linearity that was observed in the normal force. The variations are linear and give the derivatives:-

$\partial C_M/\partial \theta_{75}$ = 0.00058/° (Balance) 0.00055/° (Resolver)

$\partial C_{YAW}/\partial \theta_{75}$ = -0.000285/° (Balance) 0.000235/° (Resolver)

The data taken on Run 20 was at 80 knots and 66° incidence also, but at 500 RPM. The in plane force data with A_1 cyclic, Figure 6.26, gives the derivatives:

$\partial C_N/\partial A_1$ = 0.000107/° and $\partial C_{SF}/\partial A_1$ = 0.00026/°

compared with the data at 550 RPM from Run 21 $\partial C_N/\partial A_1$ = 0.00013/° $\partial C_{SF}/\partial A_1$ = 0.0004/°. The B_1 cyclic in plane force data, Figure 6.27, was taken with a foul warning on and the normal force data indicates a real mechanical foul.

The collective pitch sweep at 500 RPM, Figure 6.28, shows similar

normal force behavior as observed at 550 RPM in Figure 6.22. The side force data are linear and give a derivative

$$\partial C_{SF}/\partial \Theta_{75} = -0.000135/°$$

The hub moments with A_1 cyclic at 500 RPM are given in Figure 6.29 and give the derivatives

$$\partial C_M/\partial A_1 = 0.00125/° \text{ (Resolver)} \qquad 0.00124/° \text{ (Balance)}$$

$$\partial C_{YAW}/\partial A_1 = 0.0004/° \text{ (Resolver)} \qquad 0.00035/° \text{ (Balance)}$$

The pitch derivatives are a little higher than those obtained at 550 RPM (see Figure 6.24). The yaw derivatives are essentially the same.

The B_1 cyclic data, Figure 6.30, contains balance fouls; however, the resolver data is not affected and gives the derivatives:

$$\partial C_M/\partial B_1 = -0\ 00048/° \text{ (Resolver)}$$

$$\partial C_{YAW}/\partial B_1 = 0.0011/° \text{ (Resolver)}$$

The yaw derivative is close to that measured at 551 RPM, Figure 6.23, and the pitch moment derivative is a little more negative.

The hub moment derivatives with collective pitch at 500 RPM, Figure 6.31, are all higher than those obtained at 550, Figure 6.26:

$$\partial C_M/\partial \Theta_{75} = 0.00064/° \text{ (Balance)} \qquad 0.00062/° \text{ (Resolver)}$$

$$\partial C_{YAW}/\partial \Theta_{75} = -0.0003/° \text{ (Balance)} \qquad -0.00023/° \text{ (Resolver)}$$

Data in the incidence range from 35° to 55° could not be obtained because of minimal blade tip - tunnel roof clearance. The next point in the transition corridor to be examined was at 27° i_N, 551 RPM and 105 knots. The in plane force data due to cyclic pitch at this condition is given in Figures 6-32 and 6-33 and indicates the derivatives:

$$\partial C_N/\partial B_1 = -0.00136/° \qquad \partial C_{SF}/\partial B_1 = 0.0$$

$$\partial C_N/\partial A_1 = 0.00024/° \qquad \partial C_{SF}/\partial A_1 = 0.00158/°$$

The B_1 data give a force vector 290° of azimuth after the maximum blade angle input. The A_1 force vector is a little larger than the B_1 data shows and lies 281.4° after the maximum blade angle input.

The effect of collective pitch on in plane forces is shown in Figure 6-34. Much of this data has balance fouling problems and is of questionable value. The incidence sweep data, Figure 6-35, have similar problems though the side force data appear to be consistent.

The hub moment data due to cyclic at 105 knots 27° i_N are given in Figures 6-36 and 6-37. The moment derivatives with B_1 cyclic are

$\partial C_M/\partial B_1$ = -.00063/°(balance) -.0007/°(resolver)

$\partial C_{YAW}/\partial B_1$ = .00134/°(balance) .00123/°(resolver)

The moment vector lies 315.4° (balance) 319.6° (resolver) after the maximum blade angle input.

The A_1 derivatives are from Figure 6-37

$\partial C_M/\partial A_1$ = .00145/° (balance) .00140/°(resolver)

$\partial C_{YAW}/\partial A_1$ = .00033/° (balance) .00042/°(resolver)

The angle between the maximum blade angle input and the moment vector is 302.8° (balance) and 306.7° (resolver). These orientations are substantially the same as those measured at earlier transition points.

The hub moment data are given in Figure 3-38. The resolver data should be unaffected by fouls. The pitch data show more data scatter than previously observed.

The incidence sweep at 105 knots 551 RPM gave moment data shown in Figure 6-39. The balance pitch moments are obviously heavily influenced by fouling. The balance yaw data however agree closely with the resolver yaw data and indicate $\partial C_{YAW}/\partial i_N$ = -0.00011/°. The resolver pitch derivative is $\partial C_M/\partial i_N$ = .00014/°. Since a change in angle of attack essentially provides a one per rev variation in blade angle of attack about the 90°-270° axis it can be deduced that the moment vector lies 321.8° after the maximum excitation. This angle is a little higher than has been deduced from the cyclic data.

Testing was done at 140 knots at 27° i_N with a 551 RPM. This point is beyond the anticipated transition corridor limit. The in plane force data shown in Figure 6-40 due to B_1 cyclic appear to be consistent though the fouls indicated severely effect the pitch data (Figure 6-43). The side force derivative with B_1 is again zero and the normal force derivative is negative and large -0.00467/°. In view of the fact that this is much larger than the resultant due to A_1 cyclic (Figure 6-41) the in plane force data at this condition is considered untrustworthy.

The in plane force data from the incidence sweep contains two data points where no foul was indicated. These two points provide the derivatives $\partial C_N/\partial i_N$ = 0.00075/° and $\partial C_{SF}/\partial i_N$ = .00028/°.

The balance fouling problem does not appear to affect the yaw data; both balance and resolver yaw derivatives with B_1 cyclic are the same, Figure 6-43. $\partial C_{YAW}/\partial B_1 = 0.00152/°$. The resolver pitch derivative is -0.00008/°. The A_1 cyclic data yield the following derivatives:

$\partial C_M/\partial A_1 = .0013/°$ (balance) .00104/° (resolver)

$\partial C_{YAW}/\partial A_1 = .00048/°$ (balance) .0006/° (resolver)

The B_1 data shows a moment vector which lags the maximum blade angle input by 293.2° of azimuth. This is somewhat lower than the azimuthal lag indicated by the A_1 cyclic data 310.3° (balance derivatives) 320° (resolver).

The derivatives of hub moments with incidence about the 140 knot 27° i_N 551 RPM condition are shown in Figure 6-45:

$\partial C_M/\partial i_N = .00025/°$ (balance) .000248/° (resolver)

$\partial C_{YAW}/\partial i_N = -.00025/°$ (balance) -.000185/° (resolver)

These data show a moment vector azimuthal lag of 315° (balance) and 324.4° (resolver).

The data obtained at 140 knots and 10° i_N was taken at 386 RPM since in this area of transition the RPM change from 551 to normal cruise RPM will be made on the aircraft.

The in plane forces due to cyclic pitch are plotted in Figures 6-46 and 6-47:

$\partial C_N/\partial B_1 = -.00456/°$ $\partial C_N/\partial A_1 = .00245/°$

$\partial C_{SF}/\partial B_1 = .00263/°$ $\partial C_{SF}/\partial A_1 = .00524/°$

The magnitudes are larger than previously observed but this is primarily due to the nondimensionalizing parameter ($\rho \Omega^2 D^4$) dependence on RPM squared. The force vector lags the maximum blade angle input by 260° (B_1 data) 265° (A_1 data), about the same magnitude as observed in mid transition but larger than the 243.4° obtained in hover.

The in plane forces observed during the collective sweep at this test condition are shown in Figure 6-48 and give $\partial C_N/\partial \theta_{75}$ = 0.00101/° and $\partial C_{SF}/\partial \theta_{75}$ = 0.00053/°. The effect of changing incidence is shown in Figure 6-49. The incidence derivatives are

$$\partial C_N/\partial i_N = .00233/° \text{ and } \partial C_{SF}/\partial i_N = .00049/°.$$

This force vector lies 281.9° after the azimuth for maximum blade angle forcing (= 90° in this case).

The moment data due to cyclic pitch at 140 knots 10° i_N and 386 RPM are plotted in Figures 6-50 and 6-51. The derivatives obtained from these cyclic sweeps are:

$\partial C_M/\partial B_1$ = .0008/° (balance)	0.00065/° (resolver)
$\partial C_{YAW}/\partial B_1$ = .00201/° (balance)	0.00185/° (resolver)
$\partial C_M/\partial A_1$ = .00195/° (balance)	0.00197/° (resolver)
$\partial C_{YAW}/\partial A_1$ = -.00088/° (balance)	-0.00073/° (resolver)

The resultant moment vector lags the maximum cyclic blade angle input by:

268.6° (B_1, balance data)

270.6° (B_1, resolver data)

265.7° (A_1, balance data)

269.7° (A_1, resolver data)

These values are lower than previously observed at 551 RPM in transition and are primarily due to the RPM change.

The collective sweep at this condition gave the hub moments plotted in Figure 6-52:

$\partial C_M/\partial \theta_{75}$ = 0.00105/° (balance) 0.00073/° (resolver)

$\partial C_{YAW}/\partial \theta_{75}$ = -.00051/° (balance) -0.00051/° (resolver)

The hub moment data with incidence (Figure 6-53) show approximately zero moment at 10° incidence with A_1 = -2.62° and B_1 = 2.31°. The derivatives are:

$\partial C_M/\partial i_N$ = .00028/° (balance) 0.00036/° (resolver)

$\partial C_{YAW}/\partial i_N$ = -.00068/° (balance) -0.00088/° (resolver)

The maximum blade angle due to incidence change is at ψ = 90° (neglecting the effects of flapping) and results in a moment vector 290.4° of azimuth later. This moment lag is greater than that measured using cyclic pitch excitation and implies that the radial distributional differences between incidence changes and cyclic control inputs significantly affect the influence of the lag blade mode on out of plane flapping. For a single degree of freedom system the response lag would be independent of these differences.

Similar testing was performed at 170 knots $i_N = 10°$ and 386 RPM. Unfortunately balance fouling problems invalidate some of the information. The normal force due to cyclic pitch, Figures 6-54 and 6-55, are severely affected and cannot be used. The side force data seem to be consistent and give the derivatives:

$$\partial C_{SF}/\partial A_1 = .00565/° \text{ and } \partial C_{SF}/\partial B_1 = .0052/°$$

which are not much different from those measured at 140 knots at this incidence. This data however should be used with caution. Similar comments apply to the in plane force data due to collective and incidence sweeps shown in Figures 6-56 and 6-57.

The hub moments from the resolver are not affected by balance fouls and yield valid data. The balance yaw appears to remain consistent but pitch is of no value

$$\partial C_M/\partial B_1 = .0011/^{o}\text{(resolver)}$$

$$\partial C_{YAW}/\partial B_1 = .0018/^{o}\text{(resolver)} \qquad .0016/^{o}\text{(balance)}$$

from Figure 6-58. The A_1 derivatives are from Figure 6-59

$$\partial C_M/\partial A_1 = .00225/° \text{ (resolver)}$$

$$\partial C_{YAW}/\partial A_1 = -.00085/° \text{ (resolver)} \qquad -.00090/° \text{ (balance)}$$

The resultant moment vectors lie 258.6° (B_1 data) and 269.3° (A_1 data) after the maximum blade angle input. The effects of collective pitch and incidence at this condition are shown in Figures 6-60 and 6-61 and indicate

$$\partial C_M/\partial \theta_{75} = .0003/° \text{ (resolver)}$$

$$\partial C_{YAW}/\partial \theta_{75} = -.0002/° \text{ (resolver)} \qquad -.0004/° \text{ (balance)}$$

$\partial C_M/\partial i_N$ = .00025/° (resolver)

$\partial C_{YAW}/\partial i_N$ = -.001/° (resolver) -.00075/° (balance)

The resolver system used on test 416 has proved itself to be a usefull means of establishing hub moments and should be considered as a part of the flight test instrumentation.

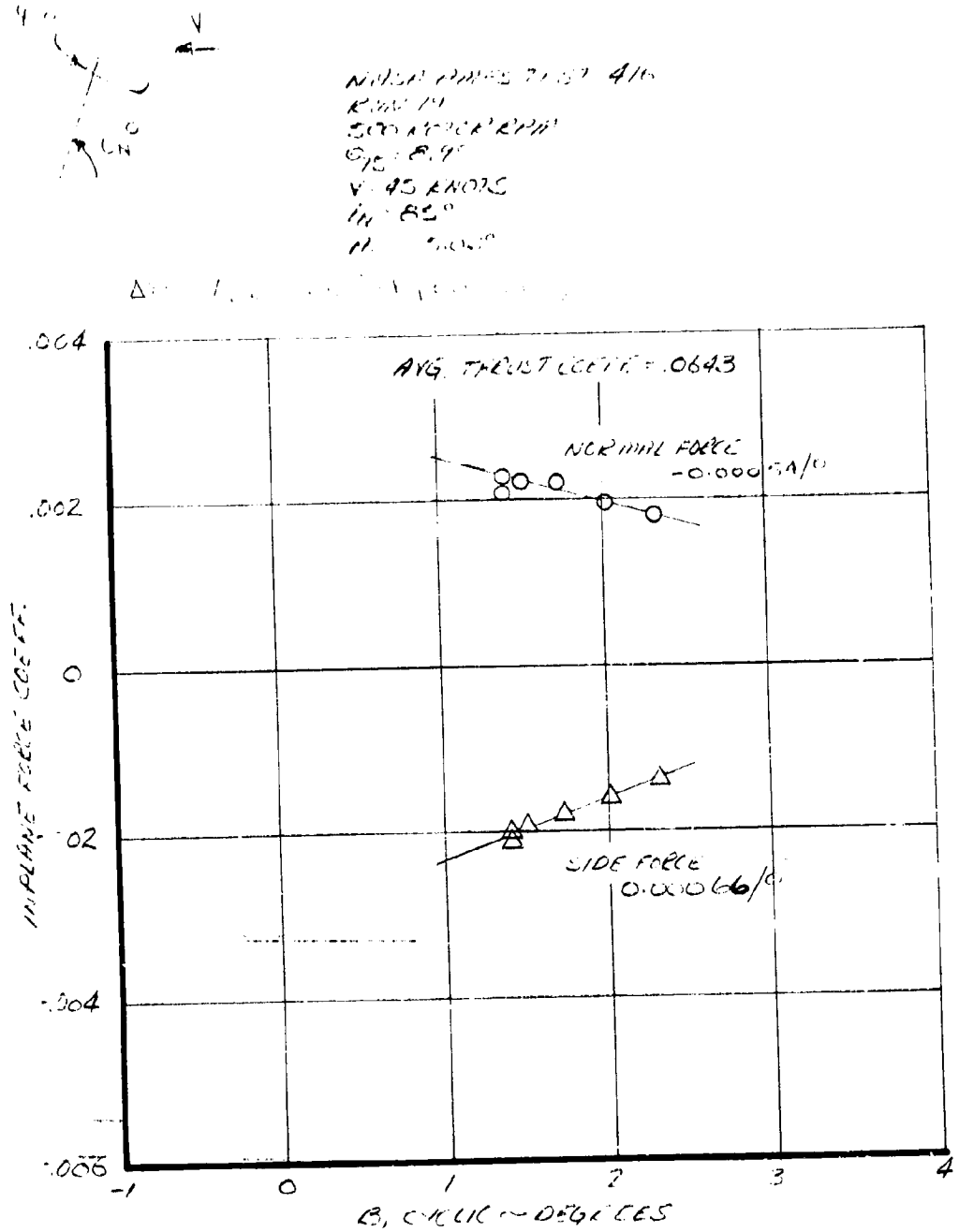

FIG. 6.8 [illegible] OF LONGITUDINAL CY[illegible] OF IN-PLANE FORCES 300 RPM - 45 KTS $\zeta_N = 85°$

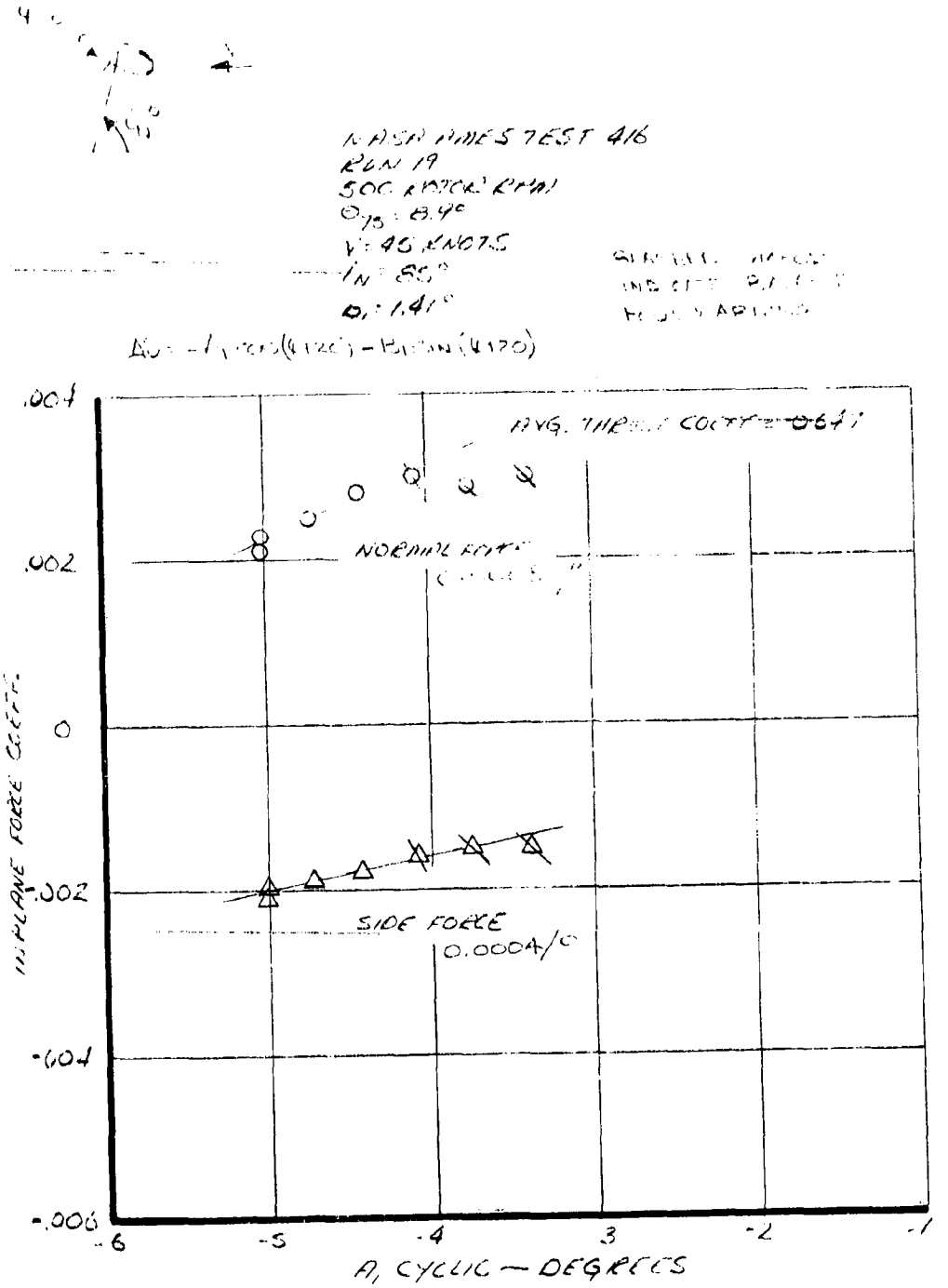

FIGURE 6.9 . EFFECT OF LATERAL CYCLIC PITCH ON ROTOR FORCES 5000 FPM 45 KTS $\gamma_N = 85°$

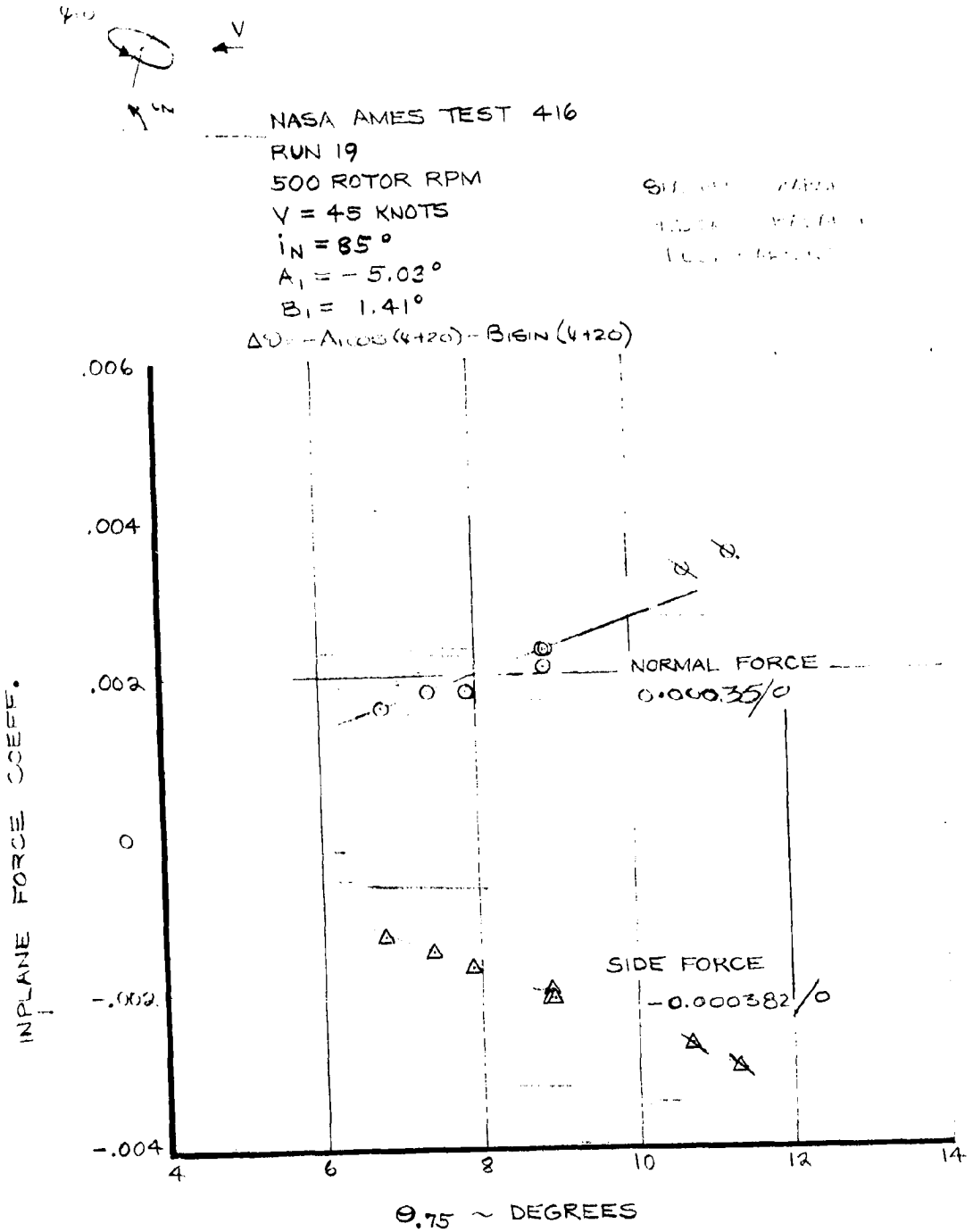

FIGURE 6.10. EFFECT OF COLLECTIVE PITCH ON IN-PLANE FORCES
500RPM 45KTS i_N = 85°

NACA AMES TEST 416
RUN 19
500 ROTOR RPM
V = 45 KNOTS
$\theta_{.75}$ = 8.9°
i_N = 85°
A_1 = -0.03°

	$\partial C_M/\partial B_1$	$-\partial C_{YAW}/\partial B_1$
BASIC	0.0	0.00105/°
RESOLVER	-0.0004 1/°	0.00105/°

$\Delta U = -A_1 \cos(\psi+120) - B_1 \sin(\psi+120)$

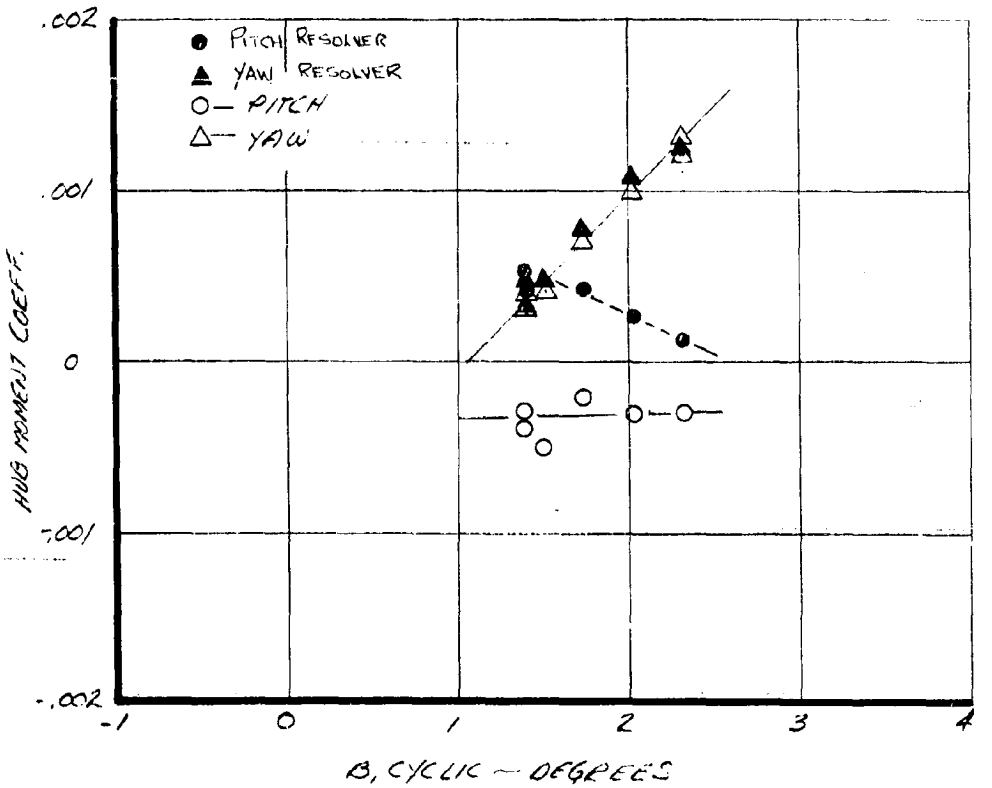

FIGURE 6.11. EFFECT OF LONGITUDINAL CYCLIC PITCH ON HUB MOMENTS 500RPM 45KTS i_N = 85°

NASA AMESTEST 4/6
RUN 19
500 ROTOR RPM
$V = 45$ KNOTS
$\theta_{.75} = 8.9°$
$i_N = 8.5°$
$\theta_1 = 1.41°$

	$\partial C_M / \partial A_1$	$\partial C_{YAW} / \partial A_1$
BARNEY	0.0012/°	0.00042/°
RESOLVER	0.00115/°	0.00055/°

$$\Delta\theta = -A_1 \cos(\psi + 120°) - B_1 \sin(\psi + 120°)$$

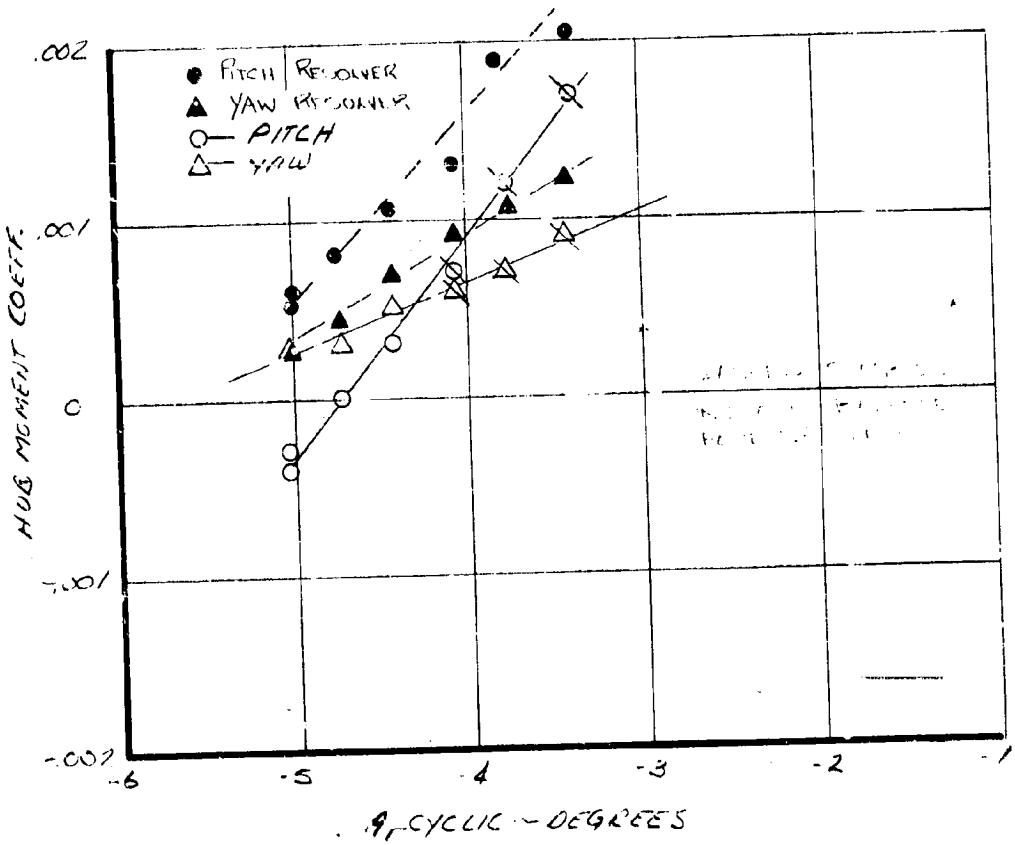

FIGURE 6.12. EFFECT OF LATERAL CYCLIC

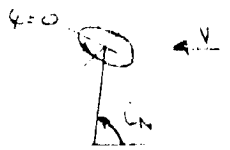

NASA AMES TEST 416
RUN 17
500 ROTOR RPM
V = 85 KNOTS
i_N = 85°
A_1 = -3.03°
B_1 = 1.41°

0·00041/° 0·00008.5/°

$$\Delta\vartheta = -A_1 \cos(\psi+20) - B_1 \sin(\psi+20)$$

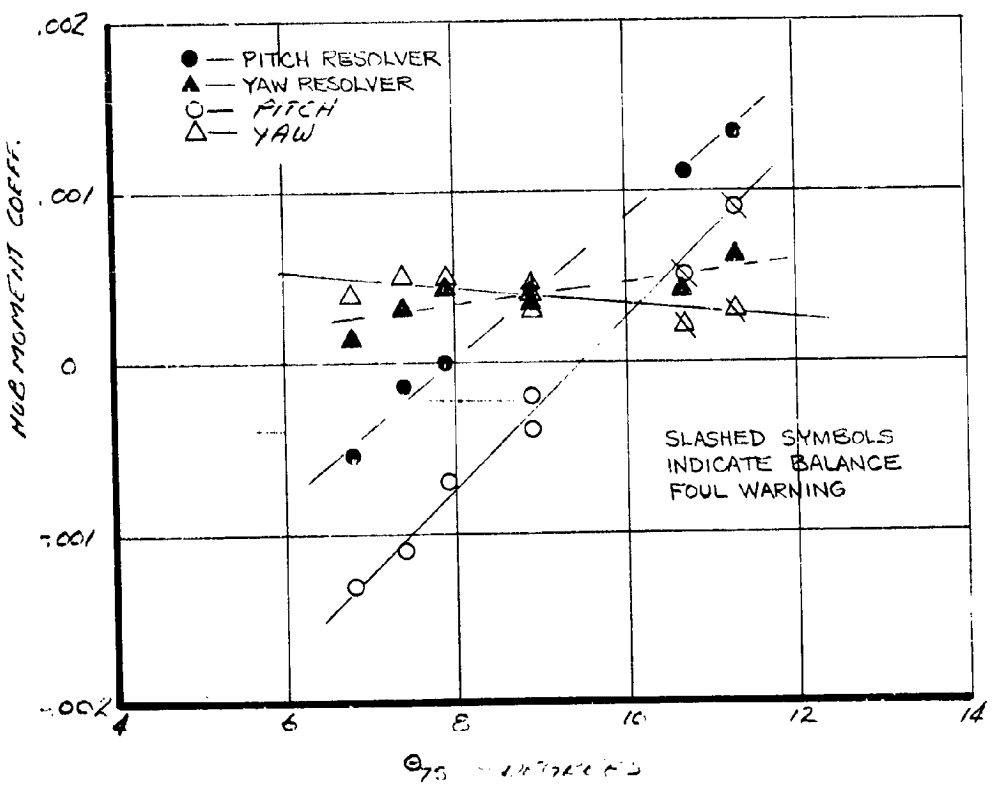

Fig. 6.13.

NASA AMES TEST 416
RUN 22
500 ROTOR RPM
$\theta_{.75} = 9.0°$
V = 76 KNOTS
$i_N = 83°$
$A_1 = -4.80°$

$\Delta\theta = -A_1 \cos(\psi + 90) - B_1 \sin(\psi + 90)$

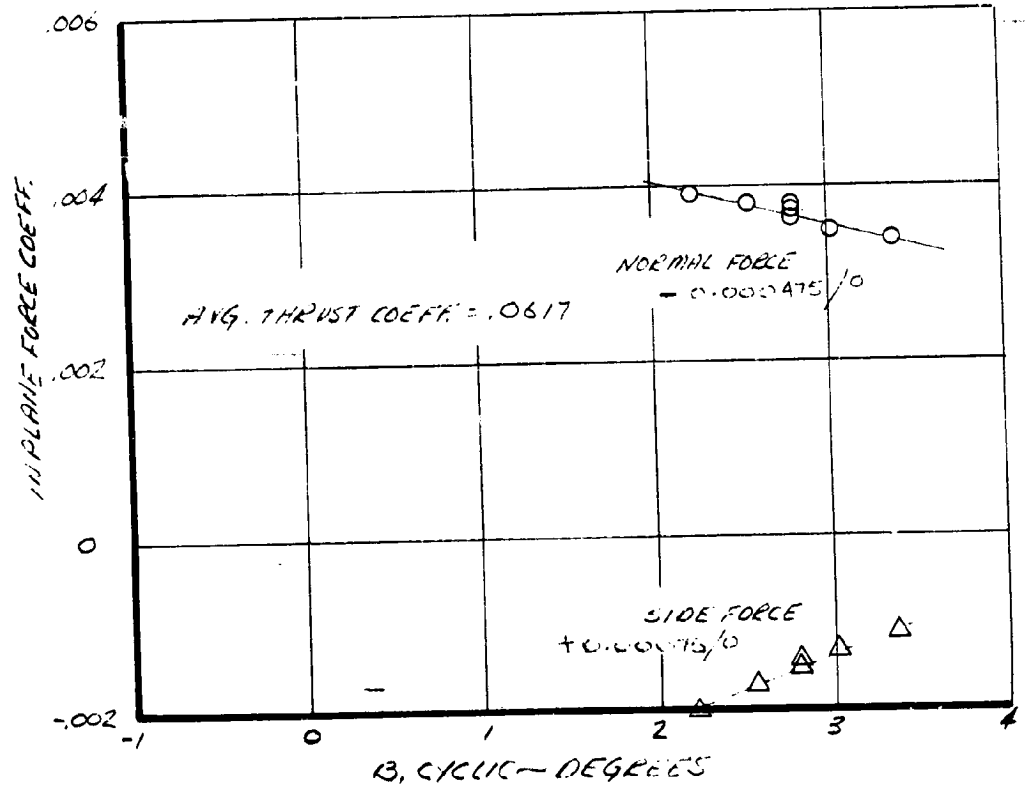

FIGURE 6.14. EFFECT OF LATERAL CYCLIC PITCH ON IN-PLANE FORCES. 500 RPM V=76 KTS $i_N = 83°$

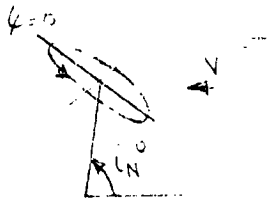

NASA AMES TEST 4/6
RUN 22
500 ROTOR RPM
$\theta_{.75} = 9.0°$
V = 76 KNOTS
$i_N = 8.3°$
$B_1 = 2.79°$

$\Delta\theta = -A_1 \cos(\psi+20) - B_1 \sin(\psi+20)$

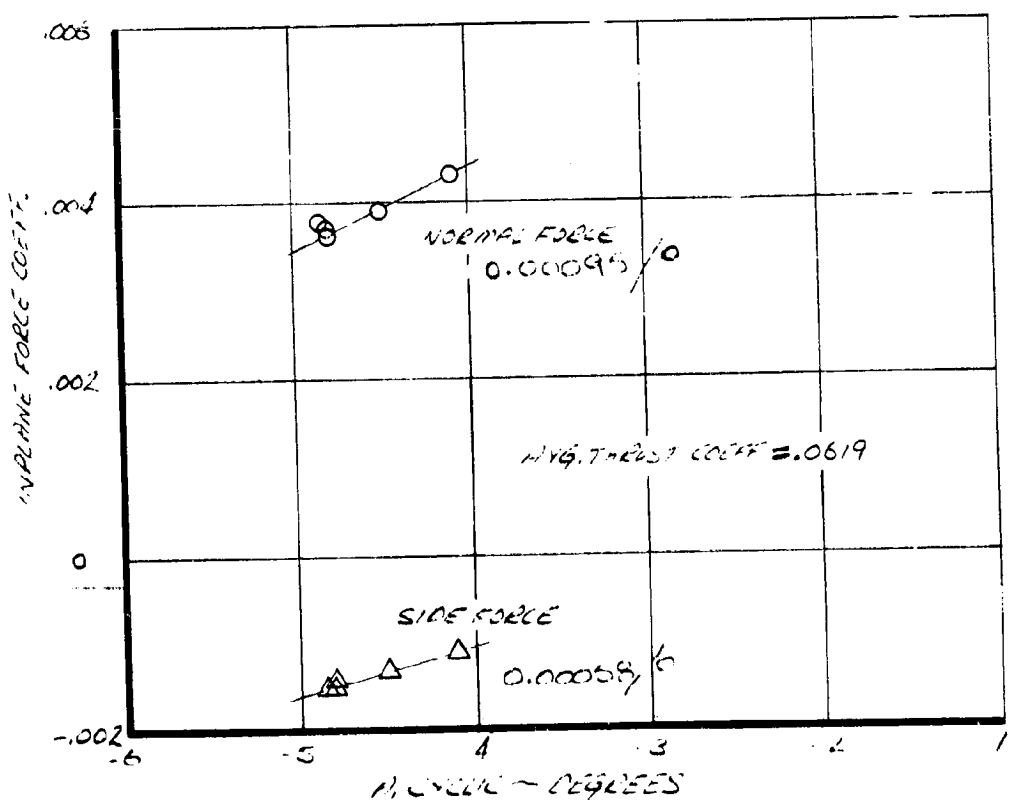

FIGURE 6.15 . EFFECT OF LATERAL CYCLIC ON IN-PLANE FORCES
500 RPM V = 76 KTS $i_N = 8.3°$

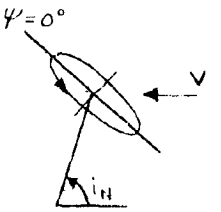

NASA AMES TEST 416
RUN 22
500 ROTOR RPM
V = 76 KNOTS
$i_N = 83°$
$A_1 = -4.84°$
$B_1 = 2.79°$

$$\Delta\theta = -A_1 \cos(\psi+20) - B_1 \sin(\psi+20)$$

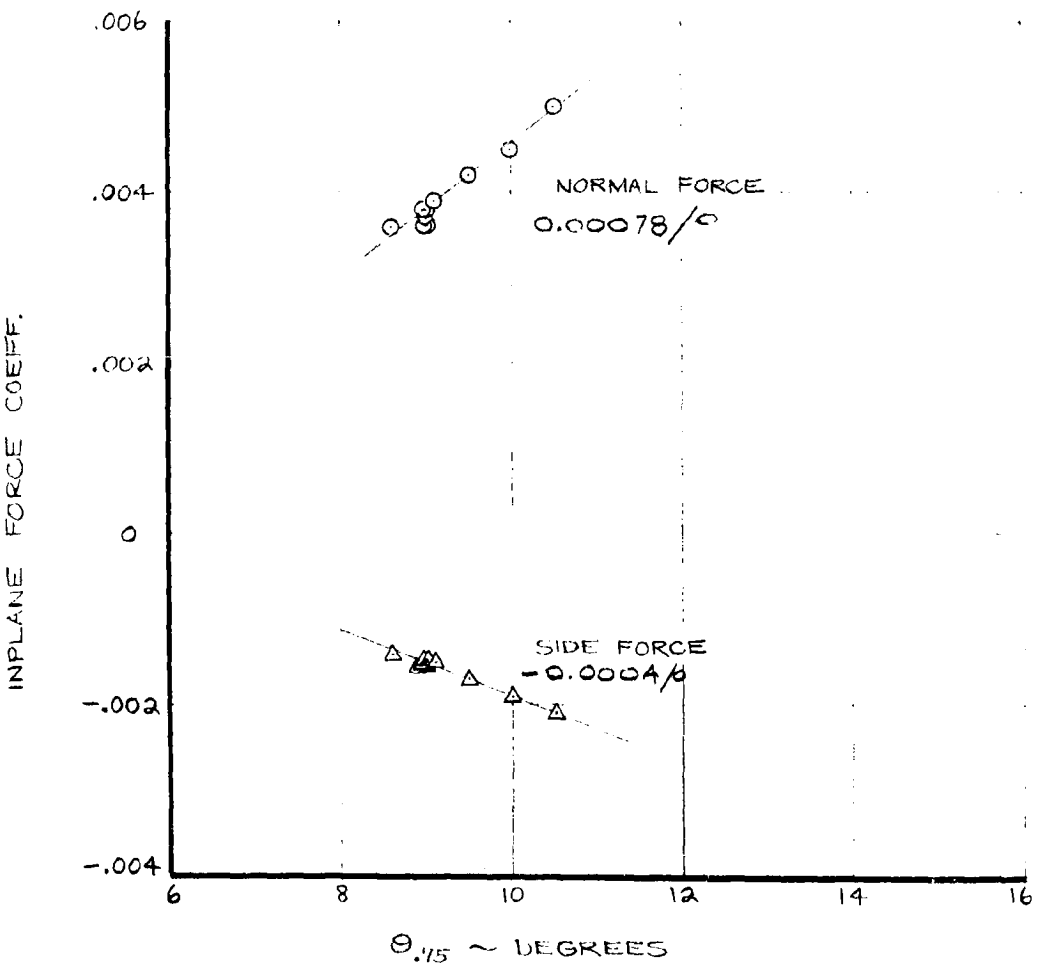

FIGURE 6.16 EFFECT OF CONTROL PITCH ON IN-PLANE FORCES
500 RPM 76 KTS $i_N = 83°$

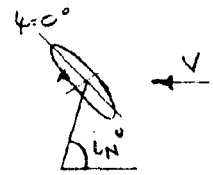

NASA AMES TEST 9/6
RUN 22
500 ROTOR RPM
V = 76 KNOTS
Θ_{75} = 9.0°
i_N = 83°
A_1 = −4.80°

	$\partial C_M/\partial B_1$	$\partial C_{YAW}/\partial B_1$
BALANCE	−0.00025/°	0.0012/°
RESOLVER	−0.00043/°	0.00105/°

$\Delta\Theta = -A_1 \cos(\psi+120) - B_1 \sin(\psi+120)$

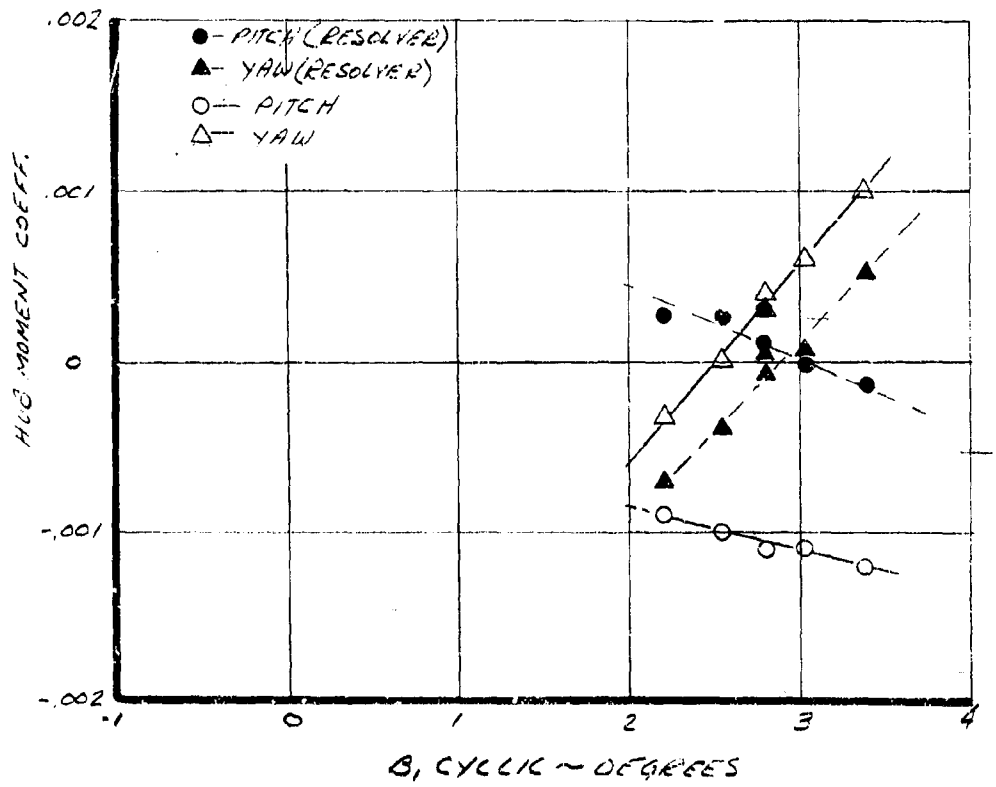

FIGURE 6-17 EFFECT OF LONGITUDINAL CYCLIC ON HUB MOMENTS
500 RPM 76 KTS i_N = 83°

NASA AMES TEST 416
RUN 22
500 ROTOR RPM
V = 76 KNOTS
$\Theta_{.75}$ 9.0°
i_N = 83°
α_s = 2.79°

	$\partial C_M/\partial A_1$	$\partial C_{YAW}/\partial A_1$
BALANCE	0.00105/°	0.0004/°
RESOLVER	0.00102/°	0.0003/°

$\Delta\Theta = -A_1 \cos(\psi+20) - B_1 \sin(\psi+20)$

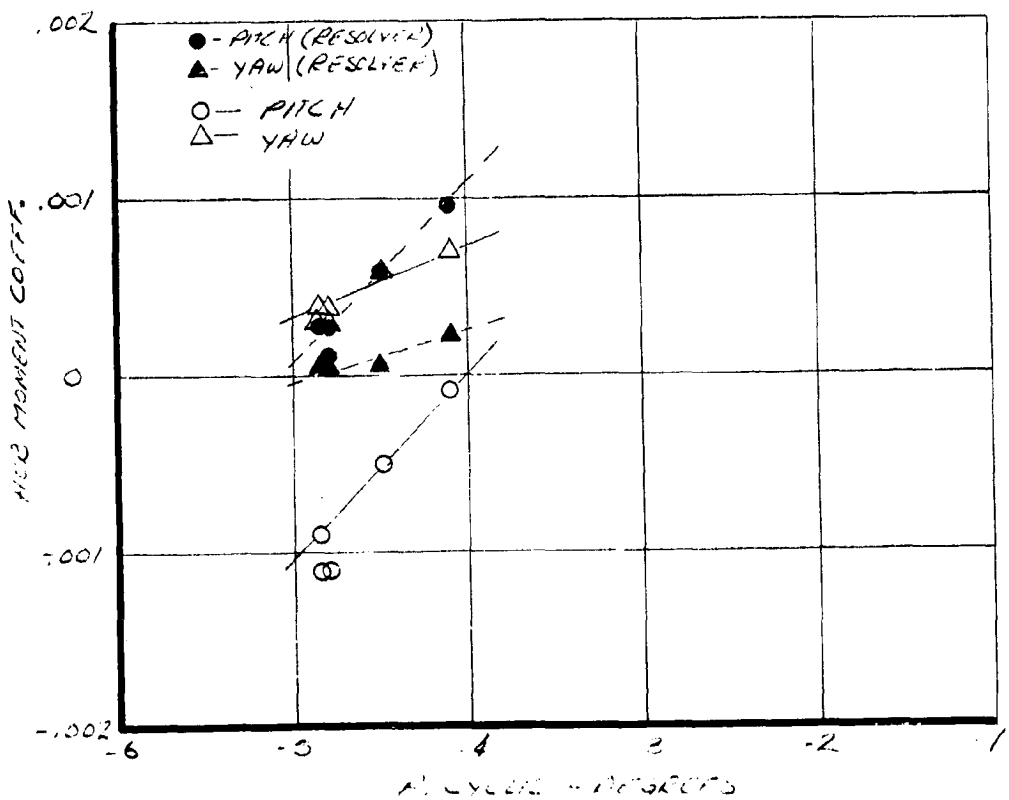

FIGURE 6.18 EFFECT OF LATERAL CYCLIC ON HUB MOMENTS
500 RPM 76 KTS i_N = 83°

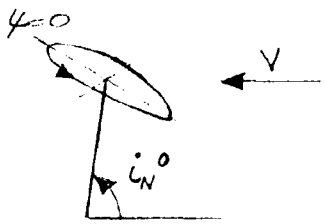

NASA AMES TEST 416
RUN 22
500 ROTOR RPM
V = 76 KNOTS
i_N = 8.3°
A_1 = −4.84°
B_1 = 2.79°

	∂CM/∂θ75	∂CYAW/∂θ75
BALANCE	0.00026/°	−0.00009.5/°
PROPELLER	0.000285/°	0.0/°

$$\Delta\theta = -A_1 \cos(\psi+20) - B_1 \sin(\psi+20)$$

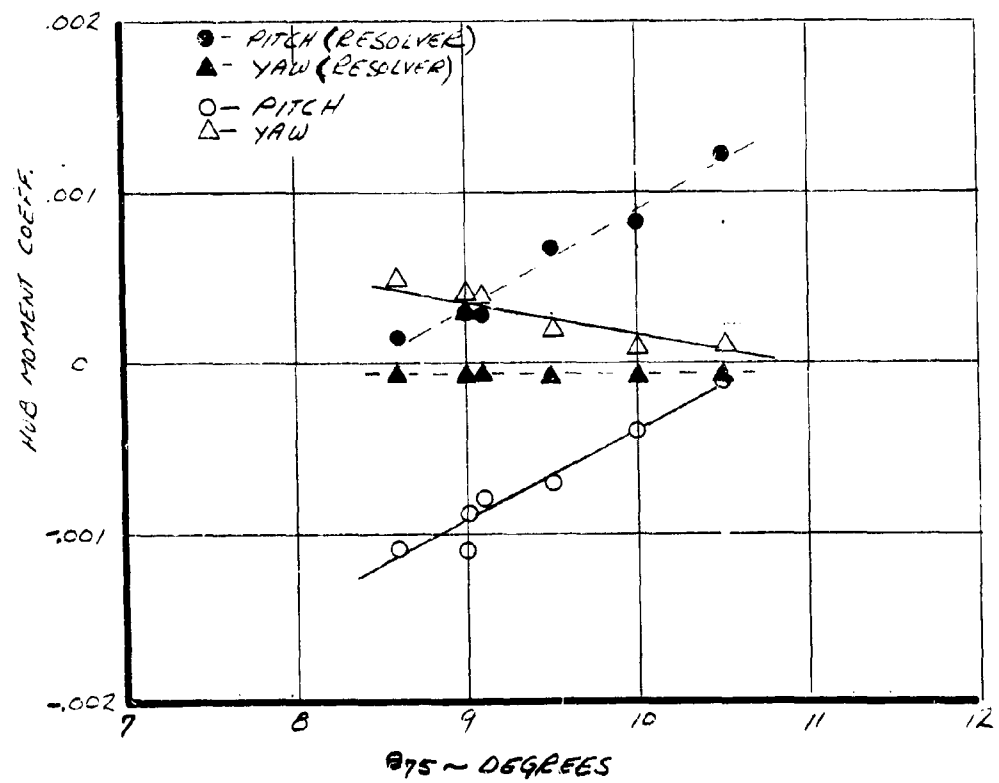

FIGURE 6.19 EFFECT OF COLLECTIVE PITCH ON HUB MOMENTS
500 RPM 76 KTS i_N = 8.3°

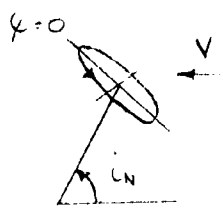

NASA AMES TEST 416
RUN 21
550 ROTOR RPM
$\theta_{.75} = 9.6°$
V = 80 KNOTS
$i_N = 66°$
$A_1 = -2.78°$

$$\Delta\theta = -A_1 \cos(\psi+120) - B_1 \sin(\psi+120)$$

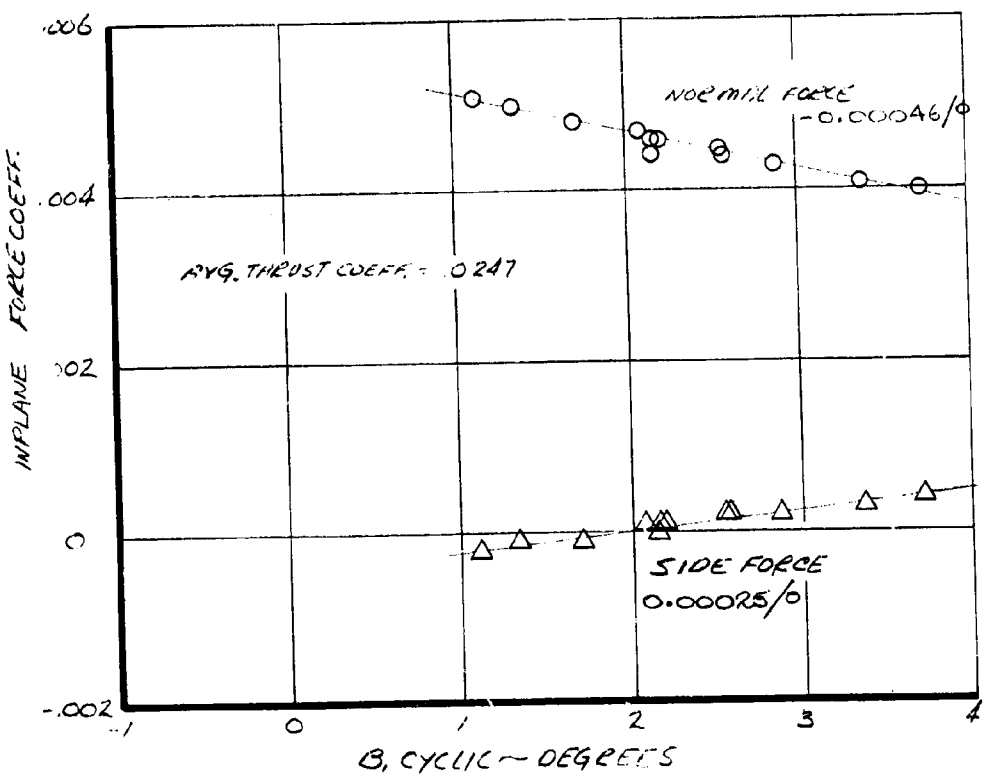

FIGURE 6.20 EFFECT OF LONGITUDINAL CYCLIC PITCH ON IN-PLANE FORCES 550 RPM 80 KTS $i_N = 66°$

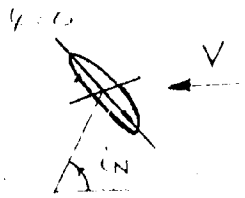

NASA AMES TEST 416
RUN 21
550 ROTOR RPM
$\Theta_{.75} = 4.6°$
V = 80 KNOTS
$i_N = 66°$
$\Theta_1 = 2.16°$

$$\Delta\Theta = -A_1 \cos(\psi+120) - B_1 \sin(\psi+120)$$

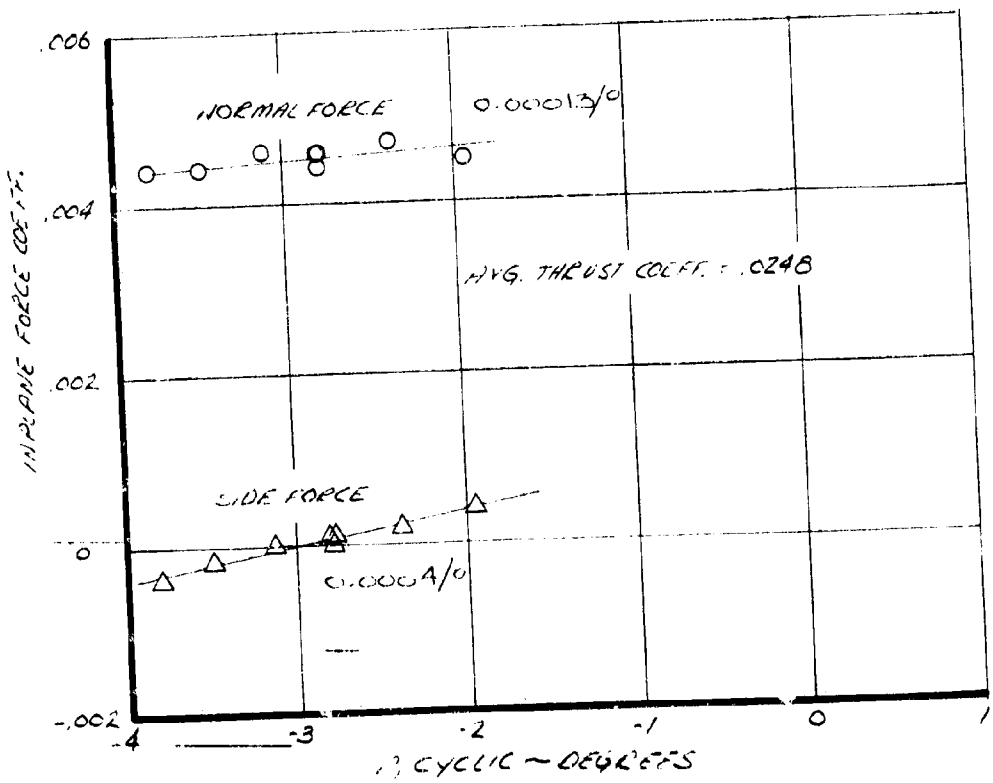

FIGURE 6.21 EFFECT OF LATERAL CYCLIC PITCH ON IN-PLANE FORCES 550 RPM 80 KTS $i_N = 66°$

NASA AMES TEST 4-16
RUN 21
550 ROTOR RPM
V = 80 KNOTS
$i_N = 66°$
$A_1 = -2.81°$
$B_1 = 2.54°$

$\Delta\theta = -A_1 \cos(\psi+20) - B_1 \sin(\psi+20)$

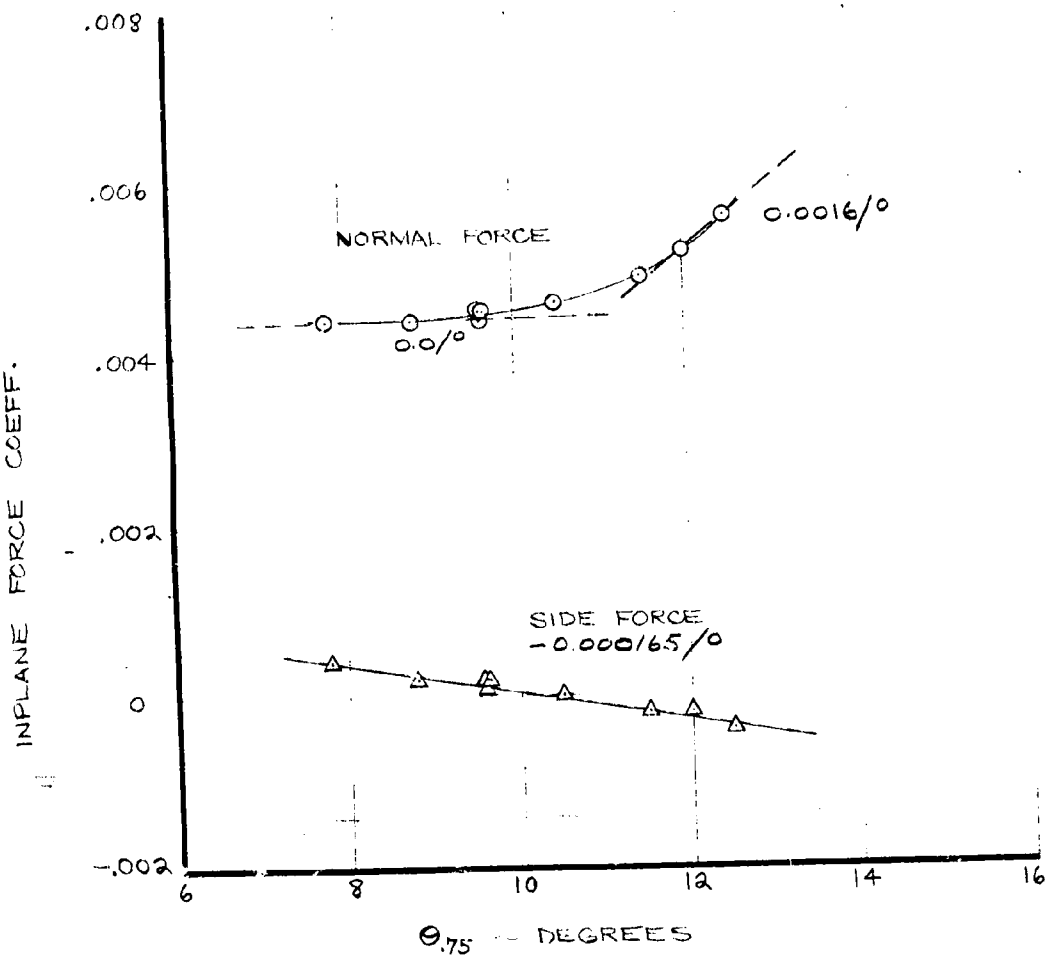

FIGURE 6.22 EFFECT OF COLLECTIVE ON IN-PLANE FORCES
550 RPM 80 KTS $i_N = 66°$

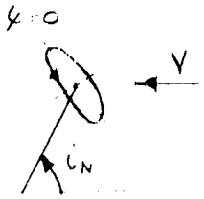

NASA AMES TEST 416
RUN 21
550 ROTOR RPM
V = 80 KNOTS
i_N = 66°
θ_{75} = 9.6°
A_1 = -2.78°

$\Delta\theta = -A_1 \cos(\psi+20) - B_1 \sin(\psi+20)$

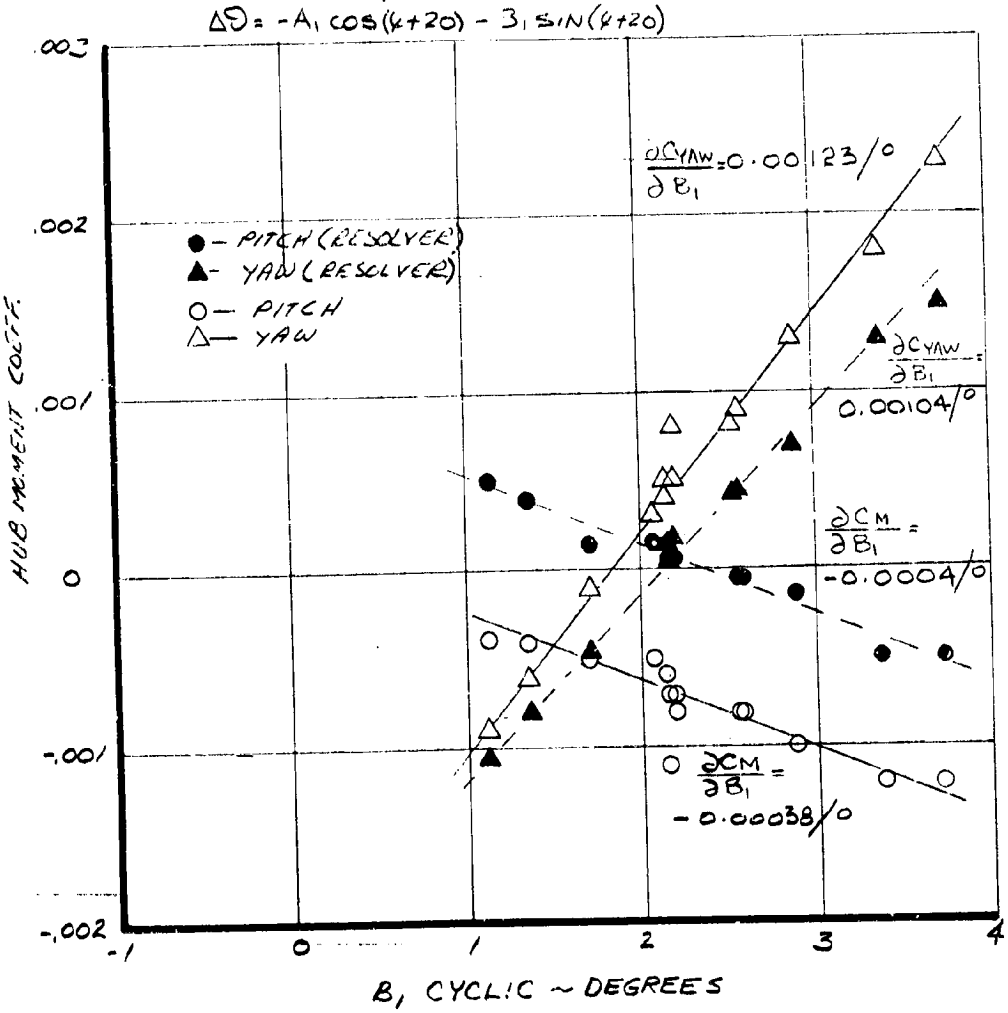

FIGURE 6.23 EFFECT OF LONGITUDINAL CYCLIC ON HUB MOMENTS
550 RPM 80 KTS i_N = 66°

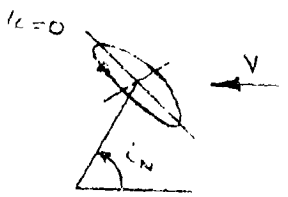

NASA AMES TEST 416
RUN 21
550 ROTOR RPM
V = 80 KNOTS
$\theta_{.75} = 9.6°$
$i_N = 66°$
$\beta_1 = 2.16°$

$\Delta\theta = -A_1 \cos(\psi+120) - B_1 \sin(\psi+120)$

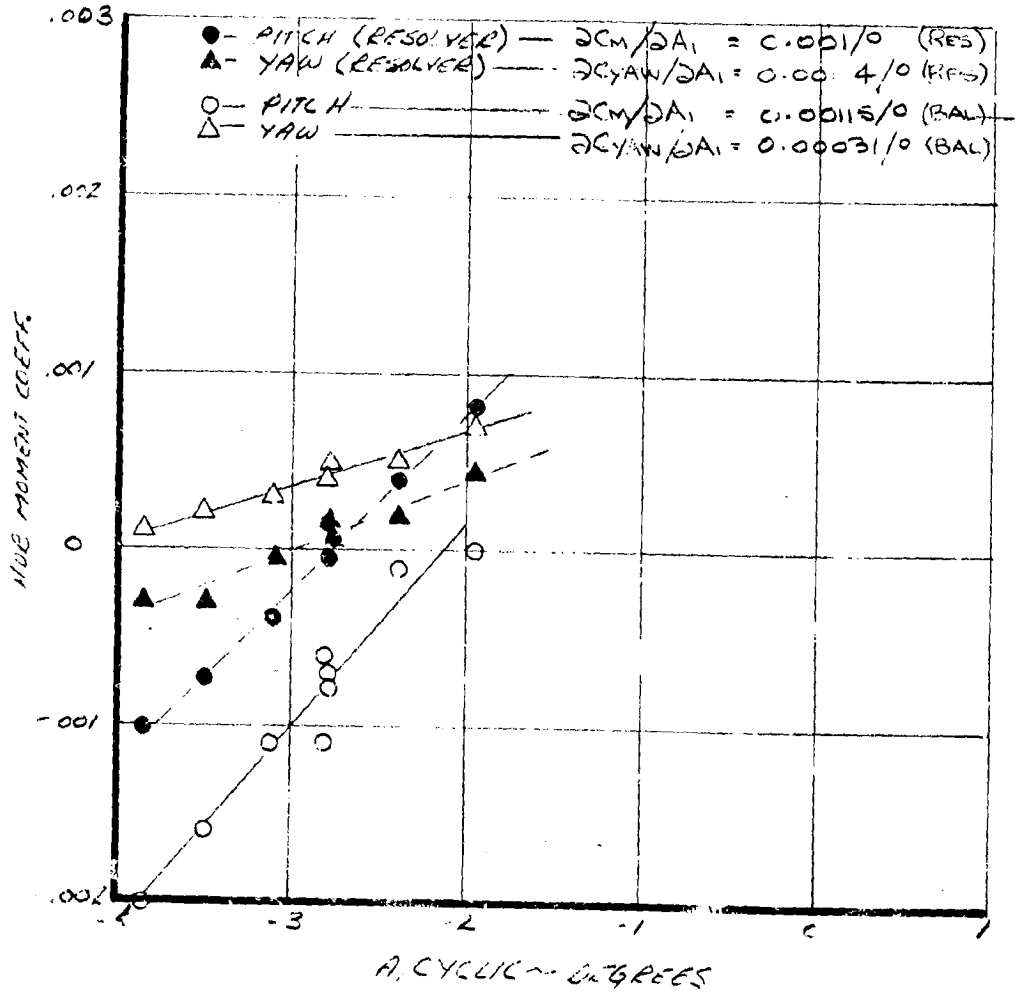

FIGURE 6.24 EFFECT OF LATERAL CYCLIC ON HUB MOMENT
550 RPM 80 KTS $i_N = 66.0°$

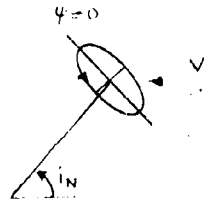

NASA AMES TEST 416
RUN 21
550 ROTOR RPM
V = 80 KNOTS
i_N = 66°
A_1 = -2.81°
B_1 = 2.54°

	$\partial C_M/\partial \theta_{.75}$	$\partial C_{YAW}/\partial \theta_{.75}$
BALANCE	0.00058/°	-0.000285/°
RESOLVER	0.00055/°	-0.000235/°

$\Delta\theta = -A_1\cos(\psi+20) - B_1\sin(\psi+20)$

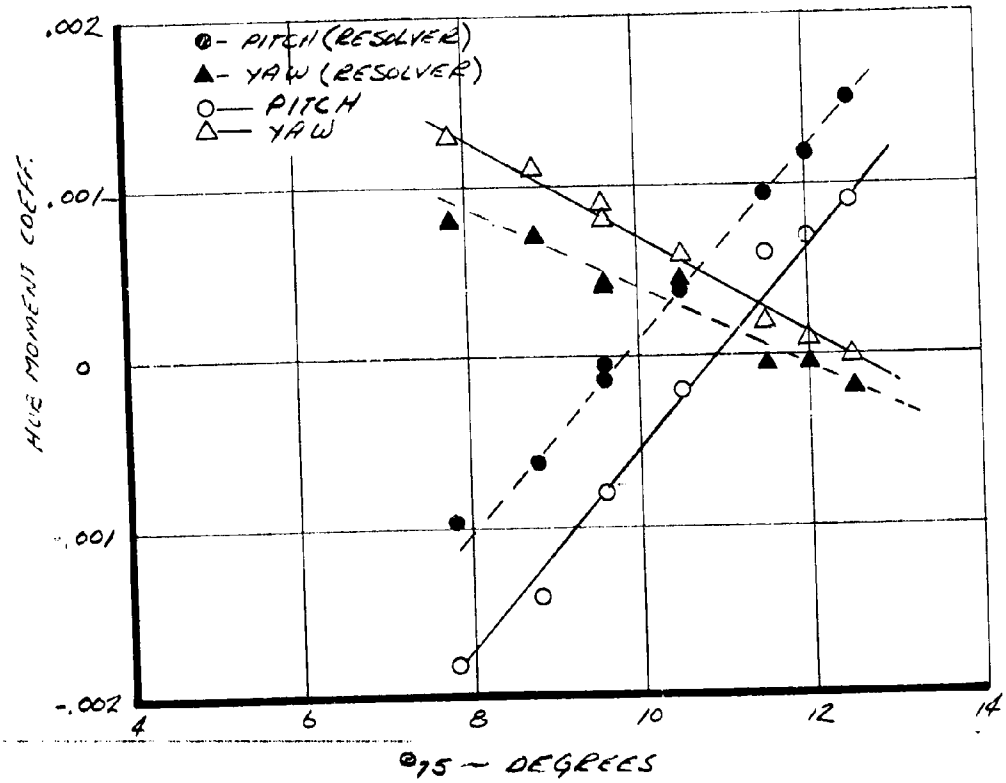

FIGURE 6.25 EFFECT OF COLLECTIVE PITCH ON HUB MOMENTS
550 RPM 80 KNOTS i_N = 66°

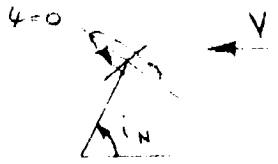

NASA AMES 7'x10' 416
RUN 20
500 ROTOR RPM
$\theta_{.75}$ = 9.8°
V = 80 KNOTS
i_N = 66°
β_1 = 2.31°

$$\Delta\theta = -A_1\cos(\psi+20) - B_1\sin(\psi+20)$$

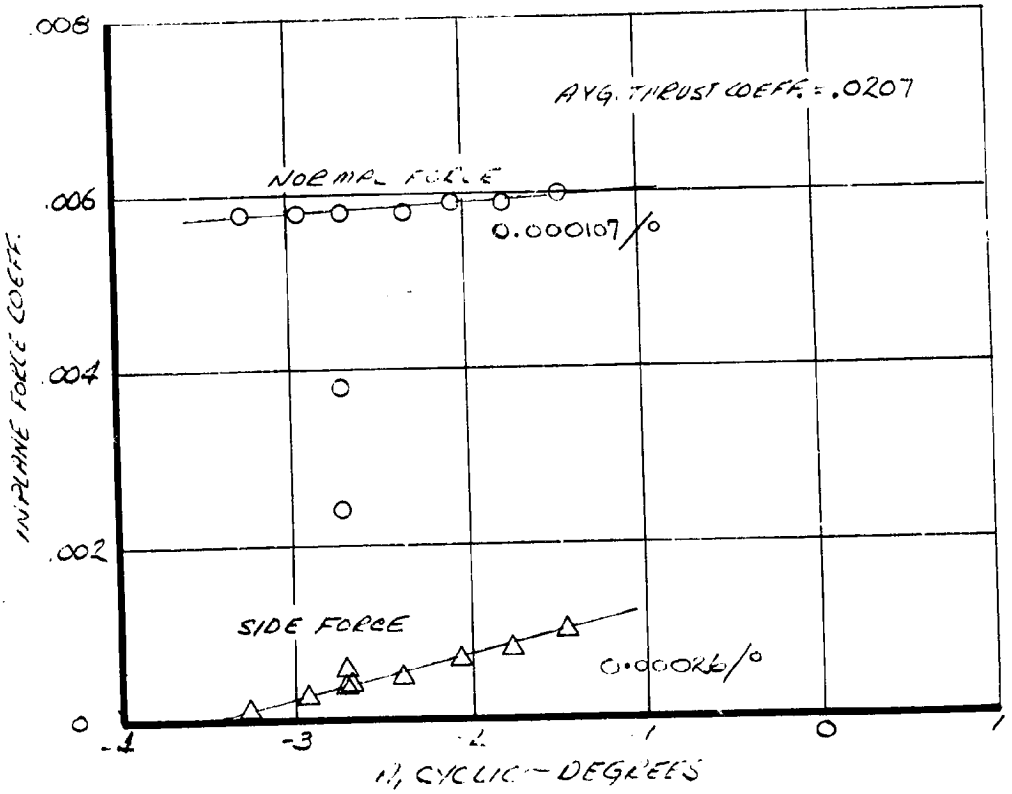

FIGURE 6.26 EFFECT OF LATERAL CYCLIC PITCH ON IN-PLANE FORCES
500 RPM 80 KTS i_N = 66°

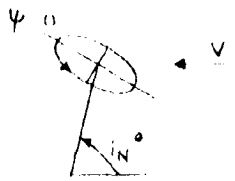

NASA AMES TEST 416
RUN 20
500 ROTOR RPM
$\theta_{.75} = 9.5°$
V = 80 KNOTS
$i_N = 66°$
$A_1 = -2.73°$

$\Delta H = -A_1 \cos(\Psi+20) - B_1 \sin(\Psi+20)$

SLASHED SYMBOLS INDICATE BALANCE FOUL WARNING

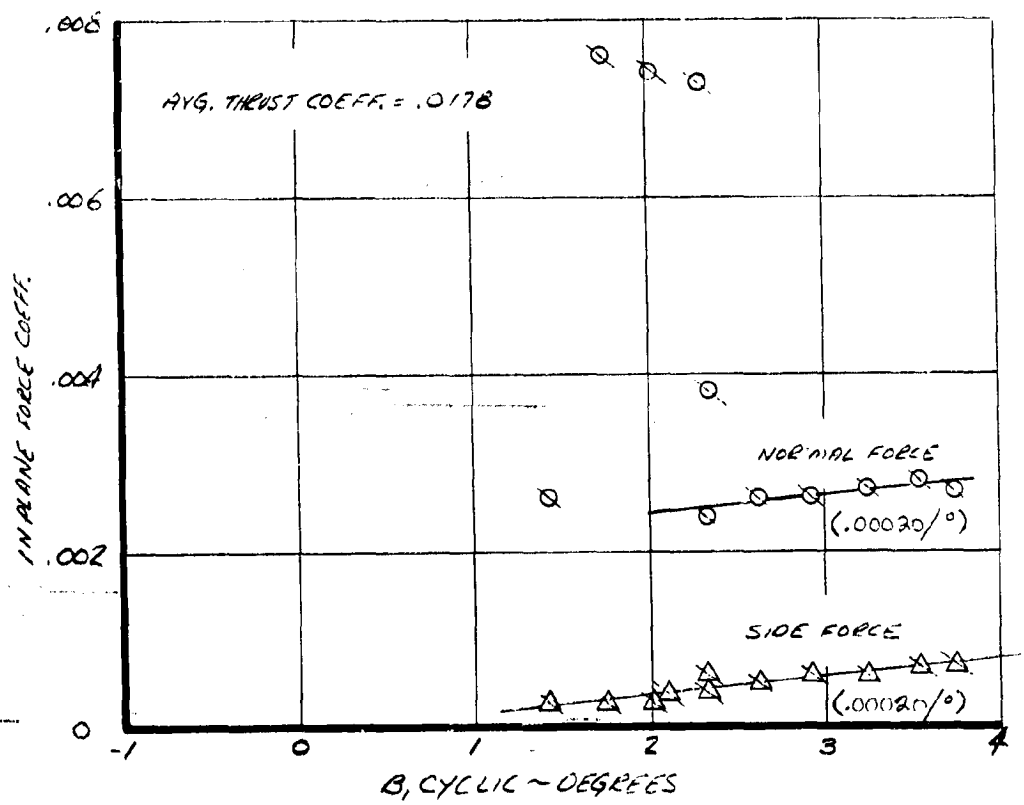

FIGURE 6.27 EFFECT OF LONGITUDINAL CYCLIC PITCH ON HUB IN PLANE FORCES 500 RPM 80 KNOTS $i_N = 66°$

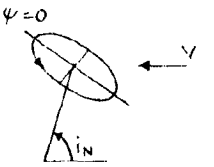

NASA AMES TEST 416
RUN 20
500 ROTOR RPM
V = 80 KNOTS
$i_N = 66°$
$A_1 = -2.73°$
$B_1 = 2.31°$

$$\Delta\theta = -A_1 \cos(\psi + 20) - B_1 \sin(\psi + 20)$$

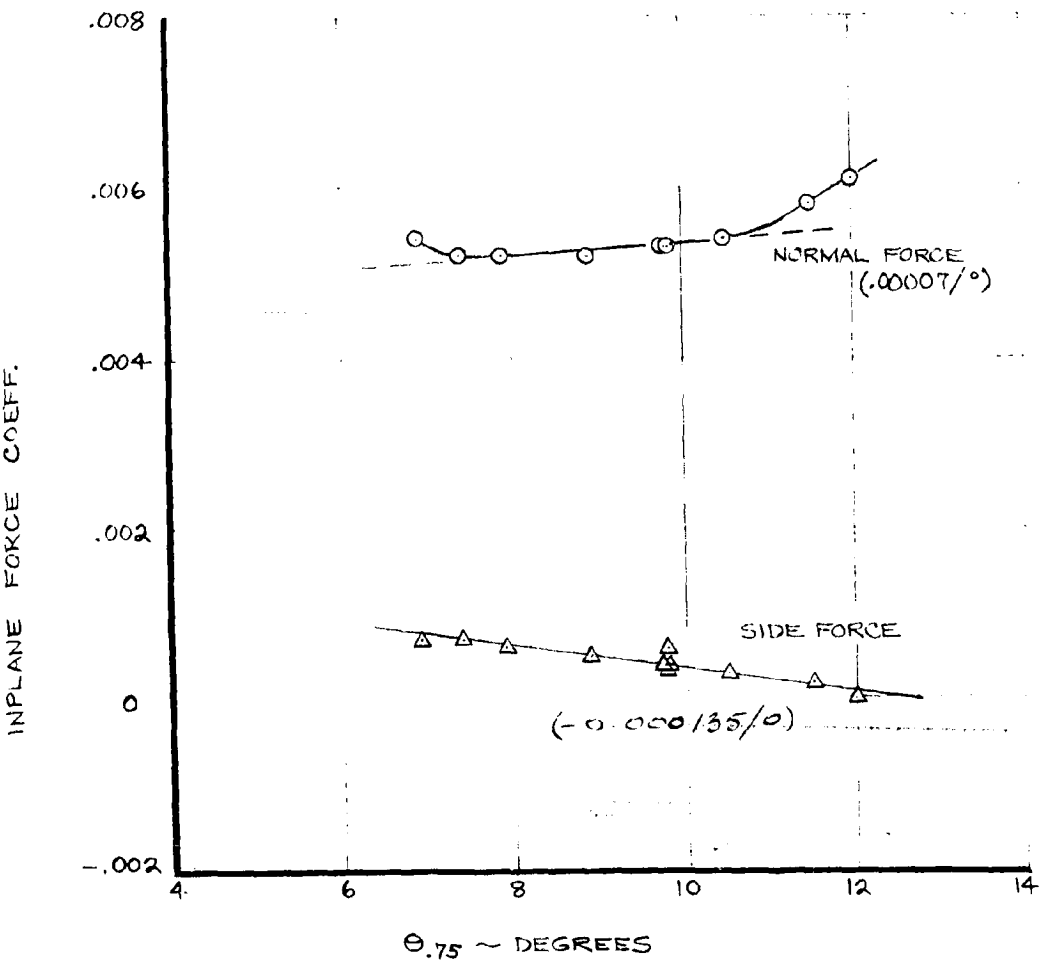

FIGURE 6.28 EFFECT OF COLLECTIVE PITCH ON HUB IN PLANE FORCES 500 RPM 80 KNOTS $i_N = 66°$

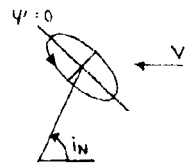

NASA AMES TEST 416
RUN 20
500 ROTOR RPM
V = 80 KNOTS
$\theta_{.75}$ = 9.8°
i_N = 66°
B_1 = 1.31°

$\Delta\theta = -A_1 \cos(\psi + 20) - B_1 \sin(\psi + 20)$

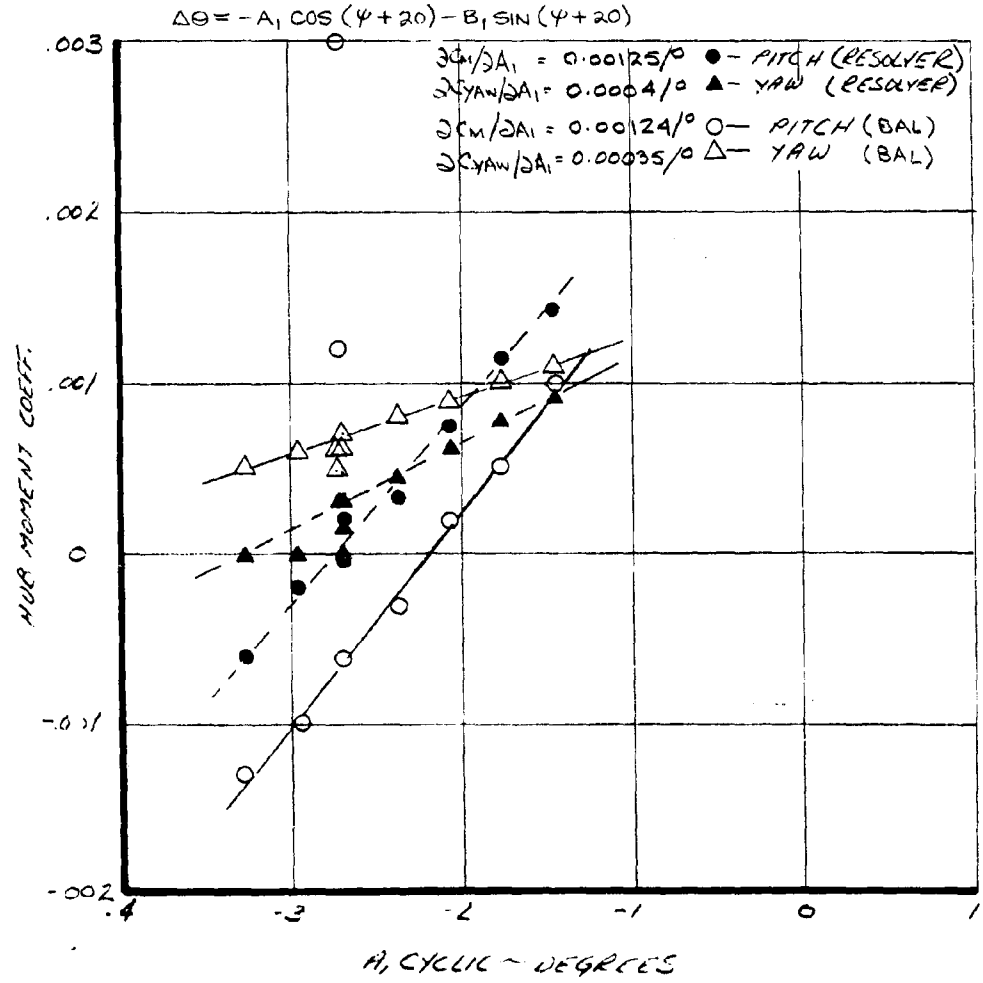

FIGURE 6-21 EFFECT OF LATERAL CYCLIC PITCH ON HUB MOMENTS
500 RPM 80 KNOTS i_N = 66°

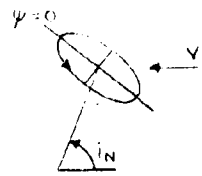

NASA AMES TEST 416
RUN 20
500 ROTOR RPM
V = 80 KNOTS
$\Theta_{75} = 9.8°$
$i_N = 66°$
$A_1 = -2.73°$

$\Delta\theta = -A_1 \cos(\psi + 20) - B_1 \sin(\psi + 20)$

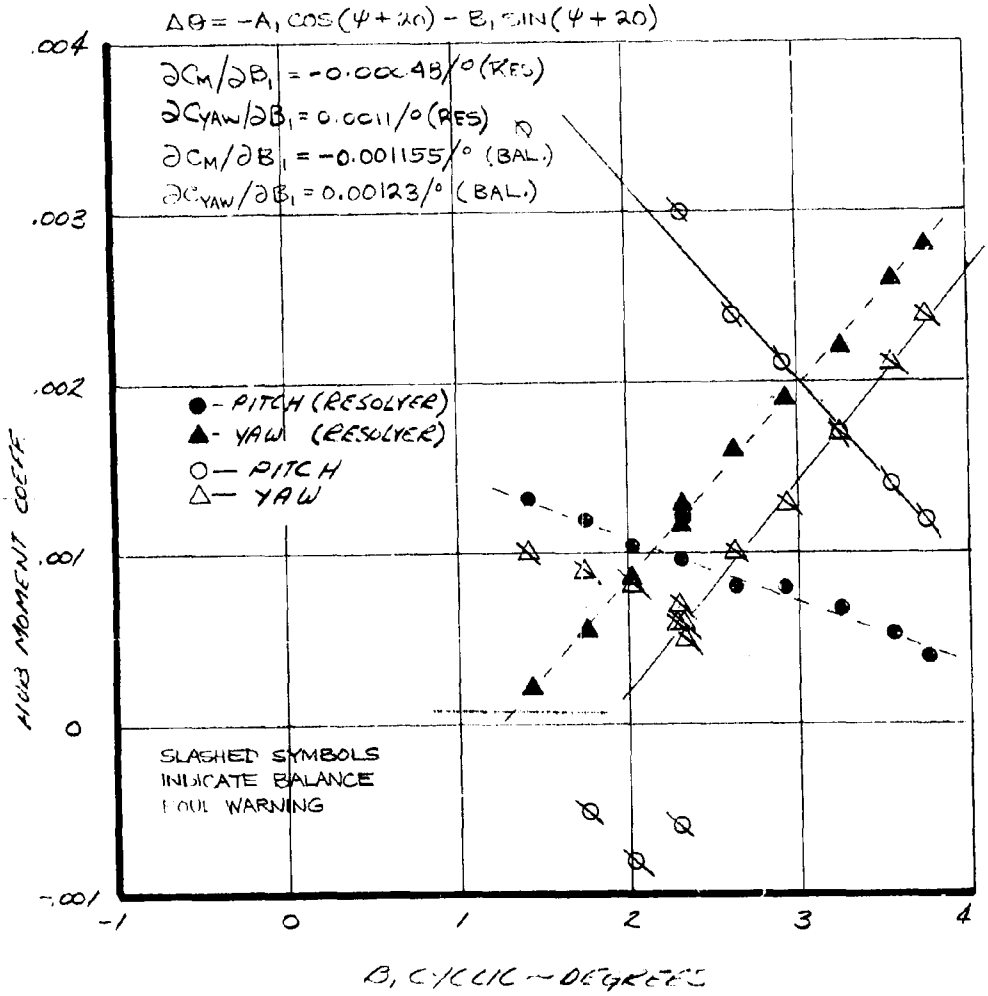

FIGURE 6.30 EFFECT OF LONGITUDINAL CYCLIC PITCH ON HUB MOMENTS 500 RPM 80 KTS $i_N = 66°$

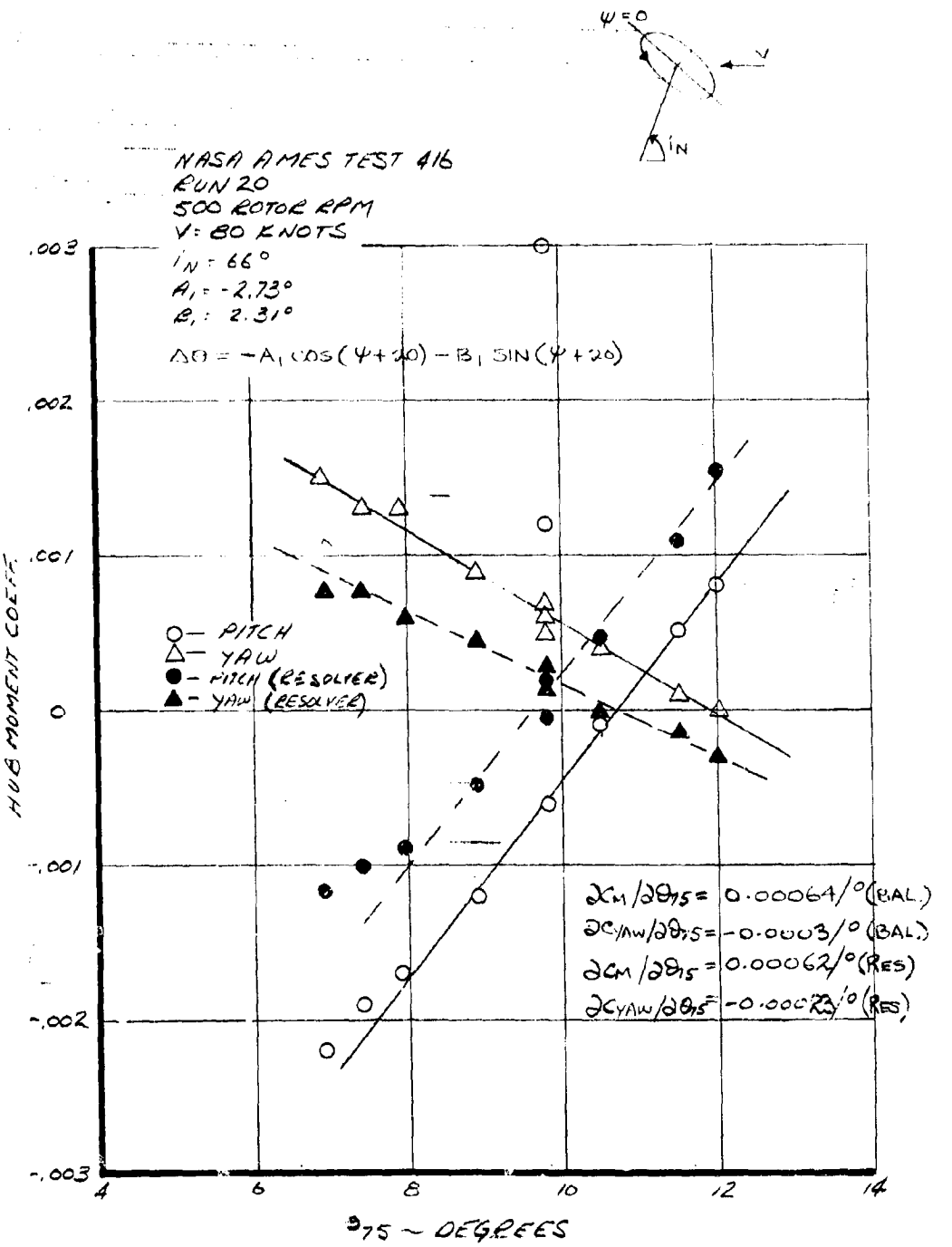

FIGURE 6.31 EFFECT OF COLLECTIVE PITCH ON HUB MOMENTS
500 RPM 80 KNOTS $i_N = 66°$

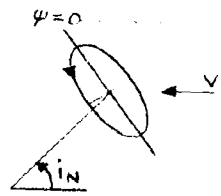

NASA AMES TEST 4-16
RUN 9
551 ROTOR RPM
V=105 KNOTS
$\theta_{.75} = 18.9°$
$i_N = 27°$
$A_1 = -2.16°$

$\Delta\theta = -A_1 \cos(\psi + 20) - B_1 \sin(\psi + 20)$

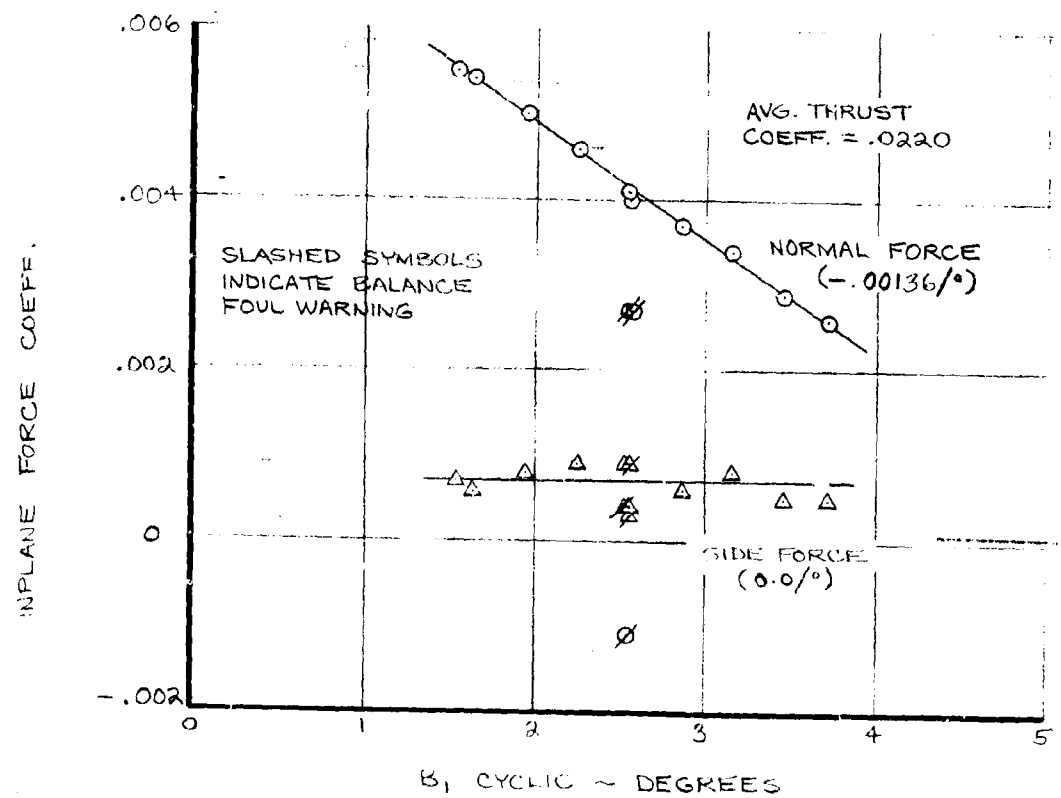

FIGURE 6-32 EFFECT OF LONGITUDINAL CYCLIC PITCH ON HUB IN PLANE FORCES 551 RPM 105 KNOTS $i_N = 27°$

NASA AMES TEST 416
RUN 9
551 ROTOR RPM
V = 105 KNOTS
$\theta_{.75} = 18.9°$
$i_N = 27°$
$B_1 = 2.56°$

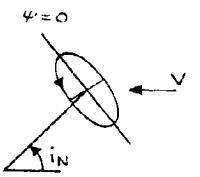

$\Delta\theta = -A_1 \cos(\psi + 20) - B_1 \sin(\psi + 20)$

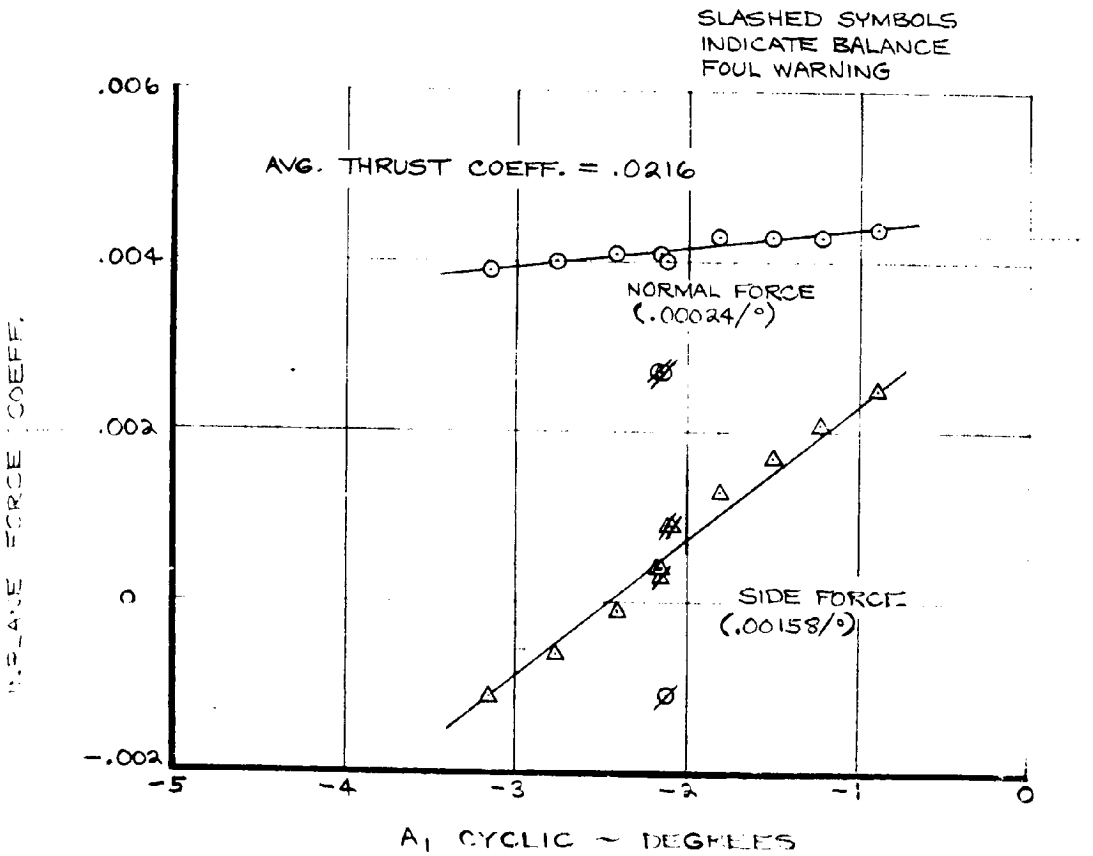

FIGURE 6-33 EFFECT OF LATERAL CYCLIC PITCH ON HUB IN PLANE FORCES 551 RPM 105 KNOTS $i_N = 27°$

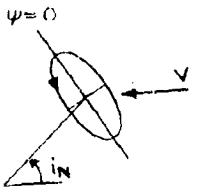

NASA AMES TEST 416
RUN 9
551 ROTOR RPM
V = 105 KNOTS
$i_N = 27°$
$A_1 = -2.16°$
$B_1 = 2.56°$

$$\Delta\theta = -A_1 \cos(\psi+20) - B_1 \sin(\psi+20)$$

SLASHED SYMBOLS
INDICATE BALANCE
FOUL WARNING

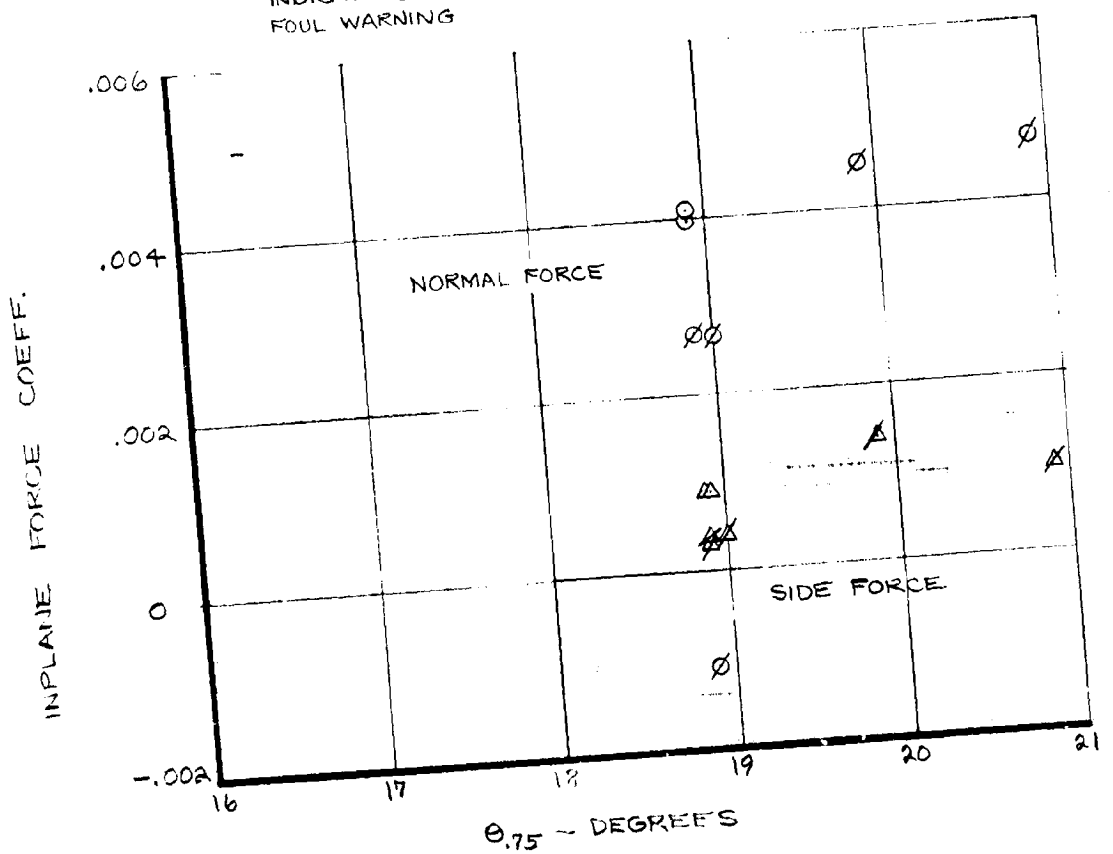

FIGURE 6-34 EFFECT OF COLLECTIVE PITCH ON HUB IN PLANE FORCES
551 RPM 105 KNOTS $i_N = 27°$

NASA AMES TEST 416
RUN 9
551 ROTOR RPM
V = 105 KNOTS
$\theta_{.75} = 18.9°$
$A_1 = -2.12°$
$B_1 = 2.56°$

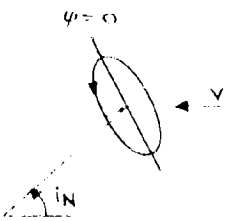

$\Delta\theta = -A_1 \cos(\psi + 20) - B_1 \sin(\psi + 20)$

SLASHED SYMBOLS
INDICATE BALANCE
FOUL WARNING

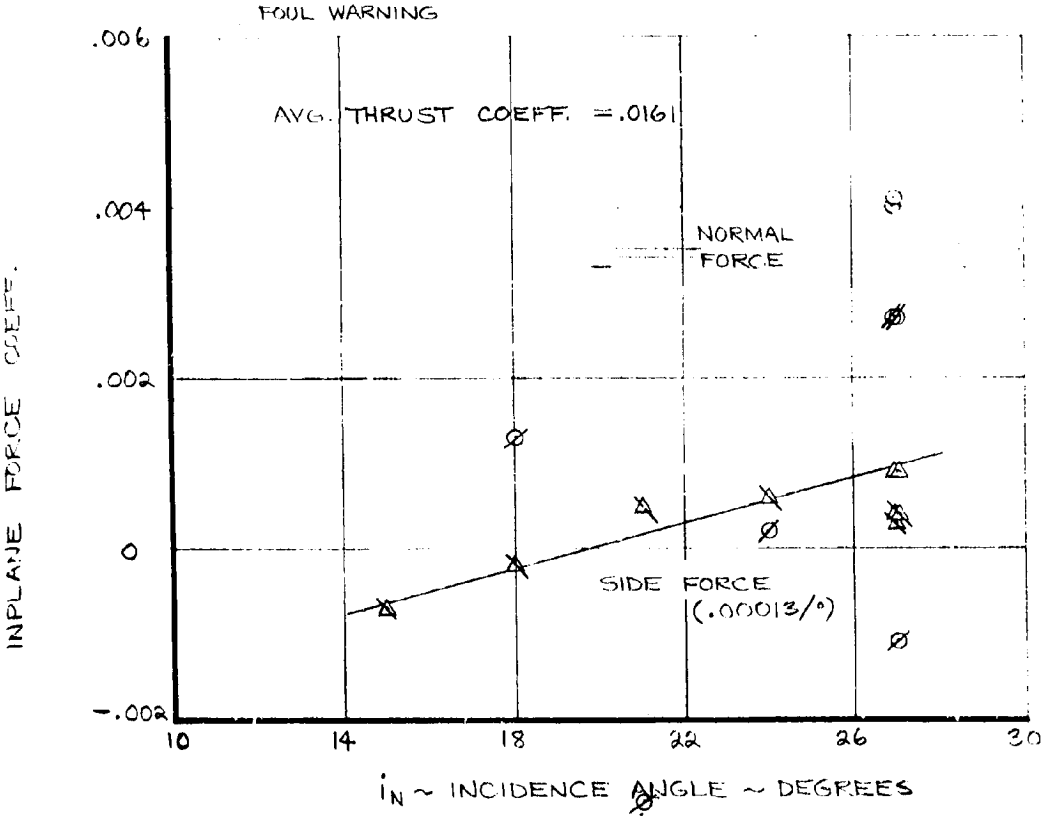

FIGURE 6-35 EFFECT OF INCIDENCE ANGLE ON HUB IN PLANE FORCES 551 RPM 105 KNOTS

NASA AMES TEST 416
RUN 9
551 ROTOR RPM
V = 105 KNOTS
$\theta_{.75} = 18.9°$
$i_N = 27°$
$A_1 = -2.16°$
$\Delta\alpha = -A_1 \cos(\psi + 90) - B_1 \sin(\psi + 90)$

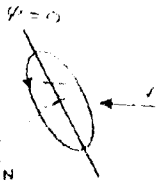

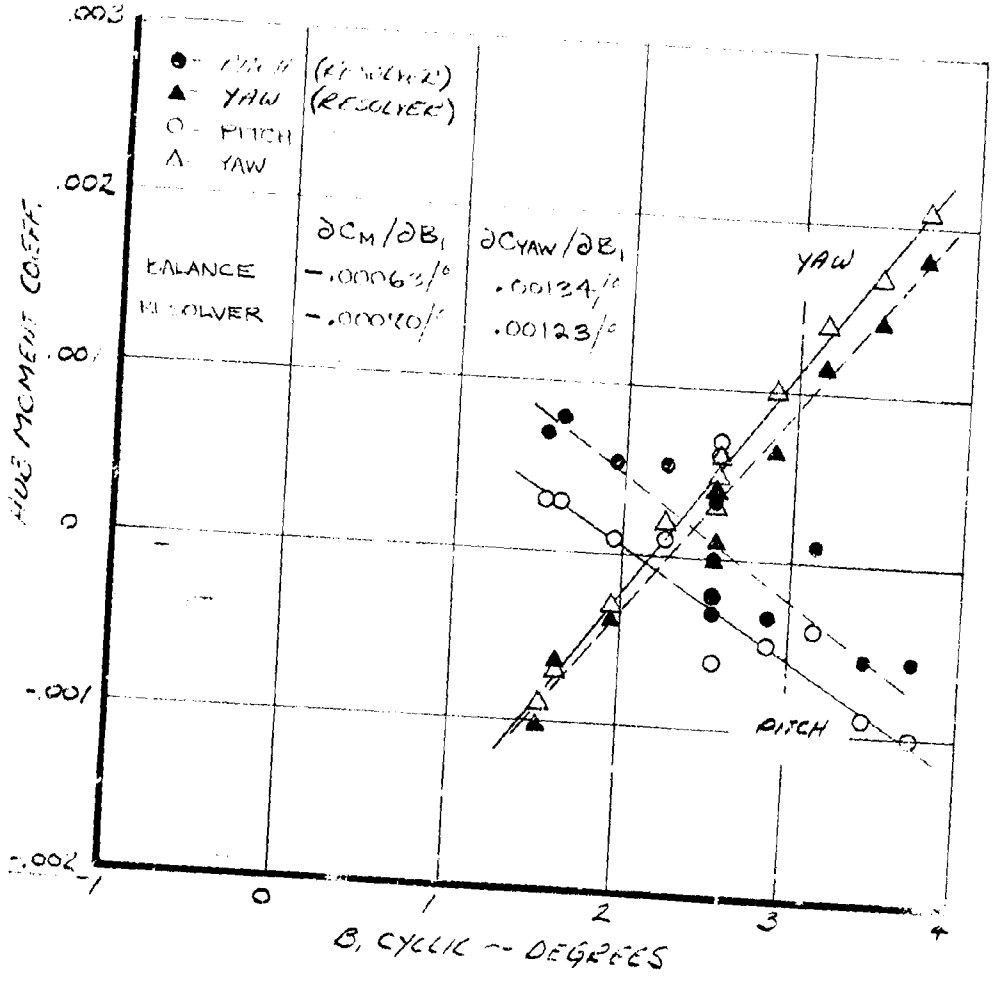

FIGURE 6-36 EFFECT OF LONGITUDINAL CYCLIC PITCH ON HUB MOMENTS 551 RPM 105 KNOTS $i_N = 27°$

NASA AMES TEST 416
RUN 9
551 ROTOR RPM
V = 105 KNOTS
θ_{TC} = 18.9°
i_N = 27°
B_1 = 2.56°

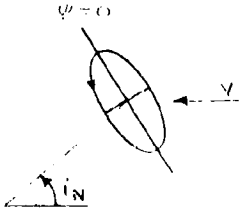

$\Delta\theta = -A_1 \cos(\psi + 30) - B_1 \sin(\psi + 30)$

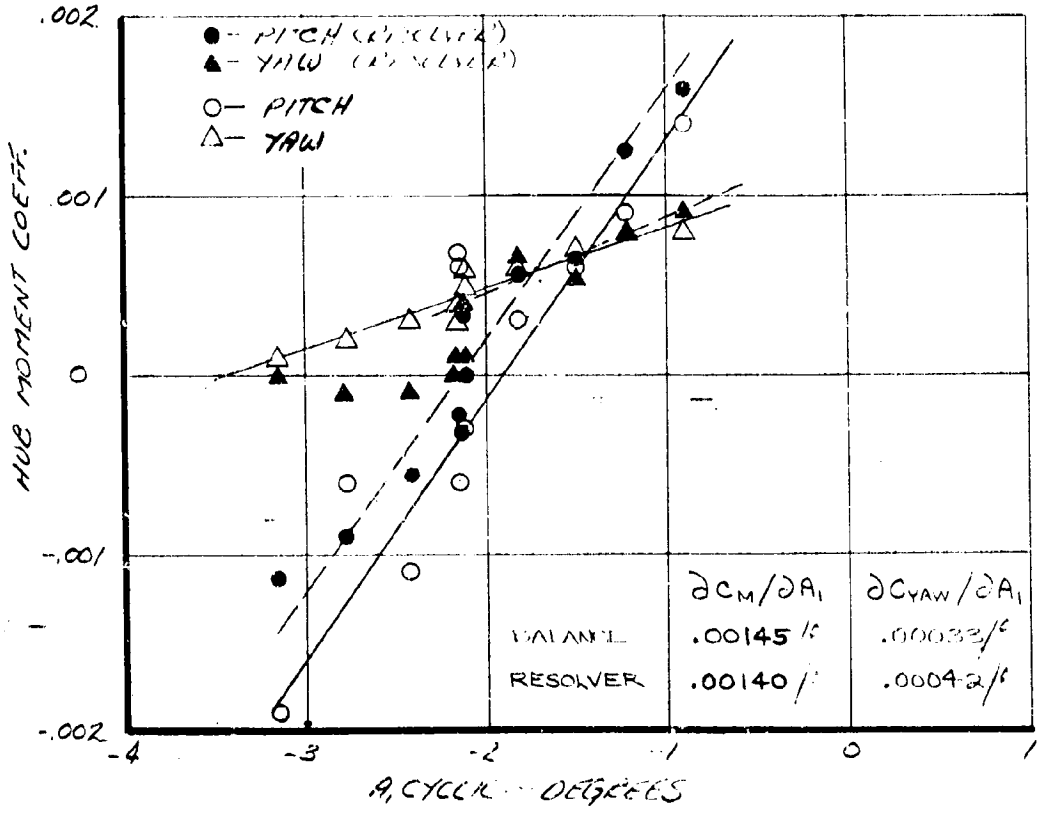

FIGURE 6-37 EFFECT OF LATERAL CYCLIC PITCH ON HUB MOMENTS
551 RPM 105 KNOTS i_N = 27°

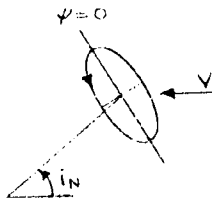

NASA AMES TEST 416
RUN 9
551 ROTOR RPM
V=105 KNOTS
i_N = 27°
A_1 = -2.12°
B_1 = 2.56°
$\Delta\theta = -A_1 \cos(\Psi+20) - B_1 \sin(\Psi+20)$

SHADED SYMBOLS
INDICATE BALANCE
FOUL WARNING

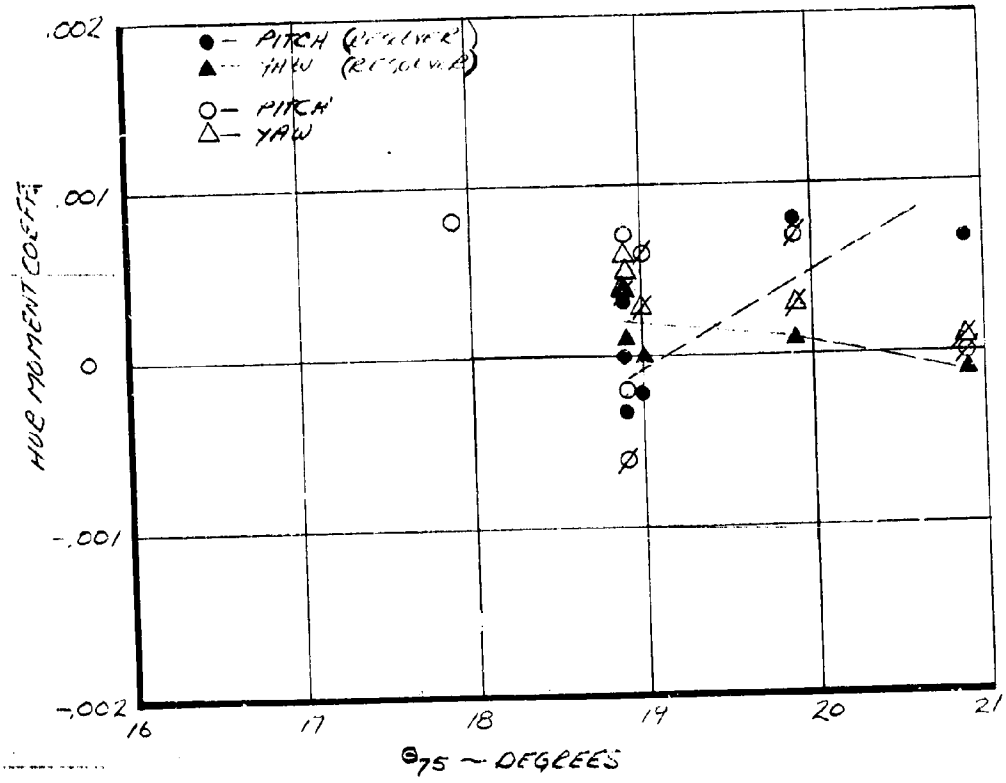

FIGURE 3-38 EFFECT OF COLLECTIVE PITCH ON HUB MOMENTS
551 RPM 105 KNOTS i_N = 27°

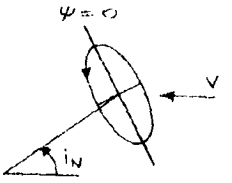

NASA AMES TEST 416
RUN 9
551 (2070.6° RPM)
V = 105 KNOTS
$\Theta_{75} = 18.9°$
$A_1 = -2.12°$
$B_1 = 2.56°$

$$\Delta\Theta = -A_1 \cos(\psi + 20) - B_1 \sin(\psi + 20)$$

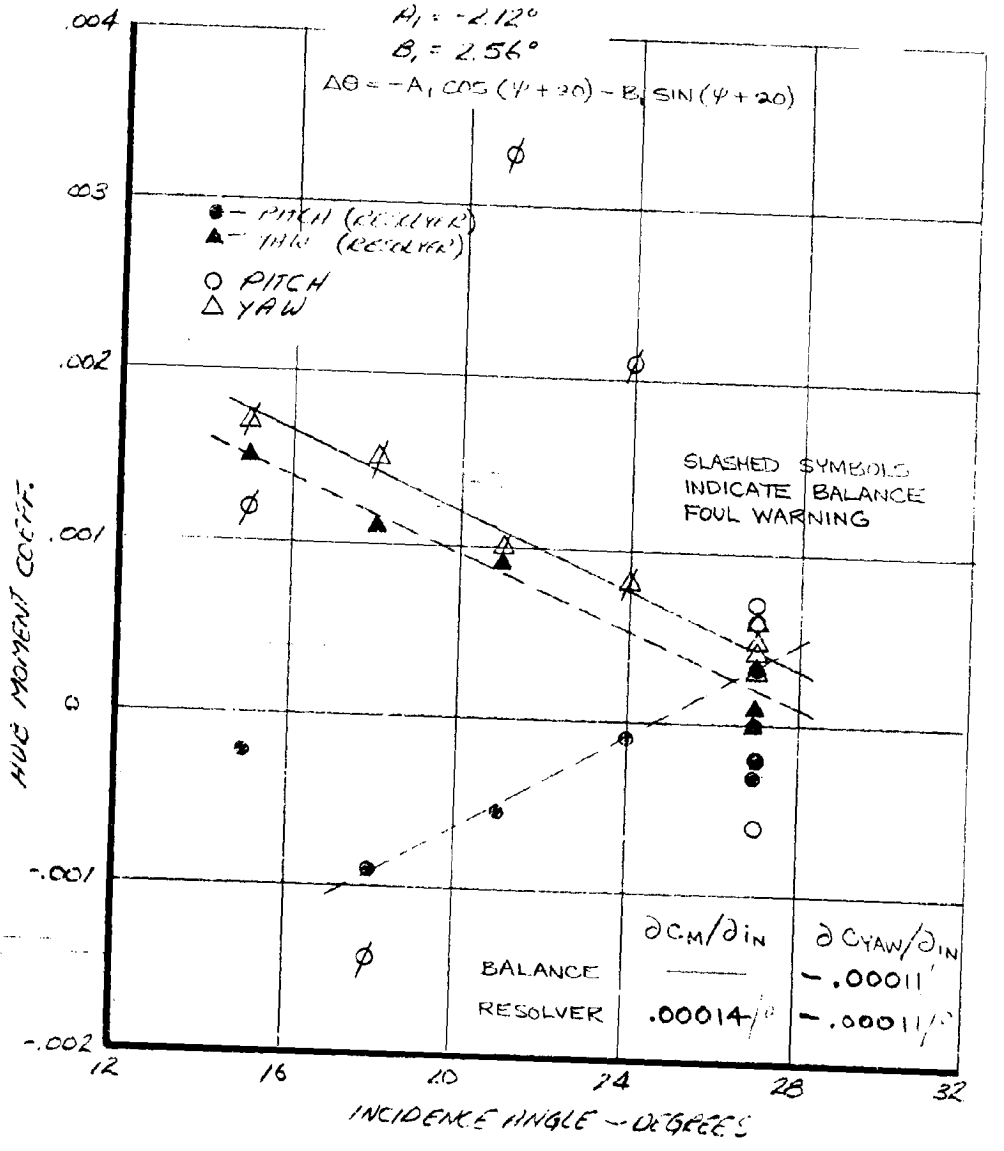

FIGURE 6-39 EFFECT OF INCIDENCE ANGLE ON HUB MOMENTS
551 RPM 105 KNOTS

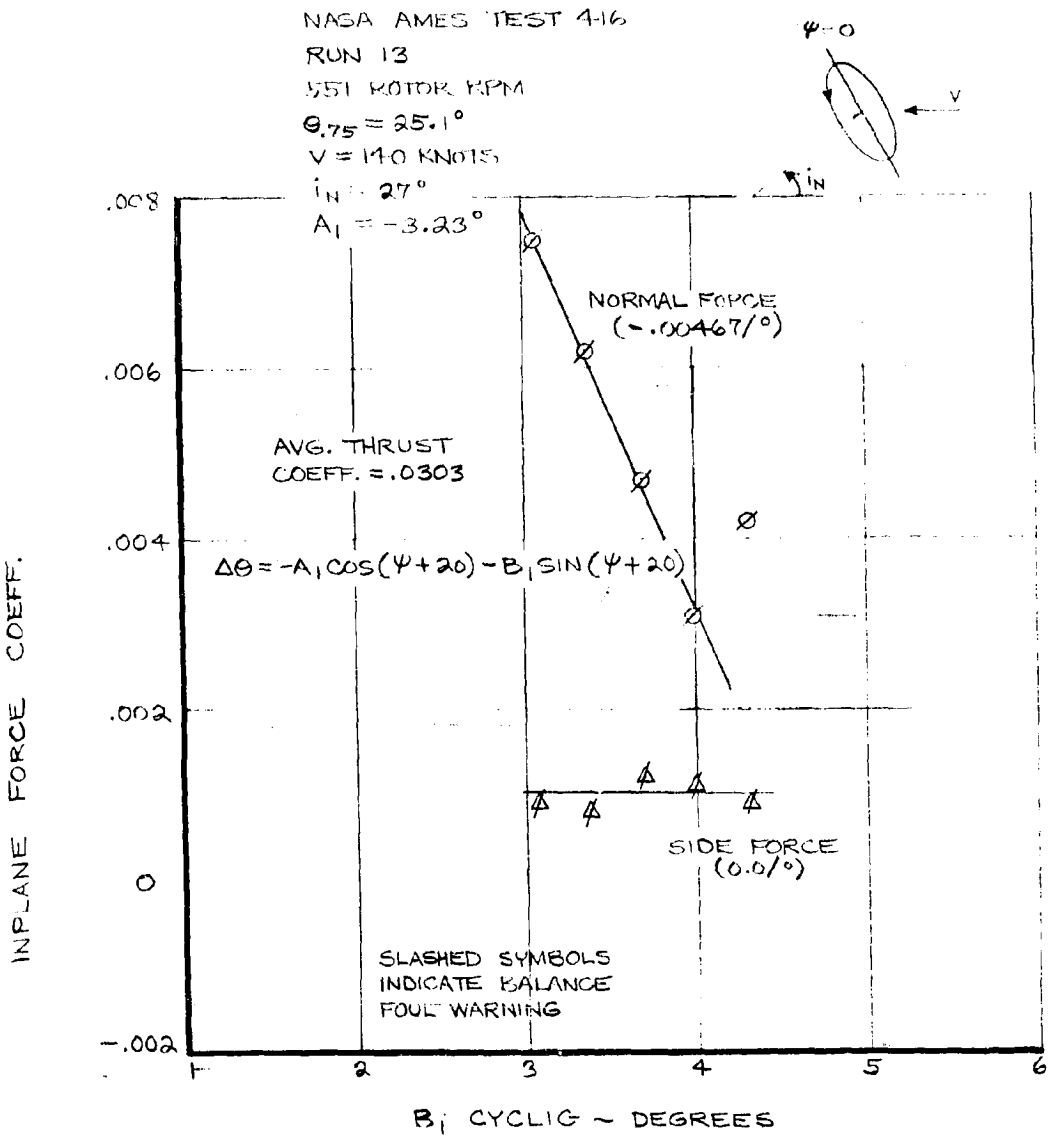

FIGURE 6-40 EFFECT OF LONGITUDINAL CYCLIC PITCH ON HUB IN PLANE FORCES 551 RPM 140 KNOTS $i_N = 27°$

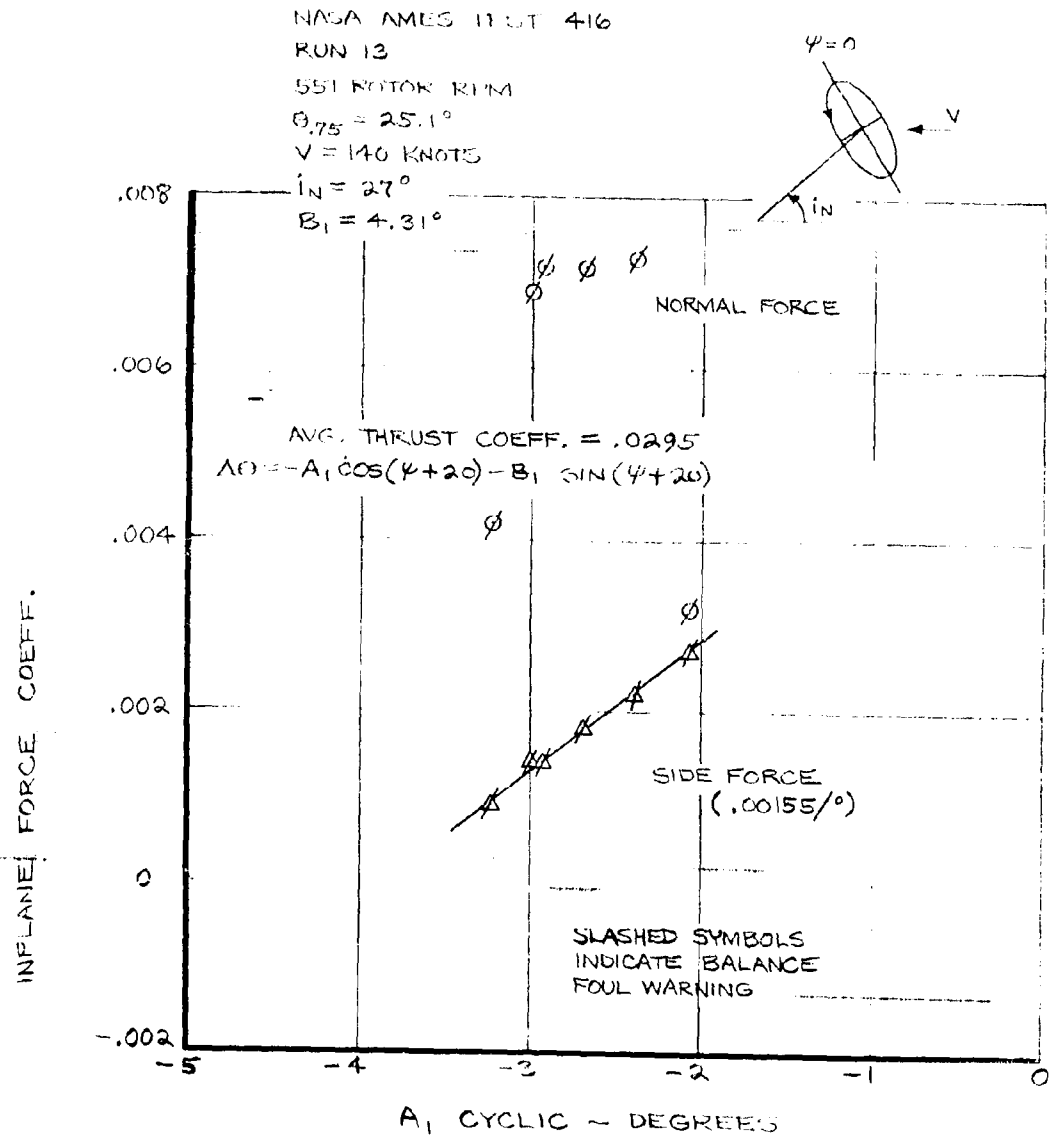

FIGURE 6-41 EFFECT OF LATERAL CYCLIC PITCH ON HUB IN PLANE FORCES 551 RPM 140 KNOTS i_N = 27°

NASA AMES TEST 416
RUN 13
551 ROTOR RPM
$\theta_{.75} = 25.1°$
V = 140 KNOTS
$A_1 = -3.23°$
$B_1 = 4.31°$
$\Delta\theta = -A_1 \cos(\psi+20) - B_1 \sin(\psi+20)$

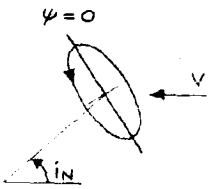

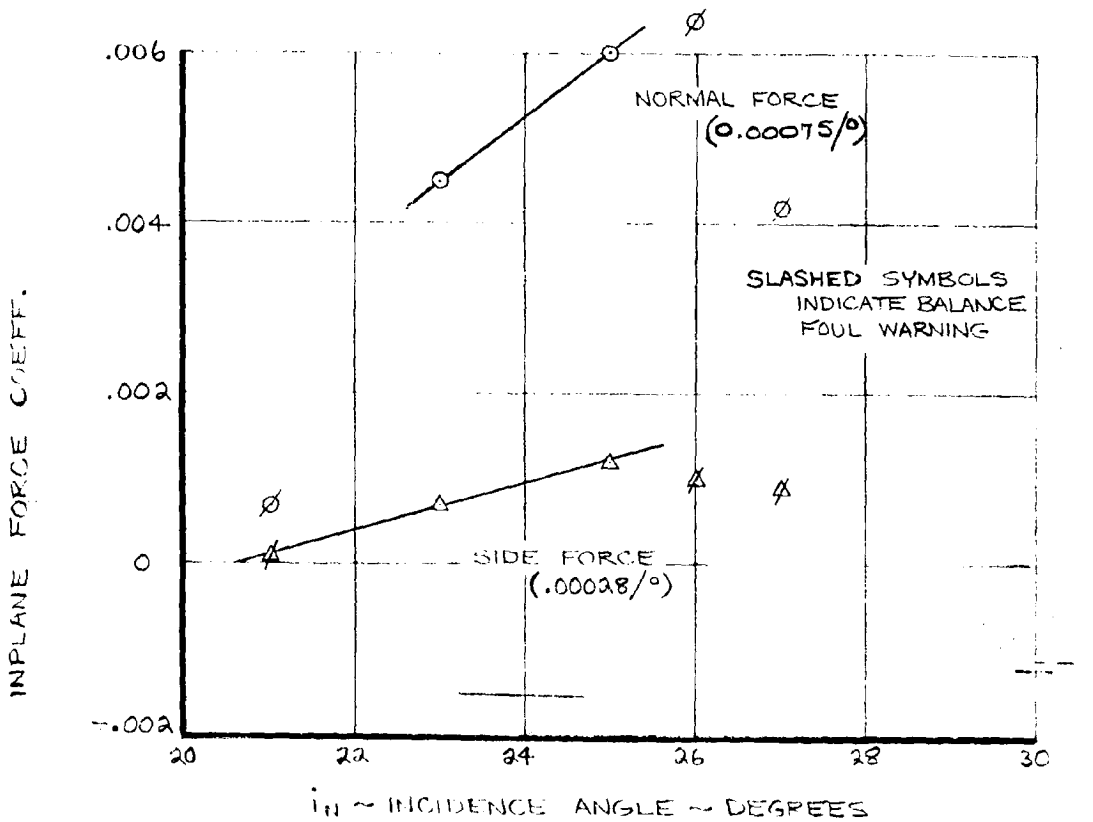

FIGURE 4-42 EFFECT OF INCIDENCE ANGLE ON HUB IN PLANE FORCES 551 RPM 140 KNOTS

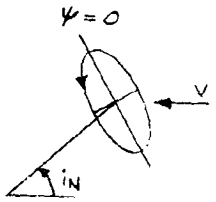

NASA AMES TEST 416
RUN 13
551 ROTOR RPM
V = 140 KNOTS
$\Theta_{.75}$ = 25.1°
i_N = 27°
A_1 = -3.23°

$\Delta\Theta = -A_1 \cos(\Psi+20) - B_1 \sin(\Psi+20)$

● – PITCH (RESOLVER)
▲ – YAW (RESOLVER)
○ – PITCH
△ – YAW

SLASHED SYMBOLS INDICATE BALANCE FOUL WARNING

	$\partial C_M/\partial B_1$	$\partial C_{YAW}/\partial B_1$
BALANCE	———	.00153
RESOLVER	-.00008	.00152

.005
.004
.003
.002
.001
0
-.001

0 1 2 3 4 5

B_1, CYCLIC – DEGREES

FIGURE 6.43 EFFECT OF LONGITUDINAL CYCLIC PITCH ON HUB MOMENTS
551 RPM 140 KNOTS i_N = 27°

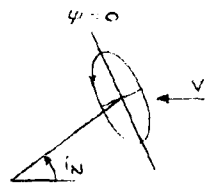

NASA AMES TEST 416
RUN 13
551 ROTOR RPM
V = 140 KNOTS
$\theta_{TS} = 25.1°$
$i_N = 27°$
$B_1 = 4.31°$

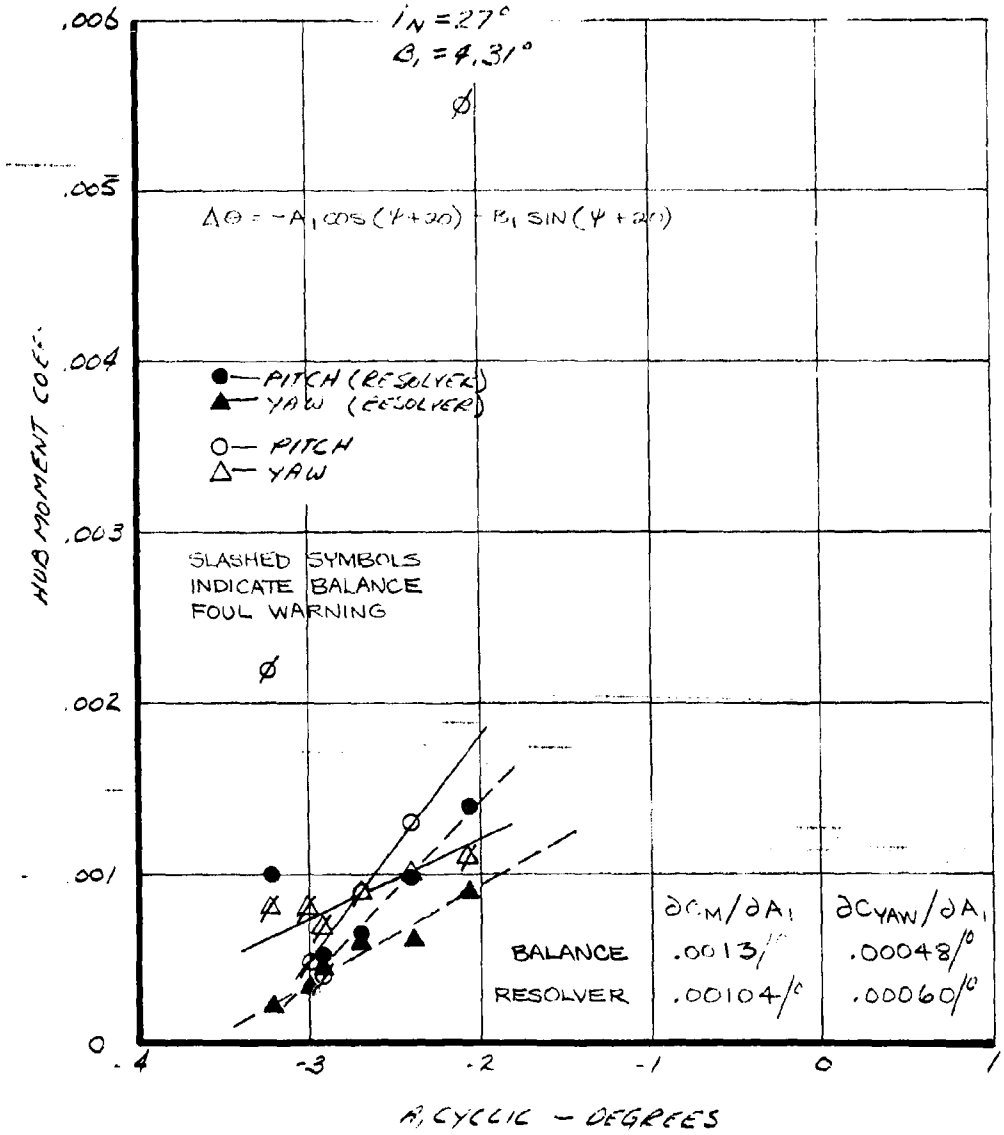

	$\partial C_M/\partial A_1$	$\partial C_{YAW}/\partial A_1$
BALANCE	.0013/°	.00048/°
RESOLVER	.00104/°	.00060/°

FIGURE 6-44 EFFECT OF LATERAL CYCLIC PITCH ON HUB MOMENTS
551 RPM 140 KNOTS $i_N = 27°$

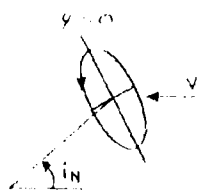

NASA AMES TEST 416
RUN 13
551 ROTOR RPM
V = 140 KNOTS
$\theta_{.75} = 25.1°$
$A_1 = -3.23°$
$B_1 = 4.31°$

$\Delta\alpha = A_1 \cos(\psi + 180) - B_1 \sin(\psi + 270)$

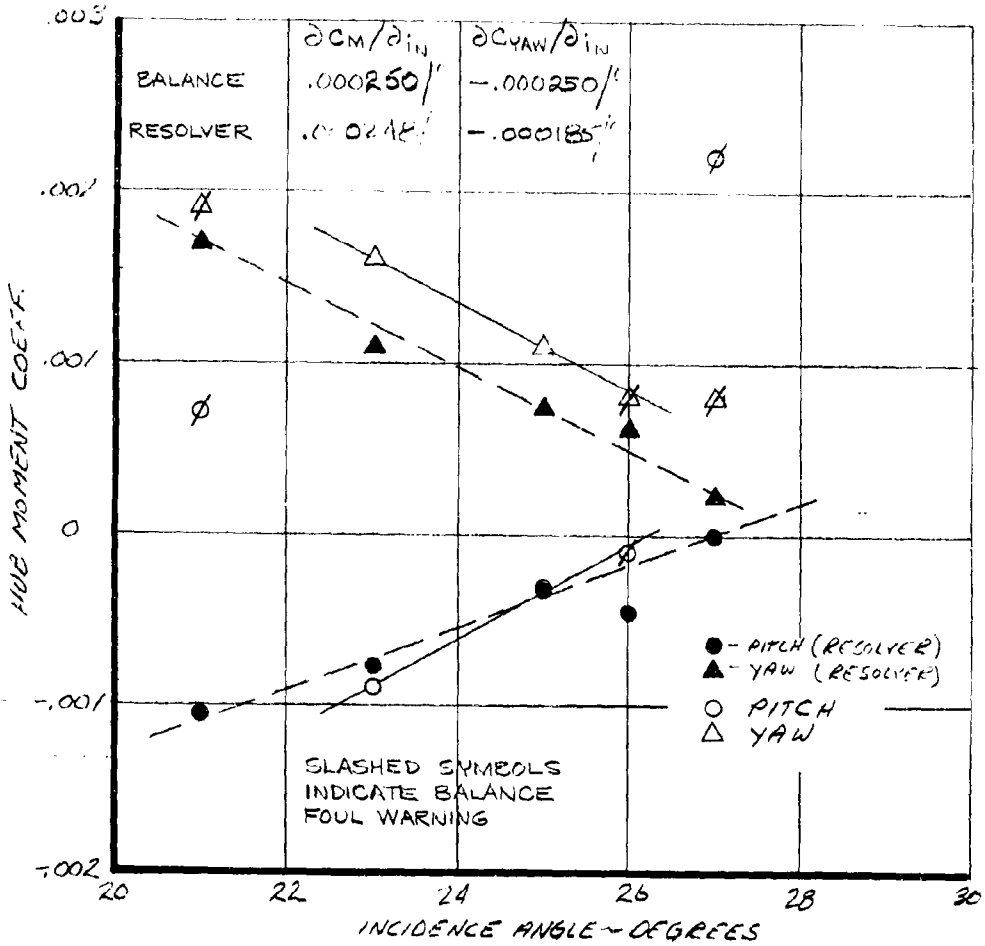

FIGURE 6-45 EFFECT OF INCIDENCE ANGLE ON HUB MOMENTS
551 RPM 140 KNOTS

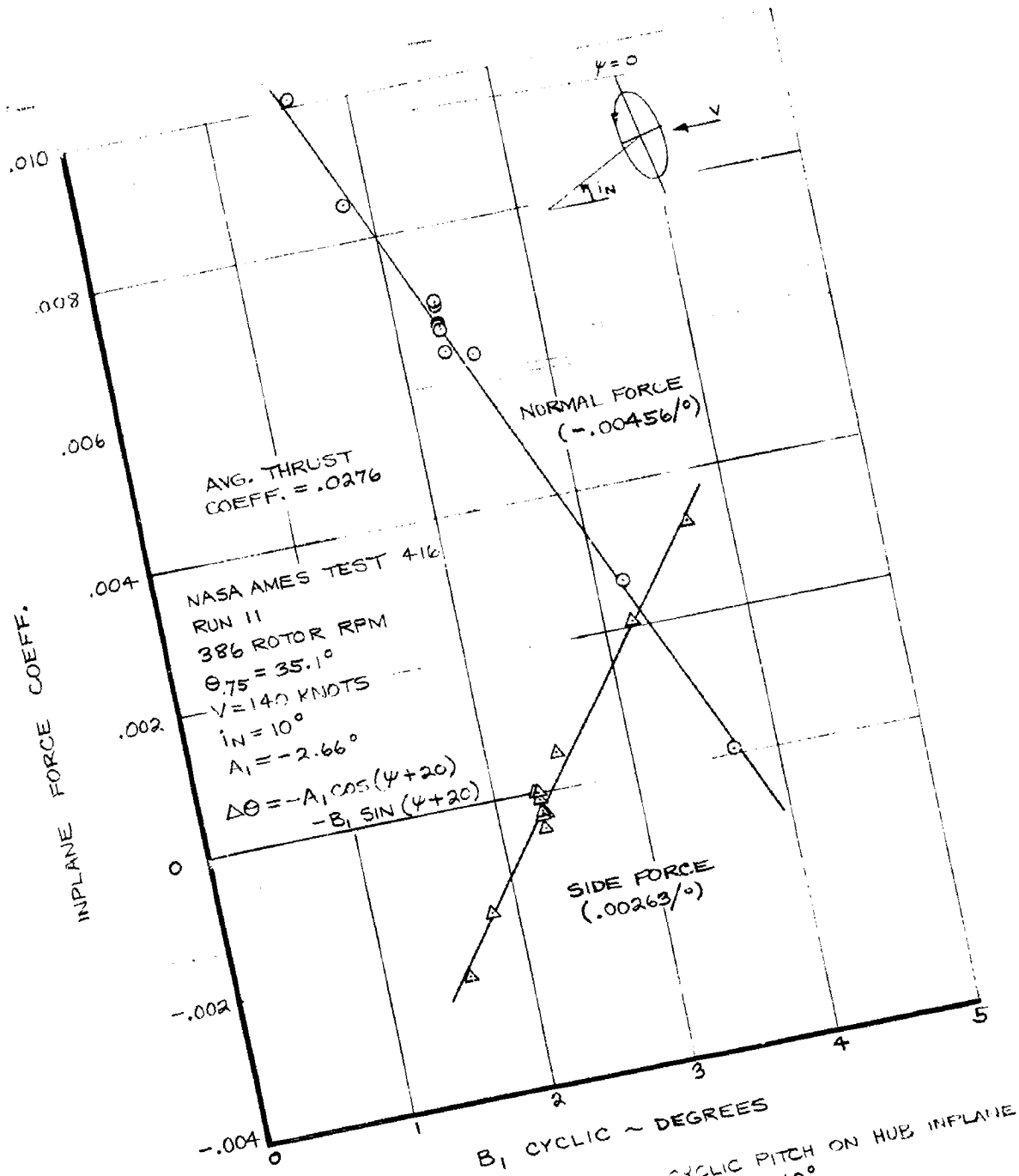

FIGURE 6-46 EFFECT OF LONGITUDINAL CYCLIC PITCH ON HUB INPLANE FORCES 386 RPM 140 KNOTS i_N = 10°

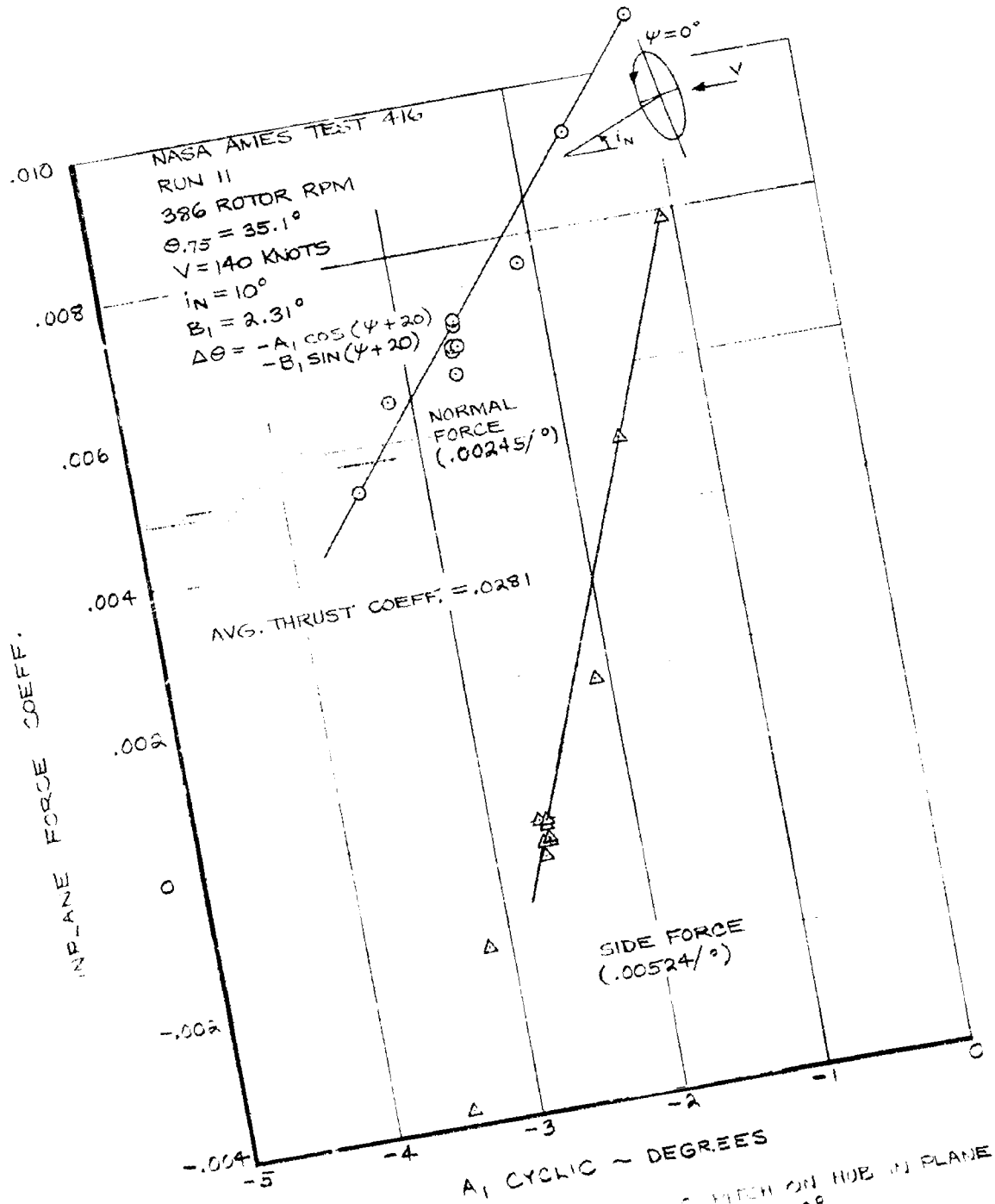

FIGURE 6-47 EFFECT OF LATERAL CYCLIC PITCH ON HUB IN PLANE FORCES 386 RPM 140 KNOTS iN 10°

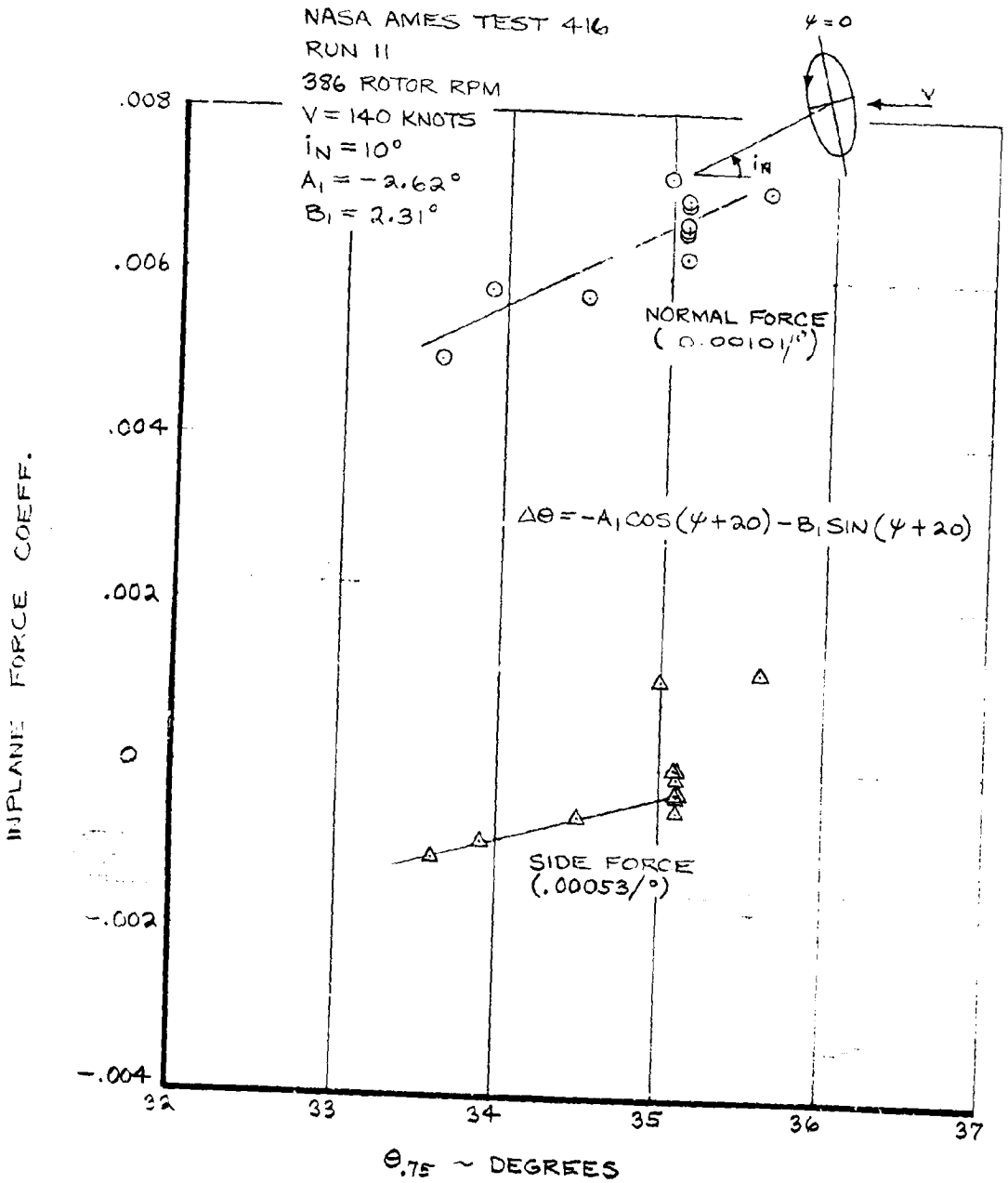

FIGURE 6-48 EFFECT OF COLLECTIVE PITCH ON HUB IN PLANE FORCES 386 RPM 140 KNOTS $i_N = 10°$

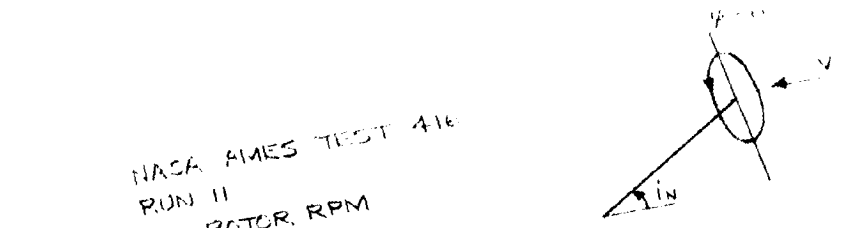

NASA AMES TEST 416
RUN 11
386 ROTOR RPM
V = 140 KNOTS
$\theta_{.75} = 35.1°$
$A_1 = -2.62°$
$B_1 = 2.31°$
$\Delta\theta = -A_1 \cos(\psi+20) - B_1 \sin(\psi+20)$

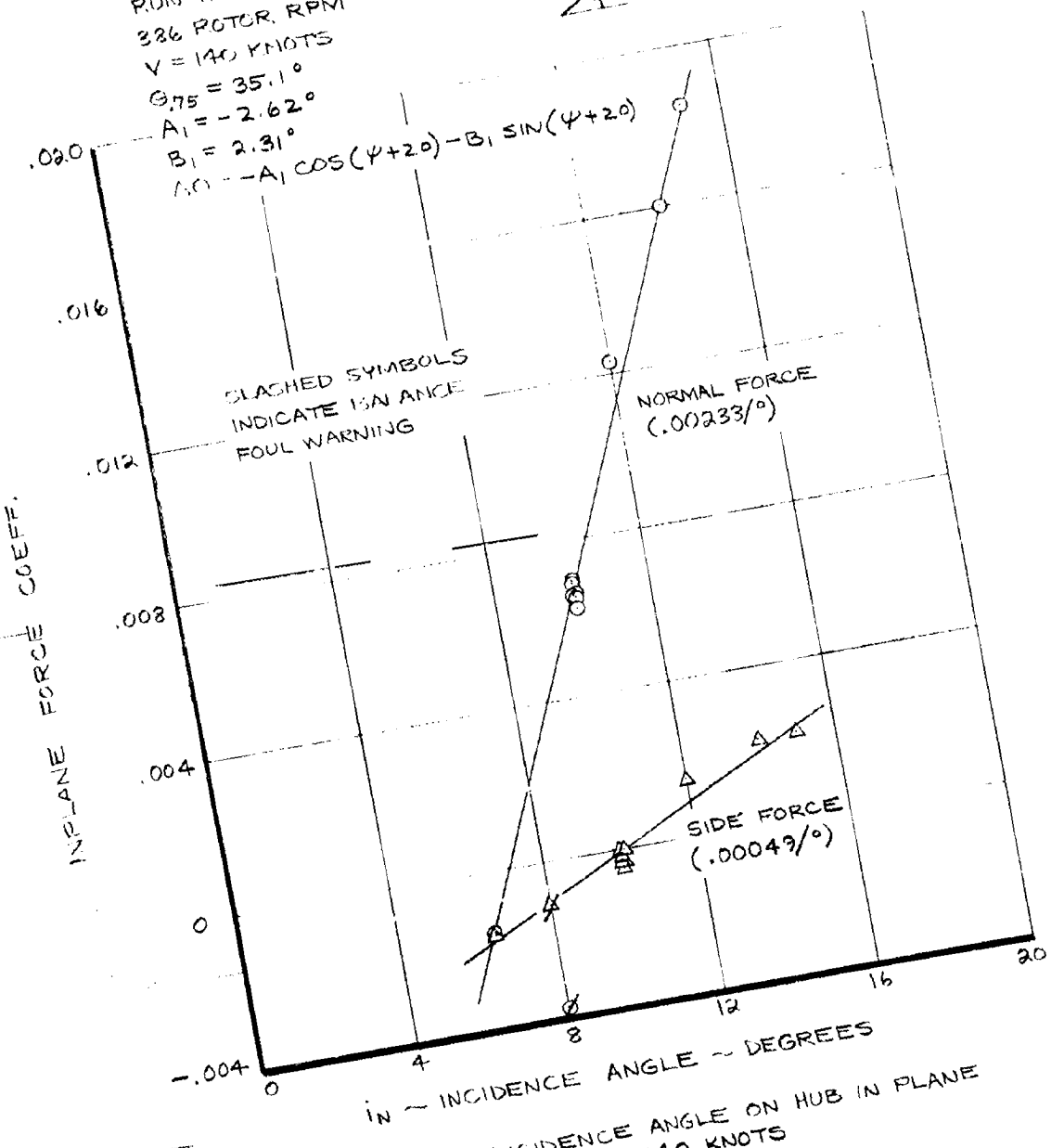

FIGURE 6-49 EFFECT OF INCIDENCE ANGLE ON HUB IN PLANE FORCES 386 RPM 140 KNOTS

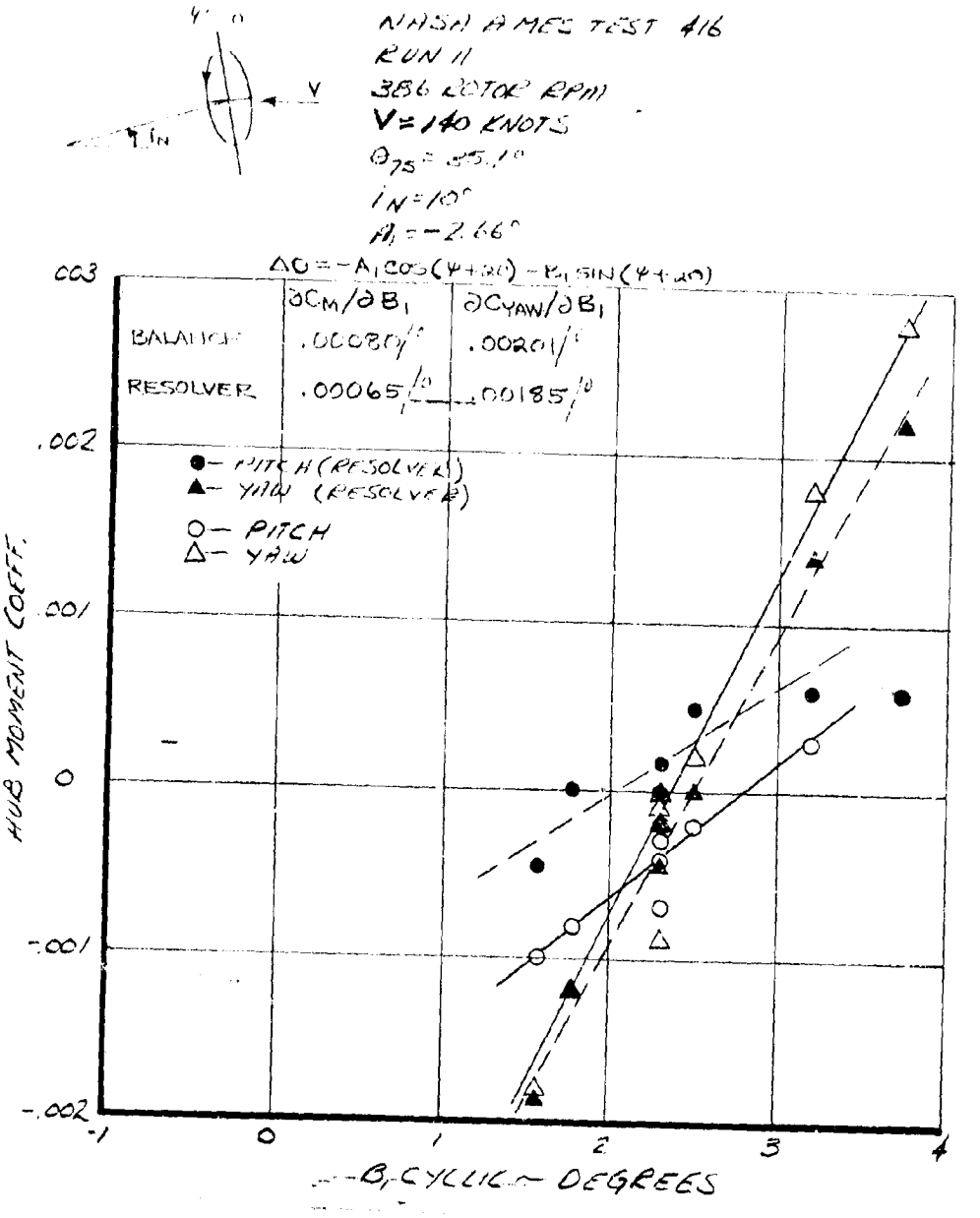

FIGURE 6-50 EFFECT OF LONGITUDINAL CYCLIC PITCH ON HUB MOMENTS
386 RPM 140 KNOTS $i_N = 10°$

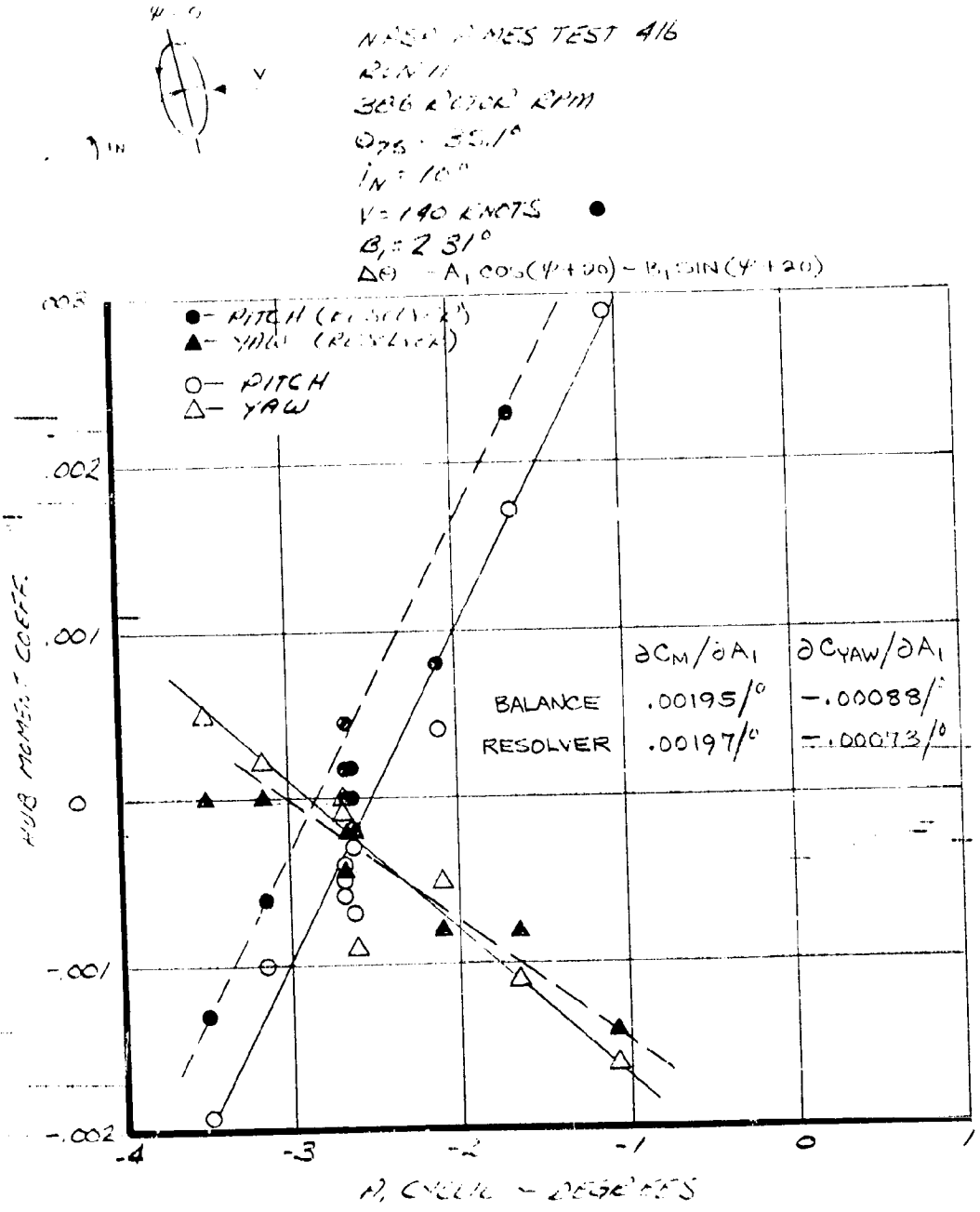

FIGURE 6-51 EFFECT OF LATERAL CYCLIC PITCH ON HUB MOMENTS
386 RPM 140 KNOTS $i_N = 10°$

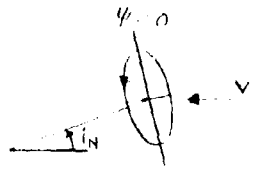

NASA AMES TEST 416
RUN 11
386 ROTOR RPM
V = 140 KNOTS
$i_N = 10°$
$A_1 = -1.62°$
$B_1 = 2.31°$
$\Delta\theta = -A_1 \cos(\psi + 30) - B_1 \sin(\psi + 30)$

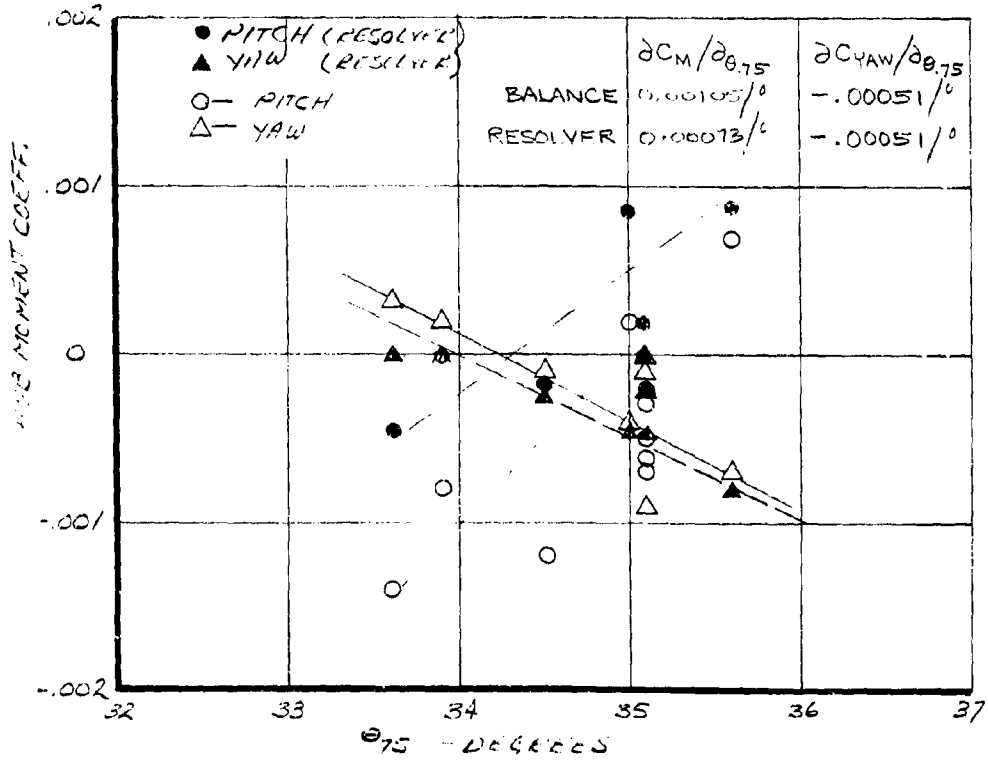

FIGURE 6-52 EFFECT OF COLLECTIVE PITCH ON HUB MOMENTS
386 RPM 140 KNOTS $i_N = 10°$

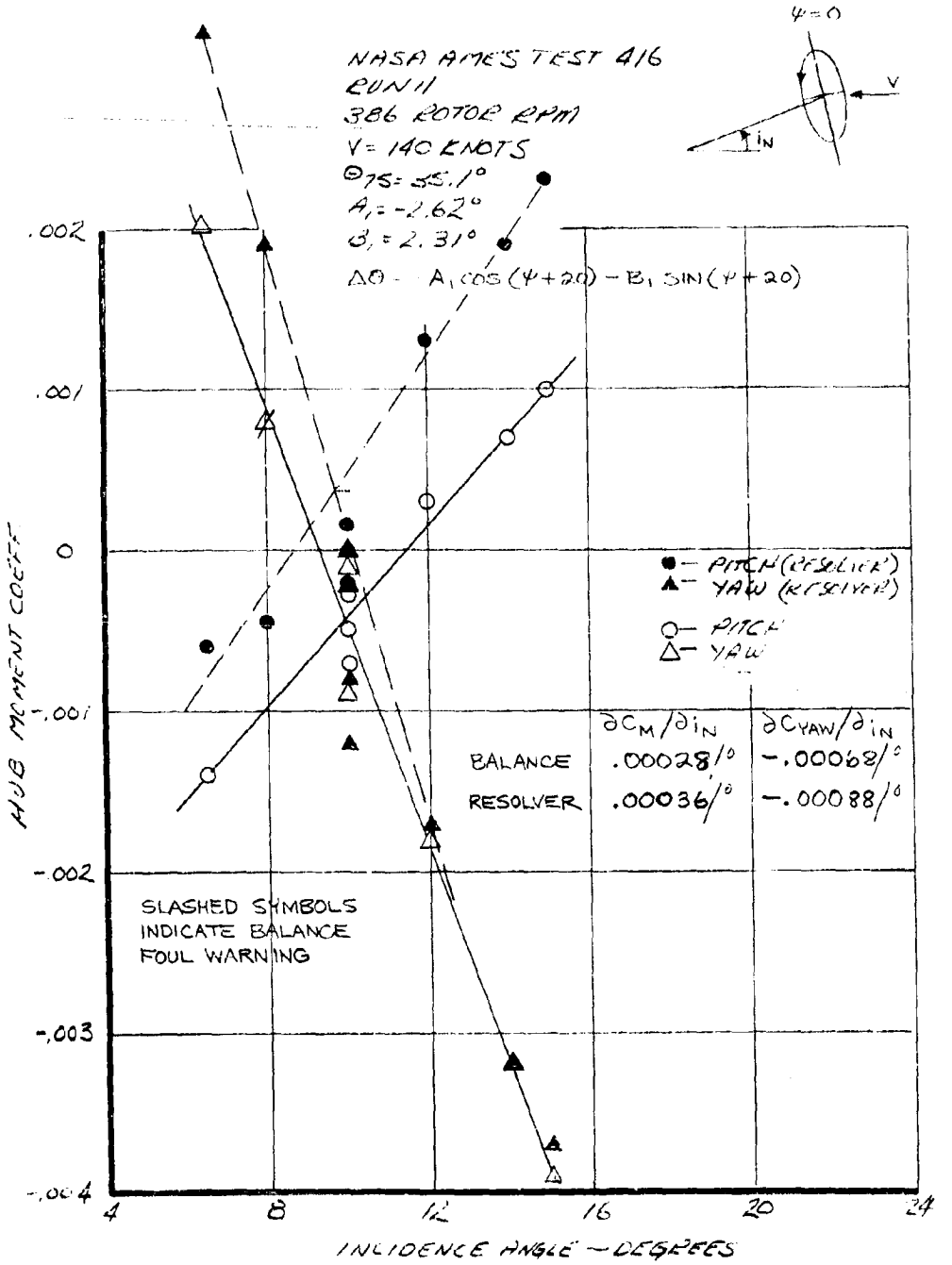

FIGURE 6-53 EFFECT OF INCIDENCE ANGLE ON HUB MOMENTS
386 RPM 140 KNOTS

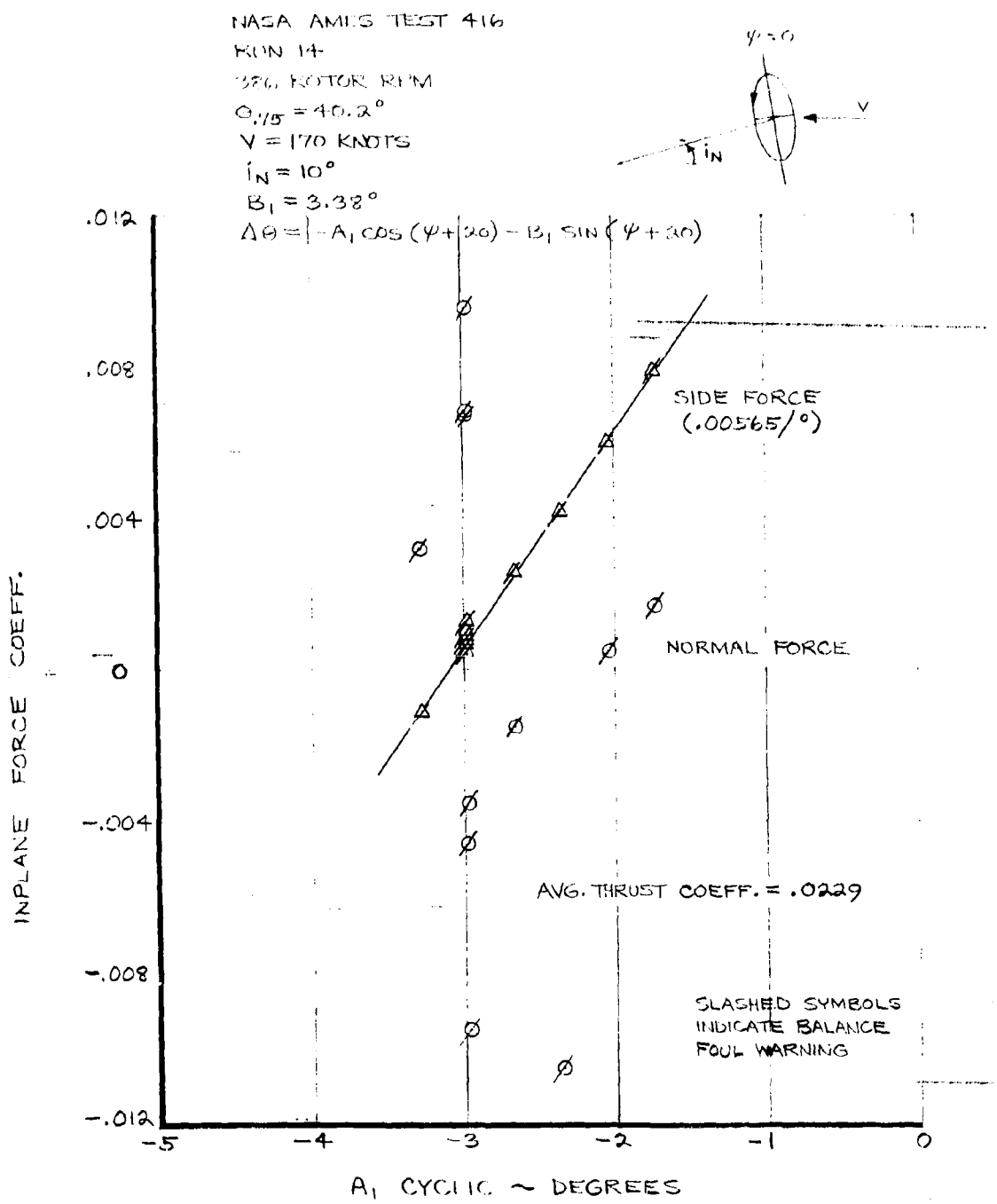

FIGURE 6-54 EFFECT OF LATERAL CYCLIC PITCH ON HUB IN PLANE FORCES 386 RPM 170 KNOTS $i_N = 10°$

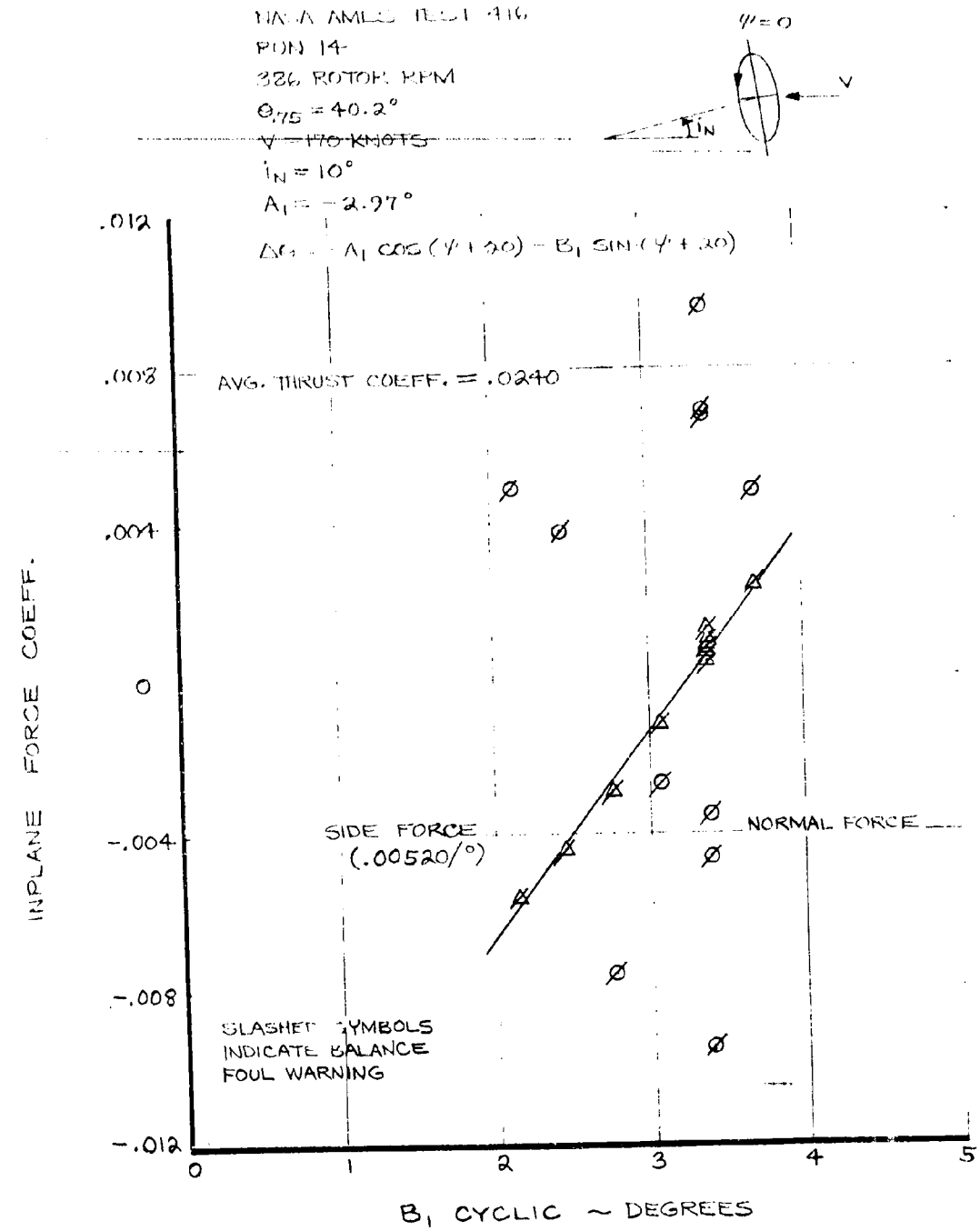

FIGURE 6-55 EFFECT OF LONGITUDINAL CYCLIC PITCH ON HUB IN PLANE FORCES 386 RPM 170 KNOTS $i_N = 10°$

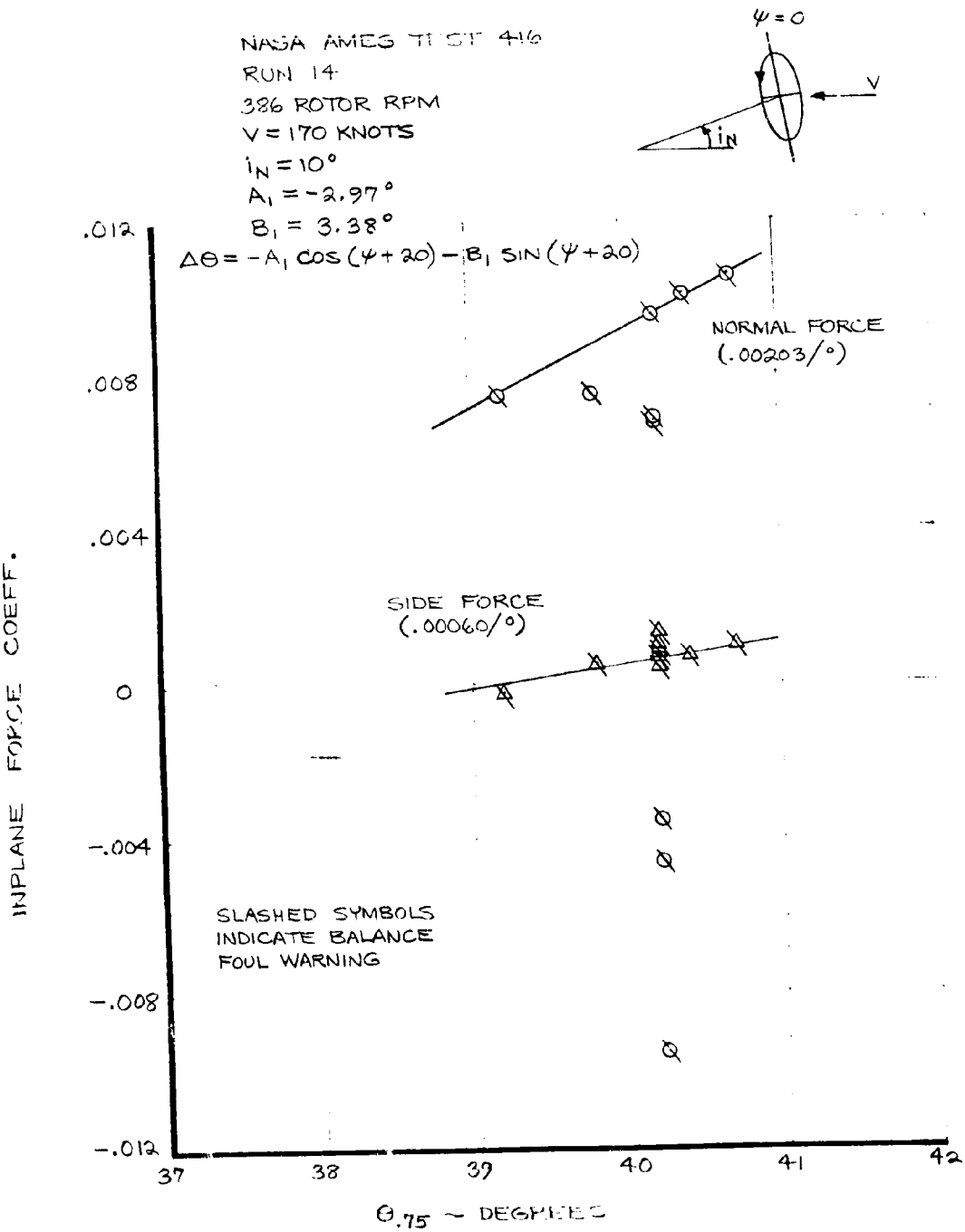

FIGURE 6-56 EFFECT OF COLLECTIVE PITCH ON HUB IN PLANE FORCES 386 RPM 170 KNOTS $i_N = 10°$

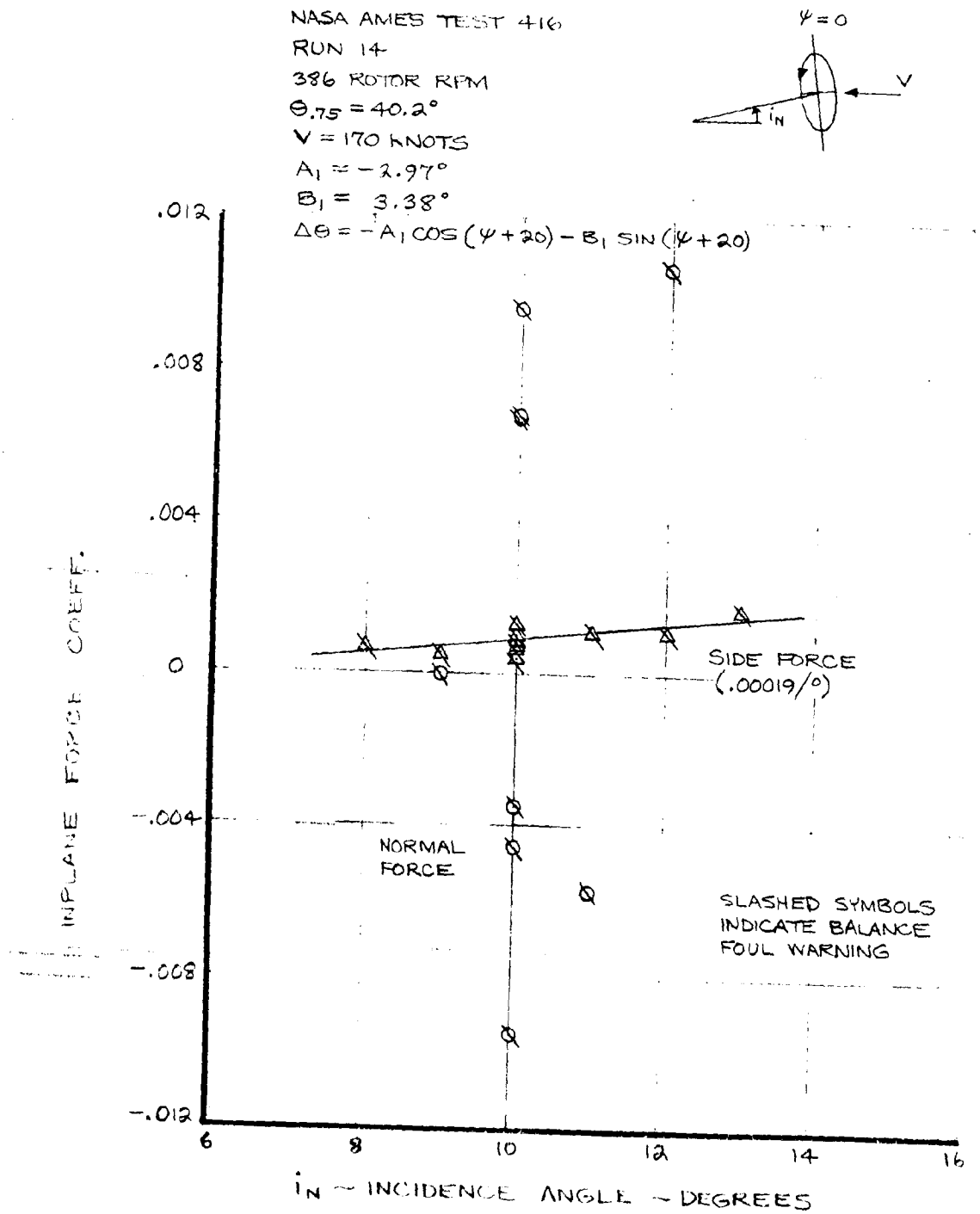

FIGURE 6-57 EFFECT OF INCIDENCE ANGLE ON HUB IN PLANE FORCES 386 RPM 170 KNOTS

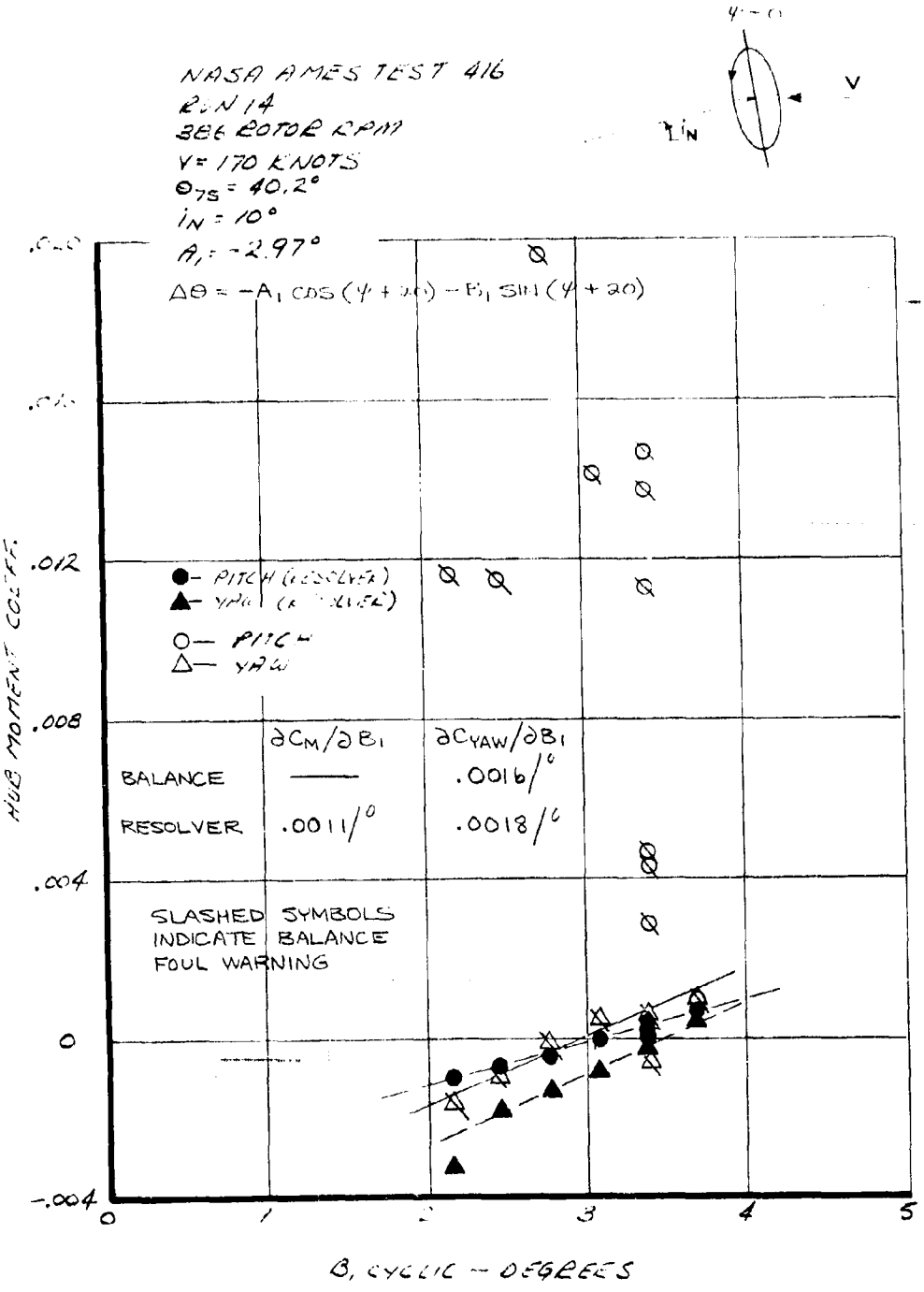

FIGURE 6-58 EFFECT OF LONGITUDINAL CYCLIC PITCH ON HUB MOMENTS 386 RPM 170 KNOTS i_N = 10°

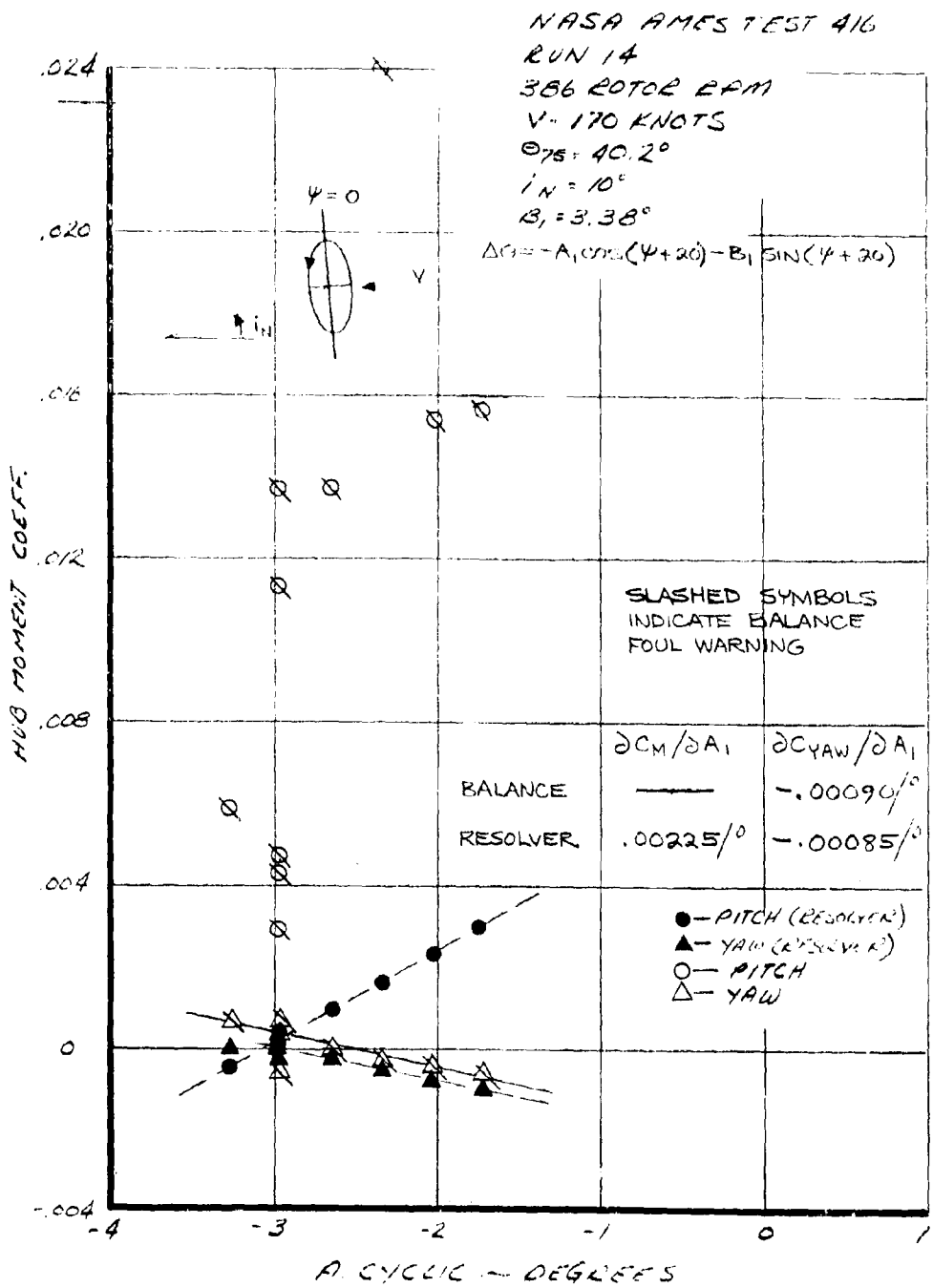

FIGURE 6-59 EFFECT OF LATERAL CYCLIC PITCH ON HUB MOMENTS
386 RPM 170 KNOTS $i_N = 10°$

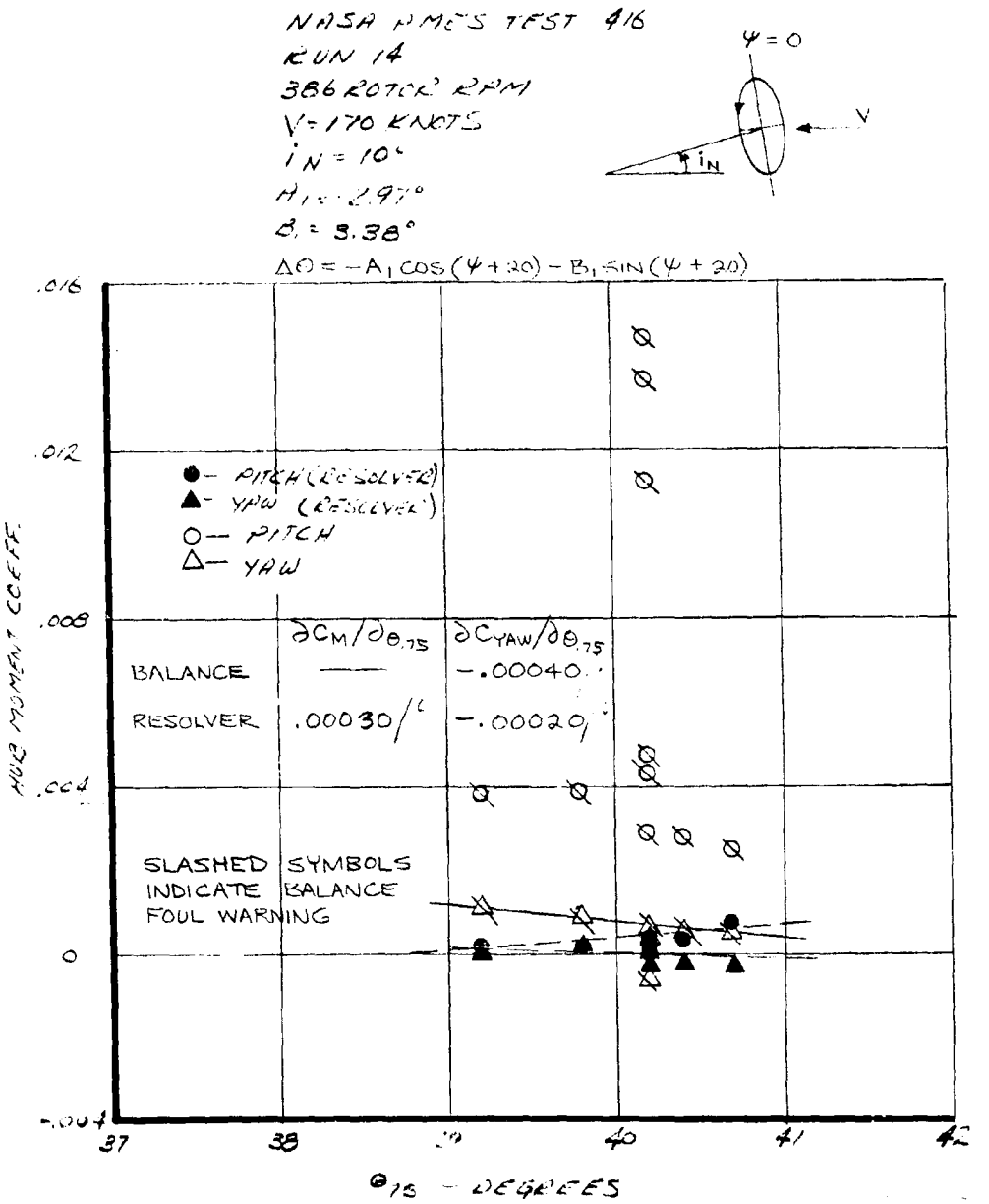

FIGURE 6-60 EFFECT OF COLLECTIVE PITCH ON HUB MOMENTS
386 RPM 170 KNOTS $i_N = 10°$

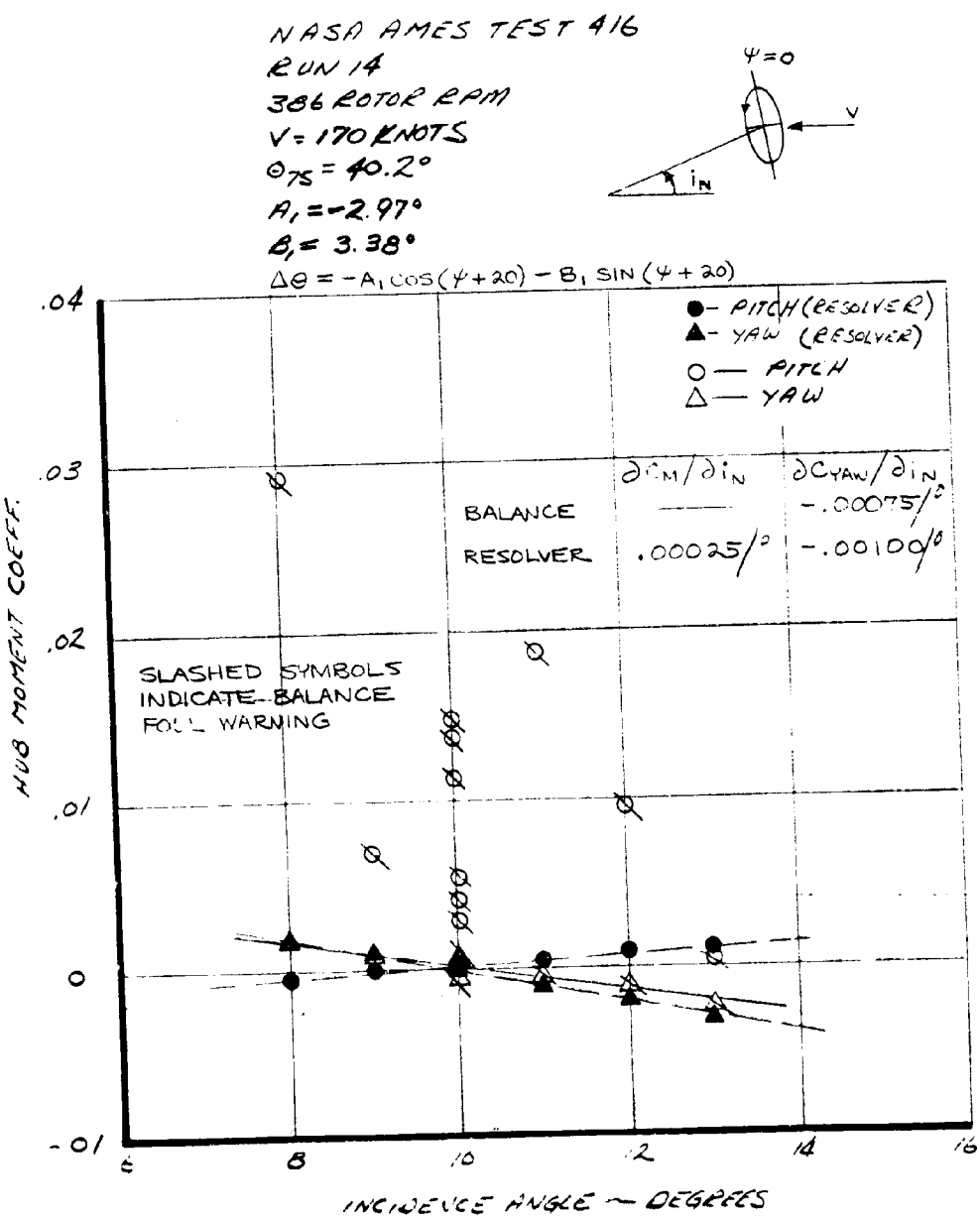

FIGURE 6-61 EFFECT OF INCIDENCE ANGLE ON HUB MOMENTS
386 RPM 170 KNOTS

6.3 Cruise Stability and Control

The data presented in this section are taken from the windmilling test (Test 410). On this test the wind tunnel balance was locked out for most of the running in order to exclude any balance dynamic effects from interfering with the wing-rotor dynamics. The investigation of the wing-rotor dynamics was the primary objective of this testing.

Forces and moments were measured at two spanwise wing stations. The locations of the measuring stations are given in Figure 2.3 and the sign convention for forces and moments shown in Figure 2.4. The sense of positive forces and moments was the same for both wing tip and wing root gages, except for wing root chord bending which is negative yaw moment in normal airplane convention. The wing and rotor are considered to be a port wing and rotor.

Effect of Angle of Attack:

In order to determine the rotor contribution to the wing forces and moments the rotors-off data was first evaluated. At the wing root station the wing was gaged to measure torsion (pitch), chord bending (yaw) and flap bending (roll). The rotor-off data is given in Figures 6-62 to 6-64. The wing root torsion data shows a derivative with angle of attack of 73.5 ft. lbs./° at 100 knots and 239 ft. lbs./° at 180 knots, showing dynamic pressure (q)

dependence as expected. The wing root flap bending shows a similar dependence in Figure 6-63, 1030 ft. lbs./degrees at 100 knots and 3350 ft. lbs./degrees at 180 knots. Wing root chord bending or (-yaw) is insensitive to angle of attack rotors-off, Figure 6-64.

The rotors-off wing tip gage data (rotors-off) is shown in Figures 6-65 to 6-67. The wing tip lift data, Figure 6-65, is the lift on the nacelle, spinner and a small portion of the wing, and is again "q" dependent giving 59 lbs./degree at 100 knots and 185 lbs./degree at 180 knots.

Wing tip yaw data (Figure 6-66) is not so well behaved. At 100 knots the data are unaffected by angle of attack. At 180 knots a blades off derivative of -42 ft. lbs./degree was obtained. This number is small by comparison with the rotor moments and the 180 knot data has been assumed (using q scaling) in analyzing the rotor on derivatives.

Wing tip pitch is not significantly affected by angle of attack blades-off and is shown in Figure 6-67.

The calibration procedure for pitch and yaw moments was such that the moments were applied at the intersection of the wing neutral axis and the rotor shaft centerline (45.58" aft of rotor disc plane). This is important to note if the wing load data are to be interpreted correctly.

The rationale for locating the yaw gage approximately 4 feet inboard, was that this position was clear of the heavy fittings associated with the shaker vane and would provide greater sensitivity than a gage with the same spanwise location as the torsion gage.

For example, the hub pitching moment due to the rotor can be derived from the equation

$$\frac{\partial PM}{\partial \alpha} = \left(\frac{\partial WTP}{\partial \alpha} - \frac{\partial WTP_{B.OFF}}{\partial \alpha}\right) - \left(\frac{\partial WTL}{\partial \alpha} - \frac{\partial WTL}{\partial \alpha}_{B.OFF}\right) \cdot \frac{45.58}{12}$$

and also

$$\frac{\partial PM}{\partial \alpha} = \left(\frac{\partial WRP}{\partial \alpha} - \frac{\partial WRP}{\partial \alpha}_{B.OFF}\right) - \left(\frac{\partial WTL}{\partial \alpha} - \frac{\partial WTL}{\partial \alpha}_{B.OFF}\right) \cdot \frac{45.58}{12}$$

The wing loads measured at 100 knots 386 RPM are given in Figures 6-68 to 6-70. The wing tip gages give a blades on pitch derivative of 450 ft. lbs./° and a wing tip lift derivative of 123.5 ft. lbs./° at 386 RPM and 100 knots. These data indicate a hub moment

$\partial PM / \partial \alpha$ = 206 Ft. Lbs./°

The wing root pitch gage (torsion) gives 520 ft. lbs./° from which a hub pitching moment of 202.5 ft. lbs./° can be derived. These data produce the rotor derivatives $\partial C_N/\partial \alpha$ = .001434/° and $\partial C_M/\partial \alpha$ = 0.000175/°.

The yaw gages are affected by hub yaw moment rotor side force, wing and nacelle drag and rotor windmilling drag. By subtracting out the blades-off derivatives and assuming that the rotor drag derivative with angle of attack is essentially zero for small angle ranges it is possible to derive a compound moment which is a function of rotor hub yaw and side force alone.

$$\frac{\partial}{\partial \alpha}\left(YAW_{HUB} + SF\ \frac{45.58}{12}\right) = \frac{\partial WTY}{\partial \alpha} - \left(\frac{\partial WTY}{\partial \alpha}\right)_{BLADES\ OFF}$$

$$= -370 - (-13) \quad \text{ft. lbs./°}$$

$$= -357 \text{ ft. lbs./°}$$

at 100 knots and 386 RPM.

The wing root chord bending derivative is of opposite sign (+ chord bending = -yaw) and shows that the rotor lateral forces relieve the wing root bending loads.

Wing load data were obtained on three separate runs of test 410 at 140 knots and the results are shown in Figures 6-71 to 6-73.

The wing root torsion data and wing tip loft Figure 6-72 imply a rotor hub pitching moment derivative of 211 ft. lbs./°. The hub derivative obtained from the tip pitch gage is 220 ft. lbs./°. The normal force from the rotor is the difference between wing tip lift (rotor on - rotors off) and indicates 141 lbs./° at 140 knots 386 RPM. These rotor derivatives in non-dimensional form are

$$\partial C_M/\partial \alpha = .000183/°$$

$$\partial C_N/\partial \alpha = .00164/°$$

Also from Figure 6-73

$$\frac{\partial}{\partial \alpha}\left(YAW + SF\ \frac{45.58}{12}\right)_{HUB} = -820 - (-25.4)$$

$$= -794.6 \text{ ft. lbs./°}$$

Runs 15 and 58, Test 410, provided angle of attack data at 192 knots and this information is plotted in Figures 6-74 to 6-76.

The rotor hub moment (pitch) derived from these data give 190 ft. lbs./° based on the tip pitch gage and 195.5 ft. lbs./° based on the wing root torsion gage. The rotor normal force is obtained from the wing tip lift and equals 331 lbs./°. These derivatives non-dimensionalized give $\partial C_M/\partial$ = .000165/°

$\partial C_N/\partial$ = 0.00384/°

The yaw moment derivative

$$\left(\text{YAW} + \text{SF} \frac{45.58}{12} \right) = -1625 \text{ ft. lbs./°} - (47.8)$$

$$= -1577.2 \text{ ft. lbs./°}$$

The rotor derivatives deduced from the wing load data are summarized in Figure 6-77. The pitching moment derivatives are positive (nose up) but decrease slightly as airspeed increases. The normal force derivative increases as airspeed increases. The rate at which the normal force derivative increases is less than airspeed squared. The compound moment of rotor hub yaw and side force is negative and increases almost linearly as airspeed increases.

Angle of attack wing loads were obtained at four airspeeds at off design RPM. The data shown in Figures 6-78 to 6-80 were taken at 190 knots and 445 RPM. The effect of increasing the RPM is to

slightly reduce the rotor normal force and the wing tip lift gage indicates 115 lbs./° compared with 123.5 lbs./° at 386 RPM.

The tip pitching moment and the root pitching moment show reductions (424 ft. lbs./° at 445 RPM, 450 ft. lbs./° at 386 RPM wing tip pitch) (490 ft. lbs./° at 445 RPM and 520 ft. lbs./° at 386 RPM). Wing root flap bending is reduced to 1620 ft. lbs./° from 1730 ft. lbs./° at 386 RPM. This reduction is due to the 8.5 lbs./° normal force as the root flap bending gage is located 12.55 ft. inboard of the rotor shaft. The wing tip yaw derivative is reduced to -234 ft. lbs./° compared with -370 ft. lbs./° at 386 RPM.

At 140 knots an angle of attack sweep was done at 420 RPM and resulted in the data shown in Figures 6-81 to 6-83. The wing tip lift is reduced by the increased RPM and results in increases in wing tip pitch, wing root pitch and wing vertical bending compared with the data at 386 RPM, Figures 6-71 to 6-73.

Figures 6-84 through 6-89 are similar data at 170 knots 400 RPM and 192 knots 450 RPM respectively.

NASA - AMES 40'x80' TEST 410

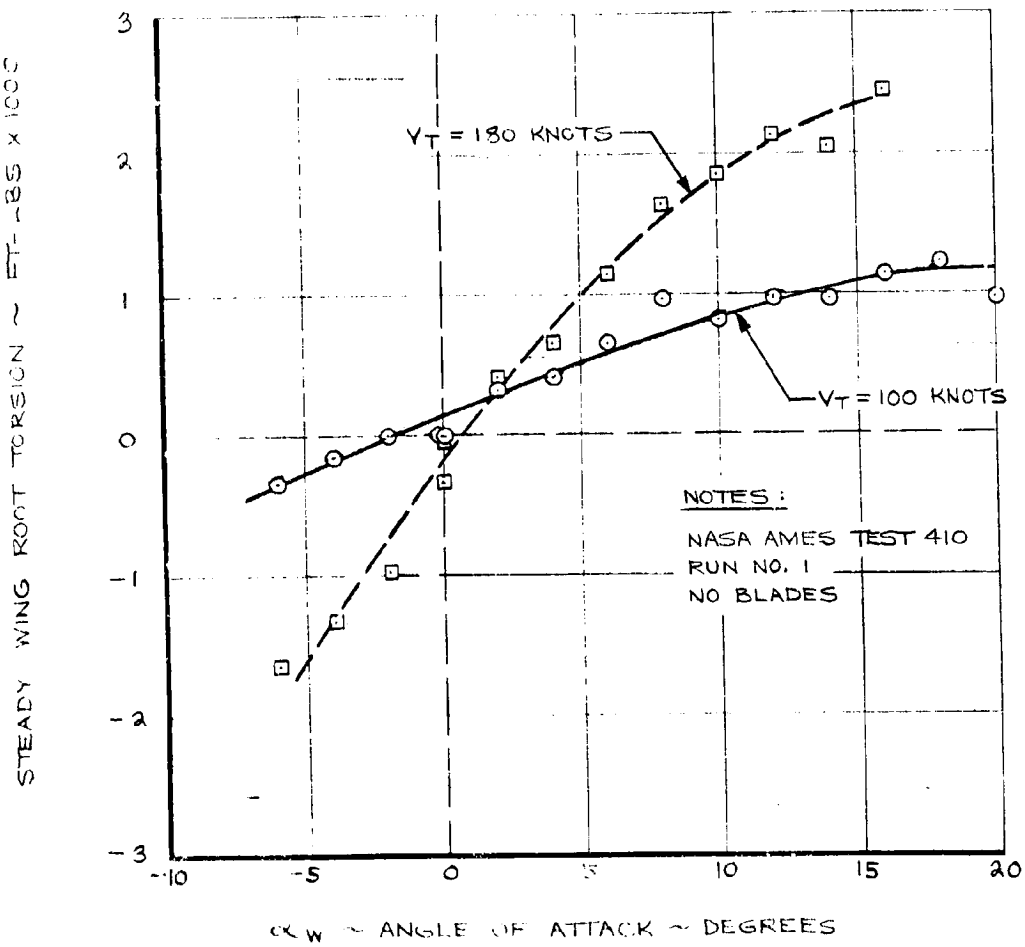

FIGURE 6.6X STEADY WING ROOT TORSION DUE TO ANGLE OF ATTACK. BLADES OFF

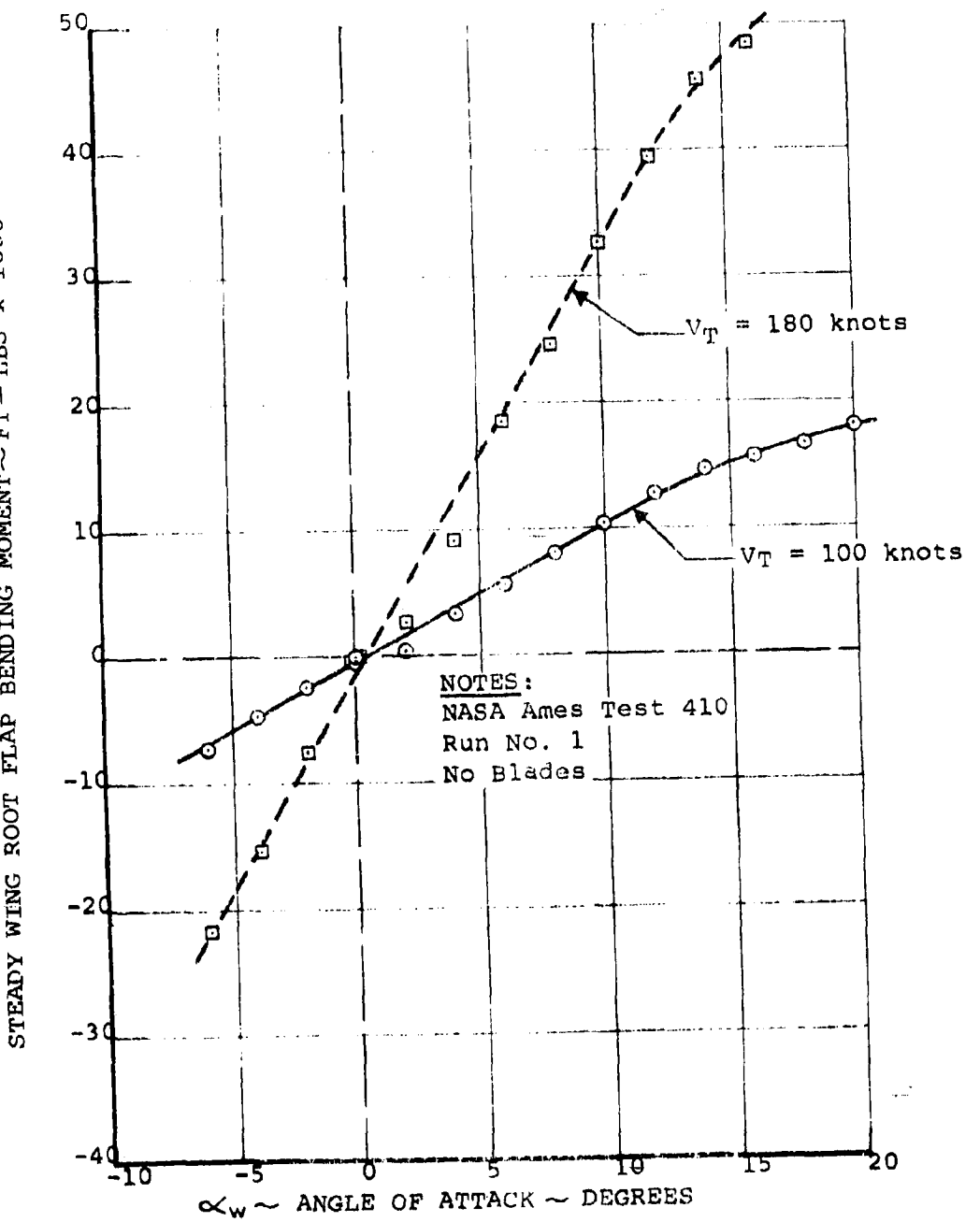

FIGURE 6.63 STEADY WING ROOT FLAP BENDING DUE TO ANGLE OF ATTACK. BLADES OFF

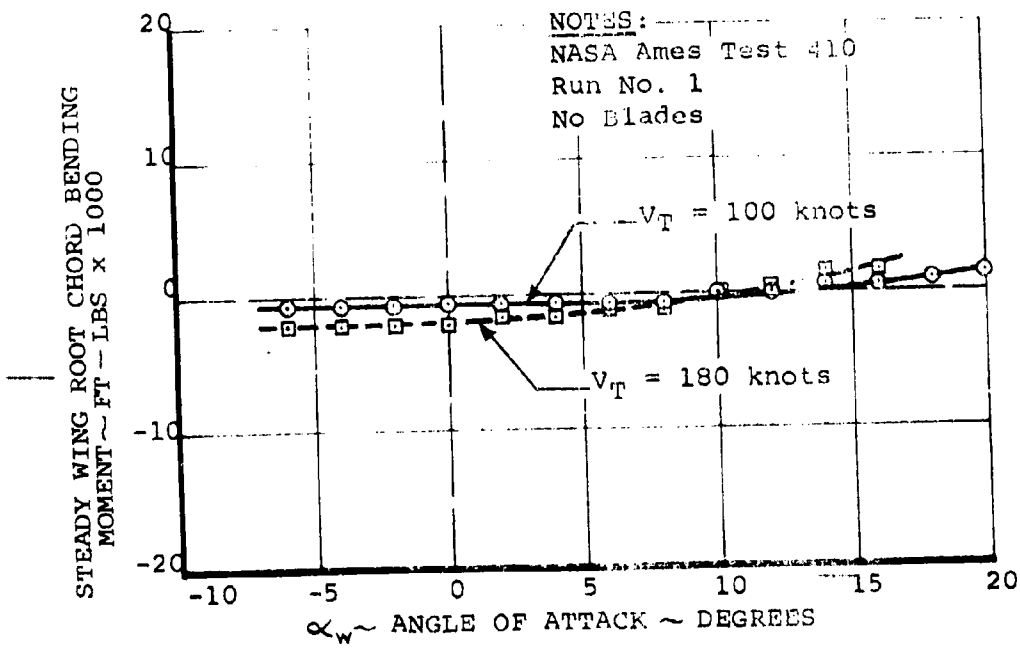

FIGURE 6.64 STEADY WING ROOT CHORD BENDING DUE TO ANGLE OF ATTACK. BLADES OFF

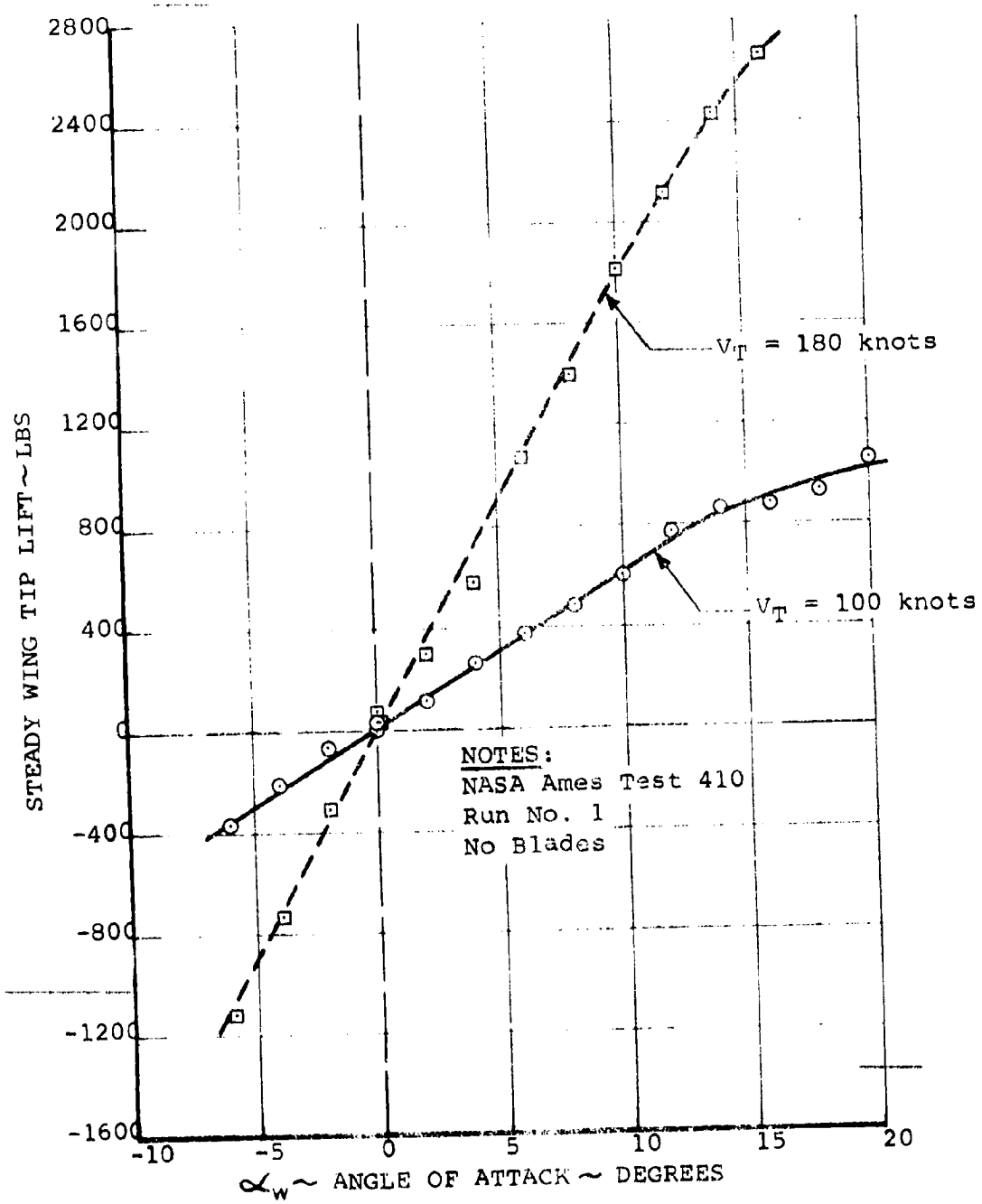

FIGURE 6.65 STEADY WING TIP LIFT DUE TO ANGLE OF ATTACK. BLADES OFF

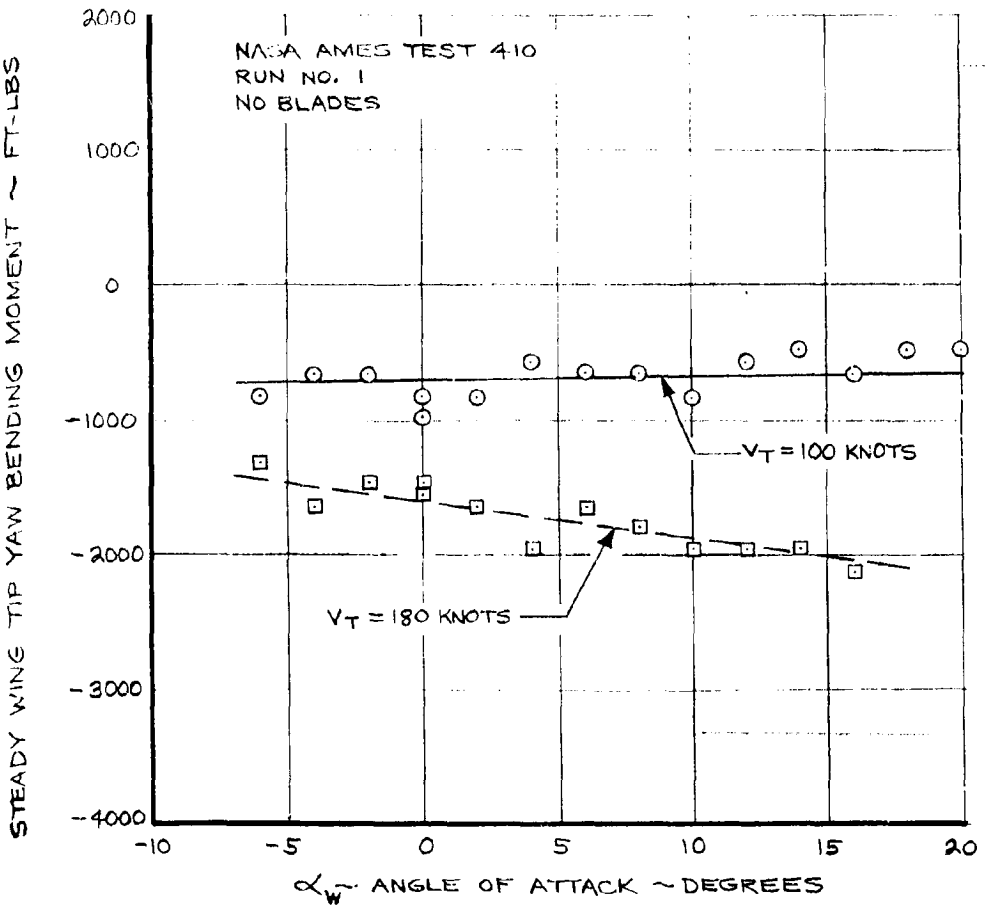

FIGURE 6.66 STEADY WING TIP YAW BENDING DUE TO ANGLE OF ATTACK. BLADES OFF

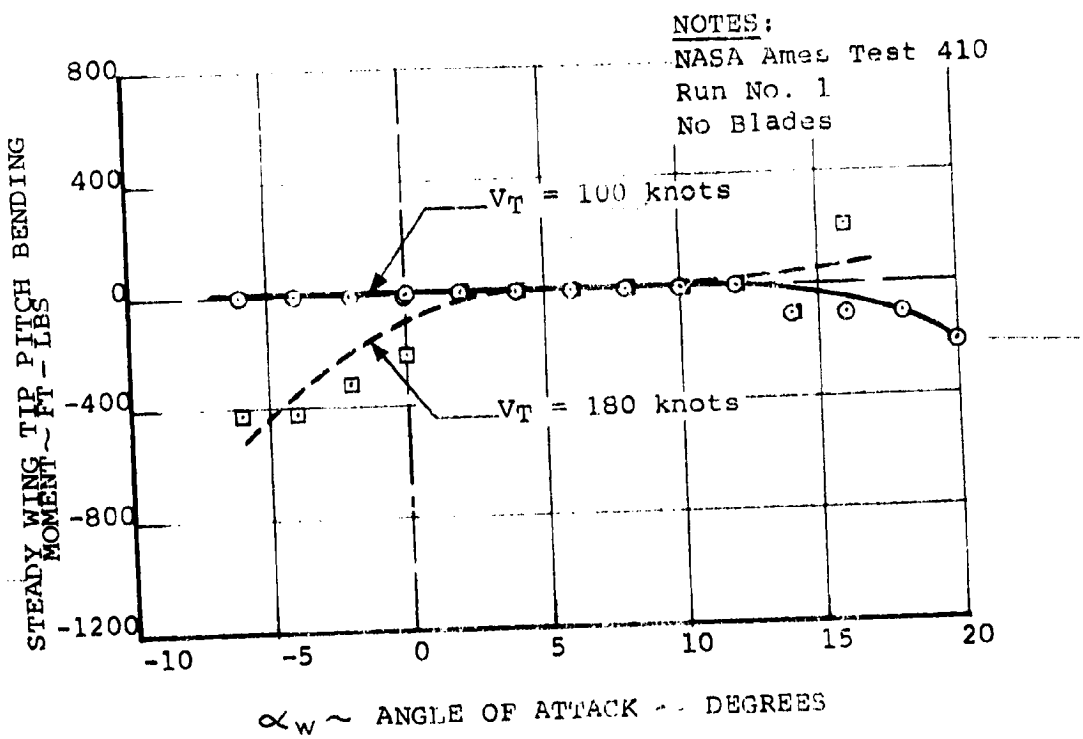

FIGURE 6.67 STEADY WING TIP PITCH MOMENT DUE TO ANGLE OF ATTACK. BLADES OFF

NASA AMES TEST 410

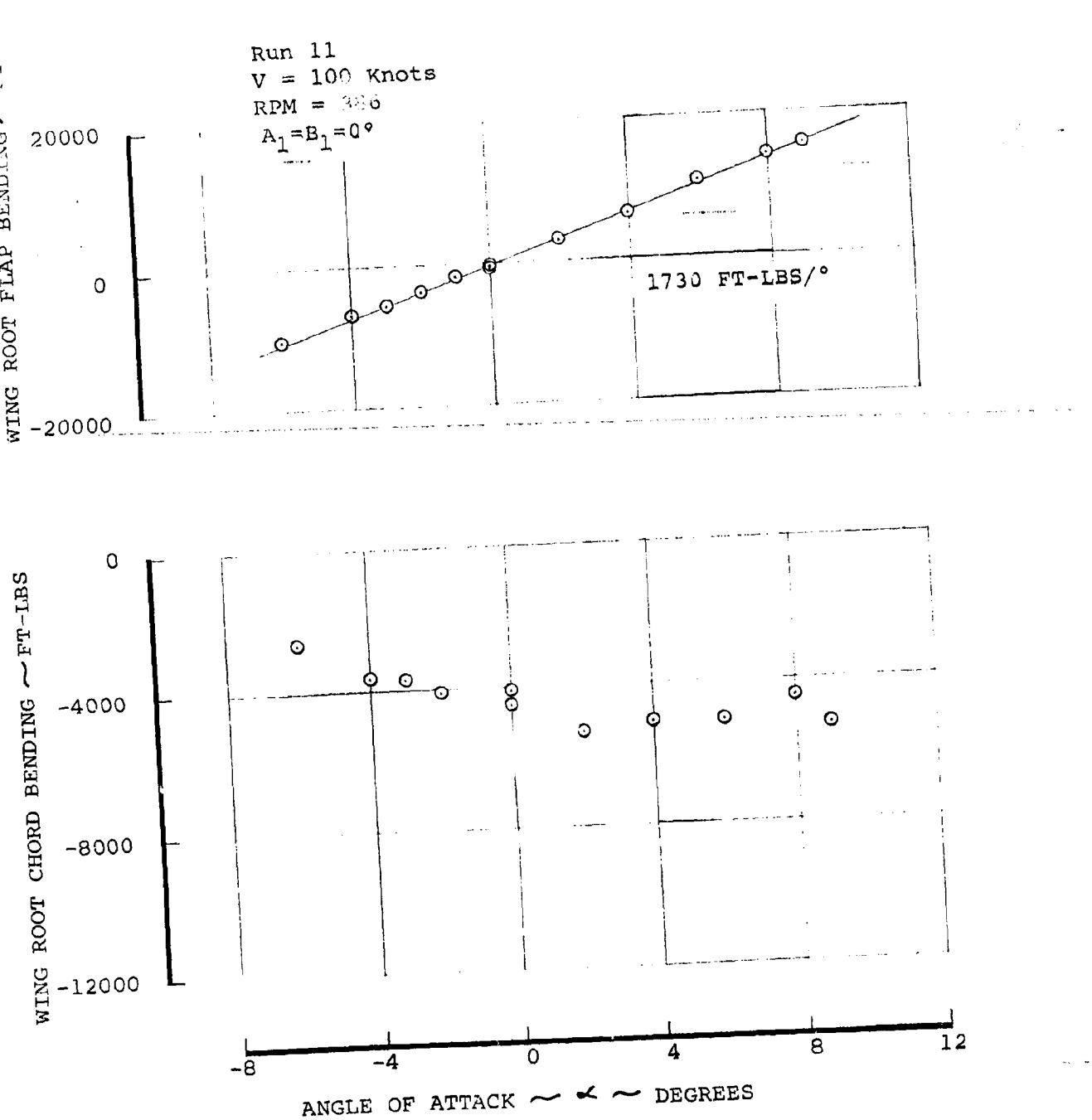

FIGURE 6.68 STEADY WING ROOT FLAP BENDING AND STEADY WING ROOT CHORD BENDING DUE TO ANGLE OF ATTACK. 100 KNOTS 386 RPM

NASA AMES TEST 410

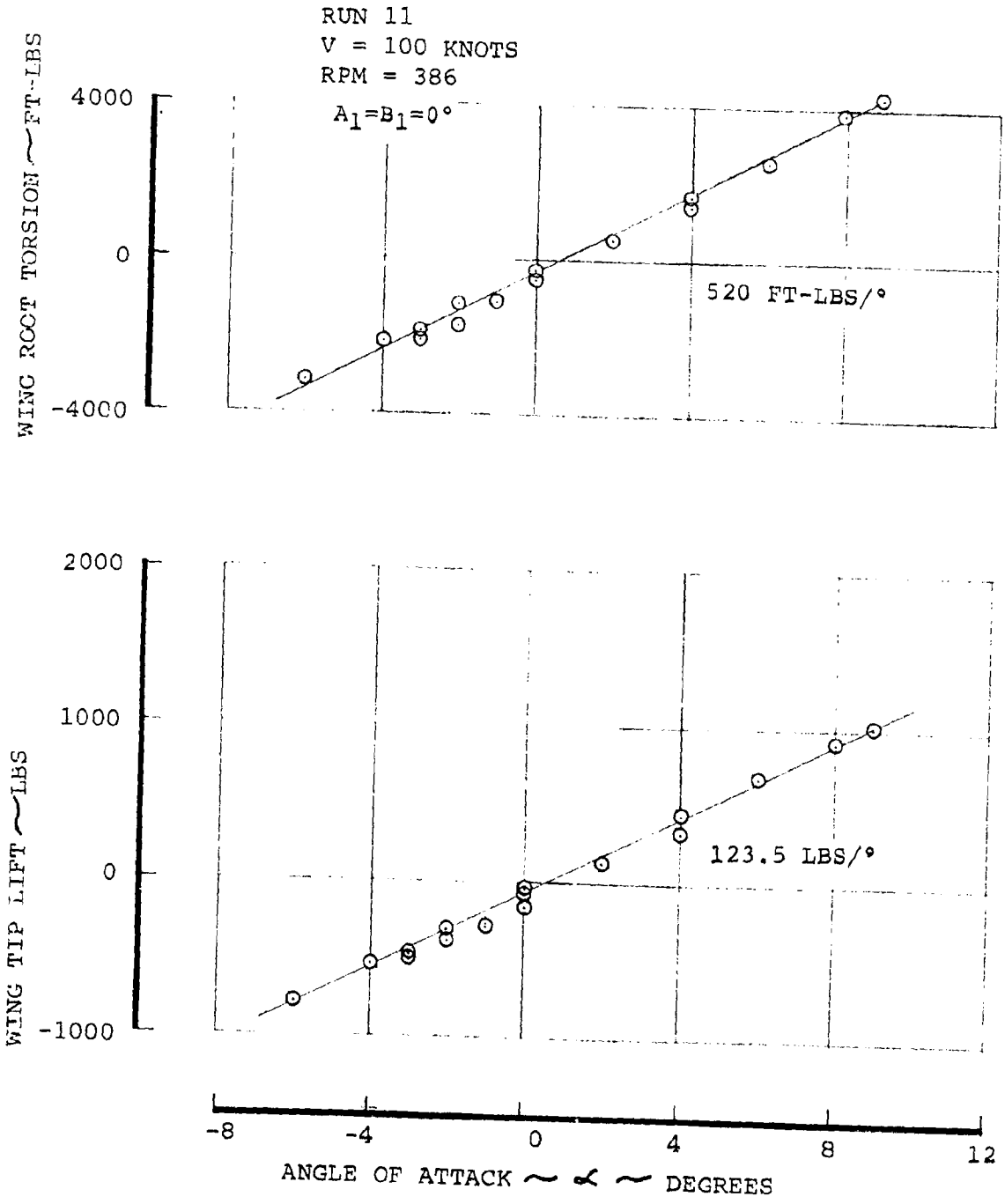

FIGURE 6.69 STEADY WING ROOT TORSION AND STEADY WING TIP LIFT DUE TO ANGLE OF ATTACK.
100 KNOTS 386 RPM

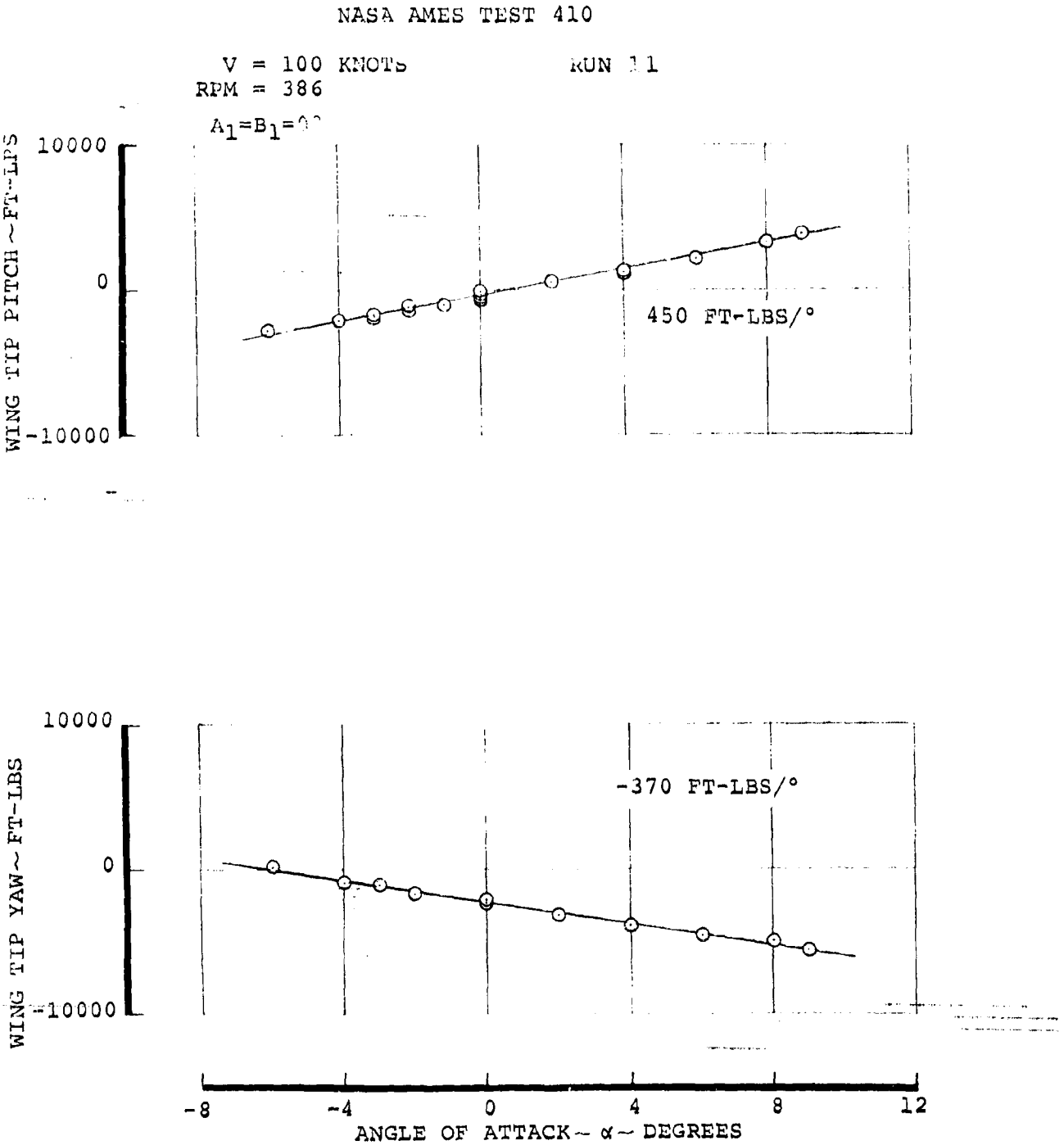

FIGURE 6.70 STEADY WING TIP PITCH AND STEADY WING TIP YAW DUE TO ANGLE OF ATTACK.
100 KNOTS 386 RPM

NASA AMES TEST 410

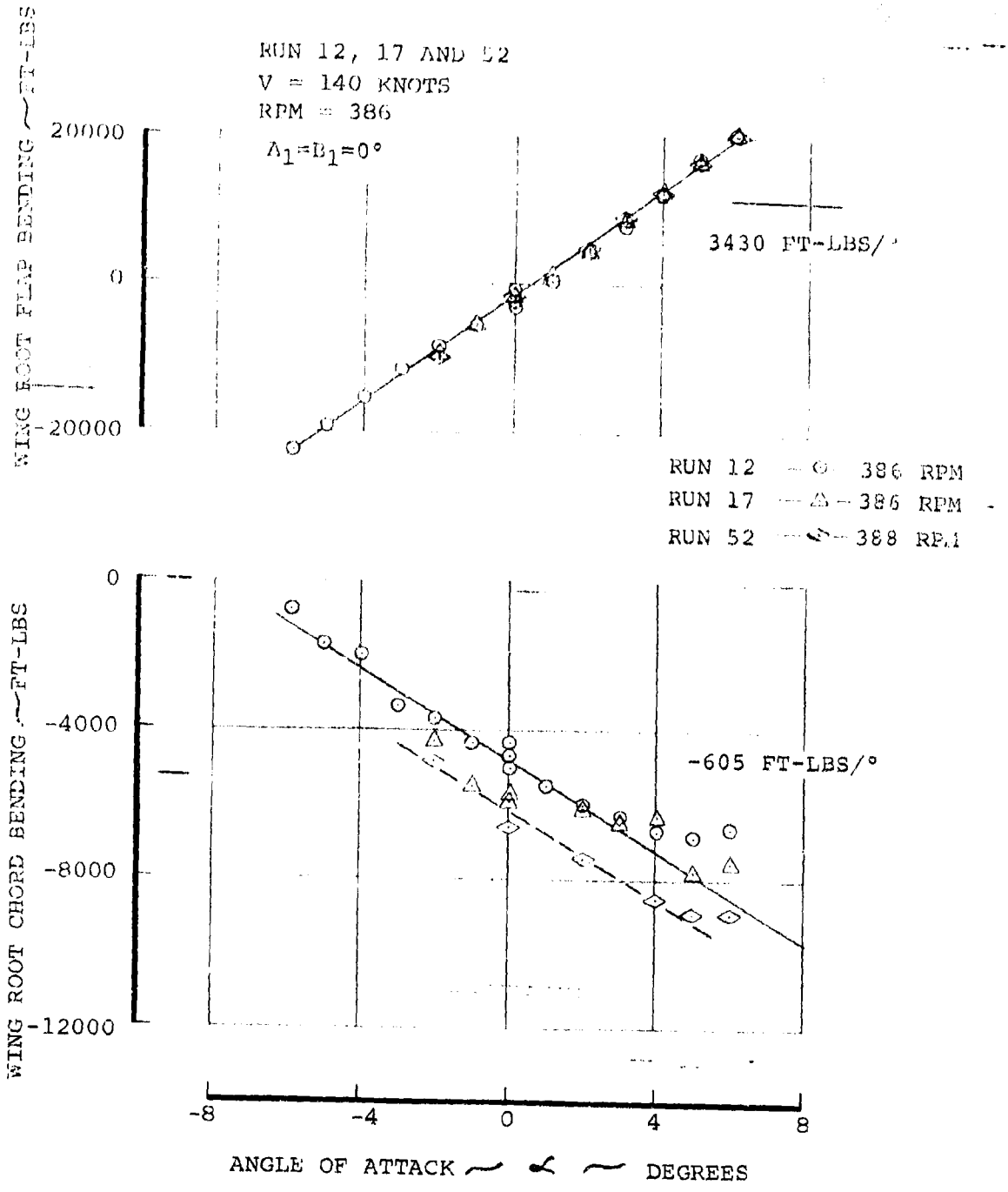

FIGURE 6-71 EFFECT OF ANGLE OF ATTACK ON STEADY WING ROOT FLAP AND CHORD BENDING. 140 KNOTS 386 RPM.

NASA AMES TEST 410

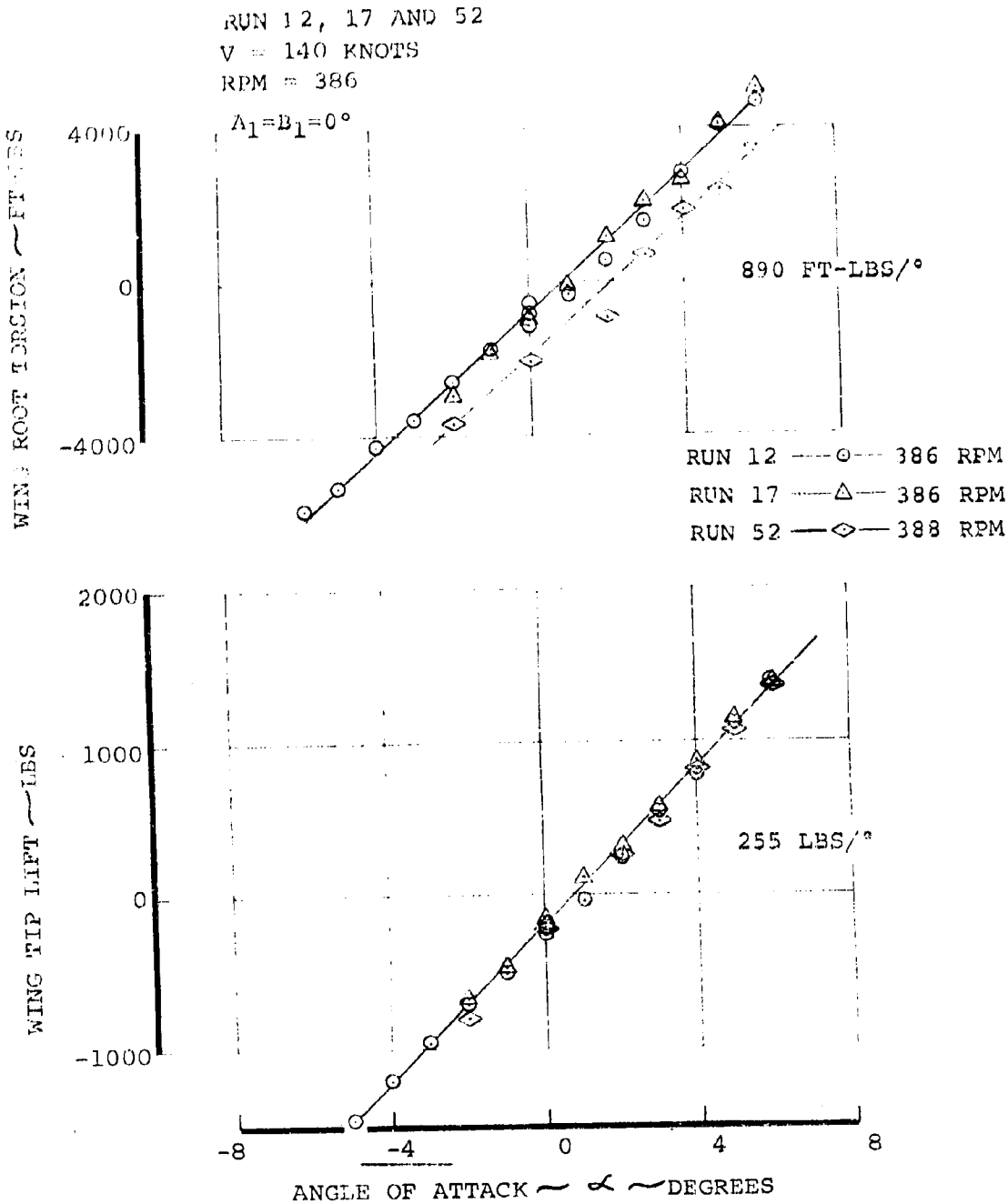

FIGURE 6-72 EFFECT OF ANGLE OF ATTACK ON STEADY WING ROOT TORSION AND STEADY WING TIP LIFT. 140 KNOTS 386 RPM.

NASA AMES TEST 410

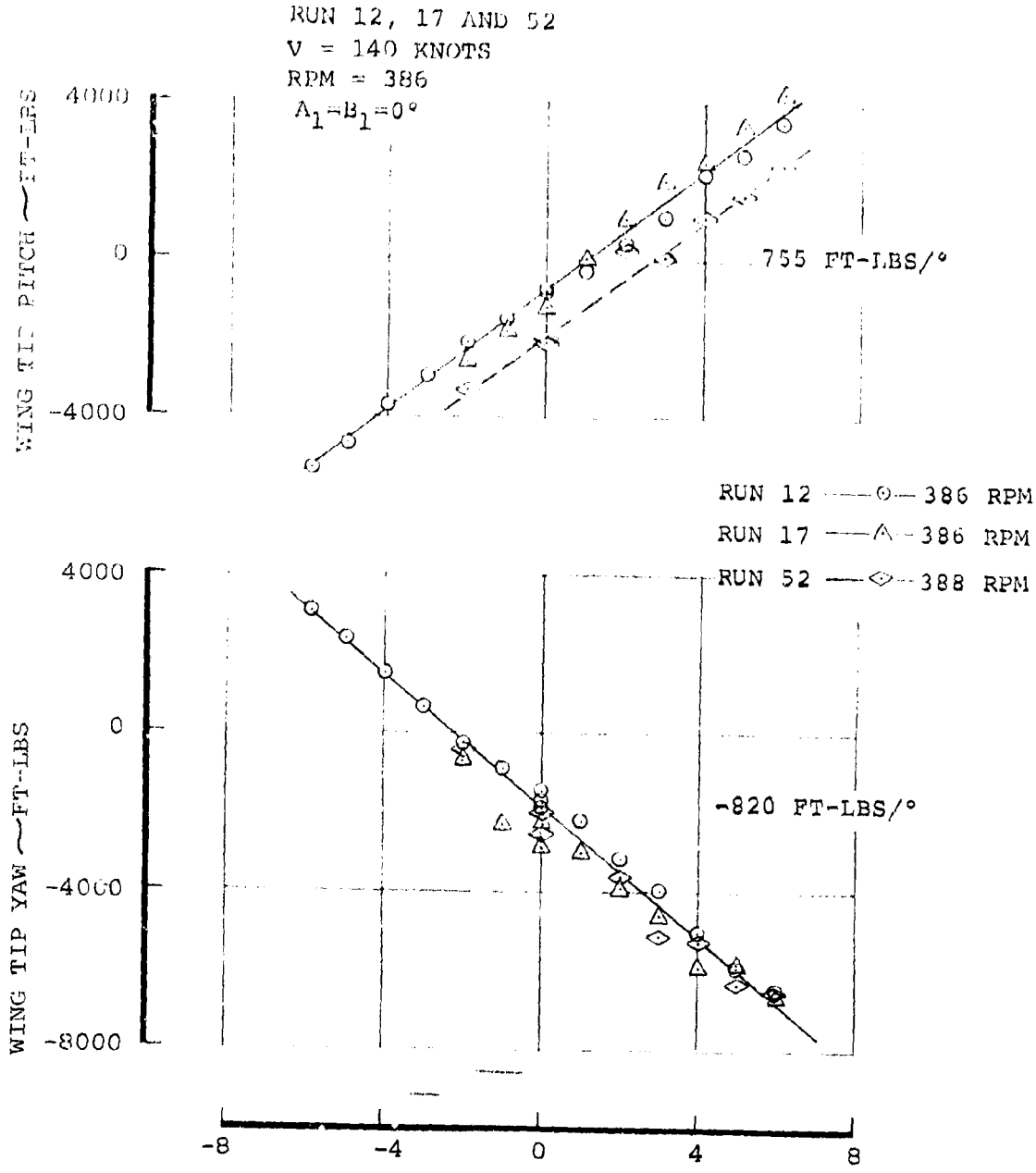

FIGURE 6-73 EFFECT OF ANGLE OF ATTACK ON STEADY WING TIP PITCH AND YAW MOMENT. 140 KNOTS 386 RPM

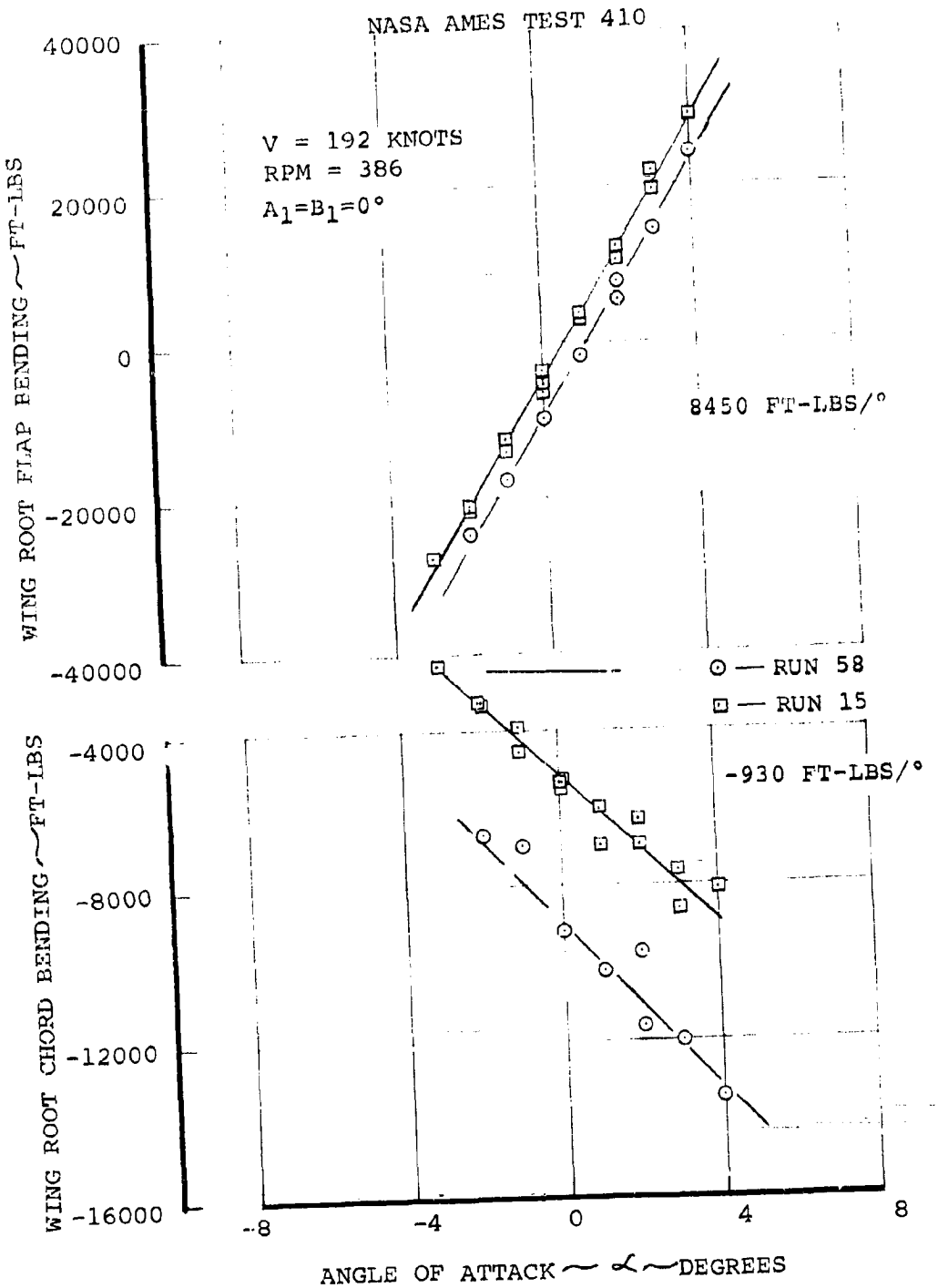

FIGURE 6.74 STEADY WING ROOT FLAP BENDING AND STEADY WING ROOT CHORD BENDING DUE TO ANGLE OF ATTACK. 192 KNOTS 386 RPM.

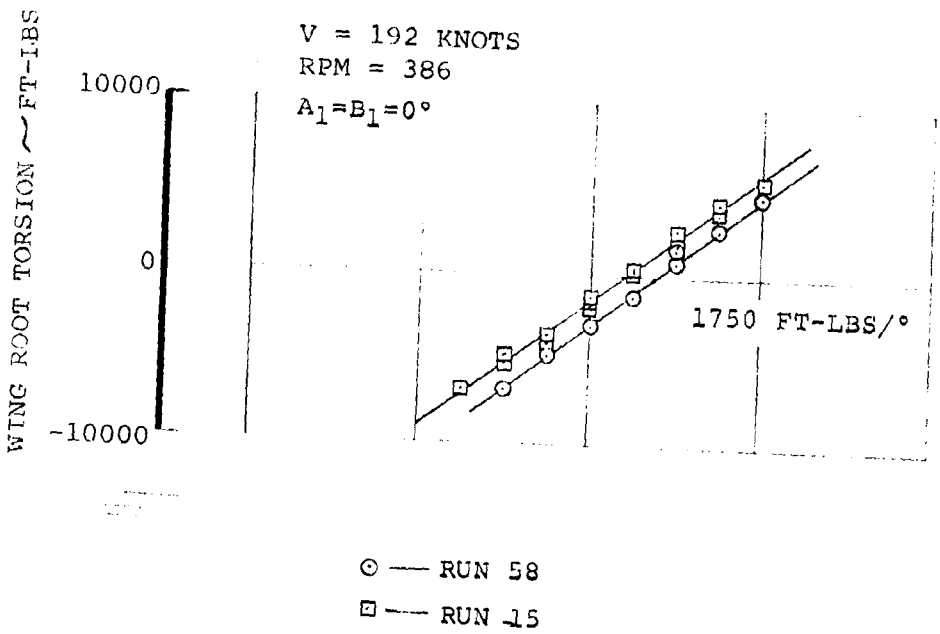

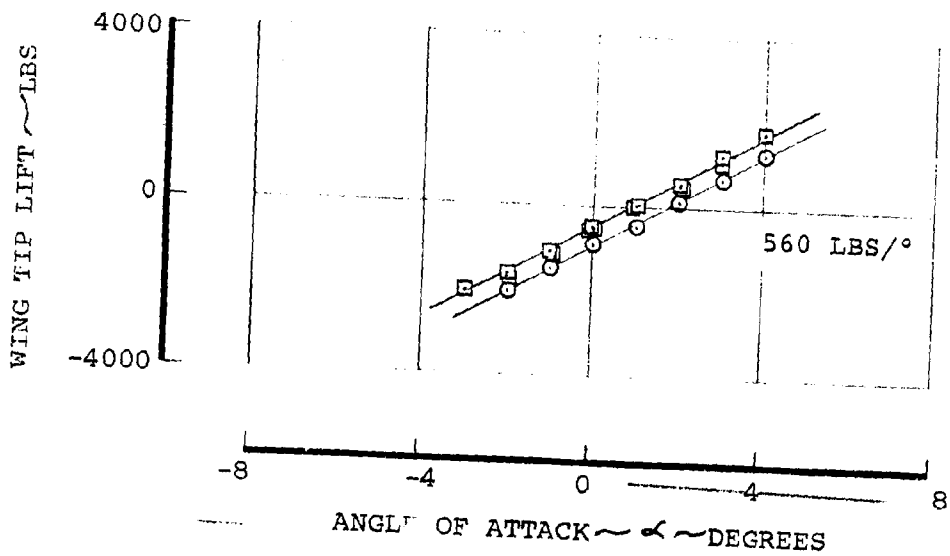

FIGURE 6.75 STEADY WING ROOT TORSION AND STEADY WING TIP LIFT DUE TO ANGLE OF ATTACK.
192 KNOTS 386 RPM

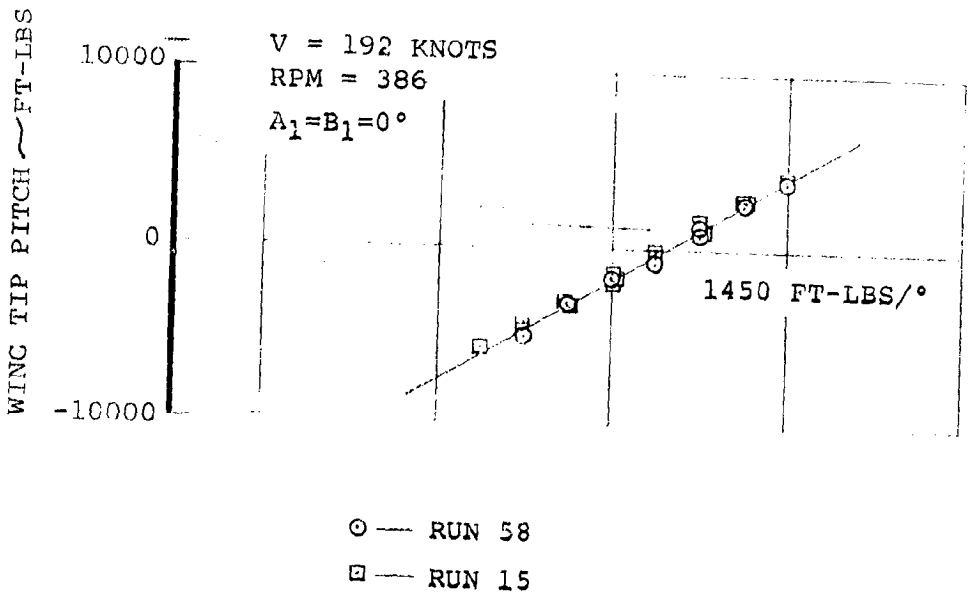

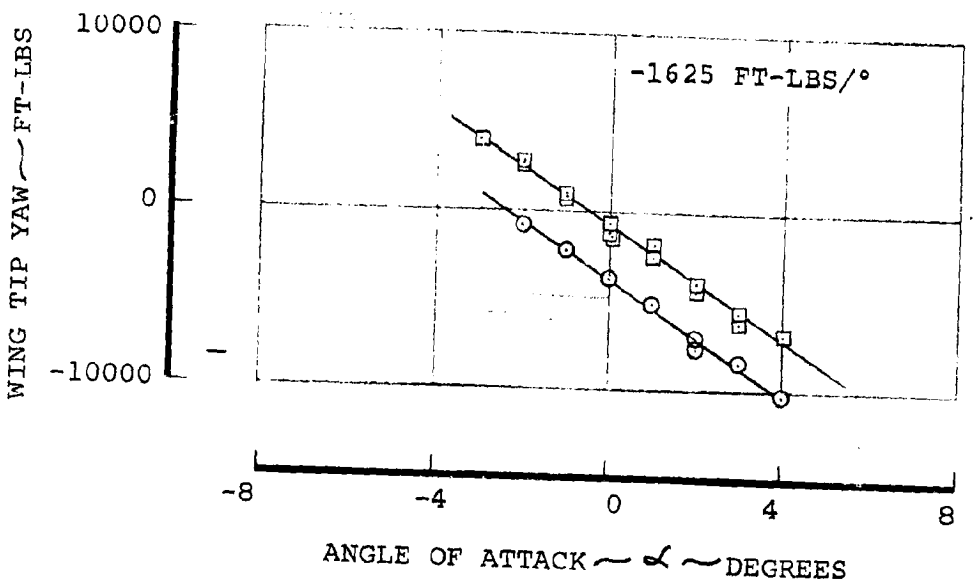

FIGURE 6.76 STEADY WING TIP PITCH AND STEADY WING TIP YAW DUE TO ANGLE OF ATTACK. 192 KNOTS 386 RPM.

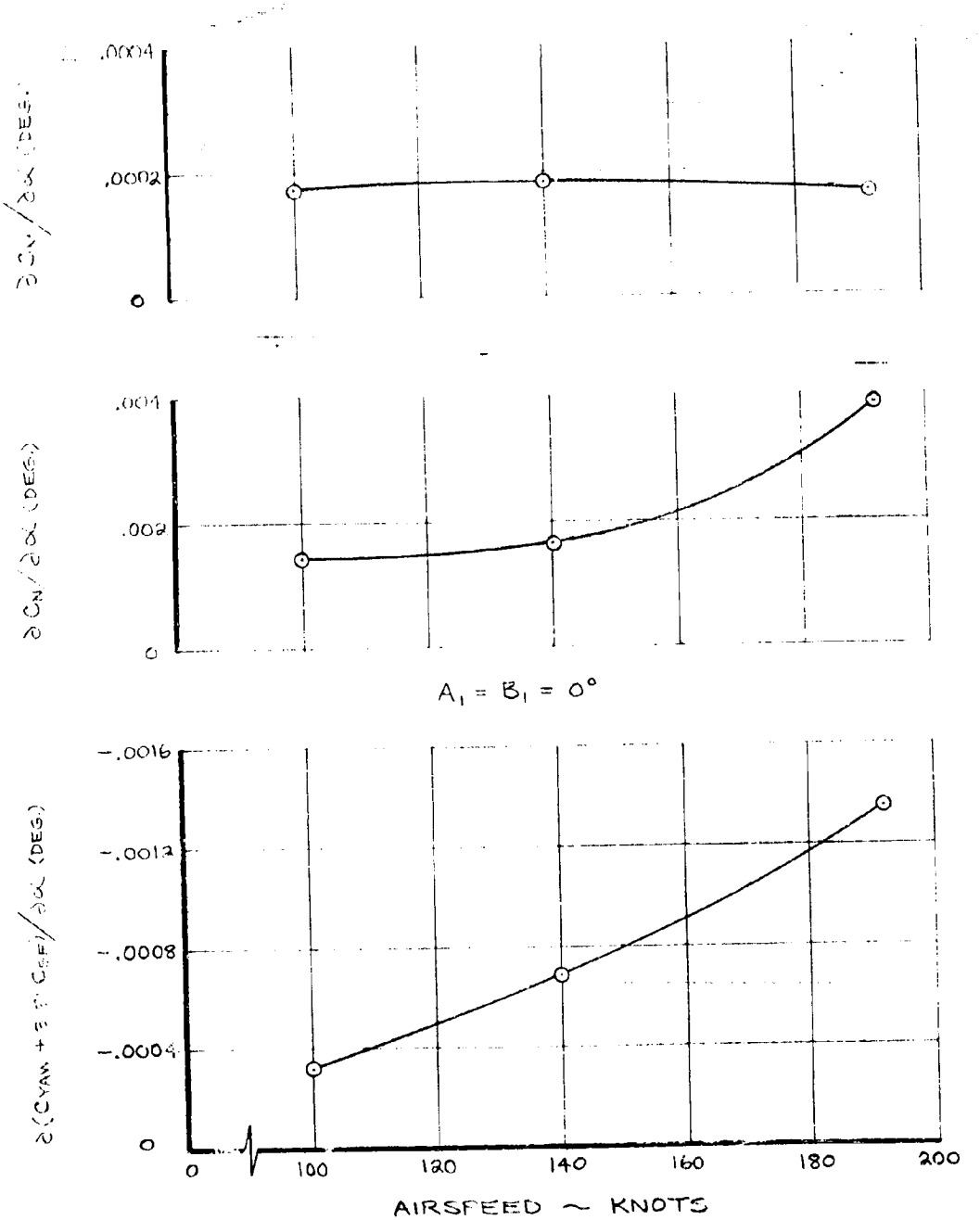

FIGURE 6.77 SUMMARY OF WINDMILLING ROTOR DERIVATIVES IN CRUISE. 386 RPM

N. ES TEST 410

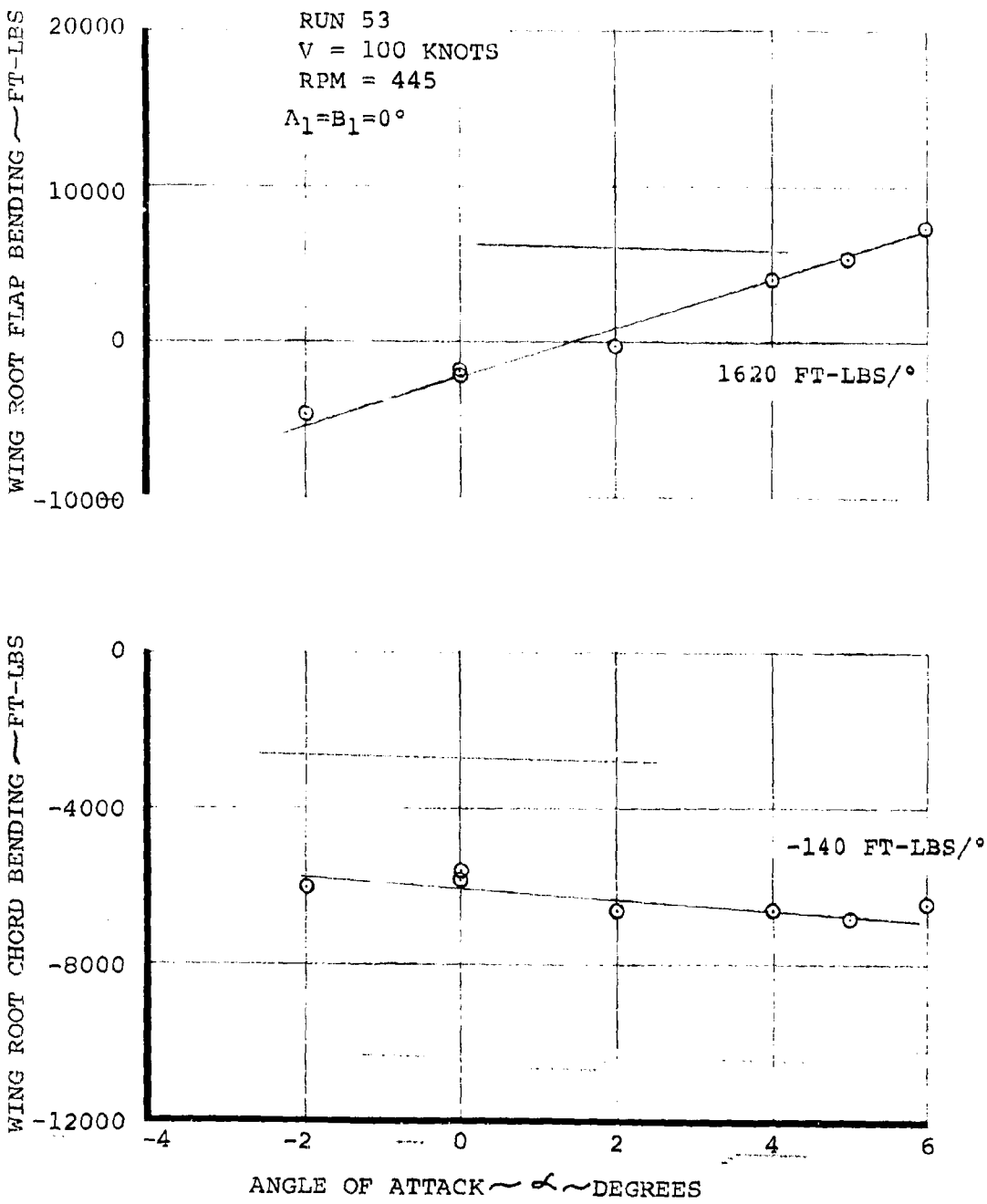

FIGURE 6-78 EFFECT OF ANGLE OF ATTACK ON STEADY WING ROOT FLAP AND CHORD BENDING 100 KNOTS 445 RPM

NASA AMES TEST 410

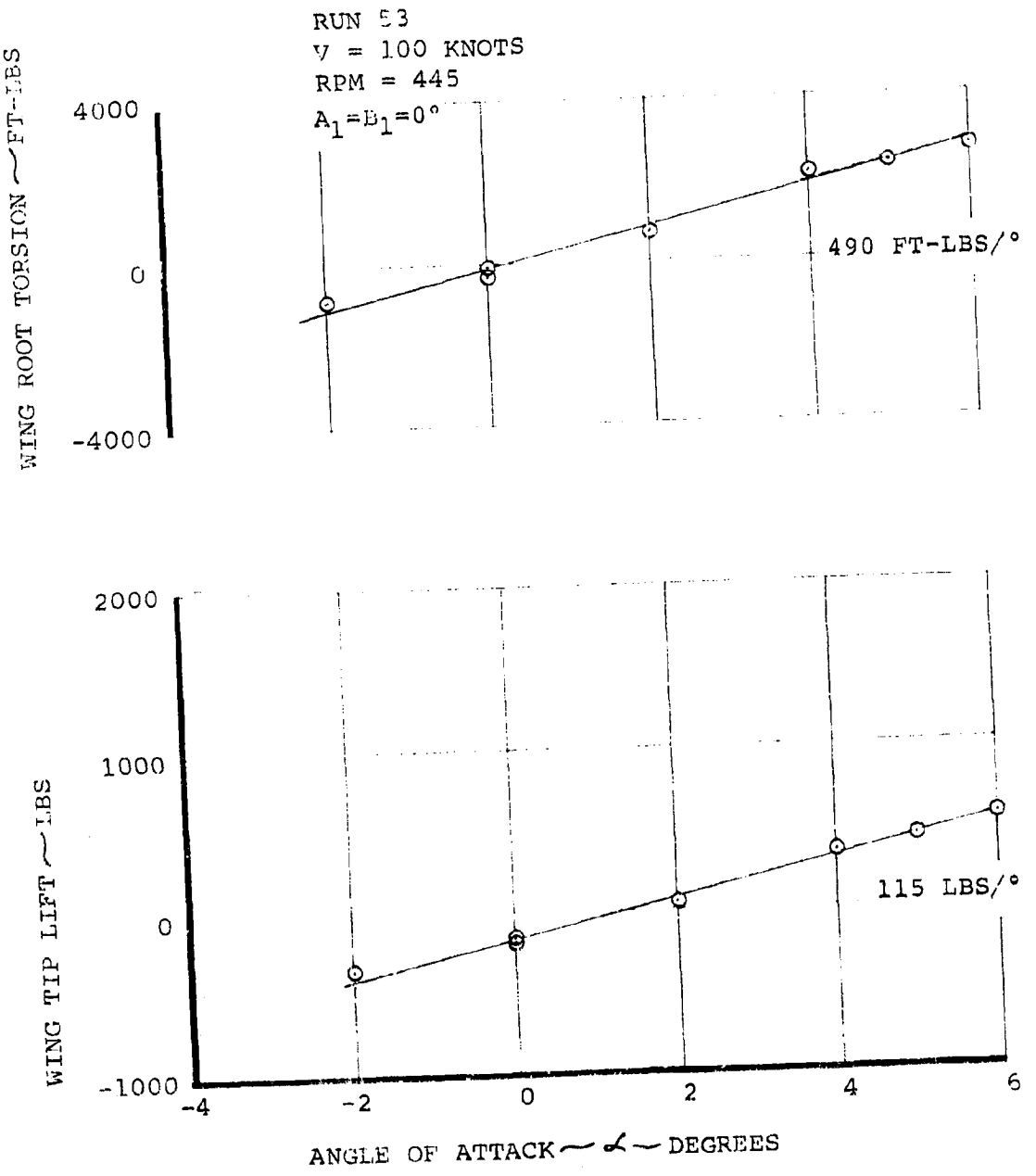

FIGURE 6-79 EFFECT OF ANGLE OF ATTACK ON STEADY WING ROOT TORSION AND WING TIP LIFT 100 KNOTS 445 RPM

NASA AMES TEST 410

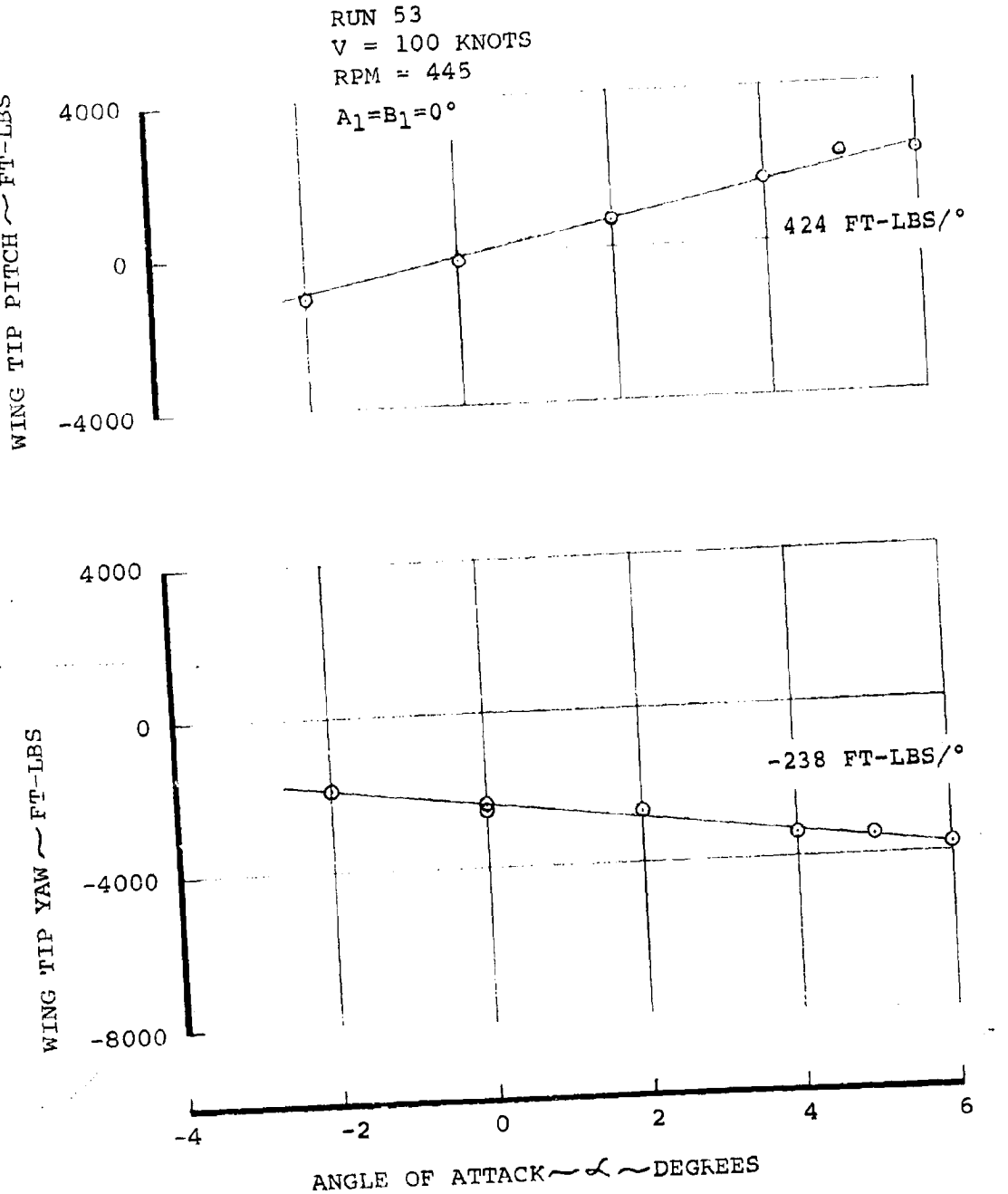

FIGURE 6-80 EFFECT OF ANGLE OF ATTACK ON STEADY WING TIP PITCH AND YAW MOMENT 100 KNOTS 445 RPM

NASA AMES TEST 410

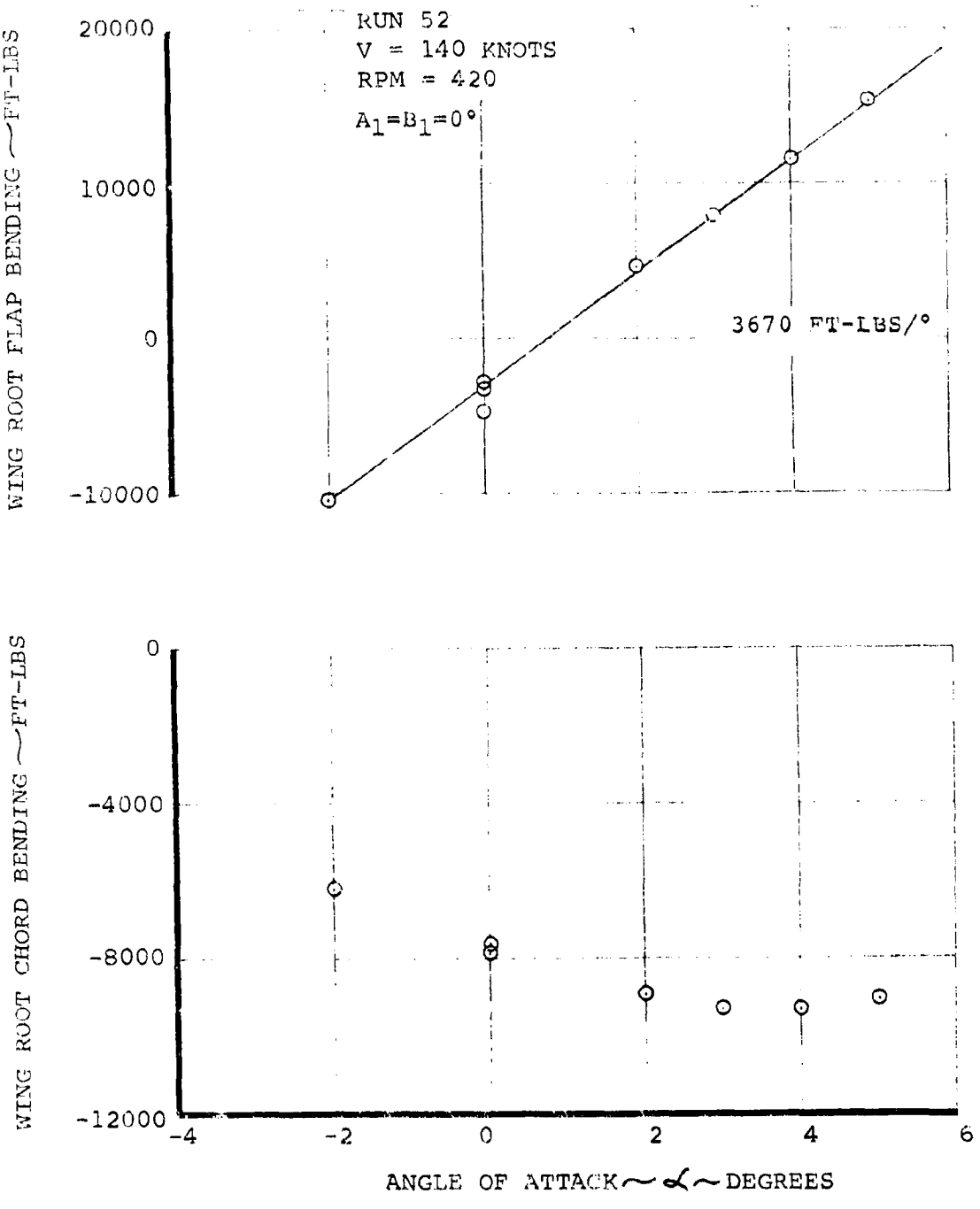

FIGURE 6-81 EFFECT OF ANGLE OF ATTACK ON STEADY WING ROOT FLAP AND CHORD BENDING 140 KNOTS 420 RPM

NASA AMES TEST 410

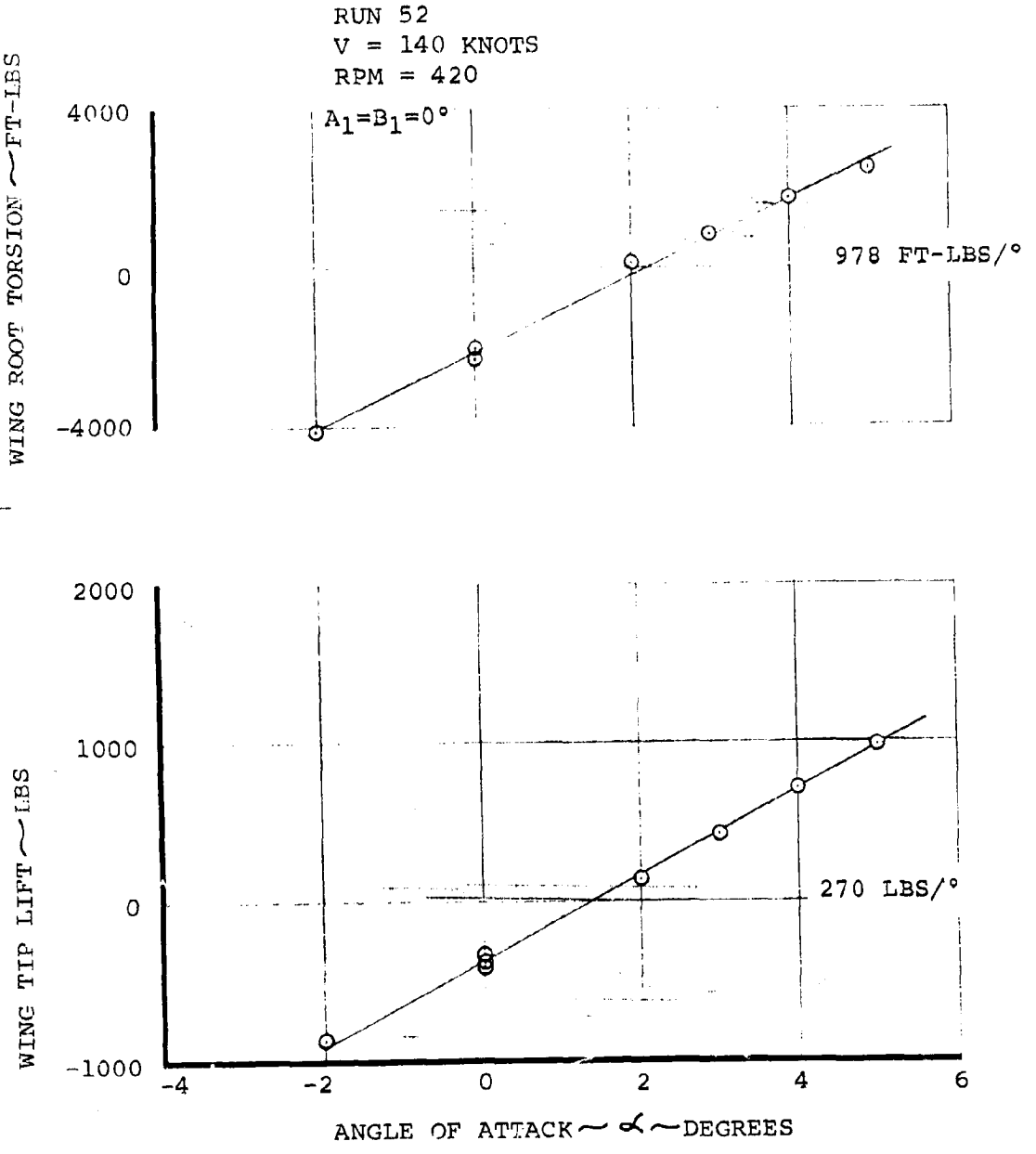

FIGURE 6-82 EFFECT OF ANGLE OF ATTACK ON STEADY WING ROOT TORSION AND WING TIP LIFT 140 KNOTS 420 RPM

NASA AMES TEST 410

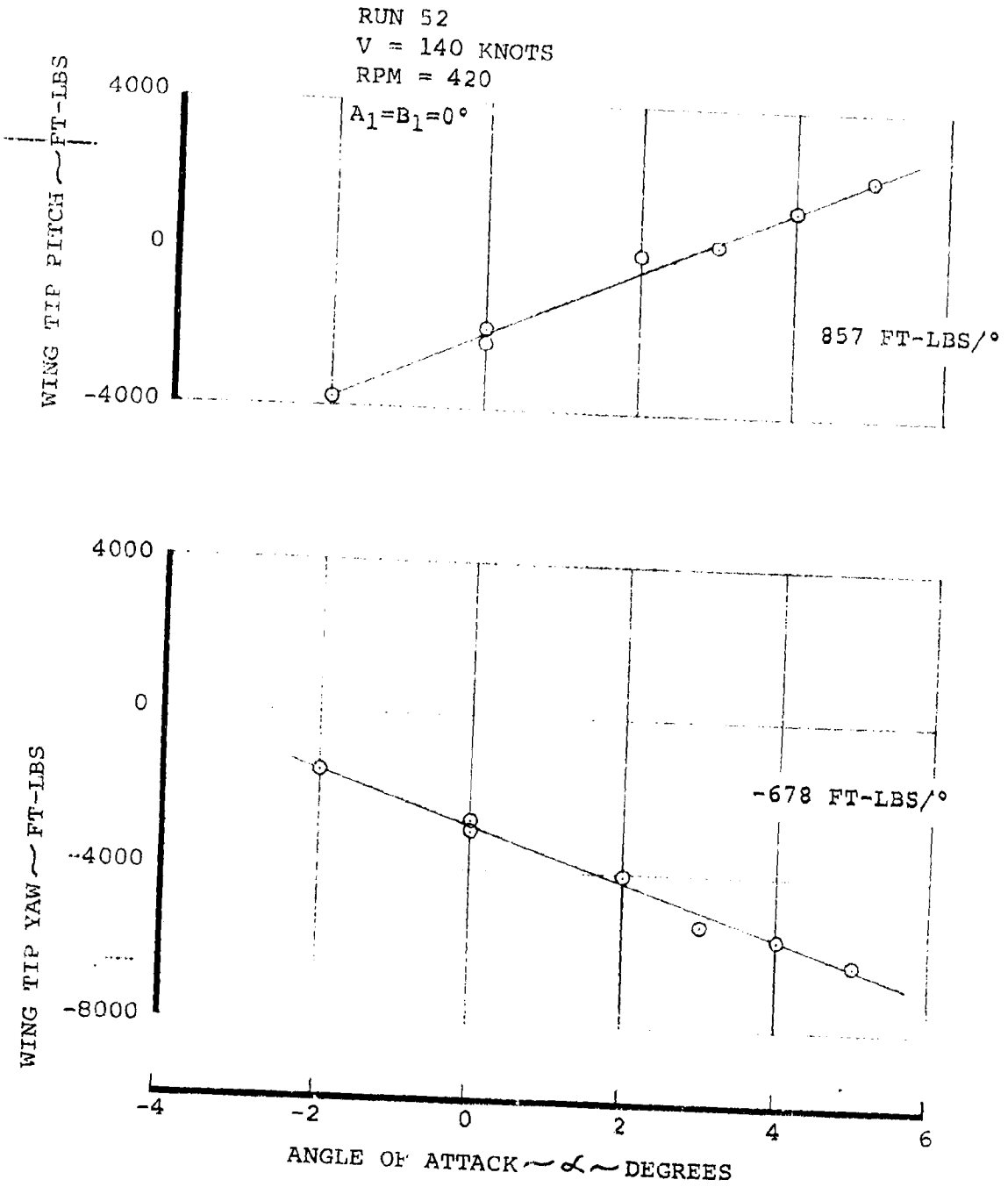

FIGURE 6-83 EFFECT OF ANGLE OF ATTACK ON STEADY WING TIP PITCH AND YAW MOMENT 140 KNOTS 420 RPM

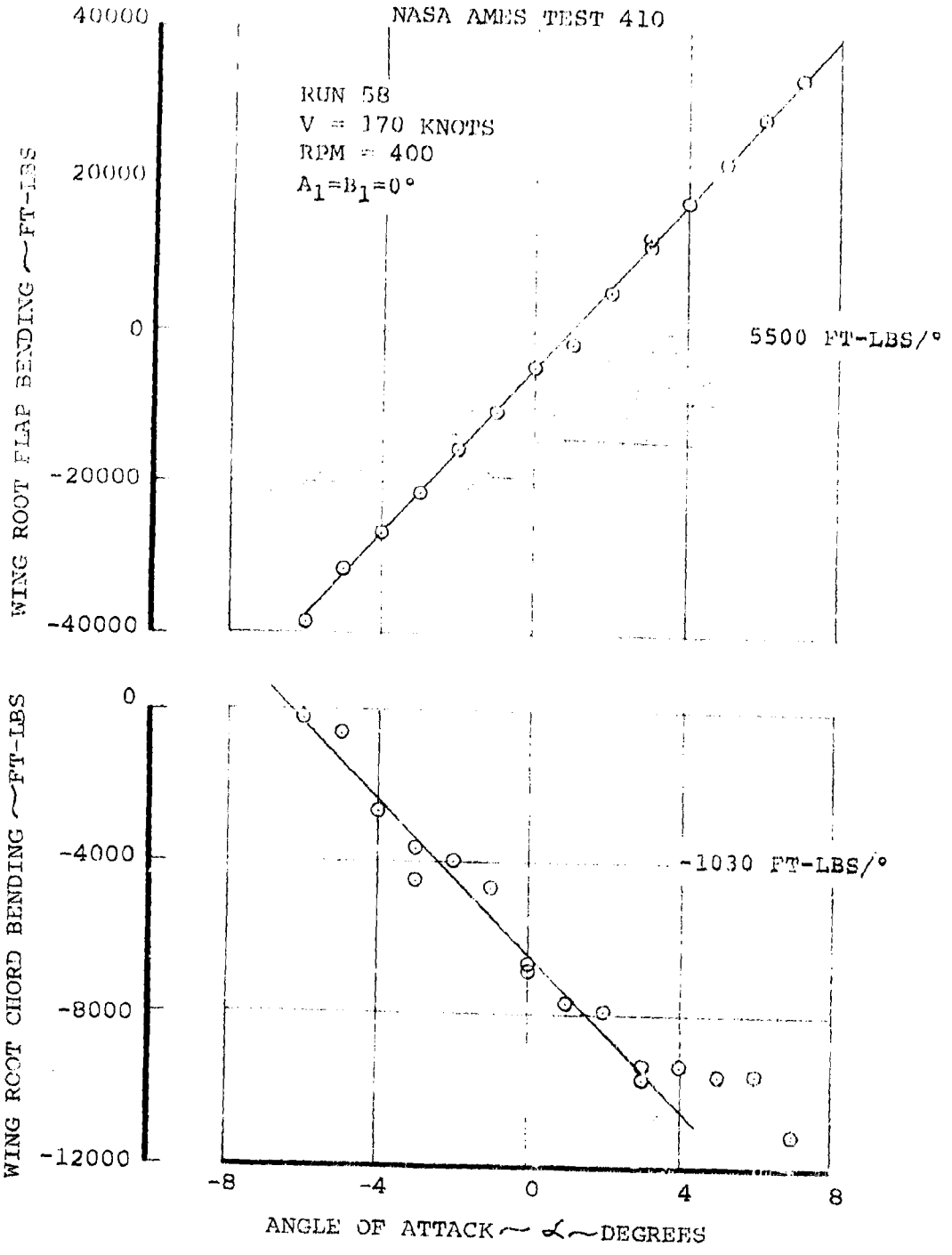

FIGURE 6-84 EFFECT OF ANGLE OF ATTACK ON STEADY WING ROOT FLAP AND CHORD BENDING 170 KNOTS 400 RPM

NASA AMES TEST 410

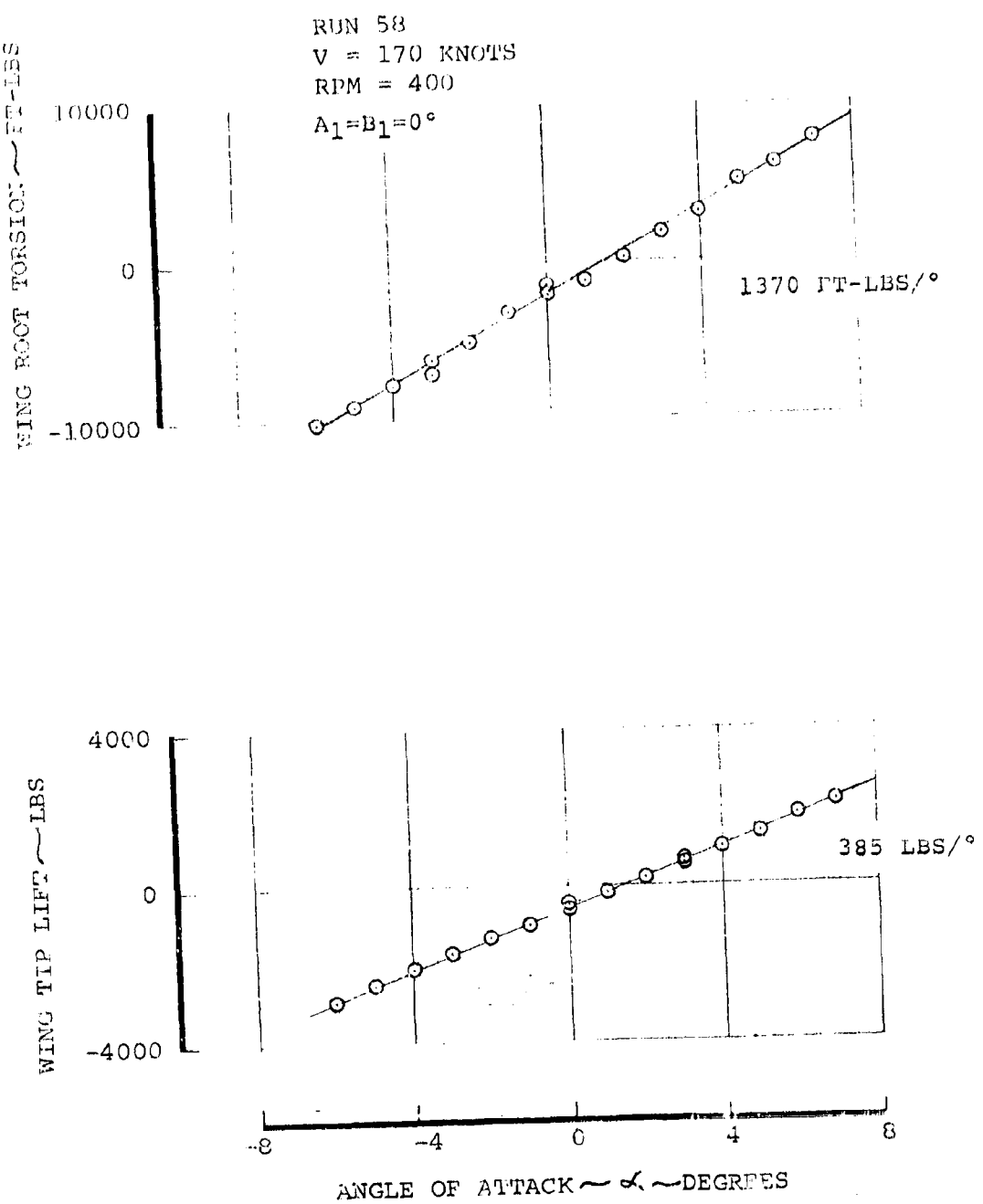

FIGURE 6-85 EFFECT OF ANGLE OF ATTACK ON STEADY WING ROOT TORSION AND WING TIP LIFT 170 KNOTS 400 RPM

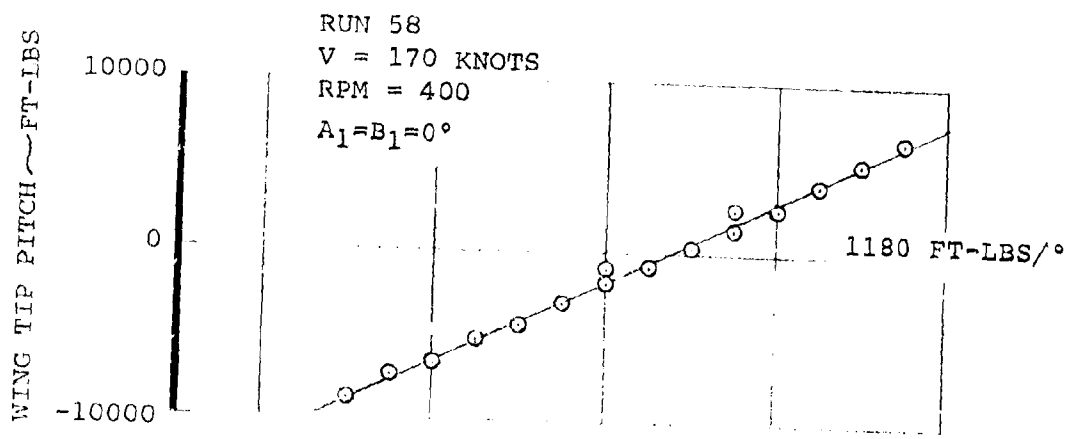

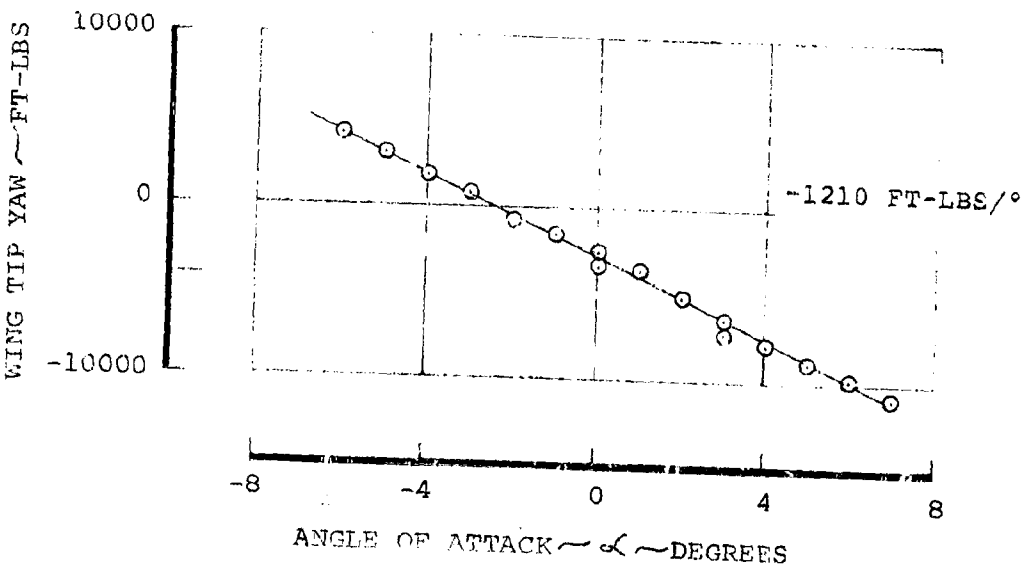

FIGURE 6-34 EFFECT OF ANGLE OF ATTACK ON STEADY WING TIP PITCH AND YAW MOMENT
170 KNOTS 400 RPM

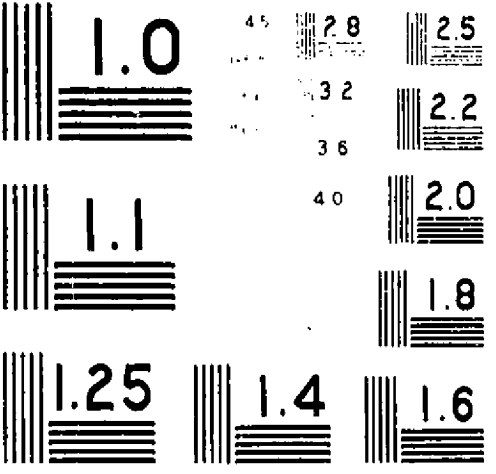

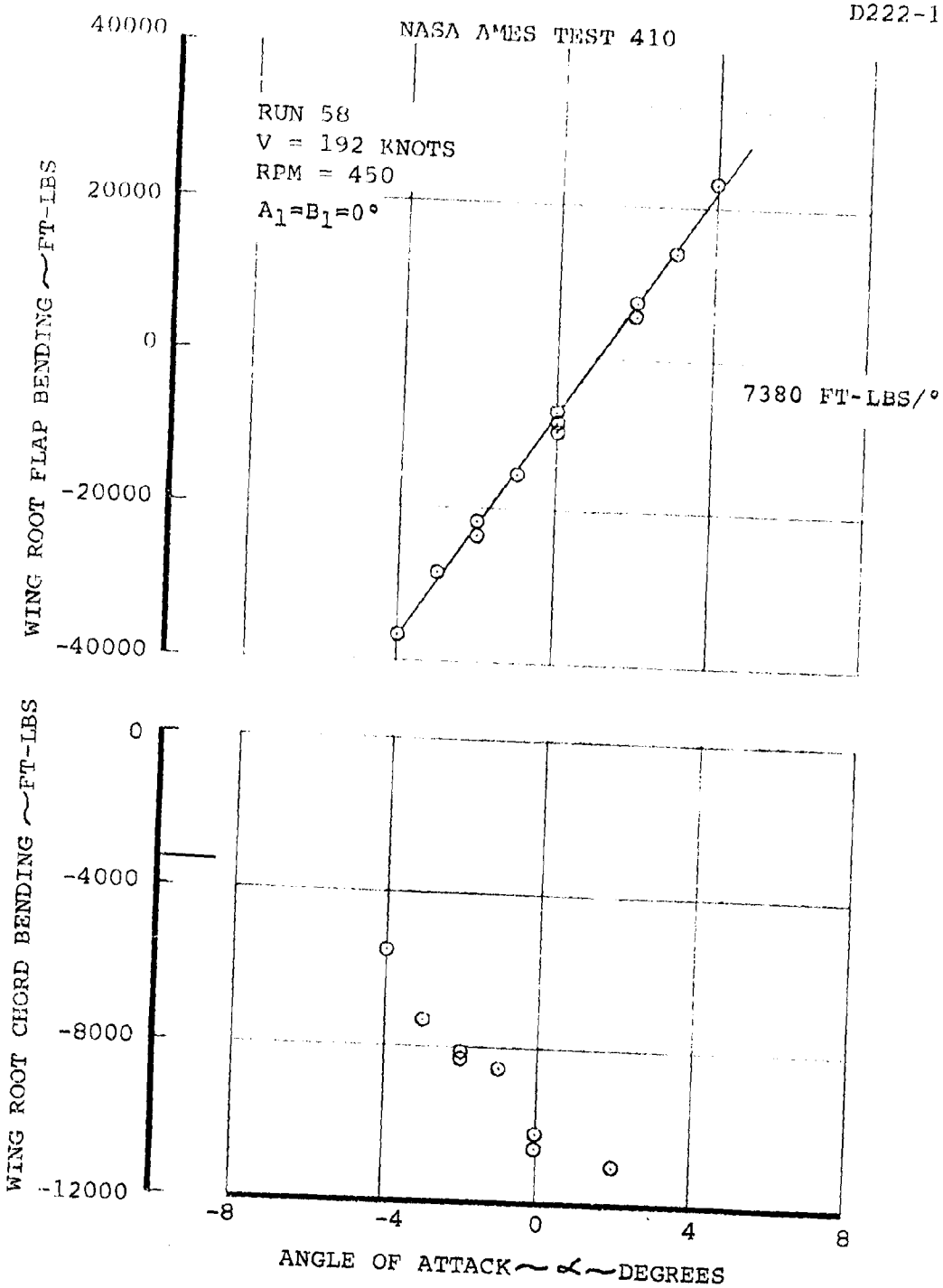

FIGURE 6-87 EFFECT OF ANGLE OF ATTACK ON STEADY WING ROOT FLAP AND CHORD BENDING 192 KNOTS 450 RPM

NASA AMES TEST 410

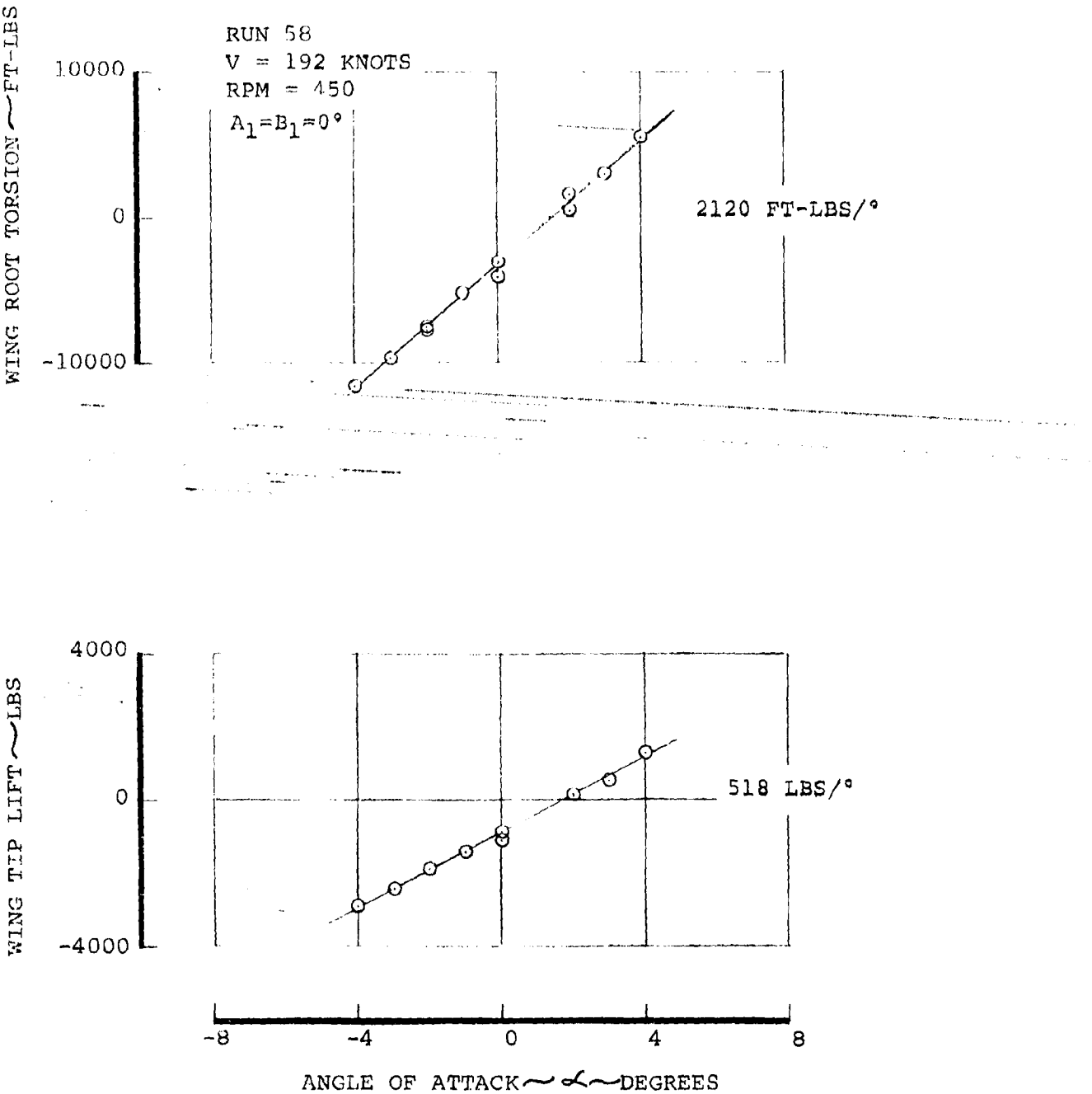

FIGURE 6-89 EFFECT OF ANGLE OF ATTACK ON STEADY WING ROOT TORSION AND WING TIP LIFT 192 KNOTS 450 RPM

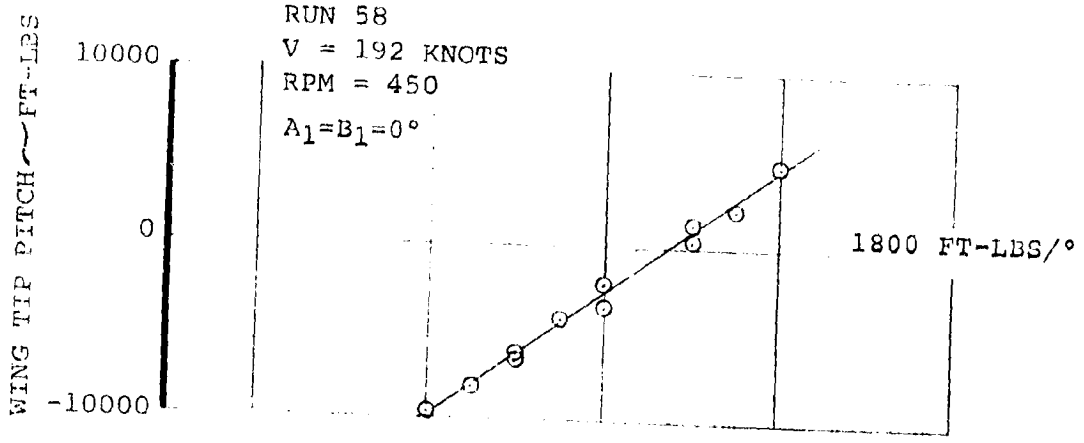

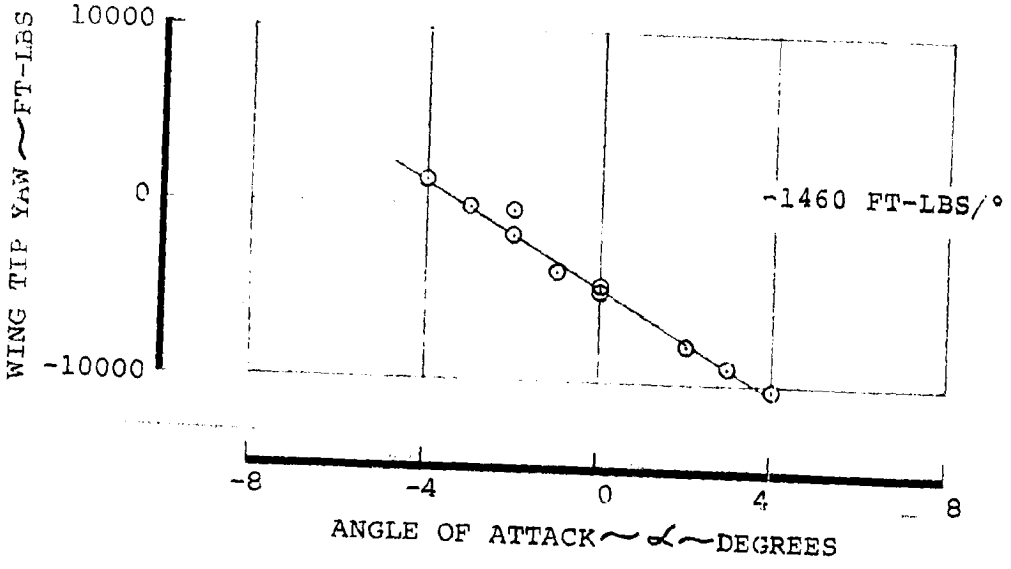

FIGURE 6-89 EFFECT OF ANGLE OF ATTACK ON STEADY WING TIP PITCH AND YAW MOMENT 192 KNOTS 450 RPM

Wing Loads Due to Cyclic Pitch

The effects of cyclic pitch on the wing loads measured on test 410 are due to the resultant changes in the rotor hub forces and moments. The cyclic pitch control inputs were made on two orthogonal axes which were 20° displaced from the conventional lateral and longitudinal axes such that

$$\Psi = -A_{1\cos}\,(\psi + 20) - B_{1\sin}\,(\psi + 20)$$

This axis system is defined in Figure 4.24 (Section 4).

The wing forces and moments measured at zero angle of attack due to A_1 and B_1 cyclic inputs at 100 knots 386 RPM are shown in Figures 6.90 through 6.95. For the cyclic pitch data there are no blades-off tares to include since the wing forces and moments blades-off are a constant. The hub pitching moment can be obtained from

$$\frac{\partial P_M}{\partial \text{CYCLIC}} = \frac{\partial \text{WTP}}{\partial \text{CYCLIC}} - \frac{\partial \text{WTL}}{\partial \text{CYCLIC}} \cdot \frac{45.58}{12}$$

and also

$$= \frac{\partial \text{WRP}}{\partial \text{CYCLIC}} - \frac{\partial \text{WTL}}{\partial \text{CYCLIC}} \cdot \frac{45.58}{12}$$

The A_1 data, Figures 6.91 and 6.92, produce rotor hub moments

$\partial P_M/\partial A_1$ = 1970 Ft. Lbs./° based on wing root pitch and

$\partial P_M/\partial A_1$ = 2145 Ft. Lbs./° based on the wing tip pitch gage.

These values give non-dimensional derivatives

$\partial C_M/\partial A_1$ = .00168 (root gage) 0.00183 (tip gage)

The normal force derivative is identical with the wing tip lift

$$\partial N_F/\partial A_1 = 106 \text{ Lbs./}^\circ \text{ or } \partial C_N/\partial A_1 = 0.00236/^\circ.$$

The wing root flap bending gage is 12.55 ft. inboard of the rotor shaft and might reasonably be expected to give increase loads at 1330 ft. lbs./° A_1. The wing root flap bending gives only 480 ft. lbs./° A_1. The wing tip yawing moment is insensitive to A_1 cyclic control.

The B_1 cyclic pitch data are given in Figures 6.93 to 6.95. The wing tip lift derivative (normal force) is -142 lbs./° and the tip and root pitch data give -180 ft. lbs./° and -275 ft. lbs./° respectively. The hub pitching moment can be deduced as before

$$\partial P_M/\partial B_1 = 361 \text{ ft. lbs./}^\circ \text{ (tip gage)}, \quad 266 \text{ ft. lbs./}^\circ \text{ (root gage)}$$

Since we have normal force data from two orthogonal cyclic pitch inputs the side force data may be deduced from symmetry considerations giving

$$\partial S_F/\partial A_1 = 142 \text{ ft. lbs./}^\circ \text{ and } \partial S_F/\partial B_1 = 106 \text{ ft. lbs./}^\circ$$

These data indicate that the orientation of the resultant in plane force vector due to cyclic pitch is 253.5° of azimuth after the maximum blade angle input.

The wing tip yaw data due to A_1 and B_1 cyclic can now be used to establish the hub yawing moments since

$$\partial WTY/\partial_{CYCLIC} = \partial YM/\partial_{CYCLIC} + 3.81 \; \partial S_F/\partial_{CYCLIC}$$

and results in

$\partial YM/\partial A_1$ = -540 Ft. Lbs./° and $\partial YM/\partial B_1$ = 2036 Ft. Lbs./° (Run 10)

The pitch and yaw moments due to A_1 cyclic indicate that the resultant moment vector occurs 275.6° after the maximum cyclic blade angle. The B_1 data gives 279.9 degrees.

These data are non-dimensionalized in the same manner as the powered test data shown in Section 8.2 and summarized in Table 6.1.

Figures 6.96 through 6.101 show wing load data at 140 knots 386 RPM. The rotor normal force data (wing tip lift) give the derivatives $\partial N_F/\partial A_1$ = 175 Lbs./° and $\partial N_F/\partial B_1$ = -217.3 Lbs./° and as before by symmetry this requires

$\partial S_F/\partial B_1$ = 175 Lbs./° $\quad$ $\partial S_F/\partial A_1$ = 217.3 Lbs./°

The orientation of the resultant force vector is almost the same as for 100 knots, 251° after the maximum cyclic blade angle.

The rotor hub pitching moment derivatives are obtained by subtracting the normal force contribution from the wing tip pitch and wing root torsion (pitch) data.

P_M/A_1 = 2883 Ft. Lbs./° (root gage) 2353 Ft. Lbs./° (tip gage)

and

P_M/B_1 = 619.9 Ft. Lbs./° (root gage) 607.9 Ft. Lbs./° (tip gage)

The hub yawing moment derivatives reduce to

$\partial Y_M/\partial A_1 = -826$ Ft. Lbs./° $\quad \partial Y/\partial B_1 = 2059$ Ft. Lbs./°

The moment vector due to cyclic occurs 270.6° (A_1 data) and 273.5° (B_1 data) after the maximum cyclic blade angle.

Figures 6.102 through 6.107 are the wing loads due to A_1 and B_1 cyclic at 192 knots 386 RPM. The rotor hub force and moment derivatives obtained from these data are

$N_F/A_1 = 338$ Lbs./° $\quad N_F/B_1 = -342$ Lbs./°

$P_M/A_1 = 2687$ Ft. Lbs./° $\quad P_M/B_1 = 893$ Ft. Lbs./° (tip data)

$P_M/A_1 = 2487$ Ft. Lbs./° $\quad P_M/B_1 = 858$ Ft. Lbs./° (root data)

$S_F/A_1 = 342$ Lbs./° $\quad S_F/B_1 = 338$ Lbs./°

$Y_M/A_1 = -1902$ Ft. Lbs./° $\quad Y_M/B_1 = 2460$ Ft. Lbs./°

The force data gives a resultant vector 245.3° after the maximum cyclic blade angle input and is consistent with the data obtained at 100 and 140 knots. The moment orientation based on the B_1 cyclic data is similarly consistent 270°. The A_1 data indicates a moment vector 254.7° after the maximum blade angle input.

This difference arises due to the fact that the wing tip yaw data at 192 give a negative derivative -600 Ft. Lbs./°, Figure 6.102, whereas at 100 and 140 knots the wing tip yaw gage data was insensitive to A_1 cyclic, Figures 6.92 and 6.98. The wing root chord bending due to A_1 also changes significantly at 192

knots (-30 ft. lbs./°, Figure 6.103) compared with 500 ft. lbs./° and 525 ft. lbs./° at 100 and 140 knots respectively (Figures 6.90 and 6.96). Bearing in mind that the positive wing chord bending convention is in the sense of negative yaw, the root chord bending appears to contradict the wing tip gage. This data needs further analysis.

The rotor hub forces and moments obtained from the cyclic sweeps of test 410 (windmilling) are summarized in non-dimensional form in Table 6.1. The effect of thrust on the rotor derivatives is shown in Section 6.2.

Additional cyclic pitch data were obtained at off-design RPM. Figures 6.108 to 6.113 are A_1 and B_1 cyclic sweeps at 100 knots 445 RPM. The wing load derivatives are shown with the test data. The rotor hub force and moment derivatives obtained from the wing load data are:

$\partial C_M / \partial B_1 = -.00016$ (root torsion)

$\partial C_M / \partial B_1 = -.00022$ (tip pitch)

$\partial C_N / \partial B_1 = -0.00201$

$\partial C_{SF} / \partial B_1 = 0.00151$

$C_{YAW} / B_1 = 0.00149$

$C_M / A_1 = 0.00168$ (root torsion)

$C_M / A_1 = 0.00216$ (tip pitch)

$C_N / A_1 = 0.00151$

$C_{SF} / A_1 = 0.00201$

$C_{YAW} / A_1 = 0.00019$

The A_1 pitch derivative deduced from the tip pitch gage is larger than that obtained from the wing root gage. Symmetry considerations would suggest that the derivative $\partial C_M / \partial A_1 = 0.00168$ from the root torsion gage is closer to the truth. The resultant moment vector occurs 298.4° (B_1 data) (294.9°, A_1 data) after the maximum cyclic blade angle. The force data give 253°. The orientation of the inplane force vector is the same as the 386 RPM data. The moment vector has shifted from 276° at 386 RPM.

Figures 6.114 to 6.119 are wing load data at 140 knots 420 RPM and the rotor hub derivatives computed from these wing loads give

$\partial C_M / \partial B_1 = 0.00009$ (root gage)

$\partial C_M / \partial B_1 = -0.00032$ (tip gage)

$\partial C_N / \partial B_1 = -0.00432$

$C_{SF} / B_1 = 0.00085$

$C_{YAW} / B_1 = 0.00161$

$C_M / A_1 = 0.00193$ (root gage)

$\partial C_M / \partial A_1 = 0.00186$ (tip gage)

$\partial C_N / A_1 = 0.00085$

$C_{SF} / A_1 = 0.00432$

$C_{YAW} / A_1 = 0.000003$

and the effect of increased RPM can be obtained by comparison with 386 RPM data of Table 6.1. The moment vector azimuthal lag from the maximum cyclic blade angle is 290.1° (A_1 data) and

301.2° (B_1 data) compared with 273° at 386 RPM. The force vector azimuthal lag is 278.9° compared with 251° obtained at 386 RPM.

Similar data at 192 knots and 300 RPM are given in Figures 6.120 to 6.125. The rotor hub derivatives at this condition are

$\partial C_M / \partial B_1 = 0.00256$ (root gage)

$\partial C_M / \partial B_1 = 0.00253$ (tip gage)

$\partial C_N / \partial B_1 = -0.00688$

$\partial C_{SF} / \partial B_1 = 0.0092$

$\partial C_{YAW} / \partial B_1 = 0.00176$

$\partial C_M / \partial A_1 = 0.00233$ (root gage)

$\partial C_M / \partial A_1 = 0.00193$ (tip gage)

$\partial C_N / \partial A_1 = 0.0092$

$\partial C_{SF} / \partial A_1 = 0.00688$

$\partial C_{YAW} / \partial A_1 = -0.00168$

At this reduced RPM the azimuthal angle between maximum blade angle input and the moment and force resultant vectors are 249° (A_1 moment data), 234.9° (B_1 moment data) and 236° force data. These orientation angles are reduced as a result of the RPM reduction.

NOTE: $\Delta\theta = -A_1 \cos(\psi+20) - B_1 \sin(\psi+20)$

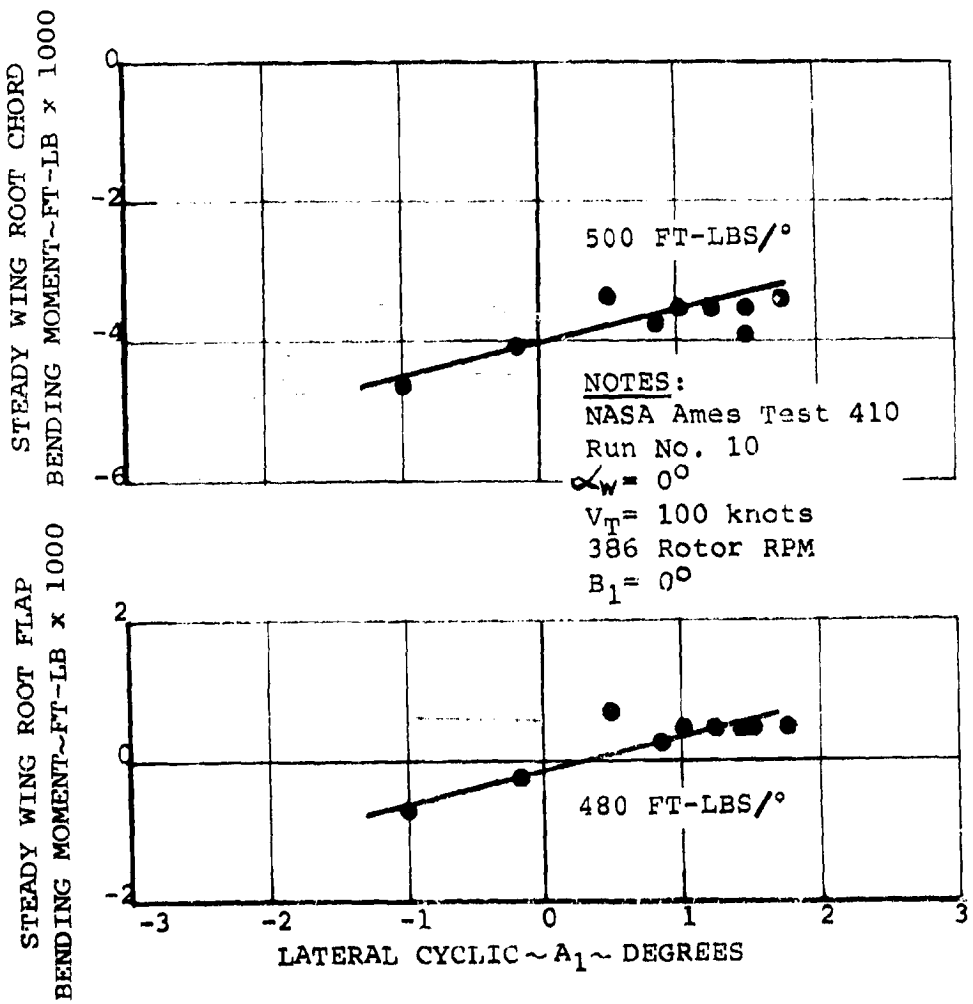

FIGURE 6-90 STEADY WING ROOT FLAP AND CHORD BENDING DUE TO A_1 CYCLIC AT 100 KNOTS 386 RPM

NOTE: $\psi = -A_1 \cos(\psi+20) - B_1 \sin(\psi+20)$

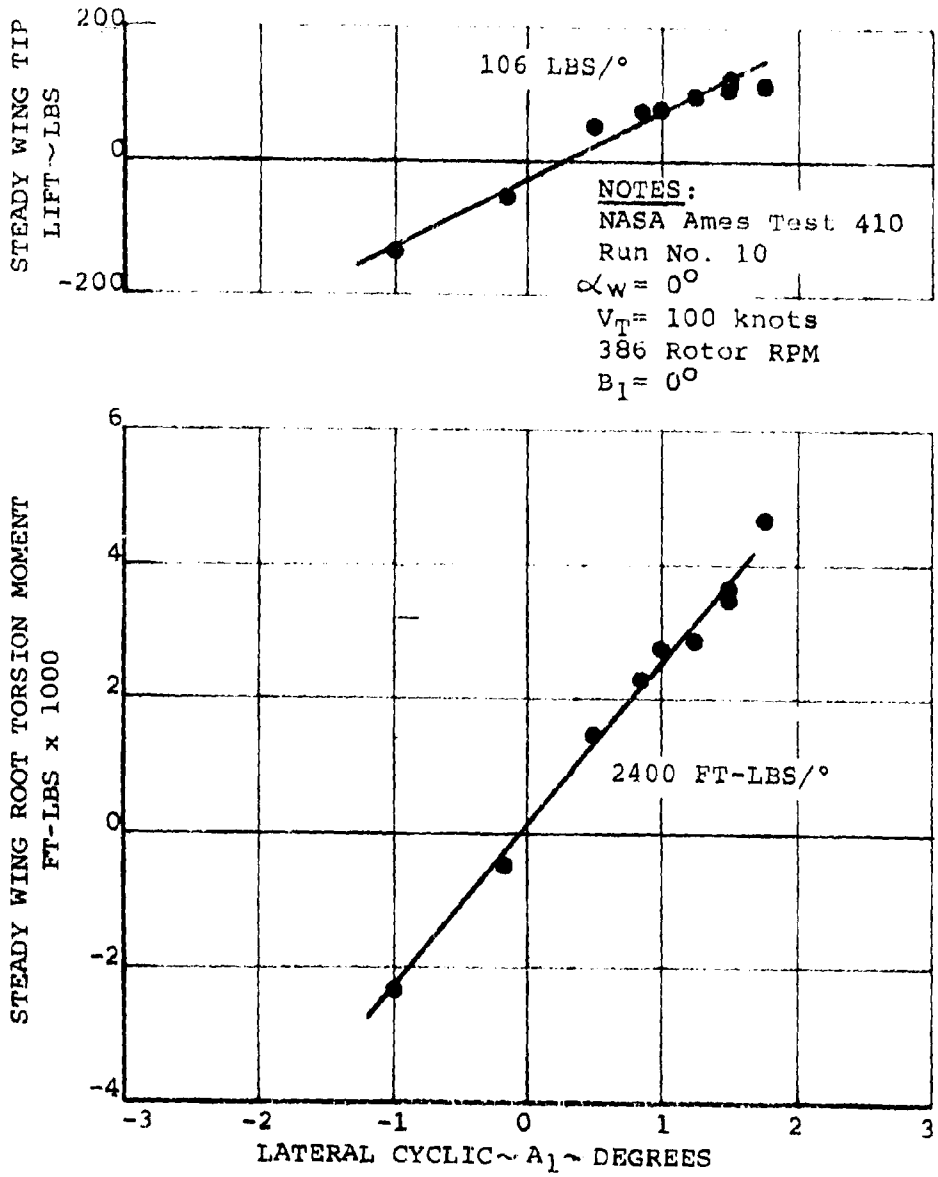

FIGURE 6-91 STEADY WING TIP LIFT AND WING ROOT TORSION DUE TO A_1 CYCLIC AT 100 KNOTS 386 RPM

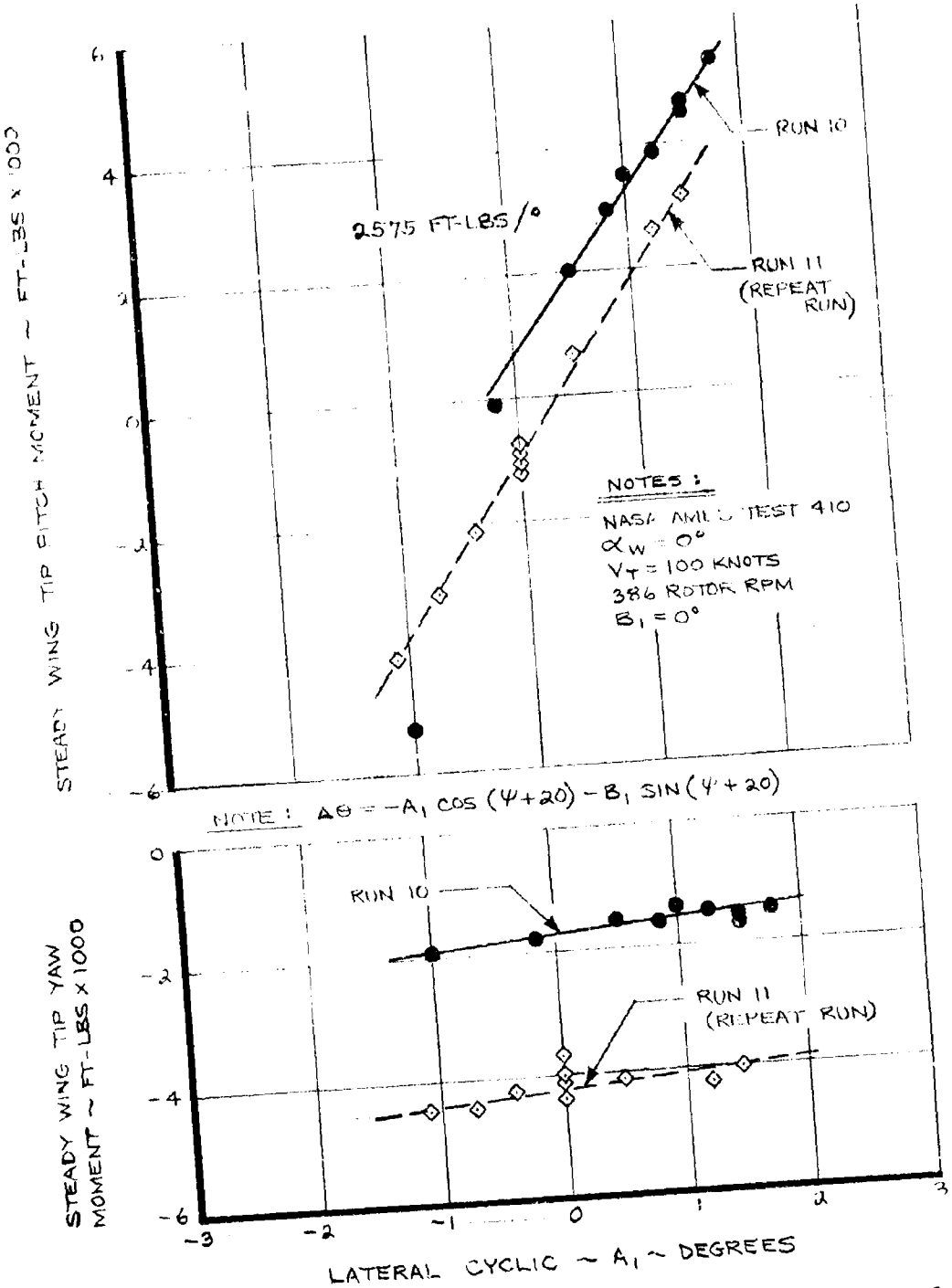

FIGURE 6-92 STEADY WING TIP PITCH AND YAW MOMENT DUE TO A_1 CYCLIC AT 100 KNOTS 386 RPM

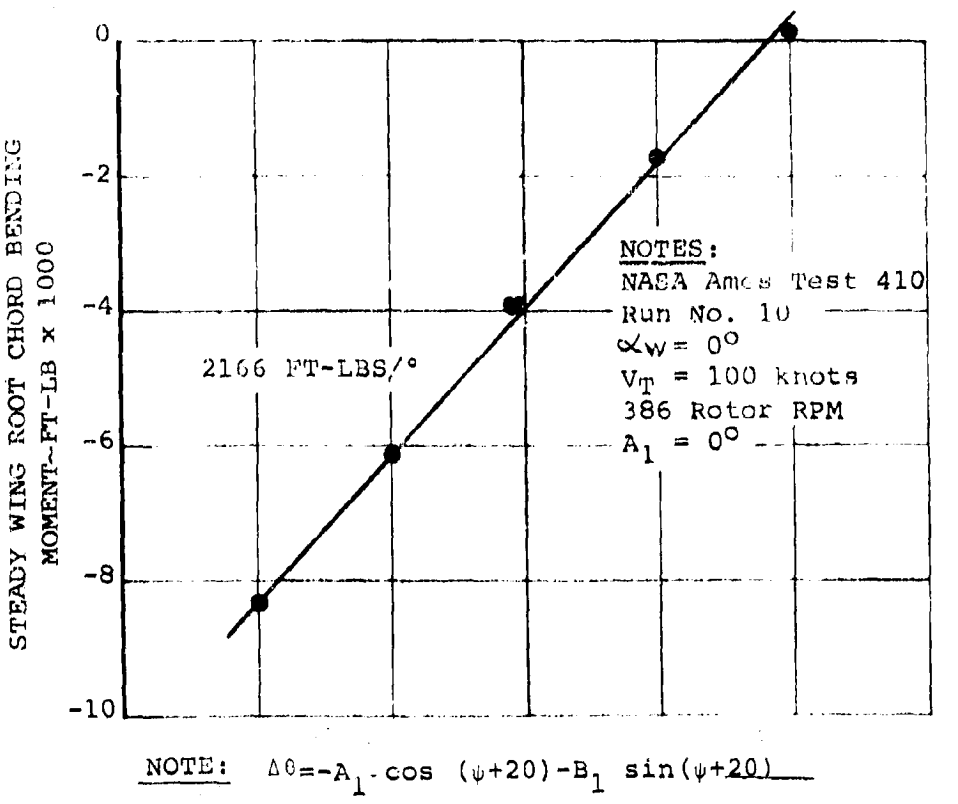

NOTE: $\Delta\theta = -A_1 \cdot \cos(\psi+20) - B_1 \sin(\psi+20)$

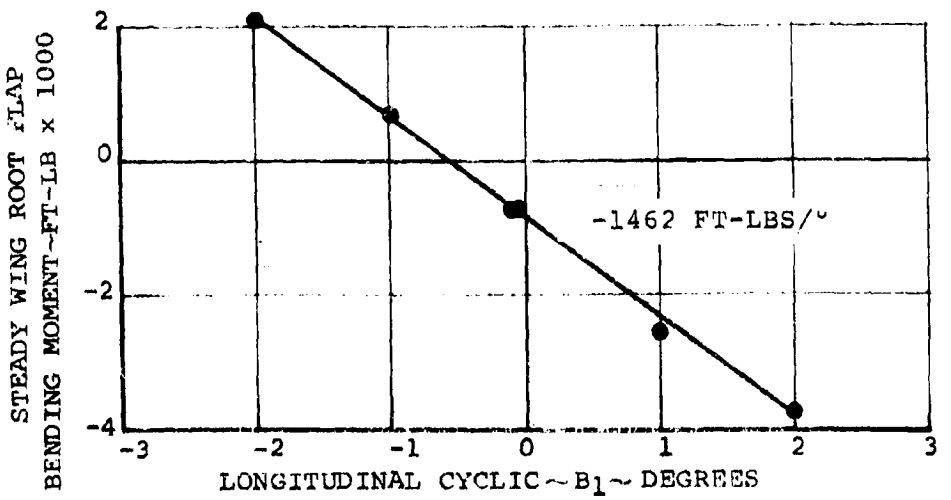

FIGURE 6-93 STEADY WING ROOT FLAP AND CHORD BENDING DUE TO B_1 CYCLIC AT 100 KNOTS 386 RPM

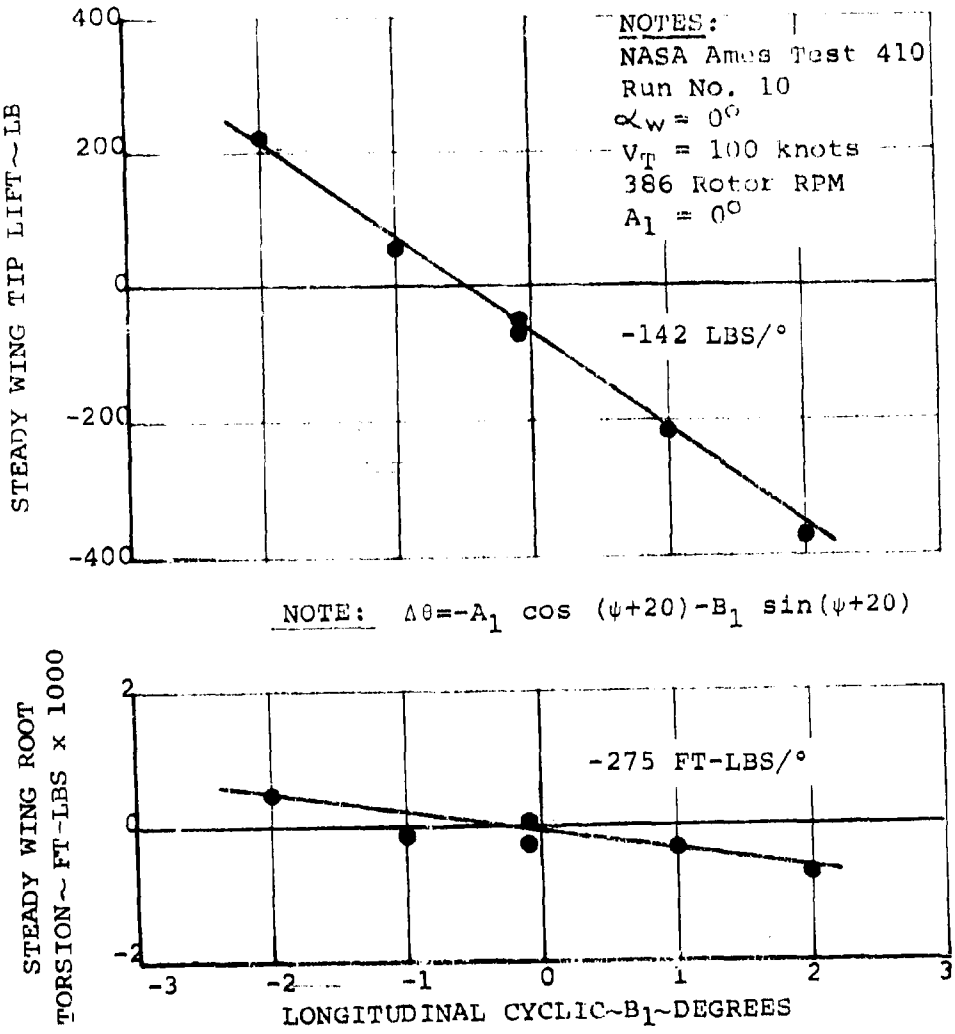

FIGURE 6-94 STEADY WING TIP LIFT AND WING ROOT TORSION DUE TO B_1 CYCLIC AT 100 KNOTS 386 RPM

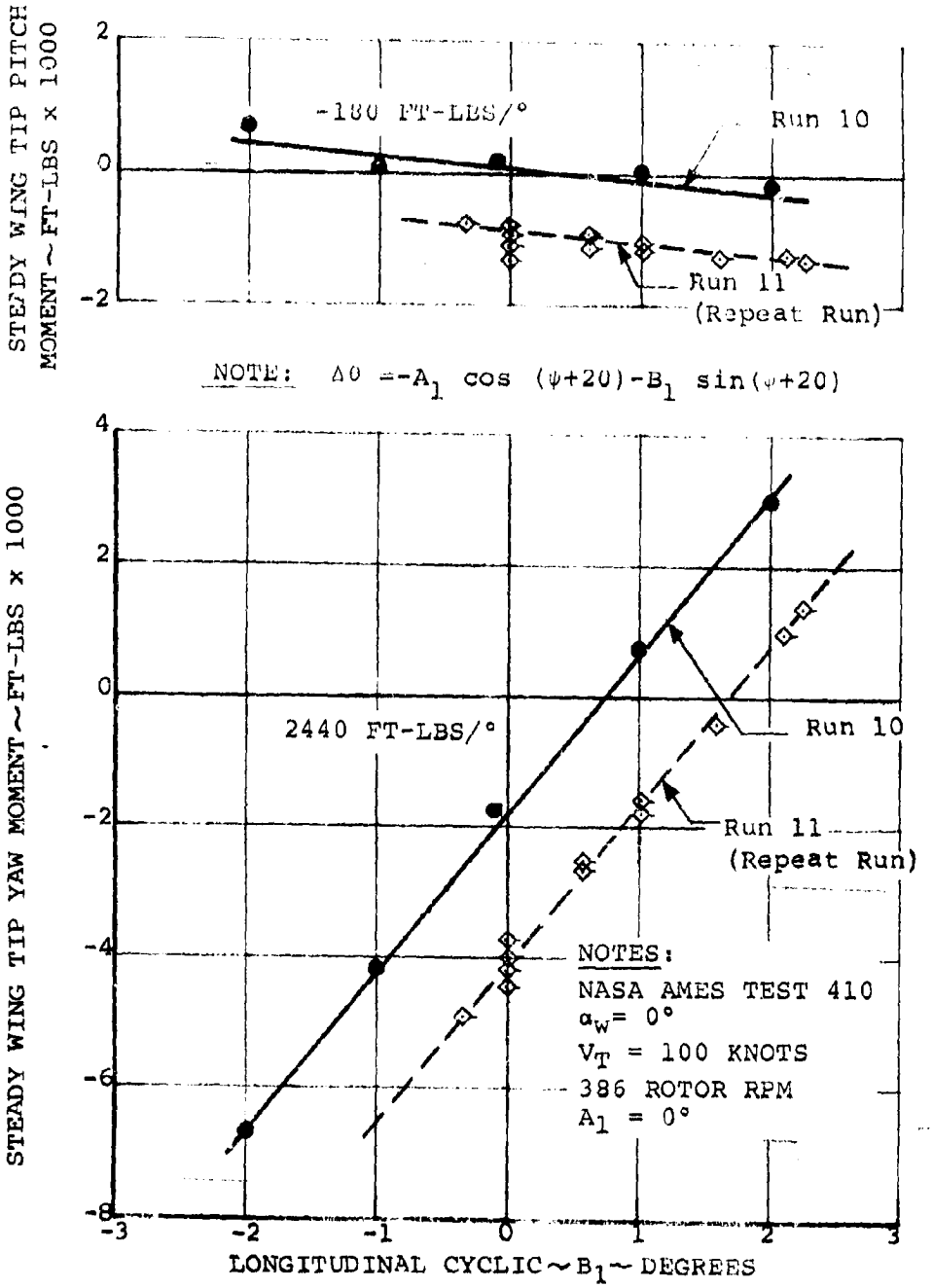

FIGURE 6-95 STEADY WING TIP PITCH AND YAW MOMENT DUE TO B_1 CYCLIC AT 100 KNOTS 386 RPM

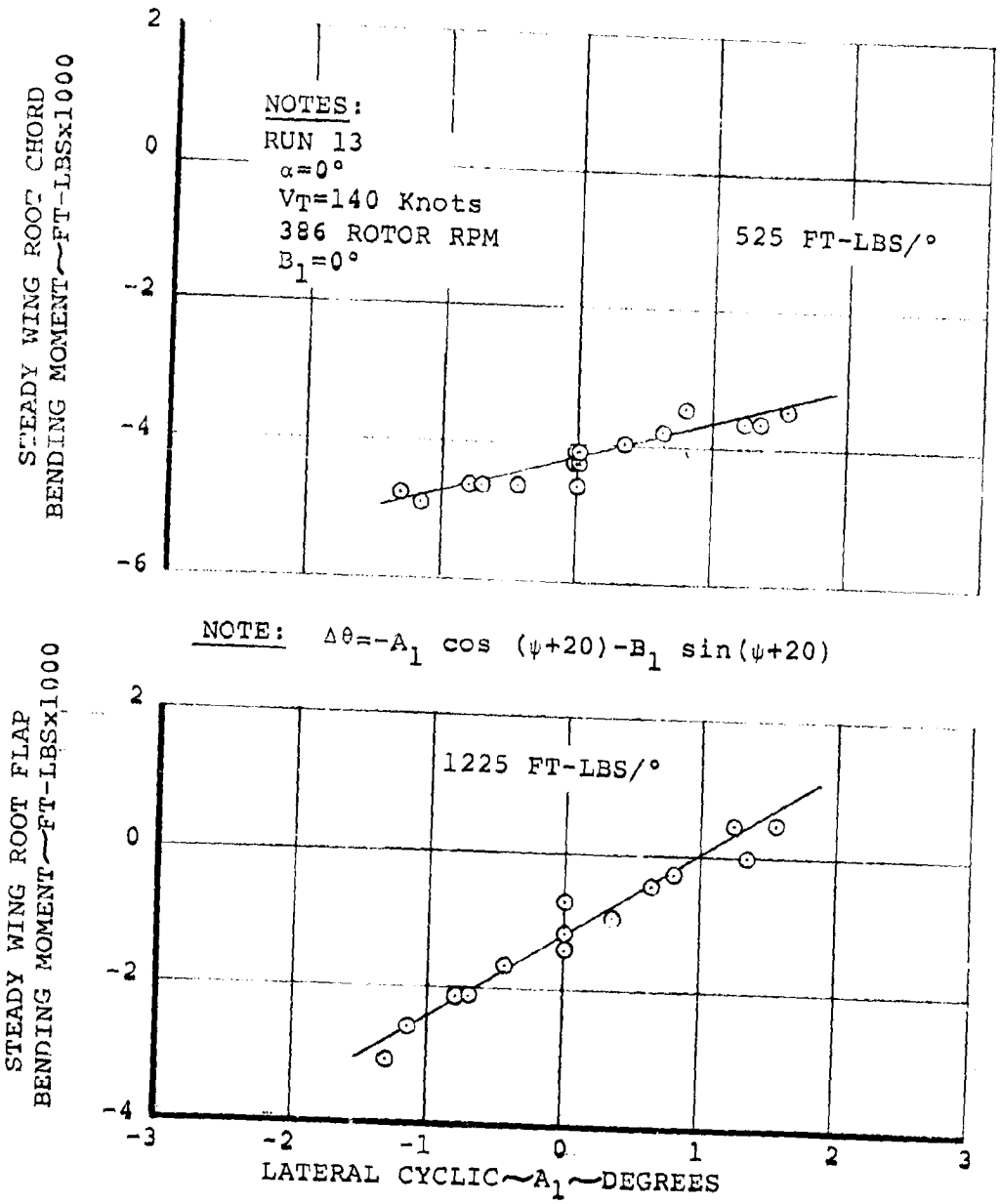

FIGURE 6-96 STEADY WING ROOT FLAP AND CHORD BENDING DUE TO A_1 CYCLIC AT 140 KNOTS 386 RPM

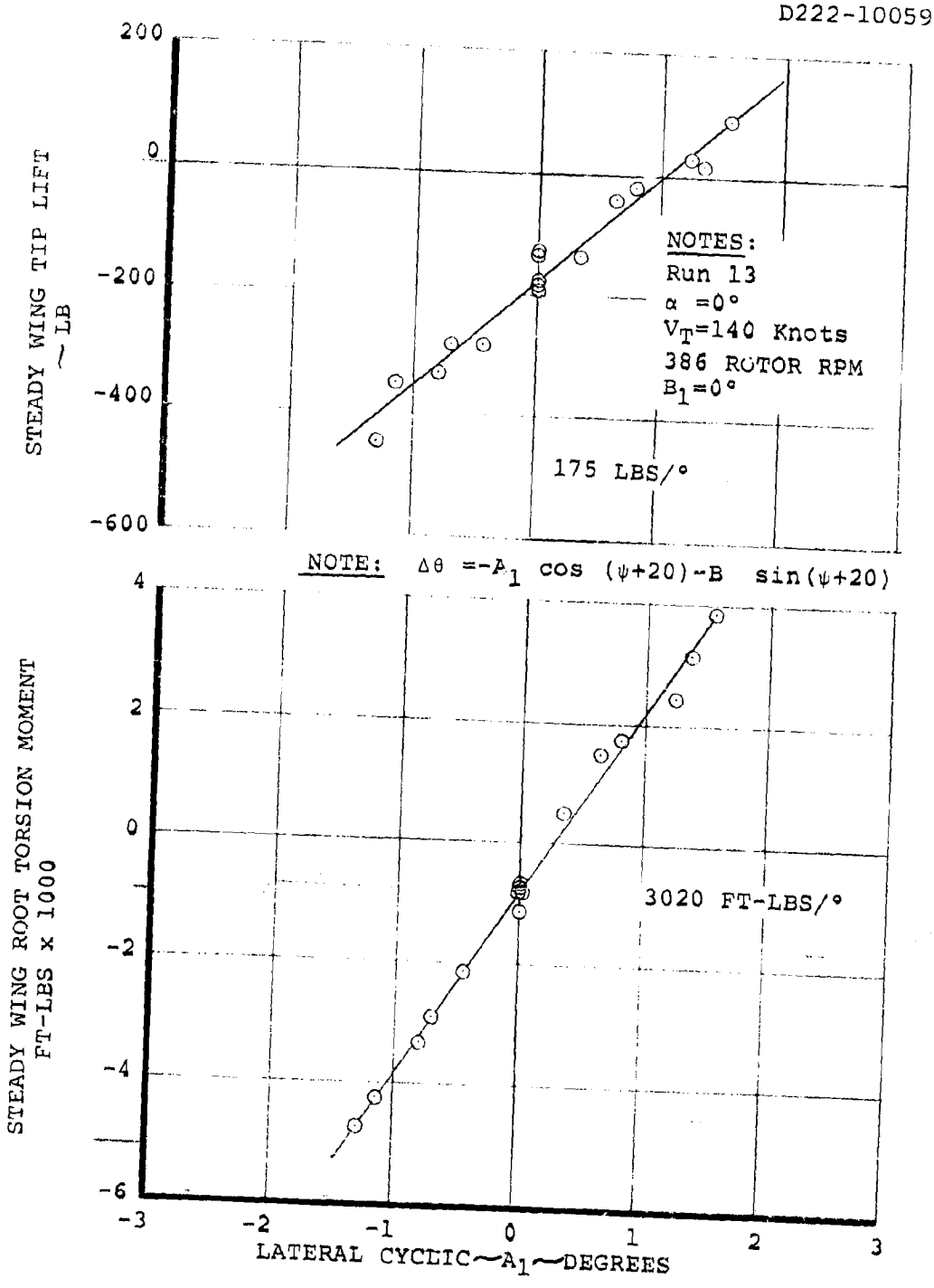

FIGURE 6-97 STEADY WING TIP LIFT AND WING ROOT TORSION DUE TO A_1 CYCLIC AT 140 KNOTS 386 RPM

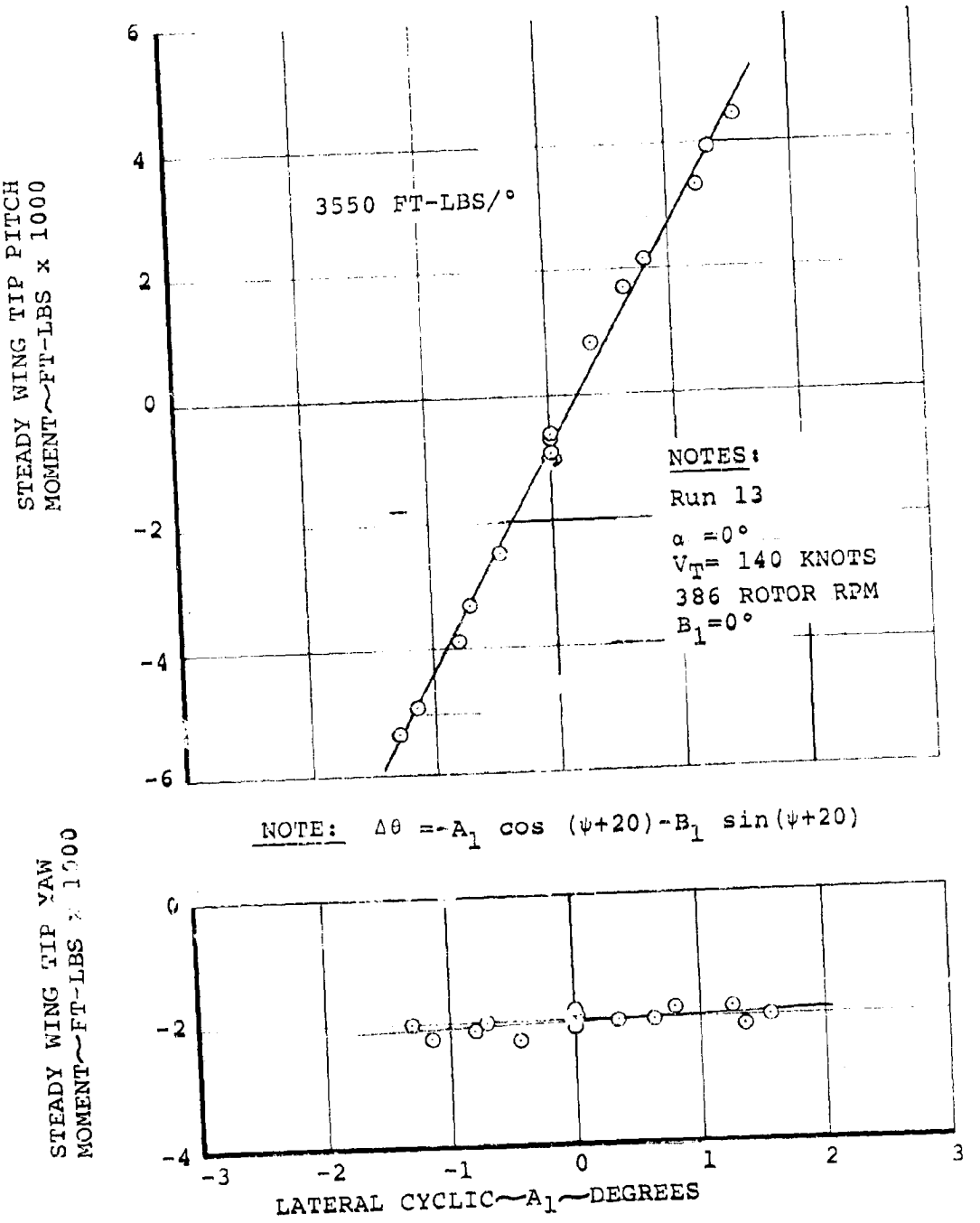

FIGURE 6-98 STEADY WING TIP PITCH AND YAW MOMENT DUE TO A_1 CYCLIC AT 140 KNOTS 386 RPM

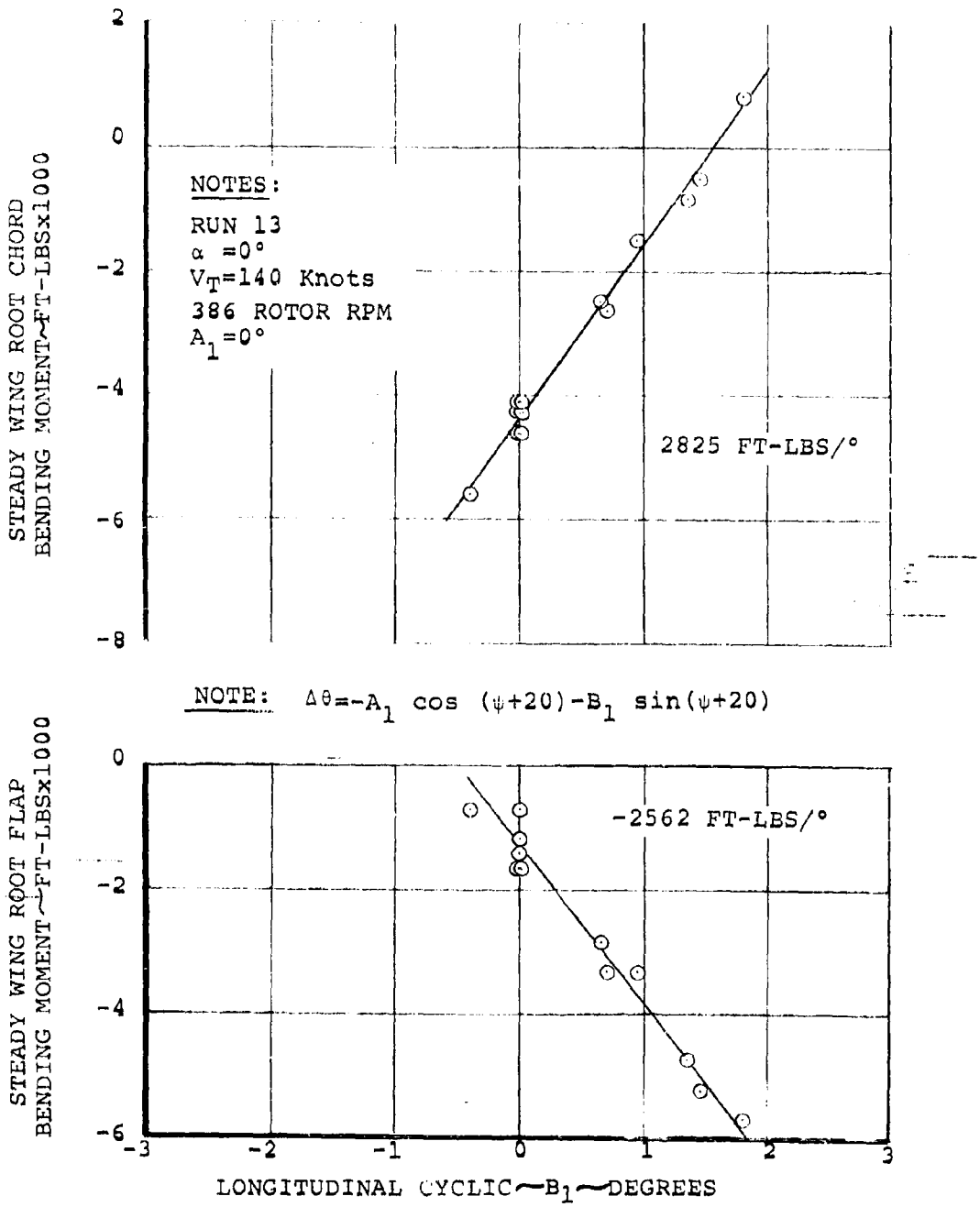

FIGURE 6-99 STEADY WING ROOT FLAP AND CHORD BENDING DUE TO B_1 CYCLIC AT 140 KNOTS 386 RPM

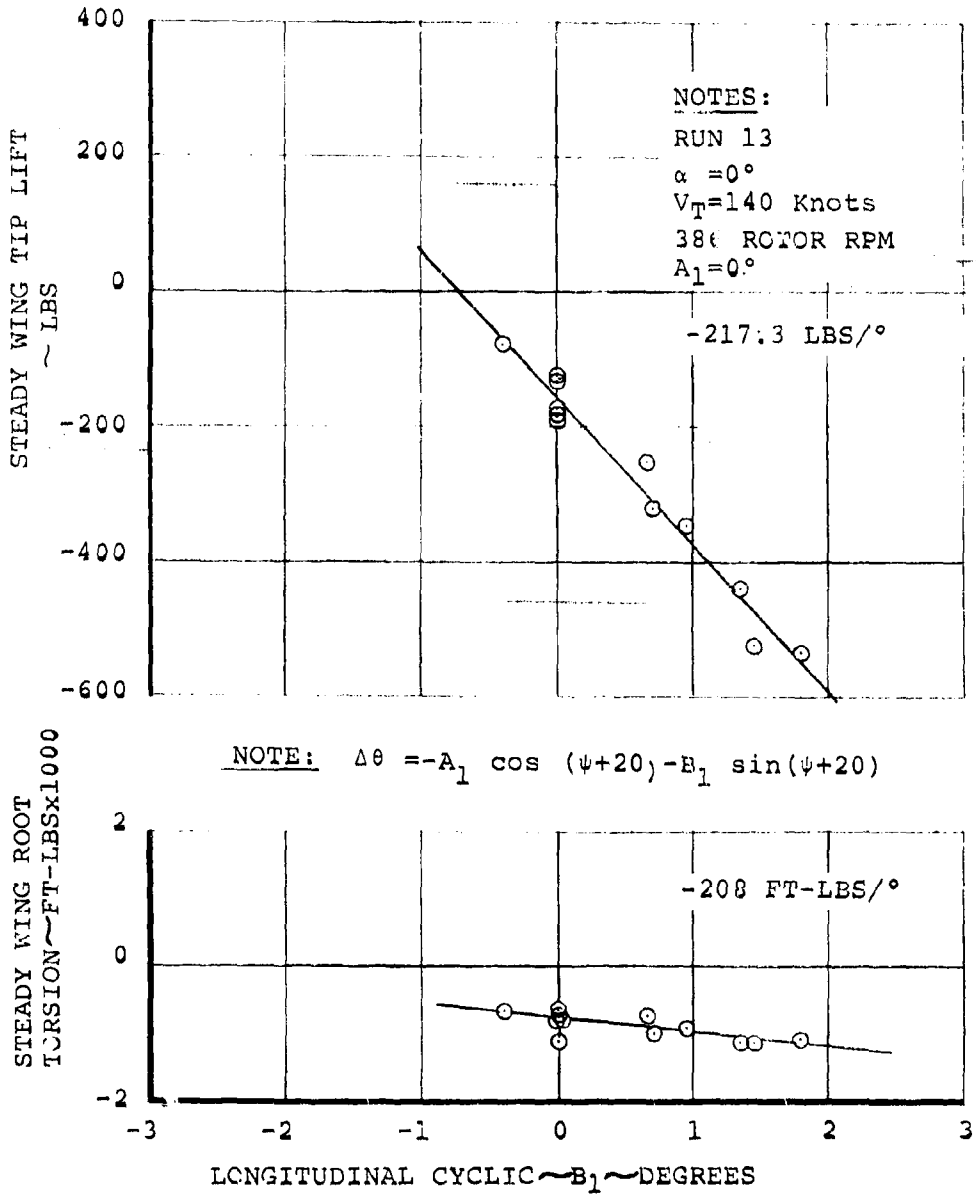

FIGURE 6-100 STEADY WING TIP LIFT AND WING ROOT TORSION DUE TO B_1 CYCLIC AT 140 KNOTS 386 RPM

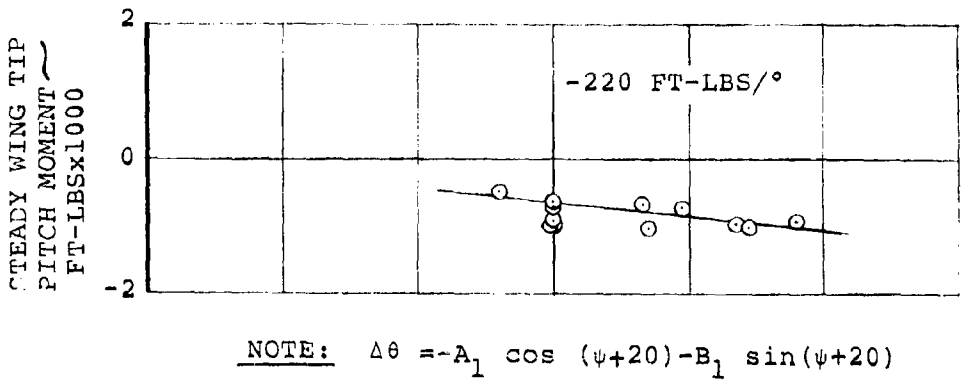

NOTE: $\Delta\theta = -A_1 \cos(\psi+20) - B_1 \sin(\psi+20)$

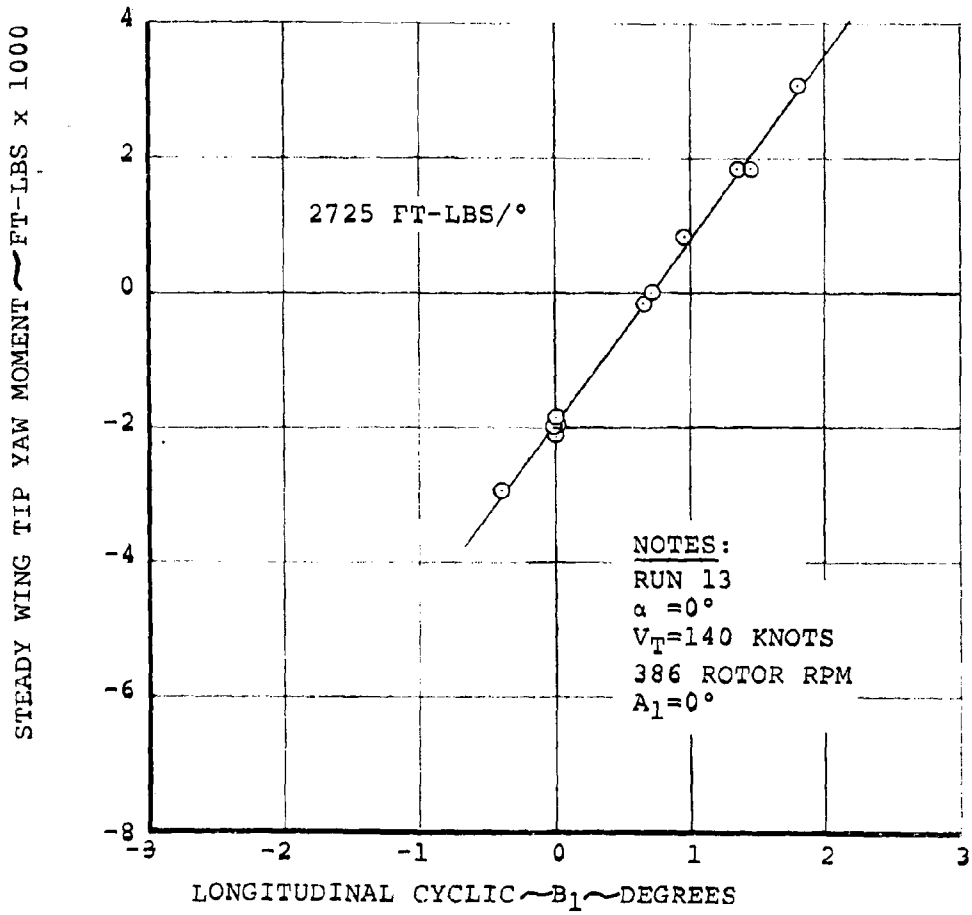

FIGURE 6-101 STEADY WING TIP PITCH AND YAW MOMENT DUE TO B_1 CYCLIC AT 140 KNOTS 386 RPM

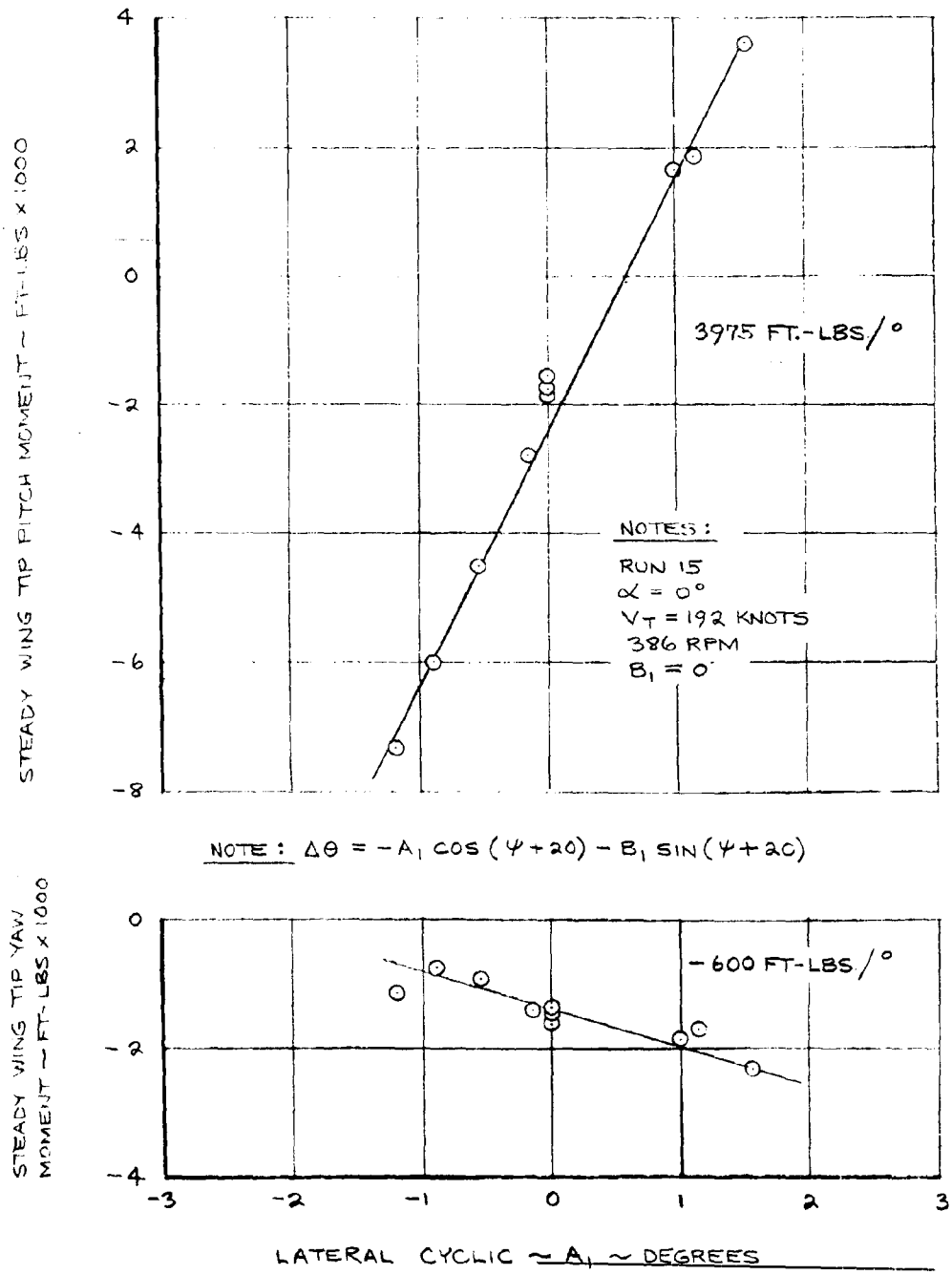

FIGURE 6-102 STEADY WING TIP PITCH AND YAW MOMENT DUE TO A_1 CYCLIC AT 192 KNOTS 386 RPM

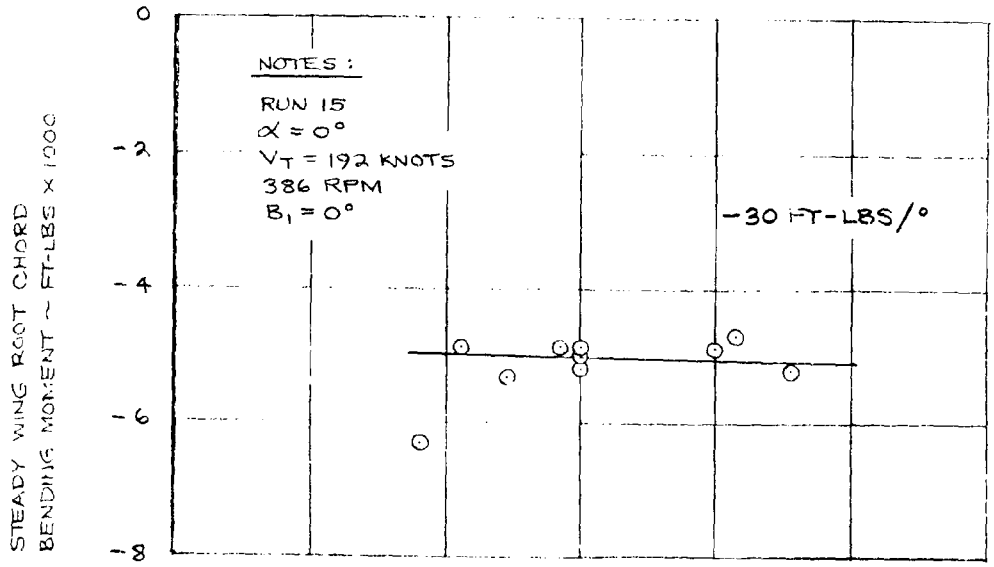

NOTE : $\Delta\theta = -A_1 \cos(\psi + 20) - B_1 \sin(\psi + 20)$

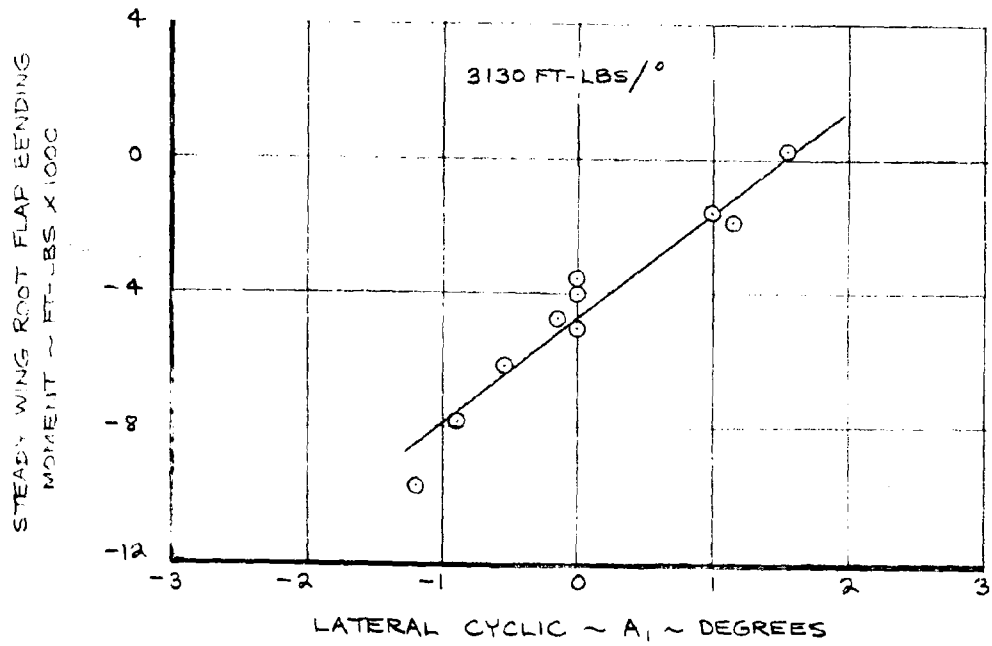

FIGURE 6-103 STEADY WING ROOT FLAP AND CHORD BENDING DUE TO A_1 CYCLIC AT 192 KNOTS 386 RPM

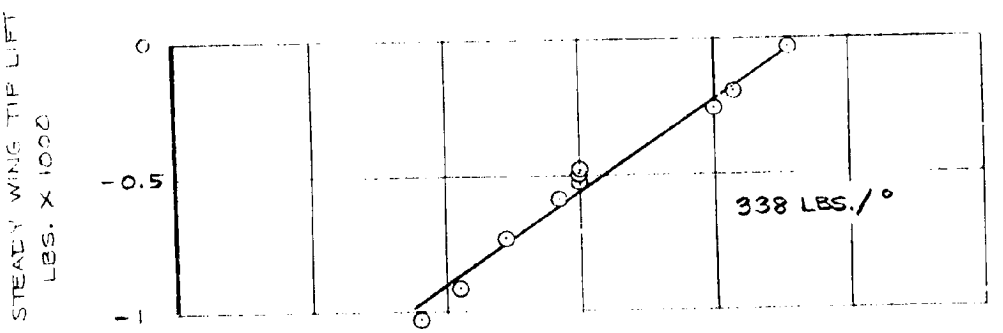

NOTE : $\Delta\theta = -A_1 \cos(\psi + 20) - B_1 \sin(\psi + 20)$

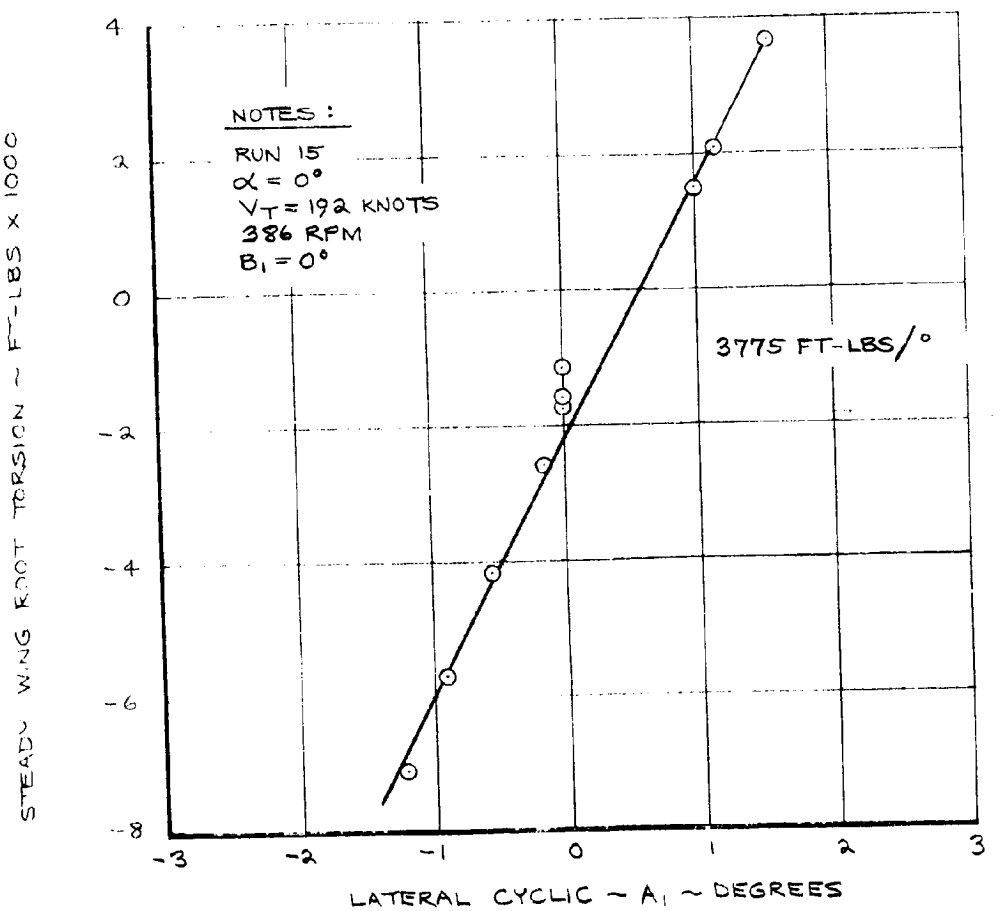

FIGURE 6-104 STEADY WING TIP LIFT AND WING ROOT TORSION DUE TO A_1 CYCLIC AT 192 KNOTS 386 RPM

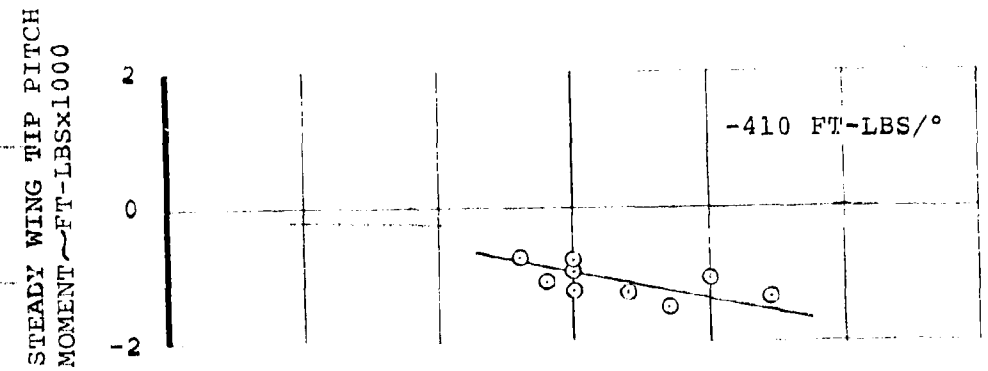

NOTE: $\Delta\theta = -A_1 \cos(\psi+20) - B_1 \sin(\psi+20)$

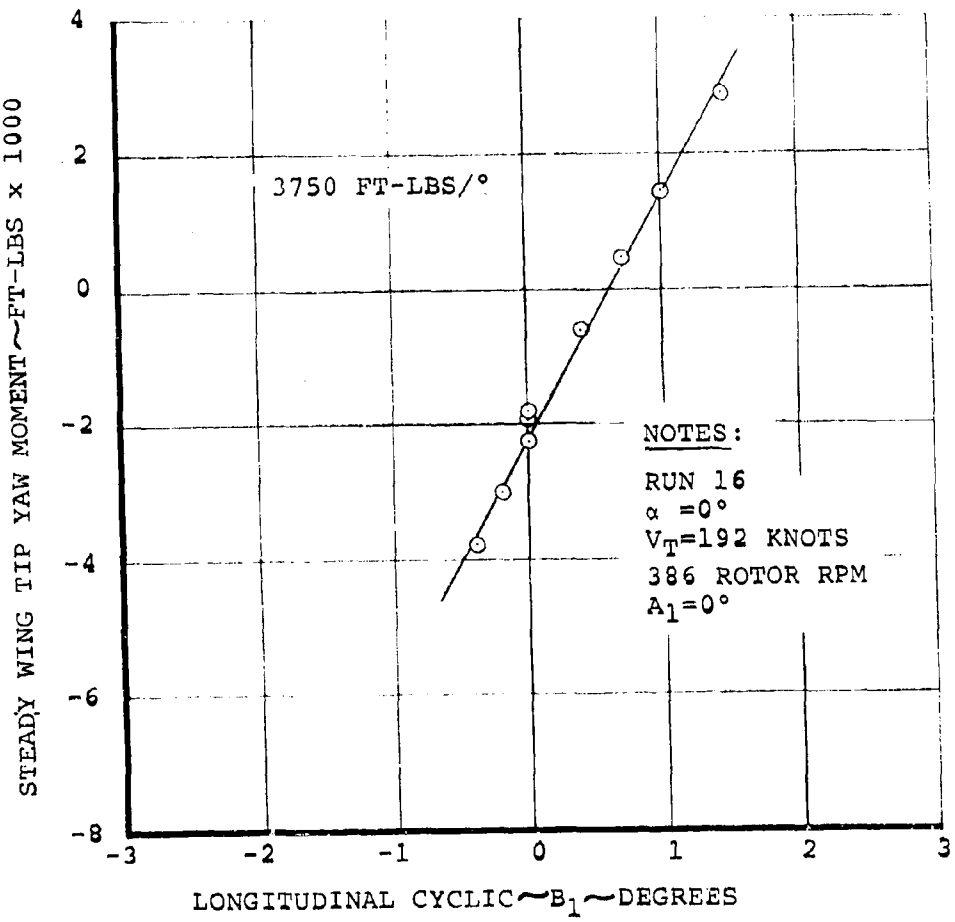

FIGURE 6-105 STEADY WING TIP PITCH AND YAW MOMENT DUE TO B_1 CYCLIC AT 192 KNOTS 386 RPM

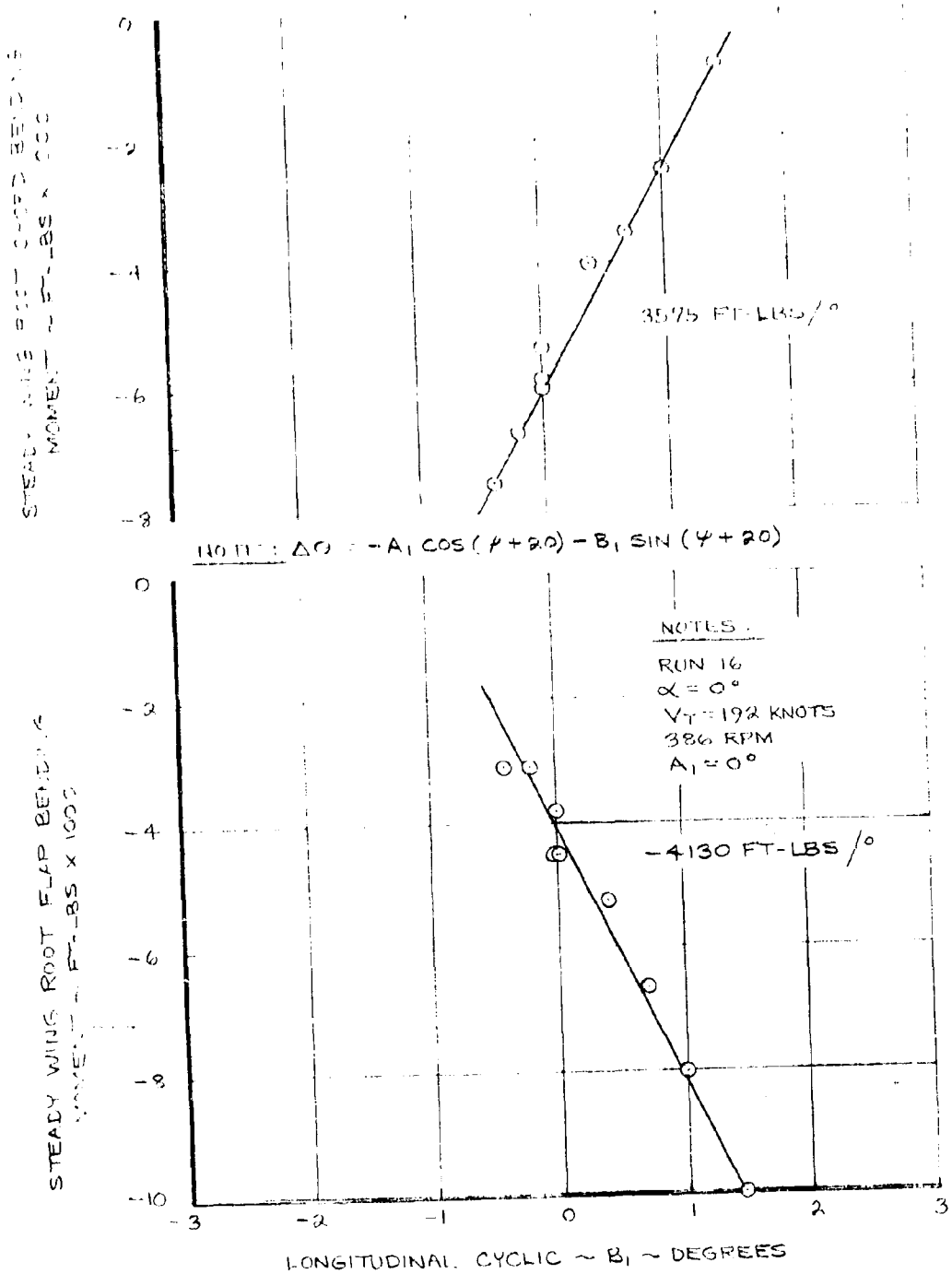

FIGURE 6-106 STEADY WING ROOT FLAP AND CHORD BENDING DUE TO B_1 CYCLIC AT 192 KNOTS 386 RPM

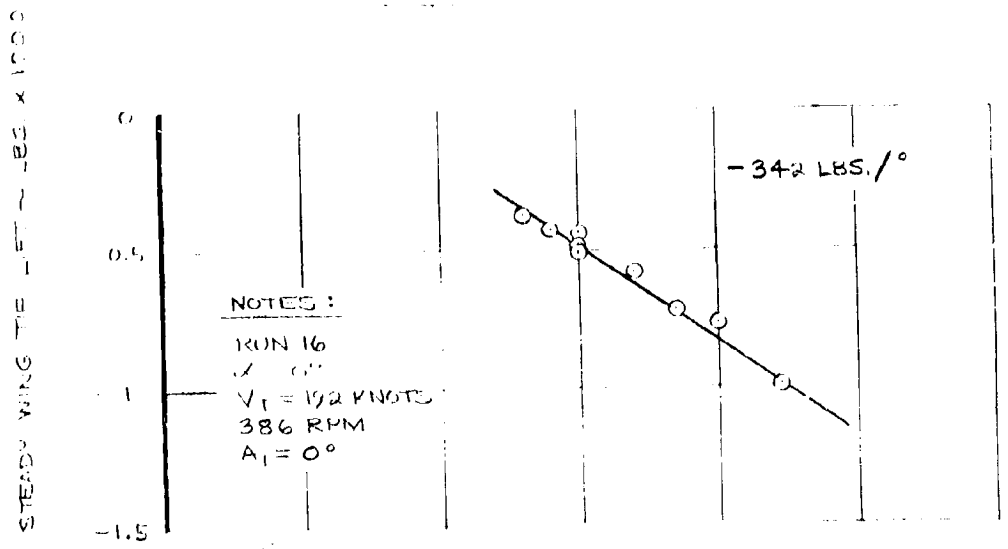

NOTE: $\Delta\theta = -A_1 \cos(\psi + 20) - B_1 \sin(\psi + 20)$

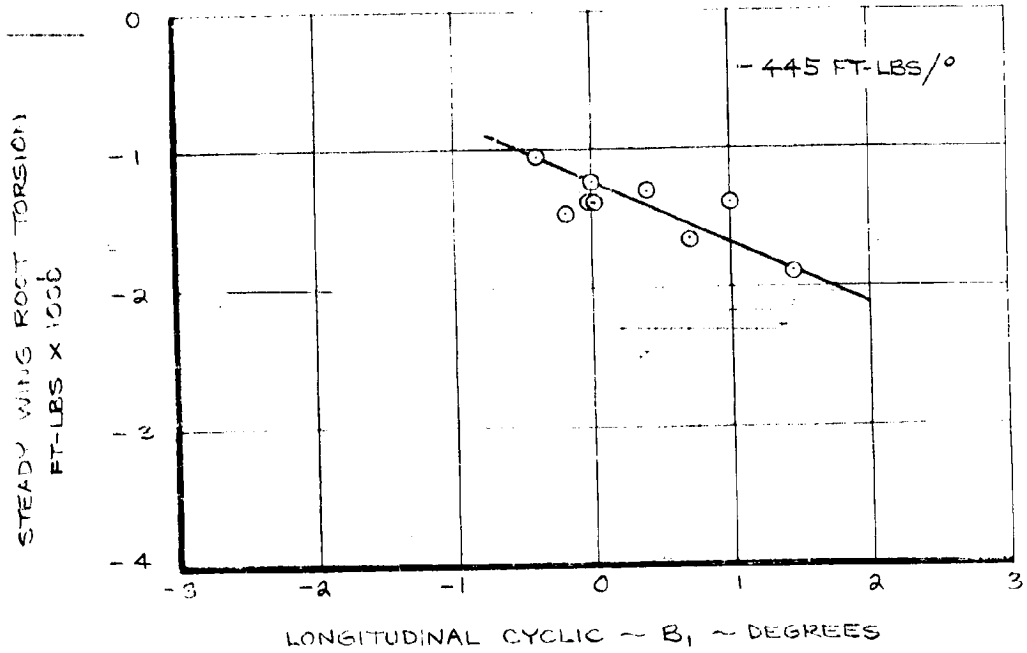

FIGURE 6-107 STEADY WING TIP LIFT AND WING ROOT TORSION DUE TO B_1 CYCLIC AT 192 KNOTS 386 RPM

-	100 Knots	140 Knots	192 Knots
$\partial C_M/\partial A_1$	0.00171	0.00201	0.0023
$\partial C_N/\partial A_1$	0.00236	0.00389	0.00752
$\partial C_{YAW}/\partial A_1$	-.00046	-.00071	-0.00163
$\partial C_{SF}/\partial A_1$	0.00316	0.00482	0.0076
$\partial C_M/\partial B_1$	0.00031	0.00052	0.00076
$\partial C_N/\partial B_1$	-0.00316	-.00482	-.00760
$\partial C_{YAW}/\partial B_1$	0.00125	0.00176	0.0021
$\partial C_{SF}/\partial B_1$	0.00236	0.00389	0.00752

Notes: 1. Wing tip pitch data used for pitch moment derivation

2. Derivatives are per degree cyclic

$$\Delta\theta = -A_{1\cos}\ (\psi + 20)\ -B_{1\sin}\ (\psi + 20)$$

Table 6.1. Summary of Windmilling Rotor Hub Force and Moment Derivatives With Cyclic Pitch in Cruise 386 RPM

NASA AMES TEST 410

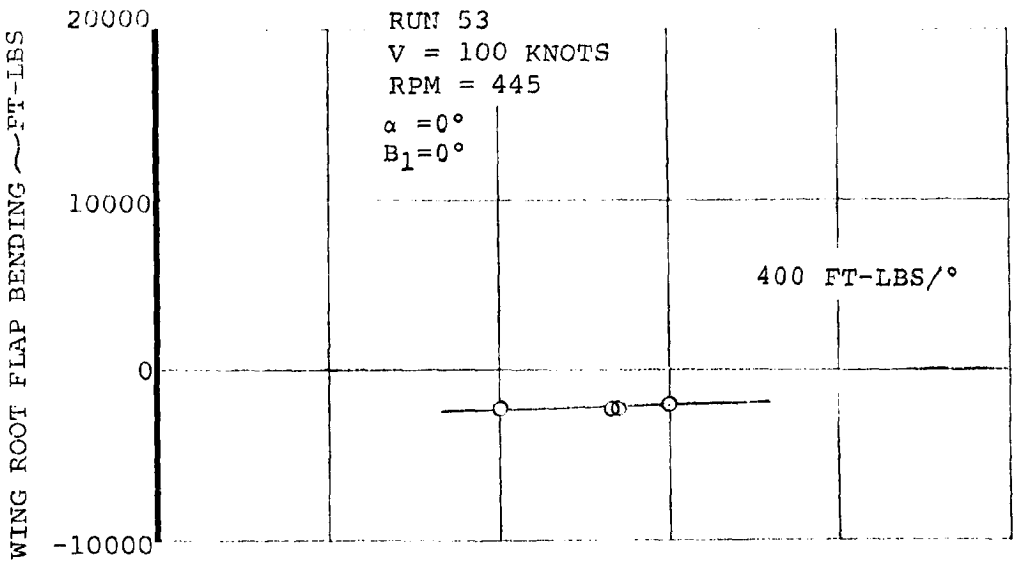

$$\Delta\theta = -A_1 \cos(\psi+20) - B_1 \sin(\psi+20)$$

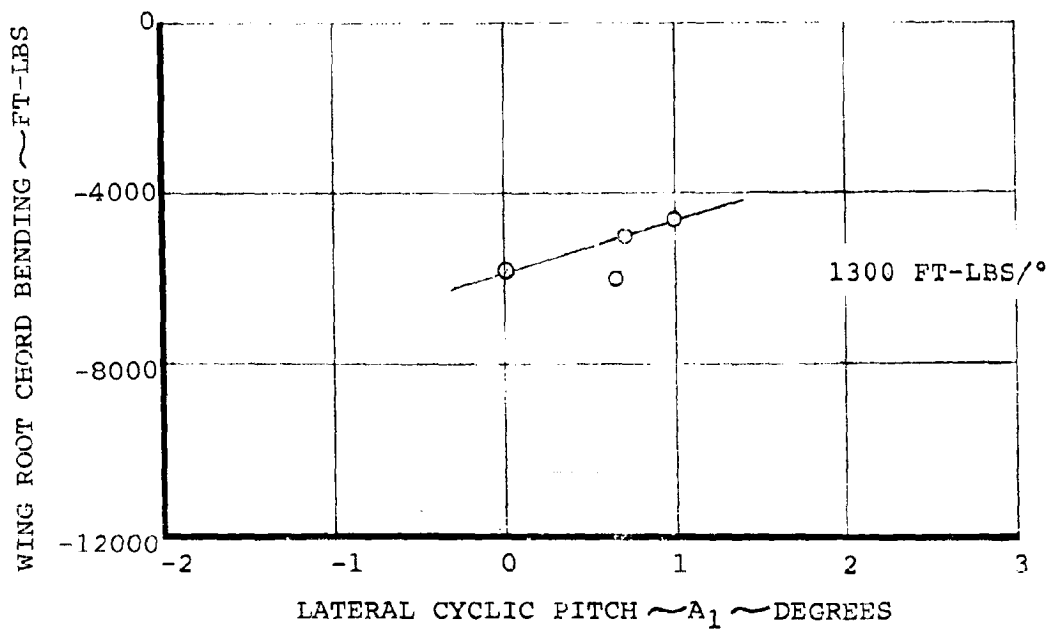

FIGURE 6-108 STEADY WING ROOT FLAP AND CHORD BENDING DUE TO A_1 CYCLIC AT 100 KNOTS 445 RPM

NASA AMES TEST 410

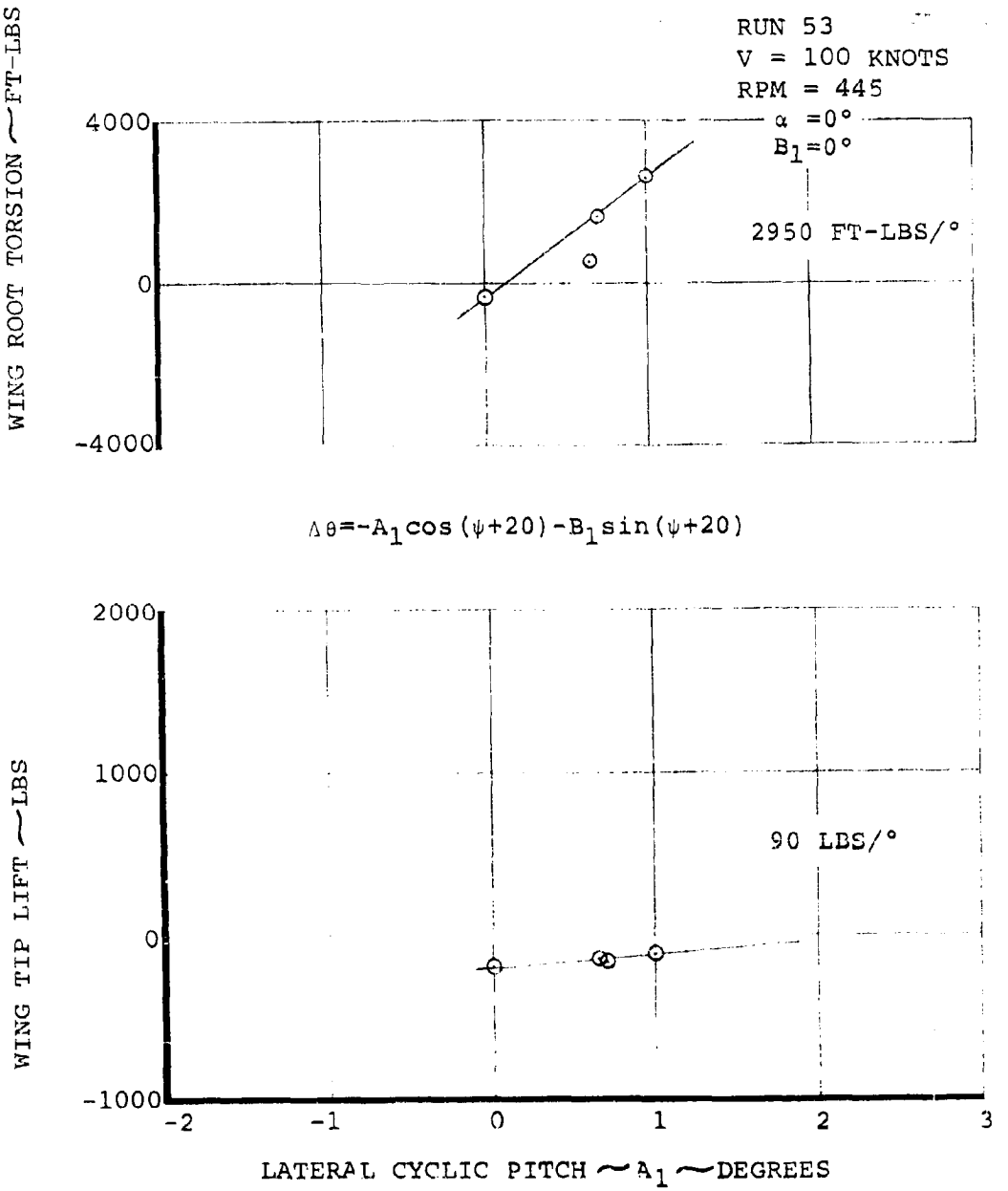

FIGURE 6-109 STEADY WING TIP LIFT AND WING ROOT TORSION DUE TO A_1 CYCLIC AT 100 KNOTS 445 RPM

NASA AMES TEST 410

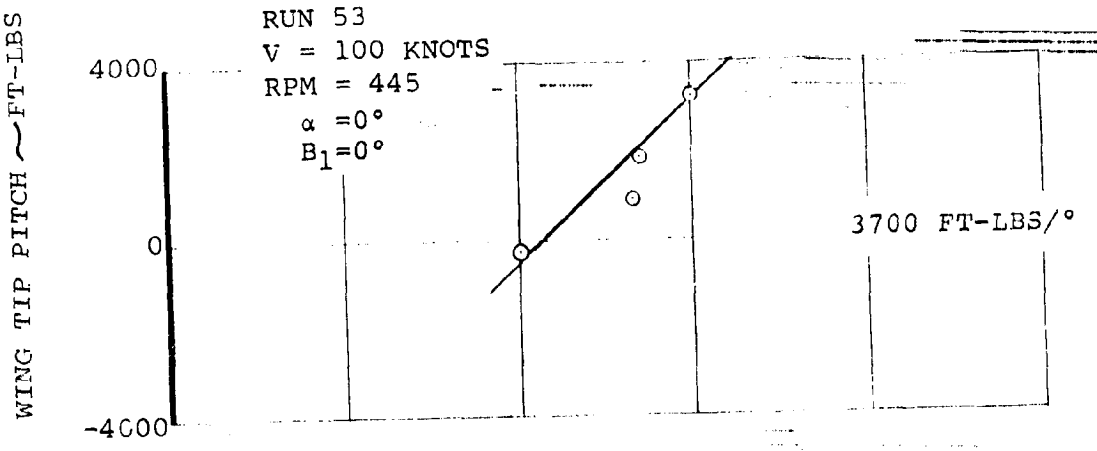

$$\Delta\theta = -A_1 \cos(\psi+20) - B_1 \sin(\psi+20)$$

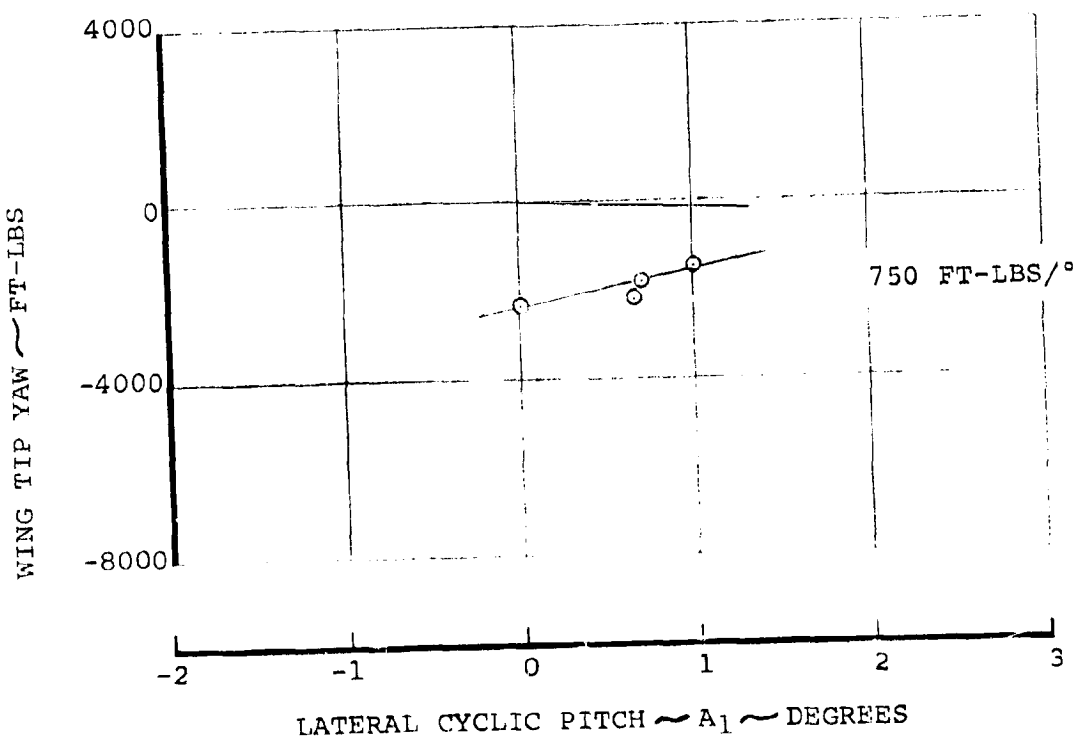

FIGURE 6-110 STEADY WING TIP PITCH AND YAW MOMENT DUE TO A_1 CYCLIC AT 100 KNOTS 445 RPM

NASA AMES TEST 410

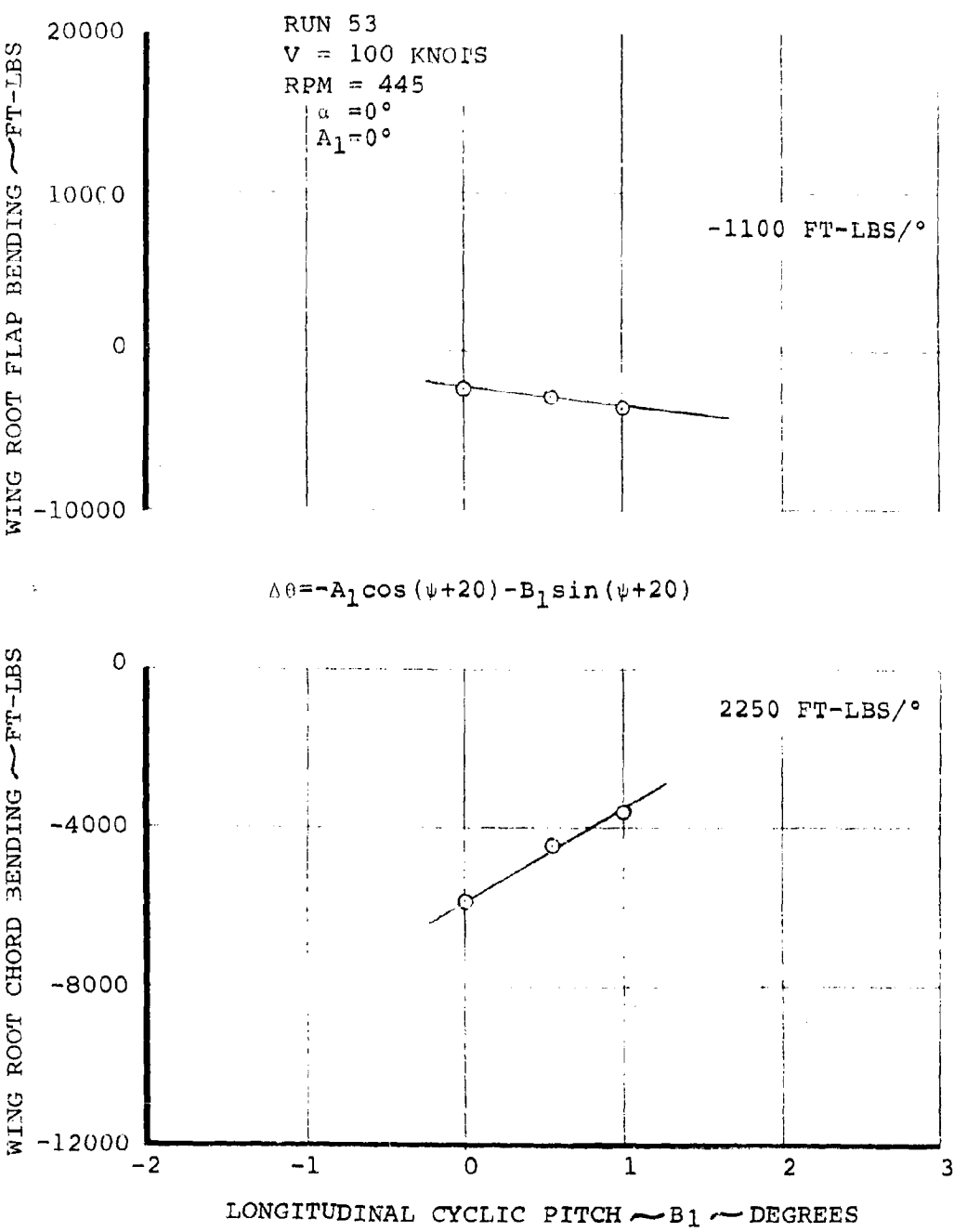

FIGURE 6-111 STEADY WING ROOT FLAP AND CHORD BENDING DUE TO B_1 CYCLIC AT 100 KNOTS 445 RPM

NASA AMES TEST 410

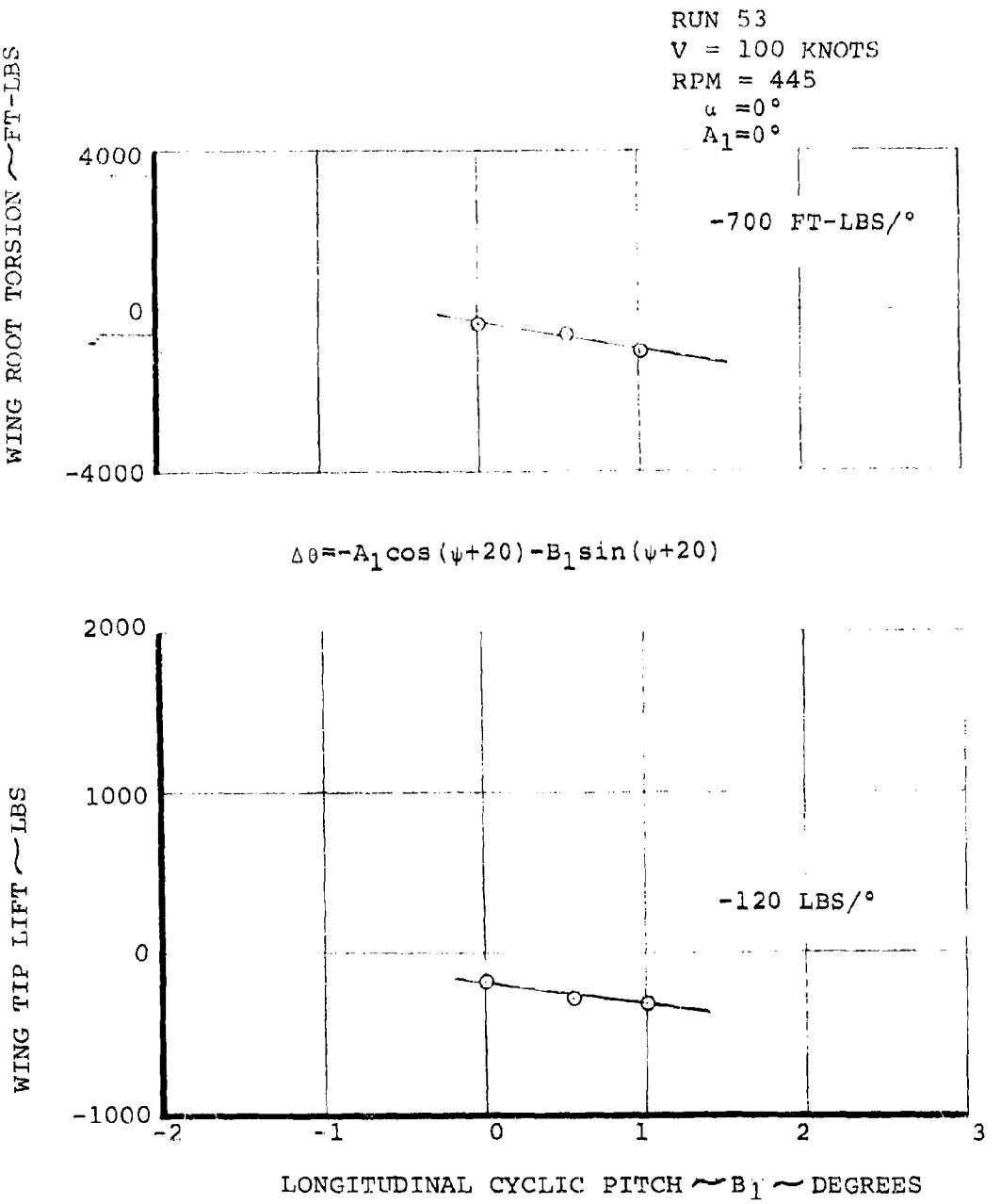

FIGURE 6-112 STEADY WING TIP LIFT AND WING ROOT TORSION DUE TO B_1 CYCLIC AT 100 KNOTS 445 RPM

NASA AMES TEST 410

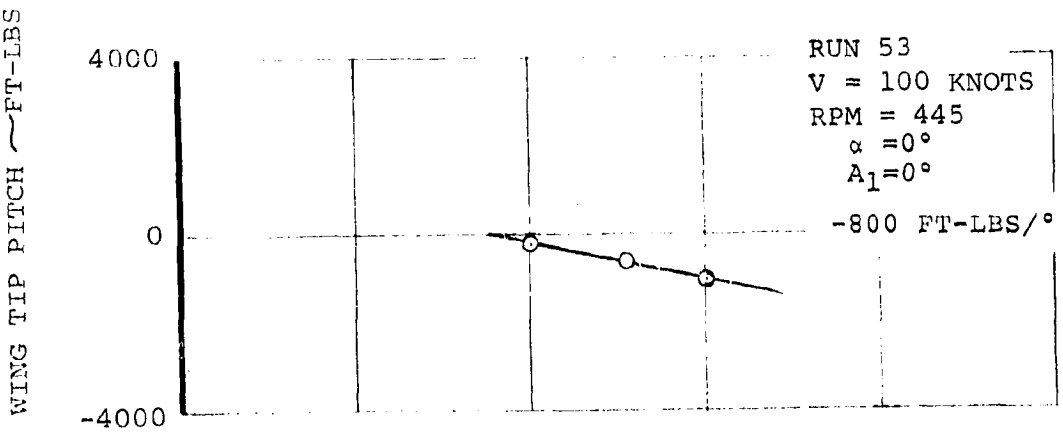

$$\Delta\theta = -A_1\cos(\psi+20) - B_1\sin(\psi+20)$$

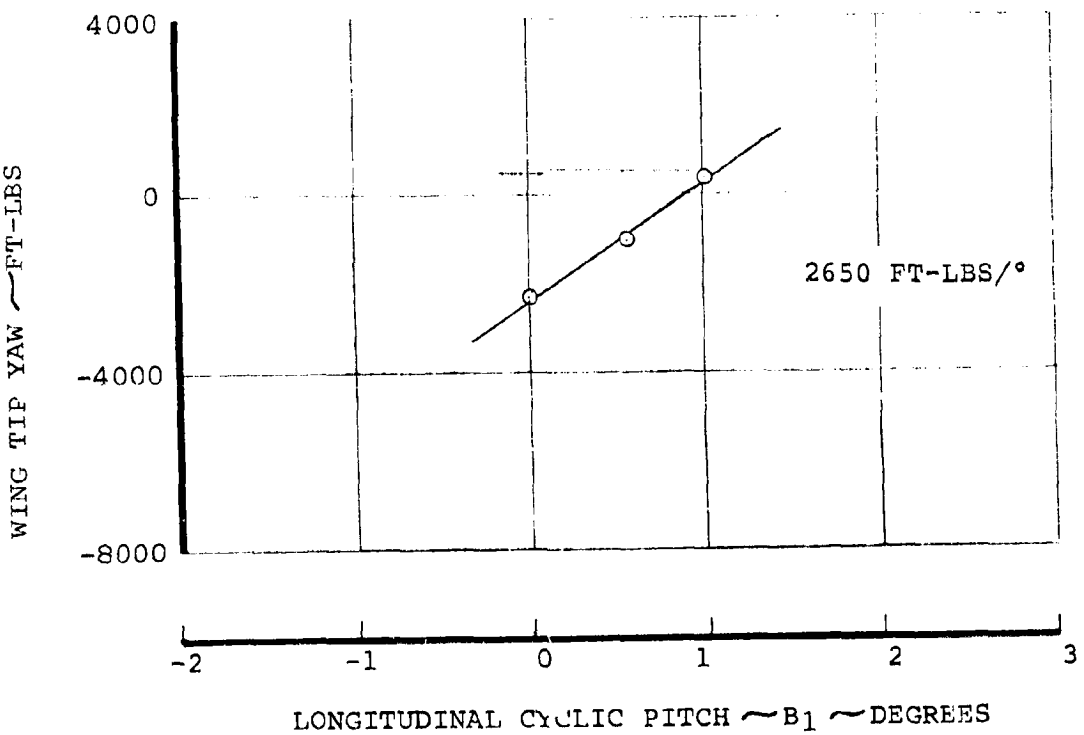

FIGURE 6-113 STEADY WING TIP PITCH AND YAW MOMENT DUE TO B_1 CYCLIC AT 100 KNOTS 445 RPM

NASA AMES TEST 410

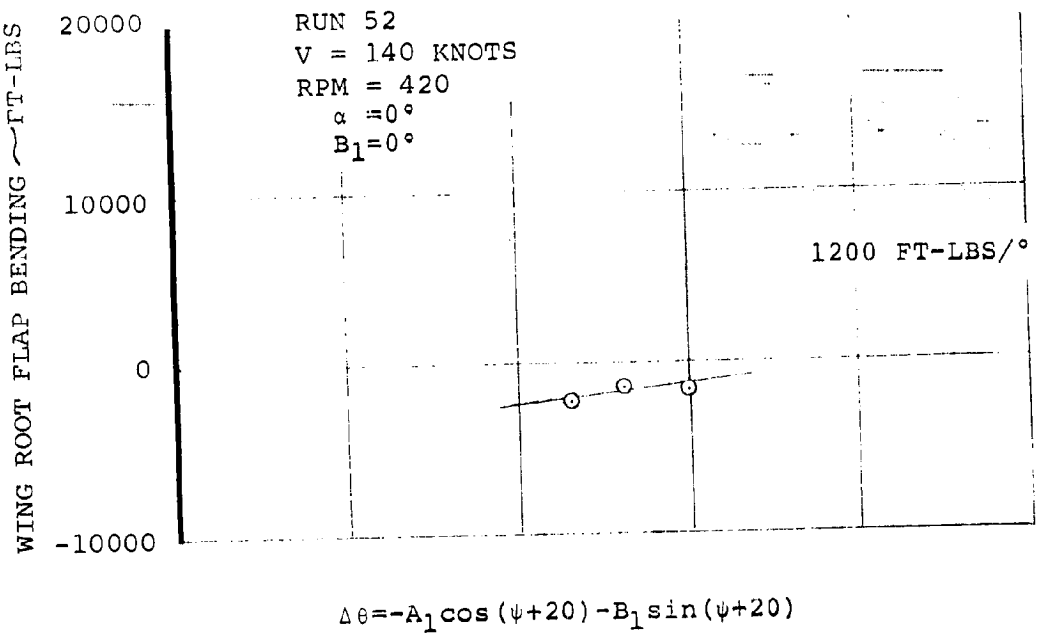

$$\Delta\theta = -A_1 \cos(\psi+20) - B_1 \sin(\psi+20)$$

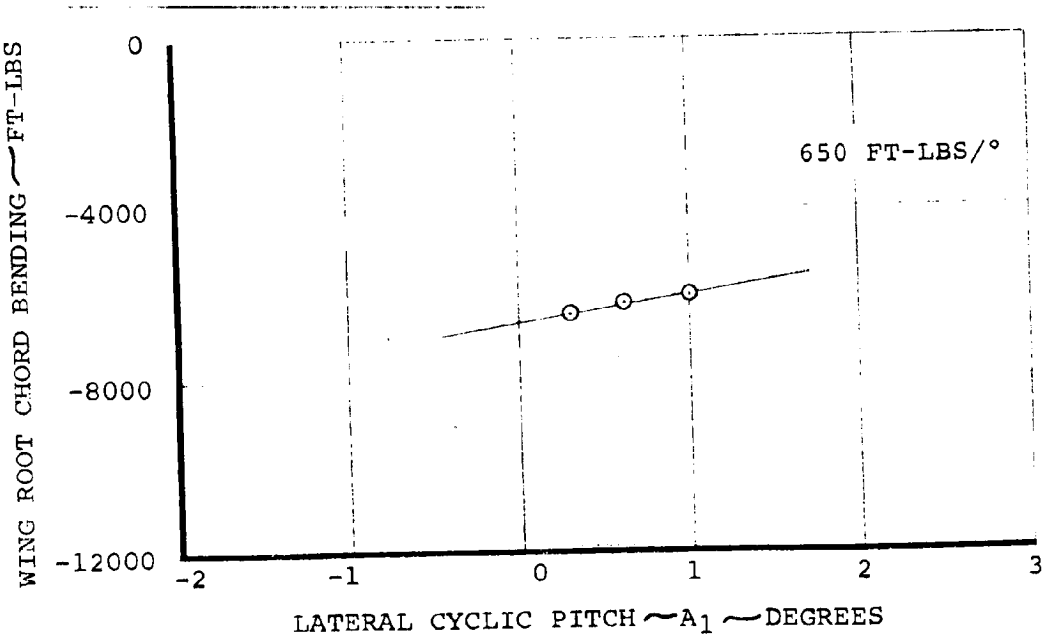

FIGURE 6-114 STEADY WING ROOT FLAP AND CHORD BENDING DUE TO A_1 CYCLIC AT 140 KNOTS 420 RPM

NASA AMES TEST 410

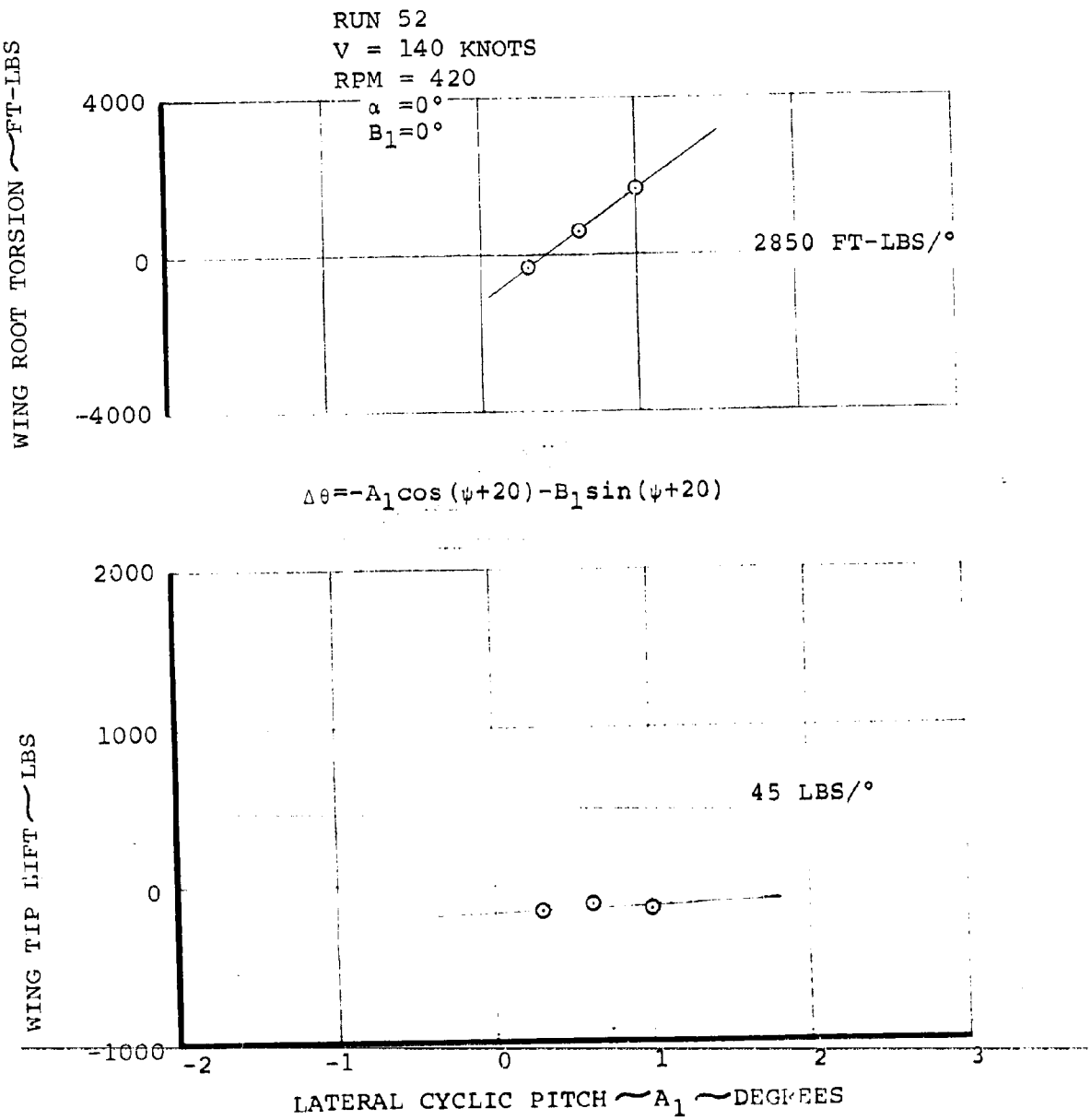

FIGURE 6-115 STEADY WING TIP LIFT AND WING ROOT TORSION DUE TO A_1 CYCLIC AT 140 KNOTS 420 RPM

NASA AMES TEST 410

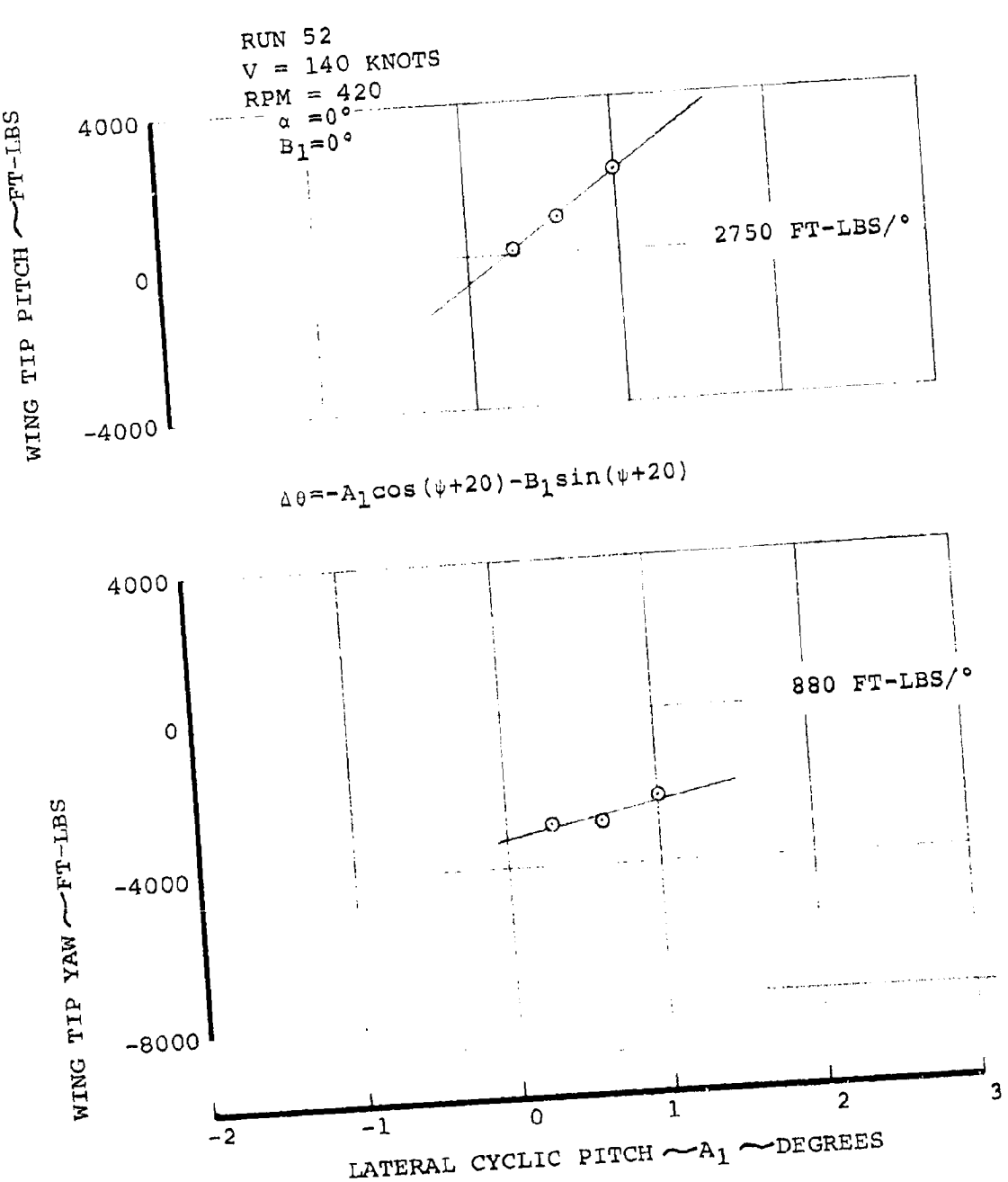

FIGURE 6-116 STEADY WING TIP PITCH AND YAW MOMENT DUE TO A_1 CYCLIC AT 140 KNOTS 420 RPM

NASA AMES TEST 410

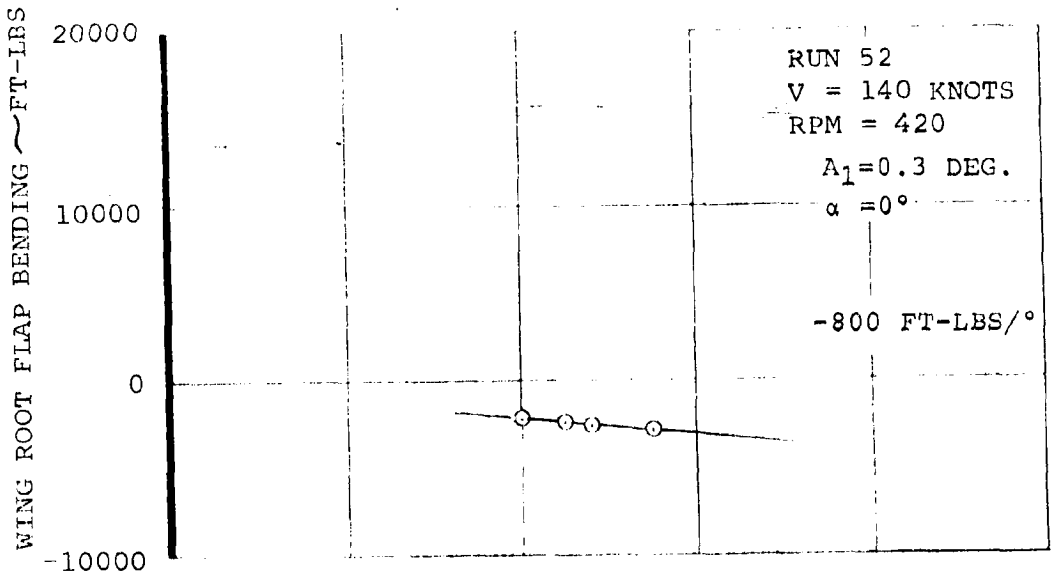

$$\Delta\theta = -A_1 \cos(\psi+20) - B_1 \sin(\psi+20)$$

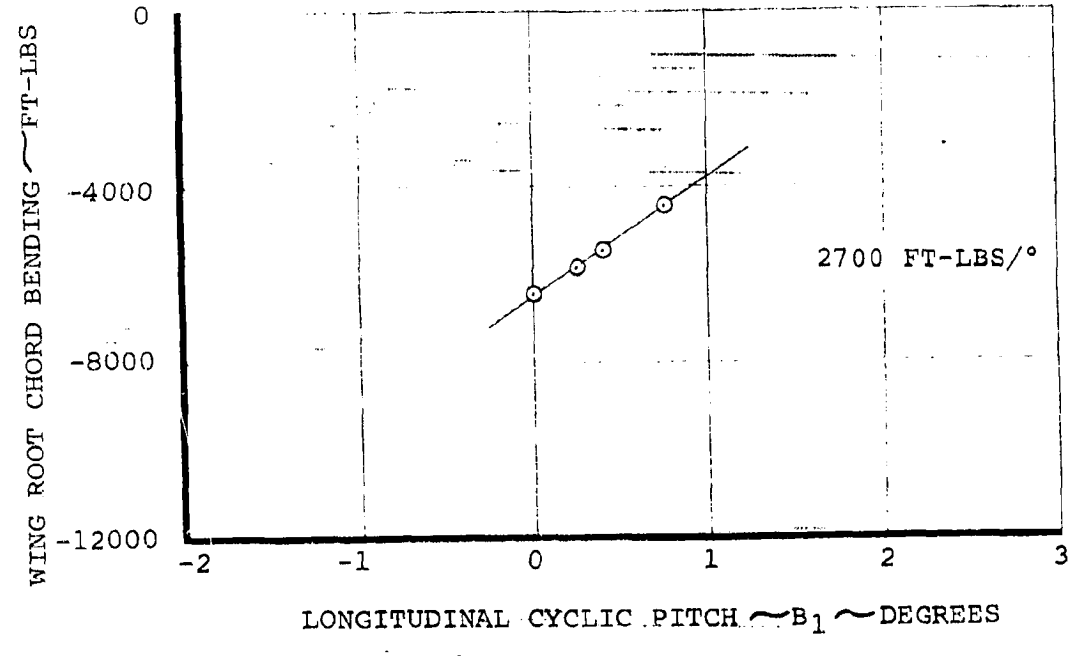

FIGURE 6-117 STEADY WING ROOT FLAP AND CHORD BENDING DUE TO B_1 CYCLIC AT 140 KNOTS 420 RPM

NASA AMES TEST 410

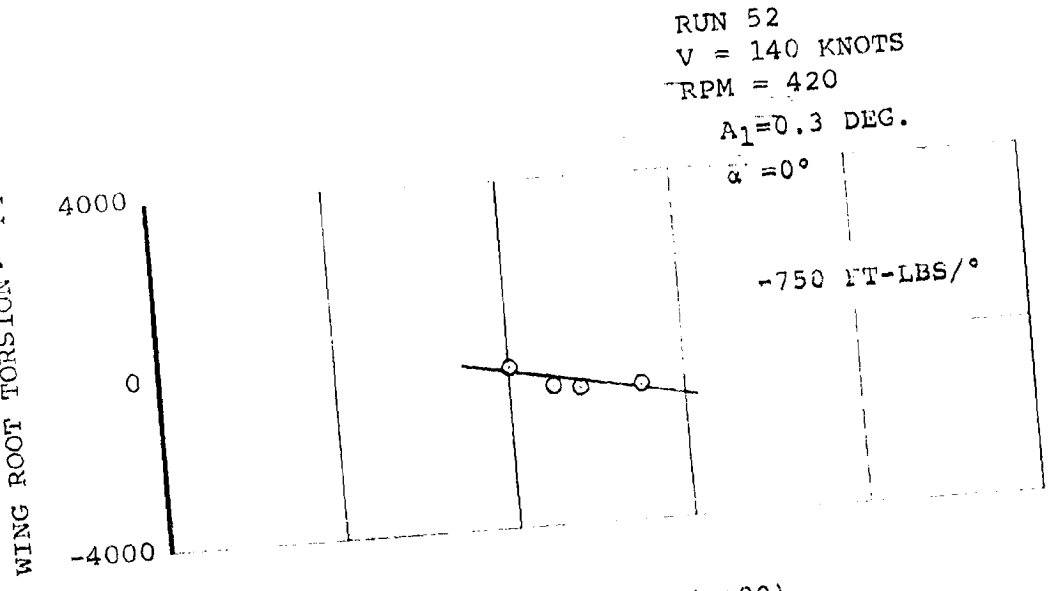

$$\Delta\theta = -A_1 \cos(\psi+20) - B_1 \sin(\psi+20)$$

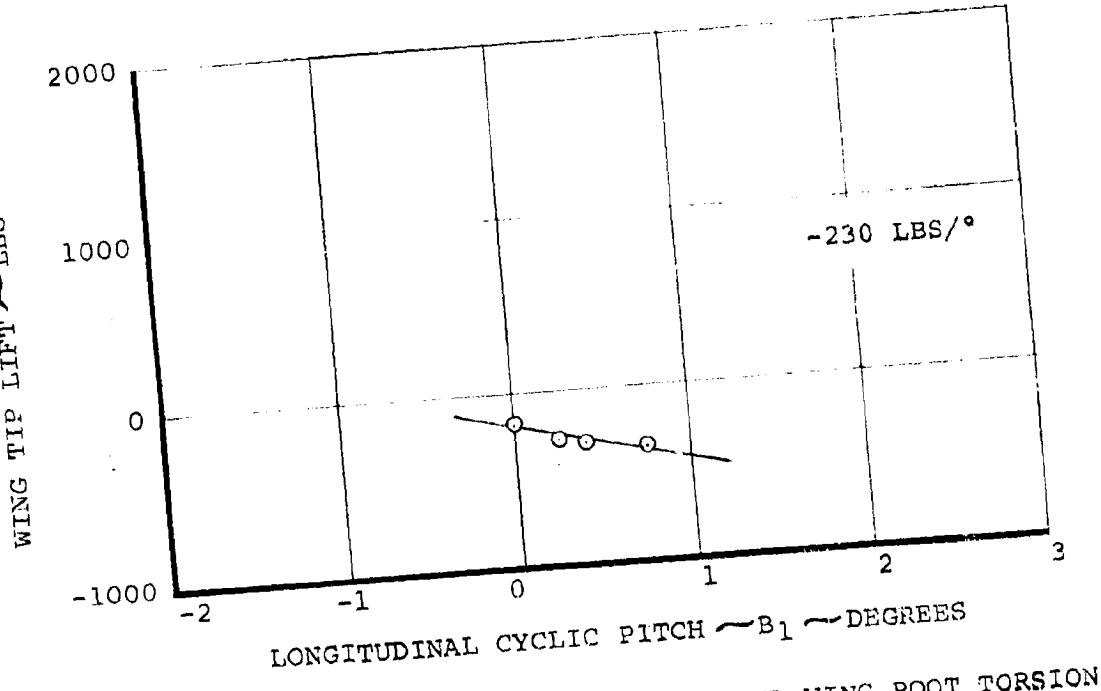

FIGURE 6-118 STEADY WING TIP LIFT AND WING ROOT TORSION DUE TO B_1 CYCLIC AT 140 KNOTS 420 RPM

NASA AMES TEST 410

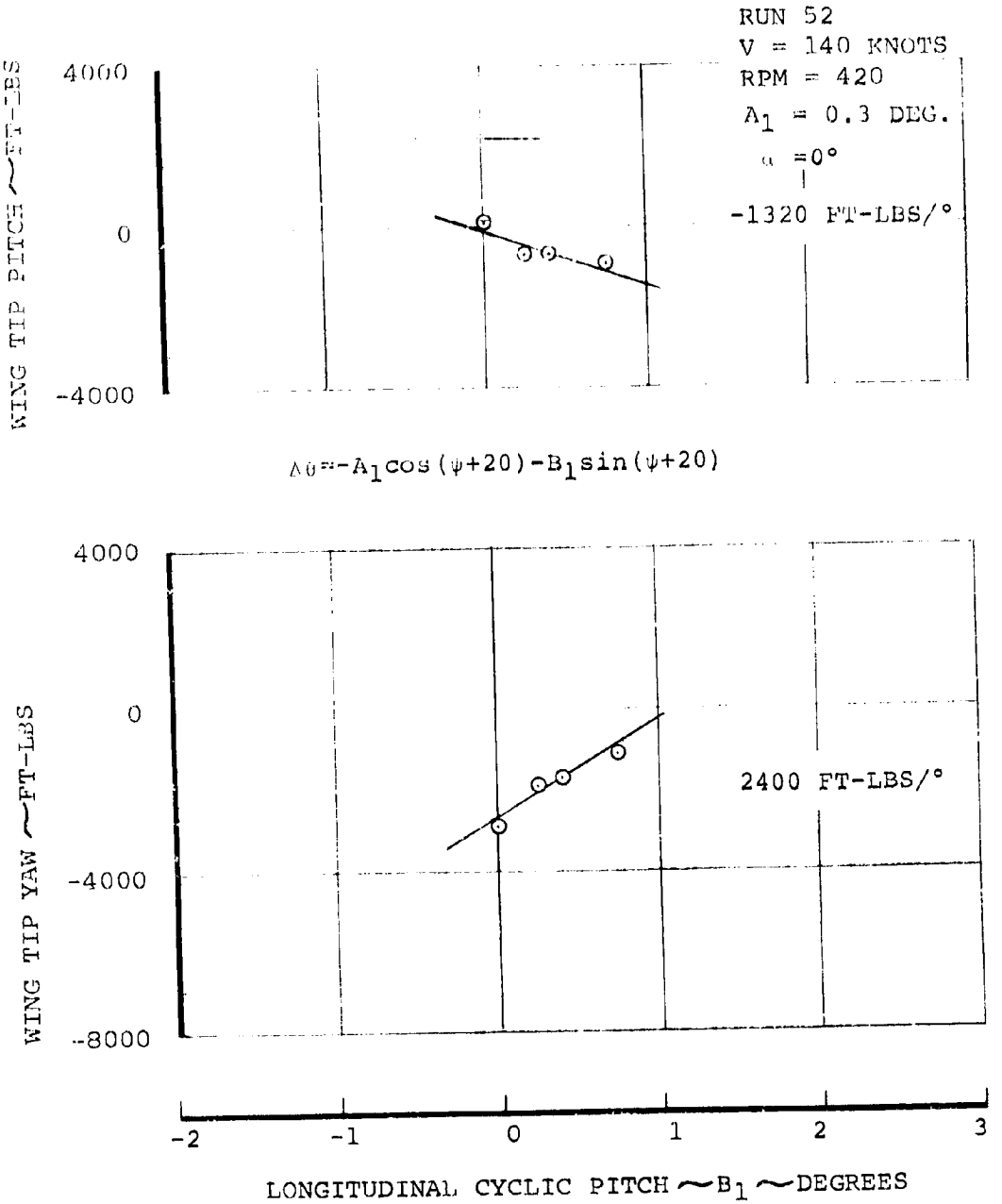

FIGURE 6-119 STEADY WING TIP PITCH AND YAW MOMENT DUE TO B_1 CYCLIC AT 140 KNOTS 420 RPM

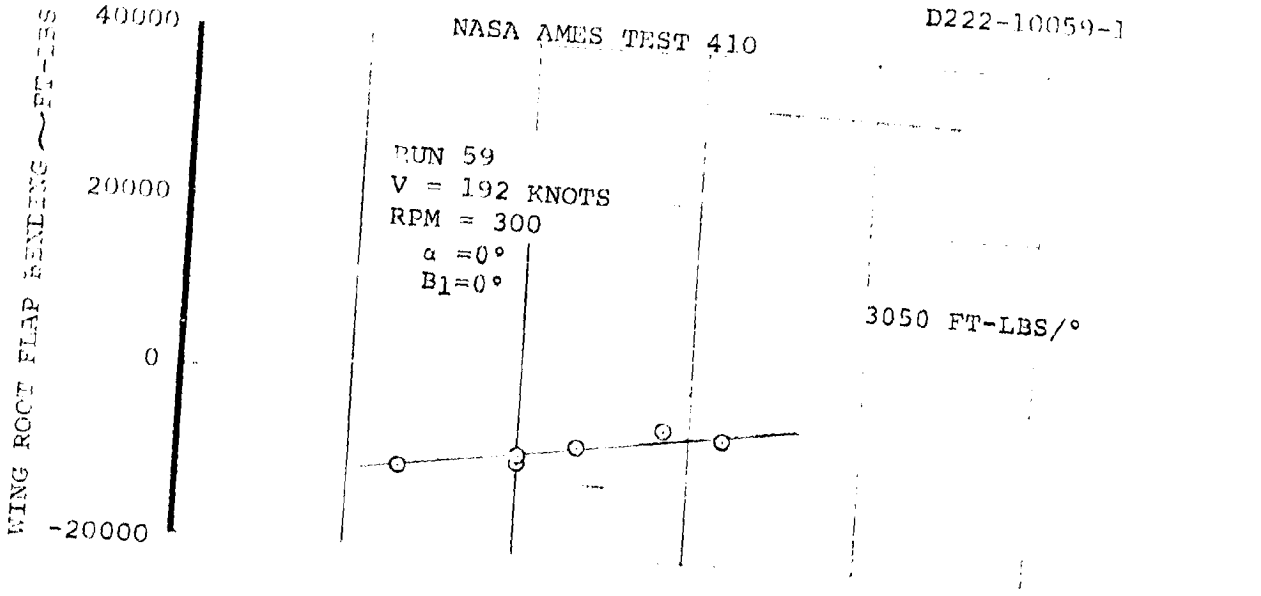

$$\Delta\theta = -A_1 \cos(\psi+20) - B_1 \sin(\psi+20)$$

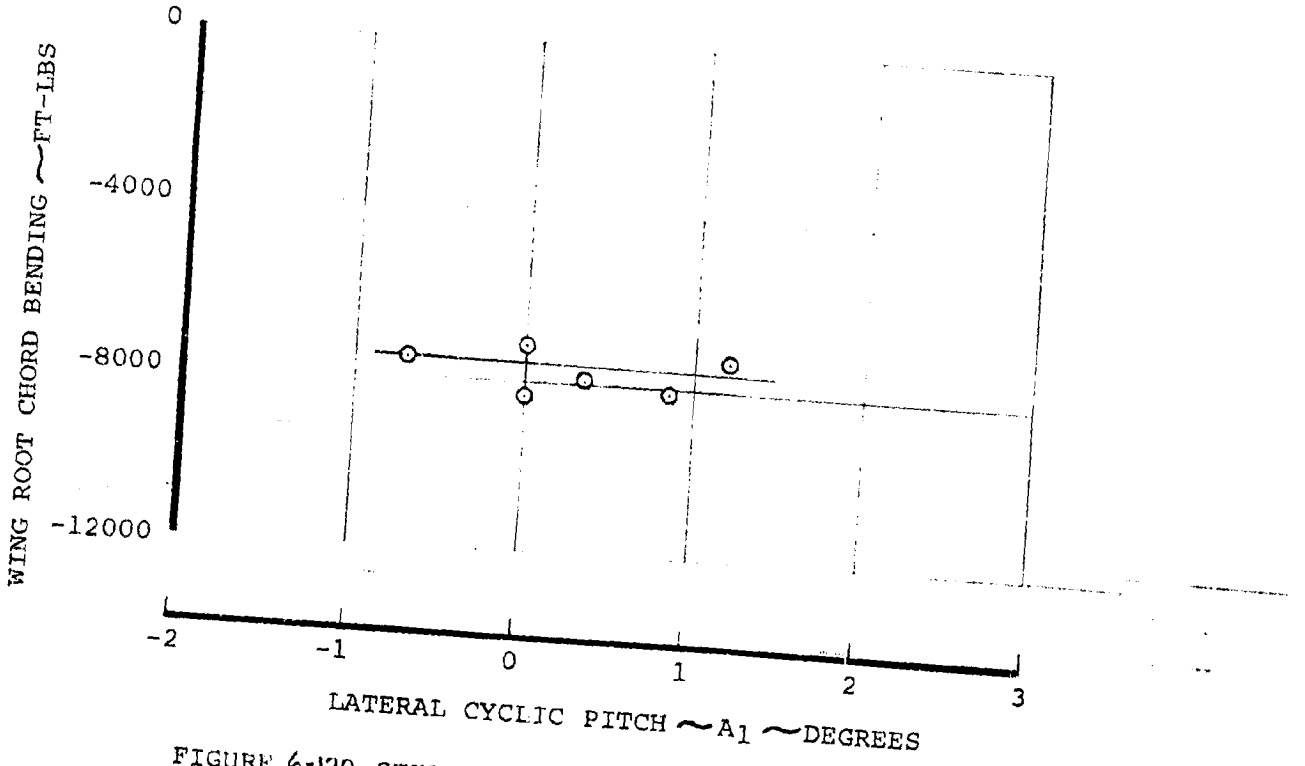

FIGURE 6-120 STEADY WING ROOT FLAP AND CHORD BENDING DUE TO A_1 CYCLIC AT 192 KNOTS 300 RPM

NASA AMES TEST 410

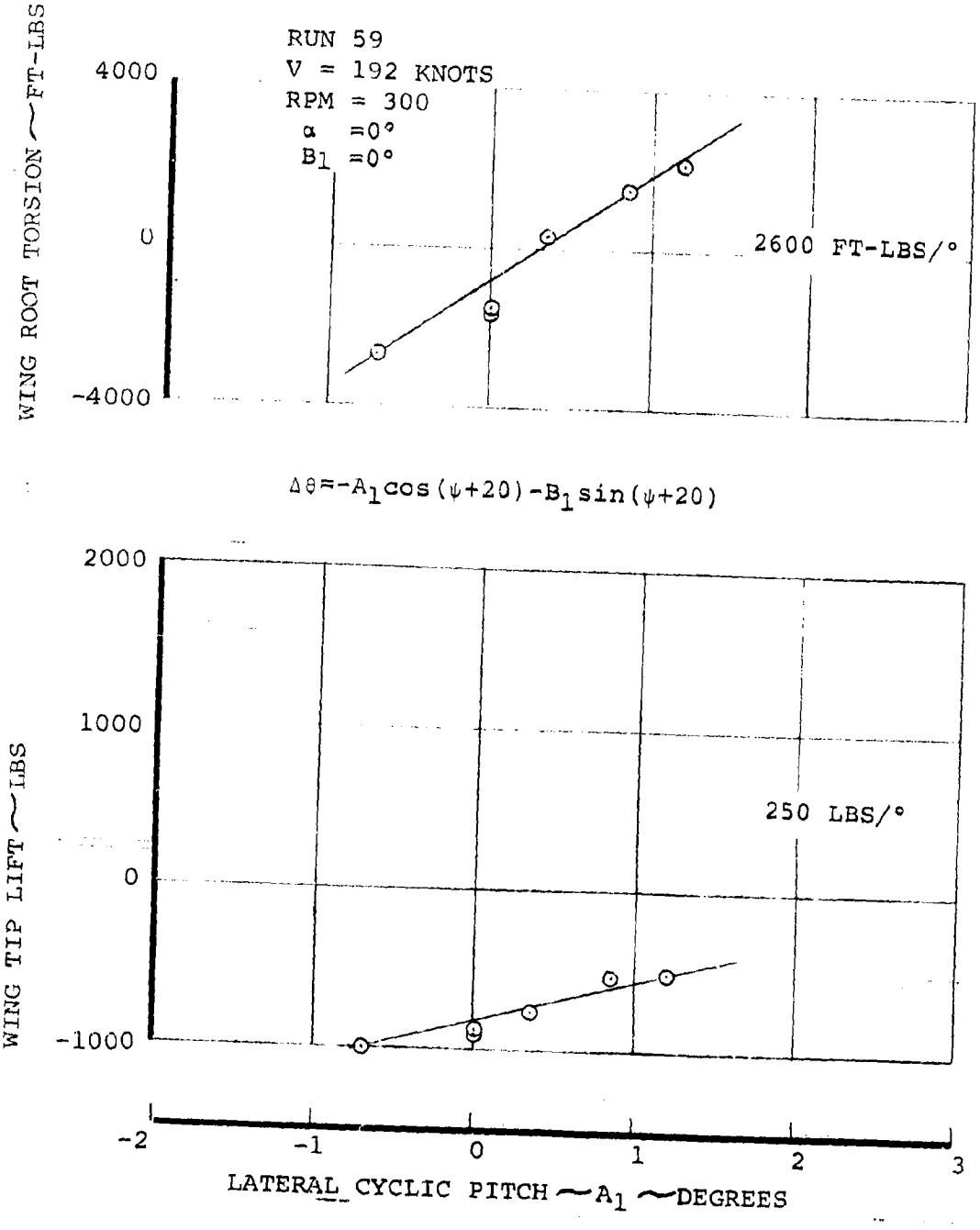

FIGURE 6-121 STEADY WING TIP LIFT AND WING ROOT TORSION DUE TO A_1 CYCLIC AT 192 KNOTS 300 RPM

NASA AMES TEST 410

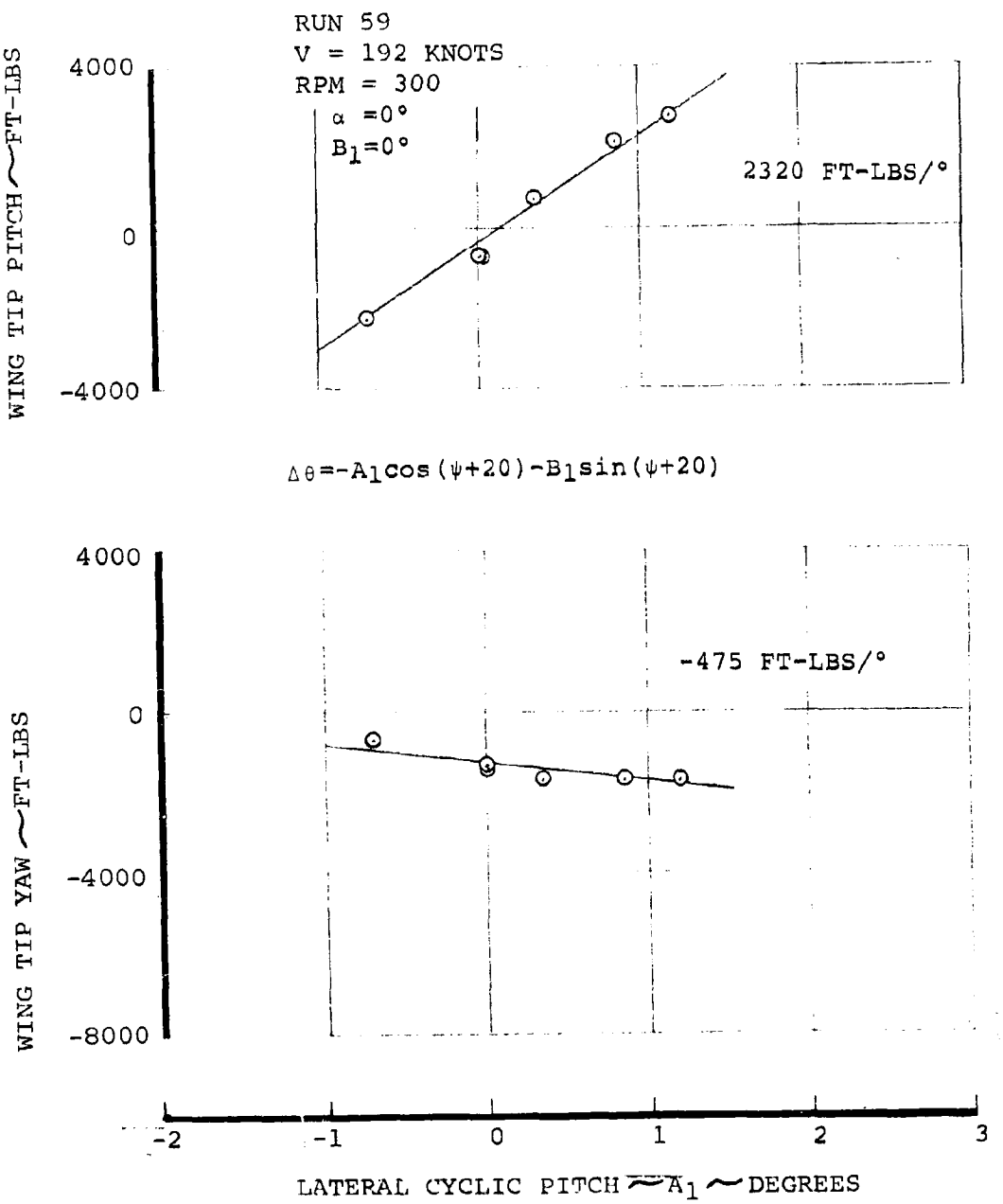

FIGURE 6-12 STEADY WING TIP PITCH AND YAW MOMENT DUE TO A_1 CYCLIC AT 192 KNOTS 300 RPM

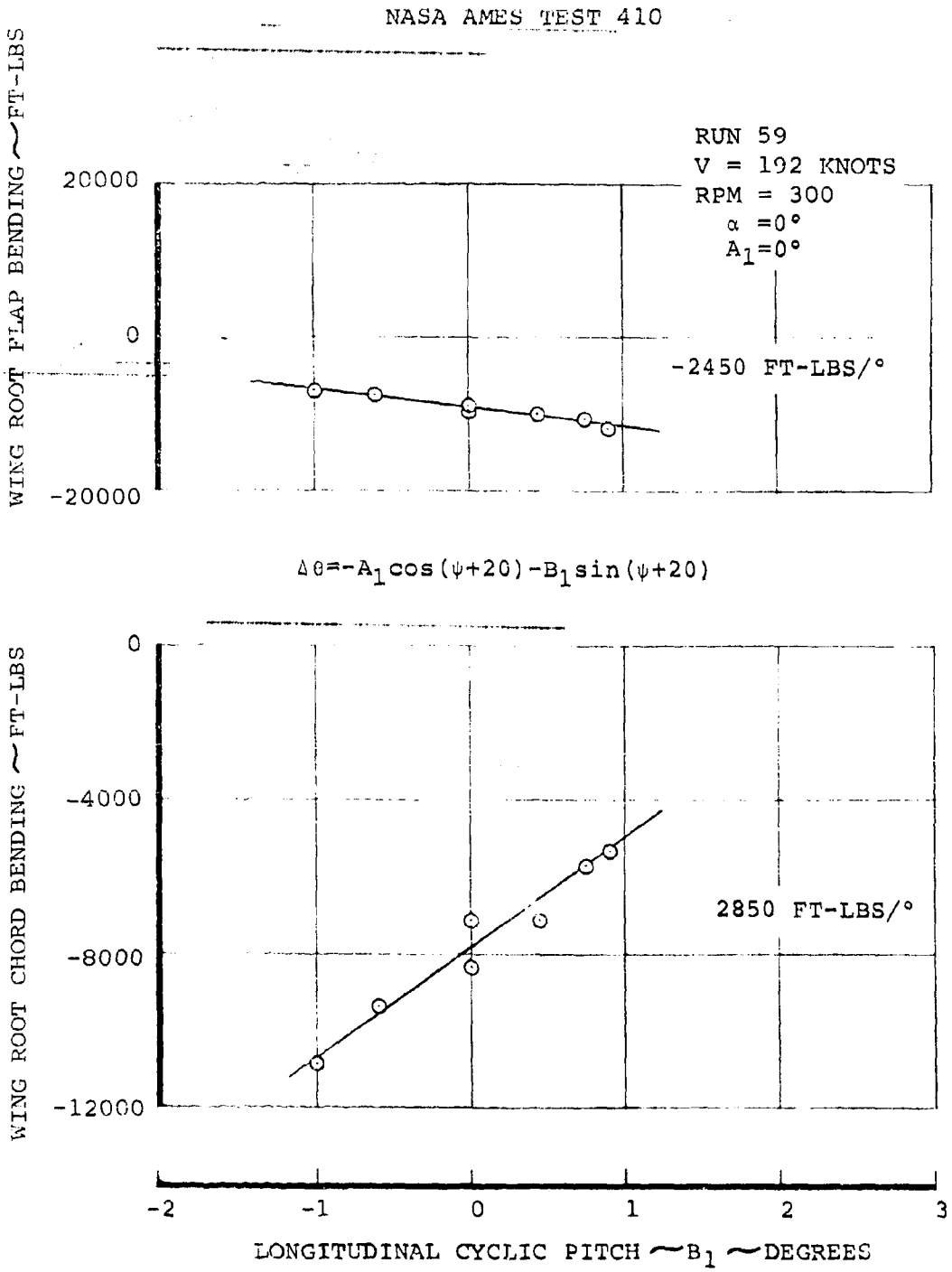

FIGURE 6-123 STEADY WING ROOT FLAP AND CHORD BENDING DUE TO B_1 CYCLIC AT 192 KNOTS 300 RPM

NASA AMES TEST 410

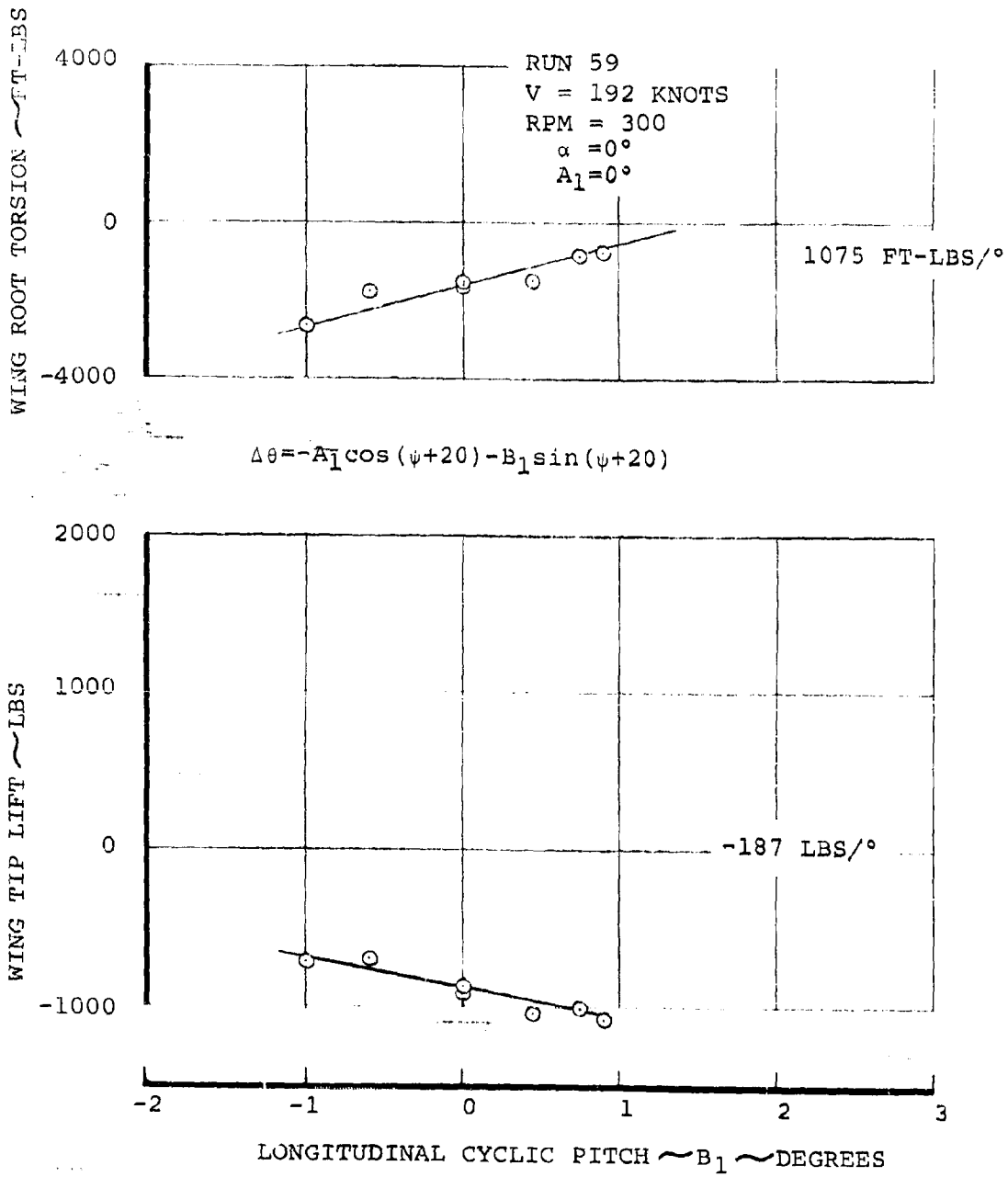

FIGURE 6-124 STEADY WING TIP LIFT AND WING ROOT TORSION DUE TO B_1 CYCLIC AT 192 KNOTS 300 RPM

NASA AMES TEST 410

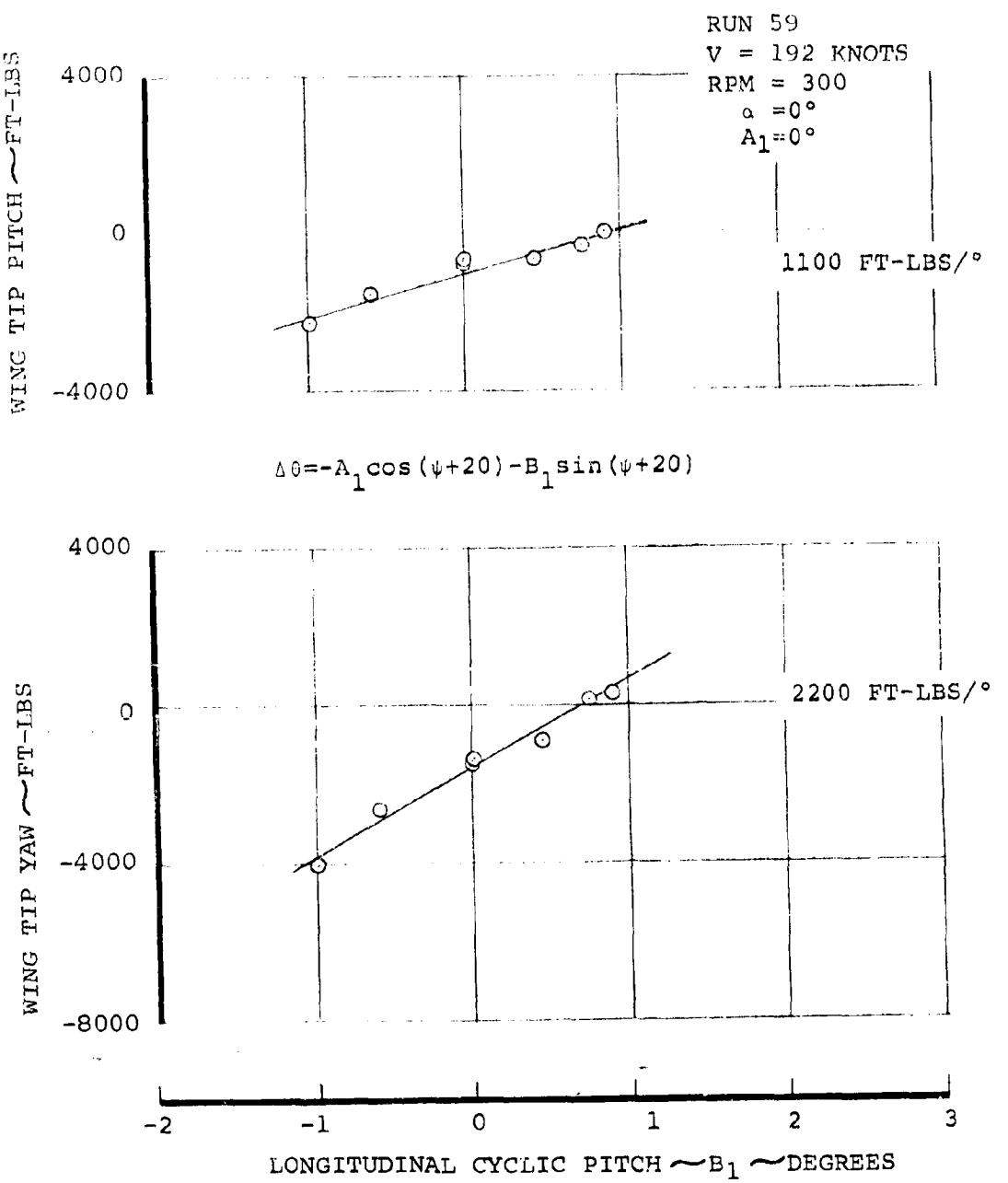

FIGURE 6-125 STEADY WING TIP PITCH AND YAW MOMENT DUE TO B_1 CYCLIC AT 192 KNOTS 300 RPM

7.0 PERFORMANCE

The performance of the tilt rotor aircraft is high both in hover and cruise flight. The compromises required in rotor design have been studied extensively under NASA Contract NAS2-6784, References 7, 8 and 20. During test 416 thrust and power data were obtained in a vertical climb condition and extrapolated to hover. Transition and low speed cruise performance was also measured and compares well with the thrust and power data predicted in Reference 15.

7.1 Performance in Hover and Vertical Climb

Test runs 7 and 15 of Test 416 were performed at zero incidence with the 40' x 80' tunnel fans stopped and in some cases with reverse tunnel fan. These data points are equivalent to a vertical climb condition and the data are plotted against climb rate advance ratio in Figures 7-1 and 7-2. The rotor was capable of driving the 40' x 80' tunnel up to about 30 kts which made low advance ratio data difficult to obtain. The data have been faired and extrapolated back to zero advance ratio on a purely empirical basis. The extrapolations shown indicate hover performance as plotted in Figure 7-3. A method of determining static efficiency is suggested in Reference 20. Values of figure of merit using this

procedure are given in Table 7-1 for Run 7 and indicate higher static figure of merit values than are predicted for this rotor.

Precise evaluation of static performance requires a more rigorous test procedure; however, the data obtained do not conflict with the predicted static rotor performance.

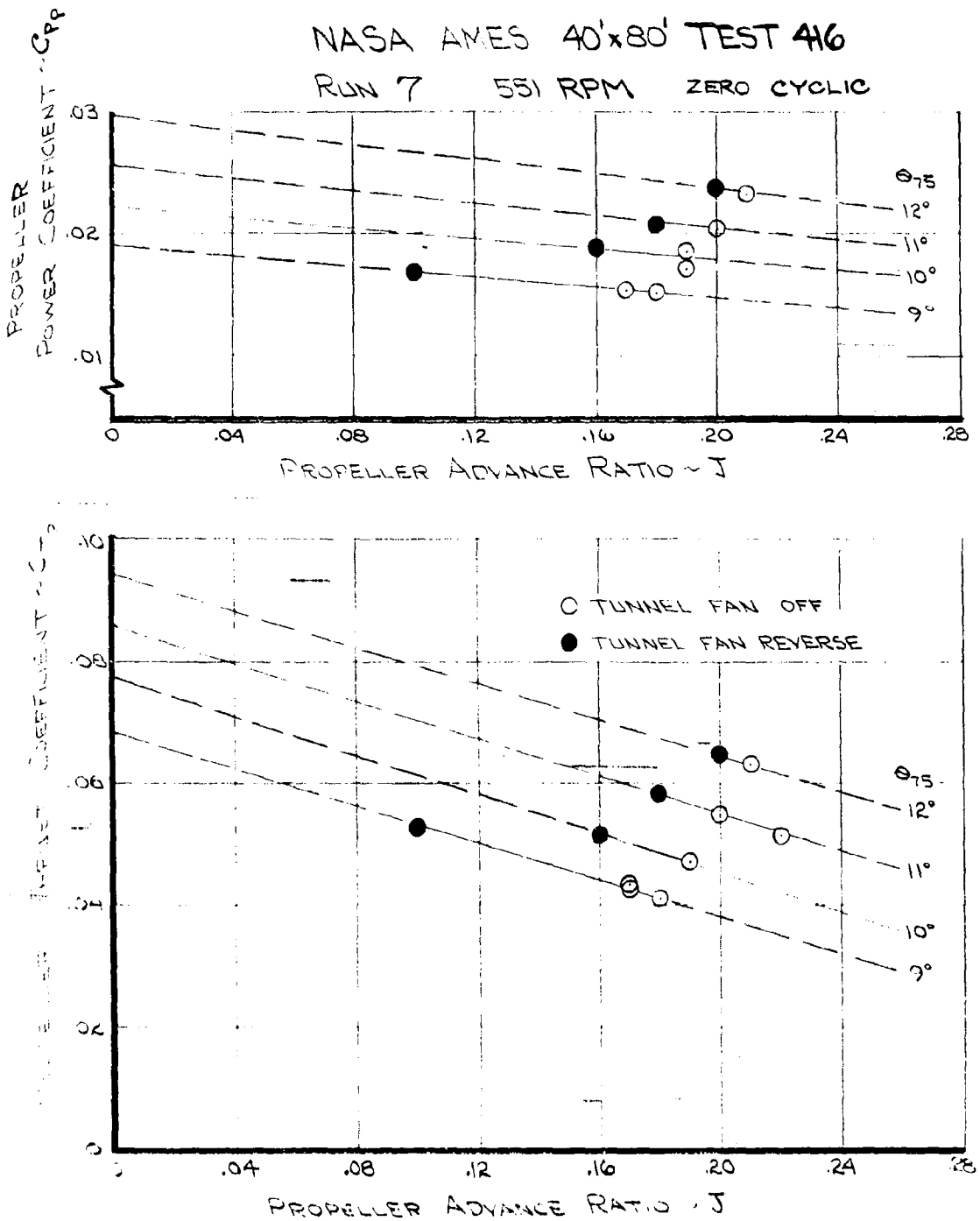

FIGURE 7-1 ROTOR PERFORMANCE IN VERTICAL CLIMB

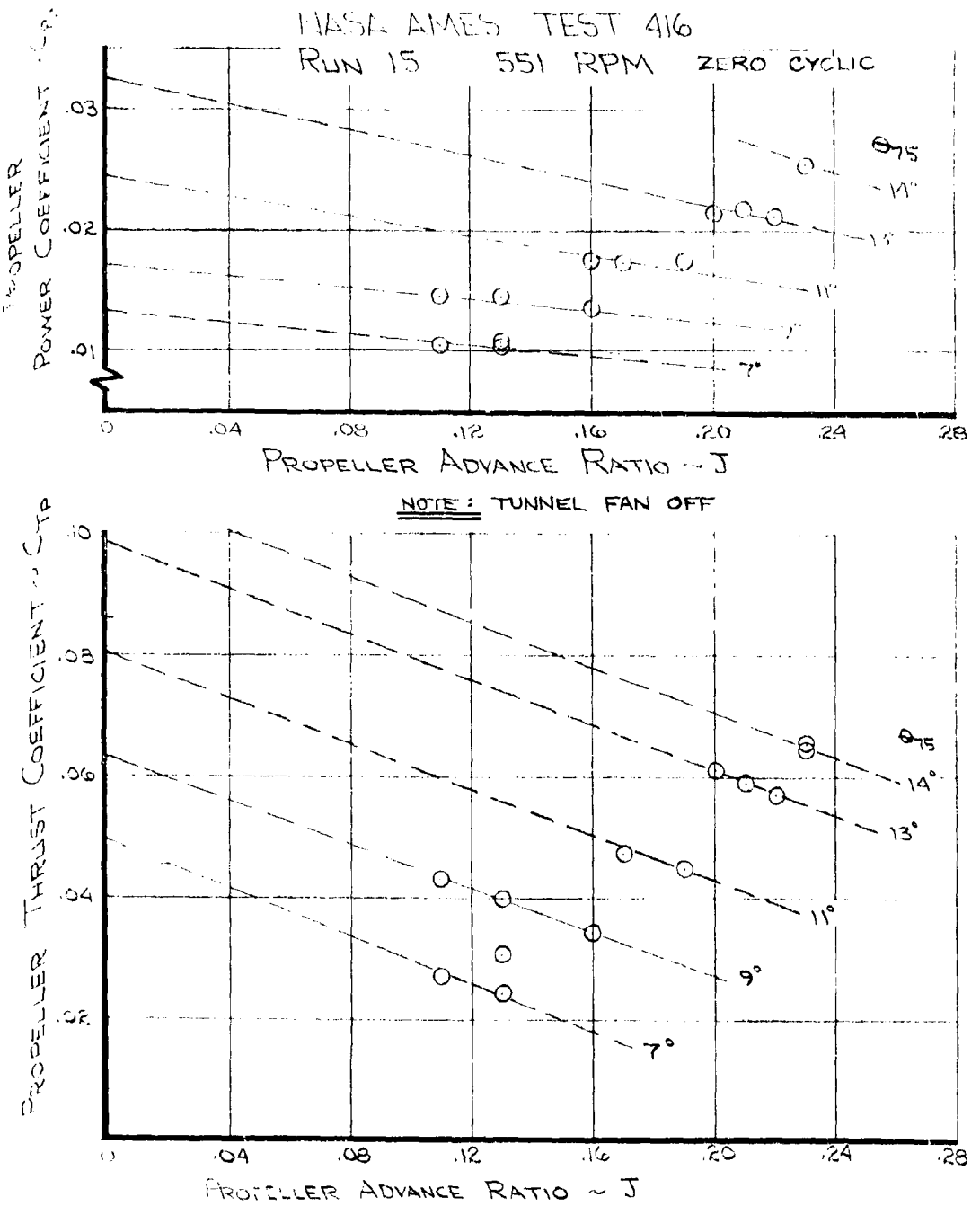

FIGURE 7-2. ROTOR PERFORMANCE IN VERTICAL CLIMB

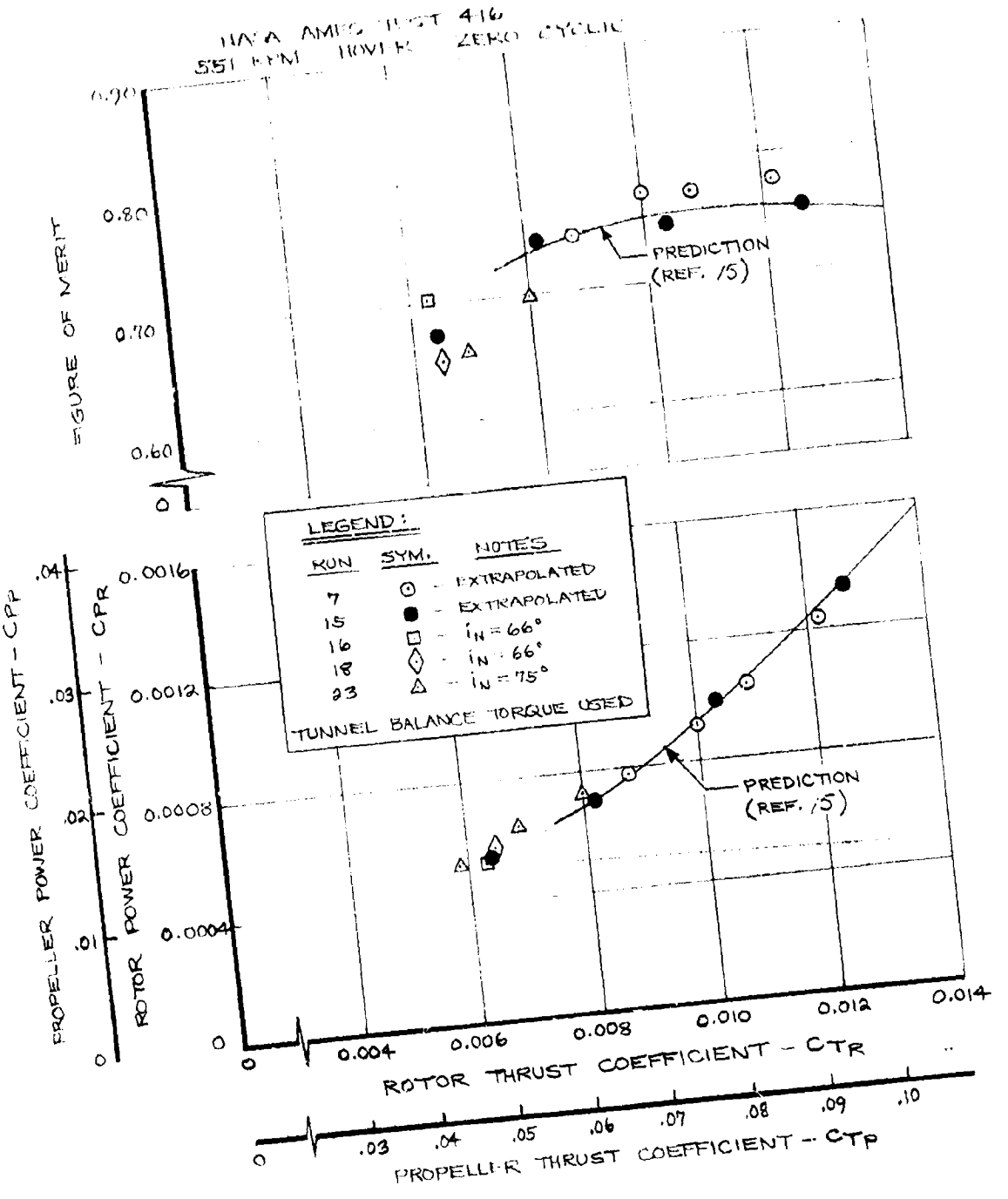

FIGURE 7-3 HOVER ROTOR PERFORMANCE

TABLE 7-1

STATIC EFFICIENCIES USING METHOD OF REFERENCE EC.

$$FM = C_T/C_P \quad \left(J/2 + \sqrt{(J/2)^2 + \frac{2\,C_T}{\pi}}\right)$$

Run 7 Data Point	$\Theta_{.75}$	C_{T_P}	C_{P_P}	J	FM
2	9	.0436	.0152	.17	.7803
3	10	.0471	.017	.19	.8104
4	11	.0517	.0176	.22	.946
6	9	.0524	.0168	.10	.7466
7	10	.0514	.0175	.16	.816
8	11	.0581	.0209	.18	.8405
9	12	.0643	.0238	.2	.8799
11	12	.0631	.0232	.21	.9009
12	11	.0551	.0203	.2	.8477
13	10	.0473	.0169	.19	.7916
14	9	.0411	.015	.18	.754

7.2 Transition Flight Performance

The transition test program consisted of excursions of collective, cyclic pitch and where possible nacelle incidence about an initial test condition. At each initial test condition cyclic pitch was adjusted to provide minimum alternating blade loads. For some test conditions the tunnel balance foul warning light was on. These data points are shown as solid symbols and should be considered with caution. The foul warning system is electrical and indicates a foul when a mechanical foul between the fairings and the balance mounted model occurs. Several times throughout the test a foul warning was traced to an electrical problem. It is not possible to identify which fouls are real. All of the data taken has been presented.

Correlation of thrust-power data obtained on Run 19, Test 416, with pretest predictions is shown in Figure 7-4. These data were obtained at 500 RPM because of rotor-test stand dynamic couplings discussed in Section 3. The effect of operating at 500 RPM as opposed to 550 RPM is shown later to be not significant. The data show lower power coefficients than predicted in the range of thrust

coefficients normally used at this flight condition. The predicted data are taken from Reference 15 .

Figures 7-5 through 7-7 show the effects of cyclic pitch and collective at 85° and 45 kts. Figures 7-5 and 7-6 show that both rotor thrust and power are insensitive to cyclic pitch changes. Figure 7-7 shows the thrust and power data with collective pitch and covers a range of thrust coefficients from 0.047 to 0.087. For this flight condition the C_T for unaccelerated 1g flight is 0.071.

The data shown in Figures 7-8 to 7-11 are for a nacelle incidence of 83° and 76 kts. This condition is not a normal flight condition since at 80 kts the unaccelerated flight schedule calls for about 55° of nacelle incidence relative to the wind. The value of C_{T_p} (.078) recorded at 10.5° θ_{75} would correspond to vertical load factors in excess of 1.8 g's dependent on fuselage angle of attack.

The predicted performance at this flight condition is verified by the measured data, Figure 7-8. The A_1 cyclic data, Figure 7-9, shows a small reduction in power as A_1 cyclic is reduced, thrust is unaffected. Figure 7-10 shows no effect of B_1 cyclic on power but a small reduction in thrust

as B_1 cyclic is increased. Thrust and power increase with collective and the data are shown in Figure 7-11.

At 66° incidence it was possible to operate at full RPM. The data from Runs 20 and 21, Figure 7-12, where obtained at 500 and 551 RPM respectively. The nondimensional performance data from these two runs is identical which provides evidence to support the earlier low RPM data. The predicted line at this condition is optimistic. The nacelle incidence is high at this speed for a normal transition and represents a condition of climbing flight. Figure 1.2-11a of Reference 21 shows a rate of climb of 3500 ft/min as computed performance. (Note optimum thrust line angle is 50° and gives 3650 ft/min rate of climb.) If the experimental thrust-power line is used the rate of climb would be 3076 ft/min. In the case of one engine inoperative the aircraft rate of climb would be 1145 ft/min. The effect of cyclic pitch at 66° incidence, 80 kts and 550 RPM is shown in Figures 7-13 and 7-14. The power coefficients are unaffected by the cyclic settings; however, the thrust data show an increase as the cyclic pitch is reduced. For an A_1 = of -3.8°, C_{T_P} = .0242 and at A_1 = -1.95°, C_{T_P} = .0258, that is, 0.00087 per degree. The B_1 data show a larger slope of .0017 per degree.

Figure 7-16 shows A_1 cyclic data at 500 RPM. These data show no effect on power and a small thrust effect (.0005 C_{T_P}/degree). The B_1 sweep at 500 RPM is shown in Figure 7-17. The balance foul warning system was on at this time and the thrust data are erratic. The collective sweep data at this condition did not have "fouling" troubles and is shown in Figure 7-18.

Correlation of predicted performance with measured data for 27° incidence and 105 kts is shown in Figure 7-19. The agreement is good; however, some of the data points where taken with a foul warning showing. These data points line up with data taken with no fouls and are thought to be reasonably accurate. The cyclic sweep data are shown in Figures 7-20 and 7-21. These data are free of foul problems. The power data are insensitive to A_1 cyclic pitch. The thrust data show a small increase as A_1 is reduced towards zero. A larger thrust change is apparent with B_1 cyclic, Figure 7-21, and the power coefficient data shows no effect except for the two lowest B_1 data points. The collective and incidence sweep data are shown in Figures 7-22 and 7-23.

Run 13 data was taken at 27° incidence and 140 kts. The foul warning light was on for nearly all of this run. The performance data are shown in Figures 7-24 to 7-27.

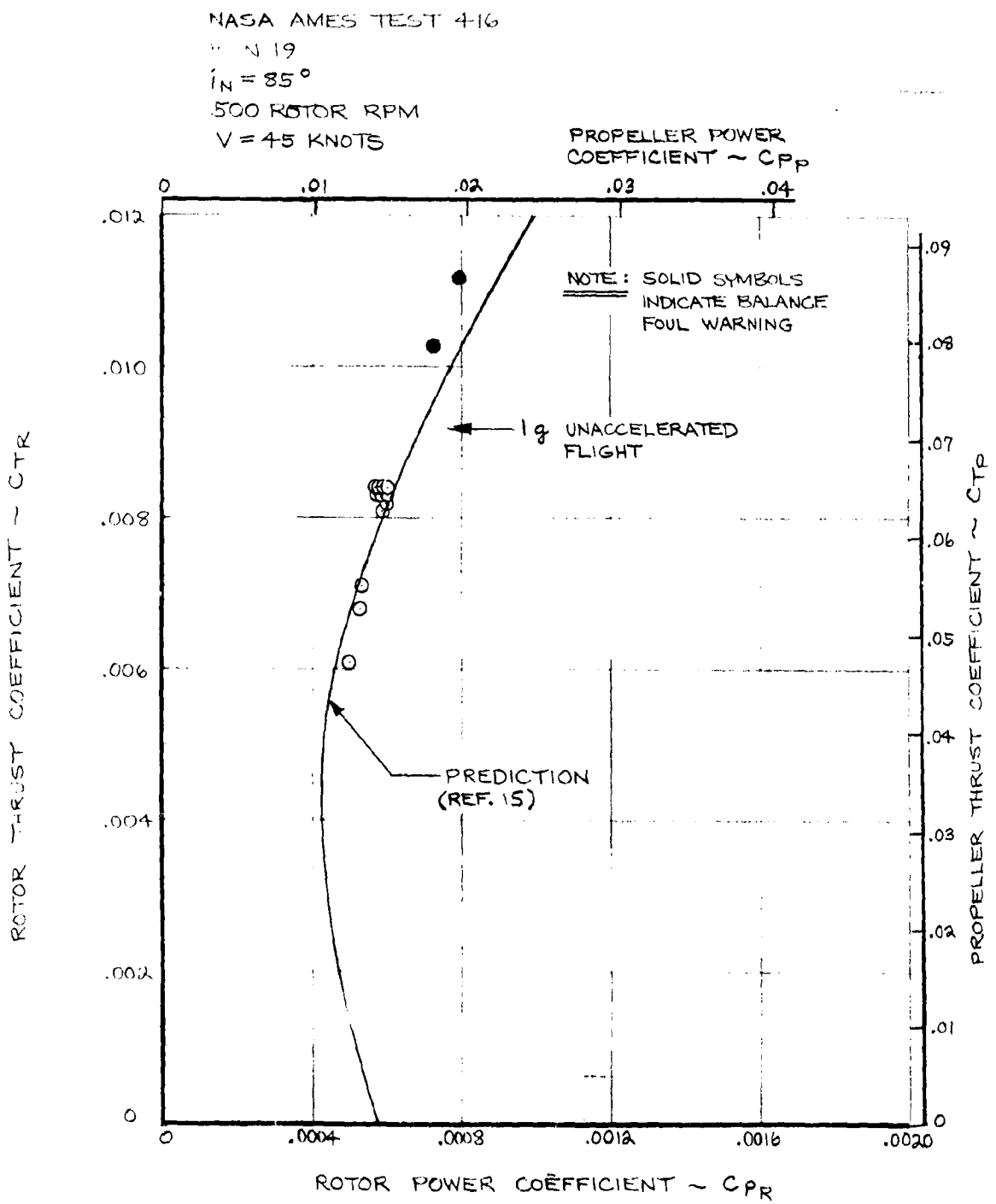

FIGURE 7-4 TRANSITION ROTOR PERFORMANCE
V = 45 KNOTS, $i_N = 85°$

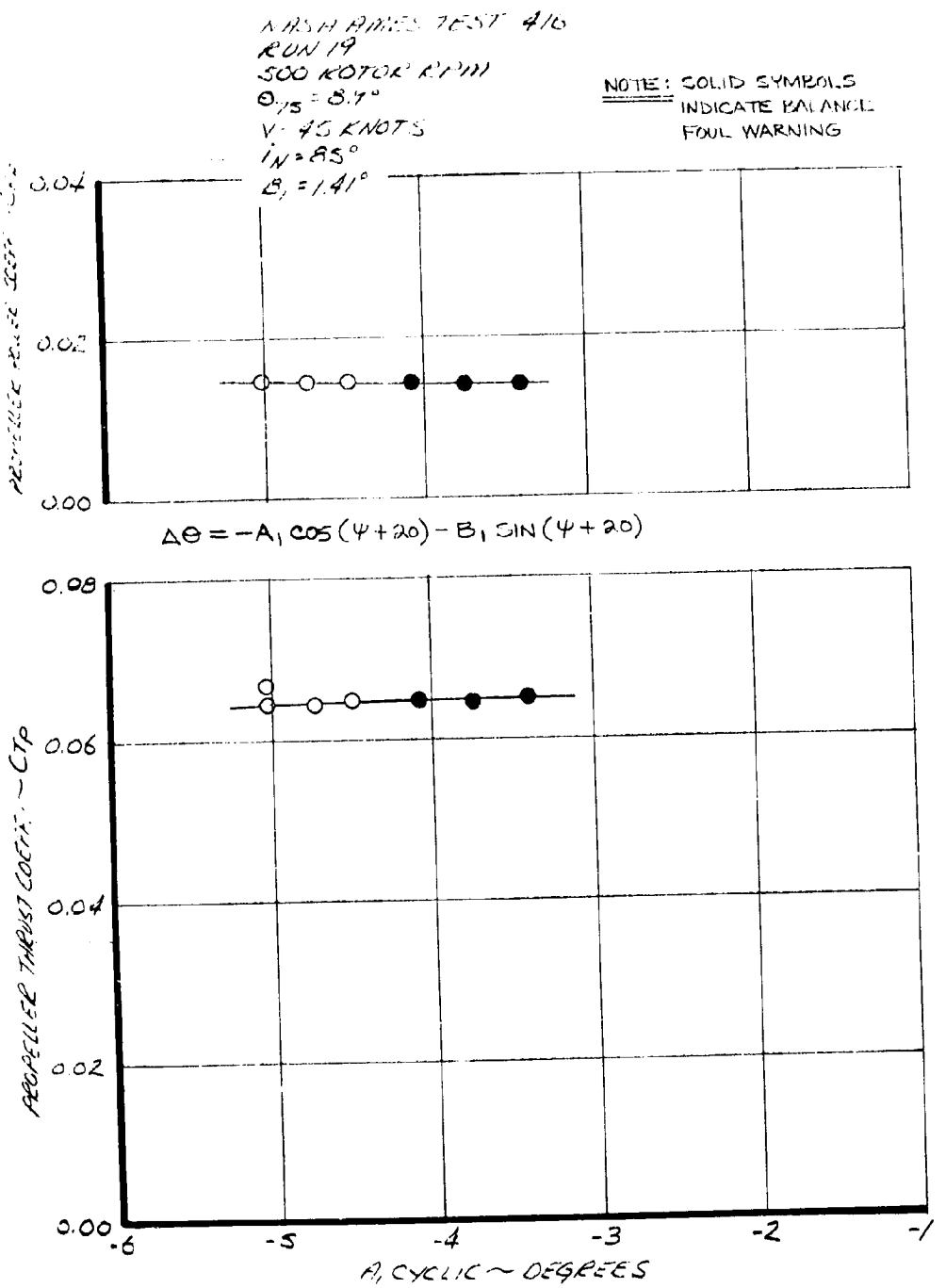

FIGURE 7-5 EFFECT OF A_1 CYCLIC ON TRANSITION ROTOR PERFORMANCE — V = 45 KNOTS, i_N = 85°

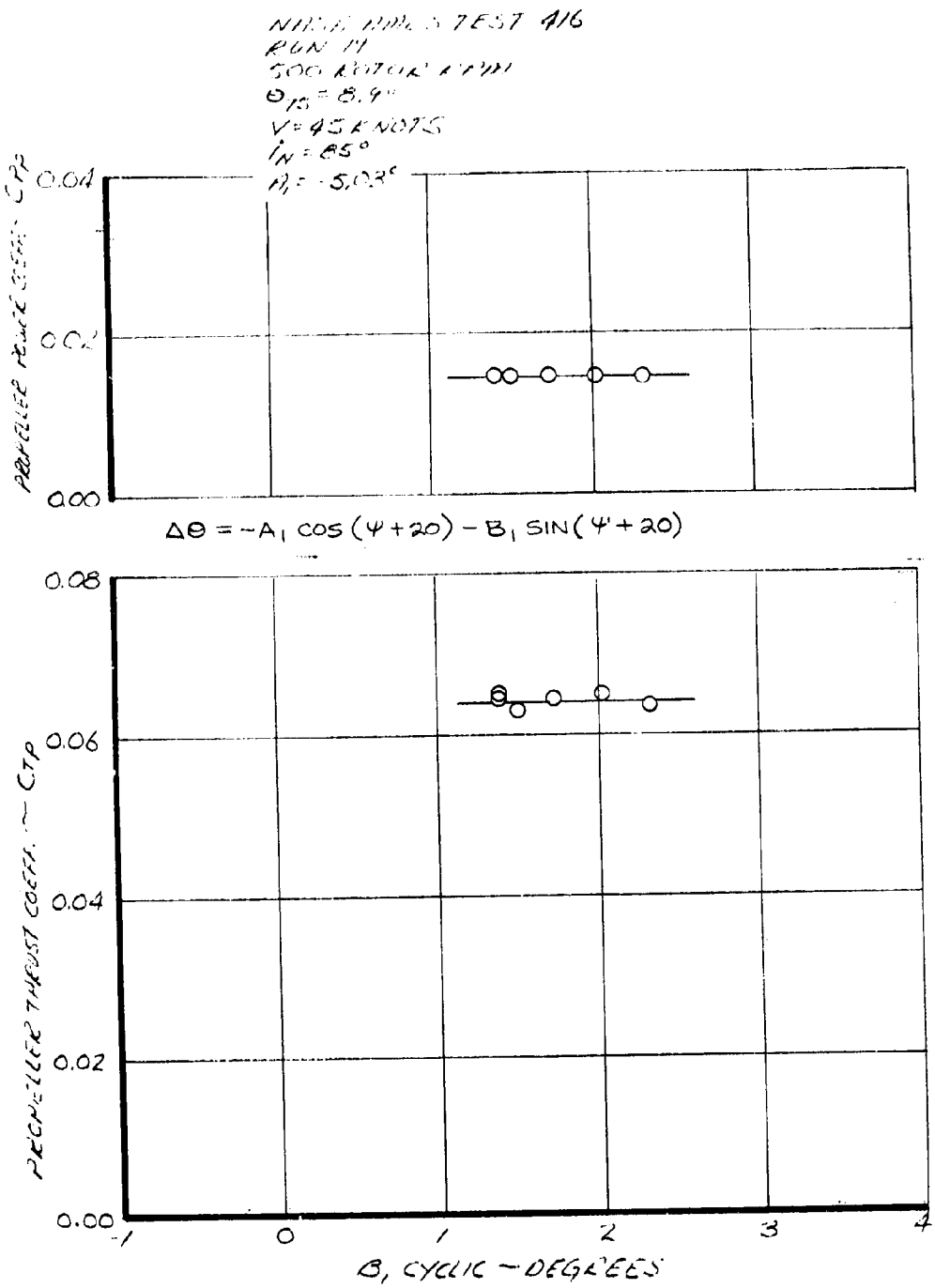

FIGURE 17-6 EFFECT OF B_1 CYCLIC ON TRANSITION ROTOR PERFORMANCE – V = 45 KNOTS, i_N = 85°

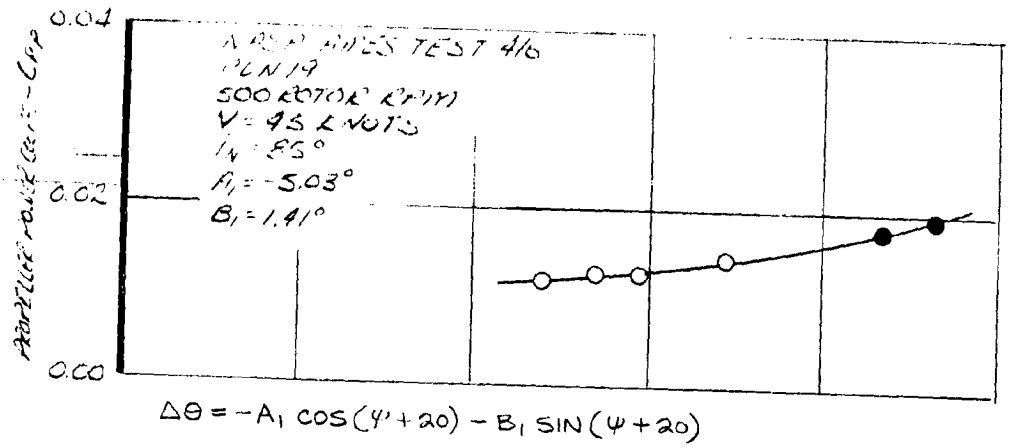

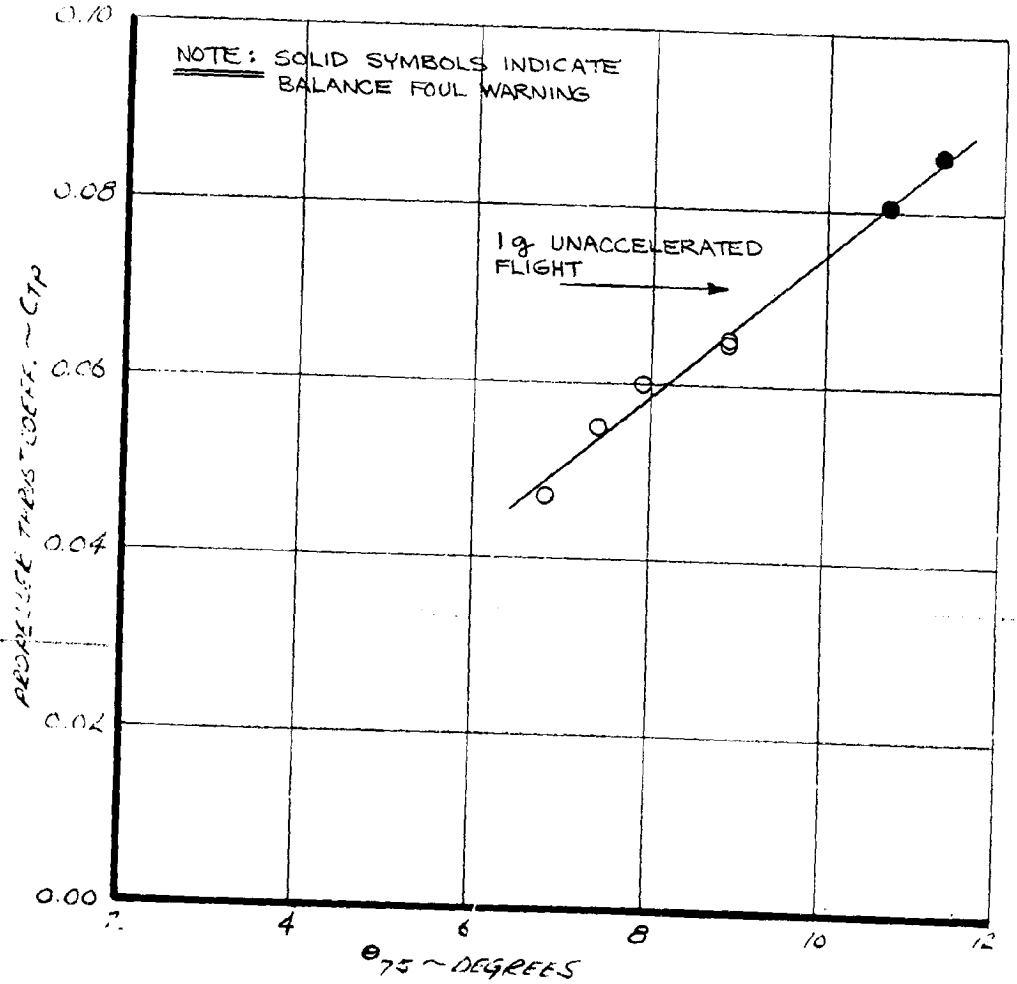

FIGURE 7-7 EFFECT OF COLLECTIVE PITCH ON TRANSITION ROTOR PERFORMANCE - V = 45 KNOTS, i_N = 85°

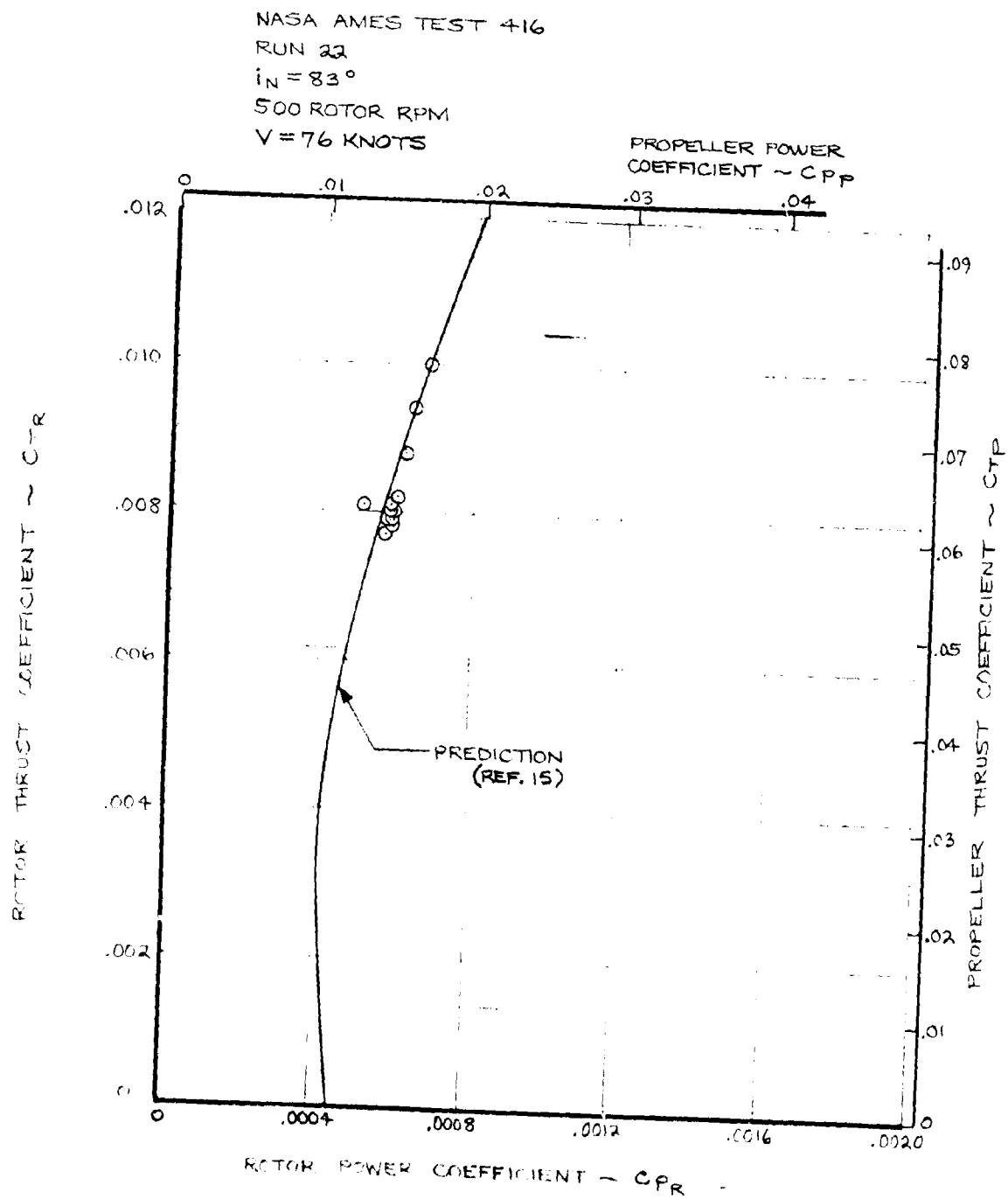

FIG. 7-8 TRANSITION ROTOR PERFORMANCE
V = 76 KNOTS, $i_N = 83°$

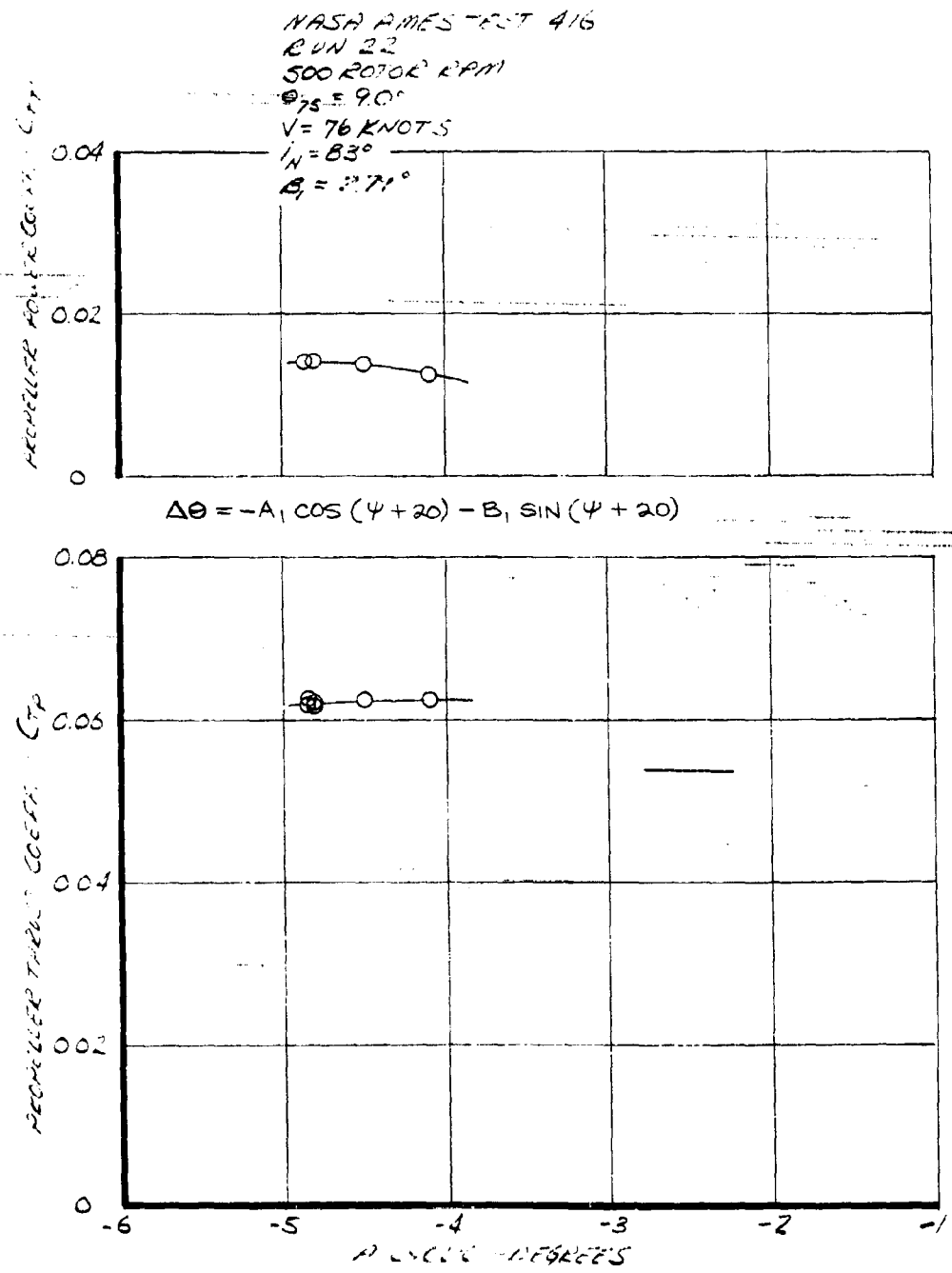

FIGURE 7-9 EFFECT OF A_1 CYCLIC ON TRANSITION ROTOR PERFORMANCE — V = 76 KNOTS, i_N = 83°

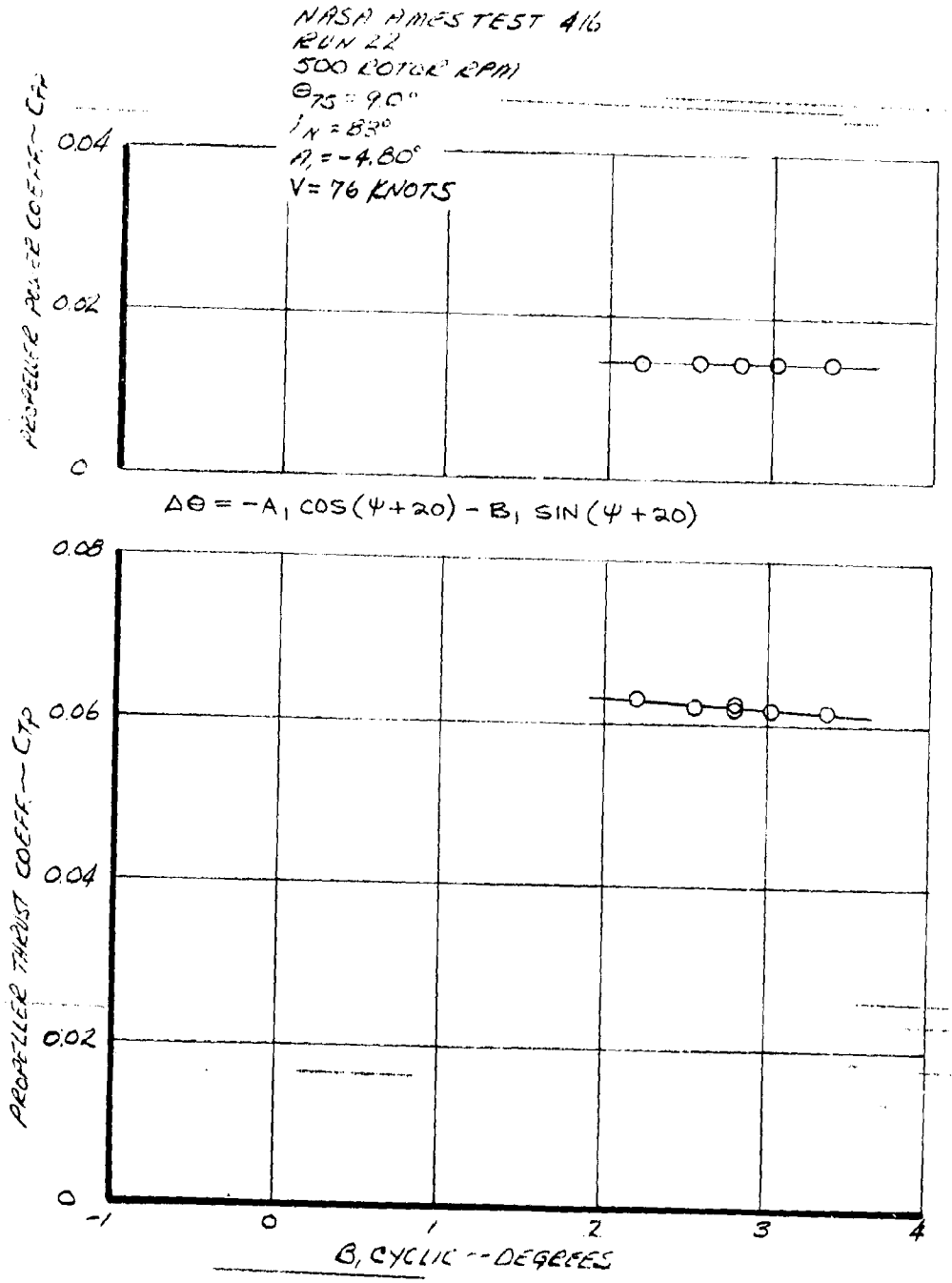

FIGURE 7-10 EFFECT OF B_1 CYCLIC ON TRANSITION ROTOR PERFORMANCE – V = 76 KNOTS, $i_N = 83°$

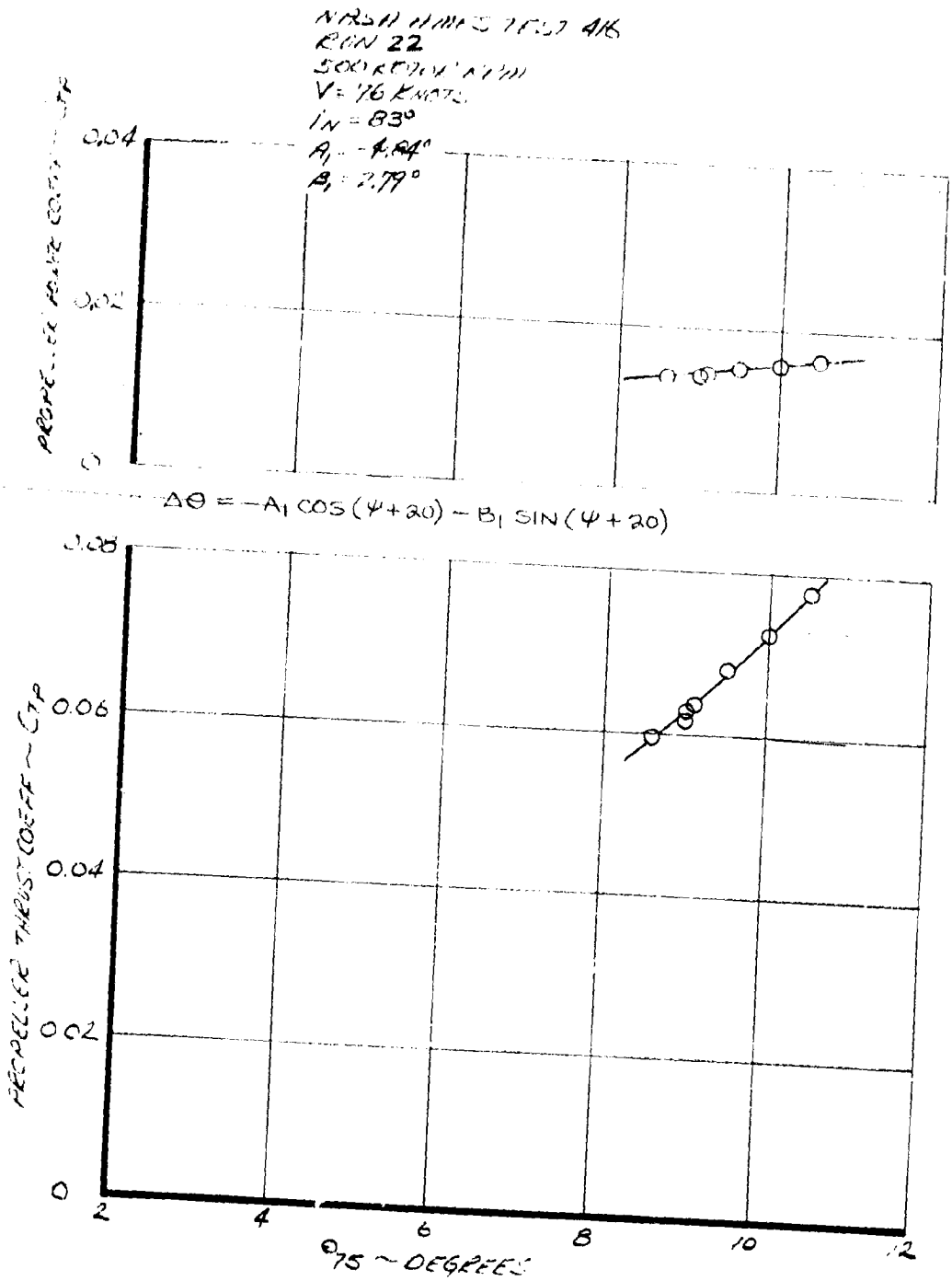

FIGURE 7-11 EFFECT OF COLLECTIVE PITCH ON TRANSITION ROTOR PERFORMANCE — V = 76 KNOTS, i_N = 83°

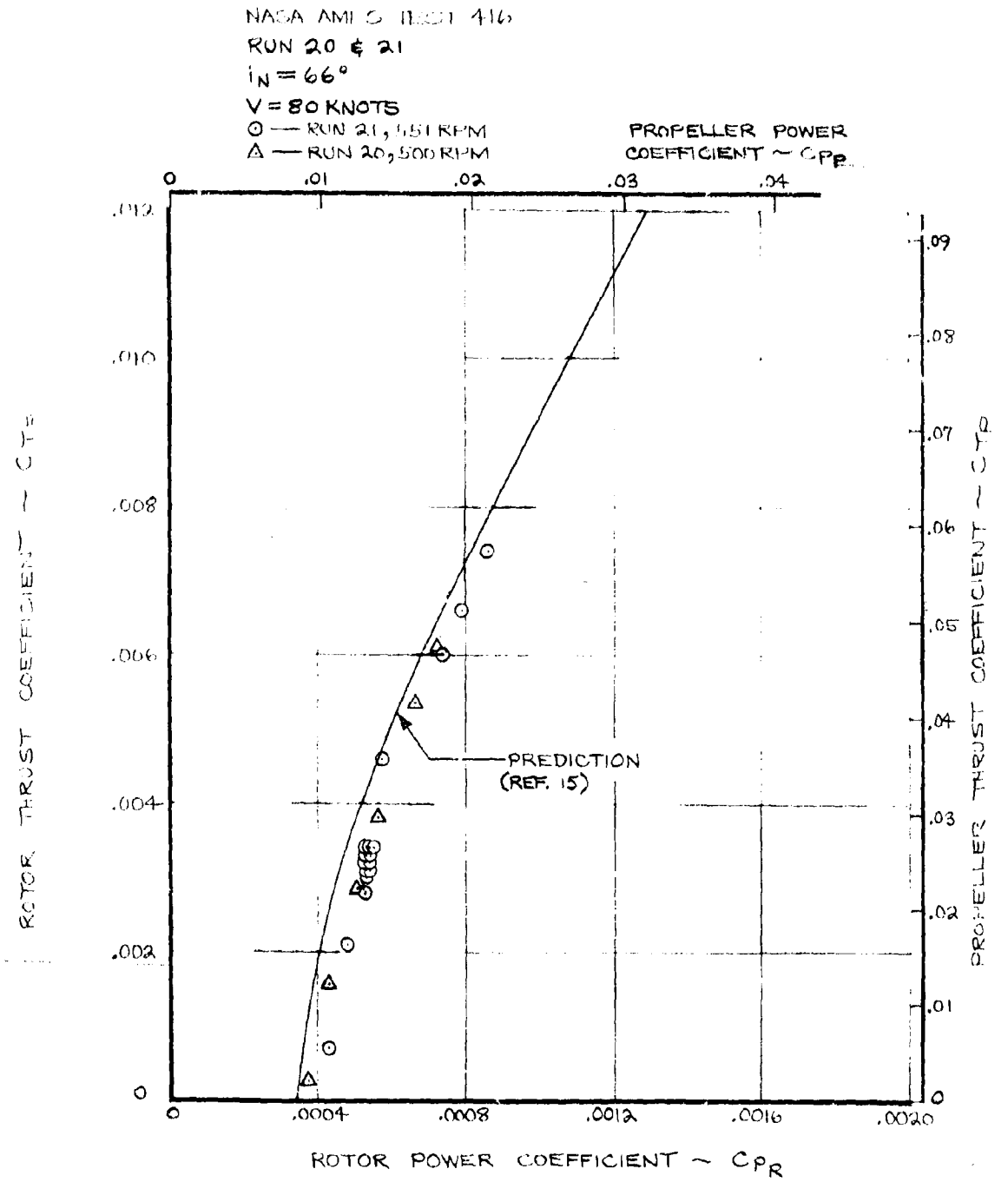

FIGURE 7-12 TRANSITION ROTOR PERFORMANCE
V = 80 KNOTS, $i_N = 66°$

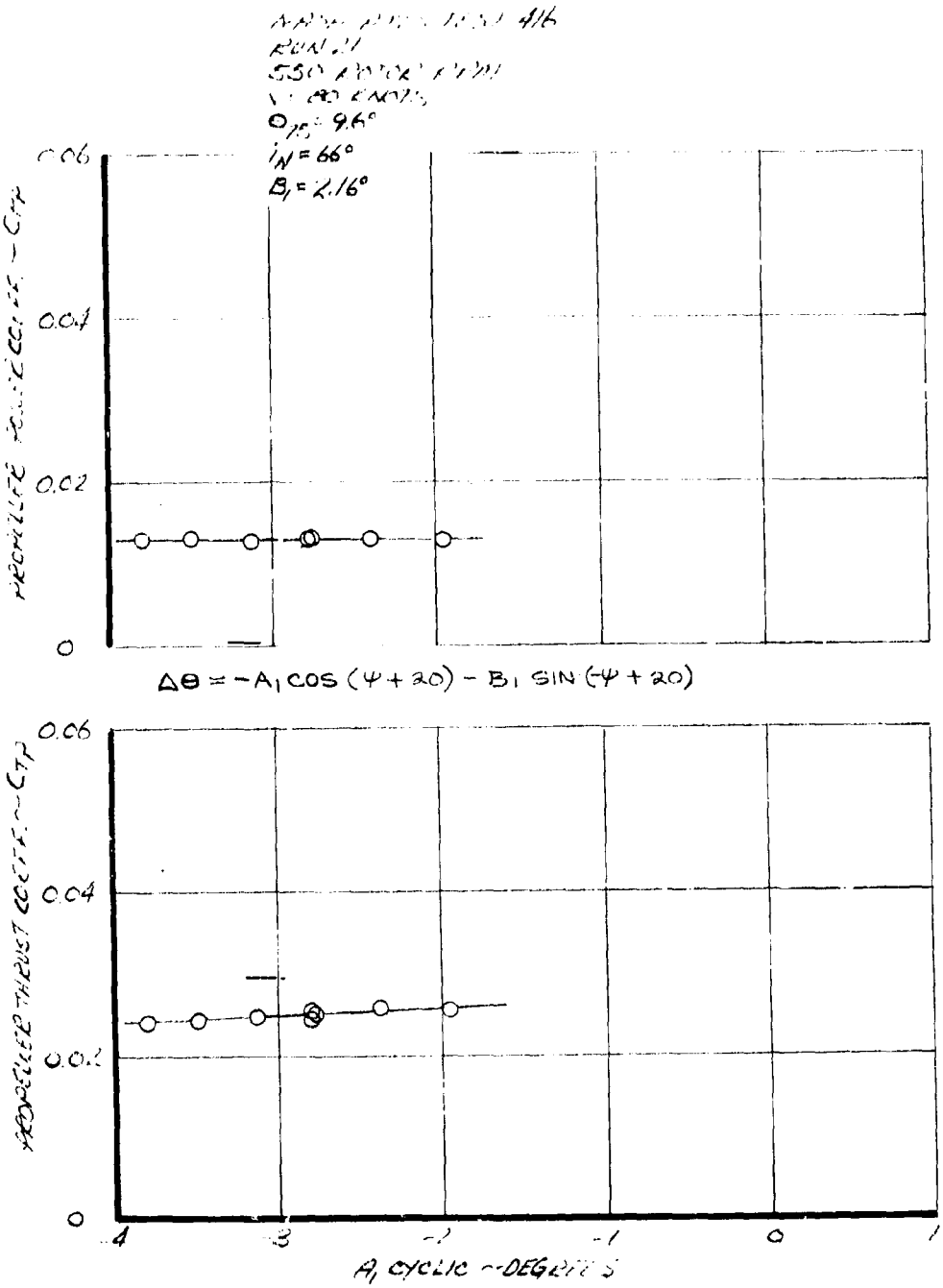

FIGURE 7-13 EFFECT OF A_1 CYCLIC ON TRANSITION ROTOR PERFORMANCE – V = 80 KNOTS, $i_N = 66°$

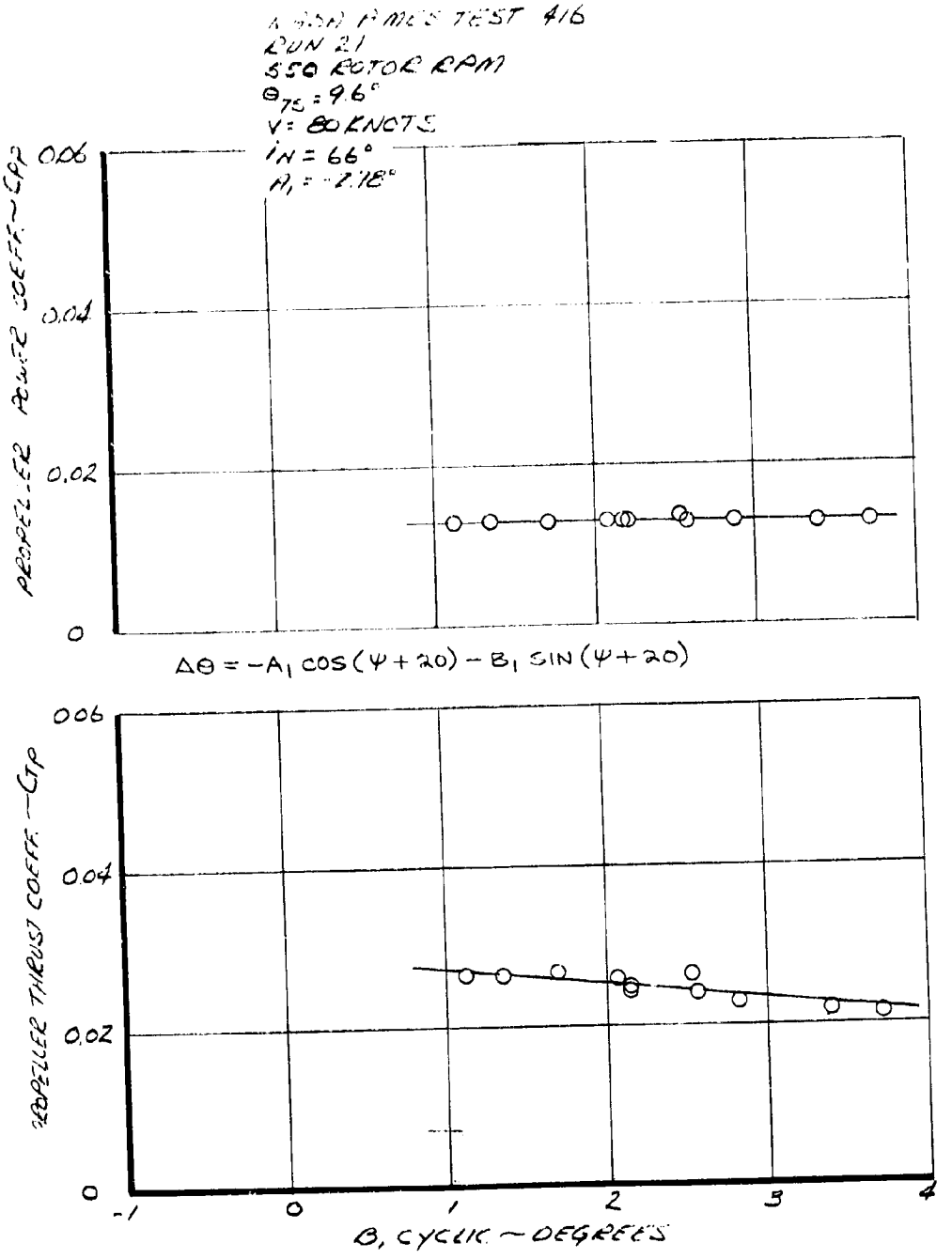

FIGURE 7-14 EFFECT OF B_1 CYCLIC ON TRANSITION ROTOR PERFORMANCE — V = 80 KNOTS, $i_N = 66°$

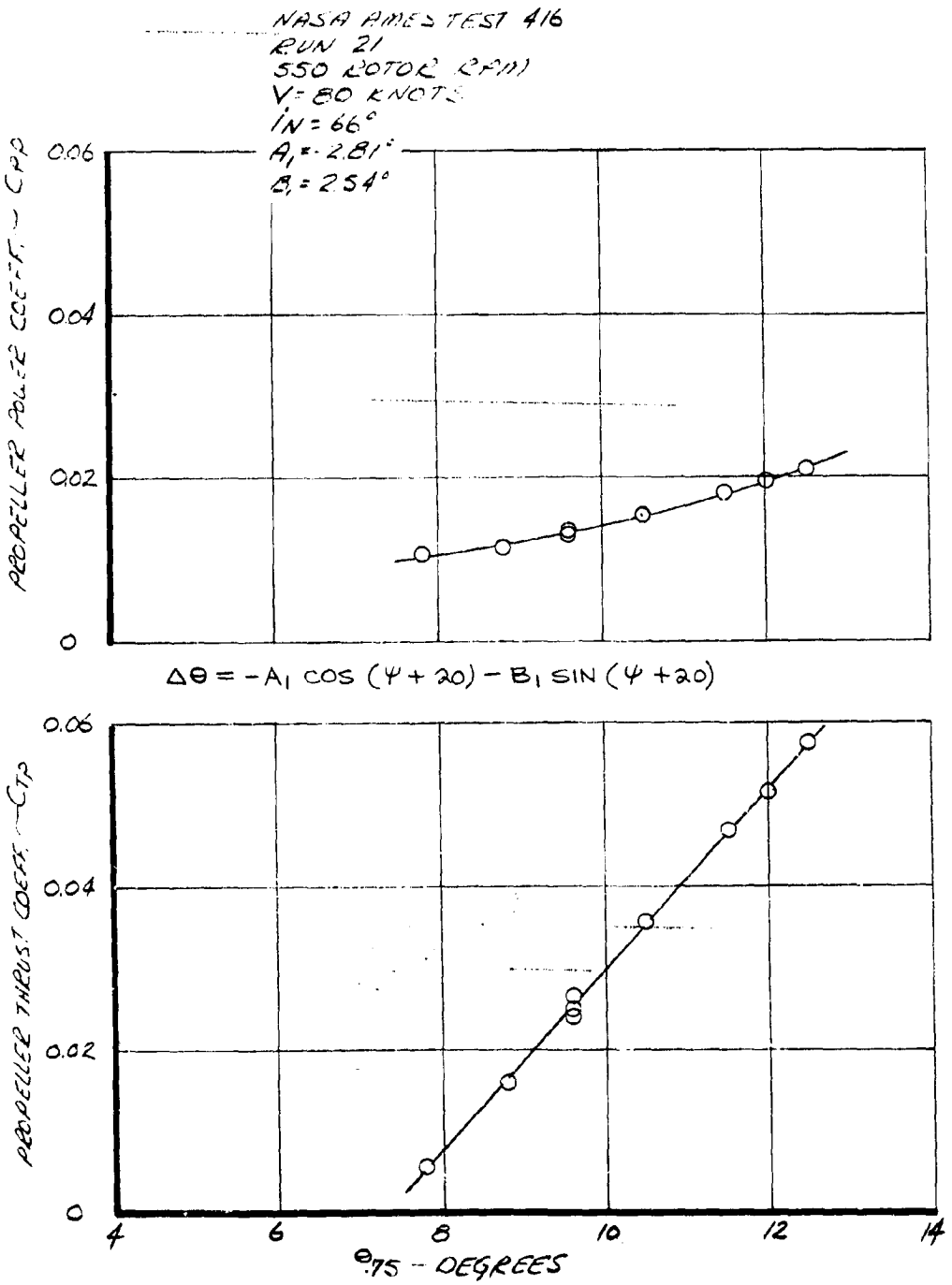

FIGURE 7-15 EFFECT OF COLLECTIVE PITCH ON TRANSITION ROTOR PERFORMANCE — V = 80 KNOTS., i_N = 66°

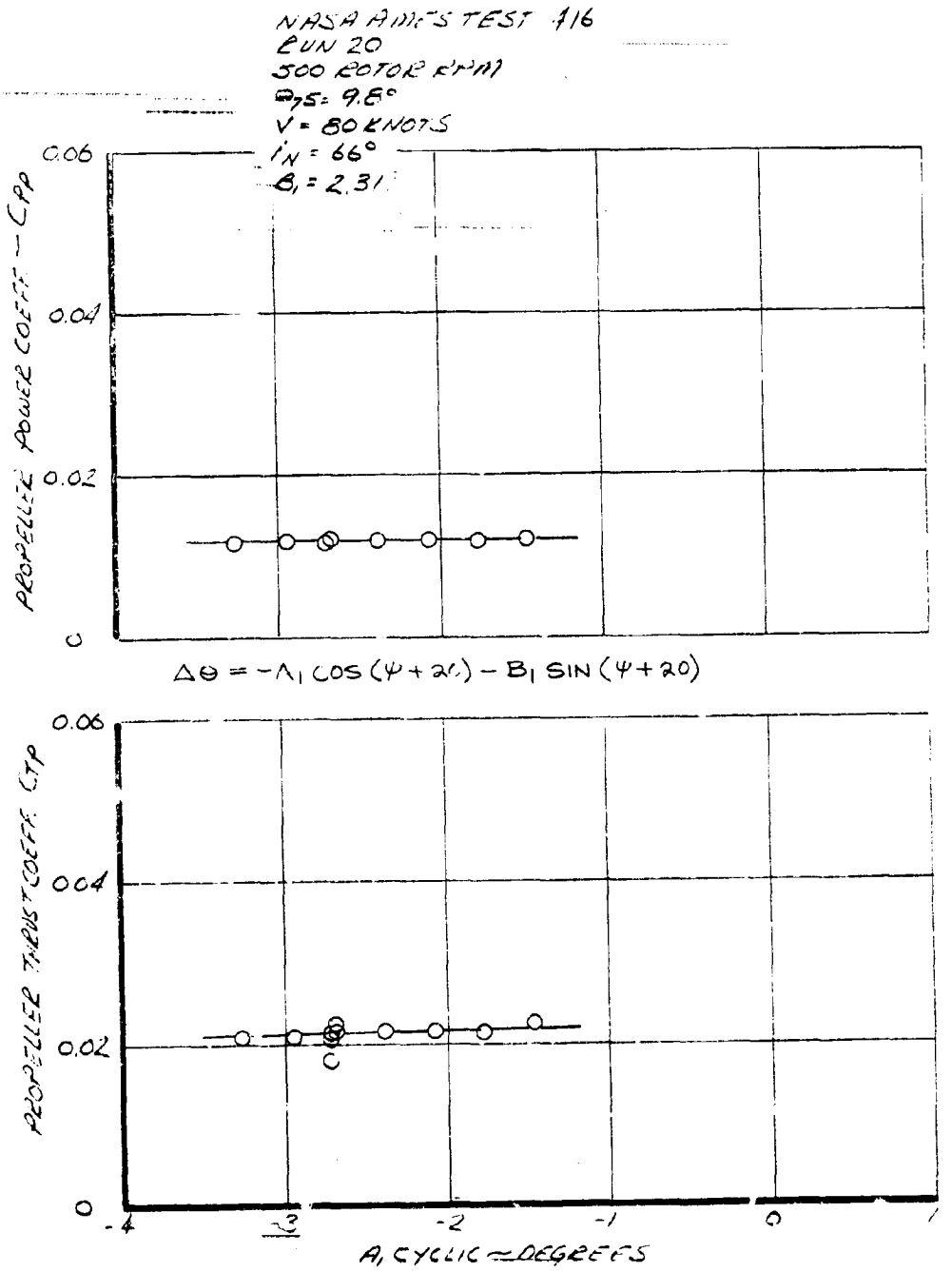

FIGURE 7-16 EFFECT OF A_1 CYCLIC ON TRANSITION ROTOR PERFORMANCE – V = 80 KNOTS, $i_N = 66°$

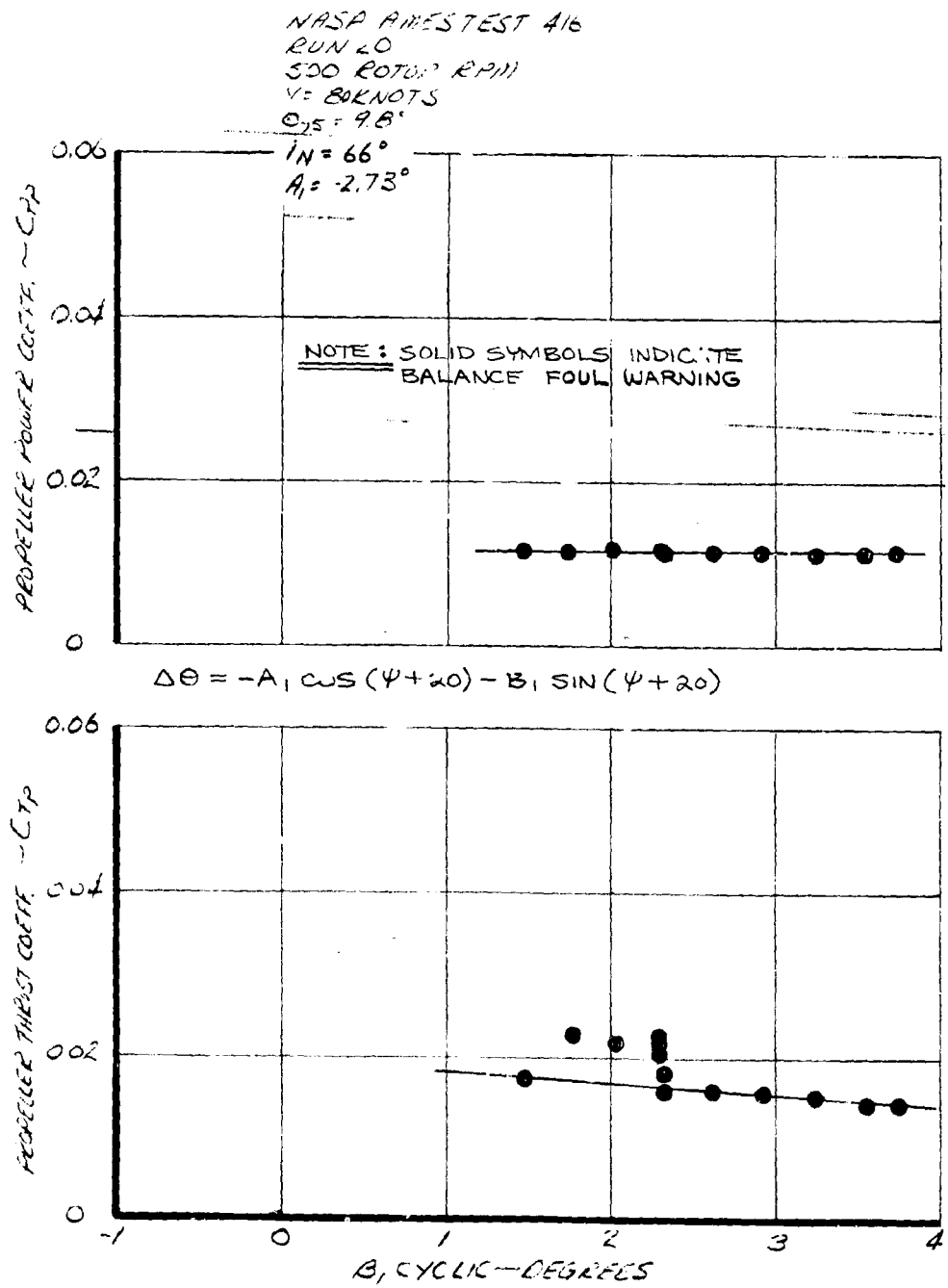

FIGURE 7-17 EFFECT OF B_1 CYCLIC ON TRANSITION ROTOR PERFORMANCE – V = 80 KNOTS, $i_N = 66°$

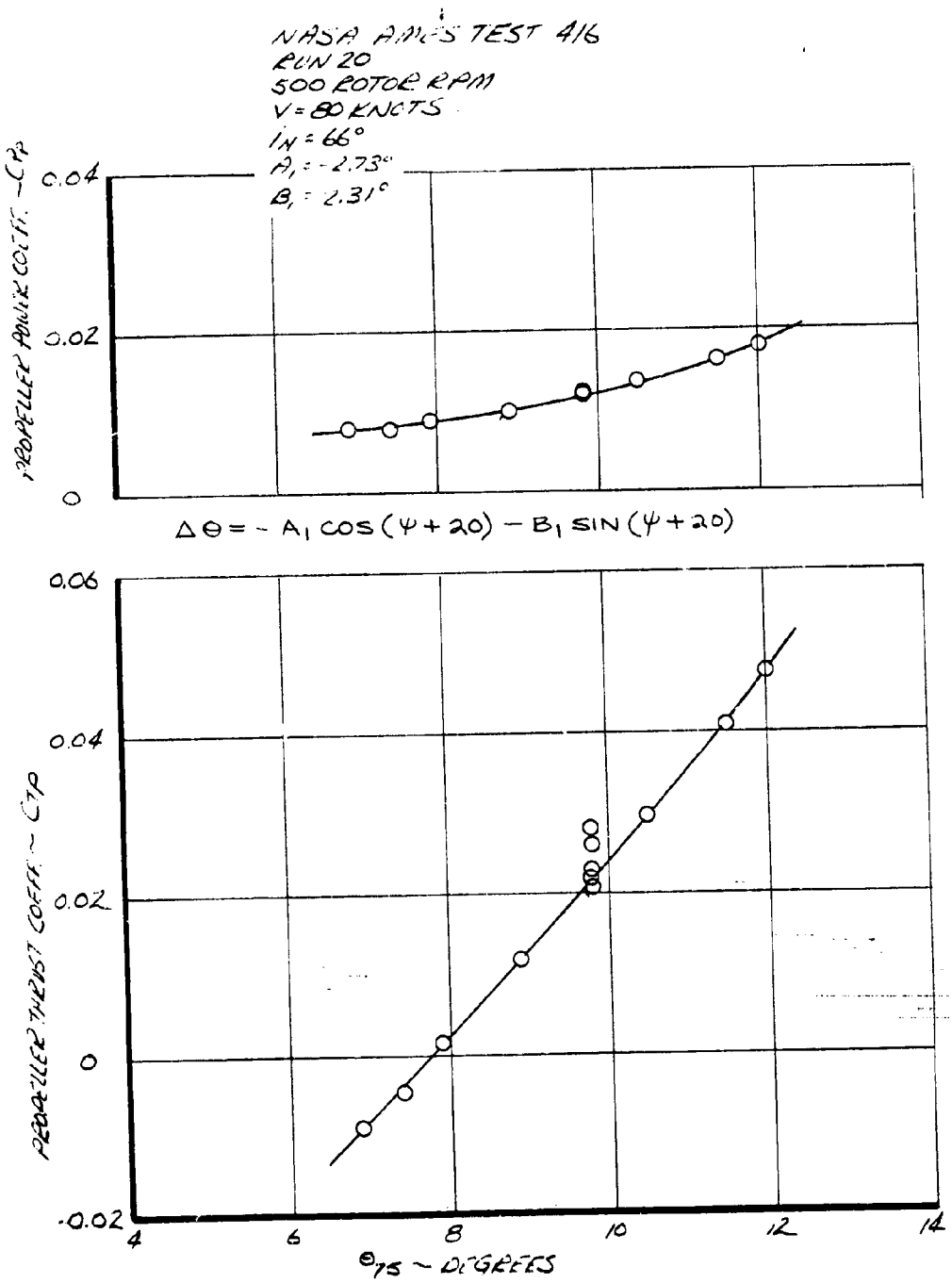

FIGURE 7-18 EFFECT OF COLLECTIVE PITCH ON TRANSITION ROTOR PERFORMANCE - V = 80 KNOTS, i_N = 66°

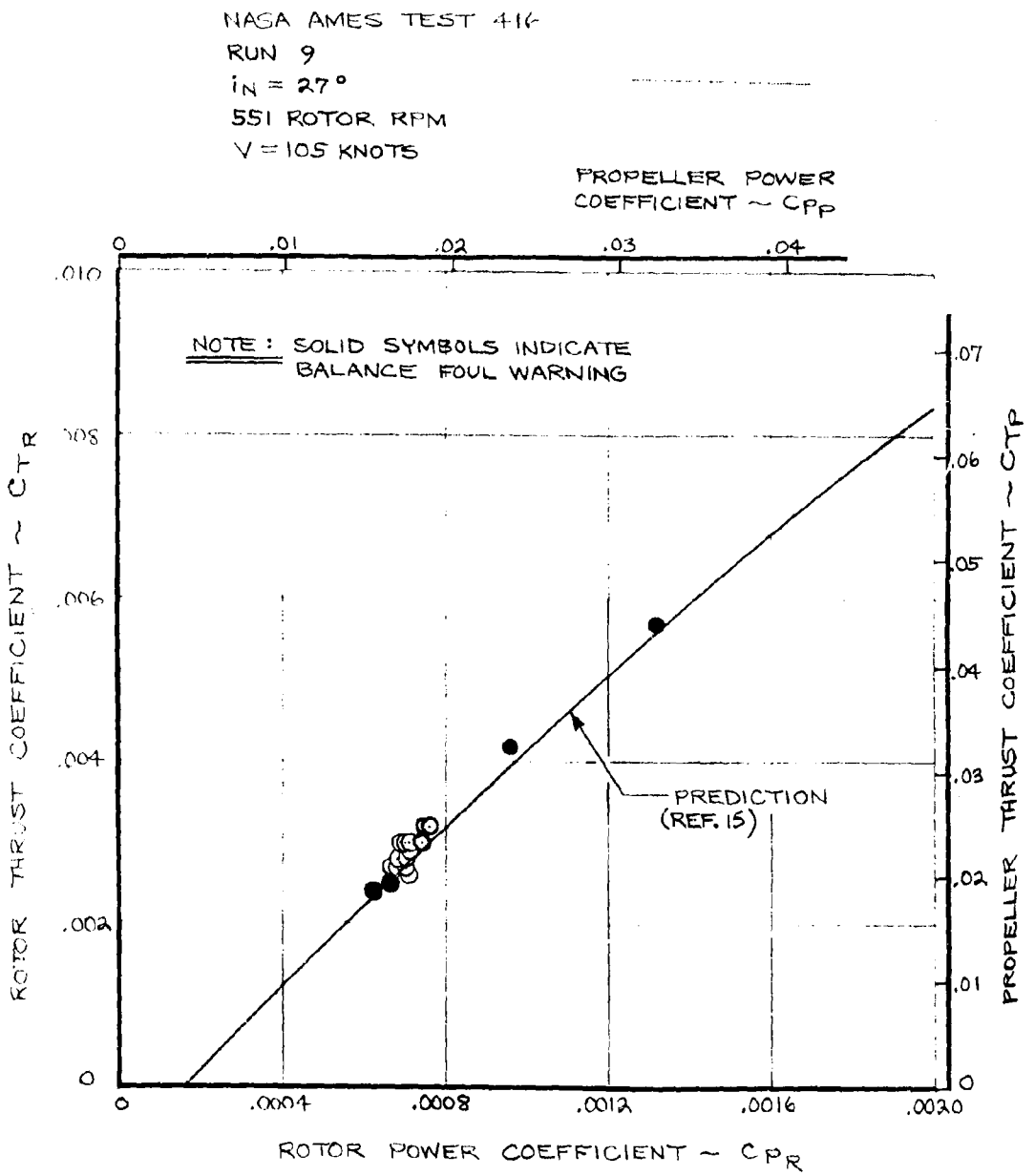

FIGURE 7-19 TRANSITION ROTOR PERFORMANCE
V = 105 KNOTS, i_N = 27°

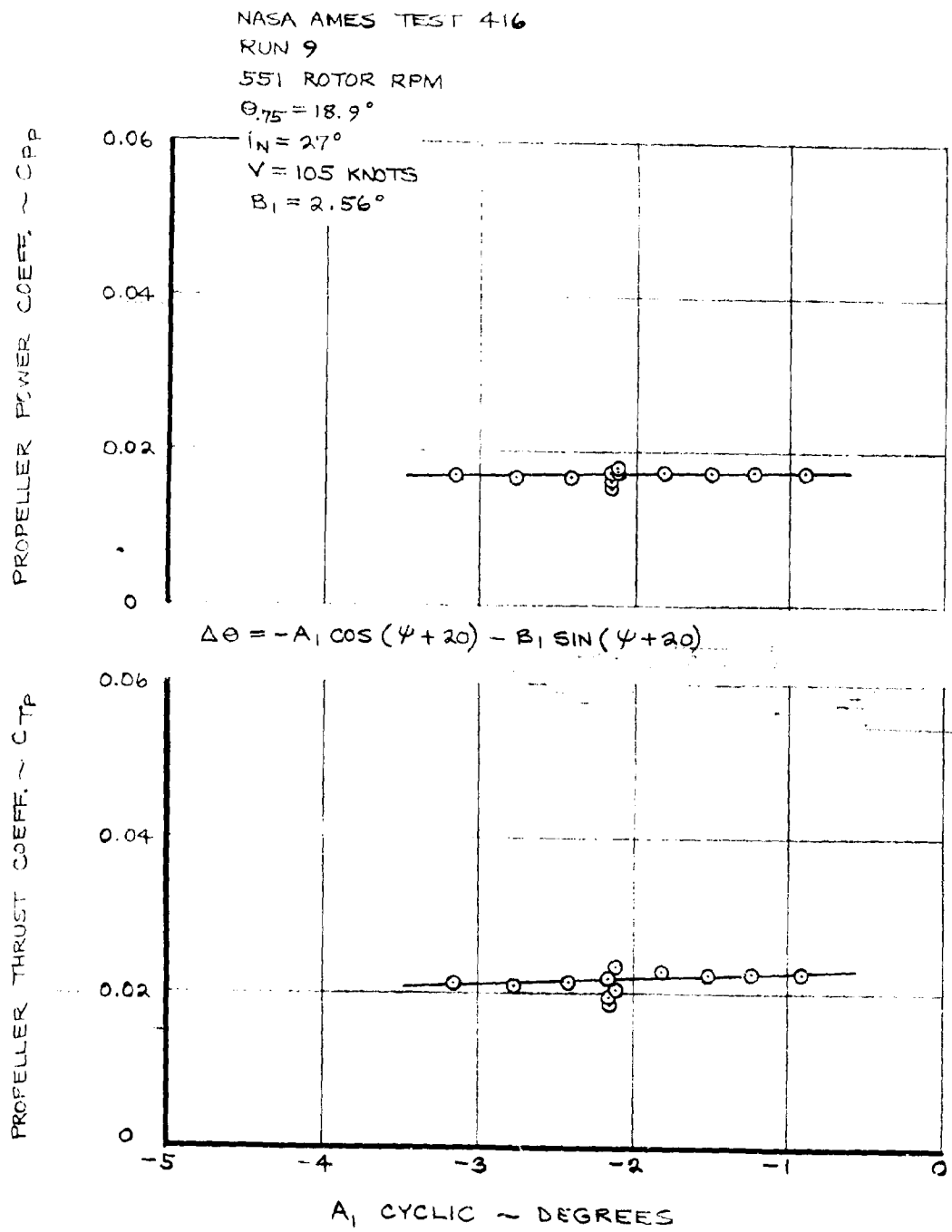

FIGURE 7-20 EFFECT OF A_1 CYCLIC ON TRANSITION ROTOR PERFORMANCE – V = 105 KNOTS, $i_N = 27°$

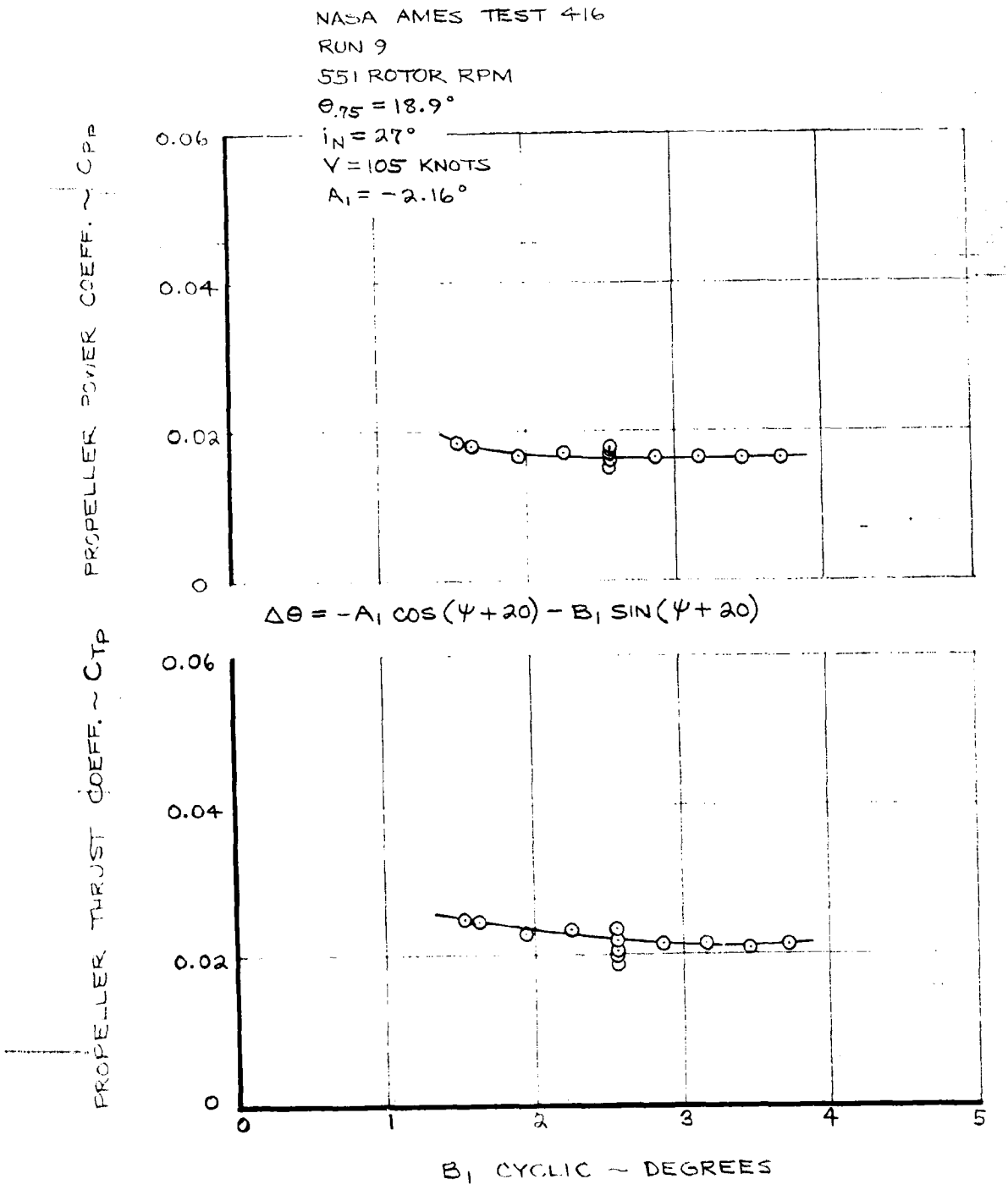

FIGURE 7-21 EFFECT OF B_1 CYCLIC ON TRANSITION ROTOR PERFORMANCE – V = 105 KNOTS, $i_N = 27°$

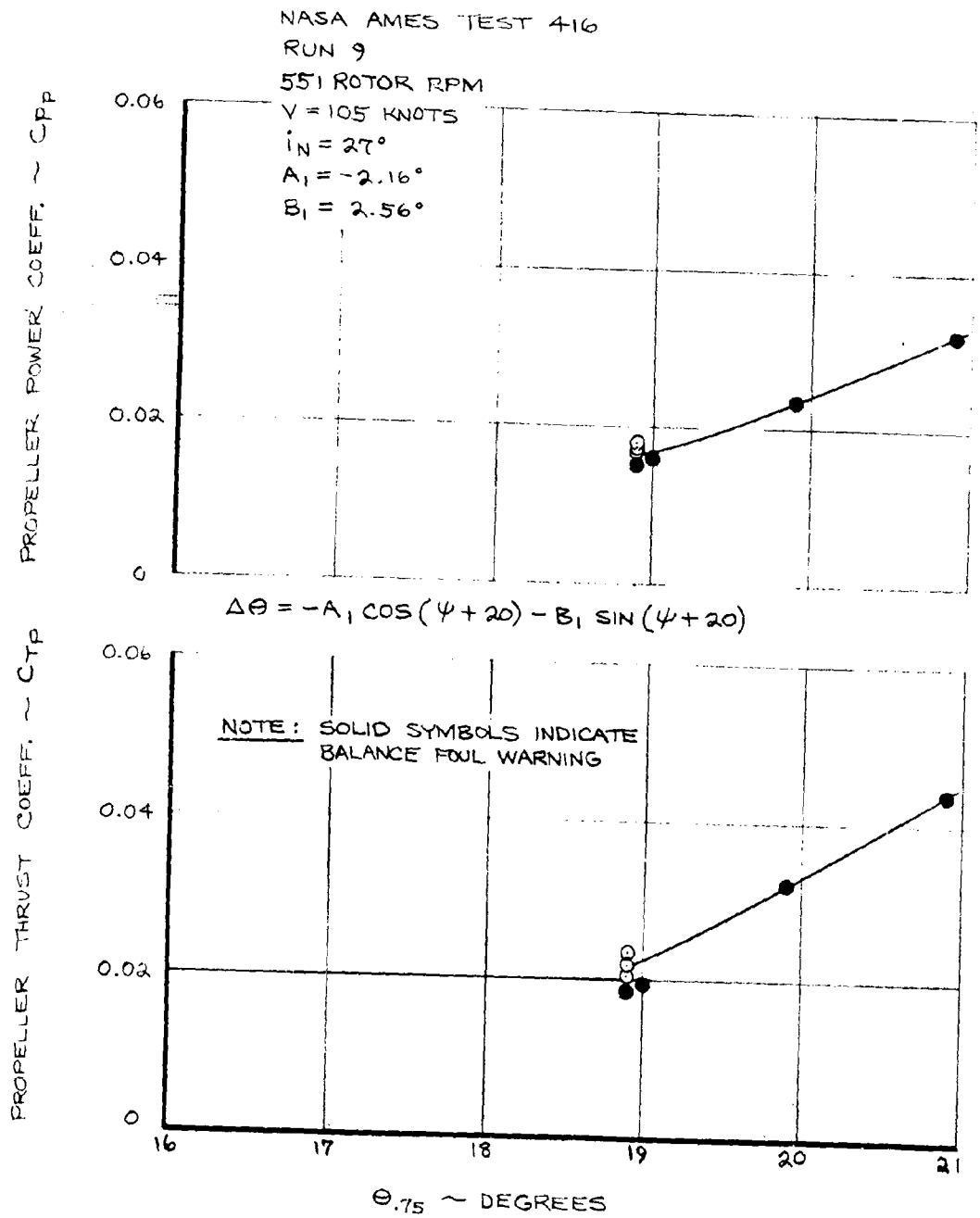

FIGURE 7-22 EFFECT OF COLLECTIVE PITCH ON TRANSITION ROTOR PERFORMANCE – V = 105 KNOTS, $i_N = 27°$

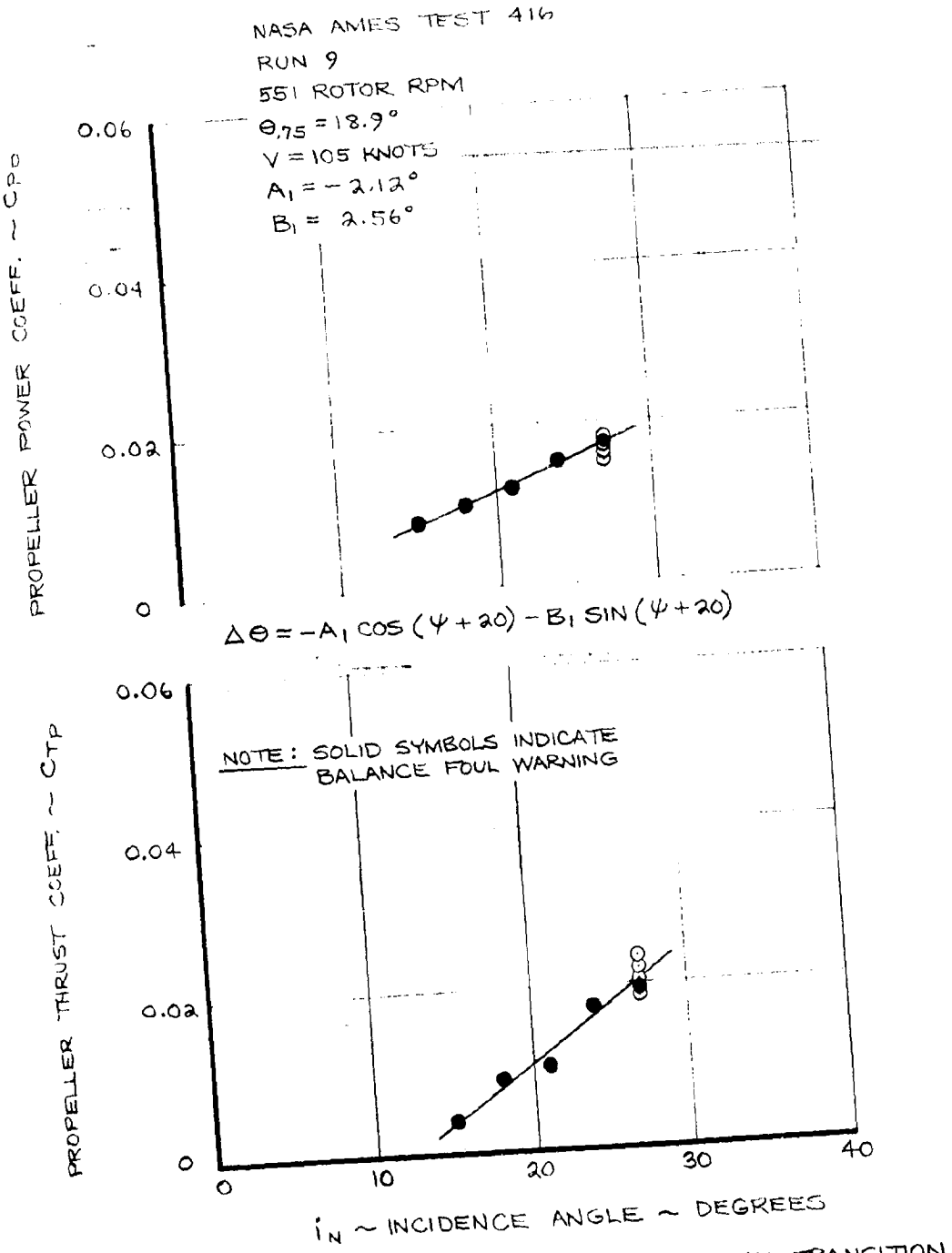

FIGURE 7-23 EFFECT OF INCIDENCE ANGLE ON TRANSITION ROTOR PERFORMANCE — V = 105 KNOTS

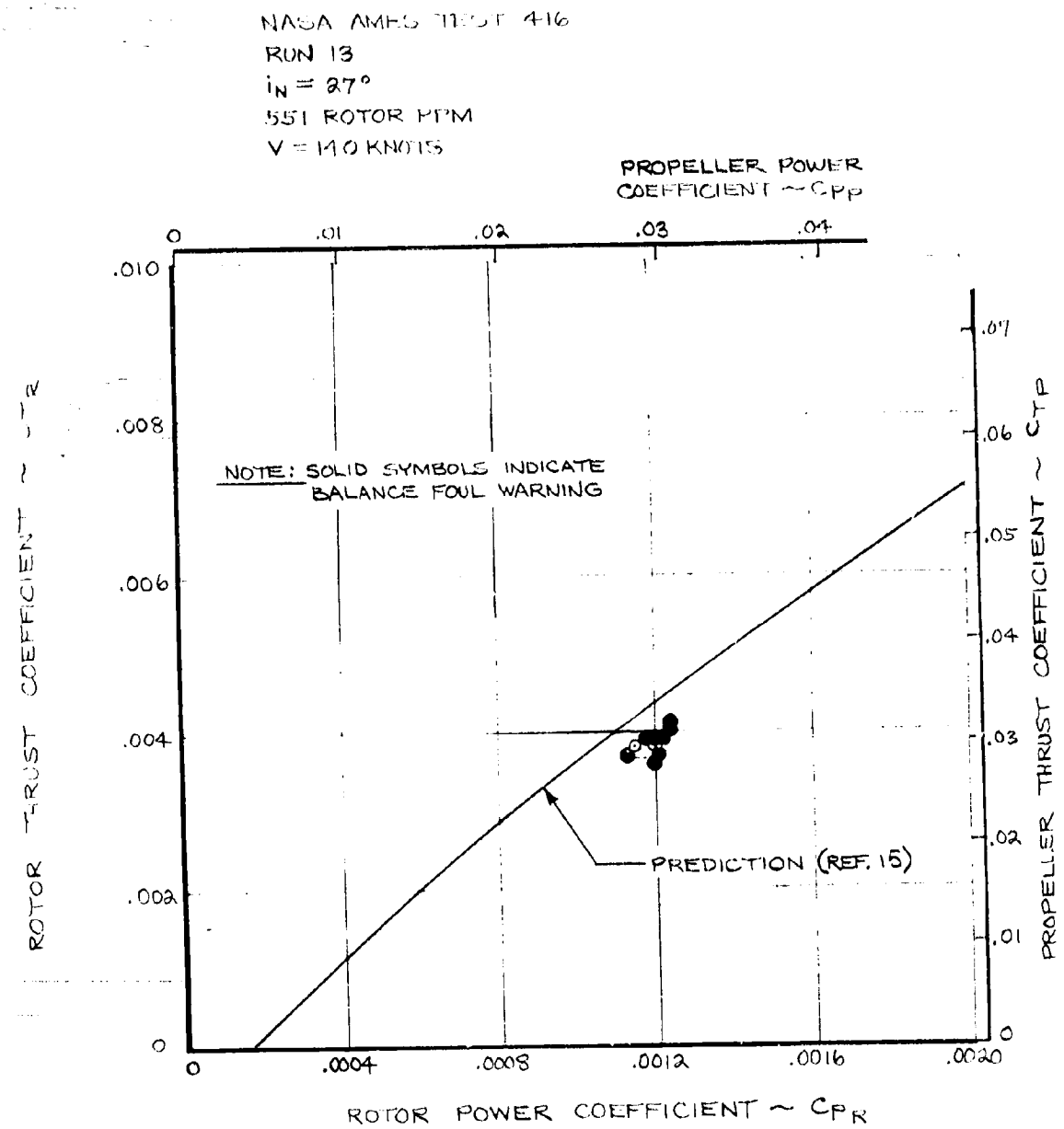

FIGURE 7-24 TRANSITION ROTOR PERFORMANCE
V = 140 KNOTS, i_N = 27°

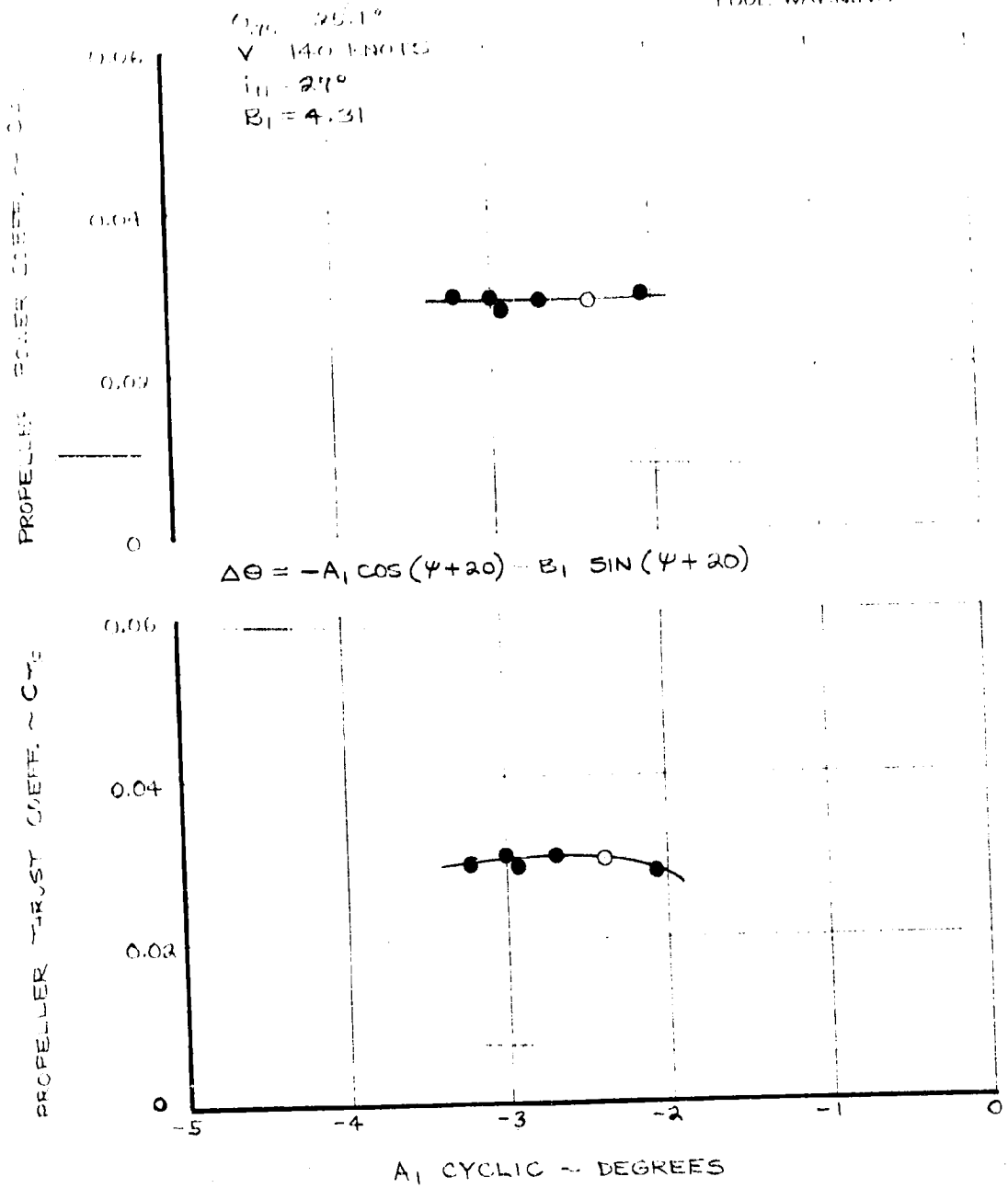

FIGURE 7-25 EFFECT OF A_1 CYCLIC ON TRANSITION ROTOR PERFORMANCE – V = 140 KNOTS, i_N = 27°

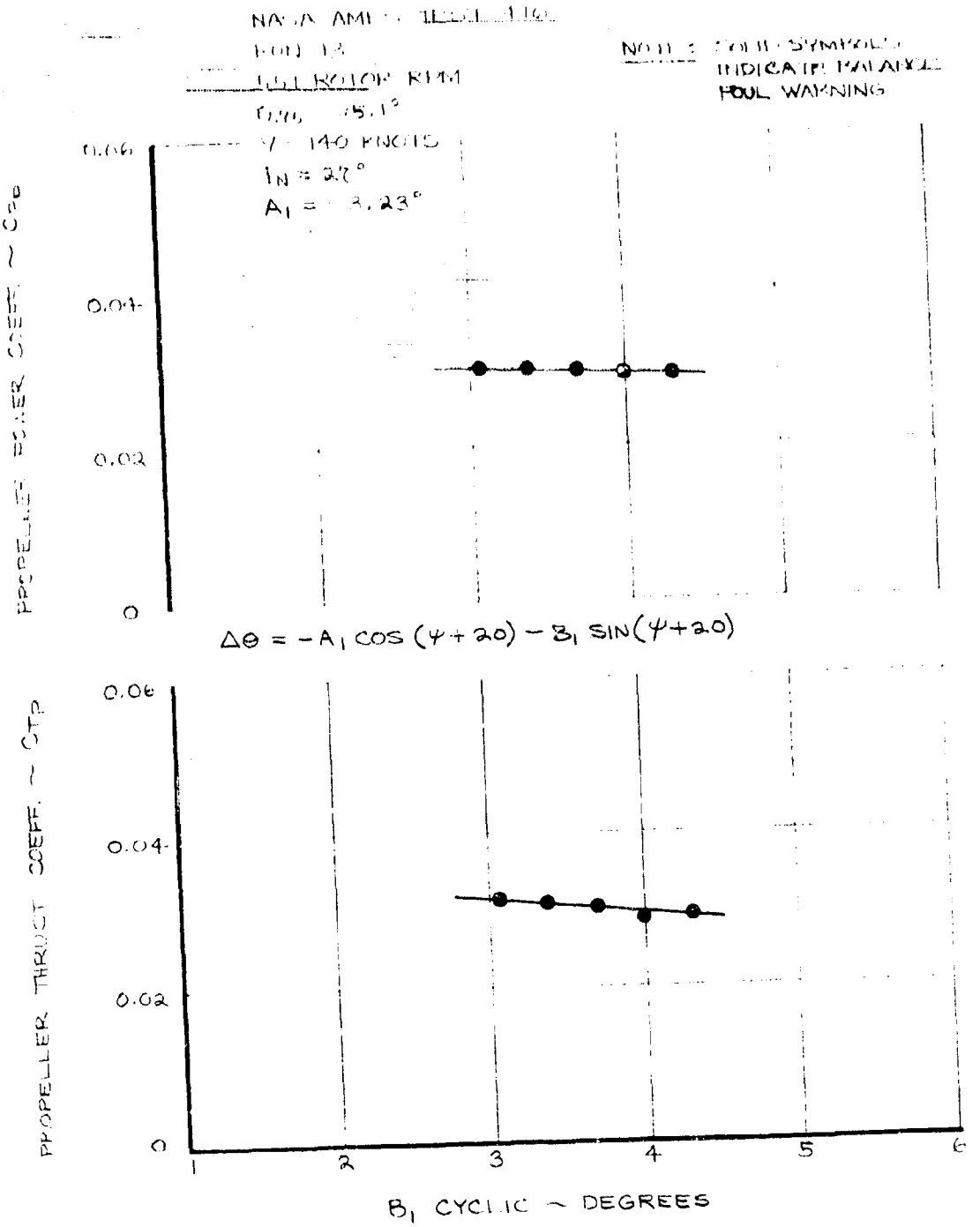

FIGURE 7-26 EFFECT OF B_1 CYCLIC ON TRANSITION ROTOR PERFORMANCE – V= 140 KNOTS, i_N = 27°

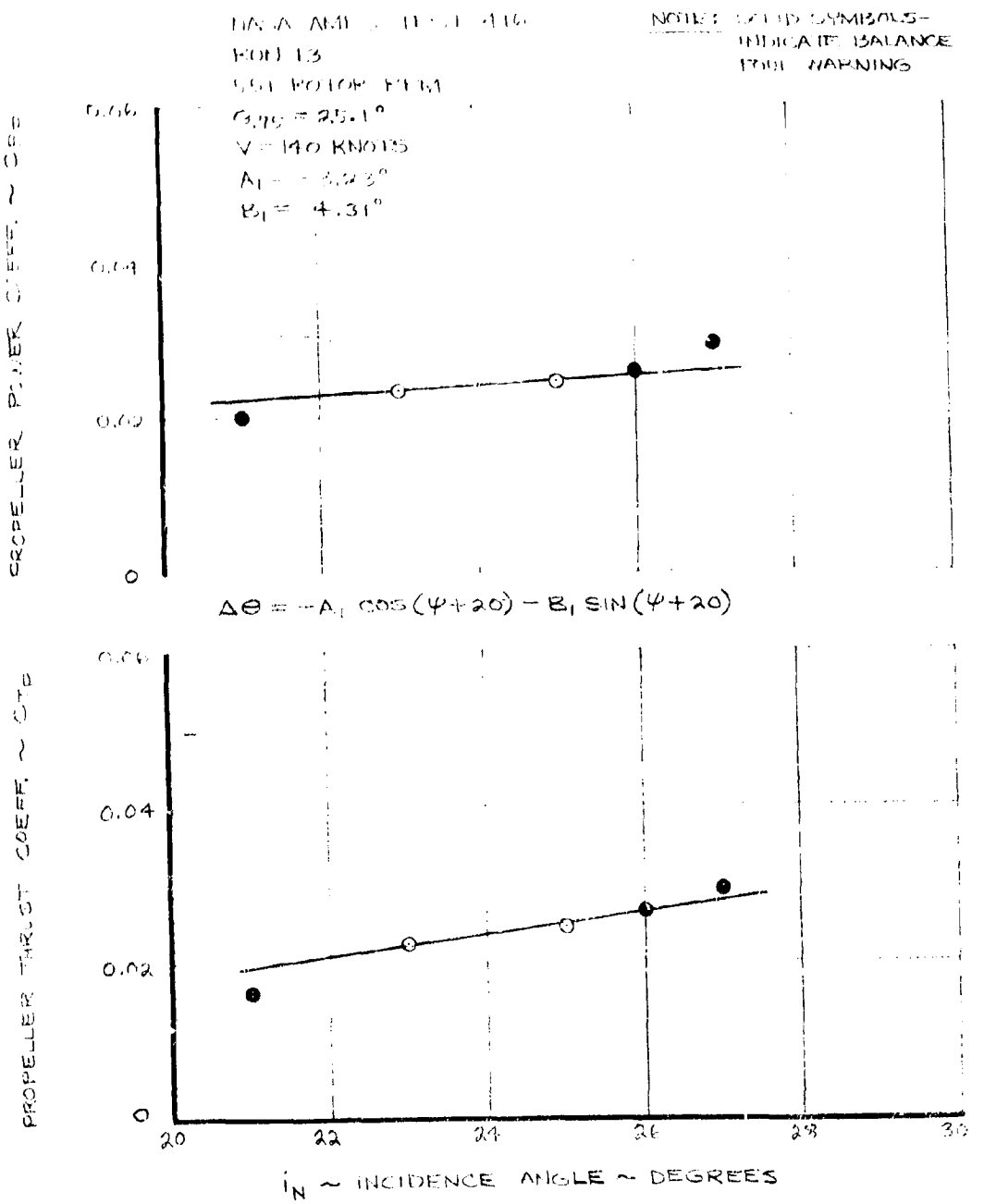

FIGURE 7-27 EFFECT OF INCIDENCE ANGLE ON TRANSITION ROTOR PERFORMANCE – V= 140 KNOTS

7.3 Cruise Performance

Rotor performance data at zero incidence and 386 RPM was obtained at 140 kts on Run 11 and is compared with predicted performance in Figure 7-28. The experimental data indicate efficiencies about 8% higher than predicted and are thought to be optimistic. It should be noted that the efficiencies quoted are propeller efficiencies (i.e., $J\ C_{T_p}/C_{P_p}$) not propulsive efficiencies.

The effects of incidence, collective and cyclic pitch on cruise performance about a minimum blade loads test condition of 10° incidence, 140 kts and 386 RPM are plotted in Figures 7-29 to 7-30. As incidence is increased, thrust and power increase due to the reduction in inflow normal to the disc (Figure 7-29).

A_1 cyclic has no effect on thrust but power required increases with cyclic pitch (Figure 7-30). For B_1 cyclic both thrust and power decrease as cyclic pitch is increased. The effect is small and would require less than 0.1° θ_{75} to correct per degree of cyclic. The collective data is shown in Figure 7-32.

Similar data was taken at 170 kts and presented in Figures 7-33 to 7-36. The foul warning system was on for this entire

run and the data scatter is indicative of a "real" foul.

Windmilling cruise performance data from Test 410 is shown in Figure 7-37 with predicted lines superimposed.

NASA AMES 40'×80' TEST 416
RUN 11 V=140 KTS 386 RPM
J=1.45

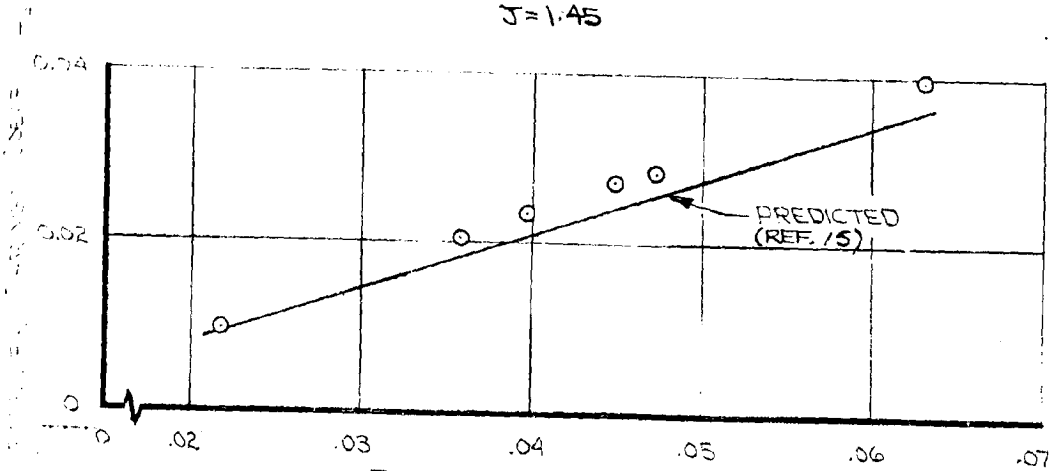

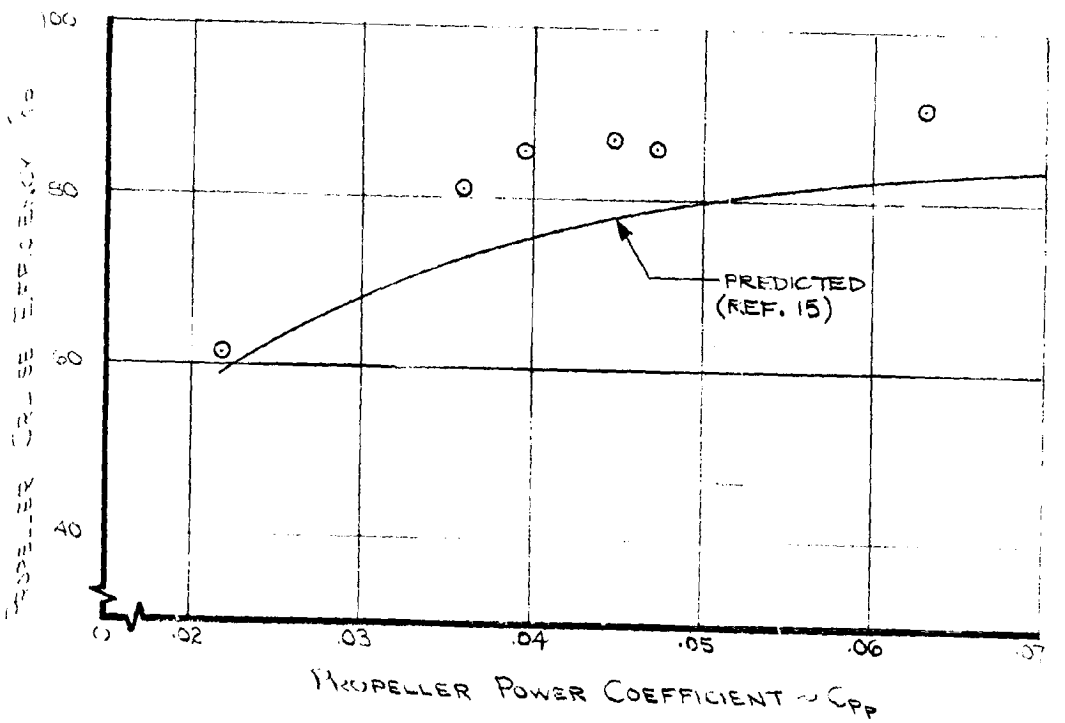

Figure 7-28. [illegible] CRUISE PERFORMANCE, V=140 KTS, i_N=0°

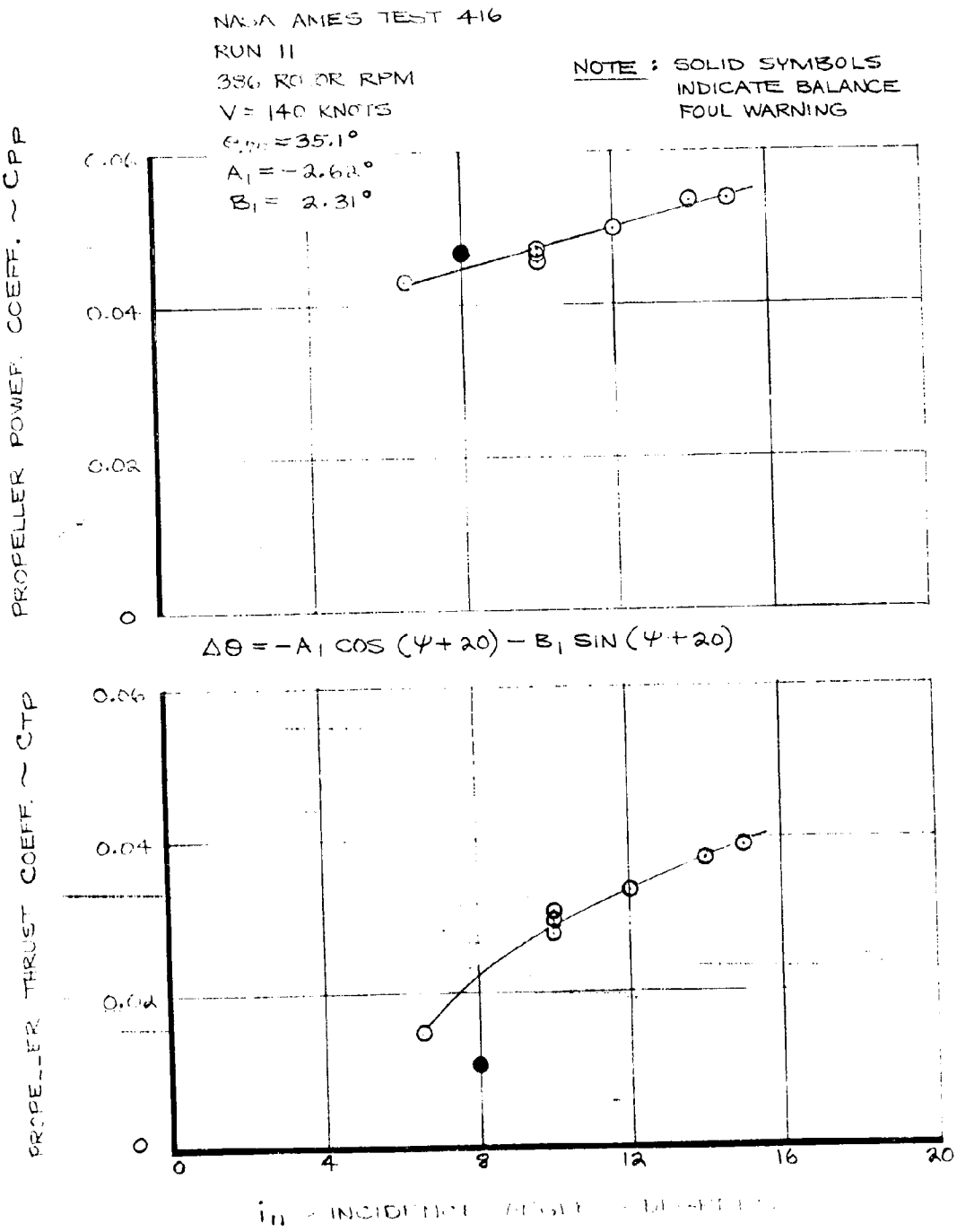

FIGURE 7-29 EFFECT OF INCIDENCE ANGLE ON CRUISE ROTOR PERFORMANCE — V = 140 KNOTS

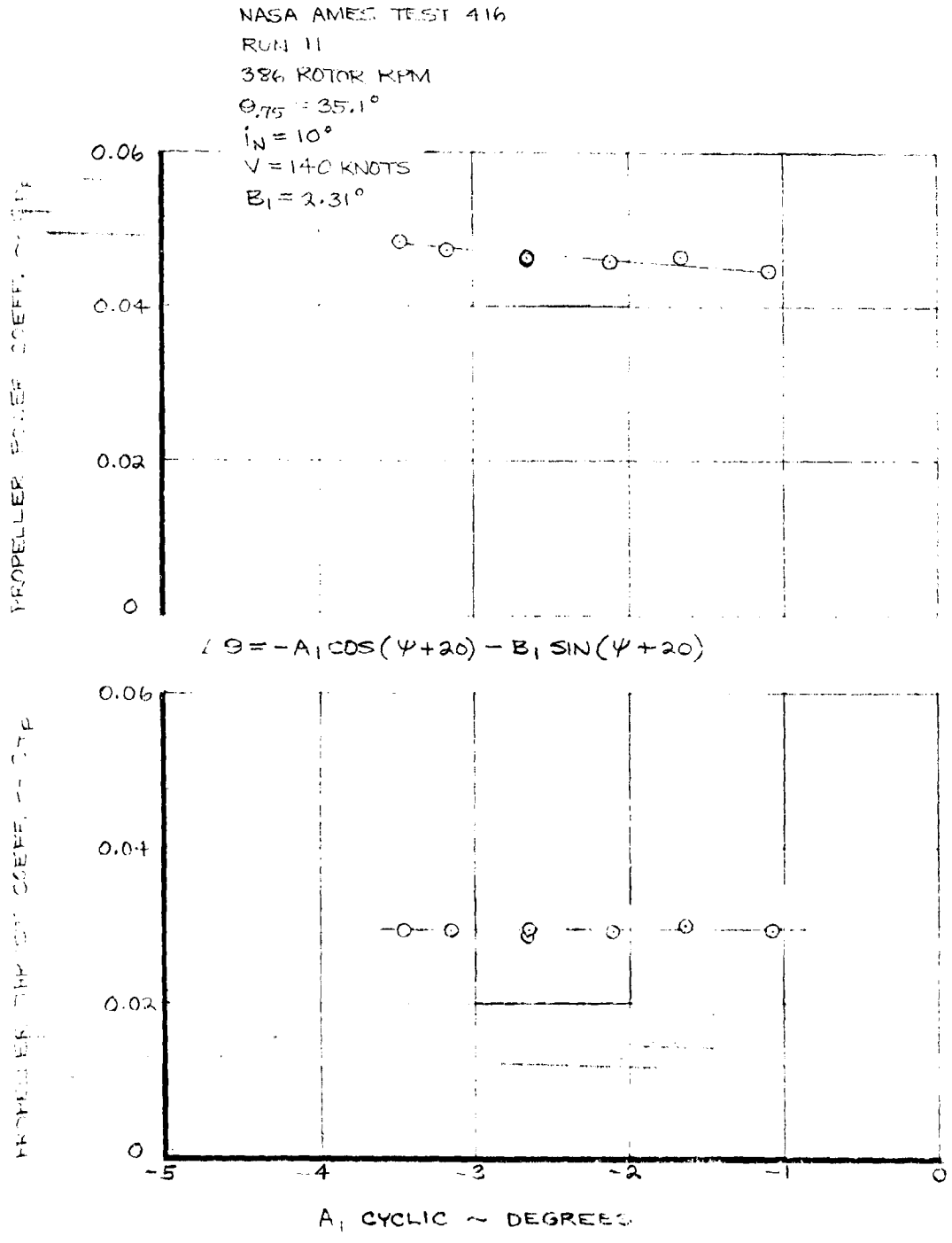

FIGURE 7-30 EFFECT OF A_1 CYCLIC ON CRUISE ROTOR PERFORMANCE - V = 140 KNOTS, $i_N = 10°$

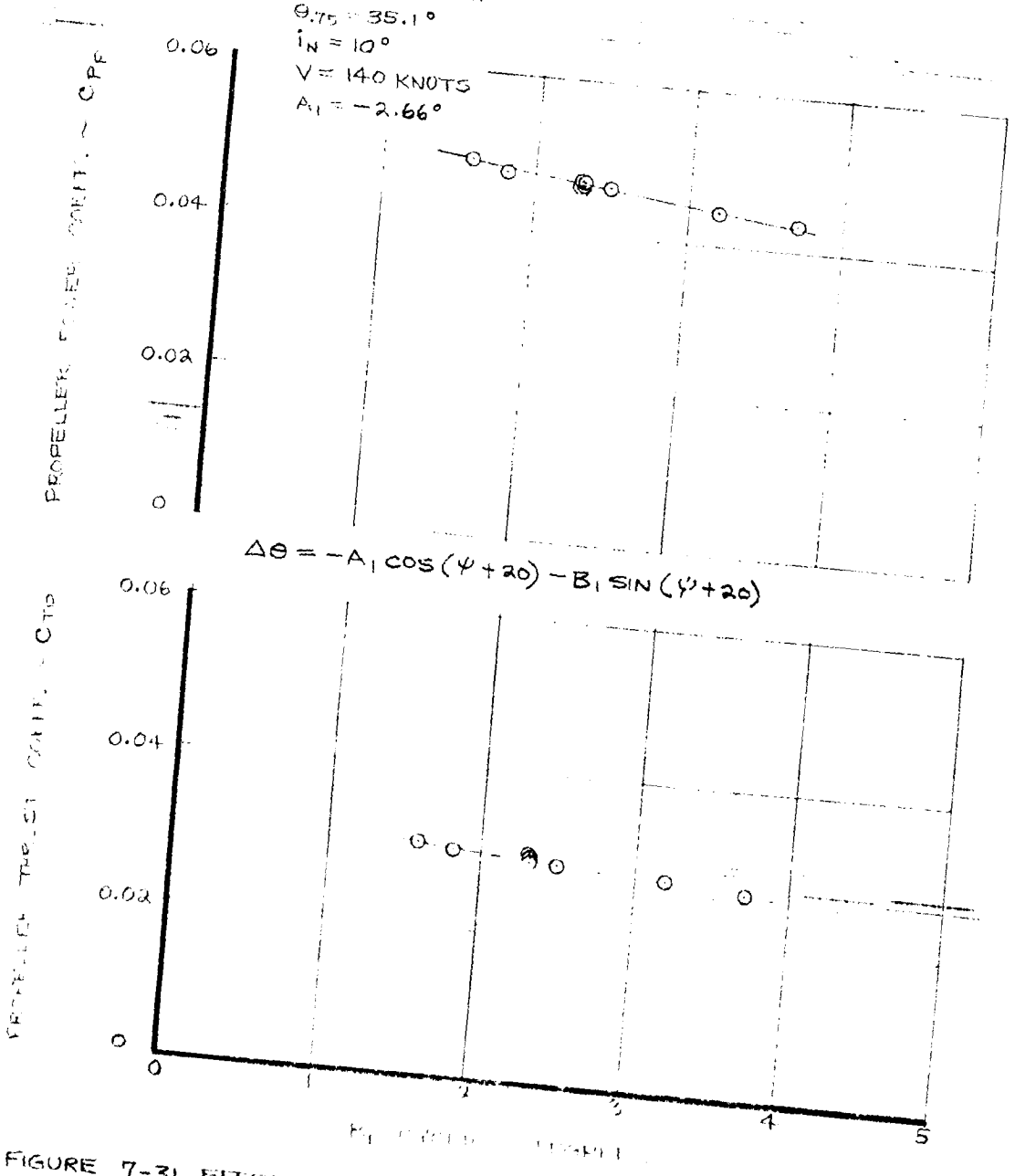

FIGURE 7-31 EFFECT OF B_1 CYCLIC ON CRUISE ROTOR PERFORMANCE – V = 140 KNOTS, i_N = 10°

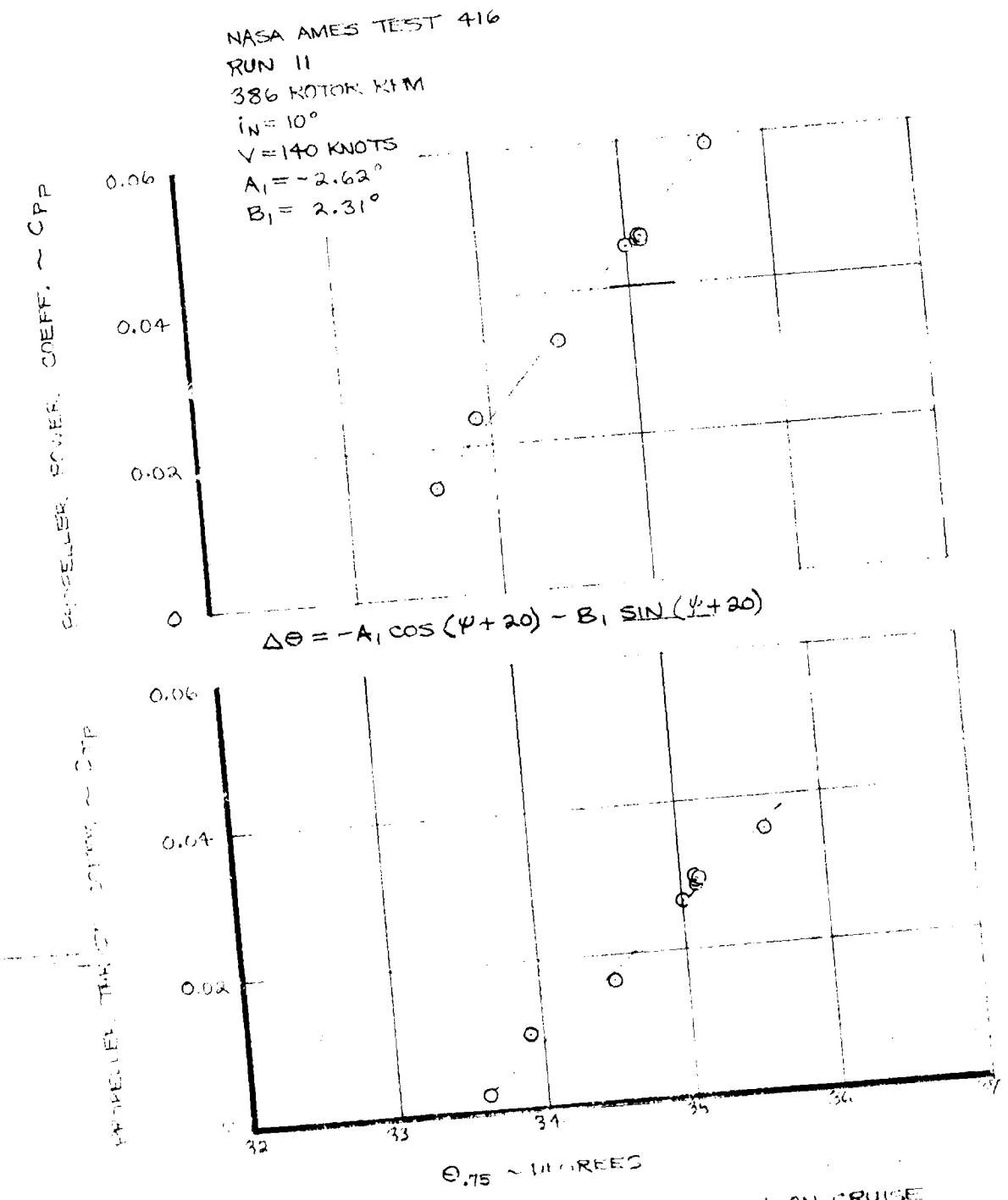

FIGURE 7-32 EFFECT OF COLLECTIVE PITCH ON CRUISE ROTOR PERFORMANCE – V = 140 KNOTS, $i_N = 10°$

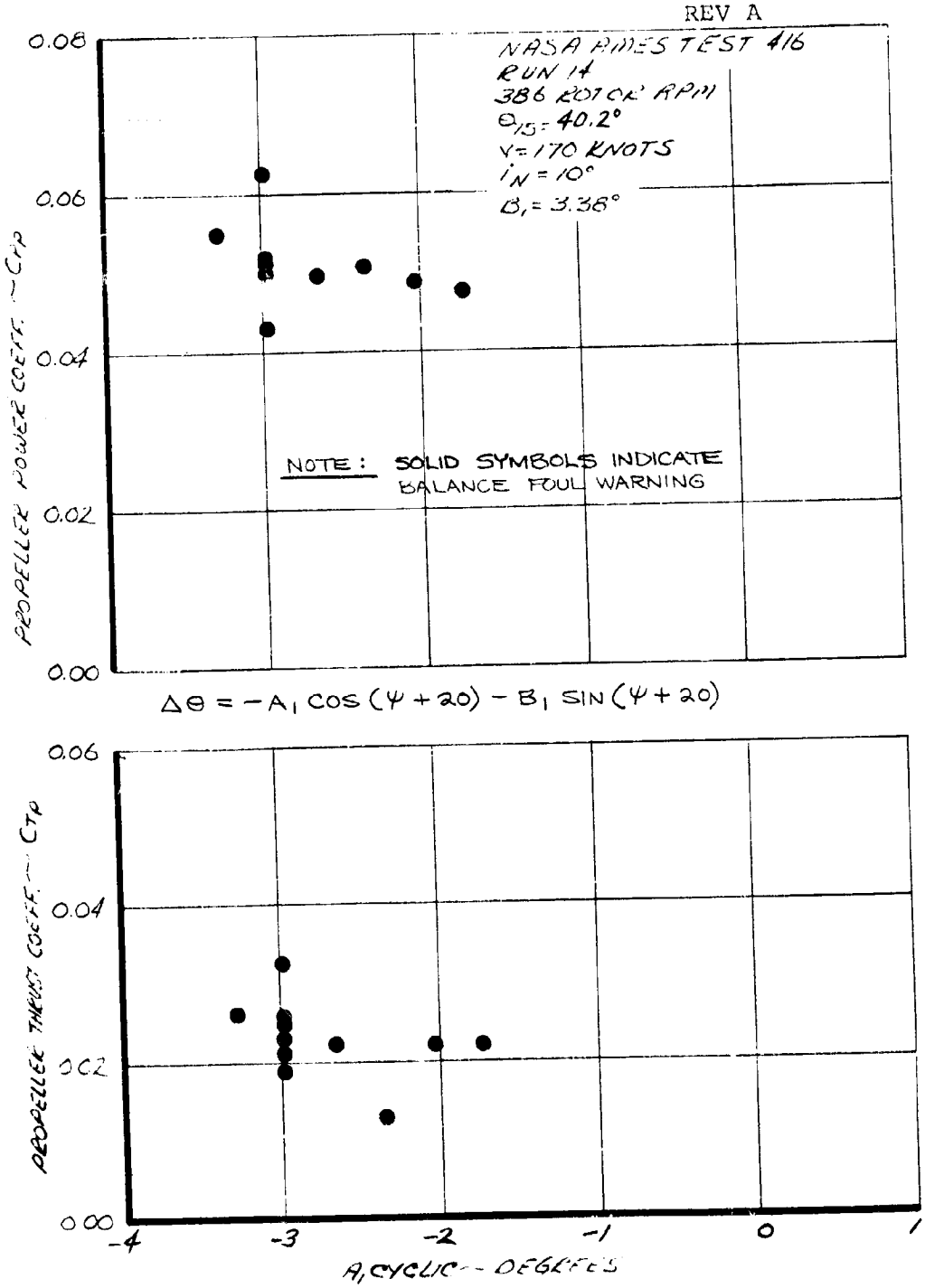

FIGURE 7-33 EFFECT OF A_1 CYCLIC ON CRUISE ROTOR PERFORMANCE — V = 170 KNOTS, i_N = 10°

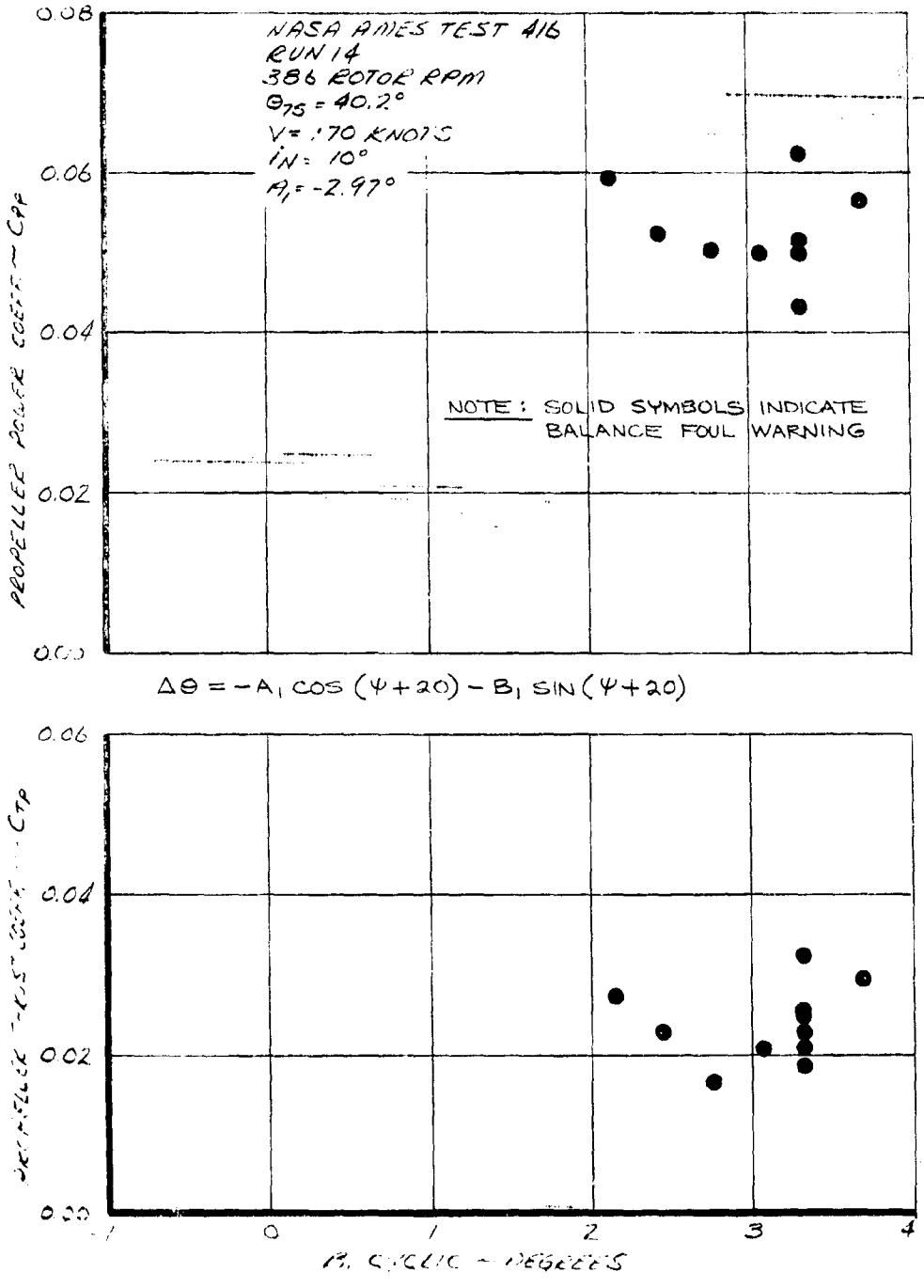

FIGURE 7-34 EFFECT OF B_1 CYCLIC ON CRUISE ROTOR PERFORMANCE – V = 170 KNOTS, i_N = 10°

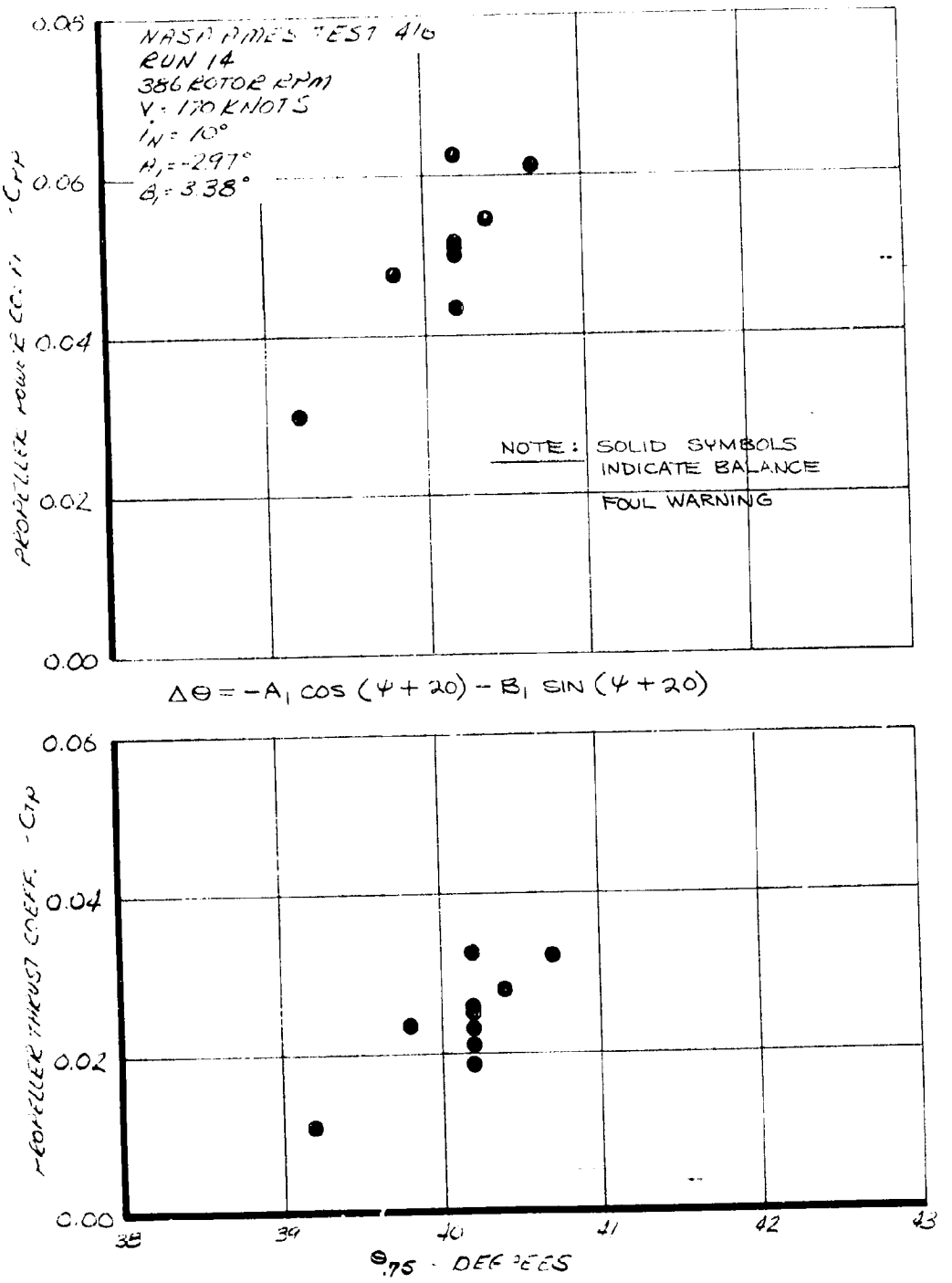

FIGURE 7-35 EFFECT OF COLLECTIVE PITCH ON CRUISE ROTOR PERFORMANCE — V = 170 KNOTS; i_N = 10°

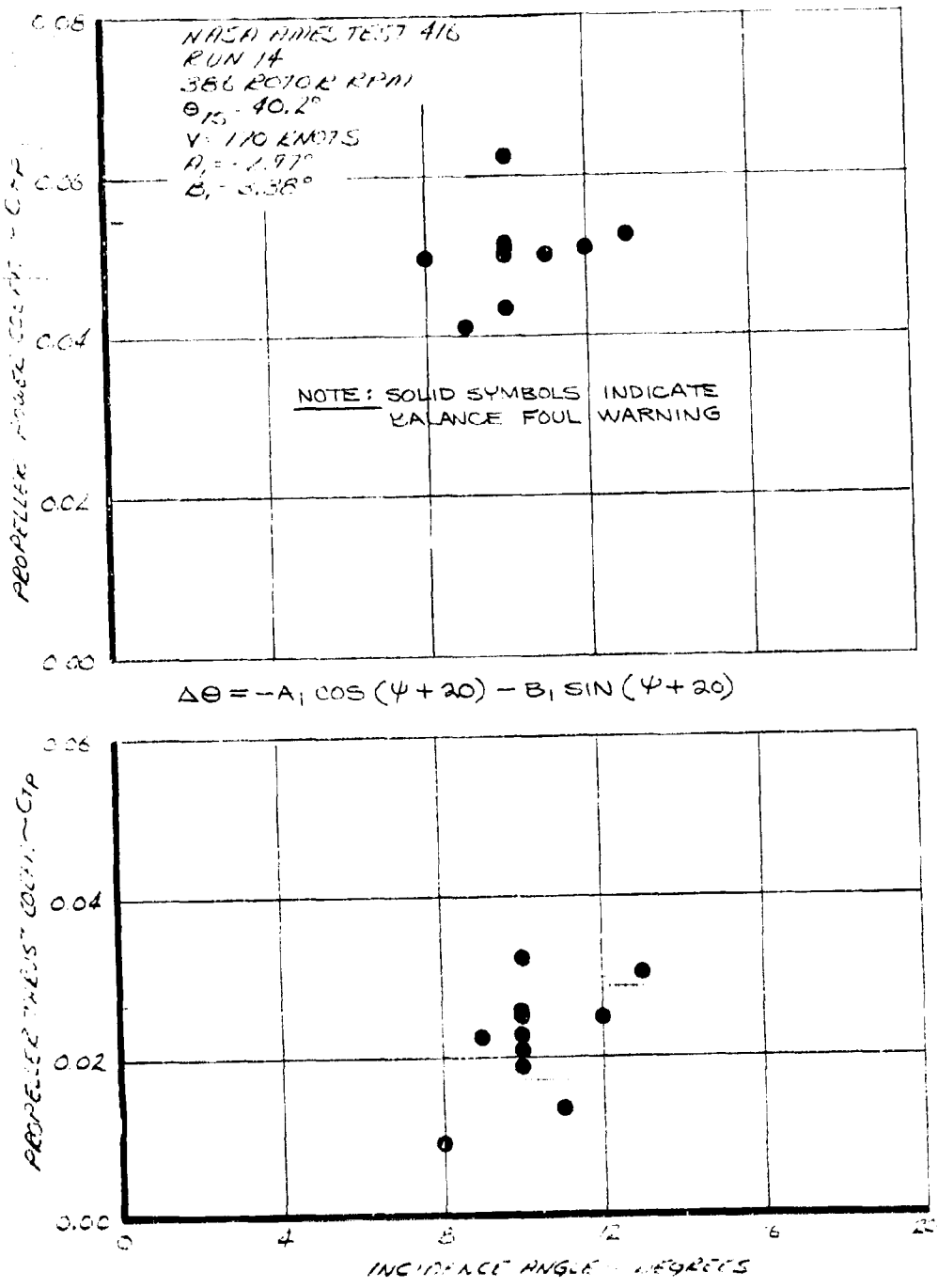

FIGURE 7-36 EFFECT OF INCIDENCE ANGLE ON CRUISE ROTOR PERFORMANCE — V = 170 KNOTS

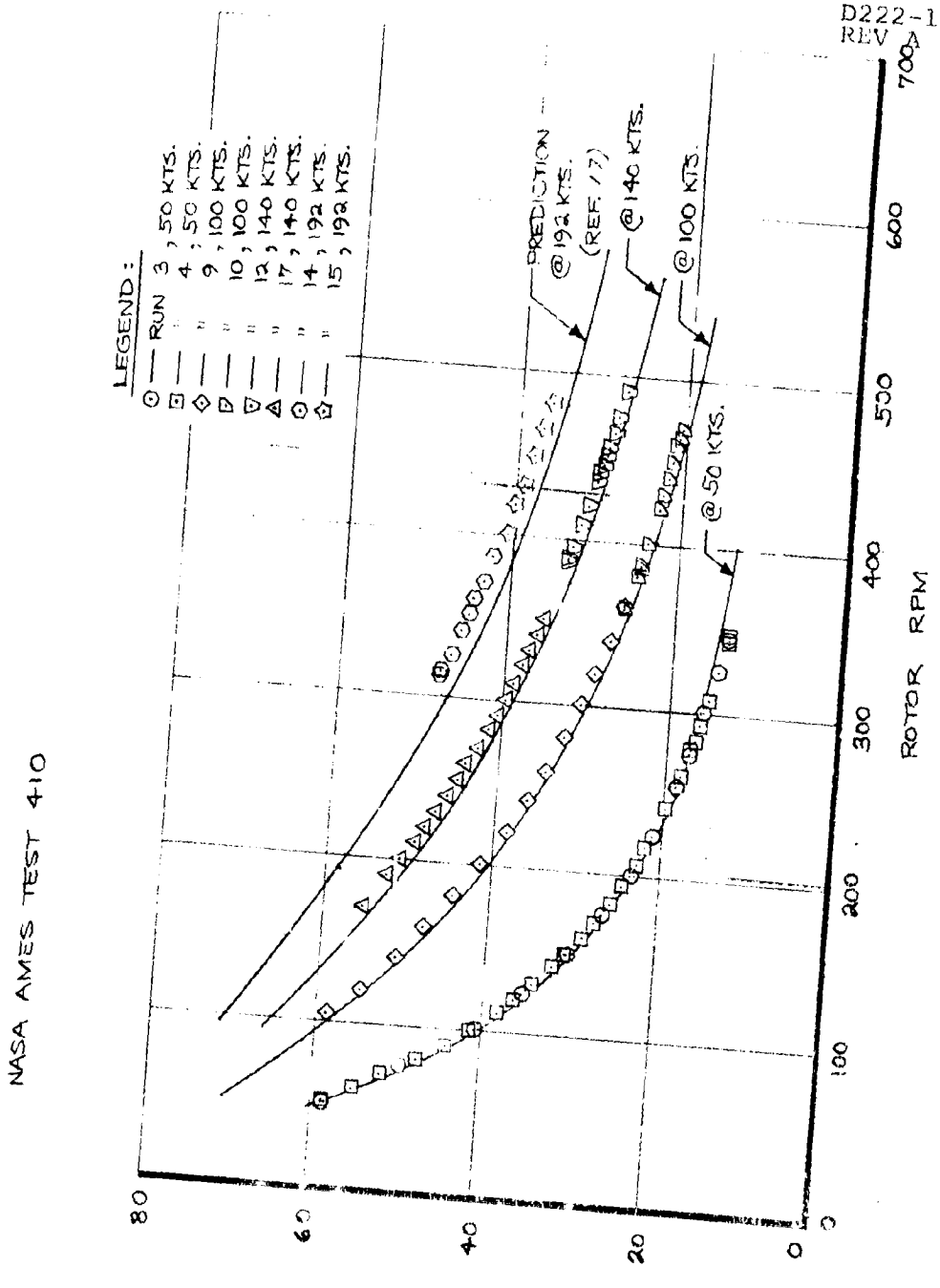

FIGURE 7-37 WINDMILLING CRUISE PERFORMANCE

6.0 FEEDBACK [illegible]
DATA

8.0 FEEDBACK TEST RESULTS

The response characteristics of the M-222 aircraft rotor and control system are such that research in the area of feedback controls to the rotor is possible over frequency ranges that cover the probable gust spectrum as well as the lower aircraft structural frequencies. Systems of this nature are not required by the M-222 but can be used to alleviate blade and wing loads due to gusts as well as shaping the aircraft response. Another potential application of feedback controls is to augment the damping of lightly damped structural modes. Some work has been done in applying systems of this type to helicopter controls (Reference 22), and experimental and theoretical studies have previously been made on tilt rotor control systems under NASA and USAF contracts as well as Boeing funded research (References 23, 24 and 25).

Two candidate systems developed on a small dynamically scaled model under NASA contract NAS2-6505 (Reference 23) were investigated on the full scale dynamic test (40 X 80-foot wind tunnel test (10). The first system (designated "low rate") was aimed at alleviating rotor loads and the second (designated "high rate") was aimed at improving damping of a lightly damped structural mode. The stability of both systems was explored on the full stiffness wing (see Section 5). These tests were performed under contract NAS2-6505.

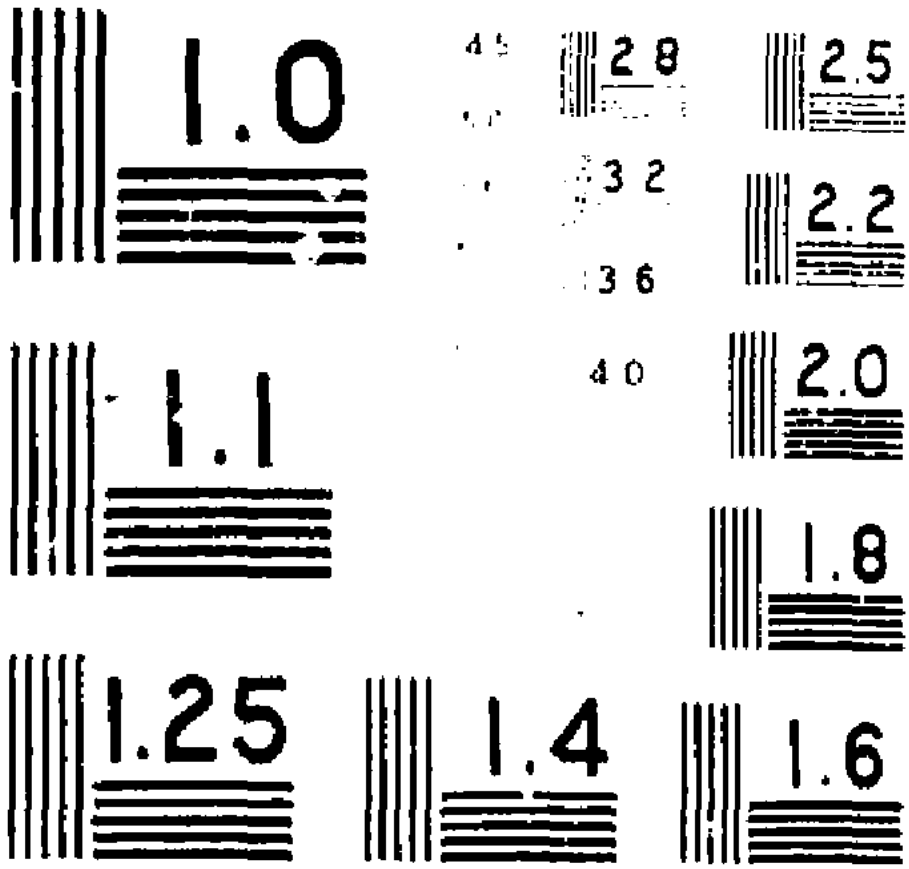

8.1 LOW RATE FEEDBACK

Propeller driven aircraft have always experienced significant blade loads during exposure to skewed flow due to steady state or transient conditions (climb, sideslip, gusts, etc.). The tilt rotor configuration has similar rotor loads (Section 4).

Technical Basis for use of Cyclic Pitch Feedback in Load Alleviation

The predominant cause of vibratory loading in prop/rotors is the blade dynamic resporse to cyclical variations in angle of attack. The two major sources of such variation are shaft tilt to the freestream and cyclic pitch control inputs. In a rotor whose shaft has an incidence relative to the freestream each blade experiences a 1 per rev sinusoidal variation in angle of attack, and a less important 1 per rev variation in dynamic pressure. The magnitude of these effects at a particular blade section is dependent on radial position. The net result of these variations is a dynamic response in the blades with associated blade shears and bending moments and hub forces and moments. Cyclic pitch imposes a 1 per rev variation in incidence and has accordingly much the same effect as shaft incidence except that the angle of attack increment is uniform across the blade and there is no directly associated variation in blade dynamic pressure. Cyclic pitch in appropriate amounts is, therefore, used to trim out the angle of attack variations

caused by shaft tilt to the relative wind. The use of cyclic pitch to trim out blade loads and for stability augmentation is established practice in the helicopter field, and the extension to tilt rotor applications is clearly indicated. The test reported here was a demonstration of how this may be done automatically using sensors providing signals proportional to the shaft angle of attack which are amplified and used to provide compensating movements of the swashplate. In principle it is desired to sense the angle of the shaft to the relative wind (α and β) and in the test this was accomplished by sensing torsional and yawing moments at the wing tip which are related linearly to α and β as discussed below.

The low rate loops tested in the 40 X 80-foot tunnel therefore differed from the airplane loops in two ways; primary sensors and loop hardware. The primary sensors used on test were wing tip pitch and yaw gages, while on the aircraft Aq and Bq sensors (angle of attack X dynamic pressure and sideslip X dynamic pressure) will be used. The second difference is the loop hardware itself which, although conceptually similar, is not the control hardware for use on the aircraft.

These systems are statically equivalent systems since Aq and Bq produce a set of hub forces and moments which themselves cause pitching and yawing moments at the wing tip. Hence the wing tip moments may be used as a measure of Aq and Bq.

Formally this may be stated as

$$M_{y_{gage}} = q\left[(F_{x_\alpha}\cdot\alpha+F_{x_\beta}\cdot\beta)\ h + M_{y_\alpha}\cdot\alpha+M_{y_\beta}\cdot\beta\right]$$

$$M_{x_{gage}} = q\left[(F_{y_\alpha}\cdot\alpha+F_{y_\beta}\cdot\beta)\ k + M_{x_\alpha}\cdot\alpha+M_{x_\beta}\cdot\beta\right]$$

where

F_x, F_y are normal and side forces normalized by q

M_x, M_y are yawing and pitching moments normalized by q

h is distance from rotor to the pitch gage

k is distance from rotor to the yaw gage

α, β are shaft angle of attack and sideslip

q is dynamic pressure

(Aq, Bq) = (αq, βq).

$$\begin{bmatrix} M_y \\ M_x \end{bmatrix}_{gage} = q \begin{bmatrix} (hF_{x_\alpha}+M_{y_\alpha}) & , & (hF_{x_\beta}+M_{y_\beta}) \\ (kF_{y_\alpha}+M_{x_\alpha}) & , & (kF_{y_\beta}+M_{x_\beta}) \end{bmatrix} X \begin{bmatrix} \alpha\cdot \\ \beta\cdot \end{bmatrix}$$

$$= \left(\begin{bmatrix} h, & o \\ o, & k \end{bmatrix} \begin{bmatrix} F_{x_\alpha}, & F_{x_\beta} \\ F_{y_\alpha}, & F_{y_\beta} \end{bmatrix} + \begin{bmatrix} M_{y_\alpha}, & M_{y_\beta} \\ M_{x_\alpha}, & M_{x_\beta} \end{bmatrix} \right) X \begin{bmatrix} \alpha \\ \beta \end{bmatrix} X \begin{bmatrix} q \end{bmatrix}$$

Hence $q \times \begin{bmatrix} \alpha \\ \beta \end{bmatrix} = \left(\quad \right)^{-1} \begin{bmatrix} M_y \\ M_x \end{bmatrix}_{gage}$.

In other words the Aq and Bq signals may be obtained from the appropriate linear combination of the pitch and yaw pivot moments, and the system demonstrated in the tunnel is in principle equivalent to that proposed for the aircraft. The advantage, from a flight vehicle point of view, of Aq and Bq sensing is reliability. Also the direct measurement of the primary source of loads eliminates the lags associated with strain gage sensing of wing response. Of course, for demonstration

purposes under static test conditions this is not an issue.

System Description:

The low rate feedback control loops used on test are shown schematically in both open and closed loop forms in Figures 8.1 and 8.2. The wing tip pitch and wing tip yaw strain gages (signal locations are given in Figure 3.2) were taken through their normal signal conditioning amplifiers and gave sensitivities of -5860 ft lbs/volt pitch and 9050 ft-lbs/volt yaw. The locations of the gages are as shown in Figure 3.2. The calibration of the gages is discussed in Paragraph 6.3. These signals were passed through low pass filters and amplifiers. Two different low pass filters were used, a first-order filter with a 0.12 Hz corner and a second order filter with a 0.75 Hz corner. The analytical form of the transfer function is given in Figures 8.3 and 8.4. The amplifiers associated with these filters were: an amplifier gain 20, the low pass filter amplifier gain 1.5, a voltage divider gain 0.835, and a final buffer amplifier gain 1.4. This system is shown schematically as one amplifier gain 35. The frequency response of both filters are given in Figures 8.3 and 8.4.

The filter output was attenuated by a variable voltage divider ("pots" with one end to ground). These potentiometers were used to control the loop gain such that 1000 counts is a gain of unity in the attenuator. The potentiometers were calibrated and found to be non-linear. The calibration data are given in Figure 8.5.

The output of the attenuators was taken through a sign change amplifier to a summing point. This point was the point at which the function generator signal was input to the loop for open loop response testing. The two signals from the pitch and yaw loops were mixed electrically to provide azimuthal rotation of the cyclic vector. Two rotary potentiometers mounted on the same shaft were used for this purpose and give the transfer equations

$$V_1' = V_1 \cos \psi_{rot} + V_2 \sin \psi_{rot}$$

$$V_2' = V_2 \cos \psi_{rot} - V_1 \sin \psi_{rot}$$

These output voltages are fed to the longitudinal and lateral actuators. The actuator transfer function is $\frac{31.8}{S + 58.2}$ degrees of cyclic per volt (see Figure 8-1), a first order lag with cut-off frequency 9.3 Hz. The rotor and wing complete the loops. The operation of the co-ordinate rotation network was checked statically and gave the data shown in Figure 8.6. For this check three degrees of cyclic were introduced using the lateral actuator with $\psi_{rot} = 0$. The equation for the first harmonic cyclic angle is

$$\Delta\theta = -A_1 \cos (\psi + 20) - B_1 \sin(\psi + 20)$$

Thus for a positive A_1 input a maximum blade angle input is obtained at $\psi = 160^{\circ}$. As ψ_{rot} increases the azimuth for maximum blade angle increases by the same amount. There is a variation in magnitude of the cyclic vector shown in Figure 8.7. On the cyclic command pots the zero cyclic position was not precisely zero volts. These small voltage offsets provide incremental signals which pass through the coordinate rotation network and cause the effect observed.

Figure 8.8 shows the phase lag response of the filter and actuator set up. For this check a signal generator input was made to the filter network and the actuator motion defined from actuator follow up pots. The filter used for this experiment was the 0.75 Hz second order filter. The resultant phase lags are almost identical with those expected from the filter in this frequency range, indicating no additional phase lags in the system.

The overall system gains in degrees of cyclic pitch per foot pound of moment in the wing were checked statically and the data are shown in Figures 8.9 and 8.10. These data were generated by loading the wing using load cells and varying the loop gain for a constant pitch or yaw moment. These calibrations were done with ψ_{rot} = 91.6. The data obtained show a discrepancy from the theoretical gain which can be attributed to the non-linearities found on the gain potentiometers (see Figure 8.5).

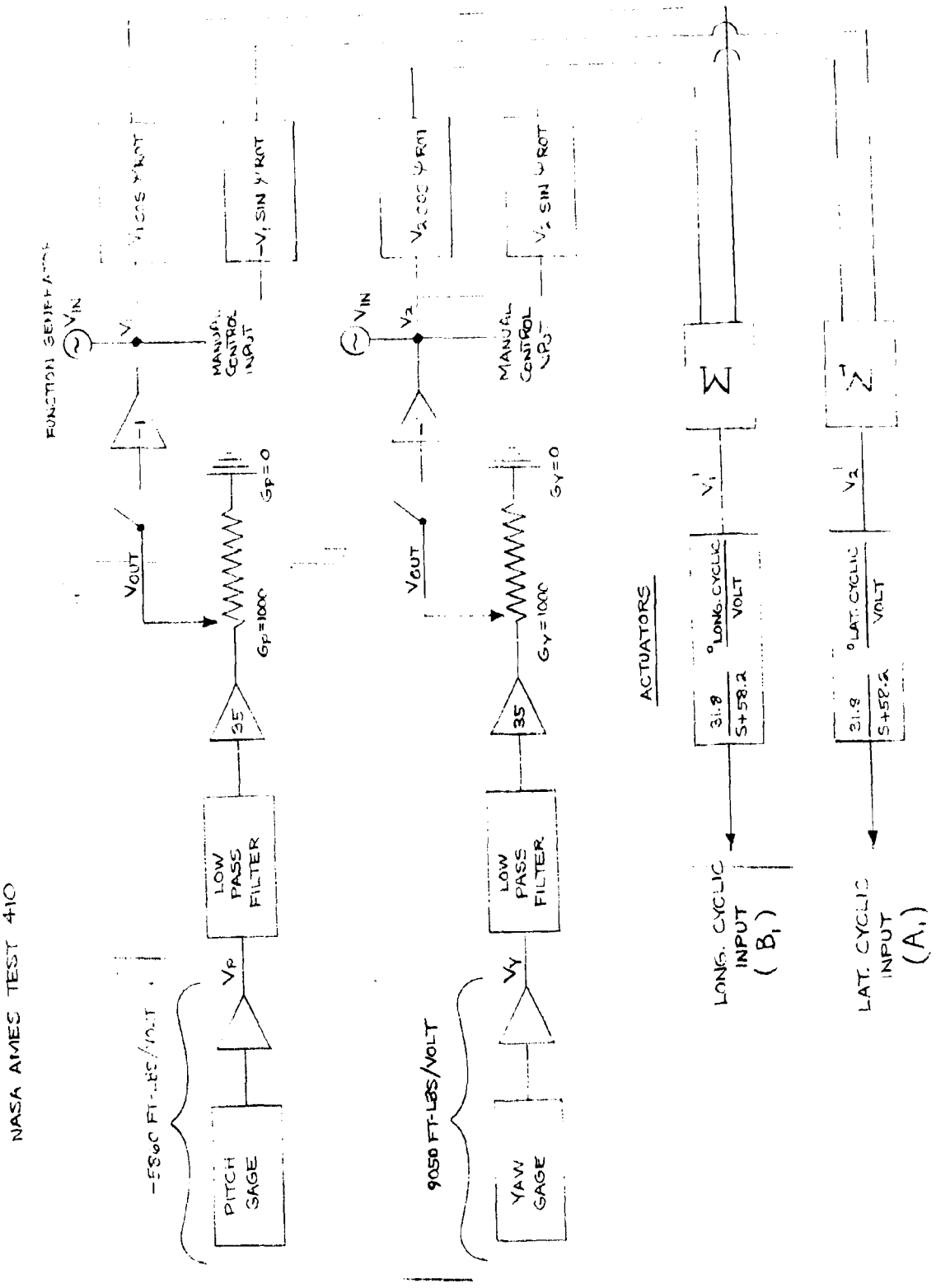

FIGURE 8-1 LOW RATE LOOPS IN "OPEN LOOP" CONFIGURATION

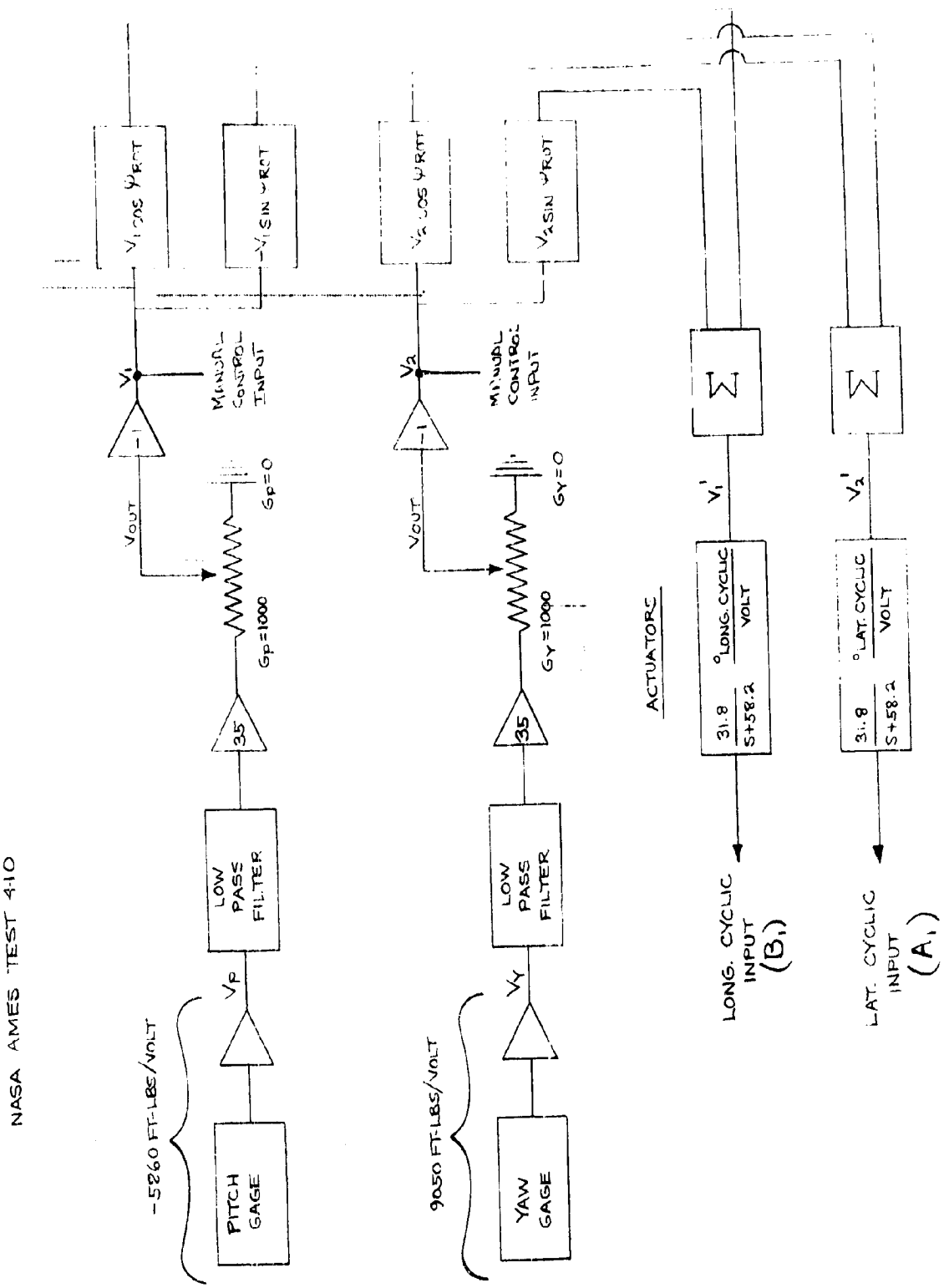

FIGURE 8-2 LOW RATE LOOPS IN "CLOSED LOOP" CONFIGURATION

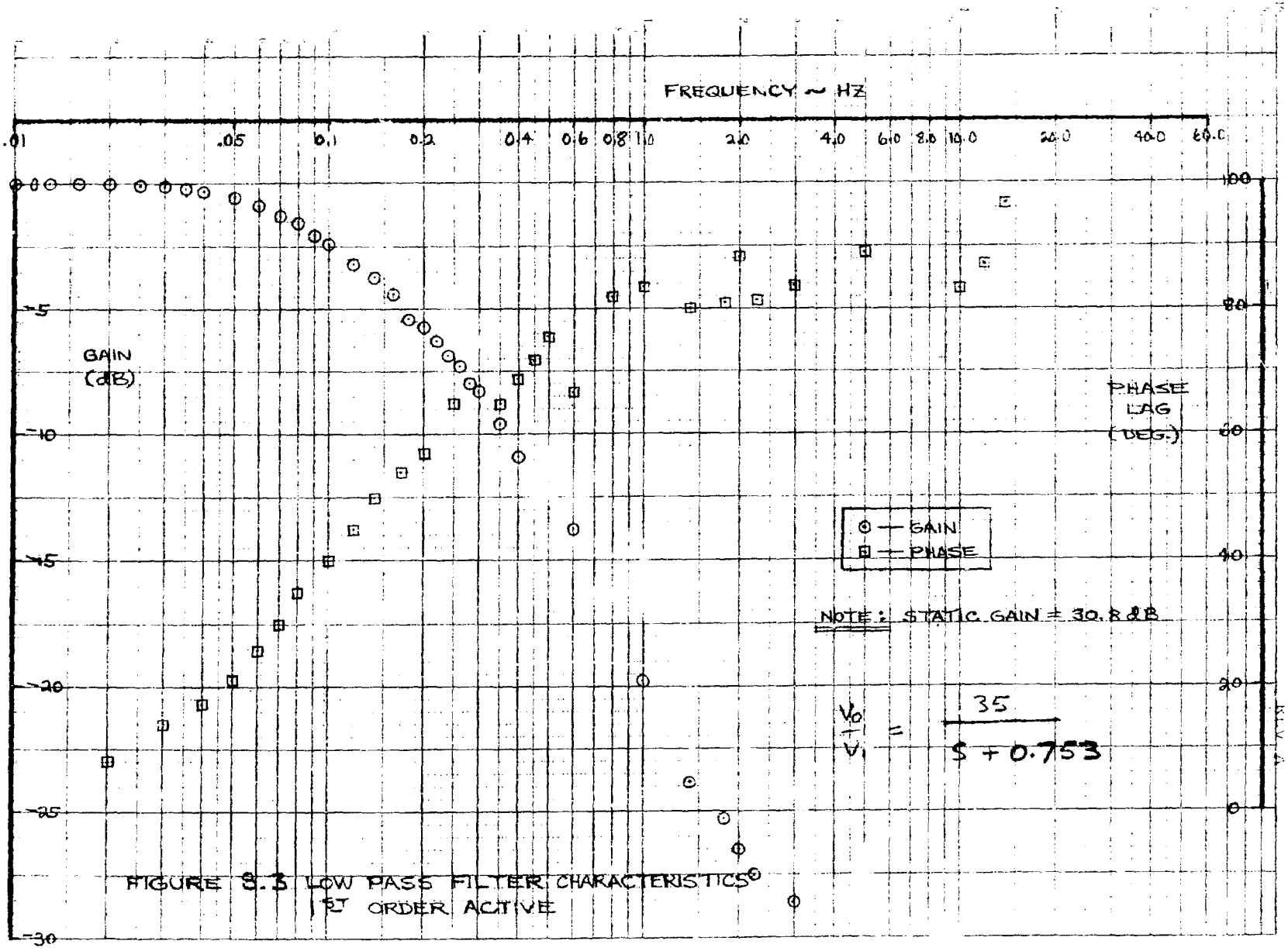

FIGURE 3.3 LOW PASS FILTER CHARACTERISTICS
1ST ORDER ACTIVE

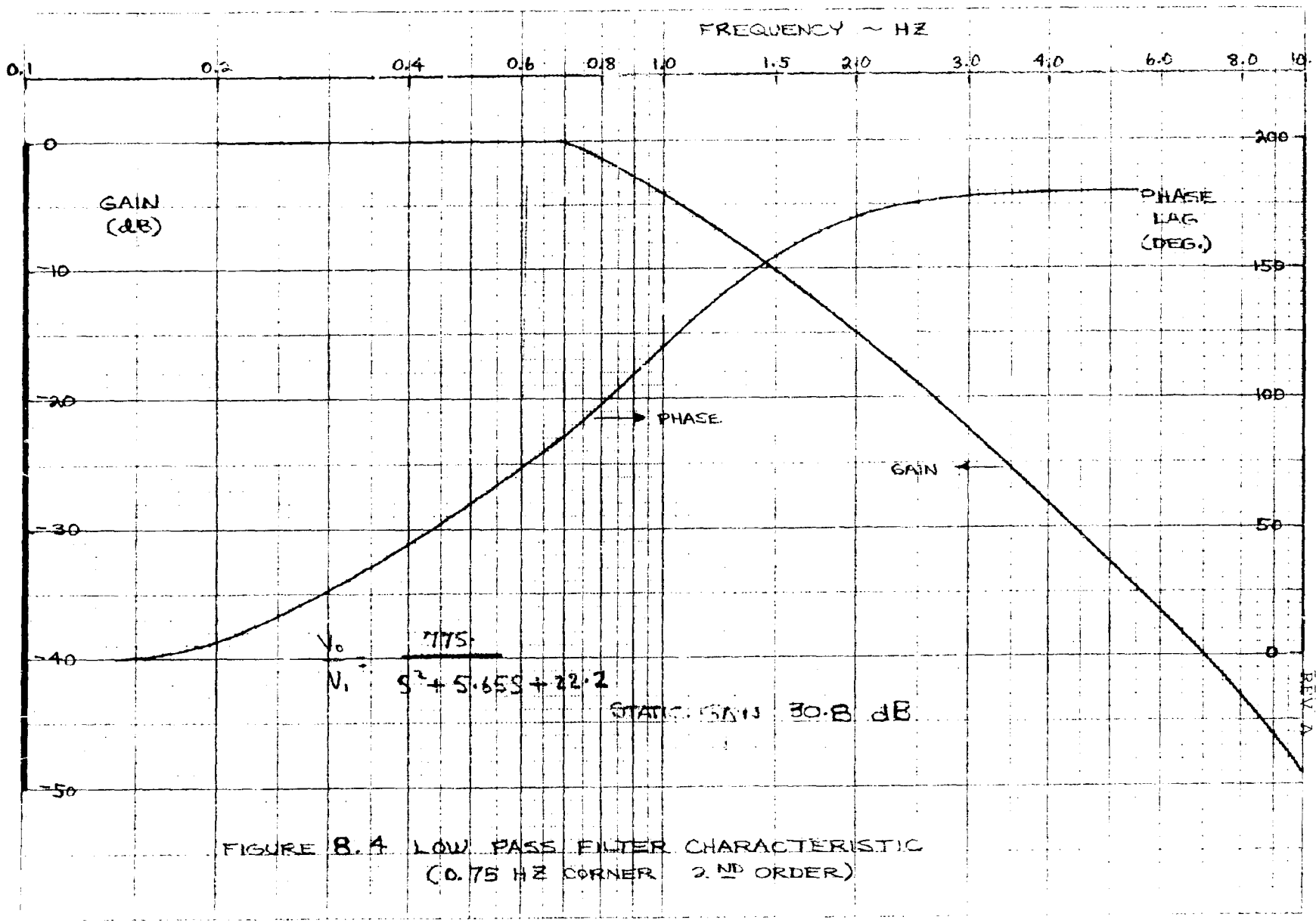

FIGURE 8.4 LOW PASS FILTER CHARACTERISTIC
(0.75 HZ CORNER 2.ND ORDER)

REV. A

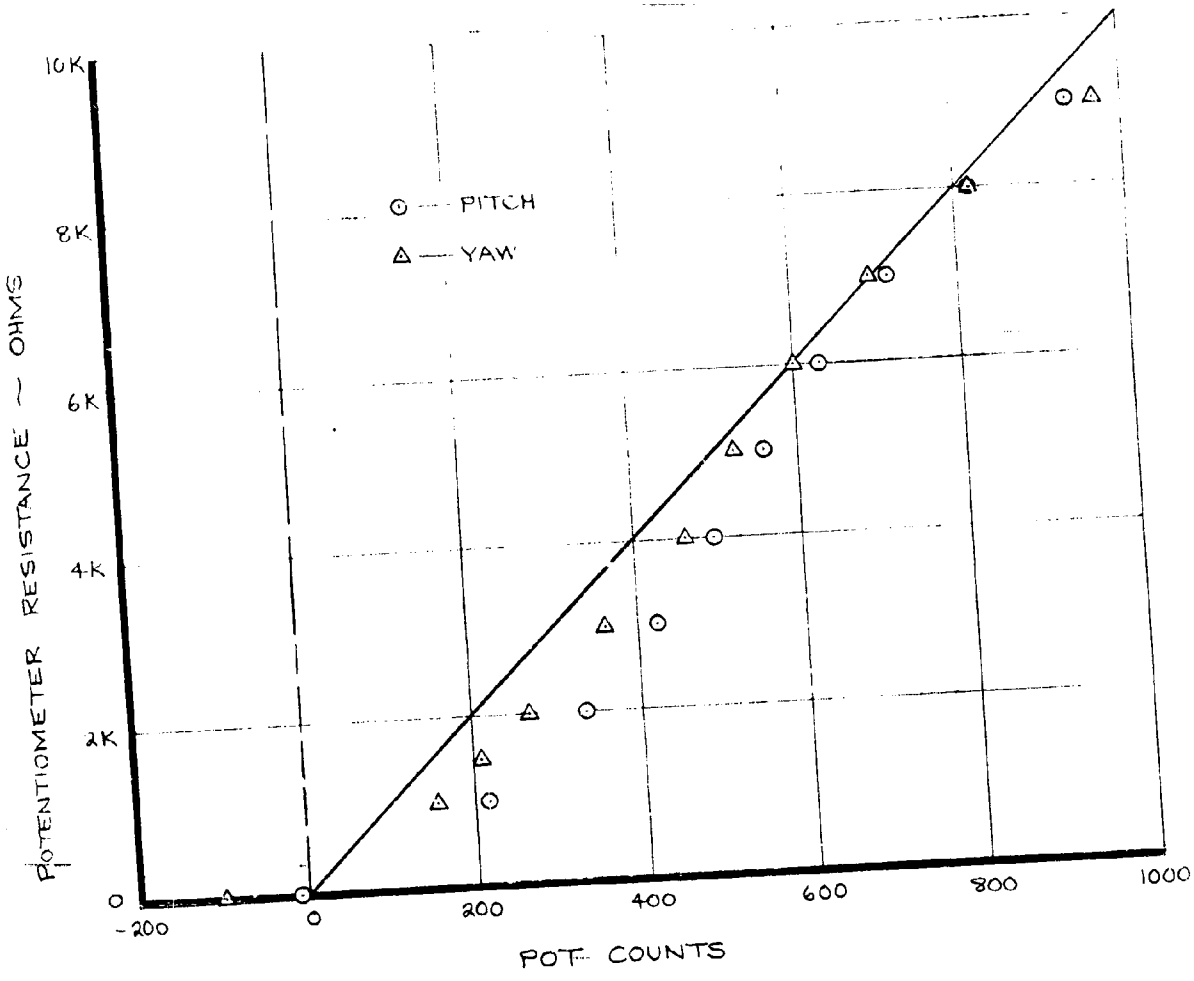

FIGURE 8.5 LOW RATE LOOP GAIN POTENTIOMETER CALIBRATIONS

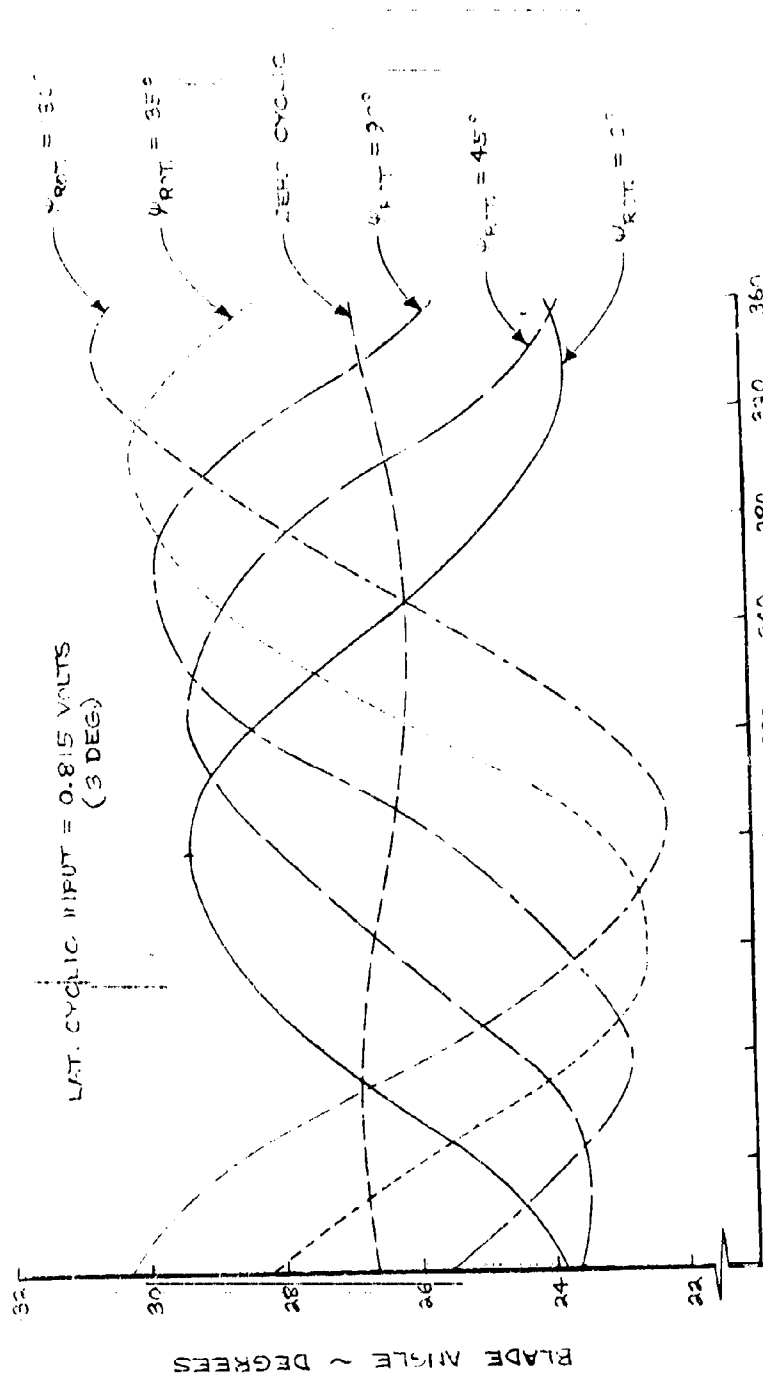

FIGURE NO. 8.6 COORDINATE ROTATION NETWORK CHECK (LATERAL)

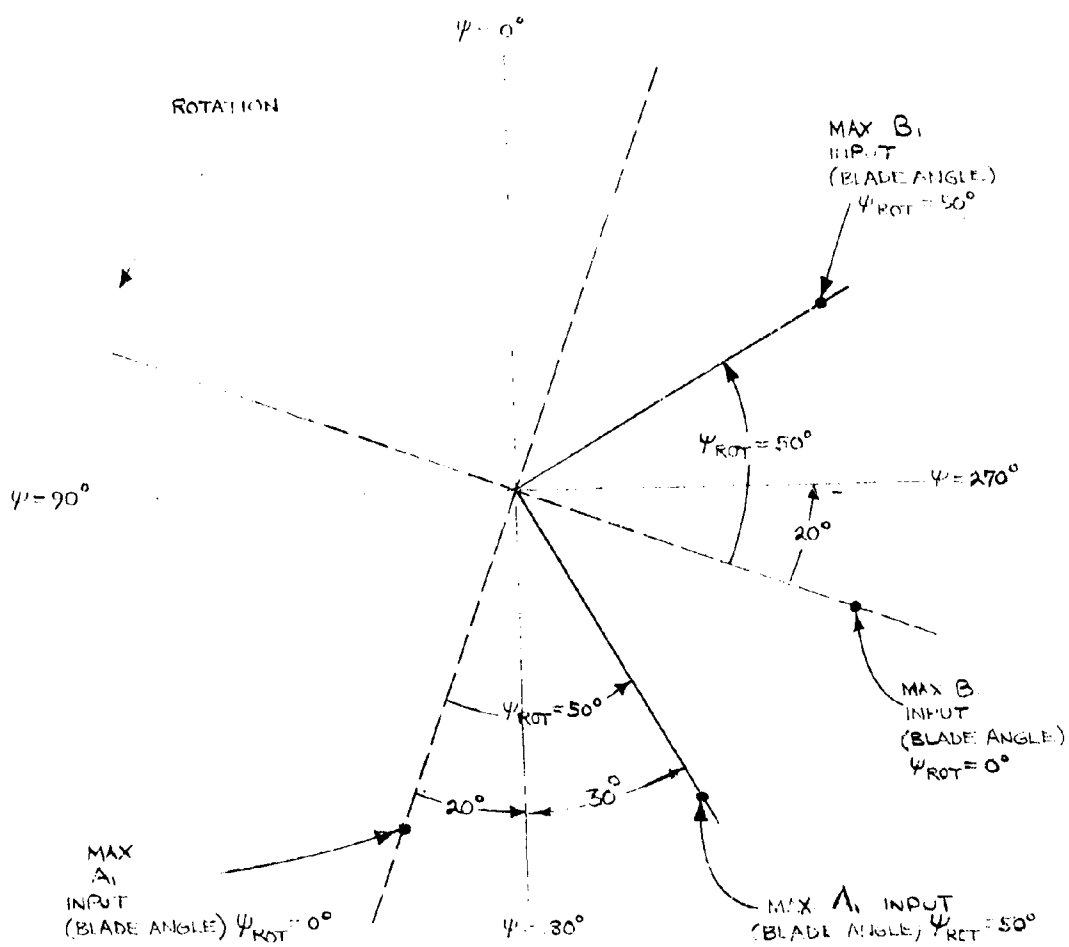

FIGURE 8-7 DEFINITION OF ψ ROTATION

PHASE LAG BETWEEN INPUT SIGNAL TO THE 2ND ORDER LOW PASS FILTER AND THE A1 ACTUATOR FOLLOW UP POT.

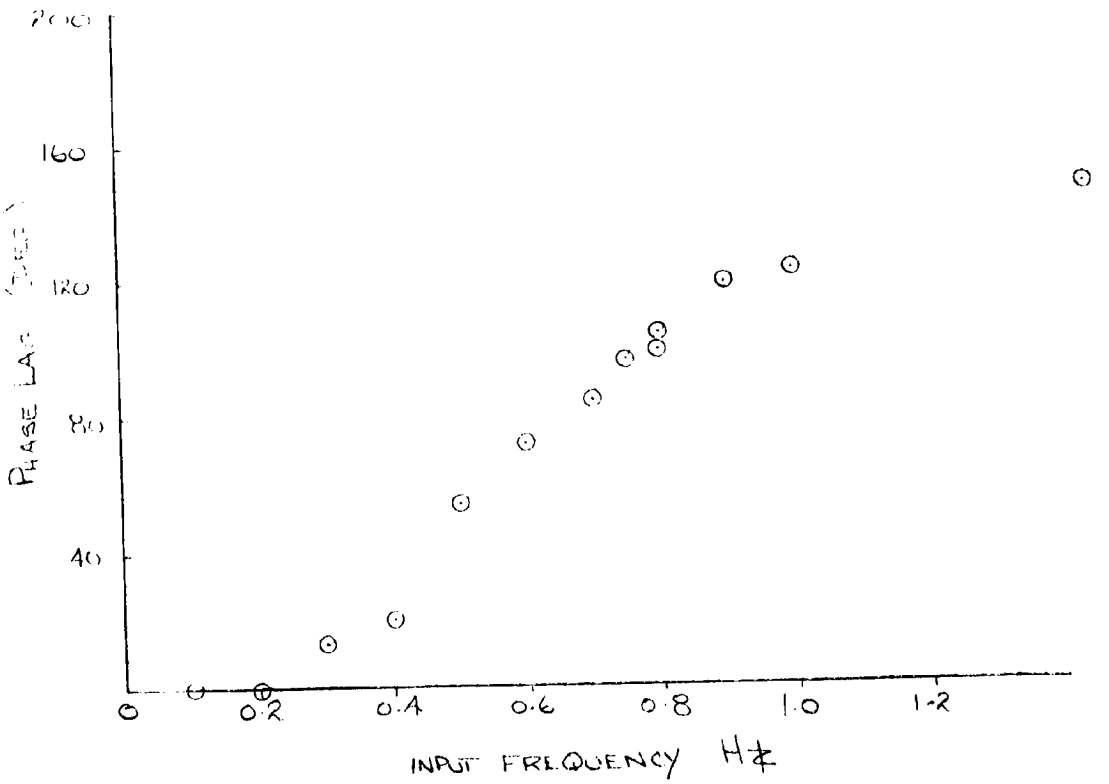

FIGURE 8.8 CONTROL SYSTEM PHASE LAG INCLUDING 2ND ORDER LOW PASS FILTER.

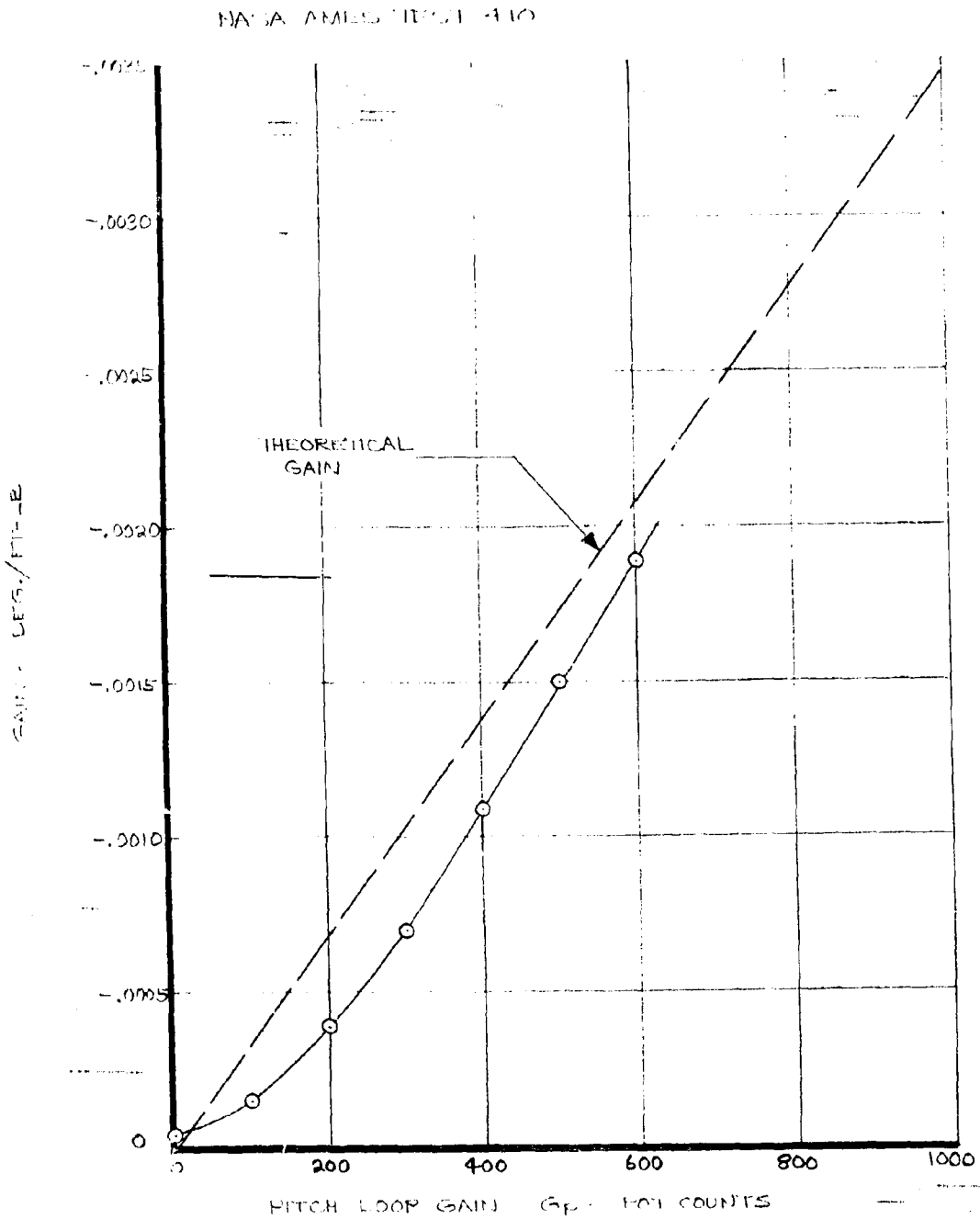

FIGURE 8-9 PITCH LOOP GAIN SETTINGS

NASA AMES TEST 410

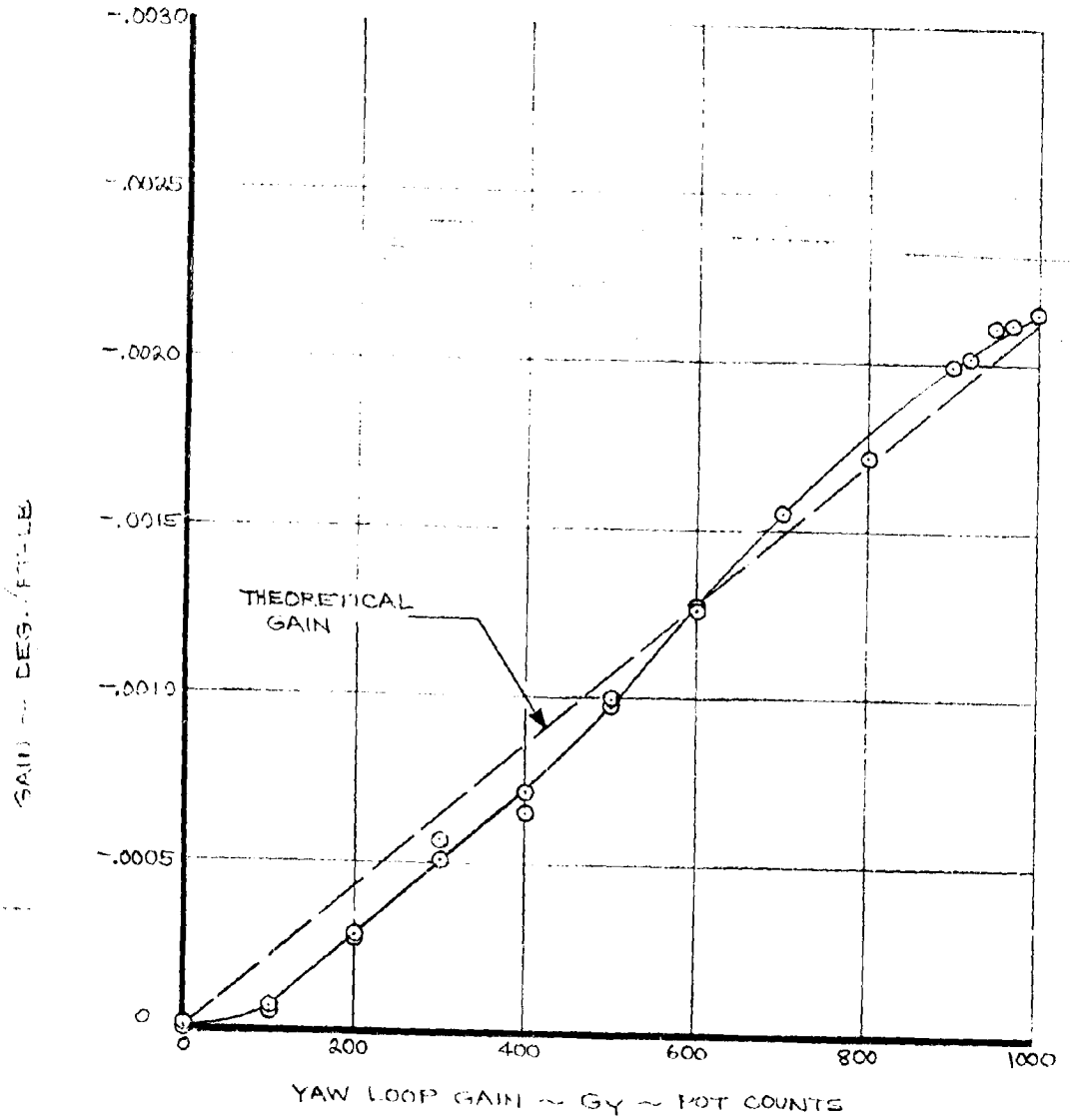

FIGURE 8-10 YAW LOOP GAIN SETTINGS

Stability Aspects of Load Alleviation System

During low rate feedback testing stability data were obtained for the loop configurations:

1. $\psi_{rot} = 91.6^{o}$ 2nd Order Low Pass Filter
2. $\psi_{rot} = 91.6^{o}$ 1st Order Low Pass Filter
3. $\psi_{rot} = 50^{o}$ 1st Order Low Pass Filter

The reason for testing three configurations was that the first ($\psi_{rot} = 91.6^{o}$) was deficient in stability and when this was rectified by filter modifications (still $\psi_{rot} = 91.6^{o}$) it was found to be deficient in performing its primary function of reducing blade loads. The third system ($\psi_{rot} = 50^{o}$) provided a successful demonstration of the use of swashplate feedback to reduce sensitivity of blade loads to angularity of flow through the disk. The first two systems tested are essentially the same; that is the selection of ψ_{rot} was based on the same assumption that a system which was designed to null the wing pitching and yawing moments would also null the blade loads. It was found that this expectation (based on earlier scaled model experience) was incorrect and that such a system could just as readily increase blade loads. This occurs because the rotor normal force due to angle of attack is large and provides the greater part of the wing tip moment. In attempting to reduce wing moments to zero by the use of cyclic, large hub moments were required and these were produced by blade root

bending moments, which appear unacceptably large at levels of gain needed to significantly reduce wing moments. The basic reason for this failure is that shaft angle and cyclic are physically different. Although they are often loosely thought of as being equivalent, the ratios of normal force to hub pitching moment produced by each may be significantly different. This question is discussed at length in Reference 24 and the relevant section is included in Appendix 3 for convenience of reference, where various system objectives and performances are explored. The net result of this fundamental difference between shaft angularity and cyclic pitch is that any one system can only meet limited (but nevertheless useful) objectives; it is not possible in general to provide a system which will null wing pitching and yawing moments, and blade lead-lag and flap bending moments all at the same time. This fact was not sufficiently understood at the beginning of the subject test. The third system tested was designed to reduce blade 1 per rev loads as reflected in hub forces and moments, and this led to ψ_{rot} of 50°. The method of arriving at this system definition is given in Appendix 3. This system was tested successfully and very significant reductions in blade load sensitivity to angle of attack were demonstrated. The three phases of testing are discussed below. The successful final configuration ($\psi_{rot} = 50^{\circ}$) is discussed first.

$\psi_{rot} = 50^{o}$ - 1st Order Low Pass Filter

The system design was selected on the basis of minimizing hub moments. Using experimental data for 192 knots, 386 RPM a ψ_{ROT} of 50-degrees was selected as optimal using the method outlined in Appendix 3. This implied pitch and yaw pot count settings in the ratio 204 to 300. A Bode diagram was determined experimentally for each loop before loop closure. Data for the pitch loop at 1000 pot counts is shown in Figure 8.11. The analytically calculated Bode diagram is also shown, showing good correlation, but indicating an unstable condition not detected experimentally. This was evident in the later loop closed testing when limit cycling occurred at high gains (pot count settings > 800) at 2.2 Hz, close to that of the wing vertical bending mode.

Two comments are in order:

(a) If the analysis had been available prior to testing, a more detailed study of the 1.8-3 Hz range would have been made experimentally, and would have indicated the need for gain restrictions.

(b) The fact that an unstable region was penetrated with limit cyclic oscillations resulting testifies to the value of limited authority systems from a safety standpoint. This is a characteristic feature of electrohydraulic systems and may be counted as an advantage of such feedback systems over systems where feedback is accomplished by mechanical linkages.

(b) continued

The other major advantage is of course the capability to change system characteristics easily.

Figure 8.13 shows calculated and experimental Bode diagrams for the yaw loop at maximum pot count settings. Here again the experimental data indicates a stable system at maximum gain, but the calculated data has an unstable characteristic in the vicinity of 4.0 Hz. However, in the light of experimental experience with the pitch loop, an on-line decision was made to restrict the yaw gain to 700 counts so that the stability issue at high gain settings was not resolved. This did not however compromise the primary objective of the test since blade loads were minimized at gains substantially lower than these.

The Bode diagram with the pitch loop closed at a pot count setting 700 and a yaw gain of 1000 counts is shown in Figure 8.14. This indicated that the system would be stable within those pot count limits, but the system was not tested above a yaw pot setting of 700.

The system discussed above was designed at maximum tunnel speed and cruise RPM. This system was $G_p = 204$, $G_y = 300$ and $\psi_{rot} =$ 50-degrees. Before testing the effectiveness of the set up at 100 knots, 386 RPM, Bode diagrams were generated. The pitch loop Bode based on test data is shown for a $G_p = 1000$ in Figure 8.15 and indicates substantial gain margin at the design gain

G_p = 204. The loop was closed with G_p = 204. The yaw Bode diagram was then generated as shown in Figure 8.16 for a yaw gain setting of 1000 with the pitch loop closed G_p = 204. This indicated a stable system with both loops closed. The yaw loop was then also closed with G_p = 300 and the system was investigated for load alleviation. Figures 8.15 and 8.16 also show the analytically developed gain and phase characteristics. The correlation between test and analysis is shown in Figure 8.15. The measured phase lag below 2 Hz is approximately 30-degrees higher than calculated and the calculated gain shows a peak at 2.3 Hz which is not found on test. Figure 8.16 shows the correlation between test and analysis with the pitch loop closed at 204 and the yaw gain open at a setting of 1000.

ψ_{rot} = 91.6° 1st Order Low Pass Filter

The interim system was based on the objective that wing tip pitch and yawing moments should be controlled by the feedback loops and that the pitch loop should control pitch with no cross coupling with yaw and vice versa. It was expected that this would be accompanied by a reduction in blade loads. This led to the selection of ψ_{rot} = 91.6°. Loop closures were preceeded by examination of the Bode characteristics of the system.

Figure 8.17 and 8.18 show the open loop Bode plots at 100 knots, 386 RPM. The data indicate adequate phase margins.

The yaw loop Bode was repeated with the pitch loop closed at a gain of G_p = 300, Figure 8.19. The stability margins were not significantly affected. Post test calculations of the frequency response have been made and are shown on Figures 8.17 and 8.18.

The experimental data show an additional lag over the theoretical line which is unexplained at this time. Figures 8.20 to 8.22 show similar data at 192 knots. Again the experimental data indicate stable systems at maximum gain. Figure 8.22 is a pitch loop Bode with the yaw loop closed (G_y = 700). These data indicate an increased response at a frequency of 1.6 Hz which is coincident with the lower blade lag mode frequency (see Figure 4.11, Section 4). Calculated response data are given in Figures 8.20 and 8.21.

This system worked reasonably well at 100 knots in that wing moments were attenuated. At 192 knots the system was less effective in reducing moments and in fact increased the alternating blade loads.

As discussed above this led to a review of the system design philosophy and it became obvious that designing the system purely to minimize wing moments was not useful because the wing moments were caused primarily by normal force. The cyclic pitch feedback was compensating for this by the application of hub moments. This is because the hub force, moment relationship produced by angle of attack is different

from that produced by cyclic pitch. The moments on the wing can be fully compensated only at the expense of increased hub moments, i.e., increased blade loads.

This led to a different approach in which the hub forces and moments were used as the criterion of system effectiveness. The hub forces and moments reflect blade shears in the plane of the rotor and out-of-plane flap bending moments respectively. Some of the same limitations still apply, i.e., the combinations of normal force, side force, pitching and yawing moment due to angle of attack and cyclic pitch do not match exactly for any ψ_{rot} so that it is not possible to null forces and moments completely by cyclic.

This is because there are physical differences in the way shaft angle of attack and cyclic pitch produce blade aerodynamic loads. However, a system which significantly compensates hub forces and moments will in most cases reduce the wing moments which partially achieves the objectives on which the above system ($\psi_{rot} = 91^{o}$, $G_p = 700$. $G_y = 700$) was based. (Note: the issue of system selection is discussed at length in Reference 24.) Recognition of the above limitations led to the final system definition ($\psi_{rot} = 50^{o}$, $G_p = 204$, $G_y = 300$).

$\psi_{rot} = 91.5^{o}$ 2nd Order Low Pass Filter

The first attempt at a low-rate feedback system was based on the expectation that reduction of wing pitching and yawing

moments would also result in reduced blade loads. This expectation had been encouraged by small scale model tests, Reference 23. In the event of full scale testing it was found that this approach not only led to increased blade loads but introduced adverse coupling between pitch and yaw which drive the system unstable at high gain values.

The desired gain settings based on calculations using the static measured rotor derivatives were $G_p = 700$, $G_y = 700$. At a pitch gain of 325 and yaw gain zero the system became unstable and the gain was returned to zero. A trace taken after the reduction of gain is shown in Figure 8.23. It should be noted that the frequency of this decaying trace is probably different from that of the actual instability.

The Bode diagram (i.e., open loop frequency response of gain and phase) for the system which went unstable is shown in Figures 8.24 and 8.25 for gains of $G_p = 350$ and 450. The data points in the region of 1 Hz indicate the existence of an instability since the phase lag is 180-degrees and the system has an overall positive gain of 5.5 db. Examination of the yaw loop Bode diagrams indicate that this system also would be unstable at gain settings in excess of 300, Figures 8.26 and 8.27. This problem was solved by using increased attenuation and reducing phase lag. This was accomplished by removal of the 0.75 Hz second order filter and

replacing it with a first order active filter. This modification stabilized the system as previously described. This permitted the testing to proceed.

Nature of the Instability

The instability frequency is significantly lower than any structural frequencies, e.g., cyclic lag, $(\Omega - W_L) = 1.55$ Hz, cyclic flap $(\Omega - W_\beta) = 1.84$ Hz and wing bending $W_V = 2.2$ Hz. The natural frequency of the 2nd order filter however was 0.75 Hz so that the instability seems to be more closely associated with the filter than the rotor airframe system.

Additional Comments

The system analyzed for stability prior to the test was not the system actually tested. That is to say pretest system definition had selected a ψ_{rot} of 54-degrees based on a combination of Princeton test data (Reference 23) and calculated derivatives. These pretest predictions are presented in Reference 26.

The calculated open loop response indicates an instability but the frequency at which the phase attains 180-degrees is significantly higher than that of the test data, that is, 2 Hz compared with approximately 1 Hz. Above 0.5 Hz there is a steady increase in the difference between the phase actually measured and that calculated. This difference is sufficiently large and of such importance that some discussion of the possible causes is required.

1. The difference in rate of change of phase in the 1.0 Hz region would be consistent with an additional first order transfer function in the loop which is not represented in the mathematical model. This would imply that the system changed over the course of the test since good correlation was obtained for other cases using essentially the same mathematical model, e.g., high rate system correlation and later testing of the low rate system.
2. Another possible explanation is that the sensitivity of system phase to $\psi_{rotation}$ is high and otherwise unimportant discrepancies between analytical and test derivatives could lead to the fairly large phase differences observed. For example the azimuthal difference between the predicted and test force vectors due to A_1 input statically may be as much as 20-degrees. This could explain the observed phase differences if the azimuth selected (91.5-degrees) were at a point where the phase was highly sensitive to azimuth. This possibility was explored analytically and only a small sensitivity to azimuth was demonstrated at $\psi_{rot} = 91.5^{o}$. However, test confirmation is not possible at this time and the actual behavior of the rotor might be such that this is the reason for the difference in the Bode diagrams.

   This second explanation of the difference between analytical and test behavior appears to be the most plausible since

2. continued

the feedback loop including the actuator was tested at the same time as the Bode diagrams and was seen to agree substantially with the mathematical model.

This experience indicates the need for the acquisition of methodical and detailed test data on rotor systems prior to system selection and the need for Bode diagram analysis prior to all loop closures.

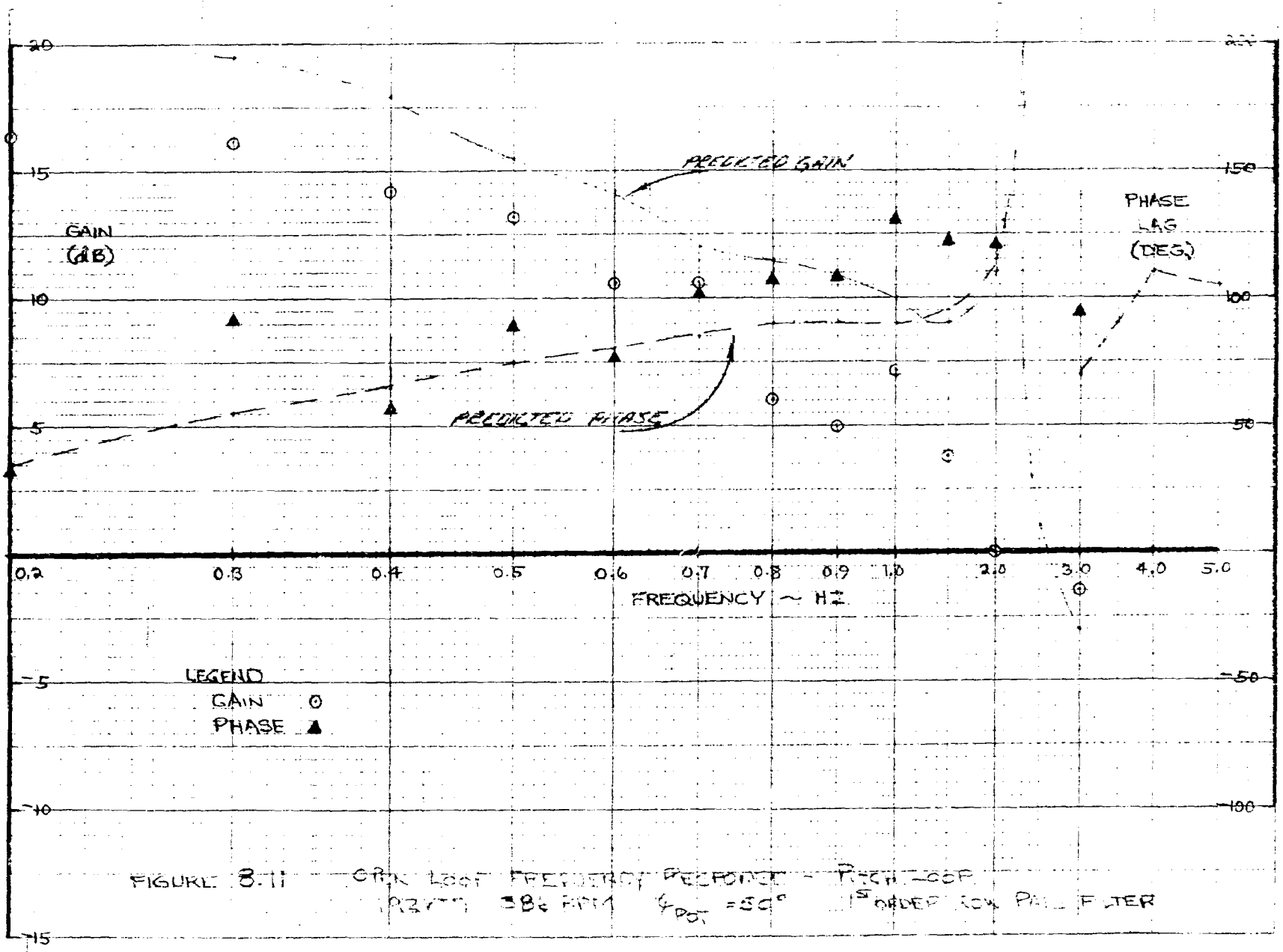

FIGURE 8.11 — GAIN LOST FREQUENCY RESPONSE - PITCH LOOP
WITH 3Db PM ϕ_{DT} = 30° 1ST ORDER RC PRE-FILTER

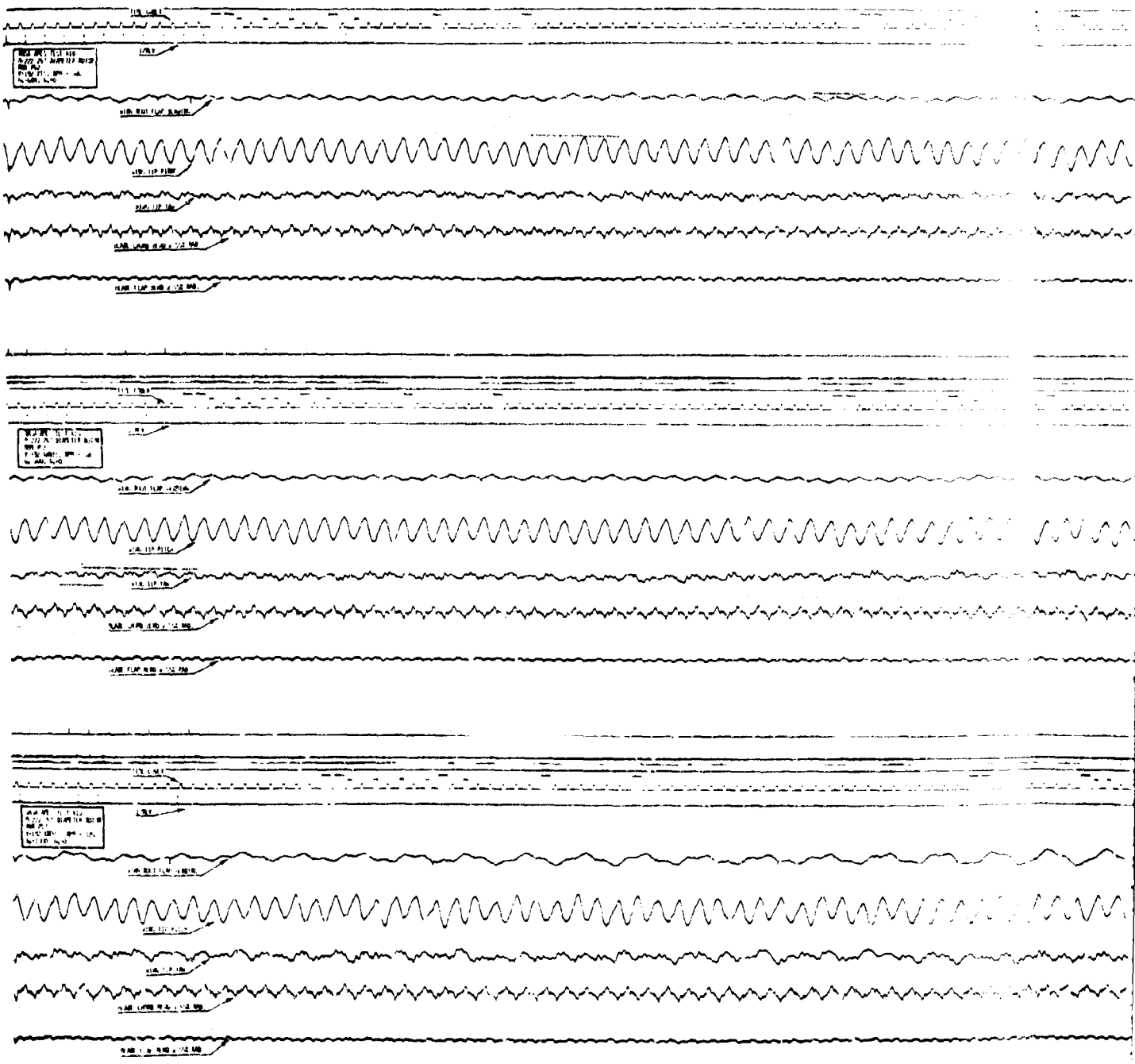

Figure 8.12. High Gain Trace Records $\zeta_{rot} = 50$, 1st Order Low Pass Filter

FOLDOUT FRAME

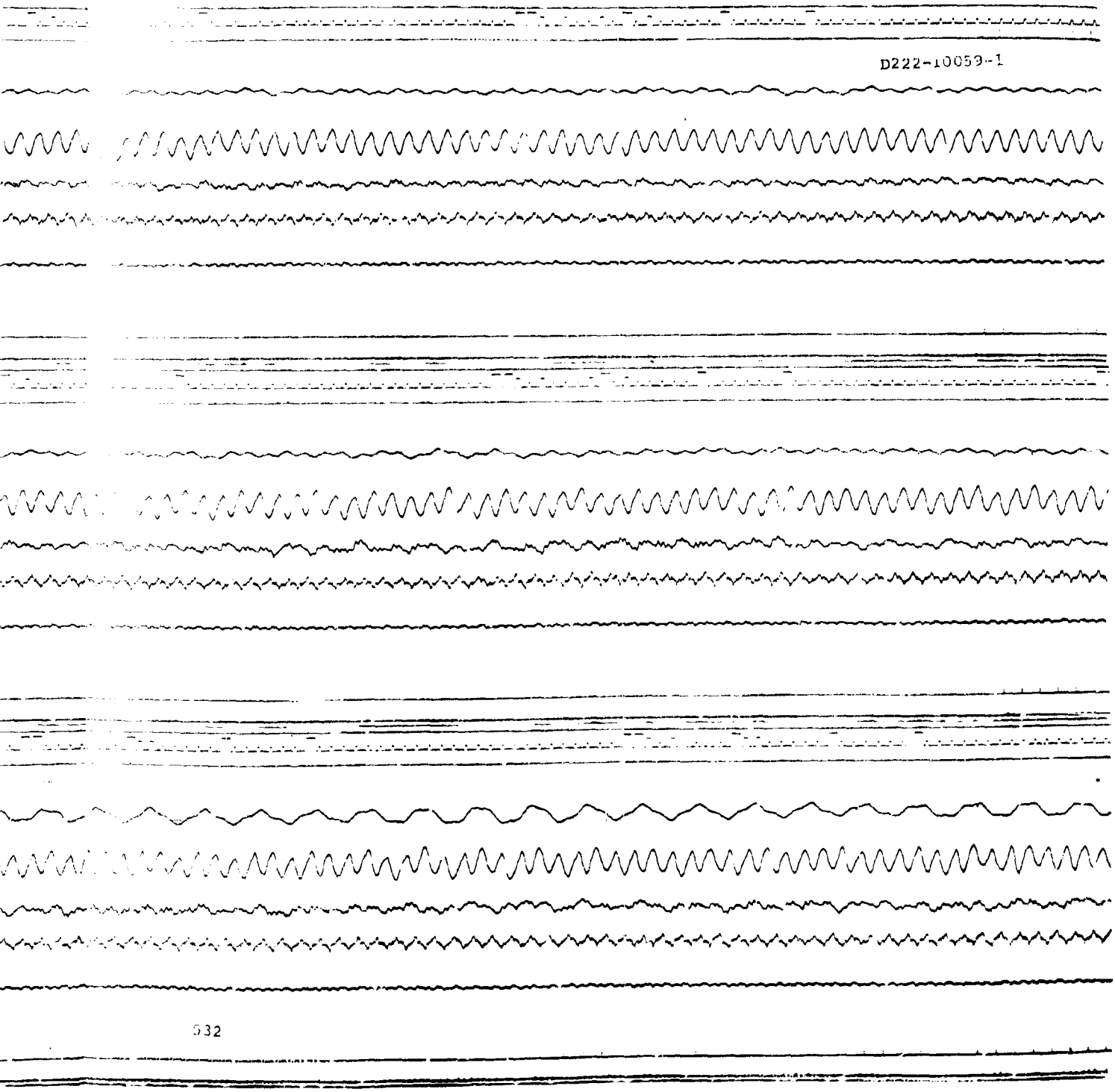

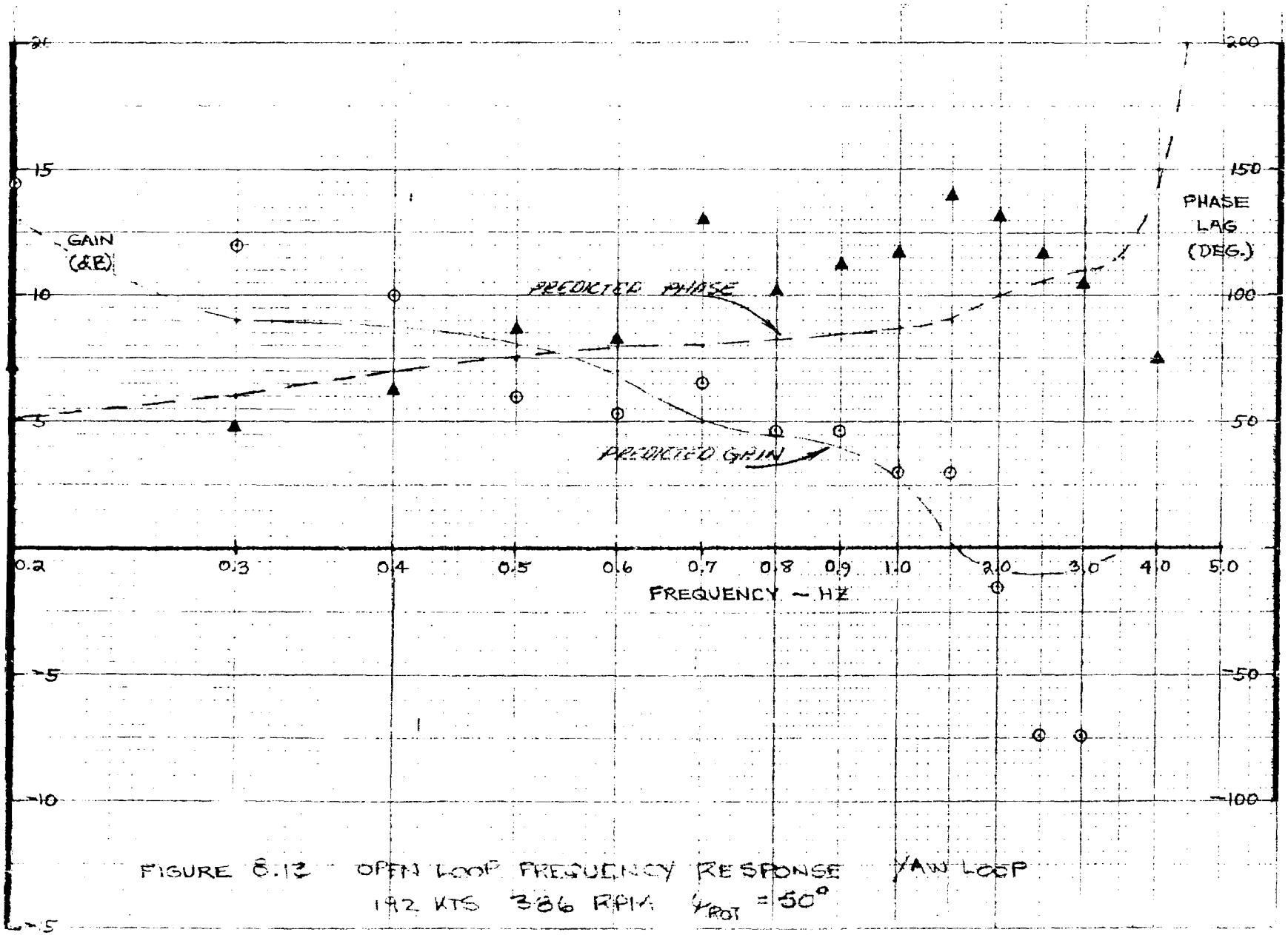

FIGURE 6.12 OPEN LOOP FREQUENCY RESPONSE YAW LOOP
192 KTS 386 RPM $\psi_{ROT} = 50°$

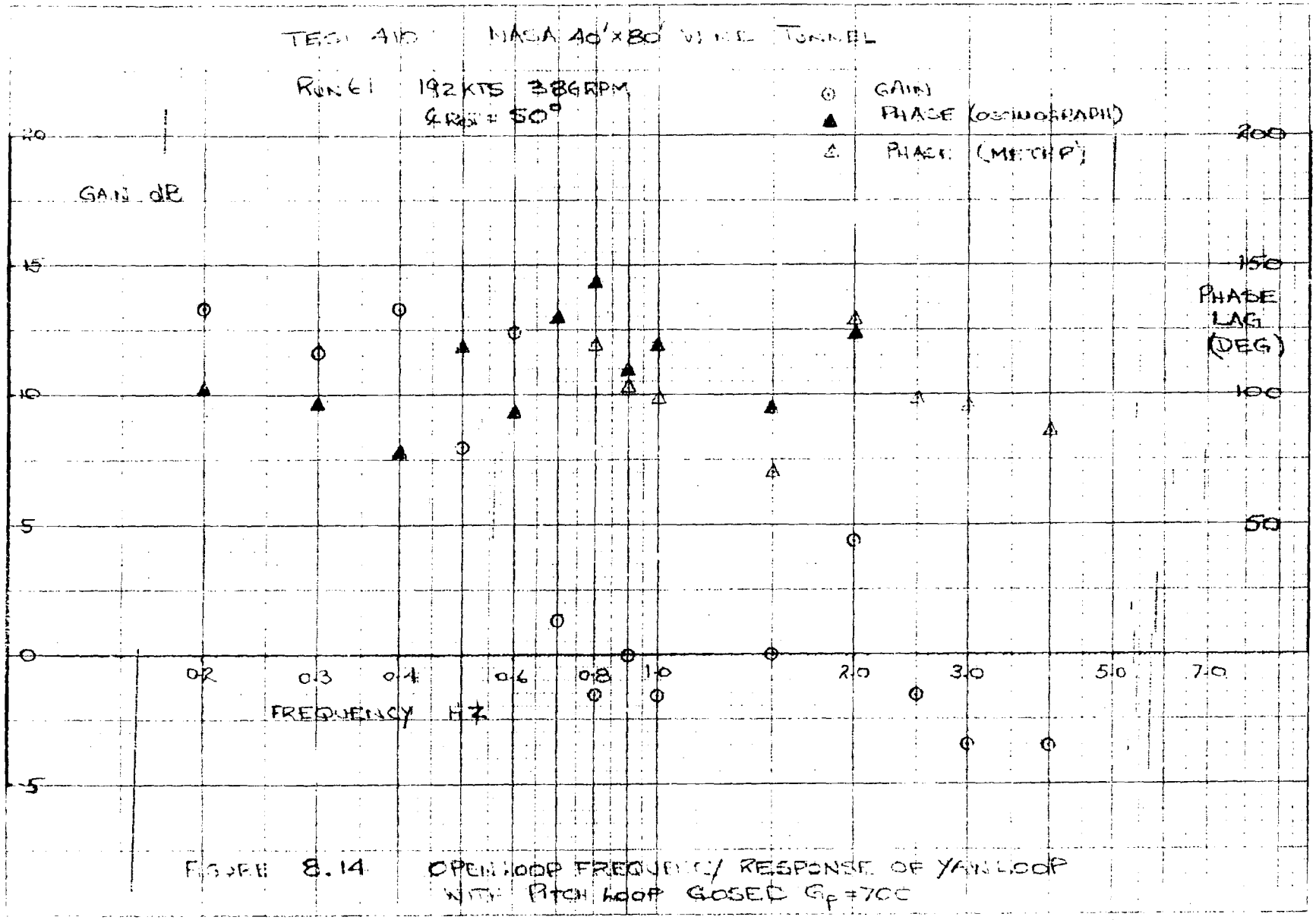

FIGURE 8.14 OPEN LOOP FREQUENCY RESPONSE OF YAW LOOP WITH PITCH LOOP CLOSED G_p = 700

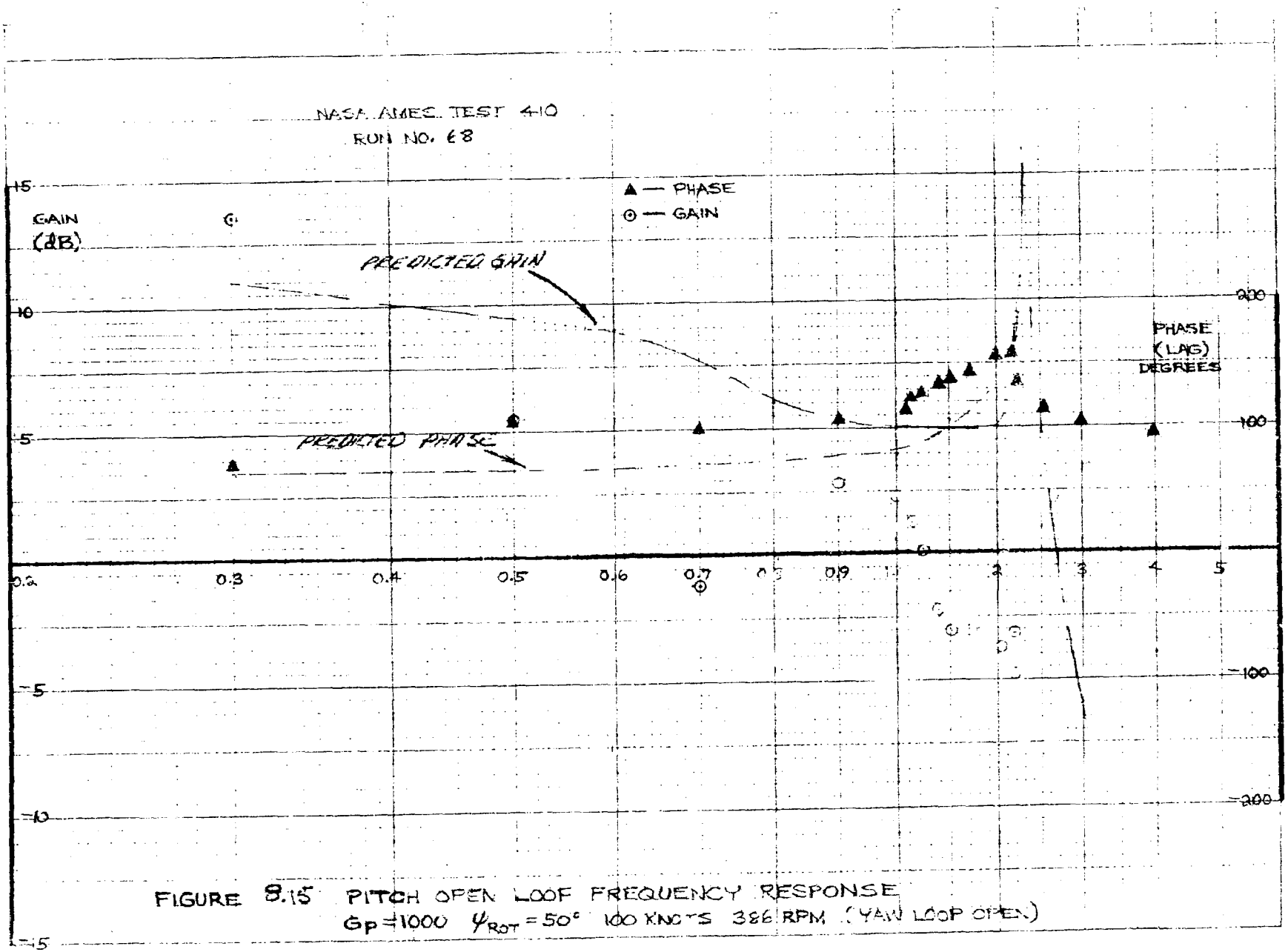

FIGURE 8.15 PITCH OPEN LOOP FREQUENCY RESPONSE
$G_P = 1000$ $\psi_{ROT} = 50°$ 100 KNOTS 386 RPM (YAW LOOP OPEN)

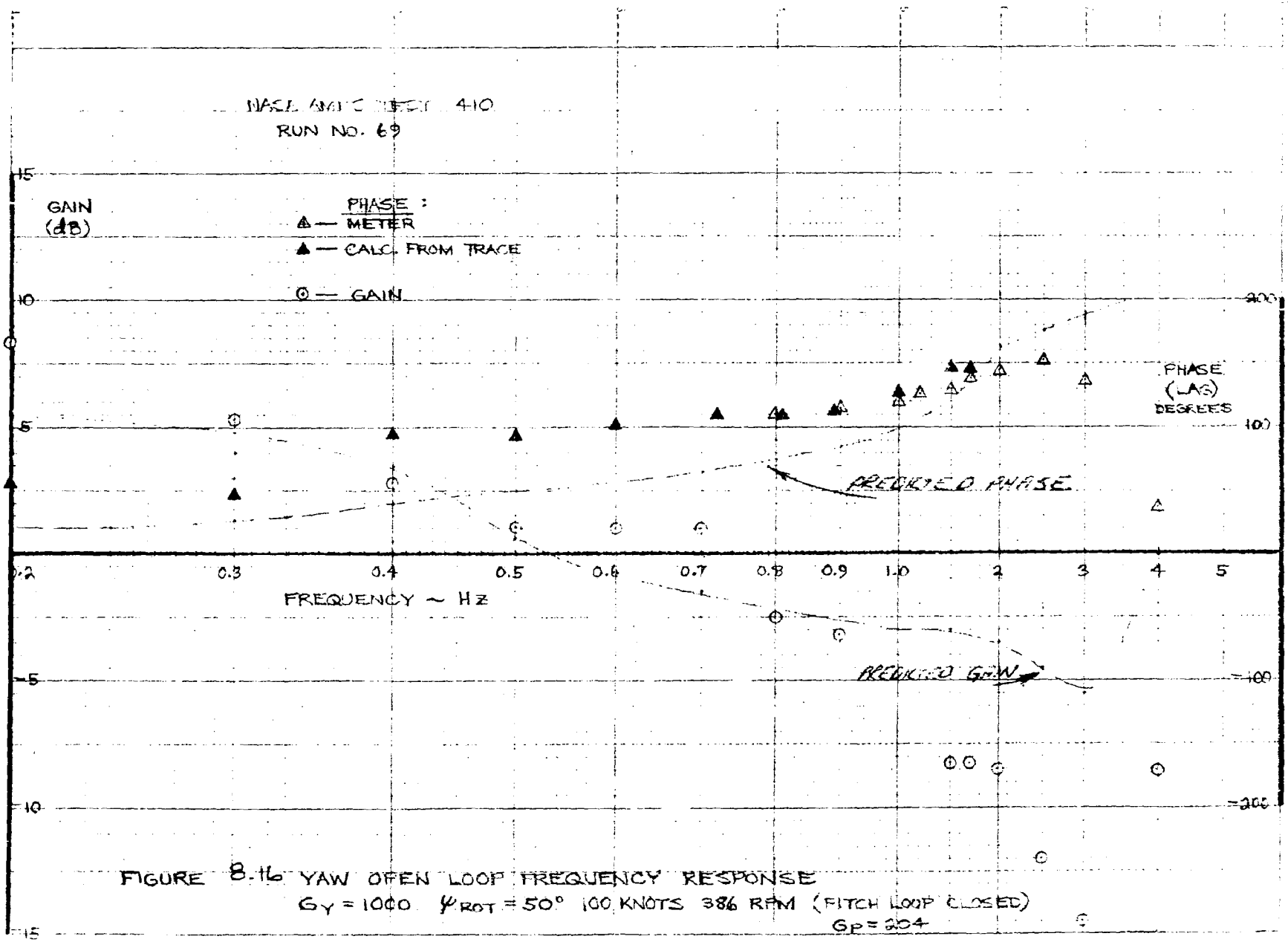

FIGURE 8.16 YAW OPEN LOOP FREQUENCY RESPONSE
$G_Y = 1000$ $\psi_{ROT} = 50°$ 100 KNOTS 386 RPM (PITCH LOOP CLOSED)
$G_P = 204$

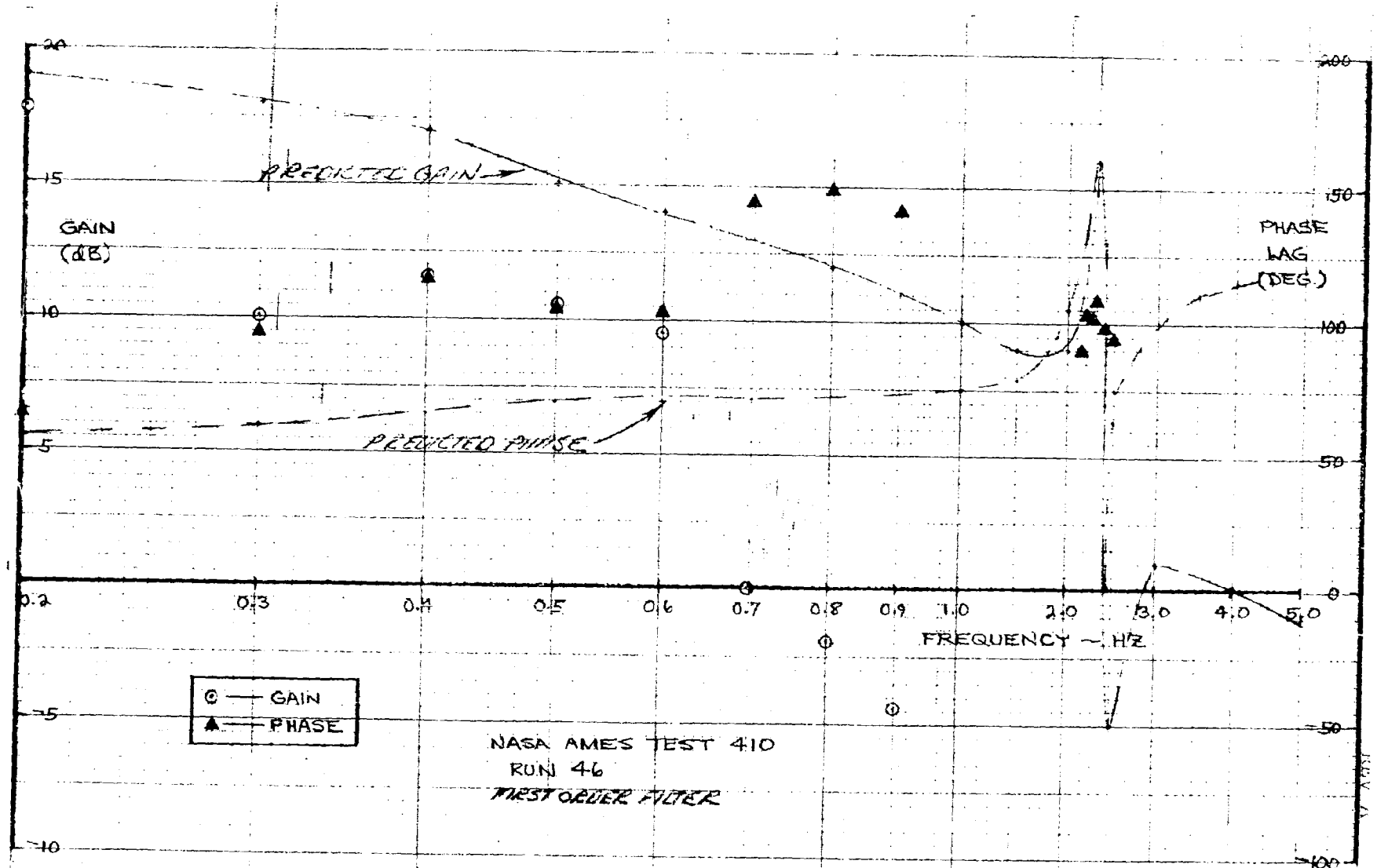

FIGURE 8.17 OPEN LOOP FREQUENCY RESPONSE PITCH LOOP (YAW LOOP OPEN)
100 KNOTS 386 RPM $\psi_{ROT} = 9.6°$

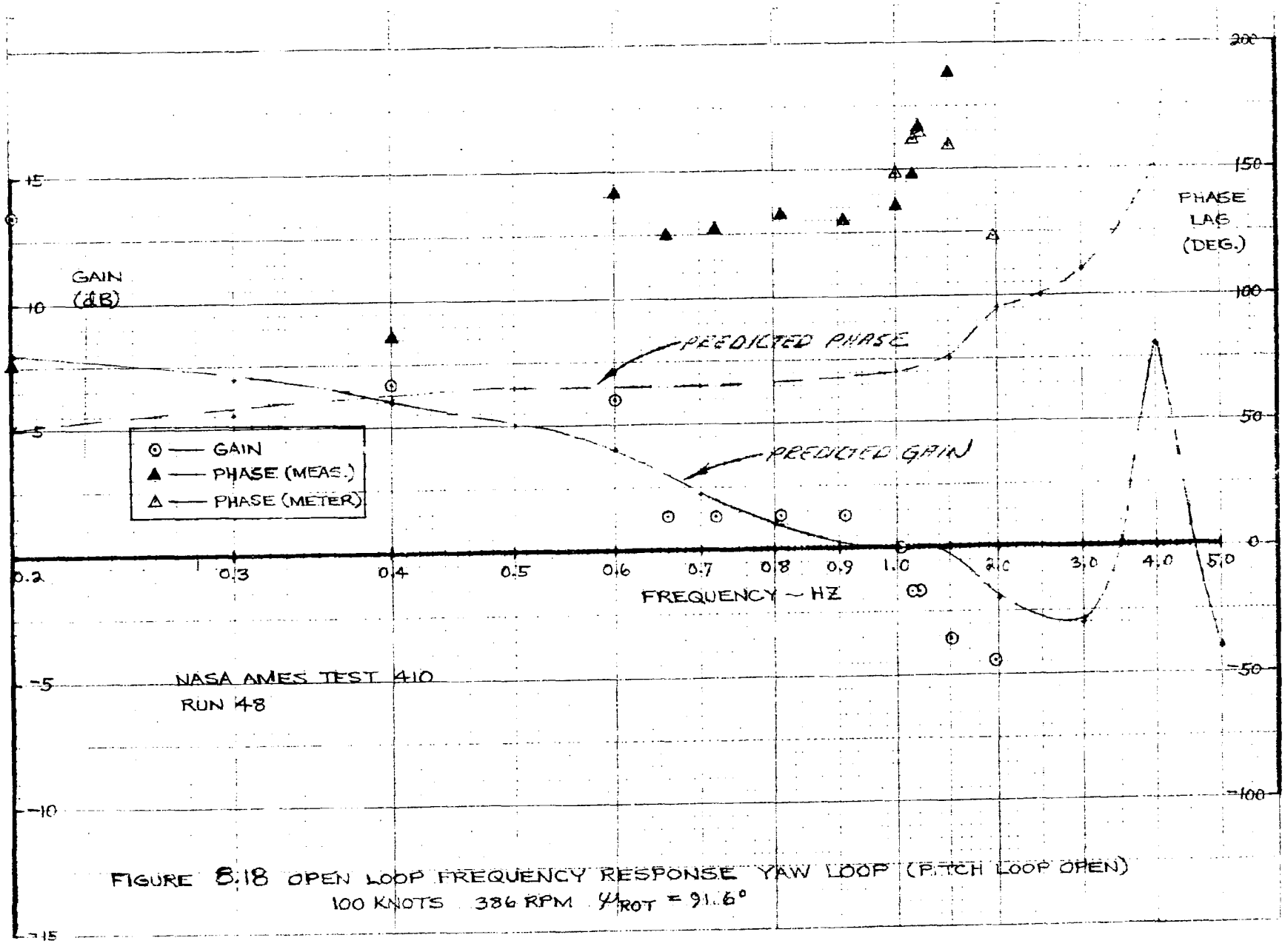

FIGURE 8.18 OPEN LOOP FREQUENCY RESPONSE YAW LOOP (PITCH LOOP OPEN)
100 KNOTS 386 RPM $\psi_{ROT} = 91.6°$

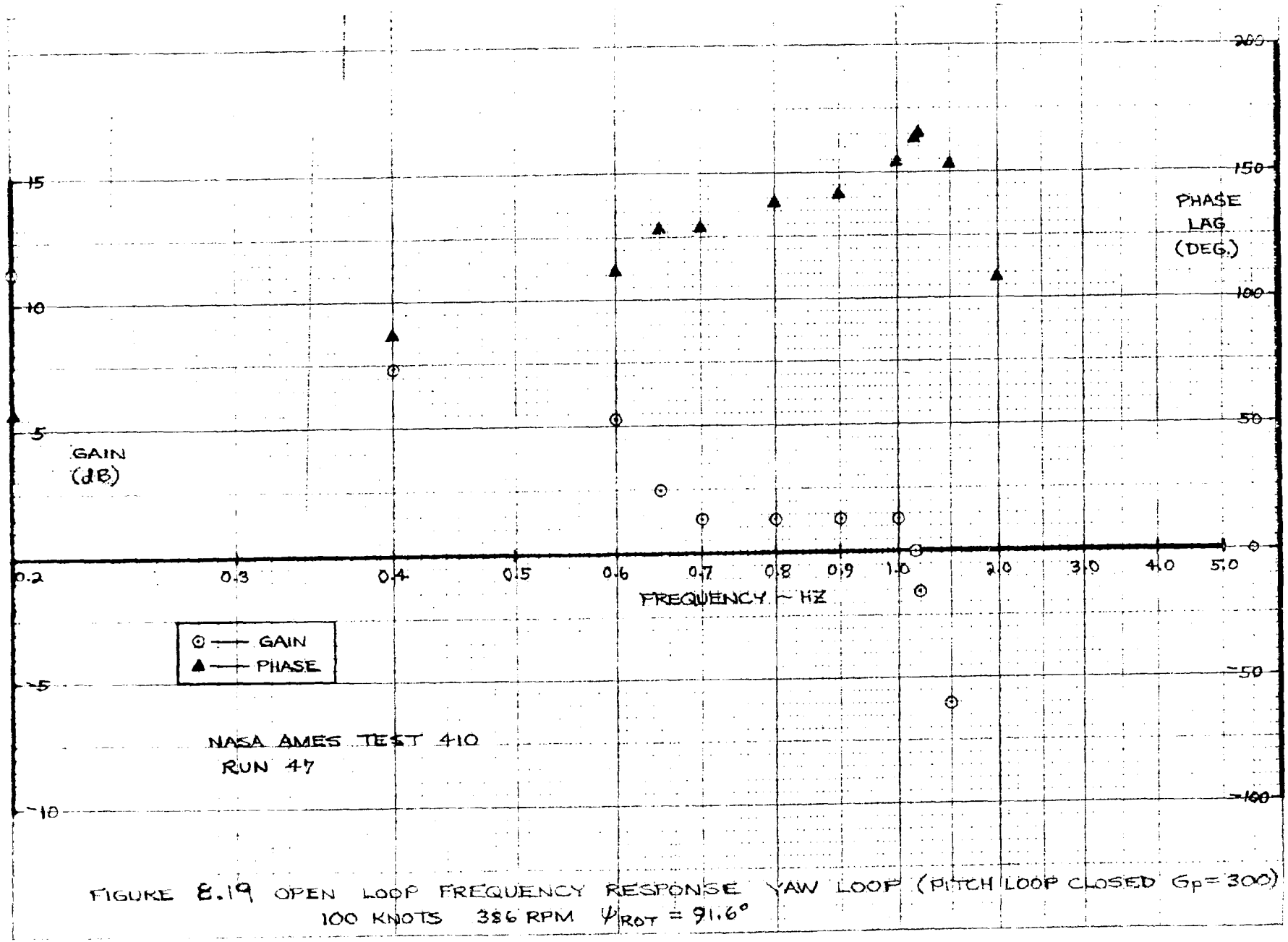

FIGURE 8.19 OPEN LOOP FREQUENCY RESPONSE YAW LOOP (PITCH LOOP CLOSED $G_p = 300$)
100 KNOTS 386 RPM $\psi_{ROT} = 91.6°$

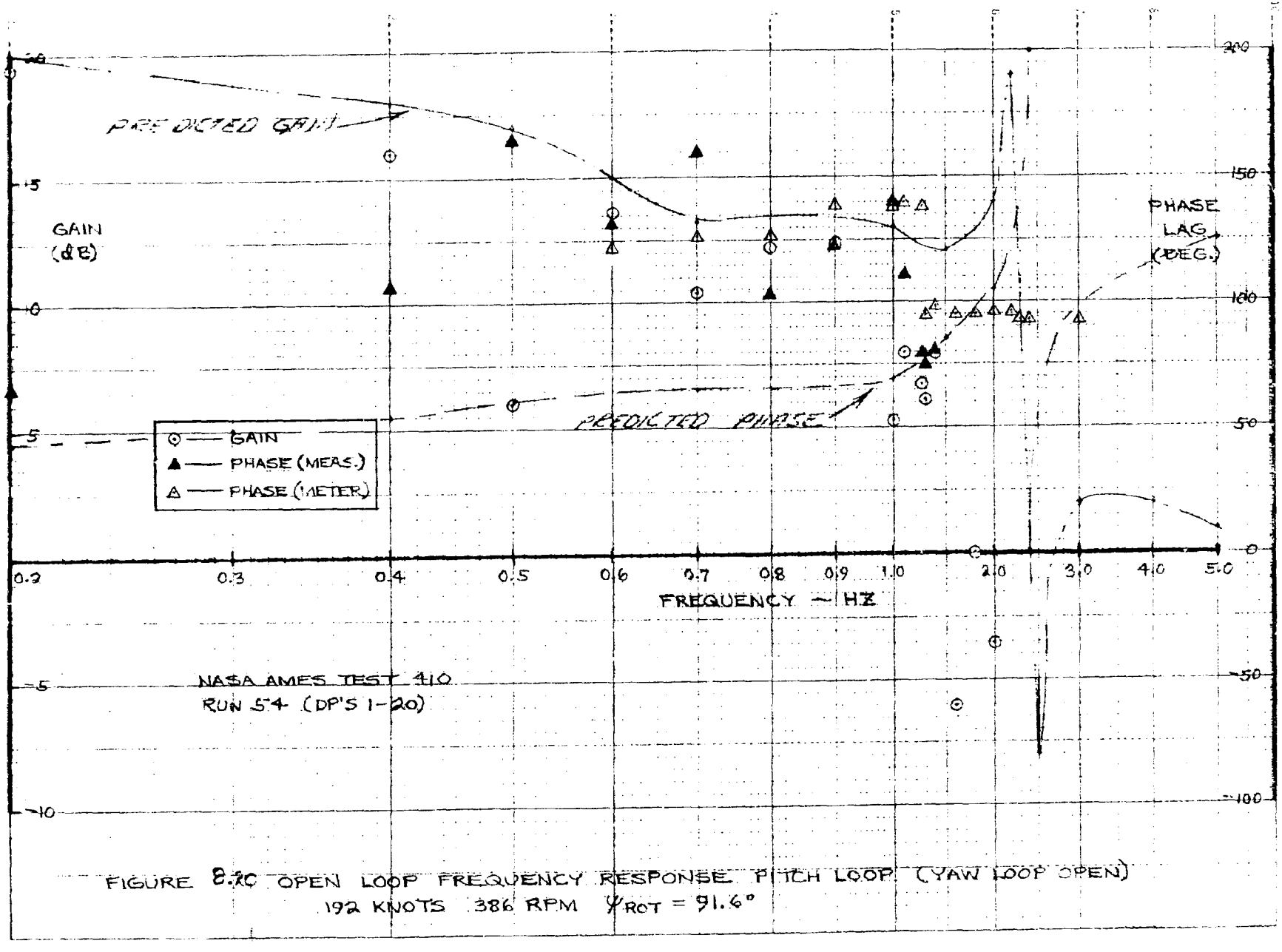

FIGURE 8.20 OPEN LOOP FREQUENCY RESPONSE PITCH LOOP (YAW LOOP OPEN)
192 KNOTS 386 RPM $\Psi_{ROT} = 91.6°$

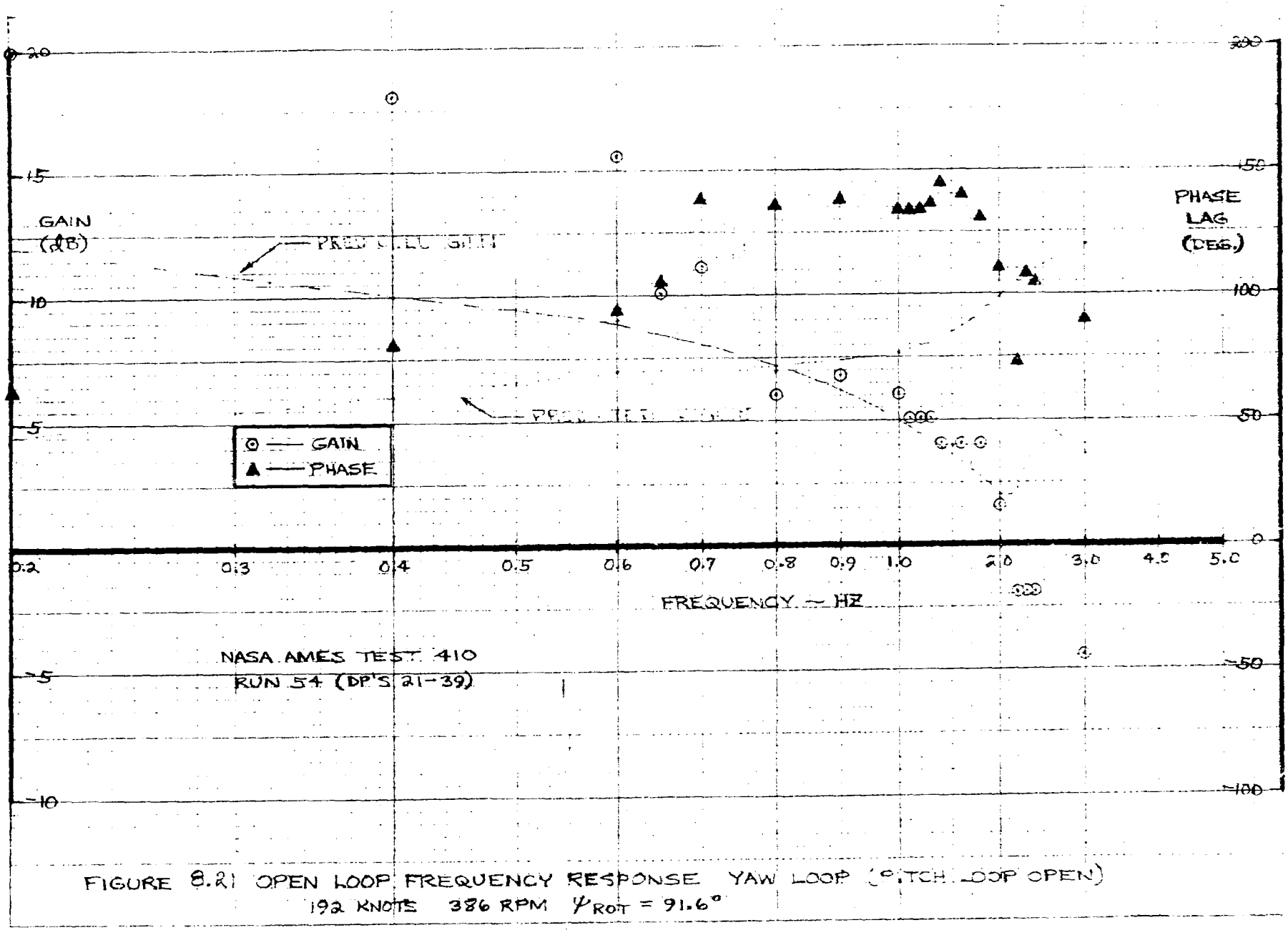

FIGURE 8.21 OPEN LOOP FREQUENCY RESPONSE YAW LOOP (PITCH LOOP OPEN)
192 KNOTS 386 RPM $\Psi_{ROT} = 91.6°$

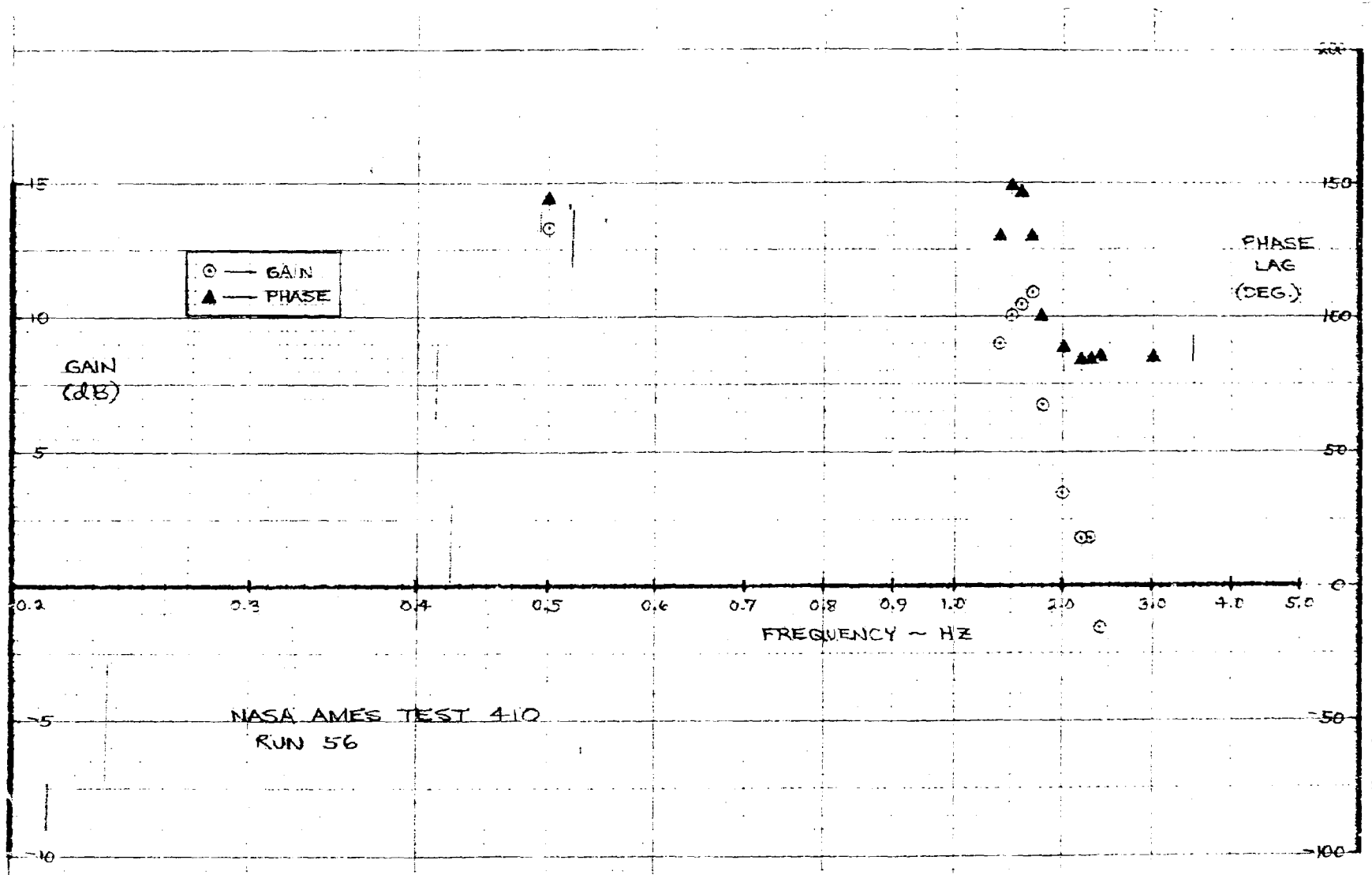

FIGURE E.22 OPEN LOOP FREQUENCY RESPONSE PITCH LOOP (YAW LOOP CLOSED G_Y = 700)
192 KNOTS 386 RPM ψ_{ROT} = 91.6°

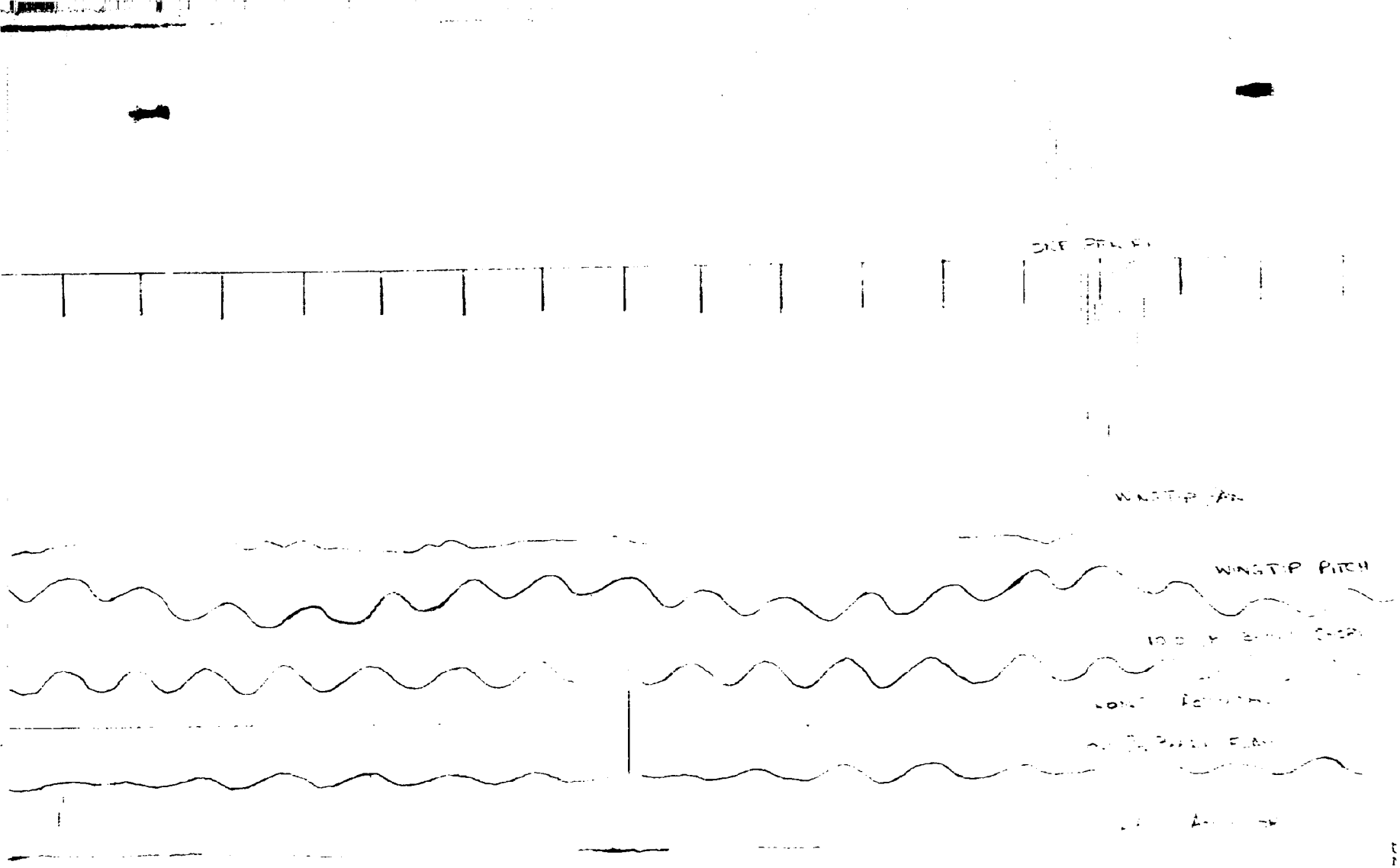

FIGURE 8.23 TRACE RECORD FOR 20 DEG TEST 410

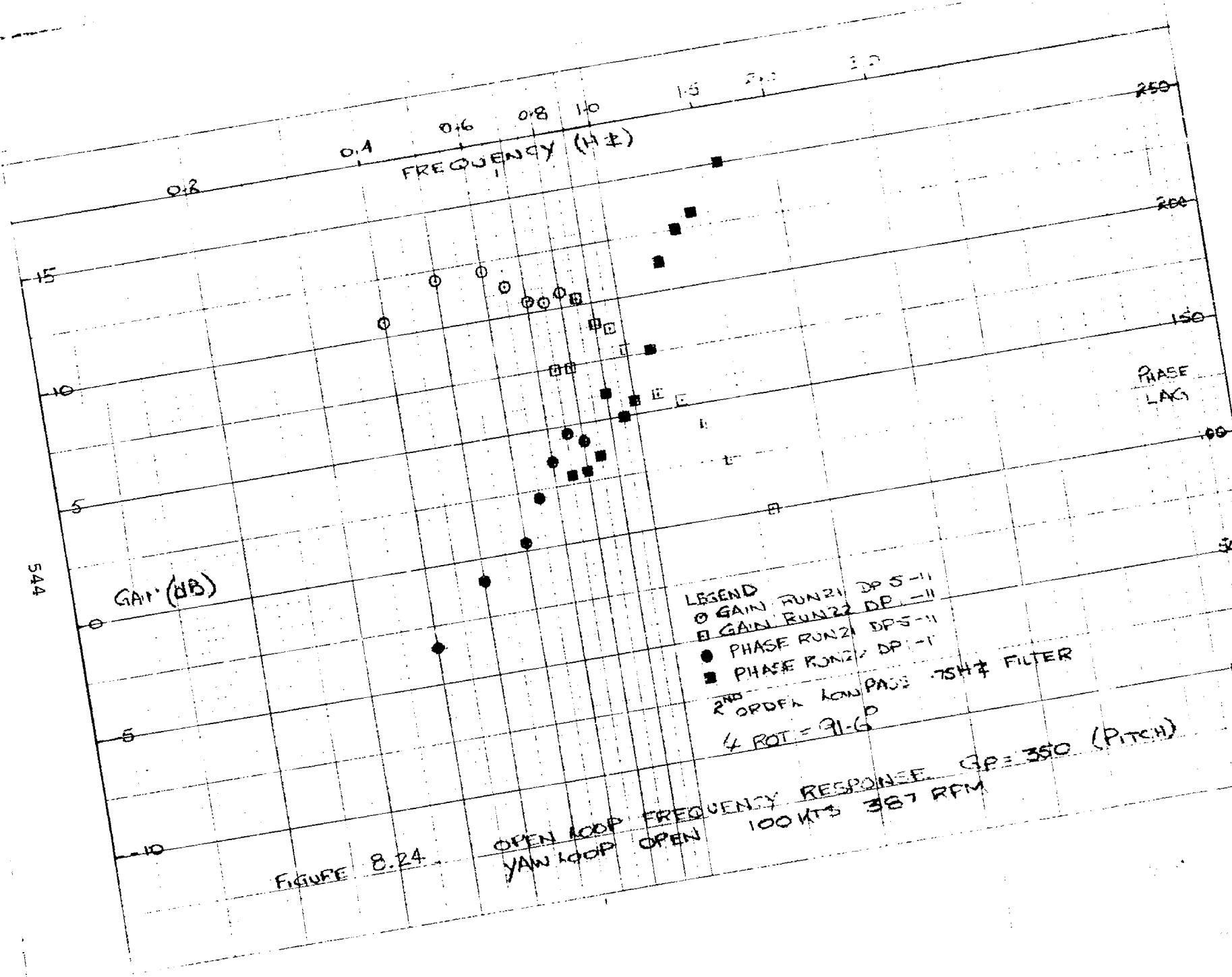

FIGURE 8.24 OPEN LOOP FREQUENCY RESPONSE GP = 350 (PITCH)
YAW LOOP OPEN 100 KTS 387 RPM

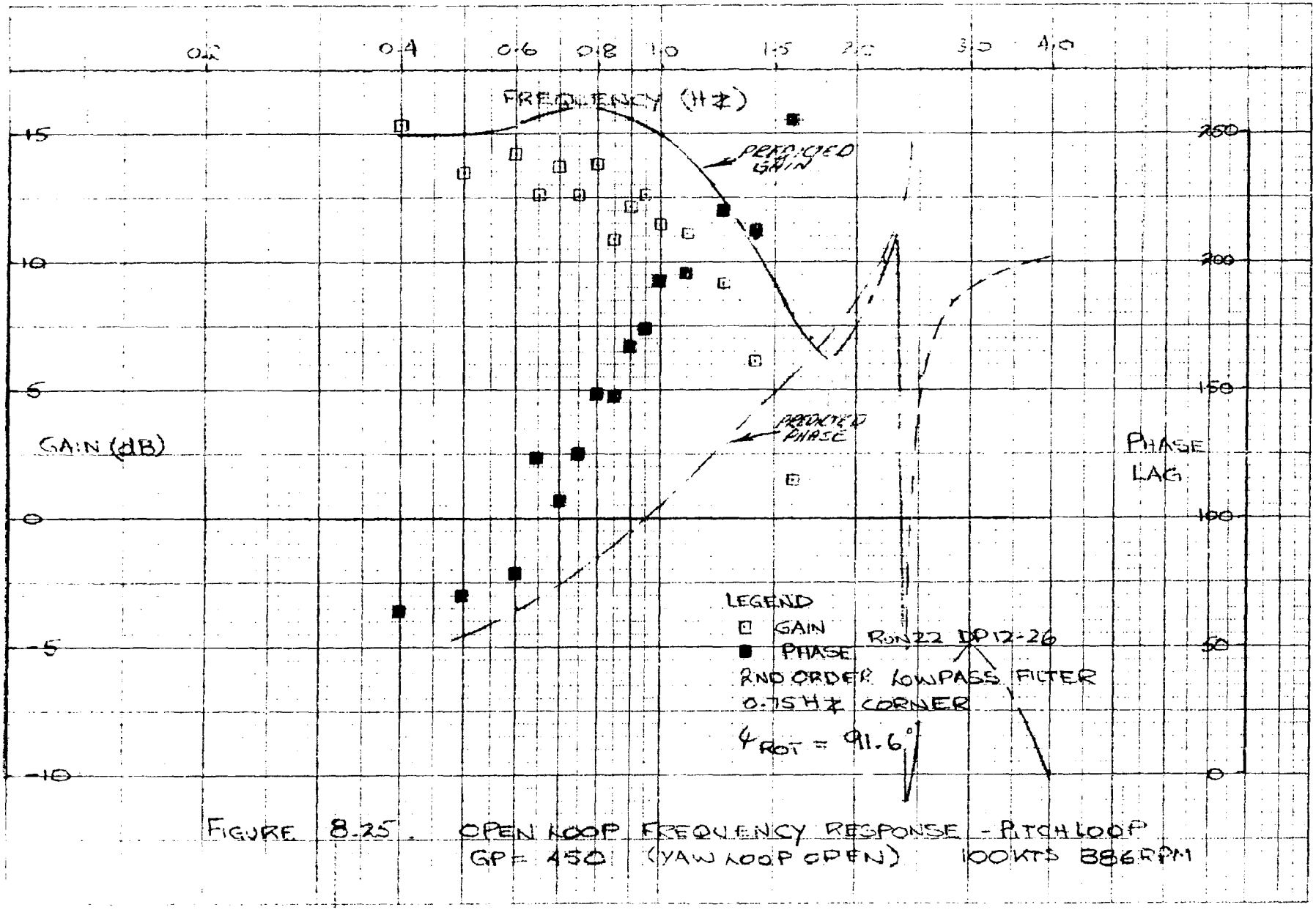

FIGURE 8-25. OPEN LOOP FREQUENCY RESPONSE - PITCH LOOP
GP = 450 (YAW LOOP OPEN) 100 KTS 386 RPM

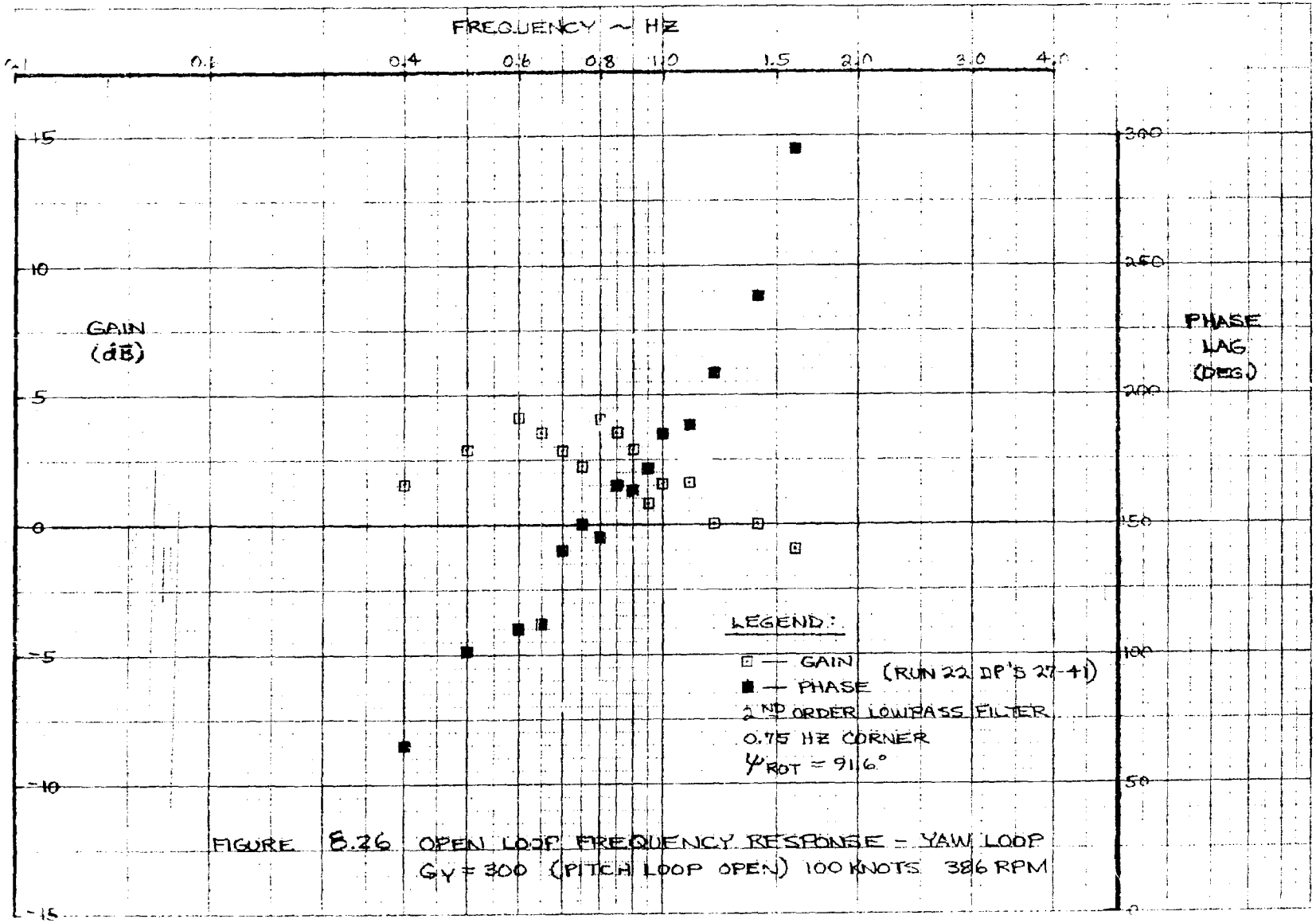

FIGURE 8.26 OPEN LOOP FREQUENCY RESPONSE - YAW LOOP
GY = 300 (PITCH LOOP OPEN) 100 KNOTS 386 RPM

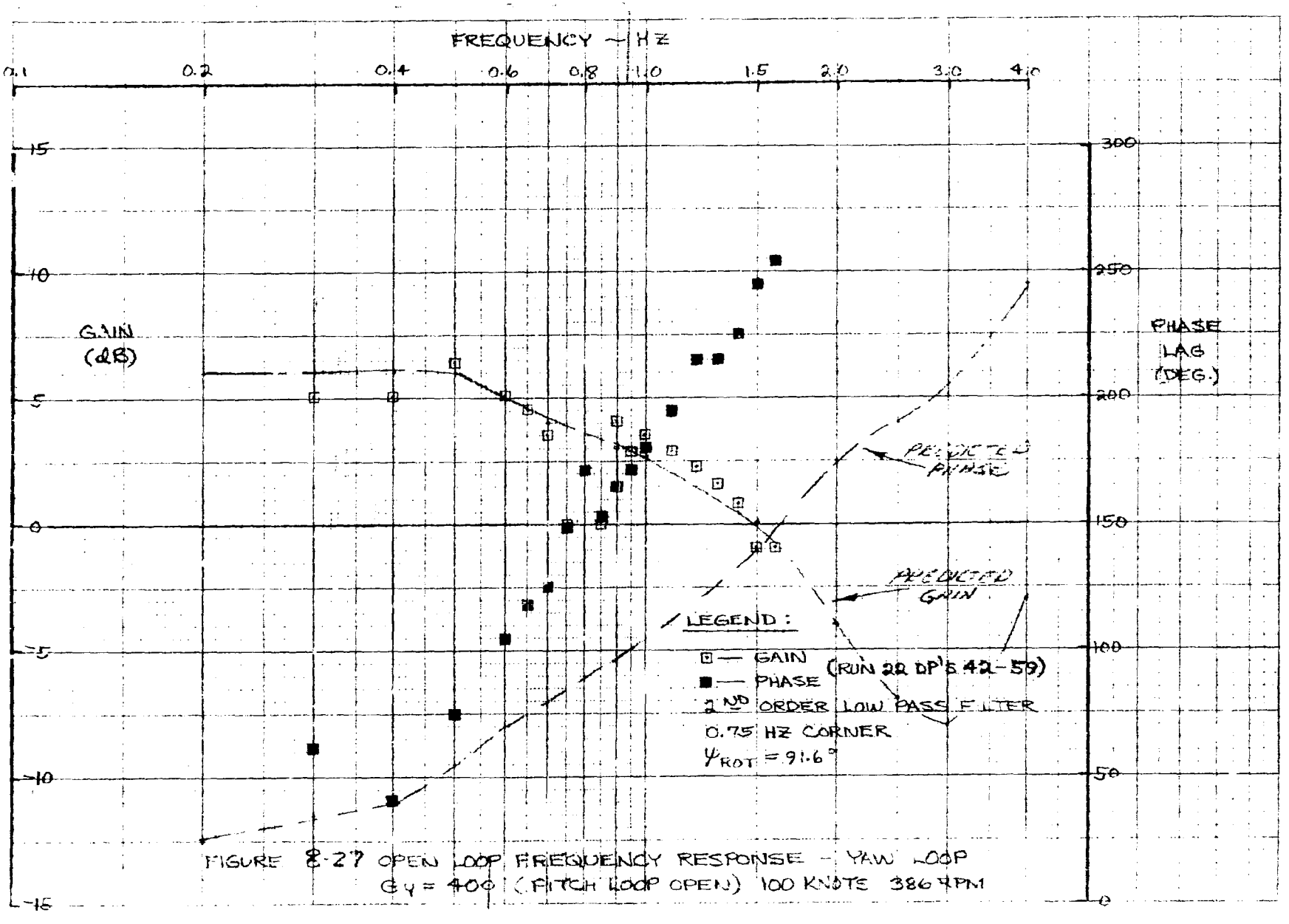

FIGURE 8-27 OPEN LOOP FREQUENCY RESPONSE - YAW LOOP
$G_Y = 400$ (PITCH LOOP OPEN) 100 KNOTS 386 RPM

Correlation With Rotor/Wing Frequency Response Date (Forward Loop)

An attempt was made to correlate with the response of the forward part of the loop; that is the response of the wing strain-gage outputs to harmonic forcing of the swashplate. It is of fundamental importance that this should be predictable; the characteristics of the other components of a feedback loop may be bench tested and calibrated. The behavior at 100 knots, 386 RPM was of interest because this speed exhibited an instability which had not been predicted. It was found that the test hardware open loop response had substantially greater lags than predicted and the issue was whether this was due to some unknown in the feedback system, or due to some inadequacy of the analysis. In order to resolve this the frequency response of the filter and actuator system was obtained by calibration. The response of the rotor-wing dynamic system can be obtained from the total loop Bode plots by subtracting the filter characteristics. Run 71 included a direct measurement of the forward loop response at 100 knots and ψ_{rot} = 50-degrees. The phase lags extracted from the Bode plots shown previously are given in Figures 8.28 and 8.29. At 192 knots the lag increases initially and then reduces again for both ψ_{rot} settings. At 100 knots the ψ_{rot} = 91.6-degrees data continues to increase the lag over the frequency range tested. Figure 8.30 shows the forward loop phase lags from Run 71 which agree with the data for ψ_{rot} = 50-degrees shown in Figure 8.29.

From these data it is concluded that information regarding the feedback part of the loop is correct and that the analysis underestimates the phase lags of the swashplate/rotor/wing system for this test condition.

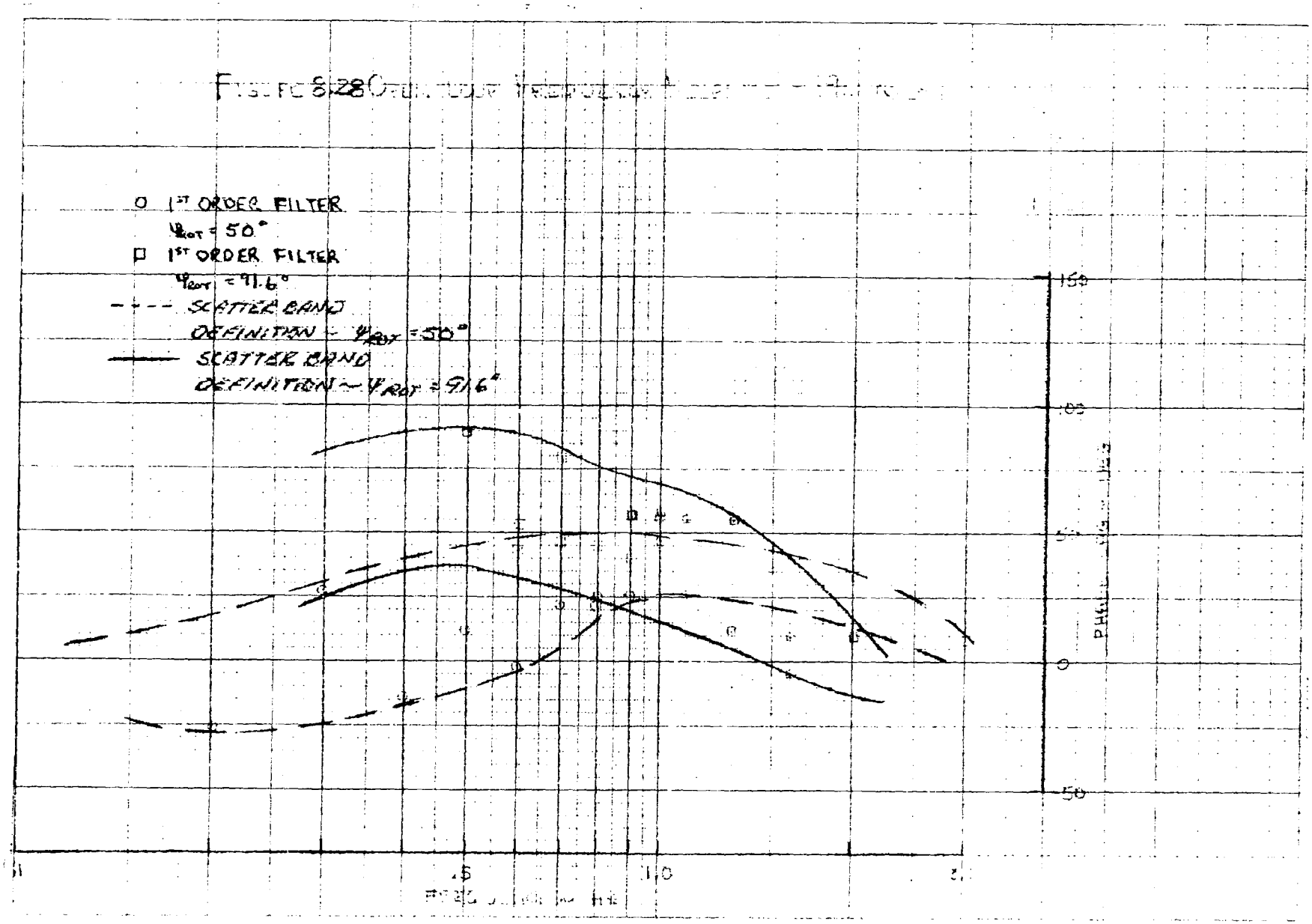
O 1ST ORDER FILTER
$\psi_{Rot} = 50°$
□ 1ST ORDER FILTER
$\psi_{Rot} = 91.6°$
- - - - SCATTER BAND DEFINITION – $\psi_{Rot} = 50°$
——— SCATTER BAND DEFINITION – $\psi_{Rot} = 91.6°$
150
100
50
0
-50
PHI
.5
1.0

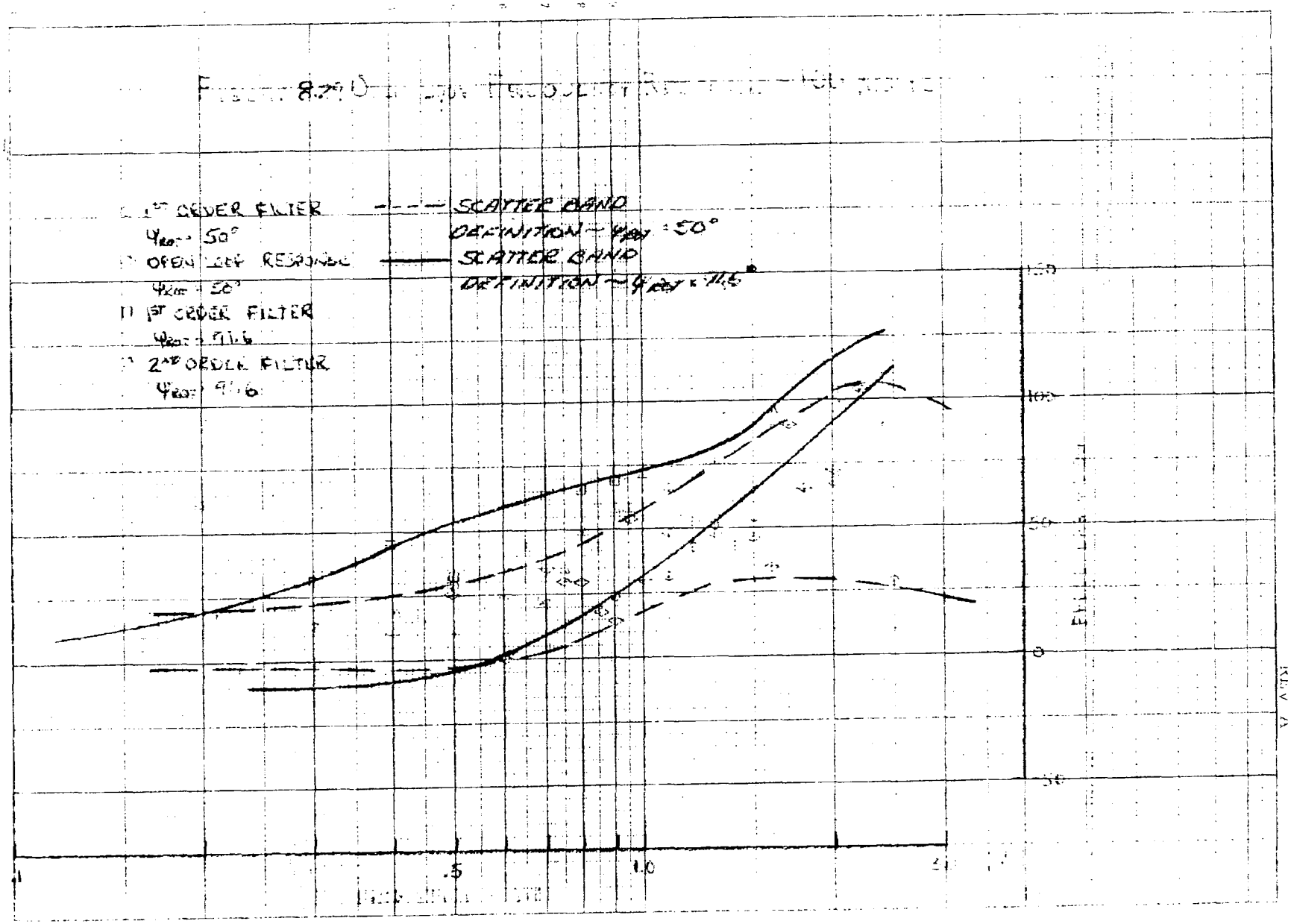
1ST ORDER FILTER
$\psi_{max} = 50°$
OPEN LOOP RESPONSE
$\psi_{max} = 50°$
1ST ORDER FILTER
$\psi_{max} = 11.6$
2ND ORDER FILTER
$\psi_{max} = 11.6$
SCATTER BAND
DEFINITION - $\psi_{max} = 50°$
SCATTER BAND
DEFINITION - $\psi_{max} = 11.6°$
.5
1.0

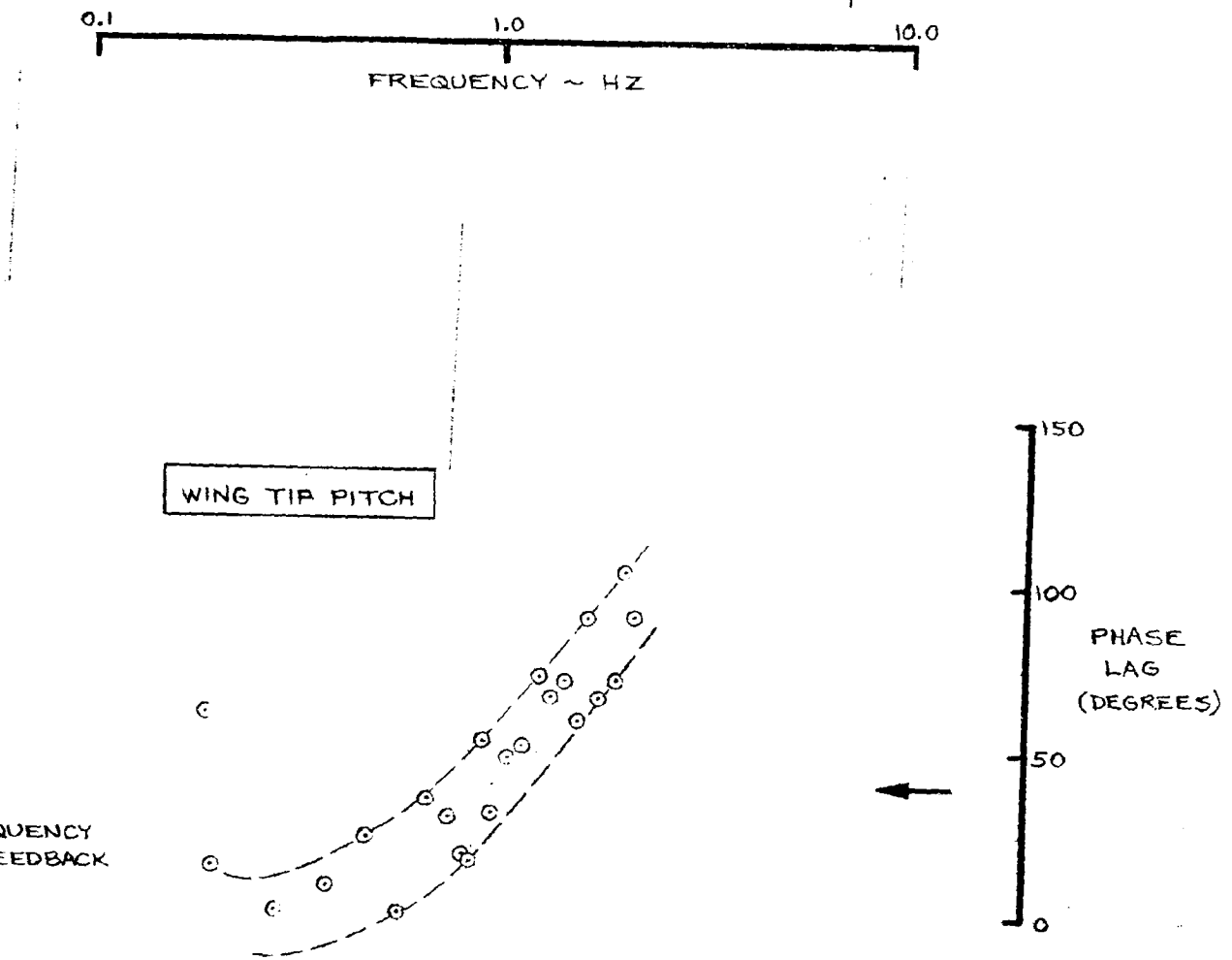

NOTES :

1. NASA TEST 410
   RUN 71
2. 386 RPM
   100 KNOTS
3. $\psi_{ROT.} = 50^{\circ}$
4. FORWARD LOOP FREQUENCY RESPONSE WITH NO FEEDBACK

FIGURE 8.30 FREQUENCY RESPONSE OF WING TORSION GAGE TO HARMONIC SWASHPLATE SHAKING

Low Rate Feedback Loop Performance

The feedback loop configuration with γ_{rot} = 50° and the 1st order filter was tested to determine the effect on wing moments and blade alternating loads due to angle of attack. Initially a matrix of pitch and yaw loop gains were run at 192 knots with a wing-rotor angle of attack of 3°. The pitch and yaw moments obtained are tabulated in Table 8.1. For this run (Run 62, Test 410) the dc level of the signals from the pitch and yaw gages were electrically adjusted to give approximately zero volts of feedback signal at zero angle of attack.

The steady wing tip pitch and yaw moments at zero incidence were negative moments as shown in Table 8.1 and also in Section 6. The strain gage bridge was offset to provide zero volts. The data presented in the table are real moments not the adjusted values sensed by the feedback loop. Thus as the pitch gain is increased the pitch moment is decreased towards zero feedback volts (i.e., -2382 ft lbs pitch).

Figures 8.31 and 8.32 are carpet plots of pitch and yaw moment derived from the data in Table 8.1. In Figure 8.31 the wing tip pitch moment is attenuated as G_p or G_y increases. The yaw moment shows large reductions due to increased yaw loop gain and a smaller effect due to the interaction of the pitch loop.

The alternating blade loads at 55%R measured on this run are tabulated in Table 8.2 and plotted in Figures 8.33 and 8.34. The alternating chord bending loads are an order of magnitude larger than the flap bending loads. Both alternating flap and chord bending reduce as the loop gains increase. The chord bending is very effectively reduced by pitch loop gain and shows the greatest reduction at $G_p = 300$. The magnitude of the alternating chord bending is about 40% of the zero gain case.

On-line a decision was made to explore the gains $G_p = 200$, $G_y = 300$ and $G_p = 400$, $G_y = 300$ further. Figures 8.35 and 8.36 show the steady wing tip moments due to angle of attack with and without low rate feedback ($G_l = 204$, $G_y = 300$) at 192 knots, 386 RPM. The yawing moment data show a significant reduction in angle of attack sensitivity around zero incidence, -630 ft lbs/° feedback on -1550 ft lbs/° feedback off. The change in slope of the yaw moment at about 1.6° is due to the saturation of the amplifier associated with the filter.

The wing tip pitch data also shows a reduction in angle of attack sensitivity prior to filter amplifier saturation, Figure 8.36, $\partial WTP/\partial \alpha$ = 970 ft lbs/° feedback on, $\partial WTP/\partial \alpha$ = 1570 ft lbs/° feedback off.

The alternating blade loads measured on this run are shown in Figures 8.37 and 8.38. The data indicate a reduction in alternating

blade stresses due to angle of attack.

Similar data for $G_p = 400$, $G_y = 300$ at 192 knots, 386 RPM, are shown in Figures 8.39 to 8.42. The wing tip pitch and yaw sensitivities are further reduced due to the increase in pitch loop gain. The angle of attack at which amplifier saturation occurs is increased due to the reduction in moments caused by the gain increase:

$\partial WTY/\partial \alpha$ = -550 ft lbs/° feedback on $G_p = 400$, $G_y = 300$

$\partial WTY/\partial \alpha$ = -1550 ft lbs/° feedback off

$\partial WTP/\partial \alpha$ = 720 ft lbs/° feedback on $G_p = 400$, $G_y = 300$

$\partial WTP/\partial \alpha$ = 1570 ft lbs/° feedback off

The alternating chord bending loads at 55%R, Figure 8.41, show a very low sensitivity to angle of attack prior to filter amplifier saturation and reduce slightly as angle of attack is increased. Above the angle of attack at which saturation occurred (about 3°) the loads increase at the same rate as the no feedback case. The alternating flap bending loads are smaller than the chord bending loads but are also reduced by the application of feedback, Figure 8.42.

The lower pitch loop gain case $G_p = 204$, $G_y = 300$ was also tested at 100 knots, 386 RPM and the data are shown in Figures 8.43 to 8.46. At 100 knots the data indicate:

- ∂ WTP/$\partial\alpha$ = 320 ft lbs/° feedback on
- ∂ WTP/$\partial\alpha$ = [illegible] ft lbs/° feedback off
- ∂ WTY/$\partial\alpha$ = -350 ft lbs/° feedback on
- ∂ WTY/$\partial\alpha$ = -330 ft lbs/° feedback off

At this tunnel speed the alternating flap bending loads (55%R) are low and there is no significant effect due to feedback, Figure 8.45. The predominant blade load is alternating chord bending shown in Figure 8.46 and in this case the loads are reduced as was observed at 192 knots.

The test successfully demonstrated that substantial reduction in both blade loads and wing tip moments can be provided by the feedback system. The effectiveness of the system as tested was limited by the early saturation of the filter amplifier used.

TABLE 8-1

NASA AMES TEST 410
26FT. DIA. ROTOR TEST, FULL STIFF WING
V=192 KNOTS, Ω=386 RPM, α=3.0 DEGREES
RUN 62 : PITCH AND YAW LOAD ALLEVIATION LOOPS CLOSED

•WHEN α=0 DEGREES
WING TIP PITCH =-2382
WING TIP YAW =-1962

• AT α=0 DEGREES
FEEDBACK LOOP VOLTAGES
ADJUSTED TO THE EQUIVALENT
OF 0 FT-LBS PITCH AND 0 FT-LBS YAW
• FEEDBACK SIGNALS BASED ON PITCH AND YAW MOMENTS PLUS D.C. ADJUSTMENT
ΔPITCH =+2382 FT-LBS
ΔYAW =+1962 FT-LBS

G_y \ G_p	0	100	200	300	400	500	600	700	800	900	1000
0	1557 / -6044		229 / -5083		-641 / -4633		-1145 / -4037		-1466 / -4025		-1741 / -4307
100	2061 / -5537	1832 / -5622	412 / -4756	92 / -4329	-458 / -3974	-916 / -3913	-1099 / -3997	-1283 / -3935	-1466 / -3581	-1833 / -3154	-2061 / -3199
200	3252 / -4795	2886 / -4272	1283 / -3749	92 / -3738	-412 / -3288	-779 / -3496	-916 / -2973	-1695 / -3108	-1924 / -2219	-1695 / -1988	-1970 / -2237
300	3619 / -4192	2519 / -3911	1649 / -3703		-275 / -2629	-870 / -2786	-779 / -2286	-1191 / -2370	-1191 / -2236	-1924 / -2832	-2153 / -2404
400	4214 / -3669	3665 / -3804	1970 / -3354	870 / -3050	-321 / -2381	-181 / -2516	-1054 / -2358	-1695 / -1981			-1878 / -2069
500	4397 / -3426	3939 / -2926	2199 / -2864	779 / -2363	-137 / -2375	-595 / -2240	-1008 / -1959	-1557 / -1824			

STEADY WING TIP PITCHING AND YAWING MOMENTS - FT-LBS

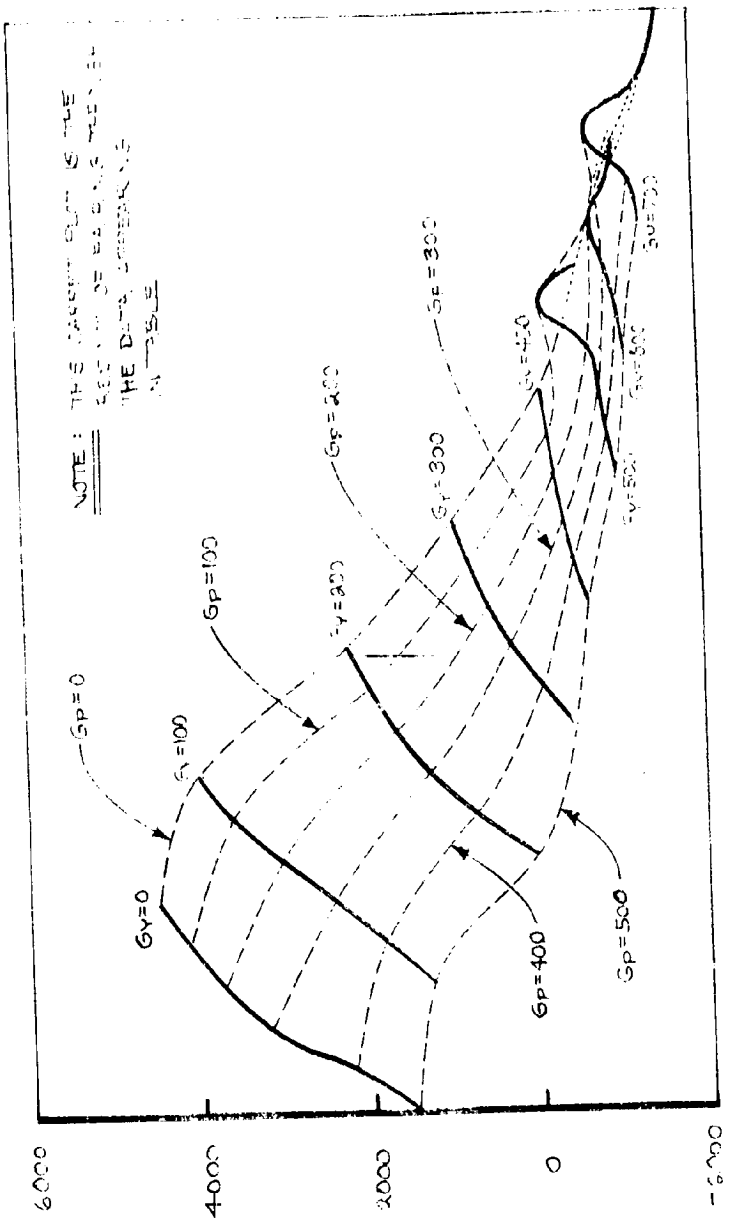

FIGURE 8-31 EFFECT OF LOAD ALLEVIATION SYSTEM GAIN ON WING TIP PITCHING MOMENT — V = 192 KNOTS, α = 3 DEGREES

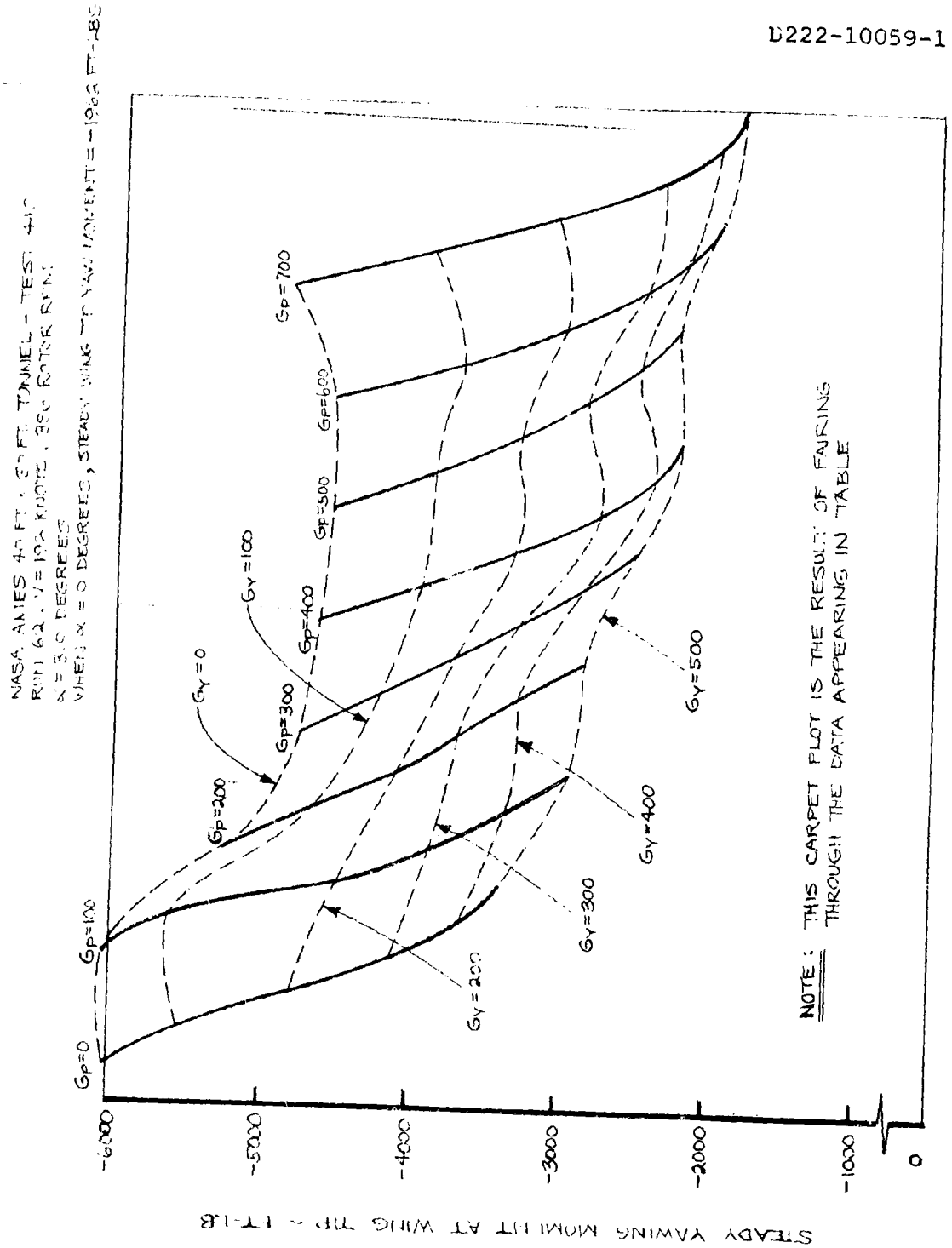

FIGURE 9.32 EFFECT OF LOAD ALLEVIATION SYSTEM GAIN ON WING TIP YAWING MOMENT - V = 192 KNOTS, α = 3 DEGREES

TABLE 8-2

NASA AMES 40 FT. x 80 FT. TUNNEL - TEST 410

26 FT. DIA. ROTOR TEST

FULL STIFF WING

V=192 KNOTS, Ω=386 RPM, α=3.0 DEGREES

RUN 62. PITCH AND YAW LOAD ALLEVIATION LOOPS CLOSED

55% FLAP AND CHORD BENDING MOMENTS (PEAK TO PEAK - IN-LBS)

G_y \ G_p	0	100	200	300	400	500	600	700	800	900	1000
0	1916 / 17593		1916 / 9969		1916 / 11729		1757 / 11729		2236 / 14075		1916 / 15247
100	1916 / 17593	1916 / 14661	1916 / 12315	1916 / 11436	1916 / 12608	1757 / 10556	1916 / 12315	1916 / 12902	1916 / 13488	1757 / 13195	1916 / 14075
200	1916 / 16714	1916 / 14954	1916 / 9969	1597 / 7917	1437 / 8503	1597 / 9090	1916 / 10550	2076 / 12315	1757 / 10556	1916 / 12315	1916 / 13488
300	1916 / 15834	1916 / 15541	1916 / 9383	1597 / 7917	1757 / 7624	1437 / 8210	1757 / 9969	1757 / 9383	1597 / 12315	1597 / 12902	1916 / 12902
400	2236 / 18766	1916 / 16420	1916 / 11729	1916 / 9090	1916 / 8210	1916 / 8210	1437 / 9969	1757 / 11142			1916 / 13195
500	1916 / 17593	1597 / 16420	1437 / 9383	958 / 7037	1437 / 8210	1278 / 8210	1916 / 10263	1757 / 11142			

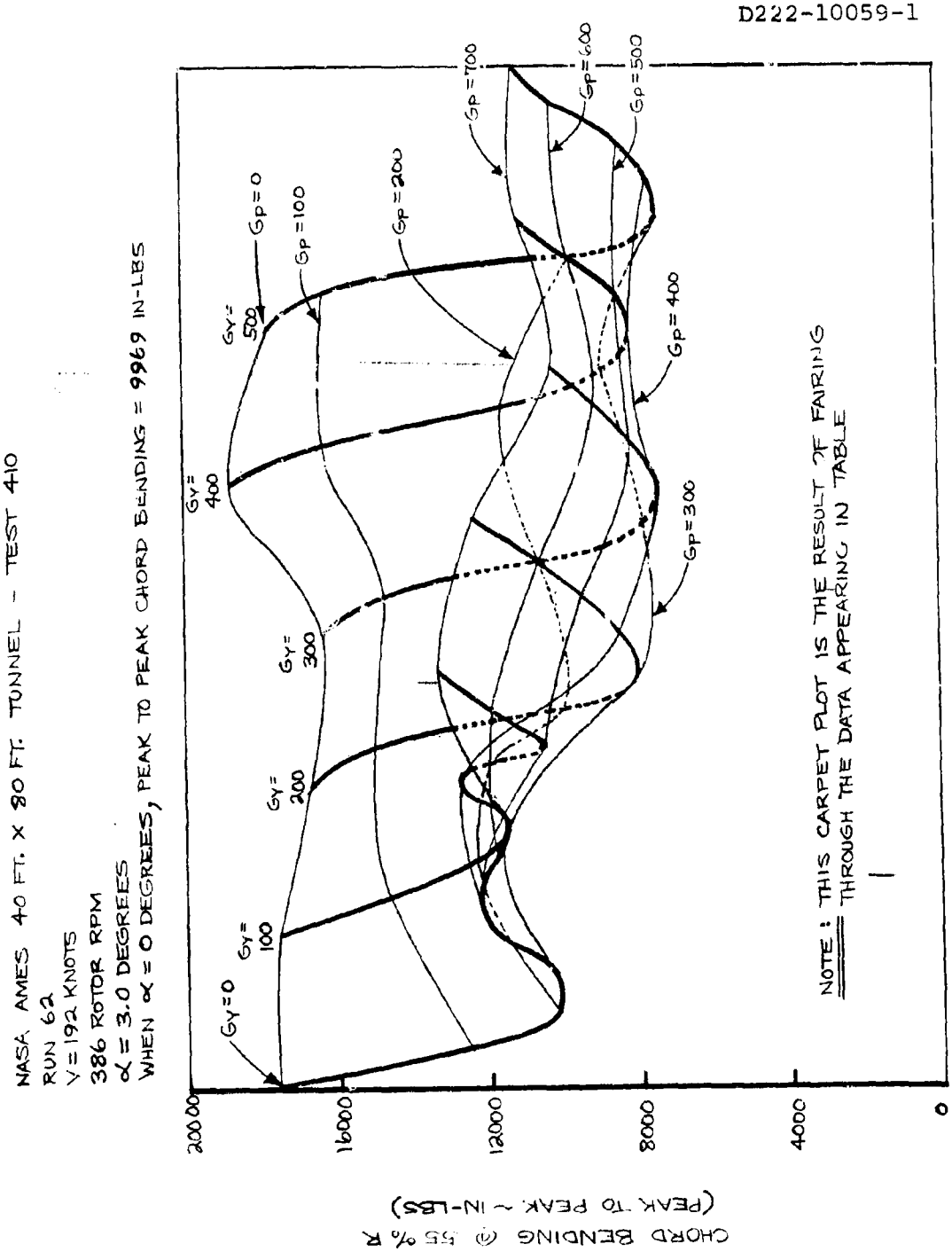

FIGURE 8.33 EFFECT OF LOAD ALLEVIATION SYSTEM GAIN ON 55% R BLADE CHORD BENDING – V = 192 KNOTS, α = 3 DEGREES

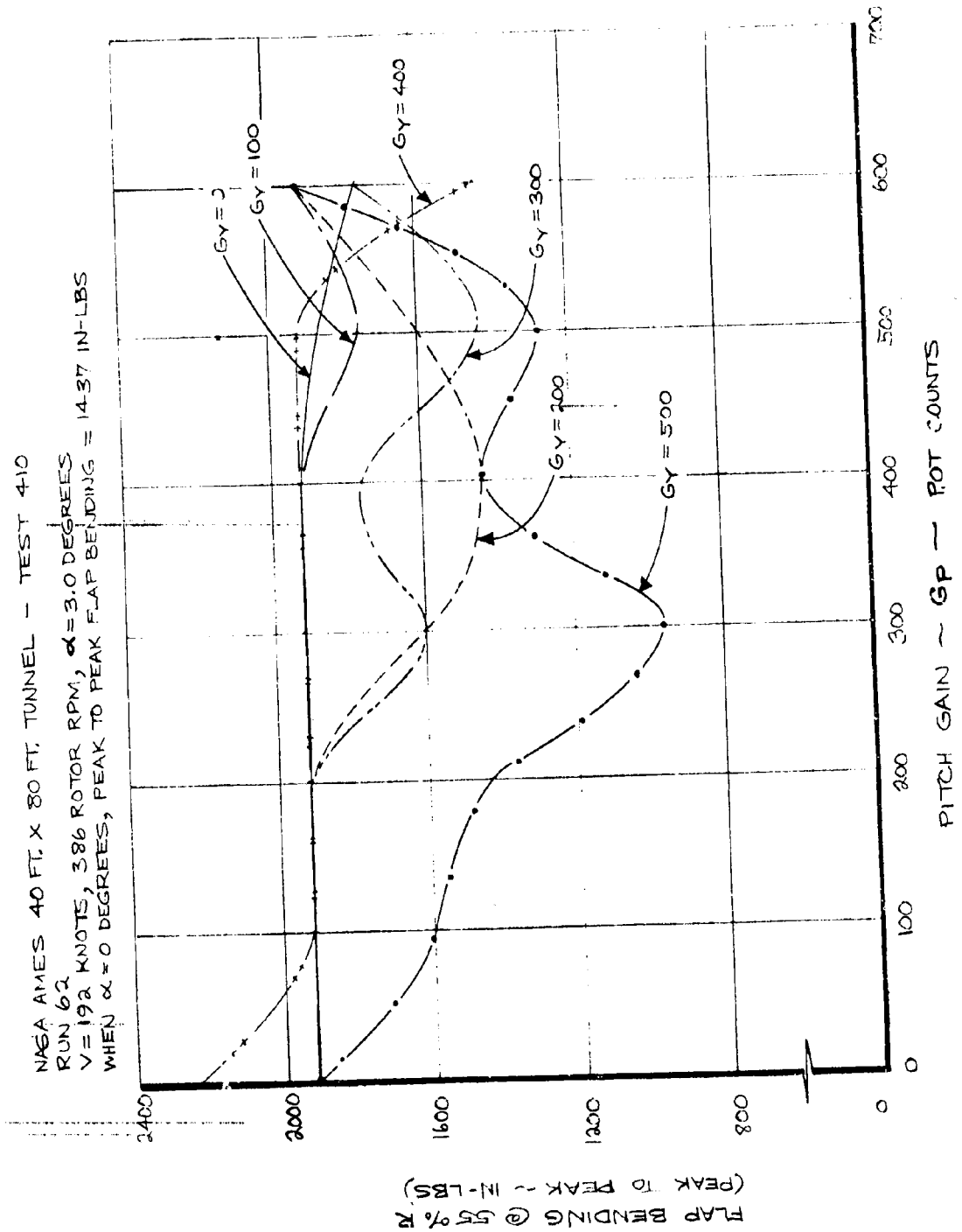

FIGURE 2-4 EFFECT OF LOAD ALLEVIATION SYSTEM GAIN ON 55 %R BLADE FLAP BENDING - V = 192 KNOTS, α = 3 DEGREES

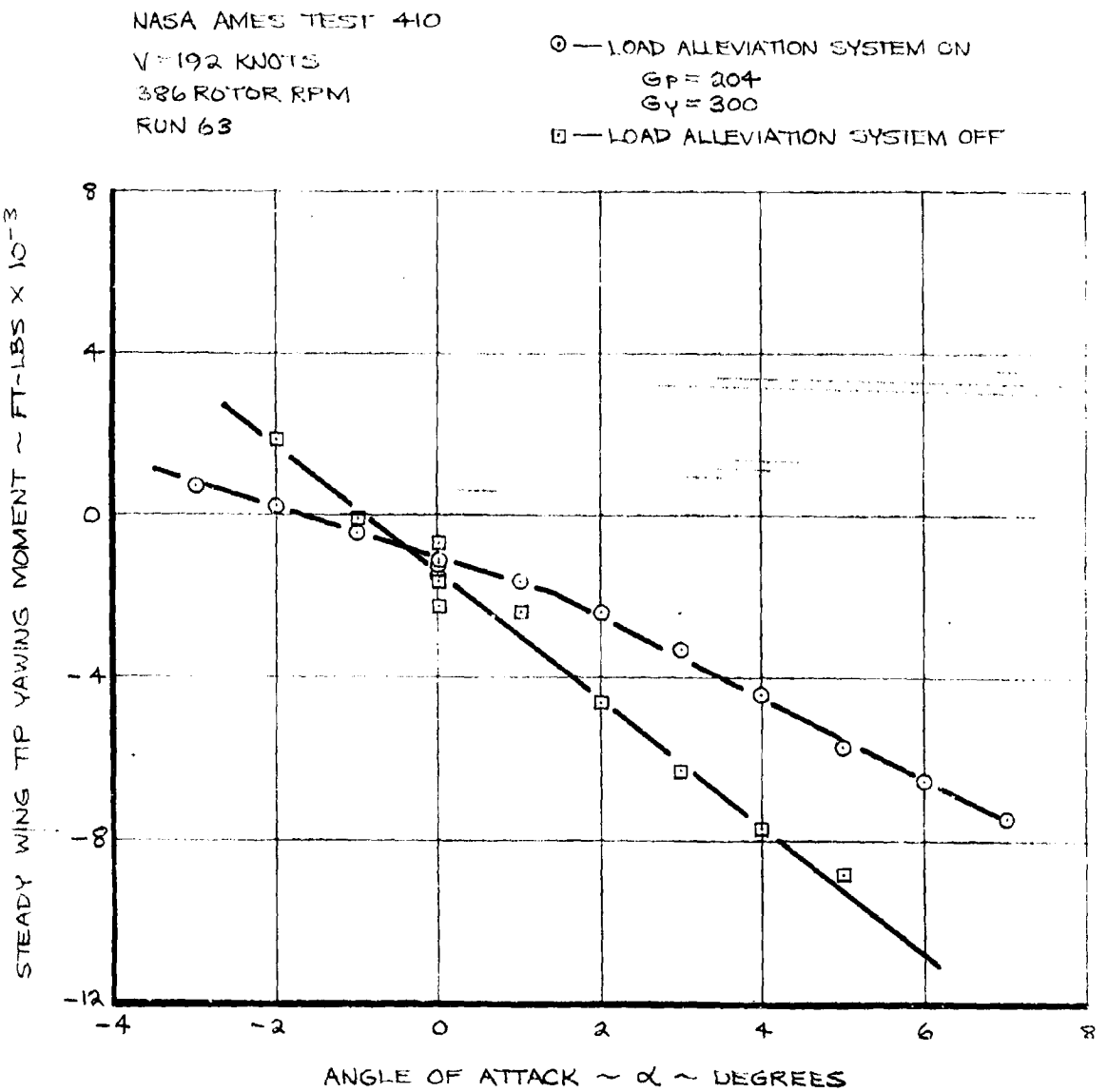

FIGURE 8.55 EFFECT OF LOAD ALLEVIATION SYSTEM ON WING TIP YAWING MOMENT — V = 192 KNOTS, Gp = 204, Gy = 300

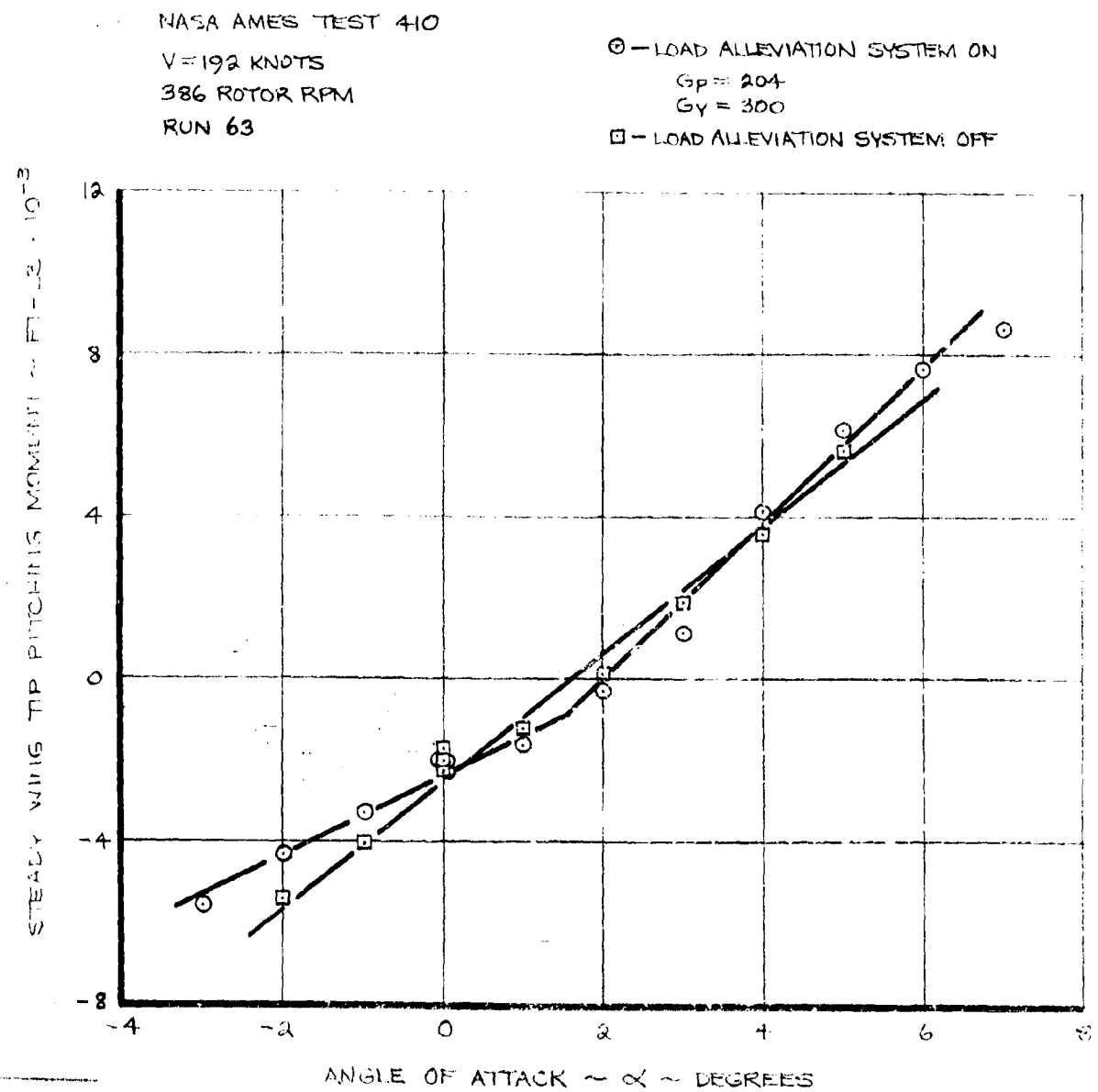

FIGURE 8-36 EFFECT OF LOAD ALLEVIATION SYSTEM ON WING TIP PITCHING MOMENT – V=192 KNOTS, Gp=204, Gy=300

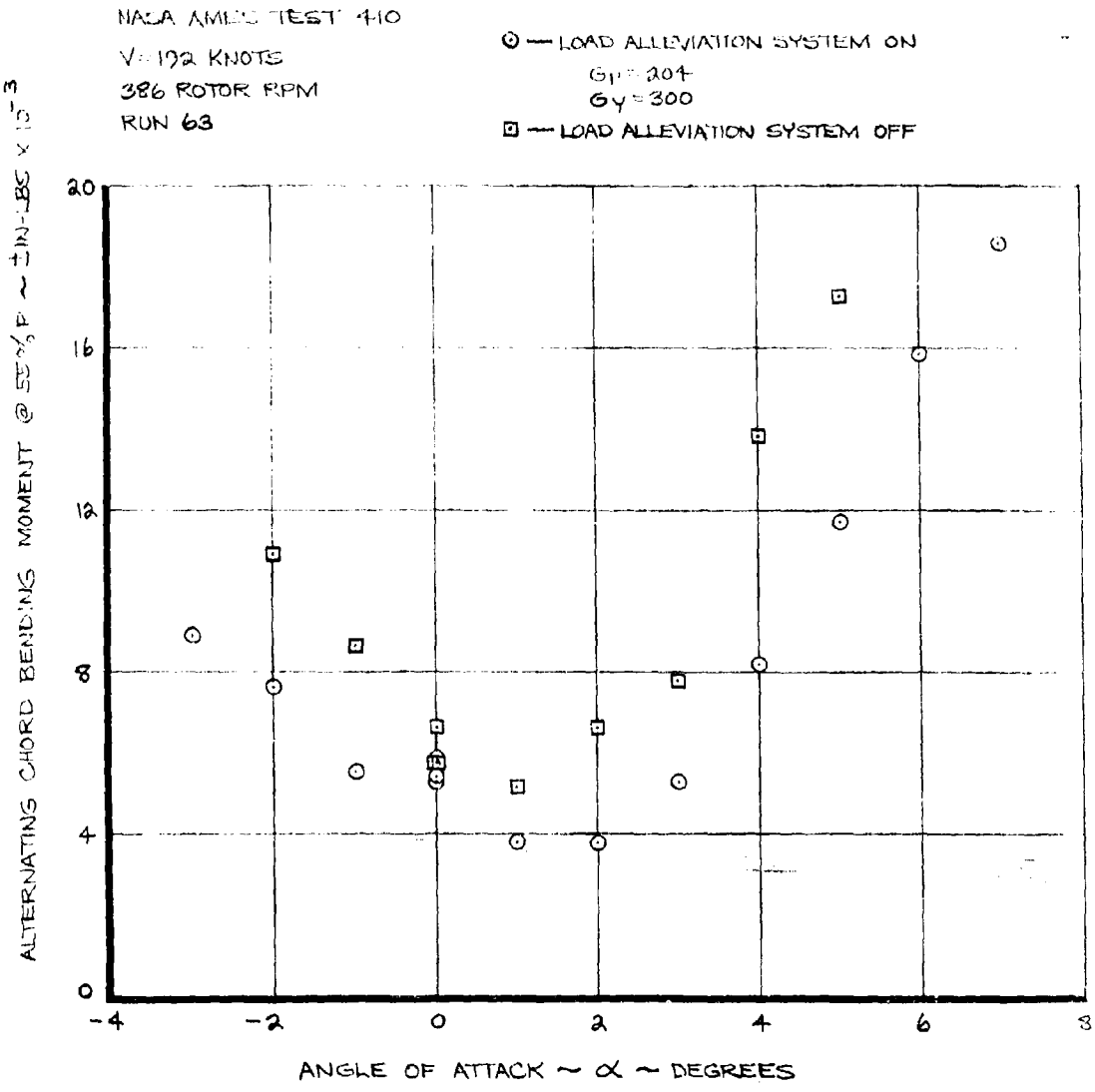

FIGURE B.27 EFFECT OF LOAD ALLEVIATION SYSTEM ON 55% R BLADE CHORD BENDING MOMENT - V = 192 KNOTS, G_p = 204, G_Y = 300

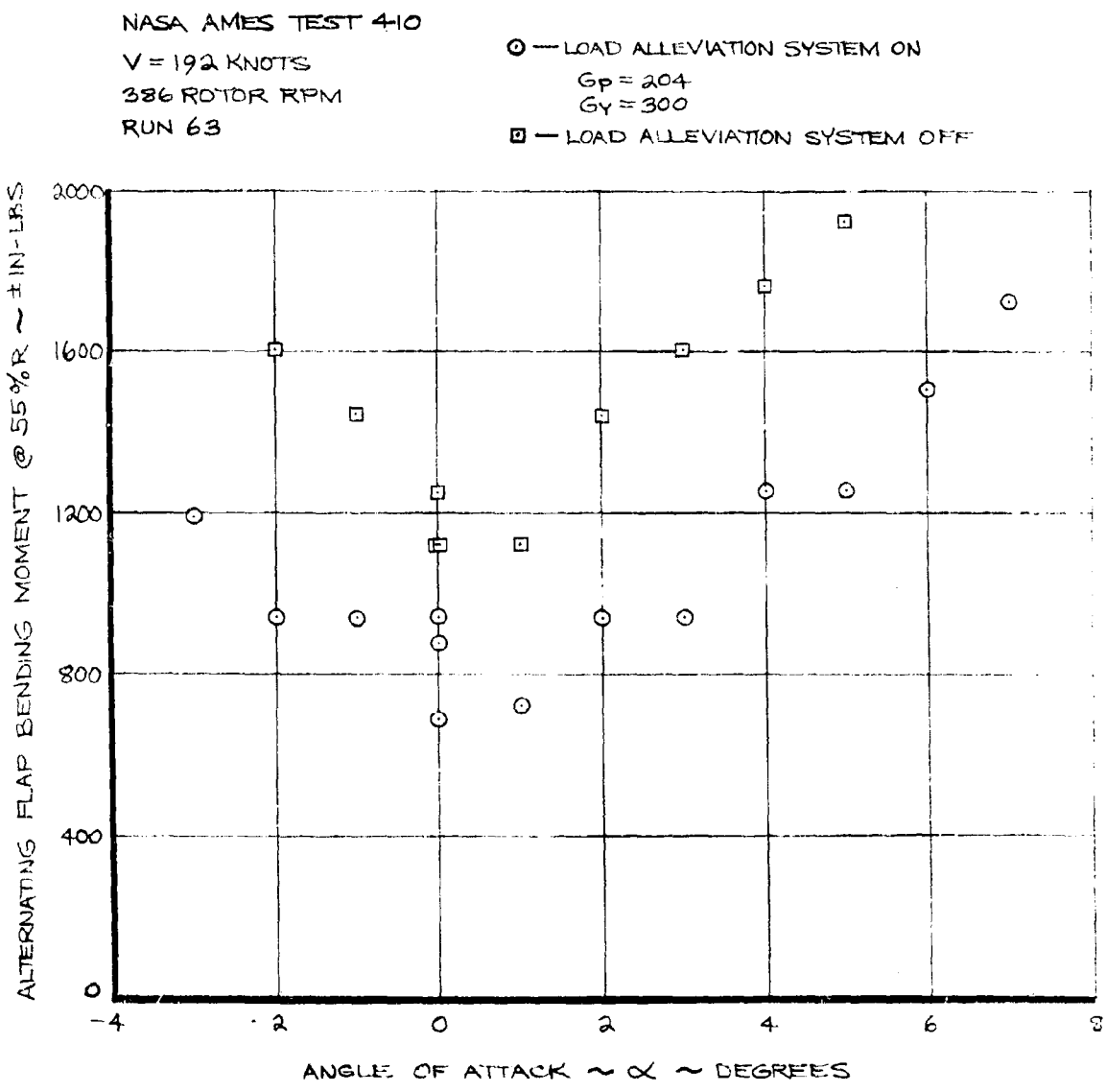

FIGURE 8.38 EFFECT OF LOAD ALLEVIATION SYSTEM ON 55% R BLADE FLAP BENDING MOMENT - V = 192 KNOTS, G_p = 204, G_y = 300

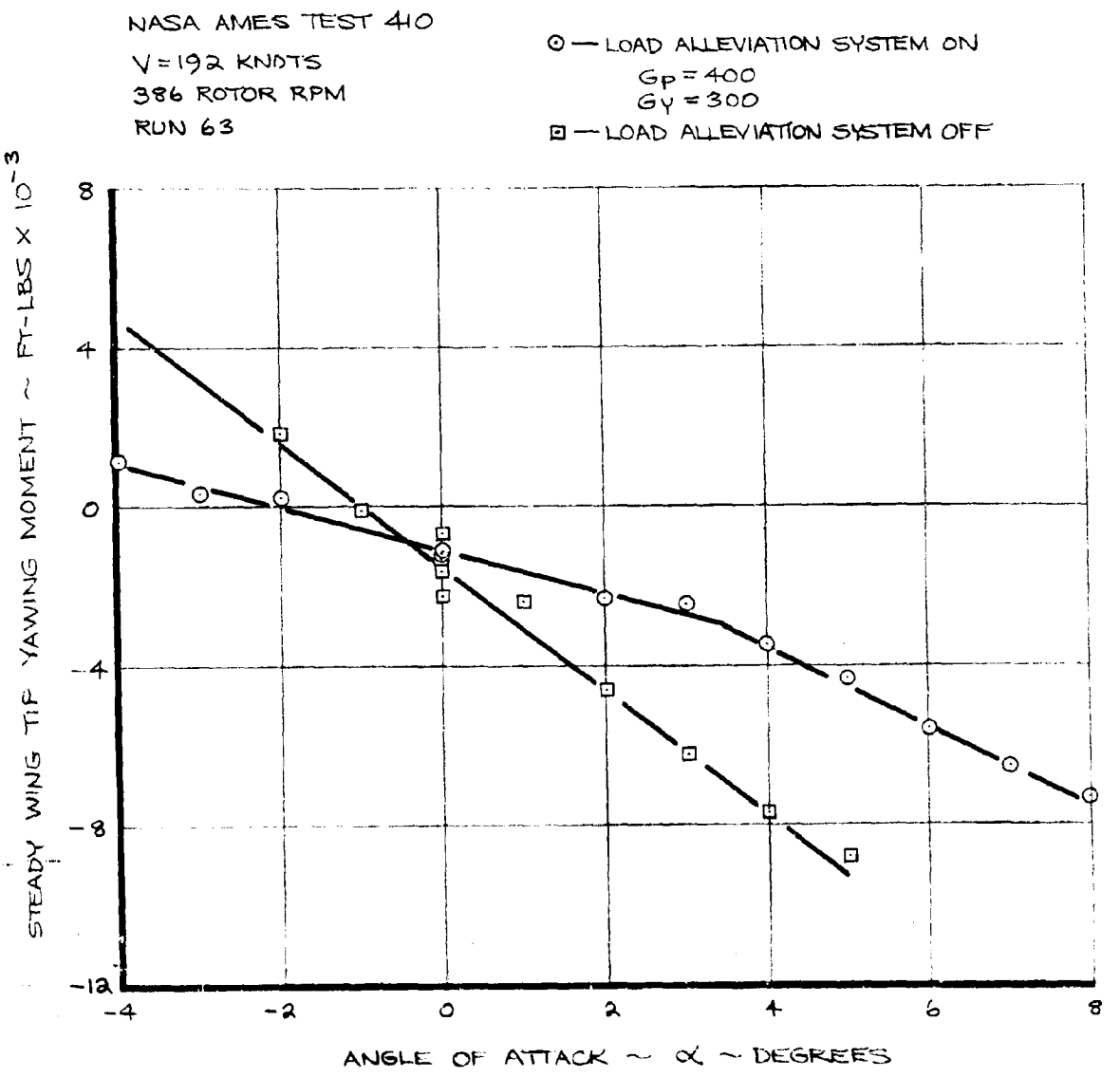

FIGURE 3.31 EFFECT OF LOAD ALLEVIATION SYSTEM ON WING TIP YAWING MOMENT - V=192 KNOTS, Gp = 400, Gy = 300

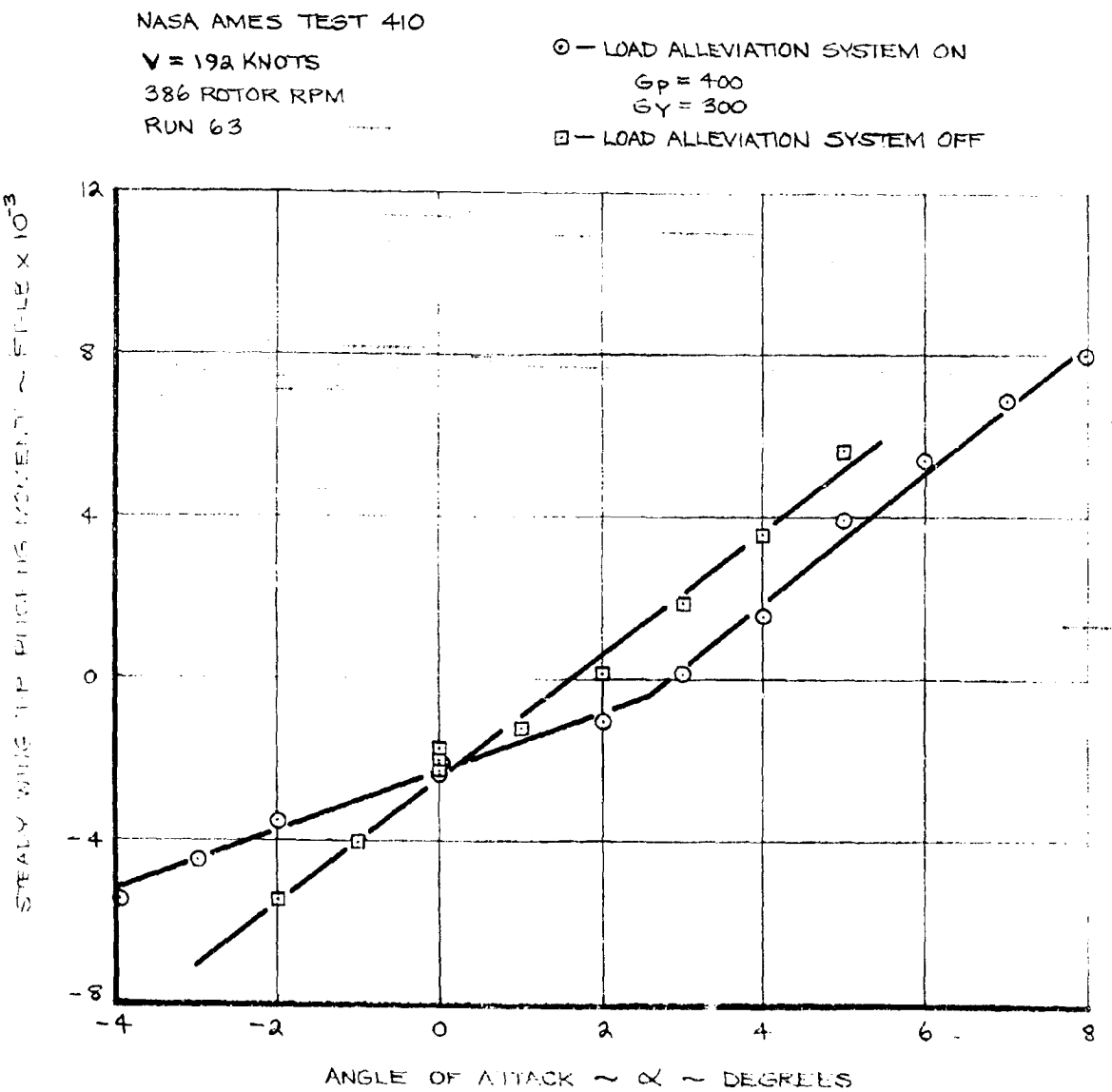

FIGURE 5.42 EFFECT OF LOAD ALLEVIATION SYSTEM ON WING TIP PITCHING MOMENT – V = 192 KNOTS, Gp = 400, Gy = 300

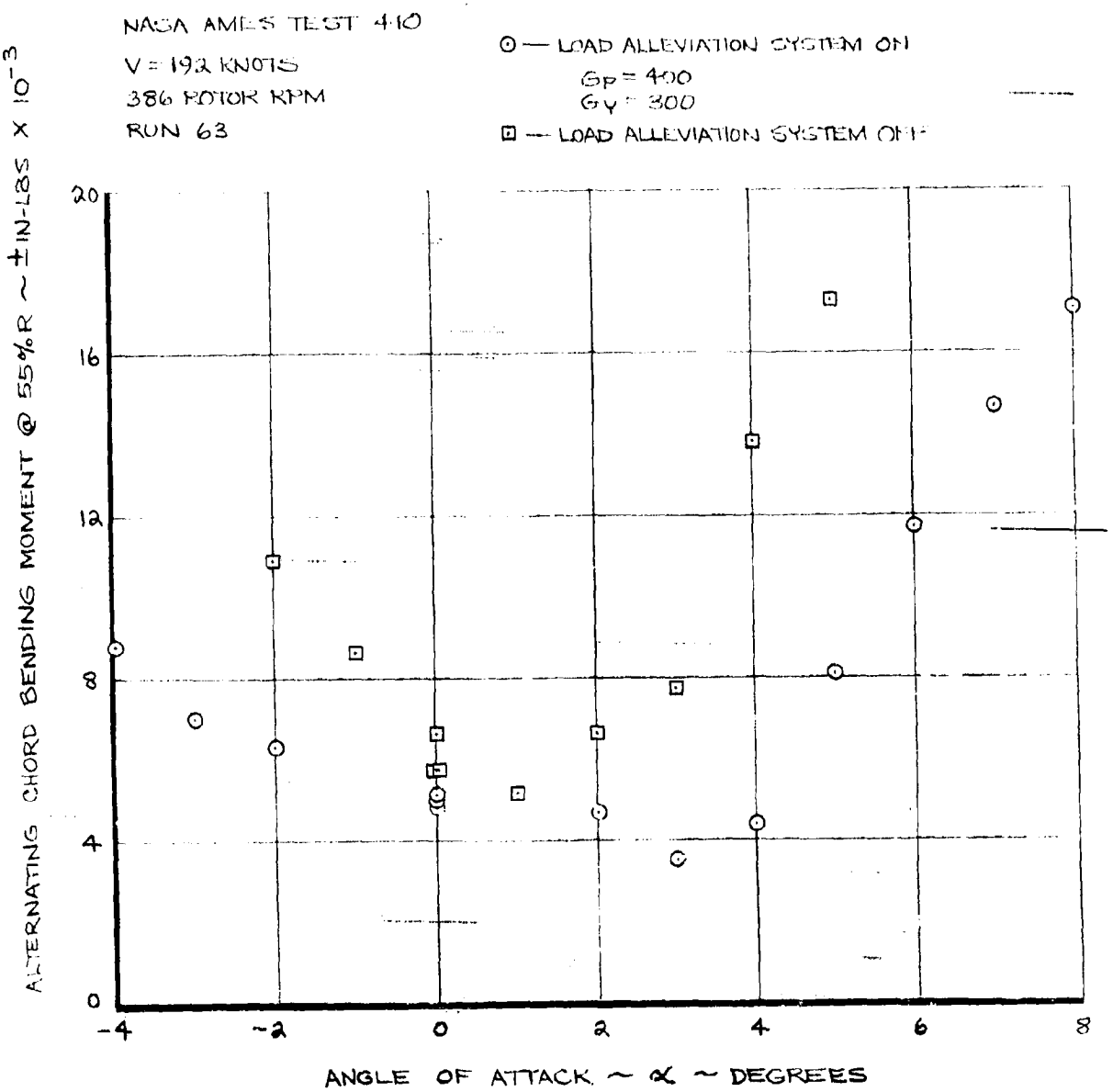

FIGURE 84 EFFECT OF LOAD ALLEVIATION SYSTEM ON 55% R BLADE CHORD BENDING MOMENT - V = 192 KNOTS, G_p = 400, G_Y = 300

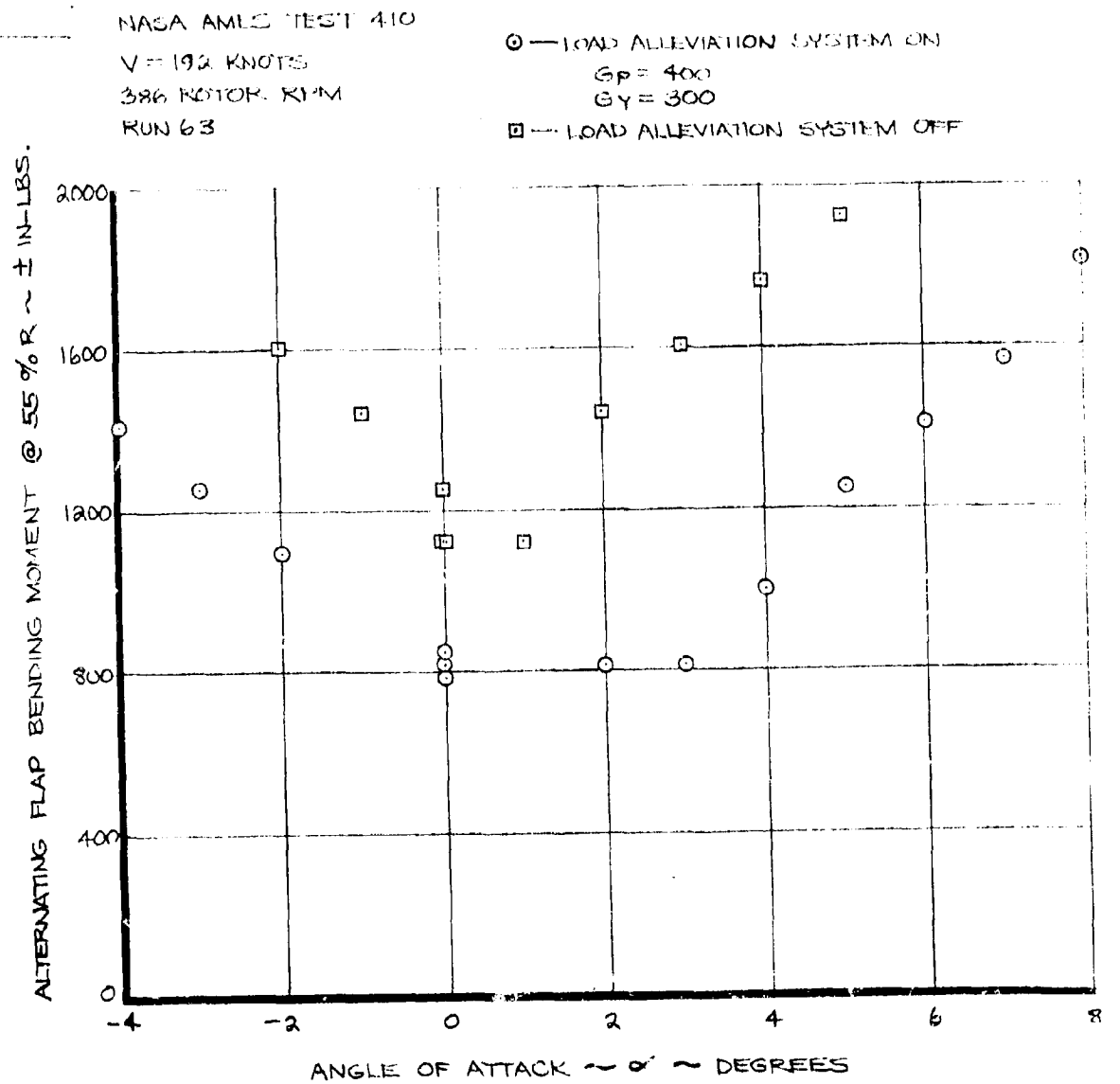

FIGURE 8.42 EFFECT OF LOAD ALLEVIATION SYSTEM ON 55% R BLADE FLAP BENDING MOMENT - V = 192 KNOTS. G_p = 400, G_Y = 300

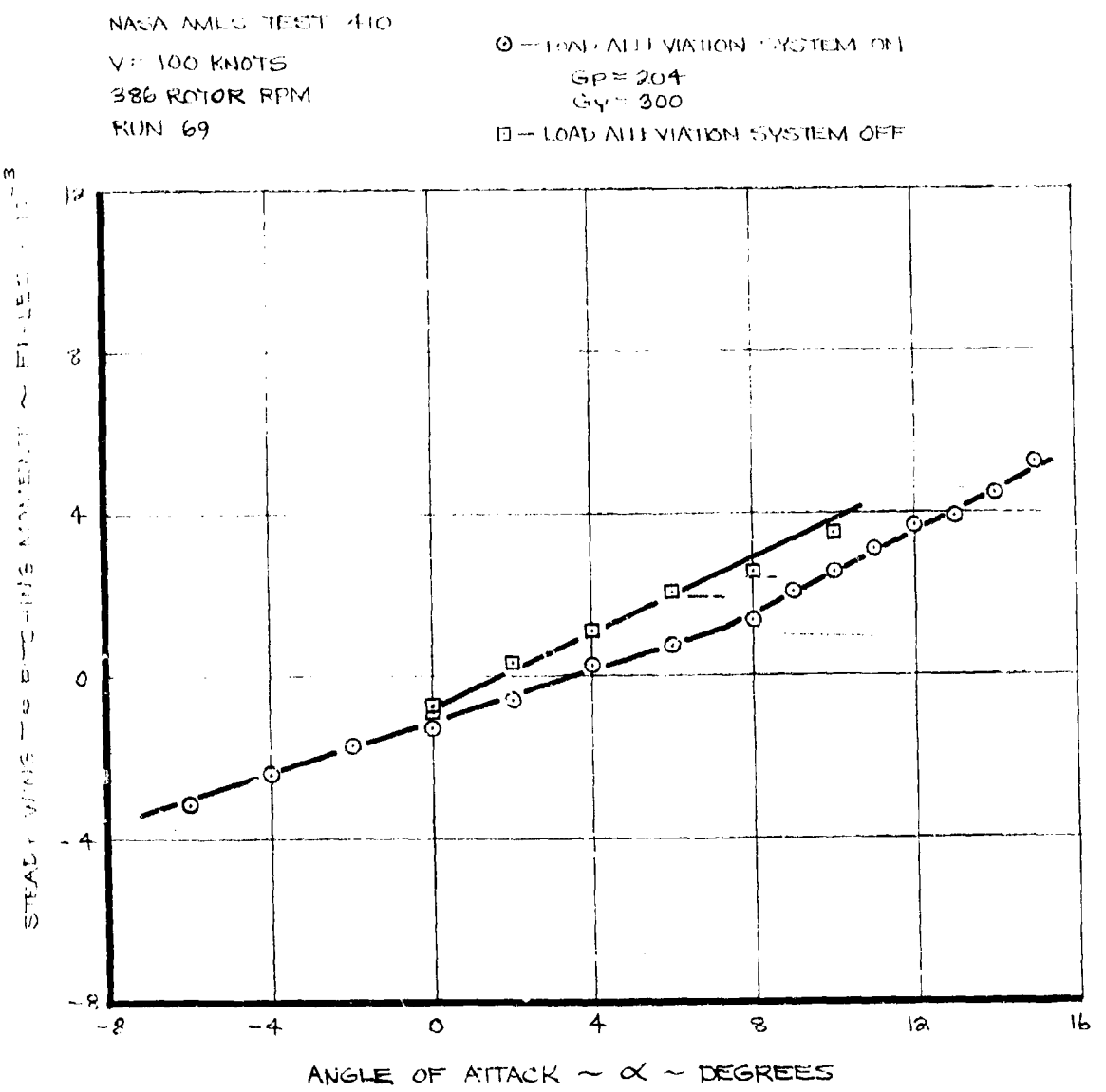

FIGURE 8.43 EFFECT OF LOAD ALLEVIATION SYSTEM ON WING TIP PITCHING MOMENT — V = 100 KNOTS, Gp = 204, Gγ = 300

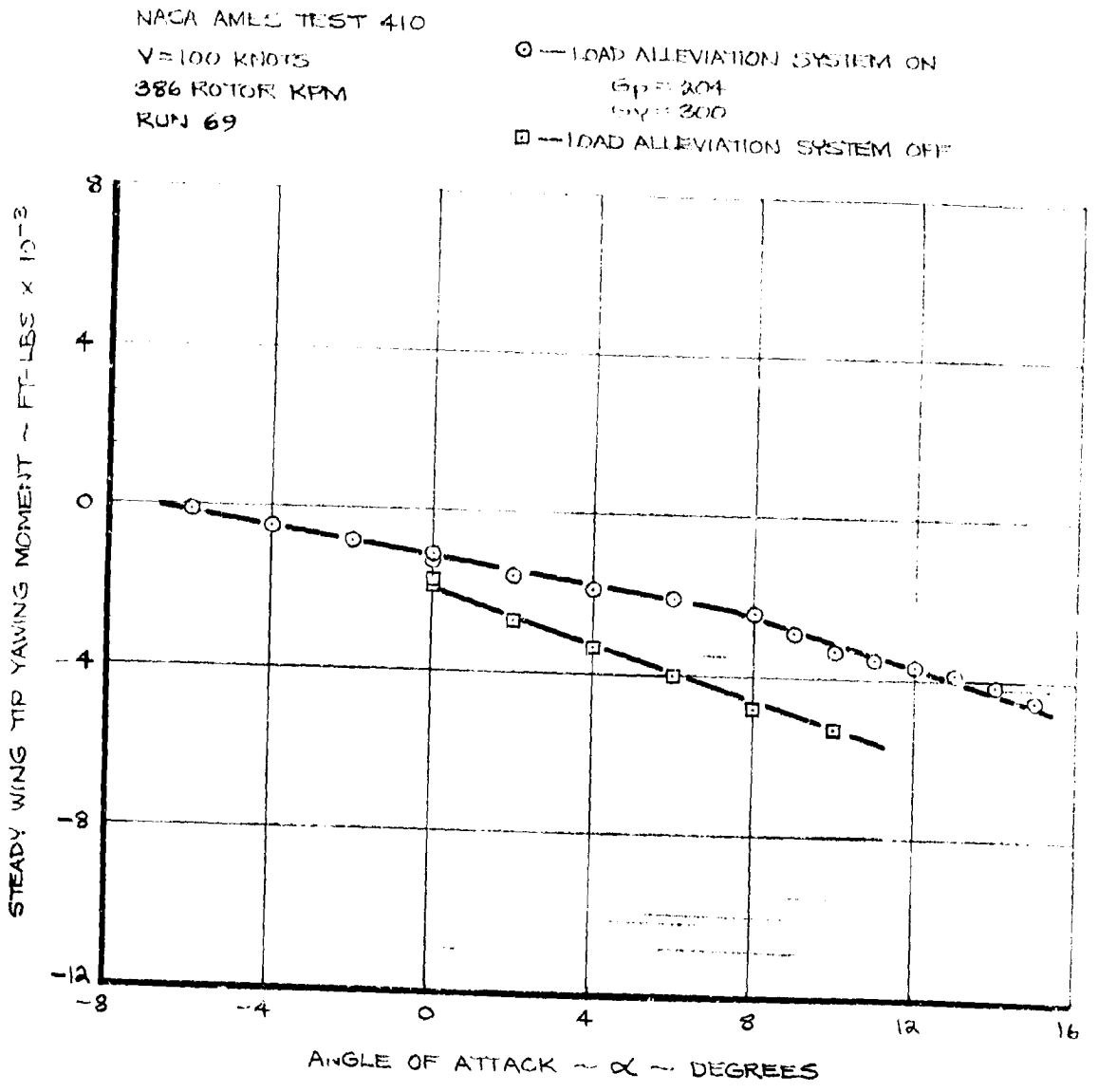

FIGURE 8.44 EFFECT OF LOAD ALLEVIATION SYSTEM GAIN ON WING TIP YAWING MOMENT -- V=100 KNOTS, Gp=204, Gy=300

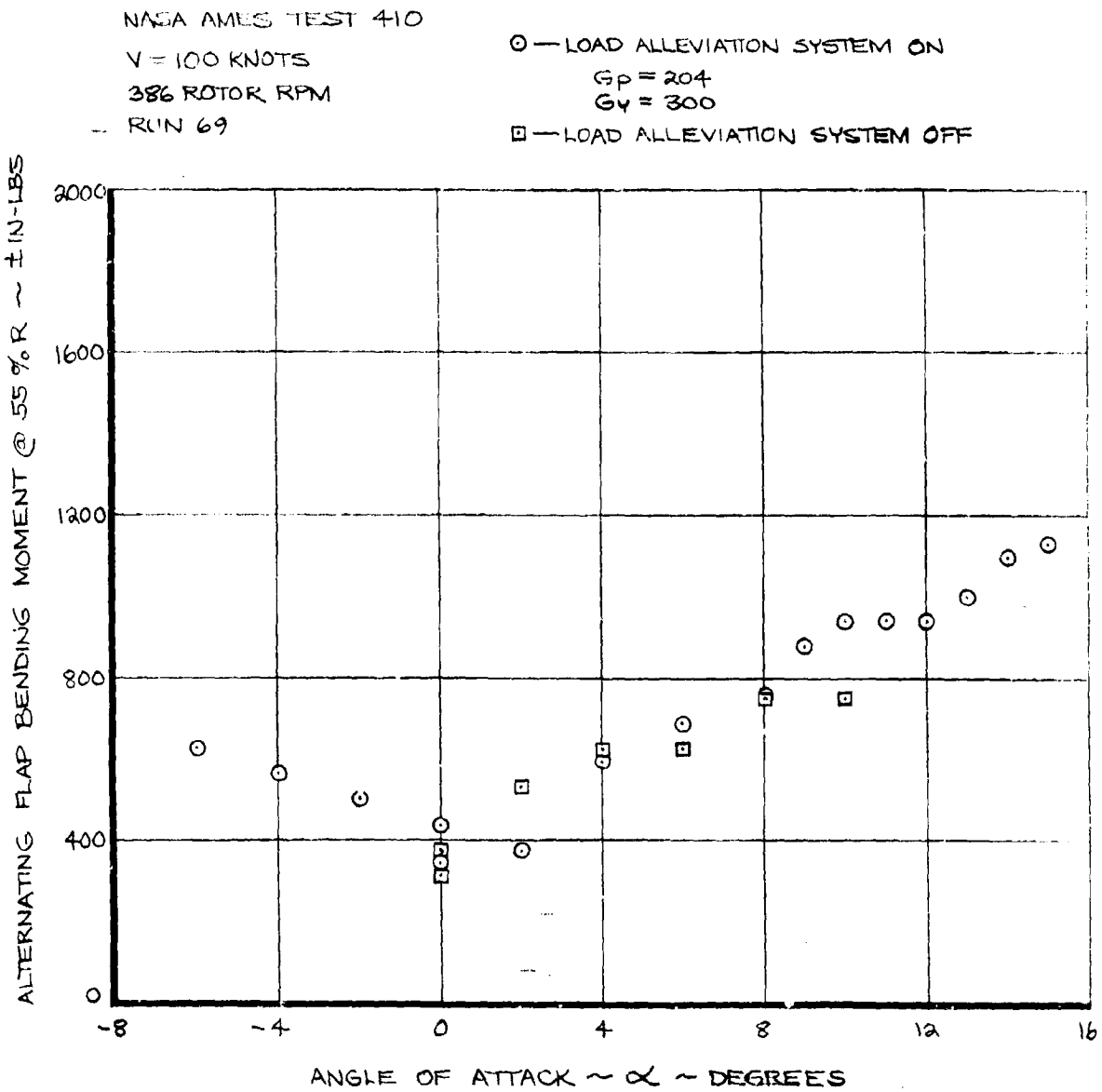

FIGURE 8.45 EFFECT OF LOAD ALLEVIATION SYSTEM ON 55 % R BLADE FLAP BENDING MOMENT — V = 100 KNOTS, G_p = 204, G_y = 300

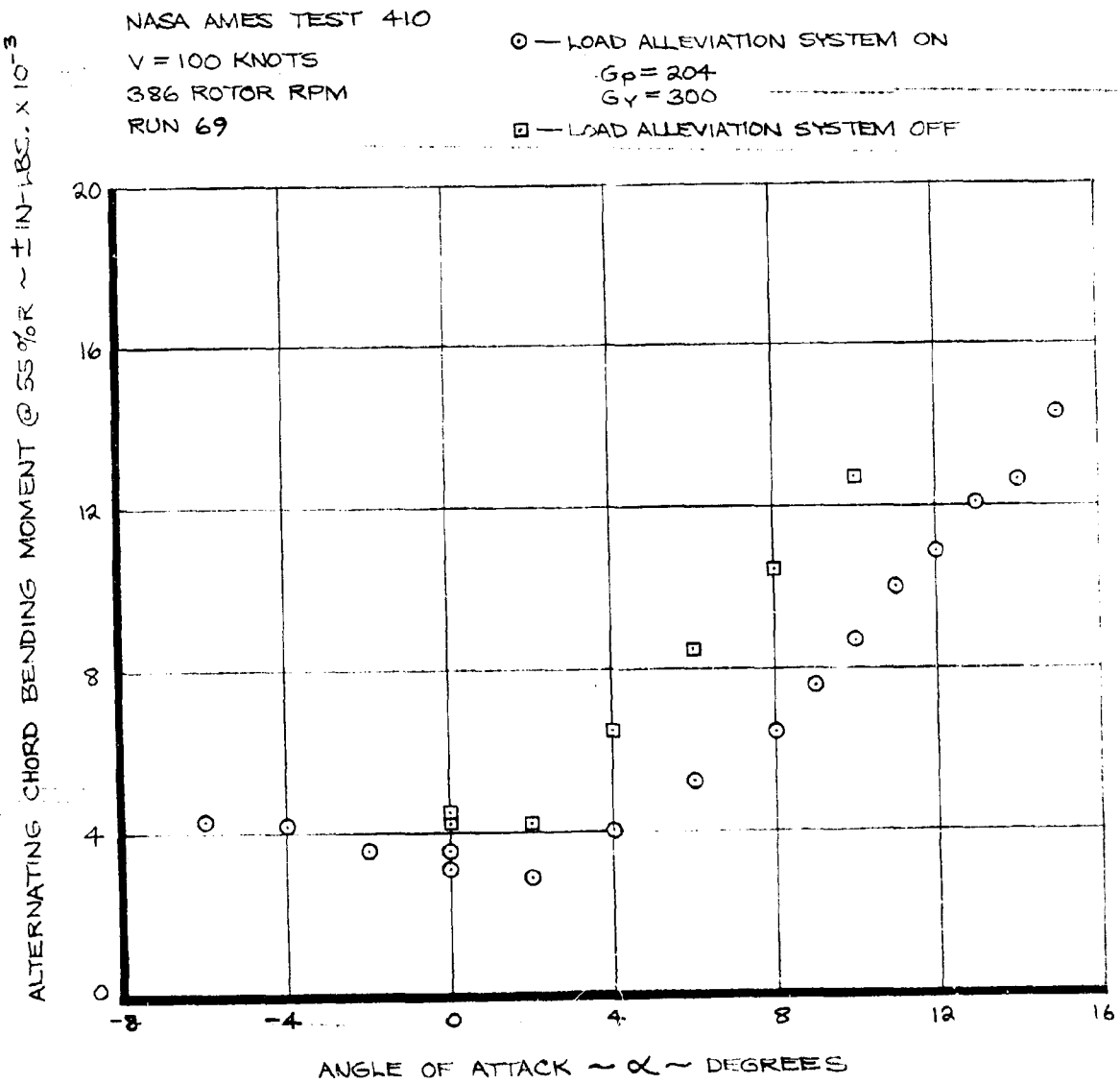

FIGURE 8.46 EFFECT OF LOAD ALLEVIATION SYSTEM ON 55% R BLADE CHORD BENDING MOMENT — V = 100 KNOTS, Gp = 204, Gy = 300

8.2 HIGH RATE FEEDBACK

The second objective of feedback testing was to investigate the use of feedback controls in augmenting aeroelastic modal damping. The designation "high rate" is relative and serves to distinguish the two types of feedback tested. The mode under investigation was the wing vertical bending mode which in earlier testing had been found to be lightly damped and had a stability boundary within the available operating condition as described and predicted in Section 3 of this document.

The sensor used in this case was an accelerometer mounted to provide nacelle vertical accelerations and located 23.24" aft of the rotor plane at the nodal point on the nacelle in the torsion mode. The feedback loop is shown schematically in Figures 8-47 and 8-48. The accelerometer output is connected to a bandpass filter with a center frequency of 2.27 Hz. The filter calibration is given in Figure 8-49. A voltage divider potentiometer was used as a gain control and a unity gain phase shifter included to allow phase adjustment of the feedback signal. The frequency response of the phase shifter is shown in Figure 8-50. The output of the phase shifter was fed into a co-ordinate rotation network and thence to the actuators as was previously done for low rate feedback. The rotor and wing dynamics complete the loop.

For these experiments the value of ψ_{rot} to be used was obtained from theoretical analysis. Figure 8-51 shows the calculated open

loop response of the loop at a frequency of 2.2 Hz and 386 RPM as a function of ψ_{ROT}. This frequency is the frequency of the air resonance mode as shown in Section 3.

A value of ψ_{ROT} = 60-degrees was selected because it gave the maximum response (considered to be the best potential damper closed loop) and also because the phase lag in the system was small as airspeed was increased from 100 to 200 knots.

Initial open loop experiments were performed and the data obtained are given in Appendix 3. These tests were interrupted by an accelerometer failure. A new accelerometer was installed and the "Bode" plots re-run.

With a ψ_{ROT} setting of 60-degrees open loop frequency response tests were performed by driving the cyclic pitch with a signal generator. With the new accelerometer an initial phase shifter setting giving 163-degrees of phase lag at ω = 2.24 Hz was used to bring the open loop phase to zero and the sign change amplifier shown in Figure 8-47 was not included. This value was based on the data of Appendix 3. The frequency response data of Figure 8-52 at 386 RPM and 192 knots shows a phase lead of 45-degrees at 2.24 Hz and peak gain and results in a relatively low phase margin on the low frequency side. Figure 8-53 shows data at 420 RPM, 192 knots and indicates a reduction in gain margin. Further increasing the RPM to 445, Figure 8-54, produces a Bode that would require gain restriction to provide a phase margin greater than 30-degrees.

These phenomena are the result of a non-optimum phase shifter setting and an additional 44-degrees of phase lag (at $\omega = 2.24$ Hz) was added by adding to the loop sign change and reducing the phase shifter to 27-degrees of phase lag giving a total of 207-degrees instead of the previous value of 163-degrees. The open loop experiments were then rechecked to ensure that the margins had been improved. These data are given at 192 knots, 386 RPM in Figure 8-55 and at 445 RPM in Figure 8-56.

Figure 8-55 shows an improvement in phase margin from 30 degrees (Figure 8-52) to 77 degrees and at maximum gain the phase shift was zero. Checks were made at the wing chord bending and torsion frequencies and the results indicated no gain levels approaching zero dB. This data was generated with the maximum available loop gain and indicates a stable system at all gain levels.

The open loop experiment was repeated at an off design RPM of 445 to determine the sensitivity of loop stability to operation at off design conditions. The phase margins for this case are different as shown in Figure 8-56. The low frequency side phase margin is reduced to 20° while the high frequency side is increased to 128°. Although the shape of the gain curve is more rounded the zero dB crossings are substantially the same; also, the peak gain is unchanged from the 386 RPM case of Figure 8-55. The major difference is in the phase plot which has about 90° more phase

lead at the maximum gain than was observed at 386 RPM. This phase change is thought to be due to the coupling between the lower blade lag mode ($\Omega - \omega_L$) and the wing vertical bending frequency. As RPM is increased these modal frequencies approach each other as shown in Sections 3 and 4 of this report.

Figures 8-57 and 8-58 show frequency response data at 100 knots airspeed at 386 and 425 RPM respectively. At design RPM (386) the gain peak is much reduced and the phase margins are large, 180° and 130° respectively. The phase at $\omega = 2.27$ is 30° lag compared with 33° lag at 192 knots (Figure 8-57). This insensitivity to airspeed was one of the reasons a ψ_{ROT} of 60° was selected.

At 425 RPM and 100 knots (Figure 8-58) the gain peak is increased presumably due to reduced damping in the air resonance mode. The phase curve swings up more sharply and crosses zero at a slightly lower frequency than for 386 RPM. The phase margins are quite adequate (65° and 82°) for loop closure with safety.

Prior to loop closure the sign change amplifier introduced to obtain 207° lag at $\omega = 2.24$ Hz was removed to provide negative feedback.

Figure 8-59 shows closed loop test data for 192 knots and design RPM.

The shaker vane was used to excite the wing vertical bending mode and the modal damping obtained from the decay after the vane oscillation was sharply stopped. The data indicates an increase in modal damping with gain increase as predicted. The gain available in the loop was 1.25-degrees of cyclic/g and this gain level provided an increase in damping from 2% critical at zero gain to approximately 10% critical at maximum gain. The data scatter are due to the presence of turbulence which makes precise evaluation of the damping difficult. Thresholds and dead zones in the system may also affect the scatter. This data is retained on magnetic tape and could be further analyzed with the use of selective filtering to yield greater precision.

The amounts of alternating cyclic pitch used prior to the vane stoppage (i.e., forced response) is also shown in Figure 8-59 and indicates as expected an increase in alternating cyclic pitch as loop gain is increased. The calibration of the cyclic exists in the system. The longitudinal actuators would not indicate any "slop" effects since they are preloaded by the steady load due to planipetal torsion from the blades. The lateral actuator can exhibit a threshold and this is felt to be of the order of 0.1-degrees or less.

Figure 8-60 shows similar data at 445 RPM, 192 knots. The damping is seen to increase at about the predicted rate up to a gain of

0.62-degrees/g gain and then reduces although never getting below the original zero gain level. This reversal was not predicted and requires further analysis. The levels of cyclic pitch are sufficiently larger than the dead band level. The reversal is unlikely to be a result of this effect.

The predicted effect of reduced airspeed is to reduce the effectiveness of the feedback loop as shown at 100 knots, 386 RPM, in Figure 8-61. The data indicates a lower growth of modal damping with gain than predicted. This may be due in part to the dead band effect since the cyclic values used are relatively low in this case.

At 100 knots and 445 RPM (Figure 8-62) the experimental damping measurements show a tendency to remain constant as gain is increased and then increase sharply at a gain level of 0.82 degrees of cyclic per 'g'. Again the cyclic values used are low and part of the reduced effectiveness could be due to the dead band. It is recommended that further theoretical analysis be performed with the measured system characteristics to investigate the effects of real components (i.e., actuator threshold and dead band, etc.) on the stability and effectiveness of the feedback loop.

The objective of these tests was to determine the effectiveness of a feedback control loop in augmenting structural modal damping. The data obtained indicates that systems of this type have large

potential and, although not necessary to current production aircraft, provide an area of valuable research for future applications.

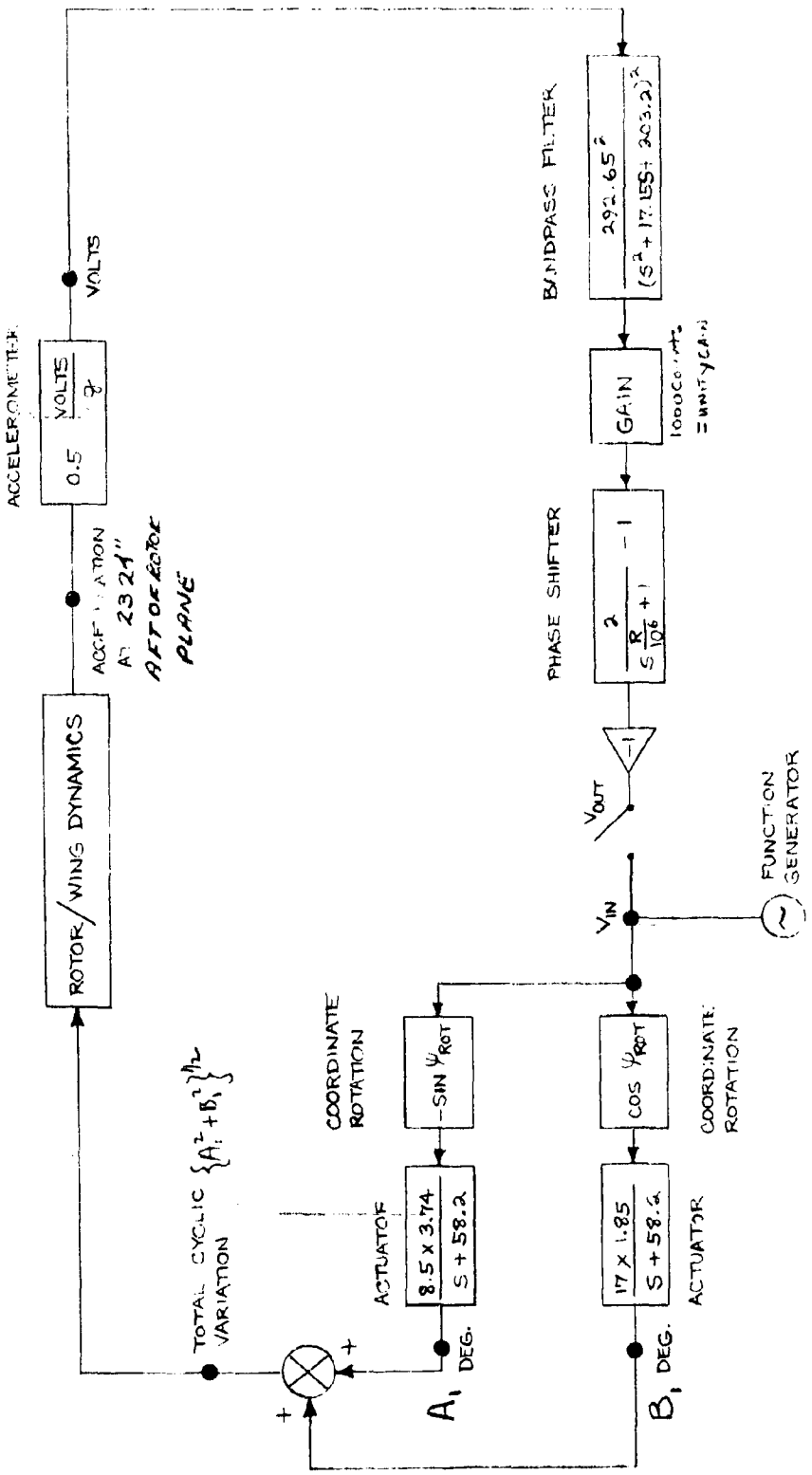

FIGURE 8.47 SCHEMATIC OF OPEN LOOP HIGH RATE FEEDBACK SYSTEM

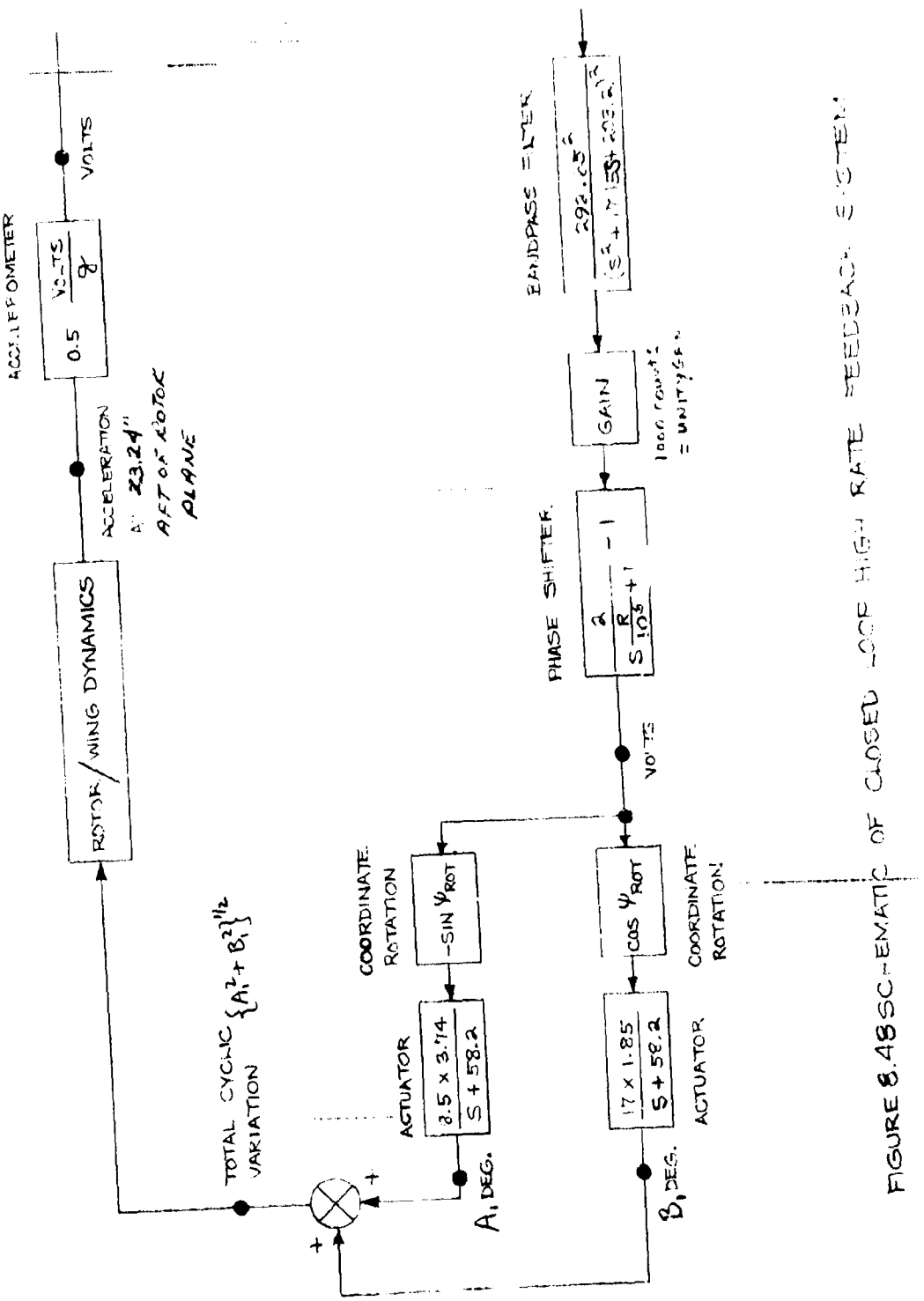

FIGURE 8.48 SCHEMATIC OF CLOSED LOOP HIGH RATE FEEDBACK SYSTEM

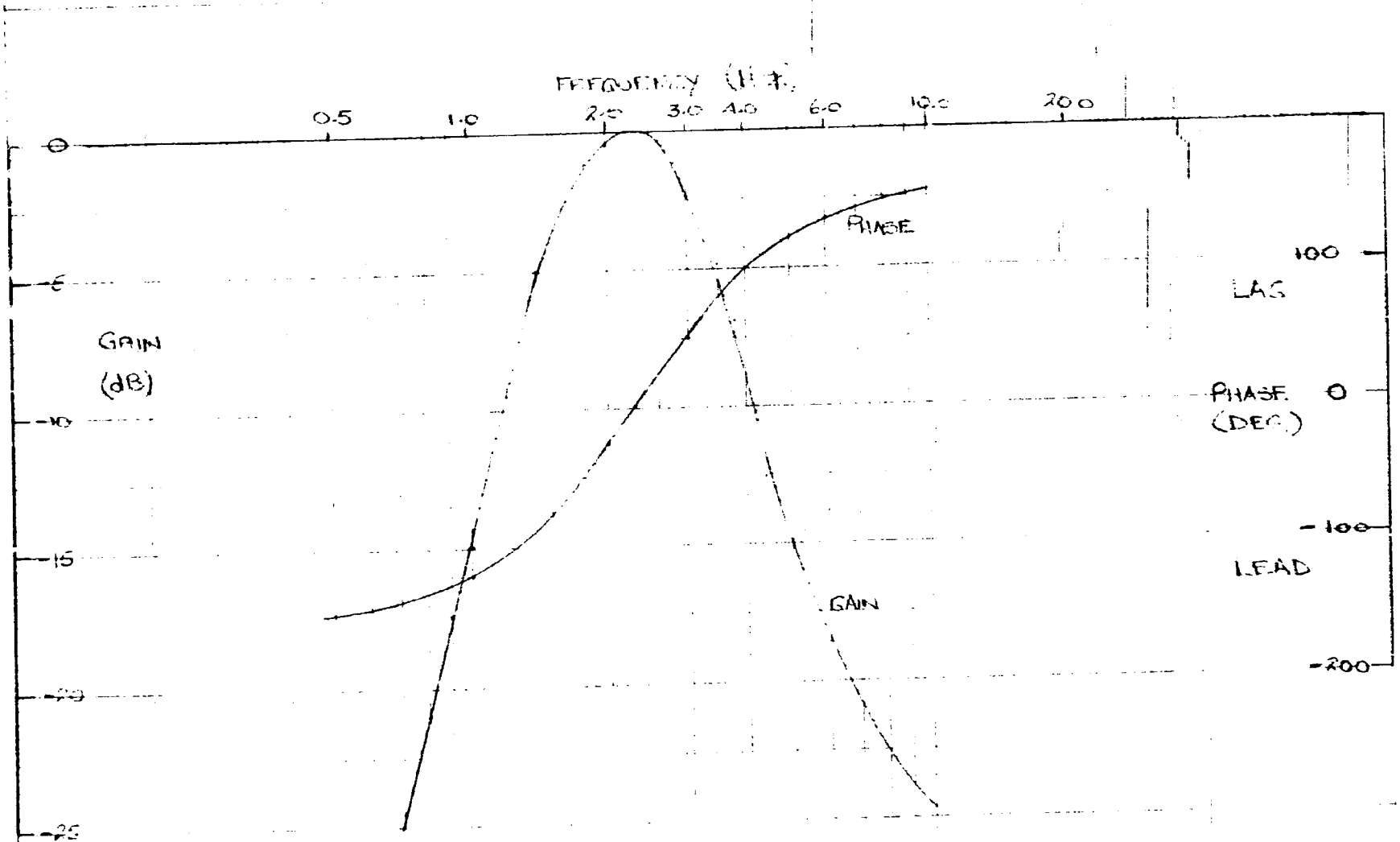

FIGURE 8-49. HIGH RATE FEEDBACK BANDPASS FILTER FREQUENCY RESPONSE

D222-10054-1

FIGURE 8.50 FH[illegible] OF PHASE SHIFT [illegible]

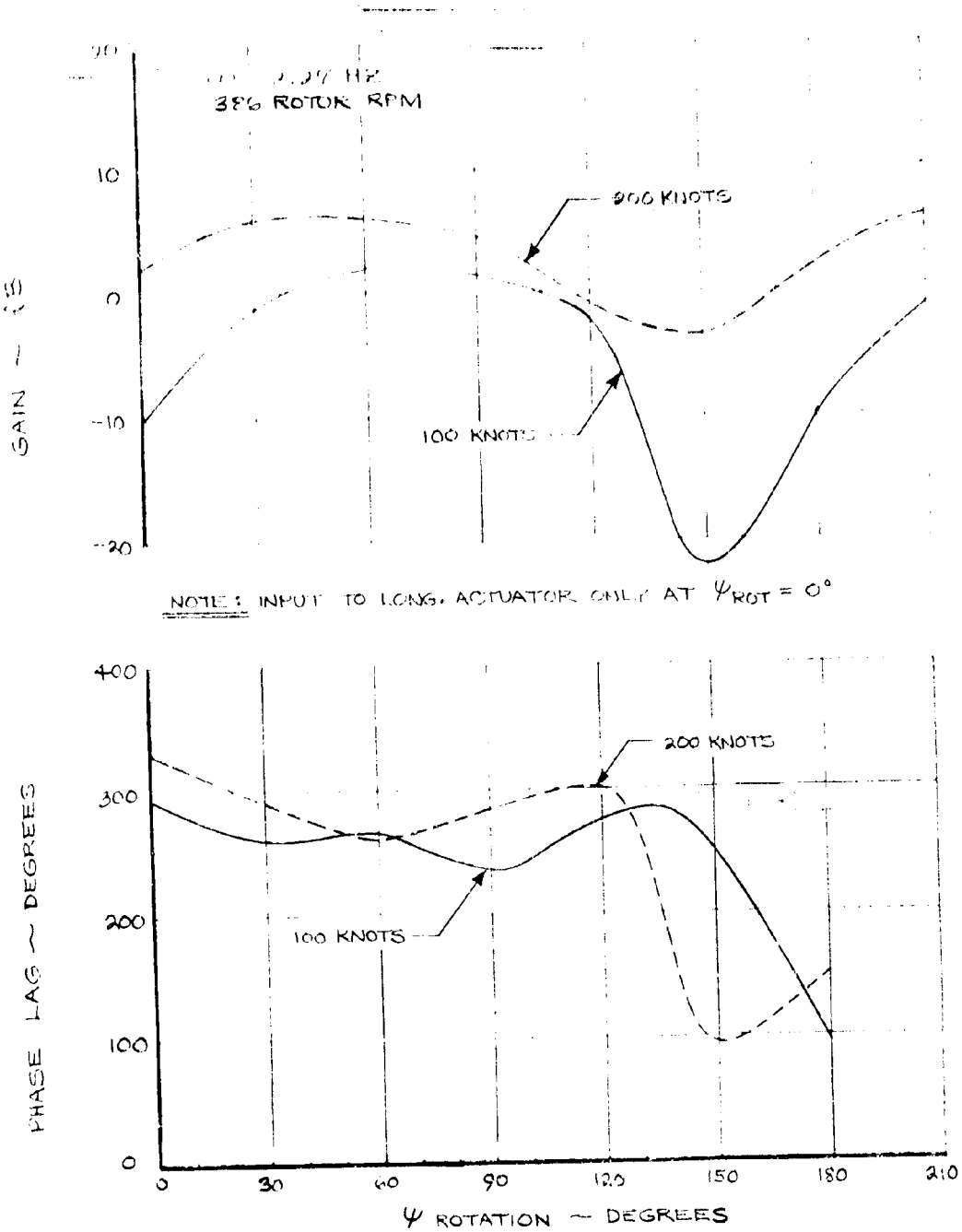

FIGURE 8.51 THEORETICAL HIGH RATE FEEDBACK OPEN LOOP RESPONSE — 2.27 HZ, 386 RPM

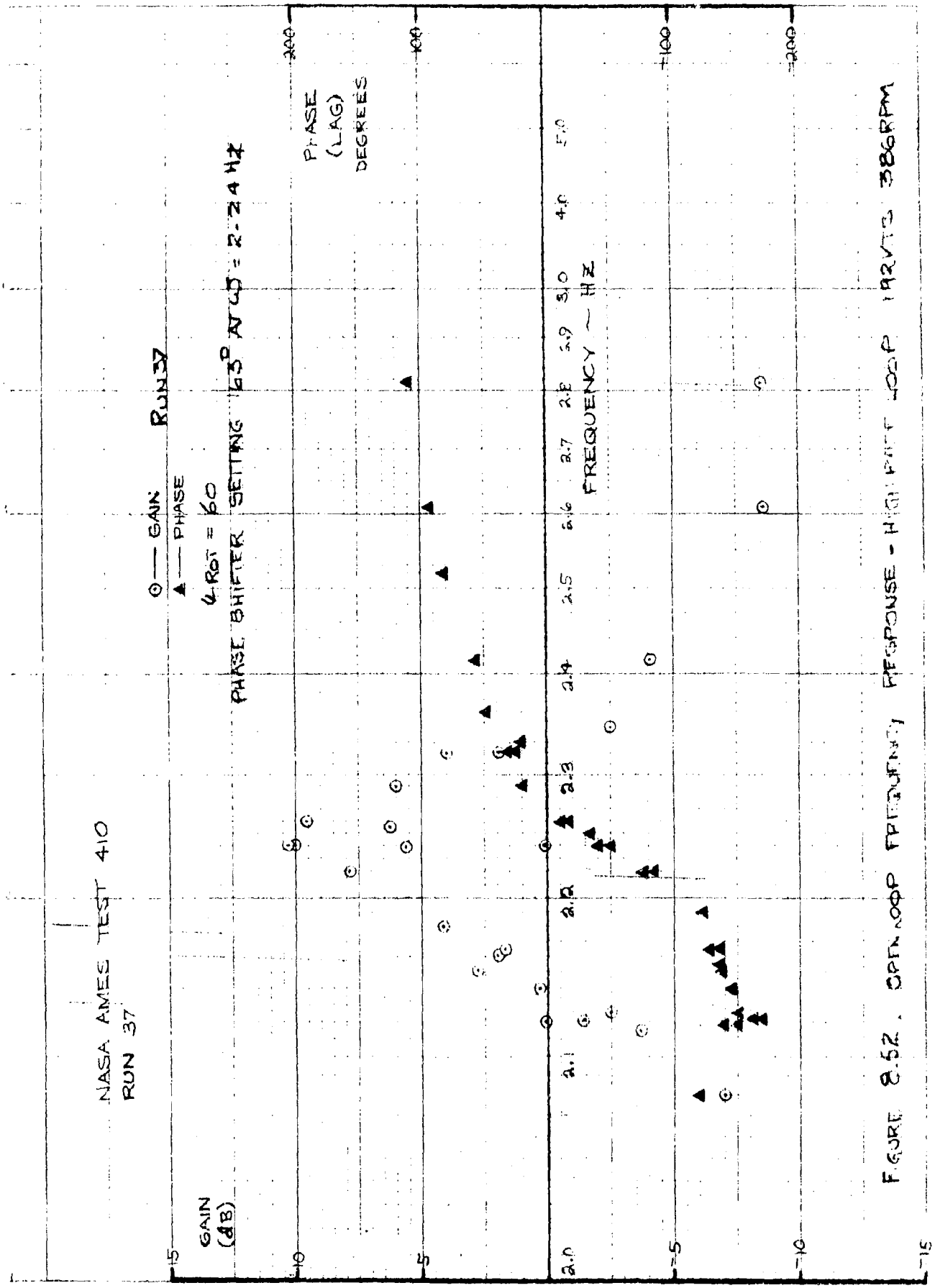

FIGURE 8.52. OPEN LOOP FREQUENCY RESPONSE - HIGH RATE LOOP 192VTS 386RPM

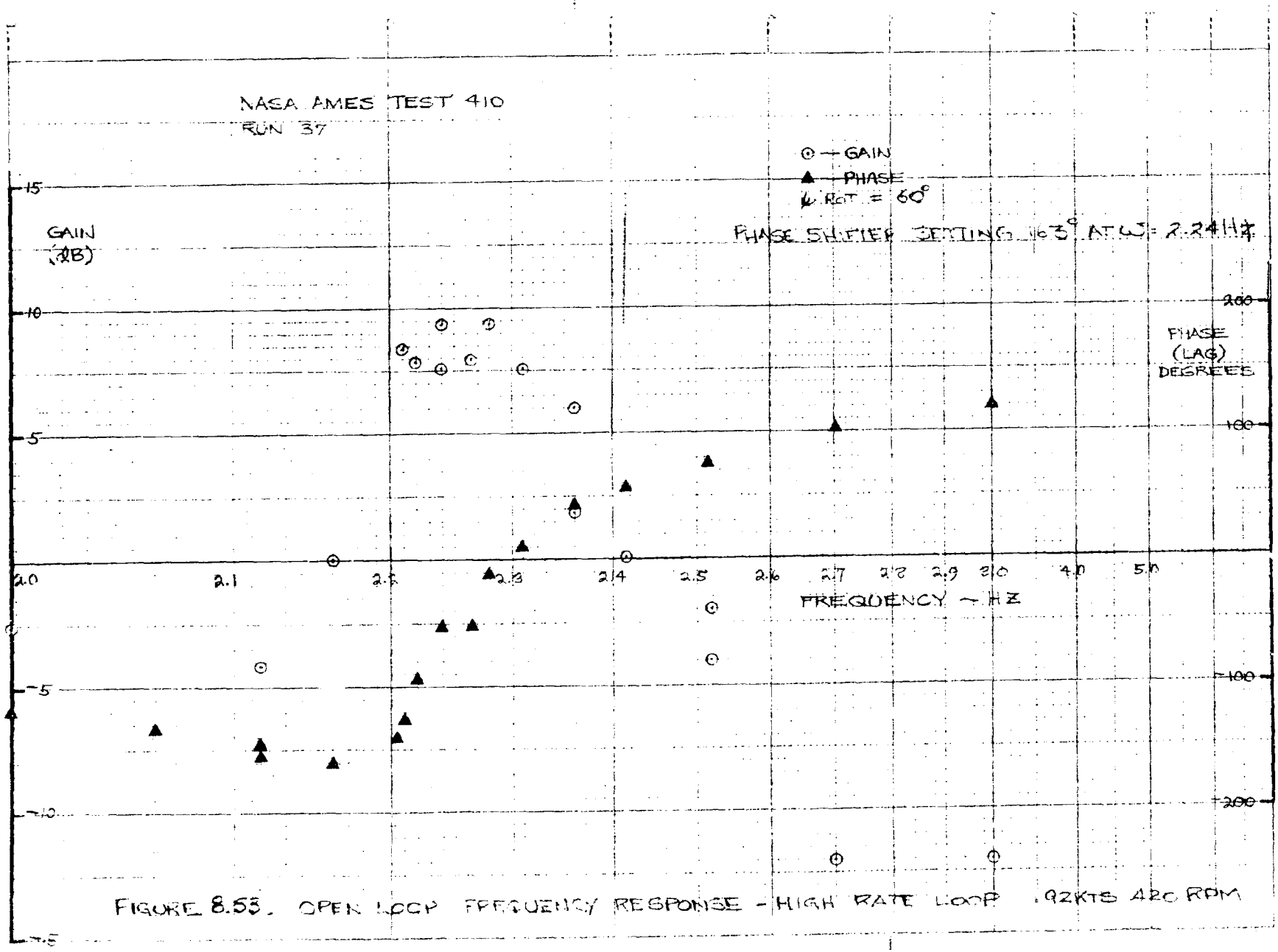

FIGURE 8.53. OPEN LOOP FREQUENCY RESPONSE - HIGH RATE LOOP .92KTS 420 RPM

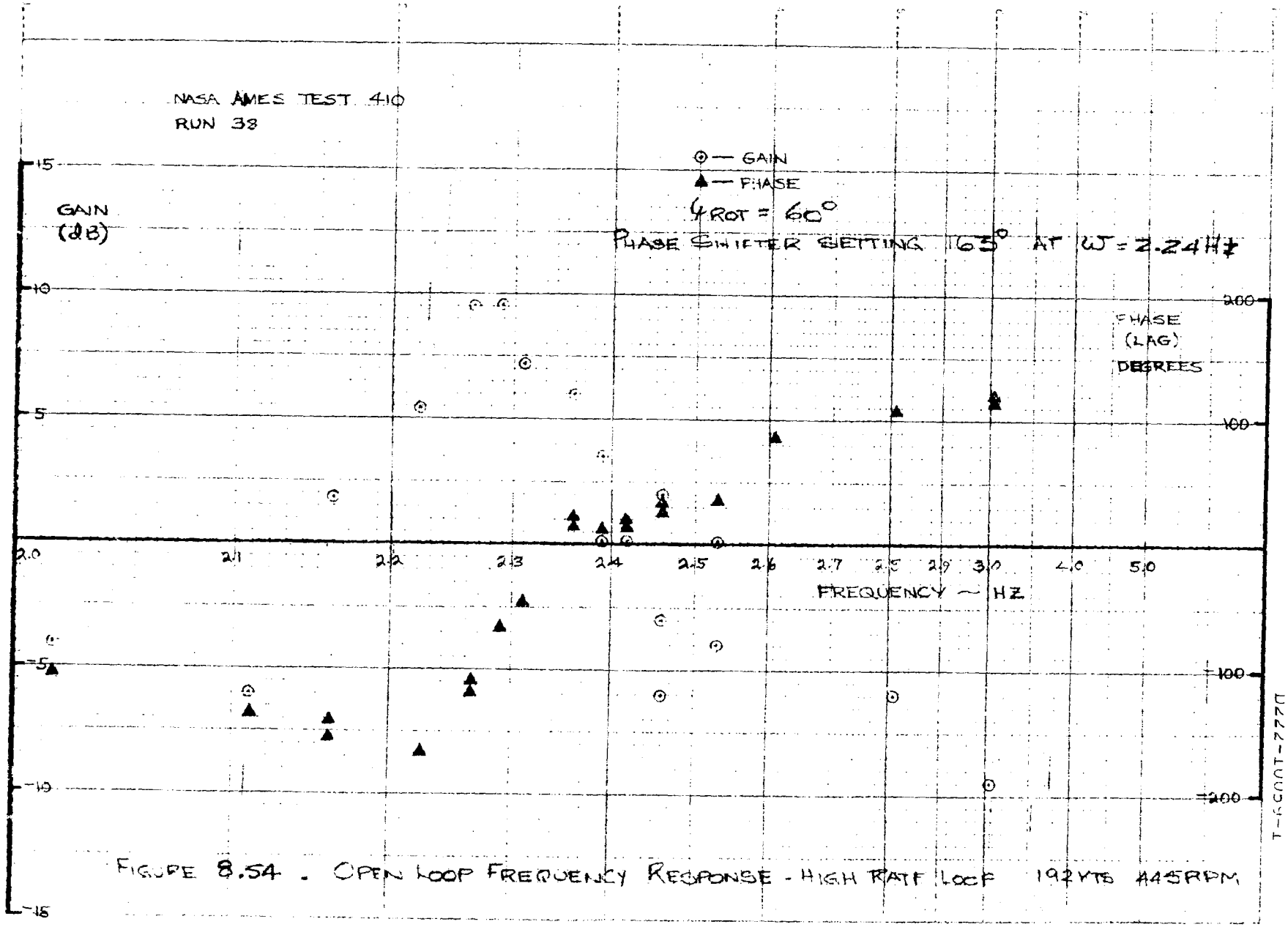

FIGURE 8.54 - OPEN LOOP FREQUENCY RESPONSE - HIGH RATE LOOP 192 KTS 445 RPM

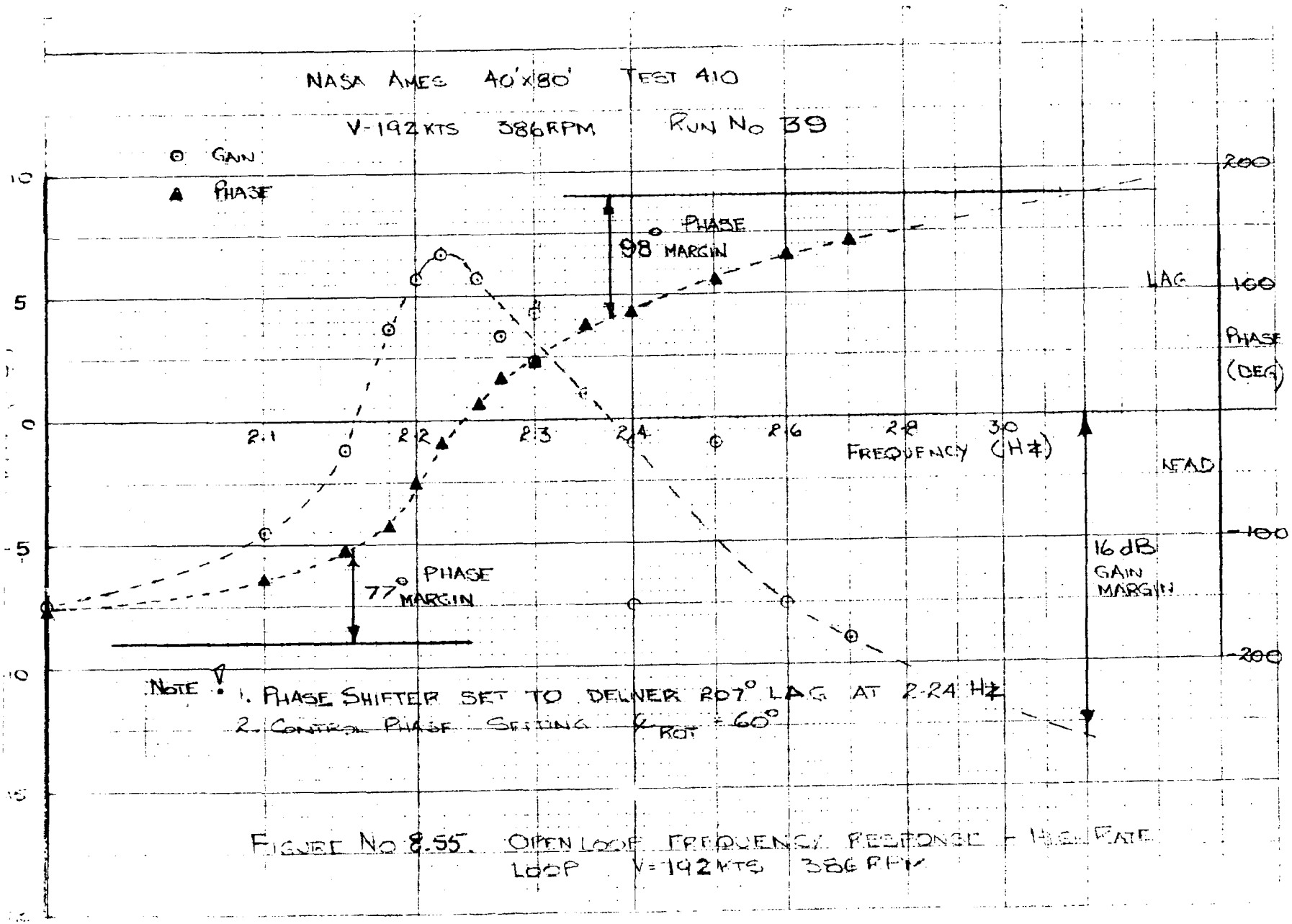

FIGURE No 8.55. OPEN LOOP FREQUENCY RESPONSE - HIGH RATE LOOP V=192 KTS 386 RPM

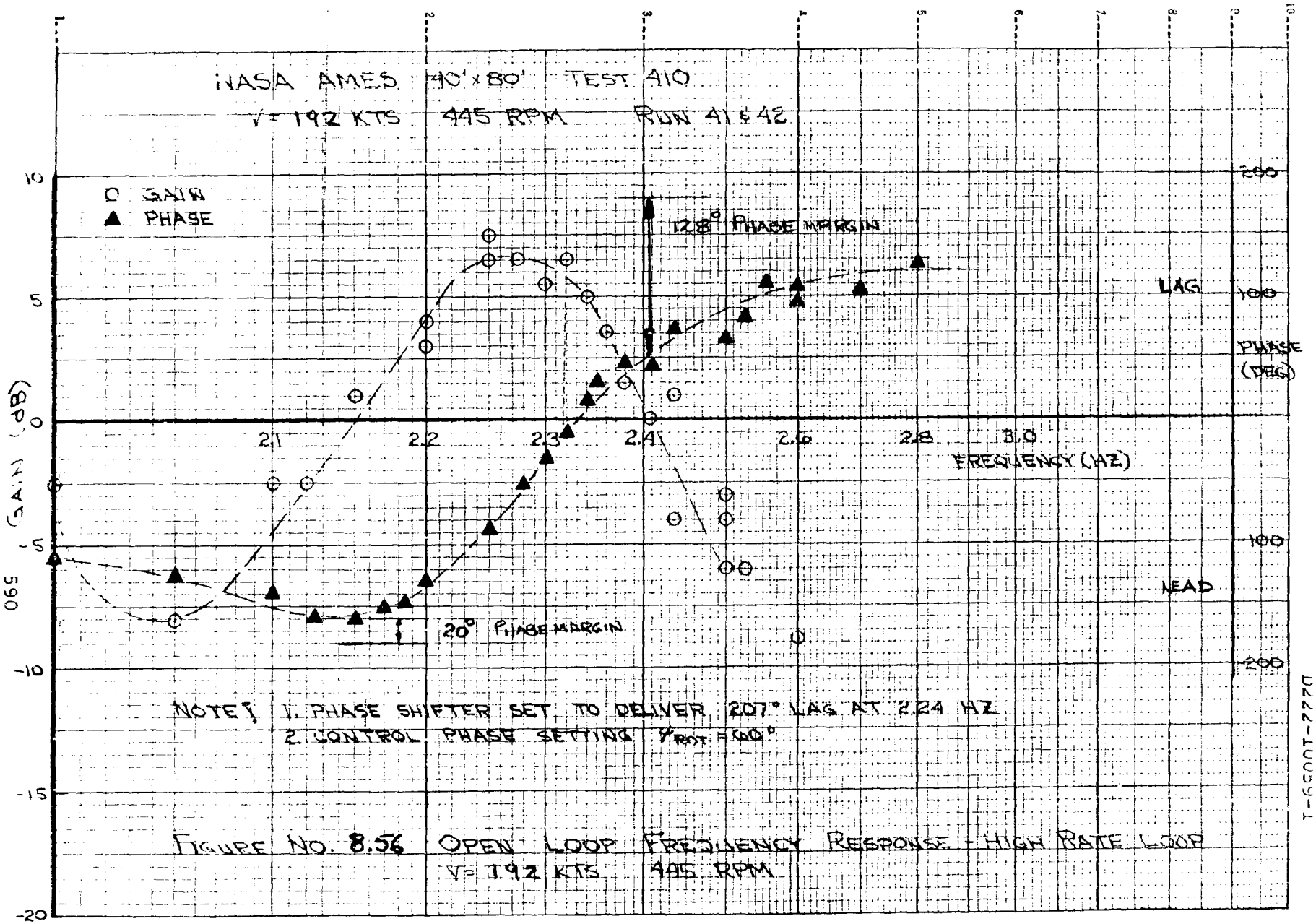

NOTE: 1. PHASE SHIFTER SET TO DELIVER 207° LAG AT 2.24 HZ
2. CONTROL PHASE SETTING $\psi_{ROT} = 90°$

FIGURE NO. 8.56 OPEN LOOP FREQUENCY RESPONSE - HIGH RATE LOOP
V = 192 KTS 445 RPM

D222-10099-1

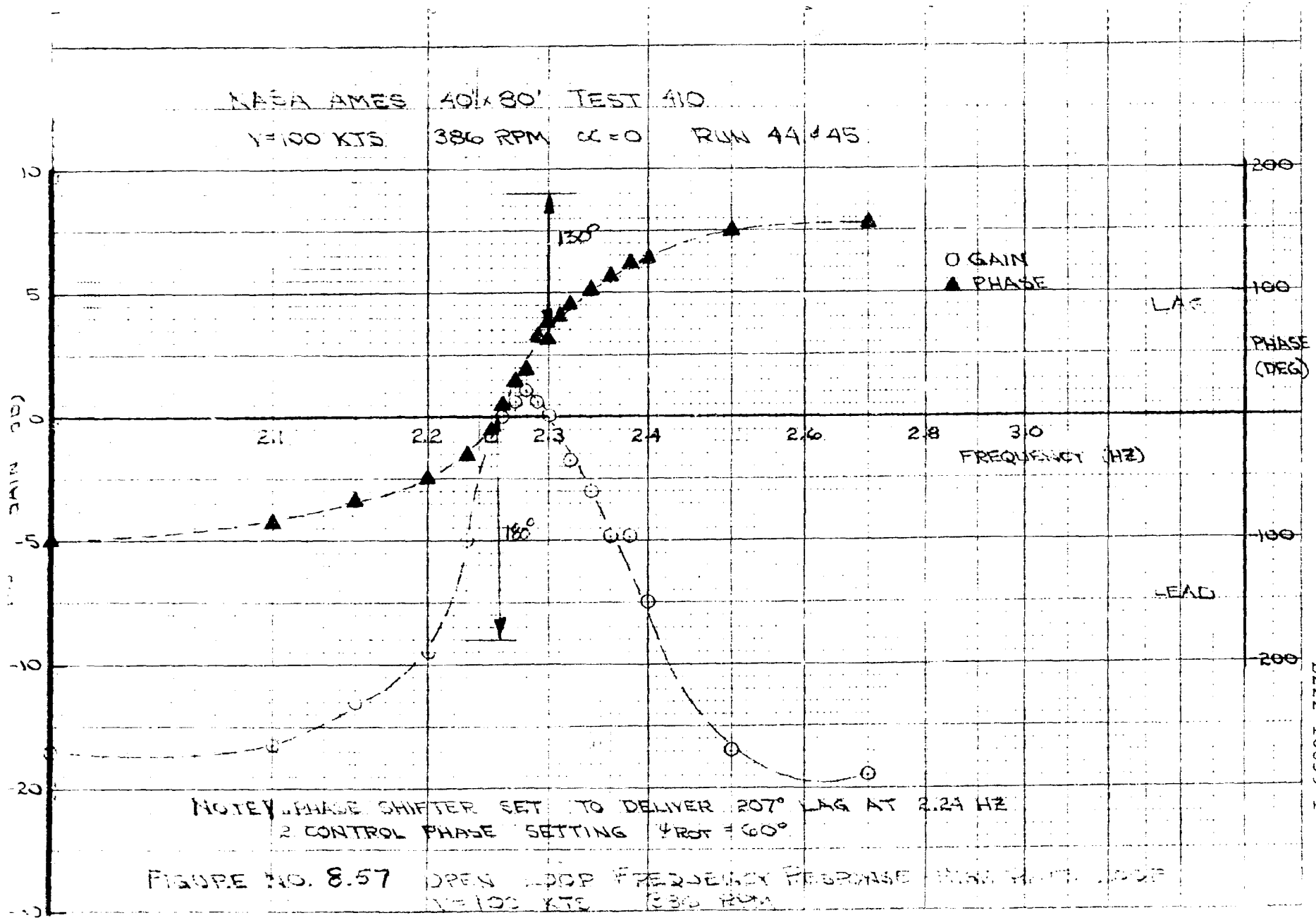

NOTE: 1. PHASE SHIFTER SET TO DELIVER 207° LAG AT 2.24 HZ
2 CONTROL PHASE SETTING ψ_{ROT} = 60°

FIGURE NO. 8.57 OPEN LOOP FREQUENCY RESPONSE [illegible]
V=100 KTS 386 RPM

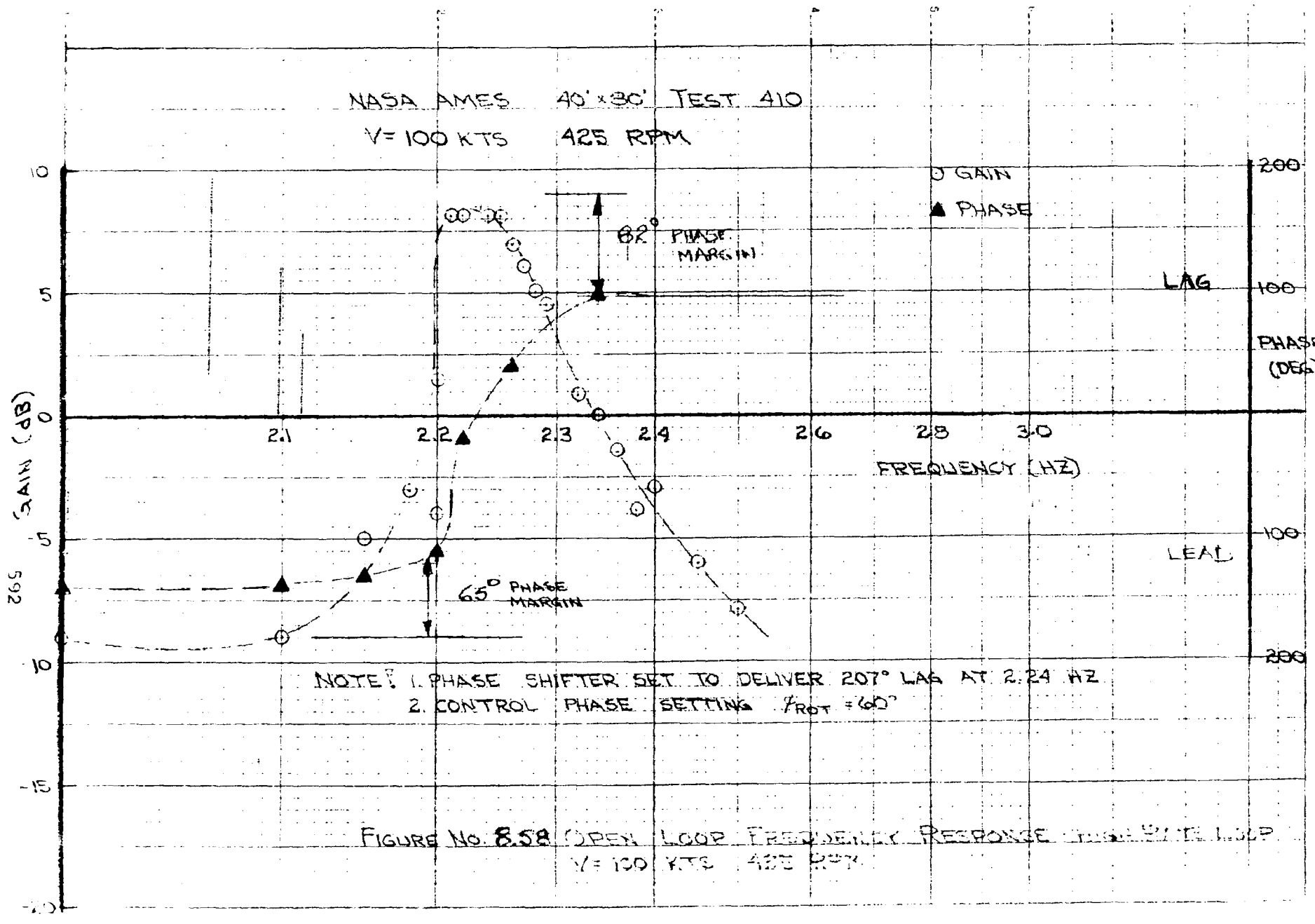

FIGURE No. 8.58 OPEN LOOP FREQUENCY RESPONSE [illegible] LOOP
V= 100 KTS 425 RPM

592

D222-10059-1

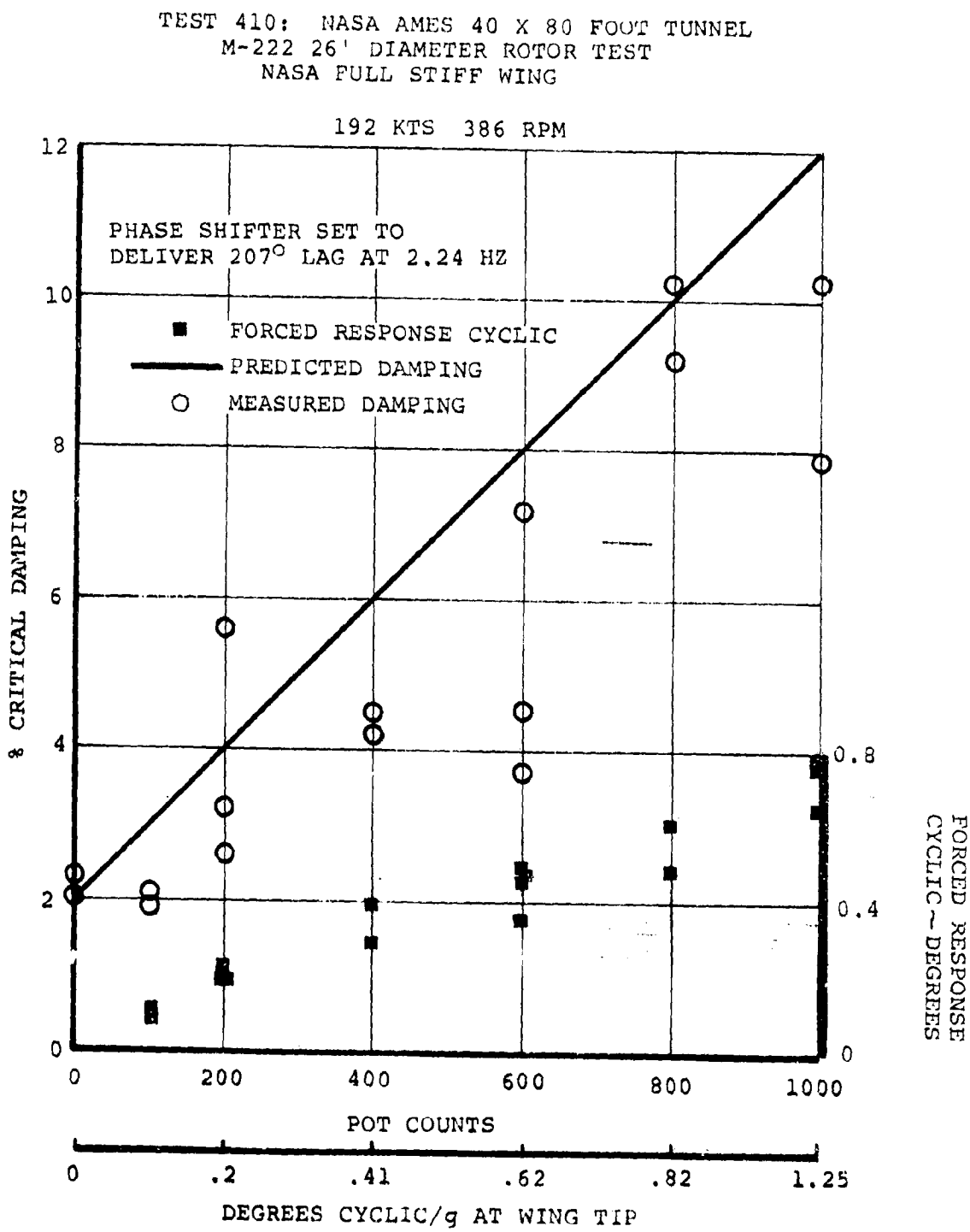

FIGURE 8.59. DAMPING VERSUS HIGH RATE SYSTEM GAIN AT 192 KNOTS, 386 RPM

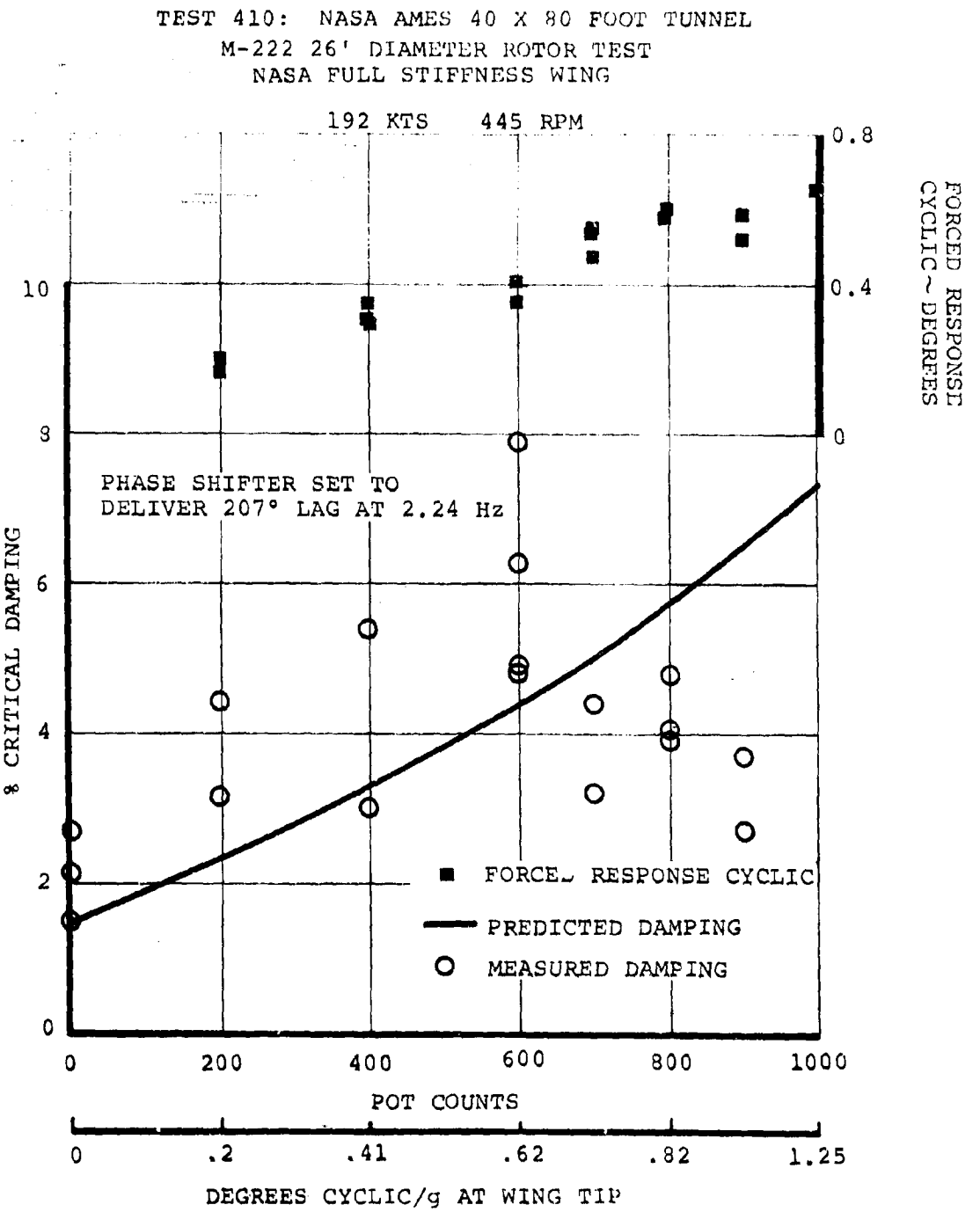

FIGURE 8.60. DAMPING VERSUS HIGH RATE SYSTEM GAIN AT 192 KNOTS, 445 RPM

TEST 410: NASA AMES 40 X 80 FOOT TUNNEL
M-222 26' DIAMETER ROTOR TEST
NASA FULL STIFF WING

100 KTS 386 RPM
RUN 45

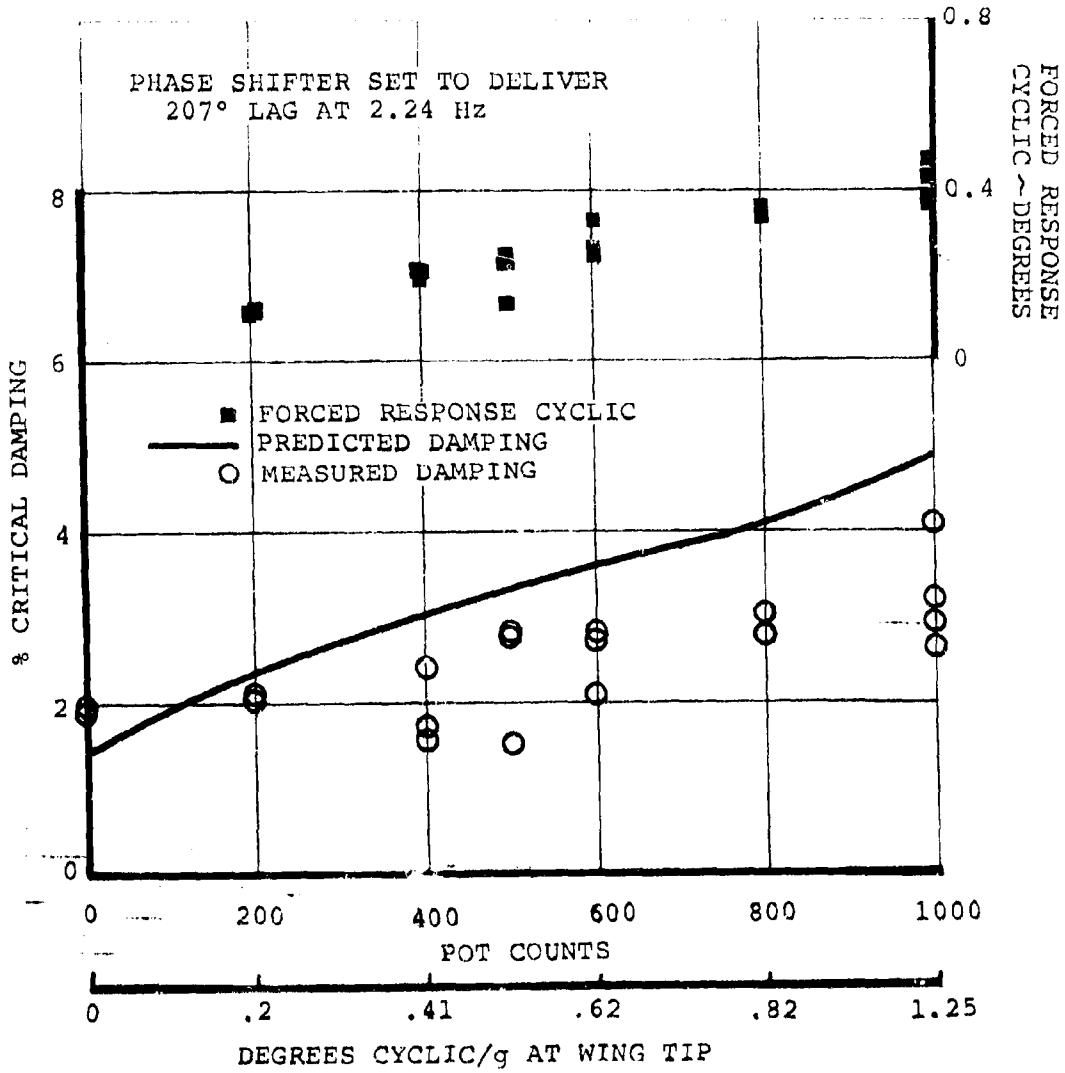

FIGURE 8.61. DAMPING VERSUS HIGH RATE SYSTEM GAIN AT 100 KNOTS, 386 RPM

TEST 410: NASA AMES 40 X 80 FOOT TUNNEL
M-222 26' DIAMETER ROTOR TEST
NASA FULL STIFF WING

100 KTS 445 RPM

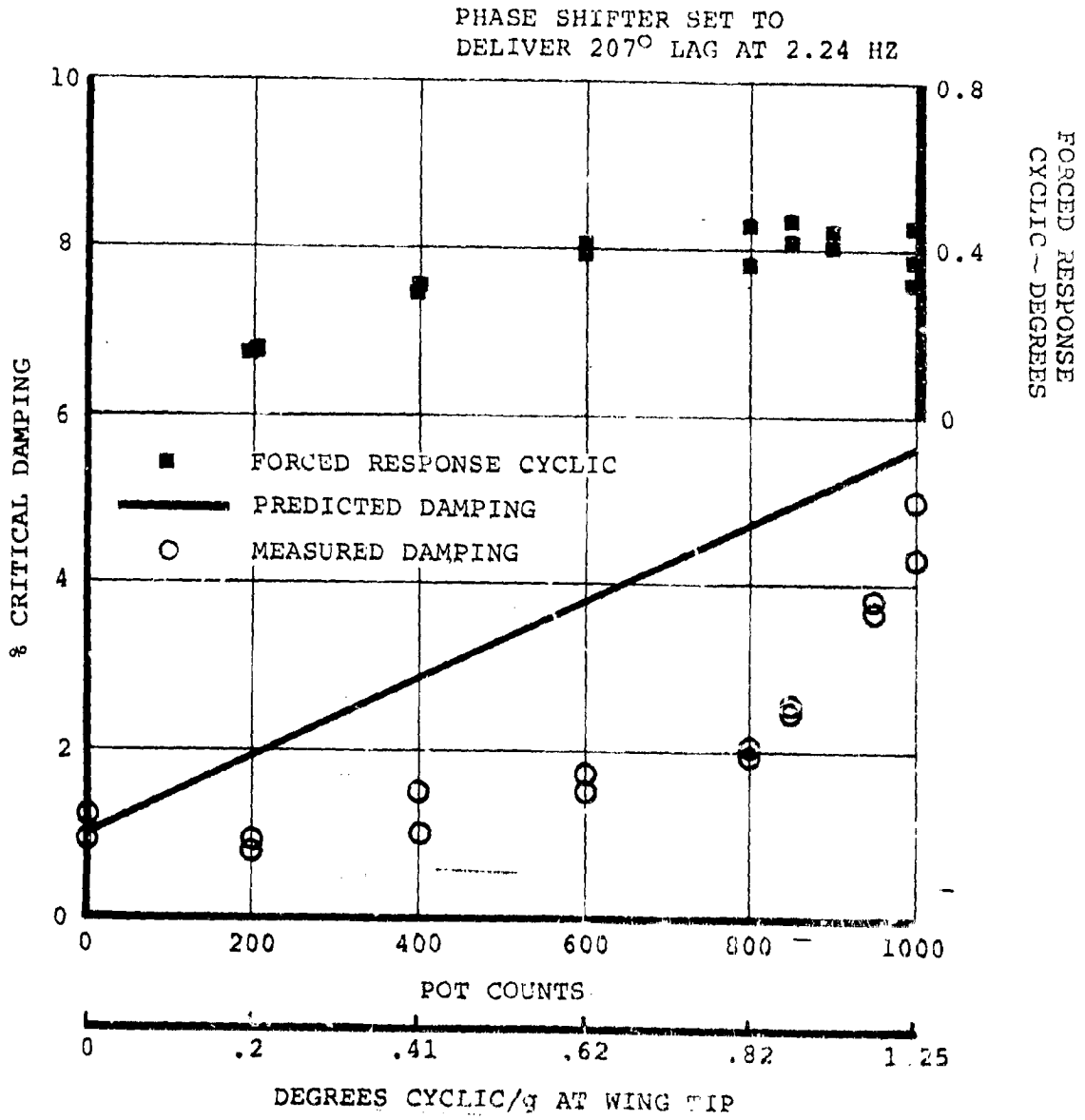

FIGURE 8.62. DAMPING VERSUS HIGH RATE SYSTEM GAIN AT 100 KTS, 445 RPM

8.3 Combined Systems

The last objective of the feedback control tests was to determine if the two types of feedback tested were compatible. Open loop frequency response experiments of the high rate loop were run at 100 and 192 knots at 386 RPM with the low rate loops closed. Figure 8.63 shows the 192 knot case with the low rate loop gains set at $G_p = 200$, $G_y = 300$. The effect of the low rate loops can be determined by comparison of this data with Figure 8.55 of Section 8.2. The phase curve is essentially unchanged; however, the gain has increased and gives zero dB crossings at higher and lower frequencies. The result is slightly reduced phase margins in the case of both systems combined. The low pass filter in the low rate loops is there to attenuate this effect and as shown in Figure 8.63 provides the combined system with adequate phase margin for stability. The open loop data of Figure 8.64 is at 100 knots and 386 RPM and show a similar effect though the phase margins are large.

The effectiveness of the high rate loop as a means of increasing the modal damping of the air resonance mode is unaffected by the low rate loop closures. The damping data obtained at 192 knots and 100 knots are shown in Figures 8.65 and 8.66 and show increasing modal damping as gain is increased at rates comparable to those measured with the high rate loop only operating.

Figures 8.67 and 8.68 show the effect of a simulated gust at 0.1 Hz with and without the feedback systems operating. The excitation was in the form of a 1-cosine cyclic input. This was achieved by introducing a sine wave signal ± 1° cyclic with a DC signal superimposed equivalent to 1° cyclic. This signal was switched in and out at the beginning and end of one cycle. The data shown are the increments in the various parameters with respect to their steady state values due to this disturbance.

The wing tip yawing moment indicates a large reduction in response due to feedback. The wing tip pitch response is small but the feedback on case is if anything slightly worse than the feedback off case. Wing tip lift (normal force) indicates a small reduction in peak amplitude due to the feedback system.

The blade loads data are shown in Figure 8.68. The alternating flap bending data are unaffected by the disturbance for both cases. The chord bending data shown are reduced by about a factor of two.

In conclusion both high and low rate systems have been made to fulfill the test objectives and can operate together without significant cross coupling between systems.

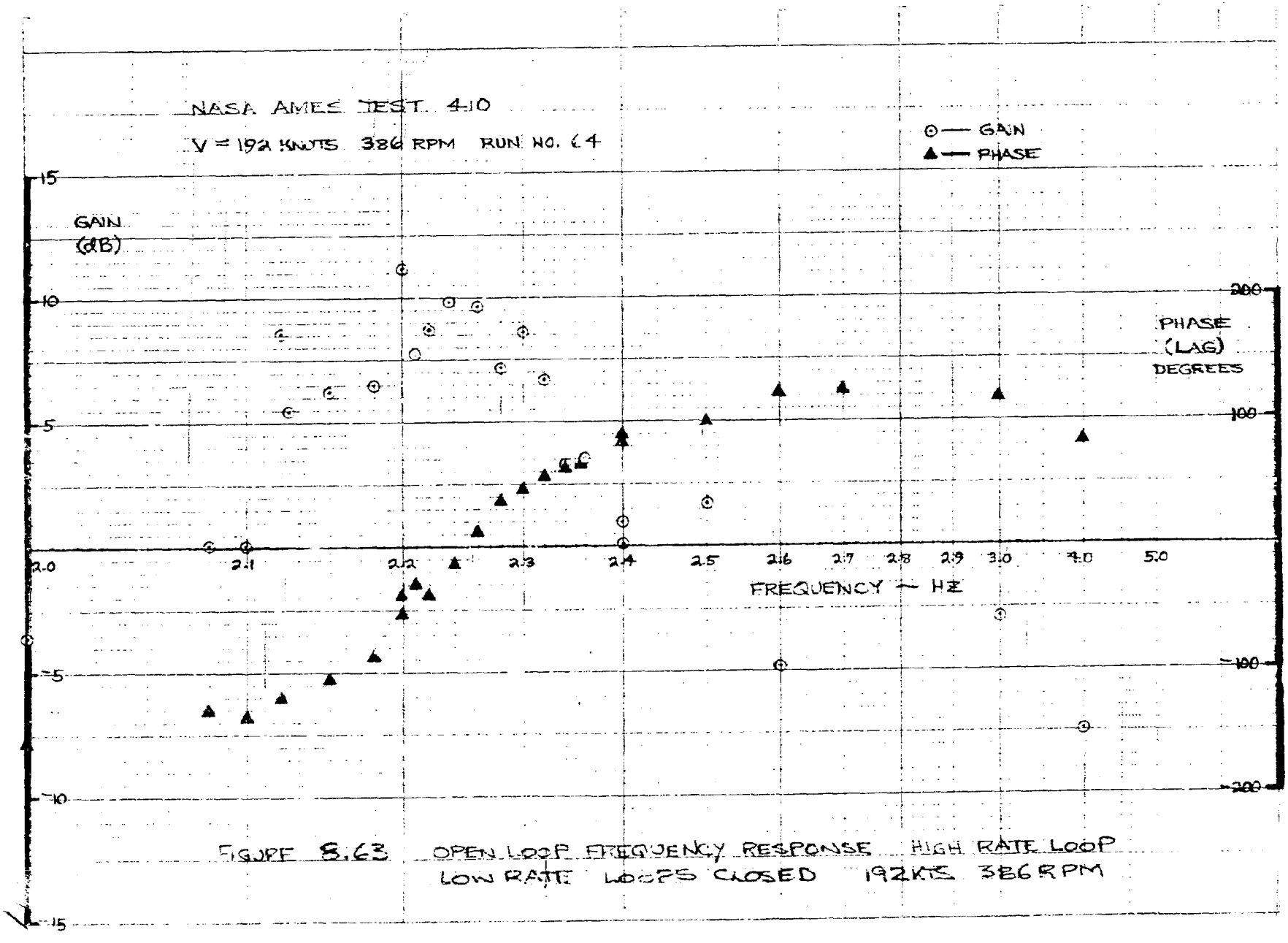

FIGURE 5.63 OPEN LOOP FREQUENCY RESPONSE HIGH RATE LOOP
LOW RATE LOOPS CLOSED 192KTS 386RPM

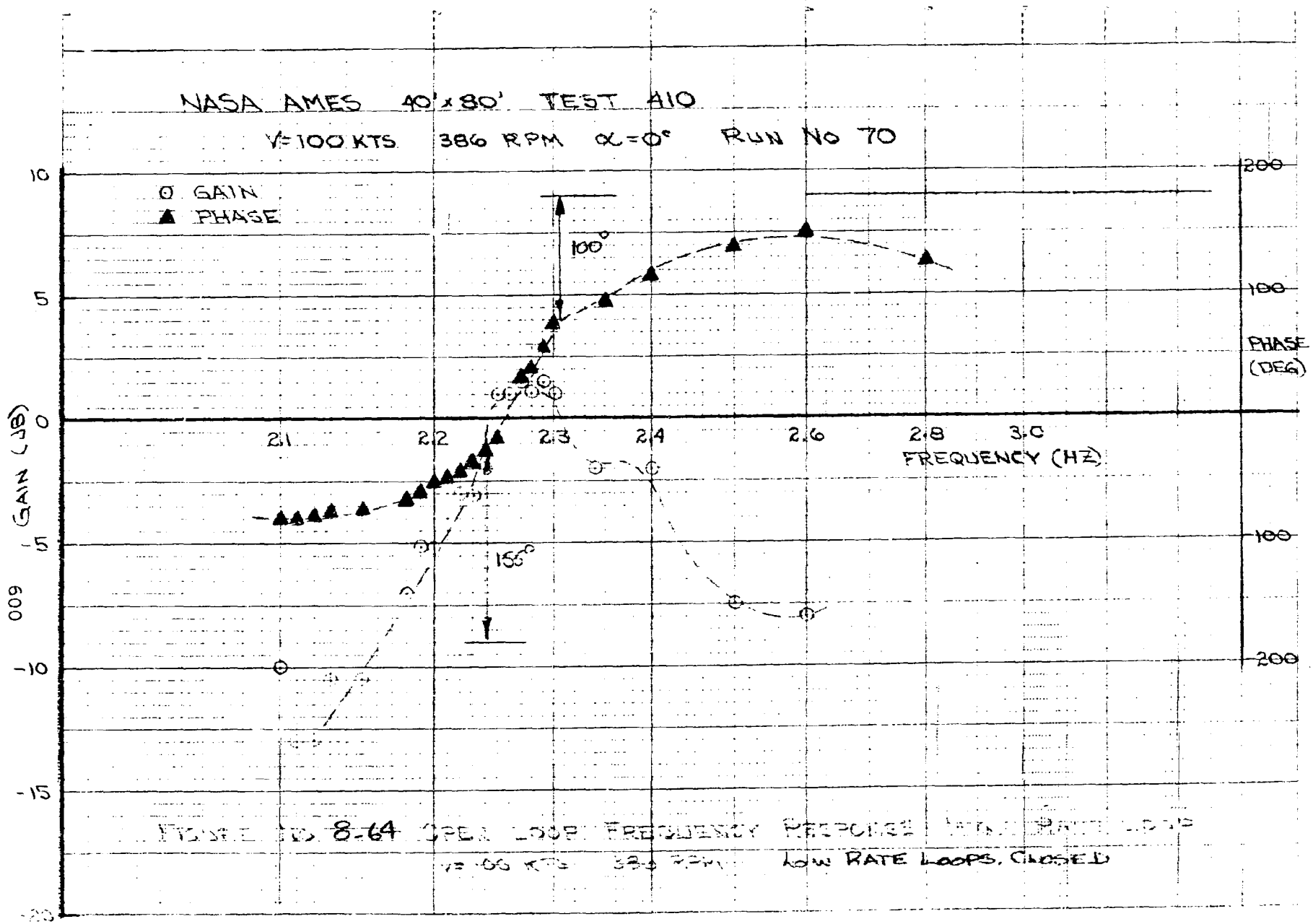
NASA AMES 40'x80' TEST 410
V=100 KTS 386 RPM α=0° RUN NO 70
GAIN
PHASE
100°
155°
10
5
0
-5
-10
-15
-20
200
100
-100
-200
PHASE (DEG)
GAIN (DB)
2.1
2.2
2.3
2.4
2.6
2.8
3.0
FREQUENCY (HZ)
8-64
Low RATE LOOPS, CLOSED

TEST 410: NASA AMES 40 X 80 FOOT TUNNEL
M-222 26' DIAMETER ROTOR TEST
NASA FULL STIFF WING
RUN 65
192 KTS 386 RPM
HIGH & LOW RATE LOOPS CLOSED
LOW RATE G_Y = 300
G_P = 204

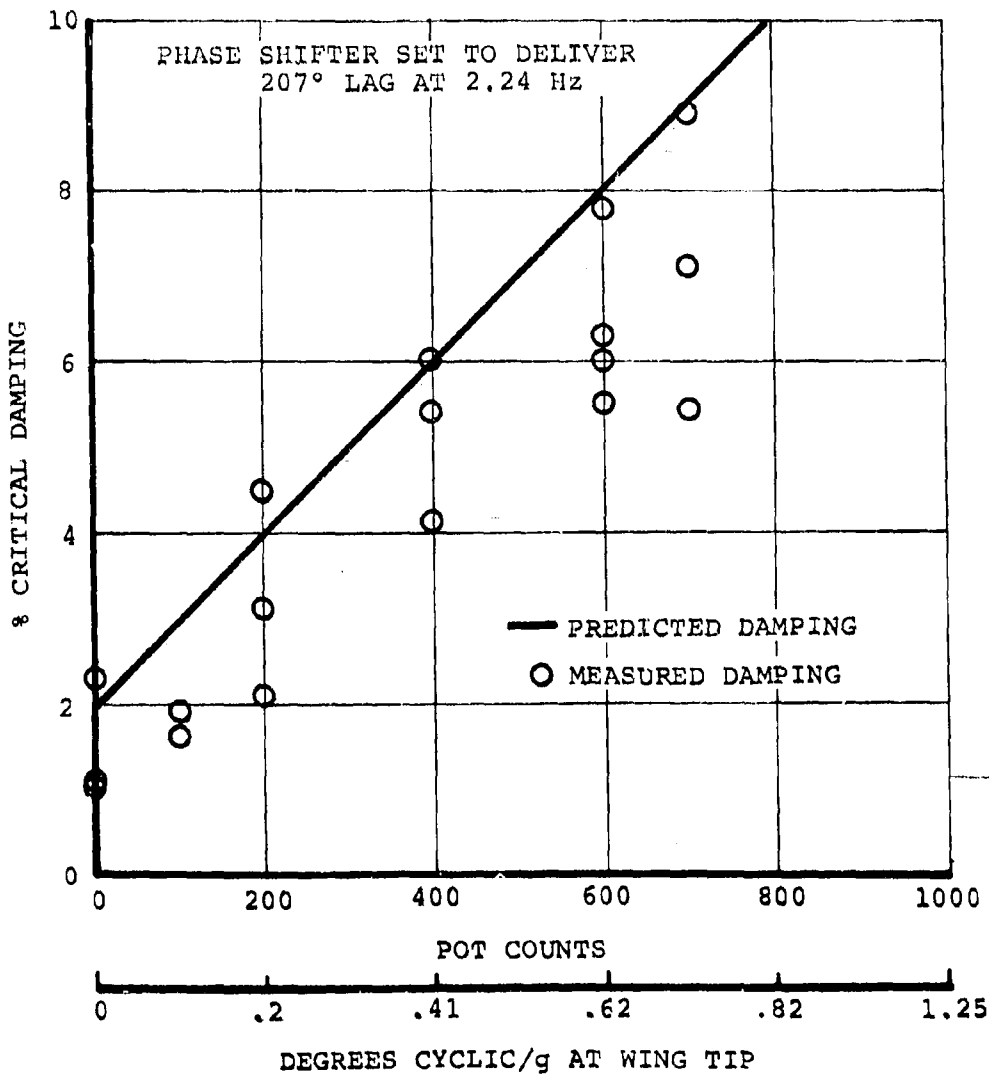

FIGURE 8.65. DAMPING VERSUS HIGH RATE SYSTEM GAIN AT 192 KNOTS, 386 RPM, WITH LOW RATE SYSTEM ACTIVE

TEST 410 : NASA AMES 40 X 80 FOOT TUNNEL
M-222 26 FT. DIAMETER ROTOR TEST
NASA FULL STIFF WING

100 KNOTS 386 RPM
RUN 70

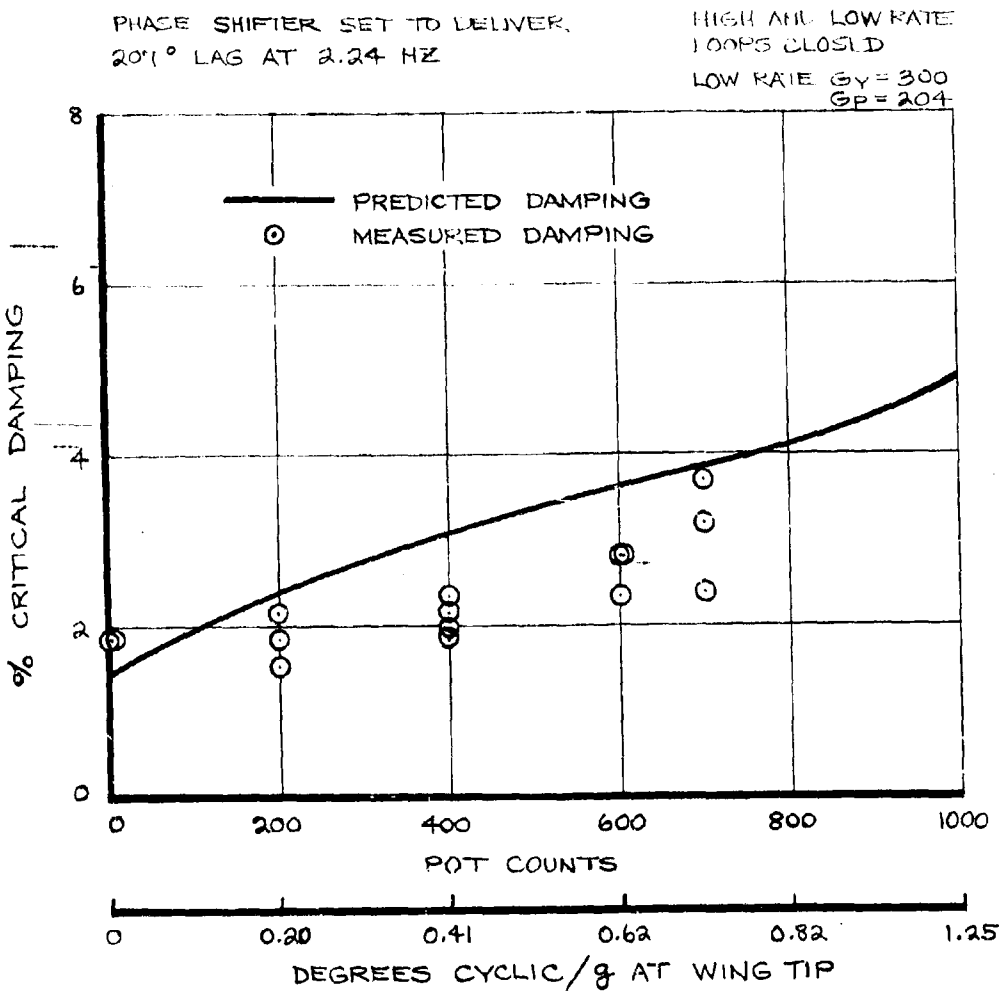

FIGURE 8.66 DAMPING VERSUS HIGH RATE SYSTEM GAIN AT 100 KNOTS, 386 RPM

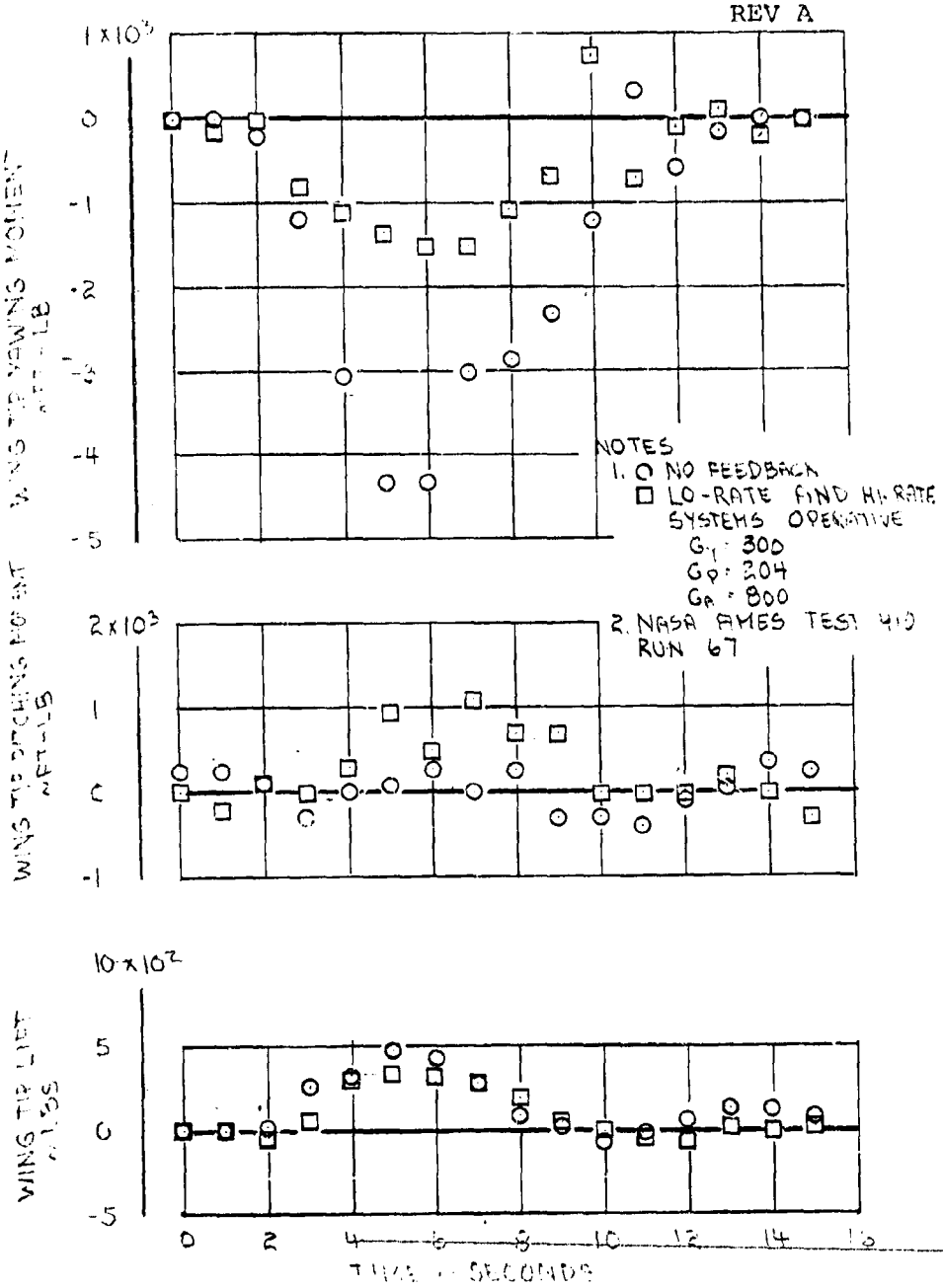

FIGURE 8.67 WING TIP FORCE AND MOMENT RESPONSES VS GUSTS TO .1 HZ SINUSOIDAL GUST

NOTES
1. ○ NO FEEDBACK
□ LO-RATE AND HI-RATE SYSTEMS OPERATIVE
G_v = 300
G_p = 204
$G_{...}$ = 800
2. NASA AMES TEST 40 RUN 67

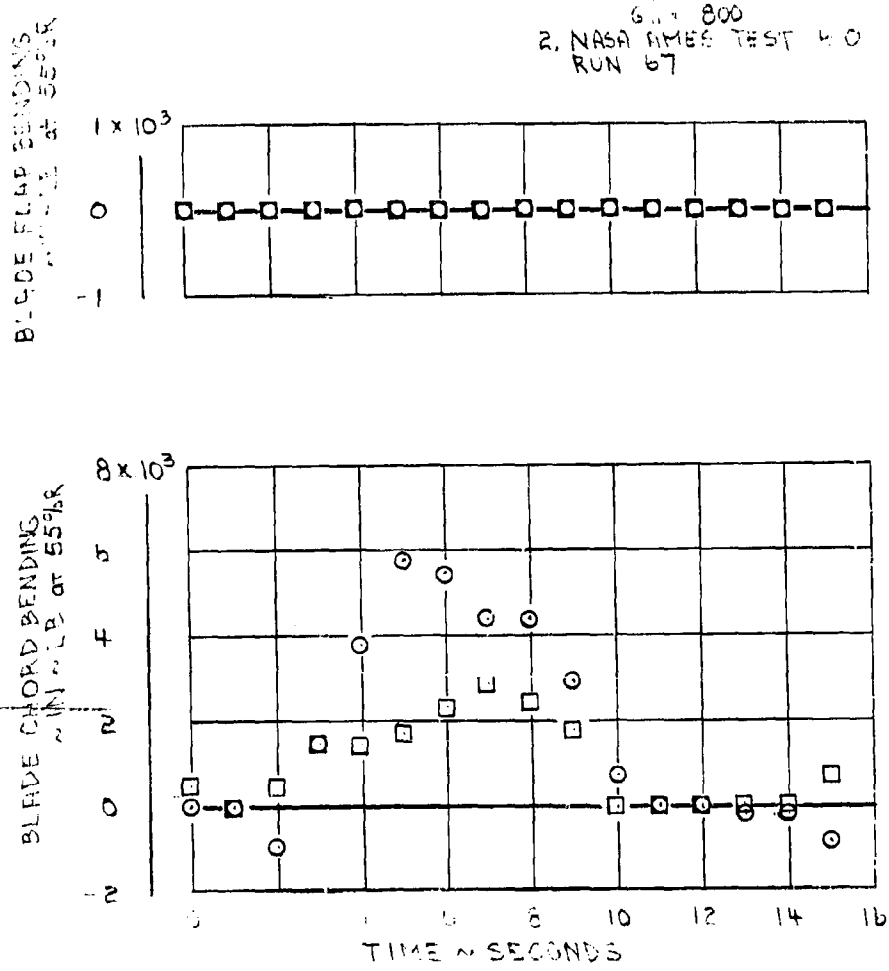

FIGURE 8.68 BLADE BENDING MOMENT TRANSIENT RESPONSE TO .1 HZ [illegible]

9.0 [illegible]

9.0 VIBRATION

9.1 Vibration

The high frequency vibration levels on the powered test stand did not at any time limit the testing. Two accelerometers were mounted just aft of the swashplate in the nacelle and two more on the powered test rig just aft of the trunnion. These stations were 124" apart. Figure 9.1 summarizes the linear 3/rev accelerations measured throughout the powered test. As expected the nacelle accelerometers indicate the highest vibration levels. These data have been converted to pitch and yaw 3/rev accelerations and are shown in Figure 9.2. These vibration levels are quite low. The data are not directly applicable to the flight vehicle since the dynamics of the test stand are reflected in the data. The data are a reasonable basis for comparison taken with other dynamic systems tested on the same rig.

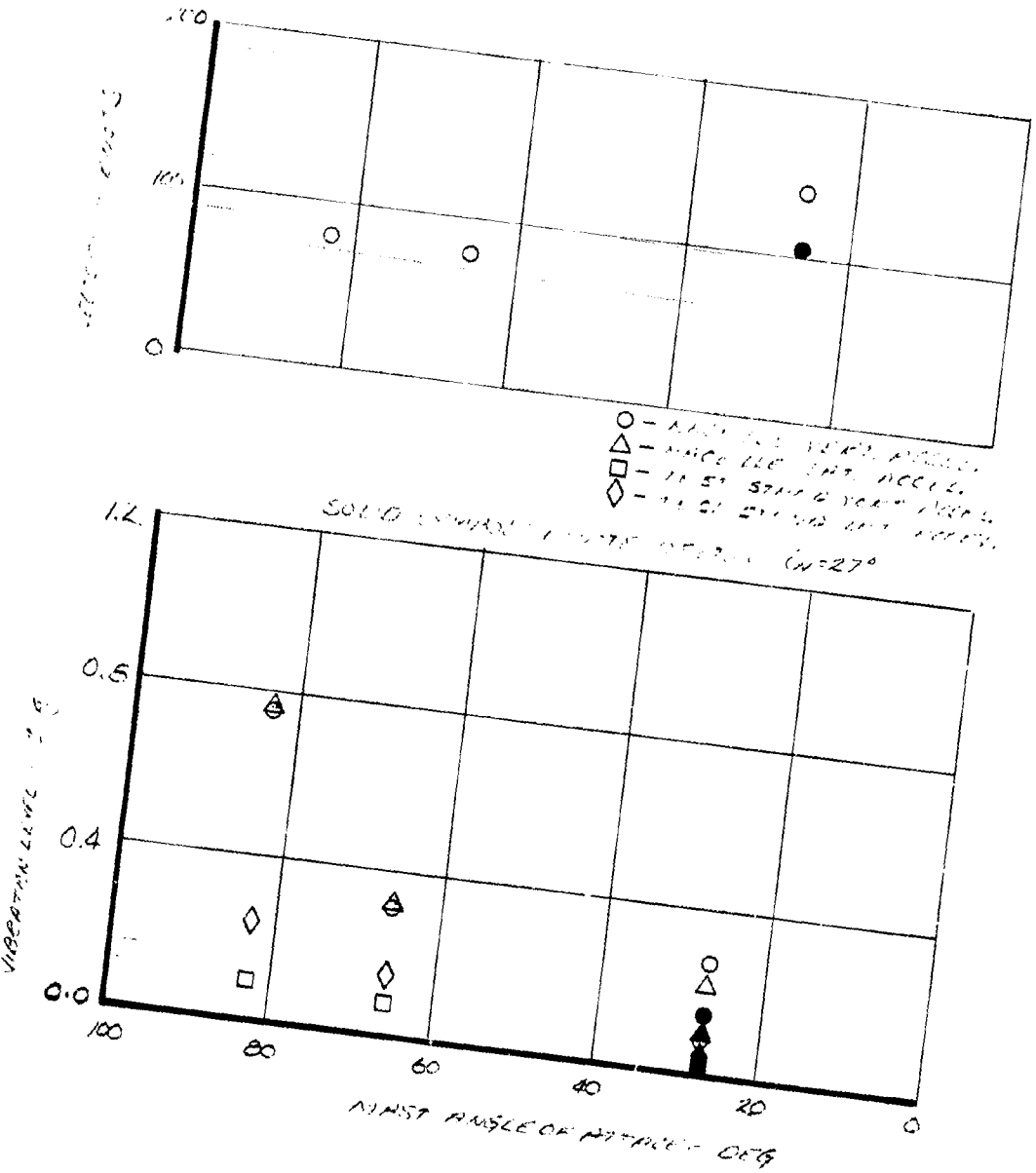

FIGURE 9-1 LINEAR 3/REV ACCELERATIONS IN TRANSITION
TEST 416

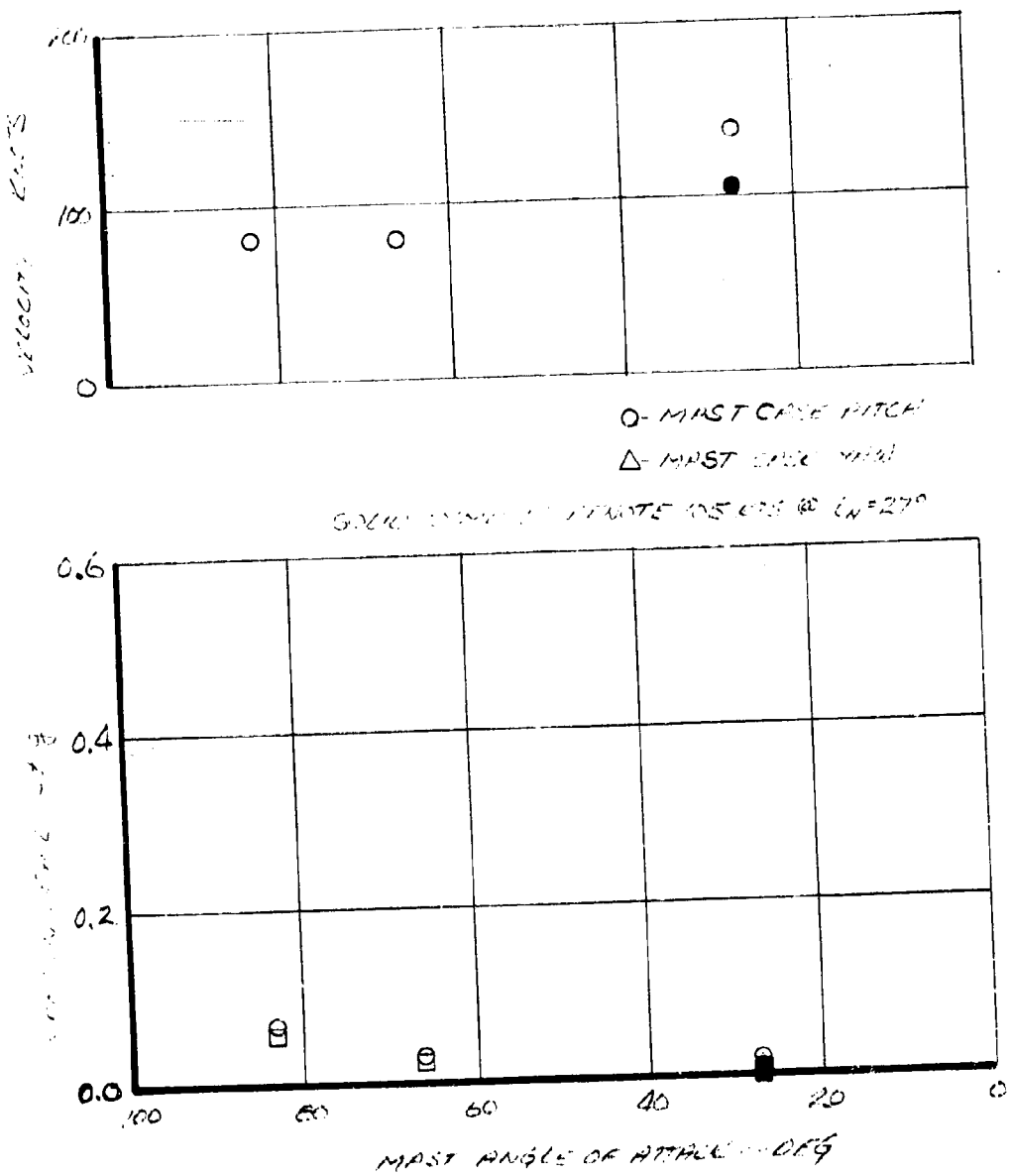

FIGURE 9.2 3/REV PITCH AND YAW ACCELERATIONS MEASURED IN TRANSITION TEST 416

10.0 CONCLUSIONS AND RECOMMENDATIONS

10.0 CONCLUSIONS AND RECOMMENDATIONS

Experimental data have been gathered to meet the objectives of the two test programs described in this document.

The dynamics data reported in Section 3 shows that for both dynamic wing test stands the experimental aeroelastic data for both air resonance and whirl flutter show excellent agreement with the predicted behavior up to the advance ratio equivalence of 400 knots.

Rotor loads (Section 4) have been measured in hover, transition and cruise up to the maximum capability of the tunnel. Preliminary correlation indicates that the loads methodology overpredicts in hover and underpredicts in cruise. Applying the measured loads data to the Model 222 tilt rotor aircraft, the predicted fatigue life is 5080 hours when no load alleviation system is used and increases to16890 hours with the use of load alleviation. See Appendix 5.

The steady pitch link loads (Section 5) agree closely with prediction. The alternating loads are less than endurance limit loads throughout the flight envelope except for one test condition in transition which was done at the anticipated boundary of the transition corridor.

Stability and control data (Section 6) have been obtained over a wide range of conditions sufficient to provide design verification and correlation.

Performance data (Section 7) correlates well with predictions. The cruise performance data exceeds the predicted levels.

Low rate feedback was used to provide load alleviation (Section 8) and operated well up to electronic filter saturation. Some difficulties were encountered in this series of tests. Some of these could have been avoided if more detailed pretest checks had been made. Procedures for system check out must be established and rigidly adhered to.

High rate feedback controls were used to augment the damping of the wing vertical bending mode. The damping was increased in some cases by 500%.

Further research in the following areas would prove valuable to the development of the tilt rotor concept:

1. Autorotation testing and entry into autorotation
2. Low rate feedback testing using the aircraft components
3. Analytical studies for correlation with the above

REFERENCES

1. "LTTAS, Light Tactical Transport Aircraft System, Volume I - Summary", Boeing Document D8-23571, July 1969.
2. "Medium Assault Transport Study, 1975 to 1980 Time Period, Volume I - Technical Analysis", Boeing Document ADR-7001, March 1970.
3. "Configuration Design Analysis of a Prop/Rotor Aircraft", Richardson, D. A. and Liiva, J., AFFDL-TR-70-44, April 1970.
4. "Detail Design of Critical Components for a Prop/Rotor Aircraft", Richardson, D. A. and Liiva, J., AFFDL-TR-70-124, July 1970.
5. "Design Studies and Model Tests of the Stowed Tilt Rotor Concept", Volume I - Parametric Design Studies; Volume II - Component Design Studies, Fry, B.L., et al, AFFDL-TR-71-62, Volumes I and II.
6. "Feasibility of V/STOL Concepts for Short Haul Transport Aircraft", Fry, B. L. and Zabinsky, J. M., NASA CR-743, September 1968.
7. "Investigation of the Performance of Low Disc Loading Tilt Rotors in Hovering and Cruise Flights", Volume I Analysis and Results, Boeing Document D160-10013-1.
8. "Investigation of the Performance of Low Disc Loading Tilt Rotors in Hovering and Cruise Flights", Volume II Wind Tunnel Program Details, Boeing Document D160-10013-2.

9. "Wind Tunnel Test of the Conversion Process of a Folding Tilt Rotor Aircraft Using a Semispan Unpowered Model", J. Magee and R. Taylor, Technical Report AFFDL-TR-72-62, Volume IV.

10. "Wind Tunnel Test of a Powered Tilt Rotor Performance Model, J. Magee, et al, Technical Report AFFDL-TR-72-62, Volume V.

11. "Wind Tunnel Test of a Powered Tilt Rotor Dynamic Model on a Simulated Free Flight Suspension System", Technical Report AFFDL-TR-72-62, Volume VI. J. Tomassoni, et al.

12. "Wind Tunnel Test of the Aerodynamics and Dynamics of Rotor Spinup and Stopping and Folding on a Semispan Folding Tilt Rotor Model", D. VanWagensveld, et al, Technical Report AFFDL-TR-71-62, Volume VII.

13. "Model 222 Tilt Rotor Aircraft Rotor Blade Structural Analysis", G. Miliziano, F. Ochs, R. Sandford, Boeing Document D222-10009-1.

14. "Assembly, Functional Test and Installation Manual for 26-Foot Diameter Rotor Test Stand", N. Weir, Boeing Document D222-10004-1, NASA Contract NAS2-6505.

15. "Test Procedures and Pretest Predictions for 26-Foot Diameter M-222 Powered Wind Tunnel Test, J. Magee, B. Fry, Boeing Document D222-10057-1, NASA Contract NAS2-6505.

16. V/STOL Dynamics and Aeroelastic Rotor-Airframe Technology", H. Alexander, et al, Technical Report AFFDL-TR-72-40, Volume II.

17. "Test Procedures and Pretest Predictions for 26-Foot Diameter M-222 Unpowered Dyanmic Wind Tunnel Test", J. Magee, D. Ekquist, Boeing Document D222-10019-1, NASA Contract NAS2-6505.

18. "Model 222 - Stress Analysis of the 26-Foot Diameter Rotor Wind Tunnel Test Stand", Boeing Document D222-10014-1, NASA Contract NAS2-6505. Y. Badrinath.

19. "M-222 26-Foot Diameter Wind Tunnel Testing System Safety Analysis", Y. Badrinath, et al, Boeing Document D222-10020-1, NASA Contract NAS2-6505.

20. "A Summary of Wind Tunnel Research on Tilt Rotors from Hover to Cruise Flight", W. L. Cook, P. Poisson-Quinton, presented at AGARD Fluid Dynamics Panel Specialists' meeting on "The Aerodynamics of Rotary Wings", Marseille, France, September 1972.

21. "Study of V/STOL Tilt Rotor Research Aircraft Program (Phase I)" Volumes 1 through 13, January 1973, Boeing Document D222-10050-1/13.

22. "Hingeless Rotor - Experimental Frequency Response and Dynamic Characteristics with Hub Moment Feedback Controls", W. A. Kuczynski, D. L. Sharpe, G. J. Sissingh, Preprint No. 612, Presented at Annual National Forum of the American Helicopter Society, May 1972.

23. "Feedback Control Tests on a Windmilling 2.81-Foot Diameter Soft In-Plane Hingeless Tilt Rotor in the Cruise Mode", Boeing Document D222-10047-1, NASA Contract NAS2-6505.

24. "V/STOL Tilt Rotor Aircraft Study, Tilt Rotor Feedback Control Technology", H. Alexander, W. Eason, et al, Boeing Document D222 10060-3, NASA Contract NAS2-6598.

25. "1/9.244 Scale Dynamic Semispan Model 222, Phase I, Wind Tunnel Test Windmilling", J. Magee, F. McHugh, et al, Boeing Document D222-10011-1.

26. "Pretest Calculations of Open Loop Frequency Response and Stability of High Rate and Low Rate Swashplate Feedback Systems of Model 222 26-Foot Rotor Test", H. Alexander, J. Morris, R. Spittle, Boeing Document D160-10019-1, NASA Contract NAS2-6505.

27. "V/STOL Tilt Rotor Aircraft Study - Mathematical Model For a Real Time Simulation of a Tilt-Rotor Aircraft", H. Rosenstein, M. A. McVeigh and P. A. Mollenkof. Boeing Document D222-10061 (NASA-CR-114601).

ANNEXURE 1

APPENDIX 1 TEST RUN LOG TEST 410

NASA Ames 40' X 80' Wind Tunnel

RUN NO.	CONFIGURATION	TYPE OF RUN	WT. TARE RUN	α_{TW} deg	$\theta_{.75}$ deg	A_1 deg	B_1 deg	a_N deg	V_T KTS	P_T IN HG	T_T °F		WIND & TIME HRS	DATE TIME
1	FULL STIFF WING NO BLADES			VARY	—	—	—	0	VARY	30.28	86/116			8/7/72

RUN NO. 1 BALANCE UNLOCKED

DATA PT.	1	2	3	4	5	6	7	8	9	10	11	12	13	14	15	16	17	18	19	20	21	22	23	24	25
α_w ~ deg.	0	-6	-4	-2	0	2	4	6	8	10	12	14	16	18	20	0	-6	-4	-2	0	2	4	6	8	10
V_T ~ KTS.	100	100	100	100	100	100	100	100	100	100	100	100	100	100	100	180	180	180	180	180	180	180	180	180	180
SHAKER FREQ CTS	—	—	—	—	—	—	—	—	—	—	—	—	—	—	—	—	—	—	—	—	—	—	—	—	—
SHAKER AMPT ~ VOLT	—	—	—	—	—	—	—	—	—	—	—	—	—	—	—	—	—	—	—	—	—	—	—	—	—

DATA PT.	26	27	28	29	30	31	32	33	34
α_w ~ deg.	12	14	16	0	0	0	0	0	0
V_T ~ KTS.	180	180	180	100	100	100	140	140	140
SHAKER FREQ. CTS	—	—	—	2	32	79	1	32	*
SHAKER AMPT. ~ VOLTS	—	—	—	5.77	2.77	5.79	8.00	2.74	*

NOTES:

WING TIP N.F. BANDEDGE FOR DATA PT. 28.

* SHAKER INOPERATIVE FOR DATA PT. 34 - DOWN FOR REPAIRS

26 FOOT DIAMETER M 222 ROTOR TEST

NASA 40X80 FT. TEST 410

FORM 4941D (1-70)

SHEET 615

NUMBER D222-10059-1
REV LTR

RUN NO.	CONFIGURATION	TYPE OF RUN	WT. TARE RUN	α_w deg	$\theta_{.75}$ deg	A, deg	B, deg	α_N deg	V_T KTS	P_T IN Hg	T_T °F		WIND ON TIME HRS	DATE TIME
2	Full Stiff Wing, No Blades			0	–	–	–	0	VARY	30.05	85/101			8/7/72
3	Full Stiff Wing, Blades On			0	Vary	0	0	0	50	30.06	81/83		1.50	8/10/72
4	Full Stiff Wing, Blades on	TRACK & BAL		Vary	Vary	0	0	0	50	30.05	83/87		.832	

PREP. | CHK. | APPR. | REVISED | DATE

FORM 4-8710-1 701

26 FOOT DIAMETER M-222 ROTOR TEST

Run No 2 Balanced Locked

Data Pt.	1	2	3	4	5	6	7	8	9	10	11	12
α_w ~deg	0	0	0	0	0	0	0	0	0	0	0	0
V_T - KTS	100	100	100	100	140	180	180	194	194	140	140	140
SHAKER FREQ CTS	2	4	32	78	1	32	78	1	78	1	78	37
SHAKER AMPT Volts	4.5	2.82	2.81	9.99	4.99	2.82	3.48	1.03	4.99	5.50	2.94	2.94

RUN NO 3 Balance Locked

Data Pt.	1	2	3	4	5	6	7	8	9	10	11	12	13
$\theta_{.75}$ (deg)	59	49.9	41.1	35.5	30.7	26.8	23.7	21.2	18.9	17.5	16.0	14.5	13.7
RPM	50	76	100	124	149	175	200	226	266	295	301	326	346
RUN NO	3	3	3	3	3	3	3	3	3	3	3	3	3
d_w (deg)	0	0	0	0	0	0	0	0	0	0	0	0	0

RUN NO. 4 BALANCE LOCKED

Data Pt.	1	2	3	4	5	6	7	8	9	10	11
$\theta_{.75}$ (deg)	59.0	55.2	52.0	47.8	44.2	41.8	38.2	36.6	34.4	32.1	30.7
RPM	51	60	70	80	90	99	112	120	130	142	150
RUN NO	4	4	4	4	4	4	4	4	4	4	4
d_w (deg)	0	0	0	0	0	0	0	0	0	0	0

Data Pt.	12	13	14	15	16	17	18	19	20	21	22	23	24	25	26	27	28	29	30	31	32	33	34
$\theta_{.75}$ (deg)	28.9	27.5	25.8	24.4	22.5	22.0	19.9	18.3	17.3	16.9	16.4	15.5	13.6	13.6	13.6	13.6	13.6	13.6	13.6	13.6	13.6	13.7	13.7
RPM	160	169	182	193	207	217	242	262	278	263	293	308	343	348	346	347	345	344	345	346	346	345	347
RUN No.	4	4	4	4	4	4	4	4	4	4	4	4	4	4	4	4	4	4	4	4	4	4	4
d_w (deg)	0	0	0	0	0	0	0	0	0	0	0	0	0	-1	-2	-3	-4	-5	-6	+1	+2	+3	0

NASA 40x80 TEST 410

NUMBER REV LTR D222-10059-1

SHEET 516

THE BOEING COMPANY

NUMBER D222-10059-1
REV LTR

RUN NO.	CONFIGURATION	TYPE OF RUN	WT. TARE RUN	DATE	TIME

Run 4 Blade Track good at 346 RPM (while blade #2 only slightly high) no unbalance noted i.e. with loadings indicated good balance.

PREP.		REVISED	DATE
CHK.			
APPR			

26 FOOT DIAMETER
M-222 ROTOR TEST

NASA 40 X 80
TEST 410

FORM 435-0 (3-70)

RUN NO.	CONFIGURATION	TYPE OF RUN	WT. TARE RUN	α_w deg	$\theta_{.75}$ deg	A_1 deg	B_1 deg	α_N deg	V_T KTS	P_T IN Hg	T_T °F		WIND ON TIME HRS.	DATE TIME
5	Full Stiff Wing, Blades On			0	VARY	0	0	0	50	30.08	73/73			8/10/72
6				0	VARY	0	0	0	50	30.14	81/84		1.00	8/11/72
7				0	VARY	0	0	0	50	30.16	85		.50	8/11/72
8				0	VARY	0	0	0	VARY	30.13	86/89		.93	8/11/72

FORM 4317 (1 70)

CHKR. | CHK. | APPR. | REVISED LATE

M-222 ROTOR TEST — 26 FOOT DIAMETER

Run 5 Data Points 1-9 $\theta_{.75}$ = 14.7 ~RPM = 320
Data Points 10-13 $\theta_{.75}$ = 14.0 ~RPM = 330

SHAKER FREQ CPS															0	2.3	0	2.3	0	2.3	0	2.3	11	9.6
ROTOR RPM	320	320	320	320	320	320	320	320	320	330	330	330	330		339	339	355	355	370	370	384	380	380	380
θ_{75}	14.7	14.7	14.7	14.7	14.7	14.7	14.7	14.7	14.7	14	14	14	14		14.3	14.3	13.6	13.6	12.7	12.7	12.3	12.2	12.2	12.2
Test Point	1	2	3	4	5	6	7	8	9	10	11	12	13		1	2	3	4	5	6	7	8	1	2
RUN NO.	5	5	5	5	5	5	5	5	5	5	5	5	5		6	6	6	6	6	6	6	6	7	7

RUN 6 SOME EVIDENCE OF FILLER BETWEEN BLADE CUFF AND BLADE COMING LOOSE.

SHAKER FREQ CPS	10.0	10.7	11.0	11.4	2.3	2.3	2.3		2.3	2.3	2.3	2.3	2.3	2.3	2.3	2.3	2.3							
ROTOR RPM	380	380	380	380	390	407	412		409	420	430	439	448	457	471	480	485							
θ_{75}	12.2	12.2	12.2	12.2	11.7	10.8	10.6		13.9	13.2	12.7	12.4	11.8	11.5	11.0	11.5	11.3							
Test Point	3	4	5	6	7	8	9		1	2	3	4	5	6	7	9	9							
RUN NO.	7	7	7	7	7	7	7		8	8	8	8	8	8	8	8	8							
V_T KTS									60	60	60	60	60	60	60	63	63							

NASA 40X80 TEST 41C

SHEET 618

NUMBER REV LTR D222-10059-1

THE **BOEING** COMPANY

NUMBER D222-10059-1
REV LTR

RUN NO.	CONFIGURATION	TYPE OF RUN	WT. TARE RUN	α_w deg	$\theta_{.75}$ deg	A_1 deg	B_1 deg	α_N deg	V_T KTS	P_T in Hg	T_T °F		Wind on Time HRS	DATE	TIME
9	Full Stiff Wing, Blades On			0	Vary	0	0	0	100	30.12	81		1.13		
10	Full Stiff Wing, Blades On			0	Vary	Vary	Vary	0	100	30.12	81		2		

Run No.	9	9	9	9	9	9	9	9	9	9	9	9	9	9	9	9	9	9	9	9	9	9	9		
Data Pt.	1	2	3	4	5	6	7	8	9	10	11	12	13	14	15	16	17	18	19	20	21	22	23		
$\theta_{.75}$	59	55	51	47.9	44.6	41.7	38.6	36.3	34.4	32.4	30.8	29.2	29.2	27.8	28.8	27.8	27.8	27.9	26.2	26.2	26.2	26.2	26.2		
SHAKER FREQ CTS	—	—	—	—	—	—	—	—	—	—	—	—	—	—	2.3	2.3	11	11	—	2.3	2.3	11	2.3		
SHAKER AMP Volts	—	—	—	—	—	—	—	—	—	—	—	—	—	—	4.99	4.99	4.99	4.99	—	4.99	4.99	4.99	4.99		
RPM	105	120	141	160	180	200	221	241	258	280	300	319	319	339	339	339	339	339	361	362	362	360	360		
Run No.	10	10	10	10	10	10	10	10	10	10	10	10	10	10	10	10	10	10	10	10	10	10	10	10	10
Data Pt.	1	2	3	4	5	6	7	8	9	10	11	12	13	14	15	16	17	18	19	20	21	22	23	24	25
$\theta_{.75}$	26.2	25.0	24.8	24.9	24.9	24.8	24.0	24.0	24.0	24.0	24.0	24.0	22.9	22.9	22.9	23	23	22.5	22.5	22.5	22.6	21.9	22	22	22
SHAKER FREQ	—	—	—	2.3	2.3	2.3	—	2.3	2.3	2.3	11	11	—	2.3	2.3	2.3	11	—	2.3	2.3	2.3	—	2.3	2.3	2.3
SHAKER AMP Volts	—	—	—	5.0	5.0	5.0	—	5.0	5.0	5.0	5.0	5.0	—	5.0	6.0	5.0	5.0	—	6.51	6.51	6.51	—	6.51	6.51	6.51
RPM	360	379	386	384	383	385	400	400	399	420	400	400	421	422	420	418	420	429	429	427	429	440	441	439	441
Lat Cyc.	0	0	0	0	0	0	0	0	0	0	0	0	0	0	0	0	0	0	0	0	0	0	0	0	0
Long Cyc.	0	0	0	0	0	0	0	0	0	0	0	0	0	0	0	0	0	0	0	0	0	0	0	0	0

PREP.			REVISED	DATE
CHK.				
APPR.				

26 FOOT DIAMETER

M-222 ROTOR TEST

NASA 40X80 TEST 410

FORM 49510 (1/70)

THE BOEING COMPANY

NUMBER D222-10059-1
REV LTR

RUN NO.	CONFIGURATION	TYPE OF RUN	WT. TARE RUN	DATE TIME

Run No.	10	10	10	10	10	10	10	10	10	10	10	10	10	10	10	10	10	10	10	10	10	10	10	10	10	10
Data Pt.	26	27	28	29	30	31	32	33	34	35	36	37	38	39	40	41	42	43	44	45	46	47	48	49	50	
Q/S	21.5	21.6	21.6	21.6	21.2	21.2	21.1	20.9	20.9	20.9	20.6	20.6	20.1	21.8	21.8	24.8	24.8	24.8	24.8	24.8	24.8	24.8	24.8	24.8	24.8	24.8
SHAKER EXCO	—	2.3	2.3	2.3	—	2.3	2.3	—	2.3	2.3	—	1	2.3	—	—	—	—	—	—	—	—	—	—	—	—	—
SHAKER AMP Volts	—	6.51	6.51	6.51	—	8.0	8.0	—	8.13	8.73	—	8.73	8.73	—	—	—	—	—	—	—	—	—	—	—	—	—
RPM	450	451	450	450	459	458	459	464	464	465	470	470	470	386	387	388	387	388	386	386	387	386	385	387	387	387
Lat. Cyc ~DEG.	0	0	0	0	0	0	0	0	0	0	0	0	0	0	0.5	1.0	1.5	1.77	1.5	1.25	.85	-.17	-.9	0	0	0
Long Cyc ~DEG.	0	0	0	0	0	0	0	0	0	0	0	0	0	0	0	0	0	0	0	0	0	0	0	1.0	1.0	2.0

Run No.	10	10	10	10
Data Pt.	51	52	53	54
Q/S	24.8	24.8	24.8	24.8
SHAKER EXCO	—	—	—	—
SHAKER AMP Volts	—	—	—	—
RPM	388	387	387	388
Lat. Cyc ~DEG.	0	0	0	10
Long Cyc ~DEG.	-.10	-2.0	-2.0	-.10

PREP.			REVISED	DATE
CHK.				
APPR				

26 FOOT DIAMETER
M-222 ROTOR TEST

NASA 40X80
TEST 410

FORM 49510 (8-70)

THE BOEING COMPANY

RUN NO.	CONFIGURATION	TYPE OF RUN	WT. TARE RUN	α_w deg	$\theta_{.75}$ deg	A_1 deg	B_1 deg	α_N deg	V_T KTS	P_T IN HG	T_T °F		WIND ON TUNNEL MPH	DATE TIME
11	Full Stiff Wing, Blades On			VARY	24.9	VARY	VARY	VARY	100	30.21	97		1.5	8/16/72

Run No.	11	11	11	11	11	11	11	11	11	11	11	11	11	11	11	11	11	11	11	11	11	11	11	11	11
Data Point	1	2	3	4	5	6	7	8	9	10	11	12	13	14	15	16	17	18	19	20	21	22	23	24	25
RPM	386	386	385	383	385	385	386	386	385	385	384	386	386	385	387	386	386	386	386	385	385	385	384	386	386
$\theta_{.75}$ deg	25.0	25.0	25.0	25.0	25.0	25.0	25.0	25.0	25.0	24.9	24.8	24.9	24.9	24.8	24.8	24.8	24.8	24.8	24.8	24.8	24.8	24.8	24.8	24.8	24.8
α_w deg	0	-2	-4	-6	-3	0	2	4	6	8	9	4	0	-3	-2	-1	0	0	0	0	0	0	0	0	0
Long DPM	.15	.15	.15	.15	.16	.15	.15	.15	.15	.15	.15	.15	.15	.15	.15	.15	.15	-.04	.15	.5	.77	1.1	1.41	1.5	.77
Lat DPM	.01	.01	.01	.01	.01	.01	.01	.01	.01	.01	.01	.01	.01	.01	.01	.01	.01	.01	.01	.01	.01	.01	.01	.01	.01

Run No.	11	11	11	11	11	11	11	11	11	11	11	11	11	11	11	11	11	11	11	11	11	11			
Data Point	26	27	28	29	30	31	32	33	34	35	36	37	38	39	40	41	42	43	44	45	46	47			
RPM	386	387	387	386	386	385	387	387	385	385	384	386	385	385	388	389	386	387	385	385	383	386			
$\theta_{.75}$ deg	24.8	24.8	24.8	24.8	24.8	24.8	24.8	24.8	24.8	24.8	24.8	24.8	24.7	24.7	24.4	24.4	24.4	24.4	24.4	24.4	24.1	24.9			
α_w deg	0	0	0	0	0	0	0	0	0	0	6	6	9	9	12	12	15	15	17	18	19	0			
Long DPM	.5	.14	.14	.14	.14	.14	.14	.14	.14	.14	.14	1.06	1.06	1.24	1.24	1.55	1.55	1.89	1.89	1.89	1.89	.15			
Lat DPM	.01	.01	.15	.35	.42	.01	-.9	-.18	-.29	0	-.01	-.08	-.08	-.15	-.15	-.25	-.25	-.29	-.29	-.29	-.29	.01			

FORM 4B510 (3-70)

			PREP
			CHK.
			APPR
			REVISED
			DATE

26 FOOT DIAMETER
M-222 ROTOR TEST

NASA 40 x 80 TEST 410

NUMBER D222-10059-1
REV LTR

SHEET 621

THE BOEING COMPANY

NUMBER D222-10059-1
REV LTR

RUN NO.	CONFIGURATION	TYPE OF RUN	WT. TARE RUN	θ_{dw} deg	θ_{1S} deg	A_1 deg	B_1 deg	θ_N deg	V_T KTS	P_T in Hg	T_T °F	WIND OR TIME MIN	DATE TYPE
12	FULL STIFF WING, BLADES ON			VARY	VARY	?	0	0	140	30.18	101/108	2.9	8/16/72

RUN NO.	12	12	12	12	12	12	12	12	12	12	12	12	12	12	12	12	12	12	12	12	12	12	12	12	12	12	12	12	12	12
DATA PT.	1	2	3	4	5	6	7	8	9	10	11	12	13	14	15	16	17	18	19	20	21	22	23	24	25	26	27	28	29	30
RPM	385	386	384	385	385	386	408	408	408	420	420	420	420	435	435	435	435	435	435	435	435	435	435	435	435	435	435	435	435	435
θ_{1S} deg	33.3	33.3	33.3	32.9	32.9	32.9	32	32	32	31.2	31.2	31.2	30.3	30.3	30.3	30.3	30.2	30.2	30.2	30.2	29.8	29.8	29.8	29.8	29.5	29.5	29.5	29.5	29.5	29.5
θ_{dw} deg	0	0	0	0	0	0	0	0	0	0	0	0	0	0	0	0	0	0	0	0	0	0	0	0	0	0	0	0	0	0
SHAKER	0	2	2	0	2	2	0	2	2	0	0	0	2	2	2	0	2	2	2	2	2	2	2	2	2	2	2	2	2	2

RUN NO	12	12	12	12	12	12	12	12	12	12	12	12	12	12	12	12	12	12	12	12	12	12	12	12	12	12	12	12	12	12
DATA PT.	29	30	31	32	33	34	35	36	37	38	39	40	41	42	43	44	45	46	47	48	49	50	51	52	53	54	55	56	57	58
RPM	435	435	435	435	435	435	435	435	435	435	435	435	435	435	435	435	435	435	435	435	435	435	435	435	435	435	435	435	435	435
θ_{1S} deg	29.5	29.5	29.5	29.5	29.5	29.5	29.5	29.5	29.5	29.5	29.5	29.5	29.5	29.5	29.5	29.5	29.5	29.5	29.5	29.5	29.5	29.5	29.5	29.5	29.5	29.5	29.5	29.5	29.5	29.5
θ_{dw} deg	0	0	0	0	0	0	0	0	0	0	0	0	0	0	0	0	0	0	0	0	0	0	0	0	0	0	0	0	0	0
SHAKER	2	2	2	2	2	2	2	2	2	2	2	2	2	2	2	0	2	2	2	2	2	2	2	2	2	2	2	2	2	2

PREP.			REVISED	DATE
CHK.				
APPR				

26 FOOT DIAMETER
M-222 ROTOR TEST

NASA 40X80
TEST 410

FORM 4851G (3-70)

THE BOEING COMPANY

NUMBER D222-10051-1
REV LTR

RUN NO.	CONFIGURATION	TYPE OF RUN	WT. TARE RUN	α_w deg	$\theta_{.75}$ deg	A_1 deg	B_1 deg	α_N deg	V_T KTS	P_T IN HG	T_T °F		WIND ON TIME HRS	DATE TIME
13	FULL STIFF WING, BLADES ON			0	33.3	VARY	VARY	0	146	30.17	85/90		.80	8/16/72
14	" " " " "			0	VARY	0	0	0	192				1.33	8/17/72

RUN NO.	13	13	13	13	13	13	13	13	13	13	13	13	13	13	13	13	13	13	13	13	13	13	13	
DATA PT	1	2	3	4	5	6	7	8	9	10	11	12	13	14	15	16	17	18	19	20	21	22	23	
A_1 deg	0	-.35	-.8	1.35	1.55	1.24	.63	0	-.44	-.8	-1.15	-1.30	-.70	0	0	0	0	0	0	0	0	0	0	
B_1 deg	0	0	0	0	0	0	0	0	0	0	0	0	0	0	-4	0	.65	.95	1.35	1.80	1.45	.70	0	

TOTAL WIND ON TIME AS OF THE END OF RUN 13 12.292 HRS.

RUN NO. 14

DATA PT	1	2	3	4	5	6	7	8	9	10	11	12	13	14	15	16	17	18	19	20					
RPM	312	315	323	326	340	340	340	350	350	350	356	356	356	370	370	370	386	386	386	386					
$\theta_{.75}$ deg	47.9	47.9	46.8	46.9	45.7	45.7	45.7	44.9	44.9	44.9	44.3	44.3	44.3	43.3	43.3	43.3	42.3	42.3	42.3	42.3					
SHAKER CPS	0	0	0	2	0	2	2	0	2	2	0	2	2	0	2	2	0	0	2	2					

26 FOOT — DIAMETER M. 222 ROTOR TEST

NASA 40x80 TEST 410

SHEET 623

FORM 49810 (3/70)

RUN NO.	CONFIGURATION	TYPE OF RUN	WT. TARE RUN	d_W deg	$\theta_{.75}$ deg	A_1 deg	B_1 deg	d_N deg	V_T KTS	P_T IN HG	T_T °F		WIND ON TIME HRS	DATE TIME
15	Full Stiff Wing, Blades on			VARY	VARY	VARY		0	152				1.00	8/17/72

RUN 15

DATA PT.	1	2	3	4	5	6	7	8	9	10	11	12	13	14	15	16	17	18	19	20	21	22	23	24	25
RPM	400	400	400	418	418	418	423	430	430	448	448	448	465	465	465	480	480	481	441	387	387	387	387	387	387
$\theta_{.75}$ deg	40.1	40.4	40.4	40.1	40.1	40.1	39.2	39.2	39.2	39.2	39.2	39.2	39.2	32.3	32.3	32.3	36.3	36.3	36.3	42.3	42.3	42.3	42.3	42.3	42.3
SHAKER, CPS	0	2	2	0	2	2	0	2	2	0	2	2	0	2	2	0	2	2	2	0	0	0	0	0	0
d_W deg	0	0	0	0	0	0	0	0	0	0	0	0	0	0	0	0	0	0	0	0	-1	-2	-3	-2	-1
A_1 deg	0	0	0	0	0	0	0	0	0	0	0	0	0	0	0	0	0	0	0	0	0	0	0	0	0

RUN 15

DATA PT	26	27	28	29	30	31	32	33	34	35	36	37	38	39	40	41	42	43
RPM	387	387	387	387	387	387	387	387	387	387	387	387	387	387	387	387	387	387
$\theta_{.75}$ deg	42.3	42.3	42.3	42.3	42.3	42.3	42.3	42.3	42.3	42.3	42.3	42.3	42.3	42.3	42.3	42.3	42.3	42.3
SHAKER CPS	0	0	0	0	0	0	0	0	0	0	0	0	0	0	0	0	0	0
d_W deg	0	1	2	3	4	3	2	1	0	0	0	0	0	0	0	0	0	0
A_1 deg	0	0	0	0	0	0	0	0	0	0	-.15	-.55	-.90	-.42	0	1.45	1.55	1.00	0

DES.				REVISED	DATE
CHK.					
APPR					

26 FOOT DIAMETER

M-222 ROTOR TEST

NASA 40X80

TEST 410

FORM 4851 0 (1/70)

RUN NO.	CONFIGURATION	TYPE OF RUN	WT. TARE RUN	α_w	θ_{TS}	A_1	B_1	q_N	V_T	P_T	T_T		WIND ON TIME	DATE TIME
				deg	deg	deg	deg	deg	KTS				HRS	
16	FULL STIFF WING, BLADES ON			VARY	4.8	VARY	VARY	0	192				1.25	8/11/72

RUN 16

DATA PT.	1	2	3	4	5	6	7	8	9	10	11	12	13	14	15	16	17	18	19	20	21	22	23	24	25
A_1 deg	0	0	0	0	0	0	0	0	0	0	.10	-.2	.5	-.10	.10	.10	-.2	-.2	-.8	-.8	-.8	-.25	-.60	-.8	-.8
B_1 deg	0	.40	.70	1.00	Hy/S	0	-.4	-.2	0	0	.25	.25	.25	0	.95	2.5	.75	.75	1.8	2.2	1.40	1.8	1.8	1.8	1.8
α_w deg	0	0	0	0	0	0	0	0	0	1	1	1	1	1	1	2	2	4	4	4	4	4	4	4	6

RUN 16

DATA PT.	26	27	28	29	30	31	32	33	34	35	36	37	38
A_1 deg	-.75	.75	-.75	-.80	-.35	-.60	0	.6	.6	1.8	[illegible]	+.6	0
B_1 deg	2.45	2.0	3.05	2.45	2.45	0	0	-.4	0	-.4	-.4	-4	0
α_w deg	6	6	6	6	6	6	-1	-1	-1	-1	-1	-1	0

26 FOOT DIAMETER
M 222 ROTOR TEST

PREP.			REVISED	DATE
CHK.				
APPR				

NASA 40X80
TEST 400

FORM 49510 (3/70)

THE BOEING COMPANY

NUMBER D222-10059-1
REV LTR

RUN NO.	CONFIGURATION	TYPE OF RUN	WT. TARE RUN	d_{HUB} deg	θ_{TS} deg	A_1 deg	B_1 deg	d_W deg	V_T KTS	P_T IN Hg	T_T °F	WIND ON TIME	DATE TIME
17	Full Stiff Wing, BLADES ON			VARY	VARY	0	VARY	0	190			1.85	8/18/72 1600

RUN 17

DATA PT	1	2	3	4	5	6	7	8	9	10	11	12	13	14	15	16	17	18	19	20	21	22	23	24	25
θ_{TS} deg	5.34	52.8	51.2	49.7	48.5	47.3	44.1	44.5	44.1	42.8	41.7	40.8	39.8	38.8	38.0	37.3	36.6	35.5	35.5	34.6	32.3	33.2	35.0	35.5	40.7
RPM	170	190	200	211	221	230	240	250	260	270	282	290	300	310	322	334	340	350	350	340	332	320	310	300	290
B_1 deg	0	0	0	0	0	0	0	0	0	0	0	0	0	0	0	0	0	0	.35	.35	.35	.35	.35	.35	.35
d_W deg	0	0	0	0	0	0	0	0	0	0	0	0	0	0	0	0	0	0	0	0	0	0	0	0	0

DATA PT	26	27	28	29	30	31	32	33	34	35	36	37	38	39	40	41	42	43	44	45	46
θ_{TS} deg	41.1	42.1	43.1	44.0	46.2	47.3	48.5	50.2	51.2	52.6	31.2	31.2	31.2	31.2	31.2	31.2	31.2	31.2	31.2	31.2	31.2
RPM	280	270	260	250	240	230	220	208	200	190	420	420	420	420	420	420	420	420	420	420	420
B_1 deg	35	35	35	.35	.35	.35	.35	.35	.35	.35	0	0	0	0	0	0	0	0	0	0	0
d_W deg	0	0	0	0	0	0	0	0	0	0	0	1	2	3	4	5	6	0	-1	-2	0

TOTAL WIND ON TIME AT THE END OF RUN 17 16.872 HRS

PREP.			REVISED	DATE
CHK.				
APPR.				

26 FOOT DIAMETER
M 222 ROTOR TEST

NASA 40X80
TEST 410

FORM 49510 (4-70)

THE BOEING COMPANY

NUMBER D222-10059-1
REV LTR

RUN NO.	CONFIGURATION	TYPE OF RUN	WT. TARE RUN	δ_{LO} deg	δ_{LS} deg	A_1 deg	B_1 deg	δ_N deg	V_T KTS	P_T in Hg	T_T °F	RPM	WIND SPD DIR KTS	DATE TIME
18	FULL STIFF WING, BLADES ON			VARY	25	0	0	0	100			387		8/21/72

ψ_{ROT} = 91.6 deg.

RUN	18	18	18	18	18	18	18	18	18	18	18	18
DATA PT	1	2	3	4	5	6	7	8	9	10	11	12
δ_{LO} deg.	0	3	3	3	3	3	3	3	3	3	3	3
PITCH GAIN CTS.	0	0	100	0	100	200	300	0	0	0	0	0
YAW GAIN CTS.	0	0	0	0	0	0	0	0	100	200	300	400

PREP.			REVISED	DATE
CHK.				
APPR				

26 FOOT DIAMETER
M-222 ROTOR TEST

NASA 40X80
TEST 410

FORM 49510 (3/70)

THE BOEING COMPANY

NUMBER D222-10059-1
REV LTR

RUN NO.	CONFIGURATION	TYPE OF RUN	WT. TARE RUN	α_w deg	$\theta_{.75}$ deg	A_1 deg	B_1 deg	α_s deg	V_t KTS	P_T IN/HG	T_T °F	ρ SLUGS/FT³	Wind on Time HRS	DATE TIME
19	Full Scale Wing, Blades On			VARY	29.1	VARY	VARY	0	100		96/103	386	1.5	8/21/72

ψ_{ROT} = 91.6 deg.

Run No	19	19	19	19	19	19	19	19	19	19	19	19	19	19	19	19	19	19	19	19	19	19
Data Point	1	2	3	4	5	6	7	8	9	10	11	12	13	14	15	16	17	18	19	20	21	22	23	24	25
A, Deg	0	-.65	-.65	-1.3	-1.3	-.65	-.65	0	.5	.5	1.0	1.0	1.5	1.5	.5	.5	.5	0	0	0	0	0	0	0	0
B, Deg	0	0	0	0	0	0	0	0	0	0	0	0	0	0	0	0	0	0	0	-.4	-.4	0	0	.55	.55
α_w Deg	0	0	0	0	0	0	0	0	0	0	0	0	0	0	0	0	0	0	0	0	0	0	0	0	0

ψ_{ROT} = 91.6 deg.

Run No	19	19	19	19	19	19	19	19	18																
Data Point	26	27	28	29	30	31	32	33	34																
A, Deg	0	0	0	0	0	0	0	0	0																
B, Deg	1.18	1.18	1.75	1.25	2.35	2.35	0	0	0																
α_w Deg	0	0	0	0	0	0	0	6	-3																

Note: TP 16 ψ was not steady

PREP.			REVISED	DATE
CHK.				
APPR				

26 FOOT DIAMETER
M-222 ROTOR TEST

NASA 40X80
TEST 410

FORM 49510 (1-72)

THE BOEING COMPANY

NUMBER D222-10059-1
REV LTR

RUN NO.	CONFIGURATION	TYPE OF RUN	WT. TARE RUN	δ_W deg	θ_{TS} deg	η_1 deg	B_1 deg	α_N deg	V_T KTS	P_T IN HG	T_T °F	ψ_{RST} deg	WIND ON TIME HRS.	DATE TIME
20	FULL STIFF WING, BLADES ON			VARY	24.6	VARY	VARY	0	100			91.6	0.4	8/24/72

RUN 20

DATA PT.	1	2	3	4	5	6	7	8	9	10	11	12	13	14	15	16	17	18	19	20	21
δ_W deg.	0	0	0	0	0	0	2	2	2	2	2	2	2	2	2	2	2	2	2	2	2
PITCH GAIN CPS	0	0	0	163	0	0	0	0	0	0	0	0	125	0	100	200	250	275	300	325	?
YAW GAIN CPS	0	218	0	0	0	0	0	0	218	0	200	?	0	0	0	0	0	0	0	0	0

NOTES:

DATA PT. 2 - OPEN LOOP INPUT - 0.2 VOLTS. YAW LOOP
4 OPEN LOOP INPUT - 0.2 VOLTS. PITCH LOOP
6 YAW LOOP CLOSED
12 PITCH LOOP CLOSED
21 SYSTEM DIVERGENT. [redacted]

PREP.			REVISED	DATE
CHK.				
APPR				

26 FOOT DIAMETER
M-222 ROTOR TEST

NASA 40x80
TEST 410

FORM 49510 (1-70)

THE BOEING COMPANY

NUMBER D222-10059-1
REV LTR

RUN NO.	CONFIGURATION	TYPE OF RUN	WT. TARE RUN	$d\omega$ deg	θ_{TS} deg	A_1 deg	B_1 deg	δ_N deg	V_T KTS	P_T IN Hg	T_T °C	$\psi_{R\&T}$ deg	WIND ON TMF KTS	DATE TIME
21	FULL STIFF WING, BLADES ON			0	24.7	VARY	VARY	0	100			51.6	-35	8/22/72
22				0	24.7	VARY	VARY	0	100			51.6	1.17	

RUN 21 - OPEN LOOP INPUT TO PITCH LOOP, RPM = 387

DATA PT	1	2	3	4	5	6	7	8	9	10	11	12	13	14	15	16	17	18	19	20	21	22	23	24	25	26
YAW LOOP GAIN CTS.	0	0	0	0	0	0	0	0	0	0	0	0	0	0	0	0	0	0	0	0	0	0	0	0	0	0
CYCLIC INPUT FREQ. CPS	0	.1	.2	.3	.4	.5	.6	.7	.75	.8	.80															
PITCH LOOP GAIN, CTS	350	350	350	350	350	350	350	350	350	350	350															

RUN 22 OPEN LOOP INPUT TO PITCH LOOP - CONTINUATION OF RUN 21, RPM = 387

DATA PT.	1	2	3	4	5	6	7	8	9	10	11	12	13	14	15	16	17	18	19	20	21	22	23	24	25	26
YAW LOOP GAIN CTS.	0	0	0	0	0	0	0	0	0	0	0	0	0	0	0	0	0	0	0	0	0	0	0	0	0	0
CYCLIC INPUT FREQ. CPS.	75	.80	.85	.90	.95	1.0	1.1	1.3	1.2	1.4	1.6	.4	.5	.6	.65	.70	.75	.80	.85	.90	.55	1.00	1.1	1.2	1.4	1.6
PITCH LOOP GAIN CTS.	350	350	350	350	350	350	350	350	350	350	350	450	450	450	450	450	450	450	450	450	450	450	450	450	450	450

RUN 22 CONTINUED - OPEN LOOP INPUT TO YAW LOOP RPM = 387

DATA PT.	27	28	29	30	31	32	33	34	35	36	37	38	39	40	41	42	43	44	45	46	47	48	49	50	51	52
YAW LOOP GAIN	300	300	300	300	300	300	300	300	300	300	300	300	300	300	300	400	400	400	400	400	400	400	400	400	400	400
CYCLIC INPUT CPS.	.4	.5	.6	.65	.70	.75	.80	.85	.90	.95	1.0	1.2	1.4	1.6	1.8	1.2	1.4	1.6	1.8	2.0	1.1	1.0	-.55	-.50	.85	.80
PITCH LOOP GAIN CTS.	0	0	0	0	0	0	0	0	0	0	0	0	0	0	0	0	0	0	0	0	0	0	0	0	0	0

* OUT OF MAG TAPE ON D.P. 50 NO MORE MAG TAPE DATA THIS RUN

PREP.		REVISED	DATE
CHK.			
APPR			

26 FOOT DIAMETER
M-222 ROTOR TEST

NASA 40X80
TEST 410

FORM 4-61-1 (1-70)

THE BOEING COMPANY

NUMBER D222-10059-1
REV LTR

RUN NO.	CONFIGURATION	TYPE OF RUN	WT. TARE RUN	δ_{LS}	δ_{TS}	A_1	B_1	δ_N	V_T	P_T	T_T	ψ_R & T	WIND ON TIME HRS	DATE TIME
				deg	deg	deg	deg	deg	KTS	IN HG				
22	CONCLUDED			0	-24.7	VARIOUS		0	100			9/6		8/22/72

RUN 22 CONCLUDED, OPEN LOOP INPUT TO YAW LOOP, RPM = 387

DATA PT.	53	54	55	56	57	58	59	60
YAW LOOP CTS. GAIN	400	400	400	400	400	400	400	400
CYCLIC INPUT CPS	.75	.70	.65	.60	.50	.40	.30	0
FREQ. PITCH LOOP GAIN CTS	0	0	0	0	0	0	0	0

DWN.			REVISED	DATE
CHK.				
APPR				

26 FOOT DIAMETER
M-222 ROTOR TEST

NASA 40X80
TEST 410

FORM 49E1C (3-70)

THE BOEING COMPANY

PREP.	CHK.	APPR.	REVISED DATE

RUN NO.	CONFIGURATION	TYPE OF RUN	WT. TARE RUN	α_W	$\theta_{.75}$	A_1	B_1	α_N	V_T	P_T IN HG	T_T	V_{ROT}	Wind on Time HRS	DATE TIME
23	Full Stiff Wing, Blades On			0	29.7			0	100	29.93	77/82	60	1	8/23/72
24	Full Stiff Wing, Blades On.			0	24.8			0	100	29.78	78/86	60	33	8/24/72

Run 23 Pot Gain = 1000 cts RPM = 386 Input = 1.1 volts o-p

Data Point	1	2	3	4	5	6	7	8	9	10	11	12	13	14	15	16	17	18	19	20	21	22	23	24	25
Frequency, Hz	0	.6	1.0	1.2	1.4	1.6	1.8	1.9	2.0	2.1	2.2	2.27	2.3	2.4	2.5	2.6	2.8	3.0	3.5	4.0	4.2	4.3	4.4	4.5	4.6

Data Point	26	27	28	29	30	31	32	33	34	35	36
Frequency Hz	6.0	7.3	8.0	9.0	10.0	10.5	11.0	11.5	12.0	12.5	13.0

C.B. ON BLADE S.N. 2 AT STAT. 22.5 % IS OUT

F.B. ON BLADE S.N. 2 AT STAT. 22.5 % IS ~~QUESTIONABLE~~ OUT

RUN 24, OPEN LOOP CHECK OF HIGH RATE FEED BACK

Data PT.	1	2	3	4	5	6	7	8	9	10	11	12	13	14	15	16	17	18	19	20	21	22	23	24	25
Freq. HZ.	0	1.9	2.0	2.1	2.15	2.20	2.22	2.24	2.26	2.28	2.29	2.30	2.31	2.32	2.33	2.35	2.37	2.39	2.45	2.50	2.55	2.60	2.70	2.80	3.00

POT GAIN = 1000,

INPUT VOLTS = 1.1 o-p VOLTS

Φ_S AT 2.32 HZ = 139° Lag.

SHEET 632

NUMBER REV LTR D222-10059-1

APPR.	CHK.	REVISED DATE	RUN NO.	CONFIGURATION	TYPE OF RUN	WT. TARE RUN	d_w deg	$\theta_{.75}$ deg	A_1 deg	B_1 deg	a_N deg	V_T KTS	P_T IN HG	T_T °F	ψ_{ROT} deg	WIND ON TIME HRS.	DATE TIME
			25	Full Stiff Wing, Blades on			0	24.7	—	—	0	100	29.66	84/82	60	1.5	8/24/72
			26	Full Stiff Wing, Blades on			0	24.7	—	—	0	100	29.83	83/86	60	1.0	
			27				0	24.7	—	—	0	100	29.83	83/86	60		

RUN 25 CLOSURE OF HIGH LOOP GAIN, SHAKER FREQUENCY AT 2.4 CPS.

DATA PT.	1	2	3	4	5	6	7	8	9	10	11	12	13	14	15	16	17	18	19	20	21	22	23	24	25
GAIN POT CTS.	0	0	0	0	100	100	200	200	300	300	300	400	400	400	200	0	200	200	200	400	400	600	600	600	600

RUN 26 OPEN LOOP & CHECK ON HIGH LOOP GAIN

DATA PT.	1	2	3	4	5	6	7	8	9	10	11	12	13	14	15	16	17	18	19	20					
INPUT VOLTS	.6	.9	.6	.9	.6	.6	.75	.8	.8	.85	.85	.85	.9	.9	.95	.95	1.0	1.0	1.0	1.0					
SHAKER FREQUENCY CPS.	.6	1.0	1.0	.6	1.2	1.4	1.6	1.8	1.7	2.0	2.2	2.24	2.265	2.29	2.32	2.365	2.41	2.61	2.8	3.05					
GAIN POT CTS.	0	0	0	0	0	0	0	1000	1000	1000	1000	1000	1000	1000	1000	1000	1000	1000	1000	1000					

RUN 27 ϕ_3 SET AT 168.5° AT 2.32 HZ. (LAG) D.P 1-3 OPEN LOOP

DATA PT.	1	2	3	4	5	6	7	8	9	10	11	12	13	14	15	16	17	18	19	20	21	22	23	24	25
INPUT VOLTS	.9	.9	.9	0	0	0	0	0	0	0	0	0	0	0	0	0	0	0	0	0	0	0	0	0	0
SHAKER FREQ CPS.	—	—	—	2.5	2.5	2.5	2.5	2.5	2.5	2.5	2.5	2.5	2.5	2.5	2.5	2.5	2.5	2.5	2.5	2.5	2.5	2.5	2.5	2.5	2.5
GAIN POT CTS.	100	100	100	0	0	0	100	100	100	0	100	200	200	200	250	300	300	350	350	350	400	400	450	450	500

RUN 27 CLOSED LOOP (HIGH RATE FEEDBACK)

DATA PT.	26	27	28	29	30	31	32	33	34	35	36
GAIN POT CTS.	500	600	600	700	700	800	800	900	900	1000	1000
AMP.											

THE BOEING COMPANY

NUMBER D222-10059-1
REV LTR

SHEET 633

RUN NO.	CONFIGURATION	TYPE OF RUN	WT. TARE RUN	d_w deg	$\theta_{.75}$ deg	A_1 deg	B_1 deg	d_N deg	V_T KTS	P_T IN HG	T_T °F	ψ_{RGT} deg	WIND ON TIME HRS.	DATE TIME
28	FULL STIFF WING, BLADES ON			0	23	—	—	0	100	29.68	80/97	60	1.37	8/25/72
29	Full Stiff Wing, Blades On			0	21.8	—	—	0	100	29.68	96/102	60	1	

RUN 28 OPEN LOOP, GAIN POT AT 1000 CTS, INPUT VOLTAGE = 1.0, RPM = 420

DATA PT	1	2	3	4	5	6	7	8	9	10	11	12	13	14	15	16	17	18	19	20	21	22	23	24	25
INPUT FREQ CPS	0	1.2	1.21	1.22	1.23	1.24	1.25	1.26	1.27	1.29	1.31	2.00	2.20	2.24	2.23	2.25	2.26	2.27	2.28	2.29	2.30	2.31	2.32	2.33	2.34

RUN 28

DATA PT.	26	27	28	29	30	31	32	33	34	35	36	37	38	39	40	41	42	43	44	45					
INPUT FREQ CPS	2.36	2.41	2.60	2.80	3.00	3.50	4.00	4.20	4.30	4.44	4.50	4.60	6.00	8.00	10.00	11.00	12.00	13.00	13.50	13.30					

Run 29 OPEN LOOP. Gain Pot at 1000cts, Input Volt Varied RPM = 444

Data Pt	1	2	3	4	5	6	7	8	9	10	11	12	13	14	15	16	17	18	19	20	21	22	23	24	25
INPUT FREQ CPS	0	2.1	2.0	2.15	2.2	2.22	2.24	2.26	2.28	2.3	2.32	2.36	2.41	2.60	2.80	3.0	3.5	4.0	4.2	4.3	4.4	4.3	4.4	4.5	4.6

Data Pt	26	27	28	29	30	31	32	33																	
INPUT FREQ CPS	6.0	8.0	9.0	10.0	11.0	12.0	14.0	14.0																	

THE BOEING COMPANY

NUMBER D222-10059-1
REV LTR

SHEET 634.

THE BOEING COMPANY

NUMBER D222-10059-1
REV LTR

PREP.	CHK.	APPR.	REVISED	DATE

RUN NO.	CONFIGURATION	TYPE OF RUN	WT. TARE RUN	α_w deg	$\theta_{.75}$ deg	A_1 deg	B_1 deg	α_R deg	V_T KTS	P_T "HG	T_T °F	ψ_{REF} deg	WIND ON TIME HRS	DATE TIME
30	Full Stiff Wing, Blades On			0	23			0	100	29.68	102/104		1.5	

Run 30 RPM = 420 OPEN LOOP

Data Pt.	1	2	3	4	5	6	7	8	9	10	11	12	13	14	15	16	17	18	19	20	21	22	23	24	25
INPUT FREQ CPS	0	0	2.285	2.20	2.338	2.31	2.32																		
SHAKER FREQ CPS								1.5	1.5	1.5	1.5	1.5	1.0	1.5	1.5	1.5	1.5	1.5	1.0	1.5	1.5	1.6	1.5	1.5	1.5
Gain Pot CPS	1000	1000	1000	1000	1000	1000	1000	0	0	0	200	200	200	400	400	400	400	600	600	600	800	800	800	1000	1000

Data Pt	26	27	28
SHAKER FREQ CPS	1.5	1.5	1.5
Gain Pot CPS	1000	400	200

SHEET 635

RUN NO.	CONFIGURATION	TYPE OF RUN	WT. TARE RUN	α_w deg	$\theta_{.75}$ deg	A_1 deg	B_1 deg	α_w deg	V_T kts	P_T in Hg	T_T °F	ϕ_{TAIL} deg	WIND ON TIME HRS	DATE TIME
31	Full Stiff Wing, Blades On			0	21.7			0	100	24.91	100	60	3	

Run 31 RPM - 444 OPEN LOOP Data PTS. 1 - 18

Data Pt	1	2	3	4	5	6	7	8	9	10	11	12	13	14	15	16	17	18	19	20	21	22	23	24	25
INPUT FREQ CPS	2.11	2.15	2.15	2.17	2.2	2.21	2.22	2.23	2.24	2.25	2.26	2.28	2.3	2.35	2.39	2.45	2.5	2.61							
SHAKER FREQ CPS																			1.5	1.5	1.5	1.5	1.5	1.5	1.5
Gain Adj CPS	1000	1000	1000	1000	1000	1000	1000	1000	1000	1000	1000	1000	1000	1000	2000	1000	1000	1000	0	0	100	100	100	100	200

Data Pt	27	28	29	30	31	32	33	34	35	36	37	38	39	40	41	42	43	44	45	46	47	48	49
SHAKER FREQ CPS	1.5	1.5	1.5	1.5	1.6	1.5	1.0	1.5	1.5	1.5	1.5	1.5	1.6	1.6	1.5	1.5	1.5	1.5	1.5	1.5	1.5	1.5	1.5
Gain Adj CPS	200	300	300	350	350	400	400	400	450	450	500	500	500	500	500	550	550	600	650	650	650	700	700

PREP.			
CHK.		REVISED	DATE
APPR			

FORM 4951-0 (J 701)

THE BOEING COMPANY

PREP.	CHK.	APPR.	REVISED	DATE

RUN NO.	CONFIGURATION	TYPE OF RUN	WT. TARE RUN	α_w deg	$\theta_{.75}$ deg	A_1 deg	B_1 deg	α_N deg	V_T KTS	P_T IN HG	T_T °F	Ψ_{ROT} deg	WIND ON TUNNEL KTS	DATE TIME
32	Full Stiff Wing, Blades On			0	29.1			0	100	29.91		60	1	

Run 32 RPM = 386 Open Loop Data Points 1 – 17

Data Pt	1	2	3	4	5	6	7	8	9	10	11	12	13	14	15	16	17	18	19	20	21	22	23	24	25
INPUT FREQ CPS	1.25	1.155	1.1	1.317	1.418	1.61	1.815	2.1	2.2	2.29	2.26	2.28	2.29	2.32	2.36	2.39	2.5								
SHAKER FREQ CPS																		1.5	1.5	1.5	1.5	1.5	1.5	1.5	1.5
Gain Pot CTS	1000	1000	1000	1000	1000	1000	1000	1000	1000	1000	1000	1000	1000	1000	1000	1000	1000	0	0	200	300	400	500	600	600

Data Pt	26	27	28	29	30	31
INPUT FREQ CPS						
SHAKER FREQ CPS	1.5	1.5	1.5	1.5	1.5	1.5
Gain Pot CTS	800	800	900	1000	1000	1000

NUMBER REV LTR

D222-10059-1

SHEET 637

THE BOEING COMPANY

RUN NO.	CONFIGURATION	TYPE OF RUN	WT. TARE RUN	α_w deg	$\theta_{.75}$ deg	A_1 deg	B_1 deg	α_N deg	V_T kts	P_T in Hg	T_T °F	ϕ RT deg	WIND ON TIME YES	DATE TIME
33	Full Stiff Wing, Blades On			0	41.9	–	–	0	190		78/19c	60	2.6	3/28/72
34	Full Stiff Wing, Blades On			0	42.1	–	–	0	190		99/134	60	.9	

FORM 4P10-13 7/70

PREP. | CHK. | APPR | DATE | REVISED

NUMBER REV LTR

D222-10059-1

SHEET 638

M-222 ROTOR TEST

26 FOOT DIAMETER

NASA 40x80 TEST 410

Run 33 RPM = 386 Open Loop Data point 1-41

Data Pt	1	2	3	4	5	6	7	8	9	10	11	12	13	14	15	16	17	18	19	20	21	22	23	24	25
INPUT FREQ CPS		81	.915	1.01	1.11	1.21	1.3	1.4	1.6	1.8	2.0	2.0	2.1	2.18	2.22	2.26	2.31	2.35	2.4	2.5	2.6	2.8	3.0	3.8	4.0
SHAKER FREQ CPS																									
Gain Pot CPS	1000	1000	1000	1000	1000	1000	1000	1000	1000	1000	1000	1000	1000	1000	1000	1000	1000	1000	1000	1000	1000	1000	1000	1000	1000

RUN 33

Data Pt	26	27	28	29	30	31	32	33	34	35	36	37	38	39	40	41	42	43	44	45	46	47	48	49	50
INPUT FREQ CPS	9.2	4.4	4.6	6.0	8.5	9.11	9.5	10.1	11.2	2.11	2.24	2.29	2.36	2.47	2.8	21									
SHAKER FREQ CPS																	1.5	1.5	1.5	1.5	1.5	1.5	1.5	1.5	1.5
Gain Pot CPS	1000	1000	1000	1000	1000	1000	1000	1000	1000	1000	1000	1000	1000	1000	1000	1000	0	0	100	100	200	200	200	200	300

RUN 33 AND 34 RUN 34 CLOSED LOOP.

Data Pt	51	52	53	54	55	56	57	58		1	2	3	4	5	6	7	8	9	10	11	12	13			
SHAKER FREQ CPS	1.5	1.5	1.5	1.5	1.5	1.5	1.5	1.5																	
Gain Pot CPS	300	400	400	400	500	500	600	600		600	600	700	700	700	700	800	800	900	900	900	0	0			
RUN No.	33	33	33	33	33	33	33	33		34	34	34	34	34	34	34	34	34	34	34	34	34			

NO ETESC taken prior to this Run ~ data runs include Runs 33 to 36 are in question

POST RUN 35 ETESC SHOWED CB ~~%~~ 22.5 % BL NO. 3 TO 25 % IN ERROR AND WING TIP LIFT TO BE 13.4 % IN ERROR.

THE BOEING COMPANY

PREP.	CHK.	APPR.	REVISED	DATE

RUN NO.	CONFIGURATION	TYPE OF RUN	WT. TARE RUN	α_w deg	$\theta_{.75}$ deg	β_1 deg	B_1 deg	α_N deg	V_T kts	P_T in Hg	T_T °F	$\%_{RPM}$	WIND ON TIME HRS	DATE TIME
35	Full Stiff Wing, Blades On			0	39.8	–	–	0	190		109/110	60	1.0	8/28
36				0	41.9	–	–	0	191			60	.5	8/28
37				0	43.3/39.5	–	–	0	190	30.05	78/124	60	1.7	8/29
38				0	37.7/42.1	–	–	0	190		103/133	60	1.9	8/29

Run 35 RPM = 419 TOTAL WIND ON TIME AT END OF RUN 38 42.092

Data Pt	1	2	3	4	5	6	7	8	9	10	11	12	13	14	15	16	17	18	19	20	21	22	23	24	25
Input Freq CPS	–	1.0	1.1	1.2	1.3	1.4	1.5	1.6	1.7	2.0	2.1	2.15	2.21	2.25	2.31	2.38	2.4	2.5	2.6	2.8	2.29	2.27	2.24	2.2	4.1

Run 36 RPM = 387

Data Pt	1	2	3	4
INPUT FREQ CPS	0	2	2000	2

Run 37 RPM = 386 TP 1-24 $\theta_{.75}$ = 42.3

Data Pt	1	2	3	4	5	6	7	8	9	10	11	12	13	14	15	16	17	18	19	20
INPUT FREQ CPS	2.07	2.12	2.12	2.16	2.22	2.26	2.30	2.36	2.29	2.4	2.54	2.6	2.8	3.0	2.18	2.24	4.0	4.11	4.2	4.31

Run 37 RPM = 420 TP 25 - 39

Data Pt	21	22	23	24	25	26	27	28	29	30	31	32	33	34	35	36	37	38	39	40
INPUT FREQ CPS	4425	8.5	9.5	13.0	2.0	2.11	2.16	2.21	2.27	2.31	2.34	2.46	2.56	2.71	3.05	2.28	2.29	2.22	2.4	

Run 38 RPM = 415 TP 1-19 $\theta_{.75}$ = 37.7 RPM = 386 TP 20-35

Data Pt	1	2	3	4	5	6	7	8	9	10	11	12	13	14	15	16	17	18	19	20	21	22	23	24	25
INPUT FREQ CPS	–	2.0	2.11	2.16	2.22	2.27	2.31	2.36	2.45	2.53	2.61	2.8	3.01	2.46	2.39	2.28	3.51	4.0	2.25	2.16	2.24	2.14	2.12	–	–

Data Pt	26	27	28	29	30	31	32	33	34	35
Gain Pt CTS	100	100	200	200	300	300	400	400	500	500

26 FOOT DIAMETER

M-222 ROTOR TEST

NASA 40X80 TEST 410

NUMBER REV LTR

D222-10059-

FORM 49410 (1-70)

SHEET 639

THE BOEING COMPANY

RUN NO.	CONFIGURATION	TYPE OF RUN	WT. TARE RUN	d_ω deg	$\theta_{.75}$ deg	A_1 deg	B_1 deg	d_N deg	V_T KTS	P_T IN Hg	T_T °F	$\psi_{R.O.T}$	WIND ON TIME HRS	DATE TIME
39	Full Stiff Wing - Blades on			0	41.7	–	–	0	192	29.84	96/128		2.10	8/29/72
40				0	41.7	–	–	0	192		107/132		1.40	8/29/72

M-222 ROTOR TEST — 26 FOOT DIAMETER

RUN 39 ROTOR RPM = 386

DATA PT	1	2	3	4	5	6	7	8	9	10	11	12	13	14	15	16	17	18	19	20	21	22	23	24	25
INPUT FREQ. CPS	0	2.14	2.25	2.33	2.24	2.12	2.12	2.00	2.10	2.15	2.18	2.20	2.22	2.24	2.00	2.10	2.15	2.18	2.20	2.22	2.24	2.27	2.30	2.35	2.40

DATA PT.	26	27	28
INPUT FREQ. CPS	2.50	2.60	2.70

NOTES RUN 39

DATA PTS. 1–7 Open loop Phase lag = 169° – Through Phase shifter

8–14 ALL BAD DATA – INCORRECT PATCHING

15–28 Open loop Phase lag = 207° – Through Phase shifter And 180° sign changer

RUN 40 ROTOR RPM = 386 FIRST 3 D.P. OPEN LOOP

DATA PT.	1	2	3	4	5	6	7	8	9	10	11	12	13	14	15	16	17	18	19	20	21
INPUT FREQ. CPS	2.15	2.20	2.35																		
~~SHAFT FREQ. CPS~~ CTS	0	0	—	0	6	100	100	200	200	200	400	400	600	600	800	800	1000	1000	1000	600	600
POT GAIN																					

MAG TAPE HAS TWO D.P. #7 FIRST ONE IS N.G.

NASA 40X80 TEST 410

SHEET 640

NUMBER REV LTR D222-10059-1

LOMM 48410 4-70

THE BOEING COMPANY

RUN NO.	CONFIGURATION	TYPE OF RUN	WT. TARE RUN	α_w deg	$\theta_{.75}$ deg	A_1 deg	B_1 deg	α_N deg	V_T KTS	P_T in HG	T_T °F	ψ_{REF} deg	WIND DIR & VMAG KTS	DATE - TIME
41	Full Shift Wing, Blades On			0	37.8	—	—	0	200	29.85		60	1.28	8/30/72
42	" " " " "			0	32.9	—	—	0	200	29.85		60	1.27	
43	" " " " "			0	21.6	—	—	0	100	29.85	104/104	60	2.00	8/30/72

PREP. | REVISED | CHK. | DATE | APPR

FORM 49510 (1-70)

26 FOOT DIAMETER M-222 ROTOR TEST

NASA 40X80 TEST 4/10

SHEET 641

NUMBER REV LTR

D222-10059-1

FB 10.5 %. BLADE NO. 3 OUT.
CB 22.5 % BLADE NO. 3 OUT RPM = 445

RUN 41 OPEN LOOP

Data Pt.	1	2	3	4	5	6	7	8	9	10	11	12	13	14	15	16	17	18	19	20	21	22	23	24	25
INPUT FREQ CPS	2.0	2.03	2.1	2.12	2.15	2.18	2.20	2.25	2.275	2.3	2.32	2.34	2.36	2.38	2.4	2.45	2.5	2.55	2.6	2.6	2.55	2.5	2.7	2.8	2.175

RUN 41 AND 42 42 IS CLOSED LOOP RPM = 445

Data Pt.	26	27		1	2	3	4	5	6	7	8	9	10	11	12	13	14	15	16	17	18	19	20	21	
INPUT FREQ	2.15	2.175		2.185	2.209	2.41	—	—	—	—	—	—	—	—	—	—	—	—	—	—	—	—	—	—	
Gain Pot CTS	—	—		1000	1000	1000	0	0	0	200	200	400	400	400	600	600	700	700	700	800	800	900	900	1000	

RUN 43 RPM = 445 FIRST 23 DIP OPEN LOOP

DATA PT	1	2	3	4	5	6	7	8	9	10	11	12	13	14	15	16	17	18	19	20	21	22	23		
INPUT CPS FREQ	2.0	2.1	2.15	2.18	2.20	2.22	2.24	2.25	2.26	2.27	2.28	2.24	2.3	2.32	2.34	2.36	2.38	2.4	2.45	2.50	2.60	2.30	2.20	2.2	2.2

DATA PT.	24	25	26	27	28	29	30	31	32	33	34	35	36	37	38	39	40	41	42	43	44				
INPUT CPS FREQ	2.2	2.2	2.26	2.34																					
GAIN POT CTS	0	1000	1000	1000	0	0	200	200	400	400	600	600	800	800	1000	1000	1000	900	900	850	850				

THE BOEING COMPANY

NUMBER D222-10059-1
REV LTR

RUN NO.	CONFIGURATION	TYPE OF RUN	WT. TARE RUN	q_w deg	$\theta_{.75}$ deg	A_1 deg	B_1 deg	α_N deg	V_T KTS	P_T IN Hg	T_T °F	ψ_R CT deg	WIND ON TIME HRS	DATE TIME
44	Full Stiff Wing Blades On			0	24.3	—	—	0	100	28.7	107/110	60	0.5	8/29/72
45	" " "			0	24.3	—	—	0	100	"	103	60	1.2	
46	" " "			0	24.3	—	—	0	100	28.4	94/105	91.6	1.1	
47	" " "			0/3	24.5	—	—	0	100	"	100/54	91.6	1.5	

RUN 44, ROTOR RPM = 387, POT GAIN = 1000, OPEN LOOP

DATA PT.	1	2	3	4	5	6	7	8	9	10	11	12	13	1	2	3	4	5	6	7			
INPUT FREQ.	.21	.215	2.20	2.23	2.25	2.27	2.24	2.30	.231	0.32	0.34	0.34	0.36	0.38	2.0	2.26	2.28	2.30	2.40	2.50	2.70			

RUN 45, ROTOR RPM = 387, FIRST 7 D/F OPEN LOOP WITH POT GAIN = 1000 CTS

DATA PT.	8	9	10	11	12	13	14	15	16	17	18	19	20	21	22	23	24	25	26	27			
POT GAIN CTS	0	0	200	200	400	400	400	500	500	500	600	600	600	800	800	800	800	1000	1000	1000			

RUN 46 ROTOR RPM = 386 P.M. GAIN POT = 1000 CTS Open Loop

DATA PT.	1	2	3	4	5	6	7	8	9	10	11	12	13	14	15	16	17	18	19	20			
INPUT FREQ CPS	.1	.2	.3	.4	.5	.6	.7	.8	.9	1.0	1.5	2.0	2.15	2.2	2.24	2.3	2.4	2.5	3.0	4.1			

RUN 47 ROTOR RPM = 386

DATA PT.	1	2	3	4	5	6	7	8	9	10	11	12	13	14	15	16	17	18	19	20	21	22			
INPUT FREQ CPS	—	—	—	—	—	—	—	—	—	—	—	.2	.4	.6	.65	.70	.8	.9	1.0	1.1K	1.24	1.50	2.0		
q_w deg.	0	3	3	3	3	3	3	3	3	0	0	0	0	0	0	0	0	0	0	0	0	0	0		
PITCH Loop GAIN	0	0	100	200	300	400	500	600	700	300	300	300	300	300	300	300	300	300	300	300	300	300	300		
YAW Loop GAIN	0	0	0	0	0	0	0	0	0	0	0	0	0	0	0	0	0	0	0	0	0	0	0		

FIRST 10 D/P OPEN LOOP Y.M AND CLOSED LOOP P.M. WITH Y.M GAIN = 0
D/P 11-22 P.M. LOOP GAIN = 300 AND OPEN LOOP Y.M.

PREP.			REVISED	DATE
CHK.				
APPR				

26 FOOT DIAMETER
M-222 ROTOR TEST

NASA 40X80
TEST 410

FORM 4951C (1-70)

APPR	CHK.	FREP.	RUN NO.	CONFIGURATION	TYPE OF RUN	WT. TARE RUN	d_W deg	θ_{75} deg	A_1 deg	B_1 deg	d_N deg	V_T KTS	P_T IN HG	T_T °F	ψ_{ROT} d'eg	WIND ON TIME HRS	DATE TIME
			48	Full Stiff Wing, Blades ON			0	24.5	VARY	VARY	0	100	29.76	94	91.6	.5	8/31/72
			49	Full Stiff Wing, Blades On			VARY	24.5	CONTROLLED BY LG-ARTS		0	100	29.76	94	91.6	.6	8.31.72 18.48
		REVISED															
		DATE															

THE BOEING COMPANY

FORM 4951D (1-70)

RUN 48 ROTOR RPM = 386 D/P 1-13 YAW LOOP GAIN POT = 1000 CTS

DATA PT	1	2	3	4	5	6	7	8	9	10	11	12	13	14	15	16	17	18	19	20	21	22	23	24	25
INPUT FREQ. CPS	0	.20	.402	.600	.660	.741	.812	.713	1.00	1.16	1.206	1.51	1.47												
A_1 deg														-.1	.47	1.0	1.37	-.6	-.1	-.6	-.1	-.1	-.1	-.6	-.1
B_1 deg														0	.03	.03	.04	-.005	0	.26	.75	1.25	1.75	-.75	0

RUN 49 ROTOR RPM = 386, YAW AND PITCH SYSTEM GAIN SWEEPS

G_P = PITCH LOOP GAIN POT CTS.
G_Y = YAW " " " "

DATA POINT	1	2	3	4	5	6	7	8	9	10	11	12	13	14	15	16	17	18	19	20	21	22	23	24	25
α_W°	0	3	3	3	3	3	3	3	3	3	3	3	3	3	3	3	3	3	3	3	3	3	3	3	3
G_P	0	0	0	0	0	0	0	0	0	100 →							→	200 →							→
G_Y	0	0	100	200	300	400	500	600	700	0	100	200	300	400	500	600	700	0	100	200	300	400	500	600	700

DATA POINT	26	27	28	29	30	31	32	33	34	35
α_W°	3 →								→	0
G_P	300 →							→	0	0
G_Y	0	100	200	300	400	500	600	700	0	0

SHEET 643

NUMBER REV LTR

D222-10059-1

THE BOEING COMPANY

NUMBER D222-10059-1
REV LTR

RUN NO.	CONFIGURATION	TYPE OF RUN	WT. TARE RUN	δ_{LON} deg	δ_{TS} deg	A_1 deg	B_1 deg	q_N deg	V_T KTS	P_T IN H2	T_T °F	$\psi_{R/T}$ deg	WIND ON TIME HRS	DATE TIME
50	Full Stiff Wing, Blades ON			VARY	245	—	—	0	100	29.26	87	9/C	1.5	8/31/72
51	Full Stiff Wing, Blades ON			VARY	343 372	—	—	0	100 / 120	29.28	81	9/C	.5	8/31/72

RUN 50 - ROTOR RPM = 386, BOTH PITCH LOOP AND YAW LOOPS CLOSED

DATA PT.	1	2	3	4	5	6	7	8	9	10	11	12	13	14	15	16	17	18	19	20	21	22	23	24	25
Gy CTS	0	0	0	0	100	200	300	400	500	600	700	0	100	200	300	400	500	600	700	0	100	200	300	400	500
Gp CTS	0	0	0	400	400	400	400	400	400	400	400	500	500	500	500	500	500	500	500	600	600	600	600	600	600
dw deg	0	0	3	3	3	3	3	3	3	3	3	3	3	3	3	3	3	3	3	3	3	3	3	3	3

RUN 50

DATA PT.	26	27	28	29	30	31	32	33	34	35	36	37	38	39	40	41	42	43	44	45	46	47	48	49	50
Gy CTS	600	700	0	0	100	200	300	400	500	600	700	0	0	0	0	700	700	700	700	700	700	700	700	700	700
Cp CTS	600	600	600	700	700	700	700	700	700	700	700	700	0	0	700	700	700	700	700	700	700	700	700	700	700
dw deg	3	3	3	3	3	3	3	3	3	3	3	3	0	2	2	2	4	6	8	5	5	10	10	11	12

RUN 51, ROTOR RPM = 280; D/P 1-7 100 KTS.

DATA PT	51	52	53	54	55	56	1	2	3	4	5	6	7	8	9	10	11	12	13	14
Gy CTS	700	700	700	700	700	700														
Cp CTS	700	700	700	700	700	700														
dw deg	13	14	15	10	6	2	0	2	4	3	-1	-2	-3	0	2	4	6	8	4	-2

D/P 8-14 100 KTS.
BALANCE UNLOCKED

PREP.			REVISED	DATE
CHK.				
APPR				

26 FOOT DIAMETER
M-222 ROTOR TEST

NASA 40X80
TEST 410

FORM 4951C-1 (7/70)

THE BOEING COMPANY

NUMBER D222-10059-1
REV LTR

SHEET 645

PREP.	CHK.	APPR.	REVISED	DATE

RUN NO.	CONFIGURATION	TYPE OF RUN	WT. TARE RUN	d_w deg	θ_{75} deg	A_1 deg	B_1 deg	d_N deg	V_T KTS	P_T IN HG	T_T °F	ψ_{a_T} deg	WIND ON TIME HRS.	DATE TIME
52	FULL STIFF WING, BLADES ON			VARY	VARY	VARY	VARY	0	140	29.80	77/103	91.6	1.5	9-1-72
53				VARY	21.6	VARY	VARY	0	100	29.80	104	91.6	.5	

28 FOOT DIAMETER
M-222 ROTOR TEST

NASA 40X80 TEST 410

RUN 52, BALANCE UNLOCKED

DATA PT.	1	2	3	4	5	6	7	8	9	10	11	12	13	14	15	16	17	18	19	20	21	22	23	24	25
ROTOR RPM	330	330	330	330	330	330	330	330	388	388	388	388	388	388	388	388	400	410	410	410	423	422	422	420	420
θ_{75} deg.	36.7	36.7	36.7	36.7	36.7	36.7	36.7	36.7	32.8	32.8	32.8	32.8	32.8	32.8	32.8	32.8	32.1	31.4	31.4	31.4	30.8	30.8	30.8	30.8	30.8
d_w deg	0	-2	2	4	5	4	2	0	0	-2	2	4	6	5	3	0	0	0	0	0	0	0	0	-2	2

RUN 53 BALANCE UNLOCKED

DATA PT.	26	27	28	29	30	31	32	33	34	1	2	3	4	5	6	7	8	9	10	11	12	13	14	15	16
ROTOR RPM	420	420	420	420	420	420	420	420	426	400	410	410	428	450	445	445	445	445	445	445	445	445	445	445	445
θ_{75} deg	30.8	30.8	31.8	30.8	30.8	30.8	30.8	30.8	30.8	21.6	21.6	21.6	21.6	21.6	21.6	21.6	21.6	21.6	21.6	21.6	21.6	21.6	21.6	21.6	21.6
d_w deg	4	5	3	0	0	0	0	0	0	0	0	0	0	0	0	6	-2	2	4	6	5	0	0	0	0
A_1 deg	0	0	0	0.3	.63	1.00	[illegible]	.3	.3	0	0	0	0	0	0	0	0	0	0	0	0	0	0	-.3	.65
B_1 deg	0	0	0	0	0	0	-4	.75	-2.5	0	0	0	0	0	0	0	0	0	0	0	0	.55	1.0	1.5	0

DATA PT.	17	18	
A_1 deg	-.7	1.0	
B_1 deg	6	0	

RUN NO.	CONFIGURATION	TYPE OF RUN	WT. TARE RUN	q_w deg	θ_{1S} deg	A_1 deg	B_1 deg	G_N deg	V_T KTS	P_T IN Hg	T_T °F	ψ_T deg	WIND ON T, MIN HRS	DATE TIME
54	FULL STIFF WING, BLADES ON			0	4.18	.3	.25	0	192	25.80	120	91.6	1.5	8/1/72

RUN 54, ROTOR RPM = 386, BALANCE UNLOCKED, G_P = 1000 G_Y = 0 D/P 1 - 20

DATA PT	1	2	3	4	5	6	7	8	9	10	11	12	13	14	15	16	17	18	19	20	21	22	23	24	25
INPUT FREQ CPS	0	.2	.4	.6	.65	.7	.8	.9	1.0	1.1	1.2	1.3	1.4	1.6	1.8	2.0	2.2	2.4	3.0	.2	.4	.6	.65	.7	

G_P=0, G_Y=1000 D/P 21 - 35 CB.0.5 BL & 3 OUT AND OFF.

DATA PT	21	22	23	24	25	26	27	28	29	30	31	32	33	34	35	36	37	38	39	40	41	42	43	44	45
INPUT FREQ CPS	.8	.6	1.0	1.1	1.2	1.3	1.4	1.6	1.8	2.0	2.2	2.3	2.4	3.0											

OPEN LOOP PITCH AND YAW BODES

PREP'D			REVISED	DATE
CHK'D				
APPR'D				

26 FOOT DIAMETER
M-222 ROTOR TEST

NASA 40X80
TEST 410

RUN NO.	CONFIGURATION	TYPE OF RUN	WT. TARE RUN	d_{LS} deg	$\theta_{.75}$ deg	A_1 deg	B_1 deg	d_N deg	V_T KTS	P_T IN HG	T_T °F	γ_{P_R} deg	WIND ON TIME HRS	DATE TIME
55	FULL STIFF WINGS, BLADES ON			2	41.7	—	—	0	192	29.8		9/16	.7	8/1/72
56	" " " "			D	41.4	—	—	0	192	29.8		9/16	1.0	8/1/72

RUN 55 ROTOR RPM = 386, BALANCE UNLOCKED D/P NO. 16 d_{LS} = 0

DATA PT.	1	2	3	4	5	6	7	8	9	10	11	12	13	14	15	16	17	18	19	20	21	22	23	24	25
G_Y CTS	0	0	100	200	300	400	500	600	700	—	—	—	300	400	—	—	—								
G_P CTS	0	—	—	—	—	—	—	—	—	0	100	200	300	400	0	—									

RUN 56 ROTOR RPM = 386, BALANCE UNLOCKED G_Y = 700 CTS

DATA PT.	1	2	3	4	5	6	7	8	9	10	11	12	13	14	15	16	17	18	19	20	21	22	23	24	25
INPUT C_{P_3} EREQ	0	0	0	-.2	-.9	-.6	.65	.7	.8	.5	1.0	1.1	1.2	1.3	1.4	1.6	1.8	2.0	2.2	2.3	2.4	3.0	.5	1.5	1.7

D/P NO. G_Y = 700 CTS CLOSED

G_P = 1000 CTS OPEN.

PREP'D				
CHK'D				
APPR				
			REVISED	DATE

26 FOOT DIAMETER
M-222 ROTOR TEST

NASA 40X80
TEST 410

THE BOEING COMPANY

NUMBER D222-10059-1
REV LTR

RUN NO.	CONFIGURATION	TYPE OF RUN	WT. TARE RUN	α_w deg	θ_{TS} deg	A_1 deg	B_1 deg	G_N deg	V_T KTS	P_T IN HG	T_T °F	ψ_T deg	WIND OR TIME KTS	DATE TIME
57	Full Stiff Wing Blades ON			2	41.6	—	—	0	190			9/6	.5	9/1/72

RUN 57 ROTOR RPM = 386 BALANCE UNLOCKED DUP NO. 1 AND 4

DATA	PT	1	2	3	4	5	6	7	8	9	10	11	12	13	14	15	16	17	18	19	20	21	22	23	24	25
Gy	CTS	—	0	0	0	200	340	340	440	500	640	700	600	500	500	400	300	200	100	100	200	300	400	500	600	700
Gp	CTS	0	0	0	100	100	100	100	100	100	100	200	200	200	200	200	200	200	200	300	300	300	300	300	300	300

$\alpha_w = 0$

DATA	PT	26	27	28	29	30	31	32	33	34	35	36	37	38	39	40	41	42	43	44	45	46	47	48	49	
Gy	CTS	700	600	500	400	300	200	100	100	200	300	400	500	600	700	700	600	500	400	300	200	100	0	0	—	
Gp	CTS	400	400	400	400	400	400	400	500	500	500	500	500	500	500	600	600	600	600	600	600	600	600	0	—	

PREP.			REVISED	DATE
CHK.				
APPR				

25 FOOT ROTOR
M-222 ROTOR TEST

NASA 40X80
TEST 410

FORM 4-8510 (3-70)

PREP.	CHK.	APPR.	REVISED DATE	RUN NO.	CONFIGURATION	TYPE OF RUN	WT. TARE RUN	d_w deg	θ_{75} deg	A_1 deg	B_1 deg	d_N deg	V_T KTS	P_T IN Hg	T_T °F	ψ_R = 0 deg	WING ON TIME HRS.	DATE TIME
				58	FULL STIFF WING, BLADES ON			VARY	VARY	0	0	0	VARY	29.86	94/136	91.6	1.5	8/5/72

RUN 58 BALANCE UNLOCKED – NASA BALANCE SIDE FORCE IS QUESTIONABLE

DATA PT.	1	2	3	4	5	6	7	8	9	10	11	12	13	14	15	16	17	18	19	20	21	22	23	24	25
d_w deg	0	-1	-2	-3	-4	-5	-6	-3	1	2	3	4	5	6	7	3	0	0	-1	-2	-3	-4	-2	0	2
V_T KTS	170	170	170	170	170	170	170	170	170	170	170	170	170	170	170	170	170	192	192	192	192	192	192	192	192
ROTOR RPM	400	400	400	400	400	400	400	400	400	400	400	400	400	400	400	400	400	450	450	450	450	450	450	450	450
θ_{75} deg	37.2	37.2	37.2	37.2	37.2	37.2	37.2	37.2	37.2	37.2	37.2	37.2	37.2	37.2	37.2	37.2	37.2								

DATA PT.	26	27	28	29	30	31	32	33	34	35	36	37
d_w deg	3	4	2	0	0	1	2	3	4	2	-1	-2
V_T KTS	192	192	192	192	192	192	192	192	192	192	192	192
ROTOR RPM	450	450	450	450	386	386	386	386	386	386	386	386
θ_{75} deg	~~42.2~~	~~42.2~~	~~42.2~~	~~42.2~~	42.2	42.2	42.2	42.2	42.2	42.2	42.2	42.2

THE BOEING COMPANY

NUMBER D222-10059-1
REV LTR

SHEET 649

RUN NO.	CONFIGURATION	TYPE OF RUN	WT. TARE RUN	d_w	$\theta_{.75}$	A_1	B_1	d_N	V_T	P_T	T_T	$\psi_{R.T.}$	WIND SPD & TIME	DATE TIME
				deg	deg	deg	deg	deg	KTS	IN HG	°F	deg	KTS	
59	Full Size Wing, Blades on			VARY	VARY	VARY	VARY	0	192	29.74	92/130	VARY	1.5	

RUN 55

DATA PT		1	2	3	4	5	6	7	8	9	10	11	12	13	14	15	16	17	18	19	20	21	22	23	24	25
A_1	deg	0	.9	.85	.6	.7	.2	-.3	-.8	-.4	-1.1	-.9	-.6	.6	-.4	.1	-.6	-.3	-.3	-.7	-.8	-.8	-.6	-.3	.1	.4
B_1	deg	0	0	-.3	-1.0	-.5	-.9	.55	.65	.15	-.5	-.55	0	-.4	-.7	-.1	-.75	-1.0	-1.0	-.75	-.9	0	.3	.55	.55	.3
ψ_{ROT}	deg	90	90	60	30	120	150	180	240	270	300	330	0	30	60	90	120	150	180	210	240	270	300	330	360	390

DATA PT		26	27	28	29	30	31	32	33	34	35	36	37	38	39	40	41
A_1	deg	.6	.6	.45	.1	0	0	.35	.85	.12	-.7	0	0	0	0	0	0
B_1	deg	0	-.4	-.7	-.1	0	0	0	0	0	0	-.6	-1	.45	.79	.9	0
ψ ROT	deg	90	60	30	0	90	90	90	90	90	90	90	90	90	90	90	90

1. BALANCE UNLOCKED
2. RPM = 386 FOR O/P 1 - 30 $\theta_{.75}$ = 42°
   RPM = 300 FOR O/P 31 - 41 $\theta_{.75}$ = 48.5°
3. d_w = 0 FOR O/P 1 - 18 AND 31 - 41
   d_w = +2° FOR O/P 19 - 30
4. VARIATION OF ψ_{ROT} # 1 IS LOW RATE SYSTEM.

PREP.			REVISED	DATE
CHK.				
APPR				

26 FOOT DIAMETER
M-222 ROTOR TEST

NASA 40 X 80
TEST 410

FORM 46810 (3/70)

THE BOEING COMPANY

PREP.			
CHK.			
APPR			
	REVISED	DATE	

RUN NO.	CONFIGURATION	TYPE OF RUN	WT. TARE RUN	α_w deg	$\theta_{.75}$ deg	A_1 deg	B_1 deg	α_N deg	V_T KTS	P_T IN HG	T_T °F	γ_{s_T} deg	WIND ON TIME HRS.	DATE TIME
60	FULL STIFF WING, BLADES ON			0	41.6	—	—	0	192	29.73	104/136	VARY	1.7	9/5/72

RUN 60

DATA PT	1	2	3	4	5	6	7	8	9	10	11	12	13	14	15	16	17	18	19	20	21	22	23	24	25
INPUT FREQ CPS	0	.2	.3	.4	.5	.6	.707	.803	.903	1.0	1.56	2.00	2.50	3.00	3.50	.2	.2	0	.2	.3	.4	.455	.556	.706	.8

1. ROTOR RPM = 386
2. G_p = 1000 CTS FOR D/P 1 - 15 AND 41 - 49 AND 0 CTS ALL OTHERS

   G_y = 0 CTS FOR D/P 1 - 15 AND 41 - 49 AND 1000 CTS D/P 17-18

   ψ_{ROT} = 50° D/P 1-32 AND 20° D/P 33 - 49

DATA PT	26	27	28	29	30	31	32	33	34	35	36	37	38	39	40	41	42	43	44	45	46	47	48	49	
INPUT FREQ CPS	.51	1.01	1.51	2.00	2.50	3.00	4.00	.2	.4	.556	.8	1.00	1.50	2.00	2.50	.20	.35	.551	.81	1.00	1.50	2.00	2.00	4.00	

3. SHAKER VANE STRAIN GAGE OUT AND OFF
4. NASA BALANCE IS LOCKED NO FORTHER NOTES UNLESS BALANCE IS UNLOCKED

26 FOOT DIAMETER

N7-222 ROTOR TEST

NASA 40X80 TEST 410

NUMBER D222-10059-1
REV LTR

SHEET 651

FORM 4951 (1-70)

THE BOEING COMPANY

NUMBER D222-10059-1
REV LTR

RUN NO.	CONFIGURATION	TYPE OF RUN	WT. TARE RUN	α_w	θ_{75}	A_1	B_1	q_∞	V_T	P_T	T_T	$\psi_{\frac{R}{T}}$	Wind on TIME	DATE TIME
				deg	deg	deg	deg	deg	KTS	IN Hg	°F	deg	HRS.	
61	Full Stiff Wings, Blades on			Vane	4.4	—	—	0	152	29.10	75/124	50	1.0	

RUN 61

DATA PT	1	2	3	4	5	6	7	8	9	10	11	12	13	14	15	16	17	18	19	20	21	22	23	24	25
G_P CTS	0	0	0	100	200	300	400	500	600	700	800	500	0	0	0	0	0	0	0	0	0	0	0	0	0
C_Y CTS	0	0	0	0	0	0	0	0	0	0	0	0	0	100	200	300	400	500	600	700	800	850	Scrub	0	0
α_w deg	0	2	3	3	3	3	3	.8	.6	.1	.7	.5	.4	3	3	3	3	3	3	3	3	3	3	3	0

DATA PT.	26	27	28	29	30	31	32	33	34	35	36	37	38	39											
INPUT FREQ CPS	.2	-.3	.4	.5	.6	.7	.8	.6	1.0	1.5	2.0	2.5	3.0	4.0											

1. BOTH PITCH AND YAW LOOPS CLOSED FOR D/P 1 - 25
   YAW LOOP OPEN AND G_Y = 1000 CTS FOR D/P 26 - 38
   PITCH LOOP CLOSED AND G_P = 700 CTS FOR D/P 26 - 38.
2. SPINNER SEAL CAME LOOSE DURING RUN - REPLACED PRIOR TO RUN 62
3. ROTOR RPM = 386

PREP.			REVISED	DATE
CHK.				
APPR.				

26 FOOT DIAMETER
M-222 ROTOR TEST

NASA 40x80
TEST 410

FORM 4-10-13-70

THE BOEING COMPANY

NUMBER D222-10059-1
REV LTR

RUN NO.	CONFIGURATION	TYPE OF RUN	WT. TARE RUN	d_W deg	θ_{TS} deg	A_1 deg	B_1 deg	d_N deg	V_T KTS	P_T IN HG	T_T °F	$\psi_{\frac{1}{2}}$ deg	WIND ON TIME HRS.	DATE TIME
62	FULL STIFF WING, BLADES ON			0/3	41.6	—	—	0	192	25.67	59/121	50	1.0	

RUN 62

DATA	PT	1	2	3	4	5	6	7	8	9	10	11	12	13	14	15	16	17	18	19	20	21	22	23	24	25
GP	CTS	0	0	20	40	60	80	100	120	140	160	180	200	220	240	260	280	300	320	340	360	380	400	420	440	460
GY	CTS.	0	0	0	0	0	0	0	100	200	300	400	500	600	700	800	900	1000	1100	1200	1300	1400	1500	1600	1700	1800

DATA	PT	26	27	28	29	30	31	32	33	34	35	36	37	38	39	40	41	42	43	44	45	46	47	48	49	50
GP	CTS	400	540	680	820	960	1100	1240	1380	1520	1660	1800	1940	2080	2220	2360	2500	2640	2780	2920	3060	3200	3340	3480	3620	3760
GY	CTS	200	340	480	620	760	900	1040	1180	1320	1460	1600	1740	1880	2020	2160	2300	2440	2580	2720	2860	3000	3140	3280	3420	3560

DATA	PT	51	52	53	54	55	56	57	58	59	60	61	62	63	64	65	66	67	68	69	70	71				
GP		700	700	600	500	400	300	200	100	0	0	100	200	300	400	500	600	700	800	900	1000	0	0			
GY		400	500	500	500	500	500	500	500	500	600	600	600	700	700	700	700	700	700	700	700	0	0			

1. ROTOR RPM = 386
2. BOTH PITCH AND YAW LOOPS CLOSED.
3. $d_W = 0$ FOR D/P 1 AND 71 FOR ALL OTHER D/P $d_W = 3$ deg.

PREP.			REVISED	DAT
CHK.				
APPR				

26 FOOT DIAMETER
M-222 ROTOR TEST

NASA 40 X 80
TEST 410

FORM 49510 (3/70)

THE BOEING COMPANY

RUN NO.	CONFIGURATION	TYPE OF RUN	WT. TARE RUN	d_w deg	$\theta_{.75}$ deg	A_1 deg	B_1 deg	a_N deg	V_T KTS	P_T IN HG	T_T °F	ψ_{ROT} deg	WIND ON TIME HRS	DATE TIME
63	FULL STIFF WING, BLADES ON			VARY	41.7	—	—	0	192	29.64	114/132	50	1.0	
64	FULL STIFF WING, BLADES ON			0/2	41.7	—	—	0	192	29.66	109/134	50/60	1.5	9/16/71

RUN 63

DATA PT.	1	2	3	4	5	6	7	8	9	10	11	12	13	14	15	16	17	18	19	20	21	22	23	24	25
d_w deg	0	-1	-2	0	1	2	3	4	5	0	0	-1	-2	-3	0	1	2	3	4	5	6	7	0	0	-2

DATA PT	26	27	28	29	30	31	32	33	34	35	36														
d_w deg	-3	-4	0	2	4	6	7	8	5	9	0														

1. ROTOR RPI = 386
2. G_P = 0 D/P 1-10, G_P = 204 D/P 11-23, G_P = 400 D/P 24-36
   G_Y = 0 D/P 1-10 G_Y = 300 D/P 11-36

RUN 64 BOTH LOW RATE LOOPS CLOSED - BODE FOR HIGH RATE LOOP

DATA PT.	1	2	3	4	5	6	7	8	9	10	11	12	13	14	15	16	17	18	19	20	21	22	23	24	25
INPUT FREQ CPS	—	—	—	—	—	—	.2	.3	.4	.6	.8	1.01	1.51	1.76	2.00	2.10	2.15	2.18	2.20	2.22	2.24	2.26	2.28	2.31	2.32
DATA PT	26	27	28	29	30	31	32	33	34	35	36	37													
INPUT FREQ CPS	2.39	2.36	2.4	2.5	2.6	2.7	3.0	2.2	4.0	2.12	2.08	2.00													

1. ψ_{ROT} LOW RATE = 50°, ψ_{ROT} HIGH RATE = 60°, G_{VA} = 0 D/P 1-6
2. ROTOR RPM = 386, G_P = 0 D/P 1-2, 100 CTS D/P 3 ALL OTHERS = 204 CTS
3. d_w = 0 FOR D/P 1 AND D/P 6-37 ALL OTHERS d_w = 2 deg
4. G_Y = 0 CTS D/P 1-2, 150 CTS D/P 3-4 ALL OTHERS G_Y = 300 CTS.
5. G_{VA} = 0 CTS D/P 1-6 AND 100 CTS ALL OTHER D/P.
6. TUNNEL LOUVERS OPEN D/P 1-4 OPEN FOR ALL OTHERS

26 FOOT DIAMETER M-122 ROTOR TEST

NASA 40 X 80 TEST 41C

NUMBER D222-10059-1
REV LTR

SHEET 654

FORM AM 10 (4-70)

THE BOEING COMPANY

NUMBER D222-10059-1
REV LTR

RUN NO.	CONFIGURATION	TYPE OF RUN	WT. TARE RUN	ϕ_w deg	θ_{TS} deg	A_1 deg	B_1 deg	ϕ_N deg	V_T KTS	P_T IN HG	T_T °F	$\psi_{R.T}$ deg	WIND ON TIME HRS	DATE TIME
65	FULL STIFF WING, BLADES ON			VARY	41.7	—	—	0	192	29.71	54/123	50/60	2.0	9/6/72

DATA PT.	1	2	3	4	5	6	7	8	9	10	11	12	13	14	15	16	17	18	19	20	21	22	23	24	25
GP CTS	0	0	0	0	0	0	0	0	0	0	0	0	0	0	OPEN	OPEN	20#	20#	20#	20#	20#	20#	20#	20#	20#
GY CTS	0	0	0	0	0	0	0	0	0	0	0	0	0	0	OPEN	OPEN	300	300	300	300	300	300	300	300	300
GYA CTS	0	1000	1000	1000	1000	1000	1000	1000	1000	1000	1000	1000	1000	1000	1000	1000	1000	1000	1000	0	0	0	0	0	102
INPUT FREQ CPS	—	2.0	2.04	2.1	2.14	2.22	2.30	2.40	2.50	2.60	2.60	2.80	2.70	3.00	OPEN	OPEN	2.22	2.08	2.24	2.40	—	—	—	—	—	—

DATA PT.	26	27	28	29	30	31	32	33	34	35	36	37	38	39	40	41	42	43	44	45	46	47
GP CTS	20#	20#	20#	20#	20#	20#	20#	20#	20#	20#	20#	20#	20#	20#	20#	0	20#	20#	20#	20#	20#	20#
GY CTS	300	300	300	300	300	300	300	300	300	300	300	300	300	300	300	0	300	300	300	300	300	300
GYA CTS	102	200	200	200	200	400	400	600	600	600	700	700	700	700	0	700	700	700	700	700	700	

1. ROTOR RPM = 386, ψ_{ROT} LOW RATE = 50°; ψ_{ROT} HIGH RATE = 60°
2. LOUVERS CLOSED D/P 1-39 42-47 OPEN FOR D/D 40-41 TO CHECK REACTIONS TO TUNNEL TURBLENCE
3. LOW RATE CLOSED HIGH RATE OPEN D/P 17-19
   LOW RATE AND HIGH RATE CLOSED D/P 20-47
4. DATA N.G. D/P 23, 28
5. D/P 1-19 HIGH RATE MODE

TOTAL WIND ON TIME AT END OF RUN 65
74.842 HOURS

26 FOOT DIAMETER M-222 ROTOR TEST

NASA 40'x80' TEST 4/10

PREP. / CHK. / APPR. / REVISED / DATE

FORM 49510-3-7/01

SHEET 655

THE BOEING COMPANY

RUN NO.	CONFIGURATION	TYPE OF RUN	WT. TARE RUN	α_w deg	$\theta_{.75}$ deg	A_1 deg	B_1 deg	α_N deg	V_T KTS	P_T IN HG	T_T °F	ψ_{Rot} deg	WIND ON TIME HRS	DATE TIME
66	Full Stiff Wing, Blades On			0	41.8			0	192	29.81	105/134	50/60	.9	
67				0	41.6			0	192	29.81	90/120	50/60	1.5	

PREP. | CHK. | APPR | DATE

REVISED

Run 66 RPM = 386 DP 2 PMS VM at tip statically balanced DP 2 PMS VM at Tip dynamically balanced

Data Point	1	2	3	4	5	6	7	8
Longitudinal deg			.25	.25	.25	.5	.5	.5
Freq cps			1.0	1.0	1.0	1.0	.5	.1

Open Loop DP 9-7 on off many cycle points Green Lead attached to Wavetek generator for Runs 66 & 67

Run 67

Data Point	1	2	3	4	5	6	7	8	9	10	11	12	13	14	15	16	17	18	19	20	21	22	23	24
Longitudinal deg		.5	.5	.5	1.0	1.0	1.0		.5	.25	.5	.5	.5	1.0	1.0	1.0		1.0	1.0	1.0	1.0	1.0	1.0	1.0
Freq cps		1.0	.5	.1	.1	.5	1.0		.1	1.0	.1	.5	1.0	.1	.5	1.0		.5	.5	.1	1.0	1.0	.5	.1

DP 1-7 were openloop Gains = 0 DP 8-24 were closed loop G_P = 204 G_y = 300 G_N = 800

DP 17 was a shaker check point zero gain DP 18-24 were one cycle Longitudinal inputs

SHEET 656

NUMBER D222-10059-1
REV LTR

FORM 10-11-13 701

THE BOEING COMPANY

PREP.	CHK.	APPR	REVISED	DATE

RUN NO.	CONFIGURATION	TYPE OF RUN	WT. TARE RUN	α_w deg	$\theta_{.75}$ deg	A_1 deg	B_1 deg	α_N deg	V_T KTS	P_s IN HG	T_s °F	ψ_{BT} deg	WIND OR TIME HRS	DATE TIME
68	Full Stiff Wing, Blades On			0,	24.5			0	100	29.85	79/	50/60	.8	
69				Vary	24.6			0	100	29.9	75/81	50/60	1.6	

Run 68 G_P = 1000 Open Loop Pitch Bode

Data Point	1	2	3	4	5	6	7	8	9	10	11	12	13	14	15	16	17	18	19
Input Freq CPS	0	.1	.3	.5	.71	.917	.917	1.118	1.12	1.21	1.41	1.51	1.71	2.01	2.21	2.21	2.83	3.0	4.0
Input Volts	.6	.6	.6	.6	.6	.6	1.0	1.0	1.0	1.0	1.0	1.24	1.24	1.24	1.0	.6	.6	.6	.6

Run 69 DP 1-17 G_P = 204 closed G_y = 1000 open

Data Point	1	2	3	4	5	6	7	8	9	10	11	12	13	14	15	16	17
Input Freq CPS	.1	.2	.3	.4	.5	.6	.7	.8	.9	1.0	1.2	1.5	1.7	2.0	2.6	3.0	4.0
Input Volts	.6	.6	.6	.6	.6	.6	.6	.6	1.0	1.0	1.0	1.24	1.24	.6	.6	.6	.6

G_P = 204 G_y = 300 Closed loop
DP 18-40 Green lead = PM Black lead = YM DP 34-40 zero Gain Open Loop

Data Point	18	19	20	21	22	23	24	25	26	27	28	29	30	31	32	33	34	35	36	37	38	39	40
α_w - deg	0	-2	-4	-6	0	2	4	6	8	9	10	11	12	13	14	15	0	2	4	6	8	10	0

NUMBER D222-10059-1
REV LTR

SHEET 657

FORM 48[illegible] (3 70)

THE BOEING COMPANY

NUMBER D222-10059-1
REV LTR

SHEET 658

FORM 4-11-1 701

PREP	CHK	APPR		REVISED	DATE

RUN NO.	CONFIGURATION	TYPE OF RUN	WT. TARE RUN	α_W deg	$\theta_{.75}$ deg	A_1 deg	B_1 deg	α_N deg	V_T KTS	P_T IN HG	T_T °F	γ_{RET}	WIND ON TIME HRS	DATE TIME
70	Full Stiff Wing, Blades On			0	24.1			0	100	29.9	88	50/60	1	
71				0	24/22			0	100	29.99		50/60	1.3	

Run 70 Green lead = 180° output from Acc. Blacklead = Function Gen. input to X_2

Data Point	1	2	3	4	5	6	7	8	9	10	11	12	13	14	15	16	17	18	19	20	21	22	23	24	25
Freq Hz	.5	1.0	2.0	2.1	.5	1.0	2.0	2.1	2.11	2.12	2.13	2.15	2.18	2.19	2.2	2.21	2.22	2.23	2.24	2.25	2.26	2.27	2.28	2.29	2.3

DP 1-31 High rate open loop Bode Low Rate Closed Loop $G_P = 204$ $G_Y = 300$ $G_N = 1000$ Input Voltage = 1 volt
DP 31-46 High rate shaker test Low Rate Closed Loop $G_P = 204$ $G_Y = 300$

Data Point	26	27	28	29	30	31	32	33	34	35	36	37	38	39	40	41	42	43	44	45	46				
Freq Hz	2.35	2.4	2.5	2.6	2.8																				
Open Loop High Rate Acc. Gain CTS	0	0	200	200	200	200	400	400	400	400	600	600	600	700	700	700									

Run 71 Open Loop: DP1-24 RPM = 386 $\theta_{.75} = 24.1$ DP 25-52 RPM = 420 $\theta_{.75} = 22.9$

Data Point	1	2	3	4	5	6	7	8	9	10	11	12	13	14	15	16	17	18	19	20	21	22	23	24	25
Freq Hz	0	.2	.2	.3	.4	.5	.6	.7	.8	.85	.9	.95	1.0	1.1	1.2	1.3	1.4	1.5	1.6	1.7	1.8	2.0	2.1	2.2	.2

DP1 & 25-39 Input Voltage = .6v DP 2-24 Input Voltage = 1.2v

Data Point	26	27	28	29	30	31	32	33	34	35	36	37	38	39											
Freq Hz	.3	.4	.5	.6	.7	.8	.85	.9	.95	1.0	1.1	1.2	1.3	1.4											

TEST #10

Data Point	40	41	42	43	44	45	46	47	48	49	50	51	52												
Shake Pot CTS	980	976	972	970	969	968	966	962	960	958	955	952	950												

FORM 4951-1-701

THE BOEING COMPANY

PREP.	CHK.	APPR	REVISED	DATE

RUN NO.	CONFIGURATION	TYPE OF RUN	WT. TARE RUN	α_w deg	$\theta_{.75}$ deg	A_1 deg	B_1 deg	α_N deg	V_T KTS	P_T IN HG	T_T °F	ψ_{EOT} deg	WIND ON TIME HRS	DATE TIME
72	Y4 Stiff Wing, Blades On			0	VARY	0	0	0	80	29.91	85	20	1.8	

Run 72

Data Point	1	2	3	4	5	6	7	8	9	10	11	12	13	14	15	16	17	18	19	20	21	22	23	24	25
Collective deg	43	43	43	35	35	35	29.3	29.3	29.3	29.3	26.1	25.1	26.1	25.1	21.8	21.8	21.8	20.6	20.6	20.6	19.1	19.1	19.1	17.9	17.6
RPM	150	150	150	200	200	200	250	250	250	250	300	300	300	300	350	350	350	370	370	370	400	400	400	430	437
Shaker CTS	958	958	958	958	958	958	958	958	958	958	958	958	958	958	958	958	958	958	958	958	958	958	958	958	958

Data Point	26	27	28
Collective deg	18.1	18.1	18.1
RPM	425	426	425
Shaker CTS	958	958	958

TEST # 410

SHEET 659

NUMBER D222-10059-1
REV LTR

THE BOEING COMPANY

FORM 4810-11 701

APPR	CHK.	PREP.	REVISED	DATE

RUN NO.	CONFIGURATION	TYPE OF RUN	WT. TARE RUN	α_w	$\theta_{.75}$ DEG	A_1 DEG	B_1 DEG	α_N DEG	V_T KTS	P_T IN Hg	T_T °F	ψ_{ROT} DEG	WIND ON TIME HRS	DATE / TIME
73	1/4 STIFF WING, BLADES ON			0	VARY	0	0	0	VARY	29.95	66	20		

RUN 73

DATA POINT	1	2	3	4	5	6	7	8	9	10	11	12	13	14	15	16	17	18	19	20	21	22	23	24	25
COLLECTIVE deg	36.1		44.7	44.7	44.7	51.6	51.6	51.8	—												→	51.8	51.8	51.8	51.8
RPM	193		193	193	193	193	193	170	—															→	170
VELOCITY KTS	80		110	110	110	140	—																	→	160
FREQ HZ			2.8	2.8	5.0	5.0	5.0		.8	.9	1.0	1.0	1.1	1.2	1.3	1.4	1.5	1.6	1.7	1.8	1.9	2.0	2.1	2.2	2.3
INPUT VOLTS								1.	1.	1.	1.	.6	—											→	.6

DATA POINT	26	27	28	29	30	31	32	33	34	35	36	37	38	39	40
COLLECTIVE deg	51.8	—					→	51.8	51.5	—				→	51.5
RPM	170	—					→	170	193	—				→	193
VELOCITY KTS	140	—												→	140
FREQ HZ	2.4	2.5	1.85	1.75	1.0	1.0	1.8	1.83	1.6	1.7	1.75	1.8	1.85	1.9	2.0
INPUT VOLTS	.6	.6	.6	.6	1.	1.	1.	1.	.6	.6	.6	.4	.4	.4	.4

DATA POINT 2 CONTINOUS POINT TRANSITION

TEST #410

SHEET 660

NUMBER D222-10059-1
REV LTR

THE BOEING COMPANY

NUMBER D222-10059-1
REV LTR

SHEET 661

FORM 4P510 (7-70)

RUN NO.	CONFIGURATION	TYPE OF RUN	WT. TARE RUN	α_W	$\theta_{.75}$ DEG	A_1 DEG	B_1 DEG	α_N DEG	Ω RPM	P_T IN Hg	T_T °F	ψ_{REF} DEG	WIND ON TIME HRS	DATE TIME
74	1/4 STIFF WING, BLADES ON			0	VARY	0	0	0	193	29.95	92	20		

RUN 74

DATA POINT	1	2	3	4	5	6	7	8	9	10	11	12	13	14	15	16	17	18	19	20	21	22	23	24	25
COLLECTIVE deg	53.0	—	—	—	—	—	—	—	—	—	—	—	—	→	53.0	54.0	55.1	55.1	56.4	56.4	56.4	56.4	56.5	56.5	56.5
VELOCITY KTS	150	—	—	—	—	—	—	—	—	—	—	—	—	→	150	155	163	163	170	170	170	170	170	170	170
FREQ HZ	1.4	1.5	1.55	1.6	1.65	1.7	1.75	1.8	1.85	1.9	2.0	2.1	2.2	2.3	2.4	1.78	1.78	1.78	1.0	1.0	1.78	1.6	1.65	1.7	1.75
INPUT VOLTS	.2	—	—	—	—	—	—	—	—	—	—	—	—	—	→	.2	.15	.2	.2	.3	.3	.3	.3	.3	3

DATA POINT	26	27	28	29	30	31	32	33	34	35	36	37	38	39
COLLECTIVE deg	56.5	56.5	56.5	56.5	57.1	57.8	—	—	—	—	—	—	→	57.8
VELOCITY KTS	170	170	170	170	175	180	—	—	—	—	—	—	→	180
FREQ HZ	1.8	1.85	1.9	2.0	1.75	1.75	1.6	1.65	1.7	1.75	1.8	1.85	1.9	2.0
INPUT VOLTS	.3	—	—	—	—	—	—	—	—	—	—	—	→	.3

DATA POINTS 19, 20, 21, 30 & 31 EXITATION WAS CHOPPED

TEST #410

THE BOEING COMPANY

RUN NO.	CONFIGURATION	TYPE OF RUN	WT. TARE RUN	α_W	$\theta_{.75}$ DEG	A_1 DEG	B_1 DEG	α_N DEG	Ω RPM	P_T IN HG	T_T °F	ψ_{AZ} DEG	WIND ON TIME HRS	DATE / TIME
75	1/4 STIFF WING, BLADES ON			0	VARY	0	0	0	193	29.95	129	20		

PREP. | CHK. | APPR. | REVISED | DATE

RUN 75

DATA POINT	1	2	3	4	5	6	7	8	9	10	11	12	13	14	15	16	17	18	19	20	21	22	23	24	25
COLLECTIVE deg	57.6	57.6	57.8	57.8	58.3	—															→	58.3	58.6	58.6	58.6
VELOCITY KTS	180	180	185	185	190	—																		→	190
FREQ Hz		1.75		1.75		1.75	1.6	1.7	1.75	1.8	1.9	2.0	.8	.9	1.0	1.1	1.2	1.3	1.4	1.5	2.1	2.2	2.3	2.4	2.5
INPUT VOLTS		.25		.3		.23	.23	.2	—															→	.2

DATA POINTS 1, 3 + 5 SHAKER COUNTS = 954

DATA POINTS 2, 4 + 6 EXITATION WAS CHOPPED

TEST #410

SHEET 662

NUMBER D222-10059-1
REV LTR

APPENDIX 2

APPENDIX 2 TEST RUN LOG TEST 416

NASA Ames 40' X 80' Wind Tunnel

FORM 4M10 (4-70)

THE BOEING COMPANY

PREP.	CHK.	APPR.	REVISED	DATE

RUN NO.	CONFIGURATION	TYPE OF RUN	WT. TARE RUN	i_N °	$V_{KT.}$	$\theta_{.75}$ °	A_1 °	B_1 °	RPM	DATE — TIME
a/	LOW Ω STAND CONFIG. NO BLADES	C/O	—	0	0	—	—	—	VAR	11/24/72
b)	✓	C/O	~	0	0	—	—	—	VAR	11/27/72
1	✓	HUB TARES	—	VAR	VAR	—	—	—	VAR	11/28/72
2	✓	✓		✓	✓				✓	✓ 2024

a) CHECKOUT RUN - BEGINNING STAND/HUB RESONANCE INVESTIGATION. RPM TO 125 ONLY. CEC DATA ONLY.

b) FUNCTIONAL CHECK-OUT RUN. RPM 80 → 349 /5 RPM APPROX.

1. AERODYNAMIC HUB TARES. ABORTED DUE TO FOULING INDICATION.

2. CONTINUATION RUN 1. FOUL RESOLVED.

q/RPM	i_N°
22/386	0, 5, 10, 14, 18, 22, 26, 30
22/450	30,
22/550	30, 14, 0
22/555	22,
22/430	14, 0
68/386	0
110/386	0

INTERMITTENT FOULING @ q = 22. STEADY FOUL @ q = 68.

INITIAL FOULING INDICATION (RUN 2) CAUSED BY FAULTY MIKE CABLE. RESOLVED. MORE FOULING @ $i_N > 5°$, $q \rightarrow 68.0$

M 222 ~ 26 FT DIA. POWERED ROTOR TEST

40' x 80'

T.416

NUMBER D222-10059-1
REV LTR

SHEET 664

RUN NO.	CONFIGURATION	TYPE OF RUN	WT. TARE RUN	i_N °	$V_{KT.}$	$\theta_{.75}$°	A_1	B_1	RPM				DATE TIME
3	LOW i_N STAND CONFIG. NO BLADES	HUB TARE	—	VAR	VAR	—	—	—	VAR				3/29/72
4	"	"		✓	✓	—	—	—	✓				✓
5	✓	✓		✓	✓	—	—	—	✓				
	✓												
	✓												
	✓												
	✓												
	✓												
	✓												
	✓												

3. CONTINUATION LOW < HUB TARES.

4. CONTINUATION LOW < HUB TARES.

PREP.	KEF.		REVISED	DATE
CHK.				
APPR				

M-222 ~ 26 FT. DIA. POWERED ROTOR TEST

40'x80'

T. 416.

FORM 4951D (3/70)

BOEING COMPANY

NUMBER D222-10059-1
REV LTR

RUN NO.	CONFIGURATION	TYPE OF RUN	WT. TARE RUN	i_N °	$V_{KT.}$	q_T NOM	$\theta^\circ_{.75}$ NOM	A_1° NOM	B_1° NOM	RPM NOM		DATE TIME
6	LOW i_N STAND CONFIG. BLADES ON	HOVER		0	0	0	9.0	0	0	VAR		12/6/72
7	✓ ✓ ✓ ✓	HOVER		0	0	0	VAR	VAR	VAR	551		✓

6/ RPM 77 → 110 / 4 D.P's. DOWN TO INVESTIGATE BLADE ∠ POT ERRATIC READOUT. POT OK.
CONTINUE RUN: $A_1 = B_1 = 0$ $\theta_{.75} \doteq 8.8°$. CYCLICS NOT ADJUSTED. 1∂ PEAK @ RPM = 290

T.P.# :	1	2	3	4	5	6	7	8	9	10	11	12	13	14	15	16	17	18
RPM. :	78	93	100	110	120	126	141	159	169	180	191	200	220	230	240	251	260	270
TP# :	19	20	21	22	23	24	25	26	27	28	29	30	31					
RPM :	276	280	296	309	335	352	380	410	437	470	500	525	550					

BLADE PITCH ∠ NOT OPERATIONAL (SLIPRING). BLADES TRACKED @ 550 RPM :- RED & YELLOW
TIPS DEAD ON, WHITE SLIGHTLY LOW. NO ADJUSTMENT REQUIRED. 9 INCREASED TO ABOUT 1.0.
BLADE #2 CB 22.5% WENT OUT AT T.P.#

7/ COLLECTIVE, A_1, B_1 VARIATIONS @ CONST RPM OF 551.

TP# :	1.	2	3	4	5		6	7	8	9	10	11	12	13	14
$\theta_{.75}$° :	SEIN UP	9	10	11	SPIN		9	10	11	12	415V	12	11	10	9
A_1° :		0	0	0	DOWN		0	0	0	0	0	0	0	0	0
B_1° :		0	0	0	MAX REVERSE 9		0	0	0	0	0	0	0	0	0
					NEW ZEROES, R-CALS										
TP# :	15	16	17	18*	19	20	21	22	23	24		REVERSE FAN TO KEEP TUNNEL '9'			
$\theta_{.75}$° :	9	9	9	9	9	9	9	9	9	9		DOWN (9 ≈ 2·0)			
A_1° :	-1	-1·5	-2·0	-2·5	-3·0	0	0	0	0	0					
B_1° :	0	0	0	0	0	0	1	1·5	2·0	2·5	(P.L. BLK. LINE)				

* FOUL INDICATION

PREP.	KEF.		REVISED	DATE
CHK.				
APPR				

M 222 - 26 FT DIA POWERED ROTOR TEST

40'x80'
T. 416

FORM 49510 (3/70)

RUN NO.	CONFIGURATION	TYPE OF RUN	WT. TARE RUN	i_N °	V_{KTS}	q_T	$\theta_{.75}$ °	A_1 °	B_1 °	RPM				DATE TIME
8	LOW i_N ° STAND CONFIG. BLADES ON			30	105		VAR	VAR	VAR	551				12/7/72
9	✓ ✓ ✓			30	105		VAR	VAR	VAR	551				12/11
10	✓ ✓ ✓			0	0	0	24.0	0	0	VAR				12/11

8. RUN ABORTED AFTER T.P. 1. SPURIOUS, & THEN LOSS OF SIGNALS ON SAFETY MONITORING GAGES (IN-PLANE & OUT OF PLANE HUB B.M.). SIGNALS BAD, OIL ON SLIPRINGS. CLEAN-UP PROCEDURE & MOD. TO RIG TO PREVENT OIL SEEPAGE INTO SLIPRING CAVITY. VALUES FOR T.P. 1 : $i_N = 30°$ $\theta_{.75}$ = A_1 = B_1 =

9. REPEAT OF RUN #8 WITH MODS. INCORPORATED. DATA. ACQUIRED :

TP#	1	2	3	4	5	6	7	8	9	10	11	12	13	14	15	16	17	18	19	20	21	22	23	24	25
$\theta_{.75}$	18.8	18.6	20	20.1	18.9	18.9	18.9	19.9	20.9	19.0	17.9	18.9	18.9	→						18.9	18.8	18.9	→		
A_1	0	-.74	-1.62	-1.6	-1.6	-1.6	-2.16	-2.12	-2.2	-2.16	-2.16	-2.08	-2.09	-2.12	-2.12	-2.12	-1.82	-1.51	-1.23	-.9	-2.42	-2.77	-3.16	-2.16	-2.16
B_1	0	-.90	1.66	1.7	1.65	1.66	2.56	2.56	2.56	2.56	2.57	2.56	2.56	2.57	2.56	2.56	2.56	2.56	2.56	2.56	2.56	2.56	2.57	2.56	2.57
i_N °	0	5	10	15	20	24	27	27	27	27	27	24	21	18	15	27	→								

TP#	26	27	28	29	30	31	32	33
$\theta_{.75}$	18.9	→						18.9
A_1	-2.12	-2.16	-2.12	-2.12	-2.12	-2.12	-2.16	-2.12
B_1	3.16	3.46	2.25	1.94	1.63	1.53	3.72	2.56
i_N °	27	→						

10. CHECKOUT RUN @ $q_T = 0$ PRIMARILY TO INVESTIGATE GROWTH OF CB 55% BLADE LOADS.
$\theta_{.75} = 24°$ (.54 DPM)

TP #	1	2	3	4	5
RPM	100	150	200	250	295

1& PEAK @ ABOUT 238.

FORM 4681D (1-70)

PREP. | DATE
REVISED | DATE
CHK. | DATE
APPR | DATE

M.222 ~ 26 FT. DIA. POWERED ROTOR TEST

40' x 80'
T. 416

SHEET 667

RUN NO.	CONFIGURATION	TYPE OF RUN	WT. TARE RUN	i_N	V_{kts}	q_T PSF	$\theta_{.75}$ °	A_1 °	B_1 °	RPM				DATE TIME
11	Low i_N ° STAND CONFIG. BLADES ON		–	10	140	70	VAR	VAR	VAR	386				12/12/72
12	✓ ✓ ✓ ✓		–	30	140		VAR	VAR	VAR	551				✓

11. DATA ACQUIRED : DID EMERGENCY SHUT DOWN CHECK-OUT @ i_N = 10°

TP # :	1	2	3	4	5	6	7	8	9	10	11	12	13	14	15	16	17	
$\theta_{.75}$:	35·1	35·6	34·0	35·1	34·7	33·7	35·1	34·9	34·75	35·1	35·6	35·1	34·5	33·9	33·4	35·0	35·0	
A_1 ° :	-·2	-·16	-·16	-·16	-·14	-·16	-·20	0	-·69	-2·62	-2·58	-2·62	-2·62	-2·62	-2·62	-2·58	-2·46	
B_1 ° :	0	0	0	0	0	0	0	1·29	1·29	2·31 →								2·31
i_N ° :	0 →						0	3	3	10 →						10	12	
TP# :	18	19	20	21	22	23	24	25	26	27	28	29	30	31	32	33	34	35	36	
$\theta_{.75}$:	35·1	35·1 →										35·0	35·1 →				35·0	35·1	35·1	
A_1 ° :	-2·62	-2·62	-2·62	-2·62	-2·62	-2·62	-2·46	-2·62	-2·44	-2·44	-2·44	-2·62	-2·46	-3·16	-3·47	-2·46	-2·11	-1·65	-1·08	
B_1 ° :	2·31 →						2·31	2·49	3·19	3·71	2·31	1·82	1·58	2·31 →					2·31	
i_N ° :	14	15	10	8	6·5	10 →													10	

12 DATA ACQUIRED : TP #: 1 2 3
$\theta_{.75}$ ° : ✓ 2·62 ✓
A_1 ° : ✓ 0 ✓
B_1 ° : ✓ 0 ✓
i_N ° : ✓ 0 ✓

RUN WAS ABORTED AFTER SUDDEN COLLECTIVE INPUT (SELF IMPOSED) CAUSED OVERLOAD TRIP ON ROTOR POWER SUPPLY. SAS WAS OFF , EM ON BEEP . PROBLEM INVESTIGATED.

T.P.# CEC TRACES DOWN.

T.P. # 1 ~ CONTINUOUS RECORD OF A PARTIAL SHUTDOWN ~ APPARENT PITCH MOTION ON STAND (WAS SHAKING CAMERA)

TP # :
$\theta_{.75}$ ° :
A_1 ° :
B_1 ° :
i_N ° :

PREP.	KEF		REVISED	DATE
CHK.				
APPR				

M. 222 ~ 26 FT. DIA. POWERED ROTOR TEST

40'x80'

T. 416

FORM 40510 (3/70)

THE BOEING COMPANY

PREP.	CHK.	APPR.	DATE
KEF			12/1/71
			REVISED
			DATE

RUN NO.	CONFIGURATION	TYPE OF RUN	WT. TARE RUN	i_N °	V_{KTS}	q_T	$\theta_{.75}$ °	A_1 °	B_1 °	RPM				DATE TIME
13	LOW L_N STAND CONFIG. BLADES ON.			27	140		VAR	VAR	VAR	551				12/13/72
14	✓ ✓ ✓ ✓ ✓			10	170		VAR	VAR	VAR	386				12/14/72

13./ DATA ACQUIRED :

TP#	1	2	3	4	5	6	7	8	9	10	11	12	13	14	15	16	17	18	19	20
$\theta_{.75}$ °	26·0	25·6	25·1	25·0	24·1	24·8	25·1	25·1	→											
A_1 °	0	-3·54	-3·47	-3·0	-3·0	-2·86	-2·93	-3·27	-3·23	-3·23	-3·23	-3·0	-2·69	-2·39	-2·07	-3·23	-3·19	-3·23	-3·19	-3·23
B_1 °	0	4·57	4·57	4·18	4·18	4·31	4·29	4·31	4·31	4·31	4·31	4·31	4·31	4·31	4·29	3·99	3·69	3·37	3·07	4·31
i_N °	0	27	27	27	27	27	27	26	25	23	21	27	27	→						27

14/

T.P#	1	2	3	4	5	6	7	8	9	10	11	12	13	14
$\theta_{.75}$ °	40·2	40·2	40·2	39·8	39·2	40·4	40·7	40·2	40·2	40·2	→			
A_1 °	0	0	-2·97	-2·93	-2·93	-2·97	-2·93	-2·93	-2·97	-2·93	-2·97	-2·93	-2·97	-2·97
B_1 °	0	0	3·38	3·38	3·38	3·37	3·38	→						
i_N °	0	0	10	10	10	10	10	10	9	8	11	12	13	10

TP#	15	16	17	18	19	20	21	22	23	24	25	26	27
$\theta_{.75}$ °	40·2	→											40·2
A_1 °	-2·66	-2·35	-2·03	-1·73	-2·97	-2·97	-2·97	-2·97	-2·97	-2·97	-2·97	-3·27	-2·97
B_1 °	3·38	→			3·38	3·07	2·76	2·45	2·14	3·69	3·38	3·38	3·38
i_N	10	10	10	10	10	10	10	10	10	10	10	10	10

M.222 - 26' DIA. POWERED ROTOR TEST

40' x 80'

T. 416

NUMBER REV LTR D222-10059-1

SHEET 669

FORM 49510 (1-70)

FORM 4811C (4-70)

THE BOEING COMPANY

PREP.	CHK.	APPR	REVISED	DATE
XCF				

RUN NO.	CONFIGURATION	TYPE OF RUN	WT. TARE RUN	i_N°	V_{KTS} NOM	q_T	$\theta_{.75}^\circ$	A_1°	B_1°	RPM				DATE TIME
15	LOW i_N STAND CONFIG. BLADES ON	HOVER (STATIC) AND ACOUSTIC	-	0°	0	0	9.00 VAR	0 0	0 0	VAR 551				12/14/72
16	HIGH i_N STAND CONFIG. BLADES ON	HOVER CHECK		6.6	0	0	9.0	0	0	VAR				12/15/72
17	✓ ✓ ✓ ✓	CHECK OUT	-	8.5	-	7.3	9.0	VAR	VAR	VAR				12/15/72

15. REPEAT HOVER RUN.

TP#	1	2	3	4	5	6	7	8	9	10	11,12	13,14	15,16	17	18	19	20,21
$\theta_{.75}$	9 (6.47V) →									7 (7.33)	11 (5.63)	13 (4.81)	14 (4.33)	13 (4.81)	11 (5.63)	9 (6.48)	7 (7.33)
A_1	0 →																
B_1	0 →																
RPM	100	150	203	255	269	308	350	551	551	551	551	551	551	551	551	551	551

NOTES: TP#5, B.L. LIMIT. R.L. LIMIT @ 1 & BETWEEN #5 & #6 (TRANSIENT CONDITION ONLY)

16.

TP#	1	2	3	4	5	6	7	8	9	10	11	12	13	14	15	16	17	18	19	20
RPM:	100	154	200	121	110	131	140	160	170	183	190	215	224	235	246	256	266	275	284	290

TP#	21	22	23	24	25	26	27	28	29	30
RPM:	300	310	330	350	370	389	410	430	451	548

~TEST RAPID SHUTDOWN

ROOF OPEN FOR RUN 16.

17. INVESTIGATION OPERATING CHARACTERISTICS, q_T ON (@ REDUCED, cf RUN CONDITION REQUM'T.) RPM → . STOPPED @ RPM = 540 AND REDUCED RPM AS STAND MODE ENCOUNTERED WITH LARGE (80%) BLADE LOADS. REPEATED INSTABILITY @ 535 RPM - TOOK CEC & TAPE DATA. CYCLICS FOR MIN LOAD CONDITIONS.

M.222 - 26' DIA POWERED ROTOR TEST

40' x 80'

T.416

SHEET 670

NUMBER D222-10039-1

REV LTR

FORM 4851 0 13 '70

THE BOEING COMPANY

PREP.	APPR.	CHK.	RUN NO.	CONFIGURATION	TYPE OF RUN	WT. TARE RUN	i_N °	V_{KTS}	q	$\theta_{.75}$ °	A_1 °	B_1 °	RPM				DATE TIME
XCF.			18	HIGH i_N STAND CONFIG. BLADES ON			85	0	0	9.0	0	VAR	VAR				12/18/72
			19	✓ ✓ ✓ ✓ ✓			85	45		VAR	VAR	VAR	500				12/19/72
12/18/72																	
REVISED																	
DATE																	

18/ 900 lb. LEAD WEIGHT REMOVED FROM DOWNSTREAM END OF NACELLE. (INCREASING STAND NAT. FREQUENCY CHECKOUT RUN FOR ESTABLISHING TEST RPM. (PITCH FREQUENCY BY ± 6%)

T.P. # :	1	2	3	4	5	6	7	8	9	10	11	12	13	14	15	16
RPM :	117	140	170	174	184	192	188	196	203	267	260	274	279	289	300	450
B_1°	0 →										-16 →					0

TP # :	17	18	19	20	21	22	23	24
RPM :	460	472	480	490	502	509	523	525
B_1°	0 →							

- LONG CEC/TAPE RECORDS @ 525 RPM APPROX. MONITORING RE-CIRCULATION EFFECTS AND/OR STAND FREQUENCY.

19/

TP #	1	2	3	4	5	6	7	8	9	10	11	12	13	14	15	16
$\theta_{.75}$°	8.9 →										9.9	10.7	11.3	7.9	7.4	6.8
A_1°	-4.67	-4.72	-4.76	-4.85	-4.85	-4.94	-4.94	-5.03 →								
B_1°	1.73 →					1.51	1.51			→		1.41 →				
	(329)	(351)	(380)	(403)	(426)	(449)	(466)	(475)	(485)	(500 NOM →						

TP #	17	18	19	20	21	22	23	24	25	26	27	28
$\theta_{.75}$°	8.9 →											
A_1°	-5.03	-4.72	-4.42	-4.08	-3.74	-3.39	-5.03 →				-4.94	-5.03
B_1°	1.41 →							1.73	2.02	2.33	2.51	1.41

M.222 a 26' DIA. POWERED ROTOR TEST

40' x 80'

T. 416

SHEET 671

NUMBER D222-10059-1

REV LTR

THE BOEING COMPANY

NUMBER D222-10059-1
REV LTR

RUN NO.	CONFIGURATION	TYPE OF RUN	WT. TARE RUN	i_N °	V_{KTS}	q	$\theta_{.75}$ °	A_1 °	B_1 °	RPM															DATE TIME
20	HIGH i_N STAND CONFIG. BLADES ON			6.6	80		VAR	VAR	VAR	500, VAR															12/19/72
21	✓ ✓ ✓ ✓	✓	✓	6.6	80		VAR	VAR	VAR	551															12/20/72

20.

TP#	1	2	3	4	5	6	7	8	9	10	11	12	13	14	15	16	17	18	19	20	21		
RPM	383	400	414	450	470	487	497	514	519	500	———												
$\theta_{.75}$ °	9.0	———						9.0	9.0	10.5	11.5	12.0	9.8	8.9	7.9	7.4	6.9	9.0	———				
A_1 °	-2.30	———			-2.55	-2.55	-2.73	-2.69	-2.65	-2.49	-2.49	-2.73	-2.69	-2.73	-2.69	-2.73	-2.69	-2.49	-2.38	-2.07	-1.77		
B_1 °	2.51	———			2.42	2.42	2.51	———															
TP#	22	23	24	25	26	27	28	29	30	31	32	33	34	35	36	37	38	39	40	41			
$\theta_{.75}$ °	9.8	———																					
A_1 °	-1.46	-2.96	-3.27	-2.73	———																		
B_1 °	2.33	2.33	2.33	2.02	1.74	1.43	2.93	2.62	2.93	3.25	3.55	3.24	2.93 (500)	(533)	(539)	(549)	(551)	(556)	(560)	(562)			

21

RPM

REPEAT RUN 21 CONDITION BUT RPM @ 551.

TP #	1	2	3	4	5	6	7	8	9	10	11	12	13	14	15	16	17	18	19	20	21	22	
RPM	386	430	456	475	498	518	———			549	549	551	550	551	550	548	———		549	———		548	———
$\theta_{.75}$ °	9.6	———										12.0	12.5	9.6	8.8	7.8	9.6	———					
A_1 °	-2.58	-2.54	-2.58	———	-2.69	-2.58	-2.73	-2.85	-2.91	———						-2.85	———	-2.81	-2.38	-1.96	-2.81	-3.12	-3.50
B_1 °	2.51	2.38	2.30	———	2.09	2.19	1.97	2.07	2.54	———						2.56	———	2.16	———				
TP #	23	24	25	26	27	28	29	30	31	32	33												
RPM	547	548	———	547	548	547	———																
$\theta_{.75}$ °	9.6	———																					
A_1 °	-3.81	-2.78	———																				
B_1 °	2.16	———	1.70	1.34	1.12	2.19	2.57	2.88	3.38	3.72	2.18												

NEW AXIAL ACCEL. WENT BAD DURING RUN. SWITCHED OFF

PREP.	KEF.		REVISED	DATE
CHK.				
APPR				

M. 222 ~ 26 FT. DIA POWERED ROTOR TEST

40 × 80

T. 416

FORM 48[illegible] 701

THE BOEING COMPANY

FORM 49810 (3/70)

RUN NO.	CONFIGURATION	TYPE OF RUN	WT. TARE RUN	i_N °	V_{KTS}	q'	$\theta_{.75}$ °	A_1 °	B_1 °	RPM	DATE TIME
22	HIGH i_N ° STAND CONFIG. BLADES ON.			83	80		VAR	VAR	VAR	500	12/20/72
23	✓ ✓ ✓ ✓ ✓			75°	0	0	9.0	0	0	VAR.	

PREP. KEF. CHK. APPR. REVISED DATE

M 222 - 26 FT. DIA. POWERED ROTOR TEST.

40' x 80' T. 416

SHEET 673

NUMBER. REV LTR D222-10059-1

22/

TP #	1	2	3	4	5	6	7	8	9	10	11	12	13	14	15	16	17	18	19	20	21	22
RPM	450	468	480	482	487	495 →			496	497	495	→				497	498 →		499	498 →		
$\theta_{.75}$°	9.0 →						9.5	10.0	10.5	9.1	8.6	9.0 →										
A_1°	-4.96	-4.39	-4.61	-4.53	-4.89	-4.84 →							-4.50	-4.80 →						-4.11	-4.80	
B_1°	2.30	2.21	1.82	2.65	2.79 →										3.03	3.37	2.80	2.55	2.21	2.79 →		

23/

TP #	1	2	3	4	5	6	7	8	9	10	11	12
RPM	442	459	478	491	498	508	519	528	538	550	552	553
$\theta_{.75}$°	9 →										10	11

STATIC CHECK RUN. ROOF DOORS OPEN CHECK FOR .66 Ω INSTABILITY INDICATION

APPENDIX 3

APPENDIX 3. ADDITIONAL FEEDBACK DATA, DESIGN PHILOSOPHY AND ANALYTICAL DERIVATIONS

This appendix includes:

A3a) additional open loop frequency response data for some non-optimum configurations obtained during Test 410.

A3b) Section 3 of Boeing Report D222-10060-3 has been extracted and included here for convenience.

A3c) derivation of ψ_{ROT} = 50-degrees for the third low rate system.

A3a - ADDITIONAL FEEDBACK DATA

The data enclosed in this section are open loop frequency response data for some non-optimum configurations obtained during Test 410.

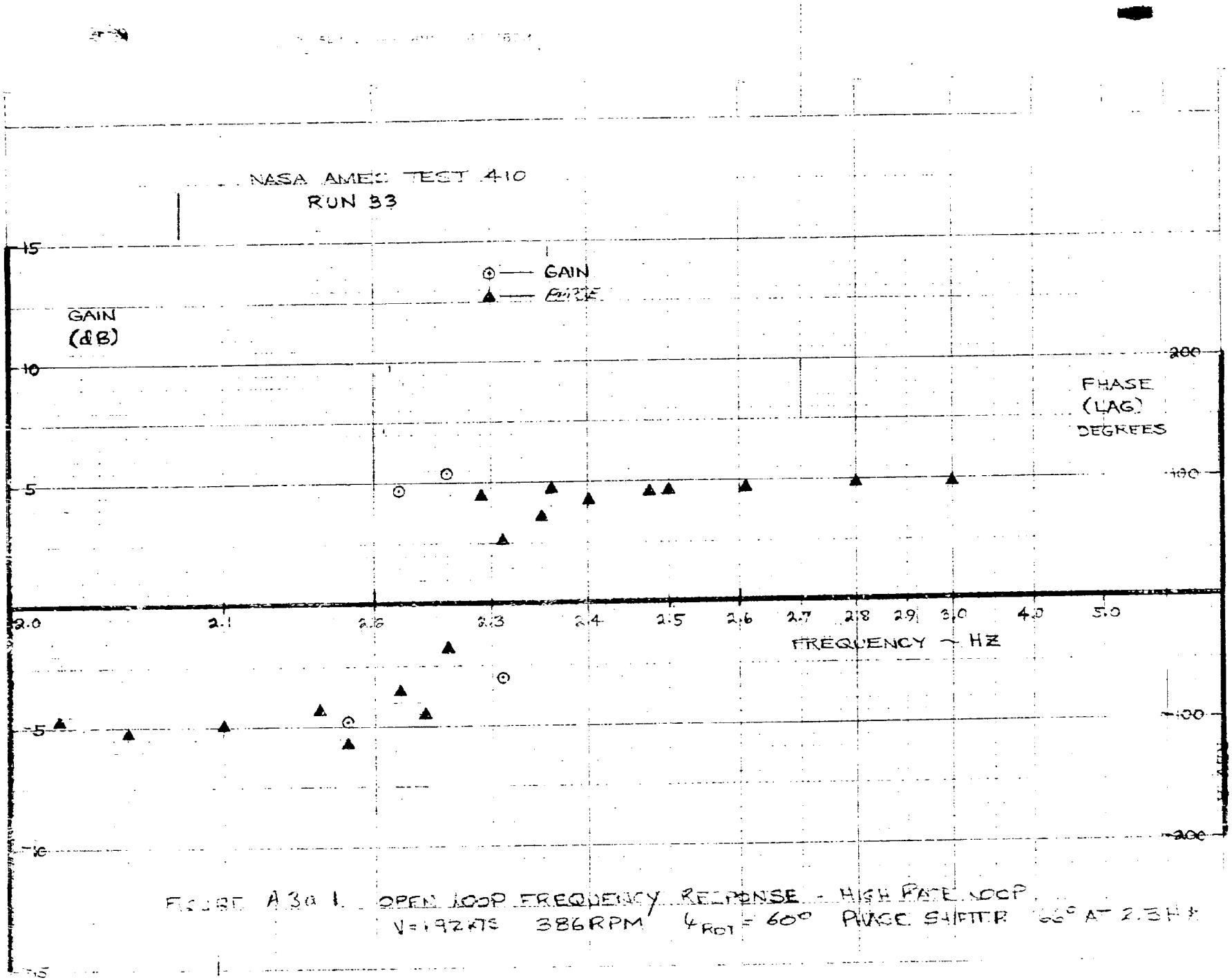

FIGURE A3a 1. OPEN LOOP FREQUENCY RESPONSE - HIGH RATE LOOP
V=192 KTS 386 RPM ψ_{ROT} = 60° PHASE SHIFTER 66° AT 2.3 Hz

D222-10059-1

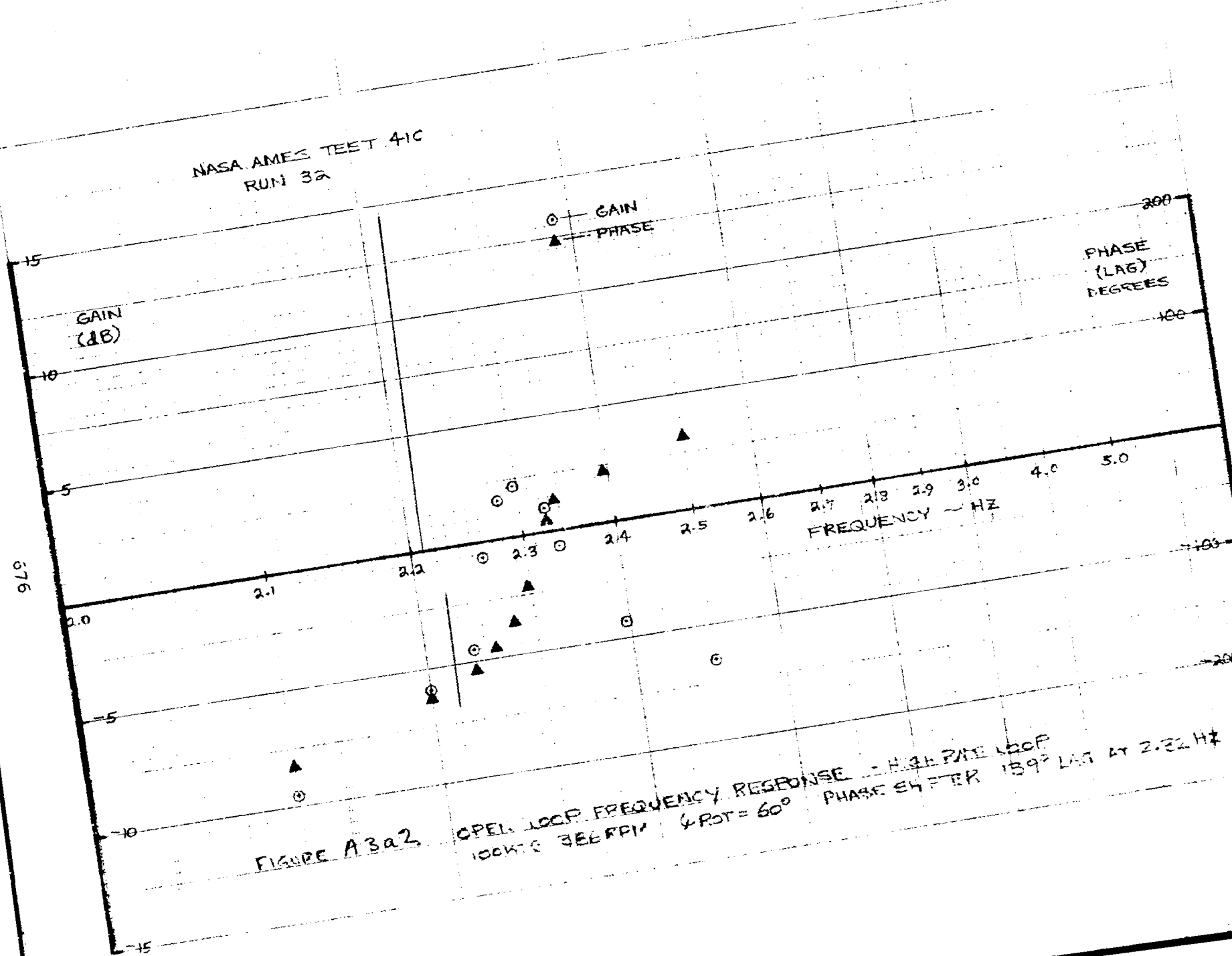

FIGURE A3a2 OPEN LOOP FREQUENCY RESPONSE - HIGH RATE LOOP
LOOKS 3 DEG/PPI $\zeta_{ROT} = 60°$ PHASE SHIFTER 159° LAG AT 2.32 HZ

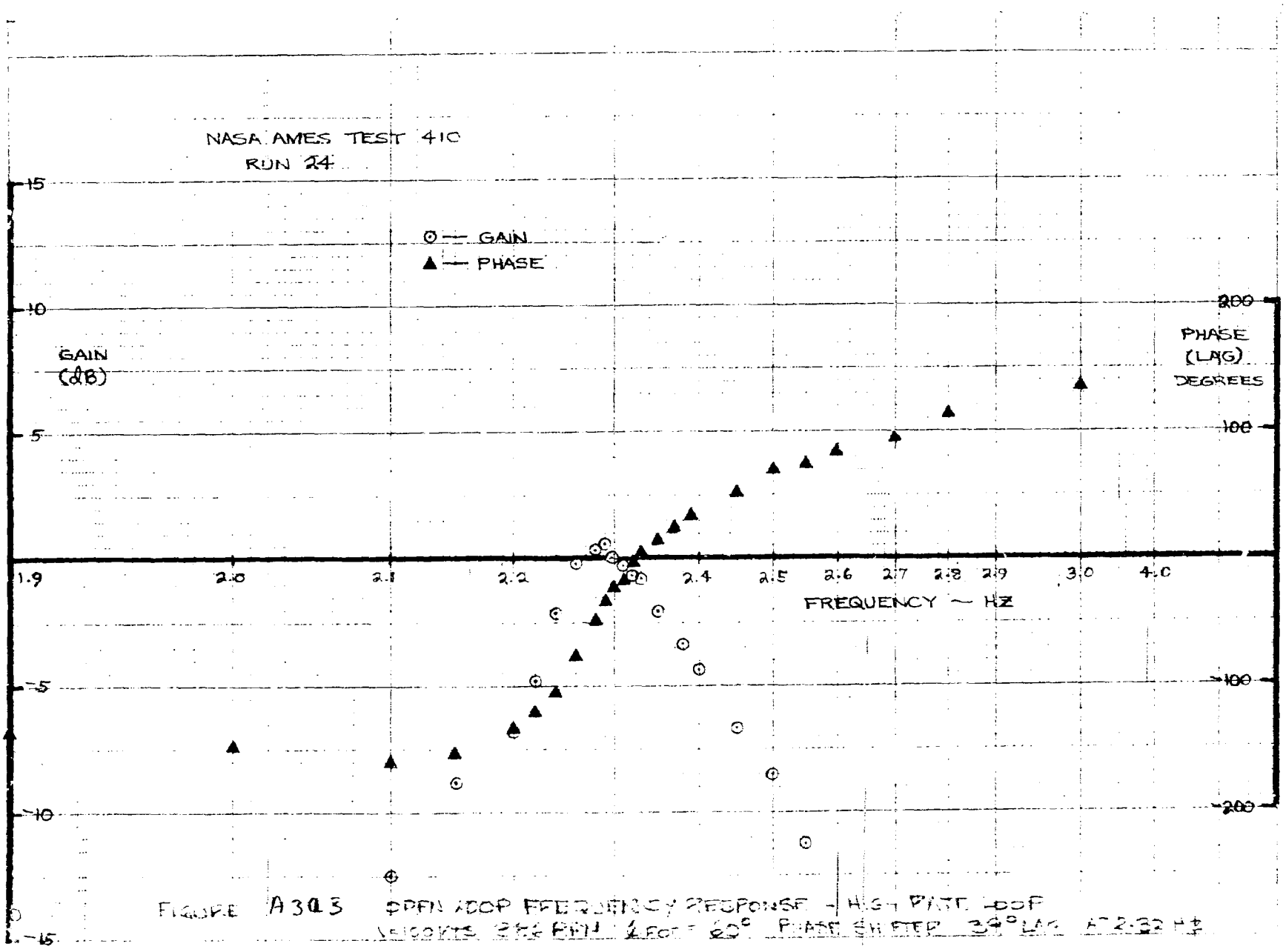

FIGURE A3.3 OPEN LOOP FREQUENCY RESPONSE - HIGH RATE LOOP
WEIGHTS 25% PRN & FOR 60° PHASE SHIFTER 30° LAG AT 2.32 HZ

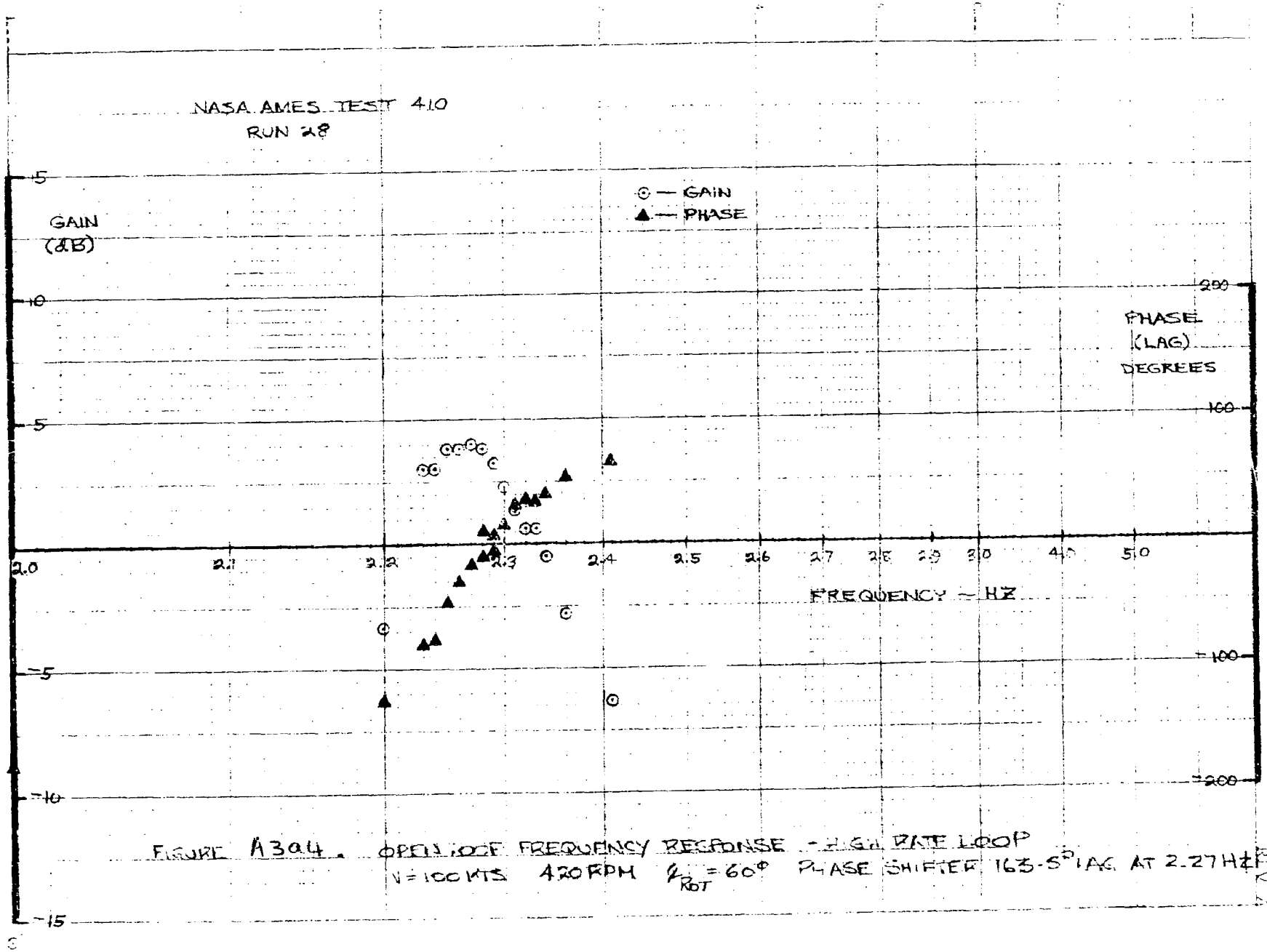

FIGURE A304. OPEN LOOP FREQUENCY RESPONSE - HIGH RATE LOOP
V = 100 KTS 420 RPM ℓ_{ROT} = 60° PHASE SHIFTER 163-S° LAG AT 2.27 HZ

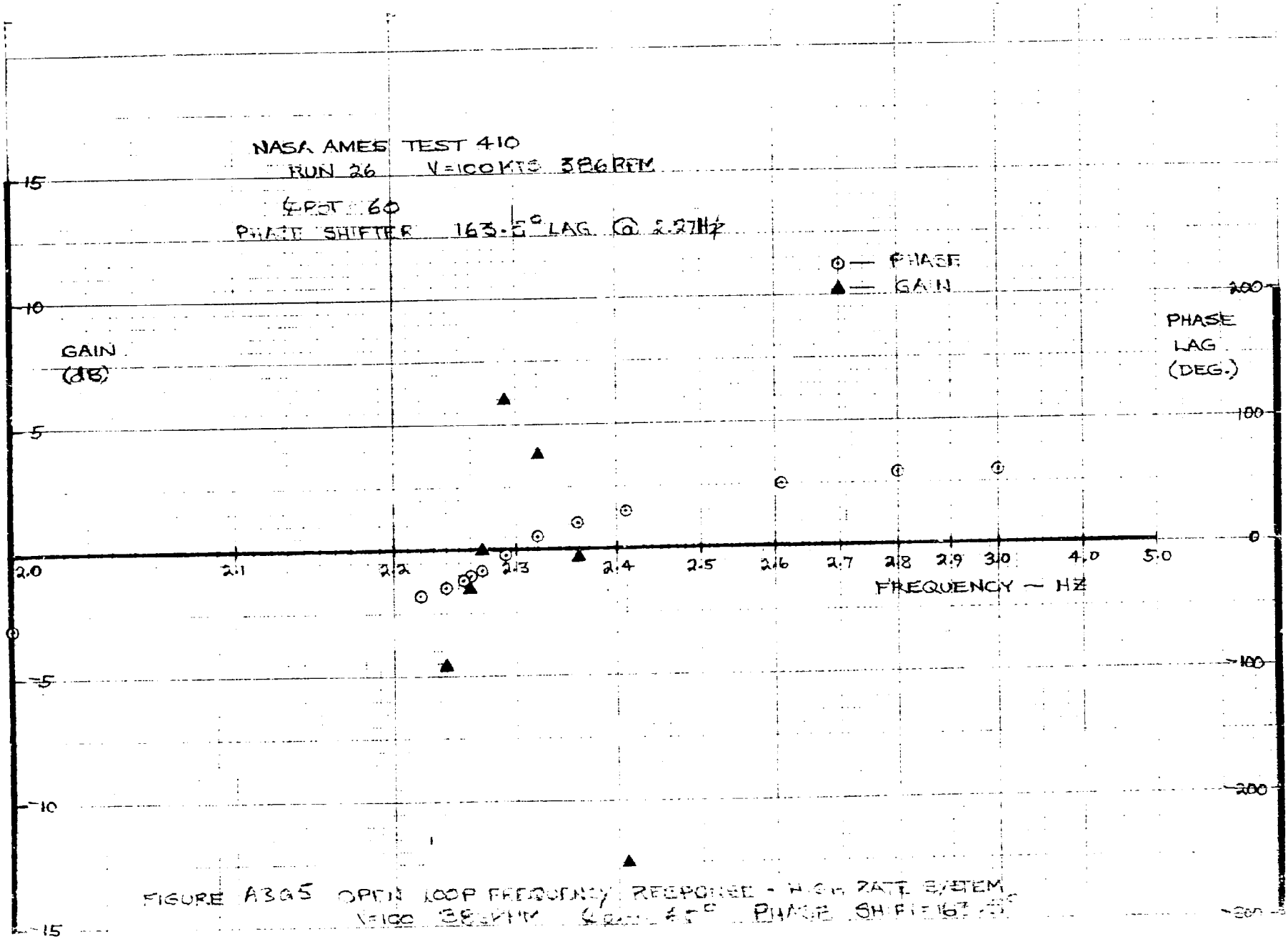

FIGURE A3.5 OPEN LOOP FREQUENCY RESPONSE - HIGH RATE SYSTEM
V=100 386 RPM [illegible] 45° PHASE SHIFT @ 1.67 HZ

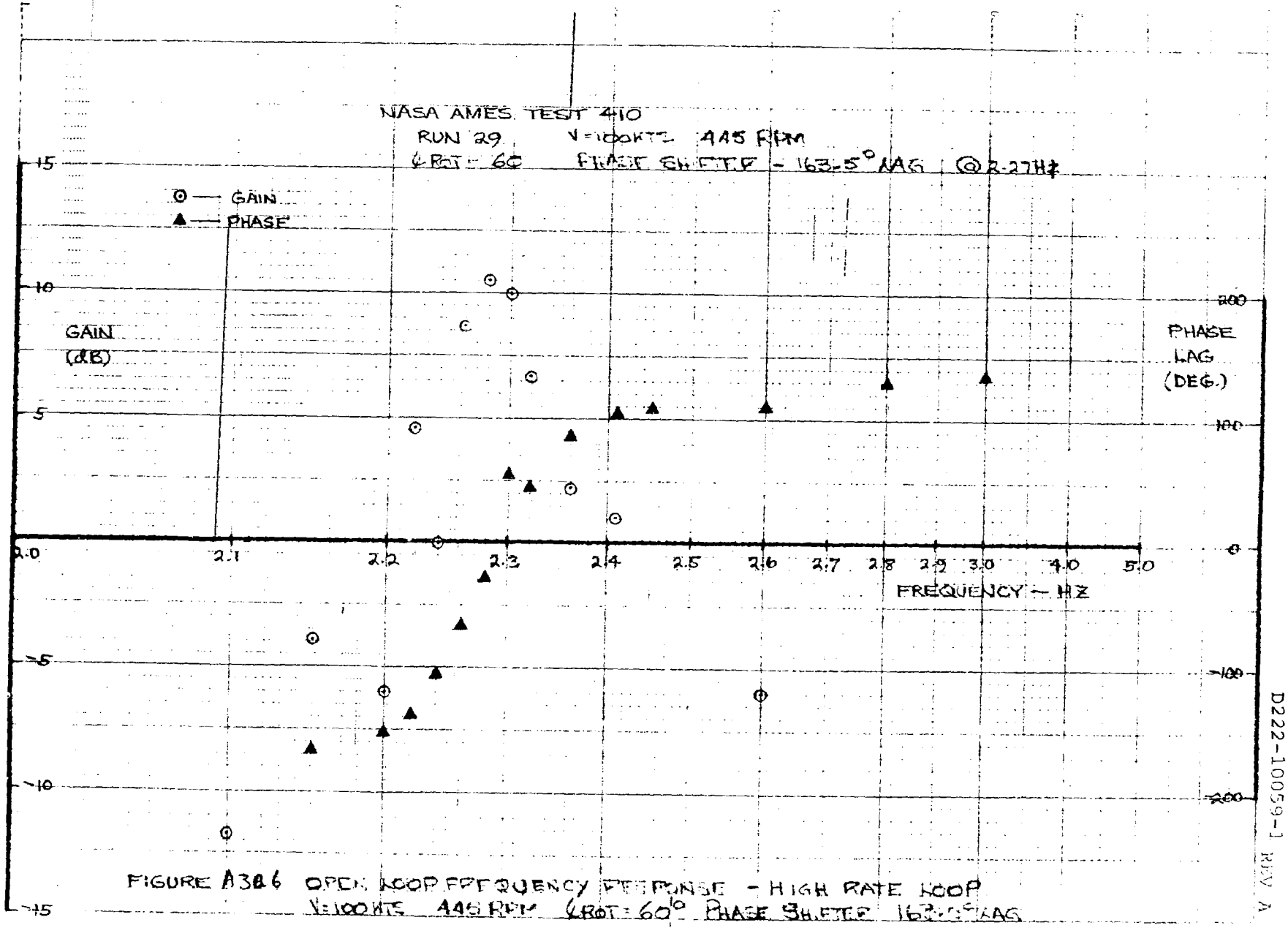

FIGURE A3&6 OPEN LOOP FREQUENCY RESPONSE - HIGH RATE LOOP
V=100 KTS 445 RPM ζ_{ROT}=60° PHASE SHIFTER 163.5° LAG

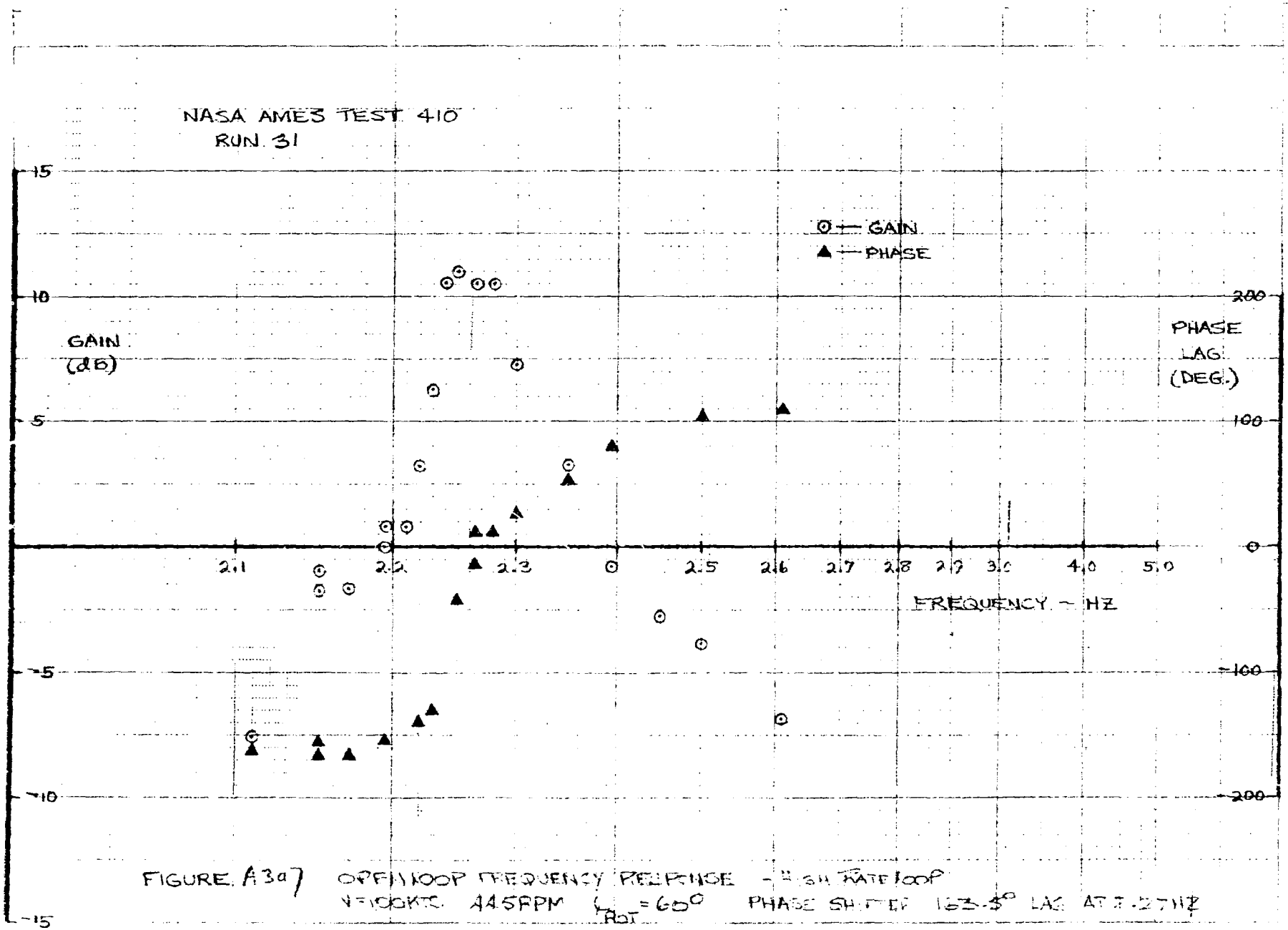

FIGURE A3a) OPEN LOOP FREQUENCY RESPONSE - HIGH RATE LOOP
V=100KTS. 445RPM $\gamma_{ROT} = 60^{\circ}$ PHASE SHIFT OF 163.5° LAG AT 2.27HZ

A3b. DESIGN PHILOSOPHY AND ANALYSIS

This section is reproduced without alteration from Boeing Document D222-10060-3. That is to say the paragraph and figure numbers remains as in the original report. This section of Appendix 3 discusses design philosophy and the compromises that are required in selecting a load alleviation or stability augmentation system.

3. BLADE LOAD ALLEVIATION AND STABILITY AUGMENTATION SYSTEMS

3.1 BACKGROUND AND OBJECTIVES OF STUDY

Tilting prop/rotor type aircraft experience significant blade loads as a result of non-axial flow in transition from hover to the cruise configuration, and in transient conditions such as maneuvers, gusts, sideslip, etc. However, since cyclic pitch is a basic feature of most tilt rotor control systems, it provides a means to significantly reduce the severity of loading conditions associated with skewed flow. This is accomplished in two ways. The first is to schedule the application of controlled amounts of longitudinal and lateral cyclic as a function of flight condition. The second, which is the primary topic of this report, is the automatic application of cyclic to reduce loads in amounts proportional to the deviations from the scheduled flight program, or to some equivalent loading in the structure caused by the deviation. Such a system will not only reduce blade loads, but will at the same time reduce the associated hub force and moment derivatives, thus increasing the static stability margin of the aircraft.

The objective of this study is to explore the use of load alleviation systems in a typical tilt rotor design, taking

into account those factors which might adversely affect performance in a practical situation. These include hardware characteristics, sensors and actuators, and the impact of dynamic transient effects as well as idealized steady state alleviation. System authority is also discussed for its impact on effectiveness at different flight conditions. The ability of a feedback control system working through the swashplate to influence the following will be analyzed:

- Reduction of blade loads and hub forces and moments under steady maneuvers and gust encounters
- Improvement of flying qualities by reducing destabilizing forces and moments from the rotors; improvement of short period response and pilot workload
- Alleviation of airframe structural loads
- Improve ride qualities by reduction of gust response accelerations

3.2 TECHNICAL BASIS FOR USE OF CYCLIC PITCH FEEDBACK IN LOAD ALLEVIATION

The predominant cause of vibratory loading in prop/rotors is blade dynamic response to cyclical angle of attack changes associated with non-axial flow caused by shaft tilt to the free stream or with cyclic pitch of the blade due to tilt of the swashplate. That is to say, in a propeller or rotor

whose shaft is inclined at an angle α to the free stream each blade experiences a sinusoidal increment of incidence of amount $\alpha \sin \Omega t$. It also experiences a sinusoidal variation in relative velocity over the blade, and both these effects combine to give a variation in dynamic pressure and in angle of attack. The net effect is to produce cyclical perturbation in the blade loads and blade dynamic response. Associated with blade response are corresponding shears, bending moments and strains. Cyclic pitch imposes a 1 per rev variation in incidence and has accordingly much the same effect as shaft incidence except that the angle of attack increment is uniform across the blade and there is no directly associated variation in blade dynamic pressure. Cyclic pitch in appropriate amounts is, therefore, used to trim out the angle of attack variations caused by shaft tilt to the relative wind. The use of cyclic pitch to trim out blade loads and for stability augmentation is established practice in the helicopter field, and the extension to tilt rotor applications is clearly indicated. There is, however, minimal discussion of such topics as scheduling of cyclic to minimize blade loads for normal flight conditions. The emphasis is on the use of automatic feedback cyclic control to counteract load occurring due to off-schedule conditions.

Such conditions occur during maneuvers and turbulence when the rotor experiences temporary departures from the trimmed unaccelerated flight condition.

3.3 TEST DEMONSTRATION OF SWASHPLATE FEEDBACK SYSTEMS

Two test programs were conducted in 1972 in which the use of swashplate feedback for load alleviation was demonstrated. The first, in May, was performed using a 1/9.622 scale model of the Model 222 rotor mounted on NASA wing in the Princeton Tunnel. The sensor system used consisted of strain gages measuring pitching moment and yawing moment in the wing. The system was demonstrated for static situations (i.e., steady wing angle of attack) and also for simulated long period gust conditions using the gust generating capability of the Princeton Tunnel. The results of this test indicated that substantial reductions in blade response were available with the correct selection of azimuth and gain. The results of this test are reported in Boeing Document D222-10047-1 (Reference 3.1). In September of the same year, the full scale version of the above model was tested in the NASA Ames 40 X 80-foot tunnel with a similar feedback system operative. This test also showed that substantial reductions in blade loads could be achieved using a swashplate feedback system. The results of this test are given in Boeing Document D222-10059-1 dated March 1973, (Reference 3.2). The results of both these tests tend to confirm the results presented in this report.

3.4 CANDIDATE SYSTEMS: CHOICE OF SENSORS

The principal feature differentiating one load alleviation system from another is the signal sensed and fed back through the swashplate. A number of potentially viable signals and sensors are tabulated in Table 3.1 along with the advantages and disadvantages of each system.

Of the sensors listed, the Aq or Bq sensor seems to offer the most advantage. The other sensors and signals would be acceptable in principle, but the issue of reliability makes strain gage systems undesirable. The Aq sensor has the additional advantage of minimum overall system lag, since each of the other signals results to a greater or lesser degree from dynamic response to the forces produced by Aq. This is not important for quasi-static cases such as steady maneuvers or long period gusts, but it could become important in dynamic situations.

A system based on Aq or Bq sensors has, therefore, been chosen for study.

TABLE 3.1. CANDIDATE SIGNALS AND SENSORS FOR LOAD ALLEVIATION SYSTEM

Signal	Sensor	For	Against
Blade Bending Moment	Strain Gage	Senses variable to be controlled	•Questionable reliability •Signal in rotating system •No phase lead
Hub Bending Moment	Strain Gage	Senses variable to be controlled	•Questionable reliability •Signal in rotating system •No phase lead
Aq, Bq Dynamic Pressure Delta Angle of Attack or Sideslip	Pressure Head	•Senses variable which is primary cause of loading •Good reliability •Previous flight experience	
Aircraft Normal, Side Acceleration	Accelerometer	Signal almost in phase with Aq	No use for unaccelerated cases such as unscheduled weight
Wing Bending Moments Torsion, Yaw	Strain Gage	•Sensor in fixed system •Direct measure of variable affecting flying qualities	•Questionable reliability •Lags introduced by wing response •Needs additional sensing to subcontract nacelle moment due to "g"

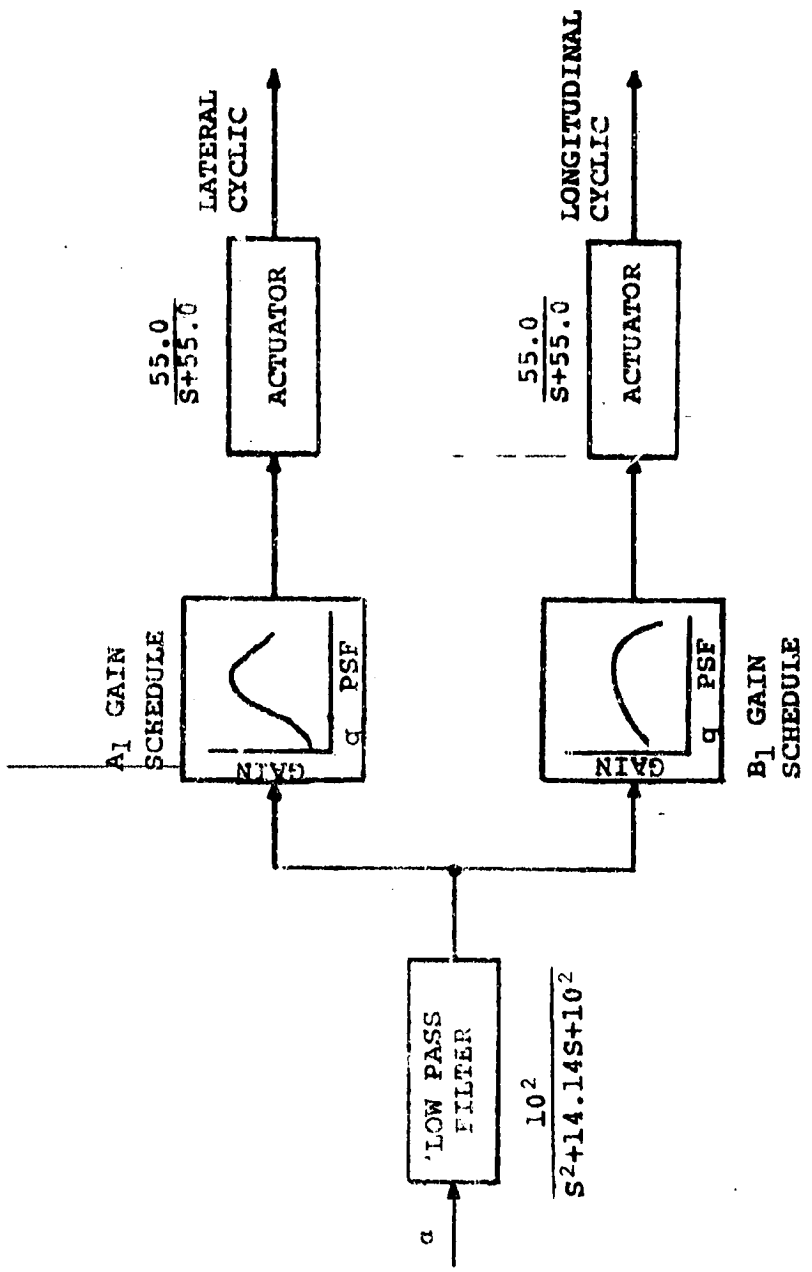

FIGURE 3.1. BLADE LOAD ALLEVIATION SYSTEM SCHEMATIC OF FEEDBACK LOOP

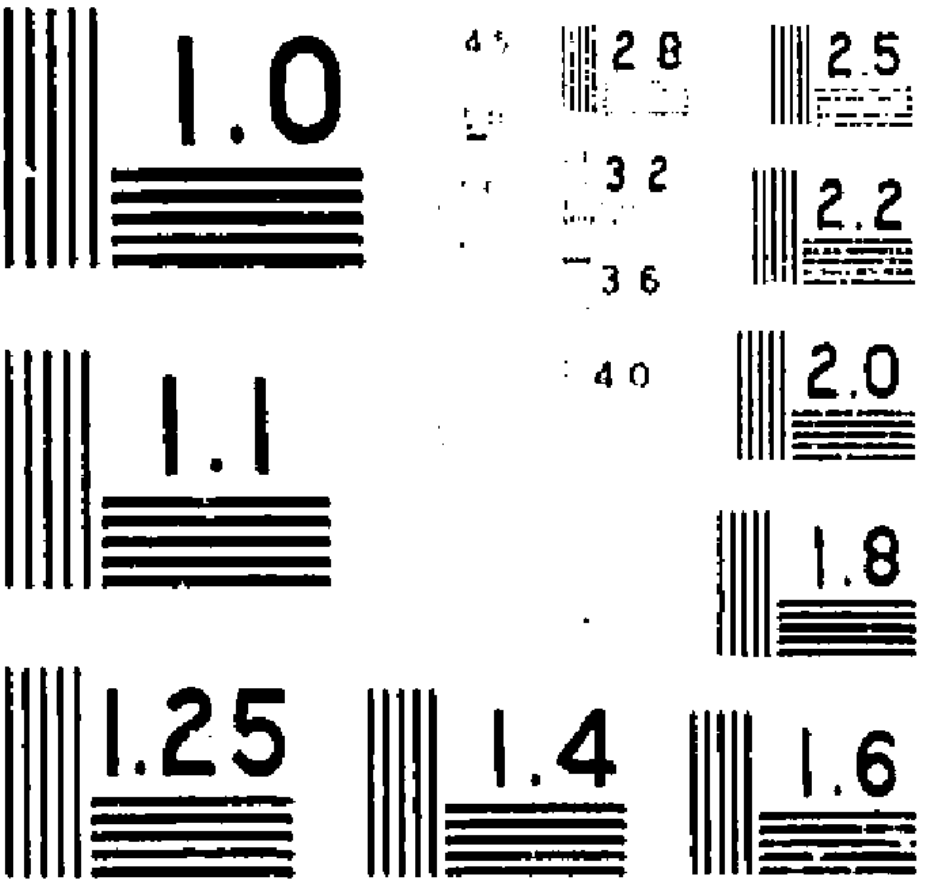

3.5 SYSTEM CHARACTERISTICS

Figure 3.1 is a schematic of the load alleviation system chosen for study.

The signal sensed is the net increment in angle of attack produced by a gust and the aircraft response. Transfer functions for filters are based on stability considerations and actuator transfer functions are typical of actual hardware. The filter has a cut-off frequency of 10 rad/sec and a damping factor of 0.707. The actuator transfer function is of first order with break frequency 55.0 rad/sec.

3.6 DESIGN OF A SYSTEM EFFECTIVE FOR QUASI-STEADY CONDITIONS

When quasi-steady conditions are considered the decision on system characteristics becomes a matter of:

- Selection of which forces or moments to control; since all hub forces and moments cannot be simultaneously brought to zero, a selection is required.
- How gain and azimuth requirements vary with flight conditions
- What signal shaping (filtering) is required to avoid destabilizing dynamic modes

3.6.1 System Designed to Null Rotor Hub Moments in Cruise

The characteristics of gain and azimuth for a system designed

to work on hub pitching and yawing moments were evaluated. Since only steady state effects are considered, the required A_1 and B_1 gain settings are solvable exactly over a range of flight conditions from knowledge of the rotor hub moment alpha and cyclic derivatives. The results are expressed in terms of azimuth and resultant gain. The azimuth angle is defined as

$$\psi = \text{Tan}^{-1} \left\{ \frac{B_1 \text{ GAIN}}{A_1 \text{ GAIN}} \right\}$$

and is a direction perpendicular to the axis about which the swashplate tilts.

Questions to be addressed in this study were:

- Does system gain and azimuth require scheduling as a function of flight conditions?
- What is the impact of the system on the hub normal force and moments?
- What is the impact on aircraft static stability?

The values of A_1 and B_1 gain required were evaluated at different speeds and altitudes from the equations for hub pitch and yaw moments:

$$M_{Y_{TOTAL}} = M_{Y_\alpha}{}^{\alpha} + M_{Y_{A_1}} A_1 + M_{Y_{B_1}} B_1 = 0$$

$$M_{X_{TOTAL}} = M_{X_\alpha}{}^{\alpha} + M_{X_{A_1}} A_1 + M_{X_{B_1}} B_1 = 0$$

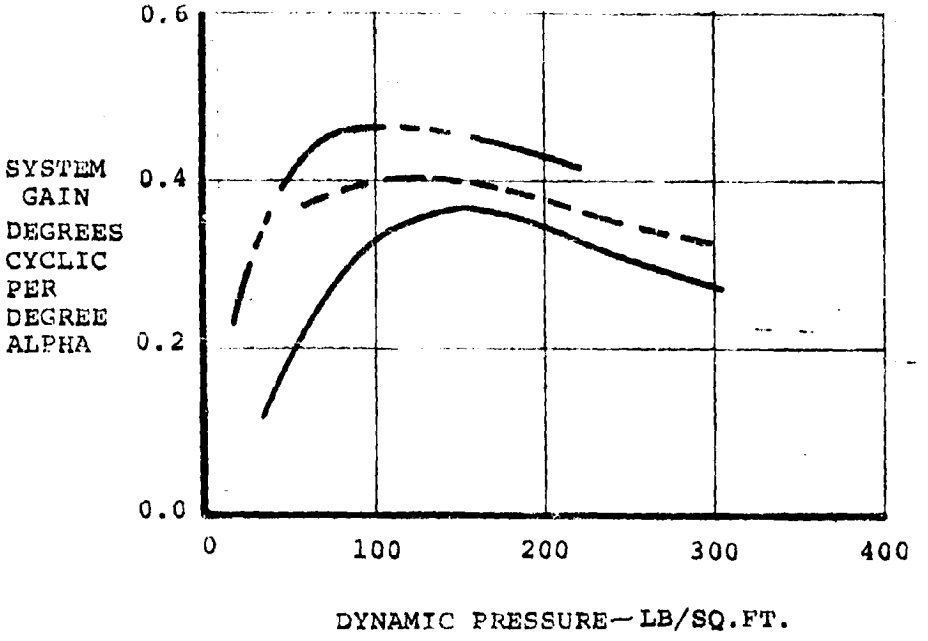

FIGURE 3.2. GAIN REQUIREMENT AS FUNCTION OF DYNAMIC PRESSURE AND ALTITUDE FOR SYSTEM DESIGNED TO ZERO-OUT HUB MOMENTS

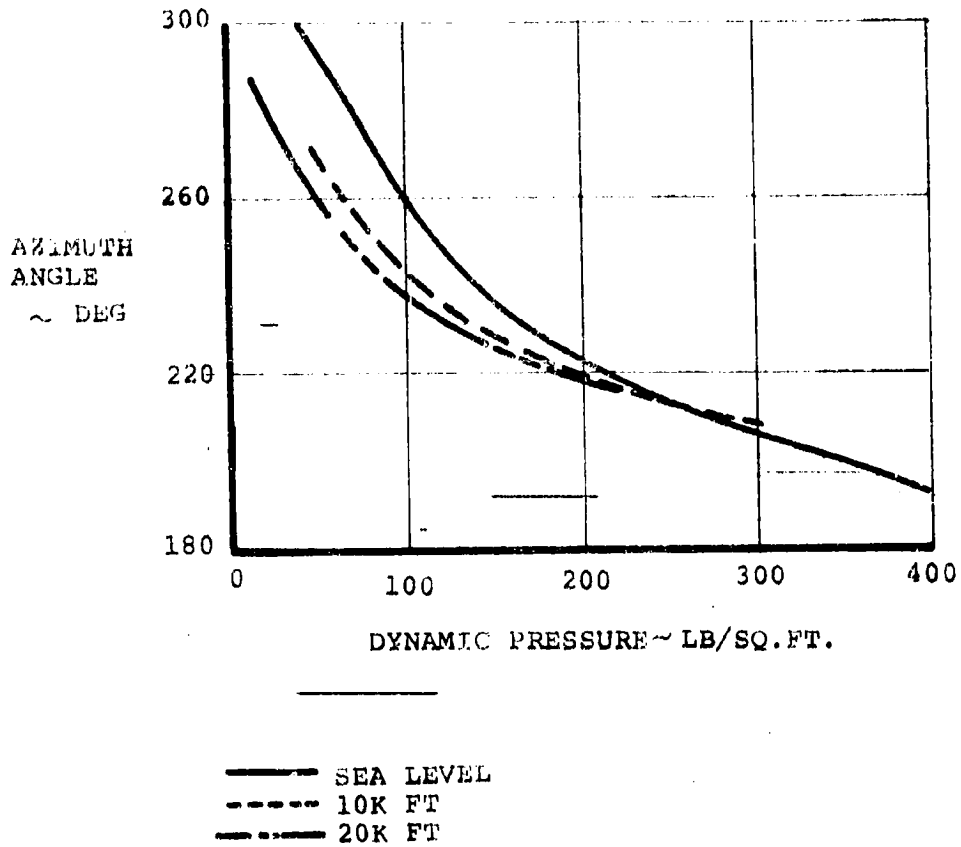

FIGURE 3.3. AZIMUTH ANGLE REQUIREMENT AS FUNCTION OF DYNAMIC PRESSURE AND ALTITUDE FOR SYSTEMS DESIGNED TO ZERO-OUT HUB MOMENTS

These equations are solved for the ratio of A_1 and B_1 to α and to each other and the answers presented in terms of net swashplate cyclic gain and azimuth. Filtering requirements were determined using Bode Diagram Techniques and system stability was confirmed by examination of root locus. The analytical methodology used is incorporated in the C-48 Flying Qualities and Aeroelastic Stability Program. Transient dynamic response was not evaluated for this system.

Figure 3.2 shows the gain required in degrees of cyclic per angle of attack, over a speed range of 100 to 300 knots at altitudes of sea level, 10,000 ft. and 20,000 ft. The associated azimuth angles required are shown in Figure 3.3 and indicate that the angle required drops from around 120° at 100 knots to 30° at 300 knots. The conclusion to be drawn from these curves is that gain and azimuth scheduling as a function of speed is required if the system objectives are to be met at all speeds. The variation with altitude is not so striking so that scheduling of gain and azimuth with altitude is probably not required. The impact of these gain and azimuth settings at sea level on the hub normal and side forces are shown in Figures 3.4 and 3.5. It is seen that normal force and side force derivatives are also reduced by

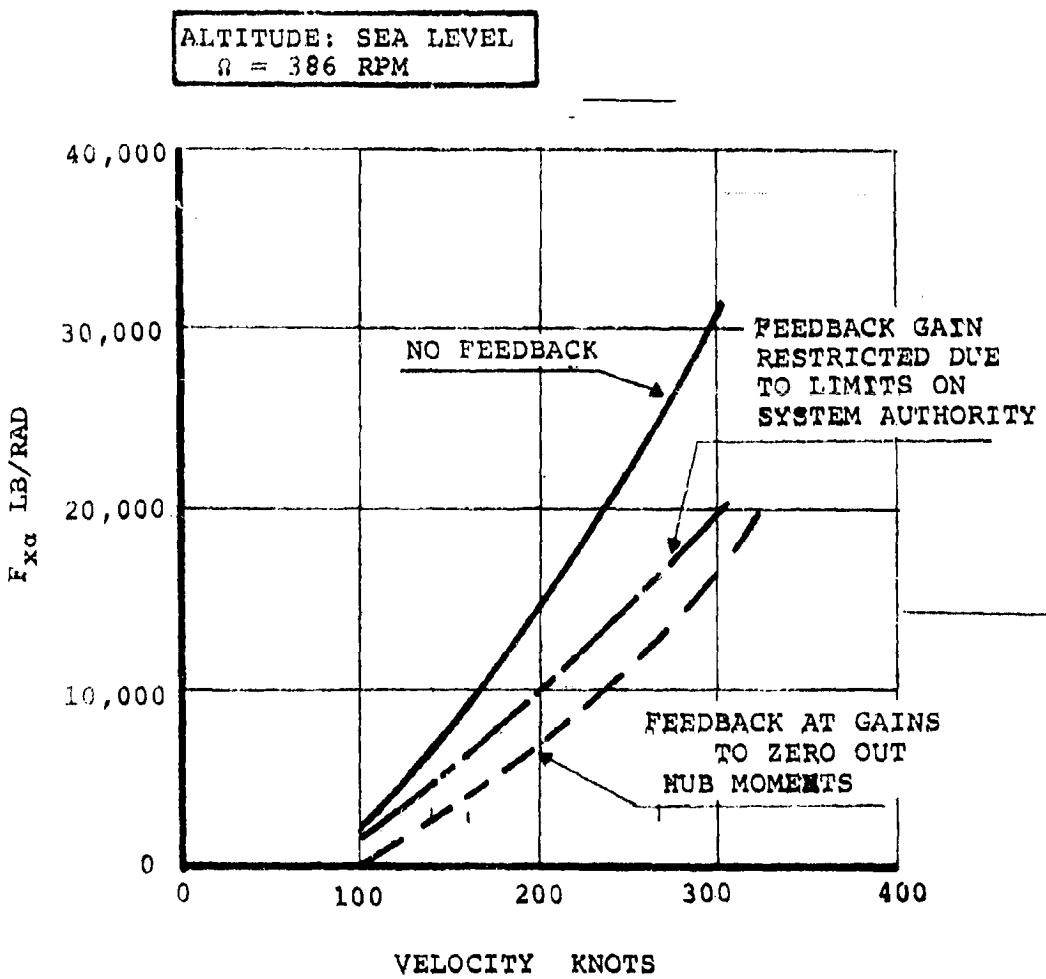

FIGURE 3.4. NORMAL FORCE DERIVATIVE WITHOUT FEEDBACK WITH UNRESTRICTED GAIN AND WITH ARBITRARY LIMIT OF 1.5° of A_1 and B_1

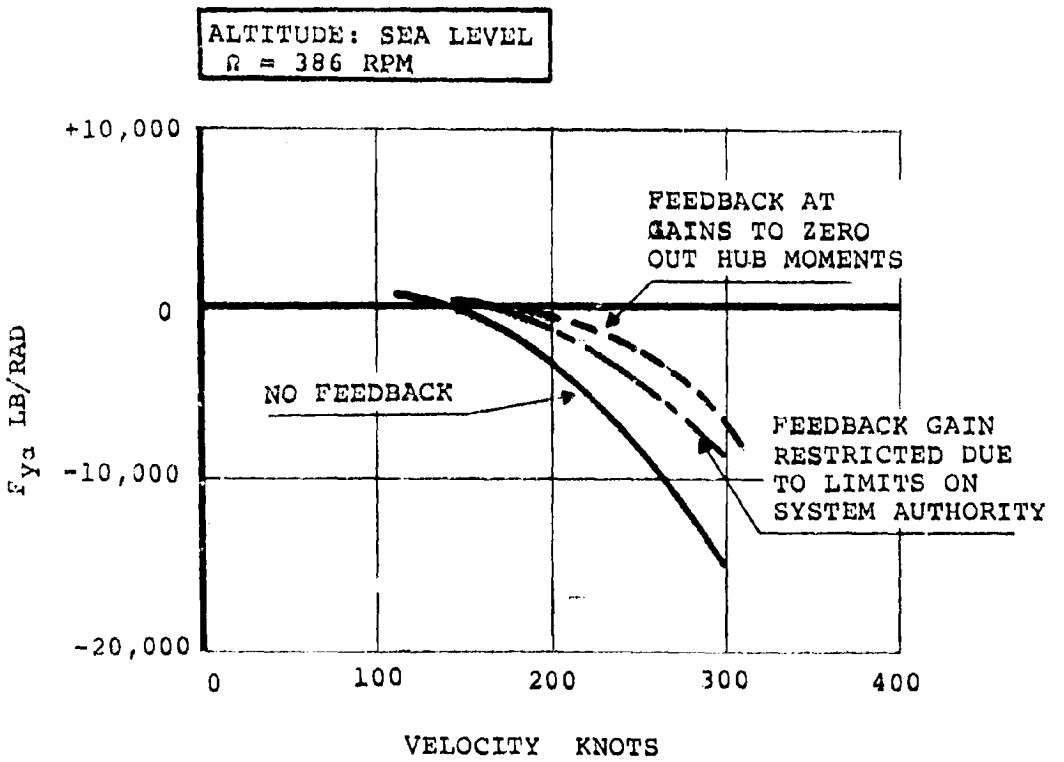

FIGURE 3.5. SIDE FORCE DERIVATIVE WITHOUT FEEDBACK, WITH UNRESTRICTED GAIN AND WITH ARBITRARY 1.5° LIMIT ON A_1 and B_1

approximately 50% at the higher speeds.

It is concluded from this study that a system can be defined which will reduce the blade flap bending moments and hub moments to zero, and that the hub normal and side forces will be reduced by the same system. This is a beneficial arrangement for blade loads but may be less acceptable from the point of view of aircraft static stability. The rotor hub pitching moment due to angle of attack is negative, i.e., nose down for low-in-plane stiffness rotors at cruise advance ratios. A reduction of hub pitching moment to zero without a similar reduction in normal force may lead to a net reduction in static margin. That is to say the objective of reduction of blade loads is not necessarily compatible with flying qualities objectives.

3.6.2 System Authority Considerations

Limits may be imposed on the authority of a feedback system because of runaway considerations. That is, unless the system is fail safe which implies triple redundancy, its authority must be less than that available to the pilot or from other control systems at each condition of flight. The stability characteristics of the aircraft will have a discontinuity when the system commands exceed the authority of the feedback

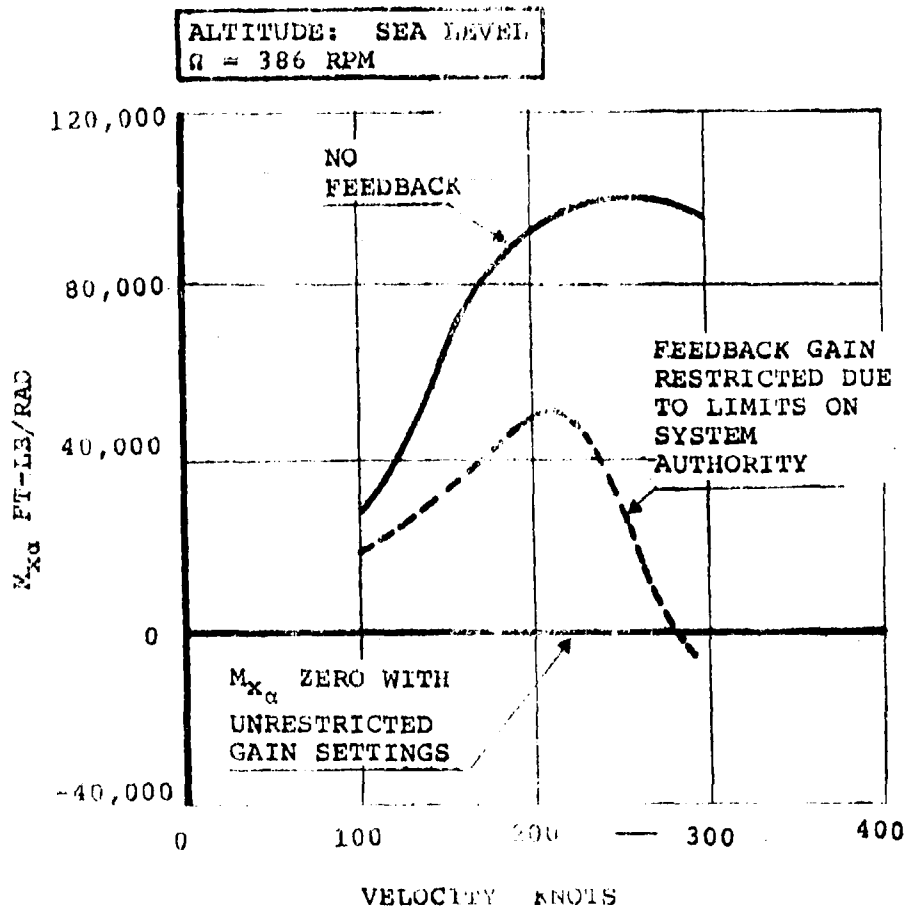

FIGURE 3.6. HUB YAWING MOMENT DERIVATIVE WITHOUT FEEDBACK AND WITH GAIN RESTRICTED FOR ARBITRARY LIMIT OF 1.5° A_1 and B_1

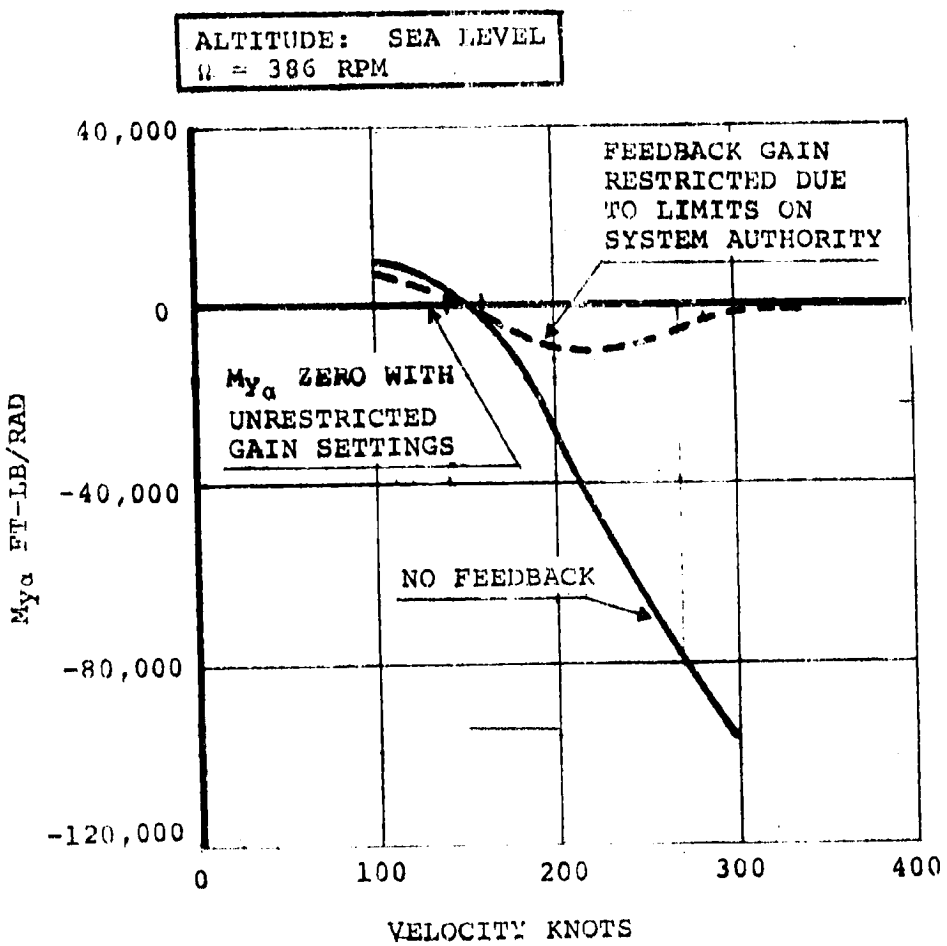

FIGURE 3.7. HUB PITCHING MOMENT DERIVATIVE WITHOUT FEEDBACK AND WITH GAIN RESTRICTED FOR ARBITRARY LIMIT OF 1.5° A_1 and B_1

system and since this would be considered unacceptable within the flight envelope the system gain will be limited so that flight envelope Aq conditions will not generate demands which exceed system authority. This places constraint on gain scheduling which is a function of speed. Figures 3.4 through 3.7 show the impact of gain restrictions set so that an arbitrary system authority of 1.5° in the A_1 and B_1 channels is not exceeded by feedback signal demands associated with maximum flight envelope conditions. It is noted that even with restrictions on gain settings there is still a significant reduction in all the hub forces and moments, reflecting a similar reduction in blade bending moments and shears. The net effect on pitching moment about the nacelle pivot is important in relation to static stability. Figure 3.8 shows the pivot pitching moment with and without feedback at sea level and 10,000 ft. At both altitudes the feedback system reduces pivot pitching moment slightly at low speed thereby increasing static margin but at high speeds the opposite is true, with a marked increase in the sea level case. This is a result of a marked reduction in negative hub pitching moment which is not accompanied by a similar reduction in positive normal force.

The net effect on static stability is to provide a slight

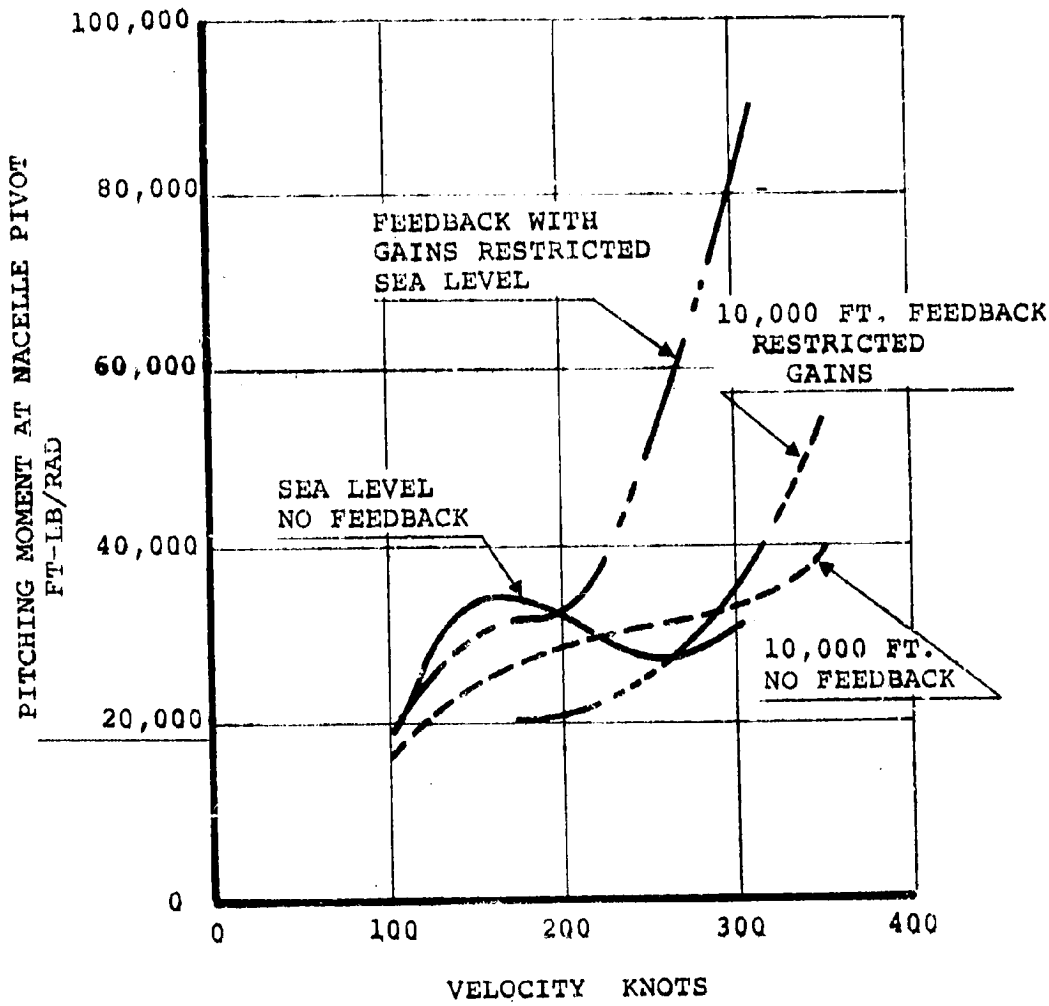

FIGURE 3.8. PITCHING MOMENT ABOUT NACELLE PIVOT WITH AND WITHOUT FEEDBACK

increase at low speed (1.2% $\bar{c}$ at 150 knots) where improvement is most useful, and to decrease the static margin by approximately 5% at 300 knots when a decrease is acceptable.

In summary this system based on a reduction of hub moments criterion also provides reductions in blade loads and normal side forces, and does not deteriorate the static stability behavior. However, scheduling of gain and azimuth with speed is required and preferably with altitude also.

Since the preceeding analysis was based on static consideration only the systems defined were cheeked for stability by inspection of their Bode Diagrams. That is the open loop response of the complete system taking account of blade dynamics and wing/pylon/fuselage flexibilities and rigid body freedoms. The diagrams for 150, 250 and 350 knots are shown in Figures 3.9, 3.10 and 3.11. Decibel levels for 350 knots are higher than at lower speeds while the phase response is similar. The levels are for unity gain in the feedback loop. The net decibel levels are obtained by subtracting the gain levels indicated. At 350 knots the phase margin is about the minimum that would be acceptable and a phase shifting network is indicated to improve this margin.

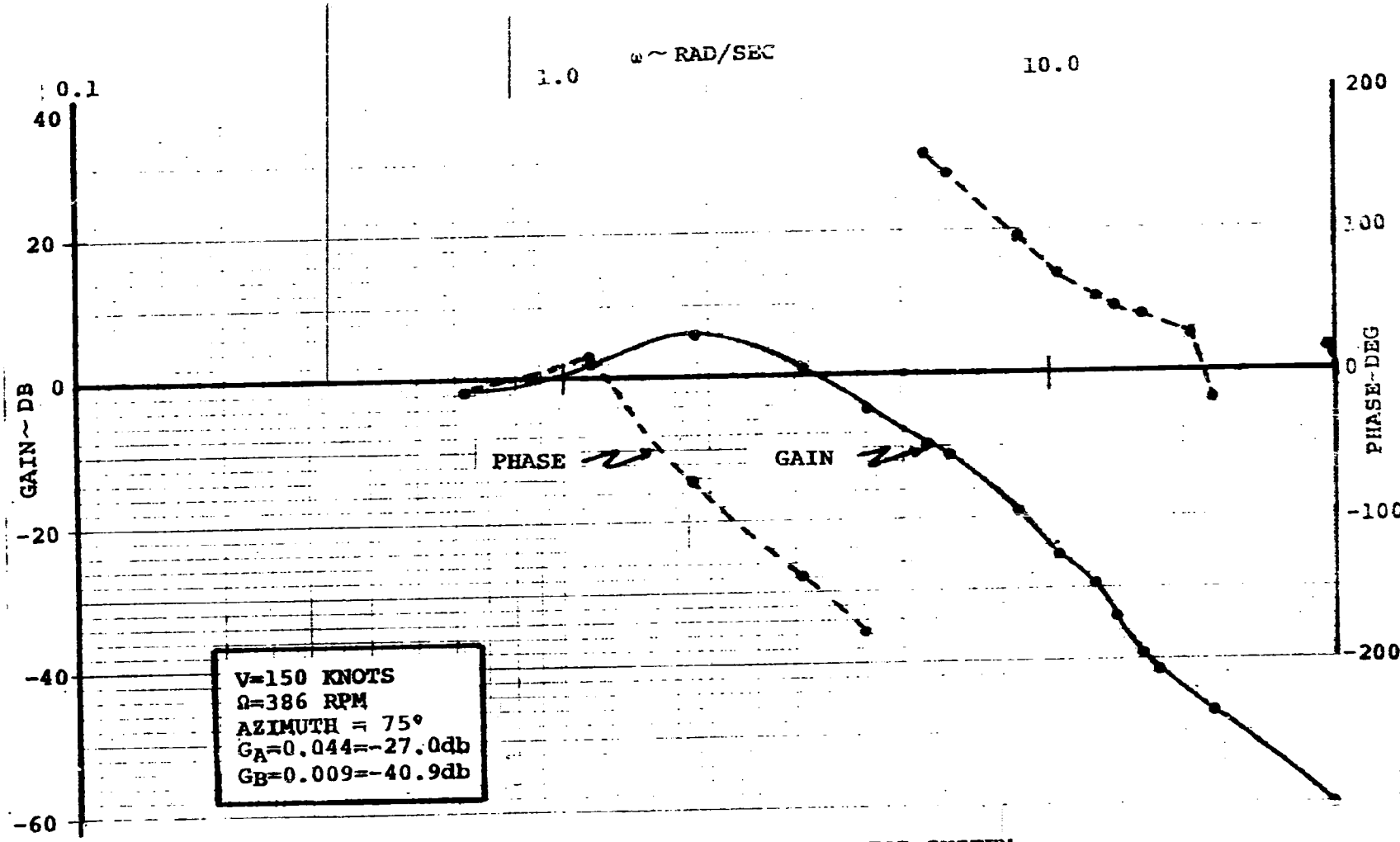

FIGURE 3.9. BODE DIAGRAMS FOR SYSTEM DESIGNED TO REDUCE HUB MOMENTS

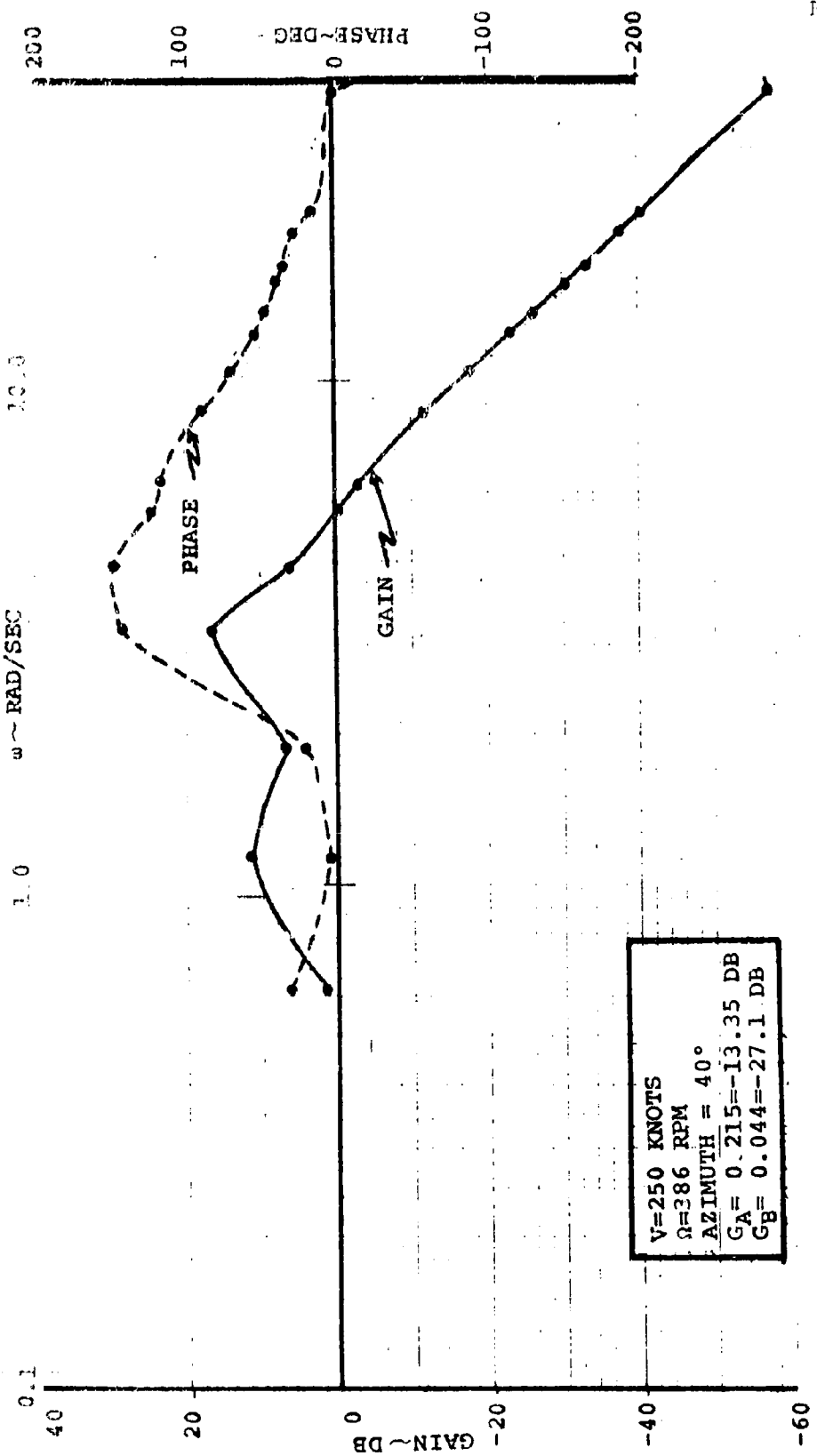

FIGURE 3.10. BODE DIAGRAM FOR SYSTEM DESIGNED TO REDUCE HUB MOMENTS

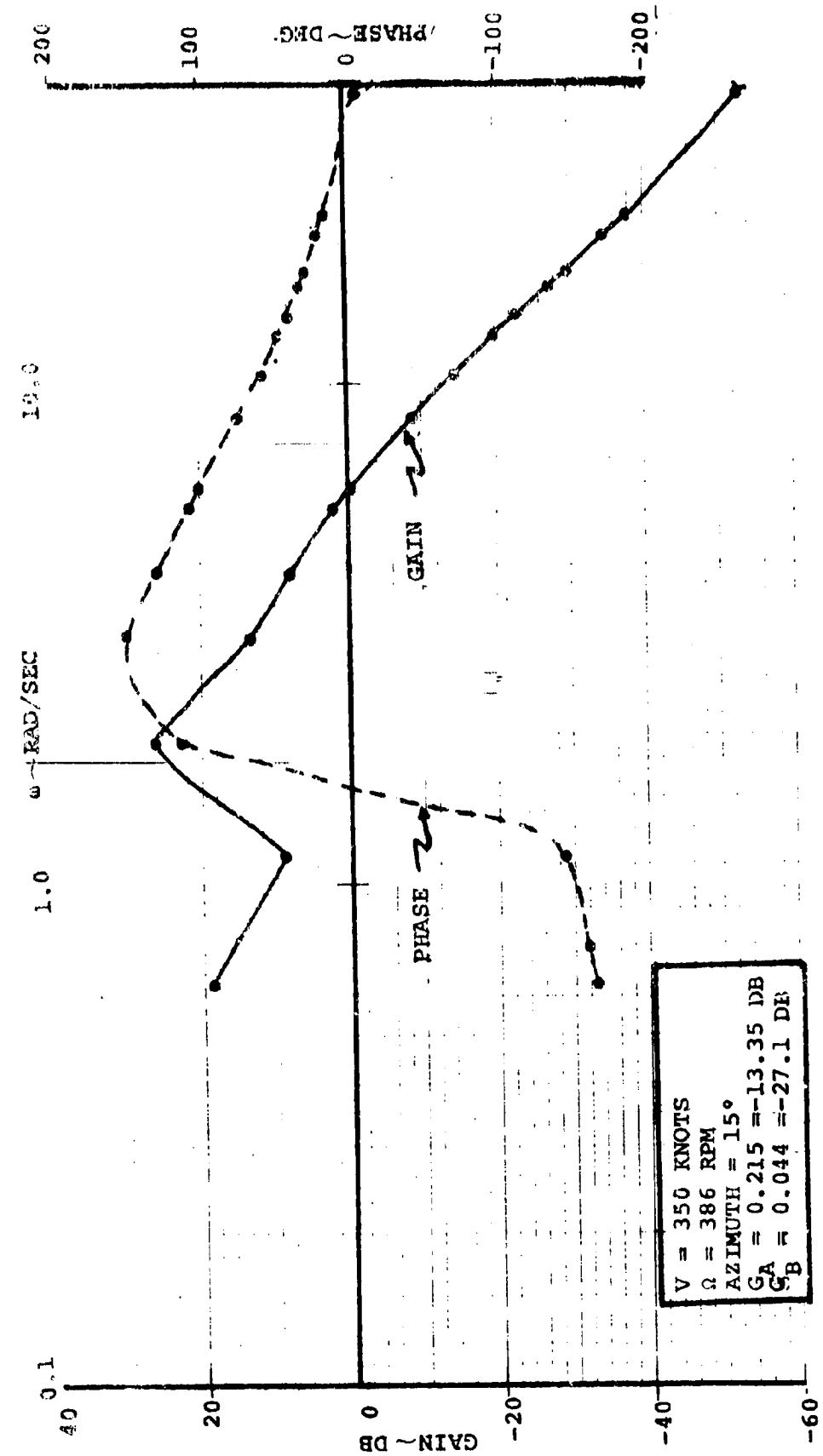

FIGURE 3.11. BODE DIAGRAM FOR SYSTEM DESIGNED TO REDUCE HUB MOMENTS

3.7 ALTERNATIVE SYSTEM DEFINITIONS

Since objectives additional to minimization of hub moments may be required and since a load alleviation system is required to operate under transient loading conditions as well as static, a more general investigation was initiated. In the preceeding study the system was designed to zero out hub moments due to steady state loading conditions and it was fortuitous that a slight improvement in static margin at low speeds came out of the system. In the present study the behavior of hub forces and moments and nacelle pivot moments are examined to see if a better approach is available. To develop a general picture of the behavior of hub forces and moments and nacelle pivot moments as functions of gain and azimuth, they were evaluated for the complete azimuth range and for a set of gain values ranging from 0 to 1.0 radian of cyclic per radian of shaft angle. Contours of forces and moments were then plotted as functions of gain and azimuth as shown in Figures 3.12 and 3.13 for 250 knots and 100 knots respectively. From these the contours for zero forces and moments and pivot moments were constructed and superimposed in Figures 3.14 and 3.15. Examination of Figures 3.12 through 3.15 permits system parameters to be selected according to different objectives. For example, if minimization of pivot moments was of

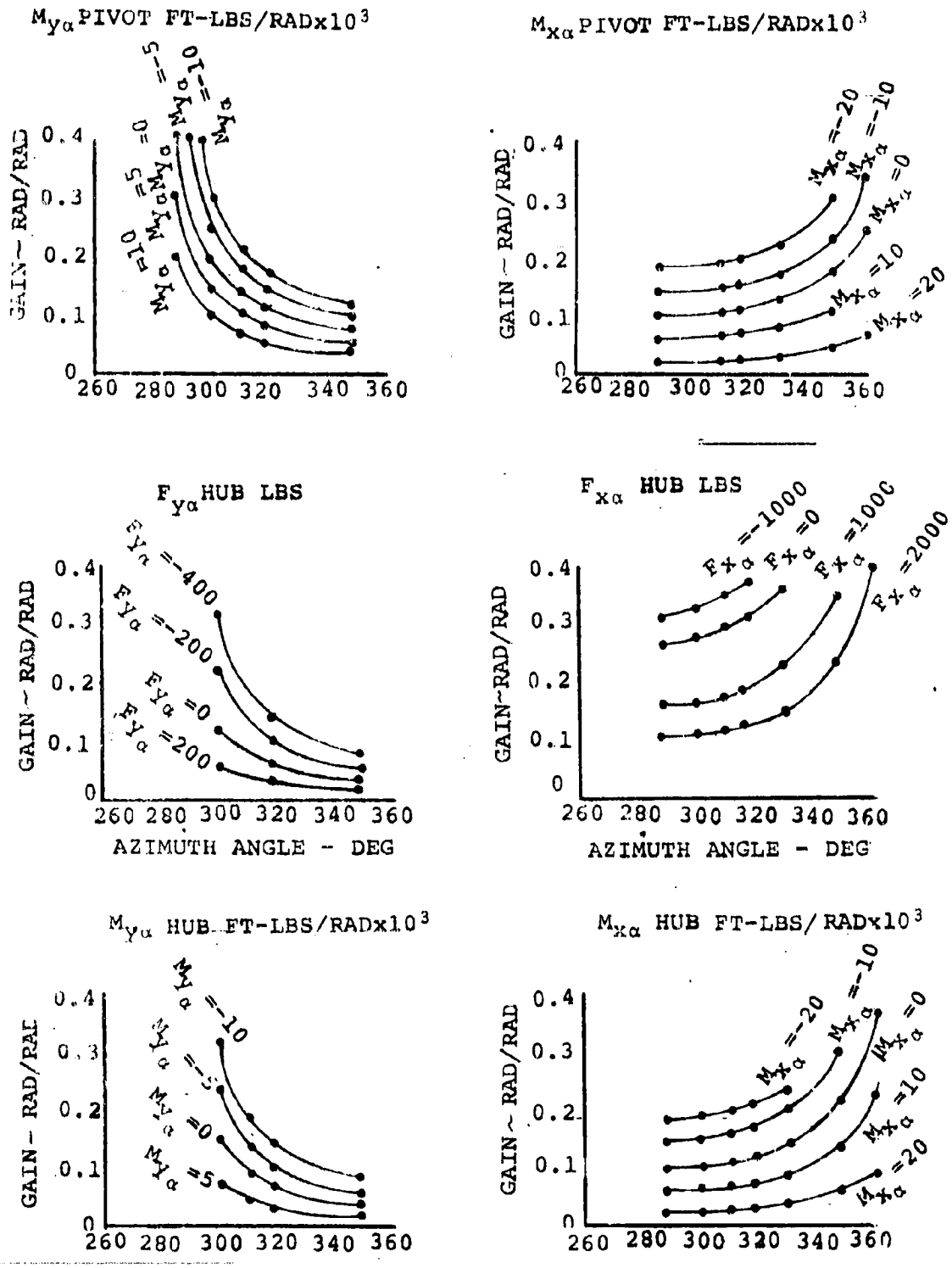

FIGURE 3.12. FORCES AND MOMENTS VS GAIN/AZIMUTH AT 100 KNOTS, 386 RPM AND SEA LEVEL.

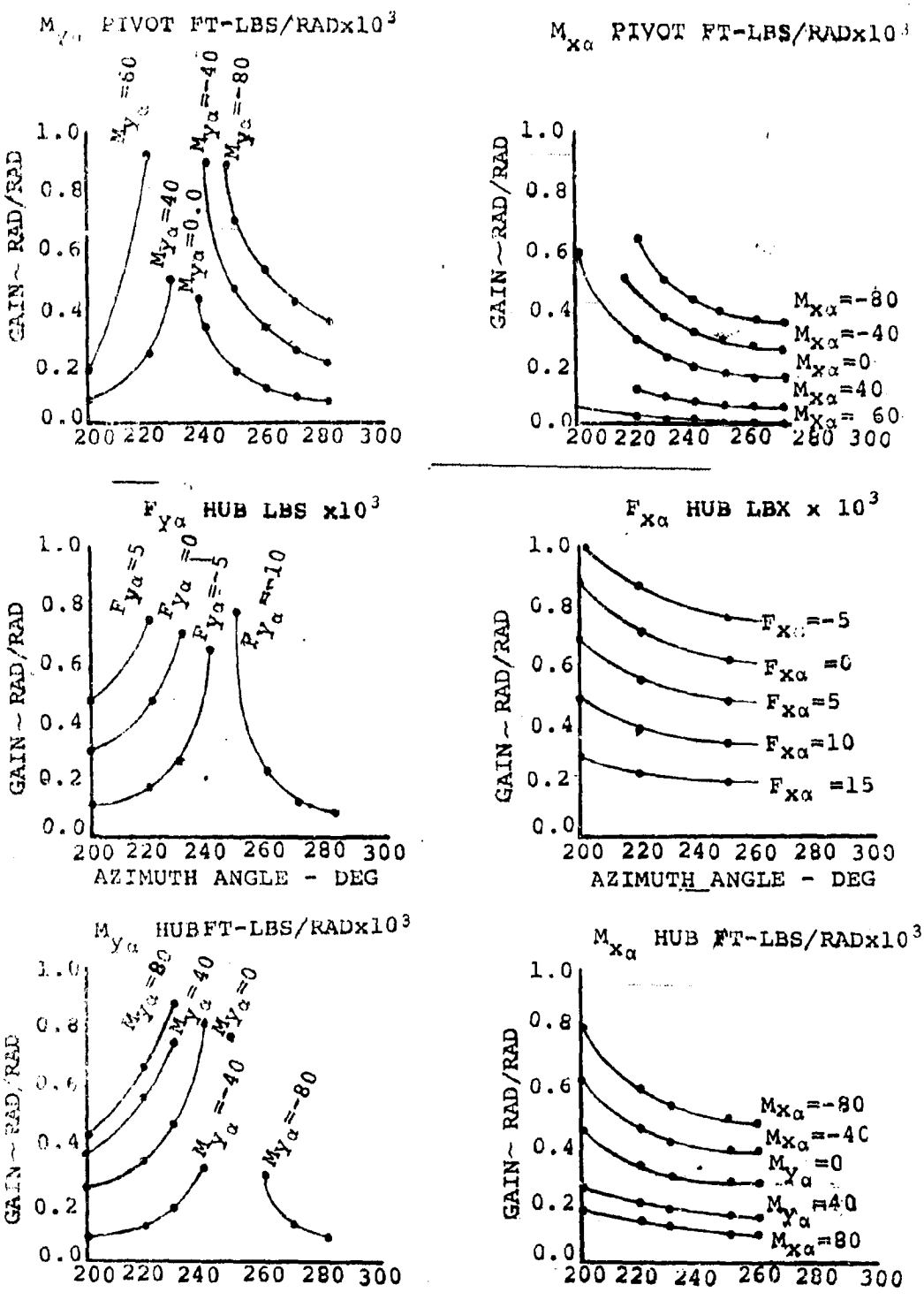

FIGURE 3.13. FORCES AND MOMENTS VS GAIN/AZIMUTH AT 250 KNOTS 386 RPM AND SEA LEVEL

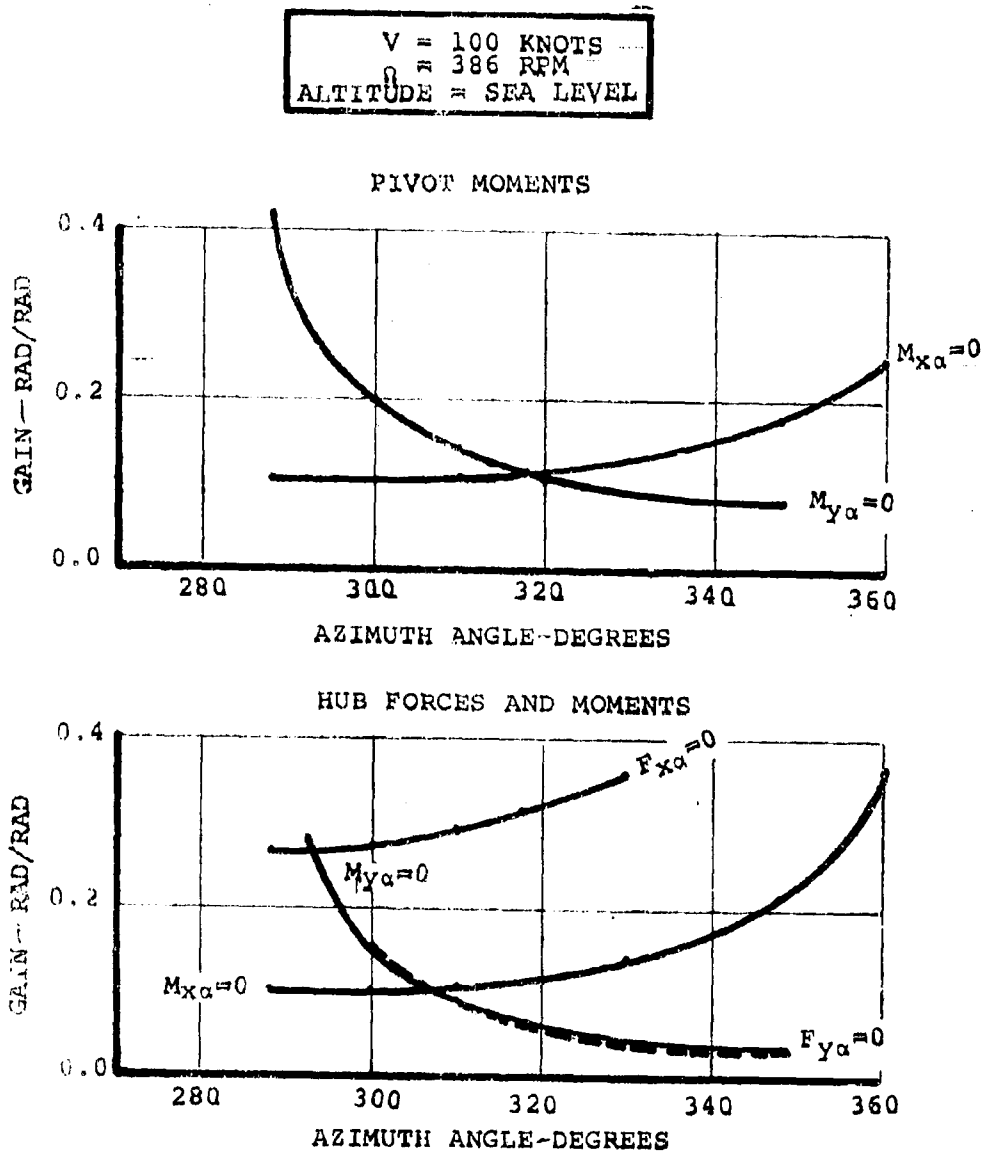

FIGURE 3.14 GAIN/AZIMUTH FOR ZERO FORCES AND MOMENTS AT 100 KNOTS

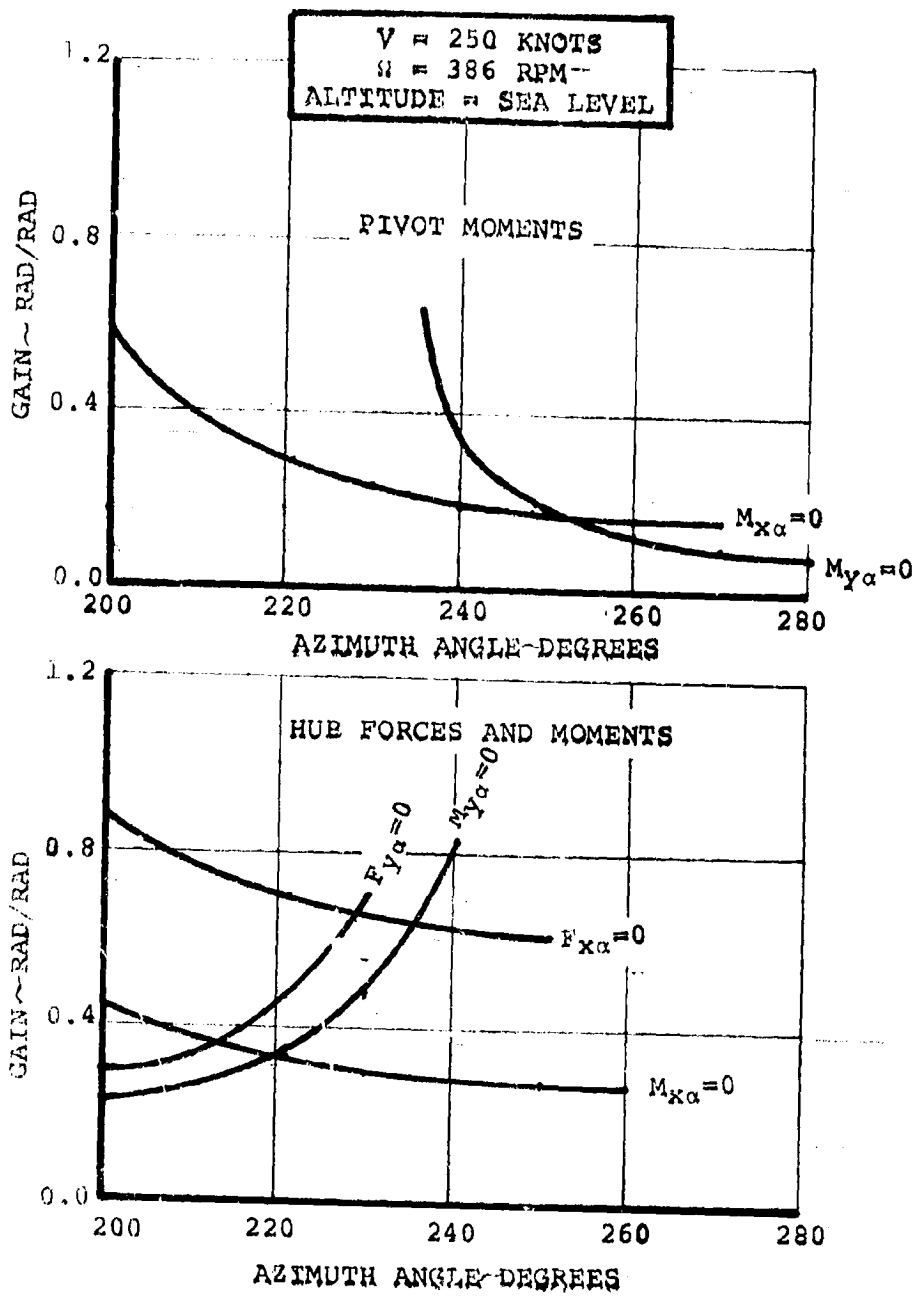

FIGURE 3.15. GAIN AZIMUTH FOR ZERO FORCES AND MOMENTS AT 250 KNOTS

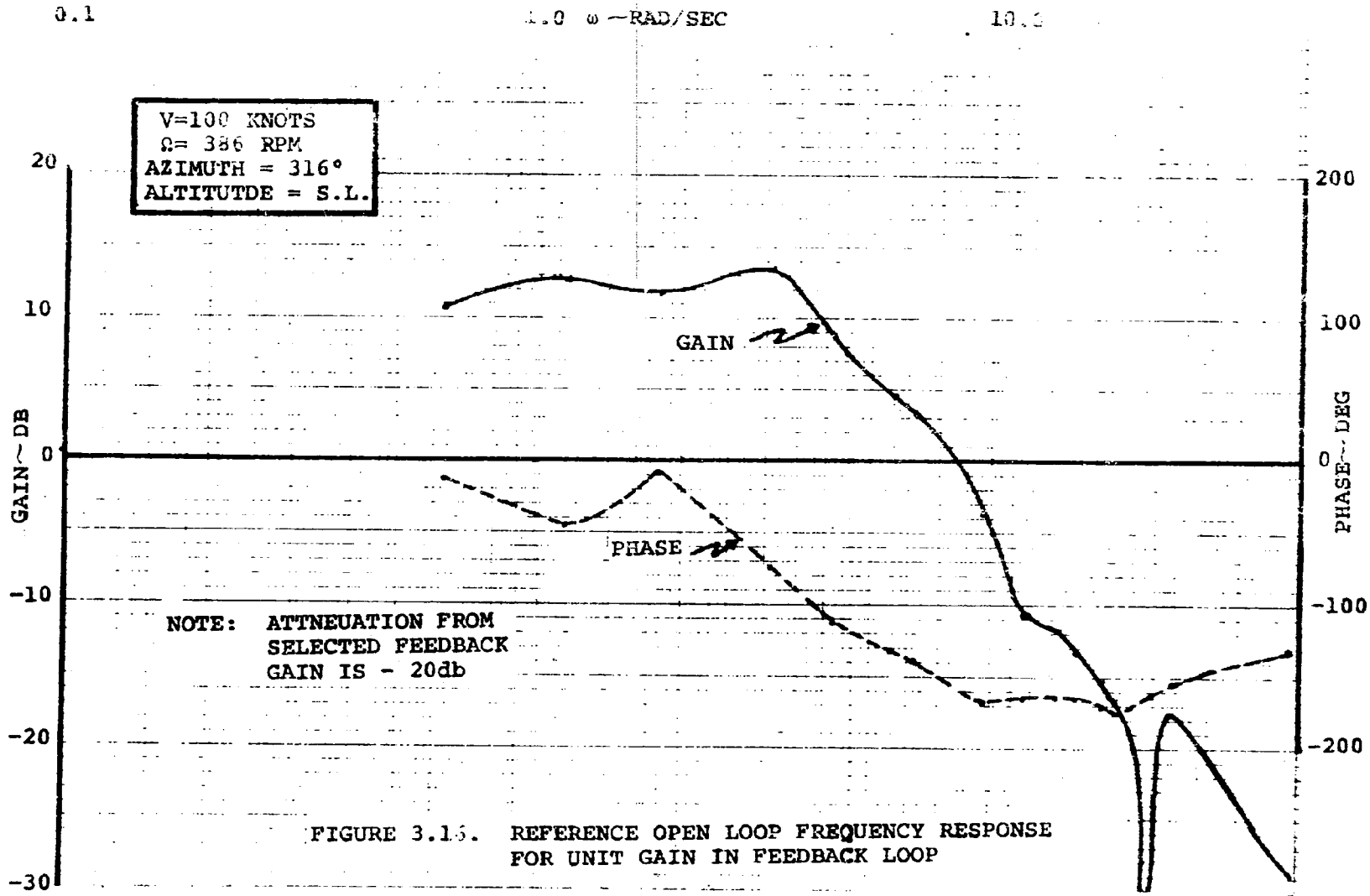

FIGURE 3.1.6. REFERENCE OPEN LOOP FREQUENCY RESPONSE FOR UNIT GAIN IN FEEDBACK LOOP

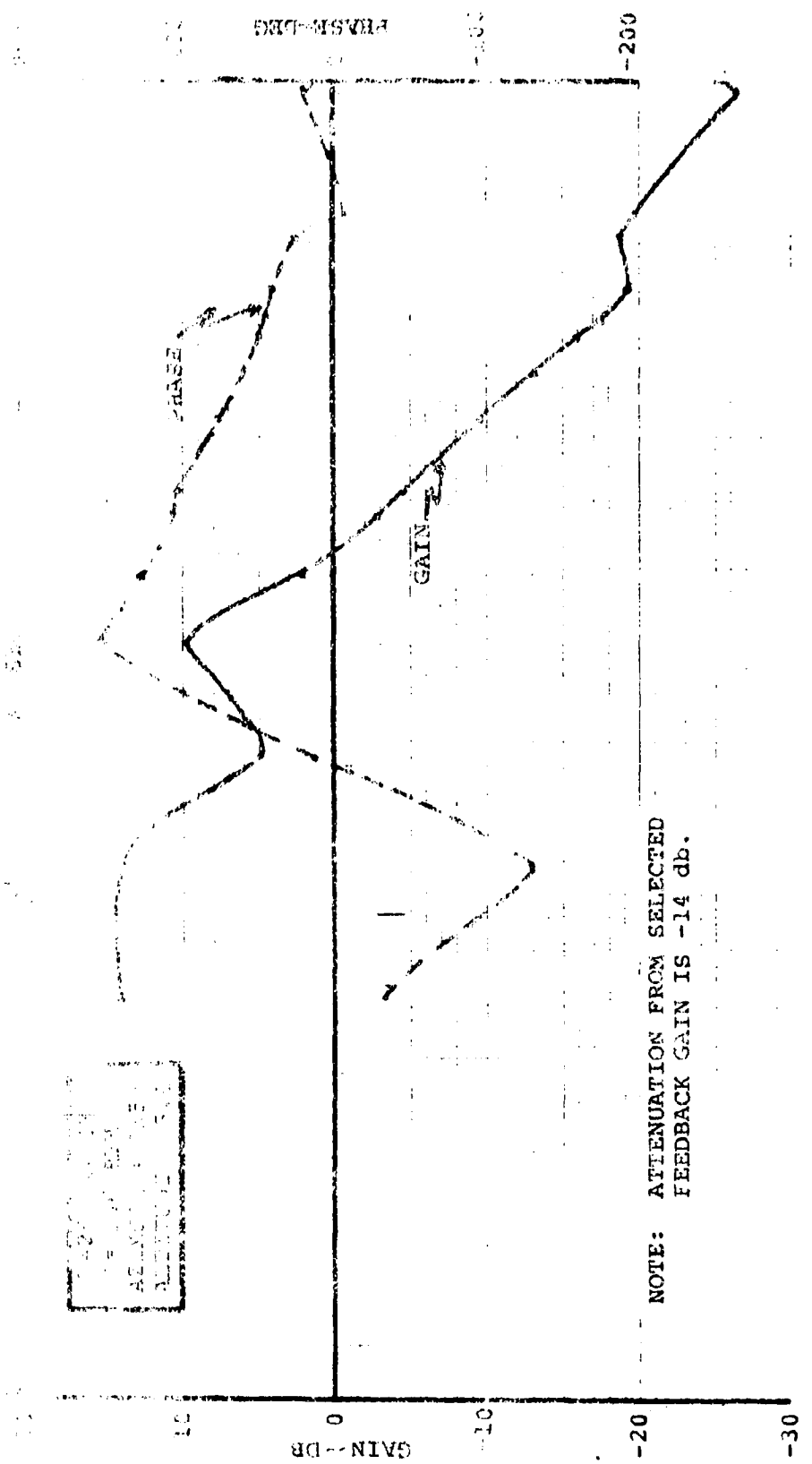

FIGURE 3.17. REFERENCE OPEN LOOP FREQUENCY RSPONSE
FOR UNIT GAIN IN FEEDBACK LOOP

overriding importance, the system gains would be set to give an azimuth of 255-degrees and a gain of around 0.2 at 250 knots with scheduling to give an azimuth of 316-degrees and gain 0.1 at 100 knots. Bode diagrams for these two conditions are given in Figures 3.16 and 3.17 and it is noted that adequate gain and phase margins exist. An attractive alternative might be to reduce the pitching moment about the pivot to zero, and at the same time minimize hub forces and moments as far as possible. Thus, by selecting an azimuth around 230 degrees and gain approximately 0.65, the pivot pitching moment is still zeroed, but so also are the hub normal and side forces and pitching moment; only the hub yawing moment remains, and it is seen from Figure 3.12 that this azimuth and gain setting will result in a hub yawing moment of approximately -100,000 ft lb/radian compared with one of approximately +100,000 ft-lb/radian when no feedback is present. There is, of course, a net reduction in total hub moment because the pitching moment has been reduced to zero. The same reasoning applies at other speeds. At 100 knots the equivalent selection is a gain setting of 0.26 and azimuth 293-degrees. In this case the total residual hub moment is approximately -30,000 ft lb/radian compared with a value without feedback, obtained by resolving 25,000 ft lb/radian of yawing moment and 10,000 ft lb/radian of pitching moment.

The above two examples do not exhaust the possibilities; for example a net nose down pivot moment might be beneficial and

this could be provided by increasing azimuth while keeping a gain setting which made F_{X_α} zero.

It is clear that this approach to the selection of feedback system gains and azimuth is a powerful and flexible tool which may be used not only to reduce rotor effects but to actively improve the static stability of the aircraft.

A3c - DERIVATION OF ψ_{ROT} = 50-DEGREES FOR THE THIRD LOW RATE SYSTEM

Designing the system such that α effects are negated by the pitch loop and β effects by the yaw loop in an uncoupled manner the equations for pitch and yaw due to α become

$$\text{(Pitch)}\quad M = M_\alpha\ \alpha + M\ (G_\rho M_{\theta_\rho} \cos\ (\psi_{ROT} + \theta_\rho - 20))$$

$$\text{(Yaw)}\quad N = N_\alpha\ \alpha + M\ (G_\rho M_{\theta_\rho} \sin\ (\psi_{ROT} + \theta_\rho - 20))$$

where M_{θ_ρ} is the resultant moment due to cyclic input derivative to cyclie and θ_ρ is the angle between the cyclic vector and the moment vector G_ρ is the pitch loop gain in degrees cyclic/ft. lb. moment

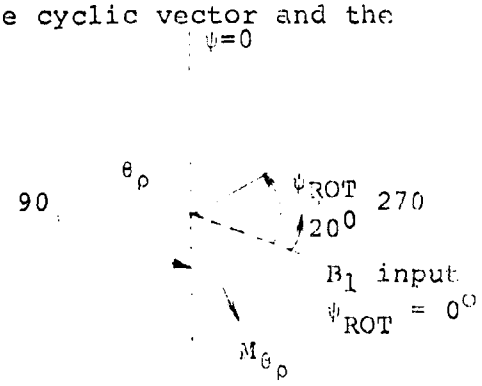

The pitch attenuation is given by

$$\frac{M}{M_\alpha \alpha} = \frac{1}{1 - G_\rho M_{\theta_\rho} \cos\ (\psi_{ROT} + \theta_\rho - 20)}$$

and the yaw attenuation

$$\frac{N}{N_\alpha \alpha} = \frac{1 - G_\rho M_{\theta_\rho} \cos(\psi_{ROT} + \theta_\rho - 20) + \frac{M_\alpha}{N_\alpha} G_\rho M_{\theta_\rho} \sin\ (\psi_{ROT} + \theta_\rho - 20)}{1 - G_\rho M_{\theta_\rho} \cos\ (\psi_{ROT} + \theta_\rho - 20)}$$

for equal attenuations

$$G_\rho M_{\theta_\rho} \cos\ (\psi_{ROT} + \theta_\rho - 20) = \frac{M\alpha}{N\alpha} G_\rho M_{\theta_\rho} \sin\ (\psi_{ROT} + \theta_\rho - 20)$$

or $$\tan(\psi_{ROT} + \theta_\rho - 20) = \frac{N\alpha}{M\alpha}$$

The pitch and yaw due to β are

$$M = M_\beta \beta + N(G_Y M_{\theta_\rho} \sin\ (\psi_{ROT} + \theta_\rho - 20))$$

$$N = N_\beta \beta + N(G_Y M_{\theta_\rho} \cos\ (\psi_{ROT} + \theta_\rho - 20))$$

Yaw attenuation

$$\frac{N}{N_\beta \beta} = \frac{1}{1 - G_Y M_{\theta_\rho} \cos\ (\psi_{ROT} + \theta_\rho - 20)}$$

Pitch attenuation

$$\frac{M}{M_\beta \beta} = \frac{1 - G_Y M_{\theta_\rho} \cos\ (\psi_{ROT} + \theta_\rho - 20) + \frac{N\beta}{M\beta} G_Y M_\theta \sin\ (\psi_{ROT} + \theta_\rho - 20)}{1 - G_Y M_{\theta_\rho} \cos\ (\psi_{ROT} + \theta_\rho - 20)}$$

For equal attenuation

$$G_Y M_{\theta_\rho} \cos\ (\psi_{ROT} + \theta_\rho - 20) = \frac{N\beta}{M\beta} G_Y M_{\theta_\rho} \sin\ (\psi_{ROT} + \theta_\rho - 20)$$

i.e., $\tan (\psi_{ROT} + \theta_p - 20) = \frac{M\beta}{N\beta}$

From symmetry $\frac{M\beta}{N\beta} = \frac{-N\alpha}{M\alpha}$

i.e., orthogonal to the pitch case.

From Section 6.0 at 192 knots

$\frac{N\alpha}{M\alpha} = -1.112$ such that

$\psi_{ROT} + \theta_p - 20 = 318.1$-degrees ($N\alpha$ negative)

$\theta_p = 276$-degrees giving a $\psi_{ROT} = 62$-degrees

On line calculations gave a value closer to 50-degrees which was the value used.

APPENDIX 4

APPENDIX 4. STRAIN GAGE RESOLVER DESCRIPTION

The tilt rotor strain gage resolver converts the signal from the flap bending moment strain gage to dc voltage levels proportional to pitching moment and yawing moment.

An electromagnetic pickoff located on the rotating hub of the nacelle generates a one per rev spike which is buffered and shaped. The conditioned one per rev signal starts a linear voltage ramp which begins at 0 v and grows to 10 v. The next one per rev signal causes the ramp to drop to 0 v rapidly and starts climbing toward 10 v again. Negative feedback in the ramp generating circuit assures a precise, linear, 0 to 10 v, one per rev ramp over a hub rotational velocity of 350 to 600 RPM.

To derive pitch and yaw components of the strain gage signal, the gage output is sampled when the number one blade is at an azimuth of 0, 90 and 270 degrees with respect to its 0 degrees reference position, thereby sampling the strain gage when its output is proportional to moments due to collective plus pitch (C + P), collective plus yaw (C + Y) and collective minus yaw (C - Y) cyclic loads.

The 0, 90 and 270 degree number one blade positions are each associated with a unique voltage level on the 0 to 10 v, one per rev ramp. Appropriate voltage threshold circuits gate three demodulators to look at the strain gage output at the proper time. Looking when the

number one blade is at 0 degrees gives the peak value of C+P; at 90 degrees the peak value of C+Y; at 270 degrees the peak value of C-Y.

In order to cancel out any in-phase harmonics of the desired signal, the strain gage is not peak sampled at precisely 0, 90 and 270 degrees, but is sampled for a time interval of 60 degrees on either side of the desired peak. This scheme effectively filters out in phase even harmonics and the 3rd, 5th, 7th and 9th in phase odd harmonics of the fundamental being sampled. The outputs of the demodulators are dc levels proportional to C+P, C+Y and C-Y flap bending moments. These three dc levels are algebraically added in order to derive dc voltage levels proportional to hub pitching moment and yawing moments.

APPENDIX 5

APPENDIX 5. SUMMARY OF APPLICATION OF EXPERIMENTAL FORCE, MOMENT AND BLADE LOAD DATA TO THE MODEL 222 AIRPLANE DESIGN.

INTRODUCTION

The test data obtained on tests 410 and 416 in the NASA 40 by 80-foot wind tunnel enables the Model 222 design to be evaluated on an experimental basis. The airplane design provides a slightly different aerodynamic and aeroelastic environment in which the rotor must operate and these differences must be considered in applying the experimental information to the aircraft.

In cruise flight the angle of attack to trim at a given maneuver load factor depends primarily on the airplane gross weight and wing lift characteristics. The rotor forces and moments have small effects on the trim attitude. With no cyclic pitch used in cruise flight the rotor operates as a conventional propeller and as seen in Section 4.0 experiences increasing alternating loads as angle of attack increases. The load factor per degree of angle of attack increases with the square of the flight speed and results in a decrease in alternating blade root strain sensitivity per g as airspeed increases. The use of cyclic pitch in cruise provides a powerful means of reducing the 1/rev component of blade alternating loads. On test, data was obtained

at 170 knots and 30-degrees incidence with modest blade loads by the judicious application of cyclic pitch. The Model 222 design incorporated an automatic cyclic pitch system using A_q and B_q sensors developed by The Boeing Company for helicopter applications. This system causes only slight changes in the aircraft attitude, but quite large reductions in blade alternating loads.

In transition the rotor hub forces and moments play a much larger role in dictating the aircraft attitude to trim and indeed many solutions to the trim equations are possible at any given airspeed. At the low speed end of transition, the airplane control surfaces are ineffective and control and trim must be effected by the rotor. This requires that the cyclic control inputs be defined by criteria other than minimum alternating loads. As airspeed increases, a larger share of the trim and control moment can be carried by the airplane surfaces and the cyclic pitch controls can be biased towards the minimum load cyclic settings. Alternating loads in transition tend to reduce as airspeed increases. The cyclic required to keep the loads at minimum levels increases with airspeed and the transition boundary based on the blade endurance limit is primarily a function of the cyclic control authority and shaping. When the maximum cyclic is used up the alternating loads increase as speed increases and constitutue a fatigue load boundary.

In hover the aircraft is trimmed and controlled entirely by the rotor. The experimental forces and moments available per degree of cyclic define the aircraft control power and the resulting alternating blade loads which eventually limit the amount of cyclic which is useable for this purpose.

It is apparent that considerably more information is required to establish the fatigue limitations of the aircraft than is given in the body of the test report. The purpose of this appendix is to summarize the analysis of the experimental data performed to date and apply the data to the Model 222 design.

ROTOR FORCES AND MOMENTS - AIRCRAFT TRIM

The experimental data given in the body of the text has been subjected to an empirical regression analysis to obtain an experimental data base from which to proceed in evaluating aircraft trim and control. Sign conventions for rotor forces and moments are given in Figure 2.6.

The cyclic derivatives measured on test were done at a constant thrust coefficient and therefore, the effect of thrust on the derivatives previously calculated and used in the Model 222 simulation has been assumed. The cyclic derivative data is

presented in Figures A.5.1 to A.5.9 and take the form of a function of advance ratio and thrust. The data points shown are test derivatives adjusted for the calculated thrust effect.

The data presented in Section 6 is relative to cyclic inputs 20-degrees prior to the classical A_1 and B_1 control axes. The data shown in Figures A.5.1 to A.5.9 are corrected to the more usual convention of

$$\Delta\theta = -A_1 \cos \Psi - B_1 \sin \Psi.$$

The derivatives are non-dimensionalized in rotor nomenclature (i.e., FORCE/$\rho\pi R^2 V_T^2$ and MOMENT/$\rho\pi R^2 V_T^2 R$).

The data indicate that cyclic effectiveness is independent of nacelle incidence. Most of the derivative data is purely a function of thrust and advance ratio. The exceptions to this general rule are the $\partial C_M/\partial B_1$ and $\partial C_Y/\partial A_1$ derivatives which exhibit a dependence on RPM, or more correctly first mode bending frequency as well as advance ratio. For RPM conditions intermediate to the operating extremes (551 RPM hover and 386 RPM cruise) linear interpolation has been used. This is supported by data obtained at off design RPM on the 26-foot rotor windmill test. An example of the RPM effect is shown in Figure A.5.9 for the yaw derivative with A_1 cyclic.

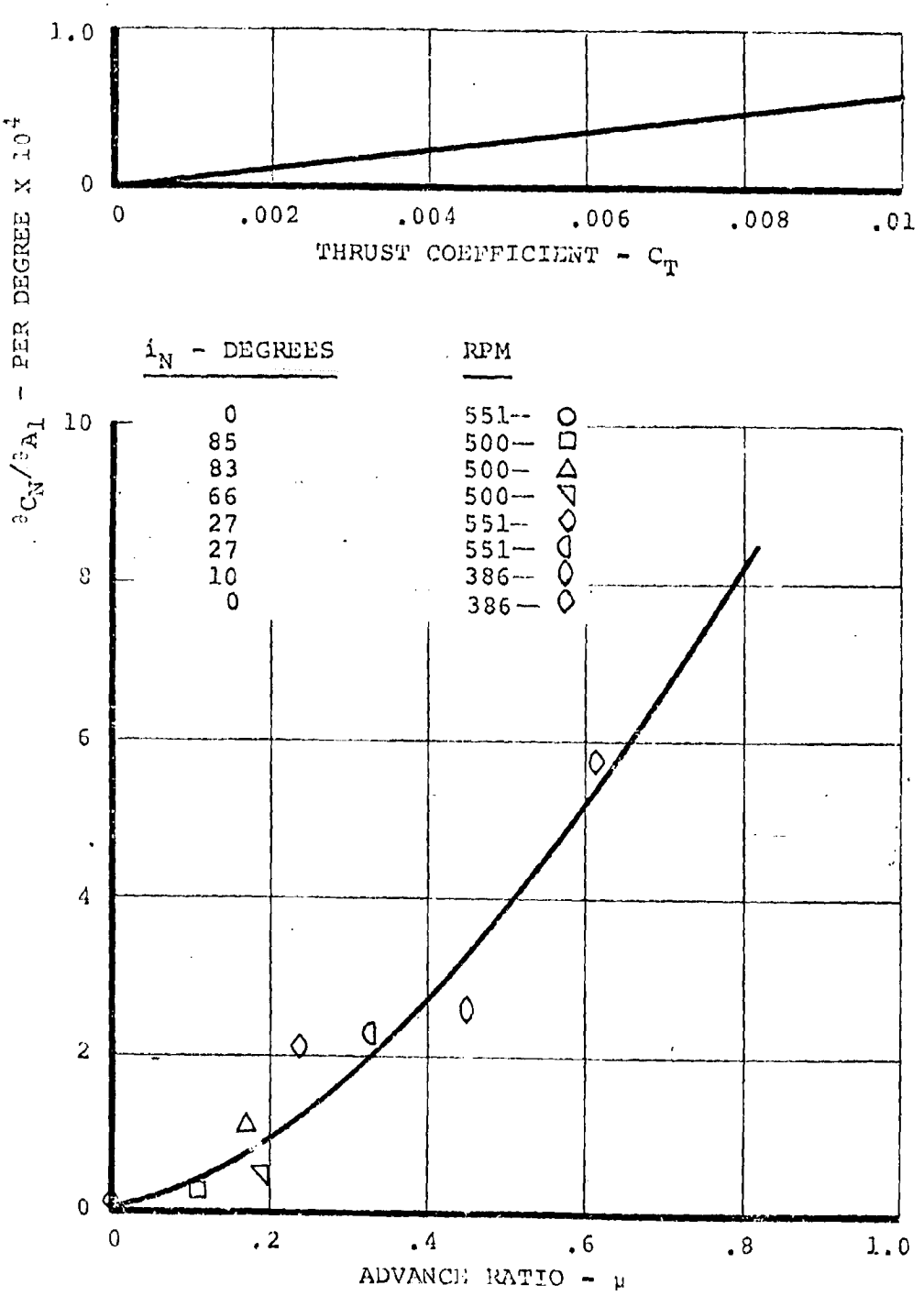

FIGURE A.5.1. CYCLIC EFFECTIVENESS - $\partial C_N/\partial A_1$

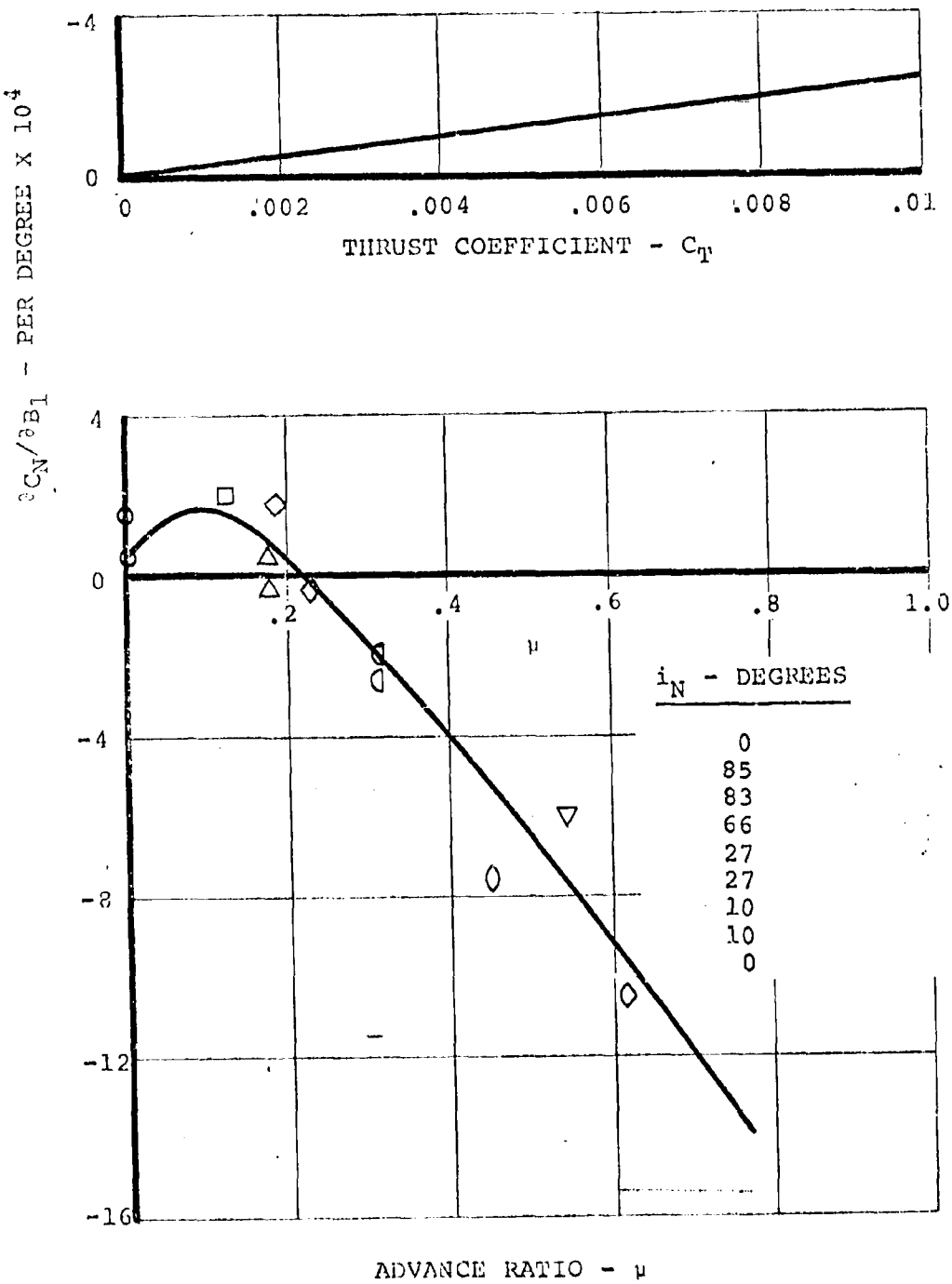

FIGURE A.5.2. CYCLIC EFFECTIVENESS - $\partial C_N/\partial B_1$

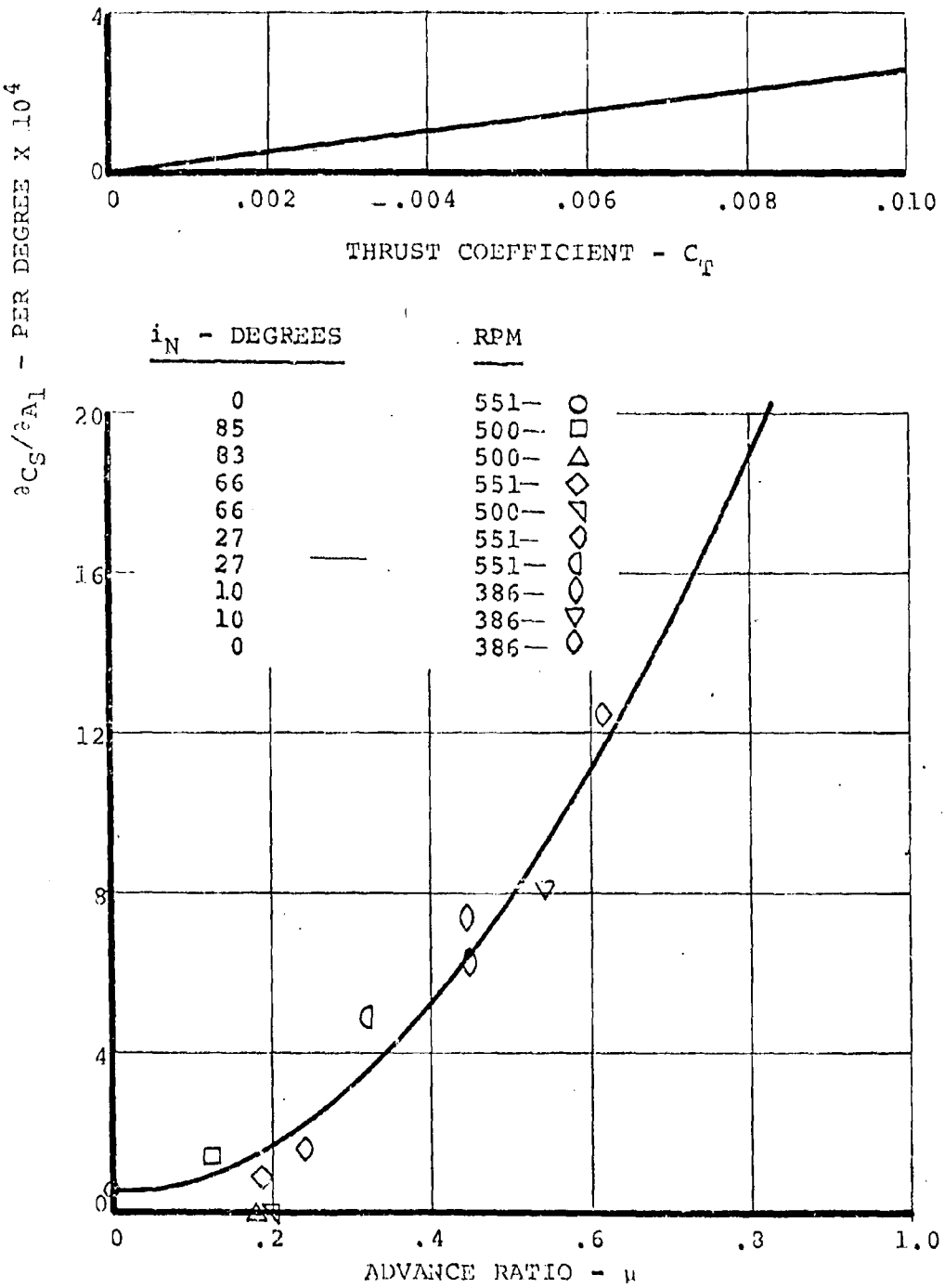

FIGURE A.5.3. CYCLIC EFFECTIVENESS $\partial C_S/\partial A_1$

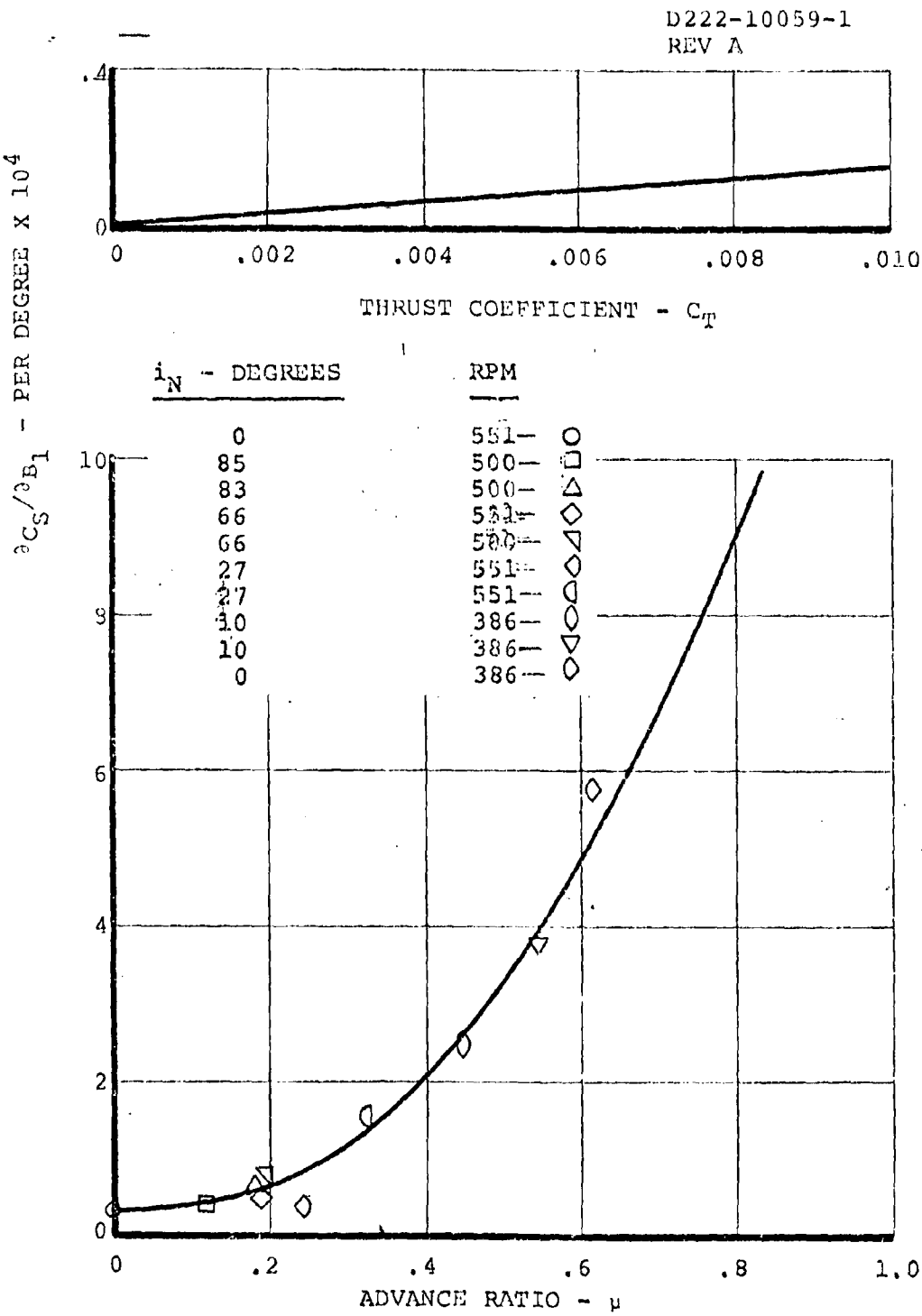

FIGURE A.5.4. CYCLIC EFFECTIVENESS - $\partial C_S/\partial B_1$

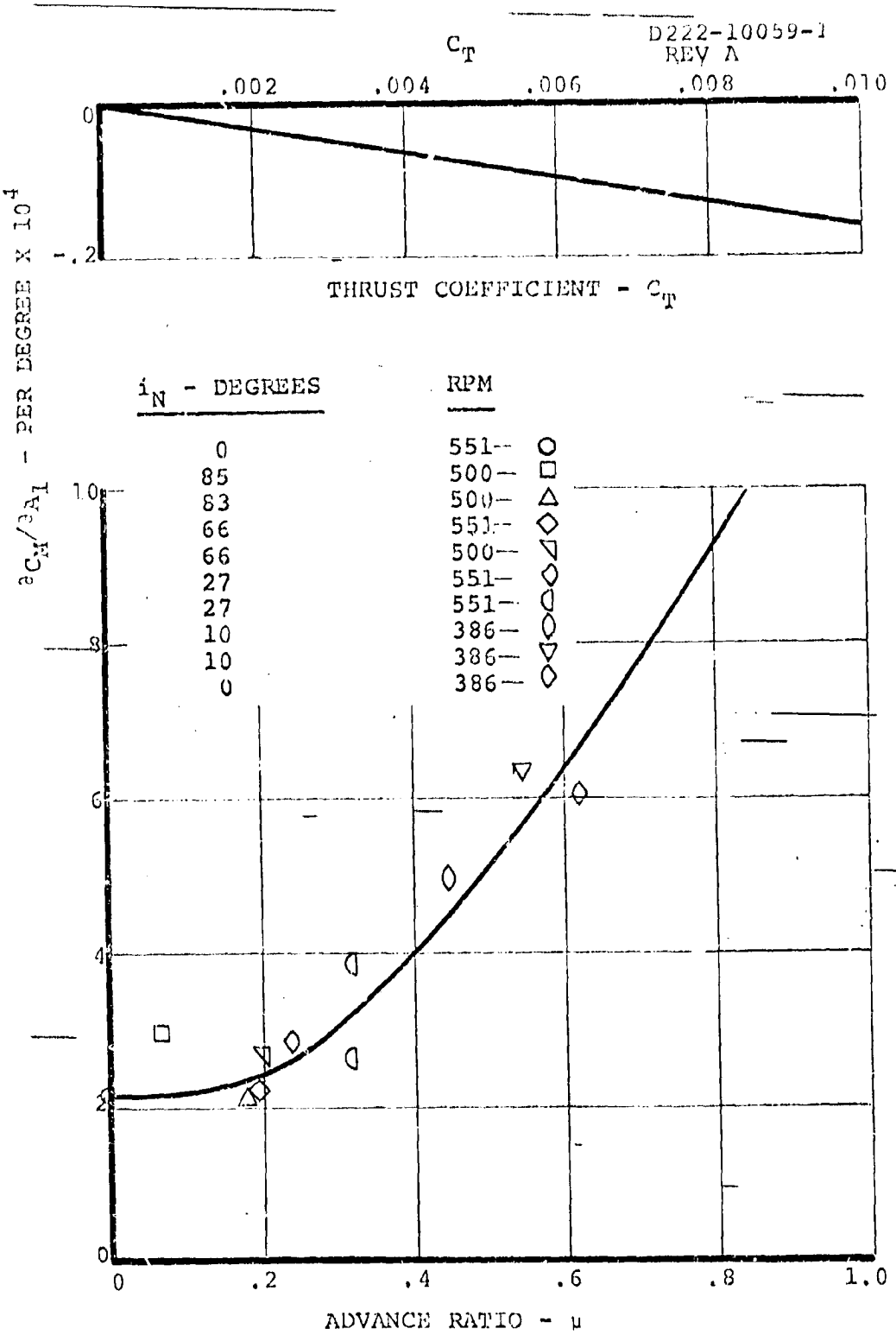

FIGURE A.5.5. CYCLIC EFFECTIVENESS $\partial C_M/\partial A_1$

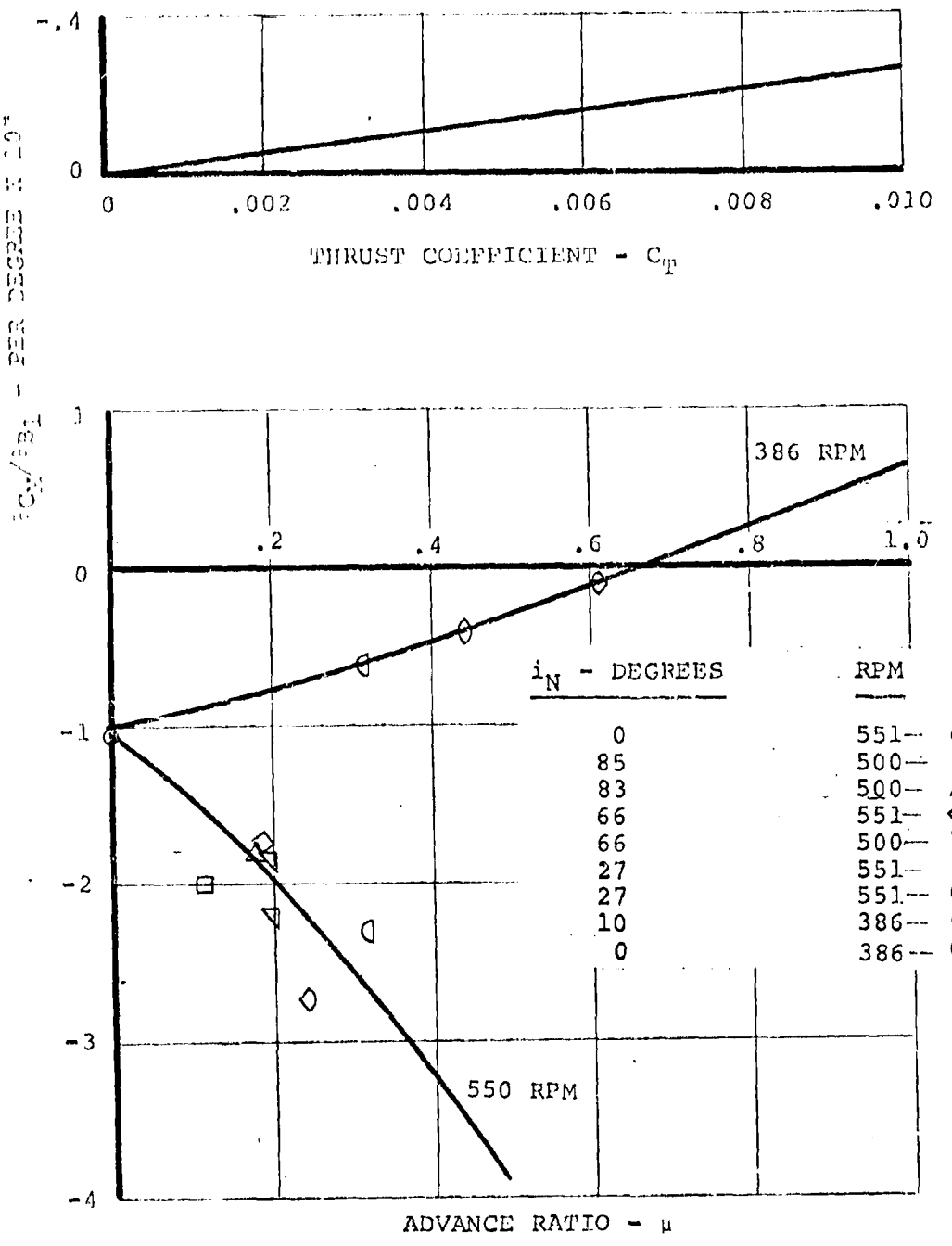

FIGURE A.5.6. CYCLIC EFFECTIVENESS $\partial C_M/\partial B_1$

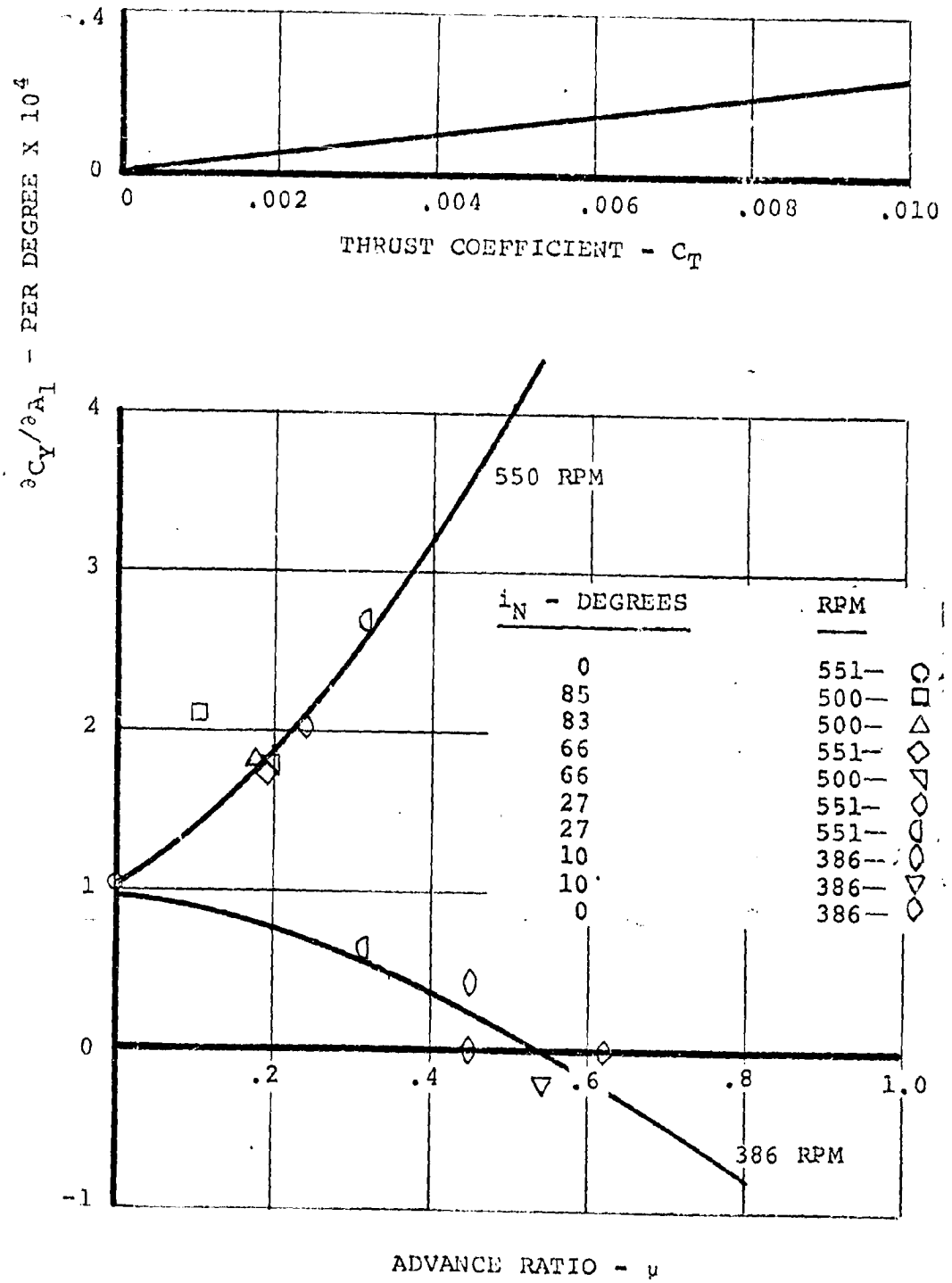

FIGURE A.5.7. CYCLIC EFFECTIVENESS - $\partial C_Y/\partial A_1$

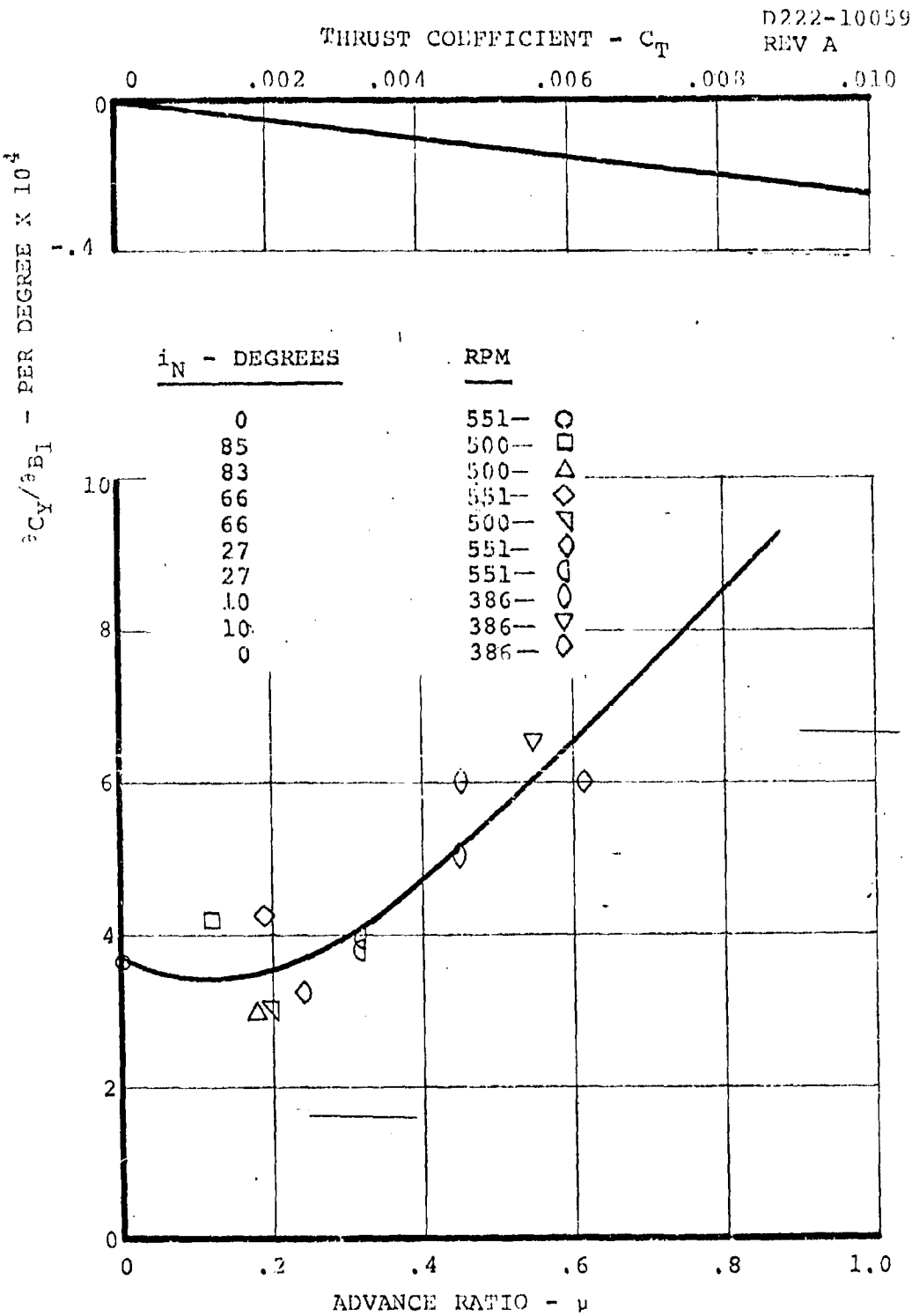

FIGURE A.5.8. CYCLIC EFFECTIVENESS - $\partial C_Y/\partial B_1$

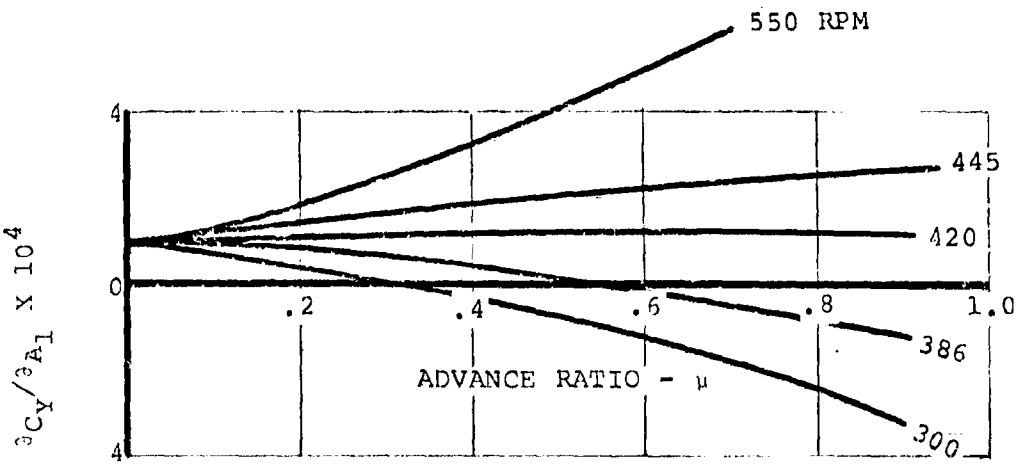

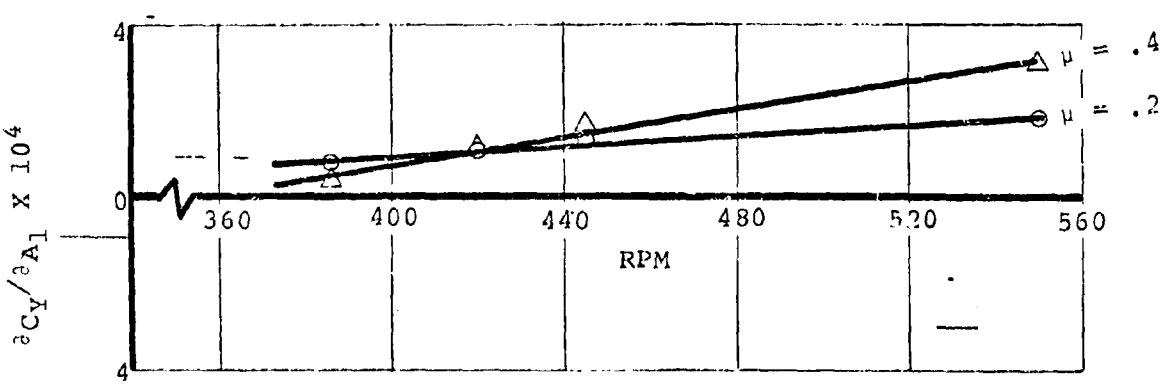

FIGURE A.3.9. EFFECT OF RPM ON YAW DERIVATIVES WITH A_1 CYCLIC

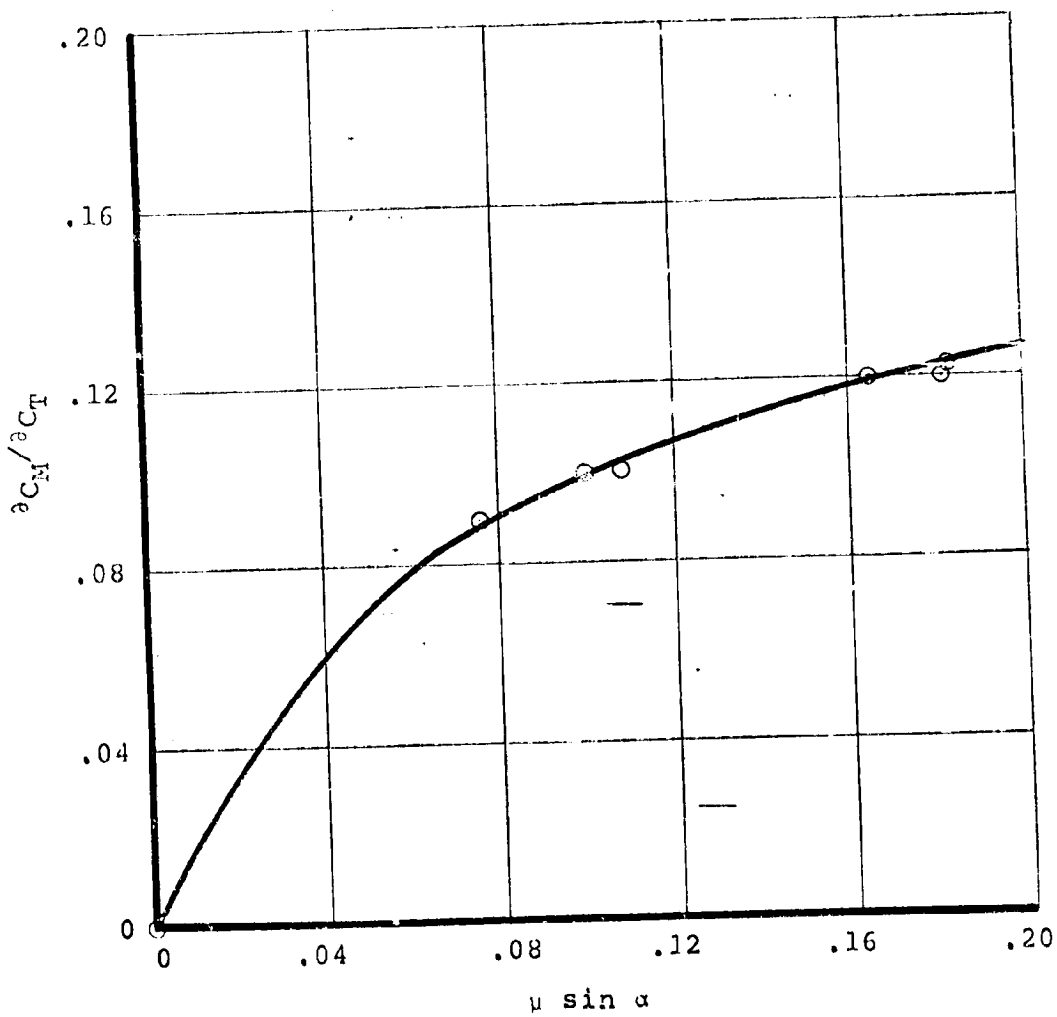

FIGURE A.5.10. EFFECT OF THRUST ON C_M

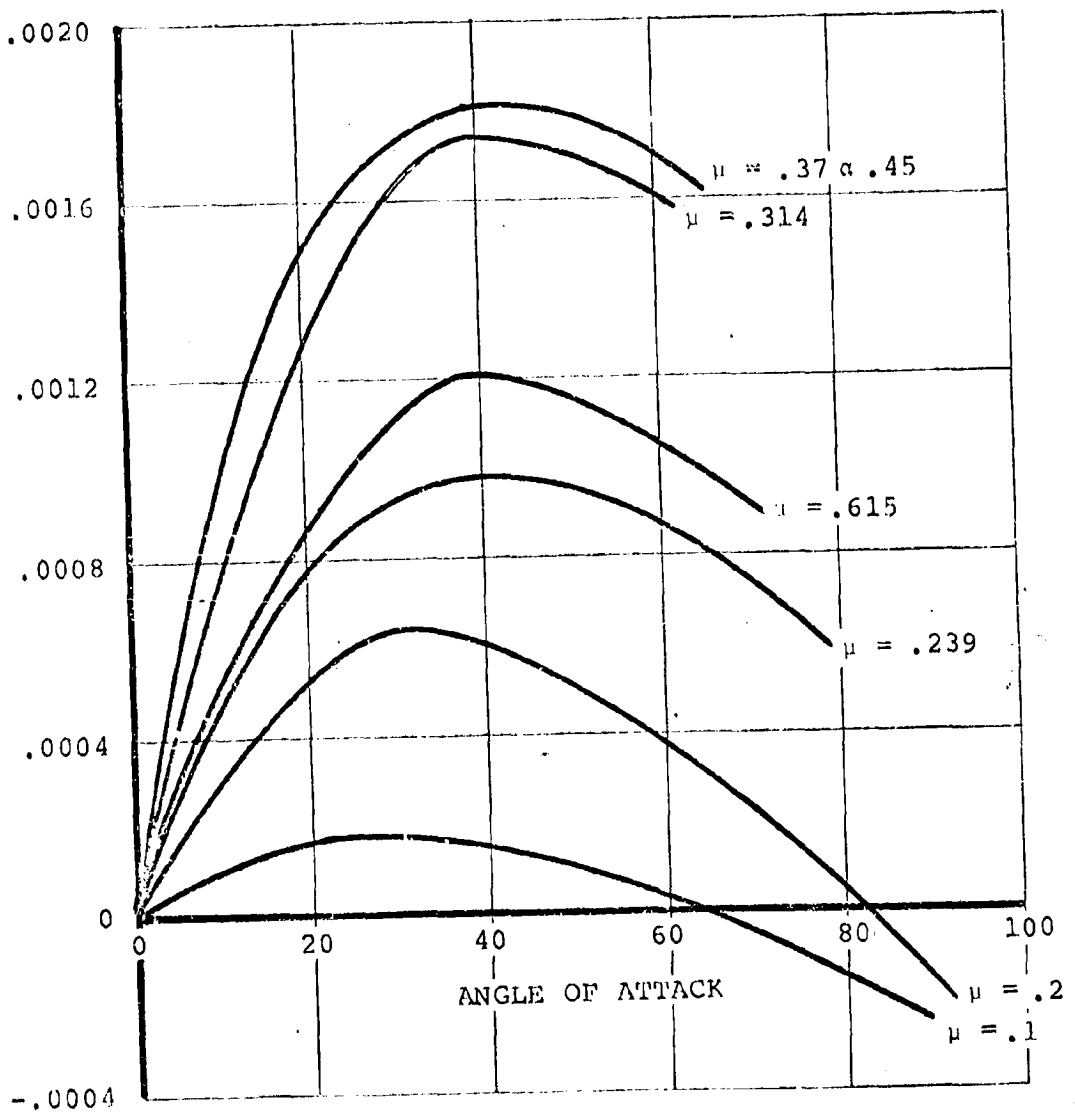

FIGURE A.5.11. VARIATION OF ROTOR HUB PITCHING MOMENT IN TRANSITION - ZERO CYCLIC PITCH - ZERO THRUST

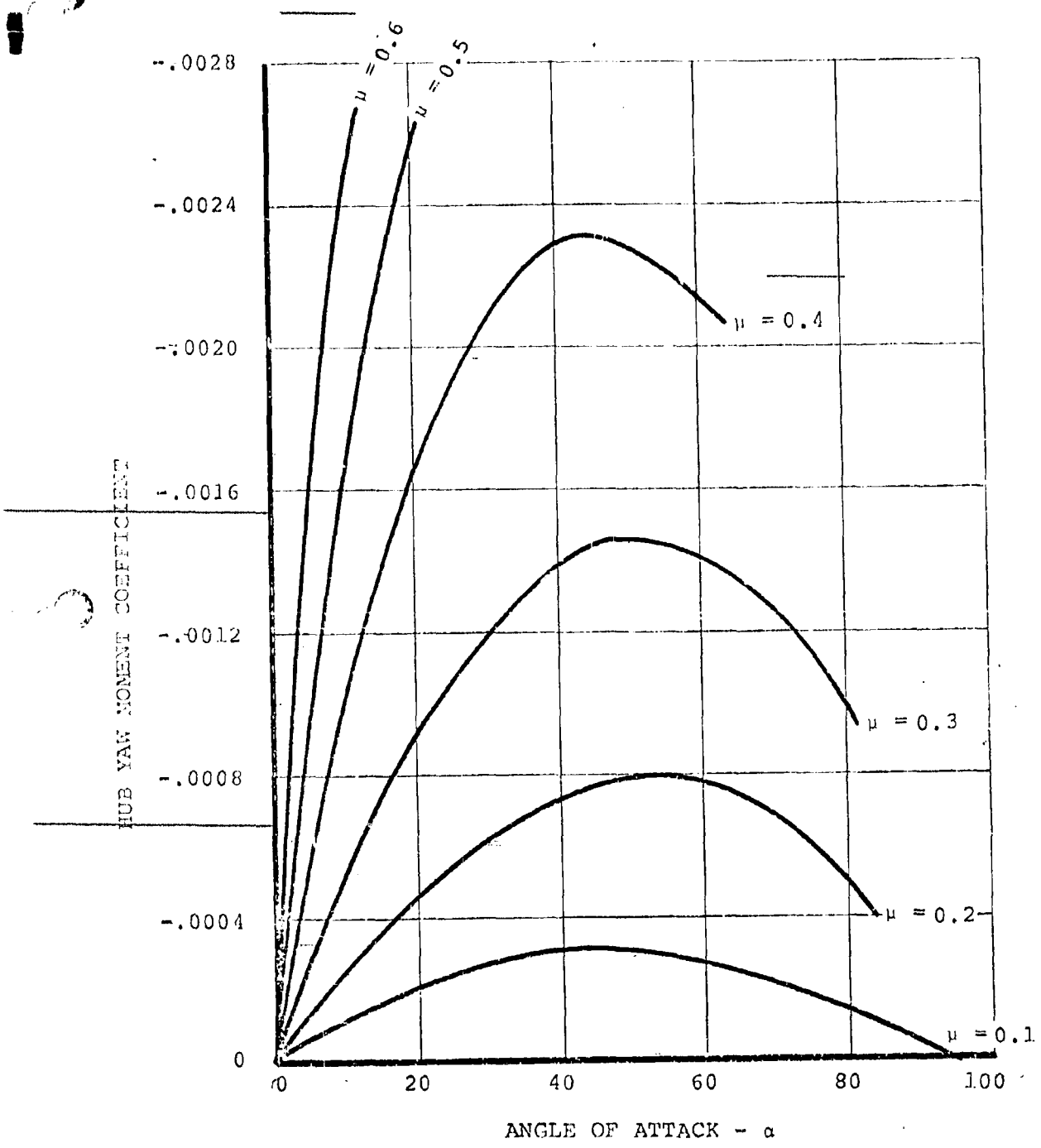

FIGURE A.5.12. VARIATION OF HUB YAW MOMENT IN TRANSITION - ZERO CYCLIC - ZERO THRUST

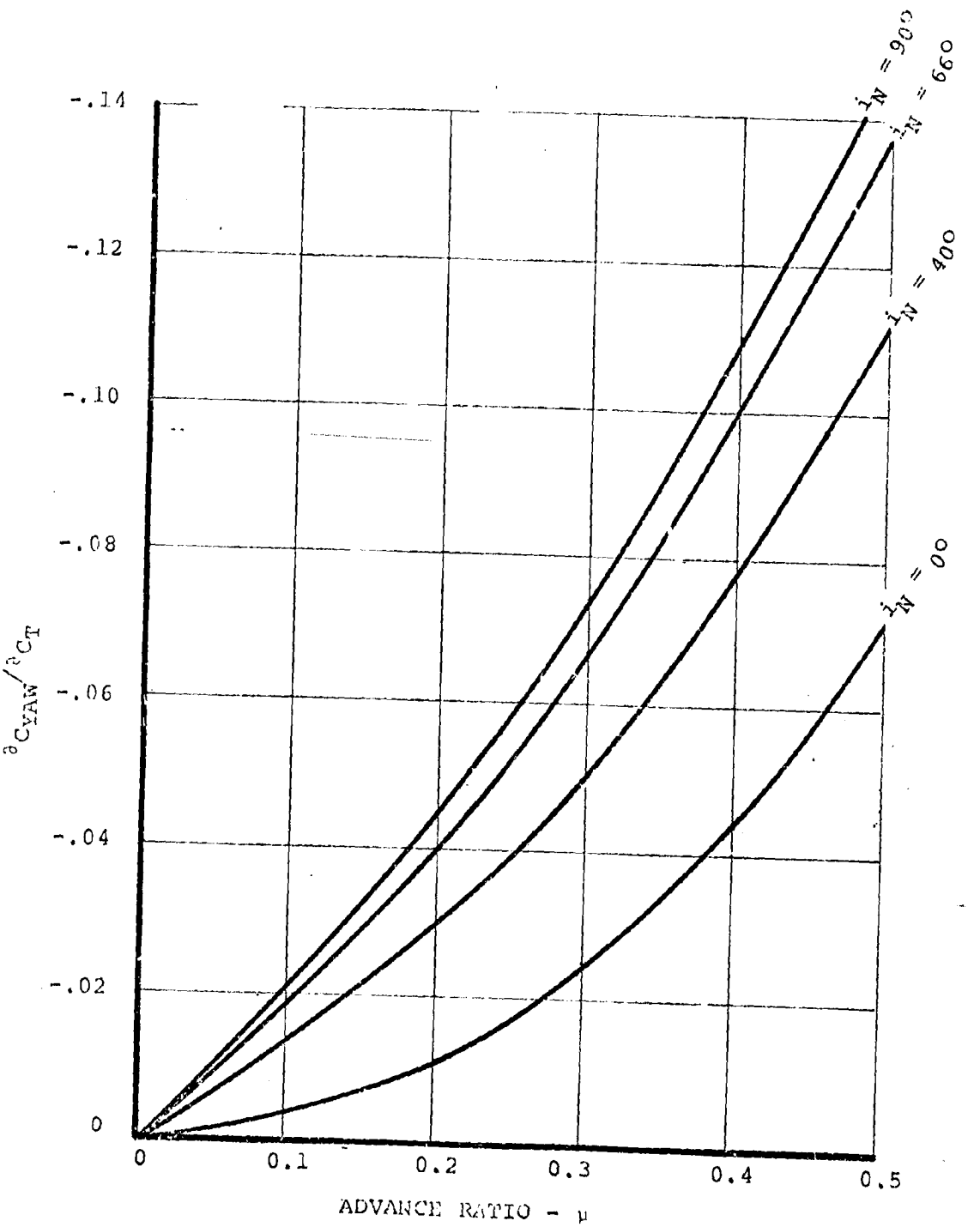

FIGURE A.5.13. EFFECT OF THRUST ON HUB YAW MOMENT IN TRANSITION

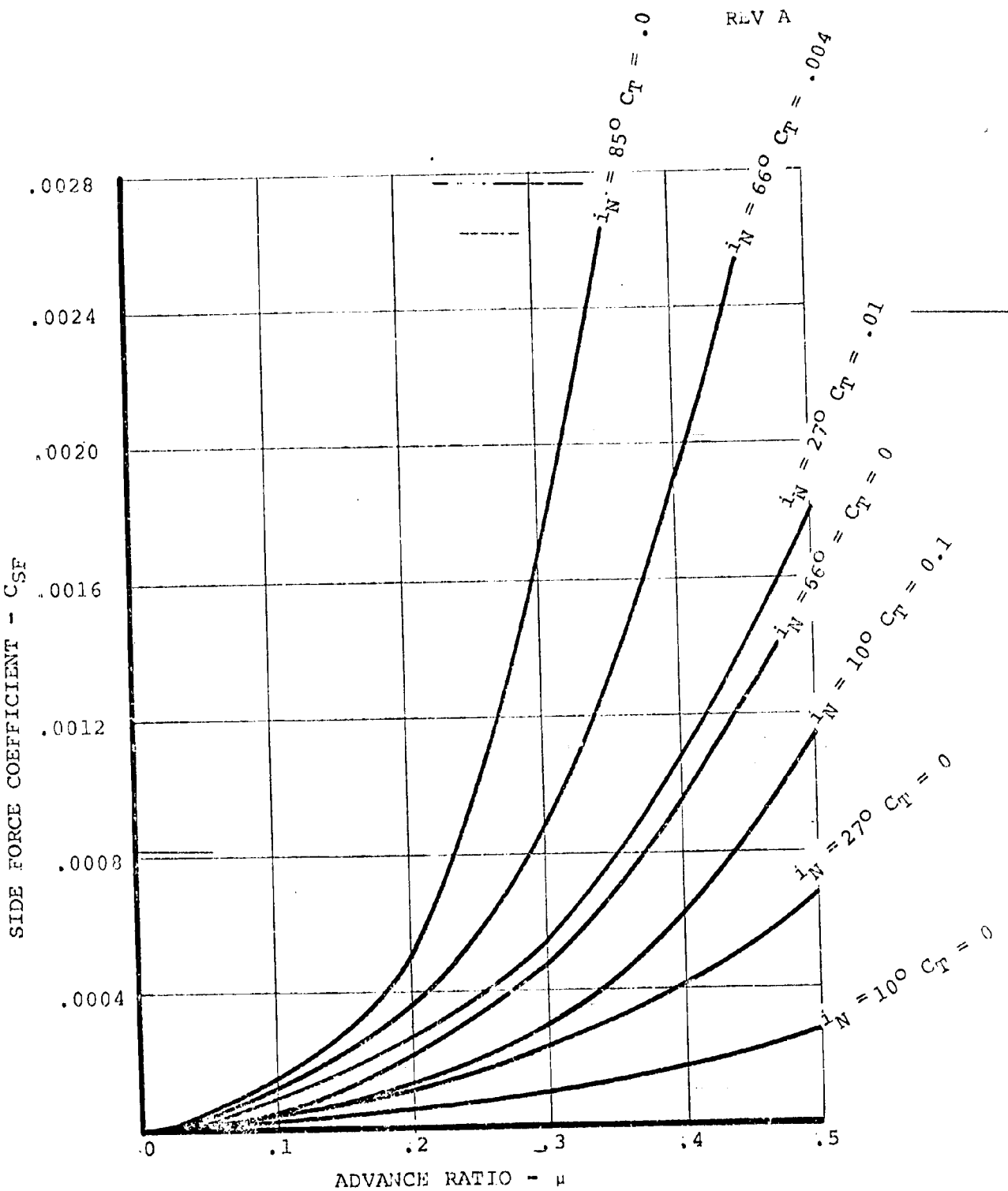

FIGURE A.5.14. ROTOR SIDE FORCE COEFFICIENT

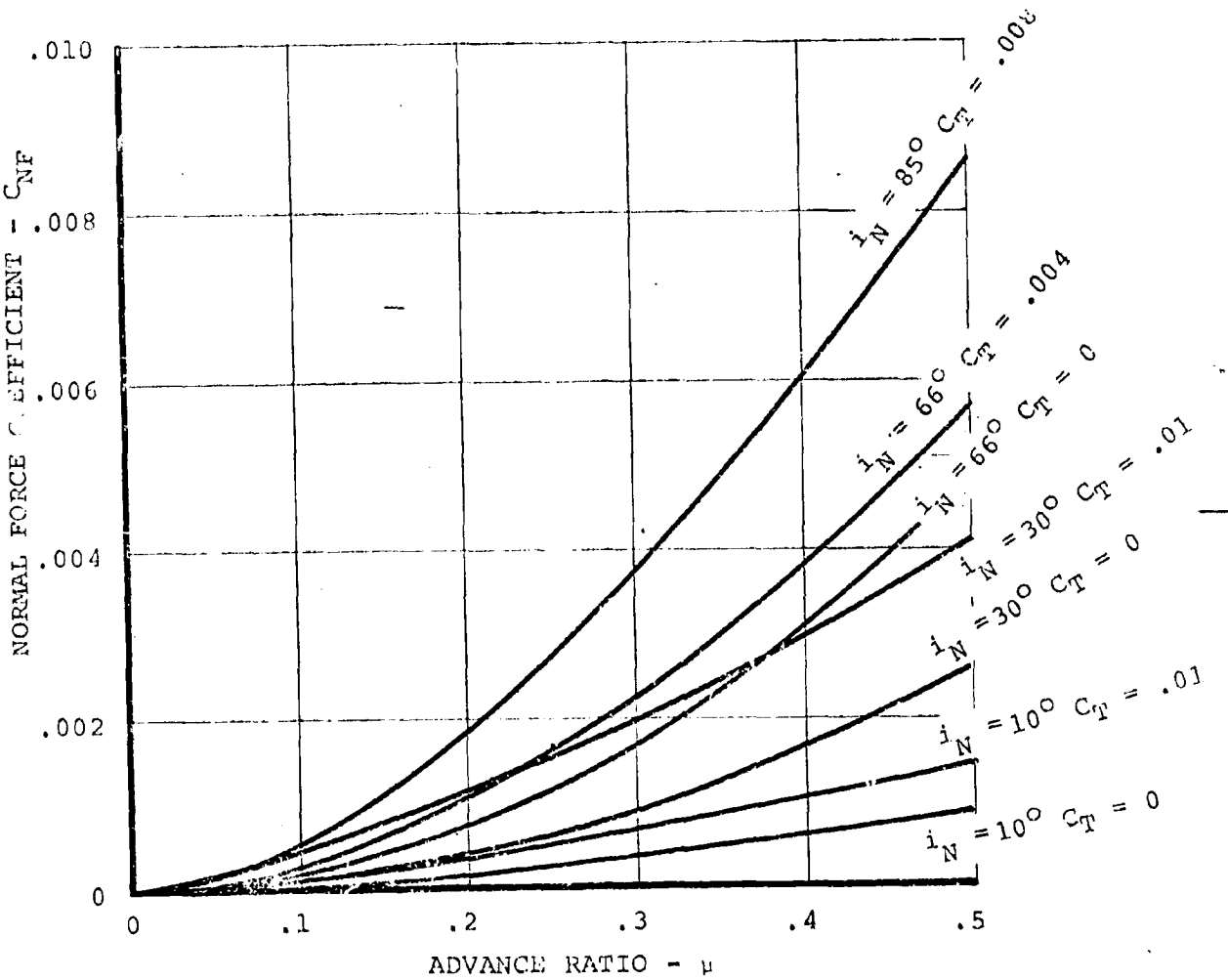

FIGURE A.5.13. ROTOR NORMAL FORCE COEFFICIENT

Using a regression technique, these cyclic derivatives have been used to derive the force and moment data due to angle of attack, advance ratio and thrust coefficient.

The effect of thrust coefficient on rotor hub pitching moment in transition arises mainly from the effect of coning due to thrust which provides longitudinal flapping excitation due to edgewise velocity.

The derivative of hub moment with respect to thrust is plotted in Figure A.5.10as a function of edgewise velocity. After correction for moment due to thrust the hub pitching moment becomes a function of angle of attack and advance ratio and is shown in Figure A.5.11. Thus, at any angle of attack and advance ratio we have

$$C_M = C_M(\alpha,\mu) + \frac{\partial C_M}{\partial C_T} C_T + \frac{\partial C_M}{\partial A_1} A_1 + \frac{\partial C_M}{\partial B_1} B_1$$

The yaw moment derivatives were treated in a similar fashion and are presented in FiguresA.5.12 and A.5.13.

$$C_{YAW} = C_{YAW}(\alpha,\mu) + \frac{\partial C_Y}{\partial C_T} C_T + \frac{\partial C_Y}{\partial A_1} A_1 + \frac{\partial C_Y}{\partial B_1} B_1$$

The rotor hub forces are shown in FiguresA.5.14 to A.5.15. The side force derivative data obtained from Reference 26 indicates linearity with thrust coefficient. The normal force data increases with thrust coefficient also and is slightly non-linear. The equations for normal force and side force are thus:

$$C_{NF} = C_{NF}(\alpha, \mu, C_T) + \frac{\partial C_{NF}}{\partial A_1} A_1 + \frac{\partial C_{NF}}{\partial B_1} B_1$$

$$C_{SF} = C_{SF}(\alpha, \mu, C_T) + \frac{\partial C_{SF}}{\partial A_1} A_1 + \frac{\partial C_{SF}}{\partial B_1} B_1$$

These forces and moments were curve fit and used in conjunction with the Model 222 flight simulation program reported in Reference 27 to obtain trim and maneuver conditions.

The thrust and power relationships are essentially the same as previously programmed into the simulator model. Correlation of experimental data and the math model is shown in Section 6.

The curve fits of cyclic effectiveness have not been used for hover calculations. The more precise force and moment data given in Section 6.0 has been used in conjunction with the calculated effect of thrust for hover control calculations.

AIRCRAFT TRIM AND MANEUVER

The force and moment data discussed above have been used to evaluate the hover trim (in terms of CG offset) using the aircraft mass and balance data given in Reference 21and is shown in Figure A.5.16. The control power per degree of cyclic in hover has similarly been evaluated and is given in Figures A.5.17 to A.5.19.

The transition and cruise trim data obtained using the experimental force and moment data is given in Figures A.5.20 to A.5.26.

BLADE LOADS

The alternating blade load radial distributions obtained on test are shown in Figures A5.27 and A5.28 as a percentage of the loads at 8.5% radius. The blade fatigue strength distributions are similarly shown. None of the alternating load data exceed the normalized strength line and demonstrate that the 8.5% radial station will be fatigue critical prior to any other radial station. It is necessary to refer bending moments to this station to evaluate fatigue life.

The 8.5% radial station has a non-circular spar cross section and thus the alternating strain experienced varies with the ratio of flap and chord bending as well as the magnitude of the resultant moment. This makes it difficult to define accurate endurance boundaries in terms of flap and chord bending since the ratio of the loads affects the answer. For this reason endurance limits are discussed in terms of total alternating strain. The interaction curves defining these relationships are given in Figure A5.29.

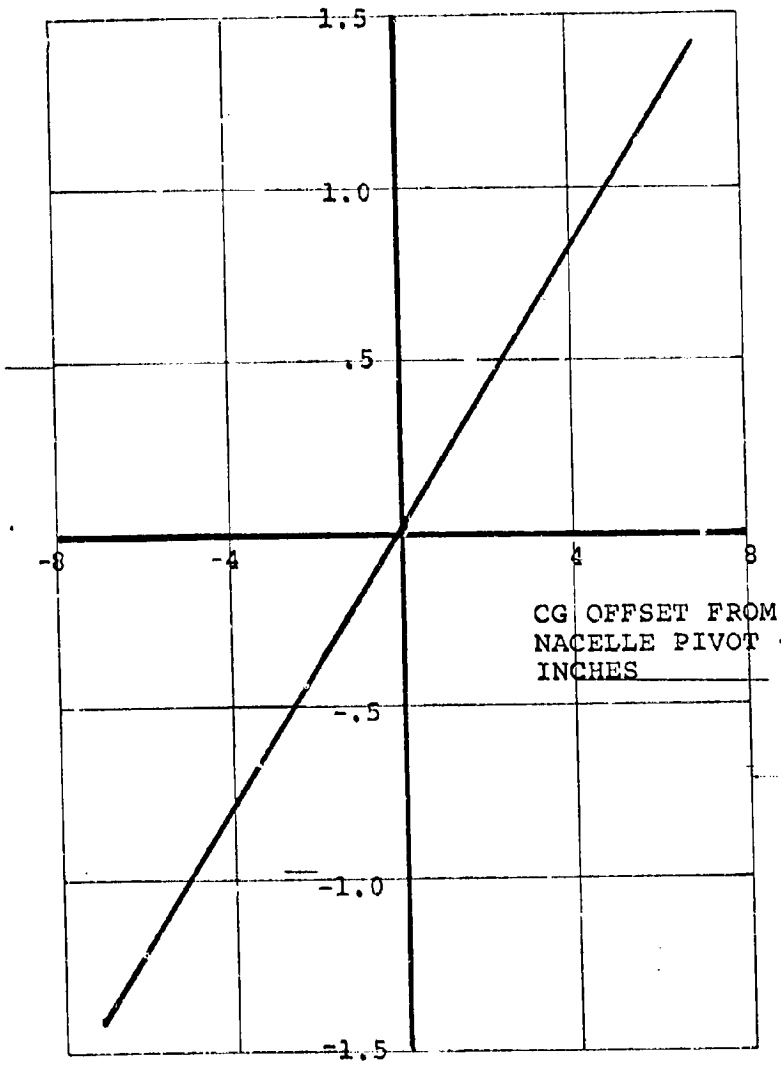

FIGURE A.5.16. CYCLIC PITCH FOR CG TRIM. FUSELAGE ATTITUDE LEVEL

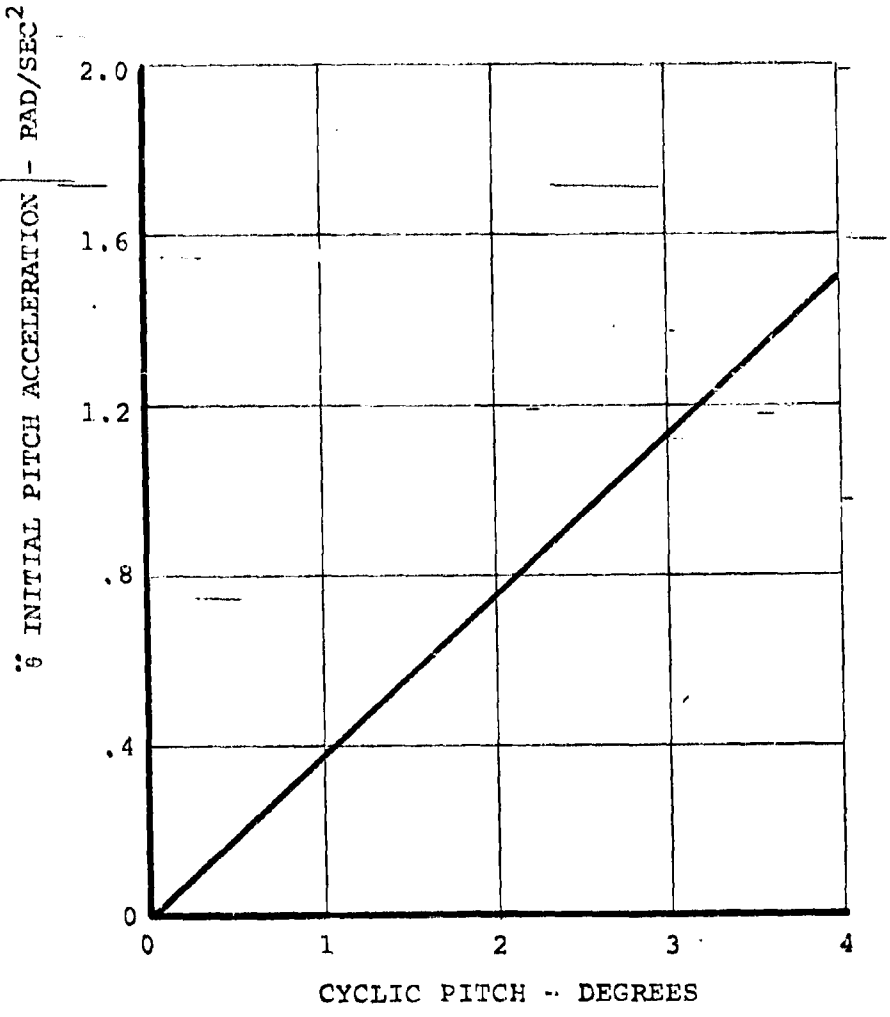

FIGURE A.5.17. PITCH CONTROL POWER IN HOVER

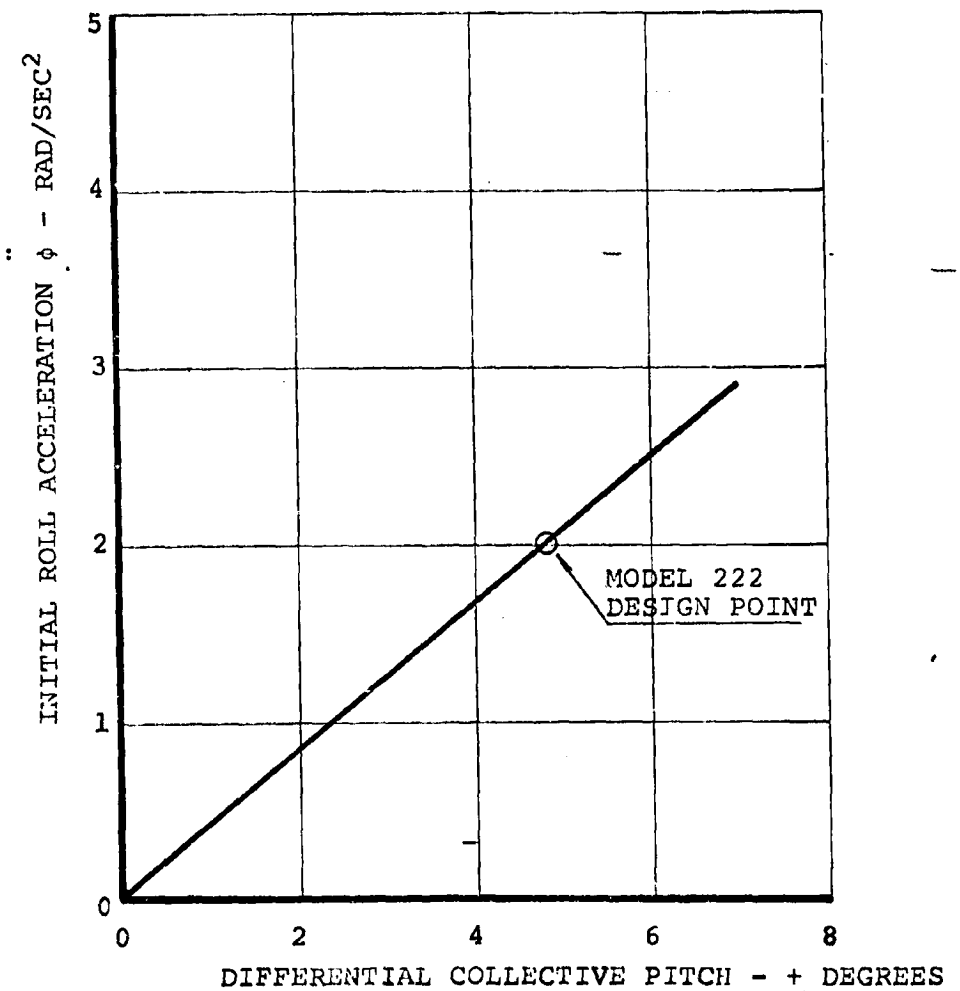

FIGURE A.5.18. ROLL CONTROL POWER IN HOVER

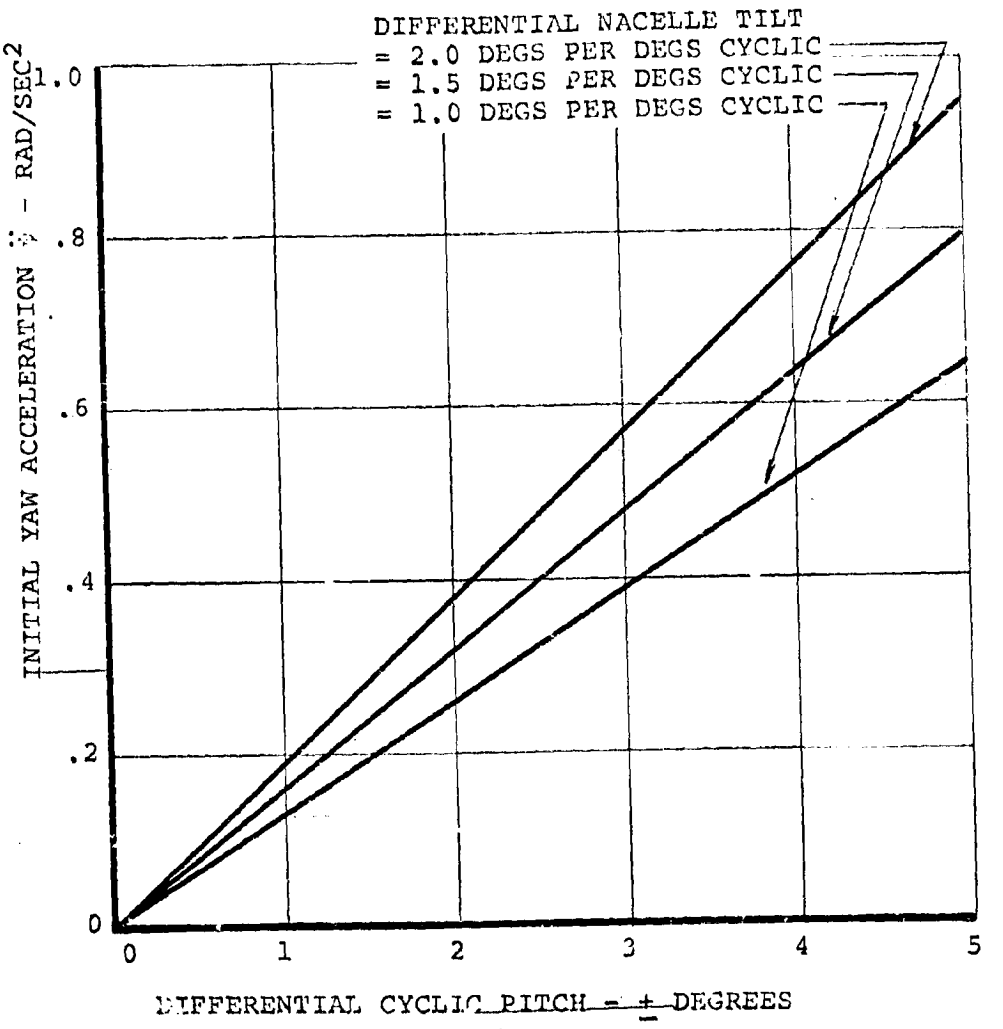

FIGURE A.5.19. YAW CONTROL POWER IN HOVER

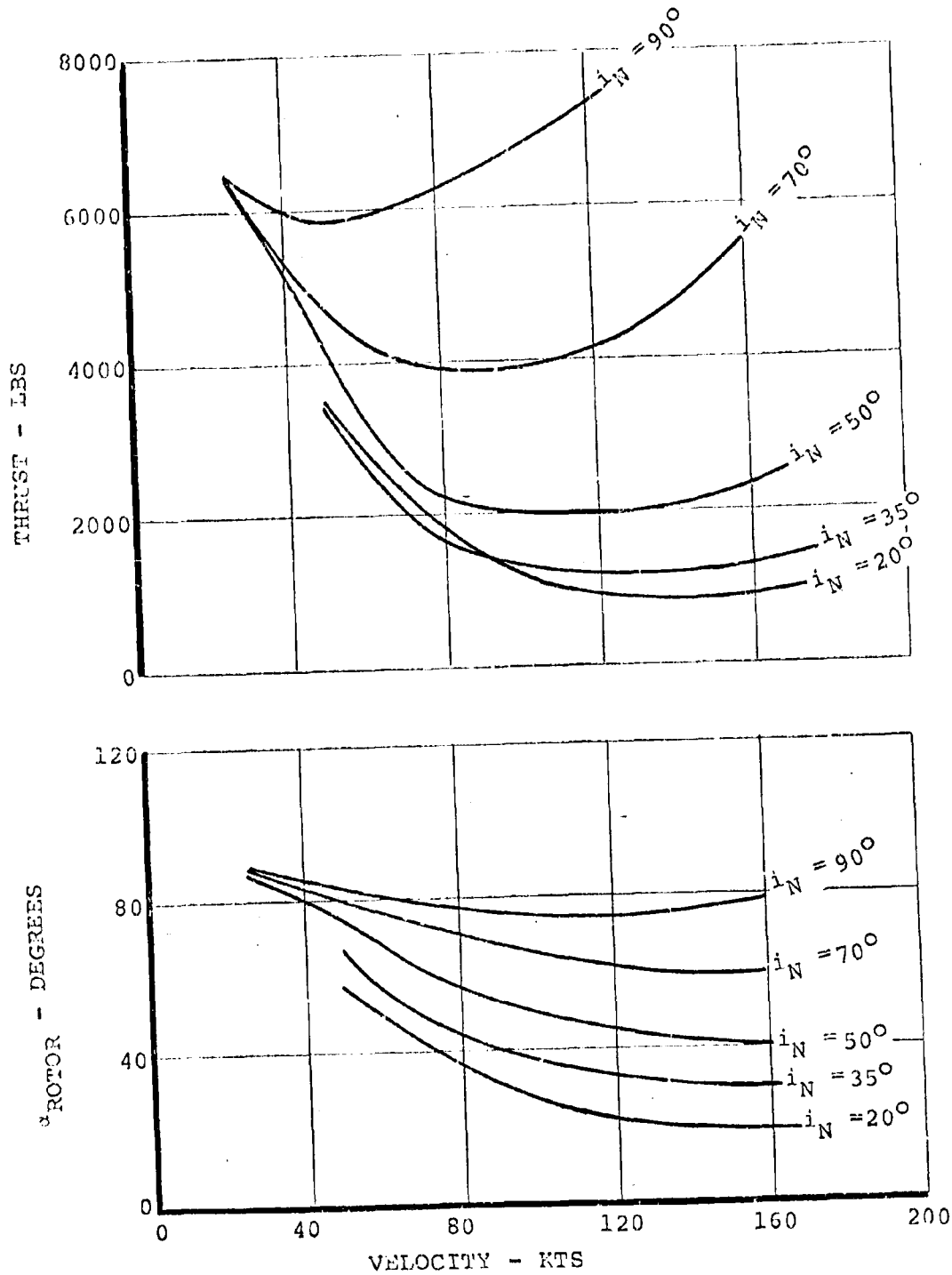

FIGURE A.5.20. MODEL 222 1g FLIGHT TRIM DATA IN TRANSITION

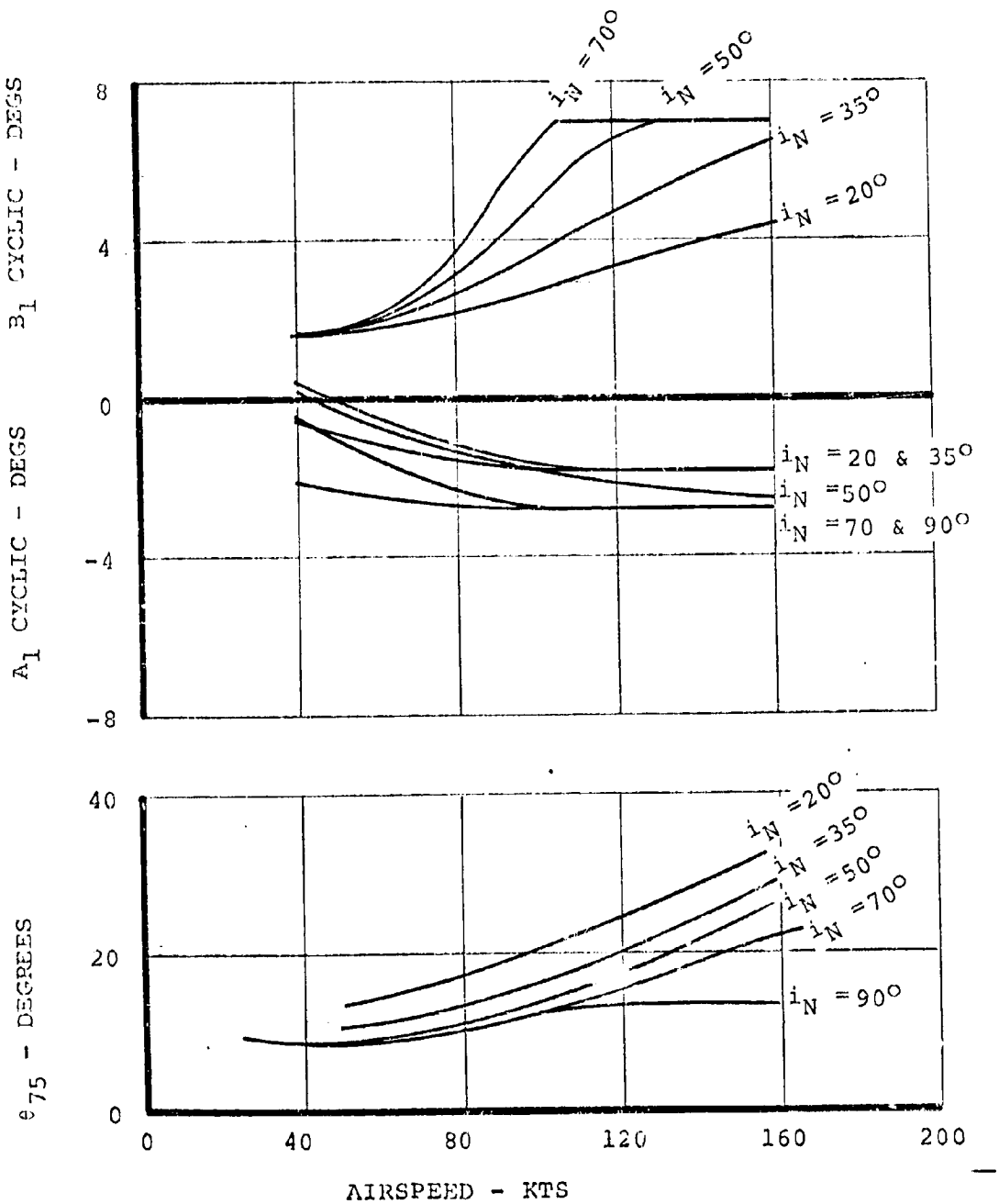

FIGURE A.5.21. MODEL 222 1g FLIGHT TRIM DATA IN TRANSITION

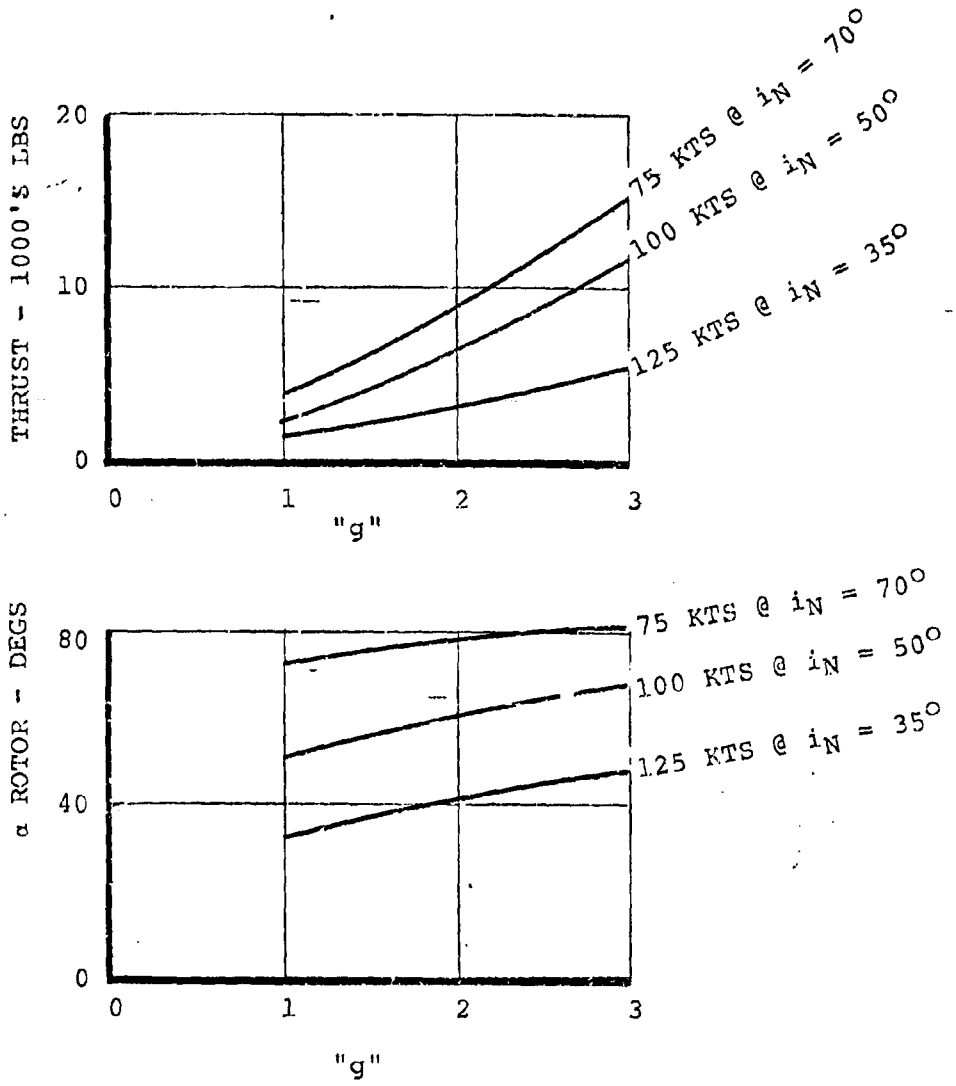

FIGURE A.5.22. EFFECT OF MANEUVER LOAD FACTOR ON ROTOR ATTITUDE AND THRUST IN TRANSITION

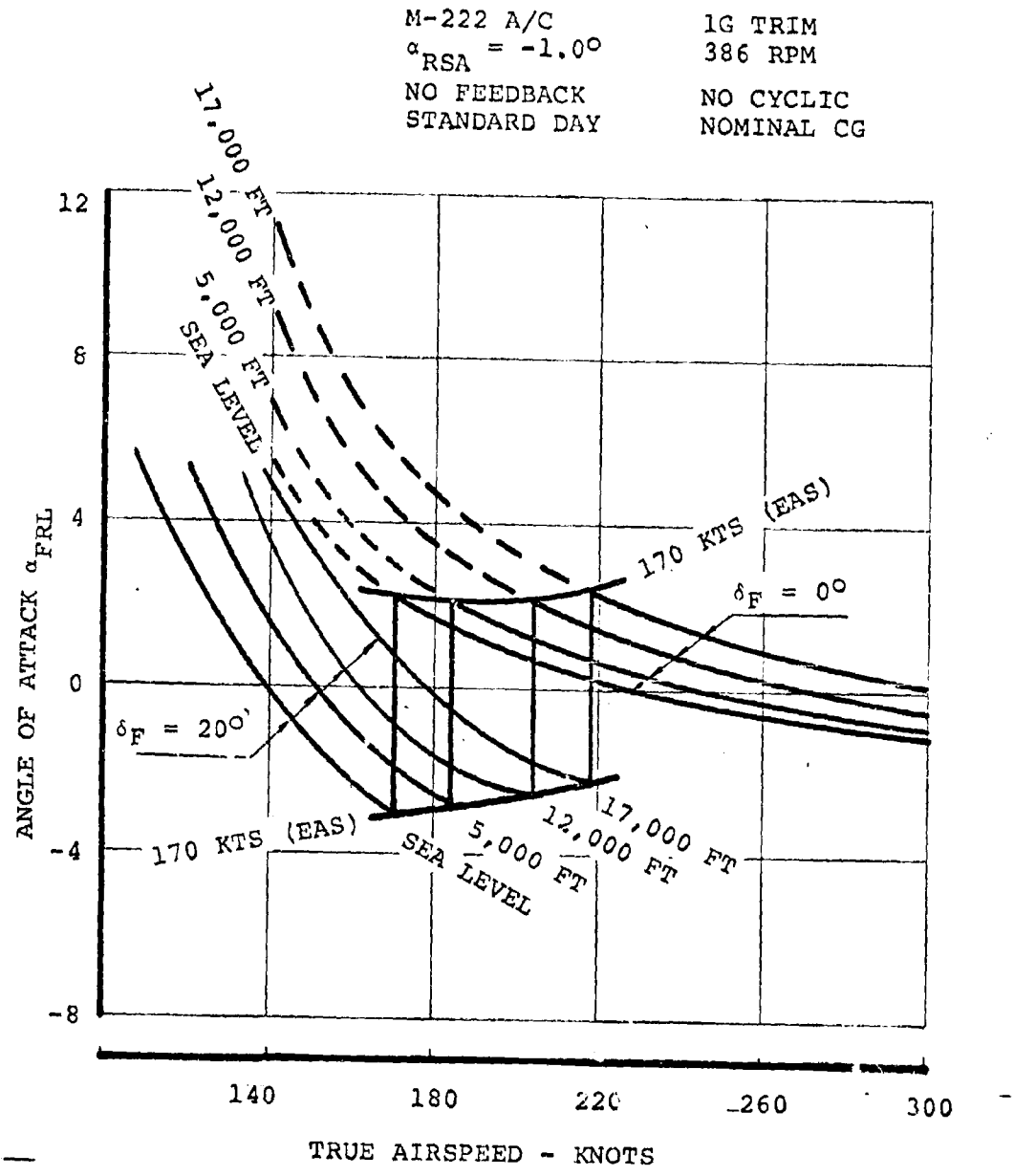

FIGURE A.5.23. FUSELAGE REFERENCE LINE ANGLE OF ATTACK FOR 1g TRIM OVER CRUISE FLIGHT ENVELOPE

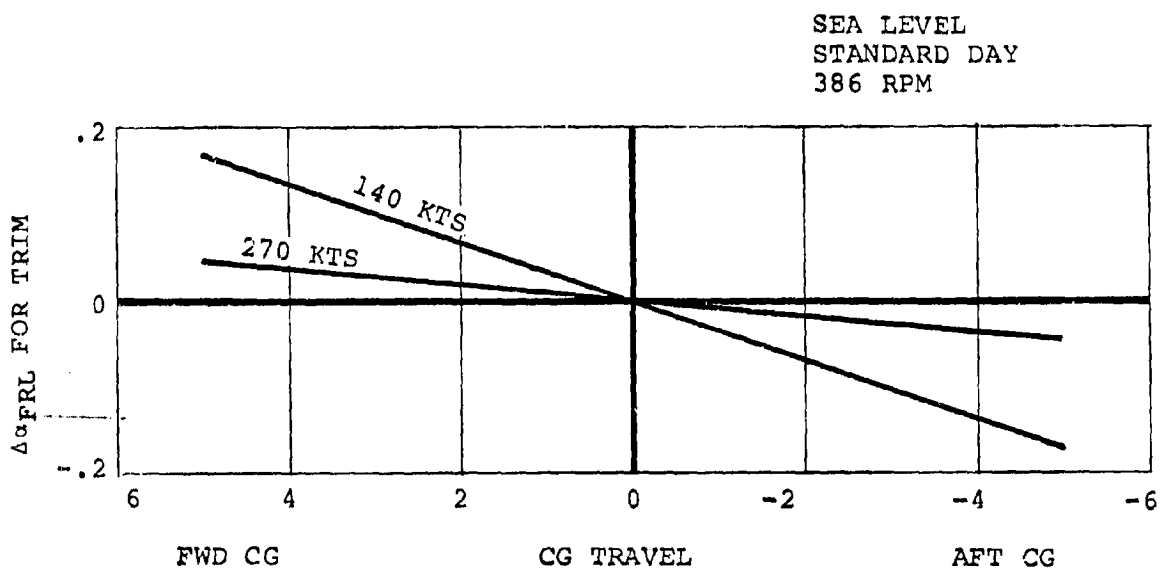

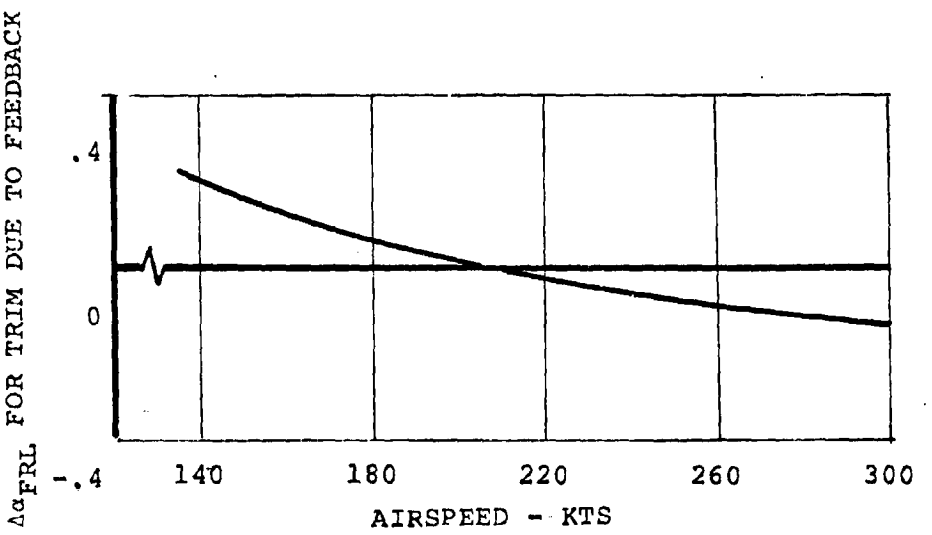

FIGURE A.5.24. EFFECT OF CG TRAVEL AND FEEDBACK ON 1G TRIM ANGLE OF ATTACK

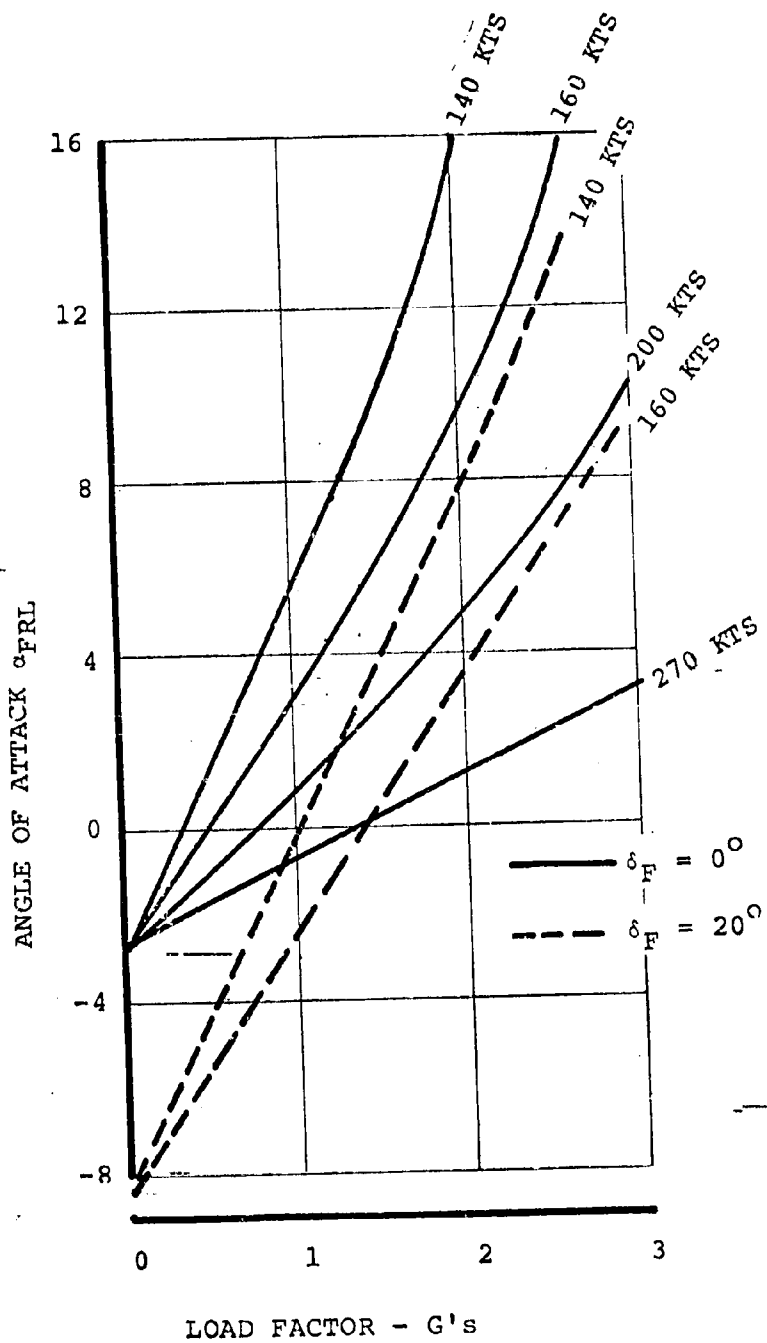

FIGURE A.5.25. ANGLE OF ATTACK VS LOAD FACTOR AS A FUNCTION OF SPEED. SEA LEVEL

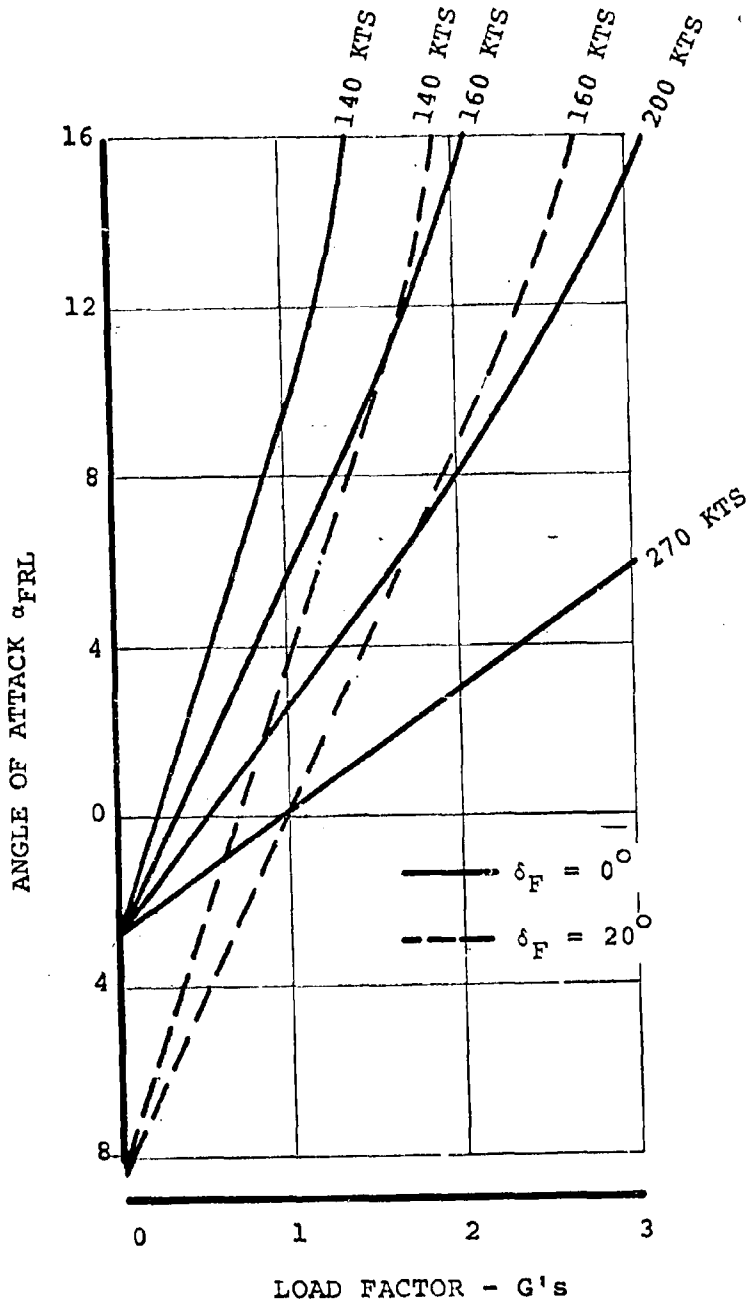

~~FIGURE A~~ 5.26. ANGLE OF ATTACK VS LOAD FACTOR AS A FUNCTION OF SPEED. 12,000 FEET

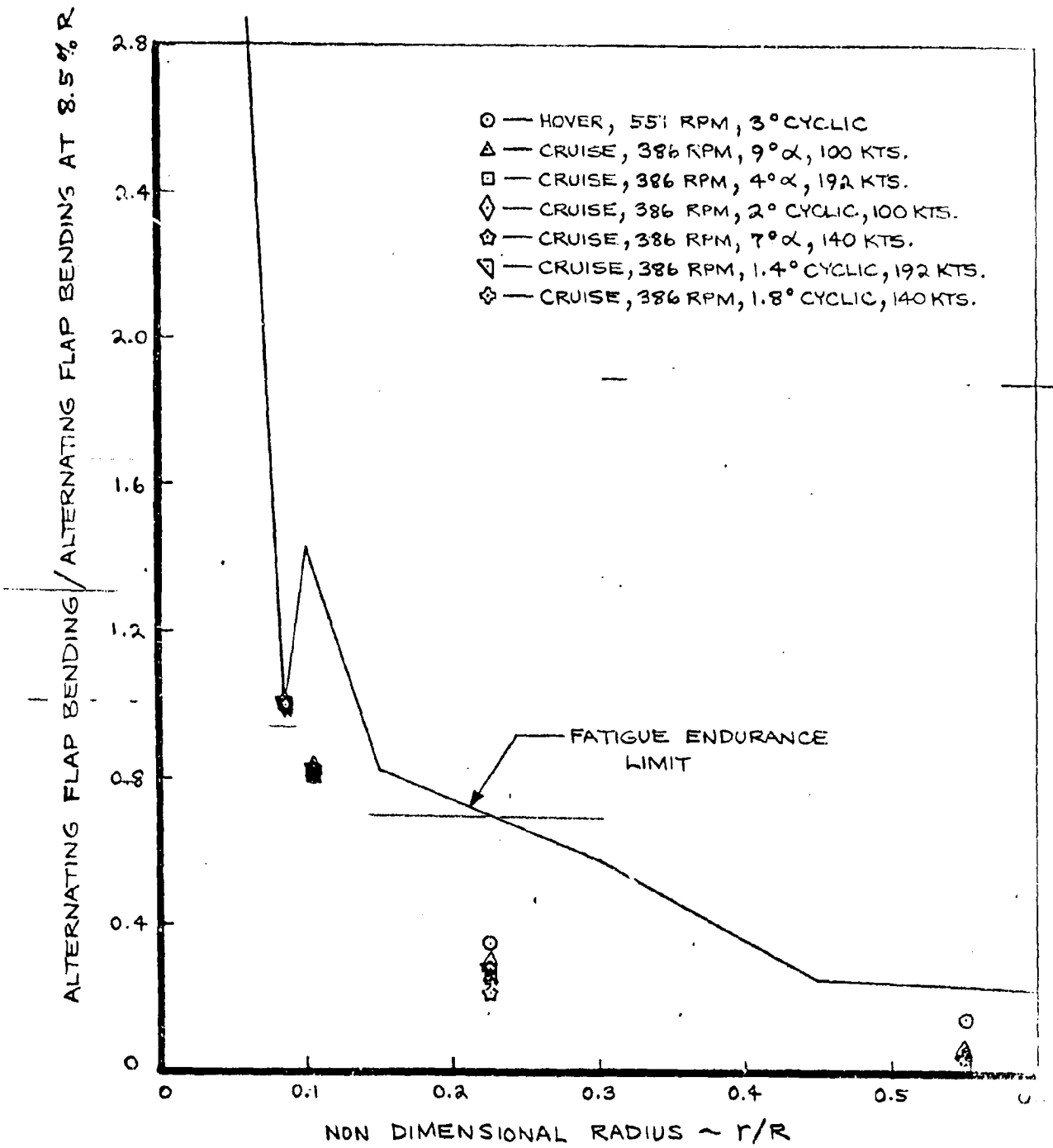

FIGURE A.5.27. NORMALIZED FLAP BENDING LOAD DISTRIBUTION

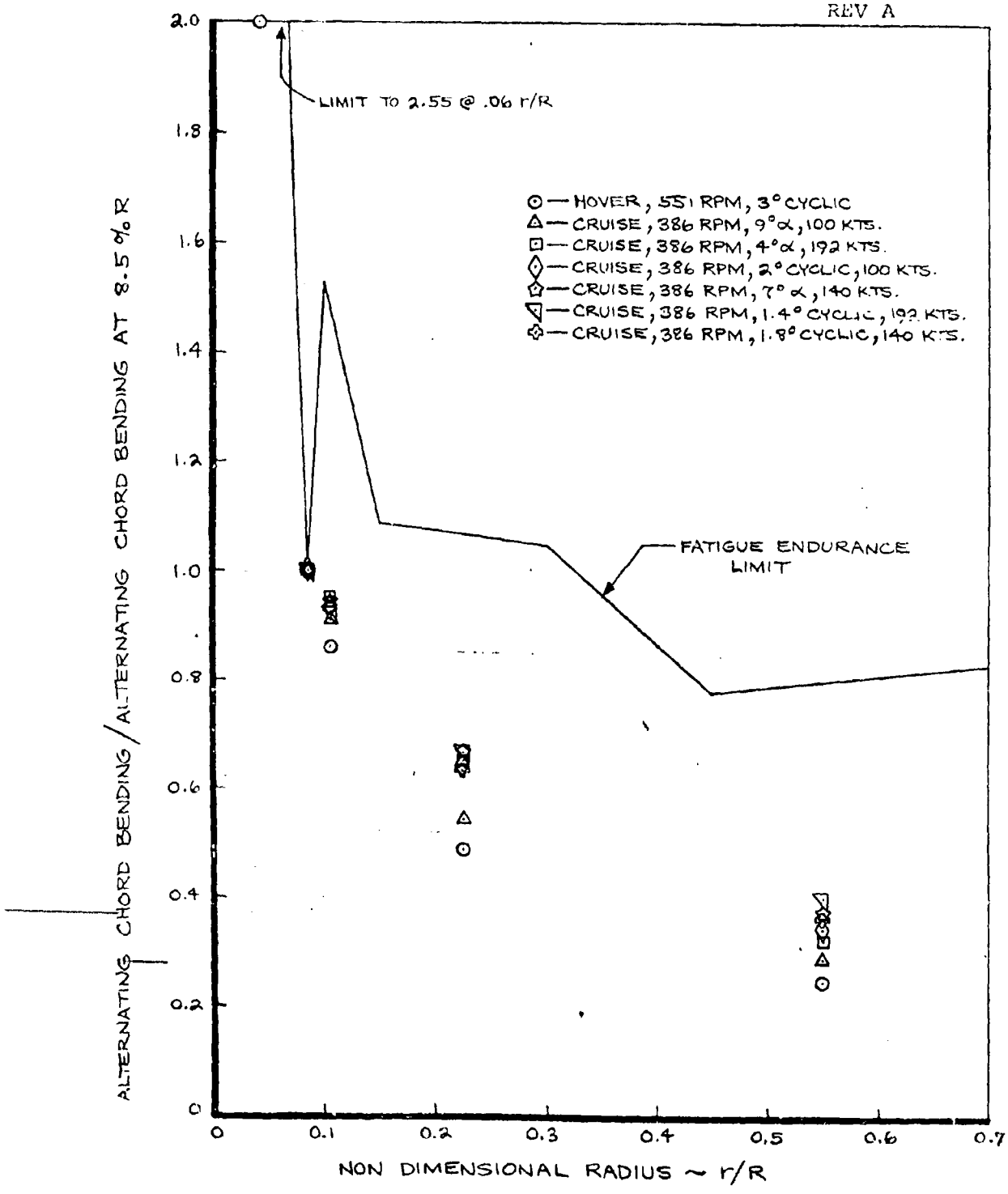

FIGURE A.5.28. NORMALIZED CHORD BENDING LOAD DISTRIBUTION

Figure A.5.29. INTERACTION OF FLAP AND CHORD FATIGUE MOMENTS AT 8.5% RADIUS FOR 551 RPM

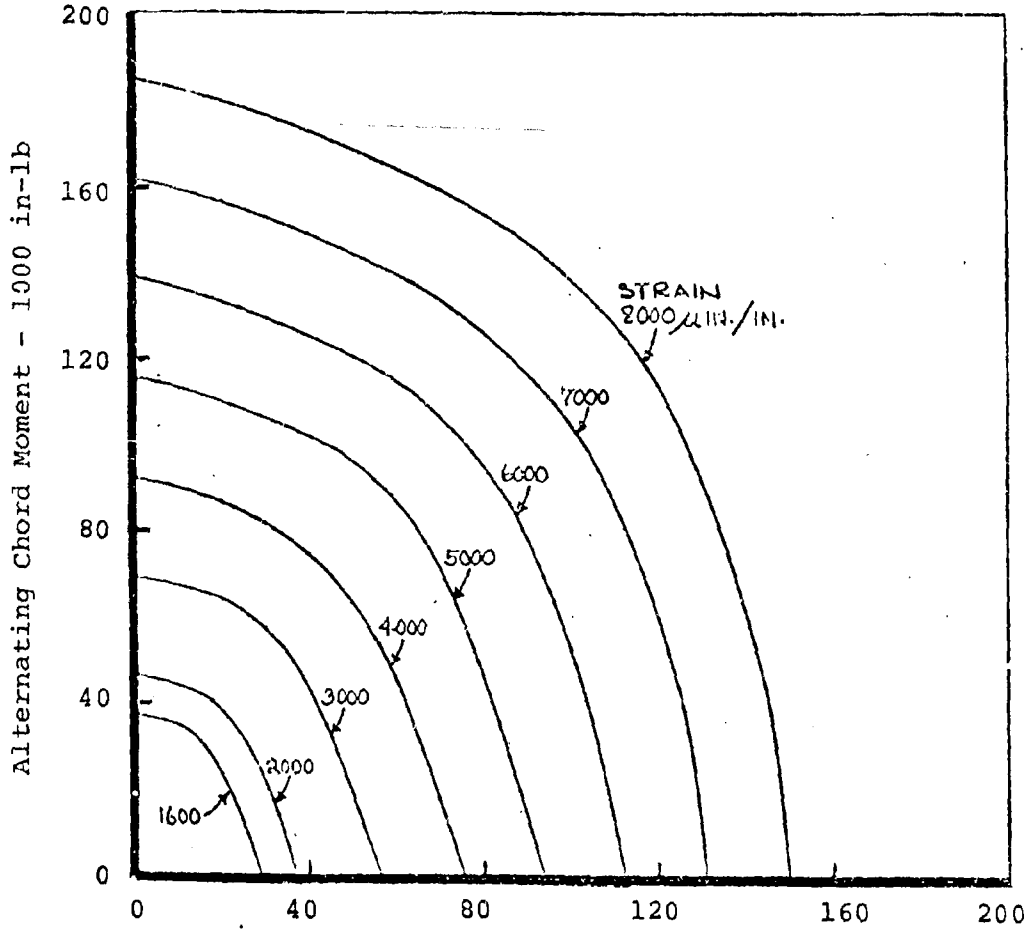

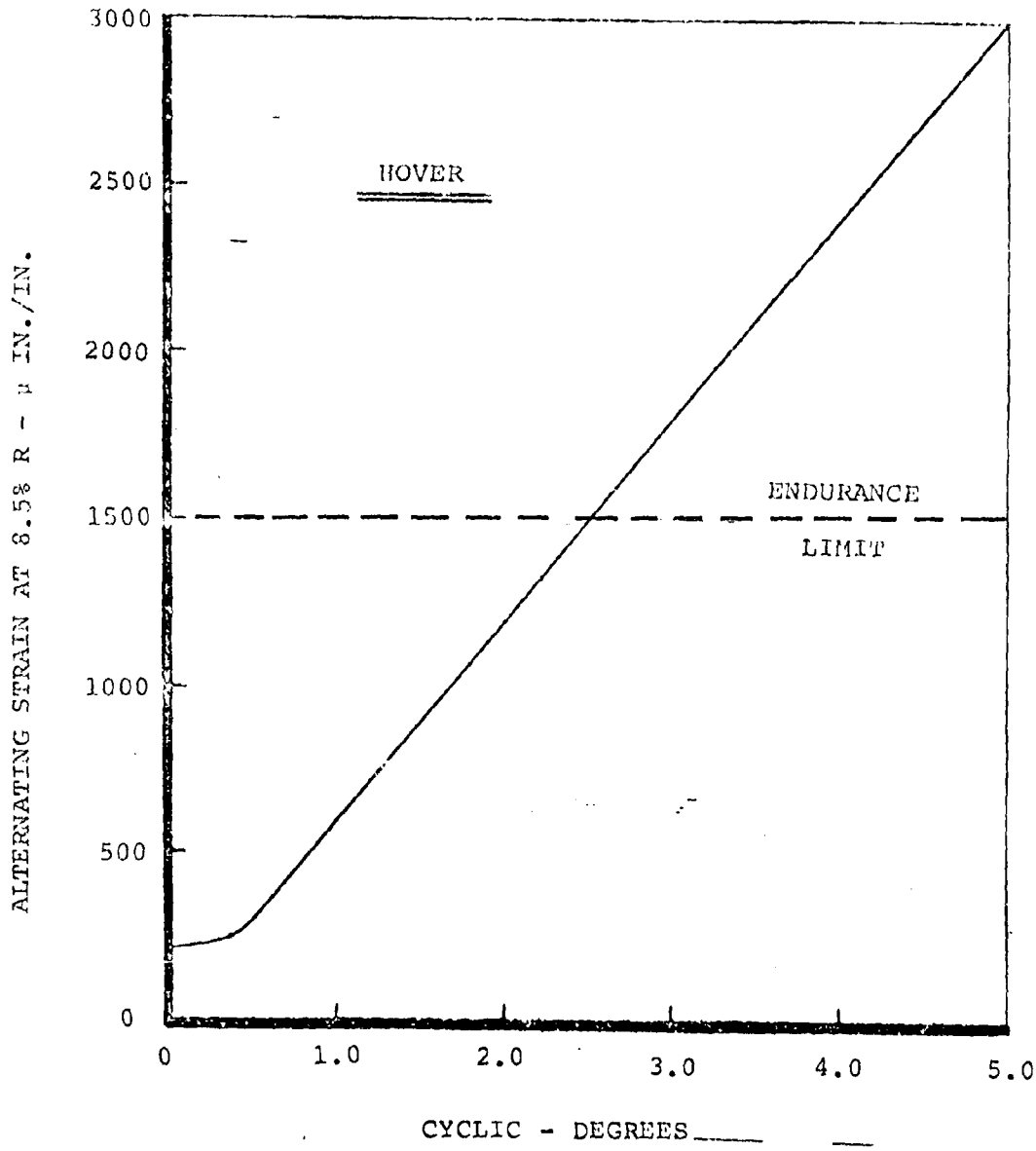

FIGURE A.5.30. ALTERNATING BLADE ROOT STRAIN DUE TO CYCLIC - HOVER 551 RPM

In hover, flap and chord bending moments were obtained at 10.5% and these data have been corrected to 8.5% R by the following ratios:

$$\frac{\partial(\text{alt chord BM})/\partial(\text{cyclic}) \quad 8.5\%\ R}{\partial(\text{alt chord BM})/\partial(\text{cyclic}) \quad 10.5\%\ R} = 1.16$$

$$\frac{\partial(\text{alt flap BM})/\partial(\text{cyclic}) \quad 8.5\%\ R}{\partial(\text{alt flap BM})/\partial(\text{cyclic}) \quad 10.5\%\ R} = 1.25$$

The ratios were obtained from load distributions in hover in Section 4.

The loads obtained at 8.5% have been converted to alternating blade root strain using the interaction curve, Figure A.5.29. The sensitivity of blade root strain to hover cyclic is given in Figure A5.30.

The transition loads present more of a problem since the 10.5%R gages became inoperative early in the test. The gages at 3.9% R were in and out of plane gages and these data have been used to deduce 8.5% R loads.

Figures A5.31 and A5.3. show minimum measured alternating bending loads at 3.9% R (in and out of plane) throughout transition. These loads were in excess of 1/rev frequency. The higher harmonic loads at 3.9% R have been assumed to act at 8.5% R. The 1/rev loads were computed using the load sensitivities obtained from the test plots

and assuming that the phasing of the loads is given by the hub moment data. These 1/rev loads were then transformed into the blade axis system to give flap and chord bending loads at 3.9% R and ratio'd to 8.5% R by the ratio's (0.69 flap, 0.845 chord) obtained from the 1/rev loads deduced in this manner were converted into alternating blade strains using Figure A.5.29.

The 1g flight alternating blade root strains in transition are shown in Figure A.5.33 and the effect of maneuver load factor for three transition conditions in Figure A.5.34.

The boundaries of the 1g flight transition corridor are given in Figure A.5.35. The 1500 μ in./in. strain line is the blade endurance load boundary.

The alternating blade bending moments in cruise with no cyclic pitch measured at 10.5% radius were corrected to 8.5% R by the ratio's 1.07 for chord bending and 1.22 for flap bending. The sensitivity of alternating bending moment to angle of attack was extrapolated using a quadratic curve fit and the resulting loads at 8.5% are shown in Figures A.5.36 and A.5.37.

To correct for altitude effects the calculated moment ratio's between altitude and sea level were used. Figure A.5.38 shows the variation of alternating bending loads with increasing altitude.

The alternating flap and chord bending at 8.5% radius define the blade root strain as before. The blade root alternating strain in cruise at sea level and 12,000 feet altitudes are shown in Figures A.5.39 and A.5.40.

These data include the interference effect of the wing test stand which was different from the Model 222 design. The upwash at the rotor for the test wing and the Model 222 wing is shown in Figure A.5.41,and was calculated using a simple lifting line representation. Accounting for the wing setting angle (2-degrees) and the rotor setting angle (-1.0-degrees) in cruise, the relationship between Model 222 fuselage reference line angle of attack and the test angle of attack can be deduced and this relationship is shown in Figure A.5.42. Using Figure A.5.42, the alternating strain for any aircraft angle can be obtained from Figures A.5.39 and A.5.40.

The alternating blade strain in 1g level flight with no cyclic pitch feedback control is given at sea level and 12,000 feet in Figures A.5.43 and A.5.44.The effect of maneuver load factor is given in Figures A.5.45 and A.5.46.

Cyclic pitch feedback as proposed in the Model 222 design reduces the alternating blade strain for 1g flight as shown in Figure A.5.47 and also reduces the sensitivity of blade alternating strain to maneuver load factor, Figure A.5.48.

3.9% RADIUS
OUT OF PLANE

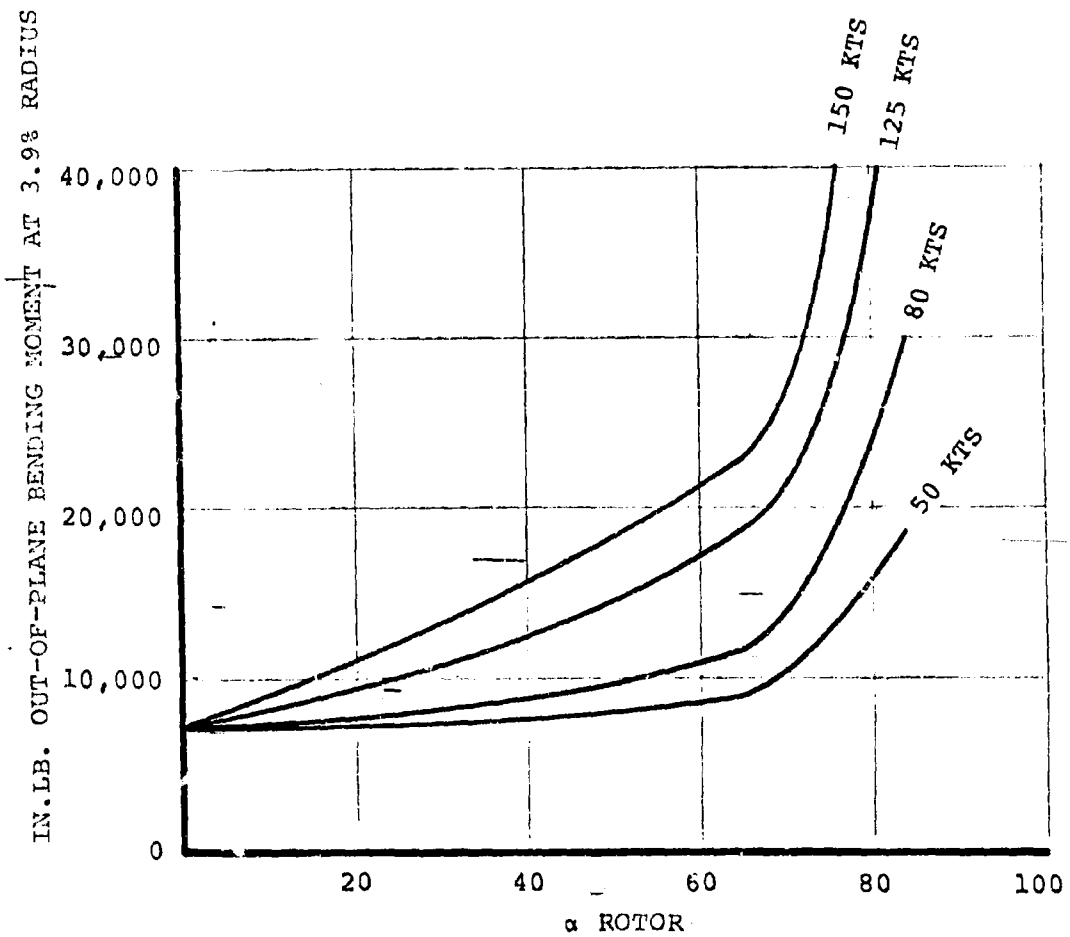

FIGURE A.5.31. VARIATION OF OUT OF PLANE MINIMUM BENDING MOMENT AT 3.9% RADIUS WITH ANGLE OF ATTACK AND SPEED IN TRANSITION

3.9% RADIUS
IN-PLANE BENDING

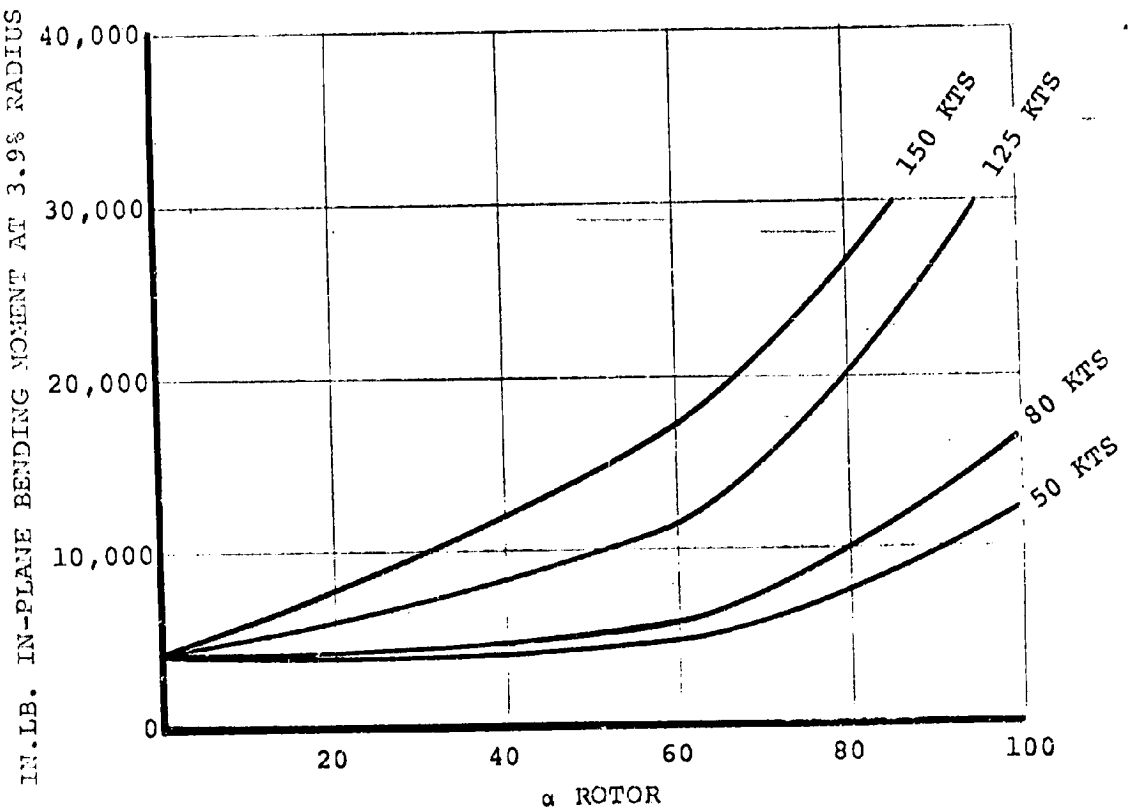

FIGURE A.5.32. VARIATION OF IN-PLANE MINIMUM BENDING MOMENT AT 3.9% RADIUS WITH ANGLE OF ATTACK AND SPEED IN TRANSITION

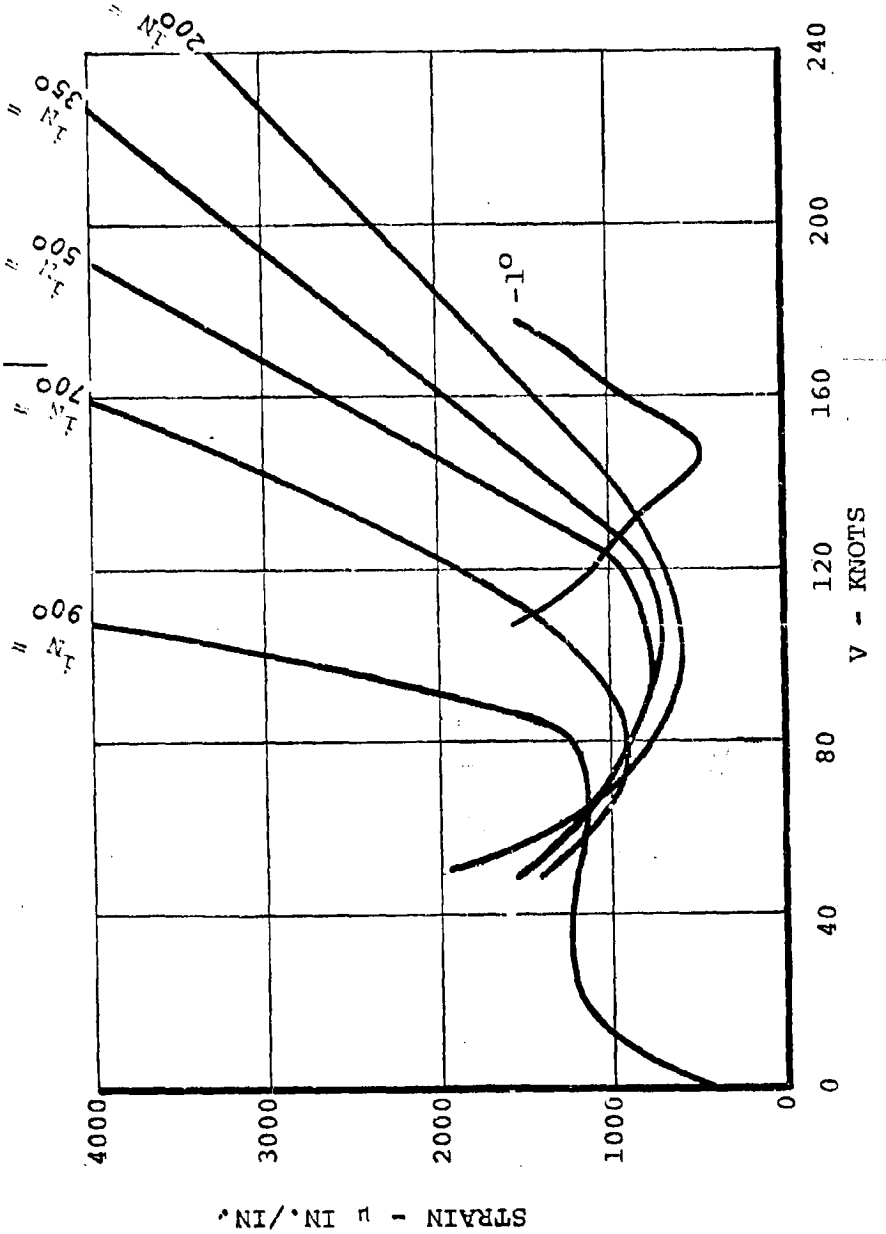

FIGURE A.5.33. ALTERNATING BLADE STRAIN IN TRANSITION
1g FLIGHT

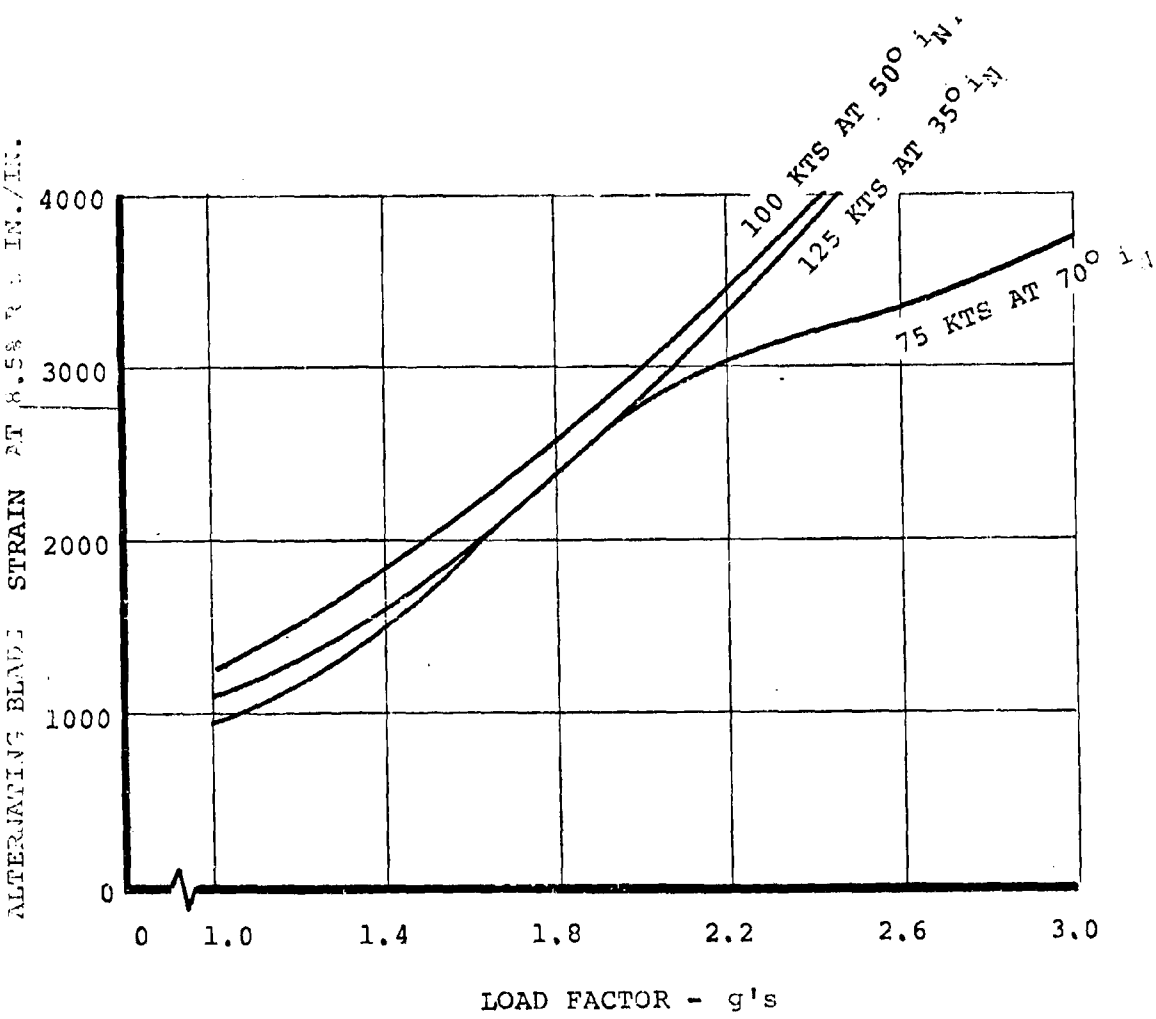

FIGURE A.5.34. EFFECT OF MANEUVER LOAD FACTOR ON ALTERNATING BLADE STRAIN IN TRANSITION

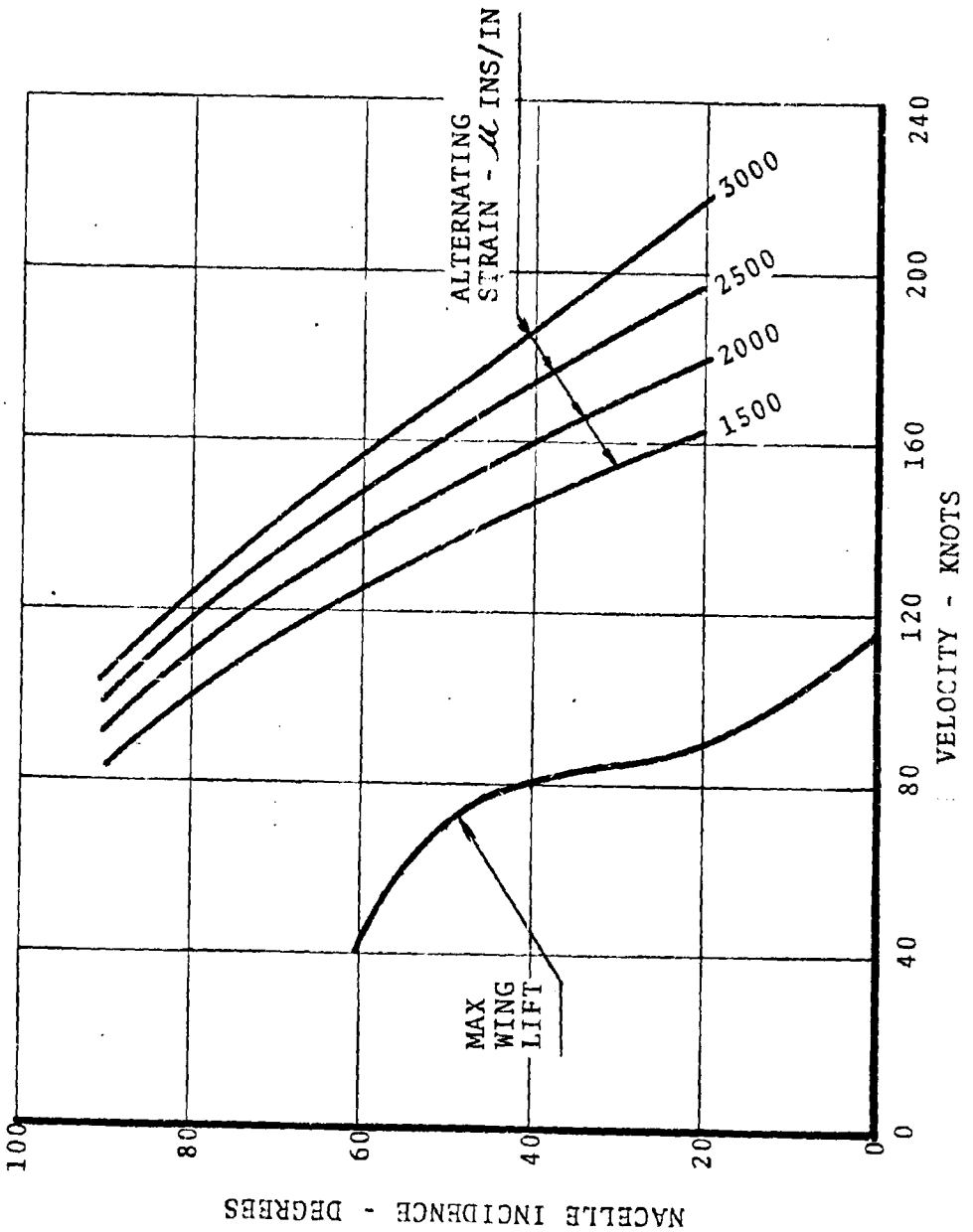

FIGURE A.5.35. ALTERNATING BLADE STRAIN BOUNDARIES FOR 1g TRANSITION FLIGHT

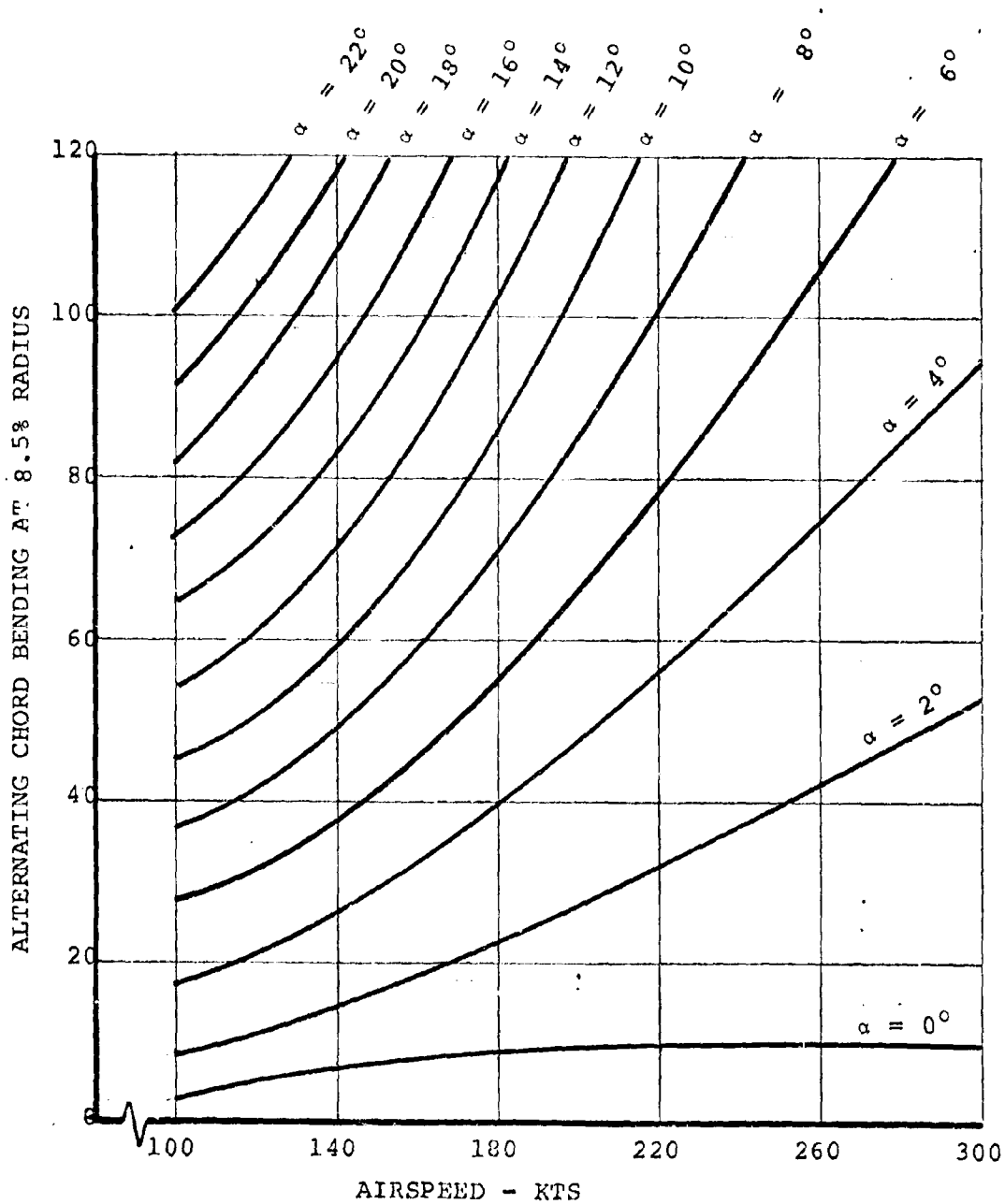

FIGURE A.5.36. BLADE LOADS IN CRUISE-ALTERNATING BLADE CHORD BENDING 8.5% R, SEA LEVEL, 386 RPM.

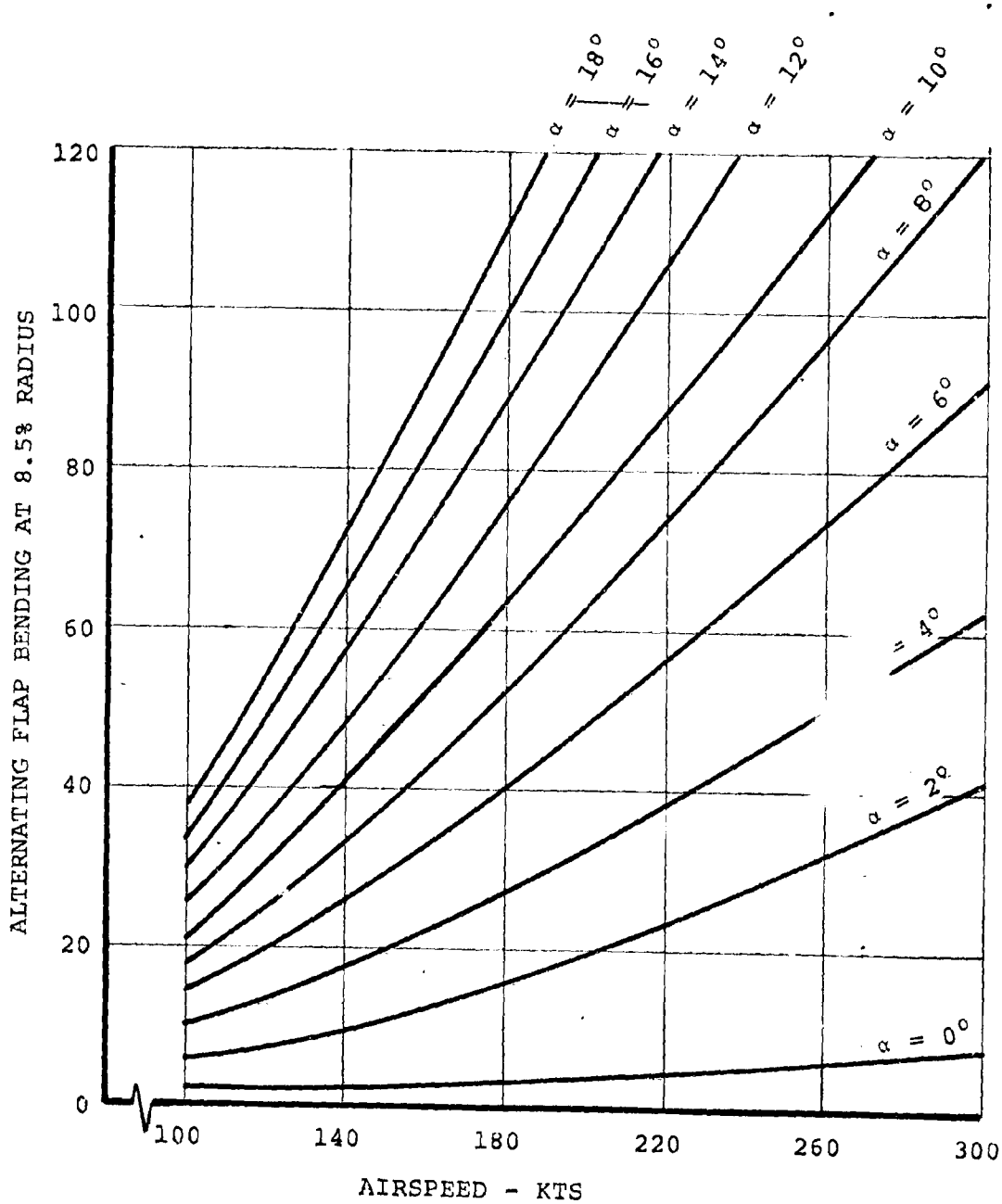

FIGURE A.5.37. BLADE LOADS IN CRUISE - ALTERNATING BLADE FLAP BENDING 8.5% R, SEA LEVEL, 386 RPM

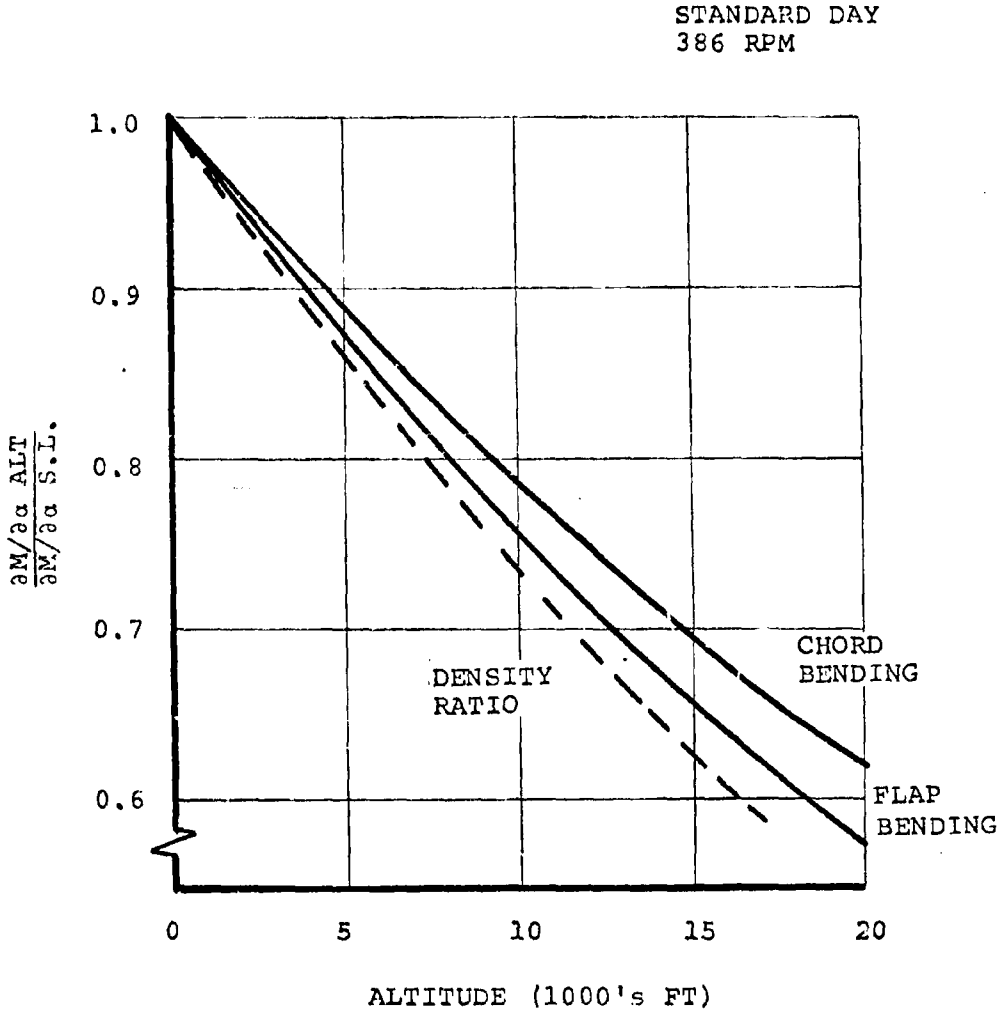

FIGURE A.5.38. EFFECT OF ALTITUDE ON BLADE BENDING MOMENTS DUE TO ANGLE OF ATTACK

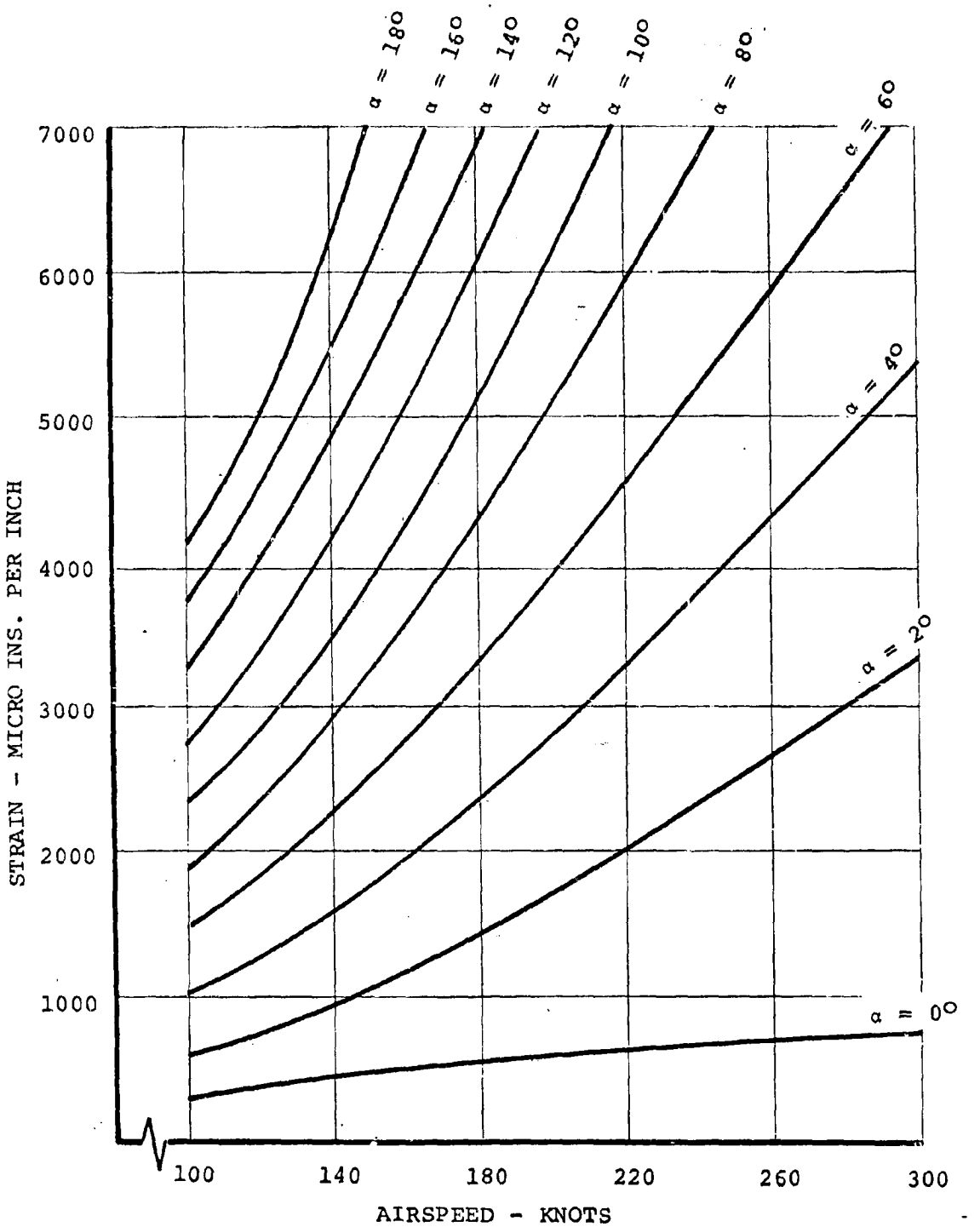

FIGURE A.5.39. ALTERNATING BLADE ROOT STRAIN IN CRUISE 85% RADIUS, 386 RPM, SEA LEVEL.

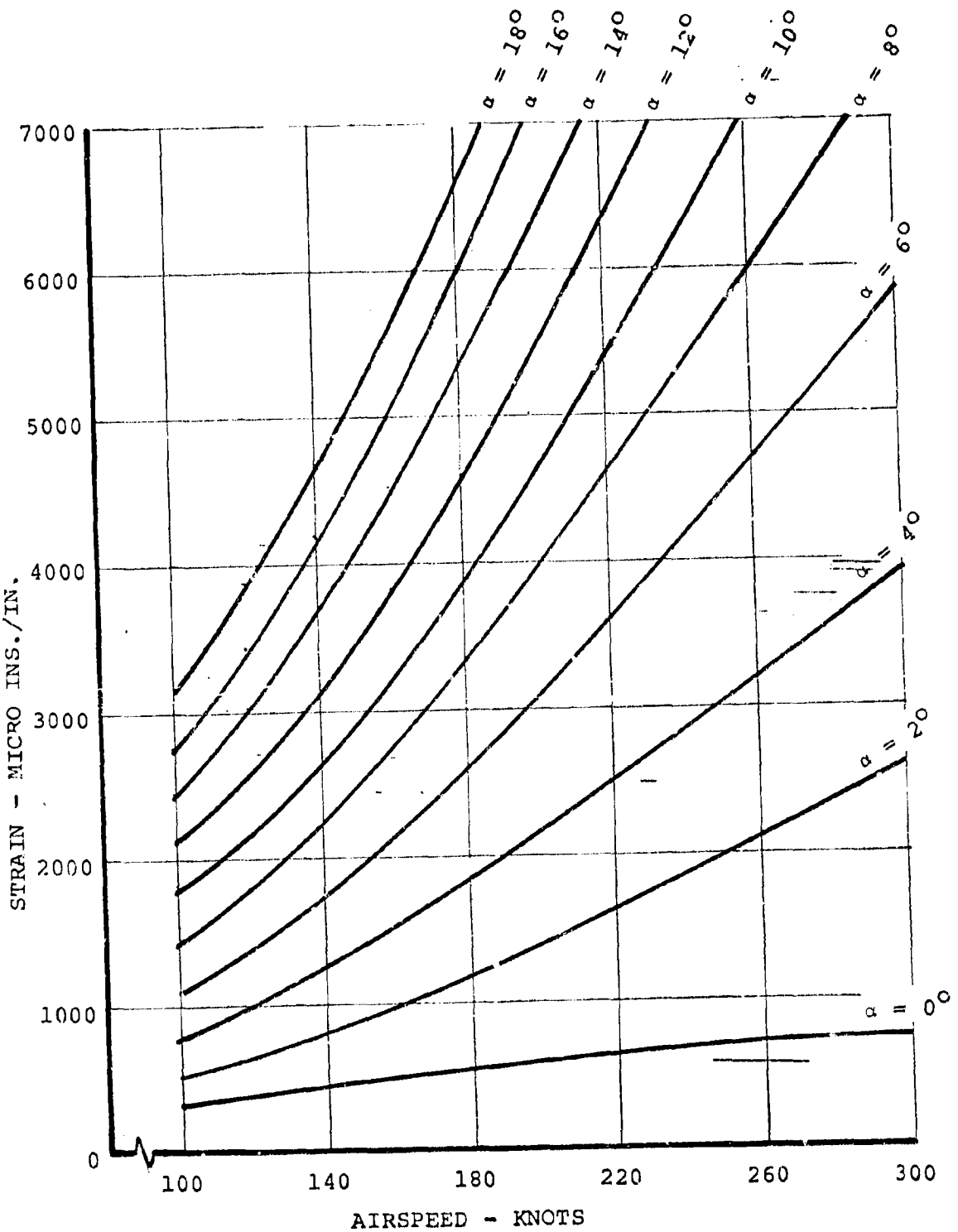

FIGURE A.5.40. ALTERNATING BLADE ROOT STRAIN IN CRUISE, 8.5% RADIUS, 386 RPM, 12,000 FEET

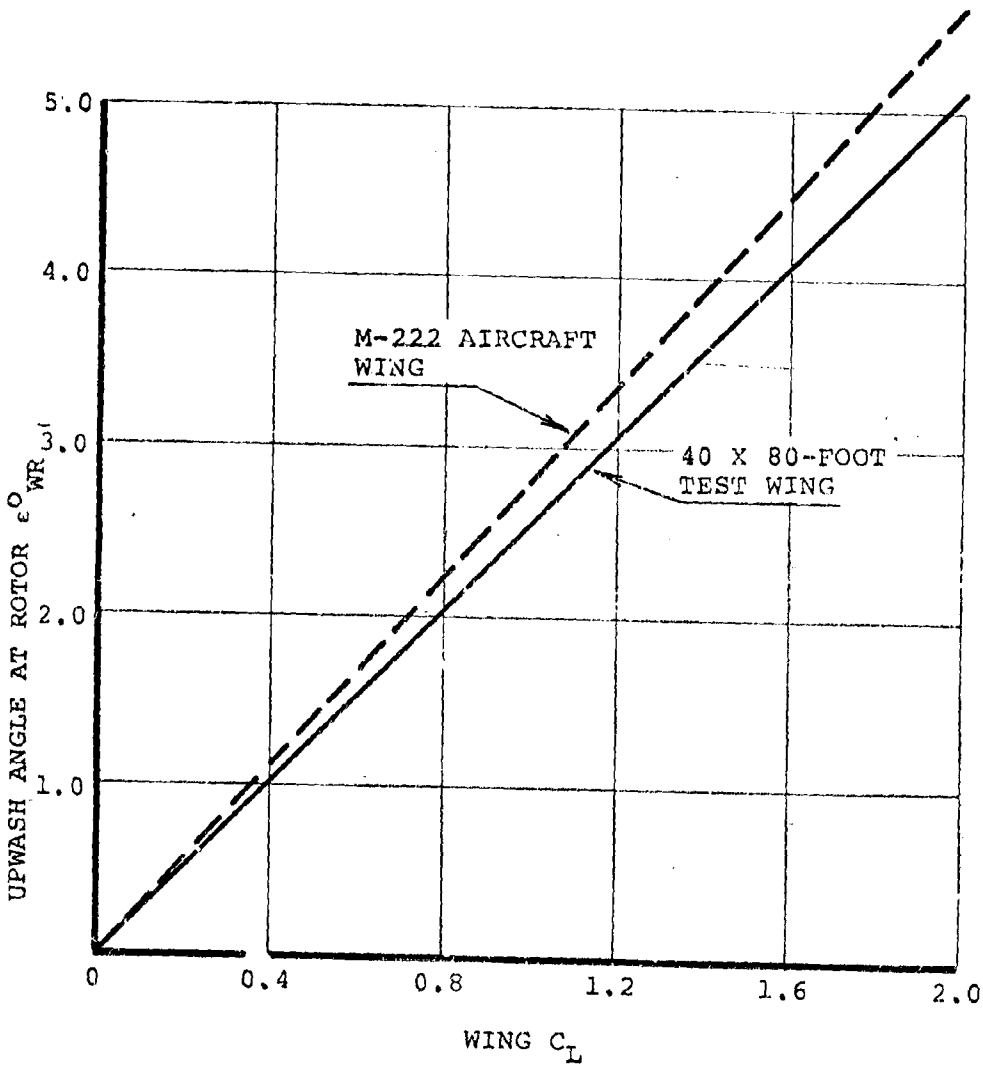

FIGURE A.5.41. COMPARISON OF WING-ROTOR EFFECTS FOR M-222 AIRCRAFT AND 40 X 80-FOOT WIND TUNNEL TEST CONFIGURATIONS

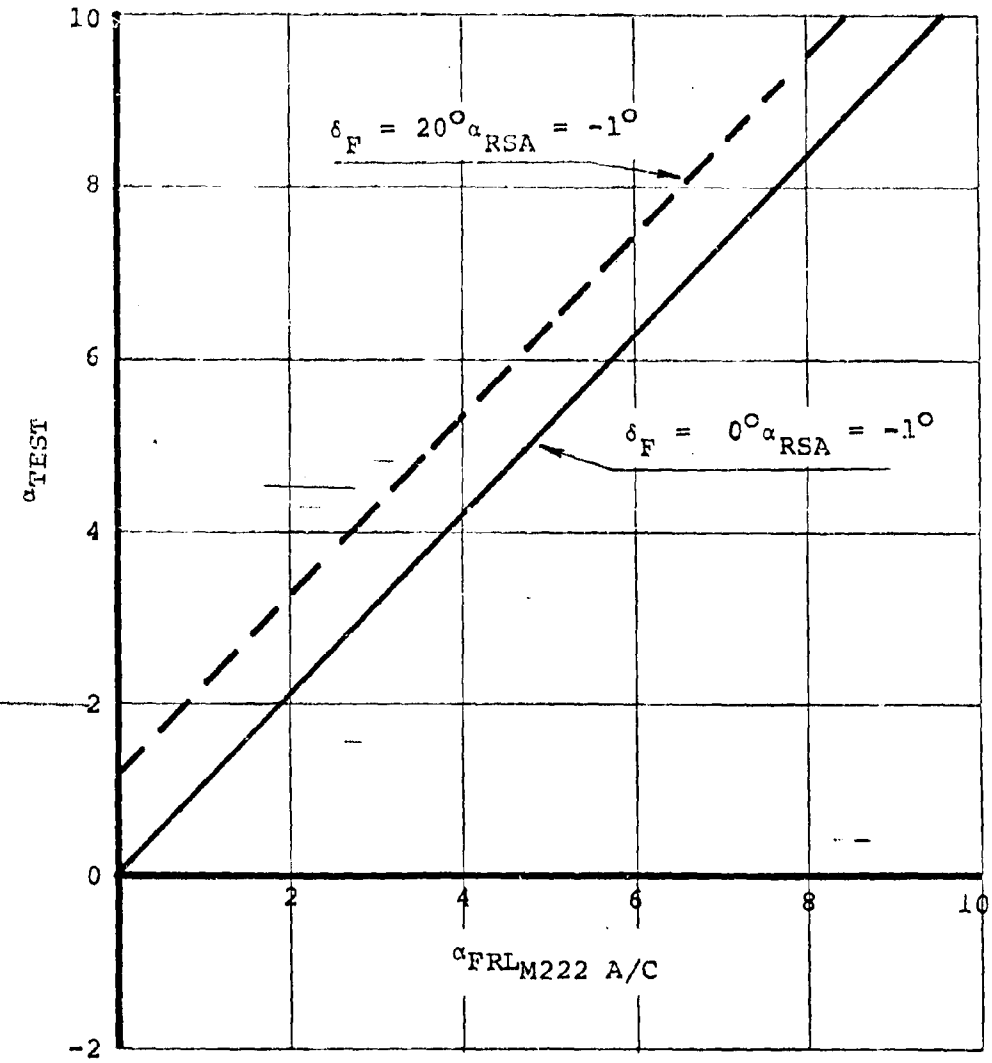

FIGURE A.5.42. RELATIONSHIP BETWEEN TEST ANGLE OF ATTACK AND MODEL 222 AIRCRAFT ANGLE OF ATTACK

M-222 1g TRIMMED CRUISE FLIGHT
386 RPM, SEA LEVEL, STANDARD DAY
$\alpha_{RSA} = -1.0^0$

- NO CYCLIC
- FEEDBACK OFF
- GW = 12,321 LBS

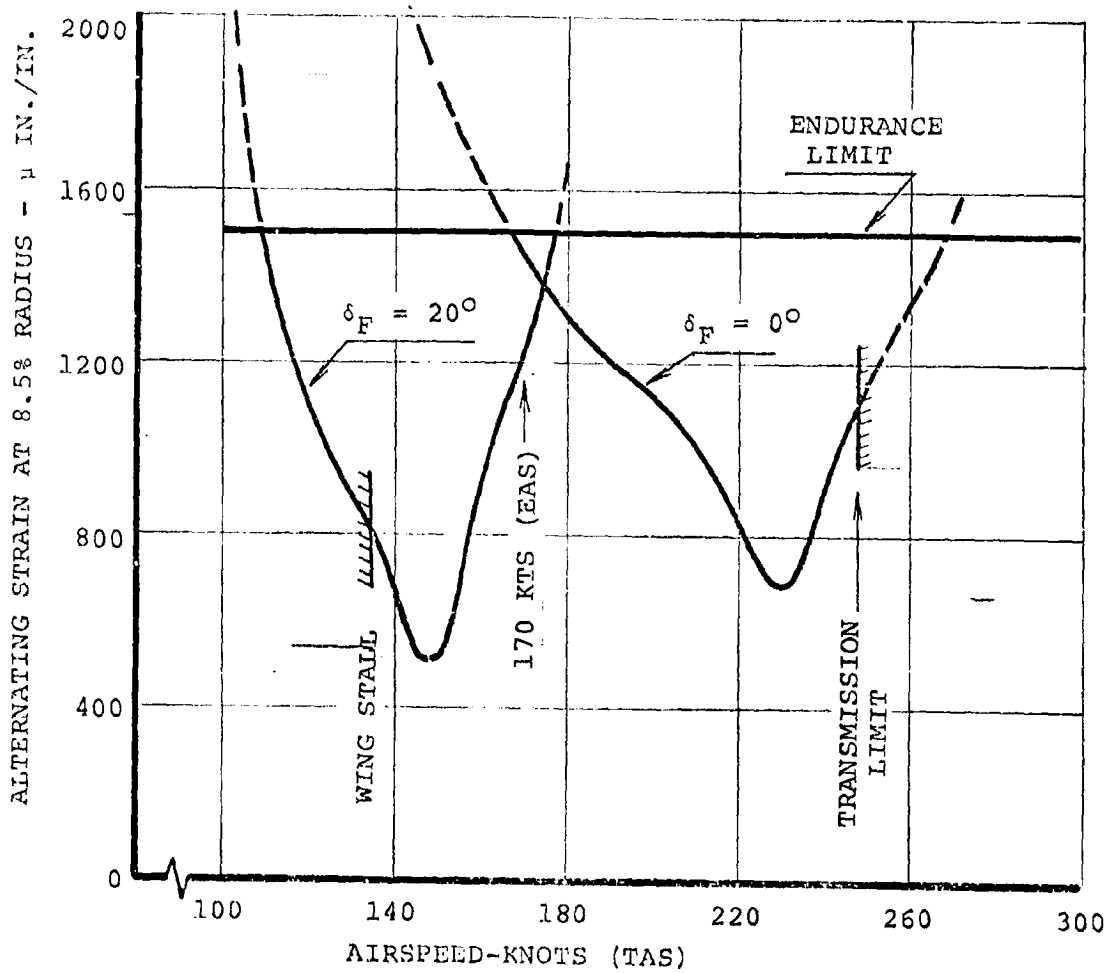

FIGURE A.5.43. ALTERNATING BLADE STRAIN AT 8.5% RADIUS FOR 1g TRIMMED FLIGHT, SEA LEVEL, STANDARD DAY, 386 RPM

M-222 1g TRIMMED CRUISE FLIGHT
386 RPM,12,000 FEET, STANDARD DAY
$\alpha_{RSA} = -1.0^{\circ}$

- NO CYCLIC
- FEEDBACK OFF
- GW = 12,321 LBS

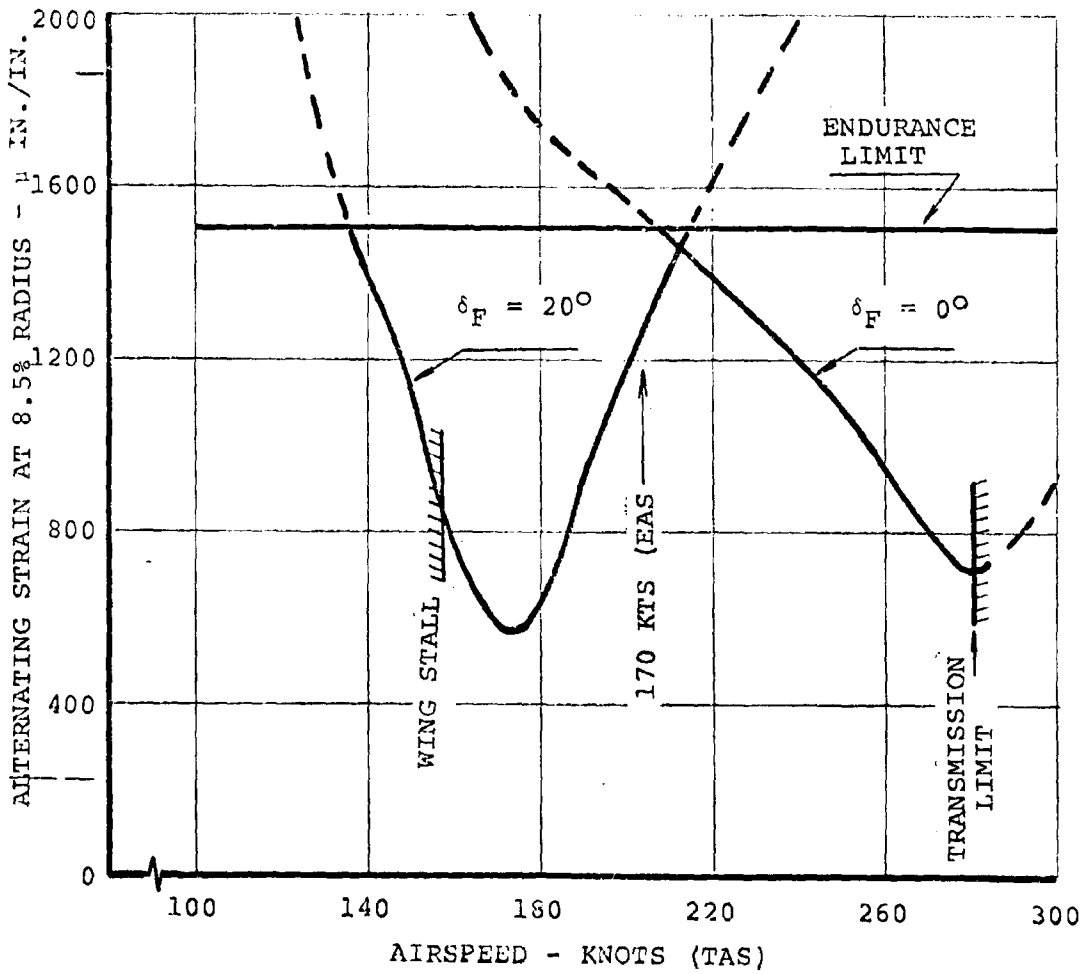

FIGURE A.5.44. ALTERNATING BLADE STRAIN AT 8.5% RADIUS FOR 1g TRIMMED FLIGHT, 12,000 FEET, STANDARD DAY, 386 RPM

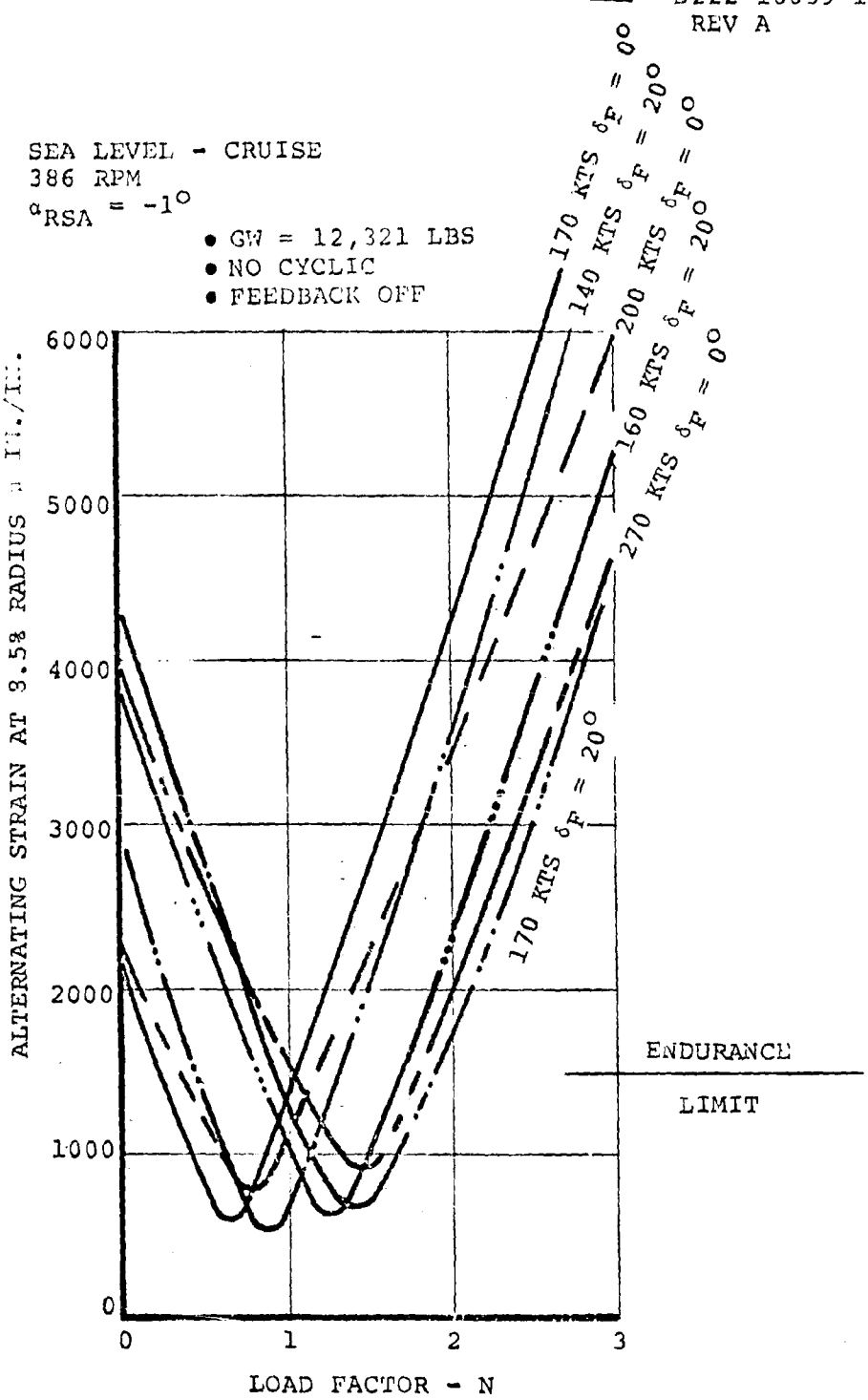

FIGURE A.5.45. EFFECT OF MANEUVER LOAD FACTOR ON ALTERNATING BLADE ROOT STRAIN

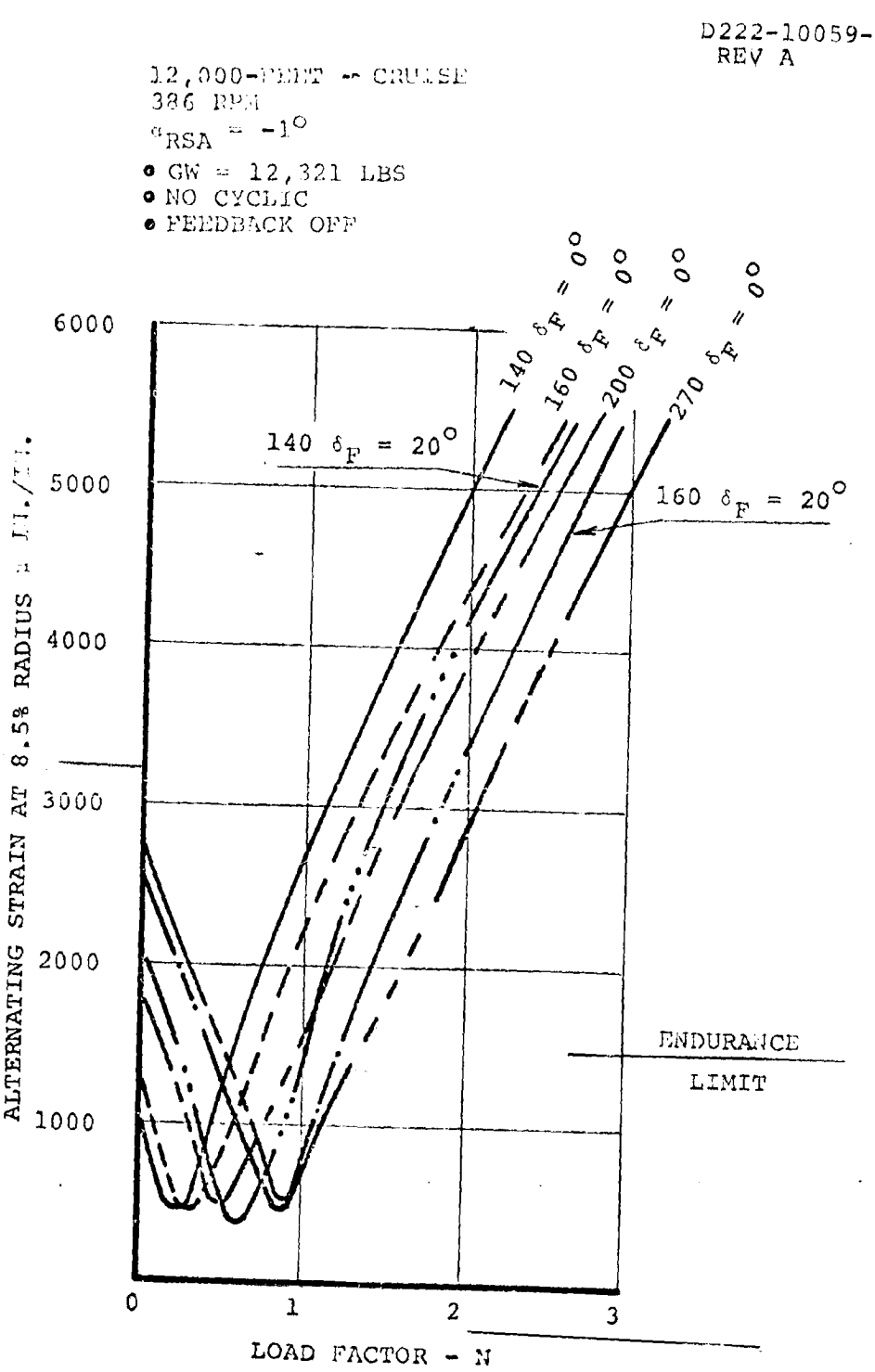

FIGURE A.5.46. EFFECT OF MANEUVER LOAD FACTOR ON ALTERNATING BLADE ROOT STRAIN

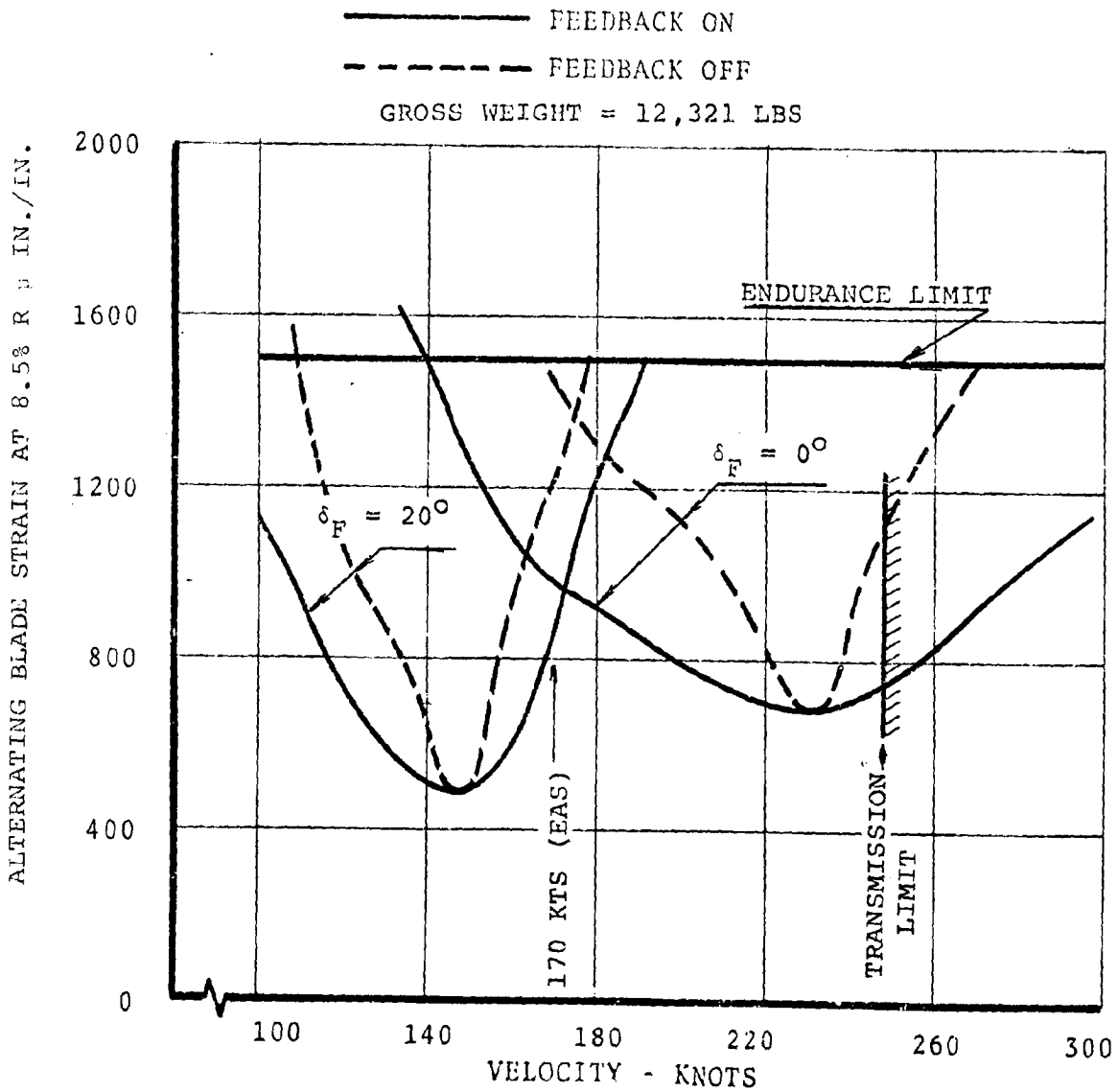

FIGURE A.5.47. 1G FLIGHT BLADE ROOT ALTERNATING STRAIN WITH AND WITHOUT FEEDBACK

SLA LEVEL
386 RPM
$\delta_{RSA} = -1^{\circ}$

FEEDBACK ON

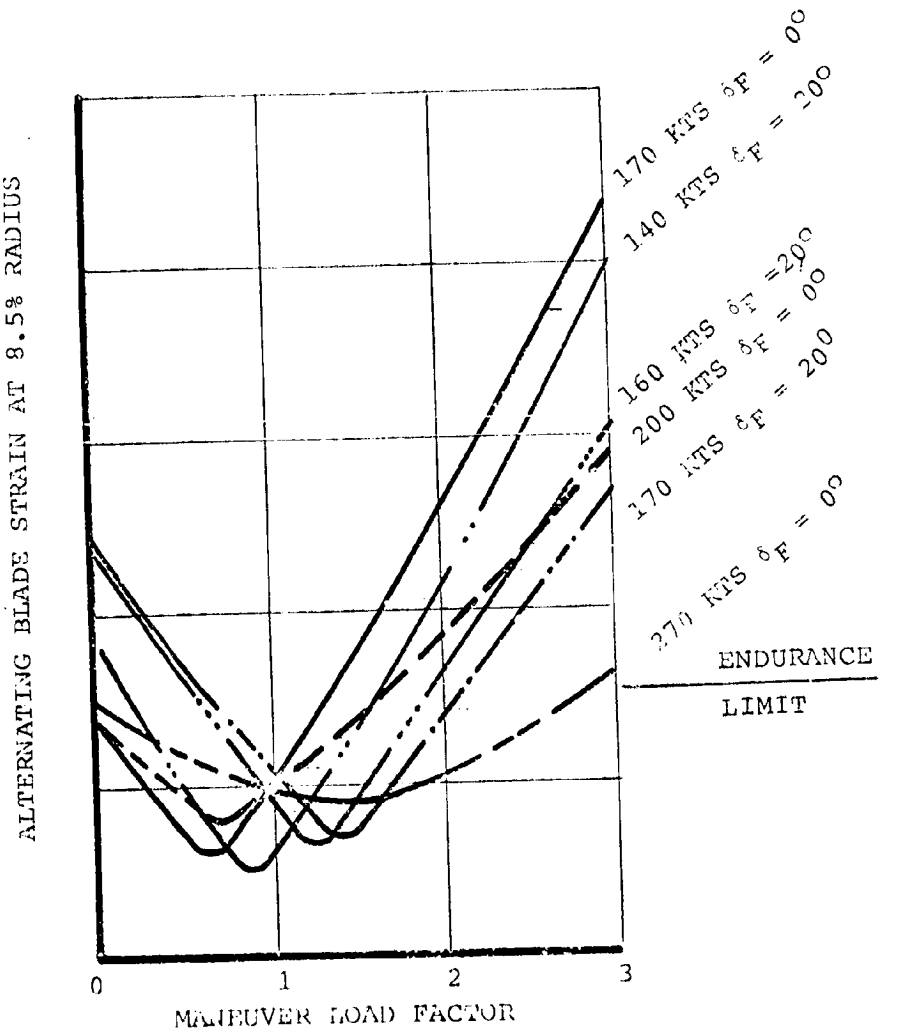

FIGURE A.5.48. EFFECT OF MANEUVER LOAD FACTOR ON ALTERNATING BLADE STRAIN - FEEDBACK ON

BLADE FATIGUE

The blade fatigue life is calculated based upon cumulative damage theory and 1000 hours of flight.

The blade root design S-N curve (mean -3σ) shown in Figure A.5.49 is based upon a full scale fatigue test failure and the curve shape taken from coupon data. A 10% coefficient of variation was used. This design curve is based upon a great deal of materials test data which is summarized in Reference 27, Volume 13.

The fatigue design condition for the blade (5×10^7 cycles endurance limit) was established from cyclic control usage in hover and transition. Control utilization data was taken from NASA TND-5342 "Simultaneous Usage of Attitude Control for Maneuvering, Determined by In-Flight Simulation". The data in this report were checked against the Journal of Aircraft, Volume IV, No. 5, September-October 1967 titled "Control Power Usage for Maneuvering in Hover of the VJ 101 Aircraft" and against data obtained during production test flights of CH-47C helicopters. The data from the three sources agreed quite well, with TND-5342 showing generally slightly higher control utilization. A summary plot from the TND is shown as Figure A.5.50. Based on these data the blade endurance limit criterion was established as follows:

> The rotor component endurance limits (fatigue strength at 5×10^7 cycles) shall be greater than the vibratory loads or stresses resulting from the following heli-

copter flight conditions:

Application of sufficient control in hover to generate .16 radians per sec yaw acceleration plus .24 radians per sec acceleration in pitch plus the maximum cyclic for CG trim. These are the maximum accelerations about each of these axes experienced during the maneuvers reported in NASA TN-5342

Since this report shows that maximum control was never applied about two axes at the same time, the requirement to consider pitch and yaw applications as simultaneous is considered conservative.

In order to determine the fatigue life of the blade, a schedule was then established for various maneuvers which might result in loads in excess of the endurance limit.

The maneuver and gust spectrum of Figure A.5.51 is based on Specification MIL-A-008866A. It was necessary to assign durations and airspeeds to each of these maneuvers. This was done in accordance with Figures A.5.52 to A.5.54. Short times are assigned to the high g maneuvers, because the aircraft does not have the performance capability to sustain them. Longer durations are assigned to the intermediate g levels which may be used for turns.

FIGURE A.5.49. S-N CURVE FOR BLADE SPAR ROOT END

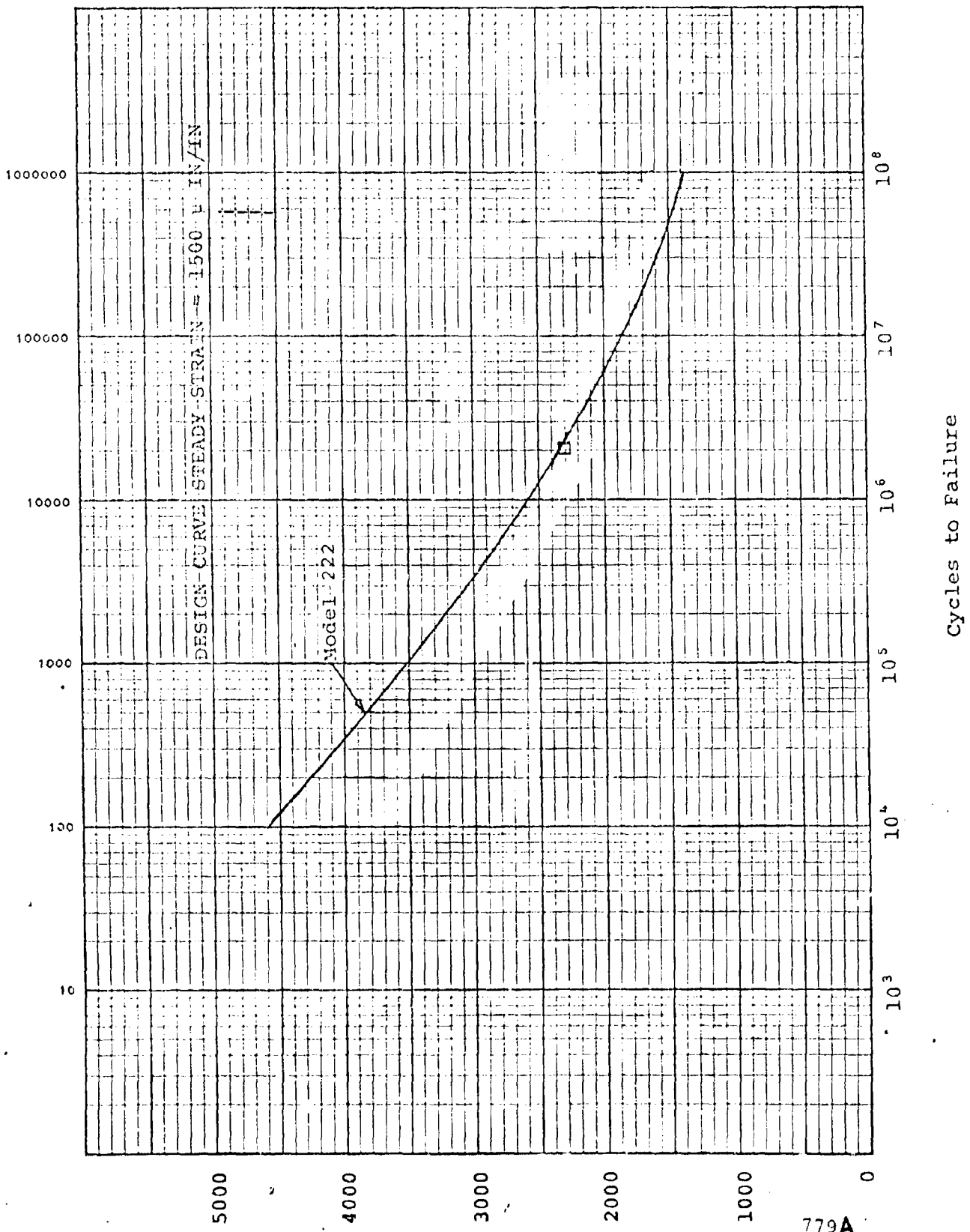

NOTE:
REF. NASA-TN D-5342

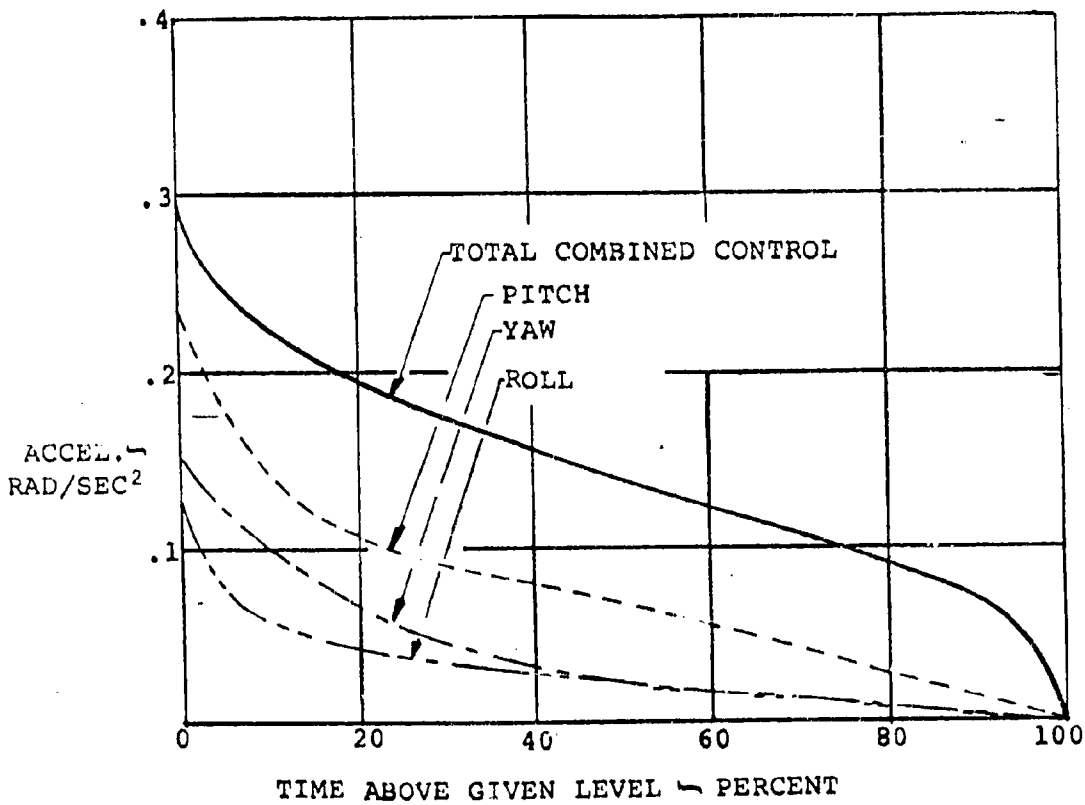

FIGURE A.5.50. TIME DISTRIBUTIONS FOR CONTROL USAGE IN S-TURNS

COMBINED GUST AND MANEUVER LOAD SPECTRUM

N_Z MAX	N_Z MIN	OCCURRENCE PER 1000 TOTAL AIRCRAFT FLIGHT HOURS
2.8	-.2	1
2.6	-.1	2.8
2.4	0	6.5
2.2	.1	20
2.0	.2	64
1.8	.3	269
1.6	.45	1683
1.4	.65	15392
1.2	.85	261495

MANEUVER AND GUST SPECTRUM BASED ON DISCRETE GUST ANALYSIS WITH MISSION PROFILE BASED ON FLYING THE ENVELOPE AT H_D = 5,000 FEET (MIL-A-008866A).

FIGURE A.5.51

BASIC FATIGUE LOADING SCHEDULE-BLADE CYCLIC SCHEDULE (SEE NOTE)

A. DEFINED MANEUVERS (FOR INITIAL FLIGHT RESEARCH PHASE)

MANEUVER	% CONTROL	CYCLIC (DEGREES)	TOTAL TIME (SECS)
Hover Yaw	100	3.5	240
Control	80	2.9	240
Power	60	2.3	240

B. ARBITRARY MANEUVERS (IN ADDITION TO THE MANEUVERS LISTED IN "A" ABOVE)

% MAX CYCLIC	CYCLIC (DEGREES)	TIME IN SECS FOR 100 FLIGHT HOURS
90	6.3	1
80	5.6	5
70	4.9	10
60	4.2	20
50	3.5	50
40	2.8	200
30	2.1	1500

NOTE: THIS SCHEDULE APPLIES FOR HOVER AND TRANSITION MODES OF FLIGHT ONLY.

FIGURE A.5.52

FIGURE A.5.53. MANEUVER AND GUST DISTRIBUTION

G MAXIMUM	% HOVER	% TRANSITION	% CRUISE	TIME/MANEUVER SECONDS
2.8	0	0	100	.5
2.6	0	0	100	.5
2.4	0	30	70	1.0
2.2	0	30	70	1.0
2.0	10	50	40	1.5
1.8	30	50	20	3.0
1.6	50	30	20	5.0
1.4	50	30	20	2.0
1.2	50	30	20	.5

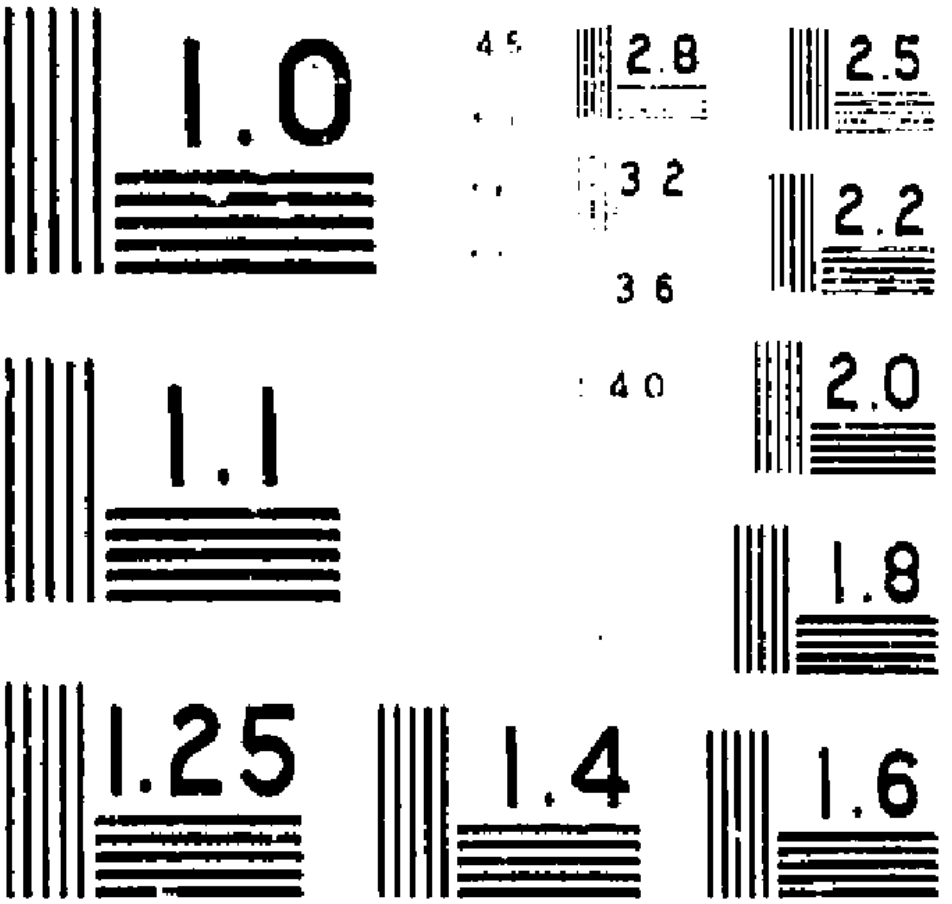

MODEL 222 MANEUVER SCHEDULE FOR 1000 FLIGHT HOURS

MAXIMUM G	MINIMUM G	VELOCITY KNOTS	ROTOR RPM	TIME IN MANEUVER SECONDS	NUMBER OF ROTOR CYCLES
2.8	-.2	270	386	.25	1.803
		200	386	.25	1.803
2.6	-.1	270	386	.7	4.503
		200	386	.7	4.503
2.4	0	270	386	1.1375	7.317
		200	386	1.1375	7.317
		170	386	1.1375	7.317
		140	386	1.1375	7.317
		125 i_N = 35°	505	.65	5.47
		100 i_N = 5°	536	.65	5.80
		75 i_N = 70°	551	.65	5.96
2.2	.1	270	386	3.5	22.51
		200	386	3.5	22.51
		170	386	3.5	22.51
		140	386	3.5	22.51
		125 i_N = 35°	505	2.0	16.83
		100 i_N = 50°	536	2.0	17.86
		75 i_N = 70°	551	2.0	18.36
2.0	.2	270	386	9.6	61.75
		200	386	9.6	61.75
		170	386	9.6	61.75
		140	386	9.6	61.75
		125 i_N = 35°	505	16.	134.6
		100 i_N = 50°	536	16.	142.9
		75 i_N = 70°	551	16.	146.9

FIGURE A.5.54

MODEL 222 MANEUVER SCHEDULE FOR 1,000 FLIGHT HOURS (CONTINUED)

G MAXIMUM	G MINIMUM	VELOCITY KNOTS	ROTOR RPM	TIME IN MANEUVER SECONDS	NUMBER OF ROTOR CYCLES
1.8	.3	270	386	40.35	259.5
		200	386	40.35	259.5
		170	386	40.35	259.5
		140	386	40.35	259.5
		125 $i_N = 35^o$	505	134.5	1132.
		100 $i_N = 50^o$	536	134.5	1201.
		75 $i_N = 70^o$	551	134.5	1035.
1.6	.45	270	386	420.7	2706.5
		200	386	420.7	2706.5
		170	386	420.7	2706.5
		140	386	420.7	2706.5
		125 $i_N = 35^o$	505	841.5	7092.
		100 $i_N = 50^o$	536	841.5	7516.
		75 $i_N = 70^o$	551	841.5	7727.
1.4	.65	270	386	1539.2	9902.1
		200	386	1539.2	9902.1
		170	386	1539.2	9902.1
		140	386	1539.2	9902.1
		125 $i_N = 35^o$	505	3078.	25909.
		100 $i_N = 50^o$	536	3078.	27500.
		75 $i_N = 70^o$	551	3078.	28269.
1.2	.85	270	386	65373.	42056.4
		200	386	65373.	42056.4
		170	386	65373.	42056.4
		140	386	65373.	42056.4
		125 $i_N = 35^o$	505	13074.	11045.
		100 $i_N = 50^o$	536	13074.	116801.
		75 $i_N = 70^o$	551	13074.	120069.

FIGURE 7.5.54 (CONTINUED)

Short durations are again assigned to the low g maneuvers which may be due to gust encounter, minor trim corrections, etc.

The maneuvers of part A of Figure A.5.52 are specific maneuvers which it is expected will be performed as part of the aircraft control evaluation.

The maneuvers of part B of Figure A.5.52 are purely arbitrary. TND-5342 would indicate no utilization of cyclic in excess of 2-degrees based on approximately 20 hours of flight. The values quoted for utilization per 100 hours are, therefore, considered reasonably conservative.

In transition three airspeed and nacelle incidence conditions have been used, 75 knots i_N = 70, 100 knots i_N = 50 and 125 knots i_N = 35-degrees. One third of the transition time is assumed to be spent at each condition.

Hover and transition maneuvers are assumed to be performed at sea level. For the nominal schedule a normal flying gross weight of 12,321 pounds has been used with nominal CG location. It is anticipated that most of the cruise flight for the research aircraft would be performed between sea level and 12,000 feet altitude, since oxygen would be required at high altitudes. For this reason the nominal fatigue schedule assumes 50% cruise time at sea level and 50% at 12,000 feet.

The cruise maneuvers are assumed to be performed at 140, 170, 200 and 270 knots. For 12,000 feet altitude the maneuvers at 140 knots are only performed up to 1.6 g's since higher load factors exceed the aircraft maximum C_L at that altitude. The higher g cases at 140 knots are assumed to be at sea level. The nominal case discussed above is performed with no cyclic control/feedback cruise and as such is a very conservative fatigue design condition.

The fatigue life data are given for hover, transition and cruise in Figures A.5.55 to A.5.58, and give

	Σ n/N X 10^6 =	11,611	hover
	Σ n/N X 10^6 =	46,840	transition (3/rev assumed)
(50% cruise time)	Σ n/N x 10^6 =	18,458	sea level cruise
(50% cruise time)	Σ n/N X 10^6 =	120,231	12,000 feet cruise
		197,140	

$$\text{calculated life} = \frac{1000}{0.197150} = 5{,}080 \text{ hours}$$

The blade fatigue life for this nominal fatigue schedule is more than five times the anticipated usage of the vehicle (1,000 hours) with no cyclic feedback system operative.

Calculations indicate that the fatigue life is in excess of 16,000 hours with the cyclic feedback system on.

FIGURE A.5.55. NOMINAL CASE - DEFINED MANEUVERS - HOVER

PART A CYCLIC	CYCLES (n)	VIB. STRAIN μ IN./IN.	(CYCLES TO FAIL. N X 10^{-6})	n/N X 10^6
3.33	2204	2010	5.8	380
2.66	2204	1580	33.0	66.7
1,998	2204	1230	300	7.3
				Σ 454.0
PART B				
6.3	92	3775	.056	1642.8
5.6	460	3350	.15	3066.6
4.9	920	2940	.37	2486.5
4.2	1840	2520	1.1	1672.7
3.5	4600	2100	4.0	1150.0
2.8	18400	1675	27.0	681.48
2.1	137000	1250	300.0	456.6
				Σ11156.8

PARTS A & B TOTAL n/N Σ X 10^6 = 11,610.8

FIGURE A.5.56. TRANSITION (NOMINAL SCHEDULE) 3/REV

LOAD FACTOR "G"	VELOCITY KNOTS	ALTITUDE FEET	CYCLES n AT 3/REV	VIBRATORY STRAIN + μ IN./IN.	CYCLES TO FAILURE $_6$ N X 10^{-6}	n/N X 10^{-6}
2.4	75		17.97	3200	.2	89.8
	100		17.41	3950	.037	470.5
	125		16.41	3850	.047	349.1
2.2	75		55.08	3050	.27	204.0
	100		53.58	3450	.13	412.15
	125		50.49	3300	.16	315.56
2.0	75		440.7	2775	.6	734.5
	100		428.7	3000	.35	1224.8
	125		403.8	2825	.53	761.8
1.8	75		3705	2375	1.8	2058.3
	100		3603	2575	1.0	3603.
	125		3396	2375	1.8	1886.6
1.6	75		23181	1950	7.5	3090.8
	100		22548	2200	3.0	7516.
	125		21245	1950	7.5	2832.6
1.4	75		84807	1500	50	1696.
	100		82500	1850	10	8250.
	125		77727	1600	30	2590.9
1.2	75		360207	1150	900	400.2
	100		350403	1300	200	1752.
	125		330135	1500	50	6602.
1.0	75			900		
	100			750		
	125			1050		

Σ 46,840.6 (3/REV)
15,613.5 (1/REV)

FIGURE A.5.57. CRUISE SEA LEVEL - NO FEEDBACK

LOAD FACTOR "G"	VELOCITY KNOTS	ALTITUDE FEET	CYCLES n	VIBRATORY STRAIN + μ IN./IN.	CYCLES TO FAILURE N X 10^{-6}	n/N X 10^{-6}
2.8	270	S.L.	1.608	4100	.028	57.42
	200		1.608	5450	.002	802.
2.6	270		4.503	3600	.08	56.28
	200		4.503	4900	.006	750.5
2.4	270		7.318	3000	.34	21.52
	200			4400	.015	487.86
	170-0°		3.659	5500	.0019	1925.
	-20°		3.659	2750	.65	5.63
	140		7.318	4850	.0085	860.9
2.2	270		22.516	2500	1.3	17.32
	200			3950	.37	60.85
	170		11.258	4850	.007	160.8
			11.258	2200	3.6	3.13
	140		22.516	4200	.023	978.9
0	270		61.76	2000	9.5	6.50
	200			3450	.12	514.6
	170		30.88	4200	.022	1403.6
			30.88	1700	19.	1.62
	140		61.76	3550	.09	686.2
1.8	270		259.58	1500	50.	5.19
	200			2950	.38	683.1
	170		129.79	3600	.08	1622.4
			129.79	1300	200.	.648
	140		259.58	2950	.4	648.9
1.6	270		2706.8	1100		
	200			2500	1.3	2082.1
	170		1353.4	3000	.35	3866.8
			1353.4	900		
	140		2706.8	2350	1.8	1503.7
1.4	270		9902.18	950		
	200			2000	6.	1650.4
	170		4951.09	2500	1.3	3808.5
			4951.09	700		
	140			1750	15.	660.1
1.2	270		6537.38	1200	500.	13.07
	200			1500	30.	217.9
	170		3268.69	1350	10.	326.8
			3268.69	850		
	140		6537.38	1220	400.	16.3
1.0	250			1100		
	200		1.16×10^6	1120	1000.	1160.
	170		$.58 \times 10^6$	1450	65.	8900.
			$.58 \times 10^6$	1220	360.	1610.
	140		1.16×10^6	680		

Σ 36,916.438

FIGURE A.5.58. CRUISE 12,000 FT. - NO FEEDBACK

LOAD FACTOR "G"	VELOCITY -- KNOTS	ALTITUDE FEET	CYCLES n	VIBRATORY STRAIN + μ IN./IN.	CYCLES TO FAILURE N X 10^{-6}	n/N X 10^{-6}
2.8	270	12,000	1.608	4600	.01	160.8
	200			5500	.0027	595.5
2.6	270		4.503	4200	.023	195.8
	200			4750	.008	562.9
2.4	270		7.318	3800	.053	138.1
	200		7.318	4700	.008	915.
	170		3.659	5350	.0025	1463.6
	170	12,000	3.659	4050	.03	121.9
	140	S.L.	7.318	4850	.007	1023.4
2.2	270	12,000	22.516	3350	.17	132.4
	200			4300	.018	1250.8
	170		11.258	4900	.0055	2046.9
	170	12,000		3600	.083	135.6
	140	S.L.	22.516	4200	.023	979.0
2.0	270	12,000	61.76	2850	.5	123.5
	200			3900	.043	1436.2
	170		30.88	4450	.015	2058.6
	170	12,000		3170	.23	134.3
	140	S.L.	61.76	3550	.09	686.2
3	270	12,000	259.58	2400	1.7	152.7
	200			4500	.013	1996.
	170		129.79	4050	.03	4326.3
	170	12,000		2710	.7	185.4
	140	S.L.		2950	.37	701.6
1.6	270	12,000	2706.8	2000	6.	451.1
	200			3100	.26	10407.
	170		1353.4	3550	.09	15037.
	170			2230	3.	451.1
	140	12,000		3300	.170	15922.2
1.4	270		9902.18	1600	30.	330.
	200			2600	.95	10423.
	170		4951.09	3100	.26	19042.
	170			1770	15.	330.1
	140			2800	.55	18002.
1.2	270		6537.4	1150	50.	130.7
	200			2000	6.	1089.5
	170		3268.69	2550	1.2	2723.9
	170			1250	300.	10.89
	140			2250	3.	2179.0
1.0	270		1.16 X 10^6	800		
	200		1.16 X 10^6	1180	600.	1935.
	170		.58 X 10^6			
	170		.58 X 10^6	1880	9.5	96700.
	140		1.16 X 10^6	1390	200.	5805.

Σ 240,463.